NUCLEAR PHYSICS

JOURNAL DEVOTED TO THE EXPERIMENTAL AND THEORETICAL STUDY OF THE FUNDAMENTAL CONSTITUENTS OF MATTER AND THEIR INTERACTIONS

EDITOR: L. ROSENFELD - COPENHAGEN
ASSOCIATE EDITOR: O. NATHAN - COPENHAGEN

VOLUME X

NORTH-HOLLAND PUBLISHING COMPANY - AMSTERDAM

NUCLEAR PHYSICS

EDITORIAL BOARD

AUSTRALIA & NEW ZEALAND:	H. Messel (Sydney), M. L. Oliphant (Canberra)
AUSTRIA:	B. Karlik, (Vienna), H. Thirring (Vienna)
BELGIUM:	M. de Hemptinne (Louvain), J. Verhaeghe (Ghent)
CANADA:	G. Volkoff (Vancouver)
DENMARK:	C. Møller (Copenhagen), S. Rozental (Copenhagen)
FINLAND:	L. Simons (Helsinki)
FRANCE:	A. Berthelot (Saclay), S. Gorodetzky (Strasbourg)
GERMANY (DEM. REP.):	G. Hertz (Leipzig)
GERMANY (FED. REP.):	W. Gentner (Freiburg i. B.), J. H. D. Jensen (Heidelberg)
GREAT BRITAIN:	S. Devons (Manchester), T. H. R. Skyrme (Harwell)
HUNGARY:	L. Janossy (Budapest)
INDIA:	H. Bhabha (Bombay), B. Peters (Bombay), R. Ramanna (Trombay)
IRISH REPUBLIC:	J. McConnell (Maynooth)
ISRAEL:	G. Racah (Jerusalem)
ITALY:	E. Amaldi (Rome)
JAPAN:	S. Kikuchi (Tokyo), S. Tomonaga (Tokyo)
MEXICO:	M. Moshinsky (Mexico)
NETHERLANDS:	H. Brinkman (Groningen), S. R. de Groot (Leiden)
NORWAY:	E. Hylleraas (Oslo), A. Lundby (Oslo), H. Wergeland (Trondheim)
POLAND:	L. Infeld (Warsaw)
PORTUGAL:	J. M. Araújo (Porto), J. R. de Almeida Santos (Coimbra)
SOUTH AMERICA:	G. Beck (Saõ Paulo), J. Leite Lopes (Rio de Janeiro)
SPAIN:	J. M. Otero (Madrid), C. Sanchez del Rio (Madrid)
SWEDEN:	O. Klein (Stockholm), K. Siegbahn (Uppsala), I. Waller (Uppsala)
SWITZERLAND:	P. Huber (Basel), P. Scherrer (Zürich)
U.A.R. & ARAB COUNTRIES:	F. El Bedewi (Alexandria), M. G. Nooh (Cairo)
U.S.A.:	H. H. Barschall (Madison, Wisconsin), V. Weisskopf (Cambridge, Mass.)
U.S.S.R.:	M. A. Markov (Moscow), I. S. Shapiro (Moscow), D. V. Skobeltzyn (Moscow)
YUGOSLAVIA:	I. Supek (Zagreb)

NUCLEAR PHYSICS

JOURNAL DEVOTED TO THE EXPERIMENTAL AND THEORETICAL STUDY OF THE FUNDAMENTAL CONSTITUENTS OF MATTER AND THEIR INTERACTIONS

EDITOR: L. ROSENFELD · COPENHAGEN

VOLUME X

FEBRUARY 1959—MAY 1959

MASTER AUTHOR INDEX VOLUMES I—X

MASTER SUBJECT INDEX VOLUMES I—X

NORTH-HOLLAND PUBLISHING COMPANY - AMSTERDAM

PRINTED IN THE NETHERLANDS

Photo Bettina, Zürich

WOLFGANG PAULI
(1900—1958)

10.C *Nuclear Physics* **10** (1959) 1—5; © *North-Holland Publishing Co., Amsterdam*
Not to be reproduced by photoprint or microfilm without written permission from the publisher

WOLFGANG PAULI
(1900—1958)

M. FIERZ
Seminar für theoretische Physik der Universität Basel

Eingegangen am 19. Januar 1959

Am 15. Dezember 1958 ist Wolfgang Pauli unerwartet gestorben. Wer ihn näher kannte, mußte zwar schon längere Zeit mit Sorgen sehen, daß ihn etwas schwer bedrückte. Er selber hatte das Gefühl in einer kritischen Situation zu stehen. Nun wissen wir, daß mit einer geheimen, schweren Krankheit der Schatten des Todes über ihn gekommen war.

Mit Pauli hat nicht nur ein bedeutender Gelehrter, sondern auch ein sehr eindrucksvoller, geheimnisvoller Mensch unsere Erde verlassen.

Wolfgang Pauli wurde am 15. April 1900 in Wien geboren. Sein Vater war dort Professor der physikalischen Chemie. Schon als Gymnasiast studiert Pauli die damals neue Relativitätstheorie Einstein's. Er sagte mir einst, er erinnere sich noch lebhaft an die Stunde, in der ihm Einstein's Gedankengang plötzlich klar geworden sei. Wie Schuppen sei es ihm von den Augen gefallen. Darum entschloß er sich auch, bei Sommerfeld theoretische Physik zu studieren und bezog nach Abschluß seiner Schulzeit die Universität in München. Im Alter von 19 Jahren veröffentlichte er zwei Arbeiten [1]) über H. Weyl's Verallgemeinerung der Einstein'schen Theorie, die zeigen, daß er diese mathematisch sehr komplizierte Theorie vollkommen beherrschte. Darum wurde ihm auch der Auftrag gegeben, den Artikel über Relativitätstheorie für die Encyklopaedie [2]) zu schreiben. So entstand ein Buch von 200 Seiten, in dem eine große und weit verstreute Literatur überlegen verarbeitet ist. Diese Arbeit hat auch heute nichts von ihrem Glanz verloren. Pauli erwies hier zum ersten Male seine kritische und zusammenfassende Gestaltungskraft, die sich erneut in seinen beiden Handbuchartikeln über Quantentheorie bewähren sollte. 1922, nach Abschluß seiner Studien in München, ging er erst nach Göttingen und von dort an's Bohr'sche Institut nach Kopenhagen. Hier vertiefte er sich in die Theorie des anomalen Zeemaneffektes [3]), eine Erscheinung die damals völlig rätselhaft war.

Pauli's Bemühungen um ihre Erklärung sollte ihn zur Entdeckung und Formulierung des nach ihm benannten Ausschließungs-Prinzips führen †.

† Vergleiche hiezu den Nobel-Vortrag [44]).

In Hamburg, wohin er 1923 als Assistent von Lenz und als Privatdozent gegangen war, wurde es ihm klar, daß von den Vorstellungen, die man sich bisher über die Multiplett-Aufspaltung der Spektralterme gemacht hatte nur richtig war, daß das Auftreten von Multipletts eng mit dem Schalenabschluß der Elektronenkonfigurationen im Atom zusammenhing. Insbesondere wies er 1924 nach, daß die Ursache der magnetischen Anomalie nicht ein resultierendes Moment der abgeschlossenen K-Schale sein könne. Er sagt in seiner Arbeit „Über den Einfluß der Geschwindigkeitsabhängigkeit der Elektronenmasse auf den Zeemaneffekt" [4]):

> „Die abgeschlossenen Elektronenkonfigurationen sollen nichts zum magnetischen Moment und zum Impulsmoment des Atoms beitragen. Insbesondere werden bei den Alkalien die Impulswerte des Atoms und seine Energieänderungen in einem äußeren Magnetfeld im wesentlichen als eine alleinige Wirkung des Leuchtelektrons angesehen, das auch als Sitz der magnetischen Anomalie betrachtet wird. Die Dublettstruktur der Alkalispektren, sowie die Durchbrechung des Larmortheorems kommt gemäß diesem Standpunkt durch eine eigentümliche, klassisch nicht beschreibbare Art von Zweideutigkeit der quantentheoretischen Eigenschaften des Leuchtelektrons zustande".

Die hier vorgeschlagene Auffassung der Komplexstruktur hat es Pauli ermöglicht, den Abschluß der Elektronengruppen im Atom zu erklären [5]). Die Zweideutigkeit der Eigenschaften der Elektronen hat nämlich zur Folge, daß zu den altbekannten Quantenzahlen, mit deren Hilfe man den Elektronenzustand beschrieb, eine neue hinzutritt, die nur zwei Werte annehmen kann. Ein in dieser Weise vollständig beschriebener Zustand ist schon „abgeschlossen", wenn er von einem einzigen Elektron besetzt ist, und zwei Elektronen sind nie im gleichen Zustand. Das ist das Pauli'sche Ausschliessungsprinzip. Während durch diese grundlegenden Untersuchungen klar wurde, daß die Multiplettstruktur der Spektralterme nichts mit einem resultierenden Impulsmoment des Atomrumpfes zu tun hat, rührt ihre Hyperfeinstruktur von einem Impulsmoment des Atomkernes her. Auch diese Erkenntnis verdanken wir Pauli [6]), der voraus sah, daß darum „das in Spektralterme geordnete Beobachtungsmaterial es ermöglichen werde, auf rein spektroskopischem Wege etwas über den Bau der Atomkerne zu erfahren".

Die „eigentümliche, klassisch nicht beschreibbare Zweideutigkeit der Eigenschaften des Elektrons" hat sich bekanntlich als Folge des Elektronenspin's erwiesen, der darum innig mit dem Ausschließungsprinzip verbunden erscheint. Freilich, damals war diese Verbindung noch unverständlich. 1940 aber konnte Pauli unter sehr allgemeinen Voraussetzungen beweisen daß alle Teilchen mit halbganzem Spin dem Ausschließungsprinzip genügen müssen [6, 24]).

Das Pauliprinzip reicht weit über den Bereich der Theorie der Atomspektren hinaus. Es ist für den Aufbau der Materie überhaupt entscheidend. Überdies aber sprengt es den Rahmen der korrespondenzmäßigen Quantentheorie und weist auf Zusammenhänge, die für uns noch im Dunkeln liegen.

1928 wurde Pauli an die Eidgenössische Technische Hochschule in Zürich berufen, der er bis an sein Lebensende treu bleiben sollte. Wie schon vorher in Hamburg, so hat er auch hier an der Entwicklung der neuen Quantenmechanik mitgearbeitet. Er hat gezeigt, wie das Wasserstoffspektrum mit Hilfe der Matrizenmechanik hergeleitet werden kann [7]) und wie der Elektronenspin wellenmechanisch beschrieben werden muß [8, 9]). Indem er die von Fermi entdeckte, und auf dem Pauliprinzip beruhende Statistik zur Erklärung des Paramagnetismus der Alkalien [10]) verwendete, legte er die Grundlage zur Quantentheorie der Metalle. Vor allem aber hat er zusammen mit Jordan [11]) und Heisenberg [12]) eine relativistische Quantentheorie der Felder entwickelt. Die mathematischen und physikalischen Schwierigkeiten, in die uns diese Theorie geführt hat, sind wohl jedem Theoretiker bekannt. Von einer befriedigenden Lösung sind wir auch heute noch weit entfernt. Pauli hat die Entwicklung mit wachem Interesse verfolgt und immer wieder eingegriffen, wenn er glaubte etwas zur Klärung der Lage beitragen zu können [13–19]).

Stets aber hat Pauli nicht nur durch seine wissenschaftlichen Publikationen, sondern auch durch persönliches Gespräch und durch einen ausgedehnten Briefwechsel eine kaum zu ermessenden kritischen und ordnenden Einfluß ausgeübt. Wie kein anderer war er fähig die reichen Ergebnisse, die eine ganze Generation erfindungsreicher Theoretiker erarbeiteten, zu einem Ganzen zusammenzufassen und so allen Gedanken ihren richtigen Platz zuzuweisen. Davon zeugen seine Handbuchartikel, vor allem derjenige über „die allgemeine Prinzipien der Wellenmechanik" [20, 21]), aus dem noch viele Theoretiker lernen werden, welches die mathematische Struktur und was der physikalische Sinn der Quantentheorie sei.

Aber nicht nur zur Quantentheorie, sondern auch zu manchem anderen Gebieten der theoretischen Physik hat Pauli fördernde Beiträge geliefert. Wier erwähen hier etwa jene kleine Arbeit zur Absorption der Reststrahlen in Kristallen [22]), die für das Verständnis der thermischen Vorgänge in Festkörpern grundlegend ist. Ja auch eine Diskussionsbemerkung, wie die Hypothese des Neutrinos [23]), konnte die größten Folgen nach sich ziehen.

Die wissenschaftlichen Ehrungen, vor allem der Nobelpreis [24]), der Pauli 1945 verliehen wurde, galten darum nicht nur dem Entdecker des Pauli-Prinzips, sondern ebensosehr dem großen Kritiker und dem Manne, der stets danach strebte, die vielen möglichen theoretischen Gesichtspunkte zu einem Ganzen zusammenzufügen.

Wie kaum ein zweiter unter den heutigen Physikern war Pauli von der

Ahnung erfüllt, daß der Versuch des Forschers, im Buche der Natur zu lesen, dazu führen muß, daß der Mensch in der Natur sein eigenes Spiegelbild erblickt. Diese Ahnung war zutiefst erlebt. Ihm waren die Grundfragen der Physik in einem geheimen und dennoch ganz lebendigen Sinne Lebensfragen. Der Harmonie, die sich in den Naturgesetzen offenbart, sollte, davon war er überzeugt, auch eine Harmonie unserer Innenwelt entsprechen.

Darum war er von den Bemühungen C. G. Jungs, die Hintergründe unserer Seele zu erhellen, tief beeindruckt. Darum besaß er auch ein eigenes ganz persönliches Verständnis für die Spekulationen der alten Naturphilosophen und Naturforscher. Die große Bedeutung solchen Spekulierens — speculum heißt der Spiegel — für die Wissenschaft hat er in seinem Aufsatz über Joh. Kepler [25]) zur erfassen gesucht †. So war Pauli ein Forscher der die große Überlieferung naturwissenschaftlichen und naturphilosophischen Denkens gültig repräsentierte. Und als solcher ist er uns, die wir seine Schüler waren, gegenübergetreten.

Freilich, er war kein Lehrer im gewöhnlichen Sinne. Seine Vorlesungen hätte sich niemand zum Muster nehmen dürfen. Sein Vortrag, anders als seine schriftliche Äußerung, war nicht glänzend. Und doch übte er einen großen Zauber auf seine Zuhörer aus. Wer überdies das Glück hatte, bei ihm als Assistent arbeiten zu dürfen, weiß welch große Förderung einem jeden dieser geniale Lehrer zuteil werden ließ. Er verstand es das, was man selber auszudenken trachtete, an's Licht zu bringen. Bei ihm glaube ich erlebt zu haben, was das Sokratische Gespräch einst war.

So wie er einen jeden mit unfehlbarer psychologischer Intuition sich selber finden ließ, so war auch sein Verhältnis zu jedem seiner zahlreichen Schüler individuell und eigentümlich. Darum haben wir alle, da er nun nicht mehr am Leben ist, einen großen Verlust erlitten.

1) Merkurperihelbewegung und Strahlenablenkung in Weyl's Gravitationstheorie. Verg. Deutsch. Phys. Ges. **21** (1919) 742.
Zur Theorie der Gravitation und der Elektrizität von Hermann Weyl. Phys. ZS **20** (1919) 457.
2) Relativitätstheorie (Teubner, Leipzig 1921).
3) Gesetzmäßigkeiten des anomalen Zeemaneffektes. ZS. f. Phys. **16** (1923) 155.
4) Über den Einfluß der Geschwindigkeitsabhängigkeit der Elektronenmasse auf den Zeemaneffekt. ZS. f. Phys. **31** (1925) 373.
5) Zusammenhang des Abschusses der Elektronengruppen im Atom mit der Komplexstruktur der Spektren. ZS. f. Phys. **31** (1925) 765.

† Vergl. auch Pauli's Artikel zum 80. Geburtstag A. Sommerfelds [26]), wo es heißt: „zu Kepler's Ellipsen hatte er auch Kepler's Geist heraufbeschworen ...".

6) The Connection Between Spin and Statistics. Phys. Rev. **58** (1940) 716; Progr. Theor. Phys. **5** (1950) 526.
Théorie quantique relativiste des particules obéissant a la statistique de Einstein-Bose. Ann. Inst. Poincaré **6** (1936) 137.
7) Über das Wasserstoffspektrum vom Standpunkt der neuen Quantenmechanik ZS. f. Phys. **36** (1929) 336.
8) Quantenmechanik des magnetischen Elektrons. ZS. f. Phys. **47** (1928) 151.
9) Diracs Wellengleichung des Elektrons und geometrische Optik. Helv. phys. acta **5** (1932) 179.
10) Über Gasentartung und Paramagnetismus ZS. f. Phys. **41** (1927) 89.
11) Zur Quantenelektrodynamik ladungsfreier Felder. ZS. f. Phys. **47** (1928) 151.
12) W. Heisenberg und W. Pauli, Zur Quantendynamik der Wellenfelder. ZS. f. Phys. **56** (1929) 1; **59** (1929) 168.
13) W. Pauli und V. Weisskopf, Über die Quantisierung der skalaren relativistischen Wellengleichung. Helv. phys. acta **7** (1934) 709.
14) Relativistic Field Theories of Elementary Particles. Revs. mod. Phys. **13** (1946) 203.
15) On Dirac's New Method of Field Quantization. Revs. mod. Phys. **15** (1943) 175.
16) Meson Theory of Nuclear Forces (New York, 1946).
17) W. Pauli und F. Villars, On the invariant Regularization in relativistic quantum theory. Revs. mod. Phys. **21** (1949) 434.
18) G. Källén u. W. Pauli, On the mathematical structure of T.D. Lee's model. Mat. Fys. Medd. Dan. Vid. Selsk. **30** (1955) 23.
19) On the Hamiltonian structure of non-local field theories. Nuovo Cimento **10** (1953) 648.
20) Handbuch der Physik **23** (Berlin 1926).
21) Handbuch der Physik **24/1**, 2. Auflage (Berlin 1933).
22) Absorption der Reststrahlen in Kristallen, Verh. Deutsch. Phys. Ges. **6** (1925) 10.
23) Rapport du Congrès Solvay (1933).
24) Exclusion Principle and Quantum Mechanics (Neuchâtel, 1947).
25) C. G. Jung und W. Pauli, Naturerklärung und Psyche (Zürich, 1952) „Der Einfluß archetypischer Vorstellungen auf die Bildung naturwissenschaftlicher Theorien bei Kepler" (Auch in englischer Übersetzung New York, 1955).
2) Sommerfeld's Beiträge zur Quantentheorie. Naturwiss. **35** (1948) 129.

8.B *Nuclear Physics* **10** (1959) 6—19; © *North-Holland Publishing Co., Amsterdam*
Not to be reproduced by photoprint or microfilm without written permission from the publisher

SYMMETRIES OF LEPTONIC INTERACTIONS

I. SAAVEDRA

Department of Theoretical Physics, University of Manchester †

Received 28 October 1958

Abstract: It is proved that leptonic processes can be described in isospace by using spinorial representations of the rotation group, and that the procedure is consistent with the general formalism and with the experimental data.

1. Introduction

The inclusion of leptons in the frame of the isospace formalism, first introduced by Salam and Polkinghorne [1]), seems to be still rather unsatisfactory. Attempts in this direction have been made by d'Espagnat, Prentki and Salam [2]) and by d'Espagnat and Prentki [3]). In ref.[2]) leptons (with respect to their weak interactions) are introduced as a three-vector (M-space) and in ref.[3]) this idea is studied by considering in M-space a three-vector and a scalar, i.e. a four-vector in the total isospace.

We will propose instead an altogether different approach. This will enable us to describe decay processes in the frame of M-space in a more unique way. On the other hand, it will not lead to the prediction of strong interactions, a danger inherent to the introduction of [4] representations for leptons ††. Finally, at least in the description of weak interactions, the problem of the electron-muon mass difference will not be introduced.

2. Spinorial Representations

Let us recall briefly that M-space is a [3] subspace of the [4] Euclidean space, orthogonal to the 4th axis. Weak interactions are invariant under any rotation in it, i.e., m and m_3 are conserved. From the definition of the space it follows that †††

$$m_3 = j_3{}^+ + j_3{}^- \tag{1}$$

and as [2]) $j_3{}^+$ can be considered (for baryons and mesons) equivalent to t_3, the 3rd component of isobaric spin and $2j_3{}^-$ equivalent to $U = S+N$

† On leave of absence from Laboratorio de Fisica Nuclear, Universidad de Chile, Santiago.

†† As a matter of fact, in the case of considering a lepton four-vector L_α it is only necessary to replace the nucleon-cascade four-vector B_α by L_α in the strong Lagrangian to predict such never observed interactions.

††† Notation: $j_3{}^+$ = eigenvalue of $J_3{}^+$, the (hermitian) operator for rotations around 3rd axis in I^+ space, etc.

(S being strangeness, N baryon number), M_3 is just Q, the electric charge. In other words, charge conservation is equivalent to invariance under rotations around the 3rd axis in M-space. Finally, as Q has only integer eigenvalues, only tensorial representations of the [3] rotation group have physical meaning, and spinorial representations (half-integer ones) have to be excluded.

Now, electric charge conservation is expressed by the fact that the total Lagrangian (including all interactions) is invariant under the transformation

$$\psi \to e^{iQ\alpha}\psi \tag{2}$$

and therefore it is this invariance which has been interpreted as a rotation invariance in M-space. But the weak Lagrangian can also be made invariant under the simultaneous transformations [4,5])

$$\begin{aligned} \psi_\nu &\to e^{i\gamma_5\alpha}\psi_\nu \\ \psi_{(a)} &\to e^{-in(a)\alpha}\psi_{(a)}, \end{aligned} \tag{3}$$

where (a) stands for any lepton field other than the neutrino, n(a) ($= +1$ or -1) being its 'neutrino charge', as defined by Umezawa and Visconti [4]) †. (This definition is extended to baryons by assuming that their neutrino charge is zero.) Therefore, one would expect to be able to interpret transformations (3) as rotations around a certain axis in an abstract space. We will prove that this is the case in the frame of the two-component neutrino theory, and also when one considers two different neutrinos, left-(L) and right-handed (R), with the definitions

$$\begin{aligned} \psi_{\nu_L} &\equiv \tfrac{1}{2}(1+\gamma_5)\psi_\nu \equiv a\psi_\nu, \\ \psi_{\nu_R} &\equiv \tfrac{1}{2}(1-\gamma_5)\psi_\nu \equiv \tilde{a}\psi_\nu, \end{aligned} \tag{4}$$

the corresponding antiparticles being given by

$$\psi^c_{\nu_L} = \tilde{a}\psi_\nu{}^c, \qquad \psi^c_{\nu_R} = a\psi_\nu{}^c, \tag{4'}$$

where ψ_ν is a four-component Dirac spinor.

In the two-component theory

$$\gamma_5\psi_\nu = \psi_\nu, \qquad \gamma_5\psi_\nu{}^c = -\psi_\nu{}^c. \tag{5}$$

Let us define an eight-component spinor

$$\Psi_\nu \equiv \begin{pmatrix} \psi_\nu \\ \psi_\nu{}^c \end{pmatrix},$$

and an 8×8 matrix

$$G_5 \equiv \underline{1} \times \gamma_5 = \begin{pmatrix} \gamma_5 & 0 \\ 0 & \gamma_5 \end{pmatrix},$$

$\underline{1}$ being the 2×2 unit matrix. Then, the transformations (eq. (3))

† The neutrino charge of the particle $\psi_{(a)}$ is positive if it interacts with a right-handed neutrino, negative if with a left-handed one.

$$\psi_\nu \to e^{\frac{1}{2}i\gamma_5\alpha}\psi_\nu, \qquad \psi_\nu{}^c \to e^{\frac{1}{2}i\gamma_5\alpha}\psi_\nu{}^c \tag{6}$$

can be written as

$$\Psi_\nu \to e^{\frac{1}{2}iG_5\alpha}\Psi_\nu = \begin{pmatrix} e^{\frac{1}{2}i\alpha} & 0 \\ 0 & e^{-\frac{1}{2}i\alpha} \end{pmatrix}\begin{pmatrix} \psi_\nu \\ \psi_\nu{}^c \end{pmatrix}. \tag{7}$$

Let us now consider an abstract space spanned out by the *two-component spinors* $\Psi_\nu = \binom{\psi_\nu}{\psi_\nu{}^c}$. In this space, with $\Sigma_3 = \left(\begin{smallmatrix} 1 & 0 \\ 0 & -1 \end{smallmatrix}\right)$, rotations around a certain axis are given by

$$\Psi_\nu \to e^{\frac{1}{2}i\Sigma_3\alpha}\Psi_\nu = \begin{pmatrix} e^{\frac{1}{2}i\alpha} & 0 \\ 0 & e^{-\frac{1}{2}i\alpha} \end{pmatrix}\begin{pmatrix} \psi_\nu \\ \psi_\nu{}^c \end{pmatrix}. \tag{8}$$

Therefore, transformations (6) (in a two-component neutrino theory) are equivalent to rotations of two-component spinors in this abstract space.

The same result holds for the left-handed and the right-handed neutrinos defined by eq. (4), namely that the transformations

$$\psi_{\nu_L} \to e^{\frac{1}{2}i\gamma_5\alpha}\psi_{\nu_L}, \qquad \psi^c_{\nu_L} \to e^{\frac{1}{2}i\gamma_5\alpha}\psi^c_{\nu_L}; \tag{9}$$

$$\psi_{\nu_R} \to e^{\frac{1}{2}i\gamma_5\alpha}\psi_{\nu_R}, \qquad \psi^c_{\nu_R} \to e^{\frac{1}{2}i\gamma_5\alpha}\psi^c_{\nu_R} \tag{9'}$$

can be considered as rotations of two two-component spinors

$$\Psi_{\nu_L} \equiv \begin{pmatrix} \psi_{\nu_L} \\ \psi^c_{\nu_L} \end{pmatrix}, \qquad \Psi_{\nu_R} \equiv \begin{pmatrix} \psi^c_{\nu_R} \\ \psi_{\nu_R} \end{pmatrix} \tag{10}$$

around a certain axis in an abstract space.

Finally, according to eqs. (3) we must also study the transformations

$$\psi^-_{(a)} \to e^{+\frac{1}{2}i\alpha}\psi^-_{(a)}, \qquad \psi^+_{(a)} \to e^{-\frac{1}{2}i\alpha}\psi^+_{(a)} \tag{11}$$

in an obvious notation.

Defining again an eight-component spinor

$$\Psi_{(a)} \equiv \begin{pmatrix} \psi^-_{(a)} \\ \psi^+_{(a)} \end{pmatrix},$$

and using Watanabe's 'chirality' representation [6]), transformations (11) can be written

$$\Psi_{(a)} \to e^{+\frac{1}{2}iX\alpha}\Psi_{(a)} = \begin{pmatrix} e^{\frac{1}{2}i\alpha} & 0 \\ 0 & e^{-\frac{1}{2}i\alpha} \end{pmatrix}\begin{pmatrix} \psi^-_{(a)} \\ \psi^+_{(a)} \end{pmatrix} \tag{12}$$

where X is the chirality operator (an 8×8 matrix)

$$X = \begin{pmatrix} \underline{1} & 0 \\ 0 & -\underline{1} \end{pmatrix} = \Sigma_3 \times \underline{1}.$$

Therefore, these transformations can also be considered as rotations of two-component spinors.

Summing up, we can say that the requirement of invariance of the weak Lagrangian under the 'generalized gauge transformation' [4]) (eq. (3)) is

equivalent to the requirement of invariance under rotations around a certain axis in an abstract space. But we know that weak interactions can be described in M-space. It is tempting, therefore, to try to identify both spaces: but, as stated before, this is not possible because only tensorial representations are allowed in the latter space.

One obvious way out of this difficulty is to try to modify eq. (1) so as to extend it to the case of leptons, the new equation reducing to the previous one for baryons and mesons. We define

$$q = m_3 + \tfrac{1}{2}n \tag{13}$$

where n is the neutrino charge. Eq. (13) implies that in Gell-Mann's scheme the electric charge would be given by $q = t_3 + \frac{1}{2}(N+S+n)$, with $n = 0$ for baryons and mesons. As q and n are integers, eq. (13) makes $m_3 = j_3^+ + j_3^-$ half-integer, i.e. *spinorial representations have been introduced for leptons.* We have written m_3 instead of $j_3^+ + j_3^-$ in order to stress the fact that in M-space the latter are meaningless, because

$$D_{j^+ j^-} \approx D_{j^+} \times D_{j^-} \approx D_{j^+ + j^-} + \ldots + D_{|j^+ - j^-|}. \tag{14}$$

In particular, for the spinorial representations $D_{\frac{1}{2}0}$('undotted') and $D_{0\frac{1}{2}}$ ('dotted'), we have

$$D_{\frac{1}{2}0} \approx D_{\frac{1}{2}} \approx D_{0\frac{1}{2}}. \tag{15}$$

Hence, undotted and dotted representations are undistinguishable, i.e. only m_3 assignments are meaningful in M-space. Use of eq. (13) gives the assignments summarized in the following table:

	m	m_3	n	q
e^-	$\frac{1}{2}$	$-\frac{1}{2}$	-1	-1
e^+	$\frac{1}{2}$	$+\frac{1}{2}$	$+1$	$+1$
μ^-	$\frac{1}{2}$	$-\frac{1}{2}$	-1	-1
μ^+	$\frac{1}{2}$	$+\frac{1}{2}$	$+1$	$+1$
ν_L	$\frac{1}{2}$	$+\frac{1}{2}$	-1	0
ν_L^c	$\frac{1}{2}$	$-\frac{1}{2}$	$+1$	0
ν_R	$\frac{1}{2}$	$-\frac{1}{2}$	$+1$	0
ν_R^c	$\frac{1}{2}$	$+\frac{1}{2}$	-1	0

If only one neutrino and antineutrino are considered (in the two-component theory), these have the same m_3 and n values as ν_L and ν_L^c, respectively.

Therefore, we define the following two-component spinors in M-space:

$$\psi_e \equiv \begin{pmatrix} e^+ \\ e^- \end{pmatrix}, \qquad \psi_\mu \equiv \begin{pmatrix} \mu^+ \\ \mu^- \end{pmatrix}, \qquad \psi_{\nu_L} \equiv \begin{pmatrix} \nu_L \\ \nu_L^c \end{pmatrix}, \qquad \psi_{\nu_R} \equiv \begin{pmatrix} \nu_R^c \\ \nu_R \end{pmatrix}, \tag{16}$$

where ψ means a two-component spinor in M-space, each component being a four-component spinor in space-time; e^+, e^-, etc., stand for lepton fields. The alternative, i.e. to consider

$$\psi'_e \equiv \begin{pmatrix} e^- \\ e^+ \end{pmatrix}, \qquad \psi'_{\nu_L} \equiv \begin{pmatrix} \nu_L{}^c \\ \nu_L \end{pmatrix}, \quad \text{etc.}$$

is also *a priori* possible, but has to be rejected because it leads to the prediction of processes (all baryon-lepton interactions) in which electric charge is not conserved. Finally, if it turns out that only one kind of neutrino occurs in nature, definitions (16) need simply be written

$$\psi_e \equiv \begin{pmatrix} e^+ \\ e^- \end{pmatrix}, \qquad \psi_\mu \equiv \begin{pmatrix} \mu^+ \\ \mu^- \end{pmatrix}, \quad \psi_\nu \equiv \begin{pmatrix} \nu \\ \nu^c \end{pmatrix}, \tag{16'}$$

as already remarked.

3. The Weak Interactions

We require the weak Lagrangian to be invariant under any rotation in both M-*space and space-time.*

From the invariance under any rotation in M-space and the conservation of electric charge follows (eq. (13)) the *conservation of neutrino charge*. This was obtained before, when we required the weak Lagrangian (in space-time) to be invariant under the generalized gauge transformation. Obviously, the opposite way around is also licit: to define electric charge by eq. (13) and require conservation of q and m_3. This amounts to the above statement.

We will consider only Fermi-type interactions, i.e. interactions between four fermion fields. Let us first discuss the interactions in which two leptons are present. Notice that the use of spinorial representations already excludes processes in which only one lepton appears (or, in general, an odd number of leptons). The interaction between four lepton fields, i.e. μ-decay, is determined by the experimental value of the Michel parameter ρ, which requires that two different neutrinos have to be emitted. As we are dealing with two kinds of neutrinos we can satisfy this requirement in four different ways, namely, with the neutrino pairs $(\nu_L \nu_R)$, $(\nu_L{}^c \nu_R{}^c)$, $(\nu_L \nu_L{}^c)$, $(\nu_R \nu_R{}^c)$. Therefore, the description of this process is now, in this sense, a matter of convention. We shall discuss it later. All other decay processes can be described as interactions in which a charged lepton (electron or muon) and a neutrino (left or right) are taking part †, and there are *a priori* 16 (plus h.c.) different lepton bilinears to be considered. Nevertheless, the conservation of neutrino charge means that terms (in M-space) like $e^{-*}\nu_R$, $e^{-*}\nu_L{}^c$, $\mu^{-*}\nu_R$, $\mu^{-*}\nu_L{}^c$, $e^{+*}\nu_L$, $e^{+*}\nu_R{}^c$, $\mu^{+*}\nu_L$, $\mu^{+*}\nu_R{}^c$, where 'star' (*) means hermitian conjugate, must be excluded.

† The approach is plainly a phenomenological one. In principle, decays in which two charged leptons are present are also possible, even though they have never been observed. In this case, from the 10 (plus h.c.) *a priori* possible bilinears the terms (in M-space) $e^{+*}e^-$, $\mu^{+*}\mu^-$, $e^{+*}\mu^-$, $e^{-*}\mu^+$ are ruled out by neutrino charge conservation (which is equivalent to electric charge when only electrons and muons are considered). It will be seen that conservation of lepton number excludes also $e^{+*}\mu^+$ and $e^{-*}\mu^-$, and therefore the only allowed bilinears are $e^{+*}e^+$, $e^{-*}e^-$, $\mu^{+*}\mu^+$, $\mu^{-*}\mu^-$.

We now go further, and *assume* conservation of lepton number l ($l \equiv$ number of leptons — number of antileptons). In doing this we notice that Konopinski's rule [7]) can again be used because the existence of two different neutrinos makes it compatible with the known value of the Michel parameter. Hence, we consider e^-, μ^+, ν_L and ν_R as leptons, e^+, μ^-, ν_L^c and ν_R^c as antileptons. If the lepton number is to be conserved, terms like $e^{-*}\nu_R^c$, $\mu^{-*}\nu_L$, $e^{+*}\nu_R$, $\mu^{+*}\nu_L^c$ must also be excluded. Therefore, the only terms we must consider are $e^{-*}\nu_L$, $\mu^{-*}\nu_R^c$, $e^{+*}\nu_L^c$ and $\mu^{+*}\nu_R$, i.e. *the electron always appears associated with the left-handed neutrino, the muon with the right-handed one*. Coming back to the four leptons interactions, we observe that its decay scheme (as far as neutrinos are concerned) is now uniquely determined by the requirement of lepton number conservation.

Finally, any four-component spinor can always be written as the sum of, so to speak, a 'left' and a 'right' term by using projection operators. Let us take, to be definite, the electron field. We have

$$e^- \equiv ae^- + \bar{a}e^- \equiv e_L^- + e_R^- \tag{17}$$

where $e_L^{-*}e_R^- = e_R^{-*}e_L^- = 0$, because $a^* = a$, $a\bar{a} = \bar{a}a = 0$, $aa = a$, $\bar{a}\bar{a} = \bar{a}$, e_L^- and e_R^- being two-component spinors. But we have shown that the electron must always appear associated with a left-handed neutrino. Let us study, then, the bilinear (M-space and space-time) $e^{-*}\gamma_4 O_i \nu_L$, where $O_i =$ scalar, vector, tensor, pseudovector or pseudoscalar couplings in space-time. From (17)

$$e^{-*}\gamma_4 O_i \nu_L = e_L^{-*}\gamma_4 O_i \nu_L + e_R^{-*}\gamma_4 O_i \nu_L,$$

and there are two cases to be considered:

(i) $O_i = \gamma_\mu, \quad \gamma_5\gamma_\mu,$
$e^{-*}\gamma_4 O_i \nu_L \equiv \overline{e_L^-} O_i \nu_L;$

(ii) $O_i = \underline{1}, \quad \gamma_\mu\gamma_\nu, \quad \gamma_5,$
$e^{-*}\gamma_4 O_i \nu_L \equiv \overline{e_R^-} O_i \nu_L$

(where $\overline{e^-} \equiv e^{-*}\gamma_4$).

Hence, in any case, we only need two components out of the four of the original spinor † and there are two possibilities: (i) to consider only e_L^- (instead of e^-), which leads to couplings (V, A), or (ii) to consider only e_R^-, which leads to couplings (S, T, P). The choice is a matter of experimental evidence, and this now seems to be conclusive in favour of the first possibility. It should be pointed out that one has this choice only when one considers the direct product of isospace and space-time as the domain of particles. If

† This result does not follow in the hypothetical case of decays into two charged leptons. Nevertheless, it can be extended as a postulate, if necessary, and it can be seen (M-space) that it excludes the same bilinears as the requirement of neutrino charge conservation.

the selection rules (for weak interactions) are required to be satisfied in M-space and space-time *separately*, case (i) is the only possible one, case (ii) being excluded by considerations of electric and neutrino charge conservation in M-space.

Similar considerations hold for e^+, μ^- and μ^+. Therefore, we conclude that we can always replace

$$e^- \to a e^-, \quad e^+ \to \bar{a} e^+, \quad \mu^- \to a \mu^-, \quad \mu^+ \to \bar{a} \mu^+, \tag{18}$$

and in consequence

$$\psi_e \to \begin{pmatrix} \bar{a}\ e^+ \\ a\ e^- \end{pmatrix} \quad \text{and} \quad \psi_\mu \to \begin{pmatrix} \bar{a}\ \mu^+ \\ a\ \mu^- \end{pmatrix}. \tag{18'}$$

We will use these results in all that follows. The replacements (18) are essentially the same as those postulated by Feynman and Gell-Mann [8]) (even though here μ^+ is the 'particle') as far as leptons are concerned. As we cannot get any conclusion regarding baryons, we shall continue considering them as four-component Dirac spinors.

If only one sort of neutrino is assumed to exist, the last considerations follow in the same way. Out of the 8 *a priori* possible bilinears, only the terms $e^{-*}\nu$, $e^{+*}\nu^c$, $\mu^{-*}\nu$ and $\mu^{+*}\nu^c$ survive after considerations of neutrino charge conservation in M-space. As the two-component theory is being used ($a\nu = \nu$, $\bar{a}\nu^c = \nu^c$), again only two-component spinors are needed for the lepton fields, i.e. the replacements (18) are still valid. Moreover, the experimental value of the Michel parameter means then that μ^- has to be considered as the 'particle', thus making neutrino charge equivalent to lepton number, and the conservation of the latter does not need to be postulated.

Summarizing, we require, then, the weak Lagrangian to be invariant under any rotation in both M-space and space-time, and the conservation of electric charge and lepton number (only electric charge if but one neutrino is considered). The interactions satisfying these requirements are given below.

3.1. FOUR-LEPTON INTERACTIONS

The μ-decay can take place according to the schemes

$$\begin{aligned} \mu^+ &\to e^+ + \nu_L + \nu_R, \\ \mu^- &\to e^- + \nu_L^c + \nu_R^c. \end{aligned} \tag{19}$$

These processes are described by

$$g_1 \psi_e^* (\underline{1} \times \gamma_4 \gamma_\mu)(\tau_i \times \underline{1}) \psi_{\nu_L} \cdot \psi_\mu^* (\underline{1} \times \gamma_4 \gamma_\mu)(\tau_i \times \underline{1}) \psi_{\nu_R} + \text{h.c.} \tag{20}$$

where $\underline{1}$ is the 2×2 unit matrix, γ_μ are the 4×4 Dirac matrices, τ_i the 2×2 Pauli matrices. Expression (20) is to be recognized as a (V—A) coupling. It is important to point out that terms like $\psi_e^* \psi_e \psi_e^* \psi_\mu$, etc., describing processes like $\mu^\pm \to e^\pm + e^+ + e^-$, etc., never observed, are excluded only by the

assumption of the conservation of lepton number. With our selection rules (20) is the *only* four-fermion interaction that can be constructed. Writing it down explicitly one gets

$$2g_1(\overline{e^+}\gamma_\mu \nu_L{}^c \overline{\mu^-}\gamma_\mu \nu_R{}^c + \overline{e^-}\gamma_\mu \nu_L \overline{\mu^+}\gamma_\mu \nu_R) + \text{h.c.} \tag{20'}$$

which is obviously invariant under transformations (3), as it should.

3.2. OTHER INTERACTIONS

As stated before, all other decay processes can be described as interactions in which a charged and an uncharged lepton field are taking part. Let us consider, e.g., the electron as the charged field. It is straightforward to prove that the scalars

$$\psi_e{}^*(\underline{1}\times\gamma_4 O_i)\psi_{\nu_L} \quad \text{and} \quad \psi_e{}^*(\underline{1}\times\gamma_4 O_i)\psi_{\nu_R} \tag{21}$$

must be rejected because they lead to the prediction of processes violating neutrino charge conservation. It is also easily proved that the vector

$$\psi_e{}^*(\underline{1}\times\gamma_4 O_i)(\tau_j\times\underline{1})\psi_{\nu_R} \tag{22}$$

is excluded by considerations of neutrino charge and lepton number conservation. Therefore, we can only define the vector

$$\psi_e{}^*(\underline{1}\times\gamma_4 O_i)(\tau_j\times\underline{1})\psi_{\nu_L} \tag{23}$$

and also, analogously, the vector

$$\psi_\mu{}^*(\underline{1}\times\gamma_4 O_i)(\tau_j\times\underline{1})\psi_{\nu_R}. \tag{24}$$

Now, nucleons and cascade particles are represented in M-space by a three-vector $\mathbf{B}$ and a scalar B_S, where, in a suitable representation [10],

$$\mathbf{B} = \begin{cases} \frac{1}{\sqrt{2}}(-\mathrm{p}+\Xi^-) \\ \frac{1}{i\sqrt{2}}(\mathrm{p}+\Xi^-) \\ \frac{1}{\sqrt{2}}(-\mathrm{n}-\Xi^0) \end{cases} \tag{25}$$

and

$$B_S = \frac{1}{i\sqrt{2}}(-\mathrm{n}+\Xi^0), \tag{26}$$

B_S being the 4th component of the vector B_α ($\alpha = 1, \ldots, 4$) in [4]-space.

In order to avoid ambiguities, we proceed to construct the corresponding bilinears starting with considerations in [4]-space. With the four-vector B_α we can form the antisymmetric tensor $B_{\alpha\beta}$, defined by

$$B_{\alpha\beta} \equiv B_\alpha{}^* B_\beta - B_\beta{}^* B_\alpha, \qquad (\alpha, \beta = 1, \ldots, 4) \tag{27}$$

which for rotations conserving the 4th axis (M-space) 'splits' into the axial vector

$$B_k{}^* B_l - B_l{}^* B_k = (\mathbf{B}^* \wedge \mathbf{B})_i \quad (i, k, l = 1, 2, 3) \tag{28}$$

and the polar vector

$$B_i^* B_S - B_S^* B_i = (\mathbf{B}^* B_S - B_S^* \mathbf{B})_i \qquad (i = 1, 2, 3). \tag{29}$$

Clearly, instead of (29) we could have considered as the polar vector

$$B_S^* B_i - B_i^* B_S = -(\mathbf{B}^* B_S - B_S^* \mathbf{B})_i. \tag{29'}$$

Nevertheless, we must use (29) because it leads to the description of β-decay of the neutron; (29'), instead, leads to the prediction of β-decay of the Ξ particle.

Therefore, the interactions between nucleons-cascade particle and leptons are accounted for through

$$g_2{}^i \psi_e^* (\underline{1} \times \gamma_4 O_i)(\tau \times \underline{1}) \psi_{\nu_L} \cdot (\mathbf{B}^* \gamma_4 O_i B_S - B_S^* \gamma_4 O_i \mathbf{B} + \mathbf{B}^* \wedge \gamma_4 O_i \mathbf{B}) + \text{h.c.} \tag{30}$$

where O_i can take the forms γ_μ and $\gamma_5 \gamma_\mu$; the explicit form of the coupling, however, remains indetermined. Expression (30) describes only ordinary β-decay and the hypothetical interaction $(\Xi^0 \Xi^- e \nu_L)$. The latter will be considered later. It *does not* predict the β-decay of Ξ particles, which was a serious drawback of the formalism as discussed in ref.[3]).

In the same way, μ-capture is described through

$$g_2{}^i \psi_\mu^* (\underline{1} \times \gamma_4 O_i)(\tau \times \underline{1}) \psi_{\nu_R} \cdot (\mathbf{B}^* \gamma_4 O_i B_S - B_S^* \gamma_4 O_i \mathbf{B} + \mathbf{B}^* \wedge \gamma_4 O_i \mathbf{B}) + \text{h.c.} \tag{31}$$

which also describes an interaction of the form $(\Xi^0 \Xi^- \mu \nu_R)$, to be considered later.

Σ particle interactions are described in [4]-space by a self dual antisymmetric tensor, i.e. a three-vector in M-space:

$$\Sigma = \begin{cases} \frac{1}{\sqrt{2}} (-\Sigma^+ - \Sigma^-) \\ \frac{1}{i\sqrt{2}} (\Sigma^+ - \Sigma^-) \\ \Sigma^0. \end{cases} \tag{32}$$

The decays $\Xi \to \Sigma + e + \nu_L$, $\Sigma \to N + e + \nu_L$, are accounted for through

$$g_3{}^i \psi_e^* (\underline{1} \times \gamma_4 O_i)(\tau \times \underline{1}) \psi_{\nu_L} \cdot \mathbf{B}^* \wedge \gamma_4 O_i \Sigma + \text{h.c.}. \tag{33}$$

The interaction

$$g_4{}^i \psi_e^* (\underline{1} \times \gamma_4 O_i)(\tau \times \underline{1}) \psi_{\nu_L} \cdot \Sigma^* \gamma_4 O_i \Lambda + \text{h.c.} \tag{34}$$

describes $\Sigma \to \Lambda^0 + e + \nu_L$, while

$$g_5{}^i \psi_e^* (\underline{1} \times \gamma_4 O_i)(\tau \times \underline{1}) \psi_{\nu_L} \cdot \Sigma^* \wedge \gamma_4 O_i \Sigma + \text{h.c.} \tag{35}$$

accounts for $\Sigma \to \Sigma^0 + e + \nu_L$.

Finally,

$$g_6{}^i \psi_e^* (\underline{1} \times \gamma_4 O_i)(\tau \times \underline{1}) \psi_{\nu_L} \cdot \mathbf{B}^* \gamma_4 O_i \Lambda + \text{h.c.} \tag{36}$$

gives the β-decay of the Λ particle, as well as the decay $\Xi^- \to \Lambda^0 + e^- + \nu_L{}^c$.

The same result holds for the muon, simply by replacing (23) by (24). The interactions (33) to (36) are, of course, all (V, A) couplings; the various coupling constants can eventually be put equal to each other.

We emphasize that the Lagrangians given are the *only* ones that can be constructed as long as we disregard charged-charged lepton bilinears. In the latter case, it can be proved that electron-muon bilinears are ruled out by neutrino charge and lepton number conservation, but interactions describing decays of the form

$$\text{baryon} \rightarrow \text{baryon} + e^+(\mu^+) + e^-(\mu^-) \tag{37}$$

can be constructed. The fact that decays of the form (37) has never been observed, suggests that some unknown selection rule is operating. Perhaps such a selection rule would not refer only to leptons, but rather to leptons and baryons. We shall come back to this point in the concluding section.

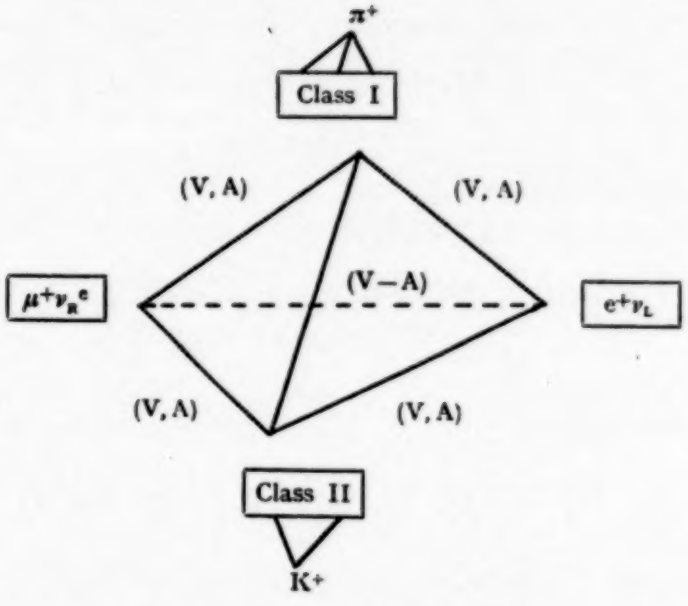

Fig. 1. Scheme of interactions.

As far as leptonic decays of pions and kaons are concerned, we know that the former undergo strong interactions, the latter intermediate ones. Their leptonic decays can then be accounted for by virtual interactions with baryon-antibaryon pairs as described by the strong interaction Lagrangian. The situation has been discussed previously by Gell-Mann and Rosenfeld [9]). The decay of the pion (π^+, say) can take place through the following pairs: ($p\bar{n}$), ($\Sigma^+\bar{\Lambda}$), ($\Sigma^+\bar{\Sigma}^0$), ($\Lambda\bar{\Sigma}^-$), ($\Sigma^0\bar{\Sigma}^-$) and ($\Xi^0\bar{\Xi}^-$); the kaon decay (K^+), through ($p\bar{\Lambda}$), ($p\bar{\Sigma}^0$), ($n\bar{\Sigma}^-$), ($\Lambda\bar{\Xi}^-$), ($\Sigma^+\bar{\Xi}^0$), ($\Sigma^0\bar{\Xi}^-$). The Puppi triangle is replaced by the tetrahedron given in fig. 1, where our results are summarized.

Class I pairs are those that interact strongly; Class II pairs undergo intermediate interactions. All the decay processes predicted by the various couplings in the tetrahedron are accounted for in the Lagrangians given above.

4. The Electromagnetic Interactions

Electromagnetic interactions are invariant under rotations around the 3rd axis in I^+ and I^- spaces, i.e. they conserve j_3^+ and j_3^-. Therefore, we must start by giving a [4] description of charged leptons. Uncharged leptons (ν_L and ν_R) do not interact electromagnetically, and for this reason do not need [4] representations. An immediate consequence of this is that they do not interact strongly either. Another consequence is that their j_3^+ and j_3^- values remain undetermined, only m_3 being meaningful.

Electrons and muons are described in M-space by the two-component spinors (16). In order to obtain their [4] representation let us recall the definition of the (hermitian) generators of the I^+ and I^- spaces:

$$J_j^+ = -\tfrac{1}{2}i(I_{kl}+I_{j4}), \qquad (j,k,l = 1,2,3) \tag{38}$$

$$J_j^- = -\tfrac{1}{2}i(I_{kl}-I_{j4}), \tag{39}$$

where the $I_{\alpha\beta}$ are (antihermitian) infinitesimal operators of the [4] rotation group. In particular, for a Dirac-type spinor representation,

$$J_3^+ = -\tfrac{1}{4}i(\Gamma_1\Gamma_2+\Gamma_3\Gamma_4), \tag{40}$$

$$J_3^- = -\tfrac{1}{4}i(\Gamma_1\Gamma_2-\Gamma_3\Gamma_4) \tag{41}$$

(where Γ_μ are 4×4 Dirac matrices), because $I_{\rho\sigma} = \frac{1}{2}\Gamma_\rho\Gamma_\sigma$ $(\rho \neq \sigma)$. Let us use the representation

$$\Gamma_j = \begin{pmatrix} 0 & -i\sigma_j \\ i\sigma_j & 0 \end{pmatrix}, \qquad \Gamma_4 = \begin{pmatrix} 0 & -\underline{1} \\ -\underline{1} & 0 \end{pmatrix}, \qquad \Gamma_5 = \begin{pmatrix} -\underline{1} & 0 \\ 0 & +\underline{1} \end{pmatrix}, \tag{42}$$

$\sigma_j (j = 1, 2, 3)$ being 2×2 Pauli matrices.

A straightforward calculation gives

$$J_3^+ = \tfrac{1}{2}\begin{pmatrix} \sigma_3 & 0 \\ 0 & 0 \end{pmatrix} \tag{43}$$

and

$$J_3^- = \tfrac{1}{2}\begin{pmatrix} 0 & 0 \\ 0 & \sigma_3 \end{pmatrix}. \tag{44}$$

According to eq. (13) the charge operator is given by

$$Q = M_3+\tfrac{1}{2}n \tag{45}$$

where $M_3 = J_3^+ + J_3^-$ and n has to be considered as the neutrino charge operator

$$n = \begin{pmatrix} \sigma_3 & 0 \\ 0 & \sigma_3 \end{pmatrix}. \tag{46}$$

Therefore,

$$Q = \begin{pmatrix} \sigma_3 & 0 \\ 0 & \sigma_3 \end{pmatrix}. \tag{47}$$

We can then attribute ψ_e(M-space) to the representation $D_{0\frac{1}{2}}$ and ψ_μ to the representation $D_{\frac{1}{2}0}$ of the rotation group, i.e., we can make the following $j_3^{\pm}$ assignments:

	e^-	e^+	μ^-	μ^+
j_3^+	0	0	$-\frac{1}{2}$	$+\frac{1}{2}$
j_3^-	$-\frac{1}{2}$	$+\frac{1}{2}$	0	0

(48)

This choice is, of course, arbitrary (in the sense that e could take the place of μ and vice-versa), but irrelevant as far as electromagnetic interactions are concerned. We now proceed to construct the four-component 'Dirac spinor'

$$\Psi \equiv \begin{pmatrix} \mu^+ \\ \mu^- \\ e^+ \\ e^- \end{pmatrix} \qquad (\epsilon\, D_{\frac{1}{2}0} \dot{+} D_{0\frac{1}{2}}), \tag{49}$$

which is our [4] representation of charged leptons. This of course implies that the bare masses of electron and muon are assumed to be equal; but no specific assumption is needed as regards their relation to the bare neutrino mass.

We assume that the 'principle of minimum electromagnetic interaction' (Gell-Mann) holds. Therefore, the electromagnetic interactions of leptons are accounted for by

$$L_{\text{e.m.}} = e\Psi^* \gamma_4 \gamma_\mu Q \Psi A_\mu, \tag{50}$$

where γ_μ are Dirac matrices acting in space-time. As

$$[J_3^+, Q] = 0, \qquad [J_3^-, Q] = 0, \tag{51}$$

$L_{\text{e.m.}}$ is invariant under the transformation

$$\Psi \to e^{i\alpha J_3^+ \alpha} \Psi \tag{52}$$

and also under

$$\Psi \to e^{i\alpha J_3^- \alpha} \Psi, \tag{53}$$

i.e. it is invariant under rotations around the 3rd axis in both I^+ and I^- space, as it should.

5. The Strong Interactions

The very introduction of [4] representations for leptons gives them, at least *a priori*, the possibility of undergoing strong interactions which may in

turn contradict experimental evidence. We must, therefore, discuss these possible interactions.

We assume all strong interactions as being of the Yukawa-type. This assumption excludes at once interactions with baryons, and we need only to consider K and π fields.

The K-meson is described in isospace by a four-vector $\varphi_\mu{}^{\mathrm{K}}$. The interaction should be of the form (the K-meson is assumed to be pseudoscalar)

$$G\Psi^*\gamma_4\gamma_5\Gamma_\mu\Psi\varphi_\mu{}^{\mathrm{K}}, \tag{54}$$

with Γ_μ given by (42) †. Writing it down explicitly, one can see that it violates electric charge as well as lepton number conservation, and therefore must be rejected.

The π-meson interactions are described with an antisymmetric self-dual tensor $\varphi^\pi_{\mu\nu}$. As for (54) it can be seen that the interaction

$$G\tfrac{1}{4}\Psi^*\gamma_4\gamma_5\Gamma_\mu\Gamma_\nu\Psi\varphi^\pi_{\mu\nu} \tag{55}$$

must also be excluded. Therefore, this formalism does not allow for strong interactions of leptons with the rest of the known particles, a fact in accordance with the experimental evidence.

6. Concluding Remarks

Concluding, we should like to emphasize the complete symmetry of the approach as far as electrons and muons are concerned. In this context, it does predict, for example, an electronic decay of the π-meson, a fact recently verified experimentally. This symmetry suggests that electron and muon are indeed one and the same particle, but the formalism does not predict a strong interaction responsible for their mass difference. (However, there is still the possibility of an intermediate interaction, which is being considered.) On the other hand, it raises the problem of explaining why only charge exchange reactions are possible in weak interactions, i.e. why decays like (37) do not occur in nature. It may well be that these two problems are not really independent.

Finally, let us remark that the formalism does not depend critically on the assumption of the existence of two different kinds of neutrinos. As a matter of fact, this assumption succeeds in making Konopinski's rule again valid, thus making the Lagrangian (20) unique, but it does not succeed in forbidding processes like (37). As stated above, the true problem seems to be that of proving that only charge exchange reactions are allowed in weak

† In (54) no Γ_4 factor is required, i.e. we must consider Ψ^* instead of $\overline{\Psi} = \Psi^*\Gamma_4$, because the space is Euclidean, and it can be shown that in this case $\Psi^*\Gamma_\mu\Psi$ is a vector, etc.

interactions. Should this be proved, the 'twin neutrinos' hypothesis would be completely unnecessary and could be replaced by the simple two-component neutrino theory.

I wish to express my thanks to Professor L. Rosenfeld for my stay in his Department, and to Dr. P. Roman to whom I am indebted in many ways. I also wish to acknowledge with thanks the scholarship awarded by the British Council which enabled me to carry out this work.

References

1) A. Salam and J. C. Polkinghorne, Nuovo Cimento **2** (1955) 685
2) B. d'Espagnat, J. Prentki and A. Salam, Nuclear Physics **5** (1958) 447
3) B. d'Espagnat and J. Prentki, Nuclear Physics **6** (1958) 596
4) H. Umezawa and A. Visconti, Nuclear Physics **4** (1957) 224
5) B. Touschek, Nuovo Cimento **5** (1957) 1281
6) S. Watanabe, Nuovo Cimento **6** (1957) 187
7) E. J. Konopinski and H. M. Mahmoud, Phys. Rev. **92** (1953) 1045
8) R. P. Feynman and M. Gell-Mann, Phys. Rev. **109** (1958) 193
9) M. Gell-Mann and A. H. Rosenfeld, Ann. Rev. of Nuclear Science **7** (1957) 407
10) P. Roman, Introduction to the Theory of Elementary Particles (North Holland Publishing Co.) to be published

8.B *Nuclear Physics* **10** (1959) 20—27; © *North-Holland Publishing Co., Amsterdam*
Not to be reproduced by photoprint or microfilm without written permission from the publisher

THE ISOBARIC SELECTION RULE FOR HYPERONS AND K-MESONS

KIMIKO NAKAGAWA
Department of Physics, University of Tokyo

Received 29 October 1958

Abstract: The weak decay processes for hyperons and K-mesons are analysed to test the isobaric selection rule $|\Delta \mathbf{I}| = \frac{1}{2}$. It is shown that only one possible type is left for the Σ-decay interaction when the rule $|\Delta \mathbf{I}| = \frac{1}{2}$, the T-invariance and the one-to-one law are assumed.

1. Introduction

The structure of interactions concerns their space-time as well as their isobaric properties. As for the space-time properties, it has been suggested in our previous paper [1]) that all the weak interactions violating the conservation of parity belong to the second kind, while the strong or electromagnetic interactions belong to the first kind. This seems to suggest that the weak interaction may play an important role in a small region $r < 10^{-17}$ cm corresponding to the very high energy region. The violation of parity conservation in weak interaction might be considered as the consequence of the structure of this small region.

It is now interesting to attempt at understanding the isobaric properties of the interaction in this small region. This is done by testing the isobaric selection rule for the hyperon decays or the K-meson decays. It is well known that the isobaric spin changes its component by $\Delta I_3 = \pm\frac{1}{2}$ in the weak decay processes for hyperons and K-mesons.

A further isobaric selection rule $|\Delta \mathbf{I}| = \frac{1}{2}$ has sometimes been suggested [2]). Experiments have once required considerably large corrections from $|\Delta \mathbf{I}| = \frac{3}{2}$ or $|\Delta \mathbf{I}| = \frac{5}{2}$ [3]). However, the situation has recently changed very much: no experiments are now found to be definitely inconsistent with the rule $|\Delta \mathbf{I}| = \frac{1}{2}$.

In section 2, an analysis of hyperon decays will be made to test the selection rule $|\Delta \mathbf{I}| = \frac{1}{2}$. It will be shown that only one possible type is left for the Σ-decay interaction as far as the rule $|\Delta \mathbf{I}| = \frac{1}{2}$, the invariance under the time reversal and the one-to-one law are assumed [4]). Further experiments on the anisotropy coefficients for the Σ-decay are necessary for proving such a type of Σ-interaction. Section 3 is devoted to the discussion

of the isobaric properties of the K-meson decay, by introducing the weak coupling of the K-meson to the nucleons and it will be shown there that the latter interaction, i.e. KNN, can explain experiments without assuming the rule $|\Delta \mathbf{I}| = \frac{1}{2}$.

Let us here list the observations used in testing the rule $|\Delta \mathbf{I}| = \frac{1}{2}$:

1) The branching ratio in the Σ^+-decay [5],

$$R_\Sigma \equiv \frac{w(\Sigma^+ \to \mathrm{p}+\pi^0)}{w(\Sigma^+ \to \mathrm{n}+\pi^+)} \approx 1. \tag{1}$$

2) The ratio of the life times of Σ^+ and Σ^- [5,6],

$$R_{\Sigma'} \equiv \frac{\tau(\Sigma^+)}{\tau(\Sigma^-)} \approx \frac{1}{2}. \tag{2}$$

3) The ratio of the anisotropy coefficients,

$$\frac{\alpha_0(\Sigma^+ \to \mathrm{p}+\pi^0)}{\alpha_+(\Sigma^+ \to \mathrm{n}+\pi^+)}. \tag{3}$$

The decay distribution function for the pions produced in the polarized hyperon decay has been known to be of the form $[1+P\alpha\cos\theta]$. Here, θ is the angle of the pion momentum relative to the polarization axis of Σ-particle in the rest system of the Σ-particle, α is the anisotropy coefficient and P is the magnitude of the polarization. It is interesting to see that the ratio $\alpha_0/\alpha_+ = \bar{P}\alpha_0/\bar{P}\alpha_+$ depends only on the interaction for the Σ-decay processes [4]. Unfortunately, information about the anisotropy coefficients is of much ambiguity [7].

4) The branching ratio in $\mathrm{K_1^0}$-decay [7],

$$R_\theta \equiv \frac{w(\mathrm{K_1^0} \to \pi^0+\pi^0)}{w(\mathrm{K_1^0})} \approx \frac{1}{3}, \tag{4}$$

5) The ratio of the decay rates $\mathrm{K^+} \to \pi^+ + \pi^0$ and $\mathrm{K_1^0} \to 2\pi$ [3],

$$R_{\theta'} \equiv \frac{w(\mathrm{K^+} \to \pi^+ + \pi^0)}{w(\mathrm{K_1^0})} \approx \frac{1}{500}. \tag{5}$$

6) The branching ratio in $\mathrm{K^+} \to 3\pi$ [3],

$$R_\tau = \frac{w(\mathrm{K^+} \to \pi^+ + 2\pi^0)}{w(\mathrm{K^+} \to \pi^- + 2\pi^+)} = 0.33 \pm 0.07. \tag{6}$$

2. The Isobaric Selection Rules for Hyperon Decay

In a previous report [4], an attempt has been made to test the isobaric selection rule $|\Delta \mathbf{I}| = \frac{1}{2}$ by assuming the one-to-one law for the Σ-decay interaction; the one-to-one law says that the coupling constants for the

parity conserving and non-conserving terms are of the same magnitude. Let us first analyse the Σ-hyperon decay without assuming the one-to-one law.

Let us assume the vector and axial vector interactions for the Σ-decay processes [4] †:

$$\begin{aligned} H &= g_1\bar{\psi}_p(a_1+b_1\gamma_5)\gamma_\mu\psi_{\Sigma^+}\partial_\mu\phi_{\pi^0} \\ &+g_2\bar{\psi}_n(a_2+b_2\gamma_5)\gamma_\mu\psi_{\Sigma^+}\partial_\mu\phi_{\pi^+} \\ &+g_3\bar{\psi}_n(a_3+b_3\gamma_5)\gamma_\mu\psi_{\Sigma^-}\partial_\mu\phi_{\pi^-}+\text{h.c.}, \end{aligned} \tag{7}$$

where the spin of Σ is assumed to be $\frac{1}{2}$, $g_i (i = 1, 2, 3)$ are real constants. Constants a_i and b_i are in general complex numbers and obey the normalization condition

$$\gamma^2|a_i|^2+|b_i|^2 = 1. \tag{8}$$

Here, γ^2 is defined to be

$$\gamma^2 \equiv \frac{(\text{s-wave part of the transition probability})/|a_i|^2}{(\text{p-wave part of the transition probability})/|b_i|^2}$$

and is calculated to be 1.4 in the lowest order approximation of the perturbational calculation.

The transition probabilities w_i and anisotropy coefficients α_i are obtained to be

$$w_i = (g_i^2/4\pi)\xi\eta, \tag{9}$$

$$\alpha_i = \text{Re}\,(a_i^* b_i)\zeta/\eta, \tag{10}$$

in the lowest order approximation of the perturbational calculation. Here, $i = 1, 2, 3$ stand for the processes $\Sigma^+ \to p+\pi^0$, $\Sigma^+ \to n+\pi^+$, $\Sigma^- \to n+\pi^-$ respectively. Constants ξ, η and ζ are

$$\xi = \frac{1}{4m_\Sigma}\left\{\frac{(m_\Sigma-m_N)^2-m_\pi^2}{m_\Sigma^2}\right\}^{\frac{1}{2}}\left\{\frac{(m_\Sigma+m_N)^2-m_\pi^2}{m_\Sigma^2}\right\}^{\frac{1}{2}},$$

$$\eta = (m_\Sigma+m_N)^2\{(m_\Sigma-m_N)^2-m_\pi^2\}$$

and

$$\zeta = 2(m_\Sigma^2-m_N^2)\{m_\Sigma^2-(m_N-m_\pi)^2\}^{\frac{1}{2}}\{m_\Sigma^2-(m_N+m_\pi)^2\}^{\frac{1}{2}},$$

where m_Σ, m_N and m_π are the masses of the Σ, nucleon and pion, respectively. According to (9) and (10), the ratios R_Σ, $R_{\Sigma'}$ and α_0/α_+ are obtained to be

$$R_\Sigma = g_1^2/g_2^2, \tag{11}$$

$$R_{\Sigma'} = g_3^2/(g_1^2+g_2^2), \tag{12}$$

† It is now evident that in Λ-decay processes the conservation of parity is violated. For the Σ-hyperon decay there is no such evidence [7]). However, it would be natural to consider that this is also true for Σ-decay. Even when the weak decay interaction is not invariant under the ordinary space inversion, the asymmetry in the decay angular distribution for the Σ-hyperon produced by the interactions, $\pi^-+p \to \Sigma^-+K^+$ or $K^-+p \to \Sigma^\pm+\pi^\mp$, should not be observed unless the hyperons are polarized.

$$\alpha_0/\alpha_+ = \mathrm{Re}\,(a_1^* b_1)/\mathrm{Re}\,(a_2^* b_2). \tag{13}$$

Here, the mass differences of the nucleons, of the pions and of the hyperons are not taken into account. Using the observed values (1) and (2), we obtain

$$g_1^2 \approx g_2^2 \approx g_3^2. \tag{14}$$

When $\alpha_0/\alpha_+ \approx 1$ [4]) is assumed, we obtain

$$\mathrm{Re}\,(a_1^* b_1) \approx \mathrm{Re}\,(a_2^* b_2). \tag{15}$$

This leads to the result

$$a_1 b_1 \approx a_2 b_2, \tag{16}$$

when the interaction is invariant under the time reversal. Interaction satisfying the rule $|\Delta I| = \frac{1}{2}$ must be an isobaric spinor [4]):

$$\begin{aligned} H_{|\Delta I|=\frac{1}{2}} &= \bar{\psi}_N \frac{1-\tau_3}{2}(A+B\gamma_5)\gamma_\mu \psi_{\Sigma i}\partial_\mu \phi_{\pi i} \\ &\quad + \left(\bar{\psi}_N \tau_i \frac{1-\tau_3}{2}\right)(A'+B'\gamma_5)\gamma_\mu \psi_\Sigma t_i \partial_\mu \phi_\pi + \text{h.c.} \\ &= \sqrt{2}\,\bar{\psi}_p (A'+B'\gamma_5)\gamma_\mu \psi_{\Sigma^+}\partial_\mu \phi_{\pi^0} \\ &\quad + \bar{\psi}_n\{(A+A')+(B+B')\gamma_5\}\gamma_\mu \psi_{\Sigma^+}\partial_\mu \phi_{\pi^+} \\ &\quad + \bar{\psi}_n\{(A-A')+(B-B')\gamma_5\}\gamma_\mu \psi_{\Sigma^-}\partial_\mu \phi_{\pi^-} \\ &\quad + \text{h.c.}, \end{aligned} \tag{17}$$

where

$$\psi_\Sigma \equiv \begin{pmatrix} \psi_{\Sigma 1} \\ \psi_{\Sigma 2} \\ \psi_{\Sigma 3} \end{pmatrix}, \qquad \phi_\pi \equiv \begin{pmatrix} \phi_{\pi 1} \\ \phi_{\pi 2} \\ \phi_{\pi 3} \end{pmatrix}, \qquad \psi_N = \begin{pmatrix} \psi_p \\ \psi_n \end{pmatrix},$$

$$\psi_{\Sigma^\pm} \equiv \frac{1}{\sqrt{2}}(\psi_{\Sigma 1} \pm i\psi_{\Sigma 2}), \qquad \phi_{\pi^\pm} \equiv \frac{1}{\sqrt{2}}(\phi_{\pi 1} \pm i\phi_{\pi 2}),$$

$$\psi_{\Sigma^0} \equiv \psi_{\Sigma 3}, \qquad \phi_{\pi^0} \equiv \phi_{\pi 3},$$

$$t_1 \equiv \begin{pmatrix} 0 & 0 & 0 \\ 0 & 0 & -i \\ 0 & i & 0 \end{pmatrix}, \qquad t_2 \equiv \begin{pmatrix} 0 & 0 & i \\ 0 & 0 & 0 \\ -i & 0 & 0 \end{pmatrix}, \qquad t_3 \equiv \begin{pmatrix} 0 & -i & 0 \\ i & 0 & 0 \\ 0 & 0 & 0 \end{pmatrix},$$

$$\tau_1 \equiv \begin{pmatrix} 0 & 1 \\ 1 & 0 \end{pmatrix}, \qquad \tau_2 \equiv \begin{pmatrix} 0 & i \\ -i & 0 \end{pmatrix}, \qquad \tau_3 \equiv \begin{pmatrix} 1 & 0 \\ 0 & -1 \end{pmatrix}.$$

Here A, B, A' and B' are in general complex numbers; they are real when the interaction is invariant under the time reversal [8]). When the interaction is invariant under the particle-antiparticle conjugation, A and A' should be out of phase by $\frac{1}{2}\pi$ from B and B' and the anisotropy coefficients should vanish unless the final state interactions are taken into account.

We can always find the solutions for A, B, A' and B' compatible with (14) and (15) when the limitations on the relative phases between the constants A, B, A' and B' are not put on. In the table are exhibited some special

TABLE

Branching ratios, the ratios of the life times and the anisotropy coefficients

A'/A	B/A	B'/A'	R_Σ	$R_{\Sigma'}$	α_0	α_+	α_-
1	± 1	∓ 1	0.88	0.44	∓ 1	0	0
-1	± 1	∓ 1	1.28	0.75	∓ 1	0	0
1	± 0.71	∓ 0.71	1.0	0.50	∓ 1	0	0
-1	± 0.71	∓ 0.71	1.0	0.50	∓ 1	0	0
-2.4	± 2.9	∓ 0.49	1.0	0.50	± 0.72	± 0.72	∓ 0.72
-2.0	± 2.0	∓ 0.5	1.3	0.59	∓ 0.69	∓ 0.73	± 0.53
0.5	± 0.5	∓ 2.0	0.80	0.44	∓ 0.53	∓ 0.89	± 0.69

solutions consistent with the relation (14). To date, no experiment has shown any violation of the invariance under the time reversal. Therefore, we are especially interested in the interaction being invariant under the time reversal. They must have the real coupling constants A, B, A' and B' and some examples of them are shown in the table. We then see that the sign of the ratio B/A is different from that of B'/A'. Let us now introduce the one-to-one law saying that

$$A^2 = B^2, \qquad A'^2 = B'^2.$$

This together with (14) leads us to the following result:

$$A^2 \approx A'^2, \qquad A/B \approx -A'/B'.$$

We see that there is only one type of interaction, viz.

$$H = g\left\{\bar{\psi}_N \frac{1-\tau_3}{2}(1+\varepsilon\gamma_5)\gamma_\mu \psi_{\Sigma i}\partial_\mu \phi_{\pi i} \pm \bar{\psi}_N \tau_i \frac{1-\tau_3}{2}(1-\varepsilon\gamma_5)\gamma_\mu \psi_\Sigma t_i \partial_\mu \phi_\pi\right\} + \text{h.c.} \tag{18}$$

when the rule $|\Delta \mathbf{I}| = \frac{1}{2}$, the one-to-one law and the time reversal invariance are assumed. Here, g is a real coupling constant and $\varepsilon = \pm 1$ [9]). The one-to-one law should be satisfied only for the interaction for the decay process $\Sigma^+ \to \mathrm{p}+\pi^0$ if the interaction (18) is formulated in terms of the coupling constants for different decay processes $\Sigma^+ \to \mathrm{p}+\pi^0$, $\Sigma^+ \to \mathrm{n}+\pi^+$ and $\Sigma^- \to \mathrm{n}+\pi^-$. The anisotropy coefficients are calculated to be

$$\alpha_0(\Sigma^+ \to \mathrm{p}+\pi^0) = -\varepsilon$$
$$\alpha_+(\Sigma^+ \to \mathrm{n}+\pi^+) = 0$$
$$\alpha_-(\Sigma^- \to \mathrm{n}+\pi^-) = 0.$$

If we assume the relation $A/B = A'/B'$ without assuming the rule $|\Delta \mathbf{I}| = \frac{1}{2}$, the one-to-one law should not depend on the expression for the interaction.

Then we obtain $\alpha_0/\alpha_+ \approx 1$ and the rule $|\Delta \mathbf{I}| = \frac{1}{2}$ should not hold.

Let us note that the fraction of the pionic decay of Λ-particle leading to $\pi^- + \mathrm{p}$ [10]),

$$R_\Lambda \equiv \frac{w(\Lambda \to \mathrm{p}+\pi^-)}{w(\Lambda)} = 0.65 \pm 0.05, \tag{19}$$

seems to support the rule $|\Delta \mathbf{I}| = \frac{1}{2}$. (The ratio R_Λ is $\frac{2}{3}$ according to the rule $|\Delta \mathbf{I}| = \frac{1}{2}$.)

3. The Pionic Decays of the K-meson: $\mathrm{K} \to 2\pi$ and $\mathrm{K} \to 3\pi$

When the weak interaction for the K-meson decay obeys the rule $|\Delta \mathbf{I}| = \frac{1}{2}$, we see

1) that the decay $\mathrm{K}^+ \to \pi^+ + \pi^0$ is forbidden if the K-meson has the spin zero and isobaric spin $\frac{1}{2}$, since the state for a π^+ and π^0 with angular momentum zero cannot have isobaric spin zero or one, and

2) that the branching ratio R_θ in K_1^0-decay is $\frac{1}{3}$. The latter is in agreement with the recent experimental results (4). The former is nearly true and only a small contribution from $|\Delta \mathbf{I}| = \frac{3}{2}$ or $|\Delta \mathbf{I}| = \frac{5}{2}$ should be put in to get a suitable decay rate; the slowness of the decay $\mathrm{K}^+ \to \pi^+ + \pi^0$ seems to be the evidence on the rule $|\Delta \mathbf{I}| = \frac{1}{2}$. However, we see in the following that there remains another possibility to account for the decay $\mathrm{K}^+ \to \pi^+ + \pi^0$ without introducing the rule $|\Delta \mathbf{I}| = \frac{1}{2}$.

Let us consider the process

$$\mathrm{K} \to \mathrm{N}+\bar{\mathrm{N}} \to \mathrm{N}+\bar{\mathrm{N}}+\pi \to \pi+\pi. \tag{20}$$

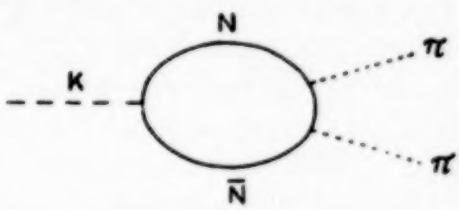

Fig. 1

The Feynman diagram for this is shown in fig. 1. Here, the interaction of the K-meson to the nucleons, KNN, violates the conservations of the strangeness and isobaric spin, and thus should be a weak interaction, which might not be invariant under the ordinary space inversion. Let us assume the absolute magnitude of its coupling constant to be of about the same value as that for the hyperon decay. It is evident that the virtual two nucleon state in the first step of the process (20) should have the isobaric spin $I = 0$ or $I = 1$. Since the other steps concern only the well-known pion-nucleon interaction for which the charge independence is shown to be rigorous, the final two pion state must have $I = 0$ or $I = 1$. On the other hand the spin-

less K-meson decay leads us to the two pion states for which $I = 0$ and $I = 2$. We thus see that the decay $K^+ \to \pi^+ + \pi^0$ should be forbidden without any restriction on the weak interaction, KNN, such as the rule $|\Delta I| = \frac{1}{2}$. The neutral K-meson decay can occur through the process (20) and the branching ratio R_θ is $\frac{1}{3}$, because the final two pions can appear only in the state of $I = 0$. Thus, if the virtual process (20) would be dominant, experimental results on the decay of the K-meson would not necessarily require the rule $|\Delta I| = \frac{1}{2}$. The fact that K^+ decays into two pions about 500 times more slowly than K_1^0 may be understood when the decay probability of K^+ through a process such as

$$K^+ \to p + \bar{\Sigma}^0 \to p + \bar{n} + \pi^0 \to \pi^+ + \pi^0 \tag{21}$$

is small compared with the process (20).

Let us now turn to the discussion concerning the 3π mode of decay of the K-meson. Considering the process

$$K \to N + \bar{N} \to N + \bar{N} + \pi \to N + \bar{N} + \pi + \pi \to \pi + \pi + \pi, \tag{22}$$

$I = 0$ and $I = 1$ states should be permitted for the final 3π system. For K^+-decay, the only possible state has $I = 1$ because of the fact that $I_z = 1$ †. The decay $K^+ \to \pi^+ + \pi^+ + \pi^-$ has been extensively studied [11]); it has been shown that the totally symmetric isobaric spin function can be used as a good approximation, since the matrix element totally symmetric in pion momenta seems to predominate in this decay. Then, the branching ratio R_τ, (6), is determined to be $\frac{1}{4}$ ††. This is in agreement with experiment (6). Taking into account the difference of the phase volumes for $K^+ \to 2\pi^+ + \pi^-$ and $K^+ \to 2\pi^0 + \pi^+$, the ratio appears to be 0.325 †††, and the agreement with the observed value becomes much better [12]). For the K_2^0 decays into 3π, it may be reasonable to assume the total symmetry for the final state wave function. We then find that the branching ratio $w(K_2^0 \to 3\pi^0)/w(K_2^0 \to \pi^+ + \pi^- + \pi^0)$ should be $\frac{3}{2}$ and taking into account the difference of the phase volumes for $K_2^0 \to 3\pi^0$ and $K_2^0 \to \pi^+ + \pi^- + \pi^0$ it should be 1.9. Experimentally, the existence of the 3π mode of decay of K_2^0 is established, but the number of the events is too small to determine the branching ratio.

The above discussions are also valid when the nucleons in (20) or (22) are replaced by baryons and Gell-Mann's global symmetry [13]) for strong π-interactions is assumed. This is because Gell-Mann's global symmetry treats (Σ^+, Y^0) and (Z^0, Σ^-) on the same footing as we have treated (p, n) and (Ξ^0, Ξ^-).

It would be worthwhile to examine what this situation becomes when four

† If in the K-decay into 3π the process (22) is dominant the isobaric properties of the K-decay are exactly the same as in the case when the rule $|\Delta I| = \frac{1}{2}$ dominates.

†† The result is not changed if the rule $|\Delta I| = \frac{1}{2}$ is assumed.

††† This effect is negligibly small for the decay $K \to 2\pi$.

fermion interactions [14]) for weak decay processes of the K-mesons are assumed. In the virtual steps for the process $K^+ \to \pi^+ + \pi^0$ we find two different ways:

a) $K^+ \to p + \bar{\Sigma}^0 \to p + \bar{n} \to p + \bar{n} + \pi^0 \to \pi^+ + \pi^0$,

b) $K^+ \to p + \bar{\Sigma}^0 \to p + \bar{\Lambda} + \pi^0 \to p + \bar{n} + \pi^0 \to \pi^+ + \pi^0$.

The processes like a) behave in the same way as the process (20) does in the isobaric spin space and therefore the decay $K^+ \to \pi^+ + \pi^0$ is forbidden when it is assumed to occur only through the process a). The process b) corresponds to the process (21). The same is true for the charged K-meson decay into three pions and for the neutral K-meson decay into two or three pions. It is then easily seen that we have the possibility to account for the K-meson decay into pions without assuming the rule $|\Delta \mathbf{I}| = \frac{1}{2}$, when four fermion interactions concerning baryons are assumed.

4. Concluding Remarks

Summarizing our results, only one possible type is left for the Σ-decay interaction when the rule $|\Delta \mathbf{I}| = \frac{1}{2}$, the invariance under the time reversal and the one-to-one law are assumed. Further experiments on the anisotropy coefficients for the Σ-decay are necessary in examining the validity of such a type of the Σ-interaction, as well as the validity of the rule $|\Delta \mathbf{I}| = \frac{1}{2}$ for the interaction leading to the Σ-decay. The anisotropy coefficients for the Σ-decay are especially important to test the isobaric selection rule $|\Delta \mathbf{I}| = \frac{1}{2}$, because of the fact that the observations on the K-decay into two or three pions do not establish the rule $|\Delta \mathbf{I}| = \frac{1}{2}$, as has been shown in section 3.

The author is grateful to Professor H. Umezawa for his inspiring discussions. The author is also indebted to Dr. M. Konuma and Dr. K. Kawarabayashi for their excellent cooperation.

References

1) H. Umezawa, M. Konuma and K. Nakagawa, Nuclear Physics **7** (1958) 169
2) G. Wentzel, Phys. Rev. **101** (1956) 1215;
G. Takeda, Phys. Rev. **101** (1956) 1547
3) M. Gell-Mann and A. Rosenfeld, Ann. Rev. Nucl. Sci. **7** (1958) 407
4) K. Nakagawa and H. Umezawa, Nuovo Cimento **8** (1958) 945
5) G. A. Snow, Proc. 7th Rochester Conf. on High-Energy Physics (1957)
6) A. Rosenfeld, Proc. 7th Rochester Conf. on High-Energy Physics (1957)
7) 1958 Annual International Conference on high energy physics at CERN (1958) 273
8) H. Umezawa, S. Kamefuchi and S. Tanaka, Prog. Theor. Phys. **12** (1954) 383
9) K. Nakagawa and H. Umezawa, Nuovo Cimento (to be published)
10) F. Eisler, N. Samios, M. Schwartz and J. Steinberger, Nuovo Cimento **5** (1957) 1700
11) R. H. Dalitz, Phil. Mag. **44** (1953) 1068
12) R. H. Dalitz, Proc. Phys. Soc. **69** (1956) 527
13) M. Gell-Mann, Phys. Rev. **106** (1957) 1296
14) R. P. Feynman and M. Gell-Mann, Phys. Rev. **109** (1958) 193

4.E *Nuclear Physics* **10** (1959) 28—32; © *North-Holland Publishing Co., Amsterdam*
Not to be reproduced by photoprint or microfilm without written permission from the publisher

THE DISINTEGRATION OF Ga^{73}

L. MARQUEZ, E. W. CYBULSKA, N. L. COSTA and I. G. ALMEIDA
Centro Brasileiro de Pesquisas Físicas, Rio de Janeiro †
and
J. GOLDEMBERG
Departamento de Física, Universidade de São Paulo, São Paulo

Received 30 October 1958

Abstract: The disintegration of Ga^{73} has been studied using gamma ray spectrometers, both alone and in coincidence; and by the absorption of the beta rays in coincidence with the most prominent gamma ray in the scintillation spectrometer. It was found that there were two gamma rays; one with an energy of 310 keV and intensity of about 90 % and one with an energy of 740 keV and an intensity of about 7 %. A self-consistent decay scheme is proposed showing one beta ray of 550 keV and intensity of about 7 %, one beta ray of 1300 keV and intensity of about 83 % and perhaps a third beta ray of 1600 keV and intensity of about 10 %. All the beta rays lead to the metastable state of Ge^{73}.

1. Introduction

The decay scheme of Ga^{73} has not been the subject of a thorough investigation. The isotope was found by Siegel and Glendenin [1]). They found that it decays with a half life of 5.0 h and they found by absorption methods that it has one beta ray of 1.35 MeV and no gamma rays. It has also been reported [2]) that it leads to the 0.53 sec Ge^{73}, the same as in decay of 76 day As^{73}. The decay of 0.53 sec Ge^{73} has been studied by several workers [2,3,4]) and it is known that it decays by the emission of two gamma rays of 53.9 keV and 13.5 keV the first with a conversion coefficient of about 8 and the second with a conversion coefficient greater than 1300.

We have found that Ga^{73} is followed by a gamma ray of 740 keV with weak intensity and by a gamma ray of 310 keV with strong intensity. The beta ray spectrum of Ga^{73} is complex and our measurements indicate that it has probably three beta ray groups. It is certain that it has two beta ray groups.

We propose a decay scheme of Ga^{73} consistent with our measurements and from this decay scheme we arrive at a value of the conversion coefficient of the 53.9 keV gamma ray in Ge^{73}.

† This work was done in part under the auspices of the Conselho Nacional de Pesquisas of Brazil.

2. Experimental Procedure

The Ga^{73} was prepared by irradiating samples of 15 g of chemically pure GeO_2 in the Betatron of Sao Paulo during one hour and at 25 cm from the target. The maximum energy of the gamma ray beam was 21 MeV. The Ga^{73} is formed by the reaction $Ge^{74}(\gamma, p)Ga^{73}$. The irradiated samples were flown to Rio de Janeiro, where the chemical processing and the measurements were done.

The irradiated GeO_2 was suspended in a small amount of water. 250 ml of 12 *N* HCl and 10 mg of Ga carrier were added and the mixture was boiled with continuous stirring. Another 100 ml of 12 *N* HCl were added and the boiling continued until the liquid was clear. All the Ge goes as $GeCl_4$. The solution was evaporated to a small volume and the samples were mounted in two different ways. For the measurements of the gamma rays, the Ga was precipitated with $K_4Fe(CN)_6$ and centrifuged in a suitable test tube to fit in the well cristal scintillation spectrometer, or the solution was evaporated to dryness at 110°C in a test tube or on a glass plate. For the measurements of the beta rays in the coincidence measurements, the concentrated Ga solution was evaporated to dryness at 110°C in plastic trays or glass plates.

The samples in the test tube were measured in a well crystal scintillation spectrometer having a NaI(Tl) crystal of $1\frac{3}{4}''$ diameter and 2'' height. The dimensions of the well are $\frac{5}{8}''$ diameter and $1\frac{1}{2}''$ height. The spectrum showed a line of 53 ± 2 keV and a line of 310 ± 5 keV. Both decayed with a half life of 5 h, showing that they were associated with the Ga^{73}. There were weaker lines at higher energy that decayed with a half life of about 14 h and belong to Ga^{72} which is also formed in the irradiation. In one of the measurements the total sample was divided exactly in two parts. In one of them the absolute activity of the 5 h beta particles was measured by the method of the well defined solid angle [5]). In the other we measured the area under the peaks of 54 keV and 310 keV. We calibrated the efficiency of the spectrometer as a function of gamma ray energy and so could express the areas under the peaks in absolute activity. If we express all the beta particles of 5 h half life as 100 %, we get for the 53 keV line 13.5 ± 2 % and for the 310 keV line 90 ± 15 %. The energy scale of the spectrometer was calibrated with well known gamma ray lines.

We measured the spectrum of the region above 310 keV very carefully in one experiment, following the decay of each point on the spectrum showed as a function of time. It was found that all the points of the spectrum showed a small component of 5 h and when this 5 h part was plotted as a function of energy for a given time, there was a peak at 740 ± 10 keV. There appeared a fictitious peak at 1050 keV, but it was shown that it was absorbed with the

half thickness of Pb corresponding to 310 keV and that it was due entirely or almost entirely to pile up of 310 keV and 740 keV.

We carried out measurement with two scintillation spectrometers in which we registered the counting rate of each of them and the coincidences. Both spectrometers were single channel pulse height analyzers. One of them had a NaI(Tl) crystal of $1\frac{3}{4}''$ diameter and 2" height; the other had a NaI(Tl) crystal of $1\frac{1}{2}''$ diameter and 1" height. They were at 1.7 cm from each other and the samples were at 1.2 cm from the first crystal. We could put absorbers between the sample and the first crystal.

The second spectrometer was set to count the line of 310 keV. The spectrum was swept with the first spectrometer. The coincidence counts showed very well the peak at 740 keV clean from the 14 h component. The pile up peak disappeared. The intensity of the 740 keV line was measured and it turned out to be about 7 % of all the beta particles.

These measurements prove the existence of at least two beta ray groups. One soft beta ray followed by the 740 keV gamma ray and then by the 310 keV gamma ray; and a harder beta ray followed by the 310 keV gamma ray only.

We made three irradiations in which coincidence measurements were carried out between the beta rays and the 310 keV gamma ray. The arrangement had a NaI(Tl) crystal of $1\frac{1}{2}''$ diameter and 1" height. The crystal was operated as single channel pulse height analyzer and it was set to count the 310 keV peak. At a distance of 2 cm from the crystal there was an end window Geiger counter and the sample was at 1.5 cm from the Geiger. Al absorbers were placed between the Geiger and the samples. The decay curve for each absorber had to be followed to correct for the 14 h beta activity. We registered the beta activity N_β, the gamma activity N_γ and the coincidences $N_{\beta\gamma}$. A curve of $N_{\beta\gamma}/N_\beta$ as a function of absorber thickness shows a ratio decreasing with the amount of absorber. The curve indicated that there must be a third group of beta particles. This conclusion is drawn from the fact that the two beta rays previously established were followed by the 310 keV gamma ray.

The curve of $N_{\beta\gamma}/N_\beta$ could be fitted with a theoretical curve having 90 % of the beta particles coincident with the 310 keV gamma ray and 10 % of a harder beta ray not in coincidence with the 310 keV gamma ray. We do not regard the existence of this third beta ray as definitely established due to the cumbersome procedure of resolving decay curves of 5 h and 14 h from which its existence was inferred. Measurements of the beta ray spectra of Ga^{73} will settle this point.

The average energy of the beta ray was determined by measuring their absorption coefficient in Al as a function of absorber thickness and gives 1.3 MeV. A curve of measured absorption coefficients as a function of maxi-

mum beta ray energy was obtained using standard beta ray sources. It follows that the energy of the main beta ray is 1.3 MeV; the energy of the softer beta ray is 0.55 MeV and the energy of the harder beta ray is 1.6 MeV.

3. Discussion

The spin and parity of the ground state of Ga^{73} is known to be $\frac{9}{2}^+$. The sequence of the gamma rays of 53.9 keV and 13.5 keV seems to be well established [4,6]) and it gives for the corresponding states the choice of spins and parities given by Welker *et al.*[3]). The spin and parity of Ga^{73} must be $\frac{3}{2}^-$ from shell model considerations. The three beta rays give log *ft* values corresponding to allowed transitions. All these enable us to construct the decay scheme shown in fig. 1. The spin and parity of the two upper levels of

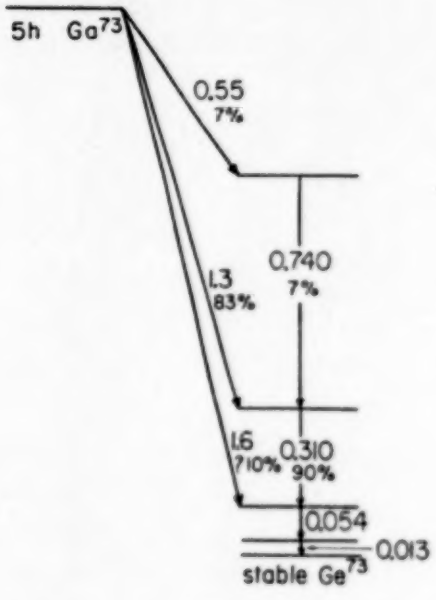

Fig. 1

the Ge^{73} that we have found as a result of this work must be $\frac{1}{2}^-$, $\frac{3}{2}^-$ or $\frac{5}{2}^-$. With the information available it is not possible to decide among them.

The only discrepancy present in this decay scheme comes from the measurement of the internal conversion coefficient of Welker *et al.*[3]) for the 53.9 keV line. Using their value of 4.7 we find that the line has an intensity of 77 %. In order to get the intensity of 100 % that it should have according to the decay scheme proposed, its conversion coefficient should be 6.4. The 13.5 keV line does not show in our measurements because its large conversion coeffiicent and the soft electrons would not come out from our relatively thick sources.

References

1) J. M. Siegel and L. E. Glendenin, NNES **9** (1950) 549
2) S. Johansson, Arkiv Fysik **4** (1952) 273
3) J. P. Welker, A. W. Schardt, G. Friedlander and J. J. Howland, Jr., Phys. Rev. **92** (1953) 401
4) R. Barloutaud, R. Ballini and M. Sartori, Compt. Rend. **237** (1953) 836
5) L. Marquez, Phys. Rev. **86** (1952) 405
6) K. Way, R. W. King, C. L. McGinnes and R. van Lieshout, Nuclear Level Schemes USAEC (1955) p. 116

2.A.1:
2.I

Nuclear Physics **10** (1959) 33—44; © *North-Holland Publishing Co., Amsterdam*
Not to be reproduced by photoprint or microfilm without written permission from the publisher

A STUDY OF THE GIANT RESONANCE REGIONS OF Be^8 AND C^{12} THROUGH THE INVERSE REACTIONS Li^7 (p, γ) Be^8 AND B^{11} (p, γ) C^{12}

D. S. GEMMELL, A. H. MORTON and E. W. TITTERTON
Research School of Physical Sciences, Australian National University, Canberra

Received 31 October 1958

Abstract: In a search for fine structure in the giant resonance of C^{12} an experiment has been carried out to determine the excitation function for the ground state gamma-rays of the reaction B^{11}(p, γ)C^{12} for protons in the energy range 4 to 7.7 MeV. The measured cross-sections can be related to the C^{12}(γ, p)B^{11} cross-sections through the principle of detailed balancing. The experiment locates the maximum of the C^{12}(γ, p) giant resonance at 22.55 ($\pm$0.1) MeV but does not resolve individual levels. The cross-section curve, however, is not smooth, and two peaks at C^{12} excitations of 21.4 and 22.1 MeV are suggested. The maximum value of the C^{12}(γ, p) cross-section is found to be (29$\pm$5) mb.

The reaction Li^7(p, γ)Be^8 was also investigated over a similar range of proton energies. Transitions to the 2.9 MeV level of Be^8 are found to predominate over those to the ground state throughout the energy range. The experiment suggests that the reaction Be^8(γ, p)Li^7, if it could be observed, would have a cross-section maximum at 22 MeV.

1. Introduction

Although the resonance absorption of gamma radiation to form a compound state is known to occur at low energies [1]) and in the case of some light nuclei at quite high excitation [2]) the reasonable surmise that the giant resonance observed in photonuclear reactions arises, at least in part, from absorption into a favoured set of energy levels has not been established with certainty. In bremsstrahlung experiments made at a fixed end-point energy, difficulties arise in obtaining high resolution detection of reaction products, of determining the energy of the gamma ray causing a given event and of identifying the state of the residual nucleus. The method of varying the end-point energy and searching for "breaks" in the yield curve has been given much attention but, unfortunately, results from various laboratories relating to the same nucleus do not, in general, agree with each other. The interpretation of such "breaks" at the present time is therefore uncertain.

Bethe [3]) pointed out that (γ, p) and (p, γ) cross-sections are related through the principle of detailed balancing, and this offers another approach to the problem. The idea has been employed by Mann and Titterton [4]) for the reactions C^{12}(γ, p)B^{11} and B^{11}(p, γ)C^{12} and by Wright *et al.*[5]) in

the case of $N^{14}(\gamma, p)C^{13}$ and $C^{13}(p, \gamma)N^{14}$; both experiments demonstrate resonance absorption in the region below the giant resonance.

Although investigation of the giant resonance through the inverse (p, γ) reaction has the great advantages that the resolution obtained is determined by the incoming protons and the energy is known precisely, it has not been exploited to date. The reason is that, until recently, variable-energy sources of protons in the range 5—15 MeV, required to cover the region, were unavailable.

Completion of the 7.7 MeV 30″ cyclotron, designed for use as the injector for the 10-GeV proton synchrotron under construction in this laboratory, provided a source of protons which, by appropriate modification of the machine, allowed an extracted beam of high energy homogeneity to be obtained. The energy could be reduced to 4 MeV in small steps by inserting aluminium foils into the beam without too great a loss of resolution.

Two reactions have sufficiently high Q-values for (p, γ) studies in this energy range to enable the giant resonance region to be covered; they are $Li^7(p, \gamma)$ $Be^8+17.2$ MeV and $B^{11}(p, \gamma)C^{12}+16.0$ MeV. This paper reports investigations of both reactions which, it was hoped, would throw light on the nature of absorption in the giant resonance region of Be^8 and C^{12}. The approximate position of the giant resonance in C^{12} is known, and since the ground state is 0^+, the levels expected to contribute most significantly to absorption in the resonance would be 1^-. C^{12} is therefore a most suitable nucleus in which to search for fine structure in the absorption curve. Be^8 is an unstable nucleus and cannot be investigated by photodisintegration techniques; it was hoped to establish the position and properties of the giant resonance for it.

2. Experimental Method

The experimental arrangement is shown in fig. 1. A beam of monoenergetic protons, extracted from the Canberra 30″ cyclotron, was focussed by means of a quadrupole lens located inside the cyclotron shield onto a very thin target outside the cell. The proton energy was varied by inserting appropriate aluminium foils in the path of the beam at the position indicated, and the gamma rays were detected at 90° by a large NaI(Tl) crystal which had to be shielded against neutrons and spurious gamma radiation.

The various components of the system will be discussed in the following paragraphs.

The Canberra cyclotron was designed for high-current beams but, for the present purpose, it was modified to obtain small, monoenergetic beams. The method is described in detail by Morton and Smith [6]); it requires that protons from the ion source shall, in their first, second and third orbits, pass through correctly located beam-defining slits of width 1, $\frac{1}{2}$ and $\frac{1}{2}$ mm respectively. This ensures that only those protons leaving the ion source during a

few electrical degrees about a particular dee voltage phase angle are accepted for acceleration. Radial movement of the second slit served to restrict the circulating current to about 10 μA, excess ions being stopped before acquiring sufficient energy to produce background radiation. An internal probe at 90° from the extractor sampled the beam at the final orbit and the current to this was adjusted to 5μA. The current to the probe was very sensitive to magnetic field fluctuations and, by stabilising it, machine conditions could be held constant over long periods of time. The remaining beam current of 5μA was

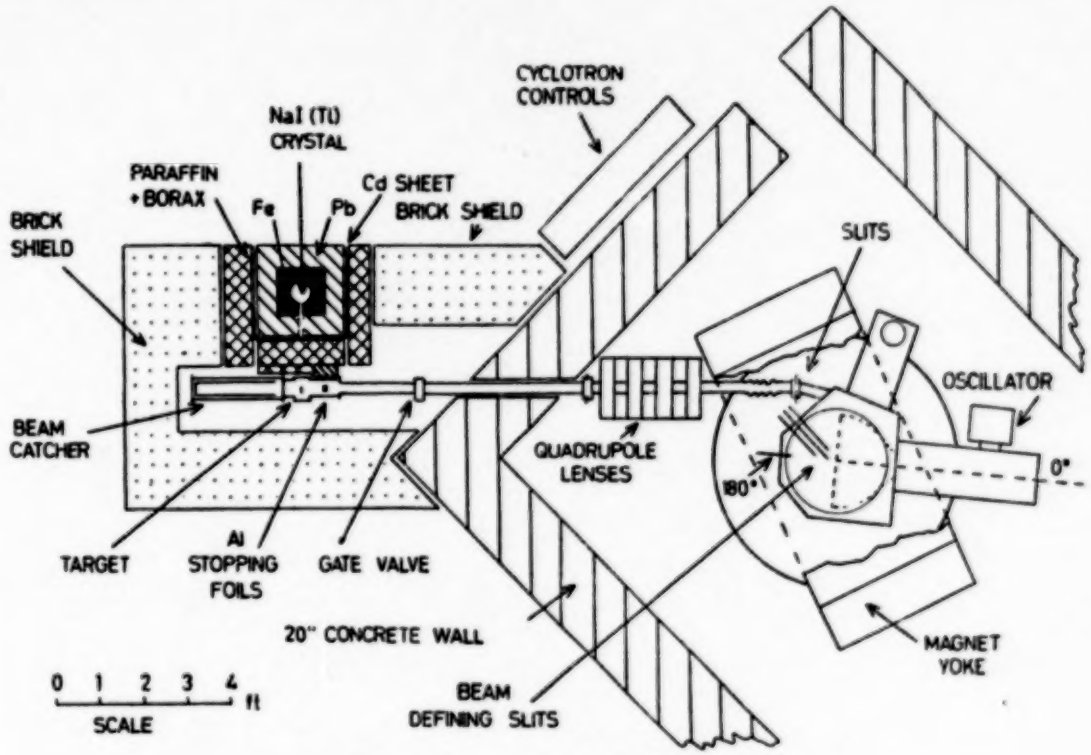

Fig. 1. Experimental arrangement.

completely extracted and limited to 1 μA by a system of narrow slits 2 mm high and 2.5 mm wide just outside the machine. The beam therefore underwent a momentum analysis in the fringing field of the machine, after which it was focussed on the target by the quadrupole lenses. Magnetic analysis of the beam reaching the target gave an energy spread of < 35 keV, and measurements[7]) made on a steeply-rising portion of the $Al^{27}(p,\gamma)$ yield curve at 7.50 MeV indicated a stability of $+0, -30$ keV over many hours of operation.

Proton energy variation was achieved by inserting 1.63 mg/cm^2 aluminium foils mounted on two movable racks, each of which could be placed in any one of seven different positions. One rack allowed any thickness of foil between 0 and 6 to be used, and the other, foil steps increasing by 7 thicknesses at a time. By this means the proton energy could be reduced from 7.7 to 3.9 MeV in 48 steps; the steps were not equal in energy, but at 7.7 MeV a

single foil corresponded to 68 keV. This method of energy variation was the only one available with this machine and has the disadvantages that the beam is spread by scattering, the energy resolution is worsened by straggling, and reactions in the foils themselves are a source of unwanted background radiation. In order to confine the beam at the target to a spot of diameter $\frac{1}{2}''$, it was found necessary to place the foil racks 5" up-beam from the target, and this made careful shielding of the detector essential. The theoretical

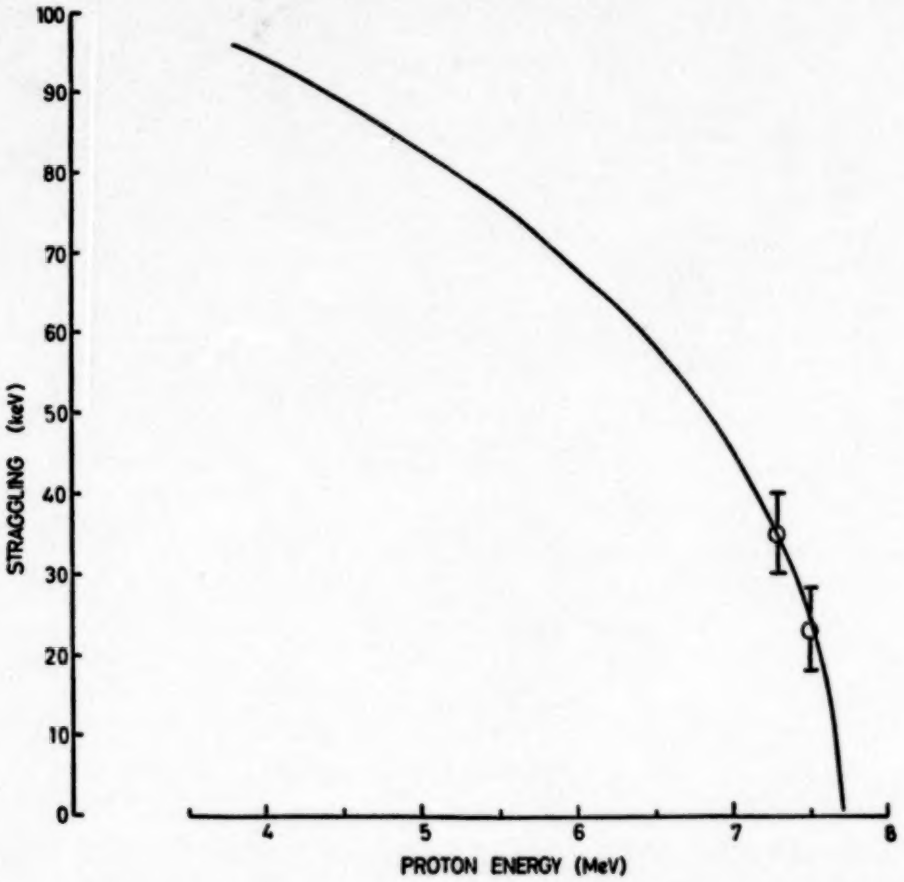

Fig. 2. Theoretical straggling curve of Bohr. The two experimental points shown are derived from magnetic analysis at proton energies corresponding to 3 and 6 stopping foils.

curve of the energy straggling [8]) is given in fig. 2; it was checked by magnetic analysis and found to hold for up to six foil thicknesses, but the angular divergence of the beam reduced the value of such measurements at lower energies and the theoretical extrapolation was assumed to hold.

Thin targets were essential both for good resolution and to keep the high-energy gamma-ray background arising from neutrons formed and captured in the target (and any backing used) to a minimum. The first boron targets were made by evaporating B_2O_3 onto a 3 mg/cm^2 gold foil, but it was found

more satisfactory to evaporate amorphous boron onto the foil by heating in vacuo in a carbon crucible. The targets used were of this type and were generally 0.8 mg/cm² in thickness. Lithium targets were made by rolling the metal, lubricated with kerosene, between brass or polythene sheets, and in this case no backing foil was necessary. The latter method enabled uniform targets of 0.001" thickness (1.4 mg/cm²) to be produced. The targets were hung in the beam and stretched by a small weight suspended from them. The beam leaving the target passed into a 2 ft long tubular "catcher" lined with lead which was connected to the beam current integrator and which stopped the protons at a sufficient distance from the detector so that radiation effects were negligible.

Detection of the high-energy quanta was carried out by a 5" diameter 4" long Harshaw NaI(Tl) crystal mounted on a 5" diameter DuMont type 6364 photomultiplier tube; the crystal axis was vertical and located 19½ inches form the target centre. Pulses from the phototube were amplified by a non-overload Higginbottom amplifier and were analysed using a 60-channel Hutchinson-Scarrott kicksorter.

The principal difficulty in the experiment arose from the background problem. There were three main sources — from the foil system (especially when many foils were inserted in the beam), from the target itself, and from pulses arising in the crystal due to the traversal of cosmic-ray μ-mesons. The foils and targets yielded neutrons through (p, n) reactions and also high-energy gamma rays (up to 14 MeV) from the capture in the crystal and its surroundings of the neutrons so produced. Neutrons reaching the crystal were found to induce in it the 25-minute I^{128} activity as well as (n, γ) reactions. The measures taken to reduce radiation at the detector are shown in fig. 1. The crystal was seated inside a steel block, 9" × 9" × 6", which in turn was surrounded by a 6" thickness of lead, through the whole of which a 1" dia. collimating hole was drilled so that gamma rays from the target could pass along a diameter of the crystal in its centre. To reduce the neutron flux, a 0.010" cadmium sheath was wrapped around the lead shield enclosing the crystal, and 8"-thick layers of a 50/50 mixture of borax and paraffin wax were placed at the sides of the assembly. An extra 3" thickness of lead was interposed between the stopping foils and the crystal just outside the foil chamber. Capture gamma rays originating at the target had to be detected through the neutron shield, and slight corrections were necessary for attenuation. The natural μ-meson flux gave a flat distribution of pulses over the energy range of interest, and this background was measured and subtracted off. To keep it small, beam currents of 1 μA were used in most of the experiments, and it was shown that under these conditions, significant pulse "pile-up" did not occur.

3. Measurements

Typical spectra taken under the experimental conditions defined above are shown in fig. 3.

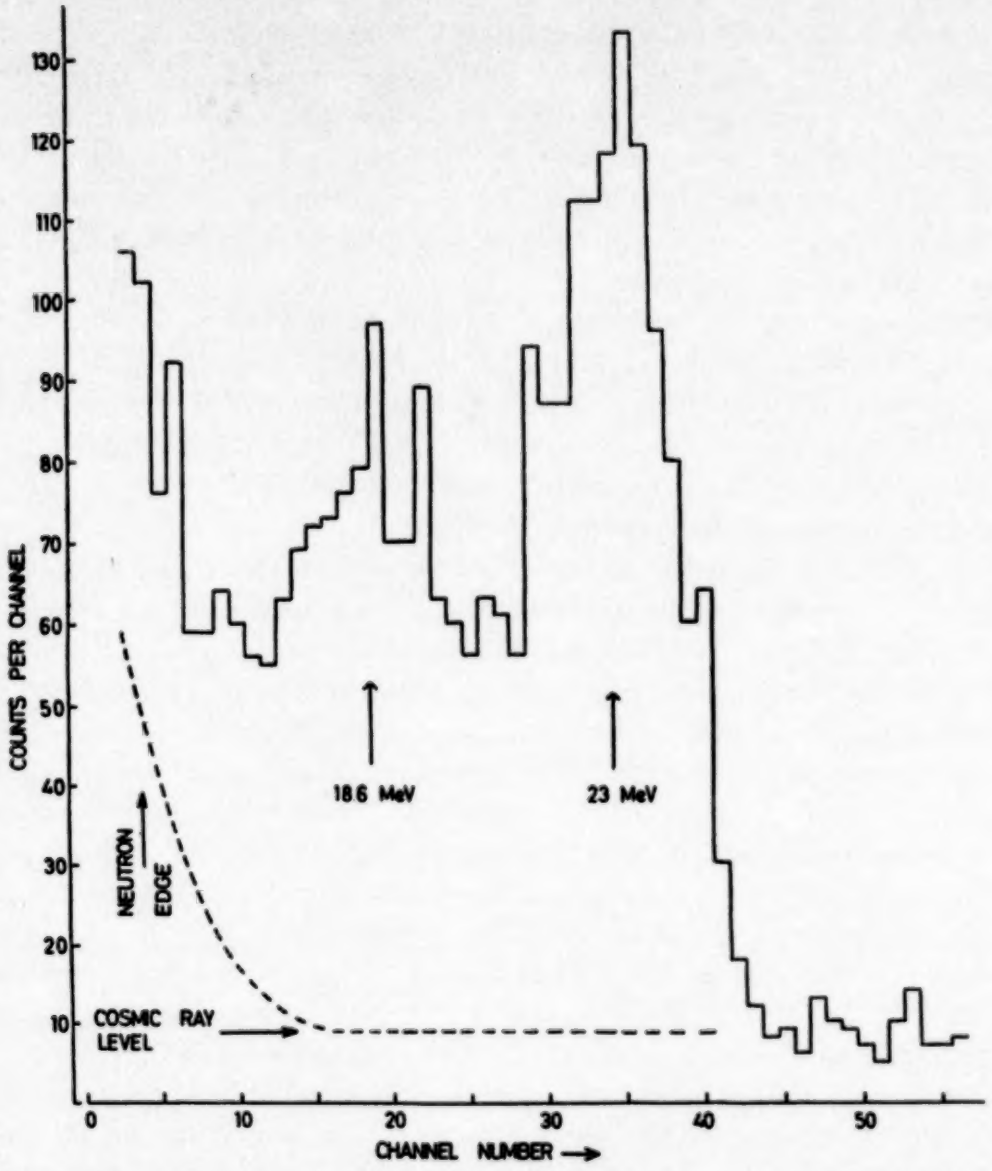

Fig. 3. (a) $B^{11}(p, \gamma)$ spectrum at $E_p = 7.7$ MeV. The dashed line represents the background level at this energy.

The resolution and calibration of the crystal for high-energy gamma rays were determined using $Li^7(p, \gamma)$ radiation at the 440 keV resonance (17.6 MeV radiation), the thick target yield being taken as 1.9×10^{-8} γ-ray/proton[9]); the resolution at this energy was approximately 15 %.

In fig. 3(a) the $B^{11}(p, \gamma)C^{12}$ spectrum at a bombarding energy of 7.7 MeV is shown with the background level marked in. The ground state and first excited state transitions are resolved at 23.0 and 18.6 MeV respectively;

the steeply-ascending counting rate in channels below 10 is due to the background effects discussed earlier. At lower proton bombarding energies the low-energy peak (first excited state transition) moved downwards in energy and merged into the background "edge", but the high-energy peak was resolved at all energies. By taking spectra at each proton energy it was

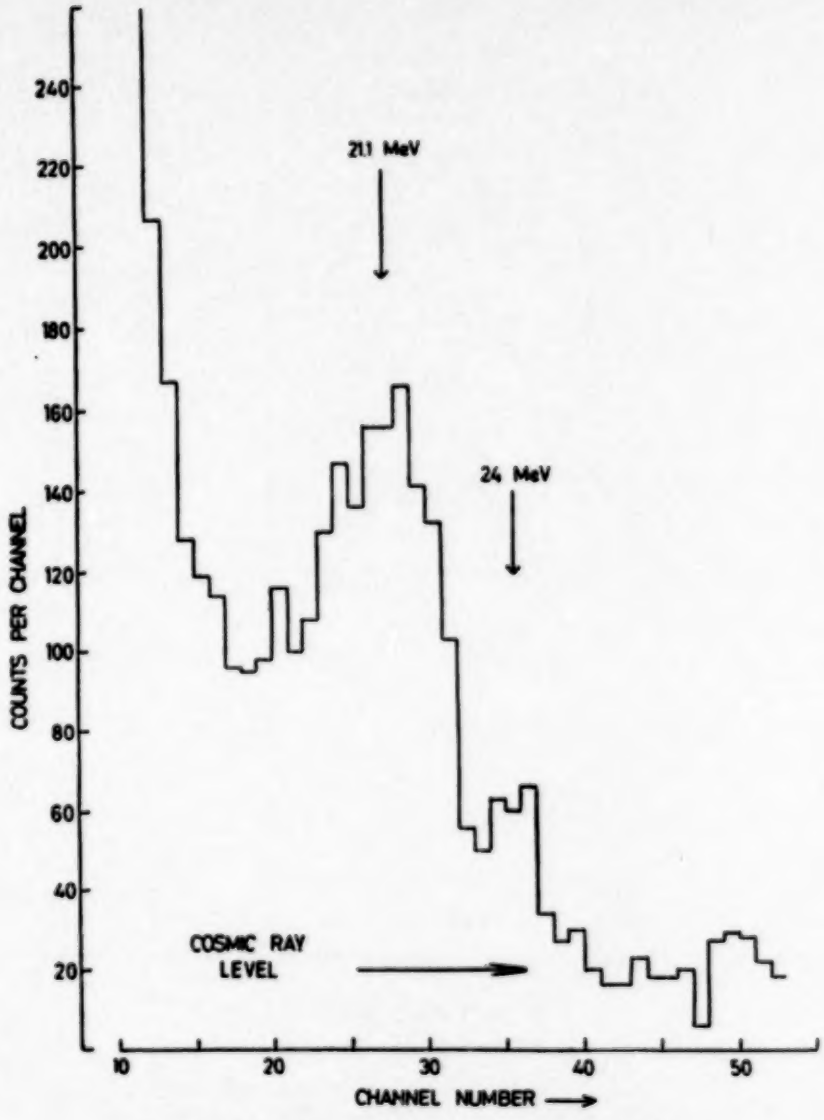

Fig. 3. (b) $Li^{7}(p,\gamma)$ spectrum at $E_p = 7.7$ MeV.

therefore possible to determine the yield of ground-state gamma rays as a function of bombarding energy. To obtain good statistics long runs were essential; each comprised starting at full energy, slowly working down to minimum and then returning to full energy, the whole run extending over a period of approximately 20 hours during which time the cyclotron was operated continuously after a warm-up period of half-an-hour. In all, a total of seventeen such runs was made with targets of boric oxide and boron of

various thicknesses, but the final result comprises the results of six runs on a 40-keV thick elemental boron target and is shown in fig. 4(a).

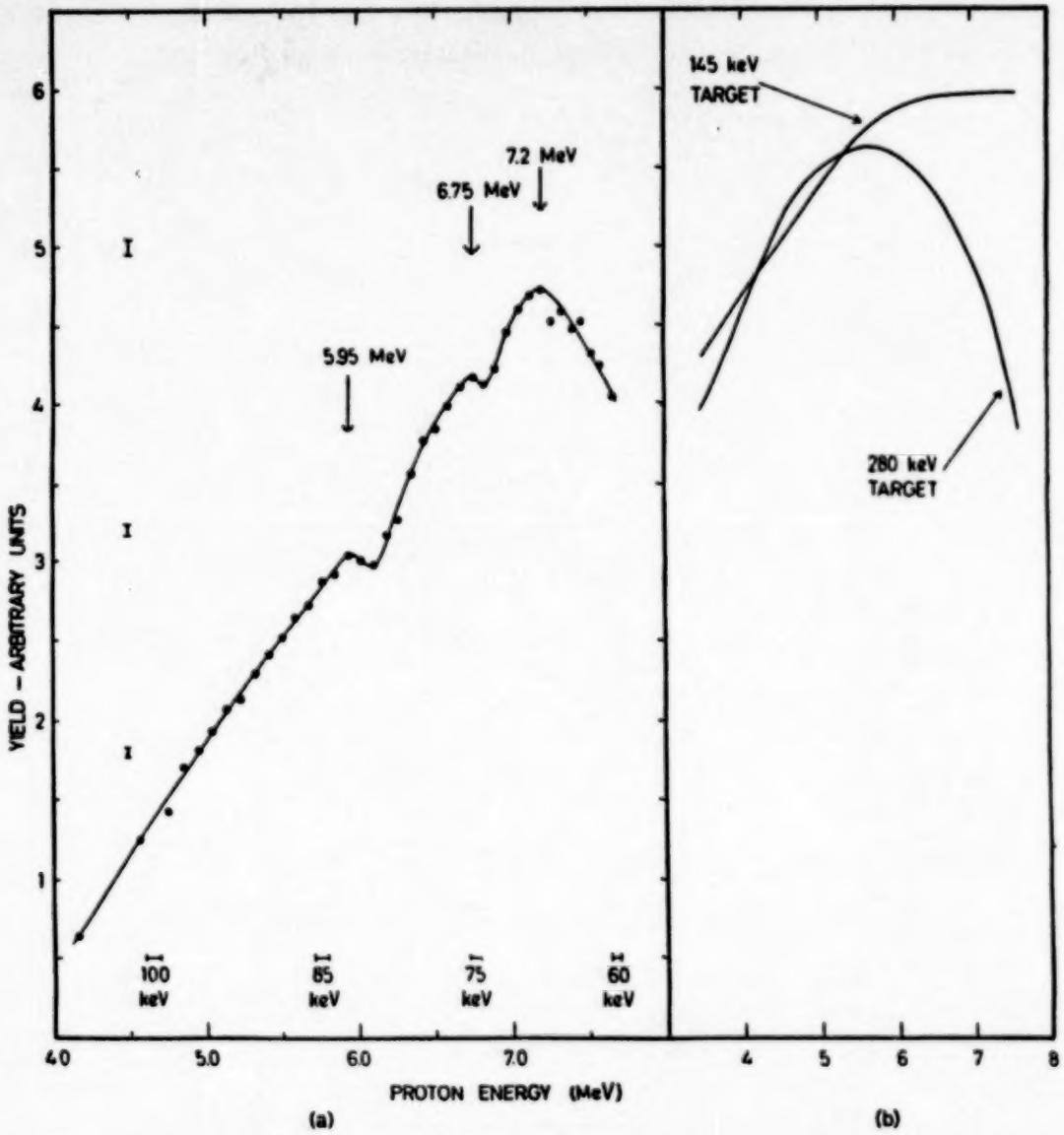

Fig. 4. (a) Yield curve for B^{11} (p, γ)C^{12} ground-state gamma rays.
(b) Two determinations of the Li^7(p, γ) yield curve.

Similar experiments were carried out with lithium targets. In this case the pulse-height spectrum at maximum energy was as shown in fig. 3(b) and the main transition was to the broad 2.9 MeV level of Be^8; the ground-state transition was not clearly resolved. Yield curves were determined as before, but the number of runs over the available proton bombarding energy range was limited to six as the cyclotron had to be dismantled and moved into position as the injector for the synchrotron. The yield curves were derived

by plotting the total number of pulses under the peaks corresponding to transitions to both the 2.9 MeV and ground states of Be^8.

In making the preliminary experiments with lithium targets it was found that the neutron production from the target was appreciably greater than that from the boron targets. This was partly due to (α, n) resctions from the (p, α) reaction occurring in the target. As a result of this enhanced background, it was necessary to use smaller beam currents to avoid distortion of the spectrum by pile-up. The two yield curves regarded to be of most significance are shown in fig. 4(b).

4. Results and Discussion

4.1. $B^{11}(p, \gamma)C^{12}$

The yield curve for ground-state gamma radiation is shown in fig. 4(a) and leads to a peak cross-section at a proton energy of 7.2 MeV of $(2.7 \pm 0.5) \times 10^{-28}$ cm^2, assuming isotropy. The measured cross-sections agree with the data of Bair *et al.*[10]) in the region of overlap and extend these data from 5.3 MeV to 7.7 MeV, revealing the position of the maximum of the giant resonance. The curve exhibits small peaks at 21.4 and 22.1 MeV excitation of the compound nucleus, but is otherwise smooth within the resolution of the experiment (indicated on the figure for various proton energies).

Application of the principle of detailed balancing yields a peak value for the photoproton cross-section of C^{12} of (29 ± 5)mb at 90°, the peak being located at (22.55 ± 0.1) MeV.

The cross-section is in agreement with that measured by Halpern and Mann [11]) who, in photodisintegration experiments, found (34 ± 8)mb at the same angle. A later Pennsylvania experiment [12]) gave some indication of fine structure in the resonance, but the statistics were not good and the interpretation was difficult since the final state of the residual nucleus was unknown. However, their histogram shows a group at 21.5 MeV, which could be identified with the peak observed in this experiment at 21.4 MeV.

The interpretation of the present result, that two compound states at 21.4 and 22.1 MeV figure in the absorption, receives some support from the work of Blaser *et al.*[13]) on the reaction $B^{11}(p, n)C^{11}$, where levels are observed at 21.3 and 21.8 MeV see fig. 5(a). Moreover, the general result is strikingly similar to that reported by the Stanford group [14]) at the Washington photonuclear conference relating to the reaction $C^{12}(e, e'p)B^{11}$. The proton distribution measured in this experiment showed a peak at about an energy of 6 MeV which was identified with the giant resonance absorption region. With the resolution available (about 170 keV) fine structure was not observed but, below the 6 MeV peak, alternate plateaux and rising portions occurred at energies in good agreement with those of the discontinuities reported here.

On the other hand, the present results are not compatible with the most recent data presented by Katz *et al.*[15]) for the "breaks" in the $C^{12}(\gamma, n)$ yield curve. In the region of C^{12} excitation between 21—23 MeV the Saskatoon

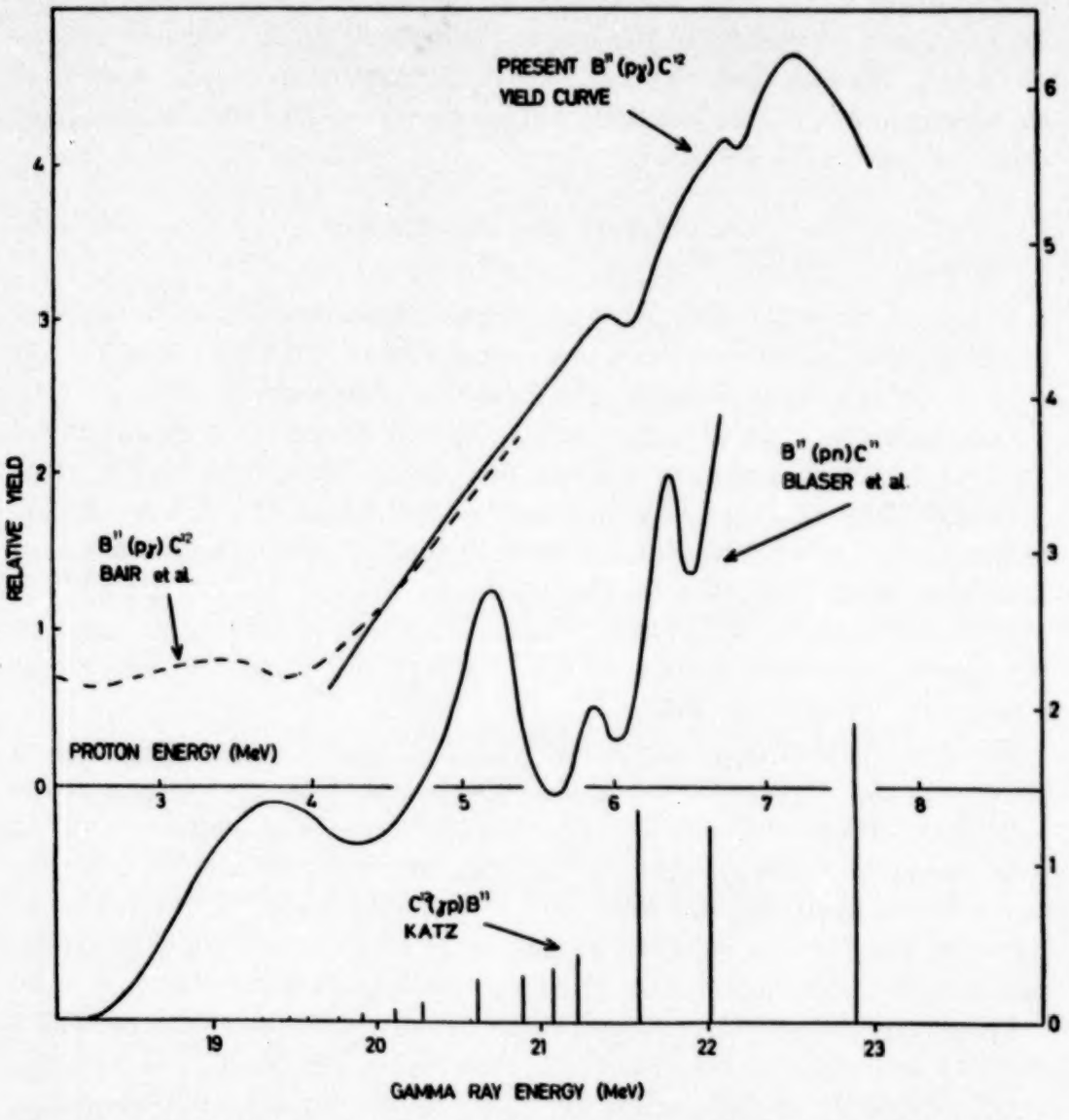

Fig. 5. (a) The $B^{11}(p, \gamma)C^{12}$ yield curve with the data of Bair *et al.*[10]), Blaser *et al.*[13]) and Katz [15]) shown for comparison.

work suggests absorption into states at 21.08, 21.22, 21.58, 22.02 and 22.88, the last three being very strong fig. 5(a). Over this region the resolution of our experiment varies from 60 to 85 keV and is good enough to have indicated such structure.

The experiment suggests that if E1 transitions to a few 1^- states of C^{12} are responsible for absorption in the giant resonance region, they must be

broad ($\Gamma \gtrsim \frac{1}{2}$ MeV); alternatively, if the widths of the states concerned are small, as is suggested by the experiments on "breaks", then the spacing must also be small ($\leqq \frac{1}{4}$ MeV). To settle the question definitely, resolution an order of magnitude better than that obtained in this experiment would be desirable.

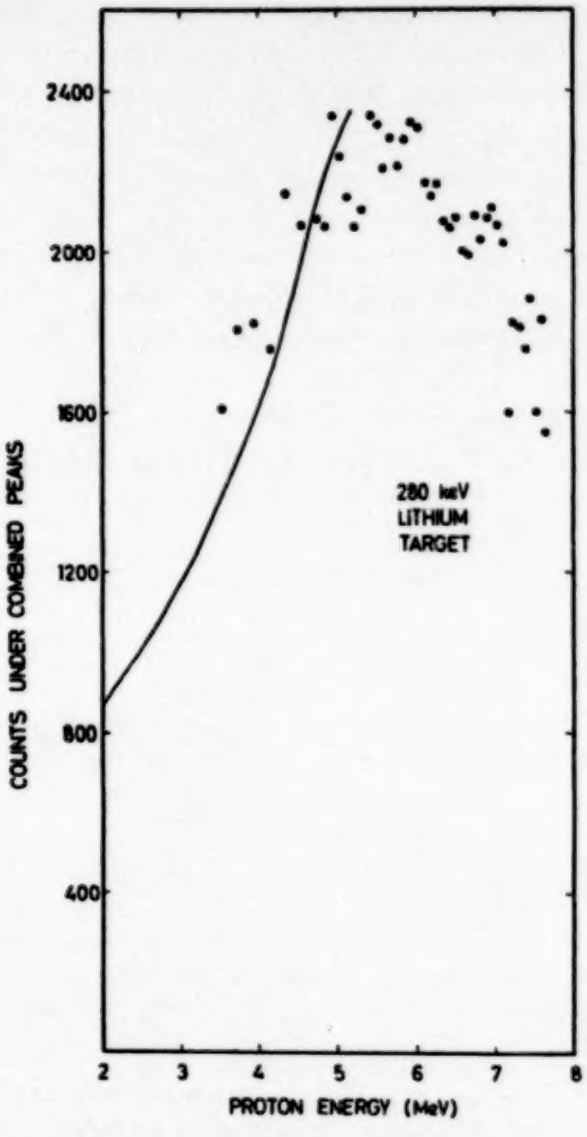

Fig. 5 (b) The most reliable $Li^7(p, \gamma)$ yield curve data showing, at lower proton energies, the fit to previous results. The full line represents the data of Bair *et al.*[17]) normalised at $E_p = 4.8$ MeV.

4.2. $Li^7(p, \gamma)Be^8$

The two yield curves obtained at lowest target currents are shown in fig. 4(b). One made with a target 145 keV thick at a beam current of 0.35 μA gave a yield curve which rises from lower proton energies and flattens off at

about 6.0 MeV proton bombarding energy. The other, made with a thicker target (280 keV) and a much lower beam current of 0.05 μA, displays a broad resonance with a maximum at a bombarding energy of 5.8 MeV. The measured value of the cross-section at the maximum was $(1.4 \pm 0.4) \times 10^{-28}$ cm^2. The experimental evidence suggested that at beam currents above 0.2 μA, pile-up and background problems were distorting the spectra, and for this reason it is believed that the yield curve taken at the lower proton beam current should be accepted. This result would indicate a maximum to the giant resonance of Be^8 at 22.3 MeV in general agreement with the suggestion of Wilkinson [16]). In fig. 5(b) the fit of the data to those of Bair *et al.*[17]), taken at lower proton energies, is shown, and agreement is within the combined errors of the two experiments.

There was no evidence for structure in the resonance, but the statistics are not good and the resolution of this experiment ranged between 300 keV and 350 keV and was considerably worse than that of the boron experiment.

The authors wish to thank Mr. R. W. Parkes for his help in operating the cyclotron, and Mr. N. F. Bowkett for operation of the 1 MeV Cockcroft-Walton accelerator.

References

1) P. B. Moon and A. Storruste, Proc. Phys. Soc. A **66** (1953) 585
2) E. W. Titterton, Prog. Nucl. Phys. **4** (1955) 1
3) H. A. Bethe, Revs. Mod. Phys. **9** (1937) section 14
4) A. K. Mann and E. W. Titterton, Proc. Phys. Soc. A **69** (1956) 917
5) I. F. Wright, D. R. O. Morrison, J. M. Reid and J. R. Atkinson, Proc. Phys. Soc. A **69** (1956) 77
6) A. H. Morton, and W. I. B. Smith, to be published
7) D. S. Gemmell, A. H. Morton and W. I. B. Smith, Nuclear Physics **10** (1959) 45
8) N. Bohr, Phil. Mag. **30** (1915) 581
9) W. A. Fowler and C. C. Lauritsen, Phys. Rev. **76** (1949) 314
10) J. K. Bair, J. D. Kington and H. B. Willard, Phys. Rev. **100** (1955) 21
11) J. Halpern and A. K. Mann, Phys. Rev. **83** (1951) 370
12) L. Cohen, A. K. Mann, B. J. Patton, K. Reibel, W. E. Stephens and E. J. Winhold, Phys. Rev. **104** (1956) 108
13) J. P. Blaser, F. Boehm, P. Marmier and P. Scherrer, Helv. Phys. Acta **24** (1951) 465
14) W. C. Barber, Washington Photonuclear Conference (May 1958)
15) L. Katz, Washington Photonuclear Conference (May 1958)
16) D. H. Wilkinson, Phil. Mag. **45** (1954) 259
17) J. K. Bair, H. B. Willard, C. W. Snyder, T. M. Hahn, J. D. Kington and F. P. Green, Phys. Rev. **85** (1952) 946

2.A.1:
2.C

Nuclear Physics **10** (1959) 45—52; © *North-Holland Publishing Co., Amsterdam*
Not to be reproduced by photoprint or microfilm without written permission from the publisher

GAMMA RADIATION FROM THE CAPTURE OF 5 TO 7.7 MeV PROTONS IN F^{19}, Na^{23}, Al^{27} AND P^{31}

D. S. GEMMELL, A. H. MORTON and W. I. B. SMITH
Research School of Physical Sciences, Australian National University, Canberra

Received 31 October 1958

Abstract: Pronounced resonances have been observed in the yield of gamma rays with variation of proton energy from 5 to 7.7 MeV in steps of 70 keV for the reactions $F^{19}(p,\gamma)Ne^{20}$, $Na^{23}(p,\gamma)Mg^{24}$, $Al^{27}(p,\gamma)Si^{28}$ and $P^{31}(p,\gamma)S^{32}$. The energy of the protons from the Canberra cyclotron was changed by interposing aluminium foils in the beam. Gamma-ray yields for transitions to the ground and first excited states of the product nuclei were measured using a large sodium iodide crystal spectrometer. Estimates of the appropriate cross-sections for these reactions are given.

1. Introduction

Radiative proton capture as described in the previous paper [1]) has been applied to a study of regions of nuclear excitation lying between 14 and 20 MeV in Ne^{20}, Mg^{24}, Si^{28} and S^{32}.

The reactions used were

$$F^{19}\ (p,\gamma)Ne^{20} + 12.9\ \text{MeV}$$
$$Na^{23}(p,\gamma)Mg^{24} + 11.7\ \text{MeV}$$
$$Al^{27}\ (p,\gamma)Si^{28} + 11.6\ \text{MeV}$$
$$P^{31}\ (p,\gamma)S^{32} + 8.8\ \text{MeV}.$$

In the resultant alpha-particle nuclei, the high binding energy of a proton, together with the 7.7 MeV available from the Canberra cyclotron, enabled maximum nuclear excitations of 20.2, 19.1, 19.0 and 16.3 MeV, respectively, to be reached.

2. Experimental Method

The general arrangement was identical with that described in the preceding paper. The Canberra 30-inch cyclotron was used as a source of 7.7 MeV protons with high energy stability and homogeneity, whose energy could be changed by the insertion of a variable number of 1.63 mg · cm^{-2} aluminium foils in the path of the extracted beam. After passing through the foils, the beam went through the target and entered a lead-lined insulated tube — the "beam catcher". The beam current to the catcher was measured and integrated. Gamma rays were detected at 90° to the proton beam using a

5″ diam. × 4″ long NaI(Tl) crystal spectrometer. The shielding against background radiation used previously was found adequate again in these experiments.

Yield curves were determined by recording gamma-ray spectra at each proton energy for a given number of protons, and by measuring the number of counts under the peaks corresponding to gamma-ray transitions to the ground and first excited states of the resultant compound nucleus. Each spectrum took 20 minutes to record with beam currents of 0.4 μA for sodium, aluminium and phosphorus, and below 0.08 μA for fluorine.

3. Results

3.1. $F^{19}(p, \gamma)Ne^{20}$

The fluorine targets were poly-tetra-fluorethylene foils 0.98 mg · cm^{-2} thick. These foils were found to suffer progressive damage produced by the

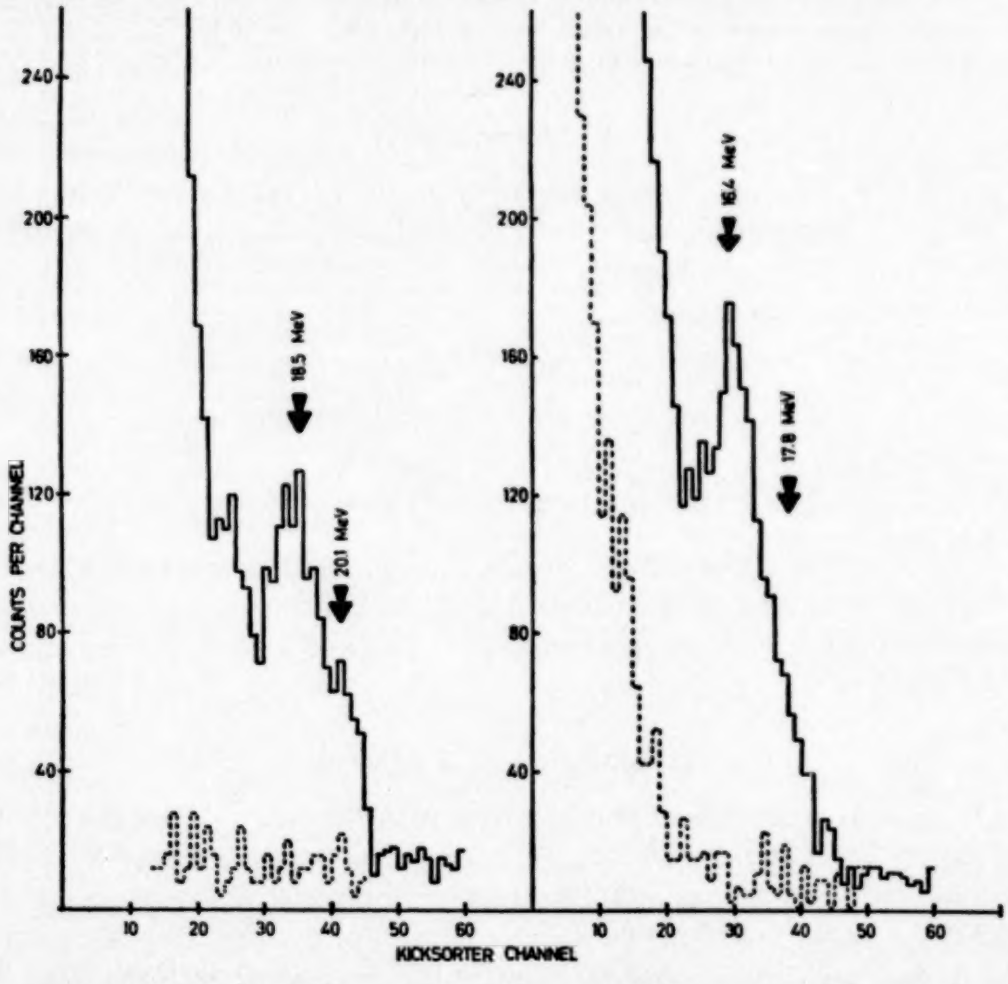

Fig. 1. Pulse height spectra produced by gamma rays from (a) the $F^{19}(p, \gamma)$ reaction at E_p = 7.63 MeV, and (b) the $Na^{23}(p, \gamma)$ reaction at E_p = 6.40 MeV. The arrows indicate transitions to the ground and first excited states of Ne^{20} and Mg^{24}. The dotted curves are the background counts with the targets withdrawn from the beam.

passage of the beam; they became brittle and, to prevent their crumbling in the region of beam impact, the beam current was kept below 0.08 μA, and after each spectrum was recorded the foil was raised so that the succeeding measurement was made on an unused section of the foil. The targets were sufficiently uniform and the running conditions constant enough for this method to give reproducible results.

A gamma-ray spectrum taken at a proton energy of 7.63 MeV is shown in fig. 1. Throughout the entire range of bombarding proton energies the gamma-ray transitions were observed to go mainly to the first excited state of Ne^{20} at 1.6 MeV above the ground state. The smaller fraction going to the ground state was observed as a shoulder on the pulse-height spectra and the ratio of intensities of the two transitions did not appear to change significantly with proton energy.

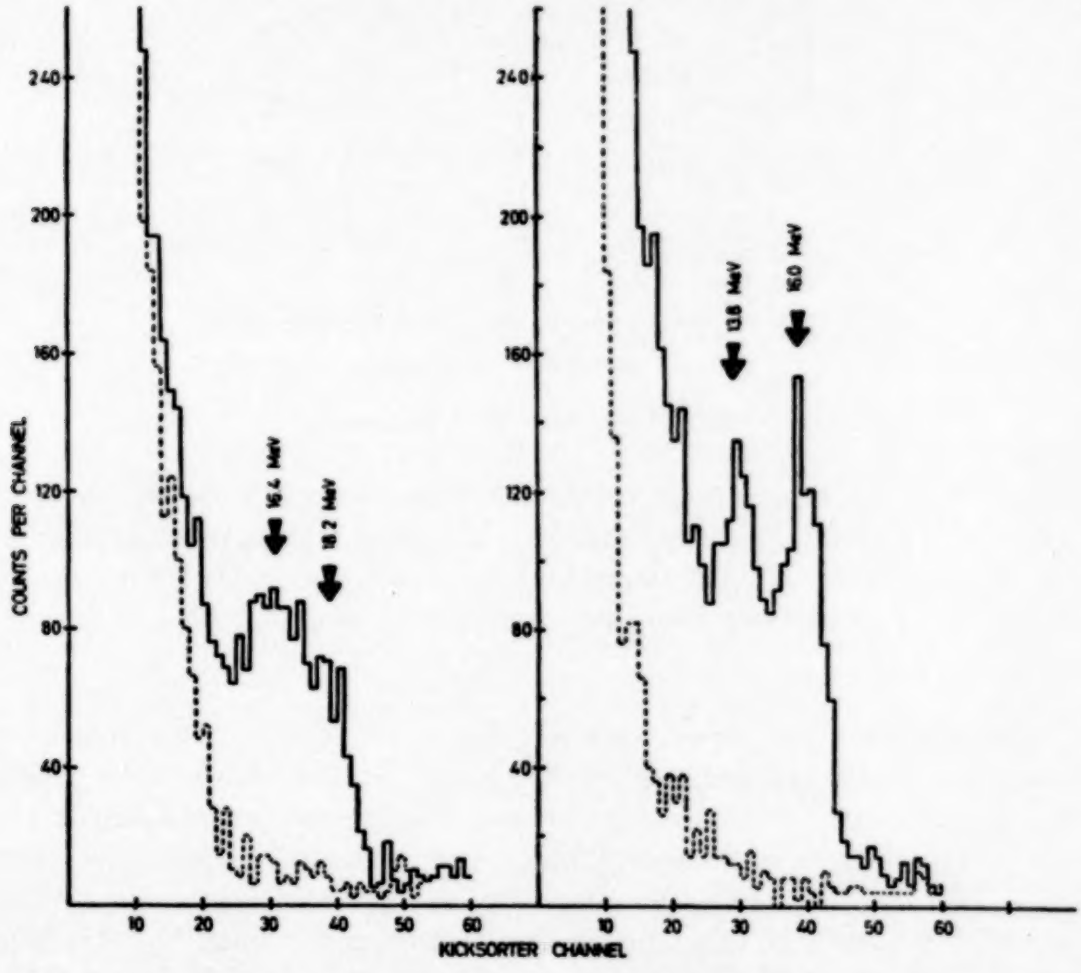

Fig. 2. Pulse height spectra produced by gamma rays from (a) the $Al^{27}(p, \gamma)$ reaction at E_p = 6.87 MeV, and (b) the $P^{31}(p, \gamma)$ reaction at E_p = 7.50 MeV. The arrows indicate transitions to the ground and first excited states of Si^{28} and S^{32}. The dotted curves are the background counts with the targets withdrawn from the beam.

In determining the yield curve the counts under the combined ground state plus first excited state peaks were recorded as a function of proton energy. Two determinations of this yield curve were made using different target foils; they agreed well and the average is shown in fig. 3. Pronounced

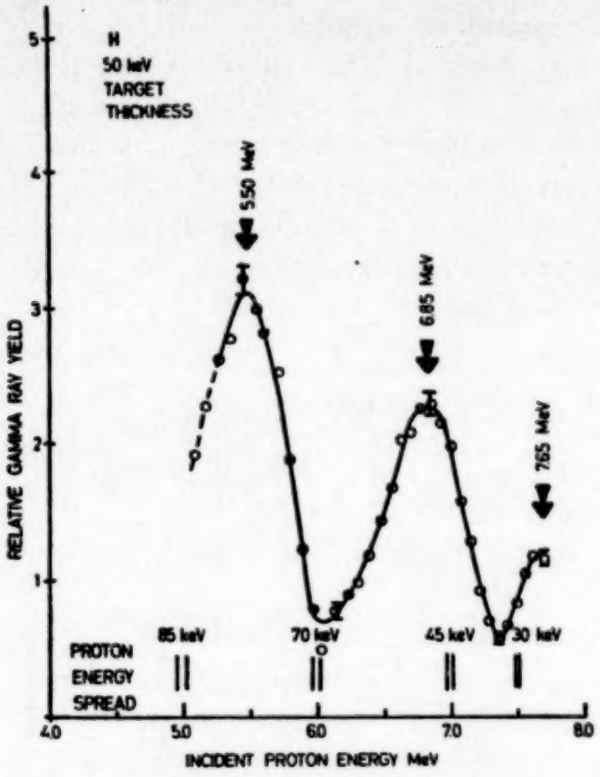

Fig. 3. Yield curve for $F^{19}(p, \gamma)Ne^{20}$.

broad resonances occur with maxima at proton energies of 5.5, 6.85 and probably 7.65 MeV. The target thickness and energy spread due to straggling are shown marked on fig. 3 at various proton energies. The 90° cross-section for the sum of the two transitions at 7.7 MeV was $(8.5 \pm 2) \times 10^{-28}$ cm^2.

3.2. $Na^{23}(p, \gamma)Mg^{24}$

Thin targets of sodium were made by rolling the metal in a kerosene bath using the technique developed for lithium described in the previous paper. Sodium foils 0.002″ thick were used in two determinations of the yield curve over the full extent of the energy range, but two additional runs were made from 7.0 to 7.7 MeV to confirm the existence of the small peak at a proton energy of 7.45 MeV. Gamma-ray transitions were predominantly to the first excited state of the residual nucleus — in this case the 1.4 MeV level in Mg^{24}. Only a small fraction of the transitions occurred to the ground state of Mg^{24}, as illustrated in the gamma-ray spectrum of fig. 1 (b) recorded at a proton energy of 6.40 MeV.

The yield curve of fig. 4 represents the average of all runs taking the total counts under the combined ground state plus first excited state peaks in the pulse-height spectra. In addition to the small peak at 7.45 MeV, a broad resonance occurs with a maximum at a proton energy of 5.95 MeV and there

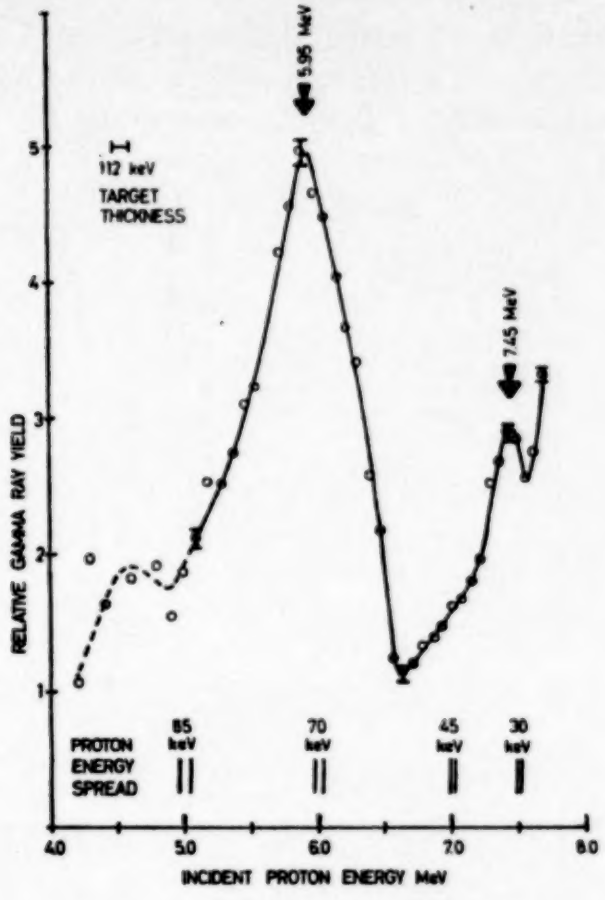

Fig. 4. Yield curve for $Na^{23}(p, \gamma)Mg^{24}$.

is an indication of a small peak at 4.6 MeV, although the rise in the background count together with the reduced energy and intensity of the gamma rays made it difficult to determine a yield curve with precision in the low proton energy region. The 90° cross-section at 7.7 MeV was $(1.4 \pm 0.4) \times 10^{-28}$ cm^2 for the sum of both transitions.

3.3. $Al^{27}(p, \gamma)Si^{28}$

An aluminium foil 1.63 $mg \cdot cm^{-2}$ thick was used as the target for this experiment and a gamma-ray spectrum recorded at 6.87 MeV proton energy is shown in fig. 2(a). Transitions for all proton energies were mainly to the first excited state at 1.8 MeV in Si^{28} with a smaller fraction to the ground state. Fig. 5 shows the yield curve derived using the sum of both transitions and represents the average of three separate determinations of the yield

curve. Peaks in the curve appear at proton energies of 6.63, 6.87 and 7.20 MeV, and possibly at 6.1 and 7.7 MeV. The 90° cross-section at 7.7 MeV was $(1.9\pm0.5)\times10^{-28}$ cm^2 for the sum of the two transitions.

3.4. $P^{31}(p,\gamma)S^{32}$

Targets were made by allowing a fine suspension of red phosphorus in alcohol with a little sugar dissolved in it to settle onto a 3 mg · cm^{-2} gold foil backing and then allowing the alcohol to evaporate; the phosphorus was

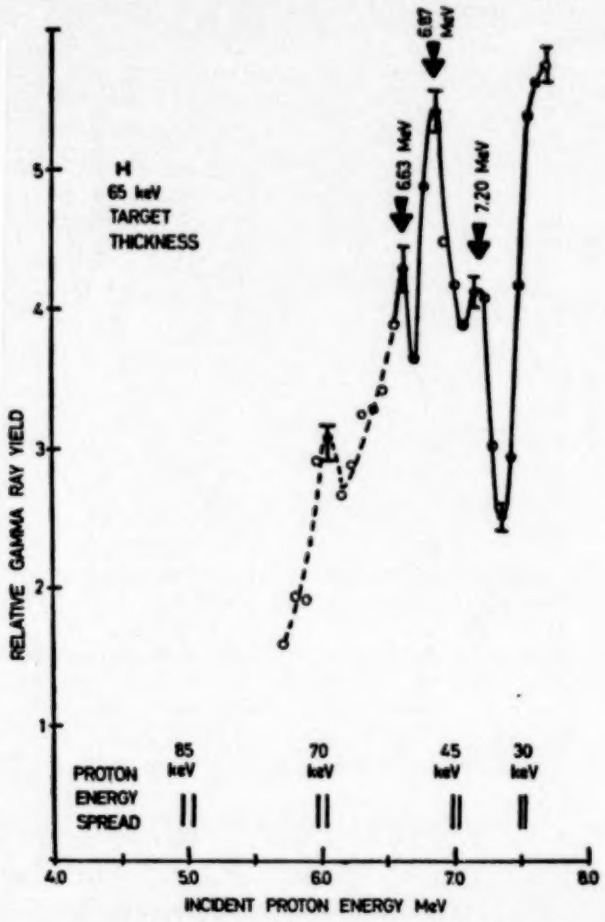

Fig. 5. Yield curve for $Al^{27}(p,\gamma)Si^{28}$.

found to adhere well to the gold backing. Three different targets, with thicknesses measured by weighing to be between 6 and 8 mg · cm^{-2}, were used in three separate determinations of the yield curve. Fig. 2(b) shows a pulse-height spectrum recorded at a proton energy of 7.50 MeV, and throughout the entire range of bombarding proton energies, transitions to the ground state and first excited state of S^{32} at 2.24 MeV occurred with about equal probability; the derived yield curve for the ground state transition is shown in fig. 6. Peaks appear at incident proton energies of 7.50, 7.15, 6.65 and

probably 5.6 MeV. The 90° cross-section at 7.7 MeV was $(0.5\pm0.2)\times10^{-28}$ cm² for ground-state transitions only.

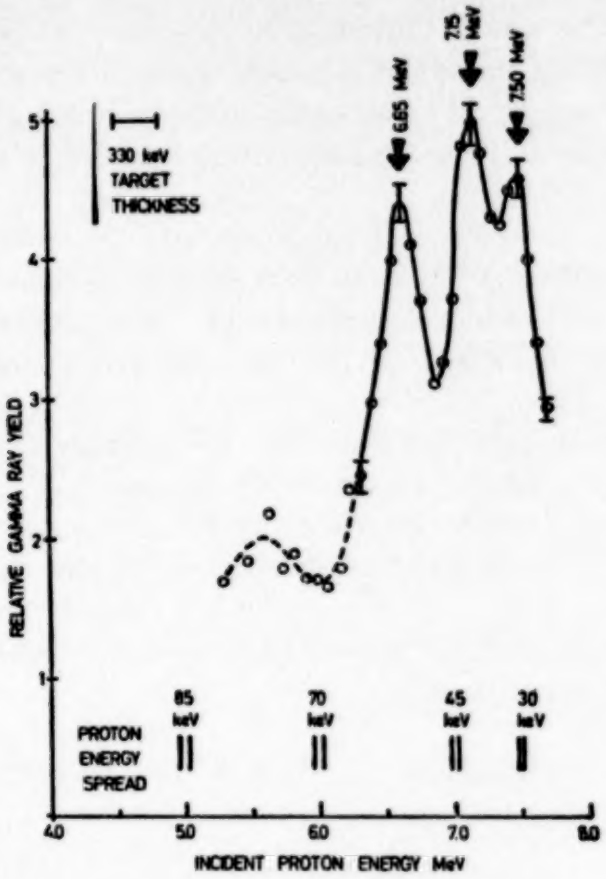

Fig. 6. Yield curve for $P^{31}(p,\gamma)S^{32}$.

4. Discussion

There is little previous information available on energy levels in the region of nuclear excitation studied in the present experiments. In the cases of $F^{19}(p,\gamma)Ne^{20}$, $Na^{23}(p,\gamma)Mg^{24}$ and $Al^{27}(p,\gamma)Si^{28}$, the levels can be compared with those found from previous measurements carried out with protons of energies up to 6.6 MeV on the reactions $F^{19}(p,n)Ne^{19}$, $Na^{23}(p,n)Mg^{23}$ and $Al^{27}(p,n)Si^{27}$.

The $F^{19}(p,n)Ne^{19}$ reaction has been studied by Blaser *et al.*[2]) using a 6.6 MeV cyclotron and examining the activity induced in stacked foils, and by Marion *et al.*[3]) using a 6-MeV Van de Graaff generator and a BF_3 counter.

The broad peak in both (p, n) yield curves at a proton energy of about 5.4 MeV could correspond with the broad peak found at 5.50 MeV in the present (p, γ) yield curve. Blaser *et al.* also determined a yield curve for the $Na^{23}(p,n)Mg^{23}$ reaction, and their broad peak at 6.00 MeV proton energy shows agreement with that found in this experiment at 5.95 MeV.

The peak at 6.1 MeV suggested in the present $Al^{27}(p, \gamma)$ result may be that observed by Blaser *et al.* at 6.17 MeV in their study of the $Al^{27}(p, n)$ reaction.

Levels in S^{32} above an excitation of 12 MeV have not been resolved previously. Whether the peaks in the present yield curves are comprised of a small number of individual broad levels or a large number of closely-spaced narrow levels could not be ascertained within the resolution of these experiments.

If the intermediate states decay by emission of E1 radiation, as is suggested by the strengths of the transitions, then these transitions will be from 1^-, 2^- and 3^- states of the compound nuclei with $T = 1$ (since all of the residual nuclei are self-conjugate with 0^+ ground states and 2^+ first excited states with $T = 0$).

It is understandable that the transitions are generally to the 2^+ state since only 1^- compound states can produce E1 transitions to the ground state, whereas 1^-, 2^- and 3^- states can decay by E1 radiation to the first excited state. Even for 1^- levels, the higher statistical weight attached to the 2^+ level will tend to favour transitions to the first excited state in spite of the increased transition probability associated with the higher energy of the ground-state gamma rays.

The authors wish to thank Mr. R. W. Parkes for his help in operating the cyclotron.

References

1) D. S. Gemmell, A. H. Morton and E. W. Titterton, Nuclear Physics **10** (1959) 33
2) J. P. Blaser, F. Boehm, P. Marmier and P. Scherrer, Helv. Phys. Acta **24** (1951) 465
3) J. B. Marion, T. W. Bonner and C. F. Cook, Phys. Rev. **100** (1955) 91

2.L:8.A *Nuclear Physics* **10** (1959) 53—59; © *North-Holland Publishing Co., Amsterdam*
Not to be reproduced by photoprint or microfilm without written permission from the publisher

THE EFFECTIVE ATOMIC FIELD FOR ELECTRON SCATTERING

E. VAN DER SPUY
Physics Department, University of Stellenbosch

Received 3 November 1958

Abstract: A discussion is given of a correction to the atomic field effective in, for example, electron polarization experiments by double scattering. The correction is aimed at suggesting an explanation of the low azimuthal asymmetry found in such experiments compared with the Mott theory. It is shown to be a many-body problem in which proper recognition of the role of the exclusion principle gives an effective modification of the screened Coulomb field normally used in electron scattering calculations, and in fact at such radii as would have an important effect on the most important phase shifts in such a scattering problem.

1. Introduction

Soon after the statement of Dirac's theory of the electron Mott [1]) applied it to the scattering of electrons by heavy atoms. His theory indicated an observable azimuthal asymmetry on double scattering of an unpolarized electron beam, which gives an experiment, in principle, for demonstrating the fourth (or spin-) degree of freedom of a "free" electron. Mott applied the Dirac theory to the case of double scattering at 90° on the unscreened Coulomb field of gold ($Z = 79$), and indicated a maximum asymmetry, for an electron energy ≈ 120 keV, of about 16 %. Calculations [2,3]) since then, taking account of the screening effect of the atomic electrons as afforded by Hartree's selfconsistent field, or approximations to it, indicated that in this region of energy screening does not have a considerable effect on the calculated asymmetry. This provides a real problem, because recent experiments [4,5]) under properly refined conditions gives asymmetries which are always significantly lower than the values calculated so far. For example, at 100 keV: 8 % (observed [5])) compared to 16 % (Mott's calculation), for double scattering at 90°.

Since the de Broglie wavelength of the electron at 120 keV is $\lambda_e = 3.54 \times 10^{-10}$ cm, and the normal screening field corrections become important at distances of the order of the first Bohr orbit radius $a_0 = 5.29 \times 10^{-9}$ cm, it is not unexpected that screening only introduces major corrections at much lower electron energies. Similarly, corrections to the Coulomb field due to nuclear size ($\approx 10^{-12}$ cm at the most) would not be effective until much higher energies.

In past discussions various unexplained deviations from the unscreened

Coulomb field were suggested. Massey and Mohr [2]) indicated that a change in the Coulomb field from $-Ze^2/r$ to $(-Ze^2/r)(1-e^{-\lambda r})$ would reduce the asymmetry by a large factor if $\lambda = 100$, in atomic units. Because this would mean changes in Coulomb field to distances as great as 5×10^{-11} cm which is $\approx$ the K-shell orbital radius for gold (6.7×10^{-11} cm), these authors felt that such a correction, if it existed, would also have affected these orbits in a major and readily observable way. It is the purpose of the discussion in this paper to indicate a correction to the Coulomb field which obeys a similar radial law, and will have a considerable effect at the above energies, but yet without affecting the normal K electrons, for example.

In principle, the discussion starts from the notion that for scattering on a heavy atom the lower orders (at least) of the incident electron partial waves each find a region in space round the nucleus which is already fully occupied in the sense of the exclusion principle, and which would in effect be repulsive to the corresponding partial component. In this sense the scattering is a many-body problem in which the operation of the exclusion principle must be fully recognized. In analogy to other many-body problems the interaction is manifestly velocity-dependent and complex. To demonstrate the forces called into play in the simplest way, the discussion below will be limited to the effect of the innermost (K-shell) electrons, and based on the following simplifying assumptions:

1. The virtual excitation of the K-shell by the electron wave may be neglected. This is perhaps not unreasonable, since the other close-lying shells are already fully occupied, and excitation to the unoccupied higher levels would occur with a sensibly lower probability. Such polarization effects will lower the repulsive effects found for the K-shell, and will be more serious for a calculation of similar effects for higher shells. We are of course considering elastic scattering only.

2. Except for the explicit allowance for electron spins, the calculation of the field correction will be non-relativistic. This is an assumption avoiding the complexities of a fully relativistic many-body problem. In this respect one realizes that if the electron energy is not too high, the relativistic theory merely corrects for the relativistic mass as a function of particle momentum, and provides a spin-orbit coupling, as fine structure effects. Thus, with a suitable limitation on the electron velocity, the present calculation will establish an approximate correction for the effect of the exclusion principle, and the spin-orbit coupling will only have a direct and hence major effect on the polarization, through its orbital motion in the modified field.

2. Theory for the K-shell Effect

On the above assumptions an electron wave incident on the K-shell alone will be governed by the following hamiltonian:

$$H = -\frac{\hbar^2}{2m}(\nabla_1^2+\nabla_2^2+\nabla_3^2)+\frac{e^2}{r_{12}}+\frac{e^2}{r_{23}}+\frac{e^2}{r_{13}} - \frac{Ze^2}{r_1}-\frac{Ze^2}{r_2}-\frac{Ze^2}{r_3}, \tag{1}$$

with an overall wave function, properly anti-symmetrized,

$$\Psi = \phi_r(1)\psi(\widetilde{23})-\phi_r(2)\psi(\widetilde{13})-\phi_r(3)\psi(\widetilde{21}), \tag{2}$$

where $\phi_r(1)$ gives the motion of the scattered electron, 1, relative to the origin, which is the heavy nucleus, and $\psi(\widetilde{23})$ is the antisymmetric wave function for the two K-shell electrons, 2, 3:

$$\psi(\widetilde{23}) = \frac{1}{\sqrt{2}}(\alpha(2)\beta(3)-\beta(2)\alpha(3))\Phi(23), \tag{2a}$$

with α, β the $+$, $-$ spin wave functions and $\Phi(23)$ the symmetric $(1s)^2$ space wave function. Since $Z \gg 1$ the motion of electrons 2 and 3 in the isolated K-shell is sensibly independent and hence we shall assume later on that

$$\Phi(23) = \phi(2)\phi(3), \tag{2b}$$

where $\phi(2)$, $\phi(3)$ are the spatially symmetric (1s) single electron wave functions.

Now, if $-E_s$, $-E_{s1}$, E are respectively the total K-shell binding energy, the single electron K-shell binding energy, and the total energy of the 3-body problem, we have

$$H\Psi = E\Psi, \tag{3}$$

$$\left\{-\frac{\hbar^2}{2m}(\nabla_2^2+\nabla_3^2)+\frac{e^2}{r_{23}}-\frac{Ze^2}{r_2}-\frac{Ze^2}{r_3}-E_s\right\}\psi(\widetilde{23}) = 0, \tag{4}$$

$$\left\{-\frac{\hbar^2}{2m}\nabla_2^2-\frac{Ze^2}{r_2}-E_{s1}\right\}\phi(2) = 0. \tag{5}$$

Now, by (3)

$$\int_{23}\psi^*(\widetilde{23})(H-E)\Psi = 0,$$

where $\int_{23}$ effects all integrations over spin and space variables of 2 and 3. Therefore, by symmetry, and normalizing $\psi(\widetilde{23})$ by $\int_{23}\psi^*(\widetilde{23})\psi(\widetilde{23}) = 1$ and using (4),

$$\left\{\frac{\hbar^2}{2m}\nabla_1^2+E-E_s+\frac{Ze^2}{r_1}-\int_{23}\psi^*(\widetilde{23})\left(\frac{e^2}{r_{12}}+\frac{e^2}{r_{13}}\right)\psi(\widetilde{23})\right\}\phi_r(1) = -2\int_{23}\psi^*(\widetilde{23})(H-E)\phi_r(2)\psi(\widetilde{13}).$$

Thus,

$$\left\{\frac{\hbar^2}{2m}\nabla_1^2+E-E_s+\frac{Ze^2}{r_1}-\int_{23}|\Phi(23)|^2\left(\frac{e^2}{r_{12}}+\frac{e^2}{r_{13}}\right)\right\}\phi_r(1)$$

$$=-P_\sigma(12)\int_{23}\Phi^*(23)(H-E)\phi_r(2)\Phi(13)$$

(where $\phi_r(1)$ contains the spin of 1 and $P_\sigma(12)$ exchanges the spin of 1 and 2)

$$=-P_\sigma(12)\int_{23}\Phi^*(23)\left\{-\frac{\hbar^2}{2m}\nabla_2^2+\frac{e^2}{r_{12}}+\frac{e^2}{r_{23}}-\frac{Ze^2}{r_2}-E+E_s\right\}\phi_r(2)\Phi(13)$$

(by the analogy of (4))

$$=-P_\sigma(12)\int_{23}\Phi^*(23)\left\{\frac{e^2}{r_{12}}+\frac{e^2}{r_{23}}-E+E_s+E_{s1}\right\}\phi_r(2)\Phi(13)$$

(by partial integration; approximately, insofar as (2b), and hence (5), holds)

$$=(E_K-E_{s1})P_\sigma(12)\int_{23}\Phi^*(23)\phi_r(2)\Phi(13), \tag{6}$$

where, to the same approximation, with $Z\gg 1$, one can neglect the contribution of e^2/r_{12}, e^2/r_{23} to the exchange integral; $E_K=E-E_s$ denotes the energy of the incident electron.

It is easy to show that the expectation value of the contributions of the latter two terms is ≈ 2 keV each, relative to ≈ 200 keV of the rest of (6), for $Z=79$, and $E_K=120$ keV, say.

Eq. (6) may be further simplified, using (2b):

$$\left\{\frac{\hbar^2}{2m}\nabla_1^2+E_K+\frac{Ze^2}{r_1}-\int_{23}|\Phi(23)|^2\left(\frac{e^2}{r_{12}}+\frac{e^2}{r_{13}}\right)\right\}\phi_r(1)$$
$$=(E_K-E_{s1})\phi(1)P_\sigma(12)\int_2\phi^*(2)\phi_r(2). \tag{7}$$

Eq. (7) may be interpreted as follows: The first three terms on the left hand side are the normal terms in the Schrödinger equation of a single particle ,1, moving in the Coulomb field $-Ze^2/r_1$. The fourth term is the normal screening correction for the effect of the K-shell electrons, and it is in fact small compared to the third, normal Coulomb term, if $Z\gg 1$. The term on the right hand side is a velocity-dependent integral interaction term which arises from the antisymmetrization of the wave-function (2) as demanded by the exclusion principle.

It is immediately clear that components of $\phi_r(2)$ which are orthogonal to $\phi(2)$ will be unaffected by this term due to the K-shell electrons. As a corollary of this, one realizes that on account of both effective spatial separation and orthogonality this term would not effect the other shells of

the atom itself, at least not to the first order. The same holds for the similar effect due to other shells as affecting the K-shell, say. This overcomes the difficulty mentioned by Mohr and Massey [2]). Thus we may proceed to discuss the right hand side of eq. (7) as applied to the scattering problem alone.

For a typical component $\alpha(1)e^{ikz}$ of the incident wave at infinity, where in the overall problem Coulomb effects may be neglected, we have in general, at all r,

$$\phi_r(1) = \sum_{l=0}^{\infty} \sum_{j=l-\frac{1}{2}}^{l+\frac{1}{2}} \frac{f_j^l(r_1)}{r_1} \left\{ g_{1j}^l Y_l^0(\theta_1, \phi_1)\alpha(1) + g_{2j}^l Y_l^1(\theta_1, \phi_1)\beta(1) \right\}, \tag{8}$$

where g_{1j}^l, g_{2j}^l are the usual Clebsch-Gordan coefficients for the composition of spin $= \frac{1}{2}$ and orbital angular momentum with quantum number l. Furthermore, with the present simplification, the (1s) spatial wave-function

$$\phi(1) = -\sqrt{\frac{Z^3}{\pi a_0^3}} \exp\left(-\frac{Zr_1}{a_0}\right), \tag{9}$$

normalized to 1 for integration over all space. The right hand side of eq. (7) is therefore

$$= (E_K - E_{s1}) \frac{Z^3}{\pi a_0^3} e^{-Zr_1/a_0} g_{1,\frac{1}{2}}^0 Y_0^0 \alpha(1) \int_0^{\infty} e^{-Zr_2/a_0} \frac{f_{\frac{1}{2}}^0(r_2)}{r_2} 4\pi r_2^2 dr_2.$$

Therefore, as already mentioned, the right hand side of eq. (7) will have no effect for components of $\phi_r(1)$ with $l > 0$. As far as the K-shell is concerned those partial waves move in the screened field indicated by the left hand side of eq. (7). For the $l = 0$ component of $\phi_r(1)$, eq. (7) reduces to

$$\begin{aligned} &\left\{ \frac{\hbar^2}{2m} \frac{d^2}{dr_1^2} + E_K + \frac{Ze^2}{r_1} - \int_{23} |\Phi(23)|^2 \left(\frac{e^2}{r_{12}} + \frac{e^2}{r_{13}} \right) \right\} f_{\frac{1}{2}}^0(r_1) \\ &\qquad = (E_K - E_{s1}) \frac{4Z^3}{a_0^3} r_1 e^{-Zr_1/a_0} \int_0^{\infty} r_2 e^{-Zr_2/a_0} f_{\frac{1}{2}}^0(r_2) dr_2. \end{aligned} \tag{10}$$

Eq. (10) again shows the K-shell effect as a velocity-dependent term, both in the coefficient $E_K - E_{s1}$ and in the integral interaction itself. Eq. (10) is an integro-differential equation of the form usual in many-body problems. To indicate the importance of the effect of the right hand side one may introduce the following considerations of what is probably its main effect.

Call $f_{\frac{1}{2}}^0(r) = f(r)$ for short. Then,

$$\begin{aligned} I &= \int_0^{\infty} r_2 e^{-Zr_2/a_0} f(r_2) dr_2 \\ &= \sum_{n=0}^{\infty} \left[\int_0^{\infty} r_2 e^{-Zr_2/a_0} \frac{(r_2 - r_1)^n}{n!} dr_2 \right] \frac{d^n f(r_1)}{dr_1^n} \end{aligned}$$

by Taylor expansion of $f(r_2)$ around the point $r_2 = r_1$. This expansion, analogous to one by Wheeler [6]), shows the velocity-dependence of the integral interaction explicitly. The following reasons may be adduced to indicate that the main effective contribution to I as used in eq. (10) is the $n = 0$ term: $r \exp(-Zr/a_0)$ is a function with a reasonably pronounced maximum at $r = a_0/Z$, in the neighbourhood of which it is roughly symmetrical. The main contribution of the right hand side of (10) will hence be in the neighbourhood of $r_1 = a_0/Z$. By the rough symmetry, odd n contributions to I will tend to be small, and since higher orders in n will be weighed down as $1/n!$ in any case, the term $n = 0$ will furnish a first approximation to the right hand side of eq. (10).

The right hand side of eq. (10), therefore,

$$\approx (E_K - E_{s1}) \frac{4Z^3}{a_0^3} r_1 e^{-Zr_1/a_0} f_{\frac{1}{2}}^0(r_1) \int_0^\infty r_2 e^{-Zr_2/a_0} dr_2$$

$$= (E_K - E_{s1}) \frac{4Z}{a_0} r_1 \exp(-Zr_1/a_0) f_{\frac{1}{2}}^0(r_1).$$

This gives an extra repulsive potential

$$= (E_K - E_{s1}) \frac{4Z}{a_0} r_1 \exp(-Zr_1/a_0). \tag{11}$$

Thus one can consider (11) as a modification of the Coulomb potential $-Ze^2/r$, such that the modified overall Coulomb potential for the s partial wave

$$= -\frac{Ze^2}{r_1}\left\{1 - (E_K - E_{s1}) \frac{4}{a_0 e^2} r_1^2 \exp(-Zr_1/a_0)\right\}. \tag{12}$$

This shows a modification which has some analogy to that tried by Massey and Mohr [2]). Stated in the form of (12) the maximum correction (to Z, say) arises where $r_1^2 \exp(-Zr_1/a_0)$ is a maximum, i.e. for $r_1 = 2a_0/Z = 1.34 \times 10^{-10}$ cm for gold, $Z = 79$; a radius where it is likely to have a big effect at λ_e corresponding to $E_K \approx 100$ keV. The correction potential itself as in (11) has a maximum at $r_1 = a_0/Z$, or half the former value. The latter is the more appropriate radius when (11) is large, as is the case for the larger E_K, because then the highest value of the correction in the curly brackets may be ≈ 1. In fact for $Z = 79$, $E_K = 120$ keV, and $-E_{s1} = 13.605\ Z^2$ eV $= 84\,909$ eV, in our approximation, the second term in the curly brackets has a highest value $= -2.61$. These details may be compared with the modification suggested by Mohr and Massey [2]). Such a large repulsive potential, at a radius where it will affect the scattering round $E_K \approx 100$ keV, will tend to reduce the phase of the s or $l = 0$ partial wave appreciably.

Note that $r = a_0/Z$ is at the maximum of the radial probability distribution corresponding to (9).

Similar effects on the other partial waves would arise from the corresponding higher shells of the atom. The calculation of these effects may, in principle, be effected in a similar manner. In the same way all inner shells especially will show important repulsive effects towards the corresponding partial waves and in fact at radii corresponding to the appropriate shell. At the energies important for polarization the effect of the exclusion principle is thus likely to be very important especially for the inner shells, and will be in a direction reducing polarization.

On account of the complex velocity-dependence of the forces the calculation of the actual effect on scattering and the azimuthal asymmetry, which normally requires a large number of phases, will be a major computational project, probably needing an electronic computer. It would be of special interest, for the investigation of the atomic scattering field, to undertake scattering and polarization calculations and experiments over an energy range corresponding to λ_e comparable with the radii of the inner electron shells.

References

1) N. F. Mott, Proc. Roy, Soc. A **135** (1932) 429
2) H. S. W. Massey and C.B.O. Mohr, Proc. Roy. Soc. A **177** (1941) 341
3) C. B. O. Mohr and L. J. Tassie, Proc. Phys. Soc. A **67** (1954) 711
4) N. Ryu, J. Phys. Soc. (Japan) **7** (1952) 125, 130
5) H. Schneider and E. Barnard, Nuovo Cimento to be published (1958)
6) J. A. Wheeler, Phys. Rev. **50** (1936) 643

7.A *Nuclear Physics* **10** (1959) 60—70; © *North-Holland Publishing Co., Amsterdam*
Not to be reproduced by photoprint or microfilm without written permission from the publisher

DISPERSION RELATIONS FOR VIRTUAL PHOTOPRODUCTION

A. A. LOGUNOV
Laboratory of Theoretical Physics, Joint Institute of Nuclear Research, Dubna, USSR
and
L. D. SOLOVYOV
Moscow State University

Received 7 May 1958

Abstract: The matrix element of lowest order (with respect to e) for electron-nucleon scattering involving π meson production is expressed through a quantity which is called the virtual photoproduction amplitude. Dispersion relations are obtained for this amplitude, it being assumed that at high energies the amplitude is independent of energy. It is shown that as a consequence of this assumption the constants entering the dispersion relations are defined by the gauge invariance condition.

1. Introduction

One of the methods which at present can be used to obtain qualitative information on strong interactions is the dispersion relation method [1]). Dispersion relations for scattering of mesons on nucleons [2, 3, 8]) and photoproduction of mesons [4–7]) have been considered by a number of authors. This method can also be employed to study more complicated processes [9]) in which along with nucleons and mesons other particles (electrons) are involved, the interaction of these particles being describable by perturbation theory. For a process of this type the Feynman diagram contains a part which corresponds to interaction between the nucleon and virtual particles (photons). A study of these parts may yield information on the structure of the nucleon.

In the present paper we consider scattering of electrons on nucleons accompanied by π meson production ($N+e \to N+e+\pi$). In the lowest approximation in e this process reduces to the emission of a virtual photon by the electron and interaction between the photon and nucleon with subsequent creation of a meson. This type of interaction between a virtual photon and nucleon will be called virtual photoproduction. The dispersion relations for the amplitude of this process are discussed in this paper. The deduction of these relations will not be considered. A general formulation of the dispersion relations is discussed and their form under some special assumptions regarding the behaviour of the amplitude in the high energy region is investigated.

It will be assumed that at high energies the amplitude as a function of energy is constant (or increases more slowly than the first power of energy). As a consequence some constants, indefinite in the general case, will enter the dispersion relations. However, due to the gauge invariance condition these constants can be uniquely expressed through integrals of the imaginary part of the amplitude. Moreover, the relativistic spin structures of the amplitude can be chosen in such a manner that the dispersion relations expressed in a relativistically invariant form will not contain (explicitly) these constants. Such are the relations (47) and (48), which are the result of the present investigation.

2. Matrix Element for Scattering of Electrons on Nucleons Involving π Meson Creation

The S-matrix element for electron-nucleon scattering involving π meson production is

$$\langle \mathrm{f}|S|i\rangle = (2\pi)^{\frac{1}{2}}\langle p's'|b_{r'}^{(-)}(p'_e)a_\rho^{(-)}(q)Sb_r^{*(+)}(p_e)|ps\rangle \tag{1}$$

where p, $s(p', s')$ are respectively the momentum and spin of the initial (final) nucleon; p_e, $r(p'_e, r')$ are the momentum and spin of the initial (final) electron; q, ρ are the momentum and kind of the meson; $b^{(-)}(b^{*(+)})$ and $a^{(-)}$ are respectively electron and meson annihilation (creation) operators. Transposing operator $b^{(-)}$ to the right and $b^{*(+)}$ to the left we obtain

$$\begin{aligned}\langle \mathrm{f}|S|\mathrm{i}\rangle = {} & \frac{(2\pi)^{\frac{1}{2}}m_e}{\sqrt{p_e^0 p_e'^0}}\bar{u}^{r'}(p'_e)\int e^{ip'_e x - ip_e y} \\ & \langle p's'|a_\rho^{(-)}\frac{\delta^2 S}{\delta\bar{\psi}_e(x)\delta\psi_e(y)}|ps\rangle \mathrm{d}x\mathrm{d}y u^r(p_e).\end{aligned} \tag{2}$$

The spinors are normalized so that $\bar{u}u = 1$. In the lowest order approximation (with respect to e)

$$\left\langle \frac{\delta^2 S}{\delta\bar{\psi}_e(x)\delta\psi_e(y)}\right\rangle_0 = -e\delta(x-y)\sum_n g^{nn}\gamma^n\int D^c(x-z)\left\langle\frac{\delta S}{\delta A_n(y)}\right\rangle_0 \mathrm{d}z \tag{3}$$

where $\langle \ldots \rangle_0$ denotes averaging over the photon vacuum and D^c is the causal Green's function. Thus (2) can be replaced by

$$\begin{aligned}\langle \mathrm{f}|S|\mathrm{i}\rangle = {} & \frac{(2\pi)^{\frac{1}{2}}m_e}{\sqrt{p_e^0 p_e'^0}}\frac{1}{k^2}\sum_n g^{nn}\bar{u}^{r'}(p'_e)\gamma^n u^r(p_e) \\ & \int e^{-iky}\langle p's'|a_\rho^{(-)}(q)\frac{\delta S}{\delta A_n(y)}|ps\rangle \mathrm{d}y\end{aligned} \tag{4}$$

where

$$k = p_e - p'_e. \tag{5}$$

Due to stability of the single-nucleon state the operator $\delta S/\delta A_n(y)$ in (4) can be replaced by $(-i)i^n(y)$, where

$$i^n(y) = i\frac{\delta S}{\delta A_n(y)}S^+ \tag{6}$$

is the electromagnetic current operator. Transposing now operator $a_\rho^{(-)}(q)$ to the right we obtain the following expression for the matrix element in the lowest order approximation in e:

$$\langle \mathrm{f}|S|\mathrm{i}\rangle = \frac{(-i)em_e}{\sqrt{2q^0 p_e{}^0 p_e'{}^0}}\frac{1}{k^2}\sum_n g^{nn}\bar{u}^{r'}(p'_e)\gamma^r u^r(p_e) \int e^{iqx-iky}\langle p's'|\frac{\delta i^n(y)}{\delta\varphi_\rho(x)}|ps\rangle dxdy. \tag{7}$$

The following Feynman diagram corresponds to it:

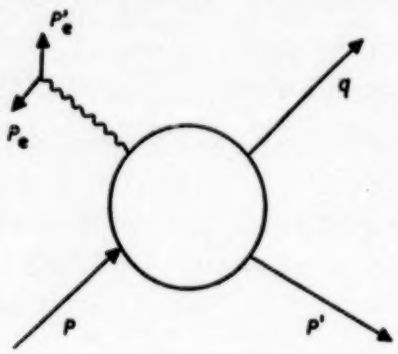

Fig. 1

3. Virtual Photoproduction Amplitude

The structure of expression (7) is similar to that for the photoproduction matrix element [4,6]). The vector

$$e^n = \bar{u}^{r'}(p'_e)\gamma^n u^r(p_e) \tag{8}$$

satisfying the condition $e \cdot k = 0$ can be called the polarization vector of a virtual photon; it may possess a time as well as a longitudinal component.

The only difference between the integral in (7) and the similar integral in the photoproduction matrix element [4,6]) is that in the given case the square of momentum k,

$$k^2 = -m_\gamma{}^2, \tag{9}$$

does not vanish. Due to the translational invariance condition this integral should contain $\delta(p+k-p'-q)$. We shall consider the pseudovector T whose components $T^n(T^0, \mathbf{T})$ are defined by the relation

$$(2\pi)^4\delta(p+k-p'-q)T^n = \sqrt{\frac{p^0p'^0}{m^2}}\int e^{iqx-iky}\langle p's'|\frac{\delta i^n(y)}{\delta\varphi_\rho(x)}|ps\rangle dxdy. \tag{10}$$

The quantity $T \cdot e$ can be called the virtual photoproduction amplitude. The matrix element considered above is then equal to

$$\langle \mathrm{f}|S|\mathrm{i}\rangle = \frac{-i(2\pi)^4 e m_e m}{\sqrt{2q^0 p_e{}^0 p_e'{}^0 p^0 p'^0}} \frac{1}{k^2} \delta(p+k-p'-q) T \cdot e. \tag{11}$$

We shall consider in future the pseudovector T. It satisfies the gauge invariance condition

$$T \cdot k \equiv T^0 k^0 - \mathbf{T} \cdot \mathbf{k} = 0 \tag{12}$$

so that $T^0 = \mathbf{T} \cdot \mathbf{k}/k^0$. Each of the three independent components of $\mathbf{T}$ corresponds to two possible orientations of the spatial nucleon spin s' relative to s. Thus T can be expressed in terms of 6 independent functions, scalar (in ordinary space).

In the coordinate system in which $\mathbf{p}+\mathbf{p}' = 0$ (in this system the quantities are denoted by the subscript p):

$$\begin{aligned} k_p{}^0 &= q_p{}^0 = E \\ \mathbf{k}_p &= \boldsymbol{\lambda} - (1+\varepsilon)\mathbf{p} \\ \mathbf{q}_p &= \boldsymbol{\lambda} + (1-\varepsilon)\mathbf{p} \end{aligned} \tag{13}$$

where $\varepsilon = (\mu^2+m_\gamma{}^2)/4\mathbf{p}^2$ and $\boldsymbol{\lambda}$ is a vector orthogonal to $\mathbf{p}$ and whose length is

$$|\boldsymbol{\lambda}| = \lambda(E) = \sqrt{E^2+m_\gamma{}^2-(1+\varepsilon)^2\mathbf{p}^2}. \tag{14}$$

In this coordinate system we therefore have two independent vectors $\mathbf{p}$ and $\boldsymbol{\lambda}$ and a spin pseudovector $\boldsymbol{\sigma}$ from which 6 (and only 6) independent pseudovectors can be set up and the spatial part T can be represented in the form

$$\begin{aligned} \mathbf{T}_p = i\boldsymbol{\sigma}L_1 + i(\boldsymbol{\sigma}\cdot\mathbf{p})\mathbf{p}L_2 + i(\boldsymbol{\sigma}\cdot\boldsymbol{\lambda})\mathbf{p}L_3 + (\mathbf{p}\wedge\boldsymbol{\lambda})L_4 \\ + i(\boldsymbol{\sigma}\cdot\boldsymbol{\lambda})\boldsymbol{\lambda}L_5 + i(\boldsymbol{\sigma}\cdot\mathbf{p})\boldsymbol{\lambda}L_6. \end{aligned} \tag{15}$$

Moreover

$$T_p{}^0 = \mathbf{T}_p \cdot \mathbf{k}_p/E. \tag{16}$$

It should be noted that for $\lambda = 0$ all vectors ($\mathbf{k}_p$, $\mathbf{q}_p$ and $\mathbf{p}$) are directed along a single straight line. Therefore $\mathbf{T}_p$ cannot depend in this case on $\boldsymbol{\lambda}/\lambda$ and hence one must have

$$\lambda^2 L_5 = 0 \quad \text{for} \quad \lambda^2 = 0. \tag{17}$$

The L_i have a known [4–7]) isobaric structure

$$L_i = \delta_{\rho 3} L_i{}^{(1)} + \tau_\rho L_i{}^{(2)} + \tfrac{1}{2}[\tau_\rho, \tau_3]_- L_i{}^{(3)} \tag{18}$$

where the $L_i{}^{(\alpha)} = L_i{}^{(\alpha)}(E, \mathbf{p}^2, m_\gamma{}^2)$ are scalars in ordinary and isobaric spaces.

4. Dispersion Relations in the Coordinate System in which $\mathbf{p}+\mathbf{p}' = 0$

Consider the dependence of $L_i^{(\alpha)}$ on energy E. The integral in (10) defines T and hence $L_i^{(\alpha)}$ for such real values of E for which $|E| \geqq E_{\text{thr}}$ where

$$E_{\text{thr}} = \sqrt{(1+\varepsilon)^2\mathbf{p}^2 - m_\gamma^2} \tag{19}$$

is the lower limit for the observable values of E.

It then follows from (10) that T does not change upon complex conjugation and the substitution

$$p' \rightleftarrows p, \qquad s' \rightleftarrows s, \qquad q \to -q, \qquad k \to -k. \tag{20}$$

In the $\mathbf{p}+\mathbf{p}' = 0$ coordinate system this corresponds to the substitution $E \to -E$, $\mathbf{p} \to -\mathbf{p}$, $\lambda \to -\lambda$, $s' \rightleftarrows s$. Thus the $L_i^{(\alpha)}$ in (15) and (18) should satisfy the symmetry conditions

$$\begin{aligned} L_i^{(\alpha)}(E) &= \mp L_i^{*(\alpha)}(-E) \qquad (i \neq 4), \\ L_4^{(\alpha)}(E) &= \pm L_4^{*(\alpha)}(-E). \end{aligned} \tag{21}$$

Here and everywhere in the future the upper sign corresponds to $\alpha = 1, 2$ and the lower to $\alpha = 3$.

The energy dependence of $L_i^{(\alpha)}$ is given by the dispersion relations. In order to write them down in accord with the method employed in ref.[1]) we should consider along with T the quantity T^+ whose components are defined by the relation

$$(2\pi)^4\delta(p+k-p'-q)T^{n+} = \sqrt{\frac{p^0p'^0}{m^2}}\int e^{iqx-iky}\langle p's'|\frac{\delta j_\rho(x)}{\delta A_n(y)}|ps\rangle dxdy \tag{22}$$

where the meson current $j_\rho(x)$ is varied with respect to the electromagnetic field $A_n(y)$. The complex conjugate of T^+ describes a process which is the inverse of virtual photoproduction. The relation between T^+ and T can be obtained, for example, by comparing the Feynman diagrams of the direct and inverse processes, as was done in ref.[10]) for real photoproduction. It is then found that T_p^+ can be obtained from T_p if in (15) and (18) $L_i^{(\alpha)}$ is replaced by $L_i^{*(\alpha)}$. The quantities T and T^+ which contain λ in the first power cannot be uniquely extended to the region of unobservable values of E. In order to remove this difficulty we shall consider instead of them the combinations

$$\begin{aligned} S^+T(\lambda) &= \tfrac{1}{2}[T(\lambda)+T(-\lambda)], \\ S^-T(\lambda) &= \frac{1}{2\lambda}[T(\lambda)-T(-\lambda)]. \end{aligned} \tag{23}$$

It is furthermore necessary to make some assumption regarding the growth of T for $E \to \infty$. We shall assume that $T(E) \to \text{const}$ for $E \to \infty$. Then by the method presented in ref.[1]) one can write the dispersion relations

$$S^+[T_p^n(E)+T_p^{n+}(E)]-\{S^+[T_p^n+T_p^{n+}]\}_{E=0} = \frac{1}{\pi i}\,\mathrm{P}\int_{-\infty}^{\infty}\frac{E}{E'(E'-E)}\,S^+[T_p^n(E')-T_p^{n+}(E')]\,\mathrm{d}E' \quad (24)$$

$$S^-[T_p^n(E)+T_p^{n+}(E)] = \frac{1}{\pi i}\,\mathrm{P}\int_{-\infty}^{\infty}\frac{1}{E'-E}\,S^-[T_p^n(E')-T_p^{n+}(E')]\mathrm{d}E'$$

for all four components of T.

Substituting the expressions for $\mathbf{T}_p$ and $\mathbf{T}_p^+$ we obtain dispersion relations for $L_i^{(\alpha)}(i\neq 5)$ and $\lambda^2 L_5^{(\alpha)}$ which contain indeterminate constants $\mathrm{Re}\,L_1^{(\alpha)}(0)$, $\mathrm{Re}\,L_2^{(\alpha)}(0)$ and $\lambda^2(0)\,\mathrm{Re}\,L_5^{(\alpha)}(0)$.

We can furthermore use condition (17) if instead of (24) we write the dispersion relations for T/λ^2. Since the $L_5^{(\alpha)}$ do not have singularities at $\lambda^2=0$ we obtain relations for $L_5^{(\alpha)}$ which do not contain indeterminate constants.

From dispersion relations (24) for T_p^0 and the requirement of gauge invariance (16) we obtain

$$S^{\pm}[(\mathbf{T}_p+\mathbf{T}_p^+)\cdot\mathbf{k}_p]=0 \quad \text{for} \quad E=0 \quad (25)$$

which yields the relation between $\mathrm{Re}\,L_1^{(\alpha)}(0)$ and $\mathrm{Re}\,L_2^{(\alpha)}(0)$ and those constants which can be derived from the dispersion relations. Making use moreover of symmetry properties (21) we obtain finally

$$\mathrm{Re}\,L_i^{(\alpha)}(E) = \mathrm{Re}\,L_i^{(\alpha)}(0)+\frac{1}{\pi}\,\mathrm{P}\int_0^{\infty}\frac{E}{E'}\left(\frac{1}{E'-E}\pm\frac{1}{E'+E}\right)\mathrm{Im}\,L_i^{(\alpha)}(E')\mathrm{d}E',\quad i\neq 4, \quad (26a)$$

$$\mathrm{Re}\,L_1^{(\alpha)}(0) = (1+\varepsilon)\mathbf{p}^2\,\mathrm{Re}\,L_3^{(\alpha)}(0)-\lambda^2(0)\,\mathrm{Re}\,L_5^{(\alpha)}(0), \quad (26b)$$

$$\mathrm{Re}\,L_2^{(\alpha)}(0) = -(1+\varepsilon)\,\mathrm{Re}\,L_3^{(\alpha)}(0) + \frac{\lambda^2(0)}{(1+\varepsilon)\mathbf{p}^2}[(1+\varepsilon)\,\mathrm{Re}\,L_5^{(\alpha)}(0)+\mathrm{Re}\,L_6^{(\alpha)}(0)], \quad (26c)$$

$$\mathrm{Re}\,L_j^{(\alpha)}(0) = \frac{1}{\pi}\,\mathrm{P}\int_0^{\infty}\frac{1\mp 1}{E'}\,\mathrm{Im}\,L_j^{(\alpha)}(E')\mathrm{d}E', \qquad j=3,5,6, \quad (26d)$$

$$(1\pm 1)\int_0^{\infty}\mathrm{Im}\,L_5^{(\alpha)}(E')\mathrm{d}E'=0, \quad (26e)$$

$$\mathrm{Re}\,L_4^{(\alpha)}(E) = \frac{1}{\pi}\,\mathrm{P}\int_0^{\infty}\left(\frac{1}{E'-E}\pm\frac{1}{E'+E}\right)\mathrm{Im}\,L_4^{(\alpha)}(E')\mathrm{d}E'. \quad (26f)$$

Eq. (26e) is a corollary of relations for $\lambda^2 L_5$ and L_5 and reflects the circumstance that for $E\to\infty$, L_5 decreases as const/λ^2, and does not possess singularities at $\lambda^2=0$.

5. Single-Nucleon Term

The integrals from 0 to ∞ in the dispersion relations reduce to integrals from $E_2 > 0$ to ∞. We shall make use of the relation

$$\frac{\delta i^n(y)}{\delta \varphi_\rho(x)} - \frac{\delta j_\rho(x)}{\delta A_n(y)} = i[i^n(y) j_\rho(x) - j_\rho(x) i^n(y)] \tag{27}$$

and the existence of a closed system of amplitudes $|l_N{}^0, \mathbf{l}\rangle$ for states with a definite momentum $\mathbf{l}$ and energy $l_N{}^0 = \sqrt{M_N{}^2+\mathbf{l}^2}$. We shall also make use of translational invariance of the current matrix elements. Then for the difference $T^n - T^{n+}$ in the integrals in (24) we obtain the expression

$$\begin{aligned} T^n - T^{n+} = 2\pi i \sqrt{\frac{p^0 p'^0}{m^2}} \\ \times \sum_N \{ &\langle p' s' | i^n(0) | l_N{}^0, \mathbf{p}-\mathbf{q}\rangle \langle l_N{}^0, \mathbf{p}-\mathbf{q} | j_\rho(0) | ps\rangle \delta(l_N{}^0 - p^0 + q^0) \\ -&\langle p' s' | j_\rho(0) | l_N{}^0, \mathbf{p}'+\mathbf{q}\rangle \langle l_N{}^0, \mathbf{p}'+\mathbf{q} | i^n(0) | ps\rangle \delta(l_N{}^0 - p'^0 - q^0). \end{aligned} \tag{28}$$

Consider now the possible values of M_N in the matrix elements in (26). From conservation of nucleon charge it follows that the minimum value of M_N corresponds to a single-nucleon state and is equal to the nucleon mass m. It is not necessary to take into account states in which photons and other non-strongly interacting particles are involved along with nucleons inasmuch as the current matrix elements in (28) are being considered in the lowest approximation in e. For the same reason the bound nucleon-meson state (π atom) can be disregarded. Therefore the next value of M_N after m corresponds to a nucleon-free meson state (in which the meson is fixed relative to the nucleon) and is equal to $m+\mu$. It is evident that all $M_N > m+\mu$ are just as important.

The dispersion relations (24) are first derived for the fictitious case when

$$\lambda^2 = E^2 + a, \qquad a > 0 \tag{29}$$

and the possibility of an analytic continuation of the dispersion relations to real values of the parameters is substantiated. In this case the intermediate states in (28) have real momenta values for any real values of $E = q^0$. Keeping this in mind we shall consider (in the $\mathbf{p}+\mathbf{p}' = 0$ coordinate system) the dependence of (28) on $q^0 = E$. This expression does not vanish only for $\sqrt{M_N{}^2+(\mathbf{p}-\mathbf{q})^2} = p^0 - q^0$ and $\sqrt{M_N{}^2+(\mathbf{p}'+\mathbf{q})} = p'^0 + q^0$. The relation between $\mathbf{q}$ and q^0 may be violated at any of the intermediate stages and μ^2 and $m_\gamma{}^2$ (in λ^2) can be regarded as numbers satisfying (29). However, we shall require that the formulas have the same form as that in which they are encountered in the dispersion relations, that is, when μ^2 and $m_\gamma{}^2$ are real. For $M_N = m$ the first δ function in (28) will not vanish if

$$q^0 = E_1 = [\mathbf{p}^2+\tfrac{1}{4}(\mu^2-m_\gamma^2)]\frac{1}{p^0} \tag{30}$$

and the second one if $q^0 = -E_1$.

For $M_N > m+\mu$ the first δ function differs from zero for $q^0 < -E_2$ and the second for

$$q^0 > E_2 = [m\mu-\mathbf{p}^2+\tfrac{1}{4}(\mu+m_\gamma^2)]\frac{1}{p^0}. \tag{31}$$

In accord with ref.[1]) it is sufficient for the existence of the dispersion relations that there exist an energy range in which (28) vanishes.

We consider 2 cases:

$$\text{(I)} \qquad 0 < E_1 < E_2 \quad \text{or} \quad m_\gamma^2-\mu^2 < 4\mathbf{p}^2 < 2m\mu+m_\gamma^2, \tag{32}$$

$$\text{(II)} \qquad 0 < -E_1 < E_2 \quad \text{or} \quad m_\gamma^2 > 4\mathbf{p}^2+\mu^2. \tag{33}$$

For $0 \leqq E < E_2$ in case I

$$T^n(E)-T^{n+}(E) = 2\pi i[m^2+\tfrac{1}{4}(m_\gamma^2-\mu^2)]\frac{1}{p^{02}}\sqrt{\frac{p^0p'^0}{m^2}} \sum_{s''}\langle p's'|i^n(0)|p-q,\, s''\rangle\langle p-q,\, s''|j_\rho(0)|ps\rangle\delta(E-E_1). \tag{34}$$

In case II

$$T^n(E)-T^{n+}(E) = -2\pi i[m^2+\tfrac{1}{4}(m_\gamma^2-\mu^2)]\frac{1}{p^{02}}\sqrt{\frac{p^0p'^0}{m^2}} \sum_{s''}\langle p's'|j_\rho(0)|p'+q,\, s''\rangle\langle p'+q,\, s''|i^n(0)|ps\rangle\delta(E+E_1) \tag{35}$$

where s'' is the space and isobaric nucleon spin in the intermediate state.

Generally speaking, the energy E_2 is smaller than the energy restricting the observable region and is identical with it only when

$$\mathbf{p}^2 = \frac{\mu^2+m_\gamma^2}{4}\,\frac{m}{m+\mu}. \tag{36}$$

Before considering the current matrix elements in (34) and (35) it should be noted that the first term in (28) vanishes in the observable region and

$$(2\pi)^4\delta(p+k-p'-q)(T^n-T^{n+}) = -i\sqrt{\frac{p^0p'^0}{m^2}}\int e^{iqx-iky}\langle p's'|j_\rho(x)i^n(y)|ps\rangle\,dxdy. \tag{37}$$

A relation between the virtual photoproduction amplitude and meson-nucleon scattering phase shifts of the same type as that for real photoproduction follows from this equation in the single-meson approximation.

The following general expressions for the matrix elements in (34) and (35)

can be written:

$$\langle p's'|i^n(0)|p''s''\rangle$$

$$= \sqrt{\frac{m^2}{p'^0 p''^0}}\,\bar{u}^{s'}(p')\{\hat{F}_e(k^2)\gamma^n + \hat{F}_\mu(k^2)\tfrac{1}{2}[\gamma\cdot k,\gamma^n]_-\}u^{s''}(p''),$$

$$k = p'-p'', \tag{38}$$

$$\langle p''s''|j_\rho(0)|ps\rangle = \sqrt{\frac{m^2}{p''^0 p^0}}\,\bar{u}^{s''}(p'')g(q^2)\gamma^5\tau_\rho u^s(p),$$

$$q = p''-p.$$

Here

$$\hat{F}_{e,\mu} = \tfrac{1}{2}(1+\tau_3)F^{(p)}_{e,\mu} + \tfrac{1}{2}(1-\tau_3)F^{(n)}_{e,\mu}; \tag{39}$$

the $F^{(p,n)}_{e,\mu}(k^2)$ are nucleon relativistic form factors (in rational units); $F_e{}^{(p)}(0) = e$ is the electric charge of the proton ($e^2/4\pi \approx 1/137$); $F_e{}^{(n)}(0) = 0$ is the neutron electric charge; $F_\mu{}^{(p)}(0) = \mu'_p$ is the anomalous proton magnetic moment; $\mu'_p = +1.78(e/2m)$; $F_\mu{}^{(n)}(0) = \mu_n$ is the neutron magnetic moment; $\mu_n = -1.91(e/2m)$, $g(\mu^2) = g$ is the meson charge; $g^2/4\pi \approx 15$.

Inserting (38) into (34) and (35) and summing over the spin of the intermediate nucleon we obtain for $0 \leqq E < E_2$ in case I

$$T^n - T^{n+} = \pi i\frac{g}{p^0}\delta(E-E_1)$$
$$\bar{u}^{s'}(p')\{\hat{F}_e(k^2)\gamma^n + \hat{F}_\mu(k^2)\tfrac{1}{2}[\gamma\cdot k,\gamma^n]_-\}\{\gamma\cdot(p'-k)+m\}\gamma^5\tau_\rho u^s(p) \tag{40}$$

and in case II

$$T^n - T^{n+} = -\pi i\frac{g}{p^0}\delta(E+E_1)$$
$$\bar{u}^{s'}(p')\gamma^5\tau_\rho\{\gamma\cdot(p+k)+m\}\{\hat{F}_e(k^2)\gamma^n + \hat{F}_\mu(k^2)\tfrac{1}{2}[\gamma\cdot k,\gamma^n]_-\}u^s(p). \tag{41}$$

We can now integrate from 0 to E_2 in relations (26), if expressions (40) and (41) are expanded in terms of structures (15) and (18). We, however, write down the final dispersion relations in a relativistically invariant form.

6. Dispersion Relations in Relativistically Invariant Form

A direct transition to the dispersion relations from a coordinate system in which $\mathbf{p}+\mathbf{p}' = 0$ to the c.m.s. is comparatively simple in the approximation $m \to \infty$. In the general case it is profitable to go over first to the dispersion relations in the relativistically invariant form.

Introducing 6 independent gauge invariant pseudovectors R_i

$$
\begin{aligned}
R_1^n &= \bar{u}^{s'}(p')\gamma^5(p^n p'\cdot k - p\cdot k p'^n)u^s(p)\\
R_2^n &= \bar{u}^{s'}(p')\gamma^5[\gamma^n(p+p')\cdot k - \gamma\cdot k(p^n+p'^n)]u^s(p)\\
R_3^n &= -\bar{u}^{s'}(p')\gamma^5[\gamma^n(p-p')\cdot k - \gamma\cdot k(p^n-p'^n)]u^s(p)\\
R_4^n &= -\bar{u}^{s'}(p')\gamma^5(\gamma^n\gamma\cdot k - \gamma\cdot k\gamma^n)u^s(p)\\
R_5^n &= \bar{u}^{s'}(p')\gamma^5[(p^n-p'^n)k^2 - (p-p')\cdot k k^n]u^s(p)\\
R_6^n &= \bar{u}^{s'}(p')\gamma^5\gamma\cdot k(\gamma^n\gamma\cdot k - \gamma\cdot k\gamma^n)u^s(p),
\end{aligned}
\tag{42}
$$

we represent T in the form

$$
T = \sum_{i=1}^{6} R_i\{\delta_{\rho 3}\Omega_i^{(1)} + \tau_\rho\Omega_i^{(2)} + \tfrac{1}{2}[\tau_\rho,\tau_3]_-\Omega_i^{(3)}\} \tag{43}
$$

where the $\Omega_i^{(\alpha)}$ are relativistically invariant functions which depend on the invariants

$$
\nu = \frac{(p+p')\cdot k}{2m}; \qquad \nu_1 = \frac{k\cdot q}{2m}; \qquad k^2 = -m_\gamma{}^2. \tag{44}
$$

T^+ can be obtained from T by substituting $\Omega_i^{*(\alpha)}$ for $\Omega_i^{(\alpha)}$. Pseudovectors R_i have been chosen so that all $\mathbf{R}_i$ contain terms with energy factors E and λ and therefore all $\Omega_i^{(\alpha)}$ for $E\to\infty$ behave as T/E, i.e., decrease under our assumption. Due to the dispersion relations for T^0 the $\Omega_i^{(\alpha)}$ do not have a singularity at $E=0$. Furthermore, complex conjugation and substitution (20) do not affect $R_{1,2,4}$ but change the sign of $R_{3,5,6}$. It is therefore evident that if T in (43) is reduced to the same form as (15), thus relating $\Omega_i^{(\alpha)}$ with $L_i^{(\alpha)}$ and the transition from (26) to the dispersion relations for $\Omega_i^{(\alpha)}$ is performed (in the $\mathbf{p}+\mathbf{p}'=0$ coordinate system) one arrives at a result of the simple form

$$
\operatorname{Re}\Omega_{1,2,4}^{(\alpha)}(E) = \frac{1}{\pi}\,\mathrm{P}\int_0^\infty\left(\frac{1}{E'-E}\pm\frac{1}{E'+E}\right)\operatorname{Im}\Omega_{1,2,4}^{(\alpha)}(E')\mathrm{d}E'. \tag{45}
$$

For $\Omega_{3,5,6}^{(\alpha)}$ the $\pm$ should be replaced by $\mp$.

In the $\mathbf{p}+\mathbf{p}'=0$ coordinate system

$$
\begin{aligned}
\nu &= \frac{Ep^0}{m}, \qquad \nu_1 = \frac{E_1 p^0}{m} = [\mathbf{p}^2+\tfrac{1}{4}(\mu^2-m_\gamma{}^2)]\frac{1}{m},\\
\nu_2 &= \frac{E_2 p^0}{m} = \mu + \frac{\mu^2-2m\nu_1}{2m}.
\end{aligned}
\tag{46}
$$

These relations can be employed to write expressions (40) and (41) for $T^n - T^{n+}$ (in the range $0\leqq\nu<\nu_2$) in a relativistically invariant form. Expanding them in terms of structures (42) and (18) we obtain the functions $\operatorname{Im}\Omega_i^{(\alpha)}$ in the range $0\leqq\nu<\nu_2$. Integrating in (45) over ν we finally obtain in case I as well as in case II

$$\operatorname{Re}\Omega^{(\alpha)}_{1,2,4}(\nu,\nu_1,m_\gamma{}^2)=\left(\frac{1}{\nu_1-\nu}\pm\frac{1}{\nu_1+\nu}\right)\mathring{\Omega}^{(\alpha)}_{1,2,4}(\nu_1,m_\gamma{}^2)$$
$$+\frac{1}{\pi}\,\mathrm{P}\int_{\mu+\frac{\mu^2-2m\nu_1}{2m}}^{\infty}\left(\frac{1}{\nu'-\nu}\pm\frac{1}{\nu'+\nu}\right)\operatorname{Im}\Omega^{(\alpha)}_{1,2,4}(\nu',\nu_1,m_\gamma{}^2)\mathrm{d}\nu'. \tag{47}$$

For $\Omega^{(\alpha)}_{3,5,6}\pm$ should be replaced by $\mp$. The coefficients $\mathring{\Omega}_i{}^{(\alpha)}$ are equal to

$$\mathring{\Omega}_1{}^{(\alpha)}=-2\mathring{\Omega}_5{}^{(\alpha)}=-\frac{f}{\mu}\,\frac{1}{2m\nu_1+m_\gamma{}^2}\begin{pmatrix}F_e{}^{(-)}\\F_e{}^{(+)}\\-F_e{}^{(-)}\end{pmatrix}\quad\begin{matrix}\alpha=1\\\alpha=2\\\alpha=3\end{matrix}$$

$$\mathring{\Omega}_2{}^{(\alpha)}=-\mathring{\Omega}_3{}^{(\alpha)}=-2\mathring{\Omega}_6{}^{(\alpha)}=-\frac{f}{2\mu}\begin{pmatrix}F_\mu{}^{(-)}\\F_\mu{}^{(+)}\\-F_\mu{}^{(-)}\end{pmatrix} \tag{48}$$

$$\mathring{\Omega}_4{}^{(\alpha)}=\frac{f}{4\mu}\begin{pmatrix}F_e{}^{(-)}+2mF_\mu{}^{(-)}\\F_e{}^{(+)}+2mF_\mu{}^{(+)}\\-F_e{}^{(-)}-2mF_\mu{}^{(-)}\end{pmatrix}$$

where

$$f=\frac{g\mu}{2m},\quad F^{(\pm)}_{e,\mu}=F^{(p)}_{e,\mu}(k^2)\pm F^{(n)}_{e,\mu}(k^2). \tag{49}$$

Setting $k^2=-m_\gamma{}^2=0$ one obtains from here dispersion relations for real photoproduction [4,6]). Approximate equations for the virtual photoproduction amplitude can be obtained from (47), (48) in a manner similar to that employed in ref.[5–7]) for real photoproduction. An investigation of these equations and comparison with the experimental data on π-meson production by electrons permits one to determine the electromagnetic form factor of the nucleon.

References

1) N. N. Bogolubov, B. M. Medvedev and M. K. Polivanov, Problems of Dispersion Relations Theory (Moscow, GTTI, in print);
N. N. Bogolubov and D. V. Shirkov, Introduction to Theory of Quantized Fields (Moscow, GTTI, 1957)
2) R. H. Capps and G. Takeda, Phys. Rev. **103** (1956) 1877
3) G. F. Chew, M. L. Goldberger, F. E. Low and Y. Nambu, Phys. Rev. **106** (1957) 1337
4) A. A. Logunov, B. M. Stepanov and A. N. Tavkhelidze, Doklady Akad. Nauk SSSR **112** (1957) no. 1
5) G. F. Chew, M. L. Goldberger, F. E. Low and Y. Nambu, Phys. Rev. **106** (1957) 1345
6) A. A. Logunov, A. N. Tavkhelidze and L. D. Solovyov, Nuclear Physics **4** (1957) 427
7) L. D. Solovyov, Nuclear Physics **5** (1958) 256
8) V. S. Kukin and A. R. Frenkin, Scientific Reports of Higher School (in press)
9) A. A. Logunov, Doklady Akad. Nauk SSSR **117** (1957) 792
10) T. Nakano and K. Nishijima, Progr. Theor. Phys. **8** (1952) 53

7.A *Nuclear Physics* **10** (1959) 71—81; © *North-Holland Publishing Co., Amsterdam*
Not to be reproduced by photoprint or microfilm without written permission from the publisher

ON THE THEORY OF DISPERSION RELATIONS FOR VIRTUAL PROCESSES

A. A. LOGUNOV

Laboratory of Theoretical Physics, Joint Institute of Nuclear Research, Dubna, USSR

Received 4 May 1958

Abstract: A deduction of the dispersion relations for virtual photoproduction is presented.

1. Introduction

Dispersion relations for virtual processes have been considered in ref.[1]). These relations permit one to investigate inelastic processes in which electrons, μ mesons, etc., participate along with strongly interacting particles (nucleons, π mesons, etc.). Examples of such processes are

$$\mathrm{e}+\mathrm{p}\to\mathrm{e}+\pi+\mathrm{n}, \qquad \gamma+\mathrm{p}\to\mathrm{e}^+ +\mathrm{e}^- +\mathrm{p}$$
$$\pi+\mathrm{p}\to\mathrm{e}^+ +\mathrm{e}^- +\mathrm{p}, \qquad \mathrm{e}+\mathrm{p}\to\mathrm{e}+\gamma+\mathrm{p}.$$

Processes of production of π-mesons in electron-nucleon collisions and their relation to virtual photoproduction were examined in ref.[2]), and the dispersion relations for virtual photoproduction were investigated. It should be especially noted that the invariant functions $F_1^{\mathrm{p,n}}(k^2)$, $F_2^{\mathrm{p,n}}(k^2)$, which characterize the electromagnetic structure of the nucleon enter the dispersion relations for this process. A consequence of this is that independent information on the electromagnetic structure of the nucleon can be derived from experimental data relating to this process.

In the present paper (which is a direct continuation of ref.[2]) and uses the same notations) we give a proof of the dispersion relations for virtual processes for the particular case of virtual photoproduction, the method of N. N. Bogolubov [3]) being used for this purpose.

2. Analytic Properties of the Virtual Photoproduction Amplitude in the Fictitious Region

For the investigation of the analytic properties of the virtual photoproduction amplitude we assume that the squares of the 4-dimensional vectors k and q have the following values:

$$k^2=\xi(\tau), \qquad \xi(\tau)=\tau-\mu^2-m_\gamma^2,$$
$$q^2=\tau, \qquad \tau<-\mathbf{p}^2(1-\varepsilon)^2. \tag{2.1}$$

We shall assume as usual that k, q, p and p' are related by the equation

$$k+p = q+p'. \tag{2.2}$$

Then in the coordinate system in which $\mathbf{p}+\mathbf{p}' = 0$ we get

$$\begin{aligned} \mathbf{k} &= \lambda\mathbf{e}-(1+\varepsilon)\mathbf{p}, \qquad 4\varepsilon\mathbf{p}^2 = \mu^2+m_\gamma^2 \\ \mathbf{q} &= \lambda\mathbf{e}+(1-\varepsilon)\mathbf{p}, \qquad \lambda = \sqrt{E^2-(1-\varepsilon)^2\mathbf{p}^2-\tau}. \end{aligned} \tag{2.3}$$

It is obvious that $\lambda^2 > E^2$ since $\tau < -\mathbf{p}^2(1-\varepsilon)^2$. This is a very important circumstance as in this case

$$\operatorname{Im} E > |\operatorname{Im}\sqrt{E^2-(1-\varepsilon)^2\mathbf{p}^2-\tau}|, \qquad \operatorname{Im} E \neq 0. \tag{2.4}$$

The retarded and advanced amplitudes of the process can be written in the form

$$\begin{aligned} T^{\mathrm{ret}}_{\alpha,\omega}\left(\frac{k+q}{2}\right) &= -\int e^{\frac{1}{2}i(k+q)x} F^{\mathrm{ret}}_{\alpha,\omega}(x)\,dx \\ F^{\mathrm{ret}}_{\alpha,\omega}(x-y) &= e^{-\frac{1}{2}i(p'-p)(x+y)}\langle p', s'|\frac{\delta i_\nu(y)}{\delta\varphi_\rho(x)}|p, s\rangle, \end{aligned} \tag{2.5}$$

$$\begin{aligned} T^{\mathrm{adv}}_{\alpha,\omega}\left(\frac{k+q}{2}\right) &= -\int e^{\frac{1}{2}i(k+q)x} F^{\mathrm{adv}}_{\alpha,\omega}(x)\,dx \\ F^{\mathrm{adv}}_{\alpha,\omega}(x-y) &= e^{-\frac{1}{2}i(p'-p)(x+y)}\langle p', s'|\frac{\delta j_\rho(x)}{\delta A_\nu(y)}|p,s\rangle. \end{aligned} \tag{2.6}$$

These amplitudes are proportional to the quantities T and T^+ introduced in ref.[2]); thus

$$T^{\mathrm{ret}} = -(p^0 p'^0/m^2)^{-\frac{1}{2}} T$$

and similarly for T^{adv} and T^+.

It may be recalled that according to the causality principle

$$\begin{aligned} F^{\mathrm{ret}}_{\alpha,\omega}(x) &= 0 \quad \text{if} \quad x \lesssim 0, \\ F^{\mathrm{adv}}_{\alpha,\omega}(x) &= 0 \quad \text{if} \quad x \gtrsim 0. \end{aligned} \tag{2.7}$$

In the reference system in which $\mathbf{p}+\mathbf{p}' = 0$ the retarded and advanced amplitudes can be written in the form

$$T^{\mathrm{ret}}_{\alpha,\omega}(E,\tau) = -\int e^{i(Ex_0-\mathbf{e}\cdot\mathbf{x}\sqrt{E^2-(1-\varepsilon)^2\mathbf{p}^2-\tau})+i\varepsilon\mathbf{p}\cdot\mathbf{x}} F^{\mathrm{ret}}_{\alpha,\omega}(x)\,dx, \tag{2.8}$$

$$T^{\mathrm{adv}}_{\alpha,\omega}(E,\tau) = -\int e^{i(Ex_0-\mathbf{e}\cdot\mathbf{x}\sqrt{E^2-(1-\varepsilon)^2\mathbf{p}^2-\tau})+i\varepsilon\mathbf{p}\cdot\mathbf{x}} F^{\mathrm{adv}}_{\alpha,\omega}(x)\,dx. \tag{2.9}$$

Since in (2.8) the integration is performed in the region

$$x_0 > |\mathbf{x}|, \qquad x_0 > 0, \tag{2.10}$$

one has

$$\begin{aligned} &\tau < -\mathbf{p}^2(1-\varepsilon)^2, \\ &\operatorname{Im} E > |\operatorname{Im}\sqrt{E^2-(1-\varepsilon)^2\mathbf{p}^2-\tau}|, \end{aligned}$$

and hence the function $S_{\pm}T^{\mathrm{ret}}(E,\tau)$ will be analytic in the upper half plane of the complex variable E. It should be recalled that $S_{\pm}$ means symmetrization or antisymmetrization with respect to the vector $\mathbf{e}$. In an analogous way it can be proved that $S_{\pm}T^{\mathrm{adv}}(E,\tau)$ is an analytic function in the lower half plane of the complex variable E. It can be shown that under certain conditions ST^{ret} and ST^{adv} are identical on a segment of the real axis of E. To prove this the behaviour of the difference of $ST(E,\tau)$ for real values of E should be investigated:

$$\begin{aligned} ST_{\alpha,\omega}\left(\frac{k+q}{2}\right) &= ST^{\mathrm{ret}}_{\alpha,\omega} - ST^{\mathrm{adv}}_{\alpha,\omega} \\ &= -S\int e^{\frac{1}{2}i(k+q)x}\{F^{\mathrm{ret}}_{\alpha,\omega}(x) - F^{\mathrm{adv}}_{\alpha,\omega}(x)\}\mathrm{d}x. \end{aligned} \tag{2.11}$$

As shown in ref.[2]) and [4]) this can be written in the form

$$\begin{aligned} ST_{\alpha,\omega}(E,\tau) = {} & 2\pi i \sum_n S\langle p', s'|j_\rho(0)|n, \lambda\mathbf{e}-\varepsilon\mathbf{p}\rangle\langle n, \lambda\mathbf{e}-\varepsilon\mathbf{p}|i_\nu(0)|p, s\rangle \\ & \cdot \delta(E+\sqrt{M^2+\mathbf{p}^2}-\sqrt{M_n{}^2+\lambda^2+\varepsilon^2\mathbf{p}^2}) \\ & - 2\pi i \sum_n S\langle p', s'|i_\nu(0)|n, -\lambda\mathbf{e}+\varepsilon\mathbf{p}\rangle\langle n, -\lambda\mathbf{e}+\varepsilon\mathbf{p}|j_\rho(0)|p, s\rangle \\ & \cdot \delta(E-\sqrt{M^2+\mathbf{p}^2}+\sqrt{M_n{}^2+\lambda^2+\varepsilon^2\mathbf{p}^2}). \end{aligned} \tag{2.12}$$

Separating the term referring to the intermediate single-nucleon state and performing elementary transformations of the δ functions we write (2.12) in the form

$$\begin{aligned} ST_{\alpha,\omega}(E,\tau) = {} & Sf_{\alpha,\omega}(E,\tau) + 2\pi i SA(p,\tau)\delta(E+E_{\mathbf{p}}) \\ & - 2\pi i SB(p,\tau)\delta(E-E_{\mathbf{p}}), \end{aligned} \tag{2.13}$$

where

$$\begin{aligned} Sf_{\alpha,\omega}(E,\tau) = {} & 2\pi i \sum_{n>1}\left|1+\frac{E_{\mathbf{p}n}}{p_0}\right| S\langle p', s'|j_\rho(0)|n, \lambda\mathbf{e}-\varepsilon\mathbf{p}\rangle \\ & \cdot \langle n, \lambda\mathbf{e}-\varepsilon\mathbf{p}|i_\nu(0)|p, s\rangle\delta(E-E_{\mathbf{p}n}(\tau)) \\ & - 2\pi i \sum_{n>1}\left|1+\frac{E_{\mathbf{p}n}}{p_0}\right| S\langle p', s'|i_\nu(0)|n, -\lambda\mathbf{e}+\varepsilon\mathbf{p}\rangle \\ & \cdot \langle n, -\lambda\mathbf{e}+\varepsilon\mathbf{p}|j_\rho(0)|p, s\rangle\delta(E+E_{\mathbf{p}n}(\tau)), \end{aligned} \tag{2.14}$$

$$\begin{aligned} SA(p,\tau) = {} & \left|1-\frac{E_{\mathbf{p}}}{p_0}\right| \sum_{s''} S\langle p', s'|j_\rho(0)|s'', \lambda\mathbf{e}-\varepsilon\mathbf{p}\rangle \\ & \cdot \langle s'', \lambda\mathbf{e}-\varepsilon\mathbf{p}|i_\nu(0)|p, s\rangle, \\ SB(p,\tau) = {} & \left|1-\frac{E_{\mathbf{p}}}{p_0}\right| \sum_{s''} S\langle p', s'|i_\nu(0)|s'', -\lambda\mathbf{e}+\varepsilon\mathbf{p}\rangle \\ & \cdot \langle s'', -\lambda\mathbf{e}+\varepsilon\mathbf{p}|j_\rho(0)|p, s\rangle, \end{aligned} \tag{2.15}$$

$$2\sqrt{M^2+\mathbf{p}^2}E_{p_n}(\tau) = M_n^2 - M^2 - 2\mathbf{p}^2 + \tfrac{1}{2}(m_\gamma^2+\mu^2) - \tau,$$
$$\sqrt{M^2+\mathbf{p}^2}E_p = \mathbf{p}^2 + \tfrac{1}{2}\tau - \tfrac{1}{4}(m_\gamma^2+\mu^2). \tag{2.16}$$

If the usual assumption is made that between M and $M+\mu$ there are no bound states in the meson-nucleon system, i.e., that

$$M_n \geqq M+\mu \qquad (n>1),$$

one finds for the scatterer momenta

$$\mathbf{p}^2 < \tfrac{1}{2}M\mu + \tfrac{1}{2}\mu^2 + \tfrac{1}{4}m_\gamma^2 - \tfrac{1}{2}\tau. \tag{2.17}$$

The function $T_{\alpha,\omega}(E,\tau)$ has the energy spectrum represented on fig. 1.

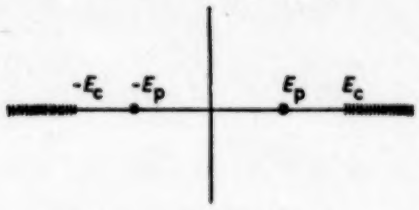

$$E_c = \frac{M\mu - \mathbf{p}^2 + \frac{1}{2}\mu^2 - \frac{1}{2}\tau + \frac{1}{4}(m_\gamma^2+\mu^2)}{\sqrt{(\mathbf{p}^2+M^2)}}$$

Fig. 1

Summing up we can say that in this section it has been proved that if

$$-V < \tau < -\mathbf{p}^2(1-\varepsilon)^2 \tag{2.18}$$

$ST^{\mathrm{ret}}(E,\tau)$ will be an analytic function in the upper half plane of E and ST^{adv} in the lower half plane of E. On the other hand if the condition

$$\mathbf{p}^2 < \tfrac{1}{2}M\mu + \tfrac{1}{2}\mu^2 + \tfrac{1}{4}m_\gamma^2 - \tfrac{1}{2}\tau \tag{2.19}$$

is valid there will always be a segment $(-E_q, E_q)$ on the real E axis for which $ST^{\mathrm{ret}}(E)$ and $ST^{\mathrm{adv}}(E)$ are identical:

$$ST^{\mathrm{ret}}(E,\tau) = ST^{\mathrm{adv}}(E,\tau), \qquad \mathrm{Im}\,E = 0, \qquad |E| < E_q. \tag{2.20}$$

Thus the set of functions $ST^{\mathrm{ret}}(E,\tau)$ and $ST^{\mathrm{adv}}(E,\tau)$ can be represented by the function

$$\widetilde{ST}(E,\tau) = \begin{cases} ST^{\mathrm{ret}}(E,\tau) & \mathrm{Im}\,E > 0 \\ ST^{\mathrm{adv}}(E,\tau) & \mathrm{Im}\,E < 0 \end{cases} \tag{2.21}$$

which is analytic over the whole complex plane of the variable E, excluding the cuts along the real axis

$$-\infty < \mathrm{Re}\,E < -E_c, \qquad E_c < \mathrm{Re}\,E < \infty, \qquad \mathrm{Im}\,E = 0, \tag{2.22}$$

and which has simple poles at the points $E = \pm E_p$ and does not increase at infinity more rapidly than a polynomial of the n^{th} degree.

Thus the Cauchy theorem, with the contour indicated on fig. 2, can be applied to the function

$$g(E,\tau)=\frac{S\tilde{T}(E,\tau)}{(E-E_0)^{n+1}} \tag{2.23}$$

where

$$\sqrt{M^2+\mathbf{p}^2}|E_0|<M\mu-\mathbf{p}^2+\tfrac{1}{2}\mu^2+\tfrac{1}{4}(m_\gamma{}^2+\mu^2)-\tfrac{1}{2}\tau(E_0\neq E_p).$$

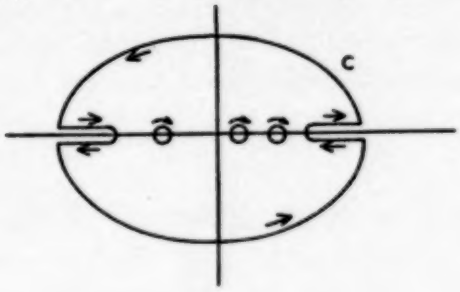

Fig. 2

When the radius of the large circle approaches infinity and the radii of the semi-circles approach zero we obtain

$$\begin{aligned}S\tilde{T}(E,\tau)=&\frac{(E-E_0)^{n+1}}{2\pi i}\int\limits_{|E'|>E_c}\frac{Sf(E',\tau)\mathrm{d}E'}{(E'-E_0)^{n+1}(E'-E)}\\&-\frac{SA(p,\tau)}{E+E_p}\left(\frac{E_0-E}{E_0+E_p}\right)^{n+1}-\frac{SB(p,\tau)}{E_p-E}\left(\frac{E-E_0}{E_p-E_0}\right)^{n+1}\\&+\sum_{0\leq r\leq n}C_r(\tau,p,E_0)E^r.\end{aligned} \tag{2.24}$$

The dispersion relations (2.24) were derived only for the fictitious range of values of τ.

3. Analytic Continuation with Respect to Variable τ

In order to change from the fictitious values of τ to the value $\tau=\mu^2$ of interest to us we must perform an analytic continuation. To do this we make use of the following result obtained in ref.[5,7]). If the variables E,τ,λ are real,

$$-V\leqq\tau\leqq(1+\rho)\mu^2 \tag{3.1}$$

and

$$0<\mathbf{p}^2<\mathbf{p}^2_{\max},$$

$$\mathbf{p}^2_{\max}=\frac{M}{M+\mu}\frac{\mu^2+m_\gamma{}^2}{4}+\tfrac{1}{2}(2M+\mu)\mu\sqrt{\tfrac{2}{3}\frac{4\mu^2+m_\gamma{}^2}{M(2M-\mu)}}$$
$$\left[1+\sqrt{\left\{1+\frac{\mu^2m_\gamma{}^2}{4\mu^2+m_\gamma{}^2}\frac{M}{(M+\mu)^2}\frac{(2M+\mu)^2+m_\gamma{}^2}{2M+\mu}\right\}}\right],\quad\text{if}\quad m_\gamma{}^2<3\mu^2,$$

then the function $f(E,\tau)$ in expression (2.13) can be represented in the form

$$Sf(E,\tau) = F_1(\tau+2E\sqrt{M^2+\mathbf{p}^2},\tau)+F_2(\tau-2E\sqrt{M^2+\mathbf{p}^2},\tau) \tag{3.2}$$

where the functions $F_i(y,\tau)$ have the following properties:

a) $F_i(y,\tau)$ are generalized functions of variable y,

b) $F_i(y,\tau)$ are analytic functions of variable τ and are regular in the region

$$-V \leqq \operatorname{Re}\tau < (1+\rho)\mu^2, \qquad |\operatorname{Im}\tau| < \rho\mu^2, \tag{3.3}$$

c) $F_i(y,\tau) = 0$ for $y < 2M\mu-2\mathbf{p}^2+\mu^2+\frac{1}{2}(m_\gamma{}^2+\mu^2)$.

We shall now demonstrate that from the representation (3.2) follows the validity of the dispersion relation (2.31) for the value

$$\tau = \mu^2 \tag{3.4}$$

of interest to us.

Let us take some negative τ, which satisfies (2.25). Then for the given τ the dispersion relations (2.31) as well as the representation (3.2) will be satisfied simultaneously. Inserting (3.2) into (2.31) we obtain

$$\begin{aligned} S\tilde{T}(E,\tau) = \phi(E,\tau) &- \frac{SA(\not{p},\tau)}{(E+E_{\mathbf{p}}(\tau))}\left(\frac{E_0-E}{E_0+E_{\mathbf{p}}}\right)^{n+1} \\ &- \frac{SB(\not{p},\tau)}{(E_{\mathbf{p}}(\tau)-E)}\left(\frac{E-E_0}{E_{\mathbf{p}}-E_0}\right)^{n+1} + \sum_{0\leq r\leq n} C_r(\tau,\not{p},E_0)\,E^r \end{aligned} \tag{3.5}$$

where

$$\begin{aligned} \phi(E,\tau) = &\frac{(E-E_0)^{n+1}}{2\pi i}\int \frac{dE''\,F_1(2E''\sqrt{M^2+\mathbf{p}^2},\tau)}{\left(E''-E-\dfrac{\tau}{2\sqrt{M^2+\mathbf{p}^2}}\right)\left(E''-E_0-\dfrac{\tau}{2\sqrt{M^2+\mathbf{p}^2}}\right)^{n+1}} \\ &+\frac{(E-E_0)^{n+1}}{2\pi i}\int \frac{dE''\,F_2(2E''\sqrt{M^2+\mathbf{p}^2},\tau)}{\left(E''-E-\dfrac{\tau}{2\sqrt{M^2+\mathbf{p}^2}}\right)\left(E''-E_0-\dfrac{\tau}{2\sqrt{M^2+\mathbf{p}^2}}\right)^{n+1}}. \end{aligned} \tag{3.6}$$

The function $\phi(E,\tau)$ will be an analytic function of E in the region in which neither of the denominators

$$\left(E''-E-\frac{\tau}{2\sqrt{M^2+\mathbf{p}^2}}\right), \qquad \left(-E''-E+\frac{\tau}{2\sqrt{M^2+\mathbf{p}^2}}\right) \tag{3.7}$$

vanishes; that is, providing that

$$\operatorname{Im}\left(\frac{\tau}{2\sqrt{M^2+\mathbf{p}^2}} \pm E\right) \neq 0. \tag{3.8}$$

It is obvious that the condition (3.8) will always be satisfied if

$$|\operatorname{Im}\tau| < 2\sqrt{M^2+\mathbf{p}^2}|\operatorname{Im}E|. \tag{3.9}$$

If the inequality (3.9) is satisfied, $\phi(E,\tau)$ will be an analytic function with respect to the variable E. Consider the analytic properties of the function $\phi(E,\tau)$ with respect to the variable τ. Since the $F_i(y,\tau)$ are analytic functions of τ in the region

$$-V < \operatorname{Re}\tau < (1+\rho)\mu^2, \qquad |\operatorname{Im}\tau| < \rho\mu^2, \tag{3.10}$$

the function $\phi(E,\tau)$ will also be analytic in this region if neither of the denominators

$$\left(E'-E_0-\frac{\tau}{2\sqrt{M^2+\mathbf{p}^2}}\right)^{n+1}, \qquad \left(-E'-E_0+\frac{\tau}{2\sqrt{M^2+\mathbf{p}^2}}\right)^{n+1} \tag{3.11}$$

vanishes in the region (3.10). If a real number is chosen for E_0, neither of the denominators (3.11) will vanish for any complex values of τ from region (3.10) and the function $\phi(E,\tau)$ will be analytic for all complex values of τ in the range (3.10). For real values of τ in the region (3.10) the denominators (3.11) will also not vanish if E_0 is chosen so that

$$|E_0| < \frac{2M\mu+\mu^2-2\mathbf{p}^2-\tau+\frac{1}{2}(m_\gamma{}^2+\mu^2)}{2\sqrt{M^2+\mathbf{p}^2}}. \tag{3.12}$$

However, since

$$\tau < (1+\rho)\mu^2, \qquad \mathbf{p}^2 < \mathbf{p}^2{}_{\max},$$

the inequality (3.12) will be satisfied if

$$|E_0| < \frac{2M\mu+\mu^2-2\mathbf{p}^2_{\max}-(1+\rho)\mu^2+\frac{1}{2}(m_\gamma{}^2+\mu^2)}{2\sqrt{M^2+\mathbf{p}^2}}. \tag{3.13}$$

Thus, if E_0 is chosen in a suitable manner, the function $\phi(E,\tau)$ will also be analytic for real values of τ from the region (3.10).

Summing up to results obtained above, we may say that if E_0 is restricted by the inequality (3.13), the integrals (3.6) will define a function $\phi(E,\tau)$ which is an analytic function in the region

$$\begin{aligned} -V < \operatorname{Re}\tau < (1+\rho)\mu^2, \qquad & |\operatorname{Im}\tau| < \rho\mu^2, \\ & |\operatorname{Im}\tau| < 2\sqrt{M^2+\mathbf{p}^2}|\operatorname{Im} E|. \end{aligned} \tag{3.14}$$

However, it has been previously established by us that the function $S\tilde{T}(E,\tau)$ is regular in the region

$$\begin{aligned} &\operatorname{Im} E > |\operatorname{Im}\sqrt{E^2-(1-\varepsilon)^2\mathbf{p}^2-\tau}|, \\ &\operatorname{Im} E < -|\operatorname{Im}\sqrt{E^2-(1-\varepsilon)^2\mathbf{p}^2-\tau}|. \end{aligned} \tag{3.15}$$

Thus the difference

$$\{S\tilde{T}(E,\tau)-\phi(E,\tau)\}(E^2-E_p{}^2(\tau)) \tag{3.16}$$

should be an analytic function of the variables E in the common part of regions (3.14) and (3.15), i.e.,

$$\begin{aligned} &-V < \operatorname{Re}\tau < (1+\rho)\mu^2, \qquad |\operatorname{Im}\tau| < \rho\mu^2, \\ &|\operatorname{Im}\tau| < 2\sqrt{M^2+\mathbf{p}^2}|\operatorname{Im} E|, \\ &|\operatorname{Im} E| > |\operatorname{Im}\sqrt{E^2-(1-\varepsilon)^2\mathbf{p}^2-\tau}|. \end{aligned} \tag{3.17}$$

However, for real $\tau < -\max[(1-\varepsilon)^2\mathbf{p}^2, 2\mathbf{p}^2]$, this difference, according to the dispersion relation (2.31), is a polynomial in E,

$$\begin{aligned} &-SA(\not{p},\tau)(E-E_{\mathbf{p}})\left(\frac{E_0-E}{E_0+E_{\mathbf{p}}}\right)^{n+1}+SB(\mathbf{p},\tau)(E+E_{\mathbf{p}})\left(\frac{E-E_0}{E_{\mathbf{p}}-E_0}\right)^{n+1} \\ &+(E^2-E_{\mathbf{p}}^2(\tau))\sum_{0\le r\le n} C_r(\tau,\mathbf{p},E_0)E^r. \end{aligned} \tag{3.18}$$

In virtue of the uniqueness of the analytic continuation it will be a polynomial in E over the complete region (3.18).

The functions $A(\not{p},\tau)$, $B(\not{p},\tau)$ and $C_r(\tau,\not{p},E_0)$ can therefore be analytically continued to a certain region of complex values of τ. It can be shown that this region contains at least the whole region

$$-V < \operatorname{Re}\tau < (1+\rho)\mu^2, \qquad |\operatorname{Im}\tau| < \rho\mu^2. \tag{3.19}$$

Indeed, let us take an arbitrary τ lying in the region (3.19). For a given $\tau_+^* = \tau_r+i\eta$, $\eta \neq 0$, we choose $E_+^* = E_r+iE_i$ so that the pair τ_+^*, E_+^* lies in the region (3.17). This can be done if E is chosen so that the following conditions be satisfied:

$$\begin{aligned} &|\operatorname{Im} E| > |\operatorname{Im}\sqrt{E^2-(1-\varepsilon)^2\mathbf{p}^2-\tau}|, \\ &|\operatorname{Im}\tau| < 2\sqrt{M^2+\mathbf{p}^2}|\operatorname{Im} E|. \end{aligned} \tag{3.20}$$

It is easy to verify that the conditions (3.20) will hold if E_r and E_i are chosen as follows:

$$E_i = \tfrac{1}{2}\eta/E_r, \qquad E_r < M, \qquad E_r^2-\tfrac{1}{4}\eta^2/E_r^2-\tau_r-(1-\varepsilon)^2\mathbf{p}^2 > 0. \tag{3.21}$$

Thus for any point $\tau_\pm^*$ from the region (3.19), $\operatorname{Im}\tau_\pm^* \neq 0$, it is always possible to find such a $E_\pm^*$ that the pairs $\tau_\pm^*$ and $E_\pm^*$ will lie in the region (3.17). A consequence of this is that the functions $A(\not{p},\tau)$, $B(\not{p},\tau)$ and $C_r(\tau,\not{p},E_0)$ will be analytic with respect to τ over the whole region (3.19) and possibly possess a cut along the real axis of τ. It can be shown that as a matter of fact this cut does not exist. Indeed, choose the real τ_r so that

$$-V < \tau_r < (1+\rho)\mu^2$$

and assume

$$\begin{aligned} &\tau = \tau_\pm = \tau_r \pm i\eta, \\ &E = E_\pm = E_r \pm i\eta/2E_r, \qquad \eta > 0; \end{aligned}$$

η is a sufficiently small number. The pairs τ_+, E_+ and τ_-, E_- will be in the

region (3.17) only if, in accord with (3.21), the following inequalities are fulfilled:

$$E_\tau^2-\tfrac{1}{4}\eta^2/E_\tau^2-\tau_\tau-(1-\varepsilon)^2\mathbf{p}^2>0, \qquad E_\tau<M.$$

However, if the points τ, E are in the region (3.17) they will also be in the broader region (3.14) in which the function $\phi(E,\tau)$ is analytic. However, such values of τ will be in the region (3.14) for which $\operatorname{Im}\tau=0$. Therefore, by continuity we have

$$\lim_{\eta\to 0}\phi(E_\pm,\tau_\pm)=\lim_{\varepsilon\to 0}\phi(E_\tau\pm i\varepsilon,\tau_\tau). \tag{3.22}$$

Using (3.6), the following important relation can be derived:

$$\begin{aligned}\lim_{\eta\to 0}\{\phi(E_+,\tau_+)-\phi(E_-,\tau_-)\}&=\lim_{\substack{\varepsilon\to 0\\ \varepsilon>0}}\{\phi(E_\tau+i\varepsilon,\tau_\tau)-\phi(E_\tau-i\varepsilon,\tau_\tau)\}\\ &=F_1(2E_\tau\sqrt{M^2+\mathbf{p}^2}+\tau_\tau,\tau_\tau)+F_2(-2E_\tau\sqrt{M^2+\mathbf{p}^2}+\tau_\tau,\tau_\tau).\end{aligned} \tag{3.23}$$

Taking into account (2.19) we get

$$\lim_{\eta\to 0}[\phi(E_+,\tau_+)-\phi(E_-,\tau_-)](E_\tau^2-E_\mathbf{p}^2(\tau))=ST(E_\tau,\tau_\tau)(E_\tau^2-E_\mathbf{p}^2(\tau)). \tag{3.24}$$

On the other hand, since E_+,τ_+ and E_-,τ_- enter the region (3.17) one can employ expressions (2.10) and (2.11) for such pairs of points; in the given case these expressions are meaningful and for $\eta\to 0$ tend to the functions $ST^{\mathrm{ret}}(E_\tau,\tau_\tau)$, $ST^{\mathrm{adv}}(E_\tau,\tau_\tau)$.

We thus obtain the following limiting relation:

$$\begin{aligned}\lim_{\eta\to 0}\{S\hat{T}(E_+,\tau_+)-S\hat{T}(E_-,\tau_-)\}&\\ =\{ST^{\mathrm{ret}}(E_\tau,\tau_\tau)-ST^{\mathrm{adv}}(E_\tau,\tau_\tau)\}&=ST(E_\tau,\tau_\tau).\end{aligned} \tag{3.25}$$

Multiplying (3.25) by $(E_\tau^2-E_\mathbf{p}^2(\tau_\tau))$ and combining with (3.24) we obtain

$$\begin{aligned}&(E_\tau^2-E_\mathbf{p}^2(\tau_\tau))\lim_{\eta\to 0}\{S\hat{T}(E_+,\tau_+)-\phi(E_+,\tau_+)\}\\ &=(E_\tau^2-E_\mathbf{p}^2(\tau_\tau))\lim_{\eta\to 0}\{S\hat{T}(E_-,\tau_-)-\phi(E_-,\tau_-)\}.\end{aligned} \tag{3.26}$$

Inasmuch as the pairs of points (E_+,τ_+) and (E_-,τ_-) lie in region (3.17), the functions on both sides in eq. (3.26) will be identical with the polynomial in E. Denoting this polynomial by $P_\tau(E)$ we can rewrite (3.26) as follows:

$$\lim_{\eta\to 0}P_{\tau_+}(E_+)=\lim_{\eta\to 0}P_{\tau_-}(E_-) \tag{3.27}$$

or by continuity

$$\lim_{\eta\to 0}P_{\tau_+}(E_\tau)=\lim_{\eta\to 0}P_{\tau_-}(E_\tau). \tag{3.28}$$

But this signifies that the function $P_\tau(E)$ is continuous when τ passes across the real axis. Since $P_\tau(E)$ is an analytic function of τ above and below the real axis it will also be an analytic function for points on the real

axis, that is, no cuts will exist. Functions $A(\tau, \not{p})$, $B(\tau, \not{p})$ and $C(\tau, \not{p}, E_0)$ will therefore be analytic in the region

$$-V < \mathrm{Re}\,\tau < (1+\rho)\mu^2, \qquad |\mathrm{Im}\,\tau| < \rho\mu^2.$$

But this means that the last three terms in the dispersion relations (2.24) are analytic functions of τ and E in the region

$$\mathrm{Re}\,\tau < (1+\rho)\mu^2, \qquad |\mathrm{Im}\,\tau| < \rho\mu^2, \qquad \mathrm{Im}\,E \neq 0. \tag{3.29}$$

Since $\phi(E, \tau)$ is analytic in region (3.14) the whole right hand side of the dispersion relations (2.24) will also be an analytic function in the region (3.14). We can therefore extend the region in which the function $S\tilde{T}(E, \tau)$ is defined so that it coincides with the right hand part throughout the entire region (3.14). However, since the point $\tau = \mu^2$ which is of interest to us is in the region (3.14) the dispersion relations (2.24) will also be valid for

$$\begin{aligned} &ST(E, \mu^2) \\ &= \frac{(E-E_0)}{2\pi i}\int_{-\infty}^{+\infty} \frac{F_1(2E'\sqrt{M^2+\mathbf{p}^2}+\mu^2, \mu^2)+F_2(-2E'\sqrt{M^2+\mathbf{p}^2}+\mu^2, \mu^2)}{(E'-E)(E'-E_0)^{n+1}}\,dE' \\ &-\left(\frac{E_0-E}{E_0+E_p}\right)^{n+1}\frac{SA(\not{p}, \mu^2)}{(E_p+E)}-\left(\frac{E-E_0}{E_p-E_0}\right)^{n+1}\frac{SB(\not{p}, \mu^2)}{E_p-E} \\ &+\sum_{0\leq r\leq n} C_r(\mu^2, \not{p}, E_0)E^r. \end{aligned} \tag{3.30}$$

It should be noted that the expression

$$F_1(2E\sqrt{M^2+\mathbf{p}^2}+\mu^2, \mu^2)+F_2(-2E\sqrt{M^2+\mathbf{p}^2}+\mu^2, \mu^2)$$

which replaces $sf(E, \mu^2)$ is identical with the latter in the region

$$E \geqq E_t$$

(E_t is the threshold energy) and is its analytic continuation to the region

$$E_c \leqq E \leqq E_t$$

in which a direct definition of function $sf(E, \mu^2)$ in terms of the integral (2.13) would be meaningless.

In order to go over to real values of E we put $E = E_r+i\varepsilon$ and let ε approach zero. Taking into account that for the extended function $S\tilde{T}(E, \tau)$ the following limiting relations hold:

$$\lim_{\varepsilon\to 0} S\tilde{T}(E\pm i\varepsilon, \tau) = ST^{\mathrm{adv}}_{\mathrm{ret}}(E, \tau), \tag{3.31}$$

we obtain

$$ST^{\substack{\text{ret}\\ \text{adv}}}(E,\mu^2) = \pm\tfrac{1}{2}ST(E^2,\mu^2) + \frac{(E-E_0)^{n+1}}{2\pi i}\,\mathrm{P}\int_{-\infty}^{\infty}\frac{sf(E',\mu^2)}{(E'-E)(E'-E_0)^{n+1}}\,\mathrm{d}E'$$
$$-\left(\frac{E_0-E}{E_0+E_p}\right)^{n+1}\frac{SA(p,\mu^2)}{E_p+E} + \left(\frac{E-E_0}{E_p-E_0}\right)^{n+1}\frac{SB(p,\mu^2)}{E-E_p} \qquad (3.32)$$
$$+\sum_{0\le r\le n} C_r(\mu^2,p,E_0)E^r.$$

The Hermitian and anti-Hermitian parts of the process amplitude are defined by the following relations:

$$D_{\alpha,\omega}(E) = \tfrac{1}{2}(T^{\text{ret}}_{\alpha,\omega}(E)+T^{\text{adv}}_{\alpha,\omega}(E)),$$
$$A_{\alpha,\omega}(E) = \frac{1}{2i}(T^{\text{ret}}_{\alpha,\omega}(E)-T^{\text{adv}}_{\alpha,\omega}(E)). \qquad (3.33)$$

Dispersion relations connecting the Hermitian and anti-Hermitian parts of the process amplitude can easily be obtained with aid of (3.32) and (3.33):

$$SD_{\alpha\omega}(E) = \frac{(E-E_0)^{n+1}}{\pi}\,\mathrm{P}\int_{-\infty}^{\infty}\frac{SA_{\alpha,\omega}(E')\mathrm{d}E'}{(E'-E)(E'-E_0)^{n+1}}$$
$$-\left(\frac{E_0-E}{E_0+E_p}\right)^{n+1}\frac{SA(\mu^2,p)}{E+E_p} + \left(\frac{E-E_0}{E_p-E_0}\right)^{n+1}\frac{SB(\mu^2,p)}{E-E_p} \qquad (3.34)$$
$$+\sum_{0\le r\le n} C_r(\mu^2,p,E_0)E^r.$$

It should be noted that

$$SA_{\alpha,\omega}(E) = 0, \qquad |E| < E_0.$$

The negative energy region in the dispersion relations (3.34) can be excluded if the following symmetry property of A is employed:

$$A_{\alpha,\omega}(E) = -P_{ss'}A_{\alpha,\omega}(-E);$$

$P_{ss'}$ is the nucleon spin state interchange operator.

It should be mentioned that the analysis of the terms $SA(p,\tau)$ and $SB(p,\tau)$ is similar to the analysis of the single-nucleon terms in the Compton effect dispersion relations [3,6]).

In conclusion I take the opportunity to express my deep appreciation to Academician N. N. Bogolubov for valuable discussions.

References

1) A. A. Logunov, Doklady Akad. Nauk SSSR **117** (1957) 792
2) A. A. Logunov and L. D. Solovyov, Nuclear Physics **10** (1959) 60
3) N. N. Bogolubov, Report at International Conference on Theoretical Physics, Seattle (1956);
N. N. Bogolubov and D. V. Shirkov, Introduction to the Theory of Quantized Fields (Gostekhizdat, 1957);
N. N. Bogolubov, B. V. Medvedev and M. K. Polivanov, Problems Encountered in the Theory of Dispersion Relations (Gostekhizdat, 1958)
4) A. A. Logunov, L. D. Solovyov and A. N. Tavkhelidze, Nuclear Physics **4** (1957) 427
5) A. A. Logunov, Scientific Reports of Higher School (in print)
6) A. A. Logunov and P. S. Isayev, Nuovo Cimento (in print)
7) V. S. Vladimirov and A. A. Logunov, report 260 of JINR (Joint Institute for Nuclear Research) (1958)

4.E *Nuclear Physics* **10** (1959) 82—89; © *North-Holland Publishing Co., Amsterdam*
Not to be reproduced by photoprint or microfilm without written permission from the publisher

ON THE HALF-LIFE OF Tl^{204}

RICHARD W. FINK
University of Arkansas †
and
BEROL L. ROBINSON
Western Reserve University ††

Received 15 November 1958

Abstract: Samples of Tl^{204} produced in different irradiations and of varying ages were counted in an end-window methane-flow beta-proportional counter for a period of 1.4 years. The decay curves for these samples are identical, and the average value of the half-life is 3.78 ± 0.04 years. Intercomparison of the ratio of K X-rays to beta-bremsstrahlung and of L X-rays to beta-bremsstrahlung between young (few months) and aged (6 years) reactor-produced, high specific activity solutions of Tl^{204} exhibited no differences which might arise from the presence of a long-lived isomeric state in thallium. Previous results are summarized.

1. Introduction

This work originated in an attempt to understand the discrepant values reported by various investigators for the half-life of Tl^{204}, as shown in table 1 (items a, d, e, f, g, h and i). Although it was by no means clear, it seemed that the half-life might be correlated with the method of activation or with the age of the sample. This led us to suspect isomerism, and the experiments described here were undertaken in an effort to evaluate this possibility. Since this work was begun, additional measurements have come to our attention, table 1 (items b, c, j, k, l and m), mostly indicating a half-life close to four years, which is confirmed by the study reported here.

Samples of Tl^{204} were produced in four different irradiations, chemically purified, mounted in a uniform fashion, and counted for a period of 1.4 years in an end-window methane-flow beta-proportional counter used for routine laboratory counting. The counter was expected to be at least stable enough to detect changes in the ratios of the activities, and in fact it turned out to be stable enough to give reliable decay constants, as judged by the internal consistency of the results. In view of its small resolving time, statistically significant data can be accumulated in short counting periods, while avoiding the uncertainties associated with dead-time corrections.

† Supported in part by the National Science Foundation and the Atomic Energy Commission.

†† Supported in part by the U.S. Air Force through the Air Force Office of Scientific Research, Air Research and Development Command.

TABLE 1

Half-life reports of thallium-204

Item	Ref.	Half-life (years)	Experimental Technique	Length of study	Age at start of study	Method of activation; comments
a	[4]	2.7	G.-M. and 4π prop. counters. Assay and reassay	15 months		(n, γ) presumably ORNL reactor
b	[5]	3.56±0.05	4π proportional counter Assay and reassay	4.5 years 3 years	2 years fresh	(n, γ) Chalk River, NRX reactor
c	[6]	4.26±0.06	Differential ionization chamber	45 days	2 years	(n, γ) USAEC, HSA*
d	[7]	2.50±0.03	Ionization chamber and Wulf electrometer	10 years		(d, p) Ohio State University cyclotron
e	[8]	3.5 ±0.5	G.-M. counters	9 months	fresh	(d, p) University of Michigan cyclotron
f	[†]	2.7		18 months		Continued study of (e); see (j)
g	[9, 12]	2.71±0.05	Type TQQ electrometer	8 months	fresh	(n, γ) Harwell thermal reactor; see (l) below
h	[10]	4.0 ±0.1	Methane-flow proportional counter	2.9 years	2.2 years	(n, γ) ORNL, HSA*
i	[11] [††]	4.1 ±0.1	Lauritsen electroscope	3.4 years	1.2 years	(n, γ) ORNL reactor
j	[†]	3.9 to 4.4	G.-M. counters			Re-analysis of data of (e) and (f)
k	[12]	mixture of 4.5 ±0.5 and 1.6 ±0.3		3 years		Continued study of (g) above.
l	[13]	3.97±0.05	4π proportional counter	3 years		
m	[14]	4.11±0.13	Ioniz. chamber with Wulf electrometer	6.3 years		
n	Present work	3.78±0.04	End-window methane-flow proportional counter	1.4 years		See table 2

* HSA refers to the high specific activity thallium-204 stock item available from Radioisotope Sales Department, Oak Ridge National Laboratory.

† Hollander, Perlman, and Seaborg, Revs. Mod. Phys. **25** (1953) 469, entry 3V45 — "A. F. Voigt, private communication to G. T. Seaborg (January, 1945)." In a private communication (October 1955), Dr. Voigt has identified the samples used for this value as being the same University of Michigan samples, counted for a more extended period. He now feels that this value is unreliable because of instrument failure, and that a re-evaluation of the valid data by the methods of least squares gives values of 3.9 to 4.4 years.

†† In a private communication (October 1955) Dr. Voigt informed us of the origin and age of the radiothallium used in this experiment.

2. Irradiations

(I) A sample of very pure thallium metal wire (Johnson, Matthey and Company, Ltd., Cat. No. JM-400) was clamped to the water cooled target plate of the Washington University Cyclotron, and irradiated in an atmosphere of helium with 250 microampere hours of 9.1 MeV deuterons. Part of this sample was mounted and counted directly and the rest was radiochemically purified specifically from Hg^{203} which was found to be present, probably due to an (n, p) reaction on Tl^{203} arising from secondary neutrons. With 200 mg of Hg^{++} holdback carrier added to a 6*N* HNO_3 solution of the thallium target wire, 30 % H_2O_2 was added and the solution boiled to oxidize the thallium to the Tl(III) state, the excess peroxide being expelled by further boiling. The solution was then evaporated several times with HCl to expel NHO_3, and finally diluted to 6*N* HCl concentration. Diisopropyl ether, freshly pre-equilibrated with 6*N* HCl, was used to extract the Tl(III) exhaustively from the aqueous substrate. After washing the organic fraction several times with 6*N* HCl containing Hg^{++} carrier, the ether fraction was mounted directly. This procedure effects a very clean separation of thallium from mercury and bismuth, but not from gold.

These low specific activity samples were prepared in March, 1955, and were 1.4 years old at the beginning of the counting period. They are designated Tl(d, p).

(II) A sample of high specific activity processed radiothallium stock solution was obtained from the Oak Ridge National Laboratory. This has been produced by irradiating reagent-grade thallium nitrate in the Oak Ridge reactor for twelve months, from April, 1950, to April, 1951, and was six years old at the beginning of the counting experiment. This sample is designated Tl(HSA).

(III) A sample of reagent grade thallium nitrate was irradiated in the ORNL high-flux reactor (LITR) for four weeks in November, 1955, and was 0.8 years old at the beginning of the experiment. This activity is designated Tl(LITR).

(IV) A standard irradiation unit was obtained from the Oak Ridge National Laboratory in February, 1956, and was 6 months old at the beginning of the experiment. This activity is designated Tl(4*N*). When fresh it exhibited the 12 day Tl^{202}(430 keV gamma) arising from the Tl^{203}(n, 2n) reaction, but no half-life intermediate between 12 days and about 4 years was discernible.

3. Counting

The counting system has a dead time of about 5 microseconds, and in the experiments described here dead-time losses did not exceed 0.8 %; in view of the small changes in the counting rates during the course of the experi-

ment, counting losses due to dead time were ignored. At least 400 000 events were counted at each point in order to assure adequate statistical significance but observed counting rates fluctuated in a random fashion some one or two percent from the decay curve fitted by least squares.

The thallium samples were counted successively for ten minute periods over an interval of 1.4 years, from August, 1956, to January, 1958. The data were reduced by the method of least squares [1]), yielding the values shown in table 2. The errors given in table 2 were determined solely from the scatter of the data [2]).

TABLE 2

Half-lives of four samples of radiothallium from least squares analysis

Sample[a]	Age at start of experiment (years)	Half-life (years)
Tl(d, p)	1.4	3.752 ± 0.049
Tl(HSA)	6	3.774 ± 0.043
Tl(LITR)	0.8	3.832 ± 0.033
Tl(4N)	few days	3.751 ± 0.034
Average		3.78 ± 0.04

[a] These samples are identified in the text.

Because the half-life discrepancy seemed to suggest the existence of a long-lived isomeric state in thallium, we undertook a set of experiments † to determine if there were a change in the K and LX-ray intensities relative to the beta intensity (a) with the age of pile-irradiated thallium, and (b) between pile-irradiated and deuteron-bombarded thallium. It was necessary to use very dilute solutions of high specific activity Tl^{204} as sources in order to avoid fluorescent-excitation of X-rays by the much more intense beta-radiation. For this reason, experiment (b) failed when we were unable to obtain sufficiently high specific activity in the cyclotron-produced material.

An intercomparison of solutions of Tl(HSA) and Tl(LITR) for the ratio of KX-rays to beta-bremsstrahlung, using an NaI(Tl) scintillation spectrometer, and LX-rays to beta-bremsstrahlung, using an argon-methane gas proportional counter [3]), showed no difference in liquid solutions having the same concentration of thallium solids (in the region below 10^{-4} molar). From this result, it is clear that there is no half-life discrepancy between young (few months) and old (6 years) reactor-produced Tl^{204}, after the initial decay of 12-day Tl^{202} which arises from the (n, 2n) reaction.

† We are indebted to Mr. M. K. RamaSwamy for preliminary work on these experiments.

4. Conclusions

It seems established that the half-life of Tl^{204}, regardless of the method of activation or the age of the sample, lies close to 4 years. The measurements reported here give a mean value of

$$T_{\frac{1}{2}} = 3.78 \pm 0.04 \text{ years.}$$

Furthermore, the experimental evidence shows that a long-lived isomeric state which could give rise to K or LX-rays is not produced in reactor-activated thallium.

The shorter half-life values obtained by the method of assay-and-re-assay [4,5]) † indicate that the solutions assayed were unstable, perhaps under the influence of beta-irradiation. It is more difficult to assess the origin of the discrepant value obtained using the differential ionization chamber [6]), except for the remote possibility that 6.7 year $Ra^{228}(MsTh_1)$ may have been present in some of the radium samples used as standards. The work of Cheng *et al.* [7]) remains an enigma.

The internal consistency of the present data, as revealed by the small uncertainty in the half-life, leads one to conclude that the end-window methane-flow beta-proportional counter is a stable instrument, well suited to long-term counting experiments of this nature. It would nonetheless be of interest to attempt to define and eliminate the sources of counting rate fluctuations of this instrument, which are ten times larger than expected statistical fluctuations and which seem to be random.

We are indebted to the following for correspondence and encouragement: Dr. Cheng Lin Sheng, Dr. A. F. Voigt, Dr. R. H. Thomas, Dr. B. H. Ketelle, Dr. G. Harbottle, and Dr. W. B. Mann; and to Dr. S. Katcoff for an enlightening conversation. Mr. Karl Dietrich Neubert and Mrs. Margery Ratner performed the least squares calculations. Mr. Alex Poularikas assisted with the counting of the samples.

† The half-life report in ref. [4]) appears in a paragraph devoted to the question of the long-term stability of very dilute solutions. The agreement of the apparent half-life with the then-accepted value was taken as an indication that the solution was indeed stable.

References

1) A. G. Worthing and J. Geffner, Treatment of Experimental Data (John Wiley and Sons, New York, 1943) p. 240 ff
2) Ref. [1]), p. 249
3) H. Schmied and R. W. Fink, Phys. Rev. **107** (1957) 1062
4) S. A. Reynolds and W. A. Brooksbank, Jr., Nucleonics **11**, no. 11 (1953) 46
5) Merritt, Campion and Hawkings, Canadian J. Phys. **35** (1957) 16
6) J. Tobailem and J. Robert, J. de phys. **16** (1955) 340

7) Cheng, Ridolfo, Pool and Kundu, Phys. Rev. **98** (1955) 231;
also L. S. Cheng, private communication (November 1955)
8) K. Fajans and A. F. Voigt, Phys. Rev. **60** (1941) 619
9) E. E. Lockett and R. H. Thomas, Nucleonics **11**, no. 3 (1953) 14
10) G. Harbottle, Phys. Rev. **91** (1953) 1234
11) D. L. Horrocks and A. F. Voigt, Phys. Rev. **95** (1954) 1205
12) R. H. Thomas, private communication (September 1955);
E. E. Lockett and R. H. Thomas, Nucleonics **14**, no. 11 (1956) 127
13) H. H. Seliger and L. M. Cavallo;
private communication from Dr. W. B. Mann (October 1958)
14) J. E. Edwards, J. Inorg. Nuclear Chem. (to be published);
private communication (September 1958)

2.B *Nuclear Physics* **10** (1959) 88—91; © *North-Holland Publishing Co., Amsterdam*
Not to be reproduced by photoprint or microfilm without written permission from the publisher

CIRCULAR POLARIZATION OF GAMMA RAYS FOLLOWING THE EMISSION OF POLARIZED HEAVY PARTICLES

J. ZIMÁNYI
Central Research Institute of Physics, Budapest

Received 4 November 1958

Abstract: The circular polarization of gamma rays following the emission of heavy particles has been calculated. It has been found that the circular polarization of gamma rays is proportional to the polarization of the emitted heavy particles. Correlation between the two polarizations can be expressed by known functions of essentially geometrical nature.

1. Introduction

In recent years the study of the polarization of scattered particles and of particles produced in various nuclear reactions has increasingly gained in interest [1]).

In the following we propose a new method for the determination of the polarization of inelastically scattered particles and particles produced in nuclear reactions.

Let us consider the following type of reactions:

$$A+a \rightarrow C \rightarrow B^*+b \rightarrow B+b+\gamma, \qquad (1)$$

where A is the target nucleus, C the compound nucleus, B* and B are residual nuclei before and after γ-quantum emission, respectively, a is the bombarding particle and b the particle emitted in the reaction. If in this process particles b are polarized, then the residual nuclei B* have also to be polarized and consequently the γ-quanta emitted by them in certain directions will be circularly polarized, the circular polarization of these γ-quanta being unambiguously correlated with the polarization of particles b.

Thus by measuring the circular polarization of those γ-quanta which are in coincidence with the particles b, we may draw conclusions as to the polarization of the latter.

2. Calculations

It is convenient to perform the calculations by means of efficiency and density tensors. In the following we shall use the symbols applied by S. Devons and L. J. B. Goldfarb in their Encyclopedia article [2]).

Let us denote the nuclear spins of A, C, B* and B by j_0, $j_1 j'_1$, $j_2 j'_2$, j_3; L_1, l_1, M_1 are angular momenta and parity quantum numbers of particle a;

L_2, l_2, M_2 those of particle b and L_3, π_3, M_3 refer to the γ-quantum. The process described in (1) can be represented as follows:

$$j_0 m_0 \xrightarrow{L_1 l_1 M_1} j_1 m_1 \xrightarrow{L_2 l_2 M_2} j_2 m_2 \xrightarrow{L_3 \pi_3 M_3} j_3 m_3 . \tag{2}$$

The correlation in question is given by

$$W = \sum_{\substack{k_1 \kappa_1 \\ F F'}} \rho_{k_1 \kappa_1}(j_1 j'_1) \varepsilon^*_{k_1 \kappa_1}(j_1 j'_1), \tag{3}$$

where $\rho_{k_1 \kappa_1}(j_1 j'_1)$ is the density tensor of the system and $\varepsilon_{k_1 \kappa_1}(j_1 j'_1)$ is the efficiency tensor of the measuring apparatus. Summation over F, F' means summing over $j_1 j'_1 j_2 j'_2 L_1 L'_1 l_1 l'_1 L_2 L'_2 l_2 l'_2 L_3 L'_3 \pi_3 \pi'_3$. $\rho_{k_1 \kappa_1}(j_1 j'_1)$ is defined by

$$\rho_{k_1 \kappa_1}(j_1 j'_1) = \sum_{m_1 m'_1} (-1)^{j'_1 - m'_1} (j_1 j'_1 m_1 - m'_1 | k_1 \kappa_1) \langle j_1 m_1 F | \rho_t | j'_1 m'_1 F' \rangle, \tag{4}$$

where $\langle | \rho_t | \rangle$ is the density matrix of the system after the process. $\varepsilon_{k_1 \kappa_1}(j_1 j'_1)$ may be expressed similarly by means of the efficiency matrices. After some calculation we obtain from (4) the following density tensor:

$$\rho_{k_1 \kappa_1}(j_1 j'_1) = Q_{AB} (-1)^{j_0 - j'_1 - L_1 + k_1} \frac{\hat{j}_1 \hat{j}'_1}{\hat{j}_0^2} W(j_1 j'_1 L_1 L'_1, k_1 j_0) \rho_{k_1 \kappa_1}(L_1 L'_1), \tag{5}$$

where

$$Q_{AB} = (j_3 || L_3 || j_2)(j_2 || L_2 || j_1)(j_0 || L_1 || j_1)(j_3 || L'_3 || j'_2)^* (j'_2 || L'_2 || j'_1)^* (j_0 || L'_1 || j'_1)^*, \tag{6}$$

$$\rho_{k_1 \kappa_1}(L_1 L'_1) = \sum_{\kappa'_1} C_{k_1 \kappa'_1}(L_1 L'_1) D^{k_1}_{\kappa_1 \kappa'_1}(\mathbf{R}) \tag{7}$$

$(j_3 || L_3 || j_2)$ etc. are symbols for the reduced matrix elements in the corresponding processes. The symbol $\hat{j}$ is used as an abbreviation for $\hat{j} \equiv \sqrt{(2j+1)}$. $\mathbf{R}_1$ denotes the rotation by which the quantization axis is turned into the direction of the bombarding beam and $C_{k_1 \kappa_1}(L_1 L'_1)$ is the particle parameter of the particles contained in the incident beam:

$$C_{k\kappa}(LL') = \sum_{\substack{\sigma \sigma' \\ \mu \mu'}} (-1)^{L' - \mu'} (LL' \mu - \mu' | k \kappa) \langle 0 \sigma | L l \mu \rangle^* \langle 0 \sigma' | L' l' \mu' \rangle \langle \sigma | \varepsilon | \sigma' \rangle. \tag{8}$$

By a somewhat lengthy but simple calculation it is found that the efficiency tensor is given by

$$\varepsilon_{k_1 \kappa_1}(j_1 j'_1) = \sum_{\substack{k_2 \kappa_2 \\ k_3 \kappa_3}} (-1)^{j_3 - j'_3 - L_3 + k_3} \hat{k}_2 \hat{k}_3 \hat{j}_1 \hat{j}'_1 \hat{j}_2 \hat{j}'_2 \varepsilon^*_{k_2 \kappa_2}(L_2 L'_2) \varepsilon^*_{k_3 \kappa_3}(L_3 L'_3)$$

$$\times (k_3 k_2 \kappa_3 \kappa_2 | k_1 \kappa_1) W(j_2 j'_2 L_3 L'_3;\ k_3 j_3) \begin{Bmatrix} j_2 j'_2 k_3 \\ L_2 L'_2 k_2 \\ j_1 j'_1 k_1 \end{Bmatrix}. \tag{9}$$

The definition of $\varepsilon_{k_2 \kappa_2}(L_2 L'_2)$ and $\varepsilon_{k_3 \kappa_3}(L_3 L'_3)$ is similar to that given by (7) for $\rho_{k_1 \kappa_1}(L_1 L'_1)$. The last factor is Wigner's symbol; for its definition see ref. [1]). By substituting (9) and (5) into (3), the correlation is found to be

$$W = \sum Q_{AB}(-1)^{j_0+j_3-j'_1-j'_2-L_1-L_3+k_1+k_3} \frac{\hat{j}_1^2 \hat{j}'^2_1 \hat{j}_2 \hat{j}''_2}{\hat{j}_0^2} \hat{k}_2 \hat{k}_3 \rho_{k_1\kappa_1}(L_1L'_1)\varepsilon^*_{k_2\kappa_2}(L_2L'_2)\varepsilon^*_{k_3\kappa_3}(L_3L'_3)$$

$$\times (k_3k_2\kappa_3\kappa_2|k_1\kappa_1)W(j_1j'_1L_1L'_1; k_1j_0)W(j_2j'_2L_3L'_3; k_3j_3)\begin{Bmatrix} j_2 j'_2 k_3 \\ L_2L'_2k_2 \\ j_1j'_1k_1 \end{Bmatrix}. \qquad (10)$$

Here the sum is to be extended over $k_1k_2k_3\kappa_1\kappa_2\kappa_3j_1j'_1L_1L'_1l_1l'_1j_2j'_2$ $L_2L'_2\ l_2l'_2L_3L'_3\pi_3\pi'_3$.

Now, let us suppose that the direction of the quantization axis coincides with that of the incident beam, i.e. $\mathbf{R}_1 = 0$, and further that the incident beam is unpolarized; let the experimental arrangement be such that the polarization of particles b is not measured, whereas the circular polarization of the γ-quanta is being measured. If we express now $\rho_{k_1\kappa_1}(L_1L'_1)$, $\varepsilon_{k_2\kappa_2}(L_2L'_2)$, $\varepsilon_{k_3\kappa_3}(L_3L'_3)$ by means of the particle parameters, we obtain from (10) the following expression:

$$W = \sum Q_{AB}(-1)^{j_0+j_3-j'_1-j'_2-L_1-L_3+k_1+k_3} \frac{\hat{j}_1^2 \hat{j}'^2_1 \hat{j}_2 \hat{j}''_2}{\hat{j}_0^2} \hat{k}_2 \hat{k}_3\, C_{k_10}(L_1L'_1)C_{k_20}(L_2L'_2)C_{k_30}(L_3L'_3)$$

$$\times (k_3k_2\kappa_3\kappa_2|k_10)D^{k_3*}_{\kappa_30}(\mathbf{R}_2)D^{k_3*}_{\kappa_30}(\mathbf{R}_3)$$

$$\times W(j_1j'_1L_1L'_1; k_1j_0)W(j_2j'_2L_3L'_3; k_3j_3)\begin{Bmatrix} j_2j'_2k_3 \\ L_2L'_2k_2 \\ j_1j'_1k_1 \end{Bmatrix}. \qquad (11)$$

Since particle parameters $C_{k0}(LL')$ are real, we have written $C_{k_20}(L_2L'_2)$ $C_{k_30}(L_3L'_3)$ instead of $C^*_{k_20}(L_2L'_2)C^*_{k_30}(L_3L'_3)$. The primed quantum numbers may take on the same values as the unprimed ones. Therefore we may sum by adding to the above formula the expression obtained by interchanging the primed and unprimed quantum numbers. Apart from the sign and the reduced matrix elements the two expressions can be reduced to the same form. By substituting the unprimed quantum numbers for the primed ones and vice versa Q_{AB} becomes its conjugate complex, Q^*_{AB}. Making use of this and by expressing $D^k_{\kappa 0}$ in terms of spherical harmonics, the expression for correlation may be written as

$$W = \sum (-1)^\lambda g C_{k_10}(L_1L'_1)C_{k_20}(L_2L'_2)C'_{k_30}(L_3L'_3)W(j_1j'_1L_1L'_1; k_1j_0)$$

$$\times W(j_2j'_2L_3L'_3; k_3j_3)\begin{Bmatrix} j_2j'_2k_3 \\ L_2L'_2k_2 \\ j_1j'_1k_1 \end{Bmatrix} S_{k_1k_2k_3}(\Omega_2\Omega_3)$$

$$\times \left[\frac{1+(-1)^{k_1+k_2+k_3}}{2}\,\mathrm{Re}\,Q_{AB} + ip_\gamma \frac{1-(-1)^{k_1+k_2+k_3}}{2}\,\mathrm{Im}\,Q_{AB}\right], \qquad (12)$$

where $C'_{k_30}(L_3L'_3)$ is now the particle parameter of the unpolarized γ-beam, from which the parity conservation factor has been omitted. p_γ is equal to $+1$ or to -1 according as the photon spin is parallel or antiparallel to its

momentum, and further

$$S_{k_1k_2k_3}(\Omega_2\Omega_3') = \sum_{\kappa} (k_3k_2\kappa-\kappa|k_10)Y^{-\kappa}_{k_2}(\vartheta_2\varphi_3)Y^{\kappa}_{k_3}(\vartheta_3\varphi_3),$$

$$\lambda = j_0+j_3-j'_1-j''_2-L_1-L_3+k_1+k_3, \tag{13}$$

$$g = \frac{\hat{j}_1^2\hat{j}''^2_1\hat{j}_2\hat{j}''_2}{\hat{j}_0^2}.$$

It has to be noted that $S_{k_1k_2k_3}(\Omega_2\Omega_3)$ is a pure imaginary quantity if the sum $k_1+k_2+k_3$ is odd and a pure real quantity if it is even. Now, let us take into account the fact that the reduced matrix elements of the gamma transitions are real quantities [3]). Then, with the abbreviation $q_{AB\bullet} = (j_2||L_2||j_1)(j_0||L_1||j_1)(j''_2||L'_2||j''_1)^*(j_0||L'_1||j''_1)^*$ the final form for the correlation becomes

$$W = \sum(j_3||L_3||j_2)(j_3||L'_3||j''_2)\,\mathrm{Re}\,q_{AB\bullet}(-1)^{\lambda}gC_{k_10}(L_1L'_1)C_{k_20}(L_2L'_2)C'_{k_30}(L_3L'_3)$$

$$\times W(j_1j''_1L_1L'_1;k_1j_0)W(j_2j''_2L_3L'_3;k_3j_3)\begin{Bmatrix} j_2j''_2k_3 \\ L_2L'_2k_2 \\ j_1j''_1k_1 \end{Bmatrix} \tag{14}$$

$$\times\left[\frac{1+(-1)^{k_1+k_2+k_3}}{2}+ip_{\gamma}\frac{1-(-1)^{k_1+k_2+k_3}}{2}\,\mathrm{tg}\,\varphi_{AB\bullet}\right]S_{k_1k_2k_3}(\Omega_2\Omega_3)$$

with

$$\mathrm{tg}\,\varphi_{AB\bullet} = \frac{\mathrm{Im}\,q_{AB\bullet}}{\mathrm{Re}\,q_{AB\bullet}}. \tag{15}$$

From formula (14) it is seen that the circular polarization of the γ-rays is proportional to the imaginary part of the same reduced matrix elements, or in other words to the tangent of the same phase angle, to which the nucleon polarization is proportional, these proportion factors being known geometrical factors. Thus from the degree of circular polarization of the γ-rays, the polarization of the nucleons b may be determined.

However, it is not necessary to calculate the polarization of particles b, as from the circular polarization of the γ quanta the same conclusions can be drawn as from the polarization of particles b.

The method described above seems suitable to extend polarization studies over fields where the usual methods cannot be applied (e.g. polarization of low energy charged particles). Moreover, by means of our method it is possible to study directly the polarization in a given process, whereas usual methods determine only the joint effect of two polarization processes.

References

1) L. Wolfenstein, Ann. Rev. Nucl. Sci. **6** (1956) 43
2) S. Devons and L. J. B. Goldfarb, Handbuch der Physik, vol. 42
3) L. C. Biedenharn and M. E. Rose, Revs. Mod. Phys. **25** (1953) 729

10.D *Nuclear Physics* **10** (1959) 92 © *North-Holland Publishing Co., Amsterdam*

BOOK REVIEWS

K. B. MATHER and P. SWAN, *Nuclear scattering* (Cambridge University Press 1958. ix—469 p. 80 s.)

This is a very welcome addition to the distinguished series of Cambridge Monographs on Physics. The rather vast subject — whose importance needs no emphasis — is not completely covered, inasmuch as the theoretical treatment based on the optical model and its derivatives is not so thorough as the discussion of simpler processes by more elaborate methods. Slightly less than half of the book is devoted to a very good description of experimental techniques. This is followed by a thorough theoretical analysis of scattering processes of increasing complexity and of their bearing on the problem of nuclear interactions. Thus we have a sequence of chapters on low-energy n-p and p-p scattering, scattering of nucleons by very light nuclei (deuteron to helium), effects of non-central forces, high-energy n-p and p-p scattering and polarization, high-energy scattering of nucleons and deuterons by light nuclei (including an account of stripping reactions), and finally resonance scattering and its description on the optical and statistical models.

The exposition is very detailed, sometimes at the risk of blurring the main features; but on the whole it is quite suitable as an introduction to the subject for advanced students. At the same time, the literature is fully surveyed in a painstaking and reasonably critical fashion, much to the benefit of the specialists, who badly need such a reliable sifting of the accumulated results of the last few years. It should be pointed out, however, that the treatment of high-energy processes is unsatisfactory; not only because it does not include the latest developments concerning the incorporation of the spin-orbit coupling into the phenomenological internucleon potential, but because it does not state sufficiently clearly the nature of the problems involved, nor stress their fundamental importance.

The typography adopted by the Cambridge Press for this book is of exquisite neatness, but how long will it yet take this venerable insular institution to become aware of the simple rules for the setting of symbols and units recommended by the SUN Commission, and followed by progressive continental publishers?

L.R.

Sonderausschuss Radioaktivität (Bundesrepublik Deutschland) Erster Bericht (Januar 1958) (George Thieme Verlag, Stuttgart 1958. 68 p. 4.50 DM)

First report of a German Government Commission on Radioactivity, composed of specialists of the various branches of physics, chemistry, biology, technology and medicine bearing on the problems raised by the increased radioactivity of the biosphere. It contains an account of the distribution and organization of the control stations established in the Federal Republic and of the first measurements, extending over the period October 1956—October 1957. The conclusions, formulated with dry objectivity, imply a serious warning of impending danger if the present situation is allowed to persist.

L.R.

Concerning A. I. AKHIEZER and V. B. BERESTETSKY'S *Quantum Electrodynamics* (this journal **6** (1957) 135) a correspondent points out that another English translation of the same book is available as publication No. AEC-tr-2876 from the Office of Technical Services, United States Department of Commerce, Washington 25, D.C. for only 2.65 dollars.

I. M. FRANK

P. A. ČERENKOV

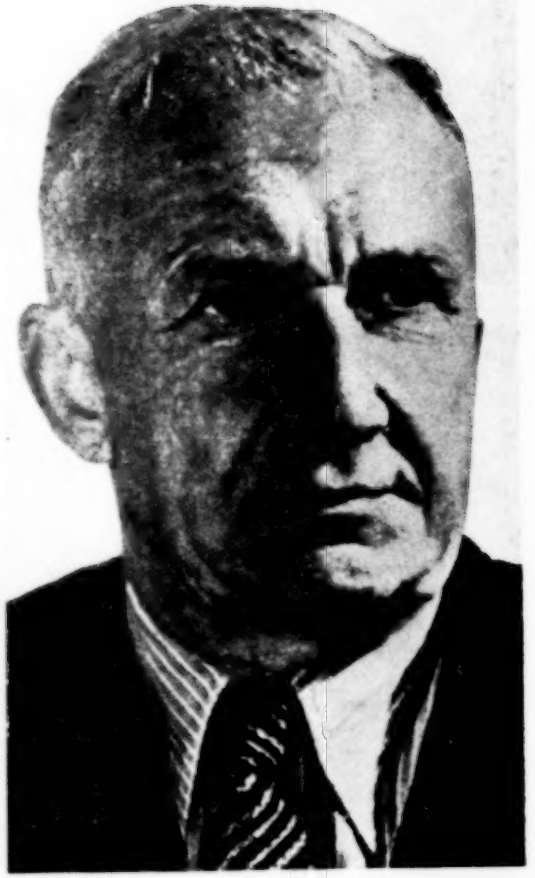

I. E. TAMM

10.A *Nuclear Physics* **10** (1959) 93—95; © *North-Holland Publishing Co., Amsterdam*

NEWS ITEMS

1958 NOBEL PRIZE FOR PHYSICS

The 1958 Nobel Prize for Physics has been awarded to three Soviet physicists, Pavel Alekseyevich Čerenkov, Ilya Mikhailovich Frank and Igor Evgenievich Tamm, for the discovery and explanation of an effect which in the U.S.S.R. is called the Vavilov-Čerenkov effect and in the West simply the Čerenkov effect.

Twenty-four years have passed since Čerenkov discovered the new phenomenon and twenty-one years since Tamm and Frank explained it. It therefore does not seem superfluous to review briefly the history of its discovery.

In 1934 P. A. Čerenkov [1]), working under S. I. Vavilov, had been investigating the luminescence of uranyl salts induced by γ-rays from radium. A strange phenomenon was encountered in these experiments, it being found that not only the salt solutions but even pure liquids weakly glowed when irradiated with γ-rays.

It had long been known that liquids emit light under γ-ray action. Čerenkov's experiments and the analysis of their results by S. I. Vavilov proved that the glow observed by Čerenkov has nothing to do with the possible presence of luminescing impurities in liquids. Thus, for example, light emission was observed in triply distilled water and the intensity of this radiation was the same as that emitted by usual pipe water prior to distillation. Moreover, it was proved that this light emission does not possess one fundamental characteristic sign of luminescence — a finite period of re-emission. Certainly, it was not possible to "quench" the new radiation by introducing in the solution strong fluorescence quenchers such as potassium iodine, silver nitrate or nitro-benzol.

Variation of the concentration of these substances, as well as changes in the temperature of the liquids, did not affect the intensity of the new radiation and already on the basis of Čerenkov's first experiments Vavilov arrived at the conclusion that the radiation could not be identified as luminescence. The first suggestions as to the nature of the new type of light emission were also made by Vavilov. Thus he pointed out [2]) that the light might be emitted by fast electrons ejected from the atoms of the liquid by γ-rays. This idea turned out to be correct. However, the mechanism of emission still remained obscure.

In order to elucidate the main properties of the new radiation P. A. Čerenkov performed a number of difficult and refined experiments. The witticism that all great discoveries are made in the dark can be taken literally in the given case.

Čerenkov, and in some cases Vavilov, carried out *visual* observations. The radiation was very weak and in order to observe it the eye had to be adapted to the dark. The investigator was forced to stay an hour or an hour and a half in the dark before commencing his daily measurements. During this time the sensitivity of the eye increased ten-thousandfold. Only after this could the measurements be started. In this case the photometric method of quenching the luminescence (previously elaborated by Vavilov and Broomberg) was applied; it was the only possible one at that time for measuring such low light intensities. Vision fatigue was so great after two or two and a half hours of such work that it was usually necessary to discontinue in order to avoid errors.

The radiation thus discovered by P. A. Čerenkov in 1934 and now called the Vavilov-Čerenkov radiation was explained by I. E. Tamm and I. M. Frank [3]) in 1937. They showed that the emission is due to electrons moving in a medium with a velocity exceeding the phase velocity of light in that medium. Their calculations involved a detailed theory of the phenomenon and the early as well as subsequent measurements of Čerenkov fully confirmed the theory.

Čerenkov radiation possesses some unique properties which make suitable its widespread

application in high energy physics. A fast particle emitting Čerenkov light "reveals" itself, as it were, to the observer. During recent years a variety of Čerenkov counters have appeared which have been used to study the very different characteristics of fast charged particles such as their velocity, magnitude of electric charge, direction of motion, total energy. Čerenkov velocity selectors have been created and with their aid the antiproton has been discovered. Čerenkov counters are employed in the Soviet Sputniks to record multicharged cosmic ray ions.

The Vavilov-Čerenkov effect is a widespread phenomenon in nature. It is encountered in many domains of physics such as in investigations on the glow of the night sky, of the cosmic radiation air showers, luminescence, plasma physics, radiowave generation on the basis of the Vavilov-Čerenkov effect, polar lights and also in investigations devoted to the development of new methods of particle acceleration.

A few words about the Prize Winners themselves. They are all workers of the P. N. Lebedev Physical Institute of the USSR Academy of Sciences. Two of them (P. A. Čerenkov and I. M. Frank) are pupils of Academician Vavilov whose untimely death was a heavy blow for science and did not permit him to share the present honour with the new Nobel Laureates.

P. A. Čerenkov was born in 1904 into a peasant family of the Voronezh Gubernia. His mother died when he was two years of age. He only graduated from school at the age of 20 since during the time of his studies he had also to work. On leaving school Čerenkov entered Voronezh University, where he graduated in 1928. The following two years were spent in teaching physics in secondary schools in Michurinsk. In 1930 he became a post-graduate student at the Physical Institute of the USSR Academy of Sciences where the worked under S. I. Vavilov. In 1935 he defended his Candidate's dissertation on "The Luminescence of Uranyl Salts Induced by γ-Rays", and in 1940 his Doctor's dissertation which was devoted to the effect now named after him. He has been active in setting up high energy electron accelerators (in particular the 265 MeV accelerator of the P.N. Lebedev Physical Institute of the USSR Academy of Sciences). During recent years Čerenkov has been studying various problems pertaining to photonuclear reactions.

I. M. Frank was born in 1908 in Leningrad. His mother was a doctor in the city hospital and his father a teacher of mathematics (subsequently Professor at the Leningrad Polytechnical Institute). In 1926, after graduating from school, Frank entered Moscow State University. His graduation thesis was carried out under the guidance of Vavilov. After completing his studies at the University Frank worked from 1930 to 1934 at the State Optical Institute in Leningrad. In 1934 he joined the Physical Institute staff. In 1935 he took his doctor's degree with a dissertation on "Elementary Processes in Optical Dissociation". In 1946 Frank was elected a corresponding member of the USSR Academy of Sciences. Frank has been continually studying various aspects of the problem of motion of charged particles in refracting media (Vavilov-Čerenkov effect, Doppler effect, transition radiation). At present he is the head of the Atomic Nucleus Laboratory at the Physical Institute. He is also known for his work on important problems in neutron physics and nuclear physics.

I. E. Tamm is an outstanding theoretical physicist. His work on the theory of metals, the theory of nuclear forces and the interaction between elementary particles, the theory of cascade processes in cosmic rays, and, of course, on the Vavilov-Čerenkov effect have received universal recognition. I. E. Tamm was born in 1895 in Vladivostok. His father was an engineer who took part in the construction of the Ussuriisk railway. In 1898 the family moved to Elizavetgrad where Tamm finished the Gymnasium in 1913. In the same year Tamm entered Edinburgh University where he studied for one year. At the beginning of the war he moved to the Physico-Mathematical Department of Moscow University. After graduation in 1918 he remained at the University to prepare for the teaching profession. From 1919 Tamm began teaching physics in higher schools in Simferopol, Odessa and (from 1922) in Moscow. In 1933 Tamm was elected a corresponding member of the USSR Academy of Sciences and in the next year he was awarded the degree of Doctor of Sciences without submitting a dissertation. Since 1934 Tamm has been working at the Physical Institute of the USSR Academy of Sciences, as head of the Theoretical Department. He was elected a Member of the Academy of Sciences in 1953.

All three Prize Winners are intensely engaged in teaching activities. During several decades I. E. Tamm was head of the Department of Theoretical Physics of Moscow State University, a Department which was essentially created by him. Frank is also a Professor of Moscow

State University and heads the Department of Radioactive Radiation. Čerenkov is a Professor of the Moscow Engineering-Physical Institute.

We extend to the new Nobel Laureates our cordial congratulations and best wishes.

References

1) P. A. Čerenkov, Doklady AN SSSR **2** (1934) 451
2) S. I. Vavilov, Doklady AN SSSR **2** (1934) 457
3) I. E. Tamm and I. M. Frank, Doklady AN SSSR **14** (1937) 107

A detailed bibliography on the Vavilov-Čerenkov effect, including many applications, can be found in T. V. Telley's book Čerenkov Radiation (Pergamon Press, 1958).

INTERNATIONAL CONFERENCE ON HIGH ENERGY ACCELERATORS AND THEIR INSTRUMENTATION

(CERN, Geneva, 1959)

An international conference on high energy accelerators and their instrumentation, sponsored by the International Union of Pure and Applied Physics (IUPAP), will be held at the CERN, Geneva, on the 21—25 September 1959. Participation is by invitation only.

Correspondence should be directed to the CERN Conference Secretariat, Geneva 23, Switzerland.

10.E *Nuclear Physics* **10** (1959) 96; © *North-Holland Publishing Co., Amsterdam*

ERRATA

B. S. Dželepow and N. N. Zhukovsky, On the gamma spectra of Ag^{110}, Sb^{124} and $Eu^{152, 154}$ (Nuclear Physics **6** (1958) 655–668)

1. In fig. 5 (p. 658) the position of the γ transition $h\nu = 1560$ keV is not indicated correctly. This transition takes place between the Cd^{110} excited levels of 2220 and 656 keV energy.

2. On p. 667 (table 4, line 7) two errors were made: a) the value of the relative intensity of the K-conversion line of the 779 keV γ-transition is incorrect; b) an error by an order of magnitude in the experimental value of α_K of this transition has been made. According to ref.[10, 13]) the relative intensity of the K-conversion line of the 779 keV transition should not be 1.5, but 2.5: the experimental value of $\alpha_K \times 10^3$ is 1.48, which corresponds to multipolarity E1.

A. Z. Dolginov and N. P. Popov, First order forbidden $\beta-\gamma$ correlation for oriented nuclei (Nuclear Physics **7** (1958) 591–598).

p. 592, line 14: write $(-1)^{S+g+J+1}$ instead of $(-1)^{S+g}$

p. 593, line 4: write $Z \gg 2A^{\frac{1}{3}}E$ instead of $Z \ll 2A^{\frac{1}{3}}E$

p. 593, eq. (11): write $(-1)^g Z^1_{01}$ instead of Z^1_{01}

p. 594, line 20: write $-3\sqrt{3}Z^1_{11}$ instead of $3\sqrt{3}Z^1_{11}$

Riazuddin, Charge dependent effects on scattering lengths of np and pp systems (Nuclear Physics **7** (1958) 217).

Multiply right-hand side of equation (8) by -4π. The last three terms in expression for M^{pp}_{ss} (eq. (10)) and the middle two terms of $V^{e.m.}_{pp}$ (eq. (11)) should be multiplied by 4π.

In eq. (12) read $\delta(-b_0/a_{pp}) = 0.0138$; in eq. (13) read $-b_0/a'_{pp} = 1.559$.

On page 222, in line 18 change 7 into 11 and in line 19 change $\Lambda = 4M$ to $\Lambda = 2.44M$.

These changes do not affect the conclusions of the paper.

Riazuddin, On the difference of π^0-nucleon and $\pi^\pm$-nucleon coupling constants (Nuclear Physics **7** (1958) 223).

In eq. (1) change + sign before C into − sign. In equation (3) 7 should read 11 and on page 224 change $\Lambda = 4M$ to $\Lambda = 2.44M$. These changes do not affect the conclusions of the paper.

K. V. Laurikainen, Phenomenological two-nucleon potentials and the deuteron (Nuclear Physics **8** (1958) 210).

The numerical values given on the second line of the table (p. 211) and, therefore, the three following lines in the text are not correct. Instead of 6 MeV, 53.5 MeV, and 0.064 the values should read: 32.5 MeV, 40.3 MeV, and 0.333. More exact calculations show also that the LS term proposed by Gammel and Thaler does not change the ground state of the deuteron as much as this rough estimate seems to indicate. A more detailed report will be published later.

8.B *Nuclear Physics* **10** (1959) 97—106; © *North-Holland Publishing Co., Amsterdam*
Not to be reproduced by photoprint or microfilm without written permission from the publisher

ON THE NUMBER OF FUNDAMENTAL FIELDS

W. THIRRING
CERN, *Geneva*
and
Seminar für theoretische Physik, Universität Bern

Received 31 October 1958

Abstract: It is investigated how many fundamental fields are needed to obtain the internal constants of the motion for strong interactions. One finds that with 3 massless Majorana fields one can get all additive constants but for getting also the multiplicative constants one has to double the number of fields. It is demonstrated that the three-field case can be excluded because of the accuracy with which parity conservation is known for strong interactions. The consequences of a γ_5-invariance are studied for the 6-field case. It is shown that in this case either all baryons have mass zero or one gets twice the empirical number of baryons. Furthermore, we find that in this case the vector and the axial vector currents of the strangeness conserving β-interaction are conserved.

1. Introduction

The usual procedure of associating a field with each stable (or metastable) particle can certainly be considered as a phenomenological approach only. If one believes in the simplicity of the fundamental interaction one has to assume that it will contain only a small number of basic fields. The attempt to reduce this number and to consider the observed particles as the low lying excited states of a system of interacting fundamental fields is limited by the observed constants of motion independent of space-time. These constants (like the electric charge) are created by the linear transformations of the basic fields which leave the Lagrangian invariant. If one considers the strong interactions only, there are 5 additive constants of this nature, namely baryon number, isobaric spin and strangeness. Furthermore there is one multiplicative constant, charge conjugation. These constants of the motion obey the same commutation rules as the linear transformations which generate them. Hence the minimum number of independent basic fields equals the rank of the smallest faithful representation of the group defined by these constants.

The linear transformations have in general to belong to the orthogonal group, except for the case of massless spin-$\frac{1}{2}$ fields for which one can admit unitary transformations. In the first section we shall investigate the minimal representation of the invariance group of the strong interactions by orthogonal and unitary matrices. It turns out that the rank of the representation is

February (2) 1959

6 in both cases. If one drops the requirement of C-invariance and insists on CP-invariance only, one can find a unitary representation of rank 3.

This case is considered in detail in the next section, where we study a model of the strongly interacting particles composed of 3 Majorana (or Weyl) fields. The interest for this case arises from the observation by several authors [1]) that the pion-nucleon interaction will automatically conserve C and P separately if we insist on CP-invariance, since parity conservation is not yet completely established for strange particle interactions. Furthermore, a similar model has been recently proposed by Heisenberg. It turns out that parity is violated for pion-nucleon interactions in spite of the CP-invariance since the nucleons are not eigenstates of parity. Although CP-invariance requires that this violation is only of the order μ/M compared with the parity conserving part, this possibility can be ruled out on grounds of existing experimental information.

In the next section we consider the representation with 6 fundamental fields. Taking spinor fields we are led to the well-known Sakata-model. Here we discuss whether the bare mass should be set equal to zero or not. The first possibility has the attractive feature that it implies conservation not only of vector but also of axial vector currents. In particular we shall prove that in the strangeness-conserving β-interaction neither the V or the A part are renormalized, and in the strangeness non-conserving current they are renormalized by the same factor. However, we shall see that in this case either the observable mass of the fermions is zero or there is a degeneracy so that we get twice as many baryons as we want. The latter possibility does not appear to be very likely, so that this suggests that some interaction will reduce the invariance group and thereby introduce a mass. In this case, however, the axial vector currents are not conserved any longer. Thus one is left with the question why we find empirically that the V and A β-interactions have almost the same strength. In some sense the zero mass case seems to be already a good approximation.

2. Representations of the Invariance Group

First we shall briefly review in this section the theory of symmetries not connected with space-time [2]).

Consider a theory with N independent fields ψ_j, each of which represents, in the case of no interaction, only one particle with given space-time characteristics. That is to say, the spin and the momentum of the particle should determine the state uniquely. This means for spin 0 that each field is a hermitian scalar field and the spin-$\frac{1}{2}$ case can be represented equivalently by a Majorana (4-component, hermitian) or a Weyl (2-component) field. We are going to choose Majorana fields since they are somewhat more

familiar. If the Lagrangian L and therefore the commutation rules are invariant under a linear transformation Λ there will be a unitary transformation $U(\Lambda)$ which effects this transformation:

$$U(\Lambda)\psi_j U^{-1}(\Lambda) = \Lambda_{jk}\psi_k. \tag{1}$$

The transformations Λ will form a group and the $U(\Lambda)$ furnish a representation of this group. Since the U leave L invariant, they commute with the 10 generators of the Lorentz group or, loosely speaking, they are constant scalars. For Λ's connected continuously with unity, e.g. $\Lambda = 1+\delta\alpha_r l^r$ with infinitesimal parameters $\delta\alpha_r$ the U can be constructed explicitly:

$$\begin{aligned} U &= 1+i\delta\alpha_r \int \mathrm{d}\sigma_\mu \pi_l{}^\mu(x) l^r_{lm}\psi_m(x) \\ &= 1+i\delta\alpha_r T^r; \end{aligned} \tag{2}$$

$\pi(x)$ is the canonical conjugate field $\delta L/\delta\psi_m(x)$. The invariance of U under the Lorentz transformation assures that for each parameter in the group there is one conserved current

$$j_\mu{}^{(r)} = \pi_l{}^\mu(x) l^r_{lm}\psi_m(x), \qquad \frac{\partial}{\partial x_\mu} j^\mu(x) = 0. \tag{3}$$

There is no conserved current associated with transformations not connected with unity, although they also represent constant scalars. Generally, the U's are multiplicative quantities, whereas the infinitesimal generators T are additive. The Lagrangian will contain the free Lagrangian L_0 which for equal bare masses can always be reduced to a unit quadratic form in the fields:

$$L_0 = \sum_{i=1}^{N} \psi_i D\psi_i, \qquad \psi_i{}^\dagger = \psi_i, \tag{4}$$

where D is some differential operator. This is invariant under the orthogonal group, i.e., $\Lambda^{\mathrm{T}} = \Lambda^{-1}$, $\Lambda^{\mathrm{T}} = \Lambda^\dagger$. A wider invariance group is obtained for spin-$\frac{1}{2}$ fields with zero mass [3]). In this case using the Majorana representation

$$\begin{aligned} &\alpha_0 = i, \qquad \alpha_1 = i\sigma_1, \qquad \alpha_2 = \sigma_2\rho_2, \qquad \alpha_3 = i\sigma_3 \\ &\beta = \sigma_2\rho_3, \qquad j_5 = \rho_2, \end{aligned}$$

we have

$$L_0 = \sum_{n=1}^{N} (\psi_n \alpha^\mu \psi_{n|\mu} - \psi_{n|\mu}\alpha^\mu\psi_n) \tag{5}$$

which is invariant under

$$\Psi \to \mathrm{e}^{(O+i\gamma_5 E)}\,\Psi \tag{6}$$

where O and E are real odd and even $N\times N$ matrices. Thus the invariance group is isomorphic to the unitary group in N dimensions. The total Lagrangian will, in general, have a smaller invariance group, which will, therefore,

be a subgroup of the orthogonal or unitary group respectively. The maximum number of additive constants is $\frac{1}{2}N(N-1)$ or N^2 for spin-$\frac{1}{2}$ and zero mass.

In the strong interactions we have 5 additive conserved quantities of the type of the T^r: baryon number N, isobaric spin $\mathbf{T}$ and displacement of the centre of charge U. They are known to satisfy the following commutation relations:

$$[N, \mathbf{T}]_- = [N, U]_- = [U, \mathbf{T}] = 0, \qquad [T_l, T_m] = i\varepsilon_{lmk} T_k. \tag{7a}$$

There is one multiplicative quantity which we take as the generalized charge conjugation R, which has as commutation properties

$$[R, \mathbf{T}]_- = [R, N]_+ = [R, U]_+ = 0. \tag{7b}$$

The Λ's corresponding to those quantities (which we will denote by small letters) obey the same commutation rules. For our two cases the τ has to be unitary (or real orthogonal), and the n, $\mathbf{t}$ and u, as infinitesimal generators, hermitian (or imaginary antisymmetric). Thus, if we want to find the theory with the least number of fundamental fields which contains those constants of the motion, we have to find matrices of the least rank which satisfy

$$\begin{aligned} &[u, \mathbf{t}]_- = [n, u]_- = [u, \mathbf{t}]_- = [\tau, \mathbf{t}]_- = [\tau, n]_+ = [\tau, u]_+ = 0, \\ &[t_m, t_l] = i\varepsilon_{mlk} t_k, \quad n^\dagger = n, \quad \mathbf{t}^\dagger = \mathbf{t}, \quad u^\dagger = u; \quad \tau^\dagger = \tau^{-1}. \end{aligned} \tag{8}$$

Except for spin-$\frac{1}{2}$ and zero mass we have the additional requirement

$$n^* = -n, \qquad \mathbf{t}^* = -\mathbf{t}, \qquad u^* = -u, \qquad \tau^* = \tau. \tag{9}$$

We start satisfying (8) by remembering that there is one two-dimensional hermitian and one three-dimensional imaginary antisymmetric representation for matrices with the properties of the $\mathbf{t}$'s, namely the Pauli matrices $\boldsymbol{\tau}$ and the $l = 1$ representation $\boldsymbol{\varepsilon}$ with $(j|\varepsilon_l|k) = i\varepsilon_{jlk}$. They will be enough for our purpose. Hermitian matrices commuting with them are multiples of the unit matrix and in order to get two linearly independent matrices n and u commuting with $\mathbf{t}$ we must go at least to $N = 3$. There we can have the representation

$$\mathbf{t} = \begin{array}{|c|c|}\hline \boldsymbol{\tau} & \\ \hline & 0 \\ \hline \end{array}, \quad n = \begin{array}{|ccc|}\hline 1 & & \\ & 1 & \\ & & 1 \\ \hline \end{array}, \quad u = \begin{array}{|ccc|}\hline 1 & & \\ & 1 & \\ & & 0 \\ \hline \end{array}. \tag{10}$$

Thus we can get all additive constants by three massless spin-$\frac{1}{2}$ fields. It is easy to convince oneself that introducing a unitary matrix τ anticommuting with n and u requires a doubling of the number of fields. For instance, one can introduce another set of independent Pauli matrices $\boldsymbol{\rho}$ and represent the

matrices as follows:

$$\mathbf{t}=\begin{array}{|c|c|}\hline \tau & \\ \hline & \\ \hline\end{array}\,,\quad n=\begin{array}{|ccc|}\hline 1 & & \\ & 1 & \\ & & 1 \\ \hline\end{array}\rho_3,\quad u=\begin{array}{|ccc|}\hline 1 & & \\ & 1 & \\ & & 0 \\ \hline\end{array}\rho_3, \tag{11}$$

$$r=\rho_1.$$

There are in fact several inequivalent representations for $N = 6$; one also satisfies (9) as follows:

$$l_1=\begin{array}{|c|c|}\hline \tau_1\rho_2 & \\ \hline & \\ \hline\end{array}\,,\quad l_2=\begin{array}{|c|c|}\hline \tau_2 & \\ \hline & \\ \hline\end{array}\,,\quad l_3=\begin{array}{|c|c|}\hline \tau_3\rho_2 & \\ \hline & \\ \hline\end{array}\,,\quad n=\begin{array}{|ccc|}\hline 1 & & \\ & 1 & \\ & & 1 \\ \hline\end{array}\rho_2 \tag{12}$$

$$u=\begin{array}{|ccc|}\hline 1 & & \\ & 1 & \\ & & 0 \\ \hline\end{array}\rho_2,\quad r=\begin{array}{|c|c|}\hline \tau_2 & \\ \hline & 1 \\ \hline\end{array}\,i\rho_3.$$

Thus to get all constants one must have 6 fields and does not need the case spin-$\frac{1}{2}$, zero mass. One can, for instance, take as basic particles P, $\overline{\text{P}}$, N, $\overline{\text{N}}$, $\Lambda, \bar{\Lambda}$, or $\Lambda, \bar{\Lambda}$, K^+K^0, $\overline{\text{K}}^0\text{K}^-$, the space-time properties then being unessential. Of course, whether such a model will actually lead to the correct masses, parities and spins of the observed particles, is a question far beyond our analysis.

In the next section we shall return to the representation (10) where there is no element R but we shall see that space inversion

$$\Psi(\mathbf{x}, t) \to i\beta\Psi(-\mathbf{x}, t) \tag{13}$$

changes the sign of N. Thus we are able to achieve CP or time-reversal invariance and we shall study whether this is compatible with our knowledge of the pion nucleon interactions. In section 4 we will return to the six-dimensional representations, particularly in view of the renormalization of the β-interaction.

3. The Three-Field Theory

In this model we have three hermitian four-component fields which we denote by P, N, Λ. Sometimes we will use $\mathcal{N}$ for the two fields P, N and Ψ for all three fields P, N, Λ. The free Lagrangian

$$L_0 = \tfrac{1}{2}(\Psi\alpha^u\Psi_{,u} - \Psi_{,u}\alpha^u\Psi), \qquad \Psi^\dagger = \Psi \tag{14}$$

is invariant under a 9-parameter group which we reduce by introducing quadratic interactions as follows:

$$L' = g_1 \mathcal{N} O_i \mathcal{N} \mathcal{N} O_i \mathcal{N} + g_2 \mathcal{N} O_i \tau \mathcal{N} \mathcal{N} O_i \tau \mathcal{N} + g_3 \mathcal{N} O_i \mathcal{N} \Lambda O_i \Lambda + g_4 \Lambda O_i \Lambda \Lambda O_i \Lambda. \tag{15}$$

The O_i are matrices in spin space commuting with γ_5 (e.g. α_i) and g_i real constants. We need not discuss the space-time form of the coupling in detail but list the invariance properties of $L = L_0 + L'$.

It admits the following unitary (or anti-unitary) transformations:

1) Continuous transformations

$$e^{i\alpha_j T_j} \mathcal{N} e^{-i\alpha_j T_j} = e^{i\alpha_j t_j} \mathcal{N} \qquad e^{i\alpha_j T_j} \Lambda e^{-i\alpha_j T_j} = \Lambda, \tag{16}$$

where $\alpha_{0,1,2,3}$ are four real parameters and the $t_{0,1,2,3}$ are the matrices $(j_5, j_5\tau_1, \tau_2, j_5\tau_3)$. For the T_j we find

$$T_j = \int d\sigma_u \mathcal{N} \alpha^u t_j \mathcal{N}; \tag{17}$$

T_0 is to be identified with U, $T_{1,2,3}$ with $\mathbf{T}$; N corresponds to

$$e^{i\alpha N} \Psi e^{-i\alpha N} = e^{i\alpha\gamma_5} \Psi, \qquad N = \int d\sigma_u \Psi \alpha^u \gamma_5 \Psi. \tag{18}$$

It appears that with these identifications we satisfy (7a). There is no transformation independent of space-time corresponding to R.

2) Space reflections

$$R\mathcal{N}(\mathbf{x}, t)R^{-1} = \beta\tau_2 \mathcal{N}(-\mathbf{x}, t), \quad R\Lambda(\mathbf{x}, t)R^{-1} = i\beta\Lambda(-\mathbf{x}, t);$$
$$R'\mathcal{N}R'^{-1} = \mathcal{N}, \quad R'\Lambda(\mathbf{x}, t)R'^{-1} = i\beta\Lambda(-\mathbf{x}, t).$$

There are two independent reflections, R satisfying (7a) and R' satisfying

$$[R', U]_- = [R', \mathbf{T}]_- = [R', R]_- = [R', N-U]_+ = 0. \tag{19}$$

3) Time-reversal

$$K\Psi(\mathbf{x}, t)K^{-1} = \beta\gamma_5 \Psi(\mathbf{x}, -t);$$
$$KNK^{-1} = N, \qquad KUK^{-1} = U; \tag{20}$$
$$KT_{1,3}K^{-1} = T_{1,3}, \qquad KT_2K^{-1} = -T_2.$$

Next we shall investigate one-particle states. We may take them to be eigenstates of N, U, T_3 but of R and R' only in the case of eigenvalue zero for N, U, T_3. Since the baryons are not simultaneous eigenstates of N and R (which induce $\Psi \to i\beta\Psi$ and $\Psi \to i\gamma_5\Psi$) there is no immediate contradiction in assuming that they have a mass $\neq 0$. This point will be further discussed in the next section. We call $U_\pm(0, m)$ the matrix element of Ψ between the vacuum $|0\rangle$ and a particle at rest $|1\rangle$ which is in an eigenstate of N, $N|1_\pm\rangle = \pm|1_\pm\rangle$, $R|1_\pm\rangle = \pm|1_\mp\rangle$:

$$U_\pm(0, m) = \langle 0|\Psi_a(0)|1_\pm\rangle. \tag{21}$$

Hence we have

$$U_\pm = \pm\gamma_5 U_\pm, \qquad U_+ = \beta U_-. \tag{22}$$

By a Lorentz transformation we see that for a state with arbitrary momentum $\mathbf{p}$ the wave functions $U_\pm(\mathbf{p}, p_0)$ satisfy

$$\begin{aligned} &\langle 0|\Psi(0)|p_\pm\rangle = U_\pm(p), \\ &U_\pm(p) \doteq \pm\gamma_5 U_\pm(p), \qquad \alpha_\mu p^\mu U_+ = m\beta U_-. \end{aligned} \tag{23}$$

Applying time-reversal we find $[p_t = (p_0, -\mathbf{p})]$

$$U^*_{t\pm}(p_t) = -U_\pm(p)\beta\gamma_5 \tag{24}$$

where U_t refers to the time-reversed state

$$|p_t\rangle = K|p\rangle, \qquad N|p_{t\pm}\rangle = \pm|p_{t\pm}\rangle. \tag{25}$$

With the aid of these formulae we shall study the general properties of one-particle matrix elements. The formalism [4]) of field theory tells us that these matrix elements of an operator O will be of the form

$$\langle p|O|p'\rangle = U_\alpha{}^*(p)\mathcal{O}_{\alpha\beta}(p, p')U_\beta(p'). \tag{26}$$

If O is hermitian we have

$$\mathcal{O}^*_{\beta\alpha}(p', p) = \mathcal{O}_{\alpha\beta}(p, p') \tag{27}$$

and time-reversal tells us, if $KOK^{-1} = \pm 0$, that

$$\begin{aligned} &\langle p|O|p'\rangle^* = \pm\langle p_t|O|p_t\rangle, \\ &\mathcal{O}(p', p) = \pm\beta\gamma_5\mathcal{O}^*(p'_t, p_t)\beta\gamma_5. \end{aligned} \tag{28}$$

For our purpose the important operator is the source density of the pion field $O_i(x)$. This can be defined as a local operator even if the pion is a compound structure [5]). It will be a vector in isobaric spin space and a scalar with respect to the proper Lorentz group. Under time-reversal it transforms like

$$KO_jK^{-1} = (-)^{j+1}O_j. \tag{29}$$

From Lorentz invariance we can infer that a matrix element of O_i between nucleon states must be of the general structure

$$\langle p_+|\mathbf{O}|p'_+\rangle = U_+{}^*(p)\tau(f_1\alpha_\mu(p-p')^\mu + f_2 i\alpha_\mu(p+p')^\mu)U_+(p'),$$

since $U_+{}^*\beta U_+ = U_+{}^*\beta\sigma_{\mu\nu}U_+ = 0$. Time-reversal eliminates the second of the two functions f_i of $(p-p')^2$:

$$f_2 = \beta\gamma_5 f_2\beta\gamma_5 = -f_2.$$

Hence we have

$$\langle p_+|\mathbf{O}|p'_+\rangle = U_+{}^*(p)\tau\alpha_\mu(p-p')^\mu U_+(p')f_1((p-p')^2). \tag{30}$$

Because of $\gamma_5 U_+ = U_+$ the matrix element equals

$$U_+{}^*[p_0 - p'_0 + \boldsymbol{\sigma}\cdot(\mathbf{p}-\mathbf{p})]U_+. \tag{31}$$

Hence in the static limit we get the usual $\boldsymbol{\sigma}\cdot\nabla$ coupling whereas the f_2-term would have given us a large coupling to s-pions. This has been eliminated by

time-reversal, and for real nucleons the f_1-terms correspond in fact to the usual pseudoscalar vertex. This can be seen by taking those linear combinations of the wave-functions (23) which obey the usual Dirac equation. Expressed in terms of those, (30) can be reduced to the $\gamma_5\phi$(or equivalently the $\gamma_5\gamma^\mu\phi_{,\mu}$) vertex. However, this is not true if one of the nucleons is virtual; hence only the part of the nuclear forces which comes from one-pion exchange conserves parity. The two-pion exchange potential would not conserve parity and it is hard to see how in such a theory parity would be a good quantum number in nuclei to the experimentally known degree. One also finds that for processes $\Lambda \to \pi+\Sigma$ or $\mathrm{p} \to \Lambda+\mathrm{K}$ the f_2-term cannot be excluded, so that a strong parity non-conservation would occur in these processes. Thus, it is safe to say that this possibility is not realized in nature.

4. The Six-Field Theory

We describe this case in the conventional way by three complex fields $\Psi = \mathcal{N}$, $\Lambda(\mathcal{N} \equiv \mathrm{P}, \mathrm{N})$. We first keep the γ_5-invariance and base our investigation on the Lagrangian

$$\begin{aligned} L_0 &= \tfrac{1}{2}(\Psi^\dagger\alpha^\mu\Psi_{,\mu} - \Psi^\dagger_{,\mu}\alpha^\mu\Psi), \\ L' &= g_1\mathcal{N}^\dagger O_i\mathcal{N}\mathcal{N}^\dagger O_i\mathcal{N} + g_2\mathcal{N}^\dagger\tau O_i\mathcal{N}\mathcal{N}^\dagger\tau O_i\mathcal{N} \\ &\quad + g_3\mathcal{N}^\dagger O\mathcal{N}\Lambda^\dagger O\Lambda + g_4\Lambda^\dagger O\Lambda\Lambda^\dagger O\Lambda. \end{aligned} \tag{32}$$

If we take again O_i commuting with γ_5 we get 10 additive constants:

(a) two kinds of $\mathbf{T}$ and U:

$$\mathrm{e}^{i(\alpha_j T_j + \bar\alpha_j \bar T_j)}\mathcal{N}\mathrm{e}^{-i(\alpha_j T_j + \bar\alpha_j \bar T_j)} = \mathrm{e}^{i(\alpha_j + \gamma_5\bar\alpha_j)\tau_j}\mathcal{N}, \qquad \mathrm{e}^{i(\alpha_j T_j + \bar\alpha_j T_j)}\Lambda\mathrm{e}^{-i(\alpha_j T_j + \bar\alpha_j T_j)} = \Lambda,$$

$$T_j = \int \mathrm{d}\sigma_\mu \mathcal{N}^\dagger\alpha^\mu\tau_j\mathcal{N}, \qquad \bar T_j = \int \mathrm{d}\sigma_\mu \mathcal{N}^\dagger\alpha^\mu\gamma_5\tau_j\mathcal{N} \quad (j = 0, 1, 2, 3), \tag{33}$$

$$\tau_0 = 1, \qquad T_0 = U;$$

(b) two kinds of N:

$$\mathrm{e}^{i(\alpha N + \bar\alpha \bar N)}\Psi\mathrm{e}^{-i(\alpha N + \bar\alpha \bar N)} = \mathrm{e}^{i(\alpha + \bar\alpha\gamma_5)}\Psi,$$

$$N = \int \mathrm{d}\sigma_\mu \Psi^\dagger\alpha^\mu\Psi, \qquad \bar N = \int \mathrm{d}\sigma_\mu \Psi^\dagger\alpha^\mu\gamma_5\Psi. \tag{34}$$

N, T_i and $\bar N$, $\bar T_i$ satisfy (7a) and

$$[N, \bar N]_- = [N, \bar T_j]_- = [\bar N, T_j] = [\bar T_i, T_j] = 0. \tag{35}$$

Now we get C and P separately:

$$\begin{aligned} &R\mathcal{N}R^{-1} = \tau_2\mathcal{N}^\dagger, \qquad R\Lambda R^{-1} = \Lambda^\dagger, \\ &[R, N]_+ = [R, \bar N]_+ = [R, T_0]_+ = [R, \bar T_0]_+ = 0, \\ &[R, \mathbf{T}]_- = [R, \bar{\mathbf{T}}]_- = 0, \end{aligned} \tag{36}$$

and

$$P\Psi(\mathbf{x})P^{-1} = i\beta\Psi(-\mathbf{x}),$$
$$[P, N]_- = [P, \bar{N}]_+ = [P, T_i]_- = [P, \bar{T}_i]_+ = 0. \tag{37}$$

Thus the barred constants are pseudoscalars.

We shall now discuss how to characterize one-baryon states. Operators which commute with the Hamiltonian, N, T_3, U and the third component of the spin are

$$P, \bar{N}, \bar{T}_3, \bar{U}. \tag{38}$$

If we assume that the particle has a non-vanishing mass, so that we can bring it to rest, we may have it in an eigenstate of P. However, the relation $[P, \bar{N}]_+ = 0$ shows that in this case there must be at least two different states belonging to the same eigenvalues of the first listed operators. Hence a non-vanishing mass is only possible if there is a degeneracy, and we get a doubling of the number of all particles. Since the other kind of particles have not yet been found, this possibility is rather speculative and we shall assume that there is no degeneracy and that the mass vanishes. On this basis we shall finally discuss matrix elements of the vector and axial vector current.

Since the baryons have now mass zero we can talk about right and left screwed neutron and proton states which we define by ($\bar{N}_{p,n} = \frac{1}{2}(\bar{T}_0 \pm \bar{T}_3)$)

$$e^{i\bar{N}_n\bar{\alpha}}|n_\pm\rangle = e^{\pm i\bar{\alpha}}|n_\pm\rangle, \qquad \langle \pm p|e^{-i\bar{N}_p\bar{\alpha}} = e^{\mp i\bar{\alpha}}\langle \pm p|. \tag{39}$$

Because of

$$\begin{aligned} e^{i\bar{\alpha}\bar{N}_n}(1+\gamma_5)ne^{-i\bar{\alpha}N_n} &= e^{i\bar{\alpha}}(1+\gamma_5)n, \\ e^{i\bar{\alpha}\bar{N}_p}p^\dagger(1+\gamma_5)e^{-i\bar{\alpha}\bar{N}_p} &= e^{-i\bar{\alpha}}p^\dagger(1+\gamma_5), \end{aligned} \tag{40}$$

only the matrix elements $\langle \pm p|p^\dagger(1+\gamma_5)\alpha_\mu|n\pm\rangle$ with $-$states will be different from zero and will be of the form

$$\langle -p|p^\dagger\alpha_\mu(1+\gamma_5)n|n_-\rangle = U_-{}^*(p')\alpha_\mu U_-(p')C((p-p')^2) = U_-{}^*(1,\sigma)U_-C. \tag{41}$$

This shows that the Fermi and Gamow-Teller matrix elements have exactly the same strength. This is not obvious since the conservation of $\bar{T}$ means only that the zero-component of the axial vector current is conserved, whereas the G.T. matrix elements refer to the space components. More generally, we have

$$\langle -p|\mathcal{N}^\dagger\alpha_\mu(1+\gamma_5)\tau\mathcal{N}|n_-\rangle = U_-{}^*\tau\alpha_\mu U_-C \tag{42}$$

and since we are dealing with eigenstates of T we must have $C(0) = 1$, i.e. no renormalization of the V and A part of the strangeness conserving current †. For $p \to \Lambda$ transitions we have by the same argument

† For the vector part, this was pointed out by Okun [7]).

$$\langle -\mathrm{p}|\mathrm{p}^{\dagger}\alpha_{\mu}(1+\gamma_5)\Lambda|\Lambda_-\rangle = U_-^*(1,\sigma)U_-\bar{C}((\not{p}-\not{p}')^2) \qquad (43)$$

but there is no conservation law which assures $\bar{C}(0) = 1$. Thus, all we can say is that for the strangeness non-conserving current the V and A interactions are renormalized by the same factor. This is indicated by the asymmetry in the Λ-decay, so that these facts seem to be realized in nature to a startlingly good approximation. Yet we know that there must be some terms in L which destroy the γ_5-invariance and produce a mass. Somehow they do not change the matrix elements significantly, which may mean that the baryon mass is only a small disturbance compared with a much heavier fundamental mass.

I am indebted to Dr. d'Espagnat for an important remark.

References

1) B. Touschek and Morpurgo (unpublished);
S. Gupta, Can. Jour. Phys. **35** (1957) 1309;
V. G. Soloview, Nuclear Physics **6** (1958) 618
2) W. Thirring, Phys. Rev. **111** (1958) 986;
S. Drell and Frautschi, preprint
3) W. Pauli, Nuovo Cimento **6** (1957) 204;
B. Touschek, Nuovo Cimento **3** (1958) 181;
F. Gürsey, Nuclear Physics **8** (1958) 675
4) H. Lehmann, K. Symanzik and W. Zimmermann, Nuovo Cimento **1** (1955) 205
5) W. Zimmermann, Nuovo Cimento **10** (1958) 597
6) L. Okun, CERN Conference Report (1958)

7.A *Nuclear Physics* **10** (1959) 107—117; © *North-Holland Publishing Co., Amsterdam*
Not to be reproduced by photoprint or microfilm without written permission from the publisher

THE RENORMALIZABILITY OF VECTOR MESON INTERACTIONS

SHELDON L. GLASHOW †
Institute for Theoretical Physics, University of Copenhagen

Received 24 November 1958

Abstract: A new and less restrictive criterion is deduced for the renormalizability of vector meson interactions. As an example, the electromagnetic interaction of a charged vector meson with unit anomalous magnetic moment is shown to be renormalizable. In order to construct a renormalizable theory of the elementary-particle decays in which such a particle plays the role of an intermediary, it is found necessary to assume an intimate connection between decay-inducing and electrodynamic interactions.

1. Kinematical Considerations

Recent advances in the study of elementary-particle decays have encouraged speculation concerning the nature of the interactions responsible for these processes. In particular, the hypothesis of an unstable vector meson whose universal interactions underlie all such decays has recently achieved some favour [1]). Those to whom renormalizability seems a desirable attribute of a quantum-field theory may object to such a theory because of the alleged unrenormalizability of most vector-meson couplings [2]). As a partial answer we shall deduce a new criterion which admits as renormalizable many interactions (among them the electrodynamics of an isolated charged vector field) that have not until now been so regarded. A suggestive connection between this renormalizability criterion and a certain limited symmetry of the Lagrange function may lead us to a renormalizable theory of a charged vector meson with appropriate decay-inducing couplings.

We must first evaluate several Green's functions associated with the propagation of a free vector field. If we are to use the formalism of Schwinger [3]), in which a variational principle yields both field equations and commutation relations, the Lagrange function must contain only first derivatives and therefore we must introduce dynamical variables Z_μ and $Z^{\mu\nu}$ which satisfy first order differential equations. The Lagrange function,

$$L = -\tfrac{1}{2}[\tfrac{1}{2}Z^{\mu\nu}(\partial_\mu Z_\nu - \partial_\nu Z_\mu) - Z_\nu \partial_\mu Z^{\mu\nu} - \tfrac{1}{2}Z^{\mu\nu}Z_{\mu\nu} + M^2 Z^\mu Z_\mu] + [\tfrac{1}{2}m_{\mu\nu}Z^{\mu\nu} - j_\mu Z^\mu], \tag{1.1}$$

† National Science Foundation Post-Doctoral Fellow.

in which M is the mass of the vector meson, includes couplings to an external vector source, j_μ, and to an external antisymmetric-tensor source, $m_{\mu\nu}$. The above form of the tensor coupling is chosen rather than the similar expression, $m^{\mu\nu}(\partial_\mu Z_\nu - \partial_\nu Z_\mu)$, for two reasons After an integration by parts the latter expression becomes identical to the vector coupling of Z_μ to an effective current $\partial_\lambda m^{\lambda\nu}$. Moreover, to include explicit derivatives in the interaction Lagrangian would destroy the canonical form of the commutation relations imp ied by L.

The first order field equations following from (1.1) are

$$\begin{aligned} Z_{\mu\nu} &= \partial_\mu Z_\nu - \partial_\nu Z_\mu + m_{\mu\nu} \\ \partial_\mu Z^{\mu\nu} &= M^2 Z^\nu + j^\nu. \end{aligned} \tag{1.2}$$

These may be combined to form second order equations for Z_μ,

$$(p^2+M^2)Z_\mu = -\left(\delta_\mu^\nu + \frac{p_\mu p^\nu}{M^2}\right) j_\nu + ip^\lambda m_{\lambda\mu}, \tag{1.3a}$$

and for $Z_{\mu\nu}$,

$$(p^2+M^2)Z_{\mu\nu} = -i(p_\mu j_\nu - p_\nu j_\mu) + (p_\mu p^\lambda m_{\lambda\nu} - p_\nu p^\lambda m_{\lambda\mu}) - (p^2+M^2)m_{\mu\nu}. \tag{1.3b}$$

With the connections

$$\mathcal{G}_\nu^\mu(x-x') = \frac{\delta Z^\mu(x)}{\delta j_\nu(x')}, \tag{1.4a}$$

$$\mathcal{G}_\lambda^{\mu\nu}(x-x') = \frac{\delta Z^{\mu\nu}(x)}{\delta j_\lambda(x')} = -\frac{\delta Z_\lambda(x')}{\delta m^{\mu\nu}(x)}, \tag{1.4b}$$

$$\mathcal{G}_{\lambda\sigma}^{\mu\nu}(x-x') = \frac{\delta Z^{\mu\nu}(x)}{\delta m_{\lambda\sigma}(x')}, \tag{1.4c}$$

the vector meson propagators are identified as

$$\mathcal{G}_\nu^\mu = -\left(\delta_\nu^\mu + \frac{p^\mu p_\nu}{M^2}\right)\frac{1}{p^2+M^2}, \tag{1.5a}$$

$$\mathcal{G}_\lambda^{\mu\nu} = -\mathcal{G}_\lambda^{\mu\nu} = -i(p^\mu\delta_\lambda^\nu - p^\nu\delta_\lambda^\mu)\frac{1}{p^2+M^2}, \tag{1.5b}$$

$$\mathcal{G}_{\lambda\sigma}^{\mu\nu} = (p^\mu p_\lambda \delta_\sigma^\nu - p^\mu p_\sigma \delta_\lambda^\nu + p^\nu p_\sigma \delta_\lambda^\mu - p^\nu p_\lambda \delta_\sigma^\mu)\frac{1}{p^2+M^2} - (\delta_\lambda^\mu\delta_\sigma^\nu - \delta_\sigma^\mu\delta_\lambda^\nu). \tag{1.5c}$$

Elimination of the vector meson field from the Lagrange function leads to an induced interaction among the currents to which Z is coupled. For $m^2 \gg -p^2$ the leading terms are $M^{-2}j^\mu j_\mu - m^{\mu\nu}m_{\mu\nu}$ and, consequently, the

vector meson can generate direct A, V and T couplings. More relevantly we note that in the limit of large momenta both (1.5a) and (1.5c) are of order one, while (1.5b) decreases with p^{-1}.

By similar means, the electrodynamic propagators in Lorentz gauge are found to be

$$\mathscr{D}^{\mu}_{\nu} = \delta^{\mu}_{\nu} p^{-2}, \tag{1.6a}$$

$$\mathscr{D}^{\mu\nu}_{\lambda} = -\mathscr{D}^{\mu\nu}_{\lambda} = -i(p^{\nu}\delta^{\mu}_{\lambda} - p^{\mu}\delta^{\nu}_{\lambda})p^{-2}, \tag{1.6b}$$

$$\mathscr{D}^{\mu\nu}_{\lambda\sigma} = (p^{\mu}p_{\lambda}\delta^{\nu}_{\sigma} - p^{\nu}p_{\lambda}\delta^{\mu}_{\sigma} + p^{\nu}p_{\sigma}\delta^{\mu}_{\lambda} - p^{\mu}p_{\sigma}\delta^{\nu}_{\lambda})p^{-2} - (\delta^{\mu}_{\lambda}\delta^{\nu}_{\sigma} - \delta^{\mu}_{\sigma}\delta^{\nu}_{\lambda}). \tag{1.6c}$$

With our choice of tensor coupling, (1.6c) satisfies $\partial_{\mu}\mathscr{D}^{\mu\nu}_{\lambda\sigma} = 0$.

Decomposing Z_{μ} into transverse and longitudinal parts,

$$Z_{\mu} = Z^{t}_{\mu} + \partial_{\mu}\Lambda, \tag{1.7}$$

where

$$\partial^{\mu} Z^{t}_{\mu} = 0,$$

we deduce for the propagators of Z^{t}_{μ} and Λ the expressions

$$\frac{\delta Z^{t}_{\mu}}{\delta j_{\nu}} = \left(\delta_{\mu\nu} - \frac{p_{\mu}p_{\nu}}{M^2}\right)\frac{1}{p^2+M^2}, \tag{1.8a}$$

$$\frac{\delta Z^{t}_{\lambda}}{\delta m^{\mu\nu}} = -\frac{\delta Z^{\mu\nu}}{\delta j_{\lambda}} = -i(p^{\mu}\delta^{\nu}_{\lambda} - p^{\nu}\delta^{\mu}_{\lambda})\frac{1}{p^2+M^2}, \tag{1.8b}$$

$$\frac{\delta\Lambda}{\delta j_{\mu}} = -\frac{p_{\mu}}{M^2 p^2}, \tag{1.9a}$$

$$\frac{\delta\Lambda}{\delta m_{\mu\nu}} = 0. \tag{1.9b}$$

2. Renormalization Criteria

We shall consider the theory of a vector meson interacting with other fields of spin not greater than one. Let the interaction Lagrange function be expressed in terms of Z_{μ} and its explicit derivatives together with those fields to which it is coupled. In the sum

$$L = \sum_{i} g_i L_i(f, b, v, s), \tag{2.1}$$

each term is a product consisting of f factors of a Fermion field, b factors of either a spinless Boson field or the electrodynamic vector potential, v factors of Z_{μ}, and s derivatives $K(F_e, B_e, V_e, \{n_i\})$ is defined as the degree of divergence of a primitive contribution of order $\prod_i (g_i)^{n_i}$ to a transition amplitude characterized by F_e external Fermions, B_e external Bosons or photons and V_e external vector mesons. Thus, a primitive divergence must satisfy $K \geqq 0$. What shall be called the 'conventional renormalizability

criterion' arises if a bound for K is evaluated in the usual manner, that is, if it is assumed that each internally propagated vector meson requires an integration over all momenta, but contributes no compensating factors of momentum from the denominator of its propagator. With the elimination of the parameters counting the numbers of internal lines, this bound is given by

$$K \leqq \bar{K} = 4-\tfrac{3}{2}F_e-2V_e-B_e+\sum_i n_i\,(\tfrac{3}{2}f+2v+b+s-4). \qquad (2.2)$$

This expression is certain to obscure any fortuitous cancellations of the gradient terms of the vector meson propagators that would reduce the value of K actually realized. To ensure that primitive divergencies exist for only a finite number of distinct values of F_e, B_e and V_e (i.e., that the theory is renormalizable), we must demand the inequality

$$n_i(\tfrac{3}{2}f+2v+b+s-4) \leqq 0 \qquad (2.3)$$

for all n_i, and consequently each term of L must satisfy the relation

$$C(L_i) = \tfrac{3}{2}f+2v+b+s \leqq 4. \qquad (2.4)$$

Since $C = 5$ for a 'Yukawa interaction' of the form $Z_\mu\bar{\psi}\gamma^\mu\psi$ and $C = 6$ for the 'minimal' electrodynamic interaction contained within $(\Pi_\mu Z_\nu-\Pi_\nu Z_\mu)^2$, we see that (2.4) is a sufficiently restrictive condition to exclude all local interactions of physical interest.

However, from (1.8) and (1.9) we notice that the difficulties encountered with the renormalization of vector-meson interactions are associated entirely with the singular propagation of the longitudinal mode. The propagator for the transverse part of Z_μ falls off with p^{-2} for large momenta, behaving in this connection identically to propagators of other boson fields. Consequently, for interactions in which only Z_μ^t participates, a sufficient criterion for renormalizability is given by

$$C' = \tfrac{3}{2}f+t+b+s \leqq 4, \qquad (2.5)$$

where t counts the number of factors of Z_μ^t appearing in the interaction. The coupling, $Z_\mu j^\mu$, of a vector meson to a conserved current differs from $Z_\mu^t j^\mu$ only by a total derivative. Thus, such a theory is renormalizable provided only that $C(j_\mu) \leqq 3$, which is easily fulfilled.

Less trivial instances in which the longitudinal mode is also excited require a renormalizability criterion that provides a limitation upon the extent of this excitation. It is the principal observation of this note that $\bar{K}$ is often an overestimate of the degree of divergence, consequently that (2.4) is an overly severe restriction upon the renormalizable interactions. An improved bound for K will emerge from a treatment that throughout deals separately with the well-behaved transverse modes and the non-physical longitudinal one.

From the field equations (1.2) follows the supplementary condition that Z_μ satisfies:

$$M^2 \partial^\mu Z_\mu = -\partial^\mu j_\mu. \tag{2.6}$$

With the decomposition (1.7) this yields a differential equation for the longitudinal part of the field:

$$M^2 \frac{\mathrm{d}^2}{\mathrm{d}x_\mu^2} \Lambda = -\partial^\mu j_\mu. \tag{2.7}$$

The solution to this equation, generally a non-local function of Z_μ^t, $Z^{\mu\nu}$, and the other fields, may be employed to eliminate Λ from the interaction Lagrange function to form an effective Lagrange function, $L'(Z_\mu^t, Z_{\mu\nu}, \ldots)$. Since perturbation theory evaluates transition amplitudes between non-interacting states, these terminal states always satisfy a free-particle supplementary condition, $\partial^\mu Z_\mu = 0$. They are thus null eigenvectors of the longitudinal part of Z_μ, and the eigenvalues of Z_μ^t provide a sufficient specification of their dependence upon the vector meson field. Consequently, the Lagrange function L' from which Λ has been eliminated still describes the system completely.

The modified renormalizability criterion is simply the requirement that the Lagrange function L', examined in the usual manner, yields a renormalizable theory. In view of the expressions (1.8) for vector meson propagators involving Z_μ^t and $Z_{\mu\nu}$, this criterion becomes simply

$$C'(L') \leqq 4, \tag{2.8}$$

where each factor of $Z_{\mu\nu}$ in L' contributes unity both to t and to s. If (2.8) is satisfied there may exist primitively divergent contributions solely to transition amplitudes for processes that satisfy

$$\tfrac{3}{2}F_e + V_e + B_e \leqq 4. \tag{2.9}$$

3. Partially-Conserved Currents

It is at this point a useful digression to introduce the definition of a certain limited symmetry property that a Lagrange function may display. Generally L may be separated into three parts,

$$L = L_K + L_I + L_M, \tag{3.1}$$

where L_K is the kinematic Lagrange function, the only term to contain explicit differentiations. It is this function that determines both the commutation properties and the expressions for generators of infinitesimal variations of the fields. With the introduction of suitable supplementary fields, L_K may be written

$$L_K = \tfrac{1}{2}(\chi \mathscr{A}^\mu \partial_\mu \chi - \partial_\mu \chi \mathscr{A}^\mu \chi). \tag{3.2}$$

L_I contains the interactions to which the fields are subjected. So that the kinematical properties of the fields do not depend upon coupling strengths, none of these interactions may contain explicit derivatives. It is also attractive to hypothesize that only dimensionless coupling constants are present in L_I, and consequently that the only admissible interactions are of the forms

$$\begin{array}{ll} \text{a. } \psi\psi\phi & \text{d. } Y_{\mu\nu}Y_\mu Y_\nu \\ \text{b. } Y_\mu\psi\psi & \text{e. } \phi^4 \\ \text{c. } Y_\mu\phi_\mu\phi & \text{f. } Y_\mu^4 \\ & \text{g. } Y_\mu^2\phi^2. \end{array} \tag{3.3}$$

Here the spinor ψ represents any spin-$\frac{1}{2}$ field, ϕ_μ and ϕ represent any spinless field, and $Y_{\mu\nu}$ and Y_μ represent any spin-one field. With the assumption that elementary-particle decays are mediated by a vector meson, these forms are sufficient to describe all interactions known to exist.

L_M contains only the mass producing terms of the theory. It has the form

$$L_M = m\bar{\psi}O_1\psi+\mu^2\phi O_2\phi+M^2Y_\mu O_3 Y^\mu, \tag{3.4}$$

in which the O_i are dimensionless matrices.

If the fields are subjected to an infinitesimal unitary transformation, $\chi \to (1+\mathcal{T})\chi$, three sorts of invariance properties of the Lagrange function may be distinguished:

1) A transformation under which L_K is invariant also leaves the commutation relations unchanged and is consequently a canonical transformation. The condition for $\mathcal{T}$ to be canonical is given by $[\mathcal{A}_\mu, \mathcal{T}] = 0$.

2) If $\mathcal{T}$ is a symmetry of the entire Lagrange function, there must correspond to it the conserved current, $J_\mu(\mathcal{T})$. For example, phase transformation of charged fields is an invariance resulting in the continuity equation for the electromagnetic current.

3) If L_K and L_I, but not L_M, are invariant then $\mathcal{T}$ will be called a 'partial symmetry' of the Lagrangian. The current corresponding to $\mathcal{T}$ is not conserved, but satisfies what shall be called a 'partial conservation law' of the form

$$\partial^\mu j_\mu = m\bar{\psi}P_1\psi+\mu^2\phi P_2\phi+M^2Y_\mu P_3 Y^\mu \tag{3.5}$$

where the P_i are dimensionless numerical matrices given by

$$P_1 = O_1\mathcal{T}-\beta\mathcal{T}\beta O_1, \qquad P_{2,3} = [O_{2,3}, \mathcal{T}]. \tag{3.6}$$

If the masses are set equal to zero, $\mathcal{T}$ becomes an invariance of the entire Lagrangian, and (3.5) a conservation law.

The relation of this discussion to that of section 2 is perhaps less obscure with the observation that in general $C'(\partial^\mu j_\mu) = C'(j_\mu)+1$, while for a partially-conserved current $C'(\partial^\mu j_\mu) = C'(j_\mu)$.

4. Some Renormalizable Interactions

An interaction of the sort $m_{\mu\nu}Z^{\mu\nu}$, where $m_{\mu\nu}$ does not itself depend upon the vector meson fields, is renormalizable only if $C(m_{\mu\nu}) \leqq 2$. There is no such antisymmetric tensor that may be constructed of spin-$\frac{1}{2}$ and spin-0 fields and their derivatives, and hence no such renormalizable local interaction.

To investigate the renormalizability of a vector interaction, $j^\mu Z_\mu$, we must first evaluate and eliminate the longitudinal part of the vector field. For such currents that $\partial^\mu j_\mu$ does not explicitly depend upon Z_μ, (2.7) yields the expression

$$\Lambda(x) = M^{-2}(x|p^{-2}|x')\partial^\mu j_\mu(x'), \tag{4.1}$$

and the effective interaction Lagrange function becomes

$$j^\mu Z_\mu^{\mathrm{t}} - \partial^\mu j_\mu(x)(x|p^{-2}|x')\partial^\nu j_\nu(x'). \tag{4.2}$$

The resulting theory is renormalizable if both the inequalities

$$C'(j_\mu) \leqq 3 \quad \text{and} \quad C'(\partial^\mu j_\mu) \leqq 3 \tag{4.3}$$

are satisfied. The first restriction requires a local j_μ to be of the form $\bar{\psi}\, O_\mu \psi$ or $\phi_\mu O \phi$. The second inequality limits $\partial^\mu j_\mu$ to the general form

$$\partial^\mu j_\mu = \bar{\psi}(O + O'\gamma_5)\psi + \mathscr{P}_3(\phi, \partial), \tag{4.4}$$

where O and O' are dimensionless matrices and $\mathscr{P}_3$ is a polynomial in ϕ and its derivatives of at most third degree. Note that (4.4) includes any 'partially-conserved current' which by definition must satisfy (3.5). So long as the first inequality of (4.3) is met, any interaction of a vector meson with a partially-conserved current will be renormalizable.

An example of a theory admitted as renormalizable by the new criterion, but excluded by the conventional one, is described by the Lagrange function

$$L = L_{\mathrm{K}}(\psi, Z) + m\bar{\psi}\psi + M^2 Z_\mu Z^\mu + g Z_\mu \bar{\psi}\gamma^\mu(i\nu + ia\gamma_5)\psi, \tag{4.5}$$

in which Z_μ is a neutral vector field and ψ is a real Fermi field with a single internal degree of freedom to which $\nu = \left(\begin{smallmatrix} 0 & i \\ -i & 0 \end{smallmatrix}\right)$ refers. The interaction current satisfies the partial-conservation law

$$\partial^\mu[\psi\gamma_\mu(\nu + a\gamma_5)\psi] = -2iam\bar{\psi}\gamma_5\psi. \tag{4.6}$$

The analogous coupling of a charged vector meson is not, by itself, renormalizable. For example, with the interaction

$$Z_\mu^k(\bar{\psi}\gamma^\mu i t_k \psi) \qquad (k = 1, 2) \tag{4.7}$$

of a charged vector meson to a $T = 1$ triplet of Fermions, the current now satisfies

$$\partial^\mu(\bar{\psi}\gamma_\mu t_k \psi) = \varepsilon^{kj3} Z_\mu^j(\bar{\psi}\gamma^\mu t^3 \psi)$$

which is not of the form (4.4), and this interaction does not qualify as

renormalizable. Thus, a renormalizable theory of the beta-interactions cannot be generated by the interactions of a charged vector meson without including appropriate self-couplings. We would like to be able to identify these self-couplings with the electrodynamic interactions of the vector meson.

5. Electrodynamic Interactions of Vector Mesons

We shall represent the charged vector meson by two real fields, with the charge given by the 2×2 antisymmetric imaginary matrix t_3. The most general linear electrodynamic coupling not involving explicit differentiations is given by

$$L_1 = ie[Z^{\mu\nu}t_3(Z_\mu A_\nu - Z_\nu A_\mu) + \gamma F^{\mu\nu} Z_\mu t_3 Z_\nu], \tag{5.1}$$

in which the first term corresponds to the usual 'minimal' interaction and an additional 'anomalous magnetic moment' interaction has been introduced. The consequent field equation for Z_μ, where Π_μ denotes $\partial_\mu + it_3 A_\mu$, is

$$(\Pi^2 - M^2)Z_\nu = -iet_3[(1+\gamma)F_{\nu\mu}Z^\mu + \Pi_\nu \tfrac{1}{2}M^{-2}((1-\gamma)F_{\lambda\sigma}Z^{\lambda\sigma} - 2\gamma j_\mu Z^\mu)]. \tag{5.2}$$

In the non-relativistic limit, and with the neglect of the last term which represents a direct self-interaction, (5.2) becomes

$$[(\tfrac{1}{2}M)\boldsymbol{\Pi}^2 - eA_0]\mathbf{Z} + (e/2M)(1+\gamma)(\mathbf{Z}\times\mathscr{H}) + (e/4M^2)(1-\gamma)\boldsymbol{\Pi}(\mathbf{Z}\cdot\mathscr{E}) = 0. \tag{5.3}$$

Evidently Z possesses a magnetic dipole moment of size $(e/2m)(1+\gamma)$ and an electric quadrupole moment of size $(e/4m^2)(1-\gamma)$, in units wherein $\hbar = c = 1$.

In order to investigate the renormalizability of this theory, we must express the longitudinal part of Z_μ in terms of the other fields, and eliminate it from the Lagrange function. Writing the interaction as

$$L_1 = ie(2Z^{\mu\nu}t_3 Z^{\mathrm{t}}_\mu A_\nu + \gamma F^{\mu\nu} Z^{\mathrm{t}}_\mu t_3 Z^{\mathrm{t}}_\nu) + L_\Lambda, \tag{5.4}$$

where L_Λ is the part of L_1 involving Λ,

$$L_\Lambda = ie(2Z^{\mu\nu}A_\nu - \gamma F^{\mu\nu} Z^{\mathrm{t}}_\nu - \gamma F^{\mu\nu}\partial_\nu \Lambda)t_3 \partial_\mu \Lambda, \tag{5.5}$$

we observe immediately that $L_1 - L_\Lambda$ satisfies the renormalization criterion (2.8). Thus the renormalizability depends entirely upon the behaviour of the longitudinal mode; it is renormalizable if $C'(L_\Lambda) \leqq 4$ or equivalently, if $C'(\Lambda) \leqq 0$.

We determine Λ from the supplementary condition Z_μ must satisfy. From (5.1) follows

$$M^2 \partial^\mu Z_\mu = iet_3 \partial_\nu [A_\mu Z^{\mu\nu} - \gamma F^{\mu\nu} Z_\mu], \tag{5.6}$$

which may be reduced with the use of the field equations to

$$M^2 \partial^\mu Z_\mu = iet_3[\tfrac{1}{2}(\gamma - 1)F^{\mu\nu} Z_{\mu\nu} - M^2 A^\mu Z_\mu]. \tag{5.7}$$

Therefore Λ satisfies the differential equation

$$(\mathrm{d}^2/\mathrm{d}x_\mu^2+iet_3 A^\mu \mathrm{d}/\mathrm{d}x_\mu)\Lambda = iet_3(A^\mu Z_\mu^{\mathrm{t}}+\tfrac{1}{2}(1-\gamma)M^{-2}F^{\mu\nu}Z_{\mu\nu}). \quad (5.8)$$

Defining an integral operator

$$(x|\Omega|x') = \int (2\pi)^{-2}\mathrm{d}^4 p \mathrm{e}^{ip(x-x')} it_3 A_\mu(x) p^{-2}p^\mu,$$

we may write the solution to (5.8) as a power series:

$$\Lambda(x) = \left(\sum_{n=0}^{\infty} \mathrm{e}^n \Omega^n\right) p^{-2} iet_3(A^\mu Z_\mu^{\mathrm{t}}+\tfrac{1}{2}M^{-2}(1-\gamma)F^{\mu\nu}Z_{\mu\nu}). \quad (5.9)$$

For each term of this series, from (2.5), we have $C' = 2$, and consequently $C'(L_\Lambda) = 6$. In general the renormalization criterion is not met. However, if γ is chosen as unity so that the second bracketed term of (5.9) vanishes, we obtain $C' = 0$ for each term. In this case, inserting (5.9) into (5.4), L' is expressed as a power series in e each of whose partial sums is characterized by $C' = 4$. From (2.9) it follows that primitive divergences exist only for transition amplitudes with $V_e \leqq 4$. Because L' is an infinite sum, there will be an infinite number of distinct primitive divergences contributing to each such amplitude. Nevertheless, the introduction of a finite number of counterterms yields a finite theory, and the electrodynamics of a vector meson with unit anomalous moment is thus shown to be renormalizable. We must emphasize that this result applies only to the isolated vector meson. If other charged fields are present, an additional term will appear in (5.7), which destroys the renormalizability.

6. Discussion

It should be observed that the choice $\gamma = 1$, besides leading to a renormalizable electrodynamics, is remarkable for certain apparently unrelated reasons. It assures that the uncorrected gyromagnetic ratio of Z_μ is two, as well as that Z_μ displays no electric quadrupole moment. Furthermore, if the Z-meson mass is to be regarded as a consequence of some unspecified interaction, then we must be able to examine the theory in the absence of this interaction. In this limit, (5.7) becomes

$$\tfrac{1}{2}(1-\gamma)t_3 F^{\mu\nu}Z_{\mu\nu} = 0.$$

Unless $\gamma = 1$, this relation conflicts with the assumed kinematical independence of the vector meson and the electrodynamic fields, hence it is only the renormalizable theory for which there exists a consistent zero-mass limit [4]).

In deriving (5.7) from (5.6) we used the relation

$$\partial_\nu(A_\mu Z^{\mu\nu}-\gamma Z_\mu F^{\mu\nu}) = \tfrac{1}{2}(\gamma-1)F^{\mu\nu}Z_{\mu\nu}-M^2 A^\mu Z_\mu. \quad (6.1)$$

Thus, with the choice $\gamma = 1$, the vector $A_\mu Z^{\mu\nu}-\gamma Z_\mu F^{\mu\nu}$ becomes what we have defined by (3.5) to be a partially conserved current. It is illuminating to

construct the infinitesimal transformation which displays the corresponding 'partial symmetry' of the Lagrange function. Defining $Z^3_\mu = A_\mu$ and $Z^3_{\mu\nu} = F_{\mu\nu}$ we may re-express (5.1) with $\gamma = 1$ as

$$L_1 = e\varepsilon^{ijk} Z_i^{\mu\nu} Z_\mu^j Z_\nu^k, \tag{6.2}$$

which is formally identical to the vector-meson interaction discussed by Yang and Mills [5]) in another context. As they observe, (6.2) is invariant under 'I-spin' rotations of the Z-meson triplet,

$$\begin{aligned} \mathbf{Z}_\mu &\to (1+i\mathbf{t}\cdot\boldsymbol{\theta})\mathbf{Z}_\mu \\ \mathbf{Z}_{\mu\nu} &\to (1+i\mathbf{t}\cdot\boldsymbol{\theta})\mathbf{Z}_{\mu\nu}. \end{aligned} \tag{6.3}$$

In our case, the identification of Z^3 with light prevents a complete symmetry of this sort. The mass producing part of L cannot produce a photon mass, hence we must have

$$L_M = -\tfrac{1}{2}M^2 Z^\mu t_3^2 Z_\mu. \tag{6.4}$$

Consequently only the t_3 rotation is an invariance of the entire Lagrange function; the other rotations are now only partial-symmetries. Of the corresponding currents,

$$j_\mu^i = \varepsilon^{ijk} Z_{\mu\nu}^j Z_k^\nu, \tag{6.5}$$

only j_μ^3, the electrical current, is conserved. The others satisfy partial-conservation laws. More succinctly, we have

$$\partial^\mu \mathbf{j}_\mu = -M^2 A^\mu t_3 \mathbf{Z}_\mu, \tag{6.6}$$

which reproduces (6.1) with $\gamma = 1$.

If other fields are introduced which also bear charge, the partial conservation of $j_\mu^{1,2}$ is destroyed. Thus, if we include nucleons, the Lagrange function

$$L_e = e\left(\sum_{i,j,k=1}^{3} \varepsilon^{ijk} Z_i^{\mu\nu} Z_\mu^j Z_\nu^k + Z_\mu^3 i\bar{\psi}\gamma^\mu \tfrac{1}{2}(\tau_3+\zeta_3)\psi\right) \tag{6.7}$$

possesses only the $|t_3|$ invariance, and does not generate a renormalizable theory. Similarly, the prototype beta-interaction

$$L_\beta = \beta \sum_{i=1,2} Z_\mu^i \bar{\psi} O_i \gamma^\mu \psi \tag{6.8}$$

(in which the O_i may refer to charge, parity, strangeness, etc.) is not renormalizable in view of the discussion near (4.7). However, it is interesting to note that by combining these two interactions we may secure a renormalizable theory. Recalling that

$$\frac{\beta^2}{M^2} \simeq \frac{10^{-5}}{m_N^2},$$

we may identify β with e providing that the vector meson mass is taken to be about thirty nucleon masses. The combined interactions may then be written

$$L_{\mathrm{W}} = e\left(\sum_{i,j,k=1}^{3} \varepsilon^{ijk} Z_i^{\mu\nu} Z_\mu^j Z_\nu^k + \sum_{i=1}^{3} Z_\mu^i \bar{\psi}\gamma^\mu O_i \psi\right), \tag{6.9}$$

where O_3 is defined as to be $\frac{1}{2}i(\tau_3+\zeta_3)$. This theory is renormalizable if the O_i constitute a representation of the rotation group,

$$[O_i, O_j] = i\varepsilon^{ijk} O_k, \tag{6.10}$$

for then the infinitesimal transformation, $\psi \to (1+\mathbf{O}\cdot\boldsymbol{\theta})\psi$, together with (6.3) constitutes a partial-symmetry of L_{W}.

From the corresponding partial-conservation law follows

$$\partial_\mu^2 \Lambda = -A^\mu t_3 Z_\mu,$$

and the arguments of section 5 may again be employed to show that the renormalization criterion is met.

To obtain a realistic theory of the decay processes, we must show that $O_{1,2}$ may contain both symmetric parity violation and the known strangeness selection rules. We must also include the existence of mesons and their strong couplings. The discussion of these points is reserved for a more speculative sequel.

I am very grateful to Prof. Julian Schwinger for first suggesting to me the hypothesis of a vector intermediary for the decay processes and for many enlightening discussions of this and related ideas. I should like also to thank Professor Niels Bohr and the members of this Institute for their kind hospitality.

References

1) E. g., J. Schwinger, Annals of Physics **2** (1957) 407;
R. Feynman and M. Gell-Mann, Phys. Rev. **109** (1958) 193;
S. L. Glashow, Harvard University Thesis (1958)
2) E.g., S. Bludman, Nuovo Cimento **9** (1958) 442;
W. Thirring, Principles of Quantum Electrodynamics (1958) 195
3) J. Schwinger, Phys. Rev. **91** (1953) 728
4) Tzou Kuo-Hsien, Compt. rend. **245** (1957) 289
5) C. N. Yang and R. Mills, Phys. Rev. **96** (1954) 190

1.D.2:
1.E.1:
3.C

Nuclear Physics **10** (1959) 118—134; © *North-Holland Publishing Co., Amsterdam*
Not to be reproduced by photoprint or microfilm without written permission from the publisher

MEASUREMENTS OF THE γ-RADIATIONS FROM Eu^{152} BY THE METHOD OF EXTERNAL CONVERSION

OVE NATHAN † and SÖLVE HULTBERG
Nobel Institute of Physics, Stockholm 50

Received 4 November 1958

Abstract: The photoline spectrum from 10 γ-rays following the decay of 12 y Eu^{152} has been studied with a double-focusing β-spectrometer, using a 2.2 mg/cm² U converter. The resulting momentum resolution was 0.6—1 %, depending on energy. The relative γ-ray intensities found are in good agreement with those obtained by Dželepow and Zhukovsky from a study of recoil electrons. Combining our γ-ray intensities and the internal conversion data of Bobykin and Novik, relative values of internal conversion coefficients of the investigated γ-rays have been determined. The multipolarity assignments obtained in this way are discussed within the framework of the unified model, and particular attention is given to the 689 keV transition in Sm^{152}. It is suggested that this radiation is of the E0+E2 type and is proceeding from a proposed 2+β-vibrational state at 811 keV to the 2+ member of the ground-state rotational band. The decay properties of the 811 keV state are discussed in some detail.

1. Introduction

The main features of the decay scheme of long-lived Eu^{152} were established in 1956 by Grodzins and Kendall [1]) who studied the radiations from neutron irradiated Eu enriched in Eu^{151}, and by Nathan and Waggoner [2]) who utilized source material composed of the natural mixture of Eu^{151} and Eu^{153}. The decay schemes proposed by these authors are almost identical, apart from a few weakly populated levels whose existence is still doubtful, and a level at 1121 keV which was incorrectly assigned to Sm^{152} instead of Gd^{154} by Nathan and Waggoner.

Additional data on the radiations from long lived Eu^{152} has recently been published by several workers. Cork *et al.*[3]), working with enriched Eu^{151}, studied the β- and γ-transitions in magnetic photographic and scintillation coincidence spectrometers. Ofer [4]) carried out γ—γ directional correlation experiments on the dominant γ-cascades in order to establish the multipole order of some of the higher energy transitions. Bobykin and Novik [5]) made a very careful investigation of the energies and intensities of the internal conversion lines by means of a double focusing spectrometer with ≈ 0.3 % resolution, and Dželepow and Zhukovsky [6]) used the Compton recoil

† Permanent address: Institute for Theoretical Physics, University of Copenhagen, Denmark

method to determine the intensities of the most prominent γ-rays. The experimental evidence produced in these studies has not required any fundamental change in the decay scheme proposed in ref.[1]) and in the spin and parity assignments given in ref.[2]). In the following we will, therefore, assume the validity of a decay scheme based on the measurements contained in refs.[1–6]) and including all transitions about whose position in the decay scheme there is agreement among the different workers. This decay scheme is shown in fig. 1 in which we have used the accurate transition energies given in ref.[5]). An additional level at 811 keV excitation energy has tentatively been included; the existence and the properties of this state, which have not been proposed previously, will be discussed below.

It may be noted that another recent experimental investigation of the decay of Eu^{152} by Bhattacherjee *et al.*[7]) has resulted in a level scheme for Sm^{152} which, on important points, differs appreciably from the scheme given in fig. 1. The reason for the underlying experimental discrepancies is not understood clearly by us, and it is particularly difficult to explain why Bhattacherjee and coworkers do not observe 122—1409 keV $\gamma-\gamma$ coincidences.

It has earlier been pointed out that several of the levels in Sm^{152} and Gd^{152} which are populated in the decay of Eu^{152} may perhaps be interpreted as collective vibrational excitations. Thus, it was suggested in ref.[2]) that the 1087 keV and 1235 keV states of the deformed nucleus Sm^{152} might be the two first members of a quadrupole vibrational band with $K = 2$ (γ-vibrations), and that, similarly, the 344 keV and 756 keV states of the spherical nucleus Gd^{152} most likely can be described as quadrupole vibrational excitations. According to the theory (see, e.g., ref.[8])) it is characteristic of vibrational excitations in both kinds of nuclei that M1 radiation is forbidden in the decay of these states, even if $\Delta I = 0$ or 1. In order to obtain a closer understanding of the character of the proposed vibrational states it is, therefore, of particular interest to determine the multipolarity of the de-exciting γ-rays as accurately as possible.

Experimentally, the multipole orders of several transitions occurring in Sm^{152} and Gd^{152} have been assigned in the usual way by relative intensity measurements of internal conversion lines and γ-lines, and using a normalization procedure in which it is assumed that the internal conversion coefficient of the 344 keV γ-ray in Gd^{152} has the theoretical value for an E2 transition. The most accurate values of the internal conversion coefficients obtained by this method are those based on the results contained in refs.[5]) and [6]), but the resolution of the Compton recoil spectrometer (2—3 %) used by Dželepow and Zhukovsky for the γ-ray measurements did not allow them to resolve all the pertinent lines and, consequently, the conversion coefficients obtained are still not accurate enough to permit an unambiguous multipolarity assignment in all the cases considered.

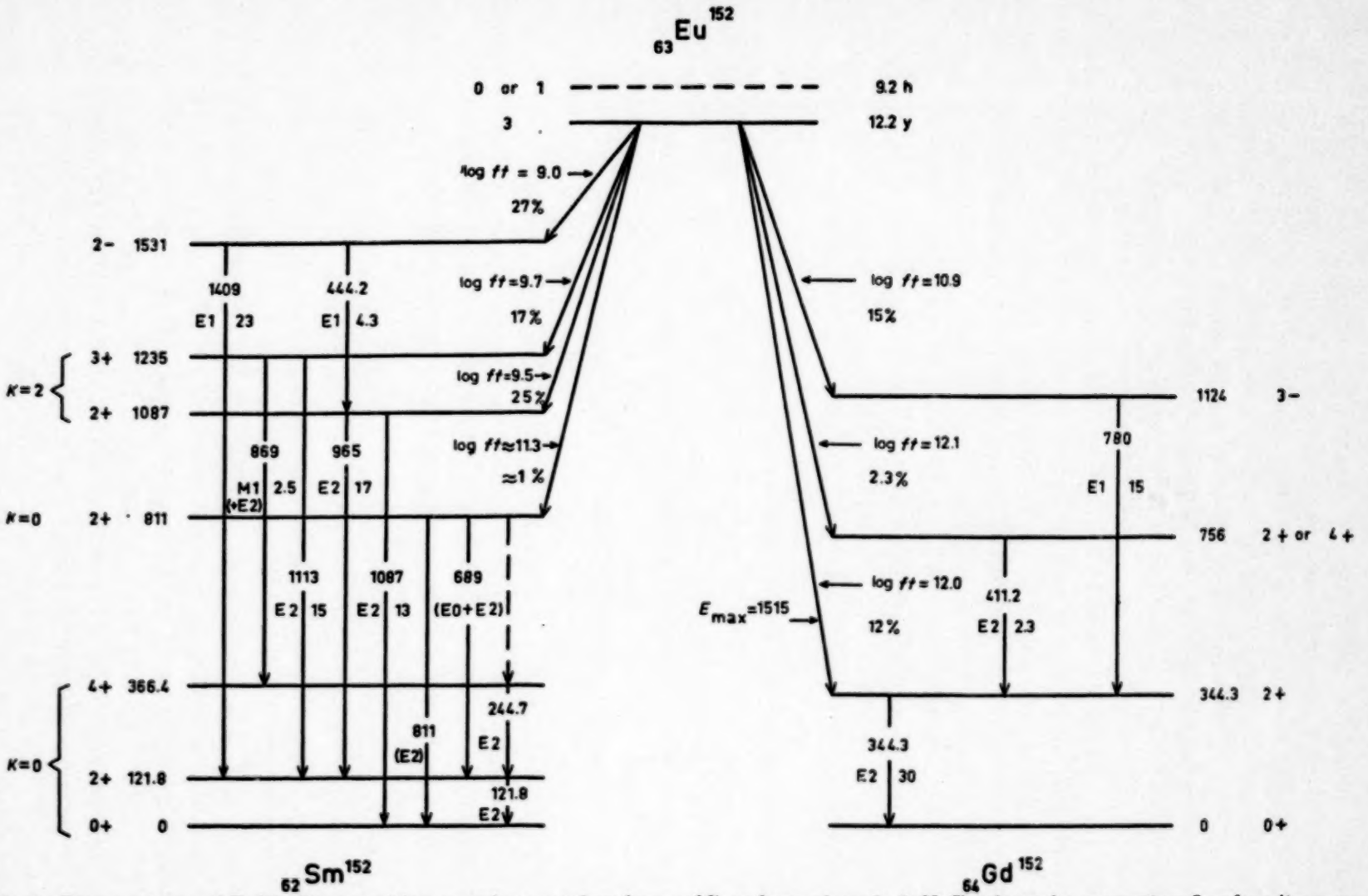

Fig. 1. Decay scheme of Eu^{152}. The transition energies are taken from ref.[5]) and are given in keV. Total angular momentum I and parity π are indicated in the conventional manner at each level. Numbers to the right of multipolarity indications give transition probabilities in per cent of all disintegrations. For the calculation of ft values in the electron capture decay, we have estimated the energy difference between the ground states of Eu^{152} and Sm^{152} to be about 1850 keV, using the transition energy reported for Eu^{152m} by Moon *et al.*[22]).

Note added in proof: A direct measurement of the latter energy difference is now available (D. E. Alburger, S. Ofer and M. Goldhaber, Phys. Rev. Letters **1** (1958) 479). The value quoted is 1859 ± 10 keV.

Supplementary knowledge of spins and multipolarities has been supplied by the $\gamma-\gamma$ directional correlation work of Grodzins [1]) and Ofer [4]) on six γ-ray cascades following the decay of Eu^{152}. However, in some of the cases, e.g. the 965—122 keV and 1113—122 keV cascades, the complexity of the γ-spectrum necessitates considerable corrections to the measured correlation functions; it would, therefore, be desirable to check the corresponding multipolarity assignments by other methods.

The purpose of this investigation is to obtain information on the multipole orders by the establishment of more accurate experimental values of the corresponding internal conversion coefficients than has been possible previously. We have chosen to study the γ-radiations by the method of photo-electric conversion, because this procedure is capable of sufficiently high resolution and, furthermore, has proved to be a very reliable tool for precise intensity determinations over large energy intervals, provided appropriate consideration is given to the angular distribution of the emitted photo-electrons (see, e.g., ref.[9])). The internal conversion spectrum was not studied in this work, since the comprehensive measurements by Bobykin and Novik in almost all cases supply sufficient information on the relevant intensities, even though these workers made use of unenriched source material. However, an additional investigation of the internal conversion spectrum of Eu^{152} with source material enriched in Eu^{151}, and similarly based on high resolution spectroscopy, would be valuable as a check on Bobykin and Novik's results.

2. Experimental Method and Results

The gamma-ray source consisted of europium oxide, enriched to about 92 % in the 151 isotope †. The material was confined to a cylindrical volume (diameter 2 mm, height 2 mm) inside an aluminium capsule, according to the standards of A.E.R.E. in Harwell for radiographic sources. The sample was irradiated in a reactor for seven weeks and was thereafter left to decay for three months to allow the short-lived activities to die away. The dose rate from the capsuled source was 5—6 mR/h at 100 cm at the beginning of the measurements.

The source was put into a large double-focusing spectrometer and a circular uranium converter U (radius 7.3 mm) of 2.19 ± 0.02 mg/cm^2 was placed in front of the source container so that the half top angle from the centre of the source to the edge of the converter was $\vartheta_0 = 65°$ (cf. ref.[9])). Photolines were then recorded with a resolution varying between 1 and 0.6 % with energy. 10 gamma-ray energies were studied in this way and

† Obtained from Stable Isotopes Division, Oak Ridge National Laboratories,

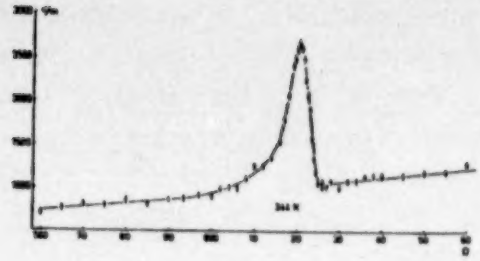

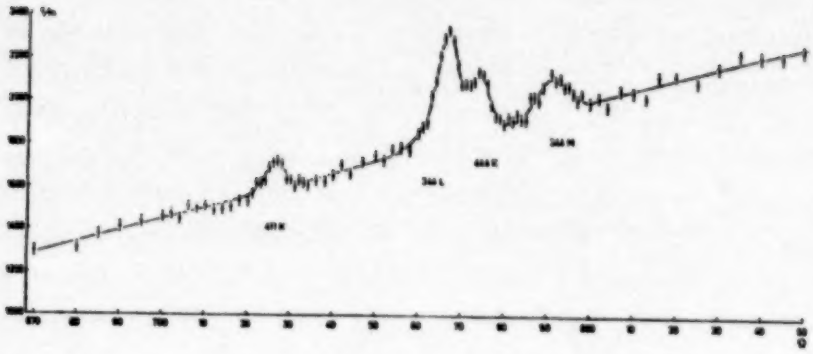

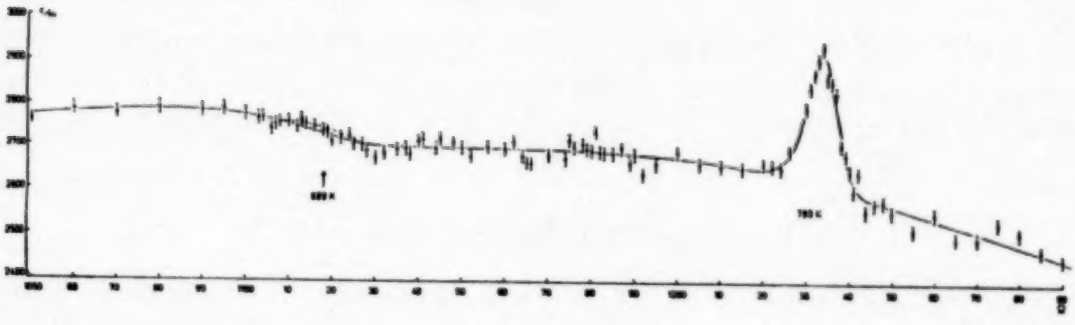

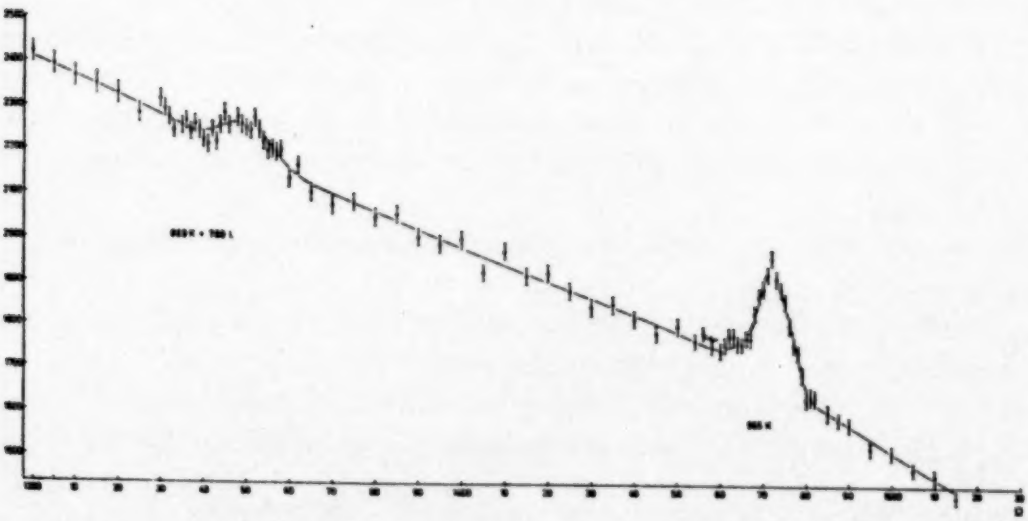

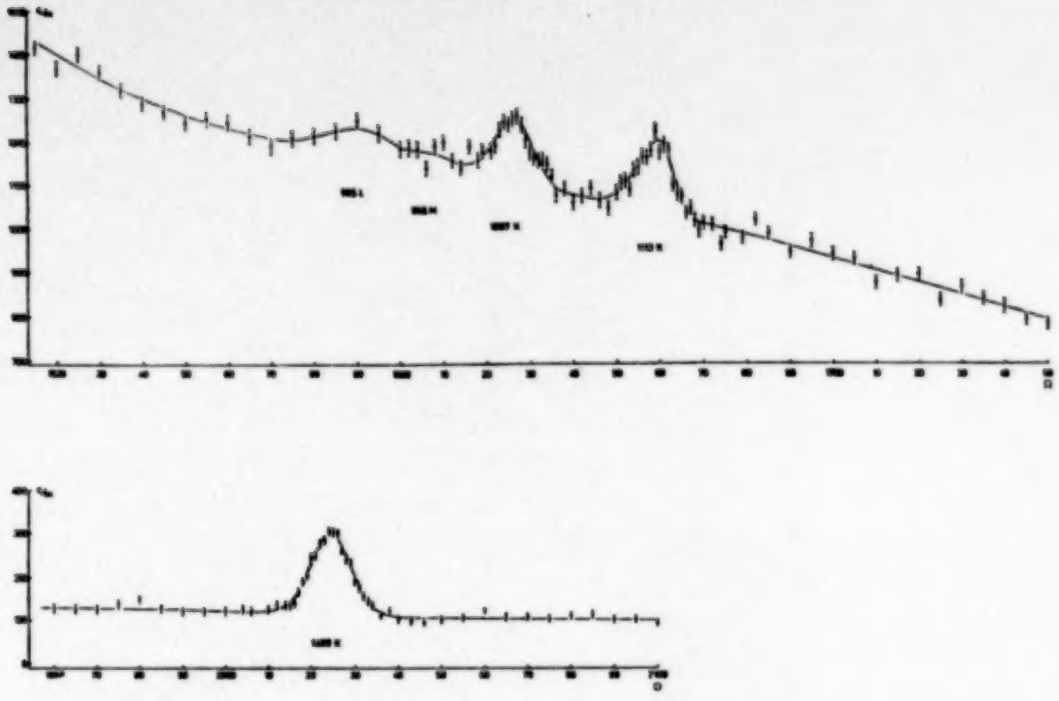

Fig. 2. Photoline spectrum from γ-rays in the decay of Eu^{152}. The photoelectrons were generated in a 2.2 mg/cm^2 U converter and recorded in a double-focusing β-spectrometer at a resolution of 0.6–1 %.

three full runs were made, one of which is shown in part in fig. 2. The region in which the interesting 689 keV photoline was expected to appear was studied with special care, 10 and 20 min readings being taken over a large interval. The continuum was carefully recorded in order to permit a correct interpolation of the backgrounds under the line profiles. Thus, it should be emphasized that in some cases the areas of the photolines shown in fig. 2 were obtained by considering energy regions even greater than those appearing in the separate drawings (cf. fig. 4 of ref.[10])).

The method for the correct deduction of γ-ray intensities from the study of photolines has been treated by Hultberg and Stockendal [9]). Their procedure was applied here to the case of $\vartheta_0 = 65°$. For the sake of illustration, the corrected photoelectric cross-sections, τ_c, are shown in fig. 3 together with the theoretical total cross-sections, τ_K, for the K-shell (compare with the case of $\vartheta_0 = 78°$ in ref.[11])). By using the (internal) conversion intensities given in ref.[5]), and by adopting

$$\varepsilon_{344K} = \alpha_2 = 3.04 \times 10^{-2},$$

relative conversion coefficients ε were obtained. The results are presented as mean values in table 1. Fig. 4 gives a diagrammatical comparison with the theoretical conversion coefficients of Sliv and Band.

TABLE 1

Comparison of experimental results for Sm^{152} and Gd^{152} with earlier investigations, reported in refs.[5]) and [6]), and with the theory of Sliv and Band (S & B)

Z	$h\nu$ (keV)	I_γ (ref.[6]))	I_γ (authors)	I_β (ref.[5]))	$\varepsilon_K \times 10^3$ (authors)	$\varepsilon_K \times 10^3$ (S & B)	Multipol. assignm.	Remarks
64	344	100	100	109.1 ±1.4	30.4	30.4	E2	ε_K is normalized
64	411	–	8±2	6.04±0.14	21 ±5	19.2	E2	
62	444	19±6	17±2	2.67±0.07	4.4 ±0.6	4.7	E1	$(K/L)_{344} = 4.7$ used †
62	689	–	<2	3.8 ±0.3	> 50	4.9 (E2)	(E0+E2)	I_β: see discussion
64	780	52±4	52±4	2.90±0.07	1.5 ±0.1	1.6	E1	
62	869	–	9±3	1.6 ±0.2	5.0 ±1.5	4.6 (M1) 2.9 (E2)	M1(+E2)	$(K/L)_{789} = 4.9$ used †
62	965	52±4	57±5	4.60±0.10	2.2 ±0.2	2.3	E2	$(K/L)_{869} = 4.9$ used †
62	1087	42±7	45±7	3.01±0.07	1.9 ±0.3	1.8	E2	
62	1113	53±7	49±7	3.13±0.08	1.8 ±0.3	1.7	E2	
62	1409	85±7	79±6	1.39±0.02	0.49±0.04	0.49	E1	

† Valid for external conversion in uranium with $\theta_0 = 65°$ (see text).

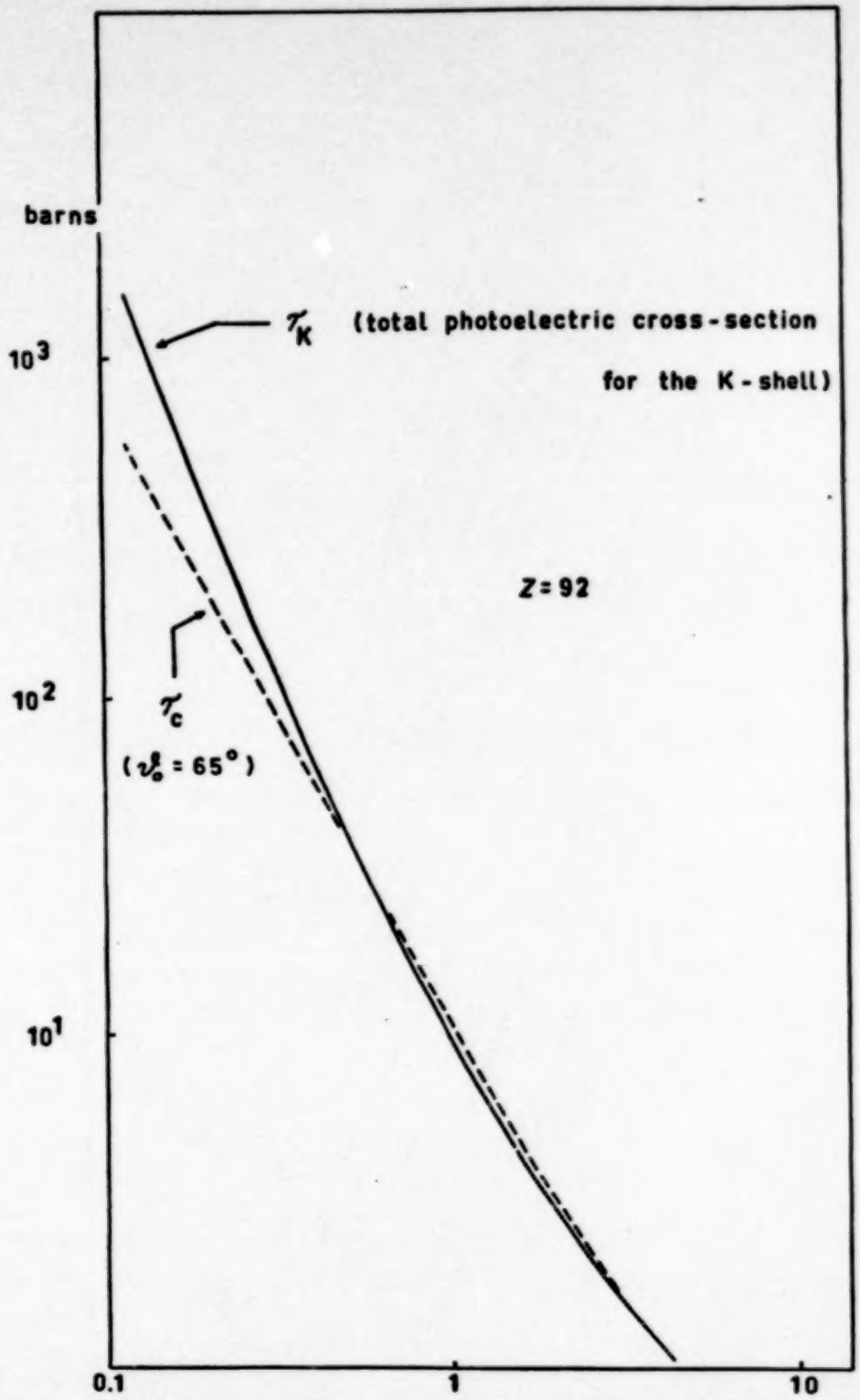

Fig. 3. Comparison (for $Z = 92$) between the tabulated total photoelectric cross-section τ_K and the corrected cross-section τ_c for $\vartheta_0 = 65°$, cf. ref.[9]) to be applied to the particular experimental set-up. The converter has circular shape.

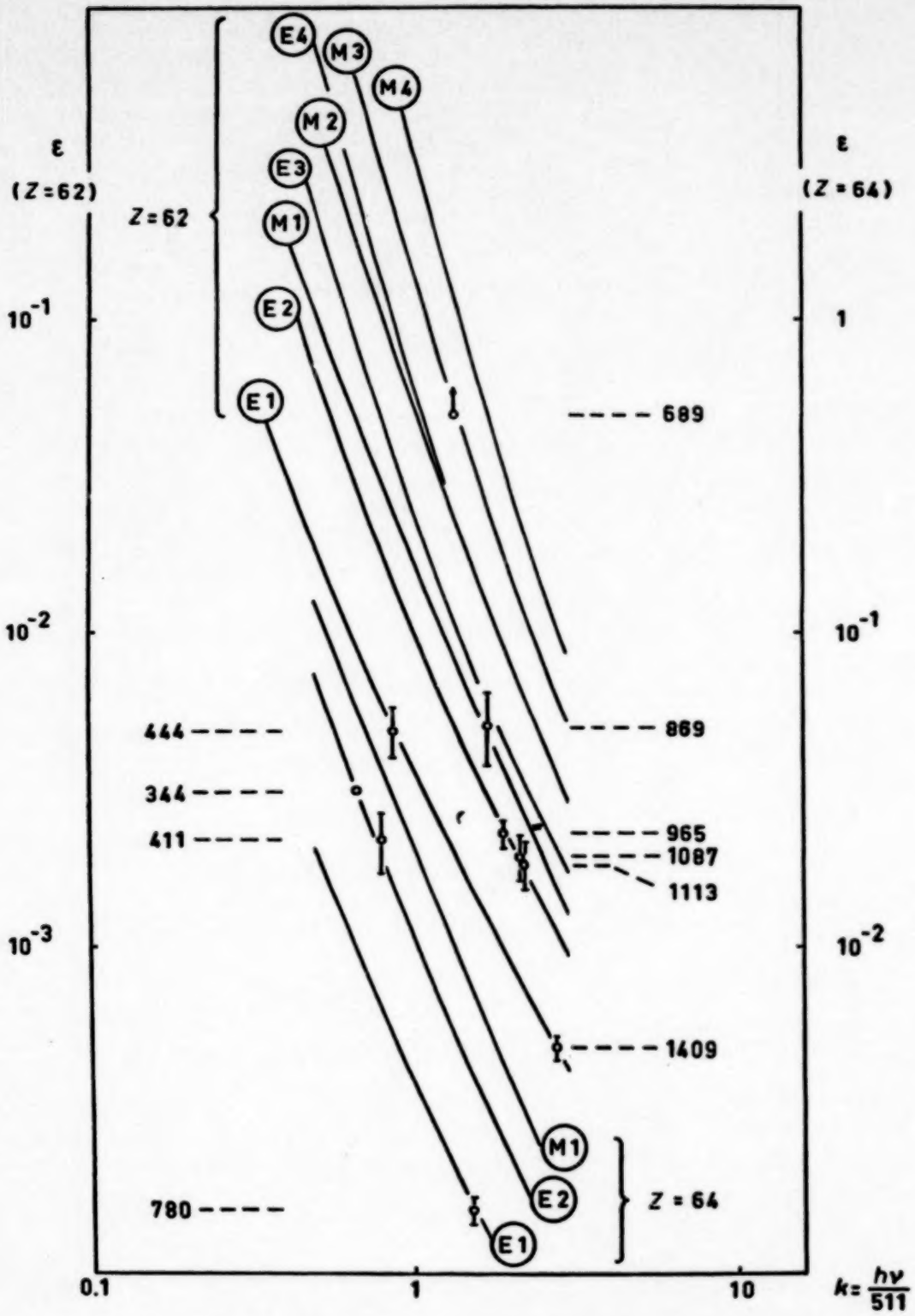

Fig. 4. Comparison of experimental and theoretical conversion coefficients for $Z = 62$ and 64. The curves represent the Sliv and Band values.

It should be observed that the agreement between our γ-ray intensities and those given by Dželepow and Zhukovsky is very satisfactory. This is interesting because Dželepow and Zhukovsky used the more infrequently employed method of studying the Compton secondaries in a magnetic spectrometer for the deduction of the Eu^{152} γ-ray intensities. The agreement is within 10 %.

From fig. 2 it can be seen that in most cases the photolines are well resolved. In only two cases do appreciable mixings between K and L lines occur. The 344 L and the 444 K photolines are partly resolved, while the 780 L and 869 K lines are unresolved. However, even in these cases the relative γ-ray intensities may be calculated, because reliable experimental information on the K/L- and K/(M+N+ . . .)-ratios in external conversion is now available (Hultberg and Sujkowski, to be published). These ratios can be obtained for any geometry of the source-converter arrangement. As the 344 K and the 780 K photolines were resolved, their corresponding L-line intensities could be estimated and subtracted from the unresolved peaks, thus giving information about 444 K and 869 K photoelectric intensities.

The upper limit for the intensity of the 689 K photoline is indicated in fig. 2. From the calculated γ-ray intensity (corresponding to the dotted line) a lower limit on the conversion coefficient was obtained.

The conversion coefficients of table 1 were obtained from

$$\varepsilon = \varepsilon_0 \cdot \frac{I_\beta}{I_\gamma}, \tag{1}$$

where

$$I_\gamma \approx \frac{A_\gamma}{\tau_K \cdot f} = \frac{A_\gamma}{\tau_c} \tag{2}$$

(cf. ref.[9])). ε_0 is the internal conversion coefficient of a transition of established multipolarity if we put $I_\beta = I_\gamma$ on an arbitrary scale for this transition (here the 344 keV transition was chosen, see above). I_β and I_γ are the relative conversion and γ-rays intensities, respectively. τ_K is the tabulated total photoelectric cross-section [12]) for the K-shell, f is a correction factor [9]), and A_γ is the area (divided by $H\rho$) of a photoline.

The accuracy of the determination of ε depends upon the possible errors in the factors of eqs. (1) and (2). An estimation of these factors has been discussed in ref. [9]) and here it need only be pointed out that in a study of *relative* conversion coefficients the error resulting from the uncertainty in the determination of $\tau_K \cdot f$ should be very small. The error in ε_0 is neglected and that in I_β is indicated in ref.[5]). The uncertainty in A_γ was estimated in each case. Adding the squares of the various errors gives the uncertainties indicated in table 1 and in fig. 4. In most cases the resulting error is completely determined by the uncertainty in A_γ.

3. Discussion

3.1. TRANSITIONS IN Gd^{152}

The experimental evidence available on the levels in Gd^{152} indicates that this nucleus with its 88 neutrons is situated inside, although at the very edge of the intermediate region between the closed shell nuclei and the deformed rare earth nuclei [2]). The even nuclei in this region are characterized by the systematic appearance of low-lying states which may be described as quadrupole vibrational excitations about a spherical equilibrium shape [8]). The first excited states always have spin and parity 2+, and the next state usually is found to be of the 0+, 2+, or 4+ type and is situated at an excitation energy 2—2.5 times that of the first excited state. The second vibrational 2+ states are generally observed to decay mainly by radiations of almost pure E2 type to the first 2+ states, while the E2 cross-over radiations to the ground states are found to be retarded by large factors.

In the case of Gd^{152}, the first excited state at 344 keV is uniquely fixed to be of the 2+ type, since the 344 keV γ-ray has E2 multipolarity. The second level occurs at 756 keV, which is at the expected position for the next member of the vibrational spectrum. This state is found to decay by a single 411 keV γ-ray whose multipolarity, according to this work, is E2 with some possible M1 admixture, in good agreement with previous K/L data [5]). No definite statement can be made, therefore, on the spin of the 756 keV state, since both of the possibilities 2+ and 4+ are consistent with this decay mode. γ—γ angular correlation measurements on the 411—344 keV cascade [1]) rule out a 0+ assignment which is also very improbable on the basis of log *ft* arguments.

3.2. TRANSITIONS IN Sm^{152}

It is a general observation [13]) that a dramatic change in nuclear structure takes place between the neutron numbers 88 and 90, which is manifested in the sudden appearance of large quadrupole deformations for nuclei with $N \geqq 90$. Sm^{152} is an even nucleus with 90 neutrons, and all information presently available indicates that it belongs to the region of strongly deformed nuclei. Thus, the two first excited states, which are of the 2+ and 4+ types, can be characterized as being the first members of a rotational band associated with the ground state. Collective excitations corresponding to vibrations about the equilibrium shape are also expected to occur in this type of nuclei, and associated with the vibrations one expects to observe rotational bands corresponding to moments of inertia of the same order of magnitude as the ground-state moment [8]). In the following we shall be concerned particularly with the lowest order shape vibrations which are of the quadrupole type, having even parity.

Two types of such quadrupole vibrations in spheroidal nuclei are predicted

by the theory: β-vibrations and γ-vibrations. The β-vibrations can be visualized as oscillations of the eccentricity about its equilibrium value and will, therefore, preserve the axial symmetry of the nucleus. In this case no angular momentum is carried by the vibrations along the nuclear symmetry axis and, consequently, the projection K of the total angular momentum along this axis is 0. The γ-vibrations involve oscillations about the symmetric equilibrium shape, and in this case $K = 2$. The rotational spectrum associated with a β-vibrational excitation is expected to consist of levels with spins 0+, 2+, 4+ . . ., while the rotational sequence for a γ-vibration is predicted to be 2+, 3+, 4+, . . . M1 radiation is forbidden in the decay of these states and the dominating decay mode is, therefore, expected to be E2 radiations to members of the ground state rotational band. However, in the decay of β-vibrational states to the ground state band, E0 transitions in competition with E2 will also be possible between states of equal spins. Electric monopole transitions are strongly hindered in the case of the γ-vibrations due to the selection rule imposed on the electromagnetic transitions by the quantum number K:

$$|K_i - K_f| = \Delta K \leqq L,$$

where L is the transition multipolarity, and i and f denote initial and final states, respectively.

Experimentally, the presence of γ-vibrational bands in deformed, even nuclei has been confirmed in a number of cases among the rare earth nuclei and among the heaviest elements. The evidence comes mainly from radioactive decay studies in which 2+ and 3+ states at about 1 MeV excitation energy have been observed systematically with the expected energy spacing and with decay properties compatible only with a $K = 2$ assignment. It may be noted that these vibrational states in general seem to contain some rotational admixtures. This is reflected by the observation of pronounced deviations from the E2 γ-branching ratios as predicted by the theory [14]) for the decay of a pure state with $K = 2$ to members of the ground state rotational band.

In contrast to the systematic observation of γ-vibrations, the experimental evidence for the presence of β-vibrational excitations is rather scanty. Among the heavy elements three β-vibrational levels have been reported, namely a 790 keV, 2+ state of Th^{232} observed in Coulomb excitation [15]), a 803 keV, 0+ state of U^{234}, and a 940 keV, 0+ state of Pu^{238}, both found in α-decay studies [15]). In the rare earth region the only evidence for the existence of β-vibrations so far is the observation of a 1450 keV, 0+ level in Er^{166} [15]) which possibly may have vibrational character.

In Sm^{152} the two levels at 1087 keV and 1235 keV have been identified previously [2,4]) as being the two first members of a γ-vibrational band.

From the present data it appears, however, that both levels probably contain admixtures of states with K values different from 2. The 1087 keV state decays by two E2 transitions to the 0+ and 2+ members of the ground state rotational band, and the ratio of the reduced γ-transition probabilities which is obtained from table 1 after correction for the fifth power energy dependence is $B(\mathrm{E2}; 2+ \rightarrow 0+) : B(\mathrm{E2}; 2+ \rightarrow 2+) = 0.44$. The theoretical value for this ratio [14]) is 0.7, assuming a pure $K = 2$ state. It may be noted that this deviation from the theoretical E2 branching ratio in the decay of the first γ-vibrational state is very normal for a deformed even nucleus in this region of the periodic table. In fact, the theoretical value 0.7 has not been reported in any case among the rare earth nuclei.

The decay properties of the second member of the γ-vibrational band also seem to deviate from the theoretical expectations. This state decays to the ground state band by the 1113 keV and 869 keV transitions, both of which are predicted by the theory to have E2 multipolarity. The experimental evidence actually favours a pure E2 assignment to the 1113 keV γ-ray, but the 869 keV radiation appears from table 1 to be M1 or a M1+E2 mixture. Unfortunately, a particularly large experimental uncertainty is associated with the determination of the internal conversion coefficient in this case. In our external conversion spectrum the 869 keV K-line and the 780 keV L-line coincide completely (see the section on experimental results), and in the internal conversion spectrum of Bobykin and Novik [5]) the K- and L-lines of the 869 keV radiation are partly mixed with the K- and L-lines of the 873 keV transition appearing in the decay of Eu^{154}. However, even considering the largest uncertainty which could reasonably well be associated with the experimental internal conversion coefficient, it seems unlikely that the 869 keV γ-ray could have pure E2 multipolarity.

The very highly converted 689 keV radiation listed in table 1 presents a particular problem in the discussion of the decay of Eu^{152}. From the works of Cork *et al.*[3]) and Bobykin and Novik [5]) the 689 keV K-conversion line can be assigned to Sm^{152}, but no coincidence experiments seem feasible on this conversion line to establish its position in the decay scheme. In the present work the corresponding γ-ray was searched for with particular care, but with a negative result. However, the transition may tentatively be incorporated in the decay scheme by the following indirect argument based on the similarity of the electron-capture decay $Eu^{152} \rightarrow Sm^{152}$ and the β-decay $Eu^{154} \rightarrow Gd^{154}$. The two daughter nuclei have the same neutron number and, on the basis of the general systematics observed in this region of the periodic table, are, therefore, expected to have similar level structures. Moreover, the ground state spins of Eu^{152} and Eu^{154} have both been measured to be 3 [16]). Actually, the proposed decay schemes present almost identical features when we consider levels in the daughter nuclei below 1.3 MeV [15]). Two

unusually highly converted radiations are observed in these decays at near-lying energies: the 689 keV transition in Sm^{152}, whose internal conversion coefficient according to this work is > 0.05, and the 693 keV transition in Gd^{154}, for which a lower limit of 0.029 is reported for the internal conversion coefficient [17]). The 693 keV internal conversion line is also observed in the electron capture decay $Tb^{154} \rightarrow Gd^{154}$, and from a detailed internal conversion and γ coincidence study of this decay it is concluded that the corresponding transition takes place between a level at 816 keV and the 123 keV, 2+ member of the ground state rotational band [18]). Weak internal conversion lines are also found in the Tb^{154} decay which probably correspond to radiations from the 816 keV level to the 0+ and 4+ members of the ground state band.

If we tentatively propose to position the 689 keV transition in Sm^{152} in the same way as the 693 keV transition in Gd^{154}, we arrive at a level in Sm^{152} at 811 keV excitation energy. The lower limit set on the 689 keV internal conversion coefficient is compatible with M3, E4 or higher multipolarity, which would involve a spin value of 5 or higher for the 811 keV state. If this were the case, M3 or E4 radiation would have to compete with radiations of lower multipole order (M1 or E2) tc the 4+ member of the ground-state rotational band, and on the basis of lifetime arguments it then appears very unlikely that the high multipole transition should be observed at all.

An alternative description of the 811 keV state, which is consistent with all the present experimental evidence, consists in considering this state as the second member of a β-vibrational band, in which case it will have spin and parity 2+, and $K = 0$. As mentioned above, such a state is expected to decay by E2 radiations to the 0+ and 4+ members of the ground state rotational band and by E0+E2 radiation to the 2+ member of this band, thus giving rise to the unusual internal conversion strength observed for the 689 keV transition. It is interesting to note that a weak internal conversion line has been reported by Bobykin and Novik at 763 keV electron energy which, if it converts in Sm, has the right energy for a transition from the 811 keV state to the ground state. Unfortunately, the expected 444 keV transition from the 811 keV level to the 367 keV, 4+ state is completely masked by the strong 444 keV, E1 transition between the 1531 keV and 1087 keV levels.

It may be noted at this point that recent measurements on the short-lived Eu^{152} isomer have revealed the presence of a 0+ level in Sm^{152} at 685 keV excitation energy, which may be interpreted as the first member of the β-vibrational band [19]). The energy separation between the two lowest members of this band thus becomes 126 keV as compared with the 122 keV energy separation in the ground state rotational band and the 148 keV

energy difference between the two first members of the γ-vibrational band. The energy difference ΔE between two members of a rotational band with spins I' and I'' is related to the moment of inertia J associated with the rotational motion by

$$\Delta E = \frac{\hbar^2}{2J}\{I''(I''+1)-I'(I'+1)\}.$$

Consequently, the observed energy differences indicate that the moments of inertia for the two vibrational bands are of the same order of magnitude as the ground state moment (about 3 % smaller in the case of the β-vibrations and about 20 % smaller for the γ-vibrational band).

In the absence of information about the Coulomb excitation cross-section or the lifetime of the 811 keV level it is not possible to estimate the absolute transition probability for the 689 keV E0 conversion electrons. From the present data we may, however, obtain the ratio of the E0 conversion rate to the E2 γ-ray rate in the $2+ \rightarrow 2+$ transition if we assume the validity of the theoretical E2 branching ratios in the decay of the 811 keV state. For a $2+$ level with $K = 0$ decaying to the $0+$, $2+$ and $4+$ members of a $K = 0$ band, the theory [14]) predicts the following ratios for the reduced E2 γ-ray transition probabilities:

$$B(\mathrm{E2};\ 2+ \rightarrow 0+) : B(\mathrm{E2};\ 2+ \rightarrow 2+) : B(\mathrm{E2};\ 2+ \rightarrow 4+) = 0.7 : 1.0 : 1.8.$$

In terms of the intensity $I_{\mathrm{e,K,811}}$ of the 811 keV internal conversion K-line the predicted intensity of the 689 keV E2 γ-ray is, therefore,

$$I_{\gamma,\mathrm{E2},689} = \frac{I_{\mathrm{e,K,811}}}{\varepsilon_{\mathrm{K,811}}} \cdot \frac{1}{0.7} \cdot \left(\frac{689}{811}\right)^5,$$

where $\varepsilon_{\mathrm{K,811}}$ denotes the internal conversion coefficient for the 811 keV E2 transition. If we insert the relative value 0.25 reported by Bobykin and Novik for $I_{\mathrm{e,K,811}}$ and the theoretical value for $\varepsilon_{\mathrm{K,811}}$, we obtain $I_{\gamma,\mathrm{E2},689} = 48$. By use of the theoretical 689 keV E2 internal conversion coefficient we can now estimate the relative intensity of the 689 keV E2 K conversion electrons to be about 0.2 in the units of Bobykin and Novik. Unfortunately, in the internal conversion spectrum published by these workers, the K lines of the 689 keV transition in Sm^{152} and the 693 keV transition in Gd^{154} are completely unresolved. We have estimated the two lines to have about the intensity ratio 5 : 4, since this is the case with the corresponding L lines, and the K/L ratios in this energy region are approximately equal for all relevant multipolarities (including E0). The relative intensity of the 689 keV K-line obtained from this estimate is ≈ 3.8 and we thus conclude that the contribution $I_{\mathrm{e,K,E0,689}}$ of E0 conversion electrons is ≈ 3.6. Hence, the ratio of the E0 conversion rate to the E2 γ-ray rate in the $2+ \rightarrow 2+$ transition is

$$\frac{I_{e,K,E0,689}}{I_{\gamma,E2,689}} \approx 0.07.$$

Since the above calculation is based on a number of assumptions which are not directly verified by experiment, the result is not considered to be more than a rough estimate. It may be noted, however, that the calculated intensity for the 689 keV γ-ray is consistent with the experimental lower limit of 0.05 for the internal conversion coefficient of the 689 keV transition.

Experimental values for the ratio of E0 conversion to E2 γ-ray emission have also been reported by the Berkeley group [20]), the values quoted being 1.0 for U^{234} and 0.5 for Pu^{238}. As these ratios are concerned with the decays of β-vibrational states of the 0+ type, they cannot be compared directly to the E0/E2 ratio obtained in the decay of the 2+ β-vibrational state of Sm^{152}. It may be reasonable, however, to make the further assumption that the reduced E2 γ-ray transition probability is of the same order of magnitude in the β-vibrational $2+ \rightarrow 2+$ transition in Sm^{152} and in the $0+ \rightarrow 2+$ transitions in the heavy elements. By correcting for the fifth power E2 energy dependence it then turns out that the 689 keV E0 transition in Sm^{152} proceeds about 0.04 times more slowly than the 803 keV E0 transition in U^{234}.

From the theoretical treatment of electric monopole transitions given by Church and Weneser [21]) it appears that E0 transition rates are expected to vary rather slowly with energy, but very rapidly with Z. A quantitative estimate of the expected variation in the E0 transition rate for an energy of about 700 keV may be obtained by inspection of fig. 1 of Church and Weneser's work. One finds that for the same value of the nuclear "strength parameter" ρ, the ratio of the E0 transition probabilities in Sm and U is expected to be about 0.01. It can thus be seen that the experimental data are consistent with the assumption that the nuclear "strength parameter" for E0 conversion is of the same order of magnitude in the decay of the 2+ β-vibrational state in Sm^{152} and in the decays of the 0+ β-vibrational states in the heavy elements, keeping in mind our above mentioned assumption about the equality of the E2 matrix elements.

The intensity of the electron capture branch leading to the 811 keV level in Sm^{152} cannot be inferred directly form the experimental data. An approximate value for the corresponding log ft value may, nevertheless, be obtained by assuming that this level is fed entirely by direct electron capture and that it decays according to our previous suggestions. A total intensity of ≈ 1 % of all disintegrations is obtained in this way for the electron capture branch to the 811 keV state, corresponding to a log ft value of about 11.3. It may be noted that the electron capture branch to the first member of the γ-vibrational band at 1087 keV has the considerably lower log ft value of 9.5,

although both states occur in the same nucleus and presumably have the same spin and parity. This can most likely be explained as a consequence of the K selection rules. The ground state of Eu^{152} is characterized by $I = K = 3$, so that $|\Delta K| = 1$ in the decay to the γ-vibrational band, while a change of K by three units is required in the decay to the β-band, resulting in a considerable retardation of the latter transition.

We like to express our sincere gratitude to Professor Aage Bohr, Copenhagen, for many stimulating discussions and for his keen interest in this problem. One of us (O.N.) also wants to thank Professor Manne Siegbahn for kind hospitality at the Nobel Institute of Physics.

References

1) L. Grodzins and H. Kendall, Bull. Am. Phys. Soc. **1** (1956) 163, 164
2) O. Nathan and M. A. Waggoner, Nuclear Physics **2** (1956) 548
3) J. M. Cork, M. K. Brice, R. G. Helmer and D. E. Sarason, Phys. Rev. **107** (1957) 1621
4) S. Ofer, Nuclear Physics **4** (1957) 477
5) B. V. Bobykin and K. M. Novik, Izv. Akad. Nauk SSSR, Ser. Fiz. **21** (1957) 1556
6) B. S. Dželepow and N. N. Zhukovsky, Nuclear Physics **6** (1958) 655
7) S. K. Bhattacherjee, T. D. Nainan, S. Raman and B. Sahai, Nuovo Cimento **7** (1958) 501
8) K. Alder, A. Bohr, T. Huus, B. Mottelson and A. Winther, Revs. Mod. Phys. **28** (1956) 432
9) S. Hultberg and R. Stockendal, Ark. f. Fysik **14** (1959) 565
10) T. Novakov, S. Hultberg and B. Andersson, Ark. f. Fysik **13** (1958) 117
11) R. Stockendal and S. Hultberg, Ark. f. Fysik **15** (1959) 33
12) G. Withe-Grodstein, Nat. Bur. Stand. Circular no. 583 (April 1957)
13) G. M. Temmer, Revs. Mod. Phys. **30** (1958) 498
14) G. Alaga, K. Alder, A. Bohr and B. Mottelson, Mat. Fys. Medd. Dan. Vid. Selsk. **29** (1955) no. 6
15) D. Strominger, J. M. Hollander and G. T. Seaborg, Table of Isotopes, Revs. Mod. Phys. **30** (1958) 585
16) M. Abraham, R. Kedzie and C. D. Jeffries, Phys. Rev. **108** (1957) 58;
A. A. Manenkov, A. M. Prokhorov, P. S. Trukhliaev and G. N. Iakovlev, Doklady Akad. Nauk SSSR **112** (1957) 623
17) J. O. Juliano and F. S. Stephens, Jr., Phys. Rev. **108** (1957) 341
18) P. Gregers Hansen, M. Jörgensen, O. Nathan, O. B. Nielsen and G. Wood, to be published
19) I. Marklund, O. Nathan, O. B. Nielsen and G. Wood, to be published
20) I. Perlman, private communication
21) E. L. Church and J. Weneser, Phys. Rev. **103** (1957) 1035
22) P. B. Moon, G. G. Shute and B. S. Sood, Phys. Rev. Letters **1** (1958) 21

2.I *Nuclear Physics* **10** (1959) 135—139; © *North-Holland Publishing Co., Amsterdam*
Not to be reproduced by photoprint or microfilm without written permission from the publisher

NUCLEAR RAMAN EFFECT

Z. MARIĆ † and P. MÖBIUS ††
Institute for Theoretical Physics, University of Copenhagen

Received 7 July 1958

Abstract: The dependence of the photo-effect on nuclear orientation is discussed. The cross-section for the excitation of rotational states in non-elastic γ-scattering by deformed nuclei is computed.

For nuclei with non-spherical equilibrium shape, the photo-effect depends on the orientation of the nucleus with respect to the direction and polarization of the photon. Thus, the giant resonance characterizing the photo-nuclear process is expected to split into two components $\omega_{\parallel}$ and $\omega_{\perp}$, corresponding to the vibrations of the nucleus parallel and perpendicular to the axis of the spheroidal nucleus [1]). Recently, experimental evidence has been obtained for such a splitting [2]).

The dependence of the photo-effect on the nuclear orientation provides at the same time a coupling to the rotational motion. We shall consider here the resulting scattering of photons with the excitation of rotational states. The phenomenon is analogous to the Raman effect in molecules. An experimental study of such processes might provide additional information about the structure of the photo-resonance in deformed nuclei.

We employ the simple collective picture of the photo-effect, and assume the absorption of the photon to lead initially to a state of ordered vibration of the nucleus with frequencies $\omega_{\parallel}$ and $\omega_{\perp}$. These vibrations have a relatively short lifetime, after which a state of more complex motion develops (formation of compound nucleus). Let us first assume that the energy of the incident photon is sufficiently large (i.e., well above the threshold for particle emission) so that we are in the excitation region where the levels of the compound nucleus overlap (level width Γ greater than level spacing D). The lifetime of the compound nucleus ($\hbar/\Gamma$) is then less than the period of motion ($\hbar/D$) and there is therefore only a small probability that the compound nucleus once formed reverts to the ordered motion of giant resonance capable of radiating to the ground state. Consequently, the emission of γ-radiation leading to the nuclear ground state, or its rotational

† On leave from the Institute for Nuclear Sciences "B. Kidrič", Belgrade, Yugoslavia.
†† Now at the Institute for Theoretical Physics, University of Göttingen, Göttingen, Germany.

excitation, arises primarily from the initial stage of the photo-process, and we can estimate the corresponding γ-scattering simply by assuming intermediate states of the giant resonance type, i.e., with energies $\hbar\omega_{\|}$ and $\hbar\omega_{\perp}$. To take into account the damping of the states, which becomes important when the photon energy is close to the resonance energies, we add the corresponding imaginary parts $-iW_{\|}$ and $-iW_{\perp}$ to these resonance energies.

If, on the other hand, the nuclear excitation energy is in the region of well-separated levels, the mechanism for the elastic and semi-elastic scattering is different, and depends on the properties of the compound nucleus.

The matrix elements for the scattering of light by a system of charged particles have the following form [3]):

$$K_{\mathrm{if}} = \sum_{n'} \frac{\langle 1\mathrm{f}|H_{\mathrm{int}}|0n'\rangle\langle 0n'|H_{\mathrm{int}}|\mathrm{i}1\rangle}{E_0 - E_{n'} + \hbar\omega_0} + \sum_{n''} \frac{\langle 1\mathrm{f}|H_{\mathrm{int}}|n''2\rangle\langle n''2|H_{\mathrm{int}}|\mathrm{i}1\rangle}{E_0 - E_{n''} - \hbar\omega}, \tag{1}$$

where 0, 1, and 2 denote the number of photons present in the particular state, i and f are the initial and final state of the nucleus, n' and n'' are the intermediate states, E_0 is the ground state energy of the nucleus, $E_{n'}$ and $E_{n''}$ are the energies of intermediate states which, according to the above consideration, represent the giant resonance states with damping effects included, and $\hbar\omega_0$, $\hbar\omega$ are the energies of incoming and outgoing radiation quanta, respectively.

The emission and absorption of the electric dipole part of electromagnetic radiation can be expressed in the usual manner, through the electric dipole moment operators, which one gets by taking the electric dipole term of the multipole expansion of the vector potential $\mathbf{A}(\mathbf{r})$ which stands in the interaction Hamiltonian

$$H_{\mathrm{int}} = -\frac{1}{c}\int \mathbf{j}_n(\mathbf{r}) \cdot \mathbf{A}(\mathbf{r})\mathrm{d}\mathbf{r}, \tag{2}$$

where $\mathbf{j}_n(\mathbf{r})$ is the nuclear current. In this representation, the matrix elements that occur in (1) have a very simple form:

$$\langle 0n'|H_{\mathrm{int}}|\mathrm{i}1\rangle = \frac{4\omega_0}{3\hbar c}\left(\frac{\pi}{R}\right)^{\frac{1}{2}}(E_{n'} - E_0)\langle n'|M(\mathrm{E}1, \mu)|\mathrm{i}\rangle \tag{3a}$$

$$\langle 1\mathrm{f}|H_{\mathrm{int}}|0n'\rangle = \frac{4\omega}{3\hbar c}\left(\frac{\pi}{R}\right)^{\frac{1}{2}}(E_{\mathrm{f}} - E_{n'})\langle \mathrm{f}|M^*(\mathrm{E}1, \mu')|n'\rangle \tag{3b}$$

and similarly for the others; here E_{f} is the energy of the final state of the nucleus, and

$$M(\mathrm{E}1, \mu) = \frac{Ze}{A}\sum_{p=1}^{Z} r_p Y_{1\mu}(\vartheta_p, \varphi_p) - \frac{Ne}{A}\sum_{n=1}^{N} r_n Y_{1\mu}(\vartheta_n, \varphi_n). \tag{4}$$

The first sum has to be taken over all protons, the second one over all

neutrons; μ and μ' are the z-components of the angular momentum of absorbed and emitted light quanta, respectively, and $M^*(\mathrm{E1}, \mu)$ means the complex conjugate of (4). (In the expression (4), the mesonic effects are neglected; see below.)

The transition probability

$$p = \frac{2\pi}{\hbar} |K_{\mathrm{if}}|^2 \rho(E) \tag{5}$$

and the cross section σ for definite polarization of light quanta are connected through the relation

$$\sigma = (2\lambda+1) \frac{\pi R c}{(\hbar\omega_0)^2} p, \tag{6}$$

where R is the radius of normalization sphere, and λ is the multipole order. The number of states in the energy interval is equal to

$$\rho(E) = \frac{R}{\pi\hbar c}. \tag{7}$$

In order to treat the dependence of the photo-nuclear interaction on the orientation of a nuclear system, one writes (4) in the system fixed in the nucleus

$$M(\mathrm{E1}, \mu) = \sum_{\nu} \mathscr{D}^1_{\mu\nu} M'(\mathrm{E1}, \nu), \tag{8}$$

where $\mathscr{D}^1_{\mu\nu}$ are irreducible representation matrices of the 3-dimensional rotation group and $M'(\mathrm{E1}, \mu)$ is the operator (4) in the system fixed in the nucleus, and one makes the separation into two parts, one of which gives rise to the dipole vibrations along the symmetry axis of a deformed nucleus ($\nu = 0$), and another one which gives rise to the dipole vibrations along the axis perpendicular to the symmetry axis ($\nu = \pm 1$). Then, one can write (1) in the form

$$K_{\mathrm{if}} = \frac{8\omega\omega_0}{9\hbar^2 c} \frac{\pi}{R} \sum_{\nu} (E_\nu - E_0) \langle \mathrm{f}|\mathscr{D}^1_{\mu\nu} M'(E1,\nu)|\nu\rangle\langle\nu|\mathscr{D}^1_{\mu'\nu} M'(\mathrm{E1},\nu)|\mathrm{i}\rangle \times \left\{ \frac{E_{\mathrm{rot}} - (E_\nu - E_0)}{E_0 - E_\nu + \hbar\omega_0} + \frac{E_{\mathrm{rot}} - (E_\nu - E_0)}{E_0 - E_\nu - \hbar\omega} \right\}, \tag{9}$$

where now ν denotes the intermediate states. E_{rot} is the energy of the rotational state in question, and it is equal to the difference between the energies of the final and initial states of the nucleus ($E_{\mathrm{rot}} = E_f - E_i$).

One can simplify the expression (9) by supposing that the energy spacing of the members of the rotational band belonging to each value of ν, i.e., to each intermediate state, is small compared to the vibrational energies ($E_{\mathrm{rot}} < E_{\|}, E_\perp$; $E_{\|} = \hbar\omega_{\|} - iW_{\|}$; $E = \hbar\omega_\perp - iW_\perp$). Then,

$$K_{\mathrm{if}} = \sum_{\nu=-1}^{+1} \langle \mathrm{f}|\mathscr{D}^1_{\mu\nu}\mathscr{D}^{\alpha'}_{\mu'\nu}|\mathrm{i}\rangle A^\nu, \tag{10}$$

where

$$A^\nu = \frac{8\omega\omega_0}{9\hbar^2 c}\,\frac{\pi}{R}\,(E_\nu - E_0)|\langle \nu||M'(\mathrm{E1},\nu)||\mathrm{i}\rangle|^2 \times \left\{\frac{E_{\mathrm{rot}}-(E_\nu-E_0)}{E_0-E_\nu+\hbar\omega_0} + \frac{E_{\mathrm{rot}}-(E_\nu-E_0)}{E_0-E_\nu-\hbar\omega}\right\}. \tag{11}$$

We use the symbols for a reduced matrix element in (11) to indicate that it is the matrix element between intrinsic states of the nucleus.

The evaluation of (11) can be done most easily by applying the sum rule for the dipole oscillator strength and by taking into account the fact that $\frac{1}{3}$ of the oscillator sum is associated with $\omega_{\|}$ and $\frac{2}{3}$ with $\omega_\perp$. Then, one obtains

$$A^0 = \frac{1}{3}\,\frac{(\omega\omega_0)^{\frac{1}{2}}}{c^2}\cdot\frac{\hbar}{RM}\,\frac{NZ}{A}\,e^2 f\left\{\frac{-E_{\|}}{-E_{\|}+\hbar\omega_0} + \frac{-E_{\|}}{-E_{\|}-\hbar\omega}\right\} \tag{12}$$

and

$$A^1 = A^{-1} = \frac{1}{3}\,\frac{(\omega\omega_0)^{\frac{1}{2}}}{c^2}\,\frac{\hbar}{RM}\,\frac{NZ}{A}\,e^2 f\left\{\frac{-E_\perp}{-E_\perp+\hbar\omega_0} + \frac{-E_\perp}{-E_\perp-\hbar\omega}\right\}, \tag{13}$$

where M is the proton mass, e the electronic charge, and the factor f takes into account the increase of the oscillator sum due to the mesonic effects [4]). The empirical value of f appears to be $f \approx 1.3$.

The integration over the rotational functions occurring in the matrix element (10)

$$\langle \mathrm{f}|\mathscr{D}^1_{\mu\nu}\mathscr{D}^1_{\mu'\nu}|\mathrm{i}\rangle$$

can be carried out easily. One sees that two of four Clebsh-Gordan coefficients that appear in the result of integration depend on the magnetic quantum numbers of the nucleus and the light quantum. If, however, in the expression for the cross section one sums over the magnetic quantum number M_{f} (the z-component of the spin of final nuclear state I_{f}) and averages over the magnetic quantum number M_1 (the z-component of the ground state spin I_1), one obtains

$$\frac{1}{2I_1+1}\sum_{\mu_1\mu_1}|K_{\mathrm{if}}|^2 = \frac{1}{3}\,\frac{2I_{\mathrm{f}}+1}{2I_1+1}\,|\sum_{j\nu}(-)^\nu A_j{}^\nu|^2, \tag{14}$$

where $A_j{}^\nu$ is equal to

$$A_j{}^\nu = \sqrt{\frac{2I_1+1}{2I_{\mathrm{f}}+1}}\,(1\nu 1-\nu|11j0)(j0I_1K_1|jI_1I_{\mathrm{f}}K_{\mathrm{f}})A^\nu. \tag{15}$$

K_1 and K_{f} are the z-components of I_1 and I_{f} in the system fixed in the nucleus; j can be 0,1 and 2; A^ν stands for (12) and (13).

Using the relation (6), one gets from (14) for the total cross-section for the inelastic scattering of γ-rays accompanied with the excitation of the rotational states (members of ground state rotational band) of strongly deformed nuclei the following expression (Raman effect):

$$\sigma_{\text{inel}} = \frac{2\pi}{108}\left(\frac{e^2}{Mc^2}\right)^2\left(\frac{NZ}{A}\right)^2\left(\frac{\hbar\omega_0}{\hbar\omega}\right)f^2 \cdot \left\{\sum_j (j0I_1K_1|jI_1I_fK_1)[(1010|11j0)\{\|\}-2(11-11|11j0)\{\perp\}]\right\}^2 \tag{16}$$

where $\{\|\}$ and $\{\perp\}$ represent the energy brackets in (12) and (13).

In particular, the cross-section for the excitation of the first rotational state of an even nucleus ($I_1 = K_1 = 0$; $I_f = 2$; $j = 0$) becomes equal to

$$\sigma_{\text{inel}}^{\text{even}} = \frac{16\pi}{27}\left(\frac{e^2}{Mc^2}\right)^2\left(\frac{NZ}{A}\right)^2 f^2\left\{\frac{E_\|^2}{E_\|^2-(\hbar\omega)^2} - \frac{E_\perp^2}{E_\perp^2-(\hbar\omega)^2}\right\}^2, \tag{17}$$

where we have further neglected E_{rot} as compared to $\hbar\omega_0$. (For odd-mass nuclei, two states will be excited, corresponding to $j = 1$ and $j = 2$.) The cross-section (17) vanishes for very small energies of incoming radiation quanta, and, of course, for non-deformed nuclei ($E_\| = E_\perp$).

In the same approximation, the resonance contribution to the cross-section for the elastic scattering becomes equal to

$$\sigma_{\text{el}}^{\text{even}} = \frac{8\pi}{27}\left(\frac{e^2}{Mc^2}\right)^2\left(\frac{NZ}{A}\right)^2 f^2\left\{\frac{E_\|^2}{E_\|^2-(\hbar\omega)^2} + 2\frac{E_\perp^2}{E_\perp^2-(\hbar\omega)^2}\right\}^2. \tag{18}$$

This formula shows explicitly the separation of the electric dipole oscillator strength into two parts.

For strongly deformed nuclei, one expects the same order of magnitude (about $10^{-25} - 10^{-24}$ cm^2) at the peak values of energy of the splitted giant resonance, and for an order of magnitude less between the peaks.

We wish to express our gratitude to Professor Aage Bohr for suggesting the problem and for enlightening discussions. Thanks are also due to Professor Niels Bohr for the hospitality granted at the Institute for Theoretical Physics. One of us (Z. M.) is indebted to the Rask-Ørsted Foundation for a grant.

References

1) Okamoto, Prog. Theor. Phys. **15** (1956) 75; Danos, Bull. Am. Phys. Soc. **2** (1956) 135
2) Fuller and Weiss, NBS Report, 5687 (April 1958); Johansson, to be published
3) Dirac, Principles of Quantum Mechanics (Oxford University Press, London, 1947)
4) Levinger and Bethe, Phys. Rev. **78** (1950) 115

8.C *Nuclear Physics* **10** (1959) 140—150; ©*North-Holland Publishing Co., Amsterdam*
Not to be reproduced by photoprint or microfilm without written permission from the publisher

AN EXAMPLE OF A FIELD THEORY WITH INDEFINITE METRIC IN HILBERT SPACE (I)

M. MARKOV
Joint Institute of Nuclear Research, Dubna, U.S.S.R.

Received 15 September 1958

Abstract: A field theory is considered in which the Green's functions have singularities not on a cone but on a hyperboloid. The metric of the corresponding Hilbert space is indefinite.

Equations of motion for the boson and fermion fields are derived. The theory goes over to the usual field theory when a certain constant (characteristic length) approaches zero.

The ultimate aim of the investigation is an attempt to find a possible reasonable interpretation of the negative energy density of the boson fields, of the negative probabilities, and of other similar features which appear in the theory, by appropriately modifying the concept of a particle coordinate so as to obtain the proposed propagation functions.

1. Introduction

At present a study of the various types of field theories possessing an indefinite metric in Hilbert space seems to be of interest. A characteristic feature of the field theory considered here is the existence of a small constant a which has the dimensions of length. This constant ensures the convergence of expressions which diverge in the usual theory. However, the most important point is that when this constant approaches zero the theory goes over to the usual theory with a definite metric.

This feature of the theory seems to indicate that the specificity of physical phenomena due to indefiniteness of the metric becomes appreciable only outside the region of applicability of the usual field theory, that is, in the immediate neighbourhood of the particles.

In the theory under consideration a finite velocity of propagation of a signal is attained by proper choice of the propagation function, the singularities of this function being removed from the cone to a hyperboloid in a time-like region.

The new propagation functions and equations of motion corresponding to them are obtained by modifying the concept of particle coordinate, it being necessary for this to change substantially the ordinary metric properties of space.

This modification of the concept of a particle coordinate permits one to offer a natural interpretation of the so-called negative probabilities which then arise or, to be more precise, of the expressions which for $a \to 0$ go over

to expressions for the probability density in the ordinary theory; other peculiar effects related to the densities of physical quantities in a space-time region located between the usual light cone and hyperboloid considered in the present theory can also be treated (II).

2. Particle Coordinate

Quantum theory has retained the concept of a particle coordinate in the sense that in quantum theory, as in classical mechanics, the possibility is not ruled out that particle states exist which can be represented by a δ-function in coordinate space.

At present the possibility of such states should be recognized as an arbitrary extrapolation of comparatively rough experience.

Let us now assume that as a consequence of a measurement of maximum precision the coordinate q of an elementary particle can be represented in the form

$$q_i = x_i + \xi_i \qquad (i = 1, 2, 3, 4), \tag{1}$$

where the distribution function $f_n(\xi)$ for ξ_i, for an experiment of highest possible precision, differs from the δ-function [1]).

This hypothesis thus violates the fundamental property of reproducibility (Wiederholbarkeit) in particle coordinate measurements [2]).

Generally speaking, it is conceivable that the function $f_n(\xi)$ may differ for different elementary particles (subscript n) and may even significantly determine their nature [1]). The function $f_n(\xi)$ does not bear any relation to the wave-function of quantum theory or to its square, it is an absolutely new quantity. Such a function $f_n(\xi)$ could be introduced into classical field theory and mechanics, as it does not contain Planck's [1]) constant.

Furthermore, let the symmetry of $f_n(\xi)$ be such that after averaging over ξ one gets

$$\bar{q}_i = x_i. \tag{2}$$

Assume, moreover, that the mean square $\overline{\xi_i^2}$ for the distribution $f_n(\xi)$ does not vanish. This signifies that the mean of the form

$$q_0^2 - \mathbf{q}^2 \tag{3}$$

can be expressed as

$$\overline{q_0^2 - \mathbf{q}^2} = x_0^2 - \mathbf{x}^2 - a_n^2 \tag{4}$$

where a_n is a constant specifying the extension of the distribution $f_n(\xi)$. Suppose that a_n^2 is a constant, i.e., is invariant under Lorentz transformations. Then instead of the usual quadratic form

$$s^2 = -x_\mu^2 = x_0^2 - \mathbf{x}^2 \tag{5}$$

a new fundamental form

$$s_n'^2 = -(x_\mu^2 + a_n^2) \tag{6}$$

will appear which is invariant under Lorentz transformations.

Let us now consider a physical world in which the usual interval $s^2 = -x_\mu^2$ is replaced by a new quadratic form $s_n'^2 = -(x_\mu^2 + a_n^2)$, the meaning of a_n^2 being that given above.

For the sake of illustration we shall consider in the following only such effects for which the constant a_n remains the same, i.e., strong † interactions; electromagnetic interactions are assumed to be of this type.

3. Classical Theory

For simplicity we shall consider one type of elementary particles †† ($a_n = a$) interacting with the electromagnetic field.

The D'Alembert equation expressed in variables of the ordinary interval $s^2 = -x_\mu^2$ can be written in the form

$$\frac{d^2 A_\mu(s)}{ds^2} + \frac{3}{s}\frac{dA_\mu(s)}{ds} = 0. \tag{7}$$

The solution of this equation is

$$A_\mu(s) = \frac{\alpha_\mu}{s^2} \tag{8}$$

where α_μ is the integration constant.

By analogy with (7) a new field equation can be written in the form

$$\frac{d^2 A_\mu(s')}{ds'^2} + \frac{3}{s'}\frac{dA_\mu(s')}{ds'} = 0 \tag{9}$$

where $s'^2 = s^2 - a^2$.

The solution of this equation is similar to that of equation (7):

$$A_\mu(s') = \frac{\beta_\mu}{s'^2}. \tag{10}$$

On the basis of a formal analogy between equations (7) and (9) and their solutions (8) and (10) one can assert that all physical quantities in the field theory under consideration when expressed in terms of s' will have the same mathematical structure as the corresponding expression in electrodynamics. We have in view here the potentials $A_\mu(s')$, Green's functions $D(s')$, $D^{(1)}(s')$ and other quantities which in ordinary electrodynamics can be expressed as functions of the interval, i.e., any of the functions $F(s) \to F(s')$.

† From this viewpoint a characteristic feature of weak interactions [1]) is the substantial change in the nature of the particles (a change in a_n signifies decay of the particle).

†† To be more precise, $a^2 = a_n^2 + a_m^2$, if the mean square of the distance between particles of type m and n is considered:

$$-\overline{(q_n - q_m)_\mu^2} = -(x_n - x_m)_\mu^2 - a_n^2 - a_m^2.$$

4. Green's Function

In accord with the foregoing the electromagnetic field propagation (Green's) function will be assumed to have the form

$$G(x-x') = \bar{D}(s')$$

or

$$\bar{D}(s') = \frac{\delta(s'^2)}{4\pi} \tag{11}$$

where

$$\begin{aligned} s'^2 &= c^2T^2-\mathbf{R}^2-a^2, \\ \mathbf{R} &= \mathbf{r}-\mathbf{r}', \qquad T = t-t'. \end{aligned} \tag{12}$$

Thus, in contrast to the Green's function of the ordinary field theory the Green's function under consideration has singularities not on a cone but on a hyperboloid (fig. 1).

Knowing the Green's function, one can determine the potential in the form

$$A_\mu(\mathbf{r}, t) = 4\pi e\int G(\mathbf{r}, \mathbf{r}'; t, t')j_\mu \mathrm{d}\mathbf{r}'\,\mathrm{d}t' \tag{13}$$

where j_μ is the current vector.

With the aid of the relation

$$\delta(s'^2) = \frac{\delta(\sqrt{R^2+a^2}+cT)+\delta(\sqrt{R^2+a^2}-cT)}{2\sqrt{R^2+a^2}} \tag{14}$$

the retarded and advanced potentials can be found in the form

$$A_\mu^{\mp}(\mathbf{r}, t) = \tfrac{1}{2}e\int\frac{\delta(\sqrt{(\mathbf{r}-\mathbf{r}')^2+a^2}\mp c(t-t'))j_\mu(\mathbf{r}', t')}{\sqrt{(\mathbf{r}-\mathbf{r}')^2+a^2}}\,\mathrm{d}\mathbf{r}'\,\mathrm{d}t' \tag{15}$$

and Coulomb's law assumes the form

$$\varphi = \frac{e}{\sqrt{r^2+a^2}}. \tag{16}$$

Function $D^{(1)}(s)$ satisfies the equation

$$\Box D^{(1)}(s) = 0. \tag{17}$$

By analogy $D^{(1)}(s')$ can be immediately written down as follows:

$$D^{(1)}(s') = -\frac{1}{2\pi s'^2}.$$

The Green's function in electrodynamics satisfies the equation (see appendix)

$$\Box\bar{D}(s) = -\delta(x-x') \equiv f(s) \tag{18}$$

where

$$\delta(x) = \prod_{i=1}^{4} \delta(x_i);$$

or, according to (7), in s-space,

$$\frac{d^2 \bar{D}(s)}{ds^2} + \frac{3}{s}\frac{d\bar{D}(s)}{ds} = f(s). \tag{19}$$

By substituting $s \to s'$ we obtain for the new Green's function a formally identical equation

$$\frac{d^2 \bar{D}(s')}{ds'^2} + \frac{3}{s'}\frac{d\bar{D}(s')}{ds'} = f(s'). \tag{20}$$

However, now $f(s') \neq \delta(x)$, and by its very nature $f(s')$ should be a function of the type of a four-dimensional δ-function which contains in its argument a constant a. However, by definition the equation for the Green's function should be of the form

$$L\bar{D}(s') = -\delta(x-x'). \tag{21}$$

In order that the right-hand side of eq. (20) assume the form $f(s) = -\delta(x-x')$ it is sufficient to act on the right and left hand sides of equation (20) by the operator $\exp(a^2\partial/\partial s'^2)$:

$$e^{a^2 \frac{\partial}{\partial s'^2}} f(s') = f(s). \tag{22}$$

The equation for the Green's function $\bar{D}(s')$ can then be written as

$$e^{a^2 \frac{\partial}{\partial s'^2}} \left(\frac{d^2 \bar{D}(s')}{ds'^2} + \frac{3}{s'}\frac{d\overline{D(s')}}{ds'} \right) = -\delta(x-x'). \tag{23}$$

Thus, the equation for the propagation function is an equation of an infinitely high order.

The important point here is that a signal from a point source located at the coordinate origin (fig. 1) is retarded to a greater extent than that in electrodynamics:

$$t = \frac{1}{c}\sqrt{r^2+a^2}.$$

As a result of averaging over the particle coordinates (q) a finite time gap $t_0 = a$ appears. This is a finite time interval during which the particle on the average retards, as it were, the start of the signal.

It is natural that this characteristic feature of the mechanism of signal propagation over a finite time interval at the initial instant of time cannot be described by a finite order equation.

A cardinal and absolutely new feature of the theory presented here is the new meaning of the propagation function. The essential point to be emphas-

ised is that in the usual theory the test body does not distort the propagation functions.

In the present theory the character of the propagation function changes in a peculiar way near the source. The singularities of the function shift from a cone to a hyperboloid. In the presence of a source the so-called "free field" is, in this sense, even a less satisfactory approximation in the present theory than in the ordinary one (not only the charge e is assumed to vanish, but also $a = 0$).

Indeed, in order to elucidate the nature of the propagation function of a source-free field, a test body should be introduced at points x and y which records the time as signal leaves x and arrives at y. However, test bodies (e.g., an elementary source) change the propagation function in the given region irrespective of the magnitude of their electric charge.

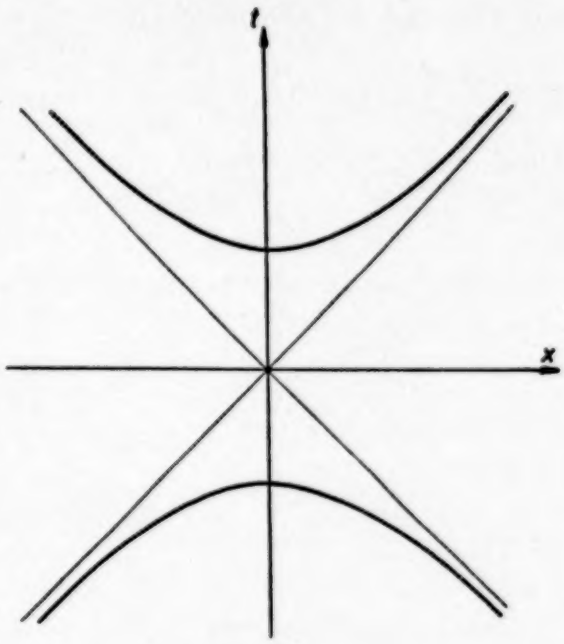

Fig. 1

The peculiar non-locality of the present theory is consistent with relativity in a curious fashion.

In a real experiment performed to determine the propagation of the field it should not be possible to obtain a signal moving with a velocity exceeding that of light: if the signal arrived at the field source at a time interval $\Delta t = a$, before that permitted in the usual theory (lower branch of hyperboloid), it would be "delayed" by the emitter (upper branch of hyperboloid).

For the same reason an emitted wave cannot appear before the absorbed one.

The idea of employing the form $s'^2 = s^2 + a^2$ instead of s^2 has repeatedly been suggested in the literature. Thus, it was proposed by Landé [3]) on the

basis of Born's principle of reciprocity and by Ingraham [4]) on considerations of conformal relativity ($a = x_5$ being a fifth coordinate). However, in all cases it was assumed that potentials similar to (15) satisfy the Maxwell equations with a distributed charge. A theory of this sort is internally inconsistent [5]). As a matter of fact, however, it is not necessary to assume a distributed charge because in the integrand in (13) the form of the Green's function can be changed without affecting the point-like nature of the charge. It is precisely this latter possibility which is exploited in the present paper. A similar idea is contained in an earlier paper by Groenewold [6]), but in outline form.

5. Propagation Function in Momentum Representation

As in the ordinary theory the propagation functions under consideration can be expressed in the form of the integrals

$$\bar{D}(s') = \frac{1}{4\pi^2}\int_0^\infty \cos(s'^2\alpha)\mathrm{d}\alpha = \frac{1}{8\pi^2}\int_{-\infty}^{+\infty} \mathrm{e}^{is'^2\alpha}\mathrm{d}\alpha, \tag{24}$$

$$D^{(1)}(s') = -\frac{1}{2\pi^2}\int_0^\infty \sin(s'^2\alpha)\mathrm{d}\alpha. \tag{25}$$

From these two functions an analogue of the causal function can be set up which satisfies the same equation: (23)

$$D_c(s') = \bar{D}(s') + \tfrac{1}{2}iD^{(1)}(s'), \qquad D_F = \frac{2}{i}D_c \tag{26}$$

or

$$D_c(s') = \frac{1}{4\pi}\int_0^\infty \mathrm{e}^{i\alpha s'^2}\,\mathrm{d}\alpha. \tag{27}$$

In the k-representation

$$D_c(k) = \frac{1}{(2\pi)^4}\,\frac{1}{4\pi^2}\int_{-\infty}^{+\infty}\mathrm{d}^4x\int_0^\infty \mathrm{e}^{i(x_\mu{}^2\alpha - k_\mu x_\mu) + i\alpha^2\alpha}\,\mathrm{d}\alpha. \tag{28}$$

After integration over x and substitution of $\beta = 1/4\alpha$ we obtain

$$D_c(k) = \frac{i}{(2\pi)^4}\int_0^\infty \mathrm{e}^{-i(k_\mu{}^2\beta - a^2/4\beta)}\mathrm{d}\beta, \tag{29}$$

$$\bar{D}(k) = \frac{1}{(2\pi)^4}\int_0^\infty \sin\left(k_\mu{}^2\beta - \frac{a^2}{4\beta}\right)\mathrm{d}\beta, \tag{30}$$

$$D^{(1)}(k) = \frac{2}{(2\pi)^4}\int_0^\infty \cos\left(k_\mu{}^2\beta - \frac{a^2}{4\beta}\right)\mathrm{d}\beta. \tag{31}$$

As the structure of the form

$$\mathbf{x}^2 + a^2 - x_0{}^2 \tag{32}$$

is similar to that of the form

$$\mathbf{p}^2+m^2-E^2 \tag{33}$$

it is natural that on changing in our case from the x-representation to k-representation the integrals for the D-function turn out to be similar to those obtained in transformations of the usual type of Δ-functions in changing from the momentum to x-representation.

In the familiar integrals [7]), m^2 is now replaced by the constant a^2. Thus, by analogy [7]), the integrals for $\bar{D}(k)$ and $D^{(1)}(k)$ one can write in the momentum representation, without performing any calculations,

$$\bar{D}(k)=\frac{a^2}{(2\pi)^4}\tfrac{1}{2}\pi\,\mathrm{Im}\,\frac{H_1^{(1)}(a\Lambda^{\frac{1}{2}})}{a\Lambda^{\frac{1}{2}}}=\begin{cases}\dfrac{a^2}{4(2\pi)^3}\cdot\dfrac{N_1(a\Lambda^{\frac{1}{2}})}{a\Lambda^{\frac{1}{2}}} & \text{for } \Lambda>0\\[2ex] \dfrac{a^2}{2\pi(2\pi)^3}\cdot\dfrac{K_1(a\sqrt{-\Lambda})}{a\sqrt{-\Lambda}} & \text{for } \Lambda<0\end{cases} \tag{34}$$

where $\Lambda=-k_\mu{}^2=k_0{}^2-\mathbf{k}^2$, and

$$\begin{aligned} D^{(1)}(k)&=\frac{1}{(2\pi)^3}\left\{\delta(\Lambda)-\tfrac{1}{2}a^2\,\mathrm{Re}\,\frac{H_1^{(1)}(a\Lambda^{\frac{1}{2}})}{a\Lambda^{\frac{1}{2}}}\right\},\\ \mathrm{Re}\,\frac{H_1^{(1)}(a\sqrt{\Lambda})}{a\sqrt{\Lambda}}&=\begin{cases}I_1(a\sqrt{\Lambda}) & \text{for } \Lambda>0,\\ 0 & \text{for } \Lambda<0.\end{cases}\end{aligned} \tag{35}$$

The asymptotic behaviour of $\bar{D}(\Lambda)$ (for $\Lambda\to\infty$) has the form

$$\bar{D}(\Lambda)\underset{\Lambda\to\infty}{\sim}\begin{cases}\dfrac{a^{\frac{1}{2}}}{4(2\pi)^3}\sqrt{\dfrac{2}{\pi}}\,\dfrac{\sin(a\Lambda^{\frac{1}{2}}-\frac{3}{4}\pi)}{\Lambda^{\frac{3}{4}}} & \text{for } \Lambda>0 \qquad (36)\\[2ex] \dfrac{a^{\frac{1}{2}}}{(2\pi)^4}\sqrt{\dfrac{2}{\pi}}\,e^{-a|\Lambda|^{\frac{1}{2}}}\dfrac{1}{|\Lambda|^{\frac{3}{4}}} & \text{for } \Lambda<0. \qquad (37)\end{cases}$$

Thus, the asymptotic behaviour of the Green's function $\bar{D}(\Lambda)$ is described either by an exponentially decreasing function of Λ or by damped oscillations.

The asymptotic behaviour of $D^{(1)}(\Lambda)$ is

$$D^{(1)}(\Lambda)\underset{\Lambda\to\infty}{\sim}\frac{1}{(2\pi)^3}\begin{cases}\delta(\Lambda)-\dfrac{a^{\frac{1}{2}}}{\sqrt{2\pi}}\,\dfrac{\cos\,(a\Lambda^{\frac{1}{2}}-\frac{3}{4}\pi)}{\Lambda^{\frac{3}{4}}} & \text{for } \Lambda>0 \qquad (38)\\[2ex] \delta(\Lambda) & \text{for } \Lambda<0. \qquad (39)\end{cases}$$

6. Indefinite Metric

An arbitrary function $F(k_\mu{}^2)$ can be represented in the form

$$F(k_\mu{}^2=)\int F(-\kappa^2)\delta(k_\mu{}^2+\kappa^2)\mathrm{d}\kappa^2. \tag{40}$$

Therefore all the D-functions described above can formally be transformed into integrals of ordinary propagation functions of the parameter κ^2 (mass parameter). For example

$$D(x) = \frac{2}{i(2\pi)^4} \int e^{ikx} dk \varepsilon(k_0) \int\int \cos\left(\kappa^2\beta - \frac{a^2}{4\beta}\right) \delta(k_\mu{}^2 + \kappa^2) d\beta d\kappa^2 \quad (41)$$

or

$$D(s') = \frac{1}{\pi} \int\int \Delta(s, \kappa^2) \cos\left(\kappa^2\beta - \frac{a^2}{4\beta}\right) d\beta d\kappa^2 \quad (42)$$

or

$$D(s') = \int \Delta(s, \kappa^2) \left\{\delta(\kappa^2) - \tfrac{1}{2}a^2 \operatorname{Re} \frac{H_1^{(1)}(a, \kappa)}{a\kappa}\right\} d\kappa^2 \quad (43)$$

or

$$D(s') = D(s) - \int \tfrac{1}{2}a^2 \frac{I_1(a\kappa)}{a\kappa} \Delta(s, \kappa^2) d\kappa^2. \quad (44)$$

From (42) it follows that a propagation function satisfying equation (23) can be represented in the form of a definite superposition of $\Delta(s, \kappa)$-functions obeying the Klein-Gordon equation. This example is particularly interesting because it is just the shift of the propagation function singularity from the cone to the hyperboloid which leads to the given type of Lehmann function

$$\rho(\kappa^2) = \int \cos\left(\kappa^2\beta - \frac{a^2}{4\beta}\right) d\beta. \quad (45)$$

This change in the propagation function apparently leads to the appearance of an indefinite metric in Hilbert space inasmuch as (45) is a function of variable sign.

The question arises as to what extent the negative metric in Hilbert space involved in the peculiar example just described can be important for real effects.

The peculiarity of this example is due to the fact that although the expanded expression of the solution in the form of (44) is meaningful, the theory nevertheless does not possess free solutions which can be ascribed to various real masses κ involved in the reactions. Another reason is that in the type of theory under consideration a small length is intrinsically involved.

Thus, "far away" from the particle (for $s^2 \gg a^2$) all relations derived in the present theory change into those of the ordinary theory. In indefinite metric theories which do not contain a length related to the interaction region, points at infinity are not preferred in any way.

7. Equations in x-Space

Equations (9) and (23) yield solutions which can be expressed as functions of the interval. A heuristic procedure can be proposed which can be used to directly write the corresponding equations in x-space.

Noting that the substitution

$$x'_\mu \to x_\mu \frac{s'}{s} \tag{46}$$

changes the quadratic form

$$s^2 \to s'^2 \tag{47}$$

one can write the D'Alembert equation as

$$\Box' A = 0 \tag{48}$$

and with the help of transformation (46) change to a (comparatively complex) equation in terms of x.

For the Dirac equation this procedure yields a new equation

$$\frac{s}{s'}\left\{\gamma_\mu \frac{\partial \psi}{\partial x_\mu} + \frac{a^2}{s^4}\gamma_\nu x_\nu x_\mu \frac{\partial \psi}{\partial x_\mu}\right\} + m\psi = 0. \tag{49}$$

According to (46) and (49) the fundamental solution of this equation, which corresponds to a plane wave in the usual theory is †

$$\psi \propto e^{ikxs'/s}. \tag{50}$$

It can be verified by substitution that solution (50) satisfies equation (48) under the usual condition

$$\sum_\mu k_\mu^2 = 0. \tag{51}$$

It should be emphasized that equations (9), (23) are translationally invariant, the source and field coordinates entering them in the form of a difference. In the expanded form of equation (48) the x have the same meaning. In this sense the equations under discussion are not "free-field" equations ($a \neq 0$).

The Lagrangian, expressions for energy tensor, current vector, the corresponding conservation laws, etc., have been found for the boson field (48) and fermion field (49) equations. These results and the physical effects connected with an indefinite metric will be discussed in a following paper of the author and A. Komar.

In conclusion the author expresses his appreciation to A. Komar and Yu. Usachov for stimulating discussions.

Appendix

The four-dimensional $\delta(x)$ function can be obtained in terms of the interval s by directly substituting $\bar{D}(s)$ in eq. (7) and writing $\bar{D}(s)$ in the parametric form

$$\bar{D}(s) = \frac{1}{8\pi^2}\int_{-\infty}^{+\infty} e^{is^2\alpha}\, d\alpha.$$

† A solution of the same type as (50) was first found by Yu. Usachov as a direct solution of the very complicated equation (48) expressed in x variables.

In the right-hand side of the equation one obtains (after substituting $\alpha = 1/4\beta$) the expression

$$\frac{1}{16\pi^2} \frac{\sin(s^2/4\beta)}{\beta^2}\Bigg|_0^\infty,$$

that is,

$$\delta(x) = -\frac{1}{16\pi^2} \frac{\sin(s^2/4\beta)}{\beta^2}$$

for $\beta \to 0$.

The same expression can be directly obtained as the real part of the integral

$$\delta(x) = \frac{1}{(2\pi)^4} \int e^{i(\beta k_\mu^2 + x_\mu k_\mu)} \, dk$$

for $\beta \to 0$.

References

1) M. Markov, Hyperons and K-Mesons (GTTI, Moscow, 1958)
2) L. Landau and R. Peierls, Zt. f. Phys. **69** (1931) 56
3) A. Landé, Phys. Rev. **56** (1939) 482; **76** (1949) 1176
4) R. Ingraham, Phys. Rev. **101** (1956) 1410
5) A. Komar and M. Markov, JETP (in press)
6) Groenewold, Physica **6** (1939) 115
7) J. Schwinger, Phys. Rev. **75** (1949) 651

1.B:2.L *Nuclear Physics* **10** (1959) 151—159; © *North-Holland Publishing Co., Amsterdam*
Not to be reproduced by photoprint or microfilm without written permission from the publisher

HIGH ENERGY NUCLEON-DEUTERON ELASTIC SCATTERING AND THE NUCLEON-NUCLEON FORCES

JERZY SAWICKI and SHIGUEO WATANABE †
Palmer Physical Laboratory, Princeton University ††

Received 20 November 1958

Abstract: The differential cross sections and the polarization are calculated for the 100 MeV and 40 MeV nucleons elastically scattered from deuterons. A kind of impulse approximation is used with the elementary scattering operators corresponding to the phase shifts resulting from Gammel-Thaler and Marshak-Signell potentials. The results for both cases are compared with the existing experimental data.

1. Introduction

The recent developments of the analysis of the elementary n-p and p-p scatterings led to successful descriptions of the cross sections and the polarization data in terms of static potentials. The potentials of Gammel and Thaler [1,2]) and Marshak and Signell [3,4]) contain central, spin-orbit and tensor forces with repulsive hard cores and seem to account for the data up to 310 MeV. It seems interesting to apply these potentials to various three-body problems. The relatively simplest problem is the high energy n-d or p-d elastic scattering. It was our aim to compute the angular distributions, cross sections and polarizations for both potentials (G-T and M-S). The comparison of the two cases seems to be the most interesting for the nuelcon polarizations since the spin dependent forces (in particular V_{LS}) differ most from each other. The sets of phase-shifts do not differ very much from each other up to about 100 MeV but the polarizations are rather sensitive to the nucleon-nucleon amplitudes and are essentially independent of the "sticking factor" — the Fourier transform of the intrinsic deuteron wave function. Recent data on the polarization of 146 MeV protons scattered by deuterons, obtained by Postma and Wilson at Harvard†††, are in qualitative agreement with our result (fig. 3). On the other hand, the angular distributions depend rather essentially on the "sticking factor" and, therefore, cannot provide a very direct test of the two-body forces assumed.

† Fellow of the National Research Council of Brazil and on leave from University of São Paulo, São Paulo, Brazil.

†† This work was supported in part by the U.S. Atomic Energy Commission and The Higgins Scientific Trust Fund.

††† Private communication.

While the calculations reported below were being in progress a paper was published on the same problem. Sakamoto and Sasakawa [5]) computed the angular distribution for 95 MeV protons using Chew's impulse approximation [6]) and Gammel and Thaler's phase shifts.

In the calculation reported below the relative phases of the two scattering amplitudes being essential, in particular for the polarization, the scattering amplitudes were computed with the use of Wu and Ashkin's [7]) eq. (17) with their Born approximation transition operators V_{12} and V_{13} replaced by the scattering operators $t_{n_0 n}$ and $t_{n_0 p}$, respectively (we are considering the n-d problem for definiteness, the incoming neutron being the particle 1 of ref. [7]). The Coulomb effect in the p-d case is important only at very small angles at the energies under consideration. The $t_{n_0 n}$ and $t_{n_0 p}$ operators correspond to the elastic ("on the energy shell") elementary scattering amplitude. The inelastic ("off the energy shell") corrections are expected to be small at such high energies ($\approx$ 100 MeV) at least for small n-d scattering angles ($\lesssim 90°$) in the spirit of the impulse approximation. The calculations are being planned for low and medium energies using "actual" t matrices correspond ng to various approximate forms [8]) represented in momentum space and substituted to the n-d scattering amplitudes with no "on the energy shell" approximation. These elementary scattering operators were first given by Wolfenstein *et al.*[9]) as operators in the spin space of the two particles, and Wright [10]) related them to phase shifts.

The present approach enables to evaluate the relative phases of the amplitudes involved in our problem as derived from two-body scattering amplitudes. The usual impulse approximation of Chew applied to this problem was confined to the use of experimental n-p and n-n cross sections only owing to the lack of knowledge of the "actual" phase-shifts at that time.

2. Calculation

The n-d scattering matrix is an operator in the spin space of the particles involved and is split in the form

$$\hat{f} = \hat{f}_{n_0 n} + \hat{f}_{n_0 p}. \tag{1}$$

The scattering operators $t_{n_0 n}$ and $t_{n_0 p}$ are properly normalized so that they reproduce the exact scattering amplitudes when applied in Born approximation. In the configuration space they are taken in the form of pseudo-potentials

$$t_{n_0 p} = -(4\pi\hbar^2/M)\hat{M}^{np}(\theta, \phi)\delta(\mathbf{r}+\tfrac{1}{2}\boldsymbol{\rho}), \tag{2a}$$

$$t_{n_0 n} = -(4\pi\hbar^2/M)\hat{M}^{nn}(\theta, \phi)\delta(\mathbf{r}-\tfrac{1}{2}\boldsymbol{\rho}), \tag{2b}$$

where M is the nucleon mass, $\mathbf{r} = \mathbf{r}_1 - \frac{1}{2}(\mathbf{r}_2+\mathbf{r}_3)$, $\boldsymbol{\rho} = \mathbf{r}_3 - \mathbf{r}_2$ as in ref. [7]); $\hat{M}^{np}$ and $\hat{M}^{nn}$ are the n-p and n-n scattering operators, as given e.g., by

Stapp *et al* [11]); we can choose a frame of reference with $\phi = 0$; θ is the centre of mass nucleon-nucleon scattering angle. Chamberlain and Stern [12]) propose a simple relation of this angle to the centre of mass n-d scattering angle. According to this relation it seems reasonable to assume the equality of both these angles at high energies. This assumption suppresses the contribution of the momentum of the intrinsic motion in the target system.

Let us first neglect the D-state admixture in the deuteron ground state. The scattering matrices can then be put in the form

$$\hat{f}_{\mathrm{n_0 n}} = \hat{M}^{\mathrm{nn}} F(q), \tag{3a}$$

$$\hat{f}_{\mathrm{n_0 p}} = \hat{M}^{\mathrm{np}} F(q), \tag{3b}$$

where $\mathbf{q} = \mathbf{K} - \mathbf{K}'$ ($\mathbf{K}$ denoting the initial and $\mathbf{K}'$ the final centre of mass momentum of the scattering neutron), and

$$F(q) = \tfrac{4}{3}\int_0^\infty \mathrm{d}\rho\, \rho^2 j_0(\tfrac{1}{2}q\rho)\Psi_0(\rho)^2 = \tfrac{4}{3} J_0, \tag{4}$$

where $\Psi_0(\rho)$ is the S-state deuteron wave function taken in the form given by Feshbach [13]):

$$\Psi_0(\rho) = \begin{cases} \dfrac{N}{\rho}\left[\mathrm{e}^{-\alpha(\rho - r_c)} - \mathrm{e}^{-\beta(\rho - r_c)}\right] & \text{for } \rho \geqq r_c \\ 0 & \text{for } \rho \leqq r_c; \end{cases} \tag{5}$$

the constants N, α, β, r_c are given in ref.[13]).

The differential cross section is given by

$$I(\theta) = \tfrac{2}{3}\tfrac{1}{4}\sum_{i=1}^{4}\sum_{j=1}^{6} |\langle j|\hat{f}|i\rangle|^2 + \tfrac{1}{3}\tfrac{1}{2}\sum_{i=5}^{6}\sum_{j=1}^{6} |\langle j|\hat{f}|i\rangle|^2 \tag{6}$$

where $\langle j|\hat{f}|i\rangle = \langle \chi_j|\hat{f}|\chi_i\rangle = f_i^j(\theta)$. Here the χ_j's are the three-body system spin-wave-functions as given in eqs. (5)-(6) of ref. [7]) †, with $i, j = 1, 2, \ldots, 6$. In computing the $f_i^j(\theta)$'s use was made of the singlet and triplet two-body amplitudes $M_{sm_s, s'm'_s}$ of the operators $\hat{M}^{\mathrm{nn}}$ and $\hat{M}^{\mathrm{np}}$. The amplitudes $M_{sm_s, s'm'_s}$ were given by Stapp *et al.* [11]) for the p-p system; the specialization for the n-p case and the generalization for the n-p case are straightforward. The explicit form of the f_i^j functions is given in the appendix.

To calculate the outgoing neutron polarization the frame of reference was chosen with the z-axis along $\mathbf{K}$ and the y-axis in the $\mathbf{K}\times\mathbf{K}'$-direction ($\phi = 0$). Then the polarization becomes

$$\begin{aligned} P(\theta) = \langle \sigma_{\mathrm{n_0 y}} \rangle_{\mathrm{av}} = [I(\theta)]^{-1}\tfrac{1}{6}\sum_{i=1}^{6} \mathrm{Im}\Big\{ & \tfrac{2}{\sqrt{3}} f_i^3 f_i^{1*} + \tfrac{2\sqrt{2}}{\sqrt{3}} f_i^1 f_i^{5*} + \tfrac{2}{\sqrt{3}} f_i^2 f_i^{4*} \\ & + \tfrac{2\sqrt{2}}{\sqrt{3}} f_i^6 f_i^{2*} + \tfrac{4}{3} f_i^4 f_i^{3*} + \tfrac{2\sqrt{2}}{3} f_i^6 f_i^{3*} + \tfrac{2\sqrt{2}}{3} f_i^4 f_i^{5*} + \tfrac{2}{3} f_i^6 f_i^{5*} \Big\}. \end{aligned} \tag{7}$$

† An independent calculation of $I(\theta)$ and $P(\theta)$ was carried out with a different representation of the spin wave-functions (direct products of the deuteron triplet spin functions and the incoming neutron spin functions): this provided a useful check.

To consider the contribution of the D-state admixture in the deuteron we replace $\Psi_0(\rho)$ by

$$\Psi_0(\rho)+\sqrt{\frac{4\pi}{2^5}}\sum_{\mu=-2}^{2}(-)^{\mu}Z_{-\mu}(\sigma_n,\sigma_p)Y_{2\mu}(\Omega_\rho)\Psi_2(\rho)$$

where $Z_\mu(\sigma,\sigma')$ is defined in Yoshida *et al.* [14]). On keeping the S-D interference term only we have

$$f_{n_0n}=\frac{4}{3}\hat{M}^{n_0n}\left[J_0-\left(\frac{5}{2}\right)^{\frac{1}{2}}J_2Z_0(\sigma_n,\sigma_p)\right], \tag{8a}$$

$$f_{n_0p}=\frac{4}{3}\hat{M}^{n_0p}\left[J_0-\left(\frac{5}{2}\right)^{\frac{1}{2}}J_2Z_0(\sigma_n,\sigma_p)\right], \tag{8b}$$

where

$$J_2=\int_0^\infty d\rho\rho^2 j_2(\tfrac{1}{2}q\rho)\Psi_0(\rho)\Psi_2(\rho).$$

The radial D-state wave function was taken in the form

$$\Psi_2(\rho)=M\{(1-A\rho)e^{-\xi\rho}-Be^{-\pi\rho}\}$$

as given by Austern [15]).

The contribution of J_2 to all the amplitudes f_i^j was found very small (less than 1 per cent): it may be neglected, as well as the contributions of the term involving $|\Psi_2(\rho)|^2$.

3. Numerical Results

The foregoing theoretical method was used to analyse the 100-MeV and 40-MeV neutron-deuteron scattering data. We calculated also the polarization of outgoing neutrons for the 100-MeV case. The approximation of our method for the 40-MeV case is not expected to be valid, excepting for small scattering angles. For the sake of comparison the sets of phase shifts corresponding to the G-T [1,2]) and M-S [3,4]) potentials were used.

In fig. 1 the comparison is given of the theoretical results for both these cases for 100-MeV neutrons with the experimental points obtained by Chamberlain and Stern [12]), for the 95-MeV protons scattered by deuterons (i.e., 190-MeV deuterons by protons). Since the Coulomb effect is important at very small angles only our theoretical results apply to the p-d scattering as well. The agreement with the data for both the angular distribution and the absolute values of the differential cross sections for all the cases is fairly good and no clear distinction between the G-T and M-S potentials can be obtained on the basis of this experiment.

In fig. 2 the comparison was made between our theory and the data by Williams and Bru sell [16]) for the 40-MeV protons scattered by deuterons. As expected the agreement is fair for small angles only (up to $\approx 60°$). The

discrepancy at very small angles (less than $\approx 15°$) is due to the interference with the Coulomb amplitude in the proton-deuteron case.

In fig. 3 the polarization of 100-MeV neutrons scattered by deuterons is shown for all the three cases. The maximum polarization occurs in every

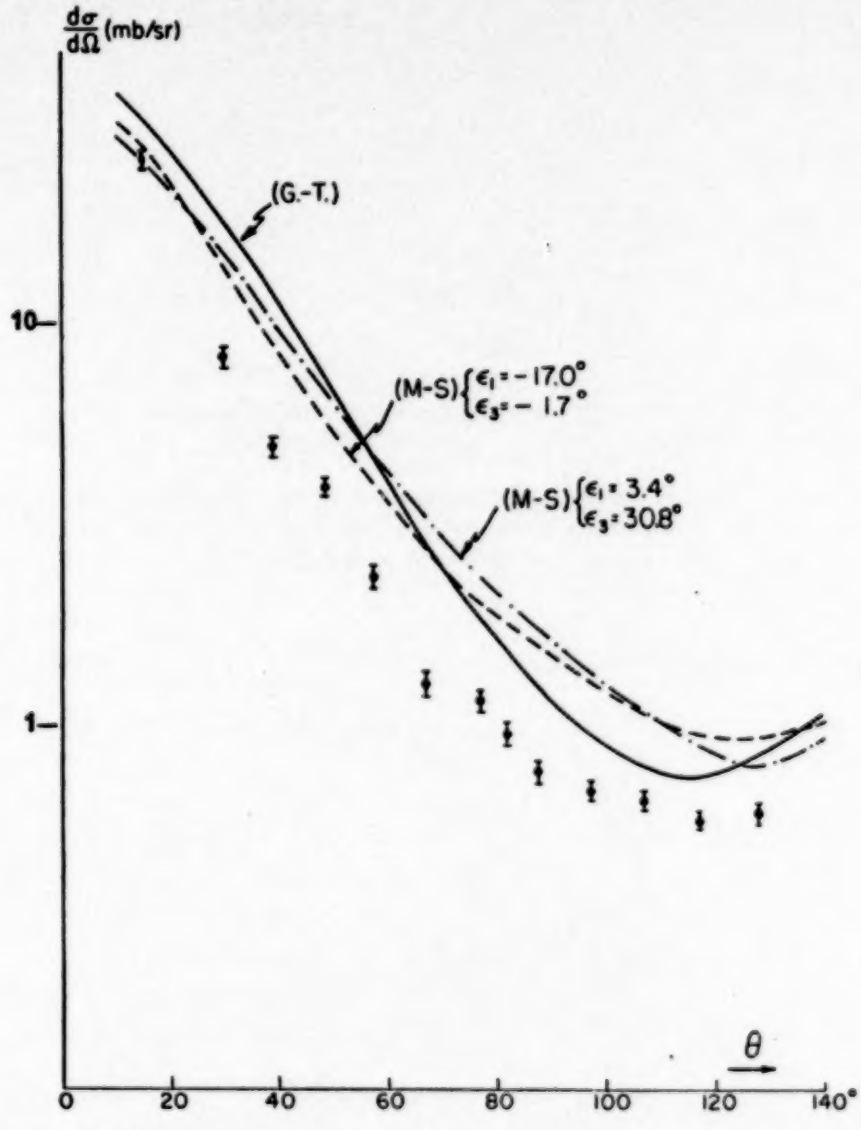

Fig. 1. The angular distribution of 100-MeV neutrons scattered from deuterons for the Gammel-Thaler potential (G-T) and the Marshak-Signell potential (M-S). The experimental points correspond to 95-MeV protons scattered from deuterons as taken from Chamberlain and Stern[13].

case at about 60° and its values are 51 percent in the G-T case and 44 percent in the M-S case for $\varepsilon_1 = 3\,4°$, $\varepsilon_3 = 30.8°$ (48 percent in the M-S case for $\varepsilon_1 = -17.0°$, $\varepsilon_3 = -1.7°$). The polarization is positive in all cases, up to about 130°.

In the theory of section 2 we used the operator $t_{n_0 n}$ antisymmetrized in the neutron coordinates and, consequently, we did not antisymmetrize our

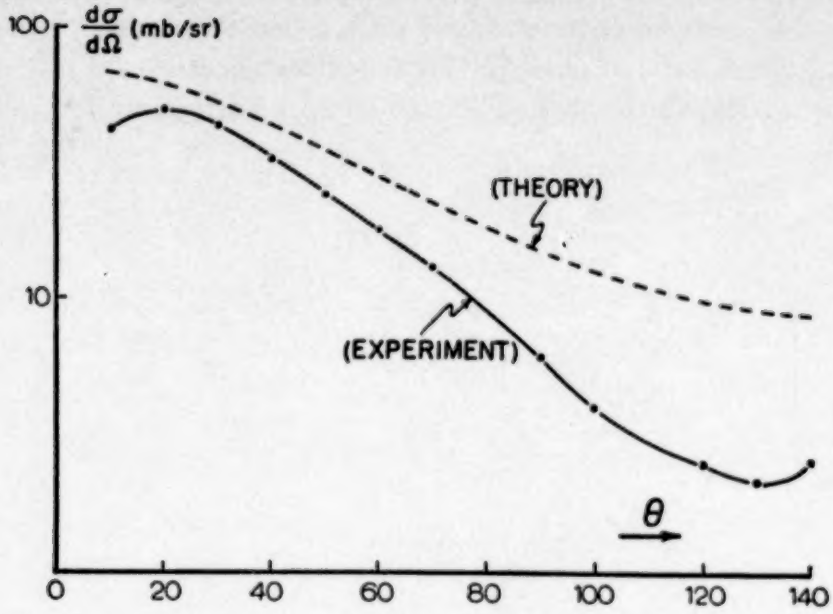

Fig. 2. The angular distribution of 40-MeV neutrons scattered by deuterons for the Marshak-Signell potential. The experimental points correspond to 40-MeV protons scattered by deuterons as taken from Williams and Brussell [16]).

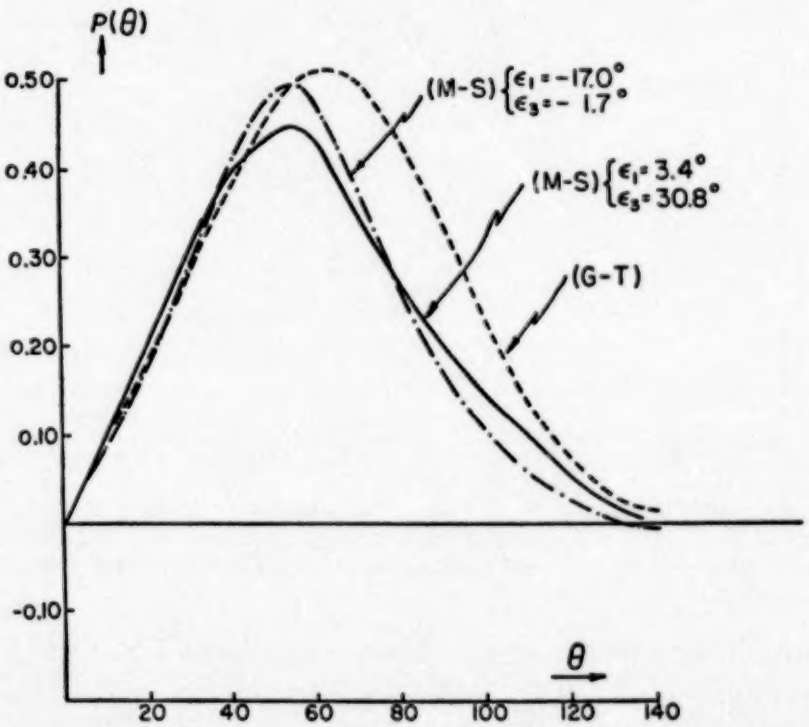

Fig. 3. The polarization of 100-MeV neutrons scattered from deuterons for the Gammel-Thaler potential (G-T) and the Marshak-Signell potential (M-S).

initial state wave-function. This procedure, however, is ambiguous in the sense that we could use the non-antisymmetrized scattering operator $t_{n,p}$ in both amplitudes and antisymmetrize the wave-function instead. This procedure, which seems to be less consistent and at least not in the spirit of

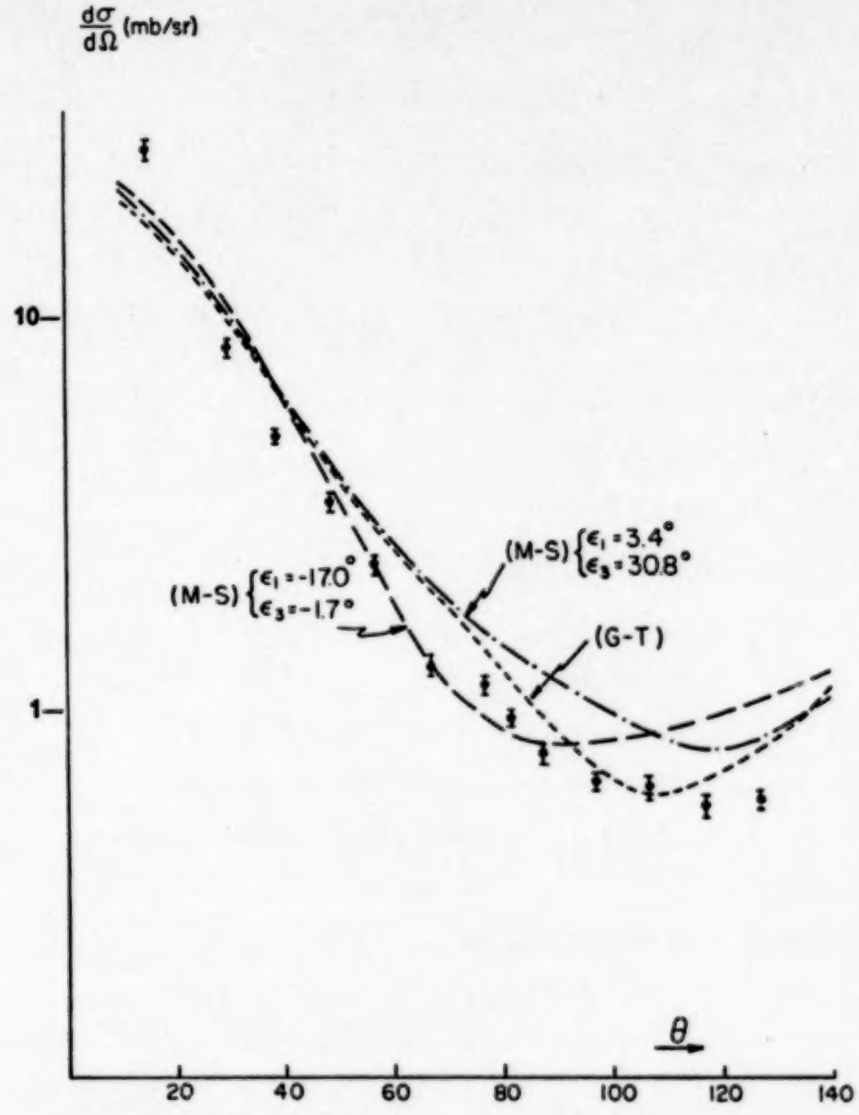

Fig. 4. The angular distribution of 100-MeV neutrons scattered from deuterons, using non-antisymmetrized t-matrix and antisymmetrized wave-function.

the impulse approximation leads to results slightly different from those discussed above. The angular distributions for this case are shown in fig. 4.

We feel indebted to Dr. J. S. Blair for helpful discussions.

Appendix

On neglecting the D-state admixture in the deuteron wave-function we can express all the non-vanishing scattering amplitudes in terms of the two body amplitudes $M_{m_s m'_s}$ with $m_s, m'_s = 0, \pm 1$, for triplet states and M_{ss} for singlet states in the form

$$f_1^1 = f_2^2 = h_1 F(q)$$

$$f_3^1 = -f_4^2 = 2\sqrt{2}\, f_6^2 = -2\sqrt{2}\, f_5^1 = \sqrt{\tfrac{2}{3}} h_2 F(q)$$

$$f_4^1 = f_3^2 = f_2^3 = f_1^4 = \sqrt{2} f_1^6 = \sqrt{2} f_2^5 = \sqrt{2} f_6^1 = \sqrt{2} f_5^2 = \frac{1}{\sqrt{3}} h_3 F(q)$$

$$f_1^3 = -f_2^4 = -2\sqrt{2}\, f_1^5 = 2\sqrt{2}\, f_2^6 = \sqrt{\tfrac{2}{3}} h_4 F(q)$$

$$f_3^3 = f_4^4 = \tfrac{1}{3}(2h_5+h_1) F(q)$$

$$f_4^3 = -f_3^4 = 4 f_5^6 = -4 f_6^5 = \frac{\sqrt{2}}{3}(h_2-h_4) F(q)$$

$$f_5^3 = f_6^4 = f_3^5 = f_4^6 = \frac{\sqrt{2}}{6}(h_1-h_5) F(q)$$

$$f_5^4 = -f_6^3 = \tfrac{1}{3}(h_4+\tfrac{1}{2}h_2) F(q)$$

$$f_4^5 = -f_3^6 = \tfrac{1}{3}(h_2+\tfrac{1}{2}h_4) F(q)$$

$$f_5^5 = f_6^6 = \tfrac{1}{12}(2h_1+h_5+9h_6) F(q)$$

where

$$h_1 = M_{11}^{np}+M_{11}^{nn}, \qquad h_2 = M_{10}^{np}+M_{10}^{nn}, \qquad h_3 = M_{1-1}^{np}+M_{1-1}^{nn},$$

$$h_4 = M_{01}^{np}+M_{01}^{nn}, \qquad h_5 = M_{00}^{np}+M_{00}^{nn}, \qquad h_6 = M_{ss}^{np}+M_{ss}^{nn}.$$

The differential cross section can be written as

$$I(\theta) = \tfrac{1}{3} F(q)^2 \{|h_1|^2+|h_2|^2+|h_3|^2+|h_4|^2+\tfrac{1}{2}|h_5|^2+\tfrac{1}{2}|h_6|^2+\tfrac{1}{8}|h_2-h_4|^2 + \tfrac{1}{16}|2h_1+h_5+h_6|^2\}.$$

The polarization can be written in the form

$$P(\theta) = \frac{F(q)^2}{I(\theta)} \frac{\sqrt{2}}{24} \operatorname{Im}\{h_4 H_4^* - h_2 H_2^*\}$$

where

$$H_4 = 10h_1-8h_3+h_5+h_6,$$

$$H_2 = 2h_1+9h_5+h_6.$$

Note added in proof: After this work was submitted for publication a preprint by L. Castillejo and L. S. Singh containing a very careful and extensive treatment of the same problem came to our attention. Their expression for $P(\theta)$ is in agreement with that of Tamor (Phys. Rev. **97** (1955) 1082, appendix A, eq. (A-3)). Our expressions for $I(\theta)$ and $P(\theta)$ coincide with theirs provided one makes use of the identity

$$M_{11}-M_{00}-M_{1-1} = \sqrt{2}\,(M_{10}+M_{01})\,\mathrm{ctg}\,\theta \qquad \text{(A1)}$$

following from the time-reversal condition (see e.g. ref. [9])) and one performs the transition to their notation. Using (A1) our $P(\theta)$ becomes

$$P(\theta) = \frac{F(q)^2}{I(\theta)}\,\frac{\sqrt{2}}{24}\,\mathrm{Im}\{(h_4-h_2)(6h_1+5h_5+h_6-4h_3)^*\}. \qquad \text{(A2)}$$

There is a slight disagreement between our numerical results of figs. 1—3 and theirs. This is due to the difference between our and their assumptions for the relation between the two-body and three-body c.m. scattering angles. Their relation $\sin\frac{1}{2}\theta_{2\text{-body}} = \frac{4}{3}\sin\frac{1}{2}\theta_{3\text{-body}}$ seems to be more consistent with the spirit of the impulse approximation. If we used this relation our theoretical curves of figs. 1—4 would be shifted a little toward smaller angles. This shift is larger for larger angles.

References

1) J. L. Gammel and R. M. Thaler, Phys. Rev. **107** (1957) 291
2) J. L. Gammel and R. M. Thaler, Phys. Rev. **107** (1957) 1337
3) P. S. Signell and R. E. Marshak, Phys. Rev. **106** (1957) 832
4) P. S. Signell and R. E. Marshak, Phys. Rev. **109** (1958) 1229
5) Y. Sakamoto and T. Sasakawa, Prog. Theor. Phys. **19** (1958) 745
6) G. Chew, Phys. Rev. **74** (1948) 809; **84** (1951) 1057
7) T. Y. Wu and J. Ashkin, Phys. Rev. **73** (1948) 986
8) G. F. Chew and M. L. Goldberger, Phys. Rev. **87** (1952) 778
9) L. Wolfenstein and J. Ashkin, Phys. Rev. **85** (1955) 947
10) S. C. Wright, Phys. Rev. **99** (1955) 996
11) H. P. Stapp, T. J. Ypsilantis and N. Metropolis, Phys. Rev. **105** (1957) 302
12) O. Chamberlain and M. O. Stern, Phys. Rev. **94** (1954) 666
13) H. Feshbach, Phys. Rev. **107** (1957) 1626
14) S. Yoshida, H. Horie and T. Tamura, Prog. Theor. Phys. **8** (1952) 341
15) N. Austern, Phys. Rev. **85** (1952) 283
16) J. H. Williams and M. K. Brussell, Phys. Rev. **110** (1958) 136

7.C *Nuclear Physics* **10** (1959) 160—165; ©*North-Holland Publishing Co., Amsterdam*

Not to be reproduced by photoprint or microfilm without written permission from the publisher

MESON PRODUCTION IN NUCLEON-NUCLEON COLLISIONS

ALLADI RAMAKRISHNAN, N. R. RANGANATHAN † and S. K. SRINIVASAN ††

Department of Physics, University of Madras, India

Received 28 November 1958

Abstract: A calculation of the amplitude for meson production in a nucleon-nucleon collision is presented using the method of Low. By making a suitable Tamm-Dancoff approximation, the matrix element for the process is expressed in terms of the two nucleon potential, pion nucleon scattering matrix element and nucleon vertex operator.

1. Introduction

It is well recognized that the description of nuclear forces depends to a very large extent on a correct theory of pion-nucleon interaction. As an initial step considerable attention has been devoted by theoreticians to the problem of meson nucleon scattering. In particular due to work of Chew [1]) Low [2]) and Wick [3]), we now have, at least what is believed to be, a correct description of the pion-nucleon scattering up to about a few hundred MeV. The agreement of this theory now known as "fixed extended source theory" with the data obtained by cyclotron experiments at Berkeley and Brookhaven is satisfactory and the resonances are predicted accurately. In view of the satisfactory agreement with experiments, the theory has been applied to the problem of nuclear forces by Gartenhaus [4]), Miyazawa [5]) and Klein and McCormic [6]) (see also ref. [7,8])). The Miyazawa-Klein potential as well as the Gartenhaus potential suitably modified by Signell and Marshak [9]) (who have added a spin orbit interaction using phenomenological arguments) have many essential features which the previous potentials lacked. Hence it is worthwhile to attempt the problem of meson production in nucleon nucleon collisions using the present knowledge of pion phenomena. We shall follow the method of Low and express the matrix element in terms of known quantities like pion nucleon scattering matrix element, nucleon potential and vertex operator.

† Atomic Energy Commission Junior Research Fellow.

†† National Institute of Sciences Senior Research Fellow. While the work here reported was in progress, this author was at the Adolph Basser Computing Labora ory and F.B.S. Falkiner Nuclear Research Laboratories, School of Physics, University of Sydney.

2. Matrix Element for the Process

Let p_1, q_1 be the energy-momentum four-vectors of the nucleons in the initial state; we require the amplitude for finding two nucleons with momenta p_2, q_2 and a meson of α-th type of momentum k. The spins of the nucleons are suppressed in this notation †. The amplitude for this process is given by

$$\langle p_2 q_2 k\alpha|S|p_1 q_1\rangle = \Big(\Phi_0, b(p_2)b(q_2)a_\alpha(k)\sum_{n=0}^{\infty}\frac{(-i)^n}{n!}\int\int\ldots\int \mathrm{d}x_1\mathrm{d}x_2\ldots\mathrm{d}x_n \cdot \mathrm{T}(L(x_1)L(x_2)\ldots L(x_n))\, b^*(q_1)b^*(p_1)\Phi_0\Big) \tag{1}$$

where $L(x)$, the interaction Lagrangian density, is given by

$$L(x) = g\bar\psi(x)\gamma_5\tau_i\psi(x)\phi_i(x)+\delta m\bar\psi(x)\psi(x) +\tfrac{1}{2}(\delta\mu)^2\phi_i(x)\phi_i(x)-\tfrac{1}{4}\lambda(\phi_i(x)\phi_i(x))^2; \tag{2}$$

here the τ_i's are the usual isobaric spin matrices and δm and $\delta\mu$ are the nucleon and meson mass renormalizations, Φ_0 is the bare vacuum and b and a are the annihilation operators for the nucleon and the meson respectively. The Lagrangian (2) leads to the meson and nucleon current operators

$$j_\alpha(x) = g\bar\psi(x)\gamma_5\tau_\alpha\psi(x)+\delta\mu^2\phi_\alpha(x)-\lambda\phi_\alpha(x)\phi_i(x)\phi_i(x), \tag{3}$$

$$J(x) = g\gamma_5\tau_i\psi(x)\phi_i(x)+\delta m\psi(x). \tag{4}$$

The S-matrix element (1) can be written as

$$\langle p_2 q_2 k\alpha|S|p_1 q_1\rangle = \frac{1}{(2\pi)^3}\int\int \mathrm{e}^{iq_2y+ikx}\,\bar w(q_2)\left(\frac{m}{2E(q_2)w(k)}\right)^{\frac{1}{2}}\mathrm{d}x \cdot\langle p_2|\Big\{(-i)^2(\mathbf{j}_\alpha(x)\mathbf{J}(y))_+-i\delta(y-x)g\gamma_5\tau_\alpha\psi(x)\Big\}|p_1 q_1\rangle \tag{5}$$

where the current operators $\mathbf{j}_\alpha(x)$, $\mathbf{J}(y)$ are in Heisenberg representation †† and $|p_1 q_1\rangle$ is the two-nucleon state vector consisting of "incoming" plane waves and "outgoing" scattered waves while $\langle p_2|$ is a one-nucleon state vector with "outgoing" plane wave and "incoming" scattered waves. $(\quad)_+$ is the time ordered product defined according to Wick [10]). The equivalence of (5) and (1) can be established by the method of Lehmann, Symanzik and Zimmerman [11]) or by the simpler approach of Low [2]). $\mathbf{j}_\alpha(x)$ and $\mathbf{J}(y)$ are given by

† Throughout this paper, we shall write a four vector as x and an ordinary vector by the corresponding bold letter $\mathbf{x}$. The scalar product of two four vectors x, y will be denoted by $xy = x_0y_0-x_iy_i = x_0y_0-\mathbf{x}\cdot\mathbf{y}$. Integrations over four dimensional volumes are denoted by $\mathrm{d}x$, those over three-dimensional volumes by $\mathrm{d}\mathbf{x}$.

†† We shall distinguish Heisenberg operators from interaction representation operators by using bold type for the former.

7.C *Nuclear Physics* **10** (1959) 160—165; © *North-Holland Publishing Co., Amsterdam*
Not to be reproduced by photoprint or microfilm without written permission from the publisher

MESON PRODUCTION IN NUCLEON-NUCLEON COLLISIONS

ALLADI RAMAKRISHNAN, N. R. RANGANATHAN † and S. K. SRINIVASAN ††

Department of Physics, University of Madras, India

Received 28 November 1958

Abstract: A calculation of the amplitude for meson production in a nucleon-nucleon collision is presented using the method of Low. By making a suitable Tamm-Dancoff approximation, the matrix element for the process is expressed in terms of the two nucleon potential, pion nucleon scattering matrix element and nucleon vertex operator.

1. Introduction

It is well recognized that the description of nuclear forces depends to a very large extent on a correct theory of pion-nucleon interaction. As an initial step considerable attention has been devoted by theoreticians to the problem of meson nucleon scattering. In particular due to work of Chew [1]) Low [2]) and Wick [3]), we now have, at least what is believed to be, a correct description of the pion-nucleon scattering up to about a few hundred MeV. The agreement of this theory now known as "fixed extended source theory" with the data obtained by cyclotron experiments at Berkeley and Brookhaven is satisfactory and the resonances are predicted accurately. In view of the satisfactory agreement with experiments, the theory has been applied to the problem of nuclear forces by Gartenhaus [4]), Miyazawa [5]) and Klein and McCormic [6]) (see also ref. [7,8])). The Miyazawa-Klein potential as well as the Gartenhaus potential suitably modified by Signell and Marshak [9]) (who have added a spin orbit interaction using phenomenological arguments) have many essential features which the previous potentials lacked. Hence it is worthwhile to attempt the problem of meson production in nucleon nucleon collisions using the present knowledge of pion phenomena. We shall follow the method of Low and express the matrix element in terms of known quantities like pion nucleon scattering matrix element, nucleon potential and vertex operator.

† Atomic Energy Commission Junior Research Fellow.

†† National Institute of Sciences Senior Research Fellow. While the work here reported was in progress, this author was at the Adolph Basser Computing Labora ory and F.B.S. Falkiner Nuclear Research Laboratories, School of Physics, University of Sydney.

2. Matrix Element for the Process

Let p_1, q_1 be the energy-momentum four-vectors of the nucleons in the initial state; we require the amplitude for finding two nucleons with momenta p_2, q_2 and a meson of α-th type of momentum k. The spins of the nucleons are suppressed in this notation †. The amplitude for this process is given by

$$\langle p_2 q_2 k\alpha|S|p_1 q_1\rangle = \Big(\Phi_0, b(p_2)b(q_2)a_\alpha(k)\sum_{n=0}^{\infty}\frac{(-i)^n}{n!}\int\int\ldots\int \mathrm{d}x_1\mathrm{d}x_2\ldots\mathrm{d}x_n \cdot \mathrm{T}(L(x_1)L(x_2)\ldots L(x_n))\, b^*(q_1)b^*(p_1)\Phi_0\Big) \tag{1}$$

where $L(x)$, the interaction Lagrangian density, is given by

$$L(x) = g\bar\psi(x)\gamma_5\tau_i\psi(x)\phi_i(x)+\delta m\bar\psi(x)\psi(x) + \tfrac{1}{2}(\delta\mu)^2\phi_i(x)\phi_i(x)-\tfrac{1}{4}\lambda(\phi_i(x)\phi_i(x))^2; \tag{2}$$

here the τ_i's are the usual isobaric spin matrices and δm and $\delta\mu$ are the nucleon and meson mass renormalizations, Φ_0 is the bare vacuum and b and a are the annihilation operators for the nucleon and the meson respectively. The Lagrangian (2) leads to the meson and nucleon current operators

$$j_\alpha(x) = g\bar\psi(x)\gamma_5\tau_\alpha\psi(x)+\delta\mu^2\phi_\alpha(x)-\lambda\phi_\alpha(x)\phi_i(x)\phi_i(x), \tag{3}$$

$$J(x) = g\gamma_5\tau_i\psi(x)\phi_i(x)+\delta m\psi(x). \tag{4}$$

The S-matrix element (1) can be written as

$$\langle p_2 q_2 k\alpha|S|p_1 q_1\rangle = \frac{1}{(2\pi)^3}\int\int \mathrm{e}^{iq_2y+ikx}\bar w(q_2)\left(\frac{m}{2E(q_2)w(k)}\right)^{\frac{1}{2}}\mathrm{d}x \cdot\langle p_2|\left\{(-i)^2(\mathbf{j}_\alpha(x)\mathbf{J}(y))_+-i\delta(y-x)g\gamma_5\tau_\alpha\psi(x)\right\}|p_1 q_1\rangle \tag{5}$$

where the current operators $\mathbf{j}_\alpha(x)$, $\mathbf{J}(y)$ are in Heisenberg representation †† and $|p_1 q_1\rangle$ is the two-nucleon state vector consisting of "incoming" plane waves and "outgoing" scattered waves while $\langle p_2|$ is a one-nucleon state vector with "outgoing" plane wave and "incoming" scattered waves. $(\ \ )_+$ is the time ordered product defined according to Wick [10]). The equivalence of (5) and (1) can be established by the method of Lehmann, Symanzik and Zimmerman [11]) or by the simpler approach of Low [2]). $\mathbf{j}_\alpha(x)$ and $\mathbf{J}(y)$ are given by

† Throughout this paper, we shall write a four vector as x and an ordinary vector by the corresponding bold letter $\mathbf{x}$. The scalar product of two four vectors x, y will be denoted by $xy = x_0y_0-x_iy_i = x_0y_0-\mathbf{x}\cdot\mathbf{y}$. Integrations over four dimensional volumes are denoted by $\mathrm{d}x$, those over three-dimensional volumes by $\mathrm{d}\mathbf{x}$.

†† We shall distinguish Heisenberg operators from interaction representation operators by using bold type for the former.

$$(-\Box+\mu^2)\phi_a(x)=g\bar{\psi}(x)\gamma_5\tau_a\psi(x)+\delta\mu^2\phi_a(x)-\lambda\phi_a(x)\phi_i(x)\phi_i(x)=\mathbf{j}_a(x), \quad (6)$$

$$(i\gamma_\mu\frac{\partial}{\partial x_\mu}-m)\psi(x)=g\gamma_5\tau_i\psi(x)\phi_i(x)+\delta m\psi(x)=\mathbf{J}(x). \quad (7)$$

Next we use translational invariance:

$$\mathbf{F}(x)=e^{iPx}\mathbf{F}(0)e^{-iPx}$$

where $\mathbf{F}(x)$ is any field operator. This yields

$$\langle p_2q_2k\alpha|S|p_1q_1\rangle=-2\pi\delta(p_1+q_1-p_2-q_2-k)\bar{w}(q_2)\left(\frac{m}{2E(q_2)w(k)}\right)^{\frac{1}{2}} \quad (8)$$
$$\langle p_2|\left\{\int e^{iq_2y}(\mathbf{j}_a(0)\mathbf{J}(y))_+dy+ig\gamma_5\tau_a\psi(0)\right\}|p_1q_1\rangle.$$

The second term is easily evaluated:

$$\langle p_2|\psi(0)|p_1q_1\rangle=(\Phi_{p_2},(S\psi(0))_+b^*(q_1)\Phi_{p_1}) \quad (9)$$

where S is the S-matrix and Φ_p's are state vectors in interaction representation. Using the relations (see, for example, ref. [2,12]))

$$\left\{\psi(0),b^*(q_1)\right\}=\frac{1}{(2\pi)^{\frac{3}{2}}}w(q_1)\left(\frac{m}{E(q_1)}\right)^{\frac{1}{2}}, \quad (10)$$

$$\left\{S,b^*(q_1)\right\}=\frac{1}{(2\pi)^{\frac{3}{2}}}\int e^{-iq_1x}w(q_1)\left(\frac{m}{E(q_1)}\right)^{\frac{1}{2}}\frac{\delta S}{\delta\psi(x)}dx, \quad (11)$$

we obtain

$$\langle p_2|\psi(0)|p_1q_1\rangle=w(q_1)\left(\frac{m}{E(q_1)}\right)^{\frac{1}{2}}\frac{1}{(2\pi)^{\frac{3}{2}}}$$
$$\left[\langle p_2|p_1\rangle-(\Phi_{p_2},\int\left(\frac{\delta S}{\delta\psi(x)}\psi(0)\right)_+e^{-iq_1x}dx\,\Phi_{p_1})\right]. \quad (12)$$

The functional derivative of S with respect to $\psi(x)$ is related to the current operator by

$$J(x)=i\frac{\delta S}{\delta\bar{\psi}(x)}S^\dagger, \qquad J(x)=i\frac{\delta S}{\delta\psi(x)}S^\dagger \quad (13)$$

so that

$$\begin{aligned}&\int\left(\Phi_{p_2},\left(\frac{\delta S}{\delta\psi(x)}\psi(0)\right)_+\Phi_{p_1}\right)e^{-iq_1x}dx\\&=-i\int\left(\Phi_{p_2},(\bar{J}(x)S\psi(0))_+\Phi_{p_1}\right)e^{-iq_1x}dx\\&=-i\int\langle p_2|(\bar{\mathbf{J}}(x)\psi(0))_+|p_1\rangle e^{-iq_1x}dx\\&=-i\int dx\Big[-\int_{-\infty}^0 e^{-iq_1x}\langle p_2|\psi(0)\bar{\mathbf{J}}(x)|p_1\rangle dx_0\\&\quad+\int_0^\infty e^{-iq_1x}\langle p_2|\bar{\mathbf{J}}(x)\psi(0)|p_1\rangle dx_0\Big].\end{aligned} \quad (14)$$

Expansion in terms of complete set of "incoming" states yields

$$\frac{1}{(2\pi)^3}\int\left(\Phi_{p_2}\left(\frac{\delta S}{\delta\psi(x)}\psi(0)\right)_+\Phi_{p_1}\right)e^{-iq_1x}dx$$
$$=-\sum_{p_n=p_1+q_1}\frac{\langle p_2|\psi(0)|n\rangle\langle n|\bar{\mathbf{J}}(0)|p_1\rangle}{E(q_1)+E(p_1)-E_n+i\varepsilon}+\sum_{p_n=p_2-q_1}\frac{\langle p_2|\bar{\mathbf{J}}(0)|n\rangle\langle n|\psi(0)|p_1\rangle}{E(p_2)-E(q_1)-E_n+i\varepsilon}. \tag{15}$$

In a similar manner, we expand the first term of the right-hand side of (8):

$$\frac{1}{(2\pi)^3}\int e^{iq_2y}\langle p_2|(\mathbf{j}_\alpha(0)\mathbf{J}(y)_+|p_1q_1\rangle dy$$
$$=-i\sum_{p_n=p_1+q_1-q_2}\frac{\langle p_2|\mathbf{j}_\alpha(0)|n\rangle\langle n|\mathbf{J}(0)|p_1q_1\rangle}{E(q_2)+E_n-E(p_1)-E(q_1)-i\varepsilon}+i\sum_{p_n=p_2+q_2}\frac{\langle p_2|\mathbf{J}(0)|n\rangle\langle n|\mathbf{j}_\alpha(0)|p_1q_1\rangle}{E(q_2)+E(p_2)-E_n+i\varepsilon}. \tag{16}$$

Defining

$$\langle p_2q_2k\alpha|S|p_1q_1\rangle=(2\pi)^4i\delta(p_1+q_1-p_2-q_2-k)\langle p_2q_2k\alpha|T|p_1q_1\rangle, \tag{17}$$

we obtain using (8), (12), (15) and (16)

$$\langle p_2q_2k\alpha|T|p_1q_1\rangle$$
$$=\bar{w}(q_2)\left(\frac{m}{2E(q_2)w(k)}\right)^{\frac{1}{2}}\Bigg[\sum_{p_m=p_1+q_1-q_2}\frac{\langle p_2|\mathbf{j}_\alpha(0)|m\rangle\langle m|\mathbf{J}(0)|p_1q_1\rangle}{E(q_2)+E_m-E(p_1)-E(q_1)-i\varepsilon}$$
$$-\sum_{p_n=p_2+q_2}\frac{\langle p_2|\mathbf{J}(0)|n\rangle\langle n|\mathbf{j}_\alpha(0)|p_1q_1\rangle}{E(q_2)+E(p_2)-E_n+i\varepsilon}-g\gamma_5\tau_\alpha w(q_1)\frac{1}{(2\pi)^{\frac{3}{2}}}\left(\frac{m}{E(q_1)}\right)^{\frac{1}{2}} \tag{18}$$
$$\Bigg\{\sum_{p_{m'}=p_1+q_1}\frac{\langle p_2|\psi(0)|m'\rangle\langle m'|\bar{\mathbf{J}}(0)|p_1\rangle}{E(q_1)+E(p_1)-E_{m'}+i\varepsilon}-\sum_{p_{n'}=p_2-q_1}\frac{\langle p|\bar{\mathbf{J}}(0)|n'\rangle\langle n'|\psi(0)|p_1\rangle}{E(p_2)-E(q_1)-E_{n'}-i\varepsilon}\Bigg\}\Bigg]$$

where we have dropped the contribution due to the first term of the right-hand side of (12) since it corresponds to the possibility where the nucleon of momentum p_1 goes unscattered, the final state meson being produced by the other nucleon.

3. Tamm-Dancoff Approximation

Equation (18) as it stands is very general in character. To make the problem simpler, we shall assume that the m and n states do not contain more than two particles. The motivation to make such a drastic assumption is twofold:

(1) If the m and n states were to contain more than two particles, we are forced to introduce a separate equation similar to (18) for double meson production amplitudes, a circumstance which we wish to avoid.

(2) Effects due to virtual pair creation are eliminated and this simplifies the evaluation of the vertex operator and other related quantities.

Of course, here we are guided by the fact that pion nucleon scattering properties are known only for energies less than a GeV.

Next we shall examine the various possibilities of m and n states:

m state: The non-vanishing contribution comes from one-nucleon and one-nucleon + one-meson states.

n state: The only state that contributes is the two-nucleon state.

m' state: Here also only the two-nucleon state gives a contribution.

n' state: The state that gives a contribution is the one-meson state.

Thus (18) can be written as

$$
\begin{aligned}
&\langle p_2 q_2 k\alpha|T|p_1 q_1\rangle \\
&= \bar{w}(q_2)\left(\frac{m}{2E(q_2)w(k)}\right)^{\frac{1}{2}}\left[\frac{\langle p_2|\mathbf{j}_\alpha(0)|p_1+q_1-q_2\rangle\langle p_1+q_1-q_2|\mathbf{J}(0)|p_1 q_1\rangle}{E(q_2)+E(p_1+q_1-q_2)-E(p_1)-E(q_1)-i\varepsilon}\right. \\
&+\int\int\frac{\langle p_2|\mathbf{j}_\alpha(0)|p'k'\beta\rangle\langle p'k'\beta|\mathbf{J}(0)|p_1 q_1\rangle}{E(q_2)+E(p')+w(k')-E(p_1)-E(q_1)-i\varepsilon}\,\mathrm{d}p'\,\mathrm{d}k'\,\delta(\mathbf{p}'+\mathbf{k}'-\mathbf{p}_1-\mathbf{q}_1+\mathbf{q}_2) \\
&-\int\int\frac{\langle p_2|\mathbf{J}(0)|p'q'\rangle\langle p'q'|\mathbf{j}_\alpha(0)|p_1 q_1\rangle}{E(q_2)+E(p_2)-E(p')-E(q')+i\varepsilon}\,\mathrm{d}p'\,\mathrm{d}q'\,\delta(\mathbf{p}_2+\mathbf{q}_2-\mathbf{p}'-\mathbf{q}') \qquad (19) \\
&-g\gamma_5\tau_\alpha w(q_1)\frac{1}{(2\pi)^{\frac{3}{2}}}\left(\frac{m}{E(q_1)}\right)^{\frac{1}{2}}\left\{\int\int\frac{\langle p_2|\psi(0)|p'q'\rangle\langle p'q'|\bar{\mathbf{J}}(0)|p_1\rangle}{E(q_1)+E(p_1)-E(p')-E(q')+i\varepsilon}\,\mathrm{d}p'\,\mathrm{d}q'\,\delta(\mathbf{p}'+\mathbf{q}'-\mathbf{p}_1-\mathbf{q}_1)\right. \\
&\left.\left.-\frac{\langle p_2|\bar{\mathbf{J}}(0)|p_2-q_1,\beta\rangle\langle p_2-q_1,\beta|\psi(0)|p_1\rangle}{E(p_2)-E(q_1)-w(p_2-q_1)+i\varepsilon}\right\}\right].
\end{aligned}
$$

Eq. (19) is an integral equation for the T-matrix amplitude of the meson production process. The first term is an inhomogeneous term and consists of the product of nucleon vertex operator and two-nucleon potential, the last two terms being exactly similar in nature. As a first approximation, we can take the T-matrix to be the sum of these three terms. As the order of each of these terms is at least f^3 (where f is the renormalized p.v. coupling constant) solution by iteration is expected to be fairly satisfactory. The solution of the T-matrix based on (19) and numerical results will be presented in a subsequent contribution.

Part of this work was done during the stay of one of us (S.K.S.) at the School of Physics, University of Sydney and he would like to take this opportunity to thank Professor Harry Messel for his hospitality. The financial support from the Atomic Energy Commission, Government of India to one of us (N.R.R.) in the form of a Junior Research Fellowship is gratefully acknowledged. These authors are also grateful to the University of Madras for facilities afforded for research.

References

1) G. F. Chew, Phys. Rev. **94** (1954) 1748, 1755; **95** (1954) 1669
2) F. E. Low, Phys. Rev. **97** (1955) 1392
3) G. C. Wick, Revs. Mod. Phys. **27** (1955) 339
4) S. Gartenhaus, Phys. Rev. **100** (1955) 900
5) H. Miyazawa, Phys. Rev. **104** (1956) 1741
6) A. Klein and B. H. McCormick, Phys. Rev. **104** (1956) 1747
7) A. Klein, Prog. Theor. Phys. **20** (1958) 257
8) Yu. V. Novozhilov, Journ. Exp. Theor. Phys. (Trans.) **6** (1958) 692
9) P. S. Signell and R. E. Marshak, Phys. Rev. **109** (1958) 339
10) G. C. Wick, Phys. Rev. **80** (1950) 268
11) H. Lehmann, K. Symanzik and W. Zimmermann, Nuovo Cimento **1** (1955) 205
12) A. A. Loganov and A. N. Tavkhalidze, Journ. Exp. Theor. Phys. (Trans) **5** (1957) 1134

1.E.5: 8.C

Nuclear Physics **10** (1959) 166—180; ©*North-Holland Publishing Co., Amsterdam*

Not to be reproduced by photoprint or microfilm without written permission from the publisher

A REMARK ON THE INTERPRETATION OF THE ELECTRON-NUCLEUS SCATTERING EXPERIMENTS

C. VILLI

Istituto di Fisica dell'Università di Trieste

and

Istituto Nazionale di Fisica Nucleare, Sottosezione di Trieste †

Received 26 November 1958

Abstract: The consequences on the interpretation of the electron-nucleus scattering data, arising from the finite size of the proton and/or of the electron, are discussed.

It is known that the angular distributions of electrons elastically scattered by nuclei have been satisfactorily interpreted in terms of non-uniform densities of the nuclear charge [1]). In this kind of analysis the effects arising from the finite size of the protons bound in the nucleus are usually neglected or accounted for in an approximate way. The object of this note, suggested by an attempt carried out by Hofstadter [2]) to allow for the finite size of the protons in C^{12}, is to emphasize the importance that the experimental information on the structure of the elementary electron-proton interaction, brought to light by Hofstadter's experiments, might have for the correct interpretation of the electron-nucleus scattering data. The following discussion will be based on the first Born approximation not because this approximation is believed to be particularly reliable, but because it is ideally suited for a rapid outline and a simple formulation of the problem. As is well known, in this approximation the differential cross-section for the elastic scattering of electrons of energy E in the angle ϑ, by a nucleus of atomic number Z, reads

$$\sigma(\vartheta) = \sigma_M(\vartheta)|F(q)|^2, \tag{1}$$

where

$$\sigma_M(\vartheta) = (Ze^2/2E)^2 \cos^2 \tfrac{1}{2}\vartheta \operatorname{cosec}^4 \tfrac{1}{2}\vartheta \tag{2}$$

is the Mott cross-section for a point nucleus and the quantity inside the vertical lines, usually called the form factor of the nucleus, is given by

$$F(q) = \int \rho(\mathbf{r}) \exp(i\mathbf{q} \cdot \mathbf{r}) d\mathbf{r}, \tag{3}$$

where $q = 2E \sin \frac{1}{2}\vartheta$ is the momentum transfer †† in the collision and the

† This research has been sponsored by the Wright Air Development Center of the Air Research and Development Command, United States Air Force, through its European Office, under Contract NO. AF 61 (052)-164.

†† A system of units where $\hbar = c = 1$ will be used throughout.

function $\rho(\mathbf{r})$, normalized to unity $[F(0) = 1]$, is generally identified with the charge distribution of the target nucleus.

For our purposes it is important to stress that the primitive and more general definition of the form factor is not given by eq. (3), but it follows naturally from the first Born approximation on which the cross-section (1) is based. In fact, elementary considerations show that the function $F(q)$ can be defined simply as the ratio between the three-dimensional Fourier transform of the radial part of the potential energy $\mathscr{V}(r) = -Ze^2f(r)$ of an electron in the Coulomb field of an extended nucleus, and the same quantity evaluated for a point nucleus. For reasons which will become clear later, the form factor defined in this way will be indicated as $"F(q)"$, i.e.

$$"F(q)" = \frac{q^2}{4\pi}\int f(r)\exp(i\mathbf{q}\cdot\mathbf{r})\mathrm{d}\mathbf{r}. \tag{4}$$

We shall now prove that from eq. (4) emerge some conceptually critical questions, which are otherwise concealed by the usual derivation of eq. (3) [2]. Integrating by parts twice the radial integral of eq. (4) and taking into account that, because of the finite size of the nucleus, we have

$$\lim_{r\to 0} rf(r) = \lim_{r\to 0}\left[r\frac{\mathrm{d}f(r)}{\mathrm{d}r}\right] = 0, \tag{5}$$

one finds

$$"F(q)" = -\frac{1}{4\pi}\int \nabla^2 f(r)\exp(i\mathbf{q}\cdot\mathbf{r})\mathrm{d}\mathbf{r}, \tag{6}$$

from which one formally gets eq. (3) $["F(q)" \equiv F(q)]$ using the Poisson equation $\nabla^2 f(r) = -4\pi\rho(\mathbf{r})$. The crucial point of the whole problem lies in the physical meaning to be attributed to the function $\rho(\mathbf{r})$, because its identification with the charge distribution of the target nucleus is by no means so obvious as may appear at first. Such an identification is physically legitimate only in so far as one implicitly assumes that the radial dependence of the electron-nucleus Coulomb potential energy arises from elementary interactions between point protons and a point electron. This fundamental circumstance, which will now be proved, reveals that it is in principle conflicting with Hofstadter's experimental evidence on the scattering of electrons by protons, to consider as the nuclear charge density the function $\rho(\mathbf{r})$, appearing in eq. (3).

To be more specific, let us assume that one proton and one electron, whose individual densities will be indicated by $\rho_p(\mathbf{r})$ and $\rho_e(\mathbf{r})$, be placed at the points $\mathbf{r}_1$ and $\mathbf{r}_2$ respectively, and construct the potential energy $V(r_{12}) = -e^2v(r_{12})$ of the electron-proton system, where $r_{12} = |\mathbf{r}_1 - \mathbf{r}_2|$ and

$$v(r_{12}) = \iint(|\mathbf{r}' - \mathbf{r}''|)^{-1}\rho_p(\mathbf{r}_1 - \mathbf{r}')\rho_e(\mathbf{r}_2 - \mathbf{r}'')\mathrm{d}\mathbf{r}'\,\mathrm{d}\mathbf{r}''. \tag{7}$$

Then, calling $r_2 \equiv r$ the distance of the electron from the centre of the nucleus, the radial dependence of the electron-nucleus potential energy is given by

$$f(r) = \int \rho(r_1) v(r_{12}) \mathrm{d}\mathbf{r}_1 \tag{8}$$

where $\rho(r)$ is the spherically symmetric distribution function of the nuclear charge. According to definition (6), for the evaluation of the form factor "$F(q)$" one must apply the operator $\nabla^2 = (\partial^2/\partial r^2) + (2/r)(\partial/\partial r)$ to eq. (8), and then perform the three-dimensional Fourier transform of the function in this way obtained. The Laplacian of $f(r)$ leads of course to the Poisson equation

$$\nabla^2 f(r) = -4\pi \, "\rho(r)", \tag{9}$$

which, however, has not the well known classical significance, because "$\rho(r)$" turns out to be a complicated functional of the nuclear density $\rho(r)$. We shall now prove that, as far as the fit of the electron-nucleus scattering data is concerned, the function "$\rho(r)$" plays — so to say — the role of an "apparent" density, which, besides the information on $\rho(r)$, foreshadows also that concerning the structure of the elementary electron-proton interaction. To see how the latter comes into play, eq. (8) should be worked out. Defining the volume element as $\mathrm{d}\mathbf{r}_1 = (2\pi/r) r_1 \mathrm{d}r_1 r_{12} \mathrm{d}r_{12}$ and taking into account that, because of the absolute value sign on the limit of r_{12}, i.e. $|r_1 - r| \leqq r_{12} \leqq r_1 + r$, the integration over r_1 must be split into two parts (a) $r_1 \leqq r$ and (b) $r_1 \geqq r$, the final expression of eq. (8) reads

$$f(r) = \frac{2\pi}{r} \left[\int_0^r r_1 \rho(r_1) \mathrm{d}r_1 \int_{r-r_1}^{r+r_1} r_{12} v(r_{12}) \mathrm{d}r_{12} + \int_r^\infty r_1 \rho(r_1) \mathrm{d}r_1 \int_{r_1-r}^{r+r_1} r_{12} v(r_{12}) \mathrm{d}r_{12} \right]. \tag{10}$$

According to definition (9), the radial part of the Laplacian, applied to eq. (10), leads to

$$"\rho(r)" = \chi(0)\rho(r) + \rho^*(r), \tag{11}$$

where

$$\chi(|r - r_1|) = \tfrac{1}{2}[(r - r_1) v(r - r_1) + (r_1 - r) v(r_1 - r)], \tag{12}$$

$$\rho^*(r) = \frac{1}{2r} \left[\int_0^r r_1 \rho(r_1) K_1(r|r_1) \mathrm{d}r_1 + \int_r^\infty r_1 \rho(r_1) K_2(r|r_1) \mathrm{d}r_1 \right], \tag{13}$$

the two functions $K_1(r|r_1)$ and $K_2(r|r_1)$ being defined as

$$K_1(r|r_1) = v(r - r_1) - v(r + r_1) + (r - r_1) \frac{\partial v(r - r_1)}{\partial r} - (r + r_1) \frac{\partial v(r + r_1)}{\partial r}, \tag{14a}$$

$$K_2(r|r_1) = v(r_1 - r) - v(r + r_1) - (r_1 - r) \frac{\partial v(r_1 - r)}{\partial r} - (r + r_1) \frac{\partial v(r + r_1)}{\partial r}. \tag{14b}$$

The normalization to unity of "$\rho(r)$" and $\rho(r)$ implies that it must be

$$\int \rho^*(r)\mathrm{d}\mathbf{r} = 1-\chi(0). \tag{15}$$

In fact, inverting the integrations over r_1 and r, one has

$$\int \rho^*(r)\mathrm{d}\mathbf{r} = 4\pi\int_0^\infty r_1\rho(r_1)\varphi(r_1)\mathrm{d}r_1 \tag{16a}$$

where

$$\varphi(r_1) = \tfrac{1}{2}\left[\int_{r_1}^\infty rK_1(r|r_1)\mathrm{d}r + \int_0^{r_1} rK_2(r|r_1)\mathrm{d}r\right]. \tag{16b}$$

Using eqs. (14) and taking into account that for large interparticle separations $v(r_{12})$ approaches to the r_{12}^{-1} law $[\chi(\infty) = 1]$, eq. (16b) yields

$$\varphi(r_1) = r_1[1-\chi(0)], \tag{17}$$

namely eq. (15) is verified. It is now easy to prove that *the necessary and sufficient condition for the identification of "$\rho(r)$" with the true nuclear charge density $\rho(r)$, i.e. $\rho^*(r) = 0$, is that the law $v(r_{12}) = r_{12}^{-1}$ holds, namely that both the proton and the electron density be described in eq.* (7) *by a delta-function.* Inspection of eqs. (13) and (14), in fact, shows that the condition $\rho^*(r) = 0$ is fulfilled provided the electron-proton potential satisfies the differential equation

$$\frac{\mathrm{d}v(x)}{\mathrm{d}x} = -\frac{v(x)}{x}, \tag{18}$$

whose solution $v(x) = x^{-1}$ is the Coulomb law.

The deceptive nature of the electron-nucleus scattering data will be clear by now. The presumptive structure of the interacting particles implies that the electron-nucleus differential cross-section is not given by eq. (1) with the form factor defined in eq. (3), but rather by the expression

$$\sigma(\vartheta) = \sigma_{\mathrm{M}}(\vartheta)|''F(q)''|^2, \tag{19}$$

where

$$''F(q)'' = F(q)+F^*(q) \tag{20}$$

is the three-dimensional Fourier transform of eq. (17). Eq. (1) is evidently a particular case of eq. (19), valid for small momentum transfer or for structureless particles. It is, then, clear that the ratio between the measured and the Mott cross-sections allows the experimental determination of the behaviour, as a function of q, of the "apparent" form factor $''F(q)''$, which disguises in a complicated manner the intrinsic features of the nuclear charge density $\rho(r)$. In the light of this circumstance, a systematic re-examination of the electron-nucleus scattering data is an important task to accomplish in order to bring to light all physical information which probably they still conceal, and to dispell the suspicion that in many cases one has attributed to the nucleus also those effects which presumably belong to the structure of the elementary electron-proton interaction. The procedure to adopt for such an

analysis is very simple, because the "apparent" density "$\rho(r)$" is nothing but the "experimental" density, so far improperly attributed to the nucleus and empirically determined from the experimental behaviour of $[\sigma(\vartheta)/\sigma_M(\sigma)]^{\frac{1}{2}}$. Hence, the charge distribution of the target nucleus is obtained by solving the integral equation (17), which in compact form reads

$$"\rho(r)" = \chi(0)\rho(r) + \frac{1}{2r}\int_0^\infty r_1\rho(r_1)K(r|r_1)\mathrm{d}r_1, \tag{21}$$

the kernel $K(r|r_1)$ being determined by the theoretical model used to construct the electron-proton interaction. Since, according to the above theorem, the validity of the Coulomb law implies $K(r|r_1) = 0$, eq. (21) discloses what the link is between the electron-nucleus and the electron-proton scattering data as far as the determination of $\rho(r)$ is concerned. The solution of the integral equation (21) is somewhat complicated by the fact that, according to eqs. (14), the integration over r_1 must be split into two parts because $K(r|r_1) \equiv K_1(r|r_1)$ for $r \geqq r_1$ and $K(r|r_1) \equiv K_2(r|r_1)$ for $r \leqq r_1$. This mathematical problem, together with the extension of the preceding considerations up to the second Born approximation, will be examined in a forthcoming paper, where it will be shown that clear-cut information on the charge distribution of the target nucleus can be obtained provided one takes into account the totality of Hofstadter's experimental evidence, namely that concerning the scattering of electrons by both nuclei and protons.

In this paper we shall restrict ourselves simply to support the above remarks with some corroborative evidence. With this aim in view, we shall examine, as an illustrative example, the limiting, and more unfavourable, case of a uniform distribution of Z protons confined into a nuclear sphere of radius R. Since in this case $\rho(r) = \rho_0 = 3/(4\pi R^3)$ for $r \leqq R$ and $\rho(r) = 0$ for $r > R$, eq. (8) becomes ($r_2 \equiv r$)

$$f(r, R) = \rho_0 \int v(r_{12})\mathrm{d}\mathbf{r}_1. \tag{22}$$

To evaluate eq. (22) it is convenient to choose the volume element $\mathrm{d}\mathbf{r}_1$ in the same way as before, and then invert the integrations over r_1 and r_{12}, using the following rules:

for $r \leqq R$:

$$\int_0^r \mathrm{d}r_1 \int_{r-r_1}^{r+r_1} \mathrm{d}r_{12} \to \int_0^r \mathrm{d}r_{12} \int_{r-r_{12}}^{r} \mathrm{d}r_1 + \int_r^{2r} \mathrm{d}r_{12} \int_{r_{12}-r}^{r} \mathrm{d}r_1 \qquad r_1 \leqq r, \tag{23a}$$

$$\int_0^R \mathrm{d}r_1 \int_{r_1-r}^{r+r_1} \mathrm{d}r_{12} \to \int_0^{R-r} \mathrm{d}r_{12} \int_r^{r_{12}-r} \mathrm{d}r_1 + \int_{R-r}^{2r} \mathrm{d}r_{12} \int_r^{2r} \mathrm{d}r_1 + \int_{2r}^{R+r} \mathrm{d}r_{12} \int_{r_{12}-r}^{R} \mathrm{d}r_1 \quad r_1 \geqq r; \tag{23b}$$

for $r \geqq R$:

$$\int_0^R \mathrm{d}r_1 \int_{r-r_1}^{r+r_1} \mathrm{d}r_{12} \to \int_{r-R}^{r} \mathrm{d}r_{12} \int_{r-r_{12}}^{R} \mathrm{d}r_1 + \int_r^{r+R} \mathrm{d}r_{12} \int_{r_{12}-r}^{R} \mathrm{d}r_1. \tag{24}$$

Performing the operations indicated, eq. (22) ultimately reads

$$f(r, R) = \frac{\pi\rho_0}{r}\left[2r\left(\int_0^{R+r} + \int_0^{R-r}\right) r_{12}^2 v(r_{12})\mathrm{d}r_{12} + \int_{R-r}^{R+r} r_{12}(R^2-r^2-r_{12}^2)v(r_{12})\mathrm{d}r_{12}\right] \quad (r \leqq R), \quad (25a)$$

$$f(r, R) = \frac{\pi\rho_0}{r}\int_{r-R}^{r+R} r_{12}(R^2-r^2-r_{12}^2+2rr_{12})v(r_{12})\mathrm{d}r_{12} \quad (r \geqq R). \quad (25b)$$

According to definition (9), the "apparent" density, following from eq. (25) is found to be:

for $r \leqq R$,

$$"\rho(r)" = \frac{\rho_0}{2r}\left[\int_{R-r}^{r+R} r_{12}v(r_{12})\mathrm{d}r_{12} - R(R+r)v(R+r) + R(R-r)v(R-r)\right], \quad (26a)$$

for $r \geqq R$,

$$"\rho(r)" = \frac{\rho_0}{2r}\left[\int_{r-R}^{r+R} r_{12}v(r_{12})\mathrm{d}r_{12} - R(R+r)v(R+r) - R(r-R)v(r-R)\right]. \quad (26b)$$

It is readily verified that eqs. (26) reduce to the mathematical expression of the step-function representing the rectangle-like shape of the assumed uniform distribution *only* when both the proton and the electron are described as point objects and, consequently, their mutual interaction is governed by the Coulomb law $v(r_{12}) = r_{12}^{-1}$. Of course, in this case eqs. (25) yield the well known result

$$f(r, R) = \frac{1}{2R}\left[3 - \left(\frac{r}{R}\right)^2\right] \quad (r \leqq R), \quad (27a)$$

$$f(r, R) = \frac{1}{r} \quad (r \geqq R). \quad (27b)$$

To be more circumstantial, let us assume that the electron-proton interaction be described by the function

$$v(r_{12}) = \frac{1-\eta e^{-kr_{12}}}{r_{12}} - \xi e^{-kr_{12}}, \quad (28)$$

which contains, as particular cases, the modified Coulomb law examined (a) by Drell [3] ($\eta = 1, \xi = 0$), (b) by Clementel and Villi [4,5] ($\eta > 1, \xi = 0$) and (c) by Hofstadter [5] ($\eta = 1, \xi = \frac{1}{2}k$). Since the function $v(r_{12})$, defined in eq. (7), is determined by the product of $\rho_p(\mathbf{r})$ and $\rho_e(\mathbf{r})$, no answer can be given to the question concerning the individual contribution of the proton and of the electron structure to the mutual interaction (28). For this reason, one can interpret the "revised" Coulomb formula (28) in terms of a proton model and, although it is conceivable that many of the facts attributed to

the proton size could pertain to a radius of the electron, eq. (28) may be thought of as obtained from eq. (7) by putting $\rho_e(\mathbf{r}) = \delta(\mathbf{r})$ and

$$\rho_P(\mathbf{r}) = k[\eta k + (kr-2)\xi]\frac{e^{-kr}}{4\pi r} - (\eta-1)\delta(\mathbf{r}). \tag{29}$$

The case (a) (Yukawa-like density of the proton) has to be ruled out because conflicting with the high energy electron-proton scattering and, as Hofstadter has discovered, only the cases (b) and (c) are capable of reproducing the data remarkably well. Since these two cases are practically indistinguishable up to the energies so far available, we shall take into account only the latter one and evaluate the "apparent" density "$\rho(r)$", following from eq. (28) for $\eta = 1$ and $\xi = \frac{1}{2}k$. In this case eqs. (26) become:

$$\text{for } r \leqq R,$$

$$"\rho(r)" = \rho_0\left[1+\tfrac{1}{2}(kR+1)e^{-kR}\cosh kr - \tfrac{1}{2}(3+kR+k^2R^2)e^{-kR}\frac{\sinh kr}{kr}\right], \tag{30a}$$

$$\text{for } r \geqq R,$$

$$"\rho(r)" = \rho_0\left[\tfrac{1}{2}kR(3+kR)\cosh kR - \tfrac{1}{2}(3+kr+k^2R^2)\sinh kR\right]\frac{e^{-kr}}{kr}. \tag{30b}$$

It is easily recognized that the last two terms in eq. (30a), and all terms in eq. (30b), represent the function indicated by $\rho^*(r)$ in eq. (17). This function of course becomes zero if one suppresses the extended structure of the proton by letting its size parameter k tend to infinity. Thus, in spite of the fact that we had intentionally confined ourselves to a uniform distribution of nuclear

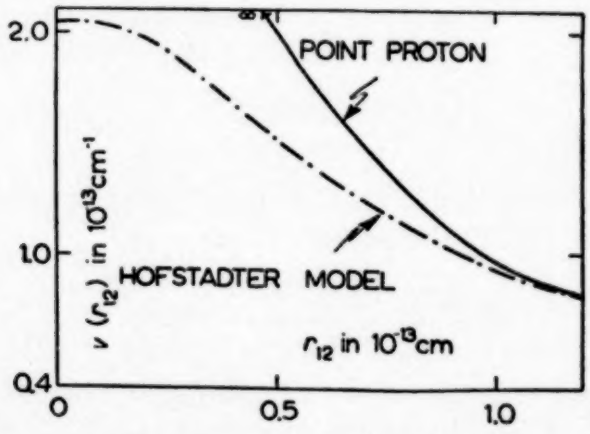

Fig. 1. Radial dependence of the electron-proton interaction for a point proton (continuous line) and for the exponential model of the proton (dotted line). The size parameter of the proton density has been computed from the relation $a_p = (12)^{\frac{1}{2}}k^{-1}$, assuming a root-mean-square radius of the proton equal to $a_p = 0.8\times10^{-13}$ cm.

charge, the radial dependence of *"$\rho(r)$" has all the characteristic features of a non-uniform distribution*, being continuous at $r = R$ and normalized to unity.

The illusory nature of "$\rho(r)$" is nevertheless evident, and its non-uniform character has indeed nothing to do with the structure of the nucleus, but it arises entirely from the exponential density of the proton, responsible for the deviation from the r_{12} law, shown in fig. 1. The radial dependence of "$\rho(r)$" is surprising: *it exhibits some of the features of a smoothed uniform density with a diffused boundary and a pronounced tail.* This disconcerting situation, visualized in fig. 2, clearly suggests that neglecting the effects arising from

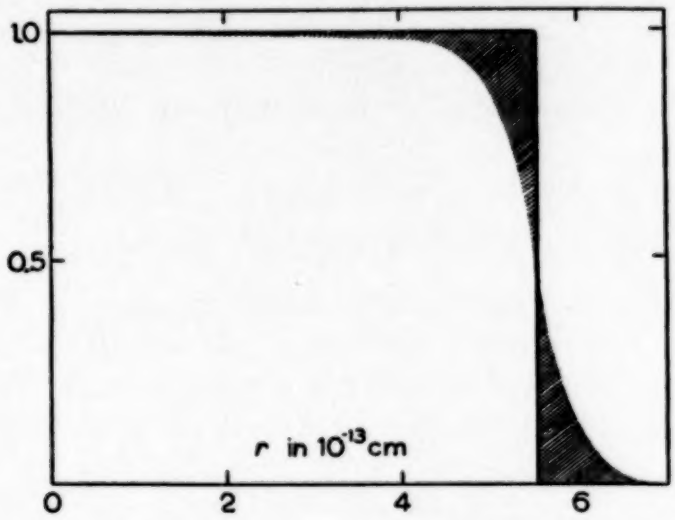

Fig. 2. The curved outline of the shadowed area shows the radial dependence "$\rho(r)$"/ρ_0 of the "apparent" density for a uniform nuclear charge distribution, brought about by the finite size of the protons. The proton has been described according to the Hofstadter exponential model. The size parameter k of the proton density has been computed from the relation $a_p = (12)^{\frac{1}{2}}k^{-1}$, assuming a root-mean-square radius of the proton equal to $a_p = 0.8\times10^{-13}$ cm. Eqs. (30) have been evaluated for $A = 100$ and $R = 1.2A^{\frac{1}{3}}\times10^{-13}$ cm.

the structure of the electron-proton interaction leads to an *overestimation* of the diffuseness of the charge distributon of the target nucleus. This is of course true also in the more realistic case when $\rho(r)$ is indeed non-uniform. For instance, inspection of eq. (21) with the kernels (14), specified according to eq. (28), namely

$$K_1(r|r_1) = 2e^{-kr}[(\eta k+k\xi r-\xi)\sinh kr_1-k\xi r_1\cosh kr_1] \quad (r\geqq r_1), \tag{31a}$$

$$K_2(r|r_1)=2e^{-kr_1}[(\eta k+k\xi r_1-\xi)\sinh kr-k\xi r\cosh kr]=K_1(r_1|r) \quad (r\leqq r_1) \tag{31b}$$

shows that "$\rho(r)$" $\leqq \rho(r)$ for $r \leqq R_0$ and "$\rho(r)$" $\geqq \rho(r)$ for $r \geqq R_0$, where R_0 is the root-mean-square radius of the "apparent" density.

From the critical content of the above remarks a question arises spontaneously, namely whether instead of interpreting the data in terms of point electrons elastically scattered by a non-uniform distribution of point protons, they could also be explained from the opposite standpoint, that extended (or point) electrons be elastically scattered by a uniform distribu-

tion of extended protons. The answer to this question can be given, without resorting to fitting subtleties, simply by taking advantage of the fact that eqs. (25) are valid whatever the radial dependence of $v(r_{12})$ may be. This remarkable circumstance suggests that we are here faced with a problem whose general mathematical nature is essentially determined by the assumed uniform character of the charge distribution. It is, in fact, readily established that the potential energy

$$\mathscr{V}(r, R) = V_0 f(r, R) \tag{32}$$

of a particle at a distance r from the centre of a system of particles uniformly distributed within a sphere of radius R, obeys the hyperbolic partial differential equation †

$$\left(\frac{\partial^2}{\partial r^2} + \frac{2}{r}\frac{\partial}{\partial r} - \frac{\partial^2}{\partial R^2} - \frac{4}{R}\frac{\partial}{\partial R}\right)\mathscr{V}(r, R) = 0, \tag{33}$$

whose solutions, derived from particular specifications of the associated Cauchy problem, are in fact given by eqs. (25) for special choices of the function $v(r_{12})$. By virtue of eq. (33) it is possible to define the "apparent" density $"\rho(r)"$ in a manner which is different from the one stated in eq. (9), namely

$$\mathfrak{D} f(r, R) = -4\pi\, "\rho(r)" \tag{34}$$

where the differential operator $\mathfrak{D}$ is given by

$$\mathfrak{D} = \frac{\partial^2}{\partial R^2} + \frac{4}{R}\frac{\partial}{\partial R}. \tag{35}$$

Eq. (34) provides us with the clue for answering the question concerning the conjectured possibility of explaining the electron-nucleus scattering data in terms of the finite size of the interacting particles only. In fact, applying the operator $\mathfrak{D}$ to both sides of eq. (4) and taking into account eq. (34), the "apparent" form factor $"F(q)"$ is found to obey the Bessel differential equation

$$(\mathfrak{D} + q^2)\, "F" = 0, \tag{36}$$

whose solutions are

$$"F(q)" = \frac{3}{qR}[C_1(q) j_1(qR) + C_2(q) n_1(qR)], \tag{37}$$

$j_1(qR)$ and $n_1(qR)$ being spherical Bessel and Neumann functions respectively, and $C_1(q)$ and $C_2(q)$ two unknown functions independent of the nuclear radius R. These functions of the momentum transfer contain the structure parameters characterizing the electron-proton interaction at small interparticle separation, and are determined by the proton model used to evaluate

† This equation is of course valid also for particles interacting through a short range field.

$v(r_{12})$. For structureless particles one has $C_1(q) = 1$ and $C_2(q) = 0$. In this case the electron-nucleus cross-section (19) identifies with eq. (1) and exhibits, in disagreement with experiment, points of zero diffraction corresponding to the zeros of the spherical Bessel function $j_1(qR)$. This disappointing circumstance, which cannot be overcome even by taking into account that $\rho^*(r)$ is different from zero, compels one to rule out the rectangle-like charge distribution. In fact, the examination of the diffraction pattern determined by eq. (37) shows that in order to wash out the minima of the cross-section, $C_1(q)$ and $C_2(q)$ should be oscillating functions of the momentum transfer. This behaviour is, however, unacceptable, because it would involve a sort of sharp boundary proton model, which is conflicting with the electron-proton scattering data. Any proton model with a diffused boundary, like the one suggested by Hofstadter or by Clementel and Villi, gives rise to an "apparent" density not sufficiently diffused to disentangle "$F(q)$" from the zeros of $j_1(qR)$ and $n_1(qR)$. The functions $C_1(q)$ and $C_2(q)$, calculated either for the case (b) and (c), depend on the momentum transfer in such a way that the cross-section still possesses points of zero diffraction, although shifted towards large angles, where "$F(q)$" exhibits a more rapid decrease than when the proton density is described by a delta-function. This circumstance suggests that a nuclear charge $\rho(r)$ less diffused than that implied by the assumption that $\rho^*(r)$ be zero, is involved in the fitting mechanism of the data. The influence on $\sigma(\vartheta)$ of the proton structure is obviously appreciable when the wave length of the impinging electron is smaller than the average interparticle separation within the nucleus. For this reason, structural effects due to the finite size of the protons are practically undetectable for scattering energies smaller than about 140 MeV. On the contrary, one should expect that at higher energies the interpretation of the data might lead, as a consequence of the neglecting of $\rho^*(r)$ in eq. (17), to a spurious energy dependence of the size parameters characterizing the spatial extension of "$\rho(r)$" $\equiv \rho(r)$. The situation shown in fig. 2 is not qualitatively altered when considering the charge distribution $\rho(r)$ extracted from the "experimental" density "$\rho(r)$" by solving the integral equation (21). One may argue that also in this case the modified Coulomb law (28) gives rise to fictitious diffuseness effects near the "surface" of the nucleus ($r \approx R_0$). An exact evaluation of these effects is therefore highly desirable for a correct description of the skin thickness of the charge density of the nucleus.

In connection with the above discussion, it is worth while calling attention to the fact that whenever in the theoretical picture of a system of interacting particles their individual structure is taken into account, effects arise which are to a certain extent indistinguishable from those due to a presumptive non-uniform character of the radial distribution of the assembly itself. To shed light in a very simple way on this peculiar circumstance, let us seek for

a solution of eq. (34) in power series of r, valid for $r \leqq R$. Since no odd power of the radial distance come into play, the power expansion reads

$$\mathscr{V}(r, R) = \sum_{n=0}^{n_{max}} \omega_n(R) r^{2n}, \tag{38}$$

where the unknown functions $\omega_n(R)$ are determined by solving the system of differential equations

$$2(n+1)(2n+3)\omega_{n+1}(R) = \mathfrak{D}\omega_n(R). \tag{39}$$

The solutions of eq. (34) having physical meaning must satisfy the evident condition $\mathscr{V}(r, \infty) = 0$. It follows that eqs. (39) cut off the expansion (38) at $n_{max} = 1$, all other coefficients being $\omega_n(R) = 0$ for $n > n_{max} = 1$. Then, the most general solution of eq. (34), in the form (38), is found to be

$$\mathscr{V}(r, R) = \frac{c_0}{3R}\left[3 - \left(\frac{r}{R}\right)^2 - \frac{c_1}{R^2}\right], \tag{40}$$

where c_0 and c_1 are two arbitrary integration constants. Since the classical expression of the electron-nucleus potential is obtained from eq. (40) by choosing $c_0 = -\frac{3}{2}Ze^2$ and $c_1 = 0$ (eq. (27a)), one is inescapably led to the conclusion that the modified potential (40) with $c_1 \neq 0$ has its only possible physical justification in the effects brought about by the finite size of the particles †. On the strength of this conclusion it is interesting to evaluate the Coulomb energy of the nucleus

$$E_C = \tfrac{1}{2}Z\int \rho(r)\mathscr{V}(r, R)\mathrm{d}\mathbf{r} \tag{41}$$

and regard $\mathscr{V}(r, R)$ as the potential energy of one proton in the Coulomb field of the remaining $(Z-1)$ ones. Assuming in this case $c_0 = +\frac{3}{2}(Z-1)e^2$, it is readily established that eq. (40) leads to the classical expression $E_C = \frac{3}{5}Z(Z-1)e^2/R^*$, provided one introduces the effective nuclear radius

$$R^* = R + \frac{5}{12}\frac{c_1}{R}, \tag{42}$$

which accounts for the fact that the square root of c_1 plays the role of a new size parameter of the system, originating in the electromagnetic structure of the proton. If this theoretical background is ignored, it is clear that the modified expression (42) could also be interpreted assuming that the nuclear

† The reader will find it interesting to examine the case when, with obvious changes in eq. (7), $v(r_{12})$ is regarded as the radial dependence of the nucleon-nucleon potential, and eq. (40) as the potential energy of one nucleon in the strong, short range field originated by the $(A-1)$ nucleons bound in the nucleus. In this case, eq. (40) is found to be consistent with the saturation prescriptions of the nuclear volume energy and density by virtue of the term in c_1. A closer inspection shows that this term, which prevents the nuclear collapse at high densities, implies in this case a dependence of the potential energy of the nucleus on the radius R which is similar to that expected to be determined by two-body forces with repulsive core.

charge, instead of being described like a sharp boundary drop of radius $R = r_0 A^{\frac{1}{3}}$, would be pictured rather like a uniform core with a tapering outward extension. In fact the former term in eq. (42) can be thought of as being related to a central core of uniform density and the latter one to a low density fringe. Thus, also in this case we are faced with effects formally attributable to a fictitious diffuseness of the nuclear charge, as shown by the shadowed area in fig. 2. The value of the parameter c_1 can be computed from eq. (42), using the energy difference between mirror nuclei in order to determine R^* and by regarding R as the radius of the equivalent uniform model consistent with the electron-nucleus scattering data. For instance, in the case of the two mirror nuclei C^{11} and B^{11} one has $R^* = 3.19 \times 10^{-13}$ cm. The value of R, extrapolated from Hofstadter's calculations [1]), is equal to 2.95×10^{-13} cm, and finally eq. (42) yields $r^* = \sqrt{c_1} = 1.11 \times 10^{-13}$ cm.

The preceding considerations suggest that accurate evaluations of the Coulomb energy of mirror nuclei might provide an indirect clue for deciding whether or not an internal structure should be attributed to the electron. In fact, the possibility of explaining the Coulomb energy of the nucleus using both the charge distributions determined from the electron-nucleus scattering data and the Coulomb interaction between protons, constructed from proton models consistent with the electron-proton scattering experiments, depends upon the prejudicial assumption that the electron is a sort of point probe, having no influence at all on the electron-proton interaction at short distances. As has been already pointed out, this assumption in no way restricts the validity of the above considerations as far as they are confined to the study of the electron-proton or electron-nucleus interaction, but it may be found to be unacceptable when considering the Coulomb energy of the nucleus and, perhaps, the scattering at very small angles of high energy protons by protons. If it is true that the electron-proton scattering data give a direct information on the structure of the proton, then, the deviation from the Coulomb law of the function $v(r_{12})$, given in eq. (28), should be thought of as entirely determined by the proton density (29). The obvious consequence of this preconceived assumption is that the proton-proton Coulomb interaction, which comes into play when calculating either the p—p Mott cross-section or E_c, is indeed obtainable from eq. (7) simply by replacing $\rho_e(\mathbf{r})$ by $\rho_P(\mathbf{r})$. To make clear this point, let us write eq. (7) as

$$v(r_{12}) = \int \rho_1(\mathbf{r}_1 - \mathbf{r}') G_2(|\mathbf{r}' - \mathbf{r}_2|) d\mathbf{r}', \tag{43}$$

where

$$G_2(|\mathbf{r}' - \mathbf{r}_2|) = \int \rho_2(\mathbf{r}_2 - \mathbf{r}'') (|\mathbf{r}' - \mathbf{r}''|)^{-1} d\mathbf{r}'', \tag{44}$$

the individual densities of the two interacting particles being defined as ($i = 1,2$)

$$\rho_i(\mathbf{r}) = a_i\phi_i(r)+b_i\delta(\mathbf{r}). \tag{45}$$

Introducing the vectors $\mathbf{x} = \mathbf{r}_2-\mathbf{r}''$ and $\mathbf{y} = (\mathbf{r}'-\mathbf{r}_2)+\mathbf{x}$, the volume element $\mathrm{d}\mathbf{r}''$ becomes equal to $(2\pi/z)xy\mathrm{d}x\mathrm{d}y$, where $z = |\mathbf{r}'-\mathbf{r}_2|$. Using the density (45) with $i = 2$, eq. (44) reads

$$G_2(z) = \frac{4\pi a_2}{z}\left[\int_0^z x^2\phi_2(x)\mathrm{d}x+z\int_z^\infty x\phi_2(x)\mathrm{d}x\right]+\frac{b_2}{z}, \tag{46}$$

and eq. (43) ultimately yields

$$v(r_{12}) = \frac{2\pi a_1}{r_{12}}\left[\int_0^{r_{12}} x\phi_1(x)\mathrm{d}x\int_{r_{12}-x}^{r_{12}+x} yG_2(y)\mathrm{d}y+\int_{r_{12}}^\infty x\phi_1(x)\mathrm{d}x\int_{x-r_{12}}^{r_{12}+x} yG_2(y)\mathrm{d}y\right]$$
$$+b_1G_2(r_{12}). \tag{47}$$

From eq. (47) one obtains the potential (28) assuming $\rho_2(\mathbf{r}) \equiv \rho_e(\mathbf{r})$ ($a_2 = 0$, $b_2 = 1$) and identifying $\rho_1(\mathbf{r})$ with the proton density $\rho_P(\mathbf{r})$, given in eq. (29). The proton-proton Coulomb potential is obtained from eq. (47) by putting $\rho_1(\mathbf{r}) \equiv \rho_2(\mathbf{r}) = \rho_P(\mathbf{r})$. In particular, assuming the Hofstadter ($\eta = 1$, $\xi = \frac{1}{2}k$) and the Clementel-Villi ($\eta > 1$, $\xi = 0$) model of the proton, the radial dependence of the p—p Coulomb interaction is found to be

$$v(r_{12}) = \frac{1}{r_{12}}\Phi(kr_{12}) \tag{48}$$

where ($kr_{12} = x$)

$$\Phi_H(x) = 1-e^{-x}(1+\tfrac{11}{16}x+\tfrac{3}{16}x^2+\tfrac{1}{48}x^3) \tag{49a}$$

for the former model, and

$$\Phi_{CV}(x) = 1-\tfrac{1}{2}\eta[4-\eta(2-x)]e^{-x} \tag{49b}$$

for the latter one. This way of constructing the Coulomb interaction between protons turns out to be conceptually wrong if the radial dependence of the electron-proton potential (28) is determined by the individual contributions of both the proton and the electron structure, *because in this case eq.* (29) *must not be interpreted as the charge distribution of the proton but rather as an "apparent" proton density "*$\rho_P(\mathbf{r})$*"*. The very reason of this circumstance is readily established by noting that also for the electron-proton scattering process the primitive definition of the form factor is still given by eq. (4), with $f(r)$ replaced by $v(r_{12})$. From this definition one obtains eq. (6) irrespective of the conditions (5), provided the delta-function singularities are accounted for when calculating $\nabla^2 v(r_{12}) = -4\pi$ "$\rho_P(r_{12})$". Assuming in eq. (47) $\rho_1(\mathbf{r}) = \rho_P(\mathbf{r})$ and $\rho_2(\mathbf{r}) = \rho_e(\mathbf{r})$, it is a simple matter to show that if the electron is not a point object, the form factor for the proton charge, determined from the experimental data, is the three-dimensional Fourier transform of the "apparent" density "$\rho_P(\mathbf{r})$". Of course, a similar situation arises also for the Mott scattering of protons by protons. In this case the fictitious

nature of the "apparent" density becomes more evident because of the identical nature of the two interacting particles. In fact, if one ignores the general definition (6), the paradoxical situation would arise that, while the target proton is believed to possess an internal structure, the incident one is implicitely assumed to be a point particle! From eqs. (9) and (48), the "apparent" density of the two-proton system is found to be

$$''\rho_{\mathrm{H}}(r)'' = \frac{k^3 \mathrm{e}^{-kr}}{192\pi}(3+3kr+k^2r^2), \tag{50a}$$

$$''\rho_{\mathrm{CV}}(\mathbf{r})'' = \frac{\eta k^2 \mathrm{e}^{-kr}}{8\pi r}(4+\eta kr-4\eta)+(1+\eta^2-2\eta)\delta(\mathbf{r}), \tag{50b}$$

and the corresponding form factors, brought about by the structure of the proton-proton Coulomb interaction, are given by

$$''F_{\mathrm{H}}(q)'' = \frac{k^8}{(k^2+q^2)^4}, \tag{51a}$$

$$''F_{\mathrm{CV}}(q)'' = \frac{(k^2+q^2)^2-\eta q^2(\eta q^2+2k^2)}{(k^2+q^2)^2}. \tag{51b}$$

The implications of eqs. (48) and (51) are expected to lead to experimental discrepancies if the electron is not a structureless particle, because one can readily prove that the true proton density $\rho_{\mathrm{P}}(\mathbf{r})$ and the "apparent" density $''\rho_{\mathrm{P}}(\mathbf{r})''$, determined from the electron-proton scattering data, are bound together by the integral equation ($b_1 = 0$)

$$''\rho_{\mathrm{P}}(\mathbf{r})'' = \chi_{\mathrm{e}}(0)\rho_{\mathrm{P}}(\mathbf{r})+\frac{1}{2r}\int_0^\infty x\rho_{\mathrm{P}}(x)K_{\mathrm{e}}(r|x)\mathrm{d}x, \tag{52}$$

which is formally similar to eq. (21). In eq. (52) the parameter $\chi_{\mathrm{e}}(0)$ and the kernel $K_{\mathrm{e}}(r|x)$ are defined according to eqs. (12) and (14) respectively, where $v(x)$ has to be replaced by the structure function of the electron $G_{\mathrm{e}}(x) \equiv G_2(x)$, defined in eq. (44) [$\rho_2(\mathbf{r}) \equiv \rho_{\mathrm{e}}(\mathbf{r})$]. Thus, the proton models suggested by Hofstadter and by Clementel and Villi refer only to the "apparent" density of the proton, and the very physical difference between them lies in the fact that, while the former implies an over-all attraction between the incident electron and the target proton, the latter implies a repulsive interaction at interparticle distances smaller than about 0.06×10^{-13} cm. Whether $''\rho_{\mathrm{P}}(\mathbf{r})''$ ought to be really identified with $\rho_{\mathrm{P}}(\mathbf{r})$, and consequently $K_{\mathrm{e}}(r|x)$ is zero (point electron), is still an open problem. The most feasible and perhaps less sophisticated way to investigate whether $K_{\mathrm{e}}(r|x)$ is, or not, equal to zero might be provided by a detailed examination of the Coulomb energies of nuclei. If the electron has a structure, one should expect it to be *impossible* to reproduce in agreement with the nuclear charge distributions,

extracted from the electron-nucleus scattering data, the energy difference between mirror nuclei, computed in terms of the proton-proton Coulomb interaction (48), *following from the assumption that* "$\rho_P(\mathbf{r})$" $\equiv \rho_P(\mathbf{r})[K_e(r|x) = 0]$. Perhaps no discrepancy will ever be so welcome, at least by those who secretly believe in the breakdown of electrodynamics.

The author is indebted to Professor R. Hofstadter for many stimulating discussions and to Professor L. Rosenfeld for the critical reading of the manuscript.

References

1) R. Hofstadter, Revs. Mod. Phys. **28** (1956) 214;
for more recent references see D. G. Ravenhall, Revs. Mod. Phys. **30** (1958) 430
2) R. Hofstadter, Annual Review of Nuclear Science, vol. VII (1957)
3) S. D. Drell, Annals of Physics **4** (1958) 75
4) E. Clementel and C. Villi, Nuovo Cimento **4** (1956) 1207
5) R. Hofstadter, F. Bumiller and M. R. Yearian, Revs. Mod. Phys. **30** (1958) 482

1.C *Nuclear Physics* **10** (1959) 181—196; © *North-Holland Publishing Co., Amsterdam*
Not to be reproduced by photoprint or microfilm without written permission form the publisher

UN DÉVELOPPEMENT DU POTENTIEL DE GIBBS D'UN SYSTÈME COMPOSÉ D'UN GRAND NOMBRE DE PARTICULES (II)

CLAUDE BLOCH et CYRANO DE DOMINICIS
Centre d'Études Nucléaires de Saclay, Gif-sur-Yvette (S & O)

Reçu le 31 Octobre 1958

Abstract: The expansion of the Gibbs potential in powers of the activity is derived with the use of the second quantization, reestablishing a result of Ward and Montroll and the link with the classical Ursell Yvon Mayer expansion. Partial summation of non-interacting "loops" leads to the expansion established in a previous paper. This expansion can be cast into a form in which a "reduced potential", temperature and activity dependent, replaces the usual interaction. All contributions are then given by the (connected) "irreducible" diagrams only.

1. Introduction

Dans la première partie de ce travail [1]) (qui sera désignée par I dans la suite), nous avons établi un développement du potentiel de Gibbs présentant de grandes analogies avec le développement établi par Goldstone [2]) pour l'énergie de l'état fondamental. Nous allons ici étudier les relations de ce développement avec le développement habituel de la mécanique statistique en puissances de l'activité

$$z = e^{\alpha}.$$

Pour cela, nous commencerons, au paragraphe 2, par établir au moyen des méthodes de la seconde quantification, le développement général du potenti l de Gibbs en puissances de l'activité. L'utilisation de la seconde quantification implique au départ le choix d'un „état de référence". Dans I, cet état était constitué par le système de particules sans interactions à la température considérée, et ce choix avait conduit à un développement ayant une dépendance plus compliquée par rapport à l'activité. Pour obtenir le développement en puissances de l'activité, nous prendrons ici comme état de référence l'état du système doublement quantifié ne contenant aucune particule. Nous serons conduits à représenter les termes du développement par des diagrammes différents des diagrammes vide-vide utilisés dans I. Les nouveaux diagrammes présentent l'aspect „d'échelles généralisées", et il est commode de les dessiner sur un cylindre pour tenir compte de l'invariance

cyclique de la trace. Chacun de ces diagrammes décrit certaines interactions d'un nombre bien déterminé de particules, et nous montrerons que la somme des contributions associées aux diagrammes connexes à N particules correspond à une constellation („cluster") de N particules de la mécanique statistique classique. Ce résultat équivalent à celui de Ward et Montroll [3]) précise le lien du développement obtenu avec les développements de Ursell, Yvon et Mayer [4]). Il faut noter que la plus grande partie des considérations développées ici ne peut être appliquée de façon naturelle qu'aux systèmes où les interactions conservent les particules.

Il est aussi possible, comme on le verra au paragraphe 3, de retrouver, à partir de ce développement, le développement établi dans I. Pour cela, il suffit d'effectuer la sommation partielle des diagrammes contenant des „spires", c'est-à-dire des lignes effectuant plus d'un tour autour du cylindre supportant le diagramme. L'effet de cette sommation partielle est de remplacer les propagateurs des particules dans le vide qui figurent dans le développement du paragraphe 2 par les propagateurs des particules au sein du système de particules indépendantes qui figurent dans le développement établi dans I.

La sommation partielle des „spires" joue un rôle très important dans l'étude du cas limite de la température nulle. Ce passage à la limite est beaucoup plus délicat à effectuer directement sur le développement en puissances de l'activité. Au contraire, le développement établi dans I conduit immédiatement lorsqu'on fait tendre la température vers zéro au développement de Goldstone de l'énergie de l'état fondamental.

Il est également important, dans le calcul de l'état fondamental, d'introduire un champ self-consistant. Bien que ceci ne soit pas l'usage courant, on peut aussi introduire un tel champ dans le calcul de la fonction de partition. Ce champ, que nous avons introduit systématiquement ici, doit conduire à de meilleures approximations, surtout à basse température. Il présente la particularité de dépendre de la température et de l'activité (paragraphes 3, 4).

2. Le Développement du Potentiel de Gibbs en Fonction de l'Activité

2.1. LE DÉVELOPPEMENT DE LA GRANDE FONCTION DE PARTITION

Pour simplifier l'écriture, nous nous limiterons à des systèmes composés de particules toutes identiques, bosons ou fermions. Les deux cas peuvent être traités d'une manière tout à fait parallèle en introduisant le symbole

$$\epsilon = \begin{cases} +1 & \text{pour les bosons,} \\ -1 & \text{pour les fermions.} \end{cases}$$

Nous écrirons l'interaction sous la forme

$$H-H_0 = V = \tfrac{1}{4}\sum_{rsmn}\langle rs|v|mn\rangle a_r^+ a_s^+ a_n a_m - \sum_{rm}\langle r|v|m\rangle a_r^+ a_m, \qquad (1)$$

où les a_m sont des opérateurs satisfaisant aux relations de commutation

$$a_m a_n - \epsilon a_n a_m = 0, \qquad a_m a_n^+ - \epsilon a_n^+ a_m = \delta_{mn},$$

et les $\langle rs|v|mn\rangle$ sont les éléments de matrice de l'interaction de deux particules pris entre les fonctions de base symétrisées ou antisymétrisées de deux particules:

$$\langle rs|v|mn\rangle = \int \varphi_r^*(1)\varphi_s^*(2)v(1,2)(1+\epsilon P_{12})\varphi_m(1)\varphi_n(2)\mathrm{d}\tau_1\mathrm{d}\tau_2; \qquad (2)$$

enfin, les $\langle r|v|m\rangle$ sont les éléments de matrice du potentiel moyen introduit dans H_0 pour la définition des états $\varphi_m, \varphi_n, \ldots$ de particules indépendantes. Dans (2), P_{12} est l'opérateur de permutation des particules 1 et 2.

Nous partirons à nouveau du développement de la grande fonction de partition en puissances de l'interaction:

$$Z(\alpha,\beta) = \sum_{p=0}^{\infty}(-)^p \int_{\beta>u_1>u_2\ldots>u_p>0} \mathrm{d}u_1\mathrm{d}u_2\ldots\mathrm{d}u_p \,\mathrm{Tr}\,\{\mathrm{e}^{\alpha N-\beta H_0}V(u_1)\ldots V(u_p)\}, \qquad (3)$$

où

$$V(u) = \mathrm{e}^{uH_0}V\mathrm{e}^{-uH_0}. \qquad (4)$$

Pour calculer la trace qui figure dans (3) nous ferons maintenant apparaître explicitement le nombre de particules figurant dans chacun des états pour lesquels on doit calculer l'élément diagonal du produit des interactions $V(u)$. Plus précisément, nous utiliserons la relation †

$$\mathrm{Tr}\,A = \sum_N \frac{1}{N!}\sum_{m_1\ldots m_N}\langle 0|a_{m_N}\ldots a_{m_1}Aa_{m_1}^+\ldots a_{m_N}^+|0\rangle, \qquad (5)$$

où $|0\rangle$ représente le *vide habituel*, c'est-à-dire l'absence de toute particule. Les sommations sur les N indices $m_1 \ldots m_N$ sont faites indépendamment les unes des autres et étendues à toutes les valeurs. Si les indices $m_1 \ldots m_N$ sont tous différents, cette méthode de sommation conduit à répéter $N!$ fois le même terme, car une permutation des opérateurs ne change pas l'état obtenu. Cette répétition est corrigée par le facteur $1/N!$. Dans le cas des bosons, certains des indices $m_1 \ldots m_N$ peuvent être égaux, et le nombre de répétitions du même terme devient inférieur à $N!$. Par exemple, dans le cas extrême où tous les indices sont égaux, il n'y a plus aucune répétition de terme, mais la relation (5) reste cependant exacte car

$$\frac{1}{\sqrt{N!}}a_m^{+N}|0\rangle$$

† Nous utiliserons la lettre N indifféremment pour désigner l'opérateur nombre de particules et le nombre de particules présentes dans un état déterminé.

est la fonction d'onde normalisée décrivant la présence de N bosons dans l'état m. On vérifie facilement que (5) reste valable lorsque certains seulement des indices sont égaux.

2.2. ÉCHELLES GÉNÉRALISÉES ET DIAGRAMMES CYLINDRIQUES

L'application de la relation (5) au développement (3) conduit à calculer la valeur probable pour le vide, de produits d'opérateurs de création et d'annihilation. Pour cela nous utiliserons le théorème de Wick habituel [5]) avec les contractions

$$a_m^{\bullet} a_n^{+\bullet} = \langle 0|a_m a_n{}^{+}|0\rangle = \delta_{mn},$$
$$a_m^{+\bullet} a_n^{\bullet} = \langle 0|a_m{}^{+} a_n|0\rangle = 0.$$

Le résultat s'exprime alors comme la somme de tous les systèmes complets de contractions entre les opérateurs figurant dans les $V(u)$ et les opérateurs introduits par la relation (5). Un tel système de contractions est commodément représenté par un diagramme de Feynman composé de N lignes de particules entièrement dirigées dans le sens des temps croissants, partant de l'instant 0 avec les états $m_1, m_2, \ldots m_A$ *dans l'ordre* et arrivant à l'instant β avec les mêmes états. La fig. 1 donne un exemple d'un diagramme de ce

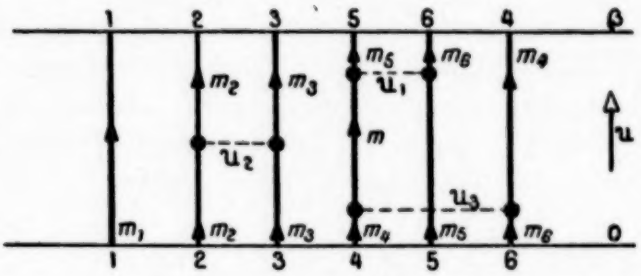

Fig. 1. Un diagramme en échelle généralisée.

genre. Pour la commodité du dessin, nous avons modifié l'ordre des états à l'instant β de telle façon que les lignes de particules ne se croisent pas et puissent être dessinées parallèles. La permutation P des états à l'instant β nécessaire pour cela est indiquée par les chiffres 1, 2, 3, 5, 6, 4. Les interactions sont représentées par des lignes horizontales joignant deux des lignes de particules. Le diagramme peut être décrit comme une *échelle généralisée.*

Il peut être commode également d'imaginer le diagramme *dessiné sur un cylindre* † tel que les instants 0 et β soient représentés par la même génératrice (fig. 2). Les lignes de particules se referment alors sur elles-mêmes en faisant une ou plusieurs fois le tour du cylindre.

Il est essentiel de se rappeler que deux diagrammes en échelle généralisée (fig. 1) que ne diffèrent que par l'ordre dans lequel les lignes de particules

† La représentation sur un tore de Ward et Montroll [3]) est commode seulement pour les diagrammes particuliers qu'ils ont considérés.

sont placées les unes à côté des autres doivent cependant être considérés comme distincts. Ils correspondent en effet à des contractions des opérateurs des $V(u)$ avec des opérateurs introduits par (5) différents.

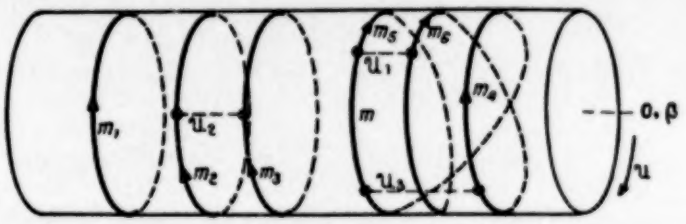

Fig. 2. Le diagramme de la fig. 1 dessiné sur un cylindre.

Désignons comme dans I par E_i l'énergie des particules présentes sur le diagramme entre les instants u_{i+1} et u_i pour $i = 1, 2, \ldots p-1$, et par E_p l'énergie entre les instants u_1 et u_p sur le cercle ou le cylindre des temps. Appelons w_i les intervalles séparant les interactions successives:

$$\begin{aligned} w_i &= u_i - u_{i+1}, \qquad i = 1, 2, \ldots p-1, \\ w_p &= \beta - u_p + u_1. \end{aligned} \tag{6}$$

Le produit des facteurs exponentiels introduits par les $V(u)$ et du facteur $\exp(-\beta H_0)$ figurant dans (3) peut s'écrire sous la forme

$$\exp(-\sum_{i=1}^{p} w_i E_i). \tag{7}$$

En résumé, la contribution au développement (3) de la grande fonction de partition associée à un diagramme s'obtient en faisant le produit des facteurs suivants:

1) *à chaque interaction est associé un élément de matrice*

$$\tfrac{1}{2}\langle rs|v|mn\rangle \quad \text{ou} \quad -\langle r|v|m\rangle;$$

2) *à chaque ligne de particule est associé le propagateur*

$$\exp(-w_m \varepsilon_m), \tag{8}$$

où ε_m est l'énergie de la ligne et w_m sa longueur mesurée sur le cylindre: le produit de tous ces propagateurs est en effet égal à (7);

3) *le facteur*

$$\frac{e^{\alpha N}}{N!}, \tag{9}$$

où N est le nombre de lignes de l'échelle, c'est-à-dire le nombre de particules intervenant pour le diagramme considéré;

4) *le facteur*

$$\epsilon^{N+l}, \tag{10}$$

où l est le nombre de boucles fermées sur le cylindre. Ce facteur résulte, comme

d'habitude, des changements de signe qui se produisent lorsqu'on amène les uns à côté des autres les opérateurs de fermions contractés. A ce signe vient s'ajouter le $(-)^p$ qui figure dans (3).

Le produit de tous ces facteurs doit enfin être intégré sur les temps ordonnés $u_1, \ldots u_p$, et sommé par rapport aux états associés aux lignes du diagramme.

Par exemple, le diagramme des fig. 1 et 2 donne la contribution

$$-\frac{e^{6\alpha}}{6!}\int_{\beta>u_1>u_2>u_3>0} du_1 du_2 du_3 \sum_{m,m_i} e^{-\beta\varepsilon_{m_1}} \tfrac{1}{2}\langle m_2 m_3|v|m_2 m_3\rangle e^{-\beta(\varepsilon_{m_2}+\varepsilon_{m_3})}$$
$$\tfrac{1}{2}\langle m_5 m_6|v|m m_5\rangle \tfrac{1}{2}\langle m m_4|v|m_4 m_6\rangle e^{-\beta(\varepsilon_{m_4}+\varepsilon_{m_5})-(u_1-u_2)\varepsilon_m-(\beta-u_1+u_3)\varepsilon_{m_6}}$$

où le premier facteur correspond à la boucle 1, la fin de la première ligne aux boucles 2 et 3, et la dernière ligne à la boucle 4, 5, 6. On a $p = 3$, $N = 6$, $l = 4$, d'où le signe $-$ pour les bosons aussi bien que les fermions.

Nous avons vu que les sommations sur les états relatifs aux lignes devaient être étendues à toutes les valeurs indépendamment les unes des autres. Dans le cas des fermions, le principe d'exclusion résulte alors du fait que lorsque deux lignes correspondent au même état, le diagramme obtenu en croisant ces lignes donne la même contribution mais avec le signe opposé.

2.3. LE DÉVELOPPEMENT DU POTENTIEL DE GIBBS

Le diagramme le plus général sera formé d'un certain nombre de *parties connexes*. Une partie connexe est ici constituée de la partie du diagramme qu'on peut atteindre en suivant les lignes d'interaction, et les lignes de particules autour du cylindre. Ainsi le diagramme des figures 1 et 2 se compose de trois parties connexes. Désignons par $\Gamma_1, \Gamma_2, \Gamma_3, \ldots \Gamma_i, \ldots$ *l'ensemble des diagrammes connexes*. Le diagramme le plus général sera de la forme

$$\Gamma = n_1\Gamma_1 + n_2\Gamma_2 + \ldots (n_1, n_2, \ldots = 0, 1, 2, \ldots). \tag{11}$$

Désignons par N_i le nombre de particules du diagramme Γ_i, de sorte que pour le diagramme Γ on aura

$$N = n_1N_1 + n_2N_2 + \ldots$$

Désignons par $Z_i(\alpha, \beta)$ *la contribution à* $Z(\alpha, \beta)$ *associée au diagramme* Γ_i suivant les règles données plus haut.

Pour un diagramme déterminé, les temps auxquels se produisent les interactions sont ordonnés d'une manière bien déterminée. Lorsqu'un diagramme est composé de plusieurs parties connexes, on peut former une *famille de diagrammes semblables* [6]) qui ne diffèrent les uns des autres que par la façon dont sont ordonnés les temps relatifs à des parties connexes différentes. Ainsi la figure 3 représente un diagramme semblable à celui de la figure 1. Lorsqu'on considère la somme des contributions provenant de tous les diagrammes d'une famille, seuls les temps relatifs aux interactions d'une

même partie connexe sont ordonnés les uns par rapport aux autres. Il en résulte que la somme de ces contributions est égale au produit des contributions Z_i des différentes parties connexes constituant le diagramme, à un facteur numérique près, cependant, provenant des $N!$ introduits par (9), que nous devons maintenant examiner.

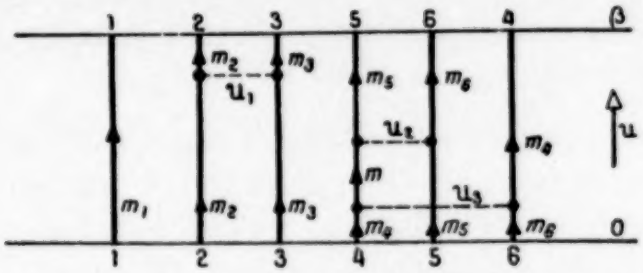

Fig. 3. Un diagramme semblable à celui de la fig. 1.

Nous avons vu que des diagrammes différant seulement par l'ordre des lignes de particules devaient être considérés comme différents. La fig. 4,

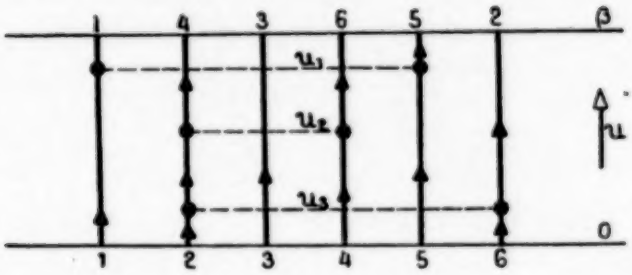

Fig. 4. Un diagramme déduit par permutation de la fig. 1.

par exemple, représente le diagramme déduit par la permutation

$$123456 \rightarrow 315246$$

du diagramme de la fig. 1. Les diagrammes déduits par permutation donnent la même contribution, et il suffit de multiplier la contribution de l'un d'eux par le nombre des diagrammes obtenus à partir d'un diagramme donné. On voit facilement que ce nombre est égal pour le diagramme (11) à

$$\frac{N!}{n_1!n_2!\ldots(N_1!)^{n_1}(N_2!)^{n_2}\ldots}.$$

Le numérateur de ce facteur fait disparaître le $N!$ introduit dans $Z(\alpha, \beta)$ par (9), alors que le dénominateur fait apparaître les $N!$ présents dans les contributions $Z_i(\alpha, \beta)$ des composantes connexes Γ_i de Γ. La somme des contributions provenant des diagrammes semblables à et déduits par permutation de Γ prend alors la forme

$$\frac{Z_1^{n_1}Z_2^{n_2}\ldots}{n_1!n_2!\ldots}.$$

En faisant la sommation sur les valeurs des exposants n_i, on obtient enfin la formule exponentielle que nous écrirons en introduisant le *potentiel de Gibbs* sous la forme

$$A(\alpha, \beta) = -\frac{1}{\beta} \sum_i Z_i(\alpha, \beta), \tag{12}$$

où, rappelons-le, la *sommation doit être étendue à toutes les contributions Z_i associées aux diagrammes connexes.*

2.4. LIEN AVEC LE FORMALISME DE URSELL, YVON ET MAYER

Le développement (12) est l'analogue du développement de Ursell, Yvon et Mayer [4]). Pour préciser l'analogie, nous allons introduire explicitement le nombre des particules des diagrammes. Nous désignerons par

$$Z_C^{(N)} = \sum_{N_i=N} Z_i \tag{13}$$

la somme des contributions à Z associées aux diagrammes connexes à N particules. Ces quantités expriment l'effet résultant de la collision simultanée de N particules. Avec cette définition, nous pouvons écrire (12) sous la forme

$$\boxed{A(\alpha, \beta) = -\frac{1}{\beta} \sum_{N=1}^{\infty} Z_C^{(N)}.} \tag{14}$$

La quantité $Z_C^{(N)}$ étant proportionnelle à $e^{N\alpha}$, on voit que (14) est le *développement du potentiel de Gibbs en puissances de l'activité* $z = e^{\alpha}$.

Désignons par

$$\boxed{Z^{(N)} = e^{\alpha N} \operatorname{Tr} \{e^{-\beta H}\}_N} \tag{15}$$

la somme des contributions à Z associées à tous les diagrammes à N particules (connexes ou non). Dans (15), N rappelle que la trace doit être calculée sur l'ensemble des états à N particules seulement.

L'expression de $Z^{(N)}$ en fonction de $Z_C^{(N)}$ s'obtient aisément en remarquant que $Z^{(N)}$ est le coefficient de $e^{\alpha N}$ dans

$$Z = \exp \{\sum_N Z_C^{(N)}\}. \tag{16}$$

D'où

$$\boxed{Z^{(N)} = \sum^{(N)} \frac{[Z_C^{(N')}]^{n'} [Z_C^{(N'')}]^{n''} \dots}{n'! n''! \dots},} \tag{17}$$

où la sommation $\sum^{(N)}$ est étendue à l'ensemble des valeurs de $n', n'', \dots$ telles que

$$\boxed{n'N' + n''N'' + \dots = N.} \tag{18}$$

Les premières relations (17) s'écrivent sous la forme bien connue

$$\begin{aligned} Z^{(1)} &= Z_C^{(1)}, \\ Z^{(2)} &= Z_C^{(2)} + \tfrac{1}{2}[Z_C^{(1)}]^2, \\ Z^{(3)} &= Z_C^{(3)} + Z_C^{(1)} Z_C^{(2)} + \tfrac{1}{6}[Z_C^{(1)}]^3, \\ &\text{etc.} \ldots . \end{aligned} \tag{19}$$

Ces relations permettent de déterminer de proche en proche les $Z_C^{(N)}$ à partir des $Z^{(N)}$, qu'on peut, tout au moins en principe, calculer à l'aide des expressions (15) pour les petites valeurs de N. Ainsi l'inversion des relations (19) donne

$$\begin{aligned} Z_C^{(1)} &= Z^{(1)}, \\ Z_C^{(2)} &= Z^{(2)} - \tfrac{1}{2}[Z^{(1)}]^2, \\ Z_C^{(3)} &= Z^{(3)} - Z^{(1)} Z^{(2)} + \tfrac{1}{3}[Z^{(1)}]^3, \\ &\text{etc.} \ldots . \end{aligned} \tag{20}$$

2.5. LA LIMITE CLASSIQUE

Pour être complets, nous allons maintenant rappeler et préciser le lien entre les développements qui précèdent et la théorie classique de l'équation d'état. Pour cela il est intéressant de considérer la limite pour $\hbar \to 0$ des quantités que nous avons introduites.

Pour une fonction $A(\mathbf{r}_1, \ldots \mathbf{r}_N, \mathbf{p}_1, \ldots, \mathbf{p}_N)$ des positions et des quantités de mouvement de N particules on a

$$\lim_{\hbar \to 0} \operatorname{Tr} A(\mathbf{r}_1, \ldots \mathbf{r}_N, \mathbf{p}_1, \ldots \mathbf{p}_N) = \frac{1}{h^{3N} N!} \int \mathrm{d}^3 r_1 \ldots \mathrm{d}^3 r_N \mathrm{d}^3 p_1 \ldots \mathrm{d}^3 p_N A(\mathbf{r}_1, \ldots \mathbf{r}_N, \mathbf{p}_1, \ldots \mathbf{p}_N), \tag{21}$$

où $h = 2\pi\hbar$. Au premier membre de cette relation, la trace est calculée sur l'ensemble des fonctions d'onde soit symétriques, soit antisymétriques, la différence entre bosons et fermions disparaissant naturellement à la limite $\hbar \to 0$. Au second membre de (21), les $\mathbf{r}_i$ et $\mathbf{p}_i$ sont des variables classiques commutant entre elles.

En appliquant (21) aux quantités (15) où l'hamiltonien peut être écrit

$$H = \sum_{i=1}^{N} \frac{\mathbf{p}_i^2}{2m} + \tfrac{1}{2} \sum_{i,j=1}^{N} v(\mathbf{r}_i - \mathbf{r}_j),$$

on obtient

$$\lim_{\hbar \to 0} Z^{(N)} = \frac{\mathrm{e}^{\alpha N}}{N!} \int \mathrm{d}^3 r_1 \ldots \mathrm{d}^3 r_N W_N(\mathbf{r}_1, \ldots, \mathbf{r}_N), \tag{22}$$

où on a posé

$$W_N(\mathbf{r}_1, \ldots, \mathbf{r}_N) = \frac{1}{\lambda^{3N}} \exp\Big[-\tfrac{1}{2}\beta \sum_{i,j=1}^{N} v(\mathbf{r}_i - \mathbf{r}_j)\Big], \tag{23}$$

avec

$$\frac{1}{\lambda} = \frac{1}{h}\int_{-\infty}^{+\infty} \mathrm{d}p\, \mathrm{e}^{-\beta p^2/2m}$$

c'est-à-dire

$$\lambda = \left(\frac{2\pi\hbar^2\beta}{m}\right)^{\frac{1}{2}}. \tag{24}$$

A partir des fonctions (23) on définit les fonctions $U_N(\mathbf{r}_1, \ldots \mathbf{r}_N)$ par les relations classiques [4])

$$\begin{gathered} W_N(\mathbf{r}_1, \ldots \mathbf{r}_N) = \sum U_{N'} U_{N''} \ldots, \\ N'+N''+ \ldots = N, \end{gathered} \tag{25}$$

où la sommation est étendue à toutes les façons de répartir les N particules en groupes de N', N'', ... particules. Si la partition de N comprend n' groupes de N' particules, n'' groupes de N'' particules, etc. ... les N particules peuvent être réparties dans ces groupes de

$$\frac{N!}{n'!\, n''! \ldots (N'!)^{n'} (N''!)^{n''} \ldots}$$

façons différentes qui donneront des contributions égales dans les intégrales (22). On voit alors que les relations (17) correspondent exactement aux relations habituelles (25), et qu'on a

$$\lim_{\hbar \to 0} Z_{\mathrm{C}}^{(N)} = \frac{\mathrm{e}^{\alpha N}}{N!} \int \mathrm{d}^3 r_1 \ldots \mathrm{d}^3 r_N U_N(\mathbf{r}_1, \ldots \mathbf{r}_N). \tag{26}$$

On démontre dans la théorie classique que les fonctions $U_N(\mathbf{r}_1, \ldots \mathbf{r}_N)$ possèdent la propriété essentielle de devenir nulles lorsque les N particules peuvent être divisées en deux ou plusieurs groupes n'interagissant pas l'un avec l'autre. Il en résulte que dans l'intégrale (26), les N points doivent rester à des distances du même ordre que la portée des interactions, les uns des autres. Ceci entraîne que les intégrales (26) sont proportionnelles au volume Ω du récipient, pour N fixe, lorsque $\Omega \to +\infty$.

La propriété correspondante pour les $Z_{\mathrm{C}}^{(N)}$ qui apparaissent en mécanique statistique quantique résulte du fait que ces quantités sont des sommes de contributions relatives à des *diagrammes connexes*. La contribution associée à un diagramme connexe s'exprime, en effet, dans la représentation $\mathbf{r}$ par une intégrale multiple étendue au volume du récipient, où les points figurant dans la fonction à intégrer sont reliés les uns aux autres soit par des termes de potentiel $v(\mathbf{r}_i - \mathbf{r}_j)$, soit par des propagateurs

$$\langle \mathbf{r}' | \mathrm{e}^{-w\mathbf{p}^2/2m} | \mathbf{r}'' \rangle = \left(\frac{m}{2\pi w\hbar^2}\right)^{\frac{3}{2}} \mathrm{e}^{-m(\mathbf{r}-\mathbf{r}'')^2/2w\hbar^2} \tag{27}$$

où w, la longueur de la ligne, varie entre 0 et $N\beta$. Ces propagateurs tendent

rapidement vers zéro lorsque la distance $|\mathbf{r}'-\mathbf{r}''|$ dépasse beaucoup $N\lambda$ où λ est la longueur d'onde de de Broglie correspondant à la température $1/k\beta$, définie par (24).

Il résulte de ces propriétés que les $Z_C^{(N)}$ sont proportionnels au volume, et qu'on peut, comme dans le cas classique, définir des coefficients b_N *indépendants du volume* dans le cas limite $\Omega \to +\infty$, en posant

$$Z_C^{(N)} = \Omega e^{\alpha N} b_N. \tag{28}$$

D'où

$$A(\alpha, \beta) = -\frac{\Omega}{\beta} \sum_{N=1}^{\infty} e^{\alpha N} b_N,$$

et

$$\lim_{h \to 0} b_N = \frac{1}{\Omega N!} \int d^3 r_1 \ldots d^3 r_N U_N(\mathbf{r}_1, \ldots, \mathbf{r}_N).$$

3. L'élimination des Spires et la Seconde Forme du Développement du Potentiel de Gibbs

3.1. L'ÉLIMINATION DES SPIRES

Nous appellerons spire:

1) *toute ligne de particule fermée sur elle-même, sur laquelle n'arrive aucune interaction* (fig. 5),

2) *tout arc de ligne de particule dont la longueur entre deux interactions consécutives est supérieure à β, c'est-à-dire à un tour autour du cylindre* (fig. 6).

Nous allons commencer par calculer la contribution au potentiel de Gibbs des spires sans interaction représentées sur la fig. 5. La contribution d'une

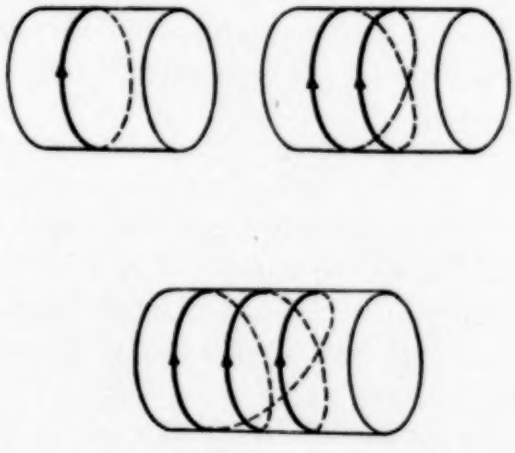

Fig. 5. Spires sans interactions.

spire entourant N fois le cylindre est d'après les règles du paragraphe précédent donnée par

$$\frac{\epsilon^{N+1}}{N!} \sum_m e^{N(\alpha-\beta\epsilon_m)}. \tag{29}$$

Une spire de ce genre peut être obtenue à partir d'un diagramme en échelle généralisée comportant N lignes, en fermant celui-ci de $(N-1)!$ façons différentes. Suivons en effet la spire dans le sens des flèches. Ceci revient à parcourir les N lignes de l'échelle dans un ordre déterminé. Les lignes jouant toutes le même rôle, puisque la spire est fermée sur elle-même, le choix de la première ligne n'est pas significatif. Ce choix fait, on peut choisir

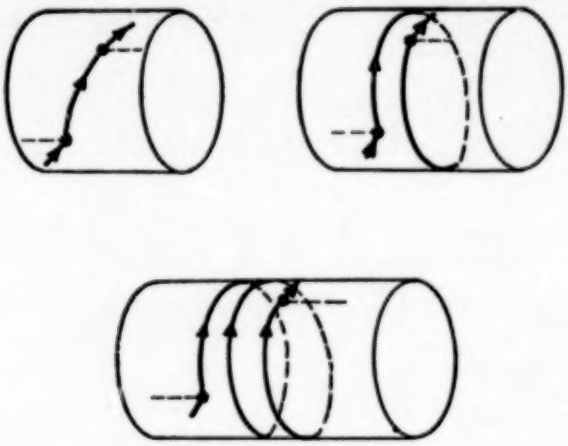

Fig. 6. L'insertion de spires dans un diagramme comprenant des interactions.

la deuxième ligne parmi les $N-1$ lignes restantes, puis la troisième parmi les $N-2$ restantes, et ainsi de suite. Ces $(N-1)!$ façons différentes de former une spire à partir d'une échelle à N lignes correspondent à des diagrammes différents, mais donnant la même contribution. Pour les inclure, il suffit de multiplier les expressions (29) par $(N-1)!$. La sommation des expressions ainsi obtenues pour $N = 1, 2, 3, \ldots$ donne pour la contribution de tous les diagrammes connexes constitués d'une spire fermée sans interaction

$$A_0 = \frac{\epsilon}{\beta} \sum_m \log\,(1-\epsilon e^{\alpha-\beta\epsilon_m}). \tag{30}$$

Nous retrouvons ainsi, naturellement, l'expression bien connue du potentiel de Gibbs pour un gaz sans interaction.

Considérons maintenant un diagramme connexe contenant des interactions. S'il contient des spires, il peut être *réduit* par remplacement des spires par des arcs de longueur inférieure ou égale à β. Nous dirons qu'un diagramme qui ne contient pas de spire est *irréductible*. Il est clair que l'ensemble des diagrammes connexes contenant des interactions peut être obtenu d'une manière biunivoque à partir des diagrammes irréductibles connexes contenant des interactions en remplaçant de toutes les manières possibles chacun des arcs du diagramme, par des spires de longueur

$$w+\beta, w+2\beta, \ldots, w+k\beta, \ldots$$

où w est la longueur de l'arc remplacé.

Cherchons quel est l'effet de l'insertion d'une spire de longueur $w+k\beta$ dans un diagramme irréductible à N particules. La nouvelle échelle aura $N+k$ lignes, et la contribution du nouveau diagramme s'obtiendra en multipliant la contribution du diagramme irréductible par le facteur

$$\frac{\epsilon^k N!}{(N+k)!} e^{k(\alpha-\beta\varepsilon_m)}$$

où ε_m est l'énergie de l'arc remplacé. Dans le nouveau diagramme en échelle, les k nouvelles lignes de la spire peuvent être placées de

$$\frac{(N+k)!}{N!\,k!}$$

façons différentes parmi les N anciennes lignes. D'autre part, la spire peut être formée par $k!$ modes de fermeture distincts de l'échelle. On peut, en effet, en suivant la boucle dans le sens des flèches depuis son point de départ, (qui, contrairement au cas des spires sans interactions, est maintenant bien défini) choisir pour faire le premier tour une quelconque des k lignes de l'échelle, puis, pour faire le second tour, une quelconque des $k-1$ lignes restantes, et ainsi de suite. Le produit de tous ces facteurs élimine toutes les factorielles, et on trouve en sommant pour les valeurs de k, le facteur correctif

$$\sum_{k=0}^{\infty} \epsilon^k e^{k(\alpha-\beta\varepsilon_m)} = \frac{1}{1-\epsilon e^{\alpha-\beta\varepsilon_m}} = f_m^+. \tag{31}$$

Nous voyons ainsi que le potentiel de Gibbs est la somme du potentiel A_0 du système sans interactions donné par (30) *et des contributions associées aux diagrammes connexes „irréductibles", c'est-à-dire sans spires, calculées selon les règles du paragraphe* 2, *mais en remplacant les propagateurs* (8) *par les propagateurs*

$$e^{-w_m\varepsilon_m} f_m^+. \tag{32}$$

3.2. IDENTITÉ DE LA SECONDE FORME DU DÉVELOPPEMENT AVEC (I,36).

Cette forme du développement de A est *exactement identique à celle qui a été établie dans I*. Pour le voir, on commencera par remarquer que *tout diagramme irréductible sur le cylindre peut être représenté par un diagramme vide-vide, sur un plan, et qu'inversement, à tout diagramme vide-vide correspond un diagramme irréductible sur le cylindre défini à une permutation près des lignes de l'échelle généralisée* (comme sur les figs. 1 et 4).

Une ligne d'un diagramme irréductible ne peut, en effet, couper plus d'une fois † la génératrice origine du cylindre correspondant aux temps

† Une ligne coupant plus d'une fois la génératrice origine ne pourrait pas être représentée sans ambiguïté sur un diagramme vide-vide plan.

0 et β. La correspondance entre les deux types de diagrammes est alors établie en représentant les lignes qui ne coupent pas cette génératrice par des lignes montantes sur le diagramme plan, et celles qui la coupent par des lignes descendantes (fig. 7).

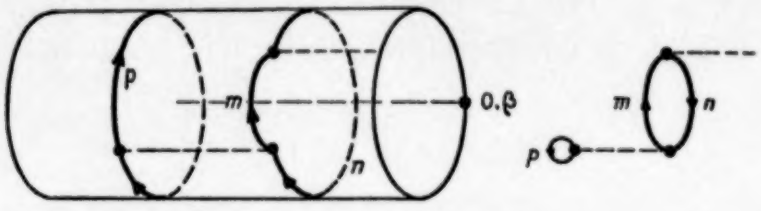

Fig. 7. La correspondance entre les diagrammes irréductibles sur le cylindre et les diagrammes vide-vide du plan.

Des diagrammes déduits par permutation tels que ceux des figs. 1 et 4 donnent le même diagramme dans le plan. La perte de cette distinction est cependant sans inconvénient car pour les diagrammes connexes irréductibles qui seuls nous intéressent ici, il existe toujours exactement $N!$ diagrammes déduits par permutations les uns des autres. On peut donc négliger la distinction entre ces diagrammes à condition de *supprimer le facteur* $1/N!$ *présent dans* (9). Lorsqu'on néglige la distinction entre les diagrammes déduits par permutation, la correspondance entre les diagrammes cylindriques irréductibles et les diagrammes vide-vide plans que nous avons définie devient biunivoque.

Considérons maintenant une ligne d'un diagramme cylindrique irréductible ayant une longueur w_m et coupant la génératrice origine. On peut lui associer le facteur

$$e^{\alpha - w_m \epsilon_m} f_m^+ \tag{33}$$

si on fractionne l'exponentielle présente dans (9) en associant un facteur e^α à chacune des lignes coupant la génératrice origine. La ligne descendante correspondante du diagramme vide-vide plan a pour longueur

$$w'_m = \beta - w_m . \tag{34}$$

Il en résulte qu'on peut mettre les facteurs (33) sous la forme

$$e^{w'_m \epsilon_m} f_m^- \tag{35}$$

où les quantités

$$f_m^- = e^{\alpha - \beta\epsilon_m} f_m^+ = \frac{1}{e^{\beta\epsilon_m - \alpha} + \varepsilon} \tag{36}$$

sont les *facteurs statistiques qui ont été associés aux lignes de trous dans I*. On notera que dans (35), l'énergie associée à la ligne de trou est bien $-\varepsilon_m$ comme dans I.

Lorsque la longueur w_m d'une ligne d'un diagramme irréductible atteint la

valeur maximum possible β, la ligne de trou correspondante a une longueur nulle; c'est une *particule passive* [2]) (voir, par exemple, la ligne p sur la figure 7).

Le nombre N de particules du diagramme cylindrique (qui figure en particulier dans (10) dans le cas des fermions) est maintenant égal au nombre h de lignes de trous du diagramme vide-vide plan.

Les transformations qui viennent d'être effectuées aboutissent au développement (I, 27). Pour obtenir la forme (I, 36) du développement du potentiel de Gibbs il ne reste plus qu'à effectuer les intégrations par rapport aux temps d'interaction $u_1, u_2, \ldots$. Ceci se fait exactement comme dans I.

3.3. L'INTRODUCTION D'UN „POTENTIEL ATTÉNUÉ" [7])

Jusqu'ici, nous avons associé les facteurs (31) résultant de l'élimination des spires aux propagateurs relatifs aux différentes lignes des diagrammes. On peut, au contraire, associer ces facteurs aux interactions. On voit alors immédiatement que le *potentiel de Gibbs est la somme du potentiel A_0 du système sans interactions et des contributions associées aux diagrammes connexes „irréductibles" calculées selon les règles du paragraphe 2, mais en remplacant partout les éléments de matrice du potentiel par les éléments de matrice d'un „potentiel atténué" $\mathscr{V}$ défini par*

$$\boxed{\begin{aligned}\langle rs|\mathscr{V}|mn\rangle &= (f_r^+ f_s^+ f_m^+ f_n^+)^{\frac{1}{2}}\langle rs|v|mn\rangle,\\ \langle r|\mathscr{V}|m\rangle &= (f_r^+ f_m^+)^{\frac{1}{2}}\langle r|v|m\rangle.\end{aligned}} \tag{37}$$

En désignant par $\mathscr{Z}^{(N)}_{\text{C.I.}}$ la somme des contributions des diagrammes connexes irréductibles à N particules calculées pour le potentiel atténué, nous pouvons écrire le potentiel de Gibbs sous la forme

$$A(\alpha, \beta) = A_0(\alpha, \beta) - \frac{1}{\beta}\sum_{N=1}^{\infty}\mathscr{Z}^{(N)}_{\text{C.I.}} \tag{38}$$

Le terme $\mathscr{Z}^{(N)}_{\text{C.I.}}$ de ce développement contient le facteur $e^{N\alpha}$, mais il dépend aussi de α par l'intermédiaire des facteurs statistiques f_m^+.

On peut définir des quantités semblables à (15):

$$\mathscr{Z}^{(N)} = e^{\alpha N}\,\mathrm{Tr}\,\{e^{-\beta\mathscr{H}}\}_N \tag{39}$$

où

$$\mathscr{H} = H_0 + \tfrac{1}{4}\sum_{rsmn}\langle rs|\mathscr{V}|mn\rangle a_r^+ a_s^+ a_n a_m - \sum_{rm}\langle r|\mathscr{V}|m\rangle a_r^+ a_m \tag{40}$$

est une sorte „d'hamiltonien atténué", mais il ne paraît pas facile de déduire d'une manière générale valable quel que soit N les $\mathscr{Z}^{(N)}_{\text{C.I.}}$ des $\mathscr{Z}^{(N)}$. Les relations (20) permettent seulement de calculer à partir des $\mathscr{Z}^{(N)}$ les quantités $\mathscr{Z}_{\text{C}}{}^{(N)}$, sommes des contributions des diagrammes à N particules connexes irréductibles ou non. Pour obtenir les $\mathscr{Z}^{(N)}_{\text{C.I.}}$, il faut encore retrancher des

$\mathscr{Z}_C^{(N)}$ les contributions des diagrammes contenant des spires. Par exemple, la figure 8 représente un diagramme qui figure dans $\mathscr{Z}_C^{(3)}$ mais pas dans $\mathscr{Z}_{C.I.}^{(3)}$ car il contient une spire désignée par m.

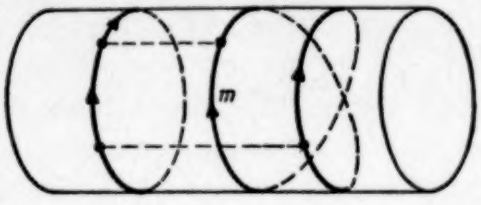

Fig. 8. Un diagramme connexe à 3 particules contenant une spire.

3.4. LES CONDITIONS DE SELF-CONSISTANCE DE HARTREE-FOCK [8])

Comme dans le cas du calcul de l'état fondamental [2]), le choix le plus simple du potentiel moyen $\langle r|v|m\rangle$ agissant sur les particules indépendantes est celui où ce potentiel compense exactement les interactions du premier ordre des particules avec les particules passives. Ceci conduit aux équations de self-consistance suivantes:

$$\langle r|v|m\rangle = \tfrac{1}{2}\sum_n f_n^-(\langle rn|v|mn\rangle - \langle rn|v|nm\rangle) \qquad (41)$$

qui généralisent les équations de Hartree-Fock. Le potentiel $\langle r|v|m\rangle$ ainsi défini dépend de α et β. Il tend vers zéro lorsque l'activité $z = e^{\alpha}$ tend vers zéro, et vers le champ self-consistant habituel de Hartree-Fock lorsque α et β tendent vers l'infini de telle façon que α/β tende vers l'énergie de Fermi.

La définition simple (41) ne peut naturellement pas être maintenue lorsque l'interaction de deux particules comporte un coeur dur. Il faut alors, comme dans la théorie de Brueckner améliorer le traitement des collisions binaires. Nous examinerons cette question dans un article prochain.

Les auteurs remercient le Professeur J. M. Blatt pour avoir attiré leur attention sur des travaux antérieurs concernant les mêmes problèmes, et Monsieur R. Balian pour d'utiles remarques sur ce travail.

Bibliographie

1) C. Bloch et C. De Dominicis, Nuclear Physics **7** (1958) 459
2) J. Goldstone, Proc. Roy. Soc. A **239** (1957) 267
3) E. Montroll et J. Ward, Physics of Fluids **1** (1958) 55
4) H. Ursell, Proc. Camb. Phil. Soc. **23** (1927) 685;
J. Yvon, Act. Sc. Ind. **203** (1935);
J. Mayer, J. Chem. Phys. **5** (1937) 67
5) G. Wick, Phys. Rev. **80** (1950) 268
6) C. Bloch, Nuclear Physics **7** (1958) 451
7) Voir aussi M. R. Schafroth, S. T. Butler et J. M. Blatt, Helv. Phys. Acta **30** (1957) 93;
J. M. Blatt et T. Matsubara, Progr. Theor. Phys. **20** (1958) 553
8) K. Husimi, Proc. Phys. Math. Soc. Japan **22** (1940) 264

8.C *Nuclear Physics* **10** (1959) 197—202; © *North-Holland Publishing Co., Amsterdam*
Not to be reproduced by photoprint or microfilm without written permission from the publisher

BOUND STATES IN MESON PAIR THEORY (A POSSIBLE PHYSICAL MODEL OF HYPERONS)

G. GYÖRGYI
Central Research Institute for Physics, Budapest

Received 2 December 1958

Abstract: Bound states in meson pair theory have been investigated in the strong cut-off lattice space approximation of Wentzel under the assumption of a vector coupling. The problem under consideration may serve as a model field theory of the "N$\overline{\text{K}}$" hyperon model suggested several years ago independently by Goldhaber and the author.

1. Introduction

Several years ago a physical model of hyperons was suggested independently by M. Goldhaber [1]) and the author [2]), according to which hyperons are considered to be bound states of nucleons and anti-K-particles ($\overline{\text{K}}$-mesons). Consequences of the model have been discussed by Christy [3]) and Zeldovich [4]). As a virtue of the model it may be mentioned that it provides a graphic physical picture for the phenomenological Gell-Mann scheme of strange particle reactions. Besides this, the model led to the prediction [2]) of the fact [5]), that while nucleons exert attractive forces on $\overline{\text{K}}$-mesons, K-mesons are repelled by them. It may be mentioned also, that even if composite models of the type discussed are not considered as providing an ultimate description of the strange particle phenomena, they may serve as guiding milestones on the way towards a unified matter theory [6,7]).

Until now, no field theory of this model has been attempted, although the importance of such a formulation has been pointed out by Wentzel [8]) as well as Rayski [9]). Wentzel even claimed that such an attempt would fail, necessarily leading to the prediction of non-existing hyperons of positive strangeness [10]). In what follows, we would like to present a field theory of the model on the basis of the following assumption: a four-vector pair coupling will be assumed to describe the interaction of the meson field and the nucleon source ensuring different signs for the interaction operators of K- and $\overline{\text{K}}$-mesons, respectively. (Another argument in favour of the vector type interaction can be found in a paper by Marx [11]).)

2. Bound States, Neglecting Isobaric Spin

The Lagrangian density describing the system consisting of a fixed nucleon source $\rho(\mathbf{r})$ and the meson field χ will be assumed according to the preceding considerations in the following form:

$$\mathscr{L} = -\operatorname{grad}\chi^+ \cdot \operatorname{grad}\chi + \frac{1}{c^2}\dot{\chi}^+\dot{\chi} - \mu^2\chi^+\chi + i\hbar\left(\frac{G}{mc^2}\right)^2\rho(\mathbf{r})(\dot{\chi}^+\chi - \chi^+\dot{\chi}) \quad (1)$$

$$\left(\mu = \frac{mc}{\hbar}\right).$$

The problem will be considered in the strong cut-off lattice space approximation introduced by Wentzel [12]), which, as a consequence of its rough character, cannot be expected to lead to quantitative results; on the other hand, it simplifies the equations to such an extent that an exact solution will be possible. Exact solutions of such a simplified problem can be useful, if, at a later stage, the problem is considered in a less simplified form.

The approximation mentioned consists in the introduction of a lattice space instead of the continuous space of the variable $\mathbf{r}$. If a lattice constant l larger than the K-meson Compton wave length $\mu^{-1} = \hbar/mc$ is assumed, one finds that 1) the first term in the Lagrangian density (1) i.e. the kinetic energy of the mesons can be neglected; 2) as far as the interaction is concerned, only one of the field operators $\chi(\mathbf{r}_s)$ attached to the different lattice points $\mathbf{r}_s$ has an essential role, namely that corresponding to the lattice point occupied by the source particle: $\chi(\mathbf{r}_0)$. Operators $\chi(\mathbf{r}_s)$ belonging to all other lattice points $\mathbf{r}_s$ satisfy free field equations. The part of the Lagrangian relevant from the point of view of the interaction can be written down in terms of the operator $\chi_0 = l^{\frac{1}{2}}\chi(\mathbf{r}_0)$ as follows:

$$L^{(0)} = \frac{1}{c^2}\dot{\chi}_0^+\dot{\chi}_0 - \mu^2\chi_0^+\chi_0 + i\hbar\left(\frac{G}{mc^2}\right)^2\rho_0(\dot{\chi}_0^+\chi_0 - \chi_0^+\dot{\chi}_0). \quad (2)$$

Here the source density $\rho(\mathbf{r}_0)$ has been denoted by ρ_0. Introducing the canonically conjugate field quantity $\pi_0 = c\partial L^{(0)}/\partial\dot{\chi}_0$ the Hamiltonian can be derived in the usual way:

$$H = \pi_0\pi_0^+ + \mu^2\left[1 + \left(\frac{G^2}{\hbar c}\right)^2\frac{\rho_0^2}{\mu^6}\right]\chi_0^+\chi_0 - i\hbar c\left(\frac{G}{mc^2}\right)^2\rho_0(\pi_0\chi_0 - \chi_0^+\pi_0^+). \quad (3)$$

Define now the creation and annihilation operators by the relations

$$\chi_0 = \frac{\hbar}{mc}(\tfrac{1}{2}mc^2)^{\frac{1}{2}}\left[1 + \left(\frac{G^2}{\hbar c}\right)^2\frac{\rho_0^2}{\mu^6}\right]^{-\frac{1}{4}}(a + b^+), \quad (4)$$

$$\pi_0 = i(\tfrac{1}{2}mc^2)^{\frac{1}{2}}\left[1 + \left(\frac{G^2}{\hbar c}\right)^2\frac{\rho_0^2}{\mu^6}\right]^{\frac{1}{4}}(a^+ - b), \quad (5)$$

$$[a, a^+] = [b, b^+] = 1. \quad (6)$$

In terms of the creation and annihilation operators the Hamiltonian assumes the following form, if symmetrized as required by charge conjugation invariance:

$$H = mc^2 \left\{ \left[\left(1 + \left[\frac{G^2}{\hbar c} \right]^2 \frac{\rho_0^2}{\mu^6} \right)^{\frac{1}{2}} + \frac{G^2}{\hbar c} \frac{\rho_0}{\mu^3} \right] (a^+ a + \tfrac{1}{2}) \right. \\ \left. + \left[\left(1 + \left[\frac{G^2}{\hbar c} \right]^2 \frac{\rho_0^2}{\mu^6} \right)^{\frac{1}{2}} - \frac{G^2}{\hbar c} \frac{\rho_0}{\mu^3} \right] (b^+ b + \tfrac{1}{2}) \right\}. \tag{7}$$

The eigenvalues of the operators a^+a, b^+b being non-negative integers, can be interpreted as the numbers N_{K}, $N_{\overline{\mathrm{K}}}$ of the K and $\overline{\mathrm{K}}$-mesons, respectively. The energy eigenvalues for states containing no K-mesons ($N_{\mathrm{K}} = 0$) but $N_{\overline{\mathrm{K}}}$ $\overline{\mathrm{K}}$-mesons are

$$E_{0N_{\overline{\mathrm{K}}}} = mc^2 \left\{ \left[1 + \left(\frac{G^2}{\hbar c} \right)^2 \frac{\rho_0^2}{\mu^6} \right]^{\frac{1}{2}} - \frac{G^2}{\hbar c} \frac{\rho_0}{\mu^3} \right\} N_{\overline{\mathrm{K}}} + E_{00},$$

$$E_{00} = mc^2 \left[1 + \left(\frac{G^2}{\hbar c} \right)^2 \frac{\rho_0^2}{\mu^6} \right]^{\frac{1}{2}}.$$

Taking into account the relation

$$(1+x^2)^{\frac{1}{2}} - x < 1 \qquad (x > 0)$$

it is easy to realize that bound states exist for $\overline{\mathrm{K}}$-mesons ($E_{0N_{\overline{\mathrm{K}}}} - E_{00} < N_{\overline{\mathrm{K}}} mc^2$). On the other hand, no bound states containing K-mesons occur ($E_{N_{\mathrm{K}}0} - E_{00} > N_{\mathrm{K}} mc^2$). If the first excited state ($N_{\mathrm{K}} = 0$, $N_{\overline{\mathrm{K}}} = 1$) is tentatively identified with the Λ-hyperon, the coupling constant can be determined from the relation

$$M_\Lambda - M_{\mathrm{N}} = m \left\{ \left[1 + \left(\frac{G^2}{\hbar c} \right)^2 \frac{\rho_0^2}{\mu^6} \right]^{\frac{1}{2}} - \frac{G^2}{\hbar c} \frac{\rho_0}{\mu^3} \right\}. \tag{9}$$

Using the values $M_\Lambda = 2181$, $M_{\mathrm{N}} = 1838$, $m = 966$ we get

$$\frac{G^2}{\hbar c} \frac{\rho_0}{\mu^3} \approx 1.2.$$

$\rho_0/\mu^3 \approx 1$ is a reasonable assumption, so one obtains for the dimensionless constant of the N-K-pair coupling the value $G^2/\hbar c \approx 1$.

3. Bound States, Assuming an Isobaric Spin Dependent Interaction

In the preceding section, isobaric spin of the interacting particles has been neglected. This rendered possible to determine the exact eigenvalues (8) of the simplified Hamiltonian (7). We proceed now to include isobaric multiplicity of the particles concerned.

The K-mesons will be described by the isospinor field: $\chi = \binom{\chi_1}{\chi_2}$. This operator is acted upon by the Pauli matrices $\vec{\tau}\left[\left(\begin{smallmatrix}0&1\\1&0\end{smallmatrix}\right), \left(\begin{smallmatrix}0&-i\\i&0\end{smallmatrix}\right), \left(\begin{smallmatrix}1&0\\0&-1\end{smallmatrix}\right)\right]$. The two charge states of the nucleon will be described using the state vectors Φ_p, Φ_n. They are transformed in the following way by the isobaric spin operator $\frac{1}{2}\vec{\vartheta}$ of the nucleon:

$$\vec{\vartheta}\,(\vartheta_+ + \vartheta_-,\ i^{-1}(\vartheta_+ - \vartheta_-),\ \vartheta_0)$$

$$\vartheta_+\Phi_p = 0, \quad \vartheta_-\Phi_p = \Phi_n, \quad \vartheta_0\Phi_p = \Phi_p,$$

$$\vartheta_+\Phi_n = \Phi_p, \quad \vartheta_-\Phi_n = 0, \quad \vartheta_0\Phi_n = -\Phi_n.$$

The operator describing the interaction of the nucleon and the meson field will be assumed to be a combination of terms containing isoscalars as well as isovectors characterizing the nucleons and mesons, respectively. In the Wentzel lattice space approximation the Hamilton-operator reduces to

$$\begin{aligned} H = {} & \pi_0\pi_0^+ + \mu^2\chi_0^+[1+S^2+3V^2+2S(S-V)\vec{\vartheta}\cdot\vec{\tau}]\chi_0 \\ & -i\mu[\pi_0(S+V\vec{\vartheta}\cdot\vec{\tau})\,\chi_0 - \chi_0^+(S+V\vec{\vartheta}\cdot\vec{\tau})\,\pi_0^+], \\ & S = \frac{G_S^2}{\hbar c}\frac{\rho_0}{\mu^3}, \qquad V = \frac{G_V^2}{\hbar c}\frac{\rho_0}{\mu^3}. \end{aligned} \tag{10}$$

The constants of the isoscalar and the isovector coupling have been denoted by G_S^2 and G_V^2, respectively. Introduce now again the emission and absorption operators defined by

$$\begin{aligned} \chi_i &= \frac{\hbar}{mc}(\tfrac{1}{2}mc^2)^{\frac{1}{2}}[1+S^2+3V^2]^{-\frac{1}{2}}(a_i+b_i^+), \\ \pi_i &= i(\tfrac{1}{2}mc^2)^{\frac{1}{2}}[1+S^2+3V^2]^{\frac{1}{2}}(a_i^+-b_i). \end{aligned} \tag{11}$$

Their effect may be vizualized through the following scheme:

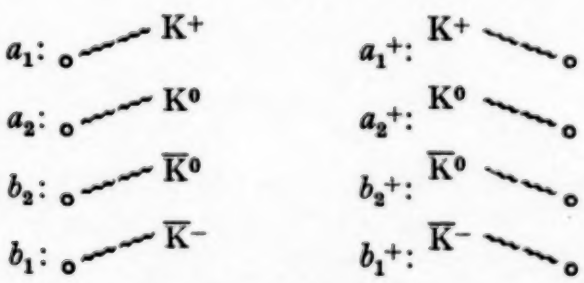

(← direction of time) (12)

The Hamiltonian generally is not diagonal in the system of one-meson states (with the only exception of the special case $G_S^2 = G_V^2$); non-diagonal terms representing pair creation processes → $\overline{K}$+K occur. *Neglecting pair creation* one finds that H possesses one-meson eigenstates with isobaric spin 0 and 1,

two-meson eigenstates with isobaric spin $\frac{1}{2}$, etc. These may be identified with the isobaric multiplets Λ, Σ, Ξ:

$$\Phi_{\Lambda^0} = \frac{1}{\sqrt{2}}(b_1^+\Phi_p + b_2^+\Phi_n);$$

$$\Phi_{\Sigma^+} = b_2^+\Phi_p, \qquad \Phi_{\Sigma^0} = \frac{1}{\sqrt{2}}(b_1^+\Phi_p - b_2^+\Phi_n), \qquad \Phi_{\Sigma^-} = b_1^+\Phi_n; \quad (13)$$

$$\Phi_{\Xi^0} = \frac{1}{\sqrt{3}} b_2^+(b_2^+\Phi_n + b_1^+\Phi_p), \qquad \Phi_{\Xi^-} = \frac{1}{\sqrt{3}} b_1^+(b_2^+\Phi_n + b_1^+\Phi_p).$$

Identifying the corresponding eigenvalues with the excitation energies of the hyperons, the following expressions are obtained for the hyperon masses:

$$M_\Lambda = M_N + m\left\{[1+S^2+3V^2]^{\frac{1}{2}} - S - 3V + 3\frac{(S-V)V}{(1+S^2+3V^2)^{\frac{1}{2}}}\right\},$$

$$M_\Sigma = M_N + m\left\{[1+S^2+3V^2]^{\frac{1}{2}} - S + V - \frac{(S-V)V}{(1+S^2+3V^2)^{\frac{1}{2}}}\right\}, \quad (14)$$

$$M_\Xi = M_N + 2m\left\{[1+S^2+3V^2]^{\frac{1}{2}} - S - 2V + 2\frac{(S-V)V}{(1+S^2+3V^2)^{\frac{1}{2}}}\right\}.$$

Here we have three experimental mass values and two unknown coupling constants. If the latter are chosen to fit M_Λ and M_Σ, the following value is obtained for M_Ξ:

$$M_\Xi = \tfrac{1}{2}(3M_\Lambda + M_\Sigma - 2M_N) = \tfrac{1}{2}(3 \cdot 2182 + 2323 - 2 \cdot 1838) = 2596. \quad (15)$$

This should be compared with the experimental value 2586.

To summarize the results: a model field theory has been formulated, in which hyperons are considered as nucleons with excited kaon fields. It has been shown, that a four-vector interaction yields bound states for $\overline{\text{K}}$-mesons but not for K-mesons, at least in the fixed source strong cut-off approximation used here. It must be mentioned that in the framework of our model, relation (15) is a consequence of charge independence (and the lack of interaction between K-mesons), and it has been found first by Christy [3]) and Zeldovich [4]) in their phenomenological discussions of the model. The author hopes to refine the treatment of the model and to extend its applications.

The major part of this work has been done during the author's stay at the Joint Institute of Nuclear Research, Dubna, USSR. Thanks are due to Prof. N. Bogolubov and Prof. V. Votruba for stimulating conversations. A report on this work was given at the Conference on the Physics of Elementary Particles, Balatonvilágos, Sept. 1958.

References

1) M. Goldhaber, Phys. Rev. **101** (1956) 431
2) G. Györgyi, JETP **32** (1957) 152
3) R. Christy, Proc. of the VIIth Rochester Conference on High Energy Nuclear Physics (1957)
4) Ia. B. Zeldovich, JETP **33** (1957) 829
5) International Conference on Mesons and Recently Discovered Particles, Padova-Venezia (1957)
6) W. Heisenberg, Revs. Mod. Phys. **29** (1957) 269
7) N. N. Bogolubov, private communication
8) G. Wentzel, remarks to the lecture of R. Christy delivered at the VIIth Rochester Conference (1957)
9) J. Rayski, private communication at the Conference on the Physics of Elementary Particles, Balatonvilágos (1957)
10) G. Wentzel, Helv. Phys. Acta **30** (1957) 135
11) G. Marx, Nuclear Physics **9** (1958/59) 337
12) G. Wentzel, Helv. Phys. Acta **13** (1940) 269

10.A *Nuclear Physics* **10** (1959) 203—204; © *North-Holland Publishing Co., Amsterdam*

NEWS ITEMS

CONFERENCE ON NUCLEAR PHYSICS AT OXFORD (8—10 APRIL 1959)

A conference on Nuclear Physics is being organized by the Physical Society at Oxford for 8th to 10th April, 1959. The following have accepted invitations to open various sections of the Conference:

Wednesday, 8th April

Morning	
E. H. S. BURHOP (University College, London)	'Recent Work on Elementary Particles Using the Visual Techniques'
W. GALBRAITH (A.E.R.E., Harwell)	'Recent Work on Elementary Particles Using Electronic Techniques'
A. SALAM (Imperial College, London)	'Theoretical Work on Elementary Particles'
Afternoon	
J. MOFFATT (Clarendon Laboratory, Oxford)	'Experimental Work on Electromagnetic Interactions'
G. E. BROWN (University of Birmingham)	'Theoretical Work on Electromagnetic Interactions'

In the afternoon there will be a parallel session of contributed papers on high energy physics. After dinner Professor H. S. W. Massey will deliver his **Guthrie Lecture** on 'Collisions'.

Thursday, 9th April

Morning	
S. S. HANNA (Clarendon Laboratory, Oxford, on leave from Argonne University)	'Resonance Interactions of Gamma Rays'
J. P. ELLIOTT (A.E.R.E., Harwell)	'Theoretical Basis of Nuclear Structure Calculations'
Afternoon	
R. J. BLIN-STOYLE (Clarendon Laboratory, Oxford)	'Lepton Theory'

Friday, 10th April

Morning	
A. E. TAYLOR (A.E.R.E., Harwell)	'Nucleon-Nucleon Interactions at Medium Energies'
R. J. N. PHILLIPS (A.E.R.E., Harwell)	'Calculation of Nucleon-Nucleon Interactions at medium Energies'
Afternoon	
J. O. NEWTON (A.E.R.E., Harwell)	'Research with Heavy Ions'

In the morning there will be a parallel session of contributed papers on low energy nuclear physics.

In the afternoon there will be a parallel session of contributed papers on the nuclear many-body problem.

Other delegates who would like to contribute should communicate immediately with Professor D. H. Wilkinson, Clarendon Laboratory, Parks Road, Oxford, if possible by the end of January.

CONFERENCE ON NUCLEAR FORCES AND THE FEW-NUCLEON PROBLEM AT UNIVERSITY COLLEGE, LONDON

(8th—11th July, 1959)

The scope of this conference is designed to cover the work at present being carried out on few-nucleon processes (3 or more, but less than about 6—12 nucleons), and the interpretation of the results in terms of two or more body forces between the nucleons.

The conference will open with a survey of the present position of the two-body nucleon-nucleon interaction obtained from consideration both of the meson theory of nuclear forces and of the nucleon-nucleon data below 200 MeV. This part will occupy the first two sessions and will consist of review papers and discussion only.

The remainder of the conference will be concerned with the few-nucleon processes below 200 MeV from both a theoretical and an experimental viewpoint, with emphasis on the extent to which the two-body nucleon-nucleon interaction can explain the experimental results. This main part of the conference will be divided between review papers and short contributions.

Further details concerning the conference can be obtained from Dr. T. C. Griffith, Department of Physics, University College, Gower Street, London, W.C. 1.

4.D *Nuclear Physics* **10** (1959) 205—212; © *North-Holland Publishing Co., Amsterdam*
Not to be reproduced by photoprint or microfilm without written permission from the publisher

K-CAPTURE TO POSITON BRANCHING RATIOS IN THE DECAY OF Ga^{68} †

M. K. RAMASWAMY ††

Dept. of Physics, The Johns Hopkins University, Baltimore, Md.

Received 20 November 1958

Abstract: K-capture to positon branching ratios have been measured in the decay of Ga^{68} using coincidence scintillation spectrometer techniques. The measured values are 1.28 ± 0.12 (to the first excited state) and 0.10 ± 0.02 (to the ground state). Assuming these decays to be pure Gamow-Teller transitions the Fierz interference terms are computed to be $b_{GT} = -0.03 \pm 0.02$ and $+0.03 \pm 0.01$ respectively (the uncertainty in the latter result arising from uncertainty in N_0, the source strength).

The ratio of positons to the first excited state and ground state of Zn^{68} has been found to be $(1.76 \pm 0.22) \times 10^{-2}$.

A search for a possible low-lying 0^+ state in Ga^{68} was made through the decay of Ge^{68} using X-ray-X-ray and X-ray-γ-ray coincidences employing NaI(Tl) crystals. Besides the 9 keV K X-ray, annihilation radiation and the known γ-ray in Ga^{68} whose energy was measured to be 1.067 ± 0.035 MeV, no other γ-ray was observed ($< 8\%$ of $1.07\,\gamma$). The number of positons per $1.07\,\gamma$ quantum was determined as 19.47 ± 2.10 by comparison with Na^{22}.

An upper limit of 0.4 % per decay was set on positon emission by Ge^{68}.

1. Introduction

The decay of Ge^{68} has been studied by Crasemann *et al.*[1]). The spin of Ga^{66} has been measured[2]) to be 0 and presumably the parity is even. The spin of Ga^{68} is most likely to be 1^+ as evidenced from allowed log *ft* values for the positon decays to Zn^{68}. This assignment has been confirmed by a recent direct measurement by Hubbs *et al.*[3]). In this region of nucleon numbers the $p_{\frac{3}{2}}$ and $f_{\frac{5}{2}}$ are close-lying in energy and since no measurements on the low-energy radiations had been reported, it seemed of interest to look for a low-lying 0^+ state in Ga^{68} by analogy with Cu^{62} [4]). If such a state did exist, it was expected that the electron capture transitions from Ge^{68} to both 0^+ and 1^+ states would be allowed and would result in a γ-ray (M1) which could be detected by X-ray—X-ray and/or X-ray—γ-ray coincidences.

This paper is divided into three sections: Section 2 deals with source preparation, section 3 the search for 0^+ state and section 4 the measurements on K/β^+ ratios.

† Supported in part by the U.S. Atomic Energy Commission.
†† On leave from Mysore University, India.

2. Source Preparation

Zinc was electroplated onto a copper backing and was bombarded for 96 μAh with 30 MeV α-particles. The investigations reported here were begun nearly 23 weeks after the bombardment in order to let all the short-lived activities decay. The zinc layer on the copper backing was dissolved in a few of conc. HCl containing Ge carrier. $GeCl_4$ was distilled on to a receiver. GeS_2 was precipitated by saturating with H_2S, then washed and dissolved in NH_4OH. Sources were prepared by evaporating drops of this solution onto a formvar backing and mounted on lucite source holders. Measurements were made on Ge^{68} in equilibrium with Ga^{68}.

3. Search for 0^+ state in Ga^{68}

The region 0 to 30 keV was studied by using thin NaI(Tl) crystals. Fig. 1 (curve *a*) shows a typical spectrum. The resolution for 9 keV K X-ray

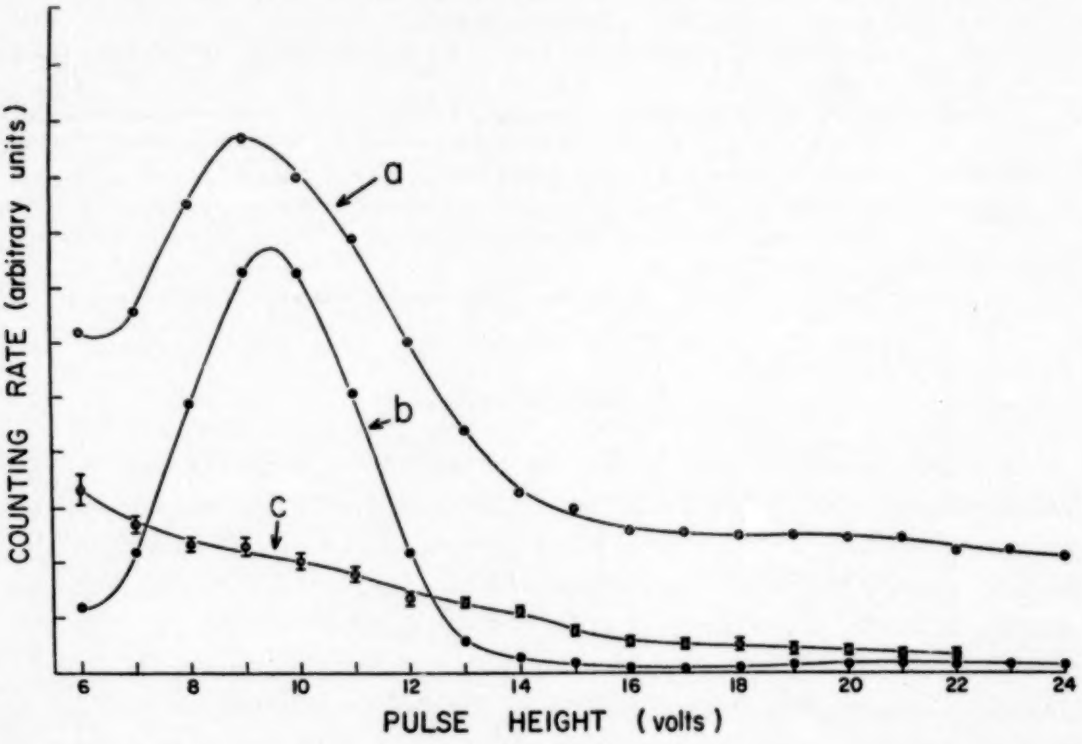

Fig. 1.

Curve a. Low-energy (0—30 keV) γ-spectrum in thin NaI(Tl) crystal taken with $Ge^{68}+Ga^{68}$ source in equilibrium.

Curve b. Pulse height spectrum of the same energy region taken immediately after separating Ga from Ge.

Curve c. Pulse height spectrum (0—30 keV) coincident with K-ray.

varied from 40 to 60 % depending on the crystal. The 5.8 keV X-ray of Fe^{55} served as energy standard. Clearly, there is no indication of any γ-ray. It is also apparent that the contribution of high-energy pulses to the X-ray is

appreciable. In order to obtain a true estimate of the intensity of the observed X-ray, the spectrum was taken with an 0.01″ aluminium absorber. By normalizing this spectrum to the original spectrum beyond the K X-ray region and subtracting this background one obtains a true estimate of the observed X-rays. The region 30 keV to 1.2 MeV was investigated by a $1\frac{1}{2}'' \times 1''$ NaI(Tl) crystal. Besides the annihilation peak and the known γ-ray around 1 MeV, whose energy was measured by a $2'' \times 2'' \times 2''$ NaI crystal to be 1.067 ± 0.035 MeV, no other γ-ray was observed ($< 8\,\%$ of 1.07 γ). Na^{22}(0.511 and 1.28 MeV), Cs^{137}(0.661 MeV) and Co^{60}(1.17 and 1.33 MeV) served as energy calibrations. To study X-ray—X-ray coincidences the Ge^{68} source was sandwiched between two photomultiplier tubes on which thin NaI crystals were mounted, covered with Al foil and sealed with light shield. Fig. 1 (curve *c*) shows the coincidence spectrum (0 to 30 keV). Most of the counts above accidentals are due to crystal scattering of higher energy pulses. This was confirmed by attenuating the X-ray in one of the channels. The 1.07 γ is too weakly converted to give any noticeable coincidences. The X-ray high energy γ-ray (up to 750 keV) coincidences were performed by replacing one of the counters by a $1\frac{1}{2}'' \times 1''$ NaI crystal counter. The results were negative. The region beyond 750 keV was not studied since the $Ge^{68} \rightarrow Ga^{68}$ decay energy can at most be 750 keV [see subsection 4.4].

A more rigorous search for this 0^+ state was attempted by separating Ge from Ga chemically, using successive ether extractions from 6 *N* HCl. Since an appreciable part (40—60 %) of Ge is also extracted into the ether layer [5]) and since the number of extractions could not be done more than twice owing to the fast growth of 68 min Ga^{68} an efficiency of 50 % or less was all that could be attained for Ge. The germanium thus separated was converted into the sulphide and rapidly transferred to the counting system. The region 0 to 30 keV was studied as a function of time with the 20 channel analyzer using a freshly cleaved thin NaI crystal. At the same time a second counter employing $1\frac{1}{2}'' \times 1''$ NaI was set on the photopeak corresponding to the annihilation radiation and its growth in Ga^{68} was studied as a function of time. Fig. 1 (curve *b*) shows the energy spectrum taken immediately after chemical separation. Clearly there is no γ-ray ($< 1\,\%$) besides the K X-ray. From the growth curve of annihilation radiation which corresponded to a 70 minute half-life an upper limit of 0.4 % per decay could be set on the positon emission by Ge^{68} (assuming the positons account for 87 % of the transitions). Horen and Meyerhof [6]) arrived at an upper limit of 0.9 %.

4. K/β^+ Ratios in the Decay of Ga^{68}

4.1. ANALYSIS OF THE METHOD

The decay scheme for Ga^{68} as given by Crasemann *et al.*[1]) is shown schematically in fig. 2. Since our measurements were made on Ga^{68} in equilibrium

with Ge^{68} the numbers of these two nuclei decaying per unit time are equal. If $f_{\beta^+}^1$ and f_ϵ^1 denote the fraction of positons and electron-captures to first

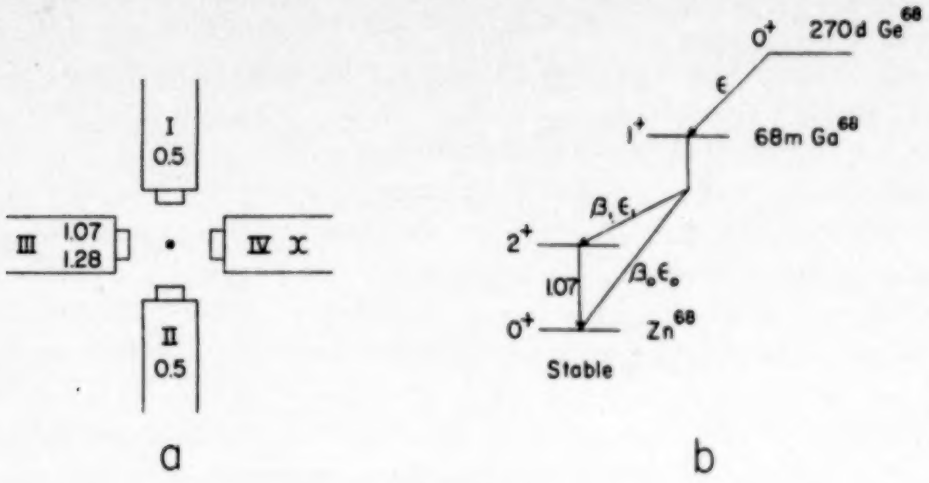

Fig. 2.

a) Schematic of experimental set up for K/β^+ measurements.
b) Ga^{68} decay scheme as given by Crasemann *et al.* [1]).

excited state and $f_{\beta^+}^0$ and f_ϵ^0 the corresponding quantities to 0^+ ground state then we have †

$$f_{\beta^+}^1+f_\epsilon^1+f_{\beta^+}^0+f_\epsilon^0=1.$$

Now consider the arrangement shown schematically in fig. 2. For the singles counting rate we have

$$N_{0.5}^{\mathrm{I}} = 2N_0E^{\mathrm{I}}(f_{\beta^+}^1+f_{\beta^+}^0) = a,$$
$$N_{1.07}^{\mathrm{III}} = N_0E^{\mathrm{III}}(f_{\beta^+}^1+f_\epsilon^1) = b,$$
$$N_{\mathrm{X}}^{\mathrm{IV}} = N_0f_{\mathrm{y}}E^{\mathrm{IV}}(f_{\mathrm{k}}^1+f_{\mathrm{k}}^0+1) = c,$$

where the superscripts denote the counters and the subscripts the radiations being measured, E = efficiency, N_0 = source strength, f_{y} = K-fluorescence yield. For the coincidences we have

$$N_{0.5,\,0.5}^{\mathrm{I,\,II}} = 2N_0E^{\mathrm{a}}(f_{\beta^+}^1+f_{\beta^+}^0) = \alpha,$$
$$N_{0.5,\,1.07}^{\mathrm{I.\,III}} = 2N_0E^{\mathrm{I}}E^{\mathrm{III}}f_{\beta^+}^1 = 2N_0E^{\mathrm{V}}f_{\beta^+}^1 = \beta,$$
$$N_{\mathrm{X},\,1.07}^{\mathrm{IV,\,III}} = N_0E^{\mathrm{IV}}E^{\mathrm{III}}f_{\mathrm{k}}^1 = \gamma,$$

where

E^{a} = combined efficiency of the two γ counters for 0.5,
$E^{\mathrm{III}'}$ = efficiency of 1.07 counter without absorber.

The preceding analysis is based on the following assumptions:

† After completion of this work we have learned from D. Horen and W. Meyerhof (private communication) that they have found additional weak electron-capture branchings ($\approx 0.37\%$) to higher excited states in Zn^{68}. This will affect our results and conclusions only slightly.

a) conversion of 1.07 γ is negligible,

b) the contribution to X-ray from pure electron capturing 12d Ge^{71} and source excitation is negligible,

c) no positons are emitted by Ge^{68},

d) the contribution to annihilation radiation due to pairs from 1.07 γ is negligible,

e) the Compton background of 1.07 has been subtracted from 0.511.

With these assumptions and with the help of the preceding relations, we get

$$f_e^1/f_{\beta^+}^1 = \frac{ab}{\alpha\beta}\frac{E^{\mathrm{a}}}{E^{\mathrm{I}}}\frac{E^{\mathrm{V}}}{E^{\mathrm{III}}} - 1 = \left[\frac{ab}{\alpha\beta}\right]_{Ge^{68}}\left[\frac{\alpha\beta}{ab}\right]_{Na^{22}} 1.11 - 1,$$

$$f_{\beta_+}^0/f_{\beta^+}^1 = [a/b]\,[1+f_e^1/f_{\beta^+}^1]\,\frac{E^{\mathrm{III}}}{2E^{\mathrm{I}}} - 1,$$

$$f_{\mathrm{k}}^0/f_{\beta^+}^0 = R\left[\frac{E^{\mathrm{III}'}c}{\gamma} - \frac{N_0 f_{\mathrm{y}} E^{\mathrm{IV}} E^{\mathrm{III}'}}{\gamma} - 1\right],$$

where

$$R = (f_{\mathrm{k}}^1/f_{\beta^+}^1)\,(f_{\beta^+}^1/f_{\beta^+}^0), \qquad f_{\mathrm{y}} E^{\mathrm{IV}} = \frac{\gamma}{b}\frac{E^{\mathrm{III}}}{E^{\mathrm{III}'}}\left[1 + \frac{1}{(f_{\mathrm{k}}^1/f_{\beta^+}^1)}\right].$$

The unknowns to be found are the various efficiencies and N_0, the source strength. We assume with negligible error that $E^{\mathrm{III}} = E^{\mathrm{III}'}$. To find the various efficiencies we replace Ga^{68} by Na^{22} which has similar and known decay scheme [7]). However, in using Na^{22} two corrections have to be made. The first is the difference in range in lucite of Na^{22} positons (0.540 MeV) and Ga^{68} positons ($\approx$ 1.90 MeV). This will affect the 0.5 solid angle. Secondly, the efficiency of $1\frac{1}{2}'' \times 1''$ NaI(Tl) crystal for 1.28 γ of Na^{22} is slightly lower than that for 1.07 γ of Ga^{68}. N_0 can be determined in principle by making a chemical separation of Ga from Ge and studying the K X-rays as a function of time. The extrapolation to zero time would then give N_0 if the fluorescence yield is known. This, however, is subject to two uncertainties a) absorption in the source, b) reckoning zero time. An approximate value of N_0 is given by $N_0 \approx 1.15\, a/2E^{\mathrm{I}}$ (if again positons account for 87 % of total decays).

4.2. THE EXPERIMENT

Fig. 2. shows the experimental set up which is self-explanatory. Counters I and II employ 2″ cube NaI and counter III $1\frac{1}{2}'' \times 1''$ NaI crystals. The use of 2″ cube crystals facilitated the evaluation of Compton contribution of 1.07 or 1.28 to 0.511 photopeak. The experimental procedure consisted simply in measuring singles and coincidences first with Ga^{68} and then under identical geometry with Na^{22}. The K X-ray peak was analyzed in the manner described in section 3.

4.3. RESULTS

Table 1 summarizes our final results, which are the average of several runs made under slightly varying conditions. All necessary corrections have been applied.

TABLE 1

Summary of final results on Ga^{68}

$f_K^1/f_{\beta^+}^1 = 1.28 \pm 0.12$	$f_{\beta^+}^1/f_{\beta^+}^0 = (1.76 \pm 0.22) \times 10^{-2}$
$f_K^0/f_{\beta^+}^0 = 0.10 \pm 0.02$	$N_{\beta^+}/N_{1.07} = 19.47 \pm 2.10$

The corrections mentioned earlier for Na^{22} were made as follows. To determine the 0.511 solid angle correction the counting rate in the annihilation peak was measured as a function of distance between source and detector. From this a correction of $(10 \pm 0.5\ \%)$ was deduced. The correction for difference in efficiency of $1\frac{1}{2}'' \times 1''$ crystal for 1.28 γ was obtained from the curves of Bell [8]). This is of the order of 8 %. It must be pointed out, however, that the corrections luckily cancel out for $f_e^1/f_{\beta^+}^1$.

From the singles γ-spectrum of Ga^{68} in 2'' cube crystal the number of positons per 1.07 γ was found to be 19.47 ± 2.10 by comparison with Na^{22}. An efficiency ratio of 0.90 ± 0.04 was assumed for 1.28 and 1.07 γ's. This result is to be compared with the value 14.4 ± 1.7 of Crasemann *et al.*[1]) and 27.3 ± 3 of Horen and Meyerhof [6]). The value for $f_{\beta^+}^0/f_{\beta^+}^1$ is in agreement with the work of the latter authors.

4.4. DISCUSSION

The failure to observe any K X-ray—K X-ray or K X-ray-low energy γ-ray or K X-ray high energy γ-ray (up to 750 keV) coincidences suggests that the 0^+ state in Ga^{68} lies either very close to the ground state (say with energy less than the K-binding energy, to which state L or K capture may occur) or that it is very high-much higher than Ge^{68}—Ga^{68} decay energy. The possibility of pure L-capture to such a low-lying state is remote.

As regards K/β^+ ratios, we would like to examine some of the assumptions we made in our analysis before comparing our results with theory. The assumption that the conversion of 1.07 γ is negligible is very reasonable. For an E2 transition of this energy the theoretical value of α_K is less than 10^{-4} [9]). This is supported by our results on X-ray—X-ray coincidences. Both the half life (12 days) and the abundance of Zn^{68} from which it was formed make the contribution from Ge^{71} negligible. Self excitation is negligible in the weak source employed. Our conclusion on positon emission by Ge^{68} justifies assumption c. This is also supported by β-decay systematics of Way and Wood [10]) or by a plot of $E_{\beta\beta}$, double β-decay energy vs/neutron number (for Zn-Ge). Linear interpolation gives 500 ± 150 keV for $Ge^{68} \rightarrow Ga^{68}$

decay if $Ga^{68} \rightarrow Zn^{68}$ energy = 2.90 MeV. The contribution to annihilation radiation due to pairs from 1.07 γ is certainly negligible [11]).

There can be no doubt that the positon decays from Ga^{68} are pure Gamow-Teller transitions. The spin of the ground state of even Zn^{68} is 0^+ and that of the first excited state 2^+ from systematics of even nuclei [12]). The spin of Ga^{68} is 1^+. Hence it becomes interesting to compare our K/β^+ ratios with theory to get an estimate of the Fierz interference term. Let R be the measured K/β^+ ratio and R_0 the theoretical value for zero interference. If $\langle W^{-1}\rangle$ denotes the expectation value of W^{-1} over the positon energy spectrum, the Fierz terms are given by [13])

$$b_{GT} = \frac{C_A C_T}{|C_A|^2+|C_T|^2} = \frac{(R/R_0)-1}{2[1+(R/R_0)\langle W^{-1}\rangle]},$$

and $\langle W^{-1}\rangle$ is given to 2 % by the expression [14])

$$\langle W^{-1}\rangle \approx \frac{5}{2W_0}\left[\frac{2W_0^3 p_0+13W_0 p_0-3(4W_0^2+1)\ln(W_0+p_0)}{2W_0^3 p_0-9W_0 p_0-(8p_0/W_0)+15\ln(W_0+p_0)}\right].$$

For the ground state positon group the available values of W_0 are 4.70 [15, 16]), 4.80 [1]) all from β-decay and 4.75 from Zn^{68}(p, n)Ga^{68} threshold [17]). For the positon group to the 2^+ state only one direct measurement exists [15]) which gives $W_0 = 2.51$. However, the γ-ray energy together with the ground state W_0 fix this value uniquely. For the γ-ray measurements we have 1.02 ± 0.02 [1]), 1.099 ± 0.015 [18]), 1.078 ± 0.005 [19]) and our own value of 1.067 ± 0.035, all in MeV. We adopt the values $W_0 = 2.59$ (to the 2^+ state) and 4.70 (to the ground state). To compute theoretical K/β^+ ratios a numerical integration of the unscreened Fermi function has been carried out using NBS tables [20]). The screening correction was obtained from the curves of Perlman *et al.* [21]). The screening correction for K-capture was taken to be $Z_k = Z-0.3$ [21]). The computed K/β^+ ratios are 1.42 (to the 2^+ state) and 0.09 (to the ground state). After correcting the measured $f_\epsilon^1/f_{\beta^+}^1$ for 8.5 % L-capture [22]) (note that for the ground state we directly get $f_k^0/f_{\beta^+}^0$) the Fierz terms are obtained as $b_{GT} = +0.03\pm0.01$ and -0.03 ± 0.02 to the ground state and 2^+ state respectively. The larger uncertainty in the former result arises from uncertainty in the value of N_0 which was based on the assumption that the positons account for 87 % of the transitions; otherwise the errors are statistical only. The latter result definitely showsthe smallness of the Fierz term.

5. Conclusions

Our failure to find a low-lying 0^+ state in Ga^{68} implies that the analogy of Cu^{62} does not hold here. The small value for the Fierz parameter is in harmony with the conclusions of Sherr and Miller [13]) on another pure Gamow-Teller emitter, Na^{22}. A more precise determination of the end-point of the low-energy positon group seems highly desirable.

It is a pleasure to acknowledge the constant encouragement of Prof. L. Madansky with whom we have enjoyed many helpful discussions. Sincere thanks are due to Prof. F. Rasetti for his kind interest and to Prof. W. S. Koski of the Chemistry Department for placing his laboratory at our disposal and for many suggestions concerning chemical separation. We have profited much from conversations with Dr. S. S. Karmarkar and our colleagues Messers D. R. Tilley and N. R. Roberson. Finally we wish to thank Drs. N. P. Heydenburg and G. M. Temmer for kindly arranging the cyclotron bombardment.

References

1) Crasemann, Rehfuss and Easterday, Phys. Rev. **102** (1956) 1344
2) Hubbs, Nierenberg, Shugart and Worcester, Phys. Rev. **105** (1957) 1928
3) Hubbs, Marrus and Worcester, Phys. Rev. **110** (1958) 534
4) Way, King, McGinnis and van Lieshout, Nuclear Level Schemes $A = 40-92$ (U.S. Government Printing Office, Washington D. C. 1955)
5) E. J. Swift, J. Am. Chem. Soc. **46** (1924) 2375
6) D. Horen and W. Meyerhof, private communication
7) P. M. Endt and C. M. Braams, Revs. Mod. Phys. **29** (1957) 683
8) P. R. Bell in Beta and Gamma Ray Spectroscopy; edited by K. Siegbahn (North-Holland Publishing Company, 1955) p. 154
9) M. E. Rose, ref. [8]), appendix 4
10) K. Way and M. Wood, Phys. Rev. **94** (1954) 119
11) C. M. Davisson, ref. [8]), p. 24
12) G. Scharff-Goldhaber, Phys. Rev. **90** (1953) 589
13) R. Sherr and R. H. Miller, Phys. Rev. **93** (1954) 1076
14) J. Gerhart, Phys. Rev. **109** (1958) 897
15) A. M. Mukerji and P. Preiswerk, Helv. Phys. Acta **25** (1952) 387
16) H. Daniel, Z. Naturf. **12a** (1957) 363
17) R. A. Chapman and J. C. Slattery, Phys. Rev. **105** (1957) 633
18) R. M. Sinclair, Westinghouse Research Report 60, 94511, 6 (1956) p. 12
19) Van Patter, Rothman, Porter and Mandeville, Phys. Rev. **107** (1957) 71
20) Tables for the Analysis of Beta-Spectra, National Bureau of Standards, Applied Mathematics Series No. **13** (U.S. Government Printing Office Washington D. C. 1952)
21) Perlman, Welker and Wolfsberg, Phys. Rev. **110** (1958) 381
22) M. E. Rose and J. Jackson, Phys. Rev. **76** (1949) 1540

8.B *Nuclear Physics* **10** (1959) 213—214; © *North-Holland Publishing Co., Amsterdam*
Not to be reproduced by photoprint or microfilm without written permission from the publisher

ON THE SECOND NEUTRAL PION

W. KRÓLIKOWSKI

Institute of Theoretical Physics, University of Warsaw

and

Institute for Nuclear Research, Polish Academy of Sciences, Warsaw

Received 8 December 1958

Abstract: The charge parity of the hypothetical second neutral pion is discussed and a possibility of absence of strong interactions for this particle is pointed out.

A number of authors [1–6]) considered recently the possibility of existence of a second neutral pion π_0^0, being a charge singulet, whereas the usual pion π^0 belongs to the charge triplet π^+, π^0, π^-. It was also pointed out [7]) that this hypothetical particle might play a role in weak interactions leading to mesonic decays of hyperons. In fact, if the field π_0^0 existed, if would be possible to group the four fields π^+, π^0, π^-, π_0^0 not only in one isotriplet ($T = 1$, $S = 0$) and one isosingulet ($T = 0$, $S = 0$), but also, alternatively, in two doublets,

$$\Pi_\alpha = \begin{cases} \pi^+ \\ \frac{1}{\sqrt{2}}(\pi^0 + i\pi_0^0) \end{cases} \quad \text{and} \quad \Pi_\alpha^* = \begin{cases} \pi^- \\ \frac{1}{\sqrt{2}}(\pi^0 - i\pi_0^0) \end{cases}, \tag{1}$$

having "apparent" isospin $T = \frac{1}{2}$ and "apparent" strangeness $S = \mp 1$. (The asterisk denotes here hermitian conjugation.) Assuming that the grouping (1) would be proper for weak interactions leading to the decays of hyperons (whereas the usual one would remain proper for strong interactions), we might interpret the Gell-Mann rule $|\Delta T_3| = \frac{1}{2}$ or $|\Delta S| = 1$ for "true" isospin and strangeness as a conservation law $\Delta T_3 = 0$ or $\Delta S = 0$ for "apparent" isospin and strangeness. Weak and strong interactions of pions might mix, of course, in some weak processes and, therefore, we would observe in these processes no rules for "apparent" isospin and strangeness.

The aim of the present note is to stress that the fields π^0 and π_0^0 (if the second exists) have charge parity $+1$ and -1,

$$C\pi^0 C^{-1} = \pi^0, \qquad C\pi_0^0 C^{-1} = -\pi_0^0, \tag{2}$$

if the combinations $\Pi^0 \equiv \Pi_2 = (\pi^0 + i\pi_0^0)/\sqrt{2}$ and $\Pi^{0*} = \Pi_2^* = (\pi^0 - i\pi_0^0)/\sqrt{2}$ behave like fields of particles and antiparticles,

$$C\Pi^0 C^{-1} = \Pi^{0*}. \tag{3}$$

(Here, C denotes the unitary operator of charge conjugation.) The proof is obvious, because we have

$$\pi^0 = \frac{1}{\sqrt{2}}(\Pi^0+\Pi^{0*}), \qquad \pi_0{}^0 = \frac{1}{i\sqrt{2}}(\Pi^0-\Pi^{0*}). \tag{4}$$

It is interesting to observe that in the case (3) the fields π^0 and $\pi_0{}^0$ are analogous to the fields $K_1{}^0$ and $K_2{}^0$ introduced by Gell-Mann and Pais [8]) (Π^0 and Π^{0*} are the analogues of K^0 and K^{0*}), but the roles of the fields in strong and weak interactions are interchanged.

An important consequence of the property (2) is the absence of (parity and charge parity conserving) Yukawa strong interactions between baryons and the second neutral pion $\pi_0{}^0$ (assuming that $\pi_0{}^0$ is pseudoscalar † like π^0), if only the corresponding strong interactions between baryons and the usual neutral pion π^0 are not forbidden. For instance, the strong interaction of $\pi_0{}^0$ with nucleons, $\bar{N}\gamma_5 N\pi_0{}^0$, is impossible.

In the theory proposed in ref. [5]) we can write

$$\pi^0 = \frac{1}{\sqrt{2}}(M_{12}+M_{21}), \qquad \pi_0{}^0 = \frac{1}{i\sqrt{2}}(M_{12}-M_{21}) \tag{5}$$

(and $\pi^+ = M_{11}$, $\pi^- = M_{22}$). Assuming relations

$$CM_{12}C^{-1} = M_{12}^* = M_{21} \quad \text{and} \quad CM_{21}C^{-1} = M_{21}^* = M_{12} \tag{6}$$

we have a theory with the property (3) (and, therefore, also (2)), in which

$$\Pi^0 = M_{12}, \qquad \Pi^{0*} = M_{21}.$$

Then, the hypothetical particle $\pi_0{}^0$ does not interact strongly (with conservation of parity and charge parity) with baryons in all the cases in which the usual neutral pion π^0 does.

† The argument remains unchanged for a scalar $\pi_0{}^0$.

References

1) B. d'Espagnat, J. Prentki and A. Salam, Nuclear Physics **3** (1957) 446 (footnote on p. 449)
2) A. M. Baldin, Nuovo Cimento **8** (1958) 569
3) A. M. Baldin and P. K. Kabir, Nuovo Cimento **9** (1958) 547
4) Y. Yamaguchi, preprint
5) W. Królikowski, Nuclear Physics **8** (1958) 461
6) W. Heisenberg, Proceedings of Geneva Conference CERN (1958)
7) W. Królikowski, Bull. Acad. Polon. Sci. **6** (1958) 417
8) M. Gell-Mann and A. Pais, Phys. Rev. **97** (1955) 1387

1.E.1:
2.B

Nuclear Physics **10** (1959) 215—219; © *North-Holland Publishing Co., Amsterdam*
Not to be reproduced by photoprint or microfilm without written permission from the publisher

SPIN AND PARITY OF THE 760 keV RESONANCE LEVEL IN THE REACTION $Si^{30}(p, \gamma)P^{31}$ AND OF THE INTERMEDIATE LEVELS IN P^{31}

LENNART SIMONS
University of Helsinki

Received 22 December 1958

Abstract: Certain triple angular correlation functions are calculated and compared with the results of triple angular correlation measurements for the reaction $Si^{30}(p, \gamma)P^{31}$. We obtain spin $\frac{5}{2}$ and even parity for the 760 keV resonance level, spin $\frac{1}{2}^+$ for the 3.51 MeV level and $\frac{5}{2}^+$ for the 2.23 MeV level.

1. Introduction

Spin and parity of the resonance level of 760 keV in $Si^{30}(p, \gamma)P^{31}$ are unknown so far [1]; of the three intermediate levels in P^{31}, which occur at γ-radiation, the 1.27 MeV level has $\frac{3}{2}^+$, the 2.23 MeV level very probably has $\frac{5}{2}^+$, whereas for the 3.51 MeV level neither spin nor parity is known (fig. 1).

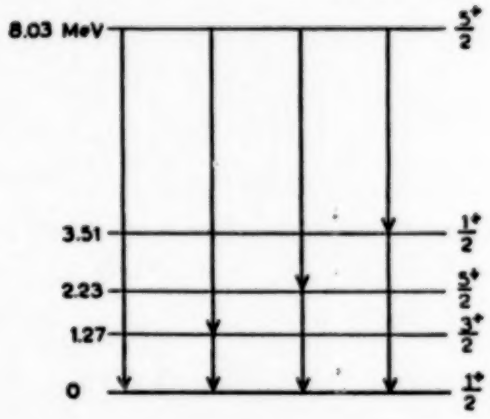

Fig. 1

A. M. Hoogenboom [2]) has performed, by means of a new exact method, triple angular correlation measurements for the 760 keV resonance in $Si^{30}(p, \gamma)P^{31}$ with relation to the three cascades originating at this resonance level in P^{31}. Each one of these cascades consists of two gamma rays and terminates in the ground state of P^{31}. The first gamma ray (γ_{12}) has been observed in a direction perpendicular to the proton beam, the other one (γ_2) in the same plane inclined at the angle θ against the proton beam. Measure-

ments of the triple correlation function $W(\theta)$ have been made for $\theta = 90°$, 45° and 0°.

2. General Discussion of Spins and Parities

Since spin and parity, $\frac{3}{2}^+$, of the 1.27 MeV level in P^{31} are considered certain, we shall start with a discussion of this cascade, which is, moreover, the most interesting one on account of its high anisotropy.

The ground states of Si^{30} and P^{31} have 0^+ and $\frac{1}{2}^+$, respectively. Since direct radiation occurs to the ground state of P^{31}, it will hardly be necessary to go any higher than $j_1 = \frac{7}{2}$ for the resonance level. But since the ground-state transition is weak, it is rather unlikely that j_1 should be $\frac{1}{2}$ or $\frac{3}{2}$. Therefore, we assume first that $j_1 = \frac{5}{2}$.

Since the intermediate level has $j_2 = \frac{3}{2}^+$, γ_2 consists of M1 radiation, possibly with slight admixture of E2. Since γ_{12} and γ_2 are approximately equal in strength, it is likely that the compound state has even parity, i.e., $j_1 = \frac{5}{2}^+$, in which case γ_{12}, too, is M1 radiation (possibly with slight admixture of E2).

3. Determination of the Spin and Parity for the Compound State using the Known Spin and Parity for the 1.27 MeV Intermediate Level

The channel spin and parity in Si^{30} is $\frac{1}{2}^+$. Therefore, when $j_1 = \frac{5}{2}^+$, the compound state will be formed only by d-wave protons, $l_1 = 2$.

For the directions for observation now concerned, there is (save for a factor independent of θ)

$$W(\theta) = 1 + B_2 \cos^2\theta + B_4 \cos^4\theta + \ldots \tag{1}$$

where, for B_ν, ν is even and $\nu_{max} \leqq 2 \min(l_2, j_2)$. Since $j_2 = \frac{3}{2}$, it is evident that, independent of the multipole order L_2 of γ_2 and independent of the other angular momenta, W will have the form

$$W(\theta) = 1 + B_2 \cos^2\theta. \tag{2}$$

Assuming that both γ-rays are pure magnetic dipoles, we obtain

$$W(\theta) = 1 - \tfrac{4}{7}\cos^2\theta, \tag{3}$$

i.e., $W(90°) = 1$, $W(45°) = \frac{5}{7} = 0.71$, $W(0°) = \frac{3}{7} = 0.43$.

In this cascade, γ_{12} has the energy 6.76 MeV and γ_2, 1.27 MeV. One of the advantages of the new method is the small amount of background. Furthermore, the γ-radiations for which coincidence measurements are carried out should yield peaks of approximately equal intensity. However, since all cascades are measured simultaneously (v. fig. 10[2]), the peaks are so closely spaced that superpositions occur; moreover, the sum peak (8.03 MeV), which furthermore has a fairly strong background, appears to disturb the

6.76 MeV peak considerably. If we subtract a given background, primarily for the 6.76 MeV peak, we find for the mean of the 1.27 and 6.76 MeV radiations: $W(0°)/W(90°) \approx 0.25 \pm 0.03$, $W(45°)/W(90°) \approx 0.60 \pm 0.05$. This is the result of an examination concerning mainly the areas but to some degree concerning the maximum ordinates.

We can thus note that the theoretical values obtained deviate to some extent from experimental conditions, and if we take into account the finite solid angle, the difference will be still greater.

The difference may be attributable to the E2 admixture. If we investigate the possibility that γ_{12} is a pure M1 and γ_2 is a mixture of M1 and E2, with the intensity ratio $I(\mathrm{E2})/I(\mathrm{M1}) = \delta^2$, we find that

$$W(\theta) = 1 - \frac{12(1+2\delta\sqrt{3}-\delta^2)}{21+10\delta\sqrt{3}+11\delta^2}\cos^2\theta. \tag{4}$$

Setting now $W(0°) = 0.25$, we obtain (disregarding the possible value $\delta = 1.26$, which is obviously too large) $\delta = 0.148$, i.e., $\delta^2 = 0.02$. Then, $W(45°) = 0.625$, which is in good agreement with the experimental value, 0.60 ± 0.05. It can be seen that a very small admixture of E2 in γ_2 is able to account for the experimental results.

If $j_1 = \frac{5}{2}$ but the parity is odd, contributions will be made only by protons with $l_1 = 3$. We have now a unique case, which occurs when $s_1 = \frac{1}{2}$, viz.

$$Z(j_1-\tfrac{1}{2},\ j_1,\ j_1-\tfrac{1}{2},\ j_1;\ \tfrac{1}{2},\ k_1) = Z(j_1+\tfrac{1}{2},\ j_1,\ j_1+\tfrac{1}{2},\ j_1;\ \tfrac{1}{2},\ k_1) \tag{5}$$

which can also be seen from Sharp's tables [3]), p. 6.

Thus, whether we consider the case $l_1 = j_1 - \frac{1}{2}$ or the case $l_1 = j_1 + \frac{1}{2}$, we obtain the same triple correlation function $W(\theta)$ and it is thus impossible to decide the parity of the compound state with the aid of $W(\theta)$. However, as has been stated before, $j_1 = \frac{5}{2}^+$ is more probable than $j_1 = \frac{5}{2}^-$ for other reasons.

For $j_1 = \frac{3}{2}^+$, $l_1 = 2$ and $j_1 = \frac{3}{2}^-$, $l_1 = 1$ we find

$$W(\theta) = 1 + \tfrac{3}{11}\cos^2\theta, \tag{6}$$

i.e., $j_1 = \frac{3}{2}$ is positively ruled out.

For the cases $j_1 = \frac{7}{2}^+$, $l_1 = 4$ and $j_1 = \frac{7}{2}^-$, $l_1 = 3$ one finds

$$W(\theta) = 1 + \tfrac{1}{17}\cos^2\theta. \tag{7}$$

This is out of the question.

There remain now only the cases $j_1 = \frac{1}{2}^+$, $l_1 = 0$ and $j_1 = \frac{1}{2}^-$, $l_1 = 1$. In these cases one finds

$$W(\theta) = 1 - 0.3\cos^2\theta, \tag{8}$$

$W(90°) = 1$, $W(45°) = 0.85$, $W(0°) = 0.70$.

It is seen that $W(\theta)$ displays an anisotropy of the same kind as in the experimental one, although it is much less pronounced. Possibly, however, a certain degree of agreement between theory and experiment may be achieved by assuming large admixtures of E2 to the gamma radiations.

However, one circumstance in support of $j_1 = \frac{1}{2}$ is that according to theory the ground state gamma radiation is then isotropic and the experiments show that $W(\theta)$ is approximately the same for 90°, 45° and 0°. But several facts speak against the possibility of $j_1 = \frac{1}{2}$; first of all the circumstance that one should then have a considerably more intensive ground state transition than that shown by the experiments, since the ground state, too, has the spin $\frac{1}{2}$.

But what is then the theoretical angular distribution function $W(\theta)$ for the ground state gamma ray when $j_1 = \frac{5}{2}$? For both $j_1 = \frac{5}{2}^+$, $l_1 = 2$ and $j_1 = \frac{5}{2}^-$, $l_1 = 3$ one finds, the multipole order of the gamma radiation being put equal to 2,

$$W = 1+\tfrac{4}{7}P_2-\tfrac{4}{7}P_4 \approx 1+6\cos^2\theta-5\cos^4\theta. \tag{9}$$

Here, the coefficients of P_2 and P_4 are equal and of opposite signs and it is therefore possible that the terms with P_2 and P_4 roughly cancel out when the solid angle correction is taken into account and, e.g., a slight admixture of radiation with the multipole order 3 is assumed. It is also possible that the experimental $W(\theta)$ for the ground state gamma ray is comparatively inaccurate because, in addition to a considerable background, contributions are made to the energy at about 8 MeV by all cascades, all of which tend to have an equalizing effect.

4. Determination of the Spin and Parity for the Intermediate Levels 2.23 and 3.51 MeV in P^{31}

We shall now investigate, for $j_1 = \frac{5}{2}^+$, the other cascades. They all are slightly anisotropic.

Since the multipole order of the gamma radiation hardly exceeds 2, the intermediate level may have the spins $j_2 = \frac{1}{2}, \frac{3}{2}, \frac{5}{2}$. According to what was just found, $j_2 = \frac{3}{2}$ yields a strong anisotropy and is therefore ruled out. $j_2 = \frac{1}{2}$ gives, theoretically, an isotropic distribution and may thus come into question. $j_2 = \frac{5}{2}$ yields

$$W(\theta) = 1-\tfrac{4}{3}\cos^2\theta+\tfrac{35}{27}\cos^4\theta, \tag{10}$$

$W(90°) = 1$, $W(45°) = \frac{71}{108} = 0.66$, $W(0°) = \frac{26}{27} = 0.963$.

The 2.23 MeV intermediate level has very probably [1]) $j_2 = \frac{5}{2}^+$. If, now, one considers the mean of the areas corresponding to the gamma rays of this cascade, we note that for $\theta = 45°$ this mean is considerably less than for $\theta = 90°$ and 0°. Therefore, one can say that the spin $j = \frac{5}{2}$ is corroborated.

Similarly, the even parity is corroborated because, if the parity were odd, the later γ-ray of the cascade would be too weak.

For $j_2 = \frac{5}{2}$, $W(0°)$ is somewhat less than $W(90°)$ but for the cascade with the 3.51 MeV intermediate level the mean of the areas is slightly higher for $\theta = 0°$ than for $\theta = 90°$. The corresponding area value for $\theta = 45°$ approximately equals that for $\theta = 90°$, while for $j_2 = \frac{5}{2}$, $W(45°) \approx \frac{2}{3}W(90°)$. The 3.51 MeV level therefore has very probably the spin $\frac{1}{2}$. The parity must then be even, because if the parity were odd, γ_{12} would hardly have the observed strength.

By the investigation of all cascades we have found further corroboration that the 760 keV resonance level has the spin $\frac{5}{2}$ and even parity.

References

1) P. M. Endt and C. M. Braams, Revs. Mod. Phys. **29** (1957) 683
2) A. M. Hoogenboom, Nuclear Instruments **3** (1958) 57
3) W. T. Sharp *et al.*, Atomic Energy of Canada Limited, Chalk River Project (1957)

3.B *Nuclear Physics* **10** (1959) 220—225; © *North-Holland Publishing Co., Amsterdam*
Not to be reproduced by photoprint or microfilm without written permission from the publisher

INTERNAL CONVERSION OF GAMMA-RAY TRANSITIONS IN As^{75}

F. R. METZGER and W. B. TODD

Bartol Research Foundation of the Franklin Institute, Swarthmore, Pennsylvania †

Received 19 December 1958

Abstract: The internal K-conversion coefficients of the 136-, 265-, 280-, 305-, and 402-keV transitions in As^{75} were measured using a lens spectrometer and scintillation counters. The E1 character of the 136- and 402-keV transitions was confirmed, and the E3 assignment to the 305-keV gamma ray was clearly established. For the 265- and 280-keV E2+M1 transitions, mixing parameters $\delta_{265} = -0.06 \pm 0.04$ and $\delta_{280} = -0.42 \pm 0.05$ were obtained on the basis of all the presently available information. The M1 transition probability of the 265-keV transition is at least one order of magnitude larger than that of the 280-keV transition while the E2 transition probabilities appear to be comparable. The spin and parity assignments made by Schardt [1]) were confirmed.

1. Introduction

Schardt [1]) has summarized the present status of our knowledge of the first few excited states of As^{75} as it emerged from studies [1,2]) of the decays of Ge^{75} and Se^{75} and from different measurements of gamma-ray transition probabilities [3,4,5]). More recently, van de Bold and coworkers [6]) confirmed the spin and parity assignments of Schardt [1]) by additional angular correlation and by direction-polarization experiments.

There remained, however, considerable discrepancies as far as the multipole mixing of the different transitions was concerned. The direction-polarization experiments [6]), for instance, suggested that the 121- and 136-keV transitions were pure E1, while the conversion measurements [2]) indicated strong mixtures. The E2 admixture to the 265-keV transition found by Schardt [2]) was also much larger than the admixture expected from the short mean life [4]) (1.6×10^{-11} sec) of this level. It appeared [4]) that most of these difficulties could be resolved if it was assumed that the old conversion coefficients [2]) were too large by a factor of ≈ 2.5. After preliminary experiments indicated that this was probably the correct explanation, the more accurate measurements to be described here were undertaken. In order to avoid the difficulties of absolute measurements, the by now well known K-conversion line of the 279-keV transition in Tl^{203} was

† Assisted by the joint program of the U.S. Office of Naval Research and the Atomic Energy Commission.

utilized for relative measurements. The close agreement of the energies of the most important transitions in As^{75} (265 and 280 keV) with that of the Tl^{203} transition made the comparison very reliable and enabled the uncertainties to be kept to a minimum.

2. Source Preparation

The Se^{75} was prepared by neutron irradiation of selenium, enriched in Se^{74} (14.1 %) [7], in the Materials Testing Reactor at Arco, Idaho. At the time of the conversion measurements the specific activity was $\approx$ 5 millicuries per milligram of enriched selenium. The circular spectrometer sources, $\approx$ 5 mm in diameter, prepared by evaporation, were very uniform and sufficiently thin to prevent any observable low energy tails on all the measured conversion lines.

The Hg^{203} sources were less satisfactory. Hg^{203} of 0.6 millicuries per milligram specific activity was obtained from Oak Ridge National Laboratory in the form of $Hg(NO_3)_2$ in HNO_3 solution and was deposited on plastic foils using insulin [8]) to improve the uniformity of the sources. The conversion lines showed some low energy tails which had to be corrected for and which represented the main source of uncertainty of the whole study. A comparison of the area under the K-conversion line with that under the Hg^{203} beta spectrum led to a conversion coefficient which agreed with the accepted value within the statistical error of the comparison measurement.

In averaging the results of six different Hg^{203} sources, the individual runs were weighted inversely proportional to the extension of the low energy tails of the conversion lines; i.e., the most uniform sources were weighted most heavily.

3. Experimental Results

3.1. CONVERSION LINE MEASUREMENTS

A lens spectrometer with 1.62 % momentum resolution was used. An anthracene crystal of 3 mm thickness, coupled to an RCA 6342 photomultiplier tube, served as the detector of the electrons. A typical portion of the conversion electron spectrum is shown in fig. 1 together with the suggested analysis into the contributions of the K and L lines of the 265- and 280-keV transitions.

In table 1 the relative internal conversion line intensities are compared with those reported by Schardt and Welker [2]). The agreement of the two sets of results is very good.

3.2. GAMMA INTENSITIES

The relative intensities of the 265-, 280-, 305, and 402-keV gamma lines were determined from an analysis of the photoelectron spectra obtained

with 0.9 and 1.8 mg/cm² gold converters. The intensities were found to be in the ratio of 100: (47±1): (2.1±0.3) : (19±2), i.e., in satisfactory agreement with previous measurements [2,6]). For the relative intensity of the 136-keV

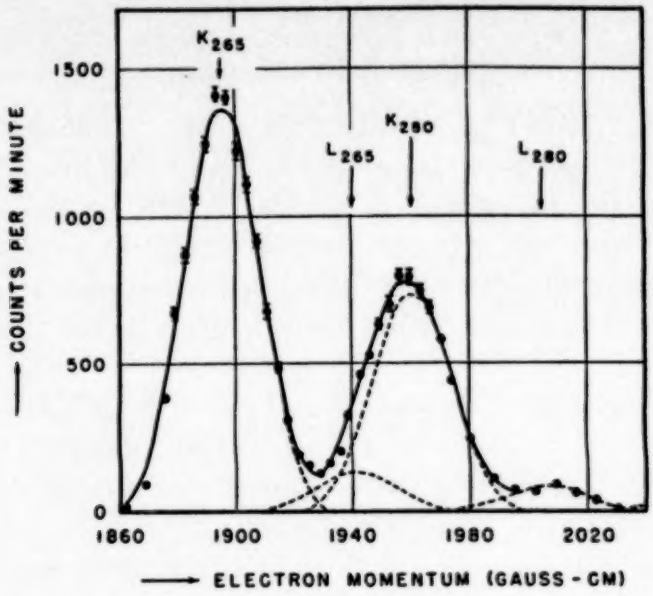

Fig. 1. Se^{75}. A portion of the internal conversion electron spectrum measured with a lens spectrometer. The dashed lines indicate the proposed decomposition of the spectrum into individual lines.

TABLE 1

Internal conversion line	Relative internal conversion electron intensity	
	Schardt and Welker	Present Work
136-K	420	377 ±20
265-K	100	100
280-K	53 ±7	53.6± 1.6
305-K	15.6±1.3 †	15.4± 0.9
402-K	3.6±0.6	3.6± 0.4

† This is a corrected value. In the original paper [3]) an incorrect scale factor had been used (Dr. Schardt, private communication).

transition a value of 90 was used. This represents a somewhat arbitrary average of the intensities given by other groups [2,6]), of a value 90±20 obtained in this laboratory from the intensity of the L photoelectron line, and of a statement by Langevin and Langevin [9]) that the direct electron capture to the 265- and 280-keV levels is smaller than 5 percent of all Se^{75} disintegrations.

For the determination of the relative gamma strengths of the Se^{75} and Hg^{203} conversion electron sources, the full energy peaks of the (265+280)-

keV radiation of Se^{75} and of the 279-keV transition from Hg^{203} were measured with a NaI scintillation spectrometer. Allowance was made for the slightly different detection efficiency for the 265-keV radiation and for the contribution of the 402-, 305-, and 199-keV transitions to the (265+280)-keV full energy peak.

3.3. CONVERSION COEFFICIENTS

In terms of the measured quantities, the conversion coefficient for a Se^{75} gamma ray of energy E is given by

$$\alpha_{Se} = \alpha^{K}_{Hg} \frac{(n_e^E)_{Se}(n_\gamma)_{Hg}}{(n_e^K)_{Hg}(n_\gamma^E)_{Se}} \qquad (1)$$

where the n_e's refer to the areas under the conversion lines (on a $N/H\rho$ vs. $H\rho$ plot) and where the n_γ's are the gamma strengths of the Se^{75} and Hg^{203} conversion electron sources. For α^{K}_{Hg}, the K-conversion coefficient of the 279-keV transition in Tl^{203}, the value 0.163 ± 0.002 was used [10,11].

Combining the results of the two preceding sections with the help of eq. (1), the conversion coefficients tabulated in the second column of table 2 were obtained. The possible multipole assignments are indicated in the last column.

TABLE 2

Internal conversion coefficients ($\times 10^3$) for As^{75}

Conversion line	Experimental present work	Theoretical [12]						Possible multipole assignments
		E1	E2	E3	M1	M2	M3	
136-K	26 ±3	26	220	1500	35	280	2100	E1 + ≦ 1.2 % M2
265-K	6.2±0.3	3.7	19	83	6.3	30	130	M1 + ≦ 1.6 % E2 90 % E1 + 10 % M2
280-K	7.0±0.4	3.2	15.6	66	5.5	25	110	85 % M1 + 15 % E2 83 % E1 + 17 % M2
305-K	45 ±7	2.5	11.5	45	4.4	19	80	E3 + ≦ 2.5 % M4 E3 + ≦ 27 % M2 51 % E2 + 49 % M3
402-K	1.2±0.2	1.2	4.6	15	2.3	8.5	29	E1 + ≦ 2.8 % M2

The conversion coefficients of table 2 are smaller by a factor of 2.4 ± 0.3 than those previously reported [2]. If this factor applies to all the conversion coefficients reported by Schardt and Welker [2], their α_K for the 97-keV transition in As^{75} is reduced to 0.75 ± 0.33. This value is in good agreement with the pure E2 character expected for this transition on the basis of the presently accepted spin assignments [1]. Similar improvements are indicated for the 199-, 121-, and the 66-keV transitions.

As a consequence of the smaller conversion coefficients the intensities of some of the low energy transitions, especially that of the 97-keV transition, are considerably reduced because they had been determined on the basis of the measured gamma intensities and the total conversion coefficients. This makes it more probable that some direct electron capture takes place to the 280-keV level. The intensity assumed in section 3.2 for the 136-keV transition already indicated some electron capture to the 265-keV level.

4. Discussion

For the E1 transitions in As^{75} (402-, 136- and, presumably, 121-keV) the new conversion coefficients lead to small M2 admixtures in agreement with the lifetime of the 402-keV level ($\approx 1.5\times10^{-9}$ sec [1,9]) and with the expected M2 transition probabilities.

For the 265- and 280-keV transitions, the second choices indicated in the last column of table 2 can be eliminated, even without recourse to the direction-polarization data [6]), on the basis of the upper limit of 8×10^{-10} sec for the half-lives [2]). The second and third possibilities indicated in table 2 for the 305-keV transition are very unlikely if one considers transition probabilities alone; they are completely eliminated once the spin value $\frac{9}{2}$ is accepted [1]).

The conversion data of table 2 restrict the mixing parameters of the 265- and 280-keV E2+M1 transitions to the ranges $|\delta_{265}| < 0.13$ and $0.33 < |\delta_{280}| < 0.44$. Additional information concerning the mixing comes from Coulomb excitation, resonance fluorescence and angular correlation experiments. Three sets of angular correlation data [2,6,13]), which differed by somewhat more than the quoted errors, were combined to obtain, in a somewhat arbitrary manner, "best" values for the coefficients of the Legendre polynomials. These "best" values were $A_2 = -0.014\pm0.008$ for the 136—265-keV cascade and $A_2 = -0.44\pm0.02$ for the 121—280-keV cascade. With these A_2 coefficients, allowing up to 0.01 percent admixture of M2 in the low energy E1 transitions of the cascades †, the mixing parameters for the 265- and 280-keV transitions were limited to the intervals

$$-0.22 < \delta_{265} < -0.096 \quad \text{and} \quad 6.3 < \delta_{265} < 26.1$$
$$-0.66 < \delta_{280} < -0.44 \quad \text{and} \quad -1.18 < \delta_{280} < -0.84.$$

For the 280-keV transition a value $\delta_{280} = -0.42\pm0.05$ was judged to reconcile both sets of experiments. This led to a mixing ratio $(E2/M1)_{280} = 0.18\pm0.04$.

For the 265-keV transition two additional independent estimates of δ were available. The first estimate was obtained by attributing the observed Coulomb excitation in the 265—280-keV region of As^{75} solely to the 265-keV level. With the $B(E2)$ value accepted by Alder *et al.* [14]) for the "280-keV"

† This is about the maximum admixture expected from lifetime considerations.

line, a lower limit of 1.0×10^{-9} sec was calculated for the partial E2 lifetime of the 265-keV transition. When this was compared with the actual lifetime of $(1.6\pm0.2)\times10^{-11}$ sec [4]), the mixing parameter was found to be limited to $|\delta_{265}| < 0.14$. A second, more severe, restriction for δ_{265} was derived from the measurement of the angular distribution of the resonance radiation [4]) which led to $|\delta_{265}| < 0.03$. The conflict between this last limit and the range of δ-values suggested by the angular correlation data is reduced by the following consideration: For $\delta_{280} = -0.42$ the angular distribution of the 280-keV resonance radiation is calculated to be of the form $W(\theta) = 1+0.92\ P_2(\cos\theta)$. With such a large coefficient of the P_2 term even a small admixture of 280-keV resonance radiation to the (265+280)-keV line in the resonance fluorescence experiment will appreciably modify the overall angular distribution. If a 4 percent admixture of 280-keV radiation is assumed, and this is the largest admixture possible on the basis of a previous analysis [4]), the coefficient of the P_2 term in the angular distribution of the 265-keV resonance radiation is reduced from 0.15 ± 0.02 to 0.118 ± 0.021. This increases the range of permissible δ-values to $-0.057 < \delta_{265} < +0.057$. While this is still outside the δ-interval allowed by the angular correlation data, the disagreement is less violent. A value $\delta_{265} = -0.06\pm0.04$ was considered to summarize all the information on the mixing of the 265-keV transition. With $\tau_{265} = 1.6\times10^{-11}$ sec, this value of δ_{265} leads to a partial E2 lifetime of 4.4×10^{-9} sec for the 265-keV transition. If the corresponding deduction from the Coulomb excitation cross section is made, the resulting $B(\mathrm{E2})$ leads to a partial E2 lifetime of 1.6×10^{-9} sec for the 280-keV transition. With $\delta_{280} = -0.42$ the total lifetime of this transition becomes 2.4×10^{-10} sec.

The authors are grateful to Drs. H. and M. Langevin for the communication of results prior to publication, and to Dr. A. W. Schardt for a helpful discussion.

References

1) A. W. Schardt, Phys. Rev. **108** (1957) 398
2) A. W. Schardt and J. P. Welker, Phys. Rev. **99** (1955) 810
3) G. M. Temmer and N. P. Heydenburg, Phys. Rev. **104** (1956) 973
4) F. R. Metzger, Phys. Rev. **110** (1958) 123
5) Robert B. Day, private communication quoted in refs. [1]) and [4])
6) H. C. van den Bold, J. van de Geijn and P. M. Endt, Physica **24** (1958) 23
7) Obtained from the Stable Isotopes Division of the U.S. Atomic Energy Commission
8) See, e.g., L. M. Langer, Rev. Sci. Instr. **20** (1949) 216
9) H. Langevin-Joliot and M. Langevin, Journ. Phys. Radium **19** (1958) 765
10) F. R. Metzger, footnote in Phys. Rev. **94** (1954) 1690
11) Nijgh, Wapstra, Ornstein, Salomons-Gobber, Huizenga and Almén, Nuclear Physics **9** (1958/59) 528
12) L. A. Sliv and I. M. Band, Acad. of Sciences USSR (Moscow Leningrad 1956), issued in the USA as report 57 ICC K1, Physics Department, University of Illinois
13) W. H. Kelly and M. L. Wiedenbeck, Phys. Rev. **102** (1956) 1130
14) Alder, Bohr, Huus, Mottelson and Winther, Revs. Mod. Phys. **28** (1956) 432

2.A.1 *Nuclear Physics* **10** (1959) 226—234; © *North-Holland Publishing Co., Amsterdam*

Not to be reproduced by photoprint or microfilm without written permission from the publisher

CROSS SECTIONS FOR SOME (n, p) AND (n, α) REACTIONS

B. D. KERN †, W. E. THOMPSON and J. M. FERGUSON

U.S. Naval Radiological Defense Laboratory, San Francisco, California

Received 24 September 1958

Abstract: The cross sections for the $Mg^{24}(n, p)Na^{24}$, $Al^{27}(n, \alpha)Na^{24}$, $Si^{28}(n, p)Al^{28}$, $Cr^{52}(n, p)V^{52}$ and $Fe^{56}(n, p)Mn^{56}$ reactions have been measured for neutrons producedby the $H^3(d, n)He^4$ reaction. The activation method was used, with the gamma rays which are emitted following beta decay being counted with a NaI(Tl) scintillation crystal. The $Mg^{24}(n, p)Na^{24}$ cross section is found to be 219 ± 26 mb at 13.0 MeV. The $Al^{27}(n, \alpha)Na^{24}$ cross section varies smoothly from 139 mb at 13.0 MeV to 106 mb at 15.7 MeV. The $Si^{28}(n, p)Al^{28}$ cross section changes smoothly from 370 mb at 12.3 MeV to 160 mb at 18.3 MeV, with a broad peak at 13.5 MeV with the maximum value of 380 mb. The $Cr^{52}(n, p)V^{52}$ cross section decreases slowly from 125 mb at 12.3 MeV to 72 mb at 18.3 MeV. The $Fe^{56}(n, p)Mn^{56}$ cross section is found to be 131 ± 15 mb at 15.3 MeV. The results are generally in agreement in those cases where previous results of others exist.

1. Introduction

Cross sections for the $Mg^{24}(n, p)Na^{24}$, $Al^{27}(n, \alpha)Na^{24}$, $Si^{28}(n, p)Al^{28}$, $Cr^{52}(n, p)V^{52}$, and the $Fe^{56}(n, p)Mn^{56}$ reactions have been measured previously for neutrons with energies near 14 MeV by several workers. Forbes [1]) and Paul and Clarke [2]) describe the results of surveys over a range of target materials at a fixed neutron energy near 14 MeV, while Cohen and White [3]) report on relative cross section measurements from 12.5 MeV to 17.5 MeV in neutron energy, with the magnitude normalized to the results of ref.[1]). Another case of a relative cross section as a function of energy is given for the $Fe^{56}(n, p)Mn^{56}$ reaction by Terrell and Holm [4]); in their work the magnitude was normalized to an average of the earlier results [1, 2]). Because of the scantiness of the data on cross sections as a function of neutron energy and the lack of good agreement among the existing cross section results, the present work was initiated. As in all the previous work mentioned above, the activation technique was used to determine the number of reactions which had taken place, but in the present work the gamma rays following the beta decay were counted rather than the beta rays themselves.

2. Experimental Apparatus and Techniques

The radioactive activation method was used, with the sample materials being irradiated with neutrons at the locations indicated in fig. 1, then

† On leave of absence from the University of Kentucky, Lexington, Kentucky.

being transferred to plastic vials which were placed in a NaI(Tl) scintillation well crystal for the counting of the gamma rays.

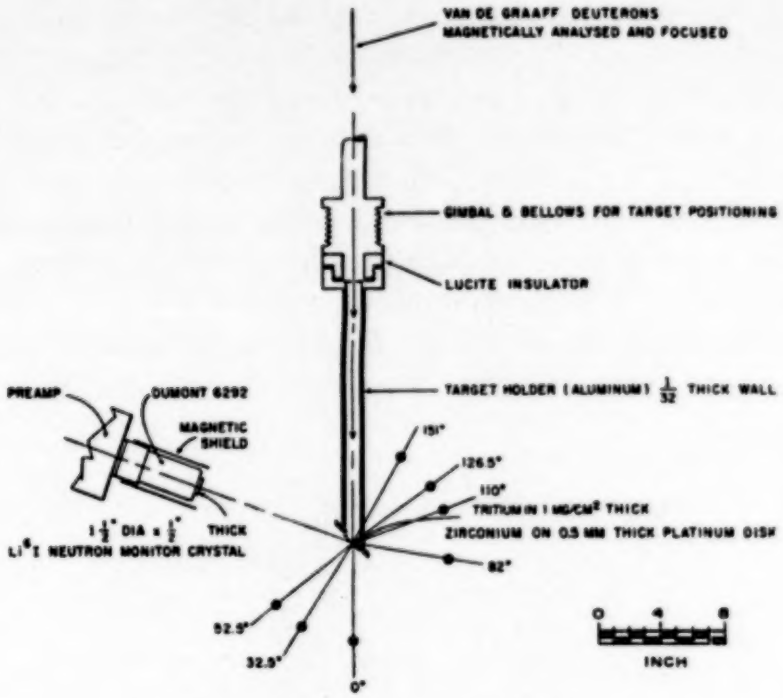

Fig. 1. Arrangement of the samples and the neutron counter.

Neutrons varying in energy from 12.33 to 18.24 MeV at the various angles at which the samples were placed were produced by the H^3(d, n)He^4 reaction, with the NRDL Van de Graaff electrostatic accelerator providing the magnetically-analyzed deuteron beam. The neutron energy was varied by selection of the deuteron energy (average values from 0.43 to 2.00 MeV) and the angular position of the sample. The target † consisted of a 0.025-inch thick platinum foil onto which had been evaporated a 1 mg/cm² layer of zirconium which was later converted to ZrH^3, with the H^3 content being approximately 0.4 curie. The time-integrated neutron flux density at each sample position was computed using as data the counts from $1\frac{1}{2}$ inches in diameter by $\frac{1}{2}$ inch in height Li^6I(Eu) scintillation counter which had earlier been calibrated [7]) by the counting of the recoil alpha particles from the H^3(d, n)He^4 reaction. In this computation the differential relative cross section values of Bame and Perry [8]) were used. The spread in neutron energy amounted to from 0.06 to 0.82 MeV and was primarily due to the loss of energy by the deuterons in passing through the zirconium layer.

The target materials (Mg, Al, Si, Cr, and Fe), in the form of the powdered

† The zirconium tritide targets were obtained from the Radioactive Isotopes Division, Oak Ridge National Laboratory.

element, were placed in cylindrical gelatin capsules (Eli Lilly and Co., Size No. 000) and attached to the end of a $\frac{1}{4}$ inch in diameter aluminium tube by a loop of fine wire. Each of eighteen available tubes was held by a light aluminium support in such a way that the sample on it could be located on a radial line through the target and at a selected distance from it. The seven samples shown in fig. 1 are held in this manner at a radial distance of 6 inches. In some irradiations the tubes were moved radially inward to reduce the distance to 5 inches. This arrangement was suitable for the Mg, Al, and Fe samples with their long-lived products, as several samples could be irradiated together and then placed in the gamma-ray counter in succession. However, the samples of Si and Cr with their shorter-lived products were irradiated at a position corresponding to one given neutron energy and then placed in the counter within 60 seconds. To increase the yield several

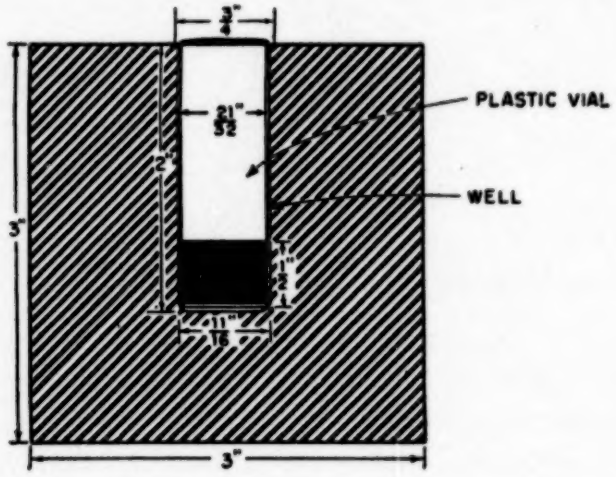

Fig. 2. Schematic diagram of the 3-in. in diameter by 3-in. in height NaI(Tl) well scintillation crystal. The radioactive sample filled the plastic vial to $\frac{1}{2}$-in. in depth.

(usually four) capsules were irradiated simultaneously. This was done by mounting the support on an optical bench to permit movement parallel to the deuteron beam's axis, with the plane of the tubes set perpendicularly to that axis. By selecting the axial position and the distance from the axis, it was possible to place several samples at equal radial distances from the target and to have all of them at the same angle relative to the beam axis where they were all irradiated by neutrons of the same energy. A typical sample contained approximately 0.1 mole of material and was irradiated with a neutron flux density of 8500 neutrons $\cdot$ cm^{-2} $\cdot$ sec^{-1} for a period which varied from about $\frac{1}{2}$(Na^{24} product) to 5(Al^{28} product) half lives.

During the irradiation the neutron flux was monitored with the calibrated $Li^{6}I$(Eu) scintillation counter; its pulse output was recorded by 50 channels

of a Penco † 100-channel pulse height analyzer and the pulses due to the $Li^6(n, t)He^4$ reaction were selected for counting. At the same time the output of the $Li^6I(Eu)$ scintillation counter went to a counting rate meter whose output was recorded on a chart as a function of the time. This was necessary as the neutron flux density was not constant in time. The continuous chart record was divided into equal time increments and each portion of the irradiation was weighted by the exponential decay factor $e^{-\lambda t}$, where λ is the radioactive decay constant of the product nucleide and t is the time from the irradiation until the beginning of the gamma-ray counting. In this way the fraction of the radioactive nuclei which survived until the beginning of the counting was determined.

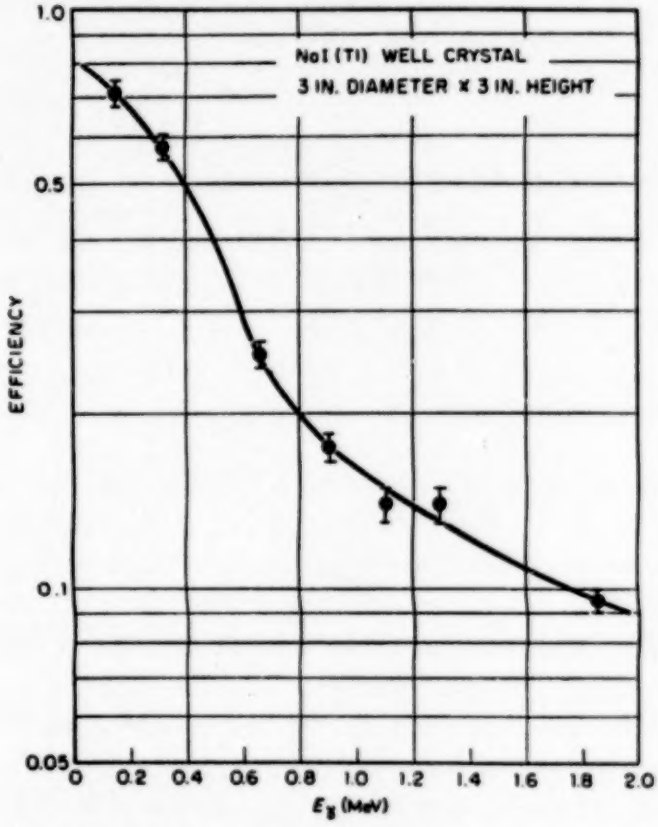

Fig. 3. The efficiency of the NaI(Tl) well crystal for gamma rays. The calibrating samples are described in the text.

The gamma rays from the activated nuclei were counted in a NaI(Tl) scintillation counter which was 3 inches in diameter and 3 inches in height. The active material was transferred from the gelatin capsules to 2.5-dram plastic vials which were inserted into a cylindrical well in the crystal, as in fig. 2. One capsule filled a vial to about $\frac{1}{4}$ of its volume. Each sample was

† Manufactured by Pacific Electric-Nuclear Co., Pasadena, California.

counted for approximately 2 half lives, except for the 14.96-hour Na^{24} and 2.58-hour Mn^{56} samples, which were counted for 120 minutes.

The efficiency of the crystal for producing a pulse corresponding to total absorption of a gamma ray as a function of the gamma-ray energy was determined by using calibrated gamma-ray sources which were prepared by the Chemical Technology Division of NRDL, using the 4π gamma-ray counting technique. These standard sources consisted of the radioactive material absorbed and dried in a bit of cotton which had then been covered by paraffin to a volume of about $\frac{1}{4}$ that of the vial, which was of the same type as that used to contain the activated samples. The efficiency curve for samples of this type is shown in fig. 3. The probable error of the points on this curve is ± 6 percent. The absolute cross sections were calculated from the counting of activated samples which filled the vials to the same height as the standard samples did; all data taken with larger volumes of material were normalized to these values.

3. Calculations and Discussion of Errors

The number n of radioactive nuclei which are present at the end of the irradiation depends on the one hand on the cross section σ; on the other hand, n may be expressed in terms of the number of gamma ray counts A:

$$\frac{\phi\sigma LWsa}{G} = n = \frac{Ae^{\lambda t_e}(1-e^{-\lambda t_c})^{-1}}{b\varepsilon}. \tag{1}$$

The remaining symbols in the equation are ϕ, the time-integrated neutron flux density at the midplane of the sample; L, Avogadro's number; W, the weight of the sample; s, the "survival factor," the fraction of the created radioactive nuclei which survive until the end of the irradiation; a, the relative isotopic abundance of the target isotope; G, the target gram atomic weight; λ, the radioactive decay constant; t_e, the time elapsed between the end of the irradiation and the start of the gamma-ray counting; b, the number of gamma rays per disintegration; ε, the efficiency of the NaI(Tl) well crystal for total absorption; and t_c, the length of time that the gamma rays are counted. From eq. (1) the cross sections have been evaluated.

A correction to the observed quantity A has been made for the self absorption of the emitted gamma rays by the sample material. This correction which increases A is in each case not greater than 12 percent. In the decay of the Na^{24} and Mn^{56}, there are gamma rays in cascade, so that at times a total energy pulse is lost from the peak in the pulse height distribution due to the addition to it of a contribution from the companion gamma ray. For this reason, the well crystal efficiency for samples emitting the Na^{24} gamma ray of 1.37 MeV was adjusted downward by 35.1 percent, and that

for the samples emitting the Mn^{56} gamma ray of 0.85 MeV, downward by 13.8 percent.

The significant sources of error and an estimate of their magnitudes are (1) uncertainty in ϕ, including statistical error in the number of counts, 7 percent; (2) uncertainty in sample position, 3 percent; (3) uncertainty in the survival factor, 1 percent; (4) uncertainty in A, due to statistical error of number of counts, 3 to 5 percent; and (5) uncertainty in the well counter efficiency, 6 to 9 percent. These uncertainties, when combined quadratically, give values which vary from 10 to 30 percent.

Accompanying the high energy neutrons there were, in small numbers, neutrons produced by the interaction of the deuteron beam with deuterium in the target. Under the conditions of the measurements, the maximum energy that these neutrons could assume was 5.3 MeV, when the highest energy deuterons were used and for the forward angles only. For the Mg^{24}(n, p)Na^{24} reaction these neutrons had energies which were below the threshold for the reaction. For the Fe^{56}(n, p)Mn^{56} reaction the neutron energy exceeded the threshold by about 0.3 MeV, but the cross section is known [4]) to be only a fraction of a millibarn at these energies and no appreciable number of reactions can occur. For the Al^{27}(n, α)Na^{24} reaction the excess is again about 0.3 MeV for a few data points; although the cross section at the lower energies was not known it was assumed to be small. For the Si^{28}(n, p) Al^{28} reaction the energy in excess of the threshold reached as high as 1.3 MeV for a few data points; the cross section was known to be small [9]) (less than 25 mb) up to 1 MeV above the threshold. For the Cr^{52}(n, p) V^{52} reaction the excess was about 1.1 MeV for a few data points; although the cross section was not known it was assumed to be small. However, for the last two reactions the cross section values for neutron energies above 17 MeV may be too large due to this possible small contribution from the contaminating H^2(d, n)He^3 neutrons.

4. Results and Discussion

The cross section values reported below are generally in agreement in those cases where earlier results of others exist.

Si^{28}(n, p)Al^{28}

Successive irradiations were made in order to cover the range of neutron energies from 12.33 to 18.24 MeV. In fig. 4, the circles show the results. The only other absolute cross section value is plotted also. In this figure, the curve shows the theoretical relative cross section curve calculated by Cohen and White [3]). It is normalized to the present results at 13.5 MeV. They used level density data for the neighboring odd-mass nucleus Al^{27} in

their calculation. They imply that because of this approximation that the good fit to their data — and now the same remark applies to the present data — may only be fortuitous.

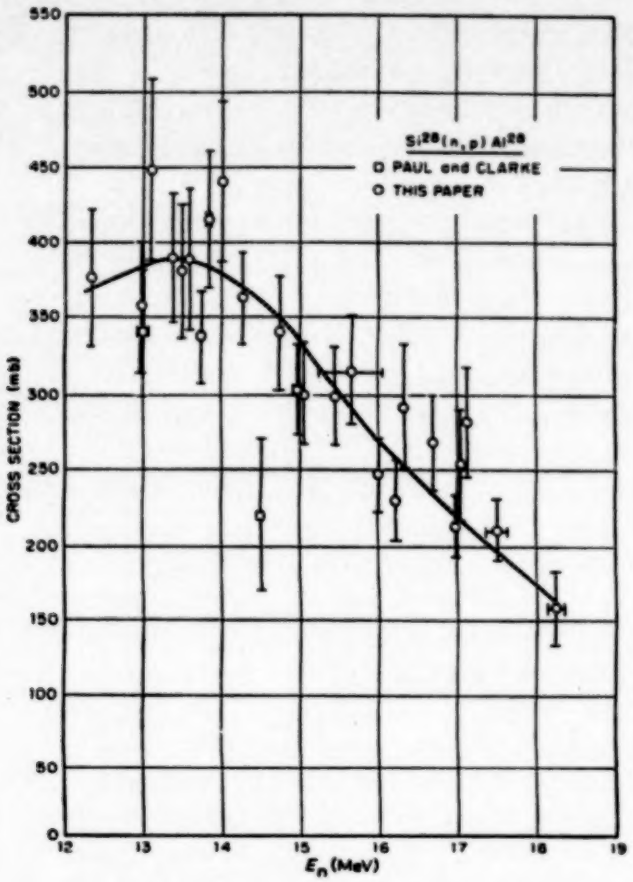

Fig. 4. Cross section for the $Si^{28}(n, p)Al^{28}$ reaction. The horizontal bars indicate the spread in neutron energy. □ is the datum from ref.[3]). The solid line is the theoretical relative excitation curve from ref.[3]), normalized to the present data.

$Cr^{53}(n, p)V^{53}$

Fig. 5 shows the cross section for the reaction for neutron energies from 12.33 to 18.24 MeV. A separate irradiation was made for each point. The only other existing value [2]) for this reaction is plotted also. The smooth curve is drawn to fit the data; there is not yet available a theoretical curve since level densities are not well known and there is a possible contribution of a direct interaction to the process.

$Al^{27}(n, \alpha)Na^{24}$

Several samples were irradiated at one time in order to cover the neutron energy interval from 13.0 to 15.7 MeV. A smooth curve has been drawn

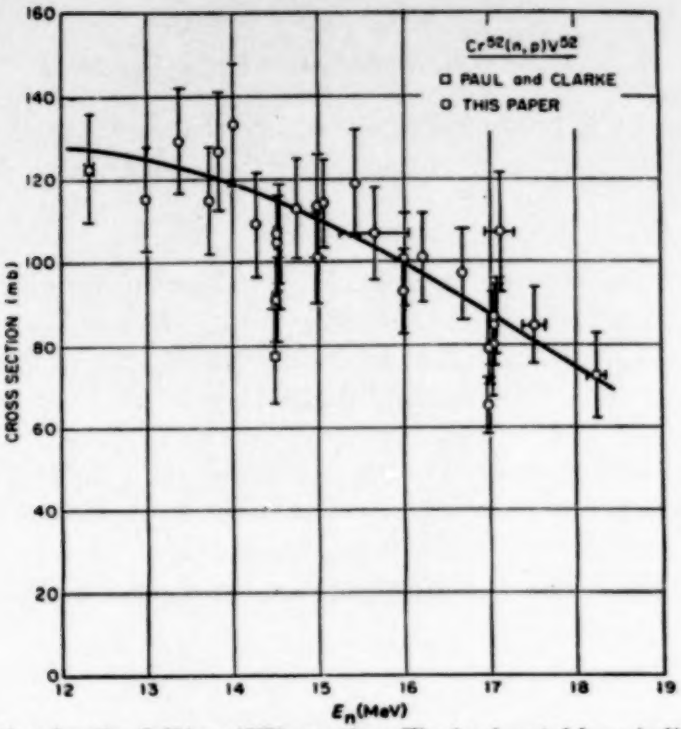

Fig. 5. Cross section for the $Cr^{52}(n, p)V^{52}$ reaction. The horizontal bars indicate the spread in neutron energy. □ is the datum from ref.[2]).

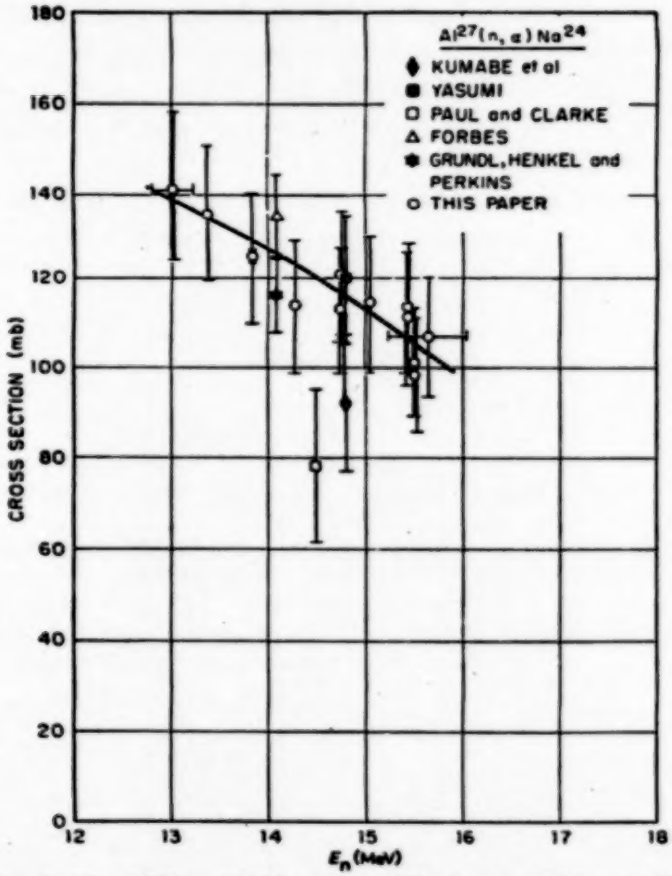

Fig. 6. Cross section for the $Al^{27}(n, \alpha)Na^{24}$ reaction. The horizontal bars indicate the spread in neutron energy. The symbols identify: ♦, ref.[8]); ■, ref.[5]); □, ref.[2]); △, ref.[1]); ✱, ref.[10]); and ○, the present results.

through the results as presented in fig. 6. The values obtained by Forbes [1], Paul and Clarke [2], Yasumi [5], and Kumabe *et al.*[6], are also plotted.

$Fe^{56}(n, p)Mn^{56}$

The cross section for this reaction was measured at only one neutron energy (15.27 ± 0.33 MeV) where the value is 131 ± 15 mb. The known experimental values are 124 ± 12 mb (at 14.1 MeV) [1], 96.7 ± 12 mb (at 14.5 MeV) [2] 144 ± 19 mb (at 14.0 MeV) [5], and 131 ± 15 mb (at 15.3 MeV) (present result). The relative excitation curve which was measured by Terrell and Holm [4] was used to determine the corresponding value at 14.3 MeV for each of the above values, and their average was found to be 127 mb. This average is 15.5 percent higher than the 110 mb value (an average of the first two) which was used by Terrell and Holm in the normalization of their excitation curve.

$Mg^{24}(n, p)Na^{24}$

The cross section was measured only at 13.03 ± 0.20 MeV, where the cross section value is 219 ± 26 mb. This sample was irradiated at the same time as the set of samples for the $Al^{27}(n, \alpha)Na^{24}$ reaction. Cohen and White [3] have obtained the excitation curve which they have normalized to a value at 14.5 MeV obtained by Paul and Clarke [2]. The present result agrees with their value of 220 mb at the corresponding point on their normalized curve.

The authors are indebted to W. M. Mallet and F. G. Watson for the operation of the Van de Graaff accelerator and to R. A. Taylor for valuable assistance with the pulse height analyzers and other electronic circuits.

References

1) S. G. Forbes, Phys. Rev. **88** (1952) 1309
2) E. B. Paul and R. L. Clarke, Can. J. Phys. **31** (1953) 267
3) A. V. Cohen and P. H. White, Nuclear Physics **1** (1956) 73
4) J. Terrell and D. M. Holm, Phys. Rev. **109** (1958) 2031
5) S. Yasumi, J. Phys. Soc. Japan **12** (1957) 443
6) I. Kumabe, E. Takehoshi, H. Ogata, Y. Tsuneoka and S. Oki, Phys. Rev. **106** (1957) 155
7) B. D. Kern and W. E. Kreger, Phys. Rev. (to be published)
8) S. J. Bame, Jr. and J. E. Perry, Jr., Phys. Rev. **107** (1957) 1616
9) J. B. Marion, R. M. Brugger and R. A. Chapman, Phys. Rev. **101** (1956) 247
10) J. A. Grundl, R. L. Henkel and B. L. Perkins, Phys. Rev. **109** (1958) 425

8.B *Nuclear Physics* **10** (1959) 235—243; © *North-Holland Publishing Co., Amsterdam*
Not to be reproduced by photoprint or microfilm without written permission from the publisher

CHARGE SYMMETRY PROPERTIES AND REPRESENTATIONS OF THE EXTENDED LORENTZ GROUP IN THE THEORY OF ELEMENTARY PARTICLES

V. I. OGIEVETSKY and CHOU KUANG-CHAO
Joint Institute of Nuclear Research, Dubna USSR

Received 17 July 1958

Abstract: The extended Lorentz group, which includes the complete Lorentz group and the charge conjugation operation, is considered. It is shown that use of irreducible projective representations of the extended group requires the existence of charge multiplets. Charge symmetry and pair production of strange particles follow from invariance under reflections and charge conjugation and from the laws of conservation of electric and baryon charges. The Pauli-Gürsey transformation is valid for free nucleons. The requirement of invariance under this transformation in the case of interaction also leads to isobaric invariance for all particles in strong interactions.

1. Introduction

As is well known, strongly interacting particles can be combined into charge multiplets (p, n; π^+, π^-, π^0; K^+, K^0 etc.). Particles belonging to a given multiplet have almost equal masses and the same spin, but possess different electric charges. The hypothesis of charge symmetry and the more stringent hypothesis of charge independence are then postulated in accord with experimental data. In the usual theory an expression of this fact is invariance under rotations in a certain formal isobaric space. Particles of a given multiplet are treated as states of a particle of a given isobaric spin, the isobaric spin projections of these states being different. The proton and neutron, for example, comprise the nucleon.

The nucleon can be described by the reducible 8-component representation of the complete Lorentz group. A similar situation (reducibility of the complete Lorentz group representation) also holds for other strongly interacting particles.

The following question now arises. If one requires that elementary particles be describable only by irreducible representations, will it then be possible to extend the Lorentz group in such a way, and find such irreducible representations of this extended group, as to lead automatically to the existence of charge multiplets and yield the charge symmetry properties? This problem is examined in the present paper.

The Lorentz group will be extended in the following way.

In quantum theory the wave functions are complex. The charge conjugation operation C which changes a particle into its antiparticle can always be represented as the product of a linear operator (matrix) and complex conjugation antilinear operator:

$$C: \quad \psi_C = C_0 \psi^*, \tag{1}$$

where C_0 is defined in such a way that ψ_C is transformed according to the same irreducible representation of the proper Lorentz group as ψ.

Besides the proper Lorentz group L, *space reflections* I, *and time reversal* T *we include in the extended group the charge conjugation operation* C.

Furthermore, along with the usual irreducible representations of the extended group we shall also consider its projective irreducible representations †.

The importance of utilization of projective representations of the complete Lorentz group has been pointed out by Gelfand and Tsetlin [1]) in connection with Lee and Yang's theory of parity doublets. The possibility of application of projective representations is connected with the uncertainty of the phase factor in the quantal wave function. After Gelfand and Tsetlin, projective representations of the complete Lorentz group were also considered by Taylor and McLennan [2]). A relation between these representations and isobaric invariance is indicated in Taylor's paper [2]). Only the complete Lorentz group was considered, and hence protons and neutrons and $\pi^{\pm}$ and π^0-mesons differ only with respect to space parity. The idea that new definitions of space-time reflections are required which would lead to charge symmetries was also expressed by Salam and Pais at the 7th Rochester Conference.

In the present paper we shall not attempt to study all the irreducible projective representations of the extended group and confine our attention to those which are required for description of strongly interacting particles. It will be shown that if nucleons, Ξ-particles and K-mesons are described by the unusual, projective representations of the extended group, and all other particles are described in the usual manner, then multiplicity, charge symmetry and pair production of strange particles follow from the standard laws of conservation of baryons, electric charge and invariance under the complete Lorentz group and charge conjugation.

In the present theory the Pauli-Gürsey transformation is assumed to

† If to each element g of group G there corresponds an operator $R(g)$ such that the product of the group elements is associated with the operator

$$R(g_1 g_2) = \alpha(g_1 g_2) R(g_1) R(g_2)$$

it will be said that a projective representation of group G is given. If $\alpha(g_1, g_2) \equiv 1$, the projective representation is of the usual type. In the projective representation anticommuting operators of the representation can be associated with the commuting group elements. In particular, the customary spinor representation is projective (operations γ_4 and $\gamma_4\gamma_5$ anticommute, whereas the space and time reflections commute).

hold for free nucleons and is related in a natural manner to isobaric invariance. The requirement that the interaction Lagrangian be also invariant under this transformation for nucleons leads to isobaric invariance in strong interactions between all types of particles.

It is not difficult to write down in this theory the interaction Lagrangian for electromagnetic fields with the aid of the charge operator. It is found that Schwinger time reversal is not valid for electromagnetic interactions and only Wigner time reversal holds.

Weak interactions in which also space parity is not conserved are more complicated and will not be considered in this article.

For the sake of concreteness we shall assume that the relative space parity of all baryons is the same and that reflection of the usual spinors is performed with the aid of operator γ_4. All bosons are assumed to be pseudoscalars. We start our discussion with nucleons.

2. Free Nucleon Field

If one demands for 4-component spinors that

$$I^2 = T^2 = C^2 = 1, \tag{2}$$

it can readily be shown that the operators I, T and C can be expressed as follows:

$$I: \quad \psi' = \gamma_4 \psi, \tag{3a}$$

$$T: \quad \psi' = i\gamma_4\gamma_5 \psi, \tag{3b}$$

$$C: \quad \psi_C = i\gamma_2 \psi^*, \tag{3c}$$

where T is the Schwinger spinor time reversal operation [3]) and matrices γ are expressed in the Pauli representation.

The following commutation relations hold for I, T and C:

$$IT = -TI, \tag{4a}$$

$$IC = -CI, \tag{4b}$$

$$TC = -CT. \tag{4c}$$

In contrast to the usual theory, in retaining relation (2) we require that relation (4a) change sign for nucleons, i.e., that the following condition be satisfied:

$$IT = TI, \quad \text{(a)}, \quad IC = -CI, \quad \text{(b)}, \quad TC = -CT, \quad \text{(c)}. \tag{4'}$$

Only 8×8 matrices satisfy commutation rules (2) and (4'):

$$\begin{aligned} I: &\quad \psi' = \tau_3 \times \gamma_4 \psi, \\ T: &\quad \psi' = 1 \times \gamma_4 \psi, \\ C: &\quad \psi_C = i\tau_3 \times \gamma_2 \psi^*, \end{aligned} \tag{5}$$

where τ is a Pauli matrix.

These operators together with the operators of the proper Lorentz group, in which γ_μ should everywhere be replaced by $1\times\gamma_\mu$, form a projective irreducible representation of the extended Lorentz group, the spinors ψ being 8-component.

In this representation the free field ψ has a uniquely defined Lagrangian †

$$L = \bar{\psi}(1\times\gamma_\mu\partial_\mu + i\tau_2\times\gamma_5 m)\psi, \tag{6}$$

where $\bar{\psi} = \psi^{*T} 1\times\gamma_4$ and the field equations have the form

$$1\times\gamma_\mu\partial_\mu\psi = -i\tau_2\times\gamma_5 m\psi. \tag{7}$$

Lagrangian (6) as well as equation (7) are invariant under two single-parameter transformation groups

$$\psi' = \exp(i\lambda)\psi, \tag{8}$$

$$\psi' = \exp(i\tau_1\times\gamma_5\lambda)\psi \tag{9}$$

and the three-parameter group

$$\psi' = a\psi + b\tau_3\times\gamma_5\psi_C, \tag{10}$$

where $|a|^2+|b|^2 = 1$.

Transformations (9) and (10) are similar to the Pauli transformations for the neutrino [4]) and differ from them only in that γ_5 is replaced by $\tau_1\times\gamma_5$ and $\tau_3\times\gamma_5$, respectively.

If we introduce the new 4-component spinors

$$\begin{aligned} \psi_p &= \frac{1}{\sqrt{2}}(\psi_1+\gamma_5\psi_2), & \psi_{p_c} &= \frac{1}{\sqrt{2}}(\psi_{C1}+\gamma_5\psi_{C2}), \\ \psi_{n_c} &= \frac{1}{\sqrt{2}}(-\gamma_5\psi_1+\psi_2), & \psi_n &= \frac{1}{\sqrt{2}}(\gamma_5\psi_{C1}-\psi_{C2}), \end{aligned} \tag{11}$$

they will be found to satisfy the familiar Dirac equation

$$\gamma_\mu\partial_\mu\psi = -m\psi \tag{12}$$

and under transformation (9)

$$\begin{aligned} \psi'_p &= \exp(i\lambda)\psi_p, & \psi'_n &= \exp(i\lambda)\psi_n, \\ \psi'_{p_c} &= \exp(-i\lambda)\psi_{p_c}, & \psi'_{n_c} &= \exp(-i\lambda)\psi_{n_c}. \end{aligned} \tag{13}$$

Thus (9) can be regarded as a gauge transformation related to the law of conservation of baryons, and ψ_p, ψ_n, ψ_{p_c} and ψ_{n_c} refer to the proton, neutron, antiproton and antineutron fields respectively.

The transformation

$$\mathrm{E}: \quad \psi' = \exp[\tfrac{1}{2}i(1\times 1+\tau_1\times\gamma_5)\lambda]\psi \tag{14}$$

should be related to the law of conservation of electric charge.

† According to Schwinger, under time reversal one has $L \to L^T$, where the transposition sign refers to Hilbert space operators [3]).

Indeed, under transformation E

$$\text{E:}\quad \begin{aligned} \psi'_{\mathrm{p}} &= \exp(i\lambda)\psi_{\mathrm{p}}, & \psi'_{\mathrm{p_c}} &= \exp(-i\lambda)\psi_{\mathrm{p_c}}, \\ \psi'_{\mathrm{n}} &= \psi_{\mathrm{n}}, & \psi'_{\mathrm{n_c}} &= \psi_{\mathrm{n_c}}. \end{aligned} \tag{15}$$

The three-parameter transformation (10) is isomorphic with rotation in isobaric space. Indeed, if we form the usually employed 8-component nucleon field $\psi_{\mathrm{N}} = \binom{\psi_{\mathrm{p}}}{\psi_{\mathrm{n}}}$ we obtain under transformation (10)

$$\psi'_{\mathrm{N}} = \exp[i(\boldsymbol{\tau}\cdot\boldsymbol{\lambda})]\psi_{\mathrm{N}} \tag{16}$$

where $\boldsymbol{\lambda}$ is a vector possessing the real components $\lambda_1, \lambda_2, \lambda_3$ and the τ are the usual two-dimensional Pauli matrices and

$$a = \cos|\boldsymbol{\lambda}| + \frac{i\lambda_3}{|\boldsymbol{\lambda}|}\sin|\boldsymbol{\lambda}|, \qquad b = \frac{\sin|\boldsymbol{\lambda}|}{|\boldsymbol{\lambda}|}(\lambda_2 - i\lambda_1). \tag{17}$$

Gürsey [5]) has pointed out that an analogous isomorphism appears when the number of components is formally doubled.

3. Interaction Between Nucleons and Ordinary Bosons

Consider first the interaction between nucleons and a neutral pseudoscalar field φ_0 with positive time parity

$$\text{I:}\quad \varphi'_0 = -\varphi_0, \qquad \text{T:}\quad \varphi'_0 = \varphi_0, \qquad \text{C:}\quad \varphi_{0\mathrm{C}} = \varphi_0. \tag{18}$$

The condition of invariance under I, T and C and transformations (9) and E uniquely yields the interaction Lagrangian (in the following only the interaction Lagrangian without derivatives will be considered)

$$\begin{aligned} L &= ig_0\bar{\psi}\tau_3 \times \gamma_5\psi\varphi_0 \\ &= ig_0(\bar{\psi}_{\mathrm{p}}\gamma_5\psi_{\mathrm{p}} - \bar{\psi}_{\mathrm{n}}\gamma_5\psi_{\mathrm{n}})\varphi_0 \\ &= ig_0(\bar{\psi}_{\mathrm{N}}\gamma_5\tau_3\psi_{\mathrm{N}}\varphi_0), \end{aligned} \tag{19}$$

i.e., the meson-proton and meson-neutron coupling constants have different signs and hence φ_0 can be assigned to a neutral π^0-meson.

If the neutral meson φ'_0 were a space pseudoscalar but would possess a negative time parity, the interaction Lagrangian

$$\begin{aligned} L &= g'_0\bar{\psi}\tau_2 \times 1\psi\varphi'_0 \\ &= ig'_0(\bar{\psi}_{\mathrm{p}}\gamma_5\psi_{\mathrm{p}} + \bar{\psi}_{\mathrm{n}}\gamma_5\psi_{\mathrm{n}})\varphi'_0, \end{aligned} \tag{20}$$

which can be ascribed to the questionable ρ_0-meson, would follow in a unique manner.

For the interaction Lagrangian between nucleons and a charged pseudoscalar boson field φ

$$\text{I:}\quad \varphi' = -\varphi; \qquad \text{T:}\quad \varphi' = \varphi; \qquad \text{C:}\quad \varphi_{\mathrm{C}} = \varphi^*$$

and we again uniquely obtain

$$\begin{aligned} L &= ig(\bar{\psi}\psi_C\varphi^* - \bar{\psi}_C\psi\varphi) \\ &= 2ig(\bar{\psi}_p\gamma_5\psi_n\varphi^* + \bar{\psi}_n\gamma_5\psi_p\varphi). \end{aligned} \tag{21}$$

Thus it may be considered that $\varphi(\varphi^*)$ refers to $\pi^-(\pi^+)$ mesons.

Charge symmetry (i.e., the possibility of simultaneously making the substitutions $\psi_p \rightleftarrows \psi_n$, $\pi^+ \rightleftarrows \pi^-$, $\pi^0 \rightleftarrows -\pi^0$) of interactions (19) and (21) is evident. The general Lagrangian for interaction with π-mesons has the form

$$\begin{aligned} L &= ig_0(\bar{\psi}_p\gamma_5\psi_p - \bar{\psi}_n\gamma_5\psi_n) \\ &+ 2ig(\bar{\psi}_p\gamma_5\psi_n\pi^+ + \bar{\psi}_n\gamma_5\psi_p\pi^-). \end{aligned} \tag{22}$$

If we now require that not only the free nucleon Lagrangian but also the nucleon interaction Lagrangian be invariant under transformations of the three-parameter group we find

$$g = g_0/\sqrt{2} = g_\pi/\sqrt{2}$$

and

$$L_\pi = ig_\pi\bar{\psi}_N\gamma_5(\tau\cdot\pi)\psi_N. \tag{23}$$

Under transformation (10) the meson fields transform as follows:

$$(\tau\cdot\pi)' = \exp[i(\tau\cdot\lambda)](\tau\cdot\pi)\exp[-i(\tau\cdot\lambda)]. \tag{24}$$

The π^+, π^- and π^0-meson masses should be the same in this case.

We have thus arrived at the usual isobarically invariant theory of interaction between π-mesons and nucleons.

4. Free K-Mesons

For bosons the usual representation of the extended Lorentz group encompasses only π-mesons. We shall describe K-mesons by the projective representation in which

$$\begin{aligned} &I^2 = 1, \qquad T^2 = -1, \qquad C^2 = 1, \\ &IT = +TI, \qquad IC = +CI, \qquad TC = +CT. \end{aligned} \tag{25}$$

The simplest irreducible representation in which these commutation rules are valid is a two-dimensional one: $\varphi = \binom{\varphi_1}{\varphi_2}$ and the operators I, T and C have the form

$$I:\ \varphi' = -\varphi, \qquad T:\ \varphi' = i\tau_2\varphi, \qquad C:\ \varphi_C = \varphi^*. \tag{26}$$

Let us identify the K^+-meson with φ_1, the $\tilde{K}^0$-meson with φ_2, K^--meson with φ_1^*, and K^0-meson with φ_2^*.

We can then relate the law of conservation of electric charge to the transformation

$$E:\ \varphi' = \exp[\tfrac{1}{2}i(1+\tau_3)\lambda]\varphi. \tag{27}$$

Indeed, under this transformation

$$\begin{aligned} K^{+\prime} &= \exp(i\lambda)K^{+}, & K^{-\prime} &= \exp(-i\lambda)K^{-}, \\ K^{0\prime} &= K^{0}, & \tilde{K}^{0\prime} &= \tilde{K}^{0}. \end{aligned} \tag{28}$$

The transformation $\varphi' = \exp(i\tau_3\lambda)\varphi$ for which

$$\begin{aligned} K^{+\prime} &= \exp(i\lambda)K^{+}, & K^{0\prime} &= \exp(i\lambda)K^{0}, \\ K^{-1} &= \exp(-i\lambda)K^{-}, & \tilde{K}^{0\prime} &= \exp(-i\lambda)\tilde{K}^{0}, \end{aligned} \tag{29}$$

corresponds to the law of conservation of hypercharge.

5. K-Meson-Nucleon Interaction. Λ and Σ Particles

We now pass to a study of the interaction between K-mesons and nucleons. Since K-mesons as well as nucleons transform according to the projective representation of the extended Lorentz group and the law of conservation of baryon charge is valid, one other baryon describable by the usual representation should necessarily be involved in the interaction. This condition inevitably leads to pair production of strange particles.

We shall first consider the case of a neutral baryon. As mentioned above, for the sake of definiteness the relative space parity of all baryons is assumed to be the same:

$$\text{I:} \quad Y'_0 = \gamma_4 Y_0. \tag{30}$$

Under the T transformation for nucleons two possibilities exist for the investigated baryon:

$$\text{T:} \quad Y'_0 = -\gamma_4\gamma_5 Y_{0_c}, \tag{31}$$

$$Y'_0 = \gamma_4\gamma_5 Y_{0_c}. \tag{32}$$

The antibaryon Y_{0_c} should be introduced in equations (31) and (32), as transformation T for nucleons anticommutes with the transformation of conservation of baryon charge (9).

If the law (31) is chosen for T, it will be found that the only type of Lagrangian consistent with invariance under the extended Lorentz group is

$$\begin{aligned} L = ig[&\bar{\psi}(1\times\gamma_5-\tau_1\times 1)(1\times 1+\tau_3\times 1)\varphi\times Y_0 \\ &-\bar{\psi}_C(1\times\gamma_5+\tau_1\times 1)(1\times 1-\tau_3\times 1)\varphi^*\times Y_0] + \text{Herm. conj.} \end{aligned} \tag{33}$$

Changing from ψ and φ to the nucleon field and K-meson field operators we obtain the familiar nucleon-Λ_0 particle interaction Lagrangian

$$L = ig_\Lambda(\bar{p}\gamma_5\Lambda_0 K^{+} + \bar{n}\gamma_5\Lambda_0 K^{0}) + \text{Herm. conj.} \tag{34}$$

The law (32) for T yields a Lagrangian which differs from expression (33) only in sign between the two terms in expression (33) and corresponds to the Σ_0-particle:

$$L = ig_{\Sigma_0}(\bar{p}\gamma_5\Sigma_0 K^{+} - \bar{n}\gamma_5\Sigma_0 K^{0}) + \text{Herm. conj.} \tag{35}$$

We thus arrive at the conclusion that under transformation T for nucleons the transformations for Λ_0 and Σ_0 differ only by sign. Considering now the interaction between nucleons and charged baryons we find it possible to set up a Lagrangian which is invariant under charge conjugation, space and time reflections and the laws of conservation of electric and baryon charges only if

$$\mathrm{T}: \begin{matrix} \Sigma^+ \to -\gamma_4\gamma_5\Sigma_C^-, \\ \Sigma^- \to -\gamma_4\gamma_5\Sigma_C^+, \end{matrix} \tag{36}$$

which implies equality of the Σ^+ and Σ^- particle masses. The Lagrangian has the form

$$\begin{aligned} L = -ig[&\bar{\psi}(1\times 1-\tau_1\times\gamma_5)(1\times 1-\tau_3\times 1)\varphi^*\times\Sigma^+ \\ &+\bar{\psi}_C(1\times 1+\tau_1\times\gamma_5)(1\times 1+\tau_3\times 1)\varphi\times\Sigma^-]+\text{Herm. conj.} \end{aligned} \tag{37}$$

In the usual notation it can be represented as follows:

$$L = ig_{\Sigma}\pm(\bar{p}\gamma_5\Sigma^+K^0+\bar{n}\gamma_5\Sigma^-K^+)+\textit{Herm. conj.} \tag{38}$$

Charge symmetry is evident.

If we furthermore require that a transformation of the Pauli-Gürsey type (10) also leave the interaction Lagrangian invariant, we get

$$g_{\Sigma^\pm} = \sqrt{2}\, g_{\Sigma_0} = \sqrt{2}\, g_{\Sigma}, \tag{39}$$

where the Σ^+, Σ^- and Σ_0 masses should be equal and the usual isobarically invariant Lagrangian

$$\begin{aligned} L = ig_{\Sigma}(&\bar{p}\gamma_5\Sigma_0K^+-\bar{n}\gamma_5\Sigma_0K^0 \\ &+\sqrt{2}\,\bar{p}\gamma_5\Sigma^+K^0+\sqrt{2}\,\bar{n}\gamma_5\Sigma^-K^+)+\text{Herm. conj.} \end{aligned} \tag{40}$$

obtains.

6. Ξ-particles

The ideas presented above admit of one other possibility. Thus, retaining the same transformation (9) for the law of conservation of baryons one can, in the projective representation (5), change, in transformation (14) which is related to the law of conservation of electric charge, the sign between 1×1 and $\tau_1\times\gamma_5$:

$$\mathrm{E}: \quad \psi' = \exp\left[\tfrac{1}{2}i(1\times 1-\tau_1\times\gamma_5)\right]\psi. \tag{41}$$

In this case one should simply replace in all formulas p by Ξ^0, n by Ξ^-, K^+ by $K^-{}_0$, K^0 by K^-. We again obtain charge symmetry properties and the requirement of invariance under Pauli-Gürsey transformations in interaction again leads to the usual isobarically invariant Lagrangians.

7. Conclusion

The plan set out at the beginning of this paper has been carried out. By introducing a new irreducible projective representation of the extended Lorentz group for nucleons and proceeding from this new representation we have been able to demonstrate that the charge symmetry properties, pair production of strong particles and multiplicity follow from the standard conservation laws whereas isobaric invariance follows from a transformation of the Pauli-Gürsey type for free nucleons. This type of invariance can be incorporated in the theory as the number of components of the wave functions which transform in accord with the irreducible representations is necessarily larger.

Weak interactions have not been studied from this viewpoint in the present paper. This is a more difficult problem and less unambiguous owing to violation of space parity.

The authors are sincerely thankful to Prof. I. M. Gelfand for valuable discussions.

References

1) I. M. Gelfand and M. L. Tsetlin, JETP **31** (1956) 1107
2) I. C. Taylor, Nuclear Physics **3** (1957) 606;
J. A. McLennan Jr., Phys. Rev. **109** (1958) 986
3) J. Schwinger, Phys. Rev. **91** (1953) 713
4) W. Pauli, Nuovo Cimento **6** (1957) 204
5) F. Gürsey, Nuovo Cimento **7** (1958) 411

9.B *Nuclear Physics* **10** (1959) 244—255; ©*North-Holland Publishing Co., Amsterdam*
Not to be reproduced by photoprint or microfilm without written permission from the publisher

SCATTERING OF μ-MESONS IN LEAD

A. I. ALIKHANIAN and F. R. ARUTYUNIAN
Physical Institute of the Academy of Sciences of Armenian S.S.R., Erevan

Received 1 September 1958

Abstract: Scattering of μ-mesons with momenta between 1.0 and 1.8×10^9 eV/c has been studied in 7 mm lead plates. The experimental angular distribution is compared with the theoretical curve for multiple scattering which takes into account the finite dimensions of the nucleus. It is shown that after introduction of all relevant corrections the experimental data satisfactorily agree with the calculations.

1. Introduction

In recent years it has been demonstrated by a number of authors that scattering of μ-mesons with momenta above 100 MeV/c does not agree with the angular distribution expected in the case of a pure Coulomb interaction between the μ-mesons and nuclei. Whittmore and Shutt [1]) who investigated scattering of μ-mesons with momenta between 0.3 and 3.1 GeV/c in a 5 mm lead plate located in a cloud chamber found that large angle scattering exceeds that predicted by Olberts theory for nuclei of finite dimensions. Surplus scattering of μ-mesons in 2 cm thick lead plates was also detected in the experiments of George, Redding and Trent [3]) carried out at a depth of 60 m water equivalent. The excess was especially pronounced at angles larger than 15°. According to the data of the aforementioned authors in the 100—300 MeV energy range the surplus scattering effective cross section is of the order of 4×10^{-27} cm^2 nucleon^{-1}.

McDiarmid [4]) working with a cloud chamber at a depth of 26 m water equivalent found that scattering in lead of μ-meson with momenta of 200—600 MeV/c agrees with the scattering theory whereas for mesons with momenta 500—1700 MeV/c the experimental data referring to angles larger than 4° significantly exceeds the number of scattering events predicted by the theory which takes into account the finite nuclear dimensions. Leontić and Wolfendale [5]) also detected a surplus number of μ-mesons scattered in lead with momenta above 285 MeV/c.

The discrepancy between the observed angular distribution of scattered μ-mesons and the theoretical distribution computed under the assumption of Coulomb scattering by nuclei of finite size has been called "anomalous scattering of μ-mesons".

In all the investigations mentioned above scattering was investigated in plates of considerable thickness in which a significant part of the mesons experienced multiple or plural scattering. Pure single scattering of μ-mesons with momenta of 100—600 MeV/c has been investigated by Kannangara and Shrikantia [6]) in photographic emulsions irradiated under a layer of earth of 60 metres water equivalent. The effective cross section for anomalous scattering derived from these measurements was $\sigma_{\text{anom.}} = (1.5 \pm 1.0) \times 10^{-27}$ cm nucleon^{-1}. Alikhanov and Eliseyev [7]) obtained a transverse cross section for anomalous scattering of the same order of magnitude. These authors studied scattering of μ-mesons with momenta between 200 and 800 MeV/c in graphite.

Alikhanian and Kirillov-Ugriumov [8]) investigated slow μ-meson scattering in thin copper plates in a narrow momentum interval from 80 to 140 MeV/c and found some surplus scattering at angles with projections exceeding 15°. Since the number of observed events was small no final conclusion concerning the existence of anomalous scattering in this energy range could be drawn.

The problem of anomalous scattering of μ-mesons is of paramount importance for the theory of elementary particles. However, the assumption of anomalous scattering of μ-meson leads to some irreconcilable contradictions with the well known properties of μ-mesons. As an example one might mention the fact that the mesoatomic X-ray spectra prove with a large degree of probability that no appreciable non-Coulomb forces exist between slow μ-mesons and nucleons.

The experimentally observed anomalous scattering of μ-mesons cannot be ascribed to non-coherent scattering involving excitation of the nuclei. Attempts to ascribe surplus scattering to the anomalous magnetic moment of the μ-meson and nucleon have also been unsuccessful.

In the present paper we present some results of an experimental investigation of scattering of μ-mesons with momenta $(1.0—1.8) \times 10^8$ eV/c in lead plates. In order to establish the existence of surplus scattering of μ-mesons on heavy nuclei a knowledge of the exact model of the nucleus is required. Experiments on scattering of fast electrons [9,10]) have been employed to determine directly from experiment the nuclear form factor for various nuclei, including that of lead.

Curves for multiple scattering on nuclei of finite dimensions have recently been computed by M. L. Ter-Mikayelian [11]) who used for this purpose the experimental values of the nuclear form factor.

Experimental data obtained in the present paper on the angular distribution of μ-mesons scattered in lead are compared with the curves for μ-mesons of various momenta computed by M. L. Ter-Mikayelian.

2. Experimental Part

Investigation of μ-meson scattering was carried out at the high altitude cosmic ray station on the Alagez mountain (3200 m above sea level) with help of a magnetic mass spectrometer in conjunction with two multiplate cloud chambers. A detailed description of the apparatus is given in ref.[12, 13]).

Particle trajectories satisfying the conditions described in ref.[8, 13]) were selected.

In the present paper we present data referring to scattering of μ-mesons of the cosmic radiation in 7 mm lead plates.

2.1. PARTICLE IDENTIFICATION

Measurement of the particle masses in the mass-spectrometer was based on momentum and range determinations.

The particle momentum was derived from the curvature of the trajectory in the magnetic field and the range from the amount of matter traversed by the particle in the chamber up to the point of stoppage. It should be mentioned that the particle range was determined with account of the entrance angle of the particles in the scattering plate and of the systematic increase of the path length as a result of multiple Coulomb scattering [14]).

812 particles with measured masses lying between 150—360 m_e were employed. The experimental mass distribution can be satisfactorily approximated by two normal distribution curves with half widths corresponding to a mean square error of 10 %.

If one assumes that all particles with measured masses smaller than $240m_e$ are μ-mesons and that particles with masses above 250 m_e are π-mesons, then the mean value of the μ-meson mass turns out to be 209 m_e and that of the π-meson 278 m_e.

An analysis of this mass spectrum with account of efficiency of the apparatus shows that not more than 2 % of π-mesons could have been included in the μ-meson group and conversely not more than 12 % of μ-mesons could have been included in the π-meson group.

The mass spectrum obtained with 5 mm and 2 mm copper plates in the chamber are given in ref. [8]). π-mesons were much more distinctly separated from μ-mesons in this case.

2.2. ANGLE MEASUREMENTS

The scattering angles in the plates were determined from the photographs with the help of a special angle measuring device and the mean value of a large number of measurements was accepted. The precision of the angle measurements is chiefly restricted by distortions in the cloud chamber (diffuseness of the particle tracks, turbulent eddies, etc.). These factors yield a mean square error in the angle of 0.6°. The magnitude of this error is the

same throughout the angle range and hence the relative error drops with increase of the angle.

The theory of multiple Coulomb scattering of charged particles usually refers to projections of the scattering angles on a plane passing through the initial trajectory. In the general case the projection of the scattering angle on the plane of the photograph differs from the projection on a plane passing through the initial trajectory; these angle projections are equal only if the trajectory prior to scattering is parallel to the photograph plane.

However, the original trajectory forms with the photograph plane some angle γ, which depends on scattering of the particle in the preceding plate and this circumstance leads to the result that the angle measured on the photograph is larger than the projection of the scattering angle on a plane passing through the original trajectory. Moreover, if the particle passes near the wall of the chamber at a sufficiently large distance from the optical axis of the photographic objective (compared with the distance between the objective and point of scattering within the chamber), then a change in the scattering angles is observed which is due to the fact that a non-orthogonal projection of the scattering angle is recorded on the photographic film. Depending on the orientation of the trajectory within the chamber this circumstance may either lead to a decrease or increase of the true scattering angle. M. I. Daion was the first to note this point.

The aforementioned discrepancy between the angles holds for trajectories of those mesons which enter the lateral parts of the chamber due to the large curvature of the trajectories in the magnetic field and which are moreover scattered in the plates through relatively large angles. The spatial pattern, i.e., the points of intersection of the trajectories with the plates was determined with the aid of a stereo-comparator for each angle separately if the meson scattering angle exceeded 20°. Knowing these intersection points one can determine the true scattering angle projection with the help of simple geometrical relations.

From the distribution of the angle difference $\Delta\theta_\varphi = \theta'_\varphi - \theta_\varphi$ (where θ'_φ is the true scattering angle projection and θ_φ is the angle directly measured on the photograph) the systematic increment of the angles directly measured on the photographs was determined and found to be 0.45°. Corrections of this magnitude were applied to all angles smaller than 20°.

2.3. MEASUREMENT OF MOMENTUM AT THE SCATTERING POINT

In order to compare the observed scattering angle with the expected one the particle momentum at the scattering point must be known. If the mass of the particle is known the momentum can be found in two ways:

1) From the residual range after scattering. The range is assumed to equal the amount of matter traversed by the particle from the centre of the

scattering plate up to the centre of the plate in which the particle is stopped.

2) From the momentum measured in the magnetic field and from the amount of matter traversed by the particle up to the point at which it is scattered.

If we denote the number of the plate in which the particle is stopped by $i = 0$ and the remaining plates are successively denoted by $i = 1, 2, 3, \ldots$ etc., we find the values of the mean momenta for plates of a same number i, as determined by each of the methods, satisfactorily agree with each other (to within 2—3 %).

The multiple Coulomb scattering distribution function was derived under the assumption that the momentum losses in the scattering plate could be neglected. However, calculations show that account of the momentum loss in the scattering plates leads to some broadening of the multiple Coulomb scattering curve. This broadening depends on the plate number i and for $i > 1$ does not exceed 5 % (depending on the location of the point at which the particle is stopped in plate $i = 0$); for $i = 1$ it varies between 5 % and ∞ and therefore scattering in plates $i = 1$ was not studied.

The residual range after scattering can therefore be determined with a maximum error $\Delta R = \frac{1}{2}t$, where t is the thickness of plate $i = 0$. A finite momentum value Δp corresponds to this ΔR and should be taken into account in plotting the scattering curves.

The corresponding corrections to the multiple Coulomb scattering curves plotted on the basis of the mean value of the momentum P_m were applied; these corrections account for uncertainty in the momentum measurements. For large scattering angles these corrections may be as high as 30—40 %.

2.4. SUBSTANCE AND THICKNESS OF THE SCATTERING PLATES

The lead plates in which the scattering occurred contained impurities which were taken into account in our calculations of the mean square scattering angle and distribution function. Thus, for example, in the presence of 7 % of antimony in the lead plates the mean square scattering angle is 1.5 % smaller than the angle computed for pure lead. The particle tracks in the cloud chamber form various angles with the normal to the scattering plates, firstly, because they enter the chamber at various angles and, secondly, because of their scattering in the plates. Thus, in essence, we are dealing not with a constant thickness, but with a certain distribution of thicknesses of the scattering plates which must be taken into account.

Suppose that for a given scattering angle θ_φ and particle momentum p there are various probabilities of observation of angle θ_φ : $f_{t_1}(\theta_\varphi)$, $f_{t_2}(\theta_\varphi)$, $\ldots$ $f_{t_k}(\theta_\varphi)$, which correspond to the various scattering plate thicknesses $t_1, t_2, \ldots, t_k$ encountered respectively with frequencies $n_{t_1}, n_{t_2}, \ldots, n_{t_k}$. Let us choose an effective thickness of the scattering plate, $t_{eff.}$ such that the

relation

$$f_{t_{\text{eff}}}(\theta_\varphi) = \frac{\sum_{i=1}^{k} n_{t_i} f_{t_i}(\theta_\varphi)}{\sum_{i=1}^{k} n_{t_i}} \tag{1}$$

be valid throughout the whole range of investigated angles. This $t_{\text{eff.}}$ (for 7 mm Pb plates) was found to equal the mean square thickness value calculated from the experimental thickness distribution and was 9 % larger than the geometrical thickness of the plates.

2.5. CORRECTION FOR GEOMETRY OF THE APPARATUS

The arrangement employed by us restricted the space in which the particle scattering could be measured. We denote by θ_φ the scattering angle projection on the plane in which the scattering is investigated and by θ_ψ the scattering angle projection on a plane perpendicular to the plane of investigation.

A consequence of this limitation of the investigation plane imposed by the geometry is that the probability of recording various scattering angles is different. This point was also noted by McDiarmid [4]) and recently by Cousins *et al.* [15]). The limitation imposed by the geometry in the plane perpendicular to the plane of investigation of scattering leads to a similar result but in this case the result depends on the scattering angle distribution function. Indeed, registration of scattered particles possessing an angle projection θ_φ will depend on the corresponding angle θ_ψ and hence the observed distribution of angles θ_φ will depend on the allowed distribution of angles θ_ψ. The effect of the apparatus geometry thus reduces to the necessity of introduction of a correction function $C(\theta_\varphi)$ which consists of two parts: $C_1(\theta_\varphi)$ and $C_2(\theta_\varphi)$; $C_1(\theta_\varphi)$ being the correction which accounts for the geometry of the apparatus in the plane of investigation of scattering and yields the probability that the scattering angle θ_φ will be observed, providing that the geometry does not impose any restrictions in the perpendicular plane.

If a particle impinges on scattering plate i at an angle γ with respect to its normal and at a distance εl from one end of the chamber (l being the length of the illuminated part of the chamber in the plane of the photograph; in the general case it is simply the length of the chamber) and if the particle is then scattered through an angle θ_φ, there will always exist a length b in plate $i+1$ such that if the particle is incident within the limits of this length it will remain within the illuminated part of the chamber at the $i-1^{\text{th}}$ plate.

If, furthermore, $\zeta(\gamma)\mathrm{d}\gamma$ is the angular distribution of the incident particles above the scattering plate one can easily prove from simple geometrical

considerations that the total relative probability for observation of angle θ_φ is

$$P(\theta_\varphi) = \int_{\varepsilon=0}^{1} \left\{ 1-\varepsilon - \frac{\varepsilon - \frac{1}{n}\operatorname{tg}\theta_\varphi}{1+n\operatorname{tg}\theta_\varphi} \right\} \frac{n\zeta[\operatorname{arctg}(n\varepsilon)-\theta_\varphi]}{[1+(n\varepsilon)^2]}\, d\varepsilon \qquad (2)$$

where $n = l/a$ (a is the distance between the plates). The correction function $C_1(\theta_\varphi)$ is thus

$$C_1(\theta_\varphi) = P(\theta_\varphi)/P(0). \qquad (3)$$

It is very difficult to obtain the exact angular distribution of the incident particles in our apparatus and hence for calculation of $C_1(\theta_\varphi)$ we have employed the experimental angular distributions of the incident particles. The function $C_1(\theta_\varphi)$ was determined by numerical integration of expression (2).

A consequence of the difference between the angular distributions of particles incident on plates of different values of i (the angular distributions moreover being different for μ- and π-mesons) is that the function $C_1(\theta_\varphi)$

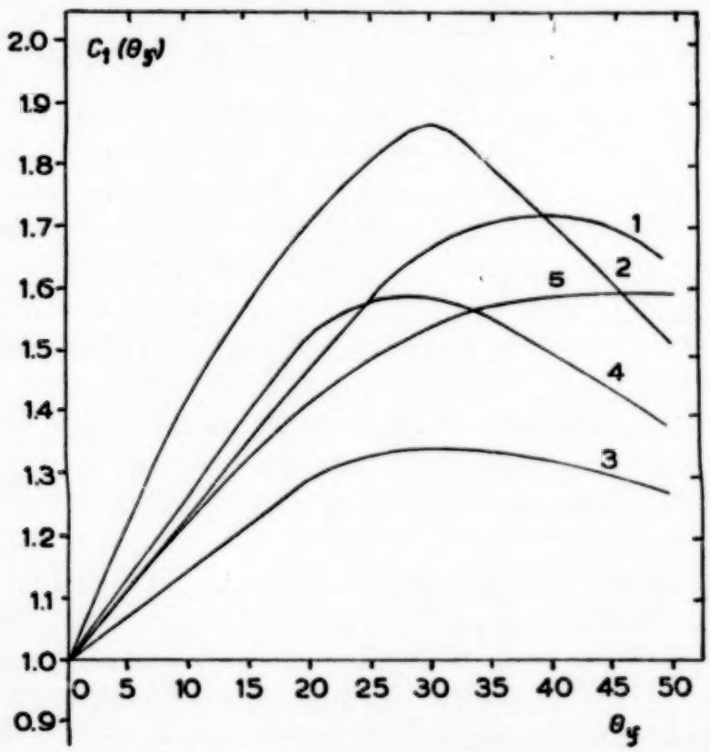

Fig. 1. Correction function.

1. μ-mesons in $(1.0-1.4)\times 10^9$ eV/c momentum range in 7 mm lead plates.
2. The same in the $(1.4-1.8)\times 10^9$ eV/c momentum range.
3. π-meson in $(1.2-1.6)\times 10^9$ eV/c momentum range in 7 mm lead plates.
4. The same in the $(1.6-2.0)\times 10^9$ eV/c momentum range.
5. $C_1(\theta_\varphi)$ under the assumption $\zeta(\gamma)d\gamma = \cos^2\gamma d\gamma$.

is not the same for μ- and π-mesons in various momentum intervals. The function $C_1(\theta_\varphi)$ for μ- and π-mesons scattered in 7 mm lead particles is represented in fig. 1. It is also depicted in the same fig. for the case when $\zeta(\gamma)\mathrm{d}\gamma = \cos^2\gamma\mathrm{d}\gamma$.

As to $C_2(\theta_\varphi)$, it is the correction function to account for the geometry of the experimental arrangement in the plane perpendicular to the plane of investigation. The multiple Coulomb scattering curve for a finite nucleus can be approximated with a high degree of accuracy by a normal distribution curve; it can readily be shown that $C_2(\theta_\varphi)$ is independent of the angle θ_φ, that is, that the probability of registration of different angles is the same. Thus, in order to compare the multiple Coulomb scattering curves with the experimental data it is only necessary to apply the correction function $C_1(\theta_\varphi)$.

3. Experimental Results and Discussion

Altogether 2337 μ-meson scattering events and 818 π-meson scattering events in 7 mm lead plates were investigated. The total μ-meson range in lead in the momentum interval $p = (1.0-1.8)\times 10^8$ eV/c was 19 m, and the total π-meson range in the $p = (1.2-2.0)\times 10^8$ eV/c interval was 6.7 m.

The experimental μ- and π-meson scattering data in 7 mm lead plates were compared with the multiple Coulomb scattering curves for point [16,17]) and extended nuclei [11]). The multiple Coulomb scattering curves for finite nuclei have been calculated by M. L. Ter-Mikayelian who used for this purpose experimental data on scattering of fast electrons by nuclei.

In order to compare the experimental results with the theoretical scattering curves all the corrections mentioned in section 2 were introduced. These corrections depend mainly on the number of the plate in which the scattering is investigated, that is, on the momentum at the scattering point and therefore the whole investigated momentum interval was divided into groups each with a momentum width of 0.2×10^8 eV/c. After application of the corresponding corrections, scattering curves for μ- and π-mesons were plotted for each group separately.

The total μ- and π-meson scattering curves in lead for all groups are represented in figs. 2 and 3. The dimensionless quantity φ is plotted along the abscissa axis; φ is defined by the relation

$$\varphi = \theta_\varphi/\chi_c B^{\frac{1}{2}}$$

where θ_φ is the projection of the scattering angle in degrees and $\chi_c B^{\frac{1}{2}}$ is a characteristic multiple Coulomb scattering angle [11]). An advantage of plotting the scattering curves in units of φ is the possibility of uniting scattering data referring to various momentum intervals and various thicknesses of the scattering plates.

The errors in figs. 2 and 3 are composed of statistical errors and of errors involved in determination of correction function $C_1(\theta_\varphi)$ inasmuch as the values of $C_1(\theta_\varphi)$ are derived from the experimental angular distributions of

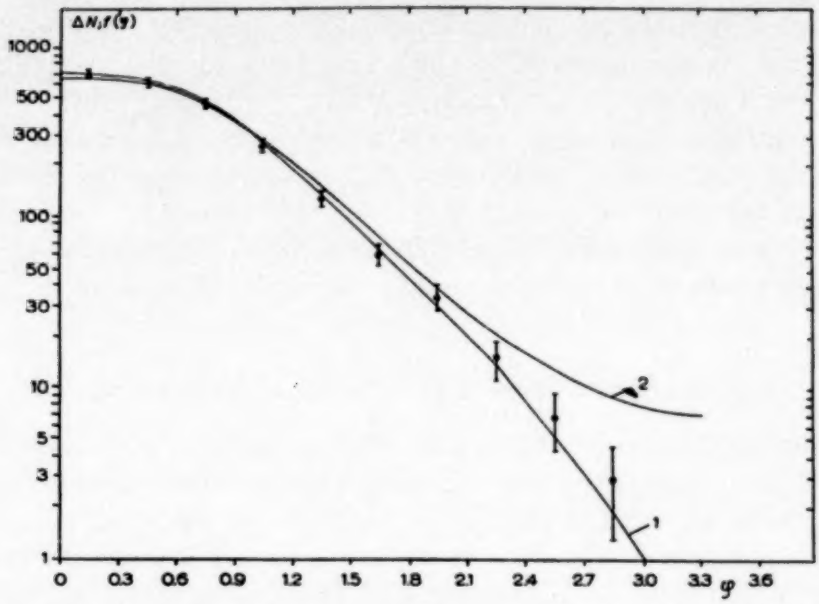

Fig. 2. Differential distribution of μ-meson scattering angle projections in 7 mm lead plates. Curves (1) and (2) are multiple Coulomb scattering curves for an extended and point nuclei respectively.

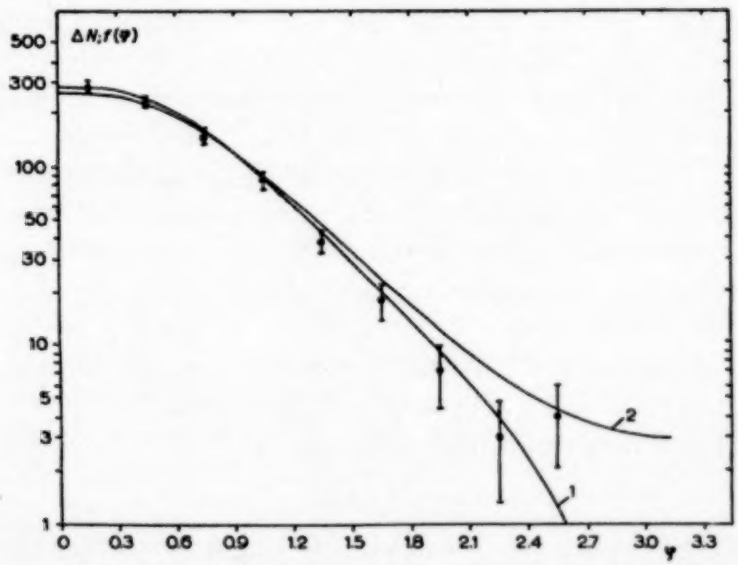

Fig. 3. Differential distribution of π-meson scattering angle projections in 7 mm lead plates. Curve 1-extended nucleus, curve 2-point nucleus.

the incident particles, $\zeta(\gamma)d\gamma$. The error in measurement of the scattering angle is not shown on the graph as it is much smaller than $\Delta\varphi = 0.3$.

It can be seen from fig. 3 that the experimental points satisfactorily fit the multiple Coulomb scattering curve for nuclei of finite dimensions.

Employing the χ^2 criterion we find that the experimental angular distribution curve satisfactorily fits the theoretical curve for a finite nucleus ($P_{\chi^2} = 95\ \%$) and sharply differs from the curve for a point nucleus ($P_{\chi^2} = 0.33\ \%$).

The experimental π-meson scattering data in lead also agree with the corresponding multiple Coulomb scattering curves. At first thought it would seem that due to diffractional scattering of π-mesons this agreement should not exist. However, it has been shown in ref.[18]), in which multiple scattering of protons was investigated, that if the proton energy and substance in which the protons are scattered are chosen so that the condition $\lambda/R \gtrsim \chi_c B^{\frac{1}{2}}$ is fulfilled (and this condition holds for the investigated π-mesons) then diffractional scattering due to absorption of the particles by nuclei can be significant only at large angles outside of the region of investigation.

To check the results obtained, scattering curves were plotted for the trajectories of μ-mesons with measured masses $< 220\ m_e$ and π-mesons with masses $> 270\ m_e$. These curves are not given here as they do not differ in any respect from the curves presented above.

An idea about the magnitude of any possible anomaly can be derived from table 1 in which data (with all corrections) are presented for the integral number of scattered μ-mesons possessing a φ value larger than a prescribed value.

TABLE 1

$\varphi >$	Number of scattered μ-mesons (exper.)	Theoretical predictions
1.5	120	119.4
1.8	59	54.0
2.1	25	22.0
2.4	10	8.2
2.7	3	3.0

The small excess of the observed number of scattered μ-mesons compared with the number predicted by Ter-Mikayelian lies within the limits of the statistical fluctuations. The total amount of matter traversed by the μ-mesons is 2.16×10^4 g/cm^2 Pb. This means that the cross section for anomalous scattering (if the latter exists) does not exceed 10^{-28} g $\cdot$ cm^2-nucleon^{-1} in the investigated momentum interval.

It should be noted that if all the corrections and refinements mentioned in section 2 (especially those to account for the geometry of the apparatus) are not applied, a large discrepancy between the experimental data and

theoretical multiple Coulomb scattering curve is obtained. In this case the experimental points even lie above the multiple Coulomb scattering curve for a point nucleus and the "μ-meson anomalous scattering" cross section turns out to be the same as that cited by various authors, i.e., $\sigma_{\text{anom.}} = (2-5)\times 10^{-27}$ cm^2/nucleon.

A very important point in the μ-meson scattering experiments is the accuracy of determination of the momentum at the point of scattering. From this standpoint, μ-meson scattering data in the (0.1—1.0) GeV range obtained by using rough methods of estimation of the momentum do not appear to be very convincing.

A circumstance of no less importance is the fact that the geometry of the experimental arrangement is usually not taken into account to a sufficient extent (or in most cases in general is neglected). The dimensions of the apparatus are often chosen arbitrarily and as a result the multiple Coulomb scattering curves may be strongly affected. Evidently, insufficient account of these two factors is the cause of the so-called "anomalous scattering of μ-mesons," at least as far as slow μ-mesons are concerned.

Be it as it may, our data indicate that if any anomaly in μ-meson scattering does exist in the investigated momentum range it must be dozens of times smaller than that alleged by various authors.

For a final solution of this problem the experiments should be carried out under conditions of single scattering.

In conclusion we consider it a pleasant duty to express our appreciation to M. Ter-Mikayelian for very fruitful discussion and for help in carrying out this work. We are also thankful to B. A. Dolgoshein and B. I. Luchkov for participation in part of the measurements and treatment of the results and to M. I. Daion and V. G. Kirillov-Ugriumov for participation in the discussion of this investigation.

References

1) W.L. Whittmore and R. P. Shutt, Phys. Rev. **88** (1957) 1312
2) S. Olbert, Phys. Rev. **87** (1952) 319
3) E. P. George, J. I. Redding and P. T. Trent, Proc. Roy. Soc. A **66** (1953) 533
4) J. B. McDiarmid, Phil. Mag. **45** (1954) 933
5) B. Leontic and A. W. Wolfendale, Phil. Mag. **44** (1953) 1101
6) M. L. T. Kannangara and G. S. Shrikantia, Phil. Mag. **44** (1953) 1091
7) A. I. Alikhanov and G. P. Eliseiev, Izv. Akad. Nauk SSSR **19** (1955) 732
8) A. I. Alikhanian and V. G. Kirillov-Ugriumov, Izv. Akad. Nauk SSSR **19** (1955) 736
9) P. Hofstadter, Revs. of Mod. Phys. **28** (1956) 214
10) L. J. Schiff, Phys. Rev. **98** (1955) 756
11) M. L. Ter-Mikayelian, JETP (in press)
12) M. I. Daion, V. M. Fedorov, G. I. Merzon and N. V. Shostakovich, Prib. Tekhn. Eksp. **1** (1957) 3

13) A. I. Alikhanian, N. V. Shostakovich, A. T. Dadayan, V. M. Fedorov and B. N. Deryagin, JETP **31** (1956) 955
14) L. Ya. Pomeranchuk, JETP **18** (1948) 759
15) J. E. Cousins, W. F. Nash and A. J. Pointon, Nuovo Cimento **6** (1957) 1113
16) G. Z. Moliere, Z. f. Naturf. **3a** (1948) 78
17) H. A. Bethe, Phys. Rev. **89** (1953) 1256
18) F. R. Arutyunian, JETP **34** (1958) 800

1.C *Nuclear Physics* **10** (1959) 256—282; © *North-Holland Publishing Co., Amsterdam*
Not to be reproduced by photoprint or microfilm without written permission from the publisher

SURFACE CORRECTIONS TO THE FERMI-THOMAS STATISTICAL THEORY

M. A. NAQVI
Department of Theoretical Physics, University of Manchester

Received 4 November 1958

Abstract: The Hartree-Fock equations are written in matrix form with the aid of the Dirac density matrix. The Fermi-Thomas theory is generalized so that these equations are explicitly satisfied for the diagonal elements and those lying near the diagonal. This procedure modifies the functional relationship between the energy and particle densities by introducing a dependence of the former on the derivatives of the particle density and on the nature of the collective field. It is shown by a simple example that the modifications appear to bring the statistical theory into better agreement with the empirically known results for the case of a local average field. They also provide a method of estimating the effects of the non-locality of the average field on the surface characteristics of a many-body system.

1. Introduction

Recently the problem of introducing surface corrections to the Fermi-Thomas statistical theory has attracted considerable attention [1–4]). In this paper we shall attempt to give a partial solution to this problem which is suitable for the applications of the statistical theory to heavy nuclei.

We shall assume first that the many-body system that we consider is held together by central, static forces only and, secondly, that we can neglect all correlation effects, i.e. that the Hartree-Fock theory is sufficient to discuss the properties of the system. We shall also assume that the system is of a saturating kind. It follows that in the volume region of the system the Fermi gas model is a good approximation and may be used to express the energy density as a function of the particle density.

The Fermi-Thomas statistical theory generalizes this relation to hold even in those regions near the surface where the density varies in space. We shall thus seek a systematic method of modifying this relation by introducing terms depending on the derivatives of the particle density and hence on surface characteristics.

Because of our assumptions, the formulae obtained are not directly applicable to finite nuclei. The nuclear forces are more complex and it seems necessary to use more refined theories of the many-body system [5]) than the Hartree-Fock scheme for calculations on nuclei. However, they

may still play a useful part, e.g. in an approximation procedure which seeks to study the finite nucleus in the Hartree-Fock scheme after the actual forces have been replaced by pseudo-potentials.

The Fermi-Thomas theory was obtained directly, as a first approximation to the Hartree-Fock equation, by Dirac [6]). We shall follow Dirac's method and try to improve the approximation to the Hartree-Fock treatment. This will lead to generalizations of the Fermi-Thomas formulae. This approach is similar to that of Kompaneetz and Pavlovsky [7]) and Theis [8]).

The self-consistent Hartree-Fock field consists of a local and a non-local part, the former arising from the direct and the latter from the exchange terms of the potential energy. In those many-body systems in which the exchange energy is a small correction (e.g. in complex atoms) it is a good approximation to base the discussion on a local collective field.

Some authors have used this approximation for calculations on nuclei [9, 10]). However, the exchange energy in nuclei forms an important fraction of the total energy and hence the effects of the non-locality of the collective field must be taken into account in calculating the surface properties.

We shall derive approximate surface corrections to kinetic and exchange energies separately for the two cases of a local and a non-local approximation to the self-consistent collective field.

Throughout this work we shall ignore spin and isospin co-ordinates (their inclusion will not affect the arguments) and take the many-body wave function to be formed by populating the lowest set of levels of the collective field with one particle per level.

Our results may be interpreted as leading to a modified Weizsäcker equation for the density, in those regions where the density varies in space. The modification will be found to depend on the shape as well as the local or non-local character of the approximation to the collective field.

2. The Hartree-Fock Scheme

2.1. THE HARTREE-FOCK EQUATION

It was pointed out by Dirac [6]) that the Hartree-Fock equations could be written as a matrix equation with the aid of the density matrix introduced by him.

For an assembly of A particles held together by pair interactions $v(\mathbf{r}_{ij})$ the Hartree-Fock equations may be written [11]) in terms of wave functions as

$$-\frac{\hbar^2}{2m}\nabla^2\psi_i(\mathbf{r})+B(\mathbf{r})\psi_i(\mathbf{r})-\int A(\mathbf{r},\mathbf{r}')\psi_i(\mathbf{r}')\mathrm{d}\mathbf{r}' = \varepsilon_i\psi_i(\mathbf{r}), \qquad (2.1)$$

where

$$B(\mathbf{r}) \equiv \int \{\sum_{i=1}^{A} \psi_i^*(\mathbf{r}')\psi_i(\mathbf{r}')\}\, v(\mathbf{r},\mathbf{r}')\mathrm{d}\mathbf{r}', \qquad (2.2)$$

and

$$A(\mathbf{r}, \mathbf{r}') \equiv v(\mathbf{r}, \mathbf{r}') \sum_{i=1}^{A} \psi_i^*(\mathbf{r}')\psi_i(\mathbf{r}). \tag{2.3}$$

The Dirac density matrix is defined as

$$\rho(\mathbf{r}, \mathbf{r}') \equiv \sum_{i=1}^{A} \psi_i^*(\mathbf{r}')\psi_i(\mathbf{r}), \tag{2.4}$$

and the particle density $n(\mathbf{r})$ is given by

$$n(\mathbf{r}) = \rho(\mathbf{r}, \mathbf{r}). \tag{2.5}$$

The equation (2.1) is a Schrödinger equation whose Hamiltonian may be written in matrix notation as

$$H'(\mathbf{r}, \mathbf{r}') = -\frac{\hbar^2}{2m}\nabla_r^2\delta(\mathbf{r}-\mathbf{r}')+B(\mathbf{r})\delta(\mathbf{r}-\mathbf{r}')-A(\mathbf{r}, \mathbf{r}'). \tag{2.6}$$

From (2.1) we can easily deduce the matrix equation

$$H'\rho = \rho H', \tag{2.7}$$

and if E' denotes the sum of the eigenvalues ε_i,

$$E' = \mathrm{tr}\, H'\rho. \tag{2.8}$$

The Hamiltonian H and energy E of the assembly are not given by (2.6) and (2.8), since in the summation over ε_i pair interactions are counted twice [11]), but by

$$H = -\frac{\hbar^2}{2m}\nabla_r^2\delta(\mathbf{r}-\mathbf{r}')+\tfrac{1}{2}B(\mathbf{r})\delta(\mathbf{r}-\mathbf{r}')-\tfrac{1}{2}A(\mathbf{r}, \mathbf{r}'), \tag{2.9}$$

$$E = \mathrm{tr}\, H\rho. \tag{2.10}$$

As can be shown directly from (2.4) the density matrix satisfies the matrix equation

$$\rho^2 = \rho, \tag{2.11}$$

and the normalization condition

$$\mathrm{tr}\, \rho = A. \tag{2.12}$$

The equation (2.11) gives the eigenvalues 0 or 1 for the matrix and its imposition satisfies the requirement of the Exclusion Principle.

It is shown by Frenkel [11]) that the minimization of either (2.10) or (2.8) with respect to variations of ρ subject to the restriction (2.11) leads to the matrix equation (2.7). This may seem surprising until we remember that in minimizing (2.8) we must treat $B(\mathbf{r})$ and $A(\mathbf{r}, \mathbf{r}')$ as fixed operators, while in minimizing (2.10) they are also varied with the variation in ρ. The Hamiltonian (2.6) specifies the self-consistent field; we shall consider approximations in which this field is replaced by a more convenient one. The two cases which we shall consider separately, will be the local field approximation

$$H_M = -\frac{\hbar^2}{2m}\nabla_r^2\delta(\mathbf{r}-\mathbf{r}')+V(\mathbf{r})\delta(\mathbf{r}-\mathbf{r}'), \tag{2.13}$$

and the non-local approximation

$$H_M = -\frac{\hbar^2}{2m}\nabla_r^2\delta(\mathbf{r}-\mathbf{r}')+D(\mathbf{r},\mathbf{r}'), \tag{2.14}$$

where the function V and the matrix D are to be suitably chosen.

These model Hamiltonians along with the equations (2.7), (2.8) and (2.11) will be used to fix aspects of the density matrix but the energy of the assembly will always be calculated from (2.9) and (2.10) so that we shall need approximations to

$$\text{diagonal element of } \left\{-\frac{\hbar^2}{2m}\nabla_r^2\delta(\mathbf{r}-\mathbf{r}')\right\}\rho, \tag{2.15}$$

$$\tfrac{1}{2}\text{ diagonal element of } \{v(\mathbf{r},\mathbf{r}')\rho(\mathbf{r},\mathbf{r}')\}\rho, \tag{2.16}$$

$$\tfrac{1}{2}\text{ diagonal element of } \{B(\mathbf{r})\delta(\mathbf{r}-\mathbf{r}')\}\rho. \tag{2.17}$$

Our aim is to express these terms, which are, respectively, the kinetic energy, exchange potential energy and direct potential energy densities, as functionals of the particle density. Since from (2.2) the direct potential energy density can be expressed in a straightforward way as a functional of the particle density, no discussion of this term is needed.

2.2. SOME PROPERTIES OF THE MATRIX EQUATIONS

There are some general features of the matrix equations (2.7)(2.11) which are best illustrated by considering a simple example.

(i) We take for H_M the local approximation (2.13) and consider a one-dimensional problem:

$$H_M = -\frac{\hbar^2}{2m}\frac{\partial^2}{\partial x^2}\delta(x-x')+V(x)\delta(x-x'). \tag{2.18}$$

The matrix equation (2.7) becomes

$$\frac{\hbar^2}{2m}\left(\frac{\partial^2\rho}{\partial x^2}-\frac{\partial^2\rho}{\partial x'^2}\right) = \{V(x)-V(x')\}\rho. \tag{2.19}$$

Regarding this as a partial differential equation for a function on the x, x' plane we consider the transformation

$$\begin{aligned} x_1 &= \tfrac{1}{2}(x'+x), & \xi &= \tfrac{1}{2}(x'-x); \\ x &= x_1-\xi, & x' &= x_1+\xi. \end{aligned} \tag{2.20}$$

The co-ordinate x_1 measures the distance along the diagonal of ρ and ξ the distance perpendicular to the diagonal. Geometrically the transformation consists of a clockwise rotation through 45° plus a deformation of the space. The matrix equation becomes

$$\frac{\hbar^2}{2m}\frac{\partial^2\rho}{\partial x_1\partial\xi} = \{V(x_1+\xi)-V(x_1-\xi)\}\rho. \tag{2.21}$$

Expanding ρ and V in a Taylor's series in ξ and equating coefficients of same powers we obtain

$$\frac{\partial}{\partial x_1}\left(\frac{\partial\rho}{\partial\xi}\right)_{\xi=0} = 0, \tag{2.22}$$

$$\frac{\hbar^2}{2m}\frac{\partial}{\partial x_1}\left(\frac{\partial^2\rho}{\partial\xi^2}\right)_{\xi=0} = 2V'(x_1)n(x_1); \tag{2.23}$$

here $n(x_1)$ is defined as in (2.5), i.e.

$$n(x_1) = \rho(x, x),$$

and the dash on V denotes its derivative with respect to its argument; we further have

$$\frac{\hbar^2}{2m}\frac{\partial}{\partial x_1}\left(\frac{\partial^3\rho}{\partial\xi^3}\right)_{\xi=0} = 4V'(x_1)\left(\frac{\partial\rho}{\partial\xi}\right)_{\xi=0}, \tag{2.24}$$

and so on.

From (2.22) we see that the matrix equation (2.21) is satisfied for the diagonal elements if ρ is an even function of ξ or symmetric under the interchange of x and x' (ρ is Hermitian by definition, the additional property of symmetry follows from the matrix equation). Equation (2.24) is now satisfied by the symmetry property. This feature of the matrix equation has been noted before [7]).

Further, if we require that the matrix equation be satisfied for elements which lie within a distance ξ from the diagonal so small that ξ^2 may be neglected, we must arrange (2.23) to be satisfied.

(ii) We consider next the Exclusion Principle restriction (2.11):

$$\int\rho(x, x'')\rho(x'', x')\mathrm{d}x'' = \rho(x, x'). \tag{2.25}$$

Using the symmetry property of ρ this becomes

$$\int\rho(x, x'')\rho(x', x'')\mathrm{d}x'' = \rho(x, x'). \tag{2.26}$$

We now assume that x' differs from x by a small quantity h and use Taylor expansions; we obtain from the different powers of h

$$\int\rho^2(x, x'')\mathrm{d}x'' = n(x), \tag{2.27}$$

$$\int\frac{1}{2}\frac{\partial}{\partial x}\rho^2(x, x'')\mathrm{d}x'' = \tfrac{1}{2}n'(x), \tag{2.28}$$

and so on. The factor $\frac{1}{2}$ on the right appears because the derivative is with respect to argument of n, which is in fact the co-ordinate x_1 in (2.20).

The equation (2.27) is the restriction for (2.25) to be satisfied for the diagonal elements. Interchanging in (2.28) the operations of differentiation and integration we see that it is satisfied as a consequence of (2.27). Thus, if we require both the matrix equations (2.25) and (2.19) to be satisfied for elements which lie within a small distance from the diagonal such that its square may be neglected, we must fulfil the restrictions (2.27) and (2.23).

(iii) We shall require transformations of the integral in (2.27) and similar integrals under the transformation (2.20). These integrals represent matrix products and the rule of matrix multiplication must be preserved in the transformation.

The geometrical interpretation of the matrices as functions on the x, x'' plane requires that we interpret the integral (2.27) as a line integral; hence for the line $x = \beta$ (say), we have

$$\int_{-\infty}^{+\infty} \{\rho^2(x, x'')\}_{x=\beta} \mathrm{d}x'' = n(\beta). \tag{2.29}$$

Then in the co-ordinates (2.20) (with x'' in place of x') this becomes

$$2\int_{-\infty}^{+\infty} \{\rho^2(x_1, \xi)\}_{x_1=\beta+\xi} \mathrm{d}\xi = n(\beta). \tag{2.30}$$

The factor 2 in (2.30) comes because the transformation (2.20) is not orthogonal, and the restriction on the integrand ensures that in the new space we are integrating the elements along line $x = \beta$ as is necessary if the left-hand-side of (2.30) is to represent an element of the product matrix. Similarly the exchange energy density, which we call f from now on, is for this simple case, from (2.16),

$$f = \tfrac{1}{2} \text{ diagonal element of } \int v(x, x'')\rho(x, x'')\rho(x'', x')\mathrm{d}x''.$$

Using symmetry of ρ and the assumption that v is a function of the distance between x and x'' only, we get

$$f(\beta) = \tfrac{1}{2}\int \{v(|x-x''|)\rho^2(x, x'')\}_{x=\beta} \mathrm{d}x''. \tag{2.31}$$

Hence under the transformation (2.20) we now get

$$f(\beta) = \int v(|\xi|)\{\rho^2(x_1, \xi)\}_{x_1=\beta+\xi} \mathrm{d}\xi. \tag{2.32}$$

These features of the matrix equations have been illustrated for the simplest case but they are perfectly general and hold with appropriate generalizations of the formulae for the non-local approximation (2.14) in the three-dimensional problem as well.

2.3. TRANSFORMATION OF CO-ORDINATES

We consider the three-dimensional analogue of (2.20) and restrict our attention to the local field approximation (2.13). The new co-ordinates are

$$\mathbf{r}_1 = \tfrac{1}{2}(\mathbf{r}'+\mathbf{r}), \qquad \boldsymbol{\xi} = \tfrac{1}{2}(\mathbf{r}'-\mathbf{r});$$
$$\mathbf{r} = \mathbf{r}_1-\boldsymbol{\xi}, \qquad \mathbf{r}' = \mathbf{r}_1+\boldsymbol{\xi}. \tag{2.33}$$

Generalizing (2.21) we get for the matrix equation (2.7)

$$\frac{\hbar^2}{2m}(\nabla_{\mathbf{r}_1}\cdot\nabla_{\boldsymbol{\xi}})\rho = \{V(\mathbf{r}_1+\boldsymbol{\xi})-V(\mathbf{r}_1-\boldsymbol{\xi})\}\rho. \tag{2.34}$$

From generalization of (2.22) we require that ρ is an even function of ξ_x, ξ_y, ξ_z in the neighbourhood of $\boldsymbol{\xi} = 0$.

(2.30) becomes

$$8\int\{\rho^2(\mathbf{r}_1, \boldsymbol{\xi})\}_{\mathbf{r}_1=\boldsymbol{\beta}+\boldsymbol{\xi}}\,\mathrm{d}\boldsymbol{\xi} = n(\boldsymbol{\beta}). \tag{2.35}$$

The model energy $E_M = \mathrm{tr}\, H_M\rho$ becomes

$$E_M = \int\left\{-\frac{\hbar^2}{8m}(\nabla^2_{\mathbf{r}_1}\rho+\nabla_{\boldsymbol{\xi}}{}^2\rho)_{\boldsymbol{\xi}=0}+V(\mathbf{r}_1)n(\mathbf{r}_1)\right\}\mathrm{d}\mathbf{r}_1. \tag{2.36}$$

The energy of the assembly E is

$$E = \int\left\{-\frac{\hbar^2}{8m}(\nabla^2_{\mathbf{r}_1}\rho+\nabla_{\boldsymbol{\xi}}{}^2\rho)_{\boldsymbol{\xi}=0}+f(\mathbf{r}_1)\right\}\mathrm{d}\mathbf{r}_1, \tag{2.37}$$

with $f(\mathbf{r}_1)$ given by the analogue of (2.32), i.e.

$$f(\mathbf{r}_1) = 4\int v(\xi)\{\rho^2(\mathbf{r}'_1, \boldsymbol{\xi})\}_{\mathbf{r}'_1=\mathbf{r}_1+\boldsymbol{\xi}}\,\mathrm{d}\boldsymbol{\xi}. \tag{2.38}$$

There is an appropriate generalization of (2.23), but as we shall need it only in a special case we shall not write down the general form.

In (2.37) we have ignored the direct potential energy term.

2.4. FERMI-THOMAS THEORY

This theory is in effect the Fermi-gas model and is rigorous when the collective field and the density are uniform in space. The wave functions are plane waves obeying periodic boundary conditions over a cubical box. The summation over eigenvalues in (2.4) is replaced by integrations in momentum space and it is easily shown that

$$\rho(\mathbf{r}_1, \boldsymbol{\xi}) = \left(\frac{3n}{32\pi\xi^3}\right)^{\frac{1}{2}} J_{\frac{3}{2}}\{2\xi(6\pi^2 n)^{\frac{1}{2}}\}; \tag{2.39}$$

$J_{\frac{3}{2}}$ is a Bessel function and n is the constant density. The equation (2.34) is satisfied since V is a constant and is independent of $\mathbf{r}_1$ and the exclusion principle by construction. The energy density is calculated from the integrand of (2.37) and is

$$\varepsilon = \frac{\hbar^2}{8m}x_0 n^{5/3}+P(n). \tag{2.40}$$

Here $P(n)$ is a function of n calculated from (2.38), the restriction on the integrand of (2.38) being no longer necessary, and x_0 is the constant

$$x_0 = \tfrac{12}{5}(6\pi^2)^{\frac{1}{3}}. \tag{2.41}$$

The Fermi-Thomas theory for a finite system takes over the form (2.40) for the energy density, i.e. we obtain for the total energy

$$E = \int \left[\frac{\hbar^2}{8m} x_0 n^{5/3}(\mathbf{r}) + P\{n(\mathbf{r})\}\right] d\mathbf{r}; \tag{2.42}$$

$n(\mathbf{r})$ is then chosen to minimize the energy subject to a normalization condition.

Since we shall deal with large but finite systems, in whose volume region we expect the Fermi gas model to be a good approximation, we shall require that the generalizations of the formulae for the energy density tend to the form (2.40) as we approach the volume region from the surface.

2.5. APPROXIMATION PROCEDURE

The procedure we shall adopt for generalizing (2.40) will be as follows:

1. We shall require that our formulae tend to (2.40) in the limit that n becomes spatially uniform.

2. We shall require that (2.35) be explicitly satisfied. This will lead to the Weizsäcker correction and the Weizsäcker equation.

3. The generalization of (2.23) will then be explicitly taken into account.

4. These restrictions will be satisfied by restrictions on the non-diagonal part of ρ (i.e. its dependence on ξ) with the aid of (2.36). The energy density will be obtained as a functional of n which is left free in the previous steps and which is then to be fixed by a minimization of (2.37).

As is evident from the remarks of section 2.2, this procedure explicitly satisfies the matrix equations for diagonal elements and those near the diagonal. In principle it is possible to go further by deriving restrictions of type (2.23) and (2.30) so that elements farther away from the diagonal are also explicitly accounted for; but in practice this may prove difficult.

3. The Weizsäcker Equation

3.1. THE WEIZSÄCKER CORRECTION

The Exclusion Principle leads to the restriction (2.35):

$$8 \int \{\rho^2(\mathbf{r}_1, \xi)\}_{\mathbf{r}_1 = \mathbf{r}+\xi} d\xi = n(\mathbf{r}). \tag{3.1}$$

We expand the integrand in a Taylor's series about $\mathbf{r}_1 = \mathbf{r}$. The terms which are odd in ξ_x, ξ_y, ξ_z do not contribute to the integral and may be dropped. Collecting the even terms and dropping the subscript on $\mathbf{r}$ after the expansion we write them as

$$\rho^2(\mathbf{r}, \xi) + \tfrac{1}{2}\left(\xi_x^2 \frac{\partial^2}{\partial x^2} + \xi_y^2 \frac{\partial^2}{\partial y^2} + \xi_z^2 \frac{\partial^2}{\partial z^2}\right)\rho^2 + \ldots \equiv F(\mathbf{r}, \xi). \tag{3.2}$$

From (3.2) and (3.1) we have the following restrictions on the unspecified

function F:

$$\{F(\mathbf{r}, \xi)\}_{\xi=0} = n^2(\mathbf{r}), \tag{3.3}$$

$$8\int F(\mathbf{r}, \xi)\mathrm{d}\xi = n(\mathbf{r}). \tag{3.4}$$

One choice that satisfies (3.3) and (3.4) is

$$F(\mathbf{r}, \xi) = \frac{3n(\mathbf{r})}{32\pi\xi^3} J_{\frac{3}{2}}{}^2[2\xi\{6\pi^2 n(\mathbf{r})\}^{\frac{1}{2}}]. \tag{3.5}$$

This choice for F is suggested by the form of the Thomas-Fermi density matrix (2.39). As we see from (3.2), in the limit when $n(\mathbf{r})$ becomes uniform in space and independent of $\mathbf{r}$, the density matrix must also become independent of position and hence F must go over into the square of the Thomas-Fermi matrix. Thus the choice (3.5) ensures that the results of this theory will go over into those of the Fermi-Thomas theory in the appropriate limit of a constant density n. In differentiating eq. (3.2) twice with respect to ξ_x, ξ_y, and ξ_z, using the fact that ρ is an even function of ξ_x, ξ_y, ξ_z, and also eq. (3.5), we obtain the relation

$$(\nabla_{\xi}{}^2\rho)_{\xi=0} = -\left\{\frac{(\nabla_{\mathbf{r}} n)^2}{n} + \nabla_{\mathbf{r}}{}^2 n\right\} - x_0 n^{5/3}. \tag{3.6}$$

In the above, x_0 is the constant given by (2.41). Substituting (3.6) into (2.36) and (2.37), we obtain for the model energy density ε_{M} and for the energy density ε of the assembly the relations

$$\varepsilon_{\mathrm{M}} = \frac{\hbar^2}{8m}\left\{\frac{(\nabla n)^2}{n} + x_0 n^{5/3}\right\} + Vn, \tag{3.7}$$

$$\varepsilon = \frac{\hbar^2}{8m}\left\{\frac{(\nabla n)^2}{n} + x_0 n^{5/3}\right\} + P(n). \tag{3.8}$$

The first term in (3.7) or (3.8) is the Weizsäcker correction to the kinetic energy. The functional $P(n)$ is the exchange energy density and its expression is from (2.38)

$$P(n) = 4\int v(\xi)\{\rho^2(\mathbf{r}_1, \xi)\}_{\mathbf{r}_1=\mathbf{r}+\xi}\mathrm{d}\xi. \tag{3.9}$$

Since the pair interaction $v(\xi)$ is an even function of ξ_x, ξ_y, ξ_z we can expand the remainder of the integrand in a Taylor's series, drop odd terms and obtain from (3.2)

$$P(n) = 4\int v(\xi)F\{n(\mathbf{r}), \xi\}\mathrm{d}\xi. \tag{3.10}$$

Since F is defined by (3.5) we see that $P(n)$ is the same functional of n as one obtains in the Fermi-Thomas theory (see section 2.4).

3.2. THE WEIZSÄCKER EQUATION

From the expression (3.7) for the energy density we obtain for the model energy E_M the relation

$$E_M = \int \left[\frac{\hbar^2}{8m} \left\{ \frac{(\nabla n)^2}{n} + x_0 n^{5/3} \right\} + Vn \right] d\mathbf{r}. \tag{3.11}$$

The normalization condition for a system of A particles is

$$\int n(\mathbf{r}) d\mathbf{r} = A. \tag{3.12}$$

The Euler equation, which minimizes E_M, subject to (3.12), with respect to density variations, is the well known Weizsäcker equation

$$\frac{\hbar^2}{8m} \left\{ \frac{(\nabla n)^2}{n^2} - 2 \frac{\nabla^2 n}{n} \right\} + \frac{5}{24} \frac{\hbar^2}{m} x_0 n^{\frac{2}{3}} + V(\mathbf{r}) = \varepsilon_0. \tag{3.13}$$

In the above ε_0 is the Lagrangian parameter and is the energy of the most energetic particle in the assembly or the value of the highest occupied level of $V(\mathbf{r})$.

3.3. DISCUSSION

The equation (3.13) was first proposed by Weizsäcker [12]) in 1935. His arguments were, however, later shown to be in error [3]). Recently, March and Young [4]) have obtained the Weizsäcker correction from the idempotency condition (2.11) on the density matrix using a somewhat different approach from ours. The Weizsäcker correction was incorporated by Gombás in his extension of the statistical theory to nuclei [13, 14]), and was made the basis by him and his collaborators for a series of investigations on the binding energies and density distributions of nuclei [15, 16, 17]). Several research workers [3, 18]) made an empirical investigation of the equation by comparing the solutions of the Weizsäcker equation with the quantal solution for some simple (local) fields $V(r)$. Their results indicated that the Weizsäcker correction over-compensates and gives too high a value for the energy.

Berg and Wilets [3]) proposed that the magnitude of the Weizsäcker term be left arbitrary and chosen so as to give the best fit to the exact solutions. They found however that the magnitude required depended on the shape of the field $V(r)$ and even for a given shape it was often the case that, while one choice made the agreement between the energies better, another was required for obtaining better agreement between the density distributions. The only definite conclusion that seems to be suggested by these investigations is that for local fields the kinetic energy is over-compensated by the Weizsäcker correction.

Meanwhile Swiatecki [9]) in his work on nuclear surface energy obtained values for surface kinetic and exchange energies. He used a local model field

which was a constant of infinite extension bounded on one side by an inclined plane, i.e.

$$V(x) = V_0 \quad \text{for} \quad x > 0,$$
$$V(x) = V_0(1+x/\lambda) \quad \text{for} \quad x < 0.$$

Several values of the slope were considered. His results showed that the surface kinetic energy was very nearly that given by the Fermi-Thomas estimate even for quite large slopes. The surface exchange energy was considerably less (for the forces used) than the Fermi-Thomas estimate.

The derivation that we have given for the Weizsäcker equation does not allow for any alteration of the magitude of the Weizsäcker term. Further, since no property of the model field has been used up to this point, this derivation holds for a non-local model field as well. However, the Thomas-Fermi part of the kinetic energy as well as the expression for the exchange energy in (3.8) follow from the special choice (3.5) and are therefore subject to alteration in the surface region.

As argued in section 2.2, the dynamical restriction (2.23) must be regarded as of equal importance to the restriction (2.27). We shall see in section 4 that this brings the theory into better agreement with the empirical results quoted above.

4. The Statistical Theory in the Local-Field

4.1. PLANE SYMMETRY

It is useful for discussing the surface effects of heavy nuclei to consider the idealized concept of Nuclear Matter. This is the hypothesis that if Coulomb forces could be switched off, infinitely large nuclei would exist as stable structures. The characteristic parameters of such large but finite systems could be obtained by an extrapolation from the data on heavy nuclei [19]). It seems plausible that in the limit of large size we may ignore effects arising from the curvature of the surface. Thus we may regard all the characteristics of the system such as particle density, energy densities, etc., to fall off (from their constant values in the interior) along the radius vector as we proceed through the surface region, but to possess no variation if at any surface point we travel a small distance along the plane perpendicular to the radius vector. We may thus discuss conditions along one axis (the x-axis, say) and generalize the results to hold along any direction from the origin. This approixmation is analogous to replacing the region in the neighbourhood of any surface point of a large sphere by a plane. The fact that the extrapolation from data on heavy nuclei suggests a constant surface thickness for large slabs of Nuclear Matter makes the approximation considered above very good for calculating the surface characteristics of such systems.

4.2. THE DYNAMICAL RESTRICTION

In the light of the arguments of the previous section, we assume

$$\rho(\mathbf{r}_1, \xi) = \rho(x_1, \xi). \tag{4.1}$$

The matrix equation for the local field model (2.34) becomes

$$\frac{\hbar^2}{2m} \frac{\partial^2 \rho}{\partial x_1 \partial \xi_x} = \{V(x_1+\xi_x) - V(x_1-\xi_x)\}\rho. \tag{4.2}$$

Differentiating this equation with respect to ξ_x, putting $\xi = 0$ and dropping the subscript on x, we get

$$\frac{\hbar^2}{2m} \frac{\partial}{\partial x} \left(\frac{\partial^2 \rho}{\partial \xi_x^2}\right)_{\xi=0} = 2\left(\frac{\partial V}{\partial x}\right) n(x). \tag{4.3}$$

This is, as could be expected, the restriction (2.23). The restriction (2.35) becomes

$$8 \int \{\rho^2(x_1, \xi)\}_{x_1=x+\xi_x} \mathrm{d}\xi = n(x). \tag{4.4}$$

As before, we expand the integrand in a Taylor's series, drop terms odd in ξ_x and the subscript on x, and write

$$\rho^2 + \tfrac{1}{2}\xi_x^2 \frac{\partial^2}{\partial x^2}\rho^2 + \ldots = F(x, |\xi|). \tag{4.5}$$

Proceeding as in section 3.1, we obtain the analogue of (3.6):

$$(\nabla_\xi^2 \rho)_{\xi=0} = -\left\{\frac{\left(\frac{\partial n}{\partial x}\right)^2}{n} + \frac{\partial^2 n}{\partial x^2}\right\} - L(x) n^{5/3}. \tag{4.6}$$

In the above we have introduced the unspecified function $L(x)$ and the assumption

$$\frac{1}{2n} (\nabla_\xi^2 F)_{\xi=0} = -L(x) n^{5/3}. \tag{4.7}$$

From the assumption that F depends only on $|\xi|$ we have

$$\left(\frac{\partial^2 F}{\partial \xi_x^2}\right)_{\xi=0} = \left(\frac{\partial^2 F}{\partial \xi^2}\right)_{\xi=0} = \tfrac{1}{3}(\nabla_\xi^2 F)_{\xi=0}, \tag{4.8}$$

and hence also the relation

$$\left(\frac{\partial^2 \rho}{\partial \xi_x^2}\right)_{\xi=0} = -\left\{\frac{\left(\frac{\partial n}{\partial x}\right)^2}{n} + \frac{\partial^2 n}{\partial x^2}\right\} - \tfrac{1}{3} L(x) n^{5/3}. \tag{4.9}$$

From (4.4), (4.5), (4.7) and (4.8) we have the following restrictions on F:

$$8 \int F(x, \xi) \mathrm{d}\xi = n(x), \tag{4.10}$$

$$\{F(x,\xi)\}_{\xi=0} = n^2(x), \tag{4.11}$$

$$\left(\frac{\partial^2 F}{\partial \xi^2}\right)_{\xi=0} = -\tfrac{2}{3}L(x)n^{\frac{5}{3}}. \tag{4.12}$$

We shall see later how $L(x)$ is to be chosen so as to fulfil the dynamical restriction (4.3).

4.3. EXCHANGE ENERGY

The exchange energy may be calulated as in section 3, eq. (3.10), if we have an explicit representation for F. We shall see in this section that it is possible to find such an explicit representation, which fulfils the relations (4.10) to (4.12) for any, unspecified, function $L(x)$.

We write F as

$$\begin{aligned} F = &\left(\frac{3n}{32\pi\xi^3}\right) J_{\frac{3}{2}}{}^2\{2\xi(6\pi^2 n)^{\frac{1}{3}}\} \\ &+ b(x)\left[n^2 e^{-4\pi n^{\frac{1}{3}}\xi^2} - \left(\frac{3n}{32\pi\xi^3}\right) J_{\frac{3}{2}}{}^2\{2\xi(6\pi^2 n)^{\frac{1}{3}}\}\right]. \end{aligned} \tag{4.13}$$

From section 2 we know that the first term in the above satisfies both (4.10) and (4.11). Similarly both the functions in the square bracket also satisfy separately these two relations. Thus (4.13) ensures that F fulfils (4.10) and (4.11). The restriction (4.12) is fulfilled if we choose $b(x)$ as

$$b(x) = \frac{L(x) - x_0}{12\pi - x_0}, \tag{4.14}$$

where x_0 is the constant given by (2.41). We further impose the condition that $L(x) \to x_0$ as we approach the volume region of constant density from the surface region. Thus all the formulae which are derived from the choice (4.13) go over into those of the Fermi-Thomas theory in the limit that n becomes a constant, i.e. in the volume region. The second term in (4.13) is the correction to the surface exchange energy resulting from the dynamical restriction (4.3). Its presence was indicated, empirically, by the results of Swiatecki [9]).

The considerations of this section solve the problem of obtaining the exchange energy density as a functional of the particle density (within the limits of the restrictions (2.23) and (2.27). The nature (local or non-local) and shape of the model field will only determine $L(x)$, the functional relationship between the exchange energy and n and L remaining as predicted from (4.13) and (3.10).

4.4. CHOICE OF AUXILIARY FUNCTION $L(x)$

From (2.36) and (4.6) we obtain the model energy ε_c contained in a cylinder of unit area placed along the x-axis:

$$\varepsilon_c = \int_{-\infty}^{+\infty} \left[\frac{\hbar^2}{8m} \left\{ \frac{\left(\frac{\partial n}{\partial x}\right)^2}{n} + L(x) n^{5/3} \right\} + V(x) n(x) \right] dx. \tag{4.15}$$

We minimize (4.15) with respect to variations of n, regarding $L(x)$ as specified i.e. not to be varied. We also restrict the variations of n so that the amount of matter contained in the cylinder remains constant and take this restriction into account by a Lagrangian parameter ε_0. The Euler equation for n is then the modified Weizsäcker equation

$$\frac{\hbar^2}{8m} \left\{ 2 \frac{\frac{\partial^2 n}{\partial x^2}}{n} - \frac{\left(\frac{\partial n}{\partial x}\right)^2}{n^2} \right\} - \frac{5}{24} \frac{\hbar^2}{m} L(x) n^{\frac{2}{3}} + \varepsilon_0 = V(x). \tag{4.16}$$

Now consider the restriction (4.3); its left side can be calculated from (4.9) and its right side from (4.16); equating the two we obtain the condition that (4.3) be fulfilled as

$$\frac{\partial L}{\partial x} = \frac{4}{n^{5/3}} \frac{\partial^3 n}{\partial x^3}. \tag{4.17}$$

The boundary condition on this equation is, from the previous section,

$$L(x) \to x_0. \tag{4.18}$$

as we approach the volume region, and x_0 is defined by (2.41).

Assuming that the exchange energy density as calculated from (3.10) and (4.13) is a functional $Q(n, L)$ of n and L we have from (2.37) for the energy density of the assembly along the x-axis

$$\varepsilon = \frac{\hbar^2}{8m} \left\{ \frac{\left(\frac{\partial n}{\partial x}\right)^2}{n} + L n^{5/3} \right\} + Q(n, L). \tag{4.19}$$

We may now generalize this expression to hold along any direction from the origin and formulate the statistical theory within the local field approximation by the expressions

$$E = \int \left[\frac{\hbar^2}{8m} \left\{ \frac{(\nabla n)^2}{n} + L(r) n^{5/3}(r) \right\} + Q(n, L) \right] d\mathbf{r}, \tag{4.20}$$

$$\frac{\partial L}{\partial r} = \frac{4}{n^{5/3}} \frac{\partial^3 n}{\partial r^3}, \tag{4.21}$$

where n is to be found by minimizing (4.20) subject to (4.21), the usual normalization condition, and the prescription that L be not varied in minimizing (4.20) with respect to density variations.

4.5. ILLUSTRATIVE EXAMPLE

To illustrate the modifications introduced into the Fermi-Thomas statistical theory we consider a semi-infinite density distribution which falls off from a constant value along the x-axis, the rate of decay being specified by one parameter λ:

$$\begin{aligned} n(x) &= n_0 \quad \text{for} \quad x > 0, \\ n(x) &= n_0 e^{-(x/\lambda)^2} \quad \text{for} \quad x < 0. \end{aligned} \tag{4.22}$$

(i) *The auxiliary function* $L(x)$

The density has a discontinuity in its second derivative at the origin; hence at $x = 0$

$$\frac{\partial^3 n}{\partial x^3} = \frac{2}{\lambda^2}\delta(x) n_0. \tag{4.23}$$

In the region $x > 0$ we have from (4.18) $L = x_0$. From (4.23) and (4.18) we obtain the boundary condition

$$L(x) = x_0 - \frac{8}{n_0^{\frac{2}{3}} \lambda^2} \quad \text{as} \quad x \to 0 \quad \text{from the left.} \tag{4.24}$$

Equation (4.17) may be solved to give

$$L(x) = \frac{1}{n_0^{\frac{2}{3}} \lambda'^2}\left\{72 - 24\left(\frac{x}{\lambda'}\right)^2\right\} e^{\frac{2}{3}(x/\lambda')^2} + x_0 - \frac{80}{n_0^{\frac{2}{3}} \lambda'^2}. \tag{4.25}$$

The dash is put on the parameter λ in (4.25), so that in the subsequent minimization we do not differentiate with respect to it, i.e. we do not vary $L(x)$.

(ii) *Kinetic energy*

We obtain for the modified Thomas-Fermi term of the kinetic energy in the surface region

$$\begin{aligned} L(x) n^{5/3} = {} & \frac{n_0}{\lambda'^2}\left(72 - 24\frac{x^2}{\lambda'^2}\right) e^{-x^2(5/3\lambda^2 - 5/3\lambda'^2)} \\ & - 80\frac{n_0}{\lambda'^2} e^{-5/3x^2/\lambda^2} + n_0^{5/3} x_0 e^{-5/3x^2/\lambda^2}, \end{aligned} \tag{4.26}$$

and for the Weizsäcker term

$$\frac{\left(\frac{\partial n}{\partial x}\right)^2}{n} = 4\frac{n_0}{\lambda^2}\left(\frac{x}{\lambda}\right)^2 e^{-x^2/\lambda^2}. \tag{4.27}$$

The surface energy per unit area is obtained by integrating along x from $-\infty$ to 0. For the surface kinetic energy T_s we get

$$T_s(\lambda, \lambda') = \frac{\hbar^2 \pi^{\frac{1}{2}}}{16m}\left[2\frac{n_0}{\lambda} + \frac{n_0}{\lambda'}\left\{72\left(\frac{5}{3}\frac{\lambda'^2}{\lambda^2} - \frac{2}{3}\right)^{-\frac{1}{2}}\right.\right.$$
$$\left.\left. -12\left(\frac{5}{3}\frac{\lambda'^2}{\lambda^2} - \frac{2}{3}\right)^{-\frac{1}{2}} - (\tfrac{3}{5})^{\frac{1}{2}}80\frac{\lambda}{\lambda'}\right\} + (\tfrac{3}{5})^{\frac{1}{2}}x_0 n_0^{\,5/3}\lambda\right]. \tag{4.28}$$

The first term in the square bracket is the Weizsäcker correction, the second term arises from the restriction (4.17) and the last term is the Thomas-Fermi estimate.

The potential energy can also be found as a function of λ and λ' and the total surface energy per unit area ε_s may be written

$$\varepsilon_s = \{\varepsilon_s(\lambda, \lambda')\}_{\lambda=\lambda'}. \tag{4.29}$$

From the considerations of section 4.4. λ is to be found from the equation

$$\left(\frac{\partial \varepsilon_s}{\partial \lambda}\right)_{\lambda'=\lambda} = 0. \tag{4.30}$$

For the kinetic energy part we obtain

$$\left(\frac{\partial T_s}{\partial \lambda}\right)_{\lambda'=\lambda} = \frac{\hbar^2 \pi^{\frac{1}{2}}}{16m}\left[-\frac{2n_0}{\lambda^2} + \frac{n_0}{\lambda^2}\{60 - 80(\tfrac{3}{5})^{\frac{1}{2}}\} + (\tfrac{3}{5})^{\frac{1}{2}}x_0 n_0^{\,5/3}\right]. \tag{4.31}$$

For kinetic energy itself, however, we have

$$(T_s)_{\lambda'=\lambda} = \frac{\hbar^2 \pi^{\frac{1}{2}}}{16m}\left[\frac{2n_0}{\lambda} + \frac{n_0}{\lambda}\{60 - 80(\tfrac{3}{5})^{\frac{1}{2}}\} + (\tfrac{3}{5})^{\frac{1}{2}}x_0 n_0^{\,5/3}\lambda\right]. \tag{4.32}$$

The numerical factor in the curly brackets in eqs. (4.31) and (4.32) is -1.978; thus for this particular case we might sum up the effects of the modifications by saying that in the equation which determines λ and hence the density distribution, the magnitude of the Weizsäcker term in the kinetic energy should be taken as twice its normal value while in the estimate of the energy itself the magnitude should be $\frac{1}{70}$ the normal value. The latter result is in good agreement with the findings of Swiatecki [9]).

It is evident, however, that these results depend very much on the functional dependence of n that is chosen and hence this example is only to be regarded as illustrative.

(iii) *Exchange energy*

A quantitative estimate of the surface exchange energy is difficult and best carried out for more realistic density distributions. We can, however, determine the sign of the correction that results from the second term in (4.13). The exchange energy f is, from (4.13) and (3.10),

$$f = f_1 + \frac{x_0}{12\pi - x_0}\left(\frac{L(x)}{x_0} - 1\right)(f_2 - f_1), \tag{4.33}$$

where

$$f_1 = \frac{12n}{32\pi}\int \frac{v(\xi)}{\xi^3} J^2_{\frac{3}{2}}\{2\xi(6\pi^2 n)^{\frac{1}{3}}\}\mathrm{d}\xi \tag{4.34}$$

and

$$f_2 = 4n^2 \int v(\xi) \mathrm{e}^{-4\pi^2 n^{\frac{1}{3}}\xi^2}\mathrm{d}\xi. \tag{4.35}$$

Now

$$\frac{x_0}{12\pi - x_0} \approx +29.4. \tag{4.36}$$

Using Gaussian interactions $v(\xi)$ of a range appropriate for nuclear forces we can show by direct calculation that $f_2 - f_1$ is always > 0 for the range of values of n to be encountered at the nuclear surface. Similarly, for an appropriate value of λ and n_0 we can show from (4.25) that $L(x)$ is mostly $< x_0$ in the surface region. Hence it appears likely that the effect of the second term in (4.33) is to reduce the estimate of the magnitude of the surface exchange energy from that given by the Fermi-Thomas theory. Thus the sign of the correction to the surface exchange energy is in agreement with the results of Swiatecki [9]).

5. The Frahn-Lemmer Equation

5.1. CHOICE OF THE NON-LOCAL FIELD

For the case of the local model field it was possible to formulate the statistical theory without any explicit reference to the field parameters. As we shall see, this is not possible when the model field is taken as non-local. The dynamical restriction which replaces (2.23) is more complex and the resulting equation for $L(x)$ which replaces (4.21) now contains the field parameters. As an approximation to the self-consistent field matrix we consider the form [20]).

$$D(\mathbf{r}, \mathbf{r}') = \frac{1}{\pi^{\frac{3}{2}} a^3} V(\tfrac{1}{2}(\mathbf{r}'+\mathbf{r}))\mathrm{e}^{-|\mathbf{r}'-\mathbf{r}|^2/a^2}. \tag{5.1}$$

There are several points worth noting about (5.1):

(i) the choice of the function V and the parameter a (which is a measure of the non-locality) must be guided by the nature of the system studied;

(ii) as $a \to 0$, $D(\mathbf{r}, \mathbf{r}') \to V(\mathbf{r})\delta(\mathbf{r}-\mathbf{r}')$; this is the local field approximation studied in the previous sections;

(iii) let us suppose that V is a constant V_0. This would be appropriate for the volume region of heavy nuclei. The Fourier transform of the Schrödinger equation corresponding to (5.1) shows that the field decays to zero for high momenta. This is consistent with the observed energy dependence of the real part of the optical model potential. This aspect was, of course, studied by Frahn [21]), who introduced the form (5.1).

5.2. THE FRAHN-LEMMER EQUATION

The single-particle Schrödinger equation corresponding to the field (5.1) is

$$\frac{\hbar^2}{2m}\nabla^2\psi_i(\mathbf{r})+\varepsilon_i\psi_i(\mathbf{r}) = \int \frac{1}{\pi^{\frac{3}{2}}a^3} V(\tfrac{1}{2}(\mathbf{r}'+\mathbf{r}))e^{-|\mathbf{r}'-\mathbf{r}|^2/a^2}\psi_i(\mathbf{r}')d\mathbf{r}'. \quad (5.2)$$

The integral in (5.2) may be simplified by the transformation

$$\mathbf{r}_1 = \tfrac{1}{2}(\mathbf{r}'+\mathbf{r}), \qquad \boldsymbol{\xi} = \tfrac{1}{2}(\mathbf{r}'-\mathbf{r}). \quad (5.3)$$

Then, as explained in section 2.2, the integral becomes

$$I = \frac{8}{\pi^{\frac{3}{2}}a^3}\int e^{-4\xi^2/a^2}\{V(\mathbf{r}_1)\psi_i(\mathbf{r}_1+\boldsymbol{\xi})\}_{\mathbf{r}_1=\mathbf{r}+\boldsymbol{\xi}}d\boldsymbol{\xi}. \quad (5.4)$$

The factor in square brackets may now be expanded in a Taylor's series about $\mathbf{r}_1 = \mathbf{r}$. Dropping first-order terms since they are odd in ξ_x, ξ_y or ξ_z and do not contribute to the integral, we have

$$\begin{aligned} I = \frac{8}{\pi^{\frac{3}{2}}a^3}\int d\boldsymbol{\xi}\, e^{-4\xi^2/a^2}[&V(\mathbf{r})\psi_i(\mathbf{r})+2\{(\boldsymbol{\xi}\cdot\nabla)V\}\{\boldsymbol{\xi}\cdot\nabla\psi_i\} \\ &+\tfrac{1}{2}\{(\boldsymbol{\xi}\cdot\nabla)^2V\}\psi_i(\mathbf{r})+2V(\boldsymbol{\xi}\cdot\nabla)^2\psi_i+\text{ higher derivatives}]. \end{aligned} \quad (5.5)$$

The analogue of the usual effective mass approximation for Nuclear Matter consists in retaining only terms up to the second order. The odd terms of the integrand in (5.5) may be dropped and the integrations carried out to obtain the approximate Schrödinger equation

$$\begin{aligned} \frac{\hbar^2}{2m}\nabla^2\psi_i(\mathbf{r})+\varepsilon_i\psi_i(\mathbf{r}) = V(\mathbf{r})\psi_i(\mathbf{r})&+\tfrac{1}{4}a^2(\nabla V)\cdot(\nabla\psi_i) \\ &+\tfrac{1}{4}a^2V(\mathbf{r})\nabla^2\psi_i+\tfrac{1}{16}a^2\psi_i(\mathbf{r})\nabla^2V. \end{aligned} \quad (5.6)$$

This equation was proposed by Frahn and Lemmer [20]), who derived it from (5.1) in a slightly different way.

We shall discuss the effects of non-locality on the statistical theory within the approximation (5.6). Thus, instead of (2.14) the model Hamiltonian is

$$\begin{aligned} H_{\mathrm{M}}(\mathbf{r},\mathbf{r}') = \Big\{-\frac{\hbar^2}{2m}+\tfrac{1}{8}a^2V(\mathbf{r})\Big\}\nabla_{\mathbf{r}}{}^2\delta(\mathbf{r}-\mathbf{r}')&+\tfrac{1}{8}a^2V(\mathbf{r}')\nabla_{\mathbf{r}}{}^2\delta(\mathbf{r}-\mathbf{r}') \\ &+\{V(\mathbf{r})-\tfrac{1}{16}a^2\nabla_{\mathbf{r}}{}^2V(\mathbf{r})\}\delta(\mathbf{r}-\mathbf{r}'), \end{aligned} \quad (5.7)$$

and the model energy is

$$E_{\mathrm{M}} = \mathrm{tr}\, H_{\mathrm{M}}\rho, \quad (5.8)$$

where ρ is, as usual, the density matrix.

5.3. SPECIFICATION OF THE FIELD PARAMETERS

In this section we shall try to specify the parameters of the model field so that it approximates the self-consistent field in heavy nuclei.

We consider, first, an infinite nucleus consisting of an equal number of neutrons and protons with paired spins held together by well-behaved Wigner and Majorana forces (in the ratio 1 : 4) with the same (Gaussian) radial dependence. We adjust the parameters of the force to reproduce the density ρ_0 and average particle energy ε_0 in Nuclear Matter by a gas model calculation. We assume the following values for the matter constants:

$$\rho_0 = 0.138\times 10^{39} \text{ particles/cm}^3,$$
$$\varepsilon_0 = -15.7 \text{ MeV}.$$

These values do not represent an accurate extrapolation from the properties of heavy nuclei, but they will serve as an illustration. It can then be shown that the constants of the Wigner force are:

$$\begin{aligned} \text{strength} &= -11.4 \text{ MeV}, \\ \text{range} &= 2.076\times 10^{-13} \text{ cm}. \end{aligned} \tag{5.9}$$

Since the Majorana force is four times the Wigner force, we obtain for the strength C and range a' of the even-state forces the values

$$\begin{aligned} C &= -57 \text{ MeV}, \\ a' &= 2.076\times 10^{-13} \text{ cm}. \end{aligned} \tag{5.10}$$

The self-consistent, single-particle equation can be then shown to be

$$-\frac{\hbar^2}{2m}\nabla^2\psi_i(\mathbf{r})+3C\int\left(\frac{3n}{4\pi|\mathbf{r}-\mathbf{r}'|^3}\right)^{\frac{1}{2}} J_{\frac{3}{2}}\{(6\pi^2 n)^{\frac{1}{3}}|\mathbf{r}-\mathbf{r}'|\}e^{-|\mathbf{r}-\mathbf{r}'|^2/a'^2} \times\psi_i(\mathbf{r}')d\mathbf{r}' = \varepsilon_i\psi_i(\mathbf{r}). \tag{5.11}$$

The first two factors of the integrand make up the Thomas-Fermi density matrix (2.39) and the third factor is the radial part of the force (see (2.3)). The parameter n is one quarter of the nucleon density. The effective mass approximation to (5.11) is found by transforming it to Fourier space and approximating the resulting momentum-dependent potential energy by a parabola. As we shall use this approximation in estimating surface energy, we require that the parabola should give correctly (i) the total potential energy and (ii) the energy of the least energetic particle, i.e. the parabola should have the same depth as the correct potential energy function. The result is that (5.11) may be written in Fourier space as

$$\left\{\frac{\hbar^2}{2m}k^2+3C(0.6634-0.0612\,a'^2k^2)\right\}\phi = \varepsilon(a'k)\phi. \tag{5.12}$$

In the above k is, as usual, the magnitude of the wave vector; we have used a value of n which is consistent with the parameters of the nucleus, and ϕ is the Fourier transform of ψ. The model field (5.1) for an infinite nucleus is

$$D(\mathbf{r}, \mathbf{r}') = \frac{V_0}{\pi^{\frac{3}{2}} a^3} e^{-|\mathbf{r}-\mathbf{r}'|^2/a^2}. \tag{5.13}$$

It is not difficult to show that the approximating process adopted in the previous section leads, for the special case (5.13), to the same result as would be obtained by taking the Fourier transform of (5.13), expanding in power series and retaining the first two terms. We, therefore, replace the parabola in (5.12) by a Gaussian function of k which is such that when expanded in a power series about $k = 0$ it gives the first two terms identical with those of the parabola in (5.12):

$$\left(\frac{\hbar^2}{2m} k^2 + 3AC\, e^{-\frac{1}{4}b^2 a'^2 k^2}\right) \phi = \varepsilon(a'k)\phi, \tag{5.14}$$

with

$$A = 0.6634, \qquad b^2 = 0.3688. \tag{5.15}$$

The inverse Fourier transform of (5.14) gives

$$-\frac{\hbar^2}{2m} \nabla^2 \psi_i(\mathbf{r}) + \frac{3AC}{\pi^{\frac{3}{2}} b^3 a'^3} \int e^{-|\mathbf{r}-\mathbf{r}'|^2/b^2 a'^2} \psi_i(\mathbf{r}')\, d\mathbf{r}' = \varepsilon_i \psi_i(\mathbf{r}). \tag{5.16}$$

Comparing (5.13)and (5.16) we find that the model field parameters are related to the force parameters by

$$V_0 = 3AC, \qquad a = a'b. \tag{5.17}$$

The problem for a finite nucleus is to specify how the function $V(\frac{1}{2}(\mathbf{r}'+\mathbf{r}))$ in (5.1) falls off from its constant value V_0 in the interior to zero as we go through the surface region. We shall assume that its decay is similar to that of the particle density. This relation is indicated by the results of Rotenberg [22]) who has carried out Hartree-Fock calculations using the same type of forces as ours. Thus, if

$$n(\mathbf{r}) = n_0 f(\mathbf{r}), \tag{5.18}$$

where $f \to 1$ as we approach the interior and n_0 is the parameter n of (5.11). Then we assume that the model field for the finite nucleus is

$$D(\mathbf{r}, \mathbf{r}') = \frac{V_0}{\pi^{\frac{3}{2}} a^3} f(\tfrac{1}{2}(\mathbf{r}+\mathbf{r}')) e^{-|\mathbf{r}-\mathbf{r}'|^2/a^2}, \tag{5.19}$$

where V_0, a are related to the force parameters from (5.17), (5.15) and (5.10).

6. The Statistical Theory in Non-Local Field Approximation

6.1. THE DYNAMICAL RESTRICTION

As in section 4 we shall restrict ourselves to those systems in which the effects of surface curvature can be ignored, and we can investigate conditions along one axis. Thus we take $V(\mathbf{r})$ in (5.7) as $V(x)$. The matrix equation

(2.7), with (5.7) as the Hamiltonian, under the transformation (2.33) becomes (see appendix 1)

$$\begin{aligned}
&\frac{\hbar^2}{2m}\frac{\partial^2\rho}{\partial x_1\partial\xi_x} - \{V(x_1+\xi_x)-V(x_1-\xi_x)\}\rho(x_1,\xi) \\
&\quad -\tfrac{1}{4}a^2\left\{V(x_1+\xi_x)\left(\frac{1}{4}\frac{\partial^2}{\partial x_1{}^2}+\frac{1}{2}\frac{\partial^2}{\partial x_1\partial\xi_x}+\tfrac{1}{4}\nabla_\xi{}^2\right)\right. \\
&\quad \left.-V(x_1-\xi_x)\left(\frac{1}{4}\frac{\partial^2}{\partial x_1{}^2}-\frac{1}{2}\frac{\partial^2}{\partial x_1\partial\xi_x}+\tfrac{1}{4}\nabla_\xi{}^2\right)\right\}\rho \\
&\quad -\tfrac{1}{4}a^2\left[\left\{\left(\frac{1}{2}\frac{\partial}{\partial x_1}+\frac{1}{2}\frac{\partial}{\partial\xi_x}\right)V(x_1+\xi_x)\right\}\left(\frac{1}{2}\frac{\partial}{\partial x_1}+\frac{1}{2}\frac{\partial}{\partial\xi_x}\right)\right. \\
&\quad \left.-\left\{\left(\frac{1}{2}\frac{\partial}{\partial x_1}-\frac{1}{2}\frac{\partial}{\partial\xi_x}\right)V(x_1-\xi_x)\right\}\left(\frac{1}{2}\frac{\partial}{\partial x_1}-\frac{1}{2}\frac{\partial}{\partial\xi_x}\right)\right]\rho \\
&\quad -\tfrac{1}{16}a^2\left\{\left(\frac{1}{4}\frac{\partial^2}{\partial x_1{}^2}+\frac{1}{2}\frac{\partial^2}{\partial x_1\partial\xi_x}+\frac{1}{4}\frac{\partial^2}{\partial\xi_x{}^2}\right)V(x_1+\xi_x)\right. \\
&\quad \left.-\left(\frac{1}{4}\frac{\partial^2}{\partial x_1{}^2}-\frac{1}{2}\frac{\partial^2}{\partial x_1\partial\xi_x}+\frac{1}{4}\frac{\partial^2}{\partial\xi_x{}^2}\right)V(x_1-\xi_x)\right\}\rho=0.
\end{aligned} \tag{6.1}$$

In (6.1) the operators appearing before V do not act on ρ. Consider this equation at $\xi_x = 0$; it is satisfied if

$$\left(\frac{\partial\rho}{\partial\xi_x}\right)_{\xi_x=0} = 0: \tag{6.2}$$

this is consistent with the assumption that ρ is an even function of ξ_x, ξ_y, ξ_z. This assumption, which makes ρ not only Hermitian but real, follows from the arguments of section 2.2. Differentiating (6.1) with respect to ξ_x and putting $\xi = 0$ we obtain the new dynamical restriction, which replaces (4.3),

$$\begin{aligned}
&\left\{\frac{\hbar^2}{2m}-\tfrac{1}{4}a^2V(x_1)\right\}\frac{\partial}{\partial x_1}\left(\frac{\partial^2\rho}{\partial\xi_x{}^2}\right)_{\xi=0}-\tfrac{1}{4}a^2\frac{\partial V}{\partial x_1}\left(\frac{\partial^2\rho}{\partial\xi_x{}^2}\right)_{\xi=0} \\
&\quad -\tfrac{1}{8}a^2\frac{\partial V}{\partial x_1}(\nabla_\xi{}^2\rho)_{\xi=0}-\tfrac{1}{8}a^2\frac{\partial V}{\partial x_1}\frac{\partial^2 n}{\partial x_1{}^2}-\tfrac{1}{4}a^2\frac{\partial^2 V}{\partial x_1{}^2}\frac{\partial n}{\partial x_1} \\
&\quad -\tfrac{1}{8}a^2\frac{\partial^3 V}{\partial x_1{}^3}n(x_1)=2\frac{\partial V}{\partial x_1}n(x_1),
\end{aligned} \tag{6.3}$$

where, as usual, n is the particle density.

In (6.3), if we put $a = 0$, we obtain the restriction (4.3) for the case of a local field. We shall henceforth drop the subscript on x.

6.2. THE GENERALIZED WEIZSÄCKER EQUATION

From (2.35) we obtain, just as in section 4.2, the relations

$$(\nabla_\xi^2 \rho)_{\xi=0} = -\left\{\frac{\left(\frac{\partial n}{\partial x}\right)^2}{n} + \frac{\partial^2 n}{\partial x^2}\right\} - L(x)n^{5/3}, \tag{6.4}$$

$$\left(\frac{\partial^2 \rho}{\partial \xi_x^2}\right)_{\xi=0} = -\left\{\frac{\left(\frac{\partial n}{\partial x}\right)^2}{n} + \frac{\partial^2 n}{\partial x^2}\right\} - \tfrac{1}{3}L(x)n^{5/3}. \tag{6.5}$$

From (6.4) and (5.8) we obtain (see appendix 2) the model energy in a cylinder of unit area placed along the x-axis:

$$\begin{aligned}\varepsilon_c = \int_{-\infty}^{+\infty} \Bigg[&\frac{\hbar^2}{8m}\left\{\frac{\left(\frac{\partial n}{\partial x}\right)^2}{n} + L(x)n^{5/3}\right\} - \tfrac{1}{16}a^2 V(x)\left\{\frac{\left(\frac{\partial n}{\partial x}\right)^2}{n} + L(x)n^{5/3}\right\} \\ &+ \tfrac{1}{8}a^2 \frac{\partial V}{\partial x}\frac{\partial n}{\partial x} + V(x)n(x) + \tfrac{1}{16}a^2 n(x)\frac{\partial^2 V}{\partial x^2}\Bigg] \mathrm{d}x.\end{aligned} \tag{6.6}$$

Minimization of (6.6) subject to some normalization condition, taken into account by an unspecified Lagrangian parameter ε_0, leads to the generalized Weizsäcker equation

$$\begin{aligned}&\left\{\frac{\hbar^2}{4m} - \tfrac{1}{8}a^2 V(x)\right\}\frac{\left(\frac{\partial^2 n}{\partial x^2}\right)}{n} - \left(\frac{\hbar^2}{8m} - \tfrac{1}{16}a^2 V\right)\frac{\left(\frac{\partial n}{\partial x}\right)^2}{n^2} \\ &- \frac{5}{3}\left(\frac{\hbar^2}{8m} - \tfrac{1}{16}a^2 V\right)L(x)n^{\frac{2}{3}} - \tfrac{1}{8}a^2 \frac{\partial V}{\partial x}\frac{\left(\frac{\partial n}{\partial x}\right)}{n} \\ &+ \tfrac{1}{16}a^2 \frac{\partial^2 V}{\partial x^2} - \varepsilon_0 = V(x).\end{aligned} \tag{6.7}$$

Now the right-hand side of (6.3) can be calculated from (6.7) and the left-hand side of (6.3) from (6.5) and (6.4); equating the two we get

$$\begin{aligned}&\left(\frac{\hbar^2}{4m} - \tfrac{1}{8}a^2 V\right) 4\frac{\partial^3 n}{\partial x^3} - \left(\frac{\hbar^2}{4m} - \tfrac{1}{8}a^2 V\right)\frac{\partial L}{\partial x}n^{5/3} \\ &- \tfrac{3}{4}a^2 \frac{\partial V}{\partial x}\frac{\partial^2 n}{\partial x^2} + \tfrac{1}{4}a^2 \frac{\partial^3 V}{\partial x^3}n(x) = 0.\end{aligned} \tag{6.8}$$

This is the new equation for L which replaces (4.21). The boundary condition in (6.8) is the same, i.e. (4.18).

Thus the formulation of the statistical theory on the basis of a non-local model field remains as at the end of section 4.4, with the relation (4.21), however, replaced by (6.8).

6.3. ILLUSTRATIVE EXAMPLE

As in section 4 we calculate the surface kinetic energy in a cylinder of unit area placed along the x-axis and use the trial function

$$\begin{aligned} n(x) &= n_0 \, e^{-(x/\lambda)^2} \quad \text{for} \quad x < 0, \\ n(x) &= n_0 \qquad\qquad\quad \text{for} \quad x > 0. \end{aligned} \tag{6.9}$$

From (5.19) and (5.17) we take

$$\begin{aligned} V(x) &= 3AC \, e^{-(x/\lambda)^2} \quad \text{for} \quad x < 0, \\ V(x) &= 3AC \qquad\qquad\quad \text{for} \quad x > 0. \end{aligned} \tag{6.10}$$

The field parameters will be taken from section 5.3 and our results will thus apply to the type of system considered in this section.

(i) *The function* $L(x)$

Because of the discontinuity in the second derivative of n at the origin, eq. (6.8) at the origin is

$$\frac{\partial L}{\partial x} = \frac{1}{n_0^{\frac{2}{3}} \lambda^2} \left\{ 8 + \frac{3}{2} \frac{AC}{(\hbar^2/(4ma^2)) - \frac{3}{8}AC)} \right\} \delta(x). \tag{6.11}$$

Thus the boundary condition on L is that as we tend to origin from the left

$$L(x) \to x_0 - \frac{8 - 4a_0}{n_0^{\frac{2}{3}} \lambda^2}. \tag{6.12}$$

From (5.10), (5.15) and (5.17)

$$a_0 = -\left(\frac{\hbar^2/(4ma^2)}{\frac{3}{8}AC} - 1 \right)^{-1} = +0.6847, \tag{6.13}$$

and x_0 is given by (2.41).

The solution of (6.8) on the basis of (6.9), (6.10) and (6.12) is

$$\begin{aligned} L(x) = {} & \frac{1}{n_0^{\frac{2}{3}} \lambda'^2} (72 - 24 x^2/\lambda'^2) e^{\frac{1}{2}x^2/\lambda'^2} - \frac{80 - 4a_0}{n_0^{\frac{2}{3}} \lambda'^2} \\ & + x_0 - \frac{1}{n_0^{\frac{2}{3}} \lambda'^2} \int_0^x \frac{32}{\lambda'} \frac{\frac{t^3}{\lambda'^3} e^{-\frac{1}{2}t^2/\lambda'^2}}{\beta + e^{-t^2/\lambda'^2}} \, dt, \end{aligned} \tag{6.14}$$

where

$$\beta = -\frac{\hbar^2/(4ma^2)}{\frac{3}{8}AC} = +0.4604, \tag{6.15}$$

and the dash is added to λ so that in the minimization of the surface energy with respect to λ we do not vary $L(x)$.

(ii) *Surface kinetic energy* T_s

The kinetic energy T_s is obtained from the relation

$$\tfrac{1}{4}T_s = \int_{-\infty}^{0} \mathrm{d}x \frac{\hbar^2}{8m}\left\{\frac{\left(\frac{\partial n}{\partial x}\right)^2}{n} + L(x)n^{5/3}\right\}. \tag{6.16}$$

The factor $\frac{1}{4}$ on the left is introduced because in this example, which refers to a nucleus in which there are four nucleons per orbital, n is $\frac{1}{4}$ of the particle density.

Carrying out the integration we obtain

$$\begin{aligned}\tfrac{1}{4}T_s(\lambda, \lambda') = \frac{\hbar^2\pi^{\frac{1}{2}}}{16m}\Bigg[2\frac{n_0}{\lambda} + \frac{n_0}{\lambda'}\Bigg\{72\left(\tfrac{5}{3}\frac{\lambda'^2}{\lambda^2} - \tfrac{2}{3}\right)^{-\frac{1}{2}} \\ -12\left(\tfrac{5}{3}\frac{\lambda'^2}{\lambda^2} - \tfrac{2}{3}\right)^{-\frac{3}{2}} - (\tfrac{3}{5})^{\frac{1}{2}}80\frac{\lambda}{\lambda'} + (\tfrac{3}{5})^{\frac{1}{2}}4a_0\frac{\lambda}{\lambda'} \\ -\frac{32}{\pi^{\frac{1}{2}}\lambda'}\int_0^{\infty}\mathrm{d}x\mathrm{e}^{-5x^2/\lambda^2}\int_0^{(x/\lambda')^2}\mathrm{d}u\frac{u\mathrm{e}^{-\frac{1}{2}u}}{\beta+\mathrm{e}^{-u}}\Bigg\} \\ +(\tfrac{3}{5})^{\frac{1}{2}}n_0^{5/3}x_0\lambda\Bigg].\end{aligned} \tag{6.17}$$

In (6.17) the first term in the square bracket arises from the Weizsäcker correction; the terms in the curly bracket are due to the dynamical restriction (6.8), and of these the first three would be present in the local field approximation; the last two terms thus represent the influence of the non-locality; the last term is the Thomas-Fermi estimate of the surface kinetic energy. From (6.17) we obtain the following results:

$$\{\tfrac{1}{4}T_s(\lambda, \lambda')\}_{\lambda'=\lambda} = \frac{\hbar^2\pi^{\frac{1}{2}}}{16m}\left[2\frac{n_0}{\lambda} - 1.968\frac{n_0}{\lambda} + 0.804\frac{n_0}{\lambda} + (\tfrac{3}{5})^{\frac{1}{2}}x_0n_0^{5/3}\lambda\right], \tag{6.18}$$

$$\left(\tfrac{1}{4}\frac{\partial T_s}{\partial\lambda}\right)_{\lambda'=\lambda} = \frac{\hbar^2\pi^{\frac{1}{2}}}{16m}\left[-2\frac{n_0}{\lambda^2} - 1.968\frac{n_0}{\lambda^2} - 3.989\frac{n_0}{\lambda^2} + (\tfrac{3}{5})^{\frac{1}{2}}x_0n_0^{5/3}\right]. \tag{6.19}$$

In both the above equations, the first term is the contribution from the Weizsäcker correction, the second that from the local and the third that from the non-local field effects manifested through the dynamical restriction (6.8); the last term is the Thomas-Fermi estimate. We may interpret these results by saying that in the estimation of the surface kinetic energy the magnitude of the Weizsäcker term should be reduced by a factor $\frac{2}{5}$ while in the equation which determines λ and hence the density, this magnitude should be increased by a factor 4.

7. Conclusion

The results of this investigation may be summarized as follows:

(1) It is possible to make a systematic generalization of the Fermi-Thomas theory so as to include surface corrections if one starts from the Hartree-Fock equations written in matrix form.

(2) The requirement that the matrix equations be satisfied for the diagonal elements and those near the diagonal leads to the formulation of the statistical theory given at the end of section 4.4, the relation (4.21) being used if the collective field is local and (6.8) if it is non-local. It remains to be seen whether the restrictions imposed are sufficient to account for the surface effects.

(3) In the above formulation of the statistical theory the Weizsäcker correction appears with its normal magnitude and is related to the Pauli exclusion principle. The results suggest, however, that it is not a good approach to rely only upon the Weizsäcker equation, either with the normal magnitude of the Weizsäcker term or by altering this magnitude in an empirical way. Other correction terms which are of the Weizsäcker type also appear and these add up in one way in the estimation of the energy and in a different way in the equation which determines the density. The magnitudes of these terms depend sensitively on the shape of the density distribution and on the local or non-local character of the collective field.

Appendix

1. DERIVATION OF THE MATRIX EQUATION (6.1)

This equation can be derived directly from the Hamiltonian (5.7), using the rules of matrix algebra, the necessary integrations being carried out with the aid of the δ functions. A less direct method is to start from the Frahn-Lemmer equation (5.6):

$$\left\{\frac{\hbar^2}{2m}\nabla_{\mathbf{r}}^2-\tfrac{1}{4}a^2V(\mathbf{r})\nabla_{\mathbf{r}}^2-V(\mathbf{r})-\tfrac{1}{16}a^2(\nabla_{\mathbf{r}}^2V)-\tfrac{1}{4}a^2(\boldsymbol{\nabla}_{\mathbf{r}}V)\cdot\boldsymbol{\nabla}_{\mathbf{r}}\right\}\psi_i(\mathbf{r}) = -\varepsilon_i\psi_i(\mathbf{r}). \quad \text{(A.1)}$$

Multiply above by $\psi_i^*(\mathbf{r}')$ and sum over i, interchanging the space operations with summation over eigenvalues, to obtain

$$\left\{\frac{\hbar^2}{2m}\nabla_{\mathbf{r}}^2-\tfrac{1}{4}a^2V(\mathbf{r})\nabla_{\mathbf{r}}^2-V(\mathbf{r})-\tfrac{1}{16}a^2(\nabla_{\mathbf{r}}^2V)-\tfrac{1}{4}a^2(\boldsymbol{\nabla}_{\mathbf{r}}V)\cdot\boldsymbol{\nabla}_{\mathbf{r}}\right\}\rho(\mathbf{r},\mathbf{r}') = -\sum_i \varepsilon_i\psi_i^*(\mathbf{r}')\psi_i(\mathbf{r}). \quad \text{(A.2)}$$

Consider the complex conjugate equation (A.1) at the point $\mathbf{r}'$, multiply by $\psi_i(\mathbf{r})$ and sum over eigenvalues, to obtain

$$\left\{\frac{\hbar^2}{2m}\nabla_{\mathbf{r}'}^2-\tfrac{1}{4}a^2V(\mathbf{r}')\nabla_{\mathbf{r}'}^2-V(\mathbf{r}')-\tfrac{1}{16}a^2(\nabla_{\mathbf{r}'}^2V)-\tfrac{1}{4}a^2(\boldsymbol{\nabla}_{\mathbf{r}'}V)\cdot\boldsymbol{\nabla}_{\mathbf{r}'}\right\}\rho(\mathbf{r},\mathbf{r}')$$
$$=-\sum_i\varepsilon_i\psi_i(\mathbf{r})\psi_i^*(\mathbf{r}'). \quad \text{(A.3)}$$

The difference of (A.2) and (A.3) is the matrix equation (2.7) in the $\mathbf{r}$, $\mathbf{r}'$ representation:

$$\begin{aligned}\Big[&\tfrac{\hbar^2}{2m}(\nabla_{\mathbf{r}'}^2-\nabla_{\mathbf{r}}^2)-\tfrac{1}{4}a^2\{V(\mathbf{r}')\nabla_{\mathbf{r}'}^2-V(\mathbf{r})\nabla_{\mathbf{r}}^2\}\\&-\tfrac{1}{4}a^2\{(\boldsymbol{\nabla}_{\mathbf{r}'}V)\cdot\boldsymbol{\nabla}_{\mathbf{r}'}-(\boldsymbol{\nabla}_{\mathbf{r}}V)\cdot\boldsymbol{\nabla}_{\mathbf{r}}\}-\{V(\mathbf{r}')-V(\mathbf{r})\}\\&-\tfrac{1}{16}a^2\{(\nabla_{\mathbf{r}'}^2V)-(\nabla_{\mathbf{r}}^2V)\}\Big]\rho(\mathbf{r},\mathbf{r}')=0.\end{aligned} \quad \text{(A.4)}$$

Equation (6.1) is obtained by transforming (A.4) to $\mathbf{r}_1$, $\boldsymbol{\xi}$ space (2.33) and noting that in this space $\rho(\mathbf{r}_1,\boldsymbol{\xi})\equiv\rho(x_1,\boldsymbol{\xi})$.

2. DERIVATION OF THE RELATION (6.6) FOR THE ENERGY

The direct procedure would be to start from (5.8). We shall, however, start from (A.2). This equation, under the transformation (2.33), becomes

$$\begin{aligned}&\left\{\frac{\hbar^2}{2m}-\tfrac{1}{4}a^2V(\mathbf{r}_1-\boldsymbol{\xi})\right\}(\tfrac{1}{4}\nabla_{\mathbf{r}_1}^2+\tfrac{1}{4}\nabla_{\boldsymbol{\xi}}^2-\tfrac{1}{2}\boldsymbol{\nabla}_{\mathbf{r}_1}\cdot\boldsymbol{\nabla}_{\boldsymbol{\xi}})\rho(\mathbf{r}_1,\boldsymbol{\xi})\\&-\{V(\mathbf{r}_1-\boldsymbol{\xi})+\tfrac{1}{16}a^2(\tfrac{1}{4}\nabla_{\mathbf{r}_1}^2+\tfrac{1}{4}\nabla_{\boldsymbol{\xi}}^2-\tfrac{1}{2}\boldsymbol{\nabla}_{\mathbf{r}_1}\cdot\boldsymbol{\nabla}_{\boldsymbol{\xi}})V(\mathbf{r}_1-\xi)\}\rho\\&-\tfrac{1}{4}a^2[\{(\tfrac{1}{2}\boldsymbol{\nabla}_{\mathbf{r}_1}-\tfrac{1}{2}\boldsymbol{\nabla}_{\boldsymbol{\xi}})V(\mathbf{r}_1-\boldsymbol{\xi})\}\cdot(\tfrac{1}{2}\boldsymbol{\nabla}_{\mathbf{r}_1}-\tfrac{1}{2}\boldsymbol{\nabla}_{\boldsymbol{\xi}})]\rho\\&=-\sum_i\varepsilon_i\psi_i^*(\mathbf{r}_1+\boldsymbol{\xi})\psi_i(\mathbf{r}_1-\boldsymbol{\xi}).\end{aligned} \quad \text{(A.5)}$$

Putting $\boldsymbol{\xi}=0$, integrating over $\mathbf{r}$, and having regard to the symmetry of ρ and the normalization of the ψ_i's, we obtain for the model energy

$$\begin{aligned}E_{\mathrm{M}}=\int\Big[&\Big\{-\tfrac{\hbar^2}{8m}+\tfrac{1}{16}a^2V(\mathbf{r}_1)\Big\}\{\nabla_{\mathbf{r}_1}^2n(\mathbf{r}_1)+(\nabla_{\boldsymbol{\xi}}^2\rho)_{\boldsymbol{\xi}=0}\}\\&+\{V(\mathbf{r}_1)+\tfrac{1}{16}a^2(\nabla_{\mathbf{r}_1}^2V)+\tfrac{1}{8}a^2(\boldsymbol{\nabla}_{\mathbf{r}_1}V)\cdot\boldsymbol{\nabla}_{\mathbf{r}_1}\}n(\mathbf{r}_1)\Big]\,\mathrm{d}\mathbf{r}_1,\end{aligned} \quad \text{(A.6)}$$

where $n(\mathbf{r}_1)$ is, as usual, the particle density. Interpreting the integrand in (A.6) as the energy density of the system, we consider a cylinder of unit is along the x_1 axis and assume that both V and n depend only on x_1 and that $\rho\equiv\rho(x_1,\boldsymbol{\xi})$. The energy in the cylinder is then given by (6.6) where the subscript on x_1 has been dropped, and the relation (6.4) has been used.

3. NOTE ON THE EVALUATION OF INTEGRALS

In order to obtain the relations (6.18) and (6.19) from relation (6.17) we have to evaluate double integrals of the type occurring in (6.17). This has been done by the approximate method of expanding the integrand of the inner integral in a Maclaurin's series upto the fifth power of the argument. The magnitudes of the terms suggest that the values given in (6.18) and (6.19) for the non-local contributions are accurate to within 10 %.

I should like to express my gratitude to Professor L. Rosenfeld for suggesting this topic, for several suggestions and discussions relating to it and for his encouragement. I wish also to thank Dr. A. R. Bodmer, Dr. B. B. Deo and Mr. Z. R. Khan for many discussions; Dr. N. H. March for a discussion on the drawbacks of the Thomas-Fermi theory, and Dr. N. V. Findler for sending me a copy of his Ph. D. thesis.

References

1) P. Gombás, Acta Phys. Hung. **3** (1954) 105
2) N. H. March, Advanc. Phys. **6** (1957) 1
3) R. Berg and L. Wilets, Proc. Phys. Soc. A **68** (1955) 229
4) N. H. March and W. H. Young, Proc. Phys. Soc. A **72** (1958) 182
5) K. A. Brueckner and J. L. Gammel, Phys. Rev. **109** (1958) 1023
6) P. A. M. Dirac, Proc. Cambr. Phil. Soc. **26** (1930) 376
7) A. S. Kompaneetz and E. S. Pavlovsky, Soviet Physics **4** (1957) 328
8) W. R. Theis, Z. Physik **142** (1955) 503
9) W. J. Swiatecki, Proc. Phys. Soc. A **64** (1951) 226
10) W. J. Swiztecki, Phys. Rev. **98** (1955) 203
11) J. Frenkel, Advanced Wave Mechanics (Oxford, Clarendon Press, 1934)
12) C. F. von Weizsäcker, Z. Physik **96** (1935) 431
13) P. Gombás, Acta Phys. Hung. **1** (1951) 329
14) P. Gombás, Acta Phys. Hung. **2** (1952) 223
15) P. Gombás, Acta Phys. Hung. **5** (1956) 511
16) P. Gombás *et al.*, Nuclear Physics **4** (1957) 448
17) N. V. Findler, Nuclear Physics **8** (1958) 338
18) R. A. Ballinger and N. H. March, Proc. Phys. Soc. A **67** (1954) 378
19) L. Wilets, Revs. Mod. Phys. **30** (1958) 542
20) W. E. Frahn and R. H. Lemmer, Nuovo Cimento **5** (1957) 1564
21) W. E. Frahn, Nuovo Cimento **4** (1956) 313
22) M. Rotenberg, Technical Report no. 6, M.I.T. (1955)

7.G *Nuclear Physics* **10** (1959) 283—293; ©*North-Holland Publishing Co., Amsterdam*
Not to be reproduced by photoprint or microfilm without written permission from the publisher

OBSERVATION OF THE BREMSSTRAHLUNG OF π-MESONS INTERACTING WITH NUCLEI

M. F. LOMANOV, A. G. MESHKOVSKY, Ya. Ya. SHALAMOV, V. A. SHEBANOV and A. F. GRASHIN

U. S. S. R. Academy of Sciences, Moscow

Received 19 August 1958

Abstract: Nuclear force bremsstrahlung of π^+-mesons has been observed in a freon bubble chamber in which 80—300 MeV π^+-mesons interacted with carbon, fluorine and chlorine nuclei. In the indicated energy range the bremsstrahlung cross section for inelastically and elastically scattered π^+-mesons as derived from 20 scattering events was found to be $(4.5^{+1.2}_{-2.0}) \times 10^{-27}$ cm^2 per fluorine nucleus. Three cases of bremsstrahlung involved absorption of the π^+-mesons by the nucleus; in two cases of bremsstrahlung charge-exchange scattering of π^+-mesons on the nucleus occurred. The bremsstrahlung cross sections for these various types of nuclear processes have been computed in the quasiclassical approximation. The values obtained from the formulas satisfactorily agree with the experimental results.

1. Introduction

Due to the strong nuclear interaction between π-mesons and nucleons bremsstrahlung of π-mesons (i.e., the emission of γ-quanta as a result of change of velocity or loss of charge) should mainly be determined by nuclear but not Coulomb forces. Bremsstrahlung of π-mesons of various energies in a nuclear force field has been considered in several theoretical papers [1–4]). Solovyov [3]), in particular, investigated the bremsstrahlung of π-mesons possessing energies close to their rest energy. It was found that in this energy region the bremsstrahlung cross section should be of the order of 10^{-28} cm^2 per nucleon.

The relatively large bremsstrahlung cross section predicted by the theory makes feasible an experimental detection of this phenomena. However, up to the present bremsstrahlung of π-mesons has not been observed experimentally. In the present work π-mesons bremsstrahlung was observed by studying the interaction between π^+-mesons and light nuclei at energies close to the rest energy.

2. Experimental Method

The experiments were performed on the synchrocyclotron of the Laboratory of Nuclear Problems of the Joint Institute of Nuclear Research. π^+-

mesons of a definite energy were sent into a bubble chamber possessing an observation volume of about 17 litres. The chamber design is shown in fig. 1. The body of the chamber, 1, is made of steel. The observation windows of the chamber are covered with 90 mm thick lucite plates, 2, which are pressed to the chamber body by steel flanges, 3. The dimensions of the observation region, 4, are $50 \times 22 \times 15$ cm^3. The particle entrance window is closed by flange, 5. The thickness of duralumin wall, 6, which has two rigidity fins, is 12 mm; its area is 10×20 cm^2.

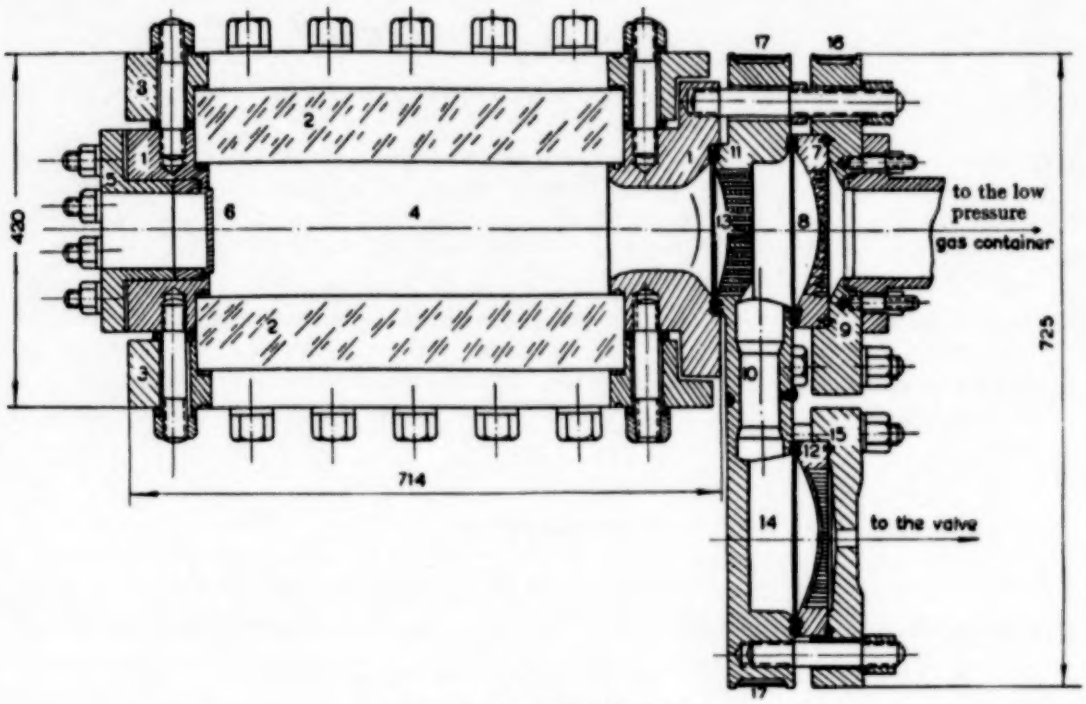

Fig. 1. Chamber design.

As Blinov *et al.*[5]) have shown, for satisfactory operation of a bubble chamber it is important to lower the pressure in the chamber to a constant controllable level. This ensures the high stability of the chamber sensitivity required in ionization measurements and also permits one to rapidly adjust the sensitivity without changing the temperature. This pressure lowering procedure was also applied in the present work. For this purpose a low pressure level device was employed which consisted of a grate, 7, rubber membrane, 8, flange, 9, and compressed gas container. A separator filled with water is placed between the low pressure level device and chamber. The separator consists of body, 10, grates, 11 and 12, rubber membranes, 13 and 14, and flange, 15. Contiguous to the separator flange is a valve employed for supply or lowering of the pressure.

The operation temperature in the chamber is maintained by passing water from a thermostat through special channels between the flanges and chamber

body and also through channels 16 and 17 in the separator and low pressure level device. The chamber is illuminated in transmitted light by two pulsed lamps. The overall dimensions of the chamber in mm are indicated in fig. 1. The weight of the chamber without the gass container and auxiliary equipment is $\approx$ 600 kg.

In selecting the working fluid for a large size chamber one should remember that operation of a large chamber is rather difficult due to the necessity of maintaining the pressure and temperature at the required level throughout a large volume. The most attractive type would seem to be a chamber working at room temperature and at relatively low pressure. It has been shown [6]) that a convenient working temperature (near room temperature) can be attained by using a mixture of freon 12 (CCl_2F_2) and freon 13 ($CClF_3$). In the present work a mixture of 54 % (by weight) of freon 12 and 46 % of freon 13 was employed. With this mixture the chamber operated at 28.5°C.

The density of the working fluid was 1.12 g/cm^2. Compared to propane or pentane which are usually employed in bubble chambers the high specific weight of this liquid and also the big size of the chamber permit one to record with a high efficiency γ-quanta converted into electron-positon pairs. For determination of the efficiency in each case the ratio of the length of the observation region in the direction of flight of the γ-quantum to the radiation length was determined. The mean efficiency deduced from these measurements was used to compute the cross sections.

In the course of the experiments the pressure in the chamber was lowered by 10—13 atm in about 15 m sec. The operation period of the chamber was about 20 sec. Photographs were made on two parallel films with a stereoscopic camera which had a base of 103 mm. Altogether three sets of measurements were carried out at initial π^+-meson beam energies (before entrance in the chamber) of 320 MeV, 234 MeV and 130 MeV. The π^+-meson beams were obtained by bombardment of polyethylene targets with an external proton beam [7]). For the 320 MeV and 234 MeV beams the field of the deflecting magnet was chosen in such a manner as to yield maximum intensity for a given thickness of the polyethylene target. The π^+-mesons obtained in this way were mainly produced in the $pp \rightarrow d\pi^+$ reaction. It was difficult to attain maximum intensity of the 130 MeV beam in this manner and the magnetic field strength finally employed was determined by calculation.

The π^+-meson energy in the first beam (320 MeV) was deduced from the kinematics of the $pp \rightarrow d\pi^+$ reaction with account of ionization losses in the polyethylene target and in the air layer between the target and chamber. The π^+-meson energy in the other two beams was deduced from the energy of the first beam and from the ratio of the corresponding magnetic field strength. The energy value E computed in this way for the 130 MeV beam satisfactorily agreed with the value derived from the energy-range curve

$R(E)$. In this case the π^+-meson range in the chamber was determined by counting the number of π-μ-e decays along the π^+-meson path in the chamber. The results are shown in fig. 2. The arrow denotes the π^+-meson range computed from the range curves on the assumption that the energy of the π^+-meson before its entering the chamber was 130 MeV.

The number of primary π-meson traversals through the chamber was determined with account of the possible presence of other types of particles in the π^+-meson beam. Proton and electron tracks on the photographs could easily be distinguished from π-meson tracks by their ionization and multiple scattering and hence any admixture of these particles could not affect the results of our measurements. About 13 % of the particles in the 130 MeV π^+-meson beam were μ-mesons. This value was derived from the experimental π- and μ-meson range data contained in the photographs.

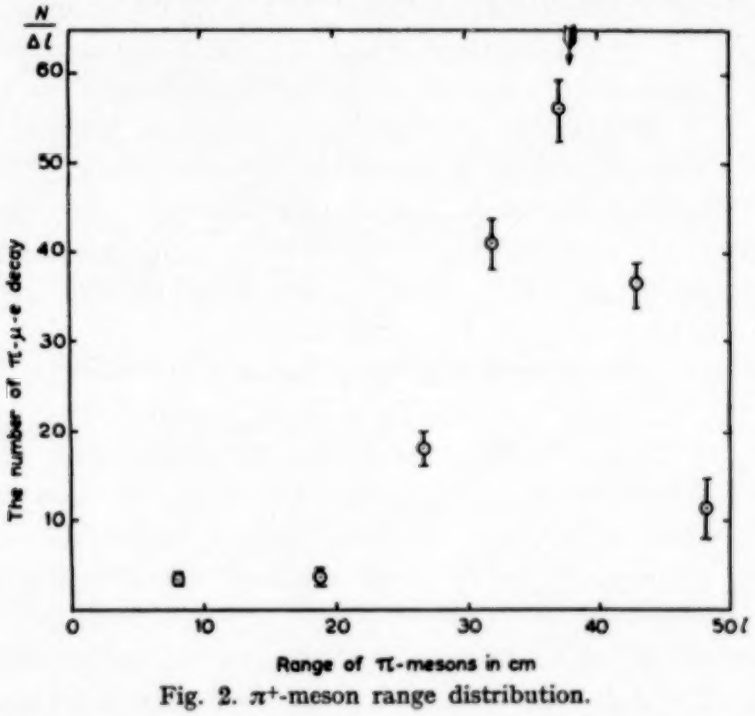

Fig. 2. π^+-meson range distribution.

The magnitude of the μ-meson admixture in the other two beams was not determined by us. To find the μ-meson contribution we used the data of Mukhin *et al.*[7]), who worked under the same experimental conditions as we did. This information on the μ-meson admixture was subsequently employed in the cross section calculations. Another correction was applied to take into account those π^+-mesons which had passed out of the beam and struck the chamber glass as a result of multiple Coulomb scattering.

In the majority of cases the energy of the charged products of π^+-meson interaction in the chamber was inferred from the particle ranges. In some cases the energy of the π-meson after interaction was determined by measuring ionization losses along the track or by measuring multiple scattering.

3. Classification of Various Types of Bremsstrahlung and Competing Processes

The following types of the radiative π-meson-nucleon interaction will be distinguished.

1. Radiative inelastic scattering of π-mesons on nuclei. In bubble chamber photographs a break is then observed on the primary π-meson track at the point of interaction and simultaneously an electron-positon pair can be seen to be emitted from the interaction point. The process can be written in the form $\pi^+ + A \rightarrow \pi^+ + \gamma + A'$ where A and A′ are the initial and final states of the nucleus. The transformation of nucleus A into nucleus A′ is accompanied by emission of protons and neutrons from nucleus A as can be inferred in most cases from the proton tracks projected from the interaction point. Another possible interpretation of such photographs is that a neutral π-meson is produced in accord with the scheme $\pi^+ + A \rightarrow \pi^+ + \pi^0 + A'$, the π^0-meson subsequently decaying into two γ-quanta, only one of which converts in the region of observation. A choice between bremsstrahlung and the alternative process can be made on basis of the following energy considerations. Let E_0 denote the kinetic energy of the π-meson before interaction, E_1 its kinetic energy after the interaction and E_p the energy of protons emitted from the nucleus. Evidently $E_0-(E_1+E_p) < \mu c^2$ (where μ is the π^0-meson mass) implies bremsstrahlung. On the other hand the inequality $E_0-(E_1+E_p) > \mu c^2$ means that either the process $\pi^+ + A \rightarrow \pi^+ + \pi^0 + A'$ or bremsstrahlung is involved and in this case further analysis is required.

2. Radiative elastic or diffraction scattering of π-mesons on nuclei in accord with the scheme $\pi^+ + A \rightarrow \pi^+ + \gamma + A$. The difference between this case and the preceding one is that no proton tracks project from the break and the π-meson is scattered through a relatively small angle. As in the preceding case the competing process is π^0-meson production by π^+-mesons in accord with the scheme $\pi^+ + A \rightarrow \pi^+ + \pi^0 + A'$. It must be assumed in the latter case that transformation of nucleus A into nucleus A′ is not accompanied by the appearance of visible tracks of the reaction products so that the measurements yield $E_p = 0$. Evidently for $E_0 - E_1 < \mu c^2$ this case should be ascribed to bremsstrahlung.

3. Radiative absorption of π-mesons in accord with the scheme $\pi^+ + A \rightarrow \gamma + A'$. The π-meson track on the photograph either terminates in a star or breaks off completely ("prongless" stars) with the simultaneous appearance of a pair on the photograph which can be traced back to the end of the π-meson track. A competing and much more probable process in this case is that of charge-exchange scattering of the π-meson in accord with the scheme $\pi^+ + A \rightarrow \pi^0 + A'$ providing (as in the preceding case) that only one

of the two π^0-meson decay γ-quanta convert in the observation region. As above, a choice between these two processes in certain cases can be made on basis of energy arguments.

4. Radiative charge-exchange scattering of the π-meson in accord with the scheme $\pi^+ + A \to \pi^0 + \gamma + A'$. The π-meson track terminates in a star or breaks off and on the photograph negaton-positon pairs can be observed which emit from the interaction point. If three pairs are observed on the photograph the process $\pi^+ + A \to \pi^0 + \pi^0 + A'$ is possible, signifying π^0-meson production with simultaneous charge-exchange of the π^+-meson and conversion of only 3 of the 4 π^0-meson decay γ-quanta.

In all of the four cases considered above the choice between bremsstrahlung and competing processes can be made not only on basis of energy balance considerations but also by studying the γ-quantum angular distribution. It will be shown in section 5 that the theory predicts most bremsstrahlung γ-quanta to be emitted predominantly in the forward direction whereas the angular distribution of π^0-meson γ-quanta should be much more isotropic.

4. Results

About 7000 photographs obtained in three sets of experiments with different initial π^+-meson energies were analyzed. 20 cases of bremsstrahlung were observed in inelastic and elastic scattering of the π^+-mesons. In 3 cases the π^+-mesons were absorbed and 2 observed events can be ascribed either to bremsstrahlung in charge-exchange scattering or to the process $\pi^+ + A \to \pi^0 + \pi^0 + A'$.

Typical photographs for bremsstrahlung processes occurring during scattering or absorption are presented in fig. 3—5. The photograph in fig. 4 can apparently be ascribed to elastic scattering bremsstrahlung because of the absence of a star at the interacting point and also because of the small scattering angle. These features are of course not sufficient to permit one to distinguish this type of event from bremsstrahlung occurring in inelastic scattering, as inelastic interaction for various reasons may not be accompanied by the appearance of visible proton tracks on the photographs.

Since we did not have a reliable criterion to enable us to choose between elastic and inelastic scattering, all 20 observed events were united into an overall bremsstrahlung process occurring during scattering. These events are presented in the table.

The energy values E_0 and E_p, presented in the table were derived from range measurements. The precision of the measurement of the energy E_0 is about 5 %. In cases Nos 9 and 12 energy E_1 was derived from the energy of the prongs of the star at the end of the scattered π^+-meson track. In two cases (Nos 10 and 19) energy E_1 was also deduced from multiple scattering

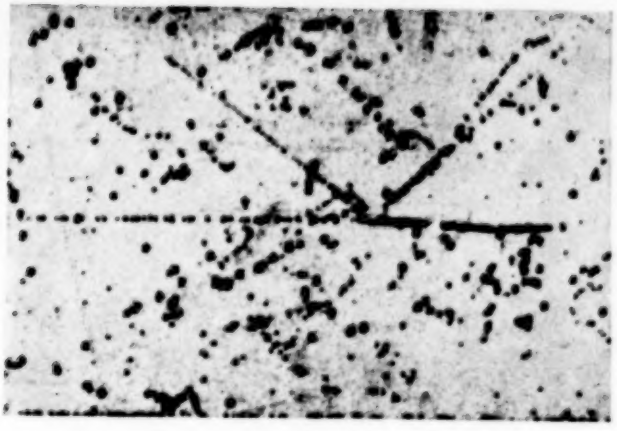

Fig. 3. Bremsstrahlung of inelastically scattered π-mesons.

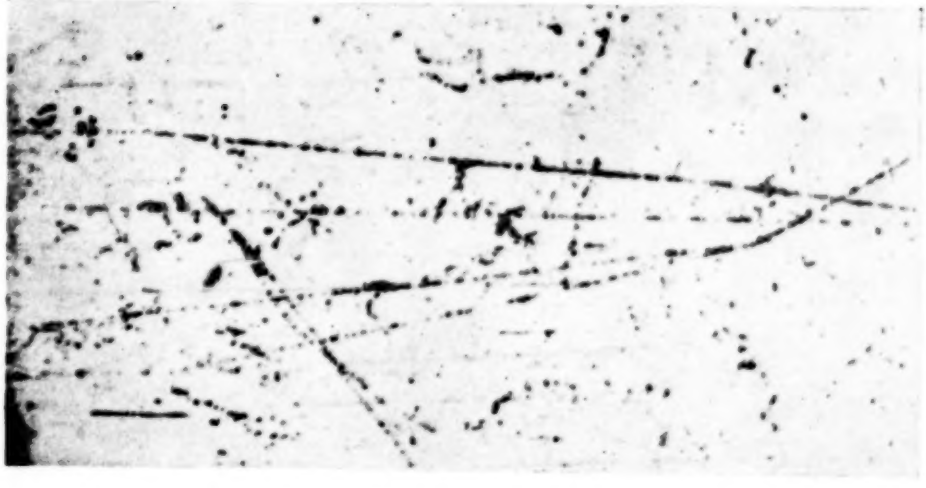

Fig. 4. Bremsstrahlung of elastically or inelastically scattered π-mesons.

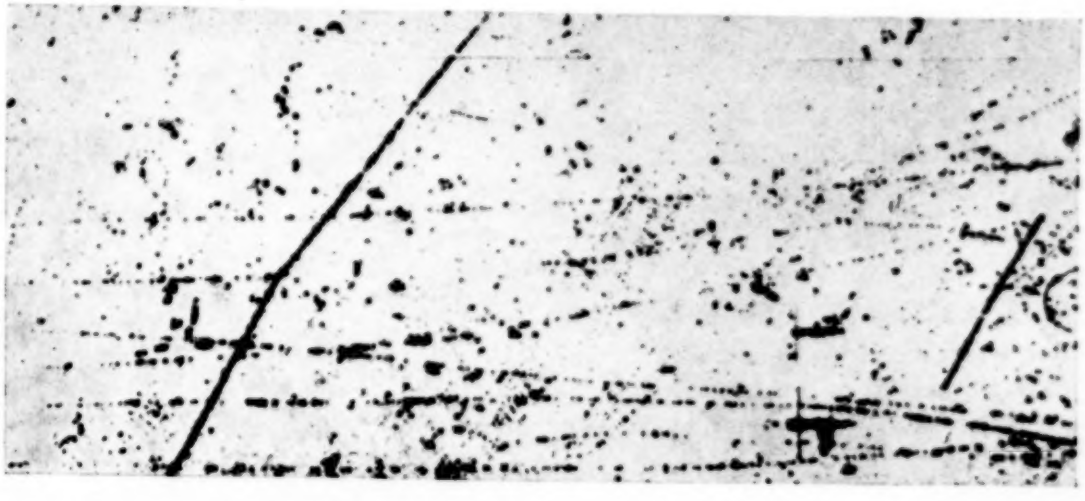

Fig. 5. Bremsstrahlung of absorbed π-mesons.

of the π^+-meson. The γ-quantum energy E_γ was estimated from the electron and positon ranges of the corresponding pair.

TABLE

Observed events of bremsstrahlung of scattered π^+-mesons

(Energy in MeV)

Nos.	π^+ meson energy				Energy of star prongs E_p	γ quantum energy E_γ	$E_0-(E_1+E_p)$
	Before scattering E_0	After scattering E_1					
		From range measurements	From ionization measurements	On basis of other measurements			
1	237	> 60	> 100		> 120	∽ 10	< 17
2	276	> 55	> 70		173	> 30	< 33
3	237	> 50	> 100		100	> 23	< 37
4	170	> 110			–	> 37	< 60
5	183	63			54	> 23	66
6	239	> 40			120	> 29	< 79
7	213	> 60	> 100		20	> 22	< 93
8	147	> 54			–	> 13	< 93
9	262			> 80	77	> 26	< 105
10	266	> 54	> 160	160±80	–	> 17	< 106
11	279	> 165			–	> 28	< 114
12	235			> 69	36	> 55	< 130
13	250	> 65	> 100		18	> 60	< 132
14	265	> 12	> 25		35	15	< 205
15	152	< 5			≈ 7	> 24	< 145
16	256	65			40	> 30	151
17	247	55			20	> 70	< 172
18	261	> 40			46	> 24	< 175
19	249	> 54		≈ 60	–	> 35	< 195
20	259	> 35			–	> 20	< 224

It can be seen from the table that for the first 13 cases the inequality $E_0-(E_1+E_p) < 140$ MeV is fulfilled and hence these events cannot be interpreted as π^0-meson creation according to the scheme $\pi^+ + A \rightarrow \pi^+ + \pi^0 + A'$ and must be ascribed to bremsstrahlung.

In the remaining 7 events (14—20) it is not excluded that $E_0-(E_1+E_p) > 140$ MeV, which signifies possible π^0-meson production. Whether these events are to be ascribed to bremsstrahlung is a question that requires special examination.

Event 14 should be ascribed to bremsstrahlung as indicated by the γ-quantum energy (15 MeV) which was determined from the ranges of the negaton and the positon and the emission angle between them. A π^0-meson decay γ-quantum cannot possess such an energy and the quantum must thus be identified as a bremsstrahlung γ-quantum.

In event 15 the initial π^+-meson energy was $E_0 = 152$ MeV which is close to the energy threshold of π-meson production by π-mesons. Since the probability of observing this process at such a value of E_0 is very small, this event has also been ascribed to bremsstrahlung.

The last 5 events can be attributed with a high degree of probability to bremsstrahlung on basis of the following two considerations. First of all, the cross section of the competing process $\pi^+ + A \to \pi^+ + \pi^0 + A'$ (which for our purpose can be estimated with a sufficient degree of accuracy from the experimental data obtained in the same chamber [8])) is such that not more than one of the five observed events could be of this type. Secondly, measurements of the angle of emission of the γ-quanta show that the radiation is emitted predominantly in the forward direction at angles of about 10—40° whereas the $\pi^+ + A \to \pi^+ + \pi^0 + A'$ process should yield an isotropic distribution of the γ-quanta.

The total bremsstrahlung cross section in elastic and inelastic scattering in the energy region from 80 to 300 MeV was computed from the 20 events presented in the table and found to equal $\sigma_s^\gamma = (4.5^{+1.2}_{-2.0}) \times 10^{-27}$ cm^2 per fluorine nucleus.

It can be seen from the table that in the 80—150 MeV energy region not one case of bremsstrahlung was observed. This can be explained first of all by the experimental conditions inasmuch as in the indicated energy region the number of π-meson traversals through the chamber was several times smaller than at higher energies. Secondly, theoretical estimations (cf. section 5) show that the radiative scattering cross section should be approximately 1.5—2 times smaller for a π-meson energy of 100 MeV than for an energy of 250 MeV.

5. Comparison of Experimental Results and Theory

Bremsstrahlung of π-mesons can be estimated with a satisfactory degree of accuracy in the quasiclassical approximation. We expand the exact expression of the differential cross section for bremsstrahlung $d\sigma_\gamma(\omega, \beta)$ obtained in relativistic quantum mechanics, into γ-quantum energies $\hbar\omega$. The first term in the expansion is of the quasiclassical form, that is, it is the product of the cross section of the corresponding non-radiative process, $d\sigma(\beta)$, by the probability of γ-quantum emission for prescribed motion of the particles, dw_γ. Here β denotes the complete set of initial and final velocities of the interacting particles.

Low [9]) has shown that the second term in the expansion of the exact expression of cross section $d\sigma_\gamma(\omega, \beta)$ can be calculated in a general form. However, if we wish to compute the total radiation there is no sense in using the second expansion term inasmuch as for $\hbar\omega/E \ll 1$ (E is the colliding

particle energy) it yields a correction of the order of $\hbar\omega/E$, which is unimportant for us. If $\hbar\omega/E \approx 1$ the contribution of the second term will be of the same order as that of the following terms in the expansion and hence one cannot be sure that use of the second expansion term in the upper part of the quantum spectrum will improve the accuracy. Moreover, this term contains the derivative of the non-derivative process amplitude with respect to energy and angle. The magnitude of this derivative cannot be determined with satisfactory accuracy from available experimental data. In accord with these remarks we shall employ only the first term in the expansion of $d\sigma_\gamma(\omega, \beta)$ for comparison of our results with the theory.

A virtue of the quasiclassical method of calculating bremsstrahlung is that the respective formulas are expressed in terms of the cross section for the exact non-radiative process, $d\sigma(\beta)$, irrespective of the model of the π-meson-nuclear interaction. This is a very important circumstance in view of the fact that there are no reliable methods for calculation of strong interactions. As regards the high energy of the γ-ray spectrum for which the quasiclassical approximation is invalid, it should be noted that for π-mesons of the energies considered here, the contribution of this part of the spectrum to the total bremsstrahlung cross section is not significant.

Assuming the nucleus to be infinitely heavy and denoting the initial and final π-meson velocities respectively by $\boldsymbol{\beta}_0$ and $\boldsymbol{\beta}_1$ and neglecting radiative energy-momentum losses, we obtain in the quasiclassical approximation

$$d\sigma_\gamma(\omega, \boldsymbol{\beta}_0, \boldsymbol{\beta}_1) \approx dw_\gamma d\sigma(\boldsymbol{\beta}_0, \boldsymbol{\beta}_1)$$
$$= \frac{1}{137}\left[\left(\frac{\boldsymbol{\beta}_0}{1-\boldsymbol{\beta}_0\cdot\mathbf{n}} - \frac{\boldsymbol{\beta}_1}{1-\boldsymbol{\beta}_1\cdot\mathbf{n}}\right)\times\mathbf{n}\right]^2 \frac{d\Omega_\gamma}{4\pi^2}\frac{d\omega}{\omega}\, d\sigma(\boldsymbol{\beta}_0, \boldsymbol{\beta}_1) \qquad (1)$$

where $\mathbf{n}$ is a unit vector along the direction of γ-ray emission, $d\Omega_\gamma$ is a solid angle element of the γ-quanta and $d\sigma(\boldsymbol{\beta}_0, \boldsymbol{\beta}_1)$ is the cross section for the corresponding non-radiative process.

For calculation of the total cross section of any of the types of bremsstrahlung with the aid of formula (1) one should insert, in accord with the classification presented in section 3, the expression for the differential cross section of the corresponding radiationless process and integrate over γ-ray energies and directions and over the final π-meson velocities.

Under the assumption of an isotropic angular dependence, the cross section for inelastic scattering of π-mesons on a nucleus can be written in the form

$$d\sigma_i(\boldsymbol{\beta}_0, \boldsymbol{\beta}_1) = \frac{\sigma_i(\boldsymbol{\beta}_0, \boldsymbol{\beta}_1)}{4\pi}\, d\Omega \qquad (2)$$

where $\sigma_i(\boldsymbol{\beta}_0, \boldsymbol{\beta}_1)$ is the total inelastic scattering cross section, the final velocity of the scattered π-meson being $\boldsymbol{\beta}_1$.

For the angular dependence the π-meson elastic scattering cross section is

$$d\sigma_d(\beta_0, \beta_1) = \frac{\sigma_d(\beta_0)}{\pi} \left| \frac{I_1\left(\frac{R}{\lambda}\theta\right)}{\theta} \right|^2 d\Omega \tag{3}$$

where R is the nuclear radius, $\cos\theta = \boldsymbol{\beta}_0 \cdot \boldsymbol{\beta}_1/\beta_0\beta_1$, $\beta_0 = \beta_1$, λ is the π-meson wavelength and $\sigma_d(\beta_0)$ is the total elastic scattering cross section.

π-meson absorption and charge-exchange scattering will be combined so that the cross section refers to stopping of π-meson charge or, more precisely, to transition of the charge to non-relativistic nucleons:

$$d\sigma_r(\beta_0) = d\sigma_a(\beta_0) + d\sigma_e(\beta_0). \tag{4}$$

Inserting now in formula (1) any of expressions (2), (3) or (4) instead of $d\sigma(\beta_0, \beta_1)$ and integrating, we obtain the required expressions for the total cross section for radiative processes. For bremsstrahlung appearing in inelastic scattering we get

$$\begin{aligned} \sigma_i^{\gamma} &= \tfrac{1}{137} \ln \frac{xE_0}{\hbar\omega_{\min}} \sum_{\beta_1} \left(\frac{1}{\beta_0} \ln \frac{1+\beta_0}{1-\beta_0} + \frac{1}{\beta_1} \ln \frac{1+\beta_1}{1-\beta_1} - 4 \right) \frac{\sigma_i(\beta_0, \beta_1)}{\pi} \\ &\approx \tfrac{1}{137} \ln \frac{xE_0}{\hbar\omega_{\min}} \left(\frac{1}{\beta_0} \ln \frac{1+\beta_0}{1-\beta_0} + \frac{1}{\beta_1} \ln \frac{1+\beta'}{1-\beta'} - 4 \right) \frac{\sigma_1(\beta_0)}{\pi}. \end{aligned} \tag{5}$$

Here $\hbar\omega_{\min}$ is the lowest measured γ-quantum energy. In our experiments $\hbar\omega_{\min} \approx 10$ MeV; β' is a certain mean velocity which the π-meson possesses after scattering. In our calculations it will be assumed that β' corresponds to the kinetic energy $\frac{1}{2}E_0$. x is a certain cut-off parameter of the γ-quantum spectrum. If one assumes $x = 1$, i.e., that the spectrum is not cut-off, the quasiclassical formulas will yield total cross section values which are higher than those derived from the exact formula $\int d\sigma_\gamma(\omega, \beta) d\omega$. By appropriately selecting the value of parameter x the quasiclassical formulas can be made to be as precise as $\int d\sigma_\gamma(\omega, \beta) d\omega$. For the π-meson energies we are dealing with the best fit is obtained with $x \approx \frac{1}{2}$.

The total cross section for radiative elastic scattering can be obtained in a similar manner:

$$\sigma_d^{\gamma} = \tfrac{1}{137} \ln \frac{xE_0}{\hbar\omega_{\min}} I\left(\beta_0, \frac{\mu c}{\hbar} R\right) \frac{\sigma_d(\beta_0)}{\pi} \tag{6}$$

where in the general case the integral $I(\beta_0, \mu cR/\hbar)$ should be evaluated numerically. In our case we can use the approximate value of this integral for $(1-\beta^2)^{-1} \gg 1$ and $2\mu cR/\hbar \gg 1$ which is $2.3/(\mu cR/\hbar)$. Finally, upon "stopping" of the charge the total bremsstrahlung cross section will be

$$\sigma_r^{\gamma} = \tfrac{1}{137} \ln \frac{xE_0}{\hbar\omega_{\min}} \left(\frac{1}{\beta_0} \ln \frac{1+\beta_0}{1-\beta_0} - 2 \right) \frac{\sigma_r(\beta_0)}{\pi} \tag{7}$$

where σ_r is the sum of the π-meson absorption and charge-exchange scattering cross sections: $\sigma_r = \sigma_a + \sigma_e$.

For comparison of our results with the theory it should be noted that for the 20 bremsstrahlung events observed for scattered π-mesons, the initial mean energy of the π^+-mesons was 234 MeV. The cross sections σ_1, σ_d and σ_r for 230 MeV mesons which we require have been measured by Dželepov *et al.*[10]). Calculations performed on basis of formulas (5) and (6) yield for the bremsstrahlung cross section of 230 MeV scattered π-mesons $\sigma_s^\gamma = \sigma_1^\gamma + \sigma_d^\gamma = 3.5 \times 10^{-27}$ cm^2 per fluorine nucleus which is in agreement with the value measured by us, $\sigma_s^\gamma = (4.5^{+1.2}_{-2.0}) \times 10^{-27}$ cm^2. The bremsstrahlung cross section for stopping of charged particles computed from formula (7), $\sigma_r^\gamma = 2.5 \times 10^{-27}$ cm^2 also agrees with our results which include 5 bremsstrahlung events of this type.

In conclusion the experimental angular distribution of bremsstrahlung γ-quanta can be compared with the theory. Emission angles of the γ-quanta were measured in each of the 20 cases presented in the table. It was found that only in two cases was the radiation directed backwards. This is the sort of distribution one would expect theoretically since formulas (1)—(3) yield a forward-backward ratio of 10.

The authors would like to express their gratitude to I. Ya. Pomeranchuk for interest in this work.

References

1) L. D. Landau and I. Ya. Pomeranchuk, JETP **24** (1953) 505
2) Yu. A. Vdovin, Doklady AN SSSR **105** (1955) 947
3) V. G. Solovyov, JETP **29** (1955) 242
4) R. E. Cutkosky, Phys. Rev. **109** (1958) 209
5) G. A. Blinov, Yu. S. Krestnikov and M. F. Lomanov, JETP **31** (1956) 762; Soviet Physics JETP **4** (1957) 661
6) G. A. Blinov, Yu. S. Krestnikov, M. F. Lomanov and Ya. Ya. Shalamov, JETP **32** (1957) 1572
7) A. I. Mukhin, E. B. Ozerov and B. Pontecorvo, JETP **31** (1956) 371
8) G. A. Blinov, M. F. Lomanov, Ya. Ya. Shalamov, V. A. Shebanov and V. A. Shchegolyev, JETP **35** (1958) 880
9) F. Low, Phys. Rev. **110** (1958) 974
10) V. P. Dželepov, V. G. Ivanov, M. S. Kozodayev, V. T. Osipenko, N. I. Petrov and V. A. Rusakov, JETP **31** (1956) 923

1.D.2:
2.H:2.L

Nuclear Physics **10** (1959) 294—305; © *North-Holland Publishing Co., Amsterdam*
Not to be reproduced by photoprint or microfilm without written permission from the publisher

INELASTIC SCATTERING FROM SEPARATED LUTECIUM ISOTOPES

B. ELBEK, M. C. OLESEN and O. SKILBREID
Institute for Theoretical Physics, University of Copenhagen

Received 11 December 1958

Abstract: Lutecium targets of high isotopic purity have been prepared in an electromagnetic isotope separator. In order to obtain thin deposits of the target material on fragile backings, a method has been developed where the ions after the separation are strongly retarded by an electrical potential on the collector. Targets prepared in this way have been used to study the Coulomb excitation of the rare odd isotope Lu^{176} and of the abundant isotope Lu^{175} by observation of inelastically scattered protons and deuterons in a magnetic spectrometer. The measured excitation energies and transition probabilities in Lu^{176} are in good agreement with the predictions of the rotational model if the ground state spin of this isotope is 7.

1. Introduction

Due to its high spin the odd isotope Lu^{176} is an interesting nucleus to study. Recent spectroscopic measurements have determined the ground state spin as 6, the values 5 or 7 not being absolutely excluded [1]). Previous spectroscopic work indicated a value of the spin $\geqq 7$ [2]). Very little is known about the level scheme, as is the case for most other odd nuclei in the region of strong deformations.

Some information about the level scheme of Lu^{176} could be obtained from the Coulomb excitation, which should reveal the two lowest states belonging to the ground-state rotational band. If the ground state has spin I_0, these two states will have spins I_0+1 and I_0+2, and their energies and reduced E2 transition probabilities should be given by the rotational theory in terms of the nuclear moment of inertia and the intrinsic quadrupole moment [3]).

By detection of inelastically scattered protons and deuterons we have studied the Coulomb excitation of Lu^{176}. In addition, more accurate data on the transition probabilities in Lu^{175} were obtained.

2. Targets

In natural lutecium the odd isotope Lu^{176} has an abundance of 2.6 %, the rest being Lu^{175}. For a reliable observation of the Coulomb excitation of the rare isotope, separated targets are therefore essential. The targets used in

our experiment were prepared in the electromagnetic isotope separator of this Institute [4]). Formerly, a sputtering technique had been used for the preparation of targets when thin backings were employed, whereas direct deposition was used on thick aluminium backings. None of these methods is applicable in the present case, where highly concentrated and chemically pure samples on thin backings are essential [5]).

In order to meet these requirements, a collection technique has been developed for the deposition of stable isotopes directly on fragile backings, which, without special precaution, would be destroyed by bombardment in the isotope separator. By this technique, the energy of the ions to be collected is reduced by an electrical potential from originally about 50 keV to about 1 keV. It is then possible to collect the ions on thin Formvar foils strengthened by a layer of evaporated aluminium. Furthermore, the material is concentrated on a very small area, and the usual penetration of the particles into the surface of the backing is prevented.

The setup used is shown on fig. 1. The ions to be collected pass a slit in an existing base plate (1). By a guard plate (2) at a negative potential of about 1kV, secondary electrons are prevented from reaching the collector. The energy of the ions impinging on the foil is adjusted by means of a corona current to the end of the resistor R, which is connected to the high voltage of the separator. In order to reduce the electrostatic forces on the foil and to yield a rather strong focusing effect, the collector electrode (3) is given the shape shown on the figure. This focusing is actually so strong that the focal point lies in front of the foil. The deposition takes place within an area of approximately 1×5 mm^2. It was found preferable to let the beam enter the collector a little off center in order to utilize the energy separation of the ions in the electrostatic field. While no investigation was made to find whether this really gives an increase in enrichment, it was found that, in fact, we do get two separate spots where the deposition occurs, the lower probably being caused by neutral atoms. Because of space-charge effects it is difficult to use beam currents higher than 5—10 μA. For the isotope Lu^{176} the maximum obtainable beam current was only about 1 μA. With this current, a target having a density of 30—40 μg/cm^2 is prepared in the course of approximately 2 hours.

3. Inelastic Scattering Measurements

The experimental arrangement was essentially the same as earlier described [5,6]). Protons and deuterons were accelerated to 4—4.5 MeV in an electrostatic generator. For energy selection a 90° analyzing magnet was used, so that the energy spread of the particles impinging on the target was about 5 keV. In most cases, the dimensions of the beam spot were 3×0.3 mm^2 and the average beam current was 0.2 μA. The small beam spot is

required to obtain full resolution of the spectrometer, but was in this case also necessary because of the rather small area on the target which was actually covered with the target material. The target was visually aligned in the target chamber so that the beam struck the densest part. It

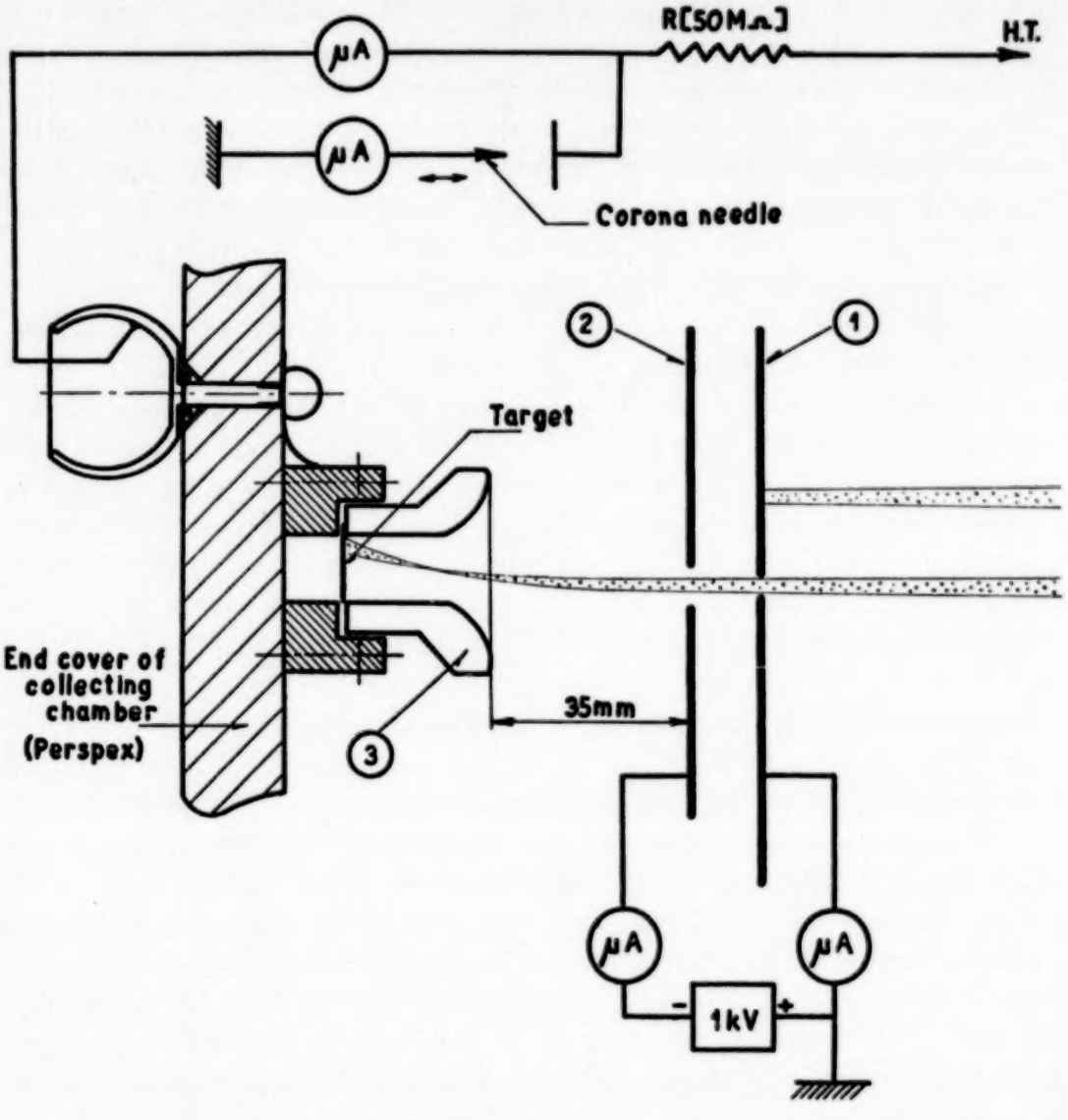

Fig. 1. Arrangement used for collecting the separated isotopes directly on a thin foil.

appeared that the slit system present in front of the target insured to a high accuracy that the beam always hit the same spot on the target, as demonstrated by the fact that no intensity variations due to beam shifts were seen. The particles scattered from the target through an angle of 145° were observed with the heavy particle spectrometer and were recorded on photographic plates with an emulsion thickness of 25 μ for proton detection and

50 μ for deuteron detection. The thicker emulsion facilitates the differentiation between simultaneously occurring (d, p) protons from the backing and the scattered deuterons of the same momentum. To increase the difference in range of these two kinds of particles, the plate was covered with a 5 mg/cm^2 absorber ensuring that the deuterons were stopped in the emulsion, whereas the protons passed through. Foils of polyvinyl chloride turned out to be the most satisfactory absorbers. They are free of wrinkles and have a convenient adhesion to the plate due to electrostatic forces.

By shifting the plate-holder laterally in the spectrograph three different exposures could be made on the same set of plates. As the elastically scattered group is very intense (in these experiments it often contained more than 10^6 tracks), a short normalizing run was recorded on the two adjacent zones of the plate before and after each long run. The normalizing exposures were about 10 μC each, whereas the long exposures ranged from 1000 to 6000 μC. Energy shifts and comparison of the proton exposures with the deuteron exposures served to distinguish inelastic groups from elastic groups due to various contaminants.

In the case of Lu^{176}, the inelastic group due to the first excited state was readily identified. The expected energy was in the range 150—200 keV (see section 4) and a group of the expected intensity was found at 184 keV. Gamma rays [7]) and conversion electrons [8]) corresponding to a level at 180 keV had earlier been observed in Coulomb excitation of natural lutecium and had tentatively been ascribed to Lu^{176}. With the energy of the first excited state known it was easy to calculate the expected position of the second excited state. For the possible values of the ground-state spin, the energy should be around 390 keV, and a group of the expected intensity was actually found at 388 keV. This group was observable only in the exposures with deuterons, as the corresponding region of the plate was obscured by strong elastic groups from chlorine in the proton exposures. The observed group was therefore identified as inelastic by changes of the bombarding energy only.

Two inelastic groups were ascribed to well-known rotational states of Lu^{175} at 113.8 and 251.0 keV [9]). These groups were present in all the exposures with a somewhat fluctuating intensity due to the varying enrichment obtained in the isotope separation. An inelastic group corresponding to an excitation energy of 83 keV was present for some of the targets and was ascribed to the first excited state in Yb^{176}, in agreement with our measurements of this isotope [10]). The presence of a small amount of Yb was also clearly visible during the isotope separation.

An elastic group corresponding to a mass number around 140 was assigned to Pr^{141}. This nucleus is expected in the target because the composite ion $Pr^{141}Cl^{35}$ has the mass 176. The intensity of this group indicated a praseo-

dymium contamination of the charging material for the isotope separator of a few parts in 10^5. This is not unlikely in view of the difficulties in obtaining absolutely pure rare-earth samples. Fig. 2 shows the spectrum of scattered deuterons from a Lu^{176} target.

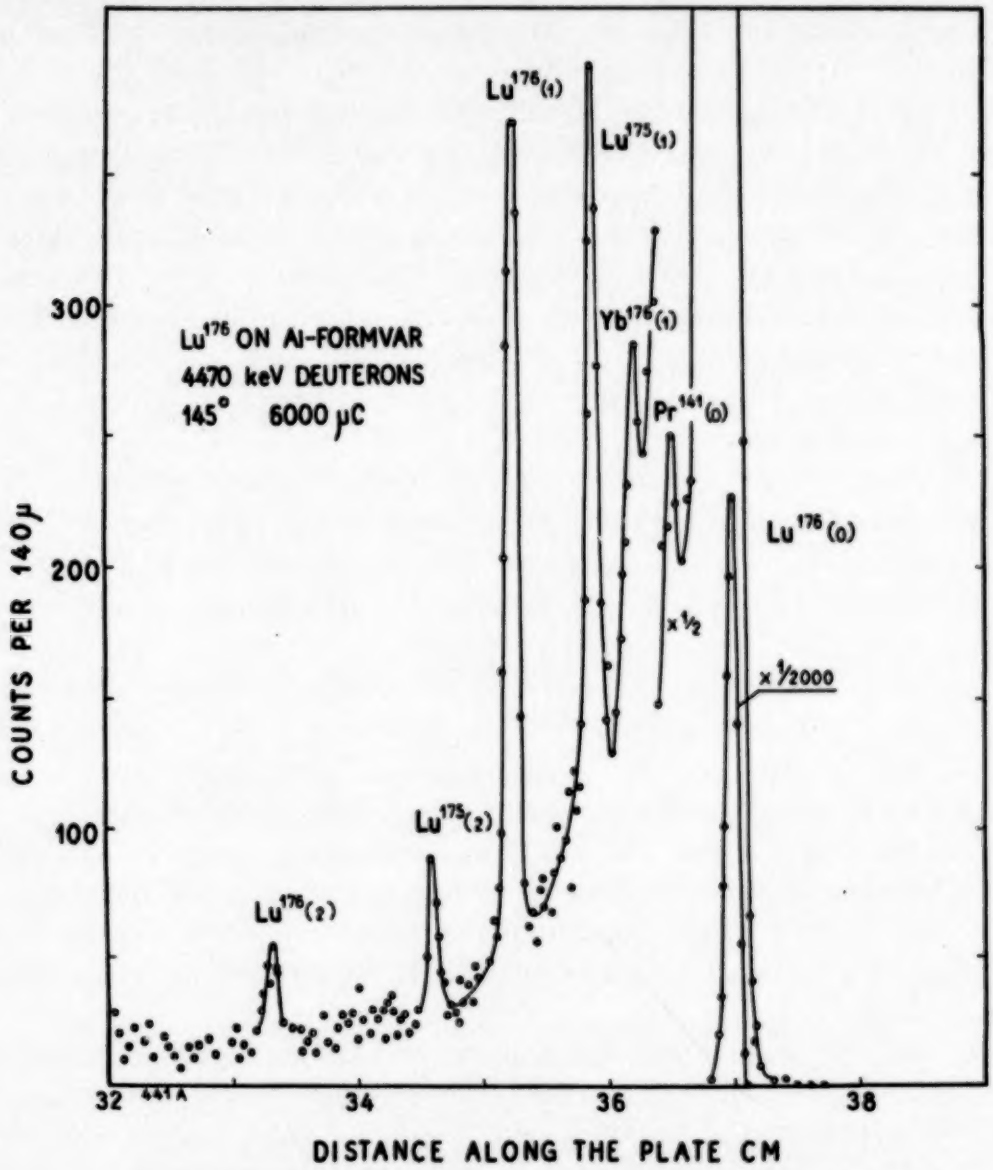

Fig. 2. Spectrum of deuterons scattered from a Lu^{176} target.

To obtain the absolute cross section for the inelastic scattering it was necessary to know the percentage of Lu^{175} and Yb^{176} present in each target, as these isotopes contribute to the elastic group which, in turn, is used in the evaluation of the inelastic cross sections. The amount of these isotopes was therefore determined from the intensities of their inelastic groups. The

corresponding absolute cross sections had been determined in a separate series of measurements also using separated targets. Usually the amount of Lu^{175} was found to be about 20 % of the total, but in some of the separations a content as low as 7 % was obtained. The content of Yb^{176} was low, the average being 5 %. These figures are in good agreement with the result of intensity measurements in the mass spectrum during the separation. An ytterbium content in the charging material (nominal purity 99.5 %) of about 0.1 % would account for the observed contamination.

Corrections like those mentioned above make of course the cross-section determinations more uncertain, but not to any serious extent. We believe that the quantity of Lu^{176} present in each target could be determined to an accuracy of a few per cent.

The energies of the excited states were obtained from the position of the corresponding groups on the photographic plates combined with the magnitude of the homogeneous magnetic field measured with a nuclear induction gauss-meter. A check on the energies determined could be obtained from the Lu^{175} groups present, as their energies are known to a high accuracy [9]). Small deviations in our energies for these groups were therefore used to correct the energies of the Lu^{176} groups, but the corrections were usually small and showed no systematic behaviour.

The measured energies and electric quadrupole transition probabilities $B(E2)$ are collected in table 1, which gives the averages of several measure-

TABLE 1

Measured excitation energies, electric quadrupole transition probabilities, and intrinsic quadrupole moments of the lutecium isotopes

Nucleus	I_0	E_1	E_2	E_2/E_1	B_1	B_2	B_2/B_1	Q_0
Lu^{175}	$\frac{7}{2}$	114	251	2.20	2.34 ± 0.10	0.57 ± 0.08	0.244	7.45
Lu^{176}	7?	184	388	2.11	1.58 ± 0.10	0.231 ± 0.015	0.146	7.38

I_0 is the ground state spin, E_1 and E_2 are the energies of the first and the second excited state, respectively, given in keV. B_1 and B_2 are the corresponding reduced transition probabilities in units of $e^2 \times 10^{-48}$ cm^4. Q_0 denotes the intrinsic quadrupole moment derived from the transition probability B_1, the unit being 10^{-24} cm^2. The errors given for the B-values are standard errors on the mean. The errors in the excitation energies are estimated to be $\pm$ 2 keV.

ments, using various targets and bombarding conditions. On Lu^{176} we have 18 exposures using 9 different targets. Table 1 also gives the ratios of the two transition probabilities and the ratio of the two excitation energies for each nucleus. These ratios are important for a comparison with the predictions of the rotational model. Fig. 3 shows the levels studied in this experiment.

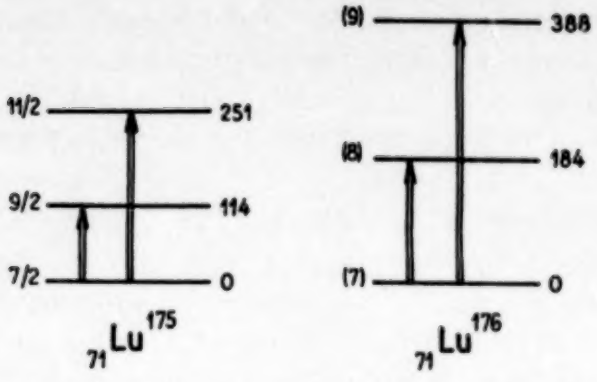

Fig. 3. Levels of the lutecium isotopes observed with inelastic scattering.

4. Discussion

4.1. MOMENTS OF INERTIA AND SPIN OF Lu^{176}

In the case of Lu^{176} we have four measured quantities: the energies of the first and second excited state, respectively, and the corresponding values of $B(E2)$. According to the rotational description, certain relations exist for these quantities. We therefore wish to discuss the data in terms of the rotational model, since they provide the possibility of testing the theoretical predictions in the specific case of odd-odd nuclei, where only little experimental material is yet available.

The excitation energies E_1 and E_2 are determined by the magnitude of the nuclear moment of inertia $\mathcal{J}$ by [3])

$$E = \frac{\hbar^2}{2\mathcal{J}}\,[I(I+1)-I_0(I_0+1)] \quad (I_0 \neq \tfrac{1}{2}). \tag{1}$$

Here, I_0 is the ground-state spin and I the spin of the excited state in question. For an odd nucleus, according to the theory, $I = I_0+1$ for the first excited state and $I = I_0+2$ for the second excited state of the ground-state rotational band.

One can obtain an approximate knowledge of the magnitude of the nuclear moment of inertia of Lu^{176} by considering the neighbouring nuclei whose excitation energies are known. For an even nucleus, the excitation energy of the first rotational state is $3\hbar^2/\mathcal{J}$, a quantity conveniently used in comparing nuclear moments of inertia. For an odd-mass nucleus the rotational energies are given by eq. (1).

In general, odd-mass nuclei have larger moments of inertia than neighbouring even nuclei. This is ascribed to Coriolis effects in the motion of the last odd particle [3]). For a single odd particle, the increase in the moment of inertia is of the order of 20 %, but to some extent appears to be determined by the orbit occupied by the odd particle. For an odd nucleus, the increase in the moment of inertia should be even more pronounced, owing to the

addition of two unpaired particles. If the effects in the moment of inertia were additive, one could get the moment of inertia of Lu^{176} from that of Lu^{175} by adding the contribution from the odd neutron. The odd neutron is presumably the same as found in Hf^{177} (cf. below), where it reduces the $3\hbar^2/\mathcal{J}$ from 89 keV for Hf^{176} to 75 keV for Hf^{177}. A similar contribution would reduce the $3\hbar^2/\mathcal{J}$ from 75 keV for Lu^{175} to 66 keV for Lu^{176}. With this estimate of the moment of inertia, the probable energy of the first excited state of Lu^{176} is 154 keV if I_0 is 6, 176 keV if I_0 is 7, and 198 keV if I_0 is 8. The experimental value, 183 keV, then favours $I_0 = 7$. However, the estimates made are not very accurate.

4.2. DEVIATIONS FROM ROTATIONAL STRUCTURE

As seen from eq. (1), the ratio of the energy of the second excited state to that of the first excited state is determined only by I_0 and equals $(2I_0+3)/(I_0+1)$. Unfortunately, this expression is rather insensitive to the value of I_0 when I_0 is large, and a very good accuracy is needed in the experimental energies to permit a determination of the ground-state spin. Thus, for a spin around 7, the ratio changes by less than 1 % for one unit change in I_0. It is of course also questionable to what extent the energy ratio is correctly given by the theory. It is known that, for most nuclei, the observed energy ratio deviates somewhat from the calculated value. The rotational theory ascribes these deviations to the coupling between rotational and intrinsic motion. Partly, there is a coupling between rotation and vibration which is assumed to account for the observed deviations in even nuclei. In addition, in odd-mass or in odd nuclei, there may be specific effects associated with a partial decoupling of motion of unpaired nucleons from the rotational motion [11]). If these couplings can be treated as perturbations, one obtains to first order for the corrections to (1):

$$\delta E = -\beta[I(I+1)-I_0(I_0+1)]^2. \tag{2}$$

The even nuclei in the region of Lu^{176} show values of $2\beta\mathcal{J}/\hbar^2$ of 5×10^{-4} (Hf^{180}: ref. [12]), Hf^{178}: ref.[13])). If we assume that the unpaired nucleons in Lu^{176} occupy the same orbits as the odd nucleons in Lu^{175} and Hf^{177}, some information on the nucleonic decoupling can be obtained from the energy levels for these nuclei. The accurate measurements of the spectra [9,14]) yield values of $2\beta\mathcal{J}/\hbar^2$ of similar magnitude as in even nuclei, indicating a relatively small contribution from the unpaired nucleons. One is then led to expect that also Lu^{176} should have a β-value comparable to that of the even nuclei. Since, for the ratio E_2/E_1, one has from (1) and (2)

$$\frac{E_2}{E_1} = \frac{2I_0+3}{I_0+1}\left(1-2(I_0+2)\frac{2\beta\mathcal{J}}{\hbar^2}\right), \tag{3}$$

one obtains an expected correction of the order of 1 %.

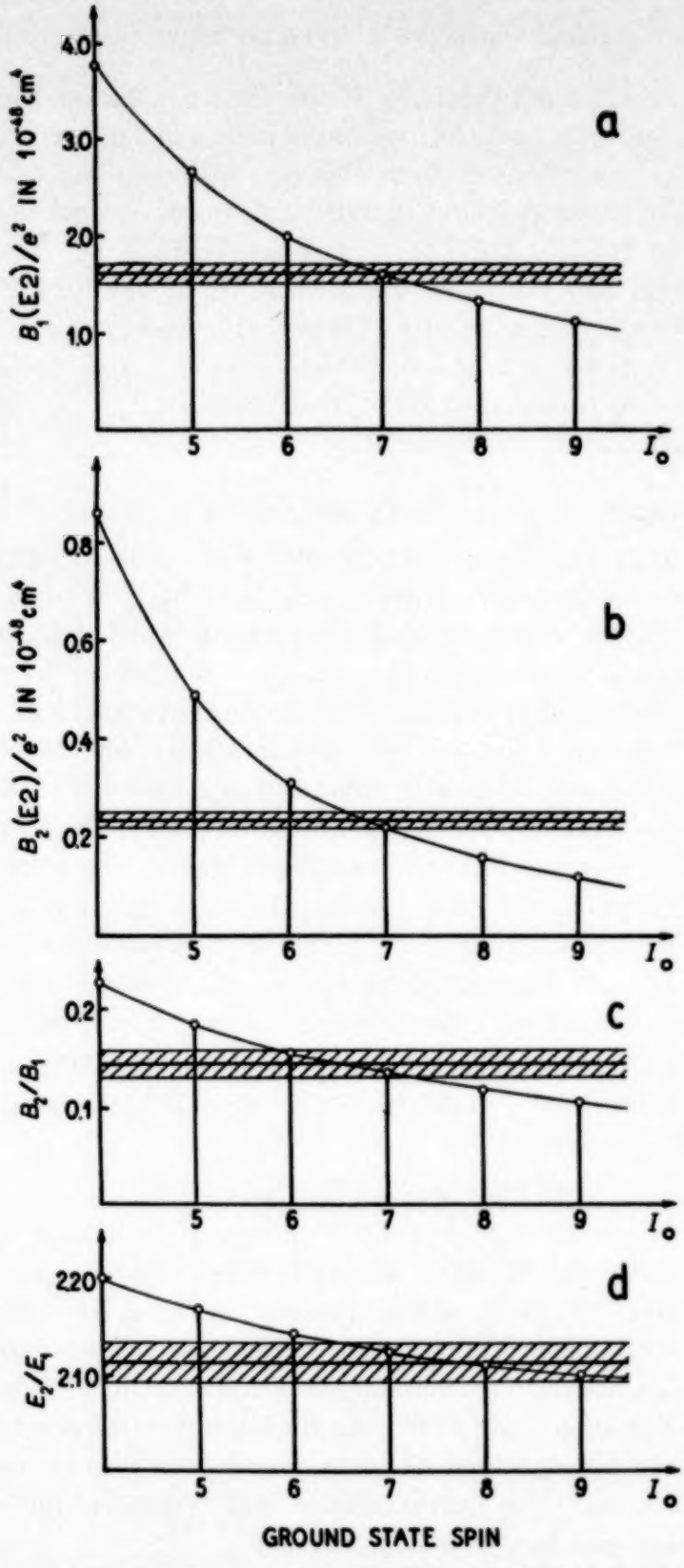

Fig. 4. The curves show the variation with ground-state spin of certain properties of the Lu^{176} levels observed by Coulomb excitation. They are based on the predictions of the collective model. The hatched areas give the experimental values.

a) Transition probability to the first excited state.
b) Transition probability to the second excited state.
c) Ratio of the transition probability of the second excited state to that of the first excited state.
d) Ratio of the energy of the second excited state to that of the first excited state.

In fig. 4d, our measured energy ratio is shown together with the uncorrected theoretical ratio for different values of I_0. The experimental value indicates a ground-state spin about 8, but the mentioned correction could bring a smaller spin value in agreement with the data.

4.3. QUADRUPOLE MOMENTS AND TRANSITION PROBABILITIES

The rotational theory gives the reduced electric quadrupole transition probabilities in terms of the intrinsic quadrupole moment Q_0 and the ground-state spin I_0. The two measured transition probabilities are therefore, in principle, sufficient for the determination of both quantities. For the comparison of our data with the theory we have found it advantageous, however, to make use of the spectroscopically measured ratio of the quadrupole moment of Lu^{176} to that of Lu^{175}. This ratio is known with reasonable accuracy [1]) and permits the determination of the intrinsic quadrupole moment of Lu^{176} from the intrinsic moment of Lu^{175} obtained in this experiment.

From atomic hyperfine structure, one determines a quadrupole moment Q related to the intrinsic quadrupole moment Q_0 through [3])

$$Q = Q_0 \frac{I_0(2I_0-1)}{(I_0+1)(2I_0+3)}. \tag{4}$$

The value of the ratio Q^{176}/Q^{175} obtained from the analysis of the hyperfine-structure patterns depends somewhat on the assumed value of the ground-state spin of Lu^{176}. For a spin of 6, the ratio Q^{176}/Q^{175} was found to be 1.43 ± 0.08 [1]). For a spin of 7, the ratio should be slightly smaller, but insufficient information is contained in the published data to make possible a determination of the change †. For the hyperfine structure terms used in earlier measurements by Schüler and Gollnow it is known that one unit increase in I_0 would decrease the ratio of the Q's by approximately 5 %, if the spin is 7 [2]). This change is relatively small considering the uncertainties in the measurements; since its actual value is unknown, we have used the ratio $Q^{176}/Q^{175} = 1.43$ also for other values of I_0 in evaluating the corresponding intrinsic quadrupole moments of Lu^{176} from the intrinsic quadrupole moment of Lu^{175} given in table 1. The anticipated transition probabilities $B(E2)$ to the first and the second excited states in Lu^{176} were then calculated, using the formulae of the rotational theory. The results of this calculation are shown in figs. 4a and 4b together with the experimental values for the transition probabilities. It is seen that the $B(E2)$ values are rather strongly dependent on I_0 and that the experimental data are in best agreement with a ground-state spin of 7. This conclusion will probably not be changed if the variation of the spectroscopical ratio of the quadrupole moments with the

† *Note added in proof:* Recently, a more detailed report on the spectroscopic measurements has been published [18]).

spin is included. This would make the curves on figs. 3a and 3b a little steeper, crossing the present curves in the point corresponding to $I_0 = 6$. The change for $I_0 = 7$ should only be a few per cent, which is much less than the experimental error.

The ratio $B_2(\mathrm{E2})/B_1(\mathrm{E2})$ is determined solely by the ground-state spin and is therefore independent of any assumptions regarding the quadrupole moments or the absolute magnitude of the transition probabilities. However, the ratio is not very strongly dependent on I_0, and both spin 6 and 7 are in agreement with the experimental data (fig. 4c).

4.4. SPINS AND MAGNETIC MOMENTS ON STRONG COUPLING SCHEME

The conclusion is then, assuming no appreciable perturbations in the rotational spectrum, that the measurements on Lu^{176} are most satisfactorily accounted for if the ground-state of this isotope is 7. This has also the reasonable consequence that the intrinsic quadrupole moments of Lu^{176} and Lu^{175} are almost equal. As spin 7 is in disagreement with the most recent spectroscopical determination, it is of interest to see how it fits with the strong coupling scheme generally valid for nuclei in this region and with other properties of the Lu^{176} nucleus. The spin of Lu^{175} is $\frac{7}{2}$ and the parity even. Here, probably, the odd proton is found in the same orbit as in Lu^{176}, whereas the odd neutron of Lu^{176} is found in Hf^{177} which also has spin $\frac{7}{2}$ and presumably odd parity. In the strong coupling limit, the two odd particles should yield spin 7 (or 0) and odd parity for the ground state of Lu^{176}.

In the same way, the magnetic moment should be determined by the moments of Lu^{175} and Hf^{177}. Using the strong coupling scheme and the usual estimate Z/A for the collective gyromagnetic ratio, one finds with $\mu^{175} = 2.20$ [1]) and $\mu^{177} = 0.61$ [15]) that μ^{176} equals 2.68. This is in good agreement with the experimental value 2.8 ± 0.3 [1]) and lends further support to the correctness of the assigned orbits for the odd particles.

4.5. β-DECAY OF Lu^{176}

Finally, it is interesting to consider the decay of the ground state of Lu^{176} to the 6^+ excited state of Hf^{176}. With the ground state of Lu^{176} being 7^- the decay must be at least first forbidden. The observed log ft for this transition is 18.9, which may be compared with about 8 as the usual value for first forbidden decays. The very large hindrance must be due to the change of the K-quantum number from 7 to 0, and the decay is thus an example of a highly K-forbidden transition [16]).

4.6. TRANSITION PROBABILITIES AND QUADRUPOLE MOMENT OF Lu^{175}

The transition probabilities for Lu^{175} compare well with earlier determinations (see compilation in ref. [3])) and their ratio 0.244 is, within the limits of error, in agreement with the rotational prediction $\frac{18}{7} = 0.257$. The

spectroscopic quadrupole moment of Lu^{175} has been given[1]) as $(5.6\pm0.5)\times10^{-24}$ cm^2 and corresponds to an intrinsic moment of $(12.0\pm1.1)\times10^{-24}$ cm^2. This does not compare too well with the value $(7.45\pm0.35)\times10^{-24}$ cm^2 we derive from the transition probabilities. The discrepancy, which is of the same order of magnitude as observed in other cases where the quadrupole moment has been determined in both ways, might be due to the lack of knowledge of the electronic wave functions necessary for obtaining the absolute spectroscopic quadrupole moment from the hyperfine structure separations [17]).

The authors wish to thank Professor Niels Bohr for the excellent working conditions at his Institute and Professor A. Bohr and Dr. B. R. Mottelson for enlightening discussions. We gratefully acknowledge the untiring assistance of Mr. P. Ambrosius-Olesen in all phases of the experiment and of Mrs. Ruth Hansen in counting the nuclear tracks in the plates.

References

1) A. Steudel, Naturwiss. **44** (1957) 371
2) H. Schüler and H. Gollnow, Z. Phys. **113** (1939) 1
3) K. Alder, A. Bohr, T. Huus, B. R. Mottelson and A. Winther, Revs. Mod. Phys. **28** (1956) 432
4) K. O. Nielsen and O. Skilbreid, Nuclear Instruments **2** (1958) 15
5) B. Elbek, K. O. Nielsen and M. C. Olesen, Phys. Rev. **108** (1957) 406
6) V. Ramsak, M. C. Olesen and B. Elbek, Nuclear Physics **6** (1958) 451
7) N. P. Heydenburg and G. M. Temmer, Phys. Rev. **100** (1955) 150
8) E. M. Bernstein and H. W. Lewis, Phys. Rev. **105** (1957) 1524
9) E. N. Hatch, F. Boehm, P. Marmier and J. W. M. DuMond, Phys. Rev. **104** (1956) 745
10) B. Elbek, M. C. Olesen and O. Skilbreid, to be published
11) A. K. Kerman, Mat. Fys. Medd. Dan. Vid. Selsk. **30** (1956) no. 15
12) J. W. Mihelich, G. Scharff-Goldhaber and M. McKeown, Phys. Rev. **94** (1954) 794(A)
13) F. F. Felber, M. A. Thesis, University of California Radiation Laboratory, Report UCRL-3618 (1956) unpublished
14) P. Marmier and F. Boehm, Phys. Rev. **97** (1955) 103
15) P. R. Speck and F. A. Jenkins, Phys. Rev. **101** (1956) 1831
16) G. Alaga, K. Alder, A. Bohr and B. R. Mottelson, Mat. Fys. Medd. Dan. Vid. Selsk. **29** (1955) no. 9
17) K. Murakawa and T. Kamei, Phys. Rev. **105** (1957) 671
18) A. Steudel, Z. Phys. **152** (1958) 599

1.D.2 *Nuclear Physics* **10** (1959) 306—310; © *North-Holland Publishing Co., Amsterdam*
Not to be reproduced by photoprint or microfilm without written permission form the publisher

HOLES IN THE 1p SHELL IN THE UNIFIED MODEL

C. S. WARKE
Tata Institute of Fundamental Research, Bombay
and
G. ABRAHAM
Atomic Energy Establishment, Trombay, Bombay

Received 28 November 1958

Abstract: The negative parity levels in nuclei of mass number $A = 13, 17, 19$ are derived on the basis of a hole in the $1p_{\frac{3}{2}}$ or $1p_{\frac{1}{2}}$ shells weakly coupled to the surface oscillations.

1. Introduction

The unified model with weak coupling has been shown to improve the single particle description of the shell model in the region where the 2s, 1d shells are filling up [1,2,3]). For F^{19} this is very similar to the improvement obtained in the shell model [4]) by taking into account all nucleons outside the closed shell O^{16} and the mixing of the 2s, 1d configurations. This suggests that there is some correspondence between the two models, which can perhaps be explained with the aid of group theory [5]).

This paper derives negative parity levels of the nuclei of mass numbers 13, 17, 19. In the first case we can compare the results with the extensive work of Lane and Radicati [6]) and Kurath [7]) based on the shell model. For the two other nuclei there is so far no shell model calculation.

In the model used here, it is necessary to know the separation of the levels due to a $1p_{\frac{3}{2}}$ hole and a $1p_{\frac{1}{2}}$ hole in the absence of coupling to collective oscillations. This is taken to be 6 MeV which is approximately the separation between the ground state and first excited negative parity state in N^{15} and O^{15}. The observed spin assignments [8,9]) are consistent with this assumption.

2. Results

2.1. $A = 17, 19$

The model for the mass 17 nuclei is the same as that [2]) for the positive parity levels in mass 19 except that the single particle in the 2s, 1d levels is replaced by a hole in the $1p_{\frac{3}{2}}$ and $1p_{\frac{1}{2}}$ shell. This means that here also $\hbar\omega$ can be taken to be 2 MeV which is nearly the $(0^+, 2^+)$ separation observed in O^{18}. The calculated energy levels are shown in fig. 1 together with the

observed levels [8,9]) of O^{17}. The energies were calculated for $P(\hbar\omega)^2 = 1.5$ and 3 and from the known value at $P = 0$, the trend is found to be nearly

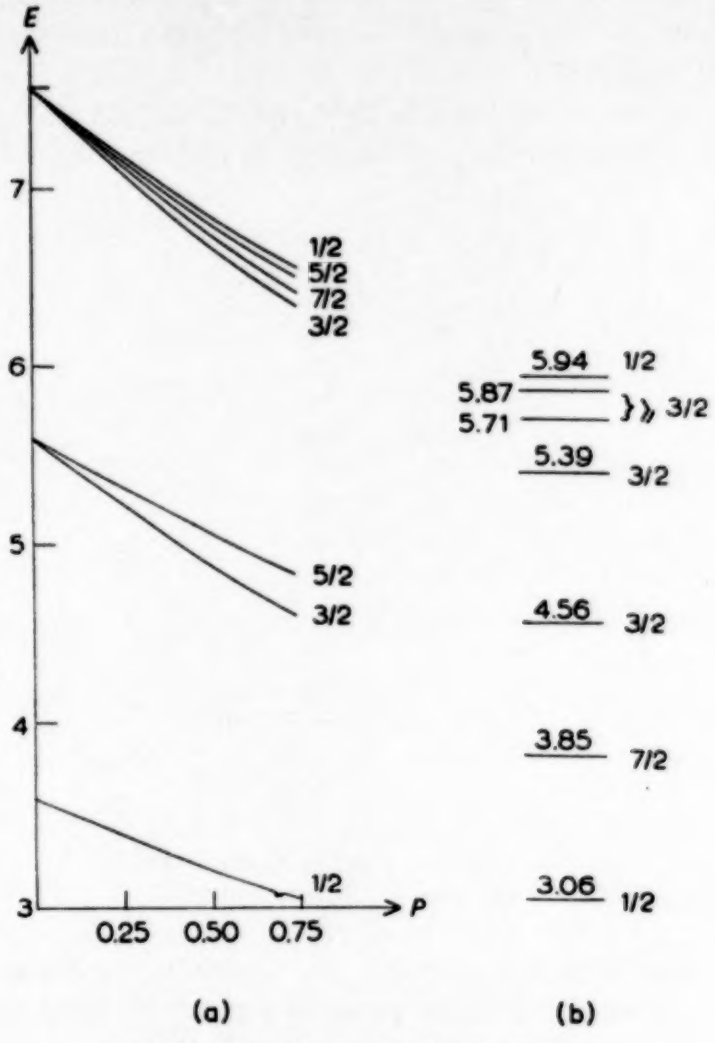

Fig. 1. Negative parity levels of O^{17}.
(a) calculated, (b) experimental.

linear in all cases. Here P is the dimensionless coupling constant

$$P = \frac{5}{32\pi} k^2 \hbar (BC)^{-\frac{1}{2}} (\hbar\omega)^{-2}. \tag{1}$$

The three lower levels arise mainly from the coupling of zero and one quanta to the $p_{\frac{1}{2}}$ hole, and the contribution of numbers of quanta greater than two is neglected. The group of four higher levels are mainly two-quanta states and therefore it is necessary to include three-quanta states. The wave-functions for three surface quanta are given in the appendix. The largest coefficient of any three-quanta term in the normalized wave-function for any level is less than 0.3 and so the energies may not be much affected by inclusion of higher quanta terms. The $\frac{3}{2}^-$, $\frac{1}{2}^-$ separation agrees with experiment for $P = 0.75$

which is the same coupling as found in F^{19}. However the $\frac{7}{2}^-$ level observed at 3.85 MeV cannot be explained in this model. In the group of four levels about 3 MeV above the low $\frac{1}{2}^-$ level, the $\frac{3}{2}^-$ and $\frac{1}{2}^-$ may be the ones observed at 5.39 and 5.94 and the $\frac{7}{2}^-$ and $\frac{5}{2}^-$ are probably the observed levels of spin $\geqq \frac{3}{2}^-$ at 5.71 and 5.87.

The F^{19} levels are proton holes in Ne^{20} with $\hbar\omega = 1.63$ MeV. For $P = 1.5$, the $\frac{3}{2}^-$ and $\frac{5}{2}^-$ levels agree in position (fig. 2) with the observed levels [8]) at

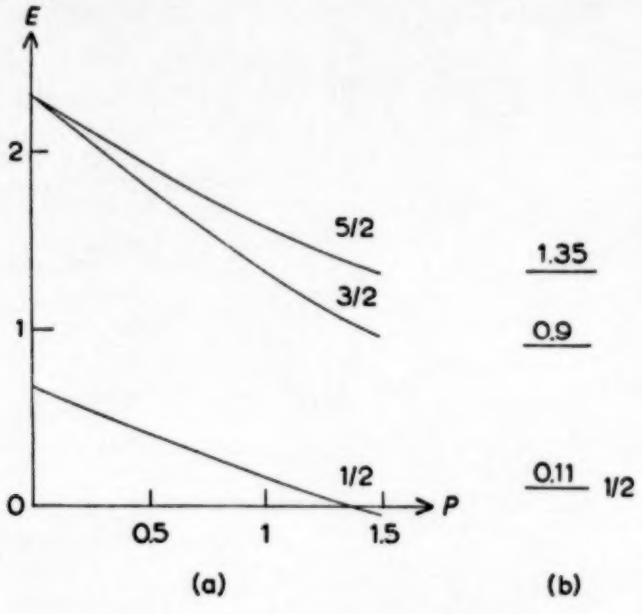

Fig. 2. Negative parity levels of F^{19}.
(a) calculated, (b) experimental.

0.9 and 1.35 MeV of undetermined spins. In strong coupling the order of these levels is reversed if as in the paper of Rakavy [10]) the decoupling parameter a is taken in the range $3 > a \geqq 1$ but is the same as here if [11]) $-1 < a < 1$. The higher levels have not been calculated here, but are expected to have the same sequence as the levels for $A = 17$, but with smaller spacing.

2.2. $A = 13$

C^{13} and N^{13} have been extensively studied [6,7]) in the shell model with coupling intermediate between jj and LS, and the agreement with experiment is very good. In this paper the negative parity levels of these nuclei are regarded as holes in doubly closed nuclei C^{14} and O^{14}. These nuclei have the expected 0^+ ground state, but no 2^+ excited state has been observed till now. However the shell model in intermediate coupling [7]) predicts this level at about 6 MeV, which is therefore assumed to be the value of $\hbar\omega$. With this choice, the $\frac{3}{2}^-$, $\frac{1}{2}^-$ separation is approximately obtained for $P = 0.22$.

The model is then tested in its prediction of the magnetic moment of C^{13} and the radiative width for the $\frac{3}{2}^-$ to $\frac{1}{2}^-$ transition in N^{13}. The results are given in table 1. The improvement to the single particle shell model is appreciable and is very similar to that given by the many-particle shell model [6,7]). The similarity extends also to the prediction of a $\frac{5}{2}^-$ level about 2 MeV above the $\frac{3}{2}^-$.

TABLE 1

	Unified model	Shell model (single particle)	Experimental
Magnetic Moment (C^{13})	0.67	0.64	0.70
Radiative Width ($\frac{3}{2}^- \rightarrow \frac{1}{2}^-$, N^{13})	0.62	0.86	(a) 0.60 (b) 0.70 ± 0.10

(a) from C^{12} (p, p) C^{12}, ref. [12]).
(b) from C^{12} (p, γ) N^{13}, ref. [13]).

3. Discussion

The main omission in the predictions of the model used here is the low $\frac{7}{2}^-$ level in O^{17} and F^{17}. It is perhaps possible to explain this level in the shell model by the coupling of a 1p hole with one proton and one neutron in the 2s, 1d shells. This is suggested by the fact that in the unified model of this paper one has either two neutrons or two protons in the 2s, 1d shells since only in such nuclei do we have the 0^+, 2^+ levels characteristic of collective oscillations. In fact it is the single proton and single neutron outside O^{16} which forms the most stable nucleus of mass 18, neglecting Coulomb energy. This shows that the correspondence between the unified model and the many-particle shell model cannot extend to all levels.

The two parameters B and C which characterize the surface oscillations of the core nucleus can be deduced from $\hbar\omega$, which is just the $2^+ - 0^+$ level separation, and the coupling constant P given by eq. (1), where k is taken to be 40 MeV (see ref. [16])). These are given in table 2. The coupling constant for

TABLE 2

A	14	16	18	20	28
$\hbar\omega$	6	7	2	1.63	1.78
P	0.22	<0.02	0.75	1.50	0.3
C	60	>560	53	33	114
$B/\hbar^2$	1.7	> 11	13	12	36

$A = 16$ (oxygen) has been obtained by F. C. Barker [14]) and that for $A = 28$ (silicon) by S. P. Pandya [15]). The parameter B is much larger than the hydro-

dynamical values [16]) for all A considered here, and C much larger than the hydrodynamical values at the doubly closed shell nuclei of oxygen and silicon. This agrees with the results for heavier nuclei [17]).

The application of the unified model to such light nuclei suggests that it may give a plausible explanation of even Li^7.

Appendix

The wave-functions of 3 quanta of surface oscillations which are necessary in these calculations are the following:

$$V_{3;0,0} = \frac{1}{\sqrt{35}} [3\phi_{02001} + 3\phi_{10020} - 2\sqrt{3}\phi_{10101} - \sqrt{3}\phi_{01110} + \sqrt{2}\phi_{00300}]$$

$$V_{3;2,2} = \frac{1}{\sqrt{7}} [\phi_{10200} + 2\phi_{20001} - \sqrt{2}\phi_{11010}]$$

$$V_{3;3,3} = \frac{1}{\sqrt{10}} [2\phi_{20010} + \sqrt{3}\phi_{03000} - \sqrt{3}\phi_{11100}]$$

$$V_{3;4,4} = \frac{1}{\sqrt{11}} [2\sqrt{2}\phi_{20100} - \sqrt{3}\phi_{12000}]$$

where the notation is the same as that of Feenberg [16]).

References

1) P. Goldhammer, Phys. Rev. **101** (1956) 1375
2) G. Abraham and C. S. Warke, Nuclear Physics **8** (1958)
3) Ivar Espe, private communication
4) J. P. Elliot and B. H. Flowers, Proc. Roy. Soc. A **229** (1955) 536
5) J. P. Elliot, Proc. Roy. Soc. A **245** (1958) 128
6) A. M. Lane and L. A. Radicati, Proc. Phys. Soc. A **67** (1954) 167
7) D. Kurath, Phys. Rev. **101** (1956) 216
8) F. Ajzenberg and T. Lauritsen, Revs. Mod. Phys. **27** (1955) 77
9) W. E. Burcham, Handbuch der Physik, Band **40** (1957) 1
10) G. Rakavy, Nuclear Physics **4** (1957) 375
11) L. Simons, Nuclear Physics **7** (1958) 209
12) H. L. Jackson and A. I. Galonsky, Phys. Rev. **89** (1953) 370
13) J. D. Seagrave, Phys. Rev. **84** (1951) 1219
14) F. C. Barker, Phil. Mag. **1** (1956) 329
15) S. P. Pandya, private communication
16) E. Feenberg, Shell Theory of the Nucleus (Princeton University Press, 1955) Ch. IX
17) K. Alder, A. Bohr, T. Huus, B. Mottelson and A. Winther, Revs. Mod. Phys. **28** (1956) 432

10.D *Nuclear Physics* **10** (1959) 311—312; © *North-Holland Publishing Co., Amsterdam*

BOOK REVIEWS

S. V. FLÜGGE (Editor), *Encyclopedia of physics*, vol. 38, part 1: External properties of atomic nuclei (Springer Verlag, Berlin-Göttingen-Heidelberg 1958. vi—471 p. 118. DM).

The title of this volume might have conveyed a precise idea several years ago, when it was natural to look upon nuclear properties from the point of view of their accessibility to measurement. Such a classification, corresponding to an early stage of the exploration of an unfamiliar domain, is now hopelessly out of date in nuclear physics; the phrase "external properties" can only be understood by examining the table of contents of the volume. The topics actually discussed in it are experimental methods by which certain nuclear characteristics: mass, spin (of ground state!), magnetic moment, quadrupole moment, can be determined. But charge distribution and shape are treated in vol. 39, excited states in vol. 40, isomerism in vol. 42, nuclear models in vol. 39 again. Clearly, when all the volumes are published, a *very* detailed index will be needed if one is ever to find what one wants!

Taken individually, the articles constitute competent monographs, profusely provided with tables, graphs and diagrams. With regard to the literature, one is entitled to expect the enumeration to be as complete and critical as possible: this expectation is not always entirely fulfilled (the article on isotopic shifts, e.g., ignores one or two quite significant papers). This is a great pity, since any paper not mentioned in such an authoritative work as this Encyclopedia has every chance of remaining overlooked in future investigations, a fate which it may not deserve at all.

L.R.

G. J. NIJGH, A. H. WAPSTRA and R. VAN LIESHOUT, *Nuclear spectroscopy tables* (North-Holland Publishing Co., Amsterdam 1959, vii—135 p. 30 fl.)

This compilation, which has been put to the test of practical use before its publication in book-form, covers the whole ground of α, β and γ spectroscopy with all its modern developments, and also includes the auxiliary mathematical and theoretical aspects. The material is presented compactly without sacrifice to completeness, and in a logical order; each section is preceded by an introduction which gives not only the description of the numerical data collected, but also in a nutshell the essentials of the subject to which they refer, with a few selected references to appropriate books or papers. The printing of the tables and graphs, as well as that of the numerous formulae in the text, is of the highest quality. The authors and the publishers both deserve congratulations for the excellent production of a most useful tool.

L.R.

B. FERRETTI (Editor), 1958 *Annual international conference on high energy physics at* CERN (CERN, Genève 1958. x—358 p. 45 fr. suisses)

The publication in book-form of the proceedings of the conference on high energy physics (traditionally known as the Rochester conference, but transferred in 1958 to Geneva) is a notable event in several respects. In the first place, it beats all records by appearing only four months after the event: this speed has been made possible by a tremendous effort of organization in the recording of the discussions during the conference; an effort which only succeeded because of the unexampled devotion of the junior CERN physicists and the secretarial staff, carrying out the work until the small hours night after night.

Secondly, it embodies in permanent form the beneficial results of the new system of reporting information inaugurated at this conference (see this journal **6** (1958) 325). The advantage of

the system of "rapporteurs" was felt in the most convincing way at the theoretical session of the conference, which for some reason was excepted from the scheme, with the consequence that (in spite of the chairman's efforts) it degenerated into an esoteric exchange of technicalities unintelligible to experimenters and theorists alike. It must be said that some of the rapporteurs did not completely avoid the mistake of assuming too much as known to the audience; in their anxiety to do justice to every bit of information entrusted to them, they tried to compress too many, often disconnected, data into their report, and allowed themselves too little time for outlining the main features and conclusions. Other rapporteurs, however, managed to strike the right balance quite successfully, and on the whole the new system has clearly demonstrated its superiority.

As regards the substance of the reports one gets the impression of a rather chequered picture. The brightest spot is the establishment on a firm basis of the form of the β-interaction, after the removal of the empirical contradictions which obscured the issue. Besides, evidence is increasing in favour of a so-called universal interaction involving four fermion fields. The state of the theory of interactions involving π (or K) meson fields, on the other hand, looks pretty desperate: the ingenious methods by which one has hitherto tried to dodge the difficulty of handling strong couplings seem to have exhausted their power, and it becomes clearer and clearer that no further significant progress can be made without some explicit consideration of strong interactions between the mesons themselves. Heisenberg's bold conceptions would yield such interactions as a by-product; but perhaps Heisenberg's approach — in spite of its conceptual beauty — is too ambitious a programme at the present stage, and a more limited effort at understanding meson couplings might have a better chance of success. The reason for the present stagnation in field theory appears to be the absence of any clue which could point in a unique way to the kind of new idea which one has to introduce; as Niels Bohr recently put it, we have not yet been confronted here with any paradox so acute that there could only be one way to remove it.

L.R.

H. R. Beck, H. Dresel and H. J. Melching, *Leitfaden des Strahlenschutzes für Naturwissenschafter, Techniker und Mediziner* (Georg Thieme Verlag, Stuttgart 1959. xi-253 pages. DM 36)

The widespread application of atomic energy has forced an ever increasing circle of specialists to take interest in the many health problems involved. This circle includes not only health physicists but also physicians, scientists and engineers of various specialisations together with lawyers, industrialists, politicians, insurance experts, administrators and military people.

The authors have succeeded admirably in providing a volume catering for all these categories in a book of a very wide scope, including chapters on basic physics, radiobiology, technical health physics, dosimetry and organisation of protection for workers and population. All this has been achieved in a volume which is by no means prohibitive in size or expense to those who are only indirectly connected with the field.

Main criticism is the preponderance of information dealing with the situation in German speaking countries. This preponderance is also felt, at least in some chapters, with regard to the references to the literature. However, in view of the advantage of keeping the volume small, the omission of any references to anglosaxon conditions and literature was probably unavoidable.

The book should be very welcome and is warmly recommended to all those categories of people mentioned above who are professionally confronted directly or indirectly with the health hazards of nuclear development.

J. A. Cohen

1.D.4 *Nuclear Physics* **10** (1959) 313—330; © *North-Holland Publishing Co., Amsterdam*
Not to be reproduced by photoprint or microfilm without written permission from the publisher

SIMPLIFIED INTERMEDIATE-COUPLING PROCEDURE IN THE 1p-SHELL

D. KURATH † and L. PIČMAN ††
Institute for Theoretical Physics, University of Copenhagen

Received 2 January 1959

Abstract: Intermediate-coupling wave functions are constructed by applying Elliott's generating procedure to intrinsic wave functions based on Nilsson's deformed-potential calculation. These are compared with wave functions from an intermediate-coupling calculation with a two-body central interaction. A strong overlap is found between the groups of low-lying states obtained by these two methods of calculation.

1. Introduction

Recently there has been much progress in establishing a connection between individual-particle and collective features of nuclei. In particular, Elliott [1]) has shown that, for the case of nucleons in a harmonic oscillator well with no spin-orbit coupling, many-particle states can be classified with the help of the group SU_3, so as to exhibit features of rotational band structure. The present paper is concerned with the question of including spin-orbit coupling for the 1p-shell, while earlier attempts have dealt with the problem by diagonalizing matrices of a two-body interaction and a spin orbit term of varying strength. A comparison is made between some of the wave functions resulting from a particular interaction calculation [2]) and those wave functions obtained by application of the generating procedure used by Elliott.

2. Procedure

A very simple way of generating many-particle states with varying strength of spin-orbit coupling is offered by Nilsson's calculation [3]) of the single-particle levels in a deformed harmonic oscillator well including spin-orbit coupling. The subsequent comparison will show that wave functions generated from the lowest-energy Nilsson states have a remarkable similarity to the wave functions of the low energy states in the intermediate-coupling interaction approach.

† Guggenheim Fellow, on leave from Argonne National Laboratory, Lemont, Illinois.
†† On leave from Institute "J. Stefan", Ljubljana, Yugoslavia.

April (1) 1959

The Nilsson picture for the 1p-shell is very simple: there are three doubly degenerate levels characterized by K, the projection of the angular momentum on the nuclear symmetry axis, whose positions as a function of deformation are shown in fig. 1. The desired number of nucleons is then put into this

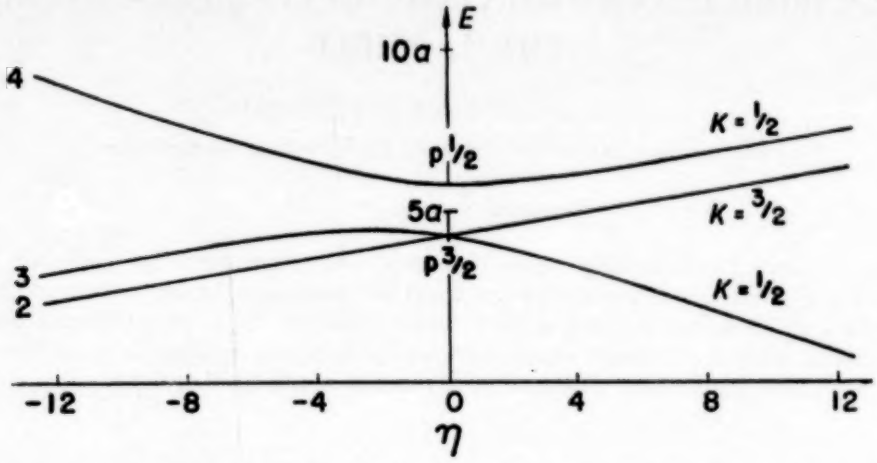

Fig. 1. Energy levels of the 1p-shell as a function of the parameter η (according to Nilsson). The energy scale is plotted in units of the spin-orbit strength a.

well, filling the lowest levels first, and one forms an anti-symmetrized many-particle state of isobaric spin T and total projection of angular momentum K, which is the sum of individual projections. This function can be expanded in the states of definite total angular momentum I, which form the basic representation for the interaction calculation

$$\chi_{K\mathfrak{p}}(R^{-1}x) = \sum_{I,s} c^{Is}_{K\mathfrak{p}}(\eta)\phi^{Is}_{K\mathfrak{p}}(R^{-1}x). \tag{1}$$

Here the functions χ and ϕ are in a frame of reference, $R^{-1}x$, oriented with respect to the laboratory frame x. The labels $\mathfrak{p}$ and s serve to allow further identification of the states, such as configuration. The coefficients $c^{Is}_{K\mathfrak{p}}$ are functions of η, the Nilsson parameter which indicates the ratio of deformation to spin-orbit strength. The η-dependence of χ is contained in the c's, ϕ being independent of η. From here on we simply follow Elliott and use the transformation property of ϕ^I under rotation

$$\phi^{Is}_K(R^{-1}x) = \sum_M \mathscr{D}^I_{KM}(R)\phi^{Is}_M(x) \tag{2}$$

to obtain the generated function from a Hill-Wheeler integral

$$\psi^I_{M(K\mathfrak{p})}(x) = N^I_{K\mathfrak{p}}(\eta)(2I+1)\int \mathrm{d}R\mathscr{D}^{I*}_{KM}(R)\chi_{K\mathfrak{p}}(R^{-1}x) \tag{3}$$

where N is a normalizing factor

$$1 = |N^I_{K\mathfrak{p}}|^2 \sum_s |c^{Is}_{K\mathfrak{p}}|^2. \tag{4}$$

The states generated in this way are then compared with those obtained from the interaction problem

$$\Phi^I_{M\lambda}(x) = \sum_s d^{Is}_\lambda(\gamma)\phi^{Is}_M(x). \tag{5}$$

Here, the coefficients d are functions of the ratio γ of the spin-orbit coupling strength to the interaction strength. (The ratio is usually written as a/K, but γ is used to avoid confusion of K's.) The γ-dependence of the Φ is contained in the d's. The label λ indicates the eigenvalue of energy from the diagonalization process, and we are interested in the low states $\lambda = \lambda_0, \lambda_1$.

3. Simple Cases

The first class of states we shall discuss are those having the following properties which lead to unambiguous simple results:

1. In the intrinsic problem, putting nucleons in the lowest possible Nilsson levels consistent with the Pauli exclusion principle, allows only one value of K for the desired value of isobaric spin T.

2. In the limit of vanishing strength of spin-orbit coupling, the functions generated from this intrinsic state become just the Wigner supermultiplet states of the lowest partition. These are the eigenstates of orbital angular momentum L which Elliott generated in his papers, vector-coupled to a spin function to form total angular momentum $\mathbf{I} = \mathbf{L}+\mathbf{S}$.

3. In the interaction problem there are no nearby states of the same (I, T) values over the entire range of γ, the parameter which measures the relative importance of spin-orbit coupling.

The states which fall into this class arise from putting two, three and four nucleons into level 3 on the right side of the Nilsson scheme, fig. 1, or putting them into level 4 on the left side. The first possibility corresponds to a prolate deformation for the beginning of the 1p-shell, and the second possibility corresponds to an oblate deformation for two, three or four holes in the shell. In making this separation we have anticipated the result which is obtained by comparing wave functions, namely, that a prolate deformation of the field is required for fewer particles than half a shell, and that an oblate field is needed for the second half of the shell.

The first property listed above is superfluous for three and four nucleons in one level, since only one state is possible; however, for two nucleons it restricts the configurations to that for $T = 1$.

The wave functions generated from these intrinsic states, according to eq. (3), are explicitly given as expansions in the states ϕ^{Is}_M which form the basic representation for the interaction calculation:

$$\psi^I_{M(K\mathfrak{I})} = N^I_{K\mathfrak{I}}(\eta) \sum_s c^{Is}_{K\mathfrak{I}}(\eta)\phi^{Is}_M. \tag{3'}$$

These generated states are given as functions of the Nilsson parameter η, and are compared with the lowest states obtained as functions of the spin-orbit parameter γ in the intermediate-coupling interaction calculation. As an example, the results for the lowest $I = 2$, $T = 0$ state of C^{12} are shown in table 1. It is quite clear that if one relates η and γ by an equation like $\eta\gamma \approx -30$, the pairs of wave functions are remarkably similar. All the components in the wave functions are well matched, and the overlap integrals in this case are 0.995 or better.

TABLE 1

Comparison of the generated and computed wave functions for the lowest ($I = 2$, $T = 0$) state of C^{12}. Numbers are coefficients of expansion in the basic set ϕ^{Is}

	η \ s	(1)	(2)	(3)	(4)	(5)	(6)	(7)	(8)
Generated	$-\infty$	0.157	0.416	−0.644	−0.172	0.100	−0.214	0.360	0.416
	−8	0.081	0.212	−0.485	−0.130	0.111	−0.237	0.400	0.682
	−4	0.032	0.084	−0.283	−0.076	0.095	−0.204	0.343	0.859
	γ \ s	(1)	(2)	(3)	(4)	(5)	(6)	(7)	(8)
Computed	0	0.165	0.410	−0.642	−0.181	0.105	−0.224	0.363	0.410
	1.5	0.133	0.335	−0.603	−0.166	0.112	−0.247	0.385	0.507
	3.0	0.102	0.264	−0.543	−0.150	0.117	−0.259	0.388	0.609
	4.5	0.075	0.201	−0.471	−0.133	0.118	−0.257	0.372	0.704
	6.0	0.055	0.152	−0.402	−0.188	0.115	−0.244	0.342	0.780
	7.5	0.041	0.115	−0.340	−0.105	0.109	−0.226	0.306	0.838

From the definitions of η and γ one finds that in the product $\eta\gamma$ the spin-orbit strength cancels out, leaving a quantity which is roughly the ratio of the deformation of the field to the interaction integral $\mathscr{K}$. Since the latter is nearly constant throughout the 1p-shell, the quantity $\eta\gamma$ is a measure of the amount of deformation needed to reproduce the effect of the two-body interaction. Therefore, the behaviour $\eta\gamma =$ constant for a given nucleus is reasonable, and one finds empirically, by comparing generated wave functions with computed ones, that it is an excellent approximation. Table 2 contains a summary of the results of such comparisons for the simple cases. Overlaps of 0.99 or better are obtained by taking the magnitude of $\eta\gamma$ roughly proportional to the number of particles (or holes) in the shell, and choosing the sign as positive (prolate field) for less than a half-full shell and negative (oblate) for more than half-full.

The exact form of the dependence of η on γ is important only in the region where the wave function changes most rapidly. In this region the form $\eta\gamma =$ constant works well, and as we go toward the LS or jj limits, it

provides a sufficiently good approximation though it is far from exact. This was investigated in the two-nucleon, $T = 1$ cases, where an algebraic derivation of the γ-dependence of η is possible. Also, the best value for $\eta\gamma$ is not exactly the same for each value of the angular momentum. Nevertheless, it is possible to choose a single value of the product $\eta\gamma$ which gives overlaps of 0.99 or better for all angular momentum states generated.

TABLE 2

Summary of simple cases with the value of the product $\eta\gamma$, which produces overlaps of 0.99 or better between generated and computed functions

Nucleus	Nilsson Config.	K, T	Generated States	$\eta\gamma$ (approximative)
He^3 C^{14}	$(3)^2$ $(4)^2$	$K = 0,\ T = 1$	$I = 0,\ 2$	$+15$ -15
Li^7† C^{13}	$(3)^3$ $(4)^3$	$K = \frac{1}{2},\ T = \frac{1}{2}$	$I = \frac{1}{2},\ \frac{3}{2},\ \frac{5}{2},\ \frac{7}{2}$	$+25$ -25
Be^8 C^{12}	$(3)^4$ $(4)^4$	$K = 0,\ T = 0$	$I = 0,\ 2,\ 4$	$+30$ -30

† For Li^7, the generated $I = \frac{5}{2}$ state is good only near the LS limit (see sec. 3).

There is one exception to this rule, namely the $I = \frac{5}{2}$ state of Li^7 which does not obey the third requirement for being a simple state. This is so because near $\gamma = 3$ there is another $I = \frac{5}{2}$ state which lies nearby in the interaction calculation. While there is good overlap near the LS limit $\gamma = 0$, and still an overlap of more than 0.98 for $\gamma = 3$, $\eta = +8$, for larger values of γ the generated function also acquires a sizeable overlap with the first excited computed state.

For all other states in this simple class, the generating procedure reproduces the wave functions of the intermediate-coupling interaction calculation to a remarkable degree, and thus effectively replaces the interaction by a deformation of the potential field.

4. Complicated Cases

While there are complications for those nuclear states which do not fall into the simple category of the previous section, there is ample evidence that one retains the basic property of being able to generate the low eigenstates of the interaction calculation from the low intrinsic states.

In the complicated cases, there are always two bands of states generated from a pair of degenerate or nearly degenerate intrinsic states of the same T,

differing by one in their values of K. The two bands then have some states of the same (I, T) in common, which is a desirable feature, since there are usually pairs of corresponding low-lying states of such (I, T) present in the interaction picture.

The major complication is that the generated pairs of states with the same (I, T) are not orthogonal, nor does either state of a pair have as good an overlap with the lowest state from the interaction calculation as occurred in the simple cases. Also the two bands give the same wave function for the state of maximum I and, while this wave function may agree with the computed interaction one, there is thus a redundancy in the generating procedure.

For a specific example of these properties, we consider the two-nucleon states with $T = 0$. These wave functions are generated from the degenerate $K = 0$ and $K = 1$ intrinsic states. From $K = 0$, we generate $I = 1,3$ while from $K = 1$ we get $I = 1, 2, 3$. The $I = 3$ functions are identical. When we compare the two $I = 1$ functions above with the two lower eigenfunctions of the interaction calculation, using $|\eta\gamma| = 12$, we get the overlaps of table 3. The following points are noteworthy, since they are common to such pairs of computed and generated functions.

TABLE 3

Overlap integrals between the low states λ_0 and λ_1, from the two-nucleon diagonalization process and the states generated from the $K = 0$ and $K = 1$ intrinsic states for $I = 1$, $T = 0$

Li^6 †	$\psi(K=1)$				$\psi(K=0)$			
	$\eta = \infty$	8	4	2.67	$\eta = \infty$	8	4	2.67
$(1, 0)\lambda_0$	0.913	0.947	0.958	0.965	0.745	0.831	0.874	0.900
$(1, 0)\lambda_1$	0.408	0.305	0.259	0.233	−0.667	−0.555	−0.478	−0.421
Sum of Intensities	1.000	0.990	0.985	0.985	1.000	0.998	0.992	0.987
N^{14}	$\psi(K=1)$				$\psi(K=0)$			
	$\eta = -\infty$	−4	−2.67	−2	$\eta = -\infty$	−4	−2.67	−2
$(1, 0)\lambda_0$	0.913	0.863	0.902	0.933	−0.745	0.756	0.874	0.925
$(1, 0)\lambda_1$	0.408	0.468	0.387	0.315	0.667	−0.655	−0.485	−0.376
Sum of Intensities	1.000	0.981	0.981	0.984	1.000	1.000	0.999	0.998

† The Li^6 functions are compared with those from the $(3)^2$ configuration with $\eta > 0$ and the N^{14} functions are compared to the $(4)^2$ configuration with $\eta < 0$. The relationship $|\eta\gamma| = 12$ is used in the comparison.

First of all, the sum of the intensities indicates that, looking at them as vectors, the two generated functions lie almost completely in the plane determined by the two computed functions. This is not so remarkable since there are only three ($I = 1, T = 0$) states in the computed problem, but this is a property which also holds in nuclei where there are many more possible states.

Secondly, since the generated states lie in the space of the computed ones, one can effectively diagonalize the interaction Hamiltonian with these generated states by finding the linear combinations which give the computed states. This leads to a strong mixing of the two generated states. In fact, an *ad hoc* procedure which gives excellent overlaps is to take the linear combination $\psi_1 \pm \psi_0$. Looking back through the generator formalism, this also corresponds to a strong mixing of the intrinsic states.

The other nucleus which has been investigated in detail is B^{11}. In this case, we form the intrinsic state with four nucleon holes in level 4 of the Nilsson diagram, fig. 1, and can put the fifth one on level 3, giving a $K = \frac{1}{2}$ state, or in level 2 giving a $K = \frac{3}{2}$ intrinsic state. The $I = \frac{1}{2}$ state generated from $K = \frac{1}{2}$ is like the simple cases, and for $\eta\gamma \approx -35$ it has overlaps of better than 0.99 over the entire range of γ.

For $I = \frac{3}{2}, \frac{5}{2}$ and $\frac{7}{2}$, there are two distinct states generated for each, while the $I = \frac{9}{2}$ state, the highest generated in either band, is again a redundant state. For $I = \frac{3}{2}$, the overlap integrals indicate that, for $\eta\gamma \approx -35$, the two generated states again lie in the plane determined by the lowest and next to lowest eigenfunctions of the interaction calculation, even though there are 13 possible states in the diagonalization. Also, as in the two-nucleon case, it requires a strong mixing of the two generated states to give the linear combinations which closely resemble the computed wave functions.

For $I = \frac{5}{2}$, the same behaviour is seen from the LS limit, $\gamma = 0$, up to $\gamma \approx 4$. Here, the interaction calculation shows a third $I = \frac{5}{2}$ level coming close to the second level. The generated excited state component acts as though these states crossed and, for larger γ-values, the generated states overlap mainly the computed ground state and second excited state. For $I = \frac{7}{2}$, the computed excited state wave function was not available, but the generated states again required strong mixing to reproduce the ground state.

If one views the generating procedure solely as a means of attacking the intermediate-coupling interaction problem, it is certainly quite useful. The wave functions of the low-lying states in the simple nuclei of section 3 are obtained without any diagonalization, and one need only compute the expectation value of the interaction Hamiltonian with these functions to obtain the nuclear spectra. For the complicated nuclei, one must diagonalize two by two matrices, but this is a great simplification over the usual diagonalization procedure in the interaction problem.

However, one would like to understand the success of the generating procedure so that one can also go beyond the simple regions. There is a further step in terms of a rotational interpretation which seems promising.

5. Rotational Considerations in the Generating Procedure

5.1. INTRODUCTION OF ROTATOR HAMILTONIAN

The presence of rotation in the generating procedure for the simple cases is not very conspicuous. The symmetric top functions, $\mathscr{D}^I_{MK}$, appear only in the role of projection operators for picking out a desired angular momentum component in the intrinsic state when one evaluates the Hill-Wheeler integral in (3). However, in order to understand the complicated cases it is desirable to view the generating function as the product of two factors:

$$g^I_{K\nu} = \mathscr{D}^I_{MK}(R^{-1})\chi_{K\nu}(R^{-1}x). \tag{6}$$

The need for mixing states in the complicated cases suggests the presence of a Coriolis coupling term, such as occurs [4]) in collective model interpretations of rotational band mixing. Hence the Hamiltonian of the generating functions should contain a rotational term and a coupling term as well as the Nilsson Hamiltonian for the intrinsic state. In the limit where the Coriolis coupling term is negligible, the generating Hamiltonian should be separable in intrinsic and rotation coordinates so that the functions $g^I_{K\nu}$ of eq. (6) are good solutions.

These requirements suggest the addition of the Hamiltonian of the axially symmetric rotator for the coupled system

$$H_{\text{rot}} = A[(I_1-J_1)^2+(I_2-J_2)^2]. \tag{7}$$

In eq. (7) the components of angular momentum refer to the nuclear coordinate axes. The I_k operates on the symmetric-top functions, $\mathscr{D}^I_{MK}$, while the sum of individual nucleon operators, $J_k = \sum j_k^{(i)}$, operates on the $\chi_{K\nu}$, the functions of intrinsic coordinates. The rotational term can be separated in the usual way into a term for which K, the projection of angular momentum on the nuclear z-axis, is a good quantum number, and the Coriolis term which mixes states differing in K by unity:

$$H_{\text{rot}} = A[I^2-I_3^2]+A[J^2-J_3^2]-A[I^+J^-+I^-J^+]. \tag{7'}$$

Since the second term operates on the intrinsic coordinates it might as well be added to the Nilsson Hamiltonian, so that the total Hamiltonian consists of the rotator of angular momentum I, an intrinsic part and a coupling term, the last term in eq. (7'). As long as the last two terms of eq. (7') have a small effect compared to the energy separation of the eigenstates $\chi_{K\nu}$ of the Nilsson Hamiltonian, the expression (6) will give good solutions for

the generating Hamiltonian. This is then apparently the situation for the simple cases of section 3, where there is a single well-isolated low state for the Nilsson Hamiltonian.

For the complicated cases of section 4 there are two states differing by unity in K in the Nilsson picture which lie close in energy, so that the last two terms of (7′) must be considered. The coupling term will mix the competing generating states and we shall see that it goes far toward removing the difficulties from the complicated cases.

5.2. APPLICATION TO THE TWO NUCLEON CASE

The inclusion of the rotational terms is simplified by noting some properties of the single-nucleon Nilsson functions. Expressing them in terms of the jj-functions $\phi_m{}^j$, the states with $K = +\frac{1}{2}$ are

$$\begin{aligned} \psi_4(+\tfrac{1}{2}) &= \alpha\varphi_{\frac{1}{2}}{}^{\frac{1}{2}}+\beta\varphi_{\frac{1}{2}}{}^{\frac{3}{2}}, \\ \psi_3(+\tfrac{1}{2}) &= -\beta\varphi_{\frac{1}{2}}{}^{\frac{1}{2}}+\alpha\varphi_{\frac{1}{2}}{}^{\frac{3}{2}}, \end{aligned} \tag{8}$$

with $-\sqrt{\frac{1}{3}} \leqq \alpha \leqq 0$ for a prolate field, $0 \leqq \alpha \leqq \sqrt{\frac{2}{3}}$ for an oblate field, and $\beta = -\sqrt{(1-\alpha^2)}$. In terms of the Nilsson parameter η,

$$2\alpha^2 = 1-(3+\tfrac{1}{3}\eta)(\eta^2+2\eta+9)^{-\frac{1}{2}}.$$

Under reversal of the 2 and 3 axes, R_1, the function ϕ_m^j becomes

$$R_1\varphi_m{}^j = i^{2j}\varphi^j_{-m}. \tag{9}$$

We select the arbitrary phases of the Nilsson functions with $K = -\frac{1}{2}$ by the requirement

$$R_1\psi_p(+\tfrac{1}{2}) = i^3\psi_p(-\tfrac{1}{2}) \quad \text{for} \quad p = 3,4. \tag{10}$$

This has the consequence of fixing the relative phases in the expansion of the intrinsic states χ_K and χ_{-K} according to (1):

$$\chi_{-K} = \sum_{I,s} c^{Is}_{-K}\psi^{Is}_{-K}. \tag{1′}$$

For the two nucleon $T = 0$ states, applying R_1 to this equation gives us

$$R_1\chi_{-K} = (i^6)\chi_K = \sum_{I,s} c^{Is}_{-K}(i)^{2I}\psi^{Is}_K.$$

Comparing this with the χ_K expansion gives us

$$c^{Is}_{-K} = (-1)^{I-1}c^{Is}_K \tag{11}$$

and shows why even I are not present in χ_0. From (11) we see that χ_1 and χ_{-1} contain the same states but have a relative phase factor of (-1) for even I.

The two-nucleon $T = 0$ generating states of the form (6) are three, g_1^I, g_{-1}^I, and $g_0{}^I$ (omitting the configuration label p). The Nilsson part of the generating Hamiltonian has the same matrix elements for all these three

states. The matrix elements of the rotational part, (7′), are

$$\begin{aligned}\langle H_{\rm rot}\rangle_{KK} &= A[I(I+1)-2K^2+\langle J^2\rangle_{KK}],\\ \langle H_{\rm rot}\rangle_{K\pm1,K} &= -A(I(I+1)-K(K\pm1))^{\frac{1}{2}}\langle J^{\pm}\rangle_{K\pm1,K}.\end{aligned} \tag{7″}$$

From the relationship (11), it is evident that the matrix elements are unchanged if the signs of the indices in (7″) are all changed. This has the consequence that the generating states obtained from diagonalizing the generating Hamiltonian occur in the combinations $g_K{}^I \pm g^I_{-K}$. In the present two-nucleon case, the generating state $g_1{}^I - g^I_{-1}$ has no matrix elements with the other combinations and so it is already a solution of the generating Hamiltonian. From (11) we see that the Hill-Wheeler integral with this generating function will give rise to only even I, and since $I = 2$ is the only even I present in χ_1 this is all that can be generated.

For the combinations $g_0{}^I$ and $g_1{}^I + g^I_{-1}$ which both give rise to odd I, namely $I = 1$ and $I = 3$, we must diagonalize the generating Hamiltonian. The necessary matrix elements for the $T = 0$ configuration with two nucleons in the number (3) Nilsson level are

$$\begin{aligned}\langle H_{\rm rot}\rangle_{11} &= A[I(I+1)-2+(2+6\beta^2)],\\ \langle H_{\rm rot}\rangle_{00} &= A[I(I+1)+(2+9\beta^4)],\\ \langle H_{\rm rot}\rangle_{10} &= -A\sqrt{I(I+1)}(\sqrt{2}(3\beta^2-1)).\end{aligned} \tag{12}$$

For two nucleons in level number (4) with $T = 0$, the matrix elements are obtained from those above by substituting α^2 for β^2, where α and β are defined in expression (8). The diagonalization of the 2×2 matrices can then be carried out.

In table 4 the functions generated for $I = 1$, $T = 0$ are again expressed in terms of the low states resulting from the interaction calculation. Comparing table 4 to table 3 where the generating Hamiltonian had no rotational term, it is clear that there is much improvement. Particularly in the LS limits the generated states are exactly the interaction ones, that is we now generate the Wigner supermultiplet states.

Then for Li^6 states, there is a steady worsening of the picture as η gets smaller, particularly for $\eta < 4$. However, if we look at fig. 1, it is evident that the intrinsic level number two gets closer to the lowest level as η approaches zero. Therefore our calculation, which treated only the states from two nucleons in level number three, could not be expected to be valid for small η. It is of interest to note that this allows us to obtain some idea of the magnitude of the rotational energy parameter A of eq. (7). Since the intrinsic energies are the same for the two generating states, the diagonalization of these intrinsic plus rotational terms is independent of A. However, when a different intrinsic state is involved, what is important is the difference

in rotational energies compared to the difference in intrinsic energies. It is difficult to get a precise evaluation, but in order for the states involving level number two to be unimportant for $\eta > 6$, as they appear to be for Li^6, one should have $A \approx 1$ MeV as a crude estimate.

TABLE 4

Overlap integrals, for two nucleons, between the low states λ_0 and λ_1, from the interaction problem and the states generated by including a rotational term in the generator Hamiltonian. Again $I = 1$, $T = 0$ and $|\eta\gamma| = 12$

Li^6	Lower Generating State				Upper Generating State			
	$\eta = \infty$	8	4	2.67	$\eta = \infty$	8	4	2.67
$(1, 0)\lambda_0$	1.000	0.996	0.992	0.990	0	0.052	0.185	0.344
$(1, 0)\lambda_1$	0	0.012	0.038	0.058	1.000	0.997	0.981	0.938
Sum of intensities	1.000	0.993	0.985	0.983	1.000	0.996	0.996	0.998
N^{14}	Lower Generating State				Upper Generating State			
	$\eta = -\infty$	−4	−2.67	−2	$\eta = -\infty$	−4	−2.67	−2
$(1, 0)\lambda_0$	1.000	0.941	0.983	0.987	0	−0.515	−0.186	−0.129
$(1, 0)\lambda_1$	0	0.288	0.102	0.081	1.000	0.856	0.972	0.979
Sum of Intensities	1.000	0.968	0.977	0.981	1.000	0.998	0.979	0.975

Of course, it is clear that the generated states are still not orthogonal, except in the *LS* limit, although the inclusion of the rotational term has removed most of the overlap. This is especially noticeable around $\eta = -4$ in N^{14}, where the two generating states (as well as the two interaction states) come quite close and repel each other. The question of redundancy in generating the state of largest I, in this case $I = 3$, is also not settled. In the *LS* limit it is taken care of with only one state generating $I = 3$, while as one goes away from this limit, one state generates it with a large amplitude, the other with a quite small one. However, since the states are normalized after being generated this difference is lost.

5.3. EFFECT ON THE B^{11} STATES

The coupled rotator terms can also be used in B^{11} to mix the $K = \frac{1}{2}$ and $K = \frac{3}{2}$ generating states. Again symmetry separates the linear combinations $g^I_K + g^I_{-K}$ which generate the states $I = \frac{3}{2}, \frac{7}{2}$ from the linear combinations $g^I_K - g^I_{-K}$ which generate the states $I = \frac{1}{2}, \frac{5}{2}, \frac{9}{2}$. This reduces the problem to

diagonalizing two 2×2 matrices, and the degree of improvement obtained by including the rotator term is quite comparable to that in the two nucleon case. Again in the LS limit ($\eta = -\infty$) the generated states are orthogonal for all I and one generates the Wigner supermultiplet states.

Away from the LS limit the two intrinsic states $K = \frac{1}{2}$ and $K = \frac{3}{2}$ are not degenerate, but are separated by something of the order of magnitude a, the spin orbit coupling strength, over the region of negative η, except near $\eta = 0$ where they are degenerate again. One might hope to determine the rotational energy parameter A, but the results are unfortunately quite insensitive to it. In a particular case in table 5 one sees the effect of varying the ratio a/A

TABLE 5

Overlap integrals for B^{11} ($I = \frac{3}{2}$, $T = \frac{1}{2}$), between the low states λ_0 and λ_1, from the interaction problem and several pairs of generated states. The ratio a/A of spin-orbit energy to rotational energy is varied for the case $\eta = -8$, $\gamma = 4.5$

	$a/A = \infty$ Rotation Term Negligible		$a/A = 4.0$		$a/A = 0.7$ Generated States Orthogonal	
	$K = \frac{1}{2}$	$K = \frac{3}{2}$	Low State	High State	Low State	High State
$(\frac{3}{2}, \frac{1}{2})\lambda_0$	0.886	0.647	0.981	0.169	0.961	−0.198
$(\frac{3}{2}, \frac{1}{2})\lambda_1$	0.441	−0.720	0.042	−0.961	−0.174	−0.962
Sum of intensities	0.979	0.937	0.964	0.952	0.954	0.965

from its value when the rotational term is neglected to its value obtained by requiring that the generated $I = \frac{3}{2}$ states be orthogonal. It is not possible to find a single value of a/A which generates orthogonal pairs of states for all I, but there is no reason why the states generated by considering only the two lowest intrinsic states should be exactly orthogonal so long as they are nearly so. The results of table 5 are typical for the various I and $\eta\gamma$ values in B^{11}. There are some broad limits placed on a/A, namely that it should lie somewhere between eight and unity, and something like four, which implies $A \approx 1$ MeV, gives reasonably good results. However, a close determination is not possible.

The indications, both in B^{11} and for the two-nucleon cases, are that including the rotational term is the major step which goes far toward removing the difficulties encountered in the complicated cases where two bands are present. It is possible that by considering the small amounts of excited generating states which the rotational term would mix into the low generating states one could obtain orthogonal non-redundant states. However,

such an extension of effort is contrary to the purpose of the present approach, which was to show how to obtain states remarkably like the low states of the interaction problem by treating only the low generating states.

6. Implications of the Generating Procedure

6.1. GENERATOR PARAMETERS

The generator Hamiltonian involves two parameters with collective interpretations. One is the rotational energy parameter A, which is $(\hbar^2/2\mathscr{I})$ where $\mathscr{I}$ is the moment of inertia of what is rotating. One would, of course, like to relate A to the experimental energy separations observed between those levels whose wave-functions are produced by the generating procedure. While the parameter A does determine the separation of the states in a band before the averaging over nuclear orientations is performed, this latter process removes the explicit presence of A, and its effect is only felt indirectly via the degree of coupling between rotational bands. In the last section we have seen that A is a very elusive parameter because the resulting wave functions are rather insensitive to it. Therefore the attempt to derive a direct or an indirect connection between A and the observed energy level spacings via the generated functions succeeds only in placing rather broad limits on the value of A.

It might appear that an alternative procedure is presented by the approach of Peierls and Yoccoz [5]). These authors present a way to obtain rotational spectra and derive the moment of inertia from the generating function, based on the assumption that the overlap between functions of different orientation is small unless the directions are very nearly the same. They expand the overlap integrals in terms of Θ, the angle between two orientations, and assume the important contributions come from small Θ. The validity of such a procedure was investigated in the present case for C^{12}. In the limit of very large η, the overlap integrals are found to be proportional to $\cos^4\Theta$. This is not a sufficiently peaked distribution to justify keeping only the low terms in the expansion of the overlap integrals, and such a procedure fails. However, the spacing of the C^{12} energy levels is exactly proportional to $I(I+1)$ in the limit of large η, so evidently one can still get such rotational behaviour even when the higher order terms in Θ contribute strongly.

It is true that the interaction calculation gives energy separations which have a rotational spacing for the wave functions one generates, when the spin-orbit coupling is not too large. In Be^8, for example, this is true for the strength of spin-orbit coupling for which the interaction calculation and experimental spectra agree quite well. Therefore one can estimate a value for A from the experimental spectrum and at least see whether this is compatible with the derived limits on A. From the $I = 0, 2, 4$ band of Be^8, the value

is $A \approx 0.5$ MeV. Such a value for A is not in contradiction with the rough estimates obtained in the previous section by considering the coupling of rotational and intrinsic motion. The analysis for B^{11}, where the broad limits on A were derived, is further complicated by the fact that the most favourable deformation is probably not cylindrically symmetric near the centre of the shell. Following a suggestion by B. Mottelson, some pilot calculations were carried out which have shown that the asymmetric deformation in B^{11} produces a band mixing that is in the same direction as the rotational coupling. This indicates that inclusion of both factors would require less of an effect from the rotational term and hence lead to a smaller value of the upper limit of A. Therefore while nothing precise can be said, the values of A from the wave-function analysis and from the experimental energy level spacings are probably quite compatible.

The second collective parameter is the amount of deformation of the potential field which is needed to reproduce the effects of the interaction. This can be evaluated by using the $\eta\gamma$ values of table 2 and Nilsson's definition of η:

$$\eta\gamma = \frac{-2\hbar\omega_0}{\mathscr{K}}\delta[1-\tfrac{4}{3}\delta^2-\tfrac{16}{27}\delta^3]^{-\frac{1}{2}}. \tag{13}$$

Here $\hbar\omega_0$ is the spacing of the oscillator levels, $\mathscr{K}$ is the central interaction integral, and δ is Nilsson's deformation parameter defined in terms of the deformed oscillator frequencies

$$\left(\frac{\omega_\perp}{\omega_Z}\right) = \frac{1+\frac{2}{3}\delta}{1-\frac{4}{3}\delta}. \tag{14}$$

If one assumes about 15 MeV for the oscillator level spacings, the first bracket on the right side of eq. (13) is about 30. Then we find that for $\eta\gamma = +15$, -15, $+30$, -30, we get $\delta = +0.47$, -0.49, $+0.70$, -0.90 respectively. These are very large deformations, so large that one must be concerned about higher order effects in δ. Such effects are not present in the wave functions where only the 1p-shell was considered. In order to obtain a reliable estimate for δ one would have to go outside this shell, and also make sure that one has a self-consistent picture. This means that the spatial distribution of the nucleons should be consistent with the potential field distribution. Such a procedure would reduce the values of δ from those we obtained above. However, the important feature is that one would still expect them to be quite large.

The determination of the physical meaning of the large deformation is a difficult question, because it occurs in the generating Hamiltonian and is effectively washed out in the averaging over nuclear orientations represented by the Hill-Wheeler integral. One must remember that the functions which

one generates give E2 matrix elements that are of the order of magnitude of single particle matrix elements, because the generated functions are nearly identical with those of the interaction calculation. There will, however, be enhancement if one goes outside the 1p-shell as seems desirable from the large indicated values of δ.

What the generating procedure emphasized is that there is a strong correlation between the positions of the 1p-shell nucleons. The effect of the interaction which it represents is that it is energetically very favourable for these nucleons to be in orbits as nearly alike as possible consistent with the Pauli principle. Already for two nucleons, as in Li^6, the effect of the other 1p nucleon is by far the most important of all the nucleons in determining the effective field for a 1p nucleon. Such an effect shows why it is possible to write the generated wave functions in "cluster" form [6,7]) (such as alpha particle plus deuteron for Li^6), because the correlations in the generating wave function are kept when one averages over orientations by integrating over dR. The use of the Nilsson model in the generating procedure shows how the preference for maximum spatial symmetry which characterizes the Wigner supermultiplet theory is extended into the regions of stronger spin-orbit coupling. As long as there is a well-isolated, lowest-energy intrinsic level, which fig. 1 shows to be true for level 3 on the prolate side and level 4 for holes on the oblate side, there will remain a strong preference for the nucleons to fill the shell in groups having very similar orbits. The Pauli principle limits the extent to which this can be done and leads to the special stability of the four-structure nuclei. This is evidently the sort of effective potential field which the interactions set up, and serves to generalize the strong spatial correlation and four-structure properties far into the region of important spin-orbit coupling. By using the $\eta\gamma$ relationships and the values of γ found desirable from a comparison of the interaction calculation with experiment, one finds that the physically significant values of η lie in the region where the lowest Nilsson level is well-isolated. This feature and its consequences are what is implied by the large values of deformation. So the interpretation of the large values of the deformation parameter is that these reflect the strong correlation within groups of 1p-nucleons which is present in the wave functions of the low states from the interaction calculation.

6.2. RELATION OF INTERACTION TO DEFORMATION

Since there is excellent agreement between the low states from the generating and interaction approaches, it is of interest to find an explicit equation relating the interaction potential to the deformation. From the simple cases where the rotational contribution is separable, the intrinsic equation is

$$[\sum_i H^i(R^{-1}x_i)]\chi_{K\nu}(R^{-1}x) = E_{K\nu}\chi_{K\nu}(R^{-1}x) \qquad (15)$$

where $H^i = H_0{}^i + kr_i{}^2 Y_0{}^2\ (R^{-1}\Omega_i)$; $H_0{}^i$ contains the spherically-symmetric harmonic oscillator Hamiltonian and the spin-orbit term, while k is proportional to the deformation. Since $H_0{}^i$ is invariant under rotation we can write

$$H^i(R^{-1}x_i) = H_0{}^i(x_i) + kr_i{}^2 \sum_\mu \mathscr{D}_{0\mu}{}^2(R) Y_\mu{}^2(\Omega_i). \tag{16}$$

Then operating with $\int dR\, \mathscr{D}^{I*}_{KM}(R)$ on eq. (15) and combining $\mathscr{D}^{I*}_{KM}(R)$ with $\mathscr{D}^2_{0\mu}(R)$ gives us

$$[\sum_i H_0{}^i(x_i) - E_{K\mathfrak{p}}] \int dR \mathscr{D}^I_{KM}(R) \chi_{K\mathfrak{p}}(R^{-1}x) = -\sum_J \left(\frac{2\mathscr{J}+1}{2I+1}\right) (\mathscr{J} 2K0|IK) \sum_i kr_i{}^2$$

$$\times \sum_m (\mathscr{J} 2mM-m|IM) Y^2_{M-m}(\Omega_i) \int dR \mathscr{D}^{I*}_{Km}(R) \chi_{K\mathfrak{p}}(R^{-1}x). \tag{17}$$

Here $(J2m_1m_2|Im_3)$ is the symbol for the vector-addition coefficient. This is clearly an equation relating the states generated from a single intrinsic state, and application of eq. (3) gives

$$[\sum_i H_0{}^i(x_i) - E_{K\mathfrak{p}}] \psi^I_{M(K\mathfrak{p})}(x)$$
$$= -\sum_J G_J(\eta) \sum_i kr_i{}^2 \sum_m (J2mM-m|Im) Y^2_{M-m}(\Omega_i) \psi^J_{m(K\mathfrak{p})}(x). \tag{18}$$

Here $G_J(\eta) = (J2K0|IK)[N^I_{K\mathfrak{p}}(\eta)/N^J_{K\mathfrak{p}}(\eta)]$, and eq. (18) is the equation obeyed by the states generated from a single intrinsic state.

On the other hand, the solution to the interaction problem obeys the equation

$$[\sum_i H_0{}^i(x_i) + \sum_{i<j} V_{ij}] \Phi^I_{M\lambda}(x) = E_{I\lambda}\, \Phi^I_{M\lambda}(x) \tag{19}$$

where $H_0{}^i(x_i)$ is the same as in eq. (18). To the extent that there is nearly complete overlap between the lowest energy solutions of eq. (19) for each I with the wave function of that I generated from $\chi_{K\mathfrak{p}}$, we can combine eqs. (18) and (19) to eliminate matrix elements of H_0 and get an approximate relationship

$$\langle I\lambda_0 M| \sum_{i<j} V_{ij} |I\lambda_0 M\rangle \approx E_{I\lambda 0} - E_{K\mathfrak{p}}$$
$$+ \sum_{J,m} G_J(\eta) (J2mM-m|IM) \langle I\lambda_0 M| \sum_i kr_i{}^2 Y^2_{M-m}(\Omega_i) |J\lambda_0 m\rangle. \tag{20}$$

This relationship expresses the fact that for the low states, the effect of the interaction is to mix in only the states within the band through a mass-quadrupole operator.

While eq. (20) places some restrictions on the form of interaction which is used for V_{ij}, these are not likely to be too stringent. There is no compelling reason to prefer the interaction which was used as a basis for comparison with the generated wave functions in the present paper. However, it does contain the feature that for two nucleons the states with spatially symmetric

wave functions lie much lower in energy than those with antisymmetric spatial dependence. This much should certainly be present in an interaction since it must be responsible for the strong correlations in the wave functions of the low states for many nucleons. This is probably the primary ingredient enabling one to obtain a relationship of the form of eq. (20).

7. Conclusions and Remaining Problems

The present study is a comparison of two methods of calculation, which has found a remarkable similarity between the wave functions of the low states in the two approaches. It is relevant for experiment because the major part of the present experimental information about the 1p-shell concerns these states, and previous comparisons have shown that the wave functions of the interaction calculation give a reasonably good picture of the experimental facts.

The results demonstrate that the agreement between the two theoretical approaches goes beyond the explanation in terms of the SU_3 groups, because the similarity in wave functions persists into regions where the supermultiplet classification breaks down and the partitions are well-mixed. The common feature which apparently links the two calculations is the presence of a strong spatial correlation among the 1p-nucleons in the low states of certain nuclei. These are the states which are generated from filling an isolated level in the Nilsson picture. The presence of the strong correlation is made evident by the large value of deformation required to generate wave functions which agree with the interaction wave functions. The large deformation results in rather well-isolated low levels so that the 1p nucleons will have very similar orbits. The mechanism for achieving strong correlation in the interaction picture is not evident, but it must come from taking best advantage of the greater binding energy of the singlet-triplet and triplet-singlet parts of the interaction †. The presence of the strong correlations in the wave functions means that a cluster description of such nuclei should be quite good for the low states.

One nucleus which we have not discussed is B^{10}. The state generated from the $K = 3$ function on the prolate side has an overlap of about 0.99 with the interaction $I = 3$ ground state. But one must really put two nucleons into the Nilsson levels two and four in all possible ways to be consistent, and this gives six intrinsic states. While it may work, the amount of labour in including the rotational term in such calculation becomes comparable with the interaction problem.

Other calculations [9, 10]) have looked outside the 1p-shell and found similar

† The relevance of this formulation of the interaction for the low states is discussed, for example, in ref. [8]).

procedures useful. An obvious extension of our procedure is to attempt to include configuration interaction by considering not only the 1p-shell, but the admixtures of 1f and 2p states which the Nilsson calculation brings in. This could bring in the E2 enhancement which seems needed for experimental agreement. It might also be a way to investigate the effect of such configuration mixing in the C^{14} beta-decay matrix element.

The authors would like to thank Dr. B. Mottelson for stimulating advice during the course of this work. We would also like to thank Drs. Aage Bohr and B. F. Bayman for valuable discussions, and Professor Niels Bohr for the hospitality of the Institute.

One of us (D. K.) gratefully acknowledges the help of a Guggenheim Fellowship, and the other (L. P.) financial support from the Ford Foundation.

References

1) J. P. Elliot, Proc. Roy. Soc. A **245** (1958) 128
2) D. Kurath, Phys. Rev. **101** (1956) 216
3) S. G. Nilsson, Mat. Fys. Medd. Dan. Vid. Selsk. **29** (1955) no. 16
4) A. K. Kerman, Mat. Fys. Medd. Dan. Vid. Selsk. **30** (1956) no. 15
5) R. E. Peierls and J. Yoccoz, Proc. Phys. Soc. A **70** (1957) 381;
J. Yoccoz, ibid. (1957) 388
6) K. Wildermuth and Th. Kanellopoulos, Nuclear Physics **1** (1958) 150
7) B. F. Bayman and A. Bohr, Nuclear Physics **9** (1958/59) 596
8) D. Kurath, Proc. Rehovoth Conf. on Nuc. Structure (1957) 46
9) M. Redlich, preprint
10) C. Levinson, private communication

8.A *Nuclear Physics* **10** (1959) 331—347; © *North-Holland Publishing Co., Amsterdam*
Not to be reproduced by photoprint or microfilm without written permission from the publisher

RELATION BETWEEN CIRCULAR POLARIZATION AND ENERGY FOR EXTERNAL BREMSSTRAHLUNG FROM BETA-RAYS

A. BISI and L. ZAPPA
Istituto di Fisica del Politecnico, Milano

Received 20 December 1958

Abstract: The relation between circular polarization of the external bremsstrahlung quanta from β-rays of ^{90}Y and their energy was investigated in Al, Cu, Ag, Pb. The degree of circular polarization was found very high; in particular, the end points of the four relations give a circular polarization $P_\gamma = 0.94 \pm 0.05$ to which corresponds a longitudinal polarization of β-rays equal to $-(0.98 \pm 0.05)v/c$. A rough calculation was made in order to compare experimental results with present theories: the predicted relations appear to be lower than the experimental ones. A detailed account of the γ-polarimeter is given.

1. Introduction

The prediction that external bremsstrahlung produced by polarized electrons can be elliptically polarized was made a few years ago by Gluckstern, Hull and Breit [1]). After the discovery of the longitudinal polarization of β-rays inferred from the lack of conservation of parity in β-decay [2, 3]), the interest on polarization effects in bremsstrahlung has grown. A number of theoretical investigations have been developed recently on bremsstrahlung cross sections for specific polarization states of the incoming and outgoing electrons [4–9]); in particular, it has been emphasized that longitudinal polarization of β-rays gives rise to circular polarization of bremsstrahlung quanta. The physical origin of the polarization effects, as pointed out by Mc Voy [9]), does not seem completely understood, however.

As far as concerns the experiments, a simple method exists to analyze the sense and the degree of circular polarization of γ-rays based on the existence of a spin-dependent part of the Compton cross section [10]). More specifically, the circular polarization can be detected through the interaction of the γ-rays with polarized electrons available in magnetized iron. The interaction leads to a comparison of the unknown screw sense associated to the γ-ray with a known screw sense associated to a polarized electron.

The circular polarization of external bremsstrahlung from β-rays was first observed by Goldhaber, Grodzins and Sunyar [11]) and subsequently by a few other authors [12, 13, 14]); their results are consistent with the existence of an

almost complete polarization, at least at the high energy end of the spectrum. However, these results do not lend themselves to an empirical polarization-energy relation which can be compared with theoretical predictions.

In the present work we report the results of our investigation (whose partial results were already published [15]) intended to establish the dependence of the circular polarization of the external bremsstrahlung produced by β-rays from ^{90}Y on both the γ-ray energy and the atomic number of the target. In fact, the target atomic number affects both the EB cross section to an extent which depends on the quantum energy, and the depolarization of the electron before radiating. Finally an attempt is made to fit the experimental results to theoretical predictions.

2. Gamma-Polarimeter

2.1. GENERAL CONSIDERATIONS

The differential and integrated Compton cross section for circularly polarized quanta from polarized electrons may be written as the sum of two terms: the first is the usual Klein-Nishina formula for unpolarized quanta and electrons, the second is sensitive to polarization. The dependence of these two terms on the quantum energy and the scattering angle practically regulates the choice of a suitable polarimeter. In our experiments the following conflicting conditions are required to be fulfilled: to collect as much outgoing radiation as possible; to obtain the maximum asymmetry as a function of magnetic field; to attain a good energy resolution; to minimize spurious effects due to degraded radiation. With that in mind we shall examine the following experimental methods:

a) *Transmission of γ-rays through magnetized and unmagnetized iron.* This method gives the best energy resolution, but the polarization term of the integrated cross section being small, large values of asymmetry can be obtained only by using long iron absorbers. This is unavoidably followed by too large a reduction of the collected radiation. Moreover the spurious effects due to degraded radiation are difficult to estimate.

b) *Forward scattering from magnetized iron for opposite field directions.* The method is convenient since the polarization term contributes appreciably to the total Compton differential cross section. Good collection of radiations can be achieved by using rotational symmetry of the scatterer, and the degraded radiation can be accounted for with reasonable accuracy. With regard to energy resolution, the finite size of the scatterer enlarges the γ lines, but this enlargement can be made quite tolerable.

c) *Backscattering from magnetized iron for opposite field directions.* The polarization term of the differential cross section is comparable to the usual one, but the intensity of the scattered radiation is weak. A serious dis-

advantage arises from the fact that the backscattered quantum energy is about the same for any energy of the primary quantum. The energy discrimination is actually prevented and so the method is impracticable.

On the basis of the preceding considerations we chose the forward scattering method.

2.2. EXPERIMENTAL SET-UP

We employed a γ-polarimeter (see fig. 1) similar to that used by Schopper [16]) and by Bohem and Wapstra [13]). The γ-rays were scattered off the inner surface of an Armco iron cylinder which can be magnetized to saturation with the help of three coils: its length is 15 cm, its internal diameter 9.5 cm and its thickness 1.5 cm. A lead plug centered in the iron cylinder was used to absorb the direct radiation from the source. The scattered quanta were detected by means of a $1\frac{1}{2}''$ dia $\times 1''$ thick NaI(Tl) crystal coupled

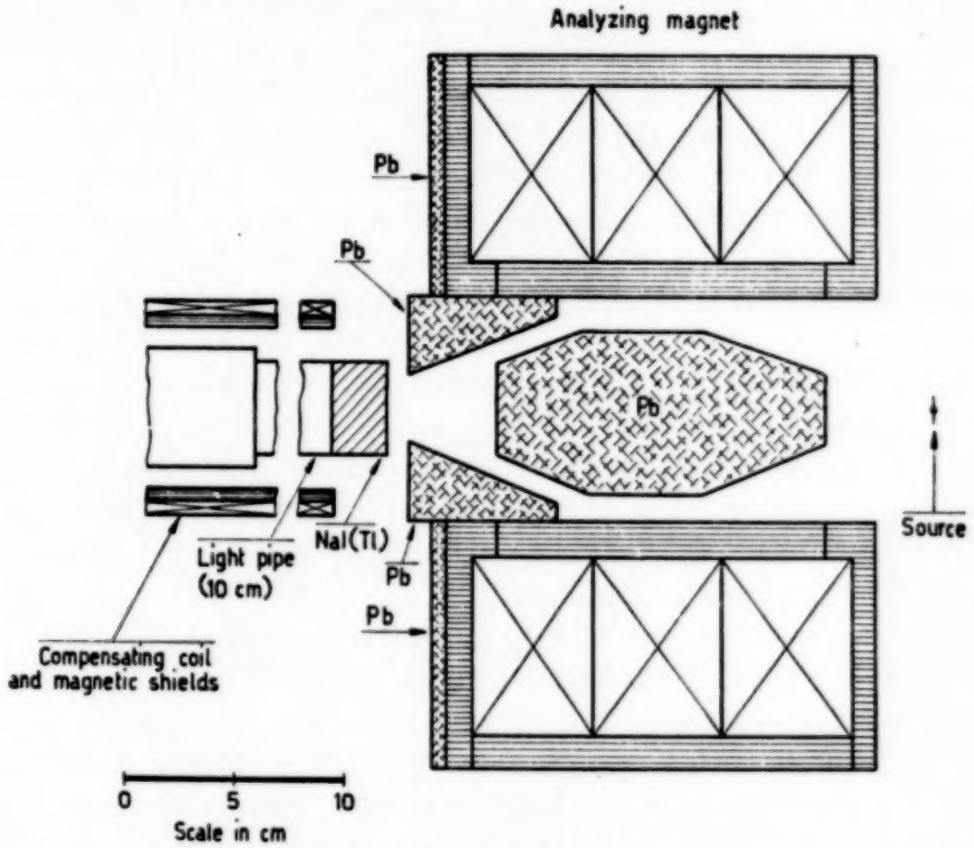

Fig. 1. Gamma polarimeter.

through a 10 cm lucite light pipe to an EMI 9514 photomultiplier. After amplification the pulses were fed into a ten channel pulse height analyzer. In order to eliminate any residual influence of the magnetic stray field on the photomultiplier, three iron shields and a compensating coil were used coaxially with the photomultiplier.

The performance of the polarimeter was investigated by using unpolarized

radiations of 0.279 (^{203}Hg), 0.511 (annihilation radiation), 0.661 (^{137}Cs), 0.835 (^{54}Mn), 1.28 MeV (^{22}Na). We report in what follows the results which will interest the discussion on the corrections to be applied to the measured asymmetries.

2.3. SCATTERER FEATURES

The iron cylinder must be of sufficient thickness to make the scattering from the magnetizing coils negligible: we have investigated the intensity of the 0.835 MeV radiation scattered from cylinders of 0.5, 1.0, 1.5, 2.0 cm thickness and found that the intensity is practically constant at thickness greater than 1.0 cm. As far as concerns the EB spectrum in particular, it was found that the scattered spectrum is the same with or without the magnetizing coils surrounding the iron cylinder.

The size of the central lead plug, sufficiently thick to stop the direct radiation, affects the transmission, the energy resolution of the polarimeter and the relative amount of the degraded radiation; in effect the relative contributions to scattering of different volume elements of the cylinder are dependent on the size of the lead absorber. We chose the best size after some trials.

The relative amount of the scattered radiation from the different annular sections of the cylinder was investigated by operating with a short cylinder (3 cm length and 1.5 cm thickness) put at different distances from the source. The central section gives far better results as far as concerns transmission, energy resolution and relative amount of degraded radiation. In our particular arrangement of fig. 1 the spectrum of scattered rays from the whole cylinder is equal to that obtained with the short cylinder in the central section, as shown in fig. 2. That offers two advantages: 1) the scattering takes place in the core of the cylinder, where the magnetization is largest and uniform; 2) the calculation of the polarimeter response to circular polarization is made easier.

Fig. 2 shows that a singly scattered γ-line is accompanied by a continuous pulse distribution arising from the doubly scattered radiation (its total contribution to the detected radiation is about 55 % at 0.835 MeV). This troublesome distribution is considerably higher when the lead conical shield placed at the end of the iron cylinder (see fig. 1) is removed. The double scattering was estimated as follows. The Armco iron cylinder was replaced with a lead cylinder of identical size, all other conditions remaining unchanged, and the scattering in lead of the above quoted monochromatic radiations was studied. The obtained pulse height spectra of radiations scattered in lead show only the presence of single scattering photoelectric peaks accompanied by their Compton distributions, as can be expected on the basis of the size of our scintillator. Then the comparison between scattering spectra in lead and iron, after normalization of photoelectric peaks, gives an estima-

tion of the spectral distribution of the double scattering as a function of the energy of the incident radiation.

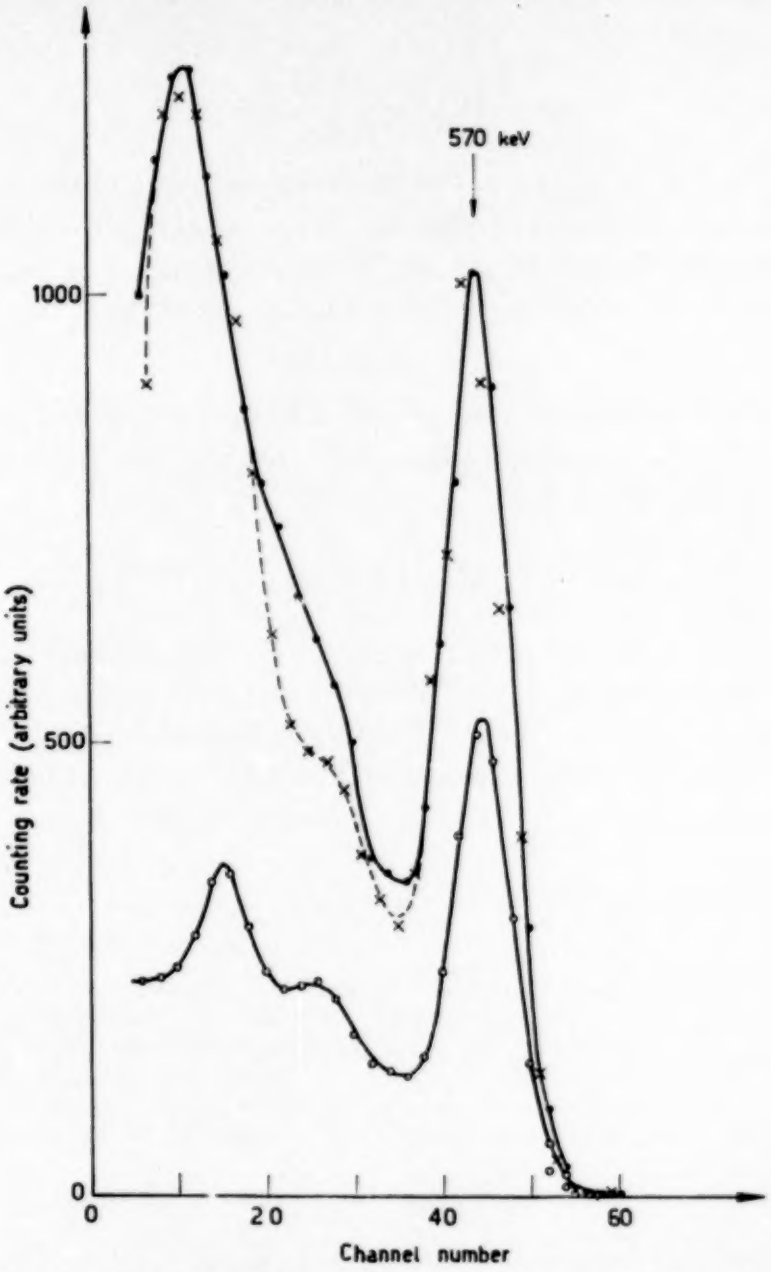

Fig. 2. Spectra of γ-rays of 835 keV energy scattered respectively by the iron (•) and lead (o) cylinders in the assembling of fig. 1 and by the short iron (x) cylinder at the central section.

2.4. ENERGY RESOLUTION

The energy resolution of the apparatus is affected by the intrinsic energy resolution of the scintillation spectrometer and by the energy spread due to the finite size of the scatterer and the detector. In order to minimize the spread due to the scintillation spectrometer, we used as short a light pipe

as possible (10 cm); the resolution of the spectrometer was investigated using a method described in a previous paper [17]). The γ-peaks fitted gaussian curves; their percentage half-width η_s depends on the energy E (in MeV) according to the equation

$$\eta_s^2 = \left(60.0 + \frac{35.5}{E}\right) \times 10^{-4}. \tag{1}$$

As regards the energy spread due to the scatterer and to finite dimensions of the crystal we have observed that the peaks of scattered radiation in the energy range between 0.2 and 0.8 MeV are nearly gaussian in shape and have a total relative half-width η_t practically independent from the energy:

$$\eta_t = 18.4 \times 10^{-2}. \tag{2}$$

Therefore the contribution of the scatterer to the total spread can be fitted approximately with a gaussian curve with a relative half-width η_p given by, according to eqs. (1) and (2):

$$\eta_p^2 = \eta_t^2 - \eta_s^2 = \left(279 - \frac{35.5}{E}\right) \times 10^{-4}. \tag{3}$$

It can be seen from eq. (3) that η_p increases with the increase in the energy of the scattered radiation. In fact the size of the effective core of the scatterer is not constant though it is larger for harder radiation.

Table 1 summarizes the features of the polarimeter, which have been discussed until now.

TABLE 1

Energy (MeV)		Transmission (10^{-4})		Degraded Radiation (%)		Energy Resolution	
primary radiation	scattered radiation	with conical lead shield	without conical lead shield	with conical lead shield	without conical lead shield	η_s %	η_p %
0.279	0.250	0.45	1.1	53	79	14.2	11.6
0.511	0.400					12.2	13.7
0.661	0.480	0.68	1.5	53	93	11.6	14.3
0.835	0.570	0.73	1.9	56	87	11.1	14.7
1.28	0.740	0.75	1.6	55	138	10.4	15.2

In table 1 the transmission is the ratio between the counting rate due to single scattered radiation, corrected for crystal efficiency, and the activity of the source; the amount of the degraded radiation is referred to that of the singly scattered radiation uncorrected for crystal efficiency.

It must not be forgotten that the features of the polarimeter described in table 1 are not instrumental constants of the given polarimeter, but they are mutually interdependent.

2.5. MAGNETIZATION OF THE SCATTERER

The magnetic induction B and the magnetic field H in the iron scatterer were measured in a conventional manner. The magnetization was found quite uniform along the cylinder with the exception of the base where it is slightly weaker (about 10 %). The number ν of polarized electrons per atom is related to B and H by the equation

$$B = H + 4\pi\nu\mu_B N$$

where μ_B is the Bohr magneton; N the number of atoms per cm^3; a correcting factor (3.4 %) was applied in order to account for the orbital contribution to B. In our working conditions ($B = 21500$ gauss) ν was equal to 2.10. The accuracy is probably better than 2 %. As we had a stabilized current supply at our disposal, no drift in the magnetization ever occurred.

2.6. EFFICIENCY OF THE POLARIMETER

The efficiency ε of the polarimeter is defined as the percentage difference in the γ counting rate for opposite field directions for a source of completely polarized γ-rays. The calculation of ε was performed as follows: let us indicate with

τ_1, τ_2 the total linear absorption coefficients for incident and scattered radiation;

$d\sigma_0$, $d\sigma_c$ respectively the usual and the spin dependent part of the differential Compton cross section in cm^2/electron for incident radiation;

σ_{c1}, σ_{c2} the spin dependent part of the integrated Compton cross section respectively for incident and scattered radiation;

$d\omega_1$, $d\omega_2$ the solid angles of the source and of a scattering point with respect to a scatterer element and a detector element;

x_1, x_2 the paths in iron respectively of the incident and scattered radiation;

f the intrinsic efficiency of the scintillator;

ν/Z the fraction of polarized electrons per atom;

N the number of iron atoms/cm^3;

N_+, N_- the counting rates for right circular polarized radiation obtained when the angle ψ between the electron spin and the direction of the incident photon is respectively lower and larger than $\frac{1}{2}\pi$;

$$\Delta = N_+ - N_-; \qquad \Sigma = N_+ + N_-; \qquad \varepsilon = 2\Delta/\Sigma.$$

By assuming that the scattered radiation is completely polarized one obtains

$$N_\pm = \int\int\int \frac{d\omega_1}{4\pi} \exp(-\tau_1 x_1 \pm N\nu\sigma_{c1}x_1) N\left(Z\frac{d\sigma_0}{d\omega_2} \pm \nu\frac{d\sigma_c}{d\omega_2}\right) dx_1 d\omega_2 \times f \exp(-\tau_2 x_2 \pm N\nu\sigma_{c2}x_2). \tag{4}$$

A very good approximation of eq. (4) can be obtained by neglecting $N\nu\sigma_{c2}$

with respect to τ_2; in fact we have $N\nu\sigma_{c2}/\tau_2 < 10^{-3}$ for the energy range under consideration ($0.5 < E < 2.5$ MeV). The approximation is even better if one considers that the scattered radiation is partially depolarized [18]). From eq. (4) it follows that

$$\begin{aligned} \frac{\Delta}{\Sigma} &= \int\int\int \frac{d\omega_1}{4\pi} \exp(-\tau_1 x_1 - \tau_2 x_2) dx_1 d\omega_2 \\ &\times f\left\{ NZ \frac{d\sigma_0}{d\omega_2} 2 \frac{\sin h}{\cos h}(N\nu\sigma_{c1}x_1) + N\nu \frac{d\sigma_{c2}}{d\omega_2} \frac{\cosh}{\sinh}(N\nu\sigma_{c1}x_1) \right\}. \end{aligned} \tag{5}$$

By considering that $N\nu\sigma_{c1}x_1 \approx 2\times 10^{-3}$ in the energy range under consideration, eq. (5) is reduced to

$$\Delta = 2N \int\int\int \frac{d\omega_1}{4\pi} \exp(-\tau_1 x_1 - \tau_2 x_2) dx_1 d\omega_2 f \frac{d\sigma_0}{d\omega_2} \left\{ ZN\nu\sigma_{c1}x_1 + \nu \frac{d\sigma_c}{d\sigma_0} \right\},$$

$$\Sigma = 2NZ \int\int\int \frac{d\omega_1}{4\pi} \exp(-\tau_1 x_1 - \tau_2 x_2) dx_1 d\omega_2 f \frac{d\sigma_0}{d\omega_2}.$$

Hence,

$$\varepsilon = 2\frac{\nu}{Z} \left\langle \frac{d\sigma_c}{d\sigma_0} + NZ\sigma_{c1}x_1 \right\rangle. \tag{6}$$

The first term of eq. (6) is given by [10])

$$\frac{d\sigma_c}{d\omega} = \tfrac{1}{2}\left(\frac{e^2}{mc^2}\right)^2 \left(\frac{k}{k_0}\right)^2 \left\{ \left(\frac{k_0}{k} - \frac{k}{k_0}\right) \cos\theta \cos\psi + \left(1 - \frac{k}{k_0}\right) \sin\theta \sin\varphi \sin\psi \right\},$$

$$\frac{d\sigma_0}{d\omega} = \tfrac{1}{2}\left(\frac{e^2}{mc^2}\right)^2 \left(\frac{k}{k_0}\right)^2 \left\{ \frac{k_0}{k} + \frac{k}{k_0} - \sin^2\theta \right\}, \tag{7}$$

where $\mathbf{k}_0$ and $\mathbf{k}$ are the initial and final photon momenta;

θ is the scattering angle,

ψ the polar angle between the electron spin $\mathbf{s}$ and $\mathbf{k}_0$,

$\frac{1}{2}\pi - \varphi$ the angle between the $(\mathbf{k}_0, \mathbf{s})$ plane and the $(\mathbf{k}_0, \mathbf{k})$ plane.

In the first of eqs. (7) the first term is the leading one.

The weighed average value (6) is dependent on the finite size of the scatterer and of the detector. In our polarimeter (see fig. 1 and section 2.3) the spread of φ about $\frac{1}{2}\pi$ and of ψ about $\frac{1}{2}\theta$ is not large; moreover the $d\sigma_c/d\sigma_0$ value is practically insensitive to the variation of ψ in the range of ψ values which are of interest, so that in eq. (7) we can put $\varphi = \frac{1}{2}\pi$ and $\psi = \frac{1}{2}\theta$. Consequently, if k_0 is considered constant, $d\sigma_c/d\sigma_0$ becomes a function of θ alone, i.e. of k or equivalently of the energy E of the scattered quantum.

We shall now consider the identity

$$NZ \int\int\int \frac{d\omega_1}{4\pi} \exp(-\tau_1 x_1 - \tau_2 x_2) dx_1 d\omega_2 f \frac{d\sigma_0}{d\omega_2} = \int A(E) dE$$

where $A(E)$ is the intensity distribution within the γ peak as detected by the scintillator. According to the results of the section 2.4, $A(E)$ can be fitted by a gaussian pulse-height distribution of relative variance constant against k_0. Therefore,

$$\left\langle \frac{d\sigma_c}{d\sigma_0} \right\rangle = \frac{1}{\delta\sqrt{2\pi}} \int \frac{d\sigma_c}{d\sigma_0} \exp\left(\frac{\bar{E}-E}{\sqrt{2}\delta}\right)^2 dE. \tag{8}$$

In the energy range under consideration the measured mean scattering angle was found to be constant and equal to $\frac{1}{4}\pi$ so that $\bar{E}$ is only a function of the incident quantum energy. In order to calculate the integral (8) we represent $d\sigma_c/d\sigma_0$ by its Taylor series development about $\theta = \frac{1}{4}\pi$ and retain the first four terms; this approximation is quite satisfactory. So the average $\langle d\sigma_c/d\sigma_0 \rangle$ becomes

$$\left\langle \frac{d\sigma_c}{d\sigma_0} \right\rangle = \left(\frac{d\sigma_c}{d\sigma_0}\right)_{\theta=\frac{1}{4}\pi} + \tfrac{1}{2}\delta^2 \left\{\frac{d^2}{dE^2}\left(\frac{d\sigma_c}{d\sigma_0}\right)\right\}_{\theta=\frac{1}{4}\pi}. \tag{9}$$

As regards the second term of eq. (6) to be averaged no particular comments are required: a graphical integration was performed. Ultimately we have for the efficiency of the polarimeter

$$\varepsilon = 2\frac{\nu}{Z}\left(\frac{d\sigma_c}{d\sigma_0}\right)_{\theta=\frac{1}{4}\pi}\left\{1+\tfrac{1}{2}\delta^2\frac{d\sigma_0}{d\sigma_c}\frac{d^2}{dE^2}\left(\frac{d\sigma_c}{d\sigma_0}\right)+NZ\sigma_{c1}\frac{d\sigma_0}{d\sigma_c}\langle x_1\rangle\right\}_{\theta=\frac{1}{4}\pi}. \tag{10}$$

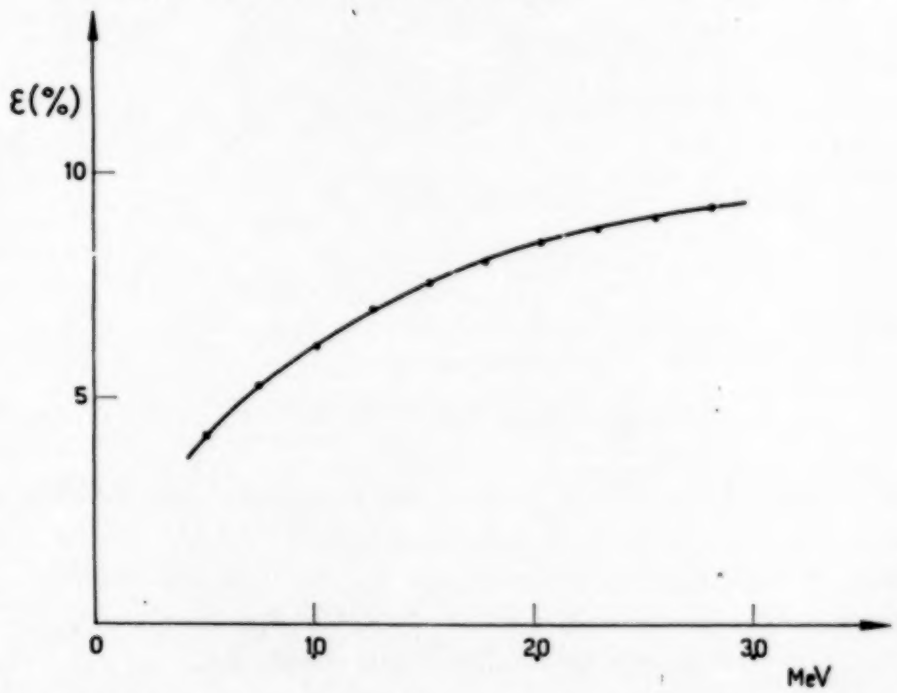

Fig. 3. Efficiency of the polarimeter aginst the energy of the incident radiation.

The last two terms in parenthesis are opposite in signs and contribute to ε to an extent of a few percent. The efficiency ε evaluated according to eq. (10)

is plotted against the energy of the primary quantum in fig. 3. The total error is certainly lower than a few percent.

3. Experimental Procedure

The source of β radiations was a disc of silver 0.05 mm thick containing uniformly dispersed 40 mC of ^{90}Sr-carbonate, backed by 0.8 mm of silver and covered by a layer of silver 0.1 mm thick. It was supplied by the Radio-

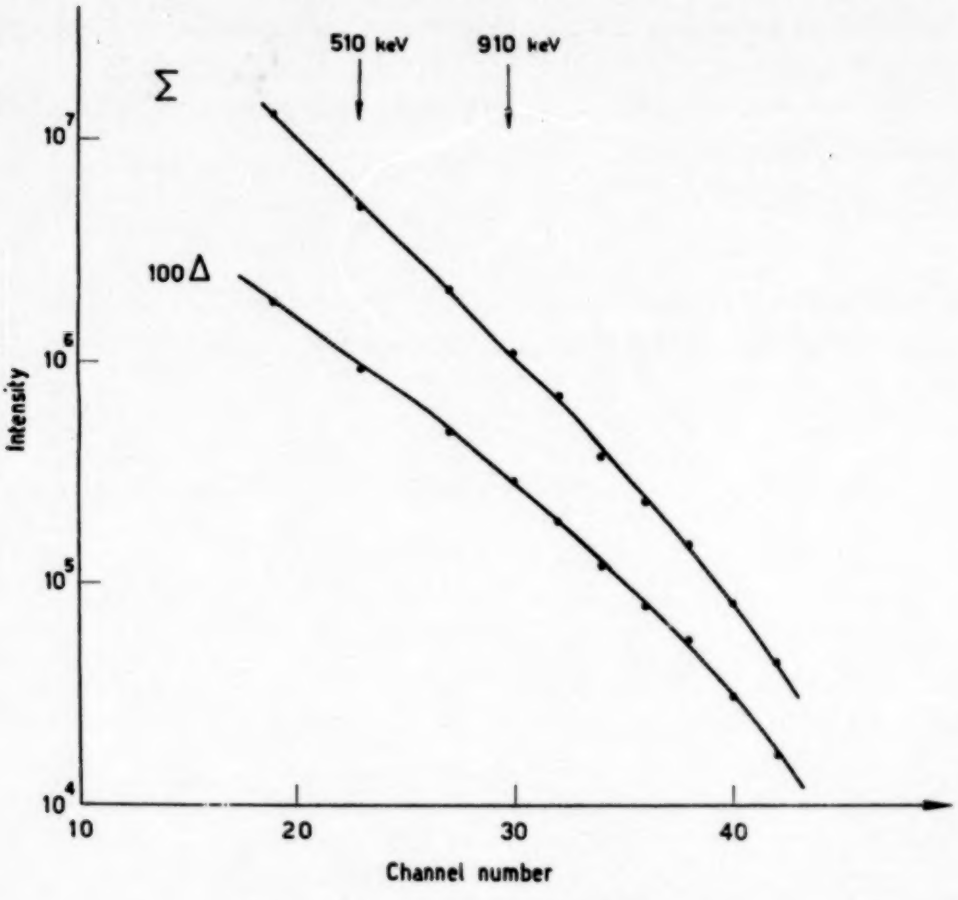

Fig. 4. Σ and Δ spectra for EB in Ag.

chemical Centre of Amersham as a sample for clinical use. The ^{90}Sr (E_{max} = 0.545 MeV) is in equilibrium with its daughter ^{90}Y, (E_{max} = 2.26 MeV). No γ-rays are present in the decay except a very week one (0.02 %) in ^{90}Y, which is very strongly converted. Foils of Al, Cu, Ag, Pb 900 mg/cm^2 thick were placed on the sample to produce bremsstrahlung.

During the measurements several runs were made, each of 6 minutes for each field direction: as a whole 5.4×10^7 pulses were counted. Energy calibrations were made approximately every five runs. Typical spectra are shown in fig. 4.

The measured asymmetries $2(N_+-N_-)/(N_++N_-)$ represent the degree of circular polarization when some corrections are applied to them. These are due to:

a) *Intrinsic energy resolution of the scintillation spectrometer.* The Δ and Σ spectra were corrected according to the equation [19])

$$N_t(E) = N_e(E) - \tfrac{1}{4}\frac{\eta_c^2}{0.693}N''_e(E), \tag{11}$$

where N_t, N_e and N''_e are respectively the intensity of the corrected spectrum, of the observed spectrum and of its second derivative.

b) *Compton electron distribution.* The subtraction of the Compton electron distributions from the Δ and Σ spectra was made by assuming a flat Compton pulse height distribution and by making use of the peak to total ratio as given by Bell [20]). In this connection it should be emphasized that we have ascertained that the values given by Bell remain practically unchanged even for sources located far from the axis of the detector.

c) *Energy spread of the polarimeter.* We used once more eq. (11) where η_c was replaced by η_p (eq. (3)) and $N_e(E)$ and $N''_e(E)$ represented the intensity of the Δ and Σ spectra already corrected for the effects just discussed, and their second derivatives.

In this way it is possible to obtain a total correcting factor converting the measured asymmetries into true ones. The correcting factors are different for different targets, the trend of Δ and Σ spectra being dependent on the atomic number of the target. At low energy the correction is mainly due to the Compton pulse distribution from the crystal, at high energy mainly to the energy spread of the polarimeter. The small amount of correction (less than 5 %) at least up to about 1.7 MeV, can be explained by considering the steepness of the measured pulse distribution at decreasing energies. At higher energy the correcting factor is larger and attains a maximum value of 0.25 for lead; in any case it is underestimated.

As regards the double scattering in the scatterer (section 2.3) no correction was applied. In fact the degraded radiation is always present in a spectral region whose upper limit corresponds to a primary energy of 1 MeV, but its relative amount (section 2.3) can be considerably reduced by the conical lead shield. However the measured asymmetries with and without the conical lead shield turned out to be practically the same.

4. Results and Discussion

The measured asymmetries, taking into account the correcting factors and the efficiency of the polarimeter (fig. 3), give the degree of circular polarization of the external bremsstrahlung quanta as a function of their

energy (fig. 5). The accuracy of the curves is better than 5 %. The polarization-energy relation for Pb is slightly different from that published previously [15]; that is due to a better approximation in the calculation of the polari-

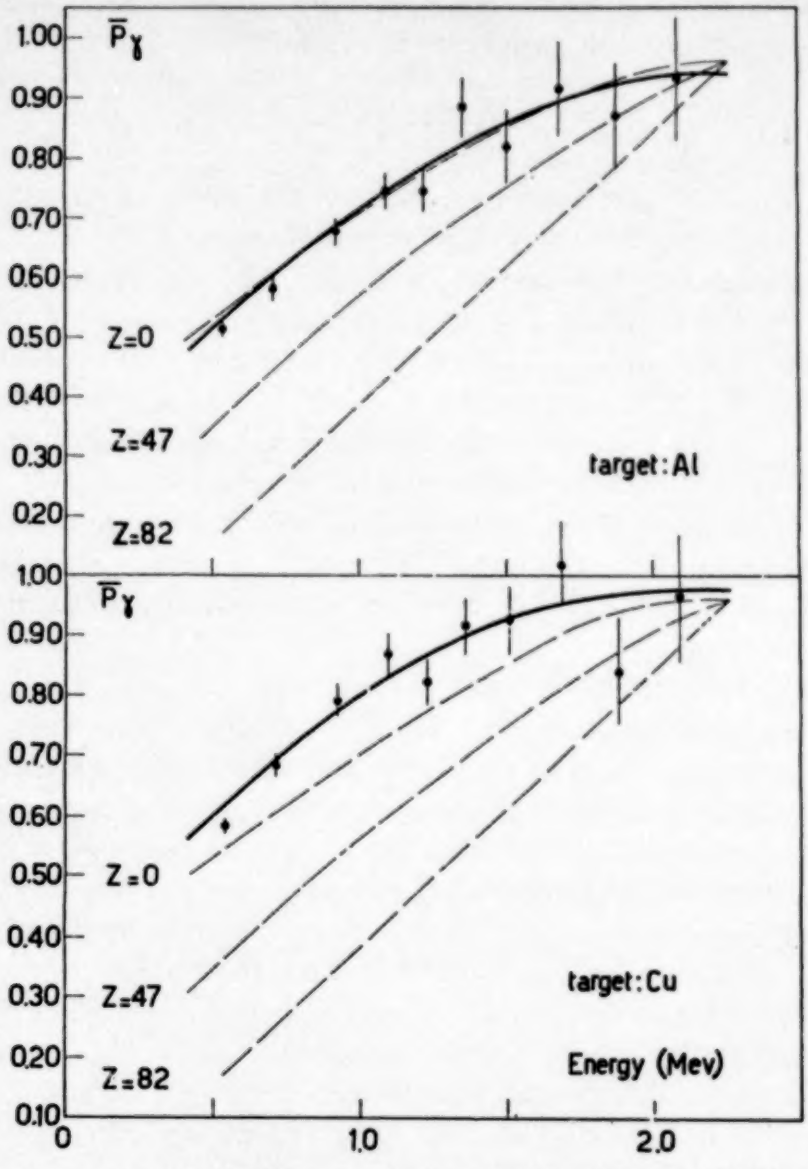

Fig. 5. Circular polarization of EB quanta as a function of their energy in different targets Al, Cu, Ag, Pb (solid curves). The quoted errors are only statistical. Dotted curves represent the predicted polarizations according to eq. (12) for $Z = 0$, 47 and 82.

meter efficiency. The polarization was found to be right, in agreement with previous measurements and theoretical previsions which require that the helicities of the EB quantum and of the radiating electron be the same.

The polarization-energy relations are dependent on the atomic number of the target (an indication of this dependence has already been found by Cohen *et al.* [14]); in particular fig. 6 and table 2 summarize this dependence for some selected energy values. In this connection it should be remembered

that the targets are actually formed by two different elements since the β-source is covered by a thin layer of Ag over which the different targets are placed and backed by a layer of Ag. This fact attenuated the Z depend-

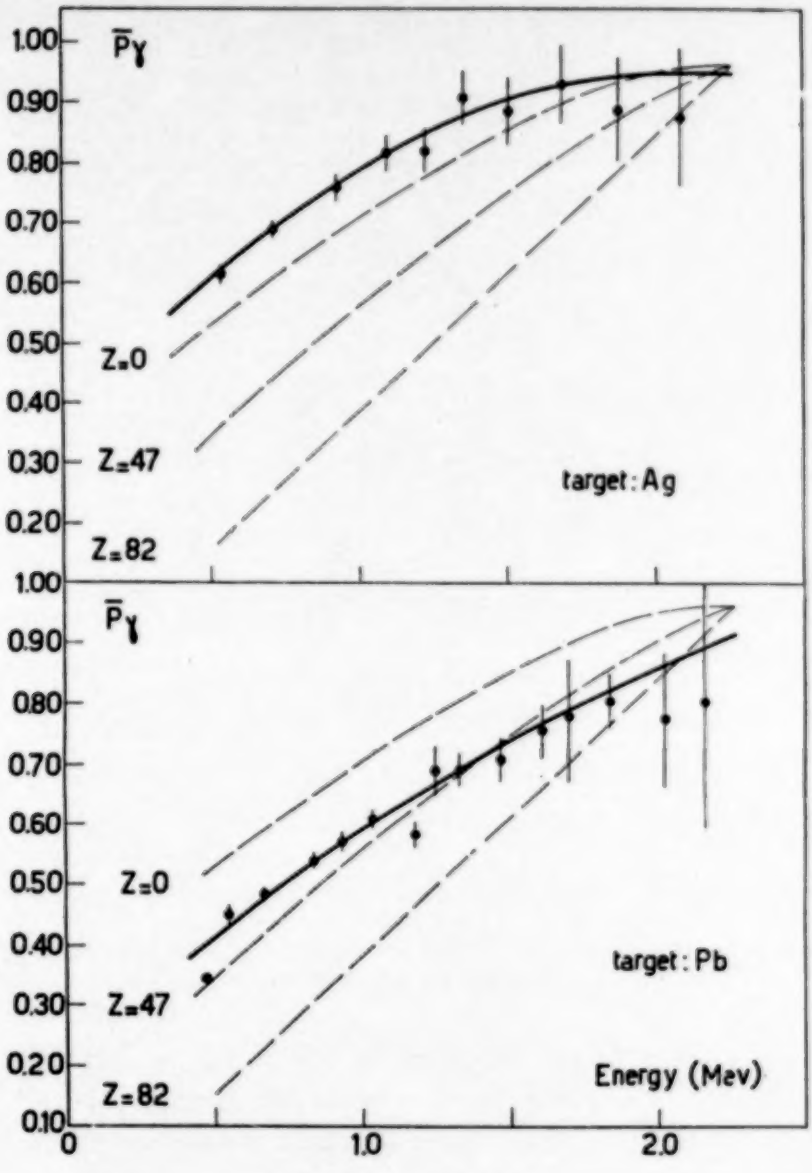

Fig. 5. (continued)

ence of the polarization to a certain extent, though not too seriously, because the radiation is emitted prevailingly forward.

At first glance the presence of a maximum in the curve of fig. 6 occurring at intermediate atomic numbers is rather surprising. However an explanation can be offered and will be made later.

Now let us make a rough calculation to compare the experimental results with theoretical previsions. The calculation is based on the following arguments:

TABLE 2

Energy of the EB quantum (MeV)	$\bar{P}_\gamma$			
	Al	Cu	Ag	Pb
0.5	0.51	0.60	0.61	0.41
1.0	0.70	0.80	0.78	0.59
1.5	0.85	0.92	0.92	0.74
2.0	0.93	0.97	0.94	0.86

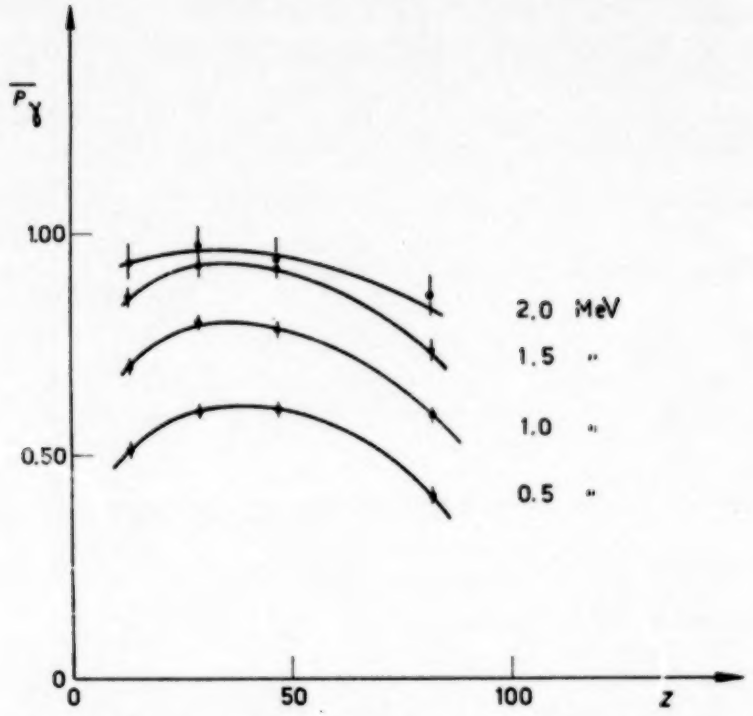

Fig. 6. Circular polarization as a function of the atomic number of the target for different energies of EB quanta.

a) The energy loss of the electrons in the target results only from inelastic collisions and is given by the Bethe-Bloch expression [21]).

b) The depolarization of monochromatic relativistic electrons is described by the following equation:

$$P = P_0 \exp\left[-\int_{E_0}^{E} \gamma \frac{\mathrm{d}x}{\mathrm{d}E}\,\mathrm{d}E\right]$$

where P_0 and P are the respective degrees of polarization of the initial electron having energy E_0 and of the electron when it has attained an energy E, $(E < E_0)$. For the quantity γ occurring in the polarization factor P we used the expression given by Rose and Bethe [22]), for a depolarizing effect arising from multiple elastic scattering. γ varies roughly as Z^2.

c) The polarization P_γ of EB quanta is proportional to the photon energy

k irrespective of the kinetic energy value of the radiating electron and of the quantum emission angle. According to McVoy [4]) and to Fronsdal and Überall [8]) that is approximately true for 2 and 2.5 MeV electrons and for emission angles between 0° and 30°. Explicity we can write

$$P_\gamma = \frac{k}{E} P_{\gamma\,\max}$$

with

$$P_{\gamma\,\max} = \left[1+\frac{1-\beta}{2-\beta}\,\frac{E+2mc^2}{E}\right]^{-1}.$$

d) The polarization of the electrons is equal to $-\,v/c$ at any energy.

Finally, an approximate expression for the EB production cross section, intermediate between that given by Bethe and Heitler [23]) and by Elwert [24]) was used:

$$\sigma_{EB} \propto \frac{Z^2}{k}\left(1-0.86\,\frac{k}{E}\right)\frac{E+mc^2}{E}.$$

By assembling all the preceding arguments and by making an integration over the β-spectrum, one obtains for the degree of circular polarization $\bar{P}_\gamma$ of an EB quantum

$$\bar{P}_\gamma = \int_k^{E_{\max}} I(E_0)\mathrm{d}E_0\,\frac{\int_{E_0}^{k} P\sigma_{EB}\,P_\gamma \mathrm{d}E}{\int_{E_0}^{k}\sigma_{EB}\,\mathrm{d}E} \qquad (12)$$

where $E_{\max}$ is the upper limit of the β-spectrum. Eq. (12) was calculated numerically for $Z = 0, 47, 82$; the results are plotted in the dotted curves of fig. 5. These curves lie below the experimental ones; in particular the experimental curves for Cu and Ag lie above that calculated for an ideal underpolarizing matter ($Z = 0$). Such a disagreement emphasizes that the assumptions on which our calculation was based are very rough and that accurate theoretical calculations are required †.

A partial qualitative explanation of this disagreement, which also accounts for the presence of the maximum in the curves of fig. 6 may be the following. If the practically linear relation between the EB spectral intensity and the atomic number Z predicted by the Bethe-Heitler theory is fulfilled, the circular polarization $\bar{P}_\gamma$ (eq. (12)) depends on Z only through the depolarizing effect. Then, $\bar{P}_\gamma$ increases with decreasing Z. On the other hand, if the EB spectral intensity deviates from the theory of Bethe and Heitler and the

† *Note added in proof:* The disagreement between the experimental and predicted curves of fig. 5 is reduced if one makes use of the calculations of Neamtan on electron dipolarization in matter instead of using the Rose and Bethe expression. For example at 511 keV energy the predicted value for Ag should be increased by 20 %. We thank dr. S. M. Neamtan for making his calculations available to us before publication.

deviation increases with the increase in quantum energy and Z, then $\bar{P}_\gamma$ becomes larger. Moreover, owing to the fact that the depolarization of the radiating electron and the EB cross section contribute to $\bar{P}_\gamma$ in a conflicting way, a maximum in the curves of fig. 6 can occur. In currently available literature there is a lack of accurate measurements of EB spectra excited by β-rays; however the work of Lidén and Starfelt [25]) on EB spectra from β-rays of ^{32}P gives a clear indication that the deviation from the Bethe-Heitler theory is in the desired direction.

As far as regards the high energy end of the polarization-energy curves, the polarization is quite insensitive to the γ and σ_{EB} values; in fact all the experimental curves converge to the same value, within the experimental errors. By extrapolating the four curves at the end point (2.26 MeV) and taking the average value, we have for the degree of circular polarization

$$\bar{P}_\gamma = 0.94.$$

On the basis of the calculation of McVoy, this limiting value indicates a longitudinal polarization of β-rays of -0.98 at $v/c = 0.98$. It is estimated that this result is affected by an experimental error not larger than 5 %. The limiting value so obtained is quite consistent with the results of previous direct measurements which give for the β-rays from ^{90}Sr+^{90}Y ($\Delta I = 2$, yes transition), a longitudinal polarization equal to $-v/c$, within about 10 % [26–29]). The direct measurements based on the Møller or Mott scattering, have covered mainly the low and the intermediate energy region of the spectrum, so that the methods employing electron scattering and the measurements of EB polarization appear to be complementary.

When this paper was drawn up, the results appeared of an investigation on the circular polarization of EB by Galster and Schopper [30]). Their experimental results agree with the present measurement as regards the polarization-energy relation for Pb. However there is disagreement as regards the Z dependence of the polarization, which was not observed by them.

References

1) Gluckstern, Hull and Breit, Phys. Rev. **90** (1953) 1026
2) T. D. Lee and C. N. Yang, Phys. Rev. **104** (1956) 254
3) Frauenfelder, Bobone, von Goeler, Levine, Lewis, Peacock, Rossi and De Pasquali, Phys. Rev. **106** (1957) 386
4) K. W. McVoy, Phys. Rev. **106** (1957) 828; **110** (1958) 1484
5) Visotsky, Kresnin and Rozentsveig, Soviet Physics, JETP **5** (1957) 883
6) A. Claesson, Arkiv Fysik **12** (1957) 569
7) H. Banerjee, Phys. Rev. **111** (1958) 532
8) C. Fronsdal and H. Überall, Phys. Rev. **111** (1958) 590
9) K. W. McVoy, Phys. Rev. **111** (1958) 1333
10) S. B. Gunst and L. A. Page, Phys. Rev. **92** (1953) 970
11) Goldhaber, Grodzins and Sunyar, Phys. Rev. **106** (1957) 828

12) H. Schopper and S. Galster, Nuclear Physics **6** (1958) 125
13) F. Bohem and A. H. Wapstra, Phys. Rev. **109** (1958) 456
14) Cohen, Wiener, Wald and Schmorak, Proc. Rehovoth Conf. Nucl. Structure (North-Holland Publ. Company, Amsterdam, 1958) p. 404
15) A. Bisi and L. Zappa, Phys. Rev. Letters **1** (1958) 332
16) H. Schopper, Phil. Mag. **2** (1957) 710
17) A. Bisi and L. Zappa, Nuclear Instruments **3** (1958) 17
18) H. Schopper, Nuclear Instruments **3** (1958) 158
19) K. Lidén and N. Starfelt, Arkiv Fysik **7** (1954) 427
20) P. R. Bell in Beta and Gamma Ray Spectroscopy edited by K. Siegbahn (North-Holland Publishing Company, Amsterdam, 1955) p. 133
21) W. Paul and H. Steinwedel in Beta and Gamma Ray Spectroscopy edited by K. Siegbahn (North-Holland Publishing Company, Amsterdam 1955) p. 1
22) M. E. Rose and H. A. Bethe, Phys. Rev. **55** (1939) 277
23) H. A. Bethe and W. Heitler, Proc. Roy. Soc. A **146** (1934) 83
24) G. Elwert, Ann. Physik **34** (1939) 178
25) K. Lidén and N. Starfelt, Phys. Rev. **97** (1955) 419
26) J. Heintze, Z. Physik **148** (1957) 560
27) Alichanov, Eliseiev, Lubimov and Eishler, Nuclear Physics **5** (1958) 588
28) Alichanov, Eliseiev and Lubimov, Nuclear Physics **7** (1958) 655
29) Benczer-Koller, Scwarzschild, Vise and Wu, Phys. Rev. **109** (1958) 85
30) S. Galster and H. Schopper, Phys. Rev. Letters **1** (1958) 330

2.B:2.D:
2.F

Nuclear Physics **10** (1959) 348—359; © *North-Holland Publishing Co., Amsterdam*
Not to be reproduced by photoprint or microfilm without written permission from the publisher

THE ENERGY AND ANGULAR DISTRIBUTION OF PROTONS FROM 14 MeV NEUTRON REACTIONS WITH Fe^{54}

D. L. ALLAN

Atomic Energy Research Establishment, Harwell, Didcot, Berks.

Received 14 January 1959

Abstract: The energy and angular distribution of protons from the reactions Fe^{54}(n, p) and Fe^{54}(n, np) at 14 MeV have been determined. The Fe^{54} angular distributions and previously published angular distributions for Cu have been corrected to the centre of mass system of co-ordinates and compared. The results indicate that there is a small contribution from the direct interaction of the incident neutrons with protons mainly in the surface of the target nucleus.

1. Introduction

In a previous paper [1]), henceforth referred to as I, the author reported some results on the energy and angular distribution of protons emitted in the reactions Cu(n, p) and Cu (n, np) at an incident energy of 14 MeV. Proton energy distributions at six angles between 25° and 150° and angular distributions for eight proton energy intervals between 2 and 14 MeV were presented. Proton groups having an energy spacing many times the known level spacing of the residual nucleus were present in the 25° energy distribution and the angular distributions exhibited a forward asymmetry which increased with increasing proton energy. Both these observations were interpreted as evidence that the Cu (n, p) reaction included a contribution from the direct interaction of the incident neutrons with the protons in the target nucleus. Similar results for a number of target nuclei have been reported recently [2–6]).

This paper presents the results of a similar study of the protons emitted from Fe^{54}. In some earlier work [7]), it was found that the 14 MeV (n, p) cross section for Fe^{54} was about five times greater than for (natural) Cu. This was attributed to the fact that, in the decay of the compound nuclei formed in these reactions, (n, p) reactions compete more favourably with (n, n′) reactions where, as is the case of Fe^{54}, the target nucleus is even. If the large Fe^{54}(n, p) cross section is a result of enhanced compound nucleus contribution, the forward asymmetries in the proton angular distributions introduced by direct interactions will be less than for Cu, provided the two reaction processes are independent. This may not be the case, however, if there is interference between the two processes (or if the direct interaction contribu-

tion to the Fe^{54} (n, p) reaction is greater for some other reason). The work reported here was undertaken for the purpose of investigating these possibilities.

2. Apparatus and Method

The apparatus, experimental procedure, and the method of deriving the results was essentially the same as described in I. The target was metallic Fe^{54} (Fe^{54}: 88.4 %; Fe^{56}: 11.2 %; $Fe^{57,58}$: 0.4 %) electrolytically deposited upon the inside of a cylindrical band 1.8 cm high, 7.5 cm diameter, formed from 0.02 in. gold sheet. This deposit formed a continuous cylindrical layer of average thickness 27 mg · cm^{-2} and width 1 cm surrounding a centrally placed photographic plate detector embedded in a copper shadow plate. Since the uniformity of the deposit could not be guaranteed to better than ± 10 %, the target was continuously rotated about the photographic plate during each exposure to neutrons by a small electric clock motor with a geared drive giving half a revolution per minute. The motor was mounted outside the vacuum chamber and at a distance of 15 cm from it in order to reduce the flux of neutrons scattered into the photographic plate.

The energy and angular distributions reported here were derived from measurements of about 19 000 tracks in six plates separately exposed to the complete Fe^{54} target. Background distributions were obtained from measurements on a single plate exposed to the target while it was masked by a 0.02 in. gold strip. This was placed so that only protons from parts of the target in the angle range $\alpha = 80° - 160°$ (see I) could reach the photographic plate. The background was very small.

3. Centre of Mass Corrections

The results have been corrected to give energy and angular distributions in the centre of mass system. For a target nucleus with $A = 54$, the centre of mass angles and solid angles differ very little from those measured in the laboratory. The energy differences ΔE between centre of mass proton energies and the energies measured in the laboratory are also small. For example, at 5 MeV, ΔE changes from +300 keV to −300 keV as the angle of observation is changed from 20° to 160°. However, the angular variation of ΔE leads to considerable distortion of the angular distributions when these are plotted between energy limits (in the laboratory system) corresponding to steeply rising or falling regions of the proton spectrum. The angular distributions have therefore been corrected for this effect †. The corrections were

† The author is grateful to Dr. L. Colli for drawing his attention to this effect (private communication).

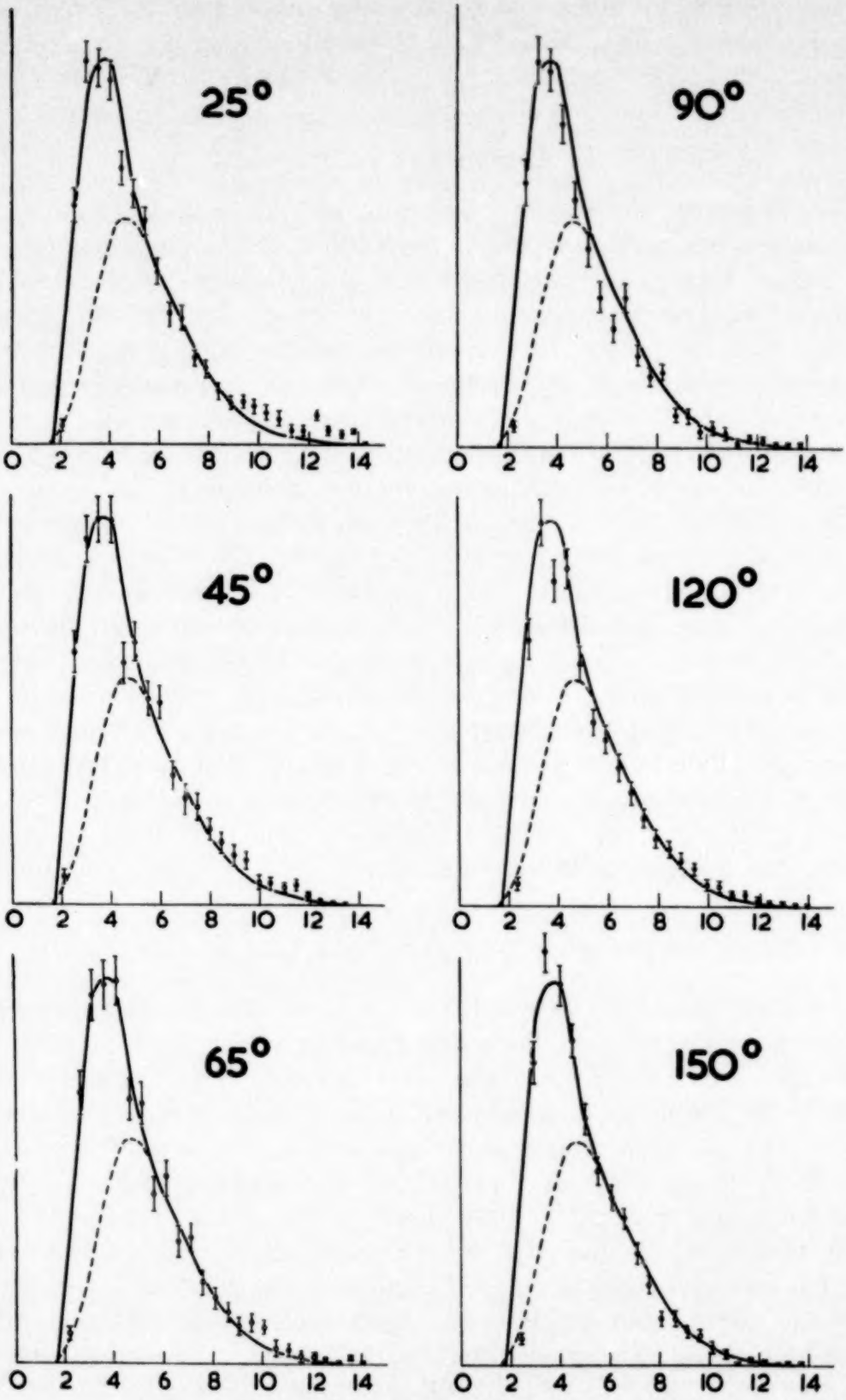

Fig. 1. Energy distributions of protons from Fe^{54}.
Ordinate: relative yield of protons (tracks/0.5 MeV energy interval)
Abscissa: Centre of mass proton energy (MeV).

computed by integrating the centre of mass proton spectrum between centre of mass energy limits appropriate to each angle point of the angular distributions. For this purpose, the solid curve in fig. 1 was used. It will be seen from this figure that this curve is a good fit to the experimental points at all angles of observation.

4. Results

4.1. PROTON ENERGY DISTRIBUTIONS

The energy spectra of the protons from Fe^{54} at six angles of observation are given in fig. 1. The ordinates give the proton yields per 0.5 MeV interval in arbitrary units; the abscissae give the proton energy in MeV in the centre of mass system. The spectra for the three lower angles cover an angular range of $\pm 10°$; the other spectra cover an angular range of $\pm 15°$.

Fig. 2 is a conventional statistical theory plot of the results from the 90°, 120° and 150° proton spectra. The ordinate is the logarithm of the proton yield divided by the product of the proton energy and the cross section for compound nucleus formation by protons given by Blatt and Weisskopf [8]). The points lie on two straight lines corresponding to the reactions Fe^{54}(n, np) Mn^{53}, and Fe^{54} (n, p) Mn^{54}. The slopes of these lines

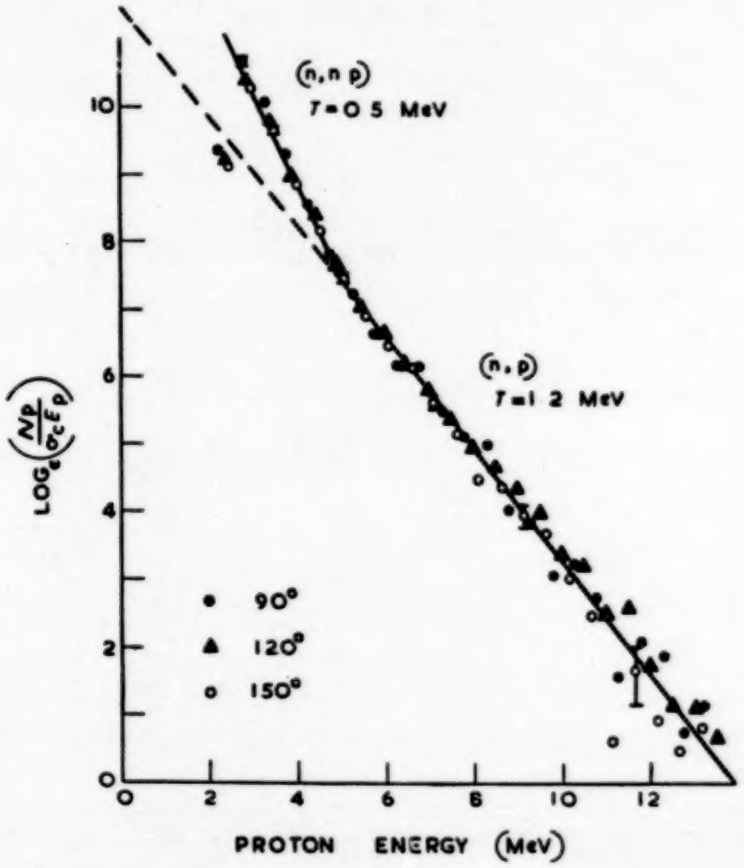

Fig. 2. Statistical theory plot for protons emitted at backward angles.

give the temperature parameters for the residual nuclei formed in these two reactions: they are $T = 0.5$ and $T = 1.2$ MeV, respectively. The continuous line appearing with each of the spectra of fig. 1 was calculated from the ordinates of points lying on these two straight lines. The curve represents the combined (n, np) and (n, p) spectrum predicted by the statistical theory on the basis of a Maxwellian proton energy distribution. The broken line in fig. 1 gives the spectrum for the (n, p) reaction alone, derived from the line $T = 1.2$ MeV in the same way. The areas under the two spectra give the relative contributions of the (n, np) and (n, p) reactions to the total proton emission cross section: they are 33 % and 67 % respectively.

4.2. ANGULAR DISTRIBUTION OF THE PROTONS

The centre of mass angular distributions of the protons from Fe^{54} are shown in figs. 3 and 4 for eight energy intervals. The horizontal broken lines

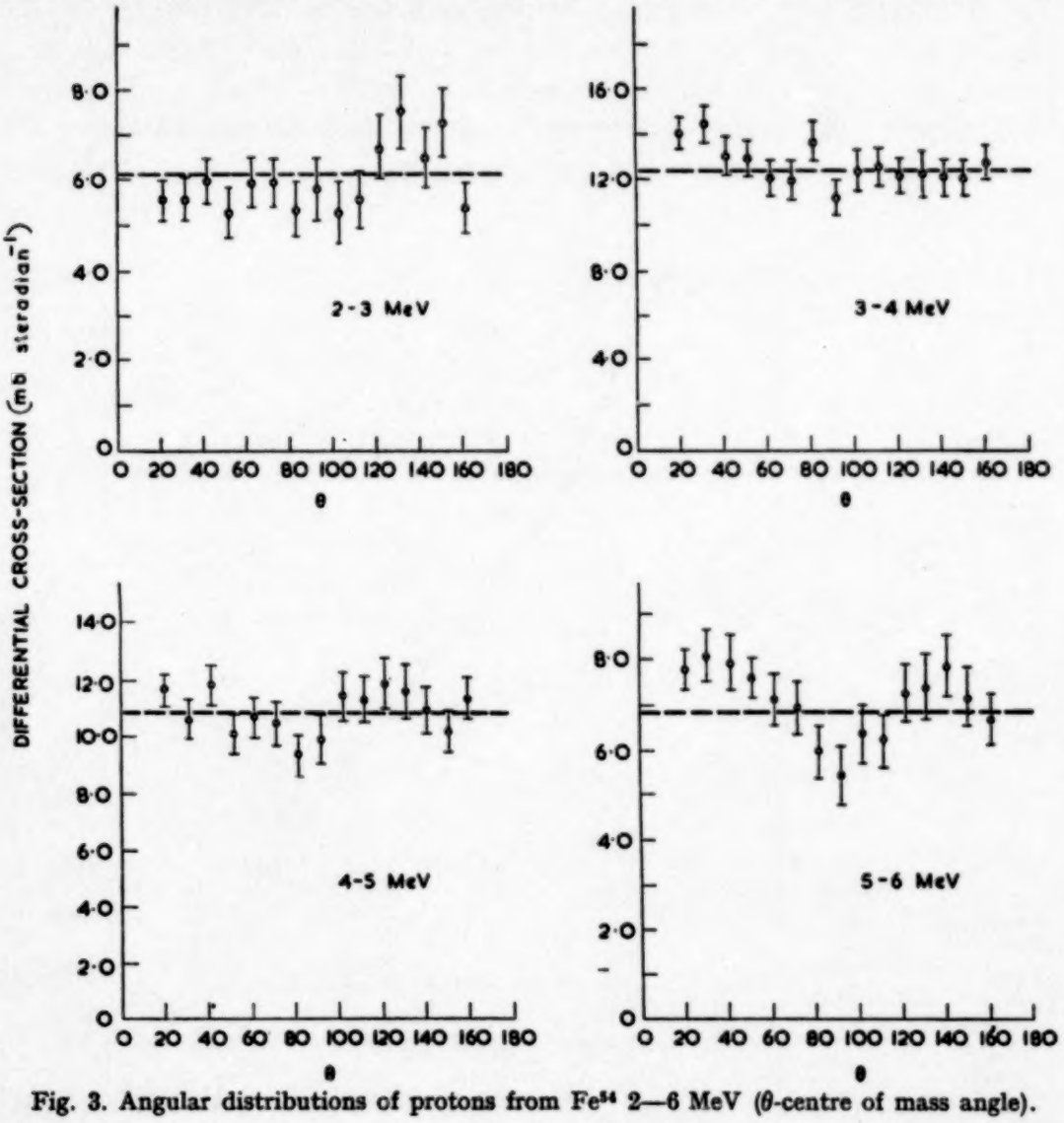

Fig. 3. Angular distributions of protons from Fe^{54} 2—6 MeV (θ-centre of mass angle).

indicate the magnitudes of the differential cross sections obtained by integrating the statistical theory spectrum (fig. 1) between the appropriate energy limits and normalising to the differential cross section over backward angles for the energy interval $E_p = 3$—4 MeV.

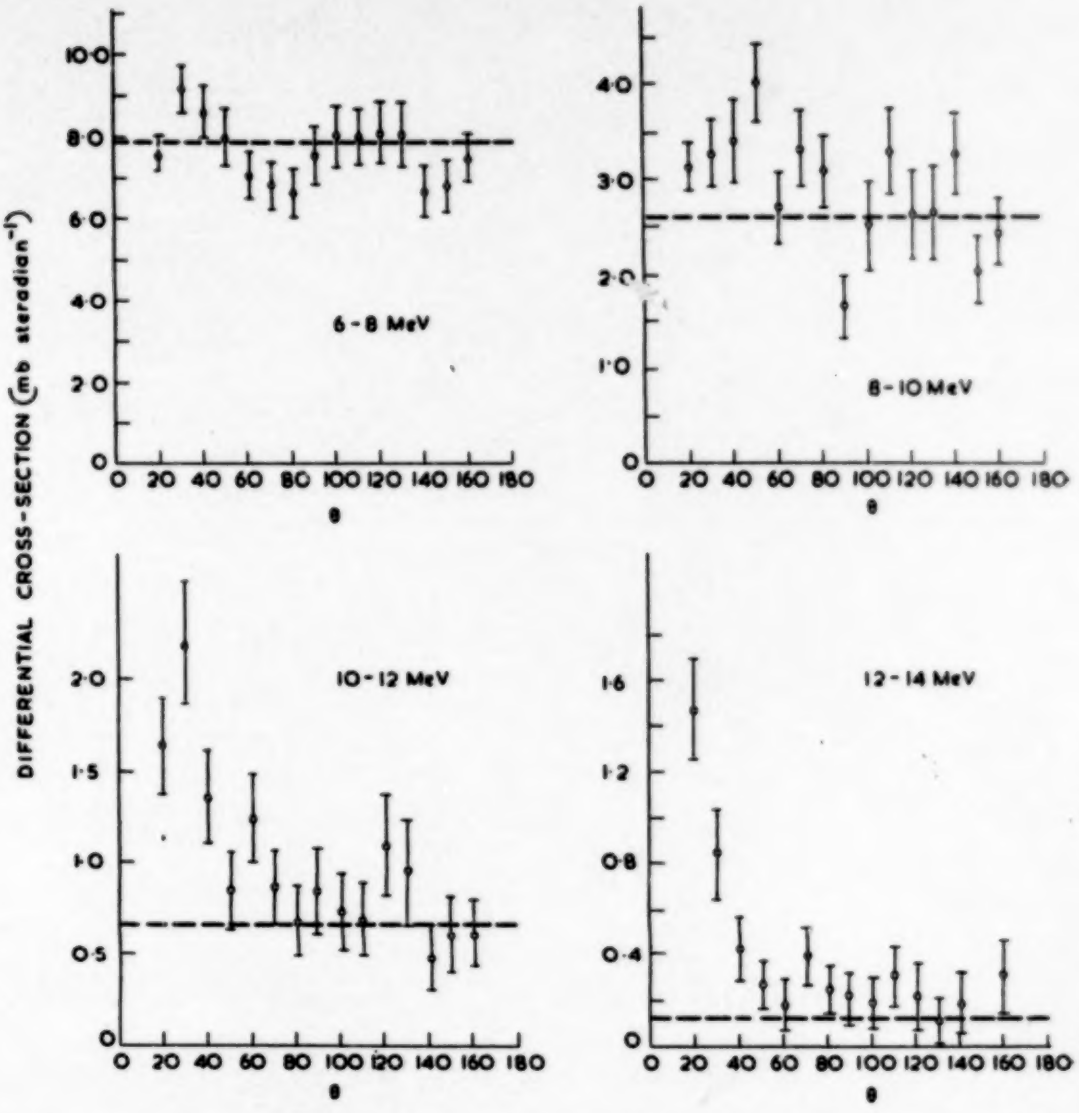

Fig. 4. Angular distributions of protons from Fe^{54} 6—14 MeV (θ-centre of mass angle).

The angular distributions of the protons from Cu were presented in I in the laboratory system of co-ordinates; the importance of the distortion introduced by the energy shift ΔE (see section 3) not being appreciated at the time these results were published. The Cu results are therefore reproduced in figs. 5 and 6 in the centre of mass system so that the Fe^{54} and Cu results can be compared. The magnitude of the Cu differential cross sections have been increased by 40 per cent in accordance with a recent recalibration of the

absolute 14 MeV neutron output. The horizontal broken lines in figs. 5 and 6 represent the statistical theory differential cross sections normalised over the backward angle points in the interval $E_p = 5$—6 MeV.

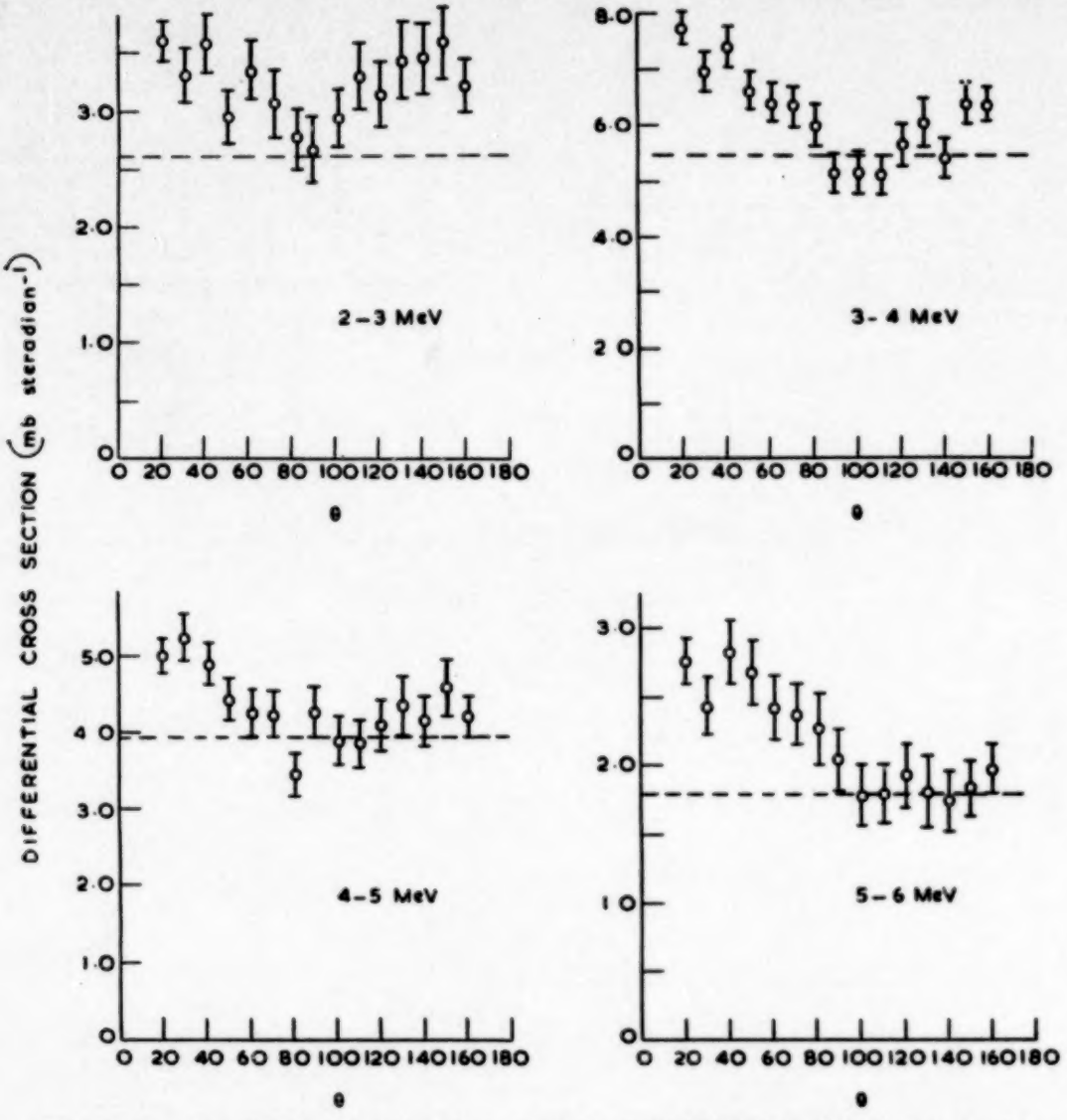

Fig. 5. Angular distributions of protons from Cu 2—6 MeV (θ-centre of mass angle).

The total proton emission cross sections and the separate (n, p) and (n, np) cross sections are given in table 1 for both Cu and Fe^{54}. The Fe^{54} cross sec-

TABLE 1

Cross sections in mb

Target	(n, p) †	(n, np) †	σ_{dir}	σ_{total}
Fe^{54}	395	195	20	610±20
Cu	98	128	20	246±10

† Compound nucleus contribution.

tions have been corrected for the contribution from the Fe^{58} present in the target; the Cu cross sections are for the natural mixture of isotopes. The total cross section for Fe^{54} is in good agreement with the results of March and Morton [6]) (600±60 mb).

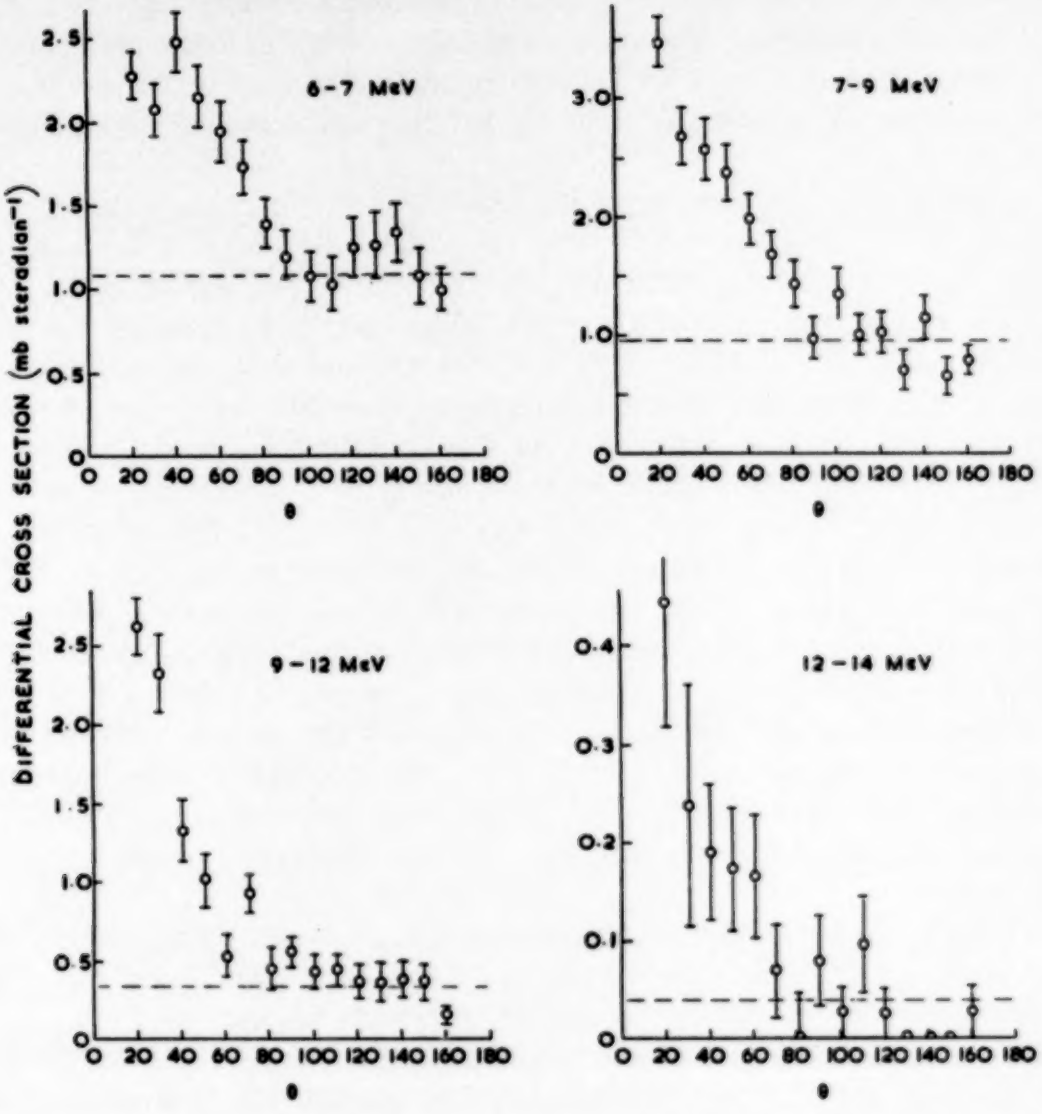

Fig. 6. Angular distributions of protons from Cu 6—14 MeV (θ-centre of mass angle).

5. Discussion

It is evident from fig. 1 that the statistical theory spectrum derived from fig. 2 fits the experimental points very well at all angles of observation. Such deviations as occur are confined to the high energy protons in the spectra at low angles. It can be concluded, therefore, that the reactions Fe^{54}(n, p) and Fe^{54} (n, np) proceed predominantly by way of compound nucleus decay. The temperature parameters, $T = 0.5$ and $T = 1.2$ MeV, deduced from fig.

2, are in good agreement with the values reported by March and Morton [6]) for the same reactions ($T = 0.45$ and 1.2 MeV).

The angular distributions of the protons from Fe^{54} (figs. 3 and 4) are roughly isotropic between $E_p = 2$ MeV and $E_p = 8$ MeV. Between $E_p = 4$ MeV and $E_p = 8$ MeV there is some evidence for a minimum around 90° and the differential cross section appears to fall towards this minimum value at 0° and 180°. For $E_p > 8$ MeV, the angular distributions exhibit a forward asymmetry which increases with E_p but they are roughly isotropic over backward angles.

The angular distributions of the protons from Cu (figs. 5 and 6) are essentially isotropic over the energy range $E_p = 2$—5 MeV. There is again evidence of a minimum at 90° but the differential cross section appears to rise to a maximum value at 0° and 180°. The slight forward asymmetries in the 3—4 MeV and 4—5 MeV angular distributions are due to underestimating the correction for distortion which is introduced by the centre of mass motion. The equivalent thickness of the Cu target foil was 1.7 MeV at $E_p = 3$ MeV and, when computing the centre of mass corrections, the proton energies were taken as those at middle depth in the foil. This procedure is approximately correct for energy intervals where the spectrum falls (or rises) linearly with energy. The corrections will be underestimated, however, where the interval begins or ends at energies corresponding to regions of the spectrum where there is an abrupt change of slope. This difficulty can be avoided if the energy interval is chosen so that the peak of the spectrum occurs in the middle of the interval. Thus, it was found that the corrected angular distribution for $E_p = 2$—5 MeV was symmetrical about 90° at which angle the differential cross section was 75 per cent of the value at 0° and 180°.

For $E_p > 5$ MeV, the distributions exhibit a forward asymmetry which becomes progressively more pronounced as E_p increases. As for Fe^{54}, the distributions are roughly isotropic over backward angles.

The fact that the Fe^{54} angular distributions are essentially isotropic for $E_p = 2$—5 MeV whereas the corresponding angular distributions for Cu exhibit minima around 90° might be a result of the difference in the relative yields of the two reactions: (n, p) and (n, np). It will be noticed from table 1 that the Cu (n, np) cross section is 30 % greater than the Cu (n, p) cross section, whereas the Fe^{54}(n, np) cross section is half the Fe^{54} (n, p) cross section. We might therefore suppose that the angular distribution of the protons from a 14 MeV (n, np) reaction has a minimum at 90° and maxima at 0° and 180°, while that of the low energy (n, p) protons is more nearly isotropic. There is a possible justification for this supposition. It has been suggested by Christy [9]) that a proton at the nuclear surface acquires an additional velocity if it is evaporated from the equator of a nucleus (that is,

the plane containing the incident particle and the centre of the nucleus). When integrated over all equatorial planes, such emission leads to a proton angular distribution having maxima at 0° and 180°. The anisotropic emission from a compound nucleus has been examined recently by Ericson and Strutinski [10]), who give both a classical and a quantal treatment of the problem. As reported above, the average kinetic energy of a proton at the nuclear surface (the nuclear temperature T) is about 2.5 times less for protons emitted in (n, np) reactions than for those emitted in (n, p) reactions. In the energy region we are considering, protons leave the nucleus with energies which are about half the Coulomb barrier height. Kinetic energy is therefore at a premium and the low nuclear temperature associated with the (n, np) reaction might lead to preferential emission from the nuclear equator and to the form of angular distribution which was supposed.

The deviations from the statistical theory spectrum and the forward asymmetry of the angular distributions of the higher energy protons can be interpreted as evidence for the occurrence of direct interactions. It is evident that the forward asymmetry is greater in the Cu angular distributions than in those for Fe^{54}. In order to compare the direct interaction contributions in reactions with these two nuclei on an absolute basis, a procedure similar to that used in I was used. It was supposed that the angular distribution of the higher energy protons emitted as a result of compound nucleus decay in (n, p) reactions is essentially isotropic. An isotropic angular distribution, representing the compound nucleus differential (n, p) cross sections (approximately, the broken lines in figs. 3—6), was therefore subtracted from the observed differential cross sections. The difference was integrated over all angles to give a cross section which will be interpreted as the direct interaction differential cross section $\partial\sigma_{dir}(E_p)/\partial E$. This procedure was followed only where the interpretation of the anisotropy of the angular distributions appeared straightforward: that is, for Cu, $E_p > 5$ MeV and for Fe^{54}, $E_p > 8$ MeV. The results are given in fig. 7, where the ordinate is $\partial\sigma_{dir}/\partial E$ in mb/MeV. The errors indicated were obtained by making the calculation for curves passing through the upper and lower bars of the statistical errors indicated on the angular distributions. It will be seen that, over the energy range where the results can be compared, the values of $\partial\sigma_{dir}/\partial E$ are the same for both Cu and Fe^{54}. Thus, the direct interaction and compound nucleus contributions are independent over this energy range.

The shape of the spectrum of direct interaction protons in fig. 7 is interesting because it suggests that these protons are ejected from the surface of the nucleus rather than from the entire volume of the nucleus. One would expect the distribution of energies transferred to the protons as a result of collisions occurring throughout the volume of the nucleus to be approximately uniform. Surface reflection effects would bias the spectrum of ejected

protons towards higher energies. In contrast, the observed spectrum is peaked towards lower proton energies. This result is consistent with the capture of the incident neutrons in the surface of the nucleus; that is, in the "exponential tails" of the states of the final nucleus. The lower proton

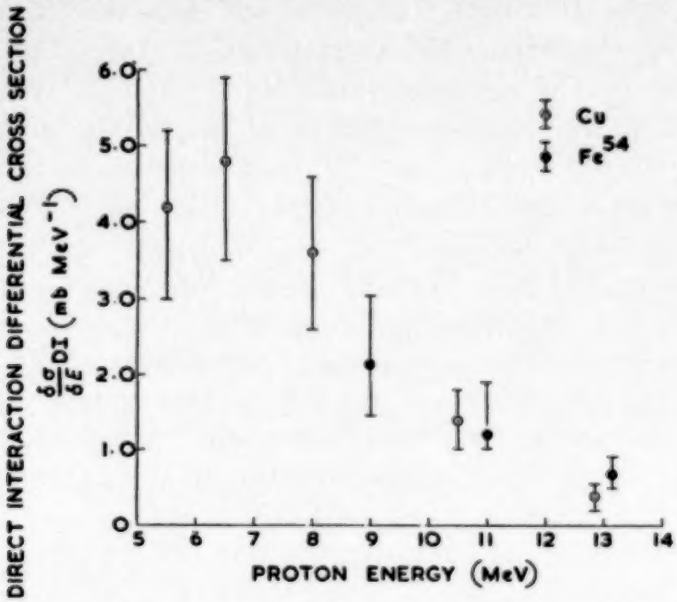

Fig. 7. Energy spectrum of direct interaction protons.

energies correspond to lower neutron binding energies in the final nucleus and therefore to more extensive tails. The differential cross section therefore increases towards lower proton energies. These results support the conclusion reached by Elton and Gomez [11]) that direct (n, p) reactions occur mainly in the nuclear surface and not in the volume.

The direct interaction cross section σ_{dir} for Cu, integrated over the energy range $E_p = 5$—14 MeV, is given in column 4 of table 1. This value probably includes most of the direct interaction contribution. The corresponding cross section for Fe^{54}, integrated over the energy range $E_p =$ 8—14 MeV, is 8 mb. For the purposes of deriving the compound nucleus cross section, the direct interaction cross section $\sigma_{dir}(Fe^{54})$, integrated over the energy range $E_p = 5$—14 MeV, is assumed to be the same as for Cu in table 1. March and Morton [6]) report a direct interaction cross section for Fe^{54} (70 mb) which is very much greater. Our lower estimate is mainly a result of the fact that we observed a much smaller degree of forward peaking in the angular distributions 7—14 MeV than did these authors.

The proton emission differential cross sections for Cu were compared with the results of Verbinski *et al.* [12]) over the energy range 6—14 MeV. The agreement is good, except in the region 120° where these authors found a differential cross section which is about 50 % greater than ours.

In conclusion, the author thanks Mrs. M. J. Bathe, Miss E. I. Harrison, Mrs. A. S. Lane and Miss P. M. Stopana for scanning the plates; Dr. K. W. Allen of A.W.R.E., Aldermaston, for providing the 14 MeV neutron irradiadtion facilities, and Dr. M. L. Smith of A.E.R.E., Harwell for preparing the Fe^{54} target. The author is also indebted to Dr. A. M. Lane for valuable discussions

References

1) D. L. Allan, Nuclear Physics **6** (1958) 464
2) R. A. Peck, Jr., Phys. Rev. **106** (1957) 965
3) L. Colli, V. Facchini and S. Micheletti, Nuovo Cimento **5** (1957) 502;
L. Colli, V. Facchini, I. Iori, G. Marcazzan, A. Sona and M. Pignanelli, *ibid* **7** (1958) 400
4) H. P. Eubank, R. A. Peck Jr. and F. L. Hassler, Nuclear Physics **9** (1958/59) 273
5) L. Rosen and A. H. Armstrong, Bull. Am. Phys. Soc. **1** (1956) 224
6) P. V. March and W. T. Morton, Phil. Mag. **3** (1958) 143
7) D. L. Allan, Proc. Phys. Soc. A **70** (1957) 195
8) J. M. Blatt and V. F. Weisskopf, Theoretical Nuclear Physics (Wiley, New York, 1952) p. 352
9) R. F. Christy, Proceedings of the University of Pittsburg Conference on Nuclear Structure (June 1957) p. 416
10) T. Ericson and V. Strutinski, Nuclear Physics **8** (1958) 284
11) L. R. B. Elton and L. C. Gomez, Phys. Rev. **105** (1957) 1027
12) V. V. Verbinski, T. Hurliman, W. E. Stephens and E. J. Winhold, Phys. Rev. **108** (1957) 779

4.E *Nuclear Physics* **10** (1959) 360—372; © *North-Holland Publishing Co., Amsterdam*
Not to be reproduced by photoprint or microfilm without written permission from the publisher

ON THE DECAY OF ^{67}Ge

R. A. RICCI † and R. VAN LIESHOUT
Instituut voor kernphysisch Onderzoek, Amsterdam

Received 15 January 1959

Abstract: The beta and gamma spectra of the nucleide ^{67}Ge, decaying with a half-life of 18.7 ± 0.5 min, were studied with scintillation techniques. Three major positon groups were found, with observed endpoint energies of 3.14 (100^+), 2.30 (40^+) and 1.6 MeV ($< 25^+$), each group probably being complex. A total of 18 gamma rays were seen in the decay (see table 1); coincidences between them were studied by the summing technique (see table 2). A tentative decay scheme is proposed (fig. 8) which incorporates the levels in ^{67}Ga known from other work.

1. Introduction

The nucleide ^{67}Ge was produced for the first time by spallation of As with 190-MeV deuterons [1]). Studies of the chemical properties and the genetic relationship with the corresponding Ga isotope established the charge and mass number of this isotope, which was found to decay with a half-life of 21 min. Further work was performed by Aten, de Vries-Hamerling and Lindner [2, 3]), who produced the activity by bombarding Zn with 15-MeV and 52-MeV alpha particles, and who reported a half life of 19 min. The positon spectrum appeared to be complex with an endpoint energy of 2.9 ± 0.3 MeV as determined by absorption. These authors report only one strong gamma ray with an energy of 170 ± 10 keV. It was established that the number of ^{67}Ge nuclei decaying by way of the 170 keV level is at least about as large as the number of nuclei decaying without an accompanying gamma ray. A preliminary investigation [5]) proved the existence of a strong gamma ray of 170 ± 3 keV in the decay of ^{67}Ge; the half-life found was 21 ± 1 min. No other conclusions could be drawn from this investigation because ^{67}Ge occurred mixed with ^{66}Ge.

The postulated level at 170 keV in ^{67}Ga was not observed by Chapman and Slattery [4]) who used the neutron threshold method to detect levels in ^{67}Ga from the (p, n) reaction on separated ^{67}Zn. In addition to the ground state, levels were found at 0.357 ± 0.007, 0.857 ± 0.020, 1.235 ± 0.015 and 1.544 ± 0.020 MeV. The 0.170 MeV gamma transition clearly does not fit into this level scheme; moreover it might be interesting to look for gamma rays arising from transitions between the reported levels.

† On leave of absence from the "Istituto di Fisica Sperimentale del Politecnico", Torino, Italia.

2. Source Preparation

The isotopes ^{66}Ge and ^{67}Ge are produced simultaneously when bombarding Zn with 52-MeV alpha particles. The two activities can be produced and studied separately by appropriately choosing the energy of the alpha-particle beam and the duration of the irradiation. Sources of ^{67}Ge were obtained in large amounts from chemically pure Zn bombarded during 5 to 10 min with 19-MeV alpha particles. ($\approx$ 0.5 to 1μAh). The targets were dissolved in 8*N* HCl, Ge and Ga carriers were added and the $GeCl_2$ was distilled into 6*N* HCl. The Ge was then precipitated as GeS and the precipitate washed out with alcohol and ether.

The contribution of ^{66}Ge and its decay product was found to be completely negligible in all sources produced in this manner. Some ^{69}Ge was always present, but due to its 40 hour half-life its contribution was easily determined and subtracted. (The initial contribution was less than 2 % in the annihilation peak, and less than 20 % in the region of 1 MeV arises from the strong gamma ray of 1.12 MeV.)

The sources were studied with scintillation counters for gamma and beta radiations and the various spectra were displayed on the 100 channel RIDL analyzer.

3. Experimental Procedure and Results

The gamma ray spectrum was measured with a conventional NaI(Tl) crystal (diameter 2.5 cm, height 2.5 cm) coupled with a 6292 DuMont photomultiplier. The energy region explored extended to about 3.6 MeV. Various sources were used; in each case the decay was followed for at least 2 hours. The half-life found in the region above 1.4 MeV was 19 ± 1 min. The spectrum between 0.3 and 1.4 MeV shows two periods of 19 ± 2 min and 40 ± 1 hours respectively, which indicates that only ^{69}Ge was present in addition to ^{67}Ge. Below 0.3 MeV the spectrum decays mainly with a half life of 18.5 ± 0.5 min, a small part having a composite half-life which is compatible with the 78 hours ^{67}Ga and the 40 hours ^{69}Ge. The growth of ^{67}Ga was evident from the presence of its characteristic gamma rays of 92 and 182 keV.

The gamma spectrum was also measured in the high energy region with a $5''\times4''$ NaI(Tl) crystal, and with the source outside and inside a well type crystal (6.2 cm diameter, height 6.2 cm, well: 0.9 cm diameter, 3.1 cm depth, coupled with a 6363 DuMont phototube); this last experiment produced some qualitative information about the possible gamma-gamma coincidences by means of the summing technique.

Fig. 1, 2, 3 and 4 show the normal spectrum in four different energy regions as measured with the 2.5×2.5 cm crystal and the analysis of the spectrum into various peaks.

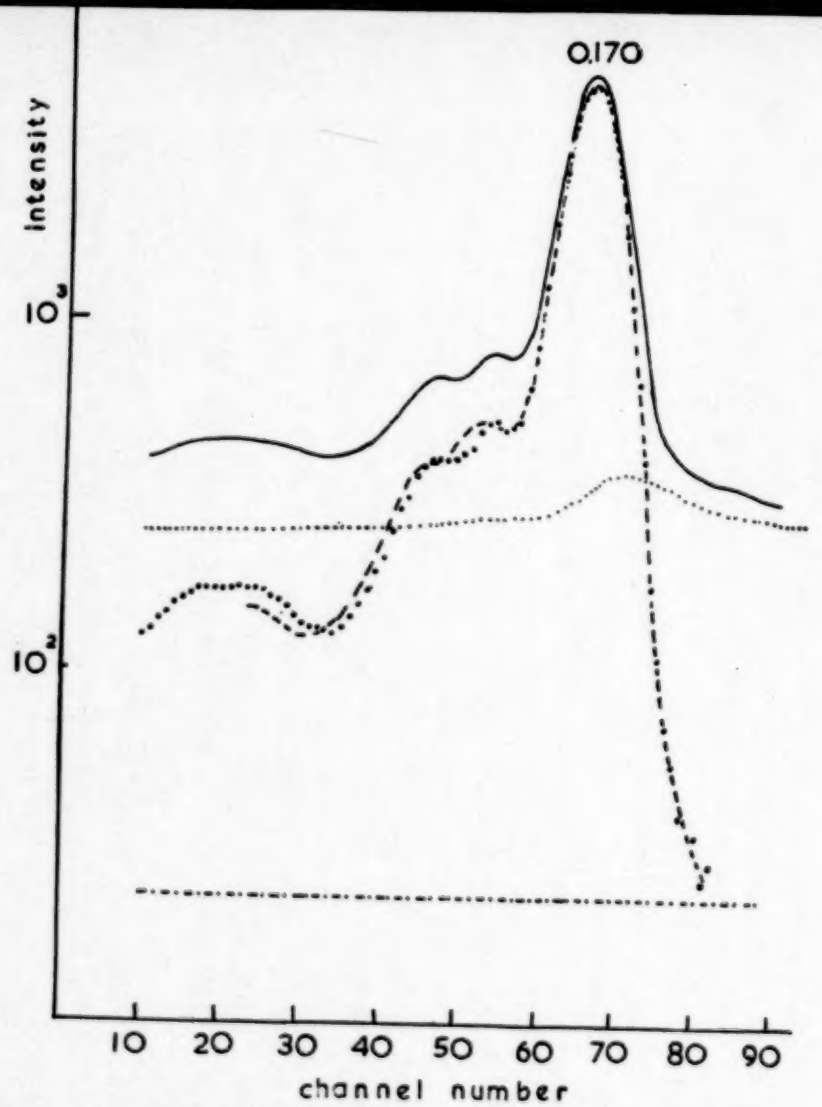

Fig. 1. Gamma scintillation spectrum of ^{67}Ge in the low energy region. The dot-dashed curve represents the contribution due to gamma rays of energy higher than 0.6 MeV; the dotted curve represents the Compton distribution of the annihilation radiation. The dots correspond to the total spectrum minus the above contributions. The 165 keV line of ^{139}Ce is drawn in for comparison (dashed curve).

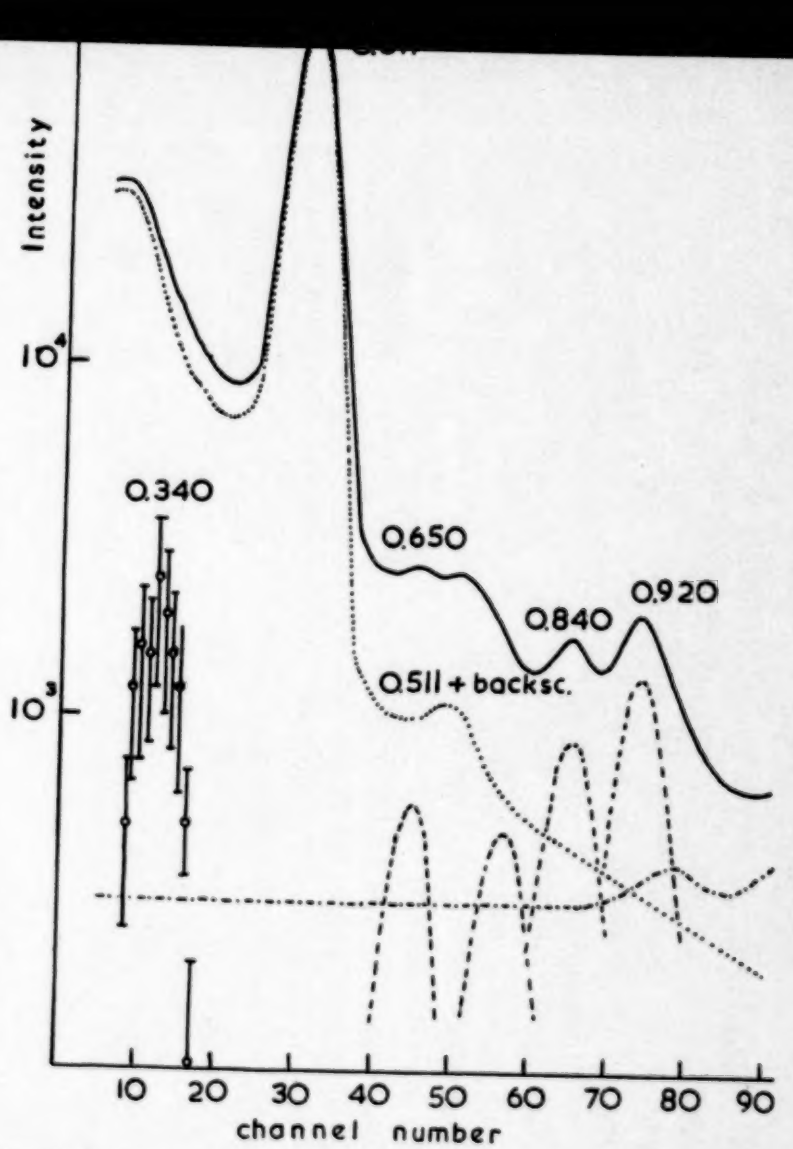

Fig. 2. Gamma spectrum in the region between 0.25 and ≈ 1 MeV. The contribution of the high energy gamma rays (dashed curve) is shown. The tail of the annihilation radiation is reported with the corresponding distribution due to annihilation of positons in flight (dotted curve), and the peak due to pile-up between the 0.511 MeV and the backscattering peak. The spectra of ^{18}F and ^{62}Cu, measured under the same conditions of geometry and backing, have been used to construct this distribution (cf. ref. [6])). The 0.340 MeV peak is shown as a result of the analysis.

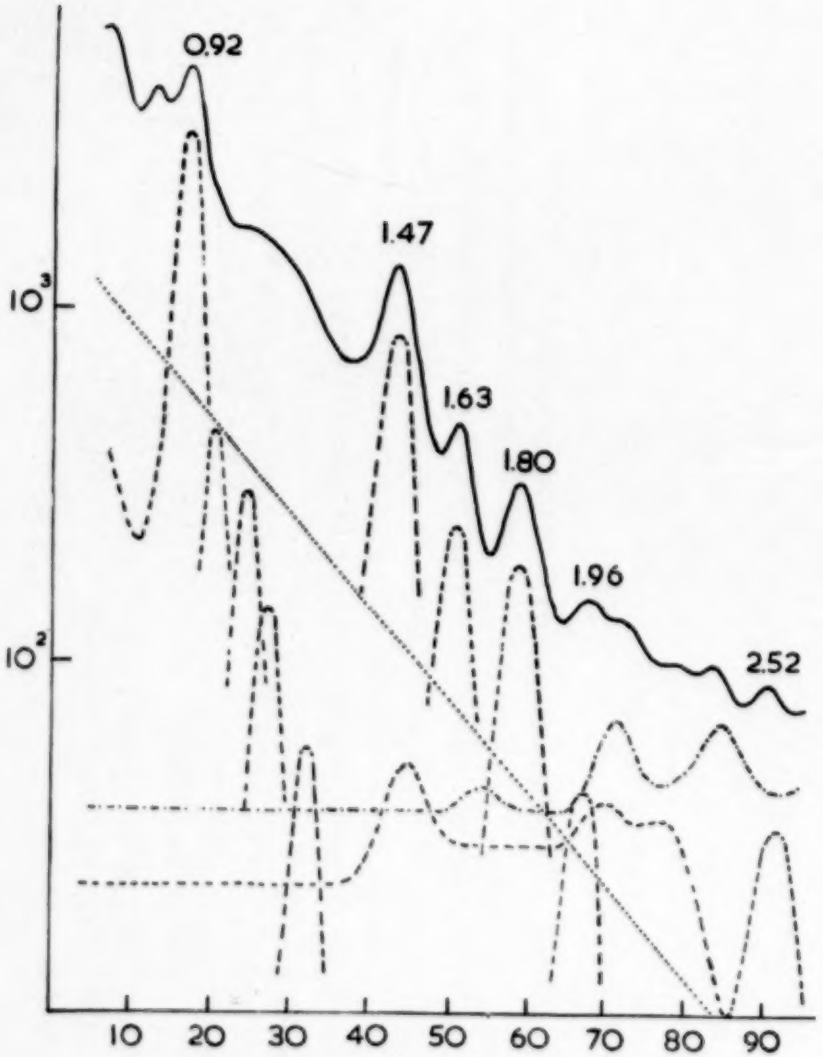

Fig. 3. High energy gamma spectrum of ^{67}Ge.
For explanation see figs. 1 and 2.

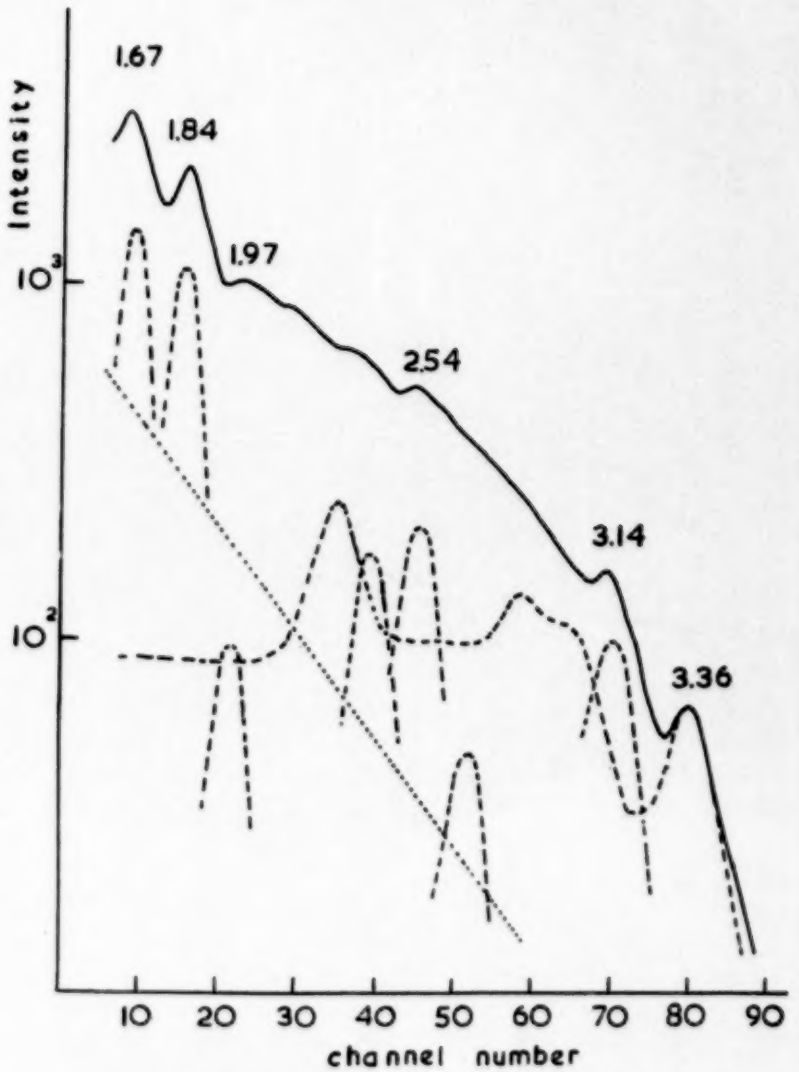

Fig. 4. High energy gamma spectrum of ^{67}Ge.
For explanation see figs. 1 and 2.

Contributions due to continuous pulse distributions, as background, bremsstrahlung and annihilation of positons in flight, have been taken into account; a detailed analysis was performed in the usual way as described in other publications [6,7]). The results of this analysis are reported in table 1.

TABLE 1

Gamma radiations from the decay of ^{67}Ge

^{67}Ge produced by Zn (19-MeV α, n) chem $T_{\frac{1}{2}} = 18.7 \pm 0.5$ min	
Energy (MeV)	Relative intensity
0.170 *5*	126 *8*
0.340 *15*	<3
$\gamma\pm$	2×100
0.650 *15*	1.9 *4*
0.750 *15*	2.2 *4*
0.840 *15*	4.9 *5*
0.920 *15*	8.7 *3*
1.00 *2*	1.0 *4*
1.10 *2*	1.0 *4*
1.16† *3*	0.6 *2*
1.27† *4*	0.3 *2*
1.48 *2*	5.8 *6*
1.65 *3*	2.2 *2*
1.83 *4*	1.9 *2*
1.98 *5*	0.5 *2*
2.53 *4*	0.8 *2*
2.70 *4*	0.2 *1*
3.13 *6*	0.5 *1*
3.39 *6*	0.4 *1*

† Both partially due to pile-up (see table 2).

In addition to the measurements performed with the well-type crystal others were done by varying the source-detector distance and also by placing Pb absorbers between the source and the detector in order to obtain more quantitative conclusions about the various summing peaks.

As an example fig. 5 shows the pulse height distributions obtained in the intermediate energy region for a variety of source-detector distances with or without a 5 mm Pb absorber; all curves are normalized to the annihilation peak. One may conclude, that the 0.69 MeV peak is mainly a summing peak which is due to coincidences between the 0.170 MeV gamma ray and the annihilation radiation. This is also shown in fig. 6, where the results of the measurements performed with the well-type crystal are presented for two different energy regions. The residual spectrum of ^{69}Ge was used to normalize the spectra obtained outside and inside the well of the crystal.

The disappearance of the 1.48 MeV peak in the summing method as shown in fig. 6 proves that the 1.48 MeV peak is certainly coincident with the 0.17 MeV gamma ray or with the annihilation radiation, because it disappears almost

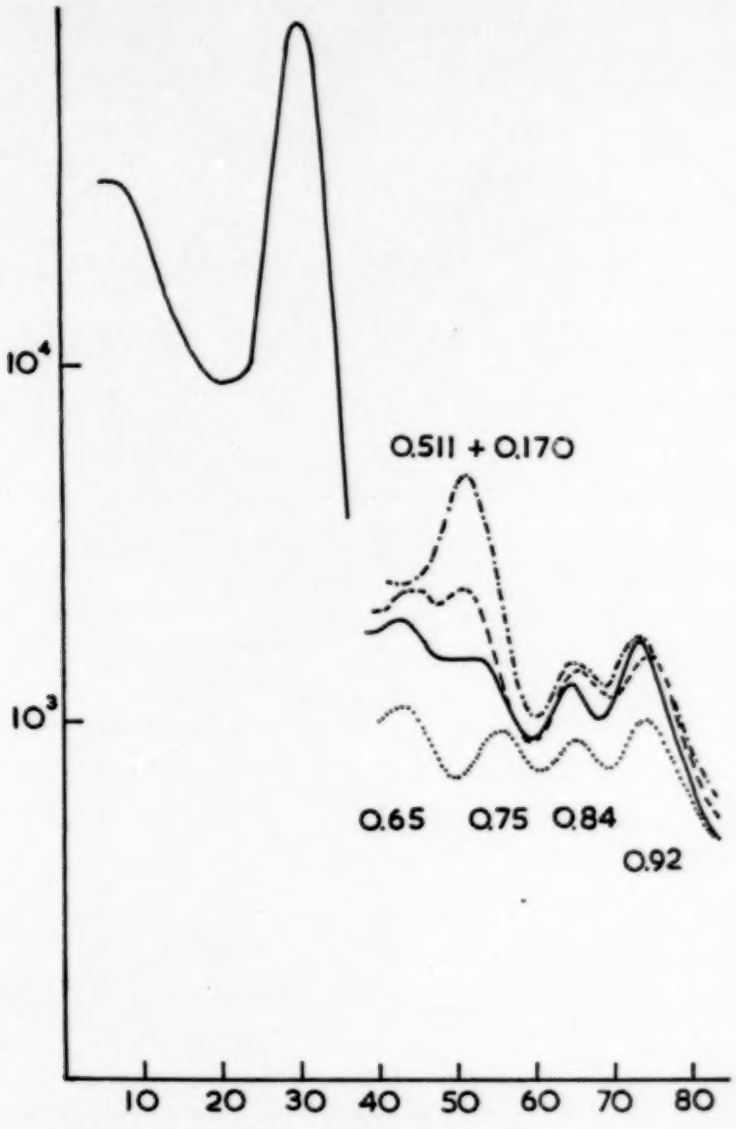

Fig. 5. Pile-up in the gamma spectrum. The different spectra have been obtained for three different source-detector distances: 6 cm (full drawn curve), 2 cm (dashed curve), 0.5 cm (dot-dashed curve) and by placing 5 mm Pb between the source and the detector (dotted curve). The different pulse height distributions have been normalized to the annihilation peak. All other contributions, namely annihilation of positons in flight and the summing peak due to the 0.511+backscattering pile-up have been subtracted here.

completely when the source is placed inside the well; such a strong coincidence cannot be explained any other way. Summing peaks also appear at 2.18 MeV and 2.36 MeV.

The conclusions drawn from the measurements are reported in table 2.

The beta ray spectrum was measured with a stilbene crystal (diameter 4 cm, height 1 cm) covered by a 200 $\mu g/cm^2$ aluminium reflector and coupled with a 6292 DuMont photomultiplier. A 3 mg/cm^2 aluminium foil was used as window.

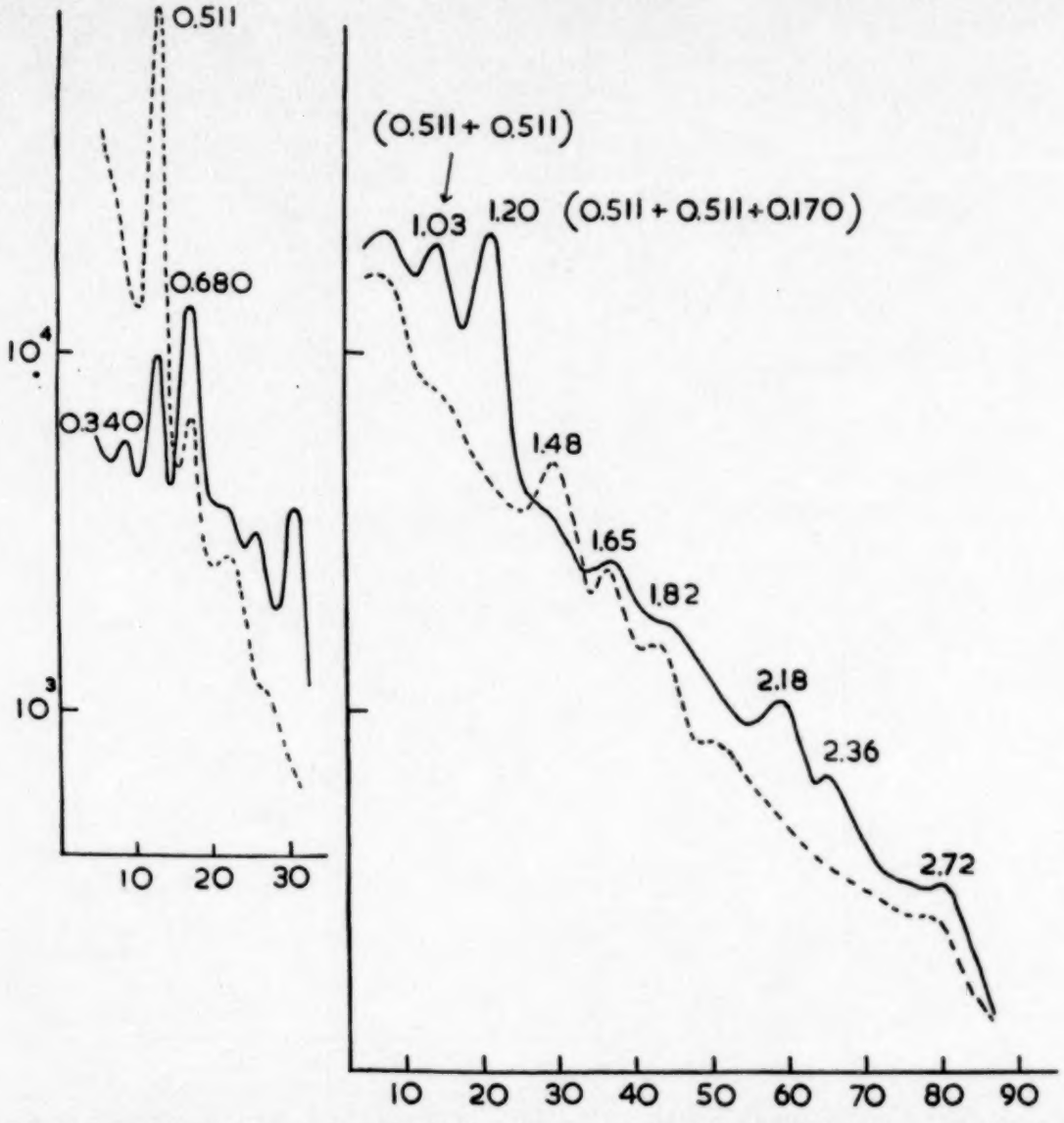

Fig. 6. Summing peaks as measured with the well-type crystal, for two different energy regions. Full curve: source inside the well, dashed curve: source at 6 cm from the crystal.

The beta scintillation spectrometer was calibrated with known conversion lines (^{137}Cs, ^{207}Bi), with the Compton edges of some gamma rays (^{88}Y, ThC) and with the endpoints of some well known negaton and positon spectra (^{32}P, $^{90}Sr+^{90}Y$, ^{63}Zn, ^{76}As, $^{62}Zn+^{62}Cu$ and ^{66}Ga).

The half-life of the beta spectrum followed over a period of 100 minutes was 18.8 ± 0.8 min for all points in the region from ≈ 0.8 to 4 MeV.

TABLE 2

Summing peaks in the gamma ray spectrum of ^{67}Ge

Technique used		Origin of the summing peak
Well crystal	Variation of geometry and absorption	
0.340 *10*		0.170+0.170
0.680† *10*	0.690† *10*	0.170+0.511
	1.16 *3*	0.170+0.920
1.20 *5*		0.170+0.511+0.511
		0.170+1.10
	1.27 *4*	0.170+0.170+0.920
		0.750+0.511
2.18 *5*	2.18 *4*	1.65 +0.511
		1.48 +0.170+0.511
2.36 *7*	2.36 *6*	1.83 +0.511
		1.65 +0.170+0.511
		2.70 +0.170
	2.90 *6*	2.53 +0.170+0.170
		1.98 +0.840

† This peak is entirely due to summing; it was erroneously listed as a real gamma ray in a previous communication to J. M. Hollander and reported as such in: D. Strominger, J. M. Hollander and G. T. Seaborg, Revs. Mod. Phys. **30** (1958) 585.

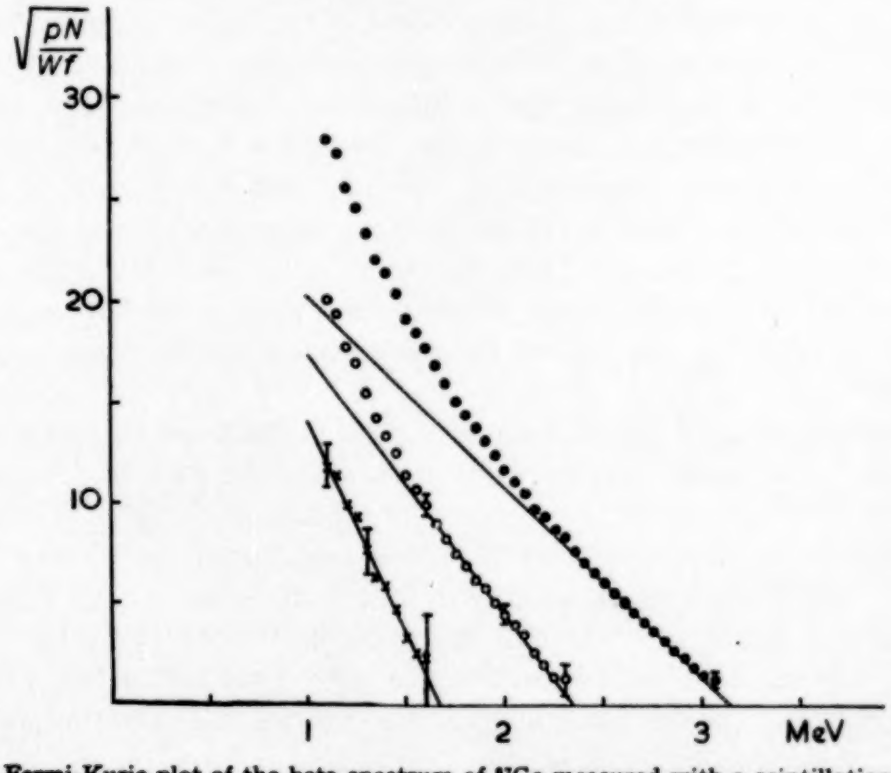

Fig. 7. Fermi-Kurie plot of the beta spectrum of ^{67}Ge measured with a scintillation spectrometer. A correction for resolution has been applied.

The Fermi-Kurie plot of the spectrum, corrected for resolution, is shown in fig. 7. It shows three components; energies and relative intensities are reported in table 3. The intensity of the lowest energy branch is probably over-

TABLE 3

Analysis of the positon spectrum of ^{67}Ge

Energy (MeV)		Relative intensity	ε/β^+ (calc)
β_1	3.14 ± 0.10	100	0.02
β_2	2.30 ± 0.20	40 ± 10	0.05
β_3	1.6 ± 0.3	< 25	0.15

estimated on account of the scattering of higher energy electrons from the crystal, whereby they only loose part of their energy in the scintillator; this effect is of importance at less than half the endpoint energy of a beta branch.

4. Discussion

A tentative decay scheme of ^{67}Ge is proposed in fig. 8. It has been built up mainly on the basis of energy and intensity matching of the various beta and gamma radiations reported above. It was found that a consistent decay scheme could be constructed including the levels in ^{67}Ga observed by Chapman and Slattery [4]). Therefore, both the results reported in this study and those of ref. [4]) will be considered in the discussion given below.

On the decay scheme all intensities are expressed in percentages per disintegration. Normalization has been achieved by using the results of table 3 and by assuming that capture to levels above 1.9 MeV is negligible, as indicated by the low intensities of gamma rays with energies > 1.9 MeV.

The presence of the intense 170 keV gamma ray proves the existence of a level of this energy. This level was not reported by Chapman *et al.* [4]) The corresponding neutron threshold for excitation of the 170 keV level was probably masked by the tail of the very strong ground state neutron threshold.

It must be assumed that the 170 keV peak is composed of two gamma transitions †, since the total intensity of the observed peak in the gamma ray spectrum is too high to be explained by the sum of the intensities of all other gamma rays plus that of the 3.14 MeV beta branch.

The 171—169 keV cascade originates at a level of 340 ± 10 keV, which could then be identical to the one at 357 ± 7 keV reported by Chapman *et al.* [4]). (There is also a slight indication of a gamma ray of this energy in the direct spectrum.) The corresponding peak in the summing spectrum may be

† To avoid confusion this 170 keV gamma ray pair will be designated as 169 and 171 keV gamma rays, the first one arbitrarily being assigned to the first excitedstate.

due to pile-up of the 169 and 171 keV gamma rays. (This summing peak is not very pronounced, since a triple sum involving the annihilation radiation, will considerably reduce its intensity.) Only a rough intensity estimate can be given for the 340 keV peak, due to its location on the Compton edge of the strong annihilation peak.

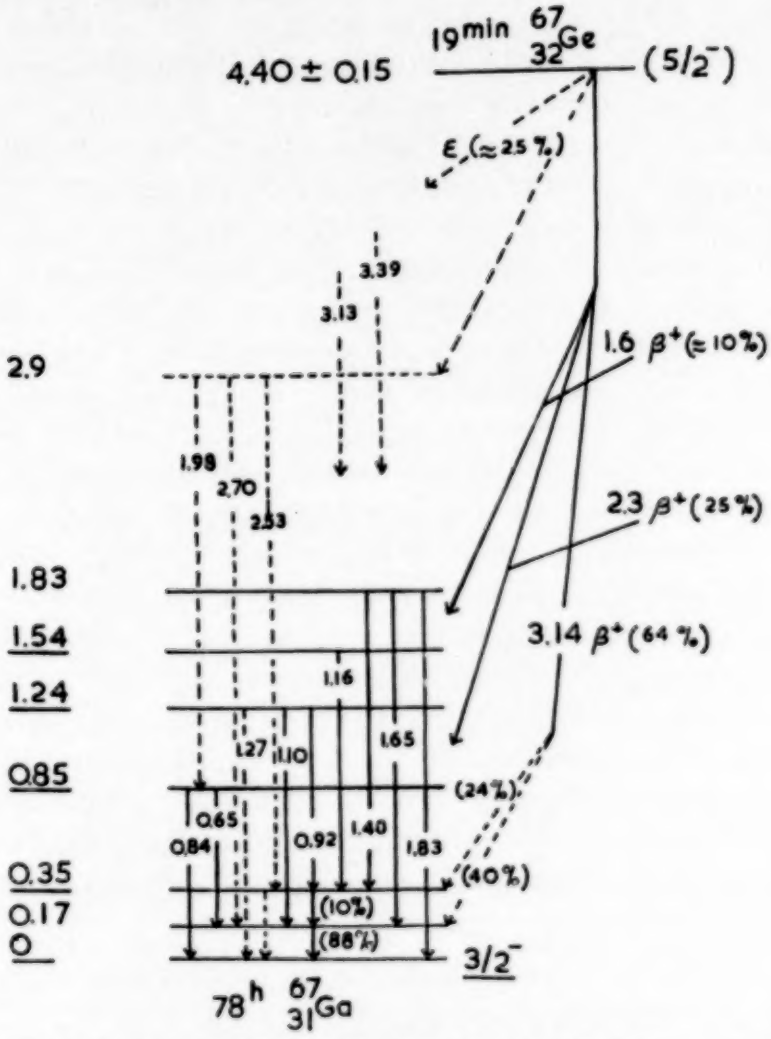

Fig. 8. Proposed decay scheme of ^{67}Ge. The levels in ^{67}Ga, found by Chapman and Slattery [4]), are underlined.

From the intensities of the various gamma rays populating the levels at 169 and 340 keV, it is obvious that the 3.14 MeV beta group must consist of two transitions. Their intensities, as well as those of the two subsequent gamma transitions, can be calculated from intensity matching; these are indicated on the decay scheme. The total disintegration energy should then be 4.40±0.15 MeV, which is in very good agreement with the value deduced from beta energy systematics [8]). Levels between 0.78 and 1.38 MeV can be populated by the second positon group of 2.30±0.20 MeV. The 0.850 MeV

level found by Chapman *et al.* [4]) lies in this region and may be deexcited by the 0.840 MeV gamma ray. The 0.650 MeV gamma ray will be assumed to be the corresponding stop-over transition to the 0.169 MeV level. Nothing can be said about a possible 0.51 MeV transition to the second excited state on account of the presence of the annihilation radiation.

The 0.850 MeV level does not exhaust the intensity of the 2.3 MeV positon group (25 ± 6 %), which should then populate other levels. The balance can only be achieved by assuming that all gamma rays with energies lower than 1.4 MeV originate from these levels. The 1.23 MeV level found by Chapman *et al.* [4]) fits here. Therefore the existence of such a level de-exciting by the 1.10, 0.92 and possibly also by the direct 1.27 MeV gamma transitions, is also indicated in fig. 8. The intensity balance with the 2.3 MeV positon group is not completely satisfactory, but this is not regarded as a major discrepancy in view of the complexity of the positon spectrum. Of course, the balance may be adjusted by postulating an 0.51 MeV transition from the 0.850 MeV level. From all these considerations it can be inferred that the 2.3 MeV positon group is complex, consisting of at least two branches.

The situation with respect to the higher levels can be well explained by postulating the existence of a level at 1.83 ± 0.04 MeV as the origin of the four gamma transitions of 1.83, 1.65, 1.48 and 1.00 MeV. The 1.54 MeV level [4]), which can also be populated by part of the 1.6 ± 0.3 MeV positon group, has also been indicated. The only gamma transition found in this work which fits here, is the 1.16 MeV gamma ray, and perhaps the 0.75 MeV gamma ray. From this it follows that the 1.6 MeV positon group should have a relative intensity of about 10 %, which is compatible with the results of the analysis of the positon spectrum. In table 4 the various beta branches are summarized with their intensities calculated on the basis of the proposed decay scheme, in addition the log *ft*-values are given.

TABLE 4

Beta branches in the decay of ^{67}Ge according to the decay scheme as proposed in fig. 8

Energy (MeV)	Intensity		log *ft*
	β^+	ε	
1.60	≈ 8 %	1.5 %	5.4
2.30	24 %	1.2 %	5.5
3.05	23 %	0.5 %	6.2
3.21	38 %	0.8 %	6.0
(3.38)	(2±6) %	–	>7.0

A level at 2.9 MeV may be present, since it would explain the existence of the 2.70, 2.53 and 1.98 MeV gamma rays populating the 0.169, 0.357 and 0.850 MeV levels; a 2.9 MeV direct transition to the groundstate is less

certain, because the 2.94 ± 0.05 MeV peak seems to be due to pile-up only.

The total intensity of these gamma rays together with the remaining 3.13 and 3.39 MeV gamma rays is about 2.5 %; this probably represents the total amount of electron capture to the higher levels of ^{67}Ga.

The total intensity of the gamma transitions leading directly to the ground state is $(98 \pm 6)\%$ according to the proposed decay scheme (1 % conversion electrons due to the 170 keV transition have been added). Therefore, not more than $(2 \pm 6)\%$ of all decays lead to the ground state. The spin of ^{67}Ga has been measured as $\frac{3}{2}^-$, that of ^{67}Ge is very probably $\frac{3}{2}^-$ or $\frac{5}{2}^-$. The transition probability of the ground state beta transition is rather small for an allowed one ($\log ft > 7.0$).

The ground state capture transition from ^{67}Ga to ^{67}Zn (ground state spin $\frac{5}{2}$) is also slowed down by an appreciable factor ($\log ft > 6.3$). Other cases involving 29, 31, 33, 35 and 37 odd nucleons are collected in table 5. The

TABLE 5

Log ft values for groundstate beta transitions within the $2p_{\frac{1}{2}}$ and $1f_{\frac{1}{2}}$ shells

Initial (final) Z		29(Cu) ($p_{\frac{1}{2}}$)		31(Ga) ($\frac{3}{2}^-$)	
Final (initial) Z		28(Ni)	30(Zn)	30(Zn)	32(Ge)
Final (initial) N					
$\Delta l = 0$	31 ($\frac{3}{2}^-$)	≈ 5	5.4		
	33 ($\frac{3}{2}^-$)	5.2	5.4		
$\Delta l = 2$	35 ($\frac{1}{2}^-$)	6.4	8.4	5.8†	>7.0
	37 ($f_{\frac{1}{2}}$)	6.6	6.3	>6.3	6.9

† See discussion in text.

slowing down of the ground state beta transitions from ^{65}Zn and ^{67}Ga is often explained by l-forbiddenness; the orbital l is assumed to be a good quantum number near a closed shell (28 particles) or subshell (38 particles). The dependence of the ft-values on the number of odd nucleons, as shown in table 5, seems to support this assumption. This table gives the log ft-values for the various ground state beta transitions between pairs of odd mass nucleides within the $2p_{\frac{1}{2}}$, $1f_{\frac{1}{2}}$ subshell. Only 29 and 31 odd protons are considered; nucleides with $Z \geqq 33$ do not decay to other members of the neutron subshell. For 31 and 33 neutrons there should be no l-forbiddenness, for $N = 35$, l-forbiddenness might be expected, for 37 neutrons one would expect a slowing-down effect. Only ^{65}Ga, decaying to ^{65}Zn, does not seem to follow the general trend evident from table 5. In view of the uncertainty

about the level scheme of ^{65}Zn in the region below $\approx$ 200 keV excitation energy, there exists still some doubt about the presence of a direct ground state beta transition between ^{65}Ga and ^{65}Zn.

We would like to thank Prof. Dr. P. C. Gugelot, Prof. Dr. A. H. W. Aten Jr. and Prof. Dr. A. H. Wapstra for their interest in this work. We are also indebted to R. K. Girgis for his help with the measurements and for many useful discussions, to Mrs. M. Lindner-Groen for performing the chemical separations and to the personnel of the synchrocyclotron for the irradiations.

This work was performed as part of the research program of the "Stichting voor Fundamenteel Onderzoek der Materie" (F.O.M.), which is financially supported by the "Nederlandse Organisatie voor Zuiver Wetenschappelijk Onderzoek" (Z.W.O.).

References

1) H. H. Hopkins Jr. and B. B. Cunningham, Phys. Rev. **73** (1948) 1406;
H. H. Hopkins Jr., Phys. Rev. **77** (1950) 717
2) A. H. W. Aten Jr., T. de Vries-Hamerling and L. Lindner, Physica **19** (1953) 1046
3) A. H. W. Aten, Jr. Physica **22** (1956) 288
4) R. A. Chapman and J. C. Slattery, Phys. Rev. **105** (1957) 633
5) R. A. Ricci and R. van Lieshout, Nuovo Cimento **4** (1956) 1592
6) R. A. Ricci, R. K. Girgis and R. van Lieshout, Nuovo Cimento, to be published
7) R. K. Girgis, R. A. Ricci and R. van Lieshout, to be published
8) K. Way and M. Wood, Phys. Rev. **94** (1954) 119;
K. Way in H. Hintenberger, Nuclear Masses and their Determination (Pergamon Press, London, 1957) p. 39

1.D.2:
6.D

Nuclear Physics **10** (1959) 373—385; © *North-Holland Publishing Co., Amsterdam*
Not to be reproduced by photoprint or microfilm without written permission from the publisher

THE γ-DEPENDENT PART OF THE WAVE FUNCTIONS REPRESENTING γ-UNSTABLE SURFACE VIBRATIONS

DANIEL R. BÈS †

Institute for Theoretical Physics, University of Copenhagen

Received 6 November 1958

Abstract: The equation for the γ-dependent part of the wave functions representing γ-unstable vibrations is solved. The general solution is a linear combination of wave functions belonging to a "basic set". The coefficients in this linear combination are expressed as polynomials in cos 3γ. Some consequences of these solutions are discussed. In the appendix, the equations for the coefficients are given in the cases $I \leqq 6$, and the explicit solutions are constructed for $\lambda \leqq 9$.

1. Introduction

A quadrupole deformation of a surface $R(\theta, \varphi)$ may be described either by the "fixed" coordinates α_μ, such that

$$R = R_0(1+\sum_{\mu=-2}^{\mu=+2} \alpha_\mu Y_{2\mu}(\theta, \varphi)) \tag{1}$$

or by two coordinates related to an intrinsic system and the three Eulerian angles θ_i, which fix the position of this intrinsic system with respect to a fixed frame of reference. The coordinates a_ν in the body-fixed system are related to the space-fixed system by the transformation

$$\alpha_\mu = \sum_\nu \alpha_\nu D^I_{\mu\nu}(\theta_i), \tag{2}$$

where $D^I_{\mu\nu}(\theta_i)$ are the transformation functions for the spherical harmonics of order I. The a_ν's satisfy the relations $a_2 = a_{-2}\ a_1 = a_{-1} = 0$. One may replace a_0 and a_2 by β and γ, defined by

$$a_0 = \beta \cos\gamma, \qquad a_2 = \frac{1}{\sqrt{2}} \beta \sin\gamma. \tag{3}$$

The equation of motion for the intrinsic coordinates has been treated by several authors. The expression for the kinetic energy was given by A. Bohr [1]):

$$T = -\frac{\hbar^2}{2B}\left\{\frac{1}{\beta^4}\frac{\partial}{\partial\beta}\beta^4\frac{\partial}{\partial\beta} + \frac{1}{\beta^2 \sin 3\gamma}\frac{\partial}{\partial\gamma}\sin 3\gamma\frac{\partial}{\partial\gamma} - \frac{1}{4\beta^2}\sum_x \frac{Q_x^2}{\sin^2(\gamma - \frac{2}{3}\pi x)}\right\} \tag{4}$$

where Q_x are angular momentum operators in the variables θ_i.

† Permanent address: Comisión Nacional de Energía Atómica, Buenos Aires, Argentina.

In the same paper, Bohr has also given the explicit solution for the free $I = 0$ waves in terms of Legendre polynomials. The case when a strong γ-dependent potential stabilizes the motion around $\gamma = 0$ or $\gamma = \pi$ is also treated there and in the following series of papers written in collaboration with B. Mottelson [2,3,4]). Wilets and Jean [5]) have discussed the case of deformation potentials independent of γ. Rakavy [6]) has given a classification of surface oscillations by group-theory which is especially suitable for γ-unstable oscillations.

In this paper, a method is outlined for the construction of the γ-dependent part of the wave functions in the case of γ-unstable vibrations.

2. Construction of the Wave Functions

Once the β-part of the wave equation is separated, it is necessary to consider only eq. (5) [5])

$$L\phi(\gamma,\theta_i) = \left[\Lambda + \frac{1}{\sin 3\gamma}\frac{\partial}{\partial\gamma}\sin 3\gamma\frac{\partial}{\partial\gamma} - \tfrac{1}{4}\sum_x \frac{Q_x^2}{\sin^2(\gamma-\frac{2}{3}\pi x)}\right]\phi(\gamma,\theta_i) = 0, \qquad (5)$$
$$\Lambda = \lambda(\lambda+3);$$

λ is an integer, called by Rakavy the "seniority". The solutions may be denoted by $\phi_{\lambda,I,M}(\gamma,\theta_i)$ when no degeneracies are present. Any eigenstate of the equation in the intrinsic coordinates is a linear combination of eigenstates of the equation in the fixed coordinates, which are of the form $e^{-\frac{1}{2}\beta^2}\Pi_{\mu=-2}^{\mu=+2}H_{n_\mu}(\alpha_\mu)$. By repeated application of the Clebsch-Gordan series, one can express this in the form $\sum_K D^I_{MK}(\theta_i)g_K(\beta,\gamma)$. It is then easily seen that only even values of K appear and, moreover,

$$g_K = (-)^I g_{-K}. \qquad (6)$$

In order to solve eq. (5) it is convenient to transform it into a system of coupled differential equations in $x = \cos 3\gamma$. This may be performed as follows:

The first solution for a given even spin is

$$\phi_{\frac{1}{2}I,I,M}(\gamma,\theta_i) = \left(\frac{\alpha_2}{\beta}\right)^{\frac{1}{2}I} = \left[\cos\gamma D^2_{M0}(\theta_i) + \sin\gamma\left(\frac{D^2_{M2}(\theta_i)+D^2_{M-2}(\theta_i)}{\sqrt{2}}\right)\right]^{\frac{1}{2}I} \qquad (7)$$

corresponding to the unique $\lambda = \frac{1}{2}I$ phonon state with $M = I$.

α_μ has two terms, one which creates a phonon and another one which annihilates a phonon. By acting with α_μ on $\phi_{\lambda,I,M}(\gamma,\theta_i)$, and making use of the properties of the Wigner coefficients, another function of the same spin can be obtained. In general, in order to obtain $\phi_{\lambda+1,I,M}(\gamma,\theta_i)$ it is necessary to orthogonalize the new wave function with respect to $\phi_{\lambda-1,I,M}(\gamma,\theta_i)$. In the case of $\lambda = \frac{1}{2}I$, there is no $\phi_{\lambda-1,I,M}(\gamma,\theta_i)$ and, thus, the new wave function is already proportional to $\phi_{\frac{1}{2}I+1,I,M}(\gamma,\theta_i)$. One repeats the procedure

until the lowest $\frac{1}{2}I+1$ functions are obtained. In the case of odd spins, the lowest wave function may be obtained by operating with α_μ on a neighbour even-spin state already known. Only $\frac{1}{2}(I-1)$ functions are needed.

These $\frac{1}{2}I+1$[or $\frac{1}{2}(I-1)$] wave functions constitute a basic set which can be used in order to construct the general solution. The wave functions

$$\phi(\gamma, \theta_i) = w(\gamma)\phi_{\frac{1}{2}I, I, M}(\gamma, \theta_i)+v(\gamma)\phi_{\frac{1}{2}(I+1)I, M}(\gamma, \theta_i)+ \ldots +u(\gamma)\phi_{I, I, M}(\gamma, \theta_i)$$

for even spin, and (8)

$$\phi(\gamma, \theta_i) = w(\gamma)\phi_{\frac{1}{2}(I+3)I, M}(\gamma, \theta_i)+v(\gamma)\phi_{\frac{1}{2}(I+5)I, M}(\gamma, \theta_i)+ \ldots +u(\gamma)\phi_{I, I, M}(\gamma, \theta_i)$$

for odd spin, are substituted in eq. (5); $w, v, \ldots u$ are functions of γ alone. In the following calculations, the different wave functions belonging to a basic set are taken to be independent, but not necessarily orthogonal to each other. The products $\phi^*_{\lambda IM}(\gamma, \theta_i)\ L\phi(\gamma, \theta_i)$ for $\lambda \leqq I$ are integrated over the Eulerian angles, and one observes that the coefficients in the resultant equations are functions only of cos 3γ and sin 3γ. One obtains a set of $\frac{1}{2}I+1$ [or $\frac{1}{2}(I-1)$] coupled differential equations, where the only variable is $x = \cos 3\gamma$. These equations can be solved by expanding $w, v, \ldots u$ as power series in x. One can work out recursion equations between the coefficients of successive terms of the series. The condition for the convergence of $\phi(\gamma, \theta_i)$ at $x = \pm 1$ makes the series terminate.

In the appendix, the equations for the coefficients are given for $I \leqq 6$, and the explicit solutions for the lowest number of phonons are constructed.

3. Special Features of the Solutions

1) There is a great similarity between the solutions for a given even I and the corresponding ones for $I+3$. This is due to the fact that both have the same number of possible K values and consequently the same number of coupled differential equations.

2) The structure of the solutions shows that each of the wave functions $\phi_{\lambda, I, M}(\gamma, \theta_i)$ with $\lambda \leqq I$ gives rise to a series of solutions with seniority $\lambda_\nu = \lambda+3\nu(\nu = 0, 1, 2, \ldots)$. These solutions may be obtained by orthogonalizing the product $\cos 3\gamma \cdot \phi_{\lambda, I, M}(\gamma, \theta_i)$ with respect to the wave functions with eigenvalue $\Lambda < \Lambda_\nu = \lambda_\nu(\lambda_\nu+3)$.

This observation is easily understandable because cos 3γ is the simplest non-trivial scalar that can be made with creation and annihilation operators, and it contains a term with three creation operators.

The previous observation allows us to predict the degeneracies to be found. Only the even-spin cases are discussed. Everything said for them can be applied to the odd spin with the same number of coupled equations.

If $I = 0$, the "basic set" of wave functions with $\lambda \leqq I$ consists of one element only, because there is only one uncoupled equation to be satisfied.

In consequence, only one series of solutions is present. The possible values of the seniority are $\lambda_\nu = 3\nu$. Indeed, the coefficient of the last term in the recurrence relations has zeros only for values of the eigenvalue $\Lambda = 9\nu(\nu+1)$. There are no degeneracies.

If $I = 2$, the "basic set" contains two terms, corresponding to the fact that two coupled differential equations are present. $\phi_{1,2,M}(\gamma, \theta_i)$ and $\phi_{2,2,M}(\gamma, \theta_i)$ give rise to two series of solutions with seniorities $\lambda_\nu = 1+3\nu$ and $\lambda_\nu = 2+3\nu$. There are no degeneracies, and no solutions with $\lambda_\nu = 3\nu$.

Three coupled differential equations and, correspondingly, three unknowns are possible if $I = 4$. For every value of $\lambda > 1$ there is a non-degenerate wave function.

In the $I = 6$ case, 2 degenerate wave functions must be present for $\lambda = 6$. One of the wave functions is obtained by applying the scalar $\cos 3\gamma$ to $\phi_{3,6,M}(\gamma, \theta_i)$ and orthogonalizing with respect to $\phi_{4,6,M}(\gamma, \theta_i)$. This solution does not give an independent unknown in the system of coupled equations. As four unknowns are admitted, another independent solution is needed and, thus, the degeneracy appears. All the states with $\lambda_\nu = 6+3\nu$ are doubly degenerate.

In the same way, one expects double degeneracy for $\phi_{7,8,M}(\gamma, \theta_i)$ and $\phi_{8,8,M}(\gamma, \theta_i)$ and, in consequence, for $\lambda_\nu = 7+3\nu$ and $\lambda_\nu = 8+3\nu$, if $I = 8$. All the $I = 10$ states are doubly degenerate, with the exception of the three first ones. The first triple degeneracy appears in $\phi_{12,12,M}(\gamma, \theta_i)$, etc.

3) A "γ-parity", π_γ, is present, corresponding to the two sets of solutions given for each case. The γ-parity may be defined as the parity of the order of the polynomial in $\cos\gamma$ and $\sin\gamma$ in which each wave function may be expressed. It is equal to the parity of λ.

The electric quadrupole operator is proportional to $\phi_{1,2,M}(\gamma, \theta_i)$ and therefore has odd parity. Any interaction which conserves the γ-parity does preserve the selection rule of the forbiddenness of the transition from the second $I = 2$ state to the ground state in any order of approximation. This fact is suggested in ref. [5]) on the basis of a first-order perturbation calculation.

The simplest interaction of this kind (aside from a constant) is $\cos^2 3\gamma$. In second-order perturbation theory, such an interaction lowers the second $2+$ level below the first $4+$ level. Therefore it is suggested that this interaction may have some relation with the experimental spectra of even nuclei in the undeformed region. Calculations in this respect are in progress.

The author wishes to express his gratitude to Professors Niels Bohr and Aage Bohr for their kindness in allowing him to work at the Institute for Theoretical Physics, Copenhagen, and for a grant. Discussions with Drs. B. Bayman, B. Mottelson, and R. Sheline have been very helpful during the

course of this work. A scholarship from Comisión Nacional de Energía Atómica, Buenos Aires, Argentina, is gratefully acknowledged.

Appendix

1. EQUATIONS FOR THE COEFFICIENTS OF SUCCESSIVE TERMS IN THE POWER SERIES EXPANSION OF $w, v, \ldots$

$$\boxed{I=0}$$

$$\phi(\gamma,\theta_i)=w;$$

w satisfies the same differential equation as the Legendre polynomials

$$9(1-x^2)\frac{d^2w}{dx^2}-18x\frac{dw}{dx}+\Lambda w=0.$$

1) $w=\sum_n a_n x^{2n}, \quad \pi=+.$

The recurrence relation for the a_n's is the following:

$$a_{n+1}18(n+1)(2n+1)+a_n(\Lambda-36n^2-18n)=0.$$

The series terminates if $\Lambda=36\nu^2+18\nu$ $(\nu=0,1,2\ldots)$.

2) $w=\sum_n a_n x^{2n+1}, \ \pi=-.$

$$a_{n+1}18(n+1)(2n+1)+a_n(\Lambda-36n^2-54n-18)=0.$$

$$\boxed{I=1}$$

No solution exists since the only possible value of K is zero, and $g_0(\gamma)=-g_0(\gamma)=0$.

$$\boxed{I=2}$$

$$\phi(\gamma,\theta_i)=(w\cos\gamma+v\cos 2\gamma)D^2_{M0}(\theta_i)+(w\sin\gamma-v\sin 2\gamma)\frac{1}{\sqrt{2}}\left(D^2_{M2}(\theta_i)+D^2_{M-2}(\theta_i)\right),$$

where w and v must satisfy the coupled differential equations

$$(\Lambda-4)w-24x\frac{dw}{dx}+9(1-x^2)\frac{d^2w}{dx^2}+12\frac{dv}{dx}=0,$$

$$6\frac{dw}{dx}+(\Lambda-10)v-30x\frac{dv}{dx}+9(1-x^2)\frac{d^2v}{dx^2}=0.$$

1) $w=\sum_n a_n x^{2n}, \ v=\sum_n b_n x^{2n+1}, \ \pi=-.$

The coefficients are determined by the recurrence relations

$$\begin{aligned}&a_{n+2}81(2n+1)(2n+2)(2n+3)(2n+4)\\&+a_{n+1}18(2n+1)(2n+2)(\Lambda-36n^2-90n-59)\\&+a_n(\Lambda-36n^2-30n-4)(\Lambda-36n^2-78n-40)=0,\end{aligned}$$

$$b_n=-a_n\frac{(\Lambda-36n^2-30n-4)}{12(2n+1)}-a_{n+1}\tfrac{3}{2}(n+1).$$

The condition that the series terminates is equivalent to $\Lambda=36\nu^2+30\nu+4$ or $\Lambda=36\nu^2+78\nu+40$.

2) $w=\sum_n a_n x^{2n+1}$, $\nu=\sum_n b_n x^{2n}$, $\pi=+$.

$$\begin{aligned}&b_{n+2}81(2n+1)(2n+2)(2n+3)(2n+4)\\&+b_{n+1}18(2n+1)(2n+2)(\Lambda-36n^2-90n-62)\\&+b_n(\Lambda-36n^2-42n-10)(\Lambda-36n^2-66n-28)=0,\end{aligned}$$

$$a_n=-b_n\frac{(\Lambda-36n^2-42n-10)}{6(2n+1)}-b_{n+1}3(n+1).$$

$I=3$

$$\phi(\gamma,\theta_i)=w\sin 3\gamma\,\frac{1}{\sqrt{2}}\,(D^3_{M2}(\theta_i)-D^3_{M-2}(\theta_i),$$

$$9(1-x^2)\frac{\mathrm{d}^2w}{\mathrm{d}x^2}-36x\frac{\mathrm{d}w}{\mathrm{d}x}+(\Lambda-18)w=0.$$

1) $w=\sum_n a_n x^{2n}$, $\pi=-$.

$$a_{n+1}18(n+1)(2n+1)+a_n(\Lambda-36n^2-54n-18)=0.$$

2) $w=\sum_n a_n x^{2n+1}$, $\pi=+$.

$$a_{n+1}18(n+1)(2n+3)+a_n(\Lambda-36n^2-90n-54)=0.$$

These solutions are the tesseral polynomials $T_\lambda{}^1(x)$ [7].

$I=4$

$$\begin{aligned}\phi(\gamma,\theta_i)=&[w(6\cos^2\gamma+\sin^2\gamma)+v\,(\sin 2\gamma\sin\gamma-6\cos 2\gamma\cos\gamma)\\&+5u\sin\gamma\sin 3\gamma]D^4_{M0}(\theta_i)\\&+[w\sin 2\gamma+v\sin\gamma+2u\cos\gamma\sin 3\gamma](15)^{\frac{1}{2}}\frac{1}{\sqrt{2}}\,(D^4_{M2}(\theta_i)+D^4_{M-2}(\theta_i))\\&+[w\sin^2\gamma+v\sin 2\gamma\sin\gamma-u\sin 3\gamma\sin\gamma](35)^{\frac{1}{2}}\frac{1}{\sqrt{2}}\,(D^4_{M4}(\theta_i)+D^4_{M-4}(\theta_i));\end{aligned}$$

w, v and u satisfy the coupled differential equations

$$-12\frac{dw}{dx}+(\Lambda-18)v-36x\frac{dv}{dx}+9(1-x^2)\frac{d^2v}{dx^2}+12\frac{du}{dx}=0,$$

$$6\frac{dv}{dx}+(\Lambda-28)u-42x\frac{du}{dx}+9(1-x^2)\frac{d^2u}{dx^2}=0,$$

$$(\Lambda-10)w-30x\frac{dw}{dx}+9(1-x^2)\frac{d^2w}{dx^2}-18\frac{dv}{dx}+10u+12x\frac{du}{dx}=0.$$

1) $w=\sum_n a_n x^{2n}$, $v=\sum_n b_n x^{2n+1}$, $u=\sum_n c_n x^{2n}$, $\pi=+$.

$$\begin{aligned}0 &= a_n(\Lambda-36n^2-42n-10)(\Lambda-36n^2-90n-54)(\Lambda-36n^2-66n-28)\\
&+a_{n+1}3(2n+1)(2n+2)\Big[(6\Lambda-216n^2-348n-148)(\Lambda-36n^2-102n-83)\\
&-(24n+10)(\Lambda-36n^2-90n-54)+(3\Lambda-108n^2-510n-622)\\
&\cdot(\Lambda-36n^2-114n-88)\frac{(9\Lambda-180n^2-330n-167)}{(9\Lambda-180n^2-690n-677)}\Big]\\
&+a_{n+2}27(2n+1)(2n+2)(2n+3)(2n+4)\Big[(3\Lambda-108n^2-174n-74)\\
&+(6\Lambda-216n^2-1068n-1408)\frac{(9\Lambda-180n^2-330n-167)}{(9\Lambda-180n^2-690n-677)}\Big]\\
&+a_{n+3}729(2n+1)(2n+2)(2n+3)(2n+4)(2n+5)(2n+6)\frac{(9\Lambda-180n^2-330n-167)}{(9\Lambda-180n^2-690n-677)},\end{aligned}$$

$$\begin{aligned}c_n &= a_n\frac{(\Lambda-36n^2-42n-10)(3\Lambda-108n^2-294n-220)}{16(9\Lambda-180n^2-330n-167)}\\
&+a_{n+1}\frac{9(2n+1)(2n+2)(3\Lambda-108n^2-318n-278)}{8(9\Lambda-180n^2-330n-167)}\\
&+a_{n+2}\frac{243(2n+1)(2n+2)(2n+3)(2n+4)}{16(9\Lambda-180n^2-330n-167)},\end{aligned}$$

$$b_n=a_n\frac{(\Lambda-36n^2-42n-10)}{18(2n+1)}+a_{n+1}(n+1)+c_n\frac{(12n+5)}{9(2n+1)}.$$

2) $w = \sum_n a_n x^{2n+1}$, $v = \sum_n b_n x^{2n}$, $u = \sum_n c_n x^{2n+1}$, $\pi = -$.

$$
\begin{aligned}
0 = {} & b_n(\Lambda-36n^2-54n-18)(\Lambda-36n^2-78n-40)(\Lambda-36n^2-102n-70) \\
& + b_{n+1}\,18(2n+1)(2n+2)\left[(\Lambda-36n^2-54n-18)(\Lambda-36n^2-126n-116)\right. \\
& \left. + (\Lambda-36n^2-174n^-2-208)(\Lambda-36n^2-150n-154)\frac{(12n+13)}{2(12n+25)}\right] \\
& + b_{n+2}\,81(2n+1)(2n+2)(2n+3)(2n+4)\left[(\Lambda-36n^2-54n-18)\right. \\
& \left. + (\Lambda-36n^2-198n-278)\frac{(24n+26)}{(12n+25)}\right] \\
& + b_{n+3}\,729(2n+1)(2n+2)(2n+3)(2n+4)(2n+5)(2n+6)\frac{(12n+13)}{(12n+25)},
\end{aligned}
$$

$$
\begin{aligned}
a_n = {} & -b_n\frac{(\Lambda-36n^2-54n-18)(\Lambda-36n^2-126n-92)}{48(2n+1)(12n+13)} \\
& -b_{n+1}\frac{9(2n+2)(\Lambda-36n^2-126n-116)}{24(12n+13)} \\
& -b_{n+2}\frac{27(2n+2)(2n+3)(2n+4)}{16(12n+13)},
\end{aligned}
$$

$$
c_n = -b_n\frac{(\Lambda-36n^2-54n-18)}{12(2n+1)} - b_{n+1}\tfrac{3}{2}(n+1) + a_n.
$$

$$\boxed{I = 5}$$

$$
\begin{aligned}
\phi(\gamma, \theta_i) = {} & (w\cos\gamma\sin 3\gamma + v\cos 2\gamma\sin 3\gamma)\frac{1}{\sqrt{2}}\left(D^5_{M2}(\theta_i) - D^5_{M-2}(\theta_i)\right) \\
& + (w\sin\gamma\sin 3\gamma - v\sin 2\gamma\sin 3\gamma)\frac{1}{\sqrt{2}}\left(D^5_{M4}(\theta_i) - D^5_{M-4}(\theta_i)\right);
\end{aligned}
$$

$$
6\frac{\mathrm{d}w}{\mathrm{d}x} + (\Lambda-40)v - 48x\frac{\mathrm{d}v}{\mathrm{d}x} + 9(1-x^2)\frac{\mathrm{d}^2v}{\mathrm{d}x^2} = 0,
$$

$$
(\Lambda-28)w - 42x\frac{\mathrm{d}w}{\mathrm{d}x} + 9(1-x^2)\frac{\mathrm{d}^2w}{\mathrm{d}x^2} + 12\frac{\mathrm{d}v}{\mathrm{d}x} = 0.
$$

1) $w = \sum_n a_n x^{2n}$, $v = \sum_n b_n x^{2n+1}$, $\pi = +$.

$$\begin{aligned}
&a_{n+2}\,81(2n+1)(2n+2)(2n+3)(2n+4)\\
&+a_{n+1}\,18(2n+1)(2n+2)(\Lambda-36n^2-126n-113)\\
&+a_n(\Lambda-36n^2-66n-28)(\Lambda-36n^2-114n-88)=0
\end{aligned}$$

$$b_n = -a_n\frac{(\Lambda-36n^2-66n-28)}{12(2n+1)} - a_{n+1}\tfrac{3}{2}(n+1).$$

2) $w = \sum_n a_n x^{2n+1}$, $v = \sum_n b_n x^{2n}$, $\pi = -$.

$$\begin{aligned}
&b_{n+2}\,81(2n+1)(2n+2)(2n+3)(2n+4)\\
&+b_{n+1}\,18(2n+1)(2n+2)(\Lambda-36n^2-126n-116)\\
&+b_n(\Lambda-36n^2-102n-70)(\Lambda-36n^2-78n-40)=0,
\end{aligned}$$

$$a_n = -b_n\frac{(\Lambda-36n^2-78n-40)}{6(2n+1)} - b_{n+1}3(n+1).$$

$I = 6$

$$\begin{aligned}
\phi(\gamma,\theta_i) =&[3\sqrt{5}w(2\cos^3\gamma+\cos\gamma\sin^2\gamma)+\sqrt{5}v(-6\cos^4\gamma+9\cos^2\gamma\sin^2\gamma+\sin^4\gamma)\\
&+14\sqrt{5}u\sin\gamma\cos\gamma\sin 3\gamma+14\sqrt{5}\,t\sin\gamma\cos 2\gamma\sin 3\gamma]D^6_{M0}(\theta_i)\\
&+[\sqrt{14}w(6\sin\gamma\cos^2\gamma+\tfrac{1}{2}\sin^3\gamma)+5\sqrt{14}\,v\sin^3\gamma\cos\gamma\\
&+\sqrt{14}u(8\cos^2\gamma+3\sin^2\gamma)\sin 3\gamma\\
&+\sqrt{14}t(8\cos^3\gamma-14\sin^2\gamma\cos\gamma)\sin 3\gamma]\tfrac{1}{\sqrt{2}}(D^6_{M2}(\theta_i)+D^6_{M-2}(\theta_i))\\
&+[3\sqrt{35}\,w\cos\gamma\sin^2\gamma+\sqrt{35}\,v(3\sin^2\gamma\cos^2\gamma+\sin^4\gamma)\\
&+2\sqrt{35}\,u\sin\gamma\cos\gamma\sin 3\gamma\\
&-2\sqrt{35}t(11\sin\gamma\cos^2\gamma-3\sin^3\gamma)\sin 3\gamma]\tfrac{1}{\sqrt{2}}(D^6_{M4}(\theta_i)+D^6_{M-4}(\theta_i))\\
&+[w\sin^3\gamma+2v\sin^3\gamma\cos\gamma-2u\sin^2\gamma\sin 3\gamma\\
&+4\,t\sin^2\gamma\cos\gamma\sin 3\gamma]\left(\tfrac{11\times 35}{2}\right)^{\frac{1}{2}}\tfrac{1}{\sqrt{2}}(D^6_{M6}(\theta_i)+D^6_{M-6}(\theta_i));
\end{aligned}$$

$$[\Lambda(49-4x^2)+72x^2-882]w+(144x^2-954)x\frac{dw}{dx}+(441-36x^2)(1-x^2)\frac{d^2w}{dx^2}$$
$$+x[-45\Lambda+1260]v+(1440x^2-630)\frac{dv}{dx}-405x(1-x^2)\frac{d^2v}{dx^2}$$
$$+[\Lambda 91(1-x^2)+3528x^2-2268]u-3906x(1-x^2)\frac{du}{dx}+819(1-x^2)^2\frac{d^2u}{dx^2}$$
$$+(\Lambda 91(1-x^2)+4914x^2-3654]xt$$
$$+(1-x^2)(1008-4914x^2)\frac{dt}{dx}+819x(1-x^2)^2\frac{d^2t}{dx^2}=0,$$

$$[-\Lambda 18x+324x]w+(396x^2-72)\frac{dw}{dx}-162x(1-x^2)\frac{d^2w}{dx^2}$$
$$+[\Lambda(4+14x^2)-392x^2-112]v-(504x^2-180)x\frac{dv}{dx}+(36+126x^2)(1-x^2)\frac{d^2v}{dx^2}$$
$$+[-14\Lambda(1-x^2)x+56(1-10x^2)x]u$$
$$+(672x^2+84)(1-x^2)\frac{du}{dx}-126x(1-x^2)^2\frac{d^2u}{dx^2}$$
$$+[-14\Lambda(1-x^2)+644-1148x^2]t+(1-x^2)x756\frac{dt}{dx}-126(1-x^2)^2\frac{d^2t}{dx^2}=0,$$

$$(\Lambda 13-234)w-378x\frac{dw}{dx}+117(1-x^2)\frac{d^2w}{dx^2}$$
$$+(-\Lambda 5x+140x)v+(210x^2-120)\frac{dv}{dx}-45x(1-x^2)\frac{d^2v}{dx^2}$$
$$+(\Lambda 32-916)u-1152x\frac{du}{dx}+288(1-x^2)\frac{d^2u}{dx^2}$$
$$+(\Lambda 32-1588)xt+(456-1608x^2)\frac{dt}{dx}+288x(1-x^2)\frac{d^2t}{dx^2}=0,$$

$$(\Lambda 13-234)xw+(90-468x^2)\frac{dw}{dx}+117x(1-x^2)\frac{d^2w}{dx^2}$$
$$+(-\Lambda 5+140)v+90x\frac{dv}{dx}-45(1-x^2)\frac{d^2v}{dx^2}$$
$$+(\Lambda 32-916)xu+(120-1272x^2)\frac{du}{dx}+288x(1-x^2)\frac{d^2u}{dx^2}$$
$$+[\Lambda(80-48x^2)t+(2592x^2-4180)]t$$
$$+x(2592x^2-3744)\frac{dt}{dx}+(1-x^2)(720-432x^2)\frac{d^2t}{dx^2}=0$$

In principle, one can proceed in the same way as before, but the coefficients in the recurrence relations get very involved. Instead, it is possible to use the eigenvalues (taken, for instance, from the discussion in section 3) and solve for the coefficients of the wave functions. As in the other cases, two parities are present:

1) $w=\sum_n a_n x^{2n}$, $v=\sum_n b_n x^{2n+1}$, $u=\sum_n c_n x^{2n}$, $t=\sum_n d_n x^{2n+1}$, $\pi=-$.

$$
\begin{aligned}
&a_{n+2}\,441(2n+3)(2n+4)+a_{n+1}(\Lambda 49-1908n^2-4770n-3744)\\
&\quad -a_n\,4(\Lambda-36n^2-54n-18)-b_{n+1}\,90(2n+3)(9n+16)\\
&\quad -b_n\,45(\Lambda-36n^2-82n-60)+c_{n+2}\,819(2n+3)(2n+4)\\
&\quad +c_{n+1}\,7(\Lambda 13-936n^2-2520n-1908)-c_n 7(\Lambda 13-468n^2-882n-504)\\
&\quad +d_{n+1}\,126(2n+3)(13n+21)+d_n 7(\Lambda 13-936n^2-2160n-1368)\\
&\quad -91d_{n-1}(\Lambda-36n^2-54n-18)=0,
\end{aligned}
$$

$$
\begin{aligned}
&\quad -a_{n+1}\,9(2n+2)(18n+13)-a_n 9(\Lambda-36n^2-26n-18)\\
&\quad +b_{n+1}\,18(2n+2)(2n+3)+b_n 2(\Lambda+90n^2+135n+17)\\
&\quad +b_{n-1}\,7(\Lambda-36n^2-108n+80)-c_{n+1}21(2n+2)(6n+1)\\
&\quad -c_n 7(\Lambda-72n^2-48n-4)+c_{n-1}7(\Lambda-36n^2-6n+2)\\
&\quad -d_{n+1}\,63(2n+2)(2n+3)-d_n 7(\Lambda-72n^2-144n-100)\\
&\quad +d_{n-1}\,7(\Lambda-36n^2-18n-82)=0,
\end{aligned}
$$

$$
\begin{aligned}
&a_{n+2}\,117(2n+3)(2n+4)+a_{n+1}(\Lambda 13-468n^2-1458n-1224)\\
&\quad -b_{n+1}\,30(2n+3)(3n+7)-b_n 5(\Lambda-36n^2-102n-70)\\
&\quad +c_{n+2}\,288(2n+3)(2n+4)+c_{n+1}\,4(\Lambda 8-288n^2-1008n-949)\\
&\quad +d_{n+1}\,24(2n+3)(24n+43)+d_n 4(\Lambda 8-288n^2-948n-799)=0,
\end{aligned}
$$

$$
\begin{aligned}
&a_{n+1}\,9(2n+2)(26n+23)+a_n 13(\Lambda-36n^2-54n-18)\\
&\quad -b_{n+1}\,45(2n+2)(2n+3)-b_n 5(\Lambda-36n^2-54n-46)\\
&\quad +c_{n+1}\,24(2n+2)(24n+17)+c_n 4(8\Lambda-288n^2-492n-229)\\
&\quad +d_{n+1}\,720(2n+2)(2n+3)+d_n 4(\Lambda 20-1152n^2-2448n-1981)\\
&\quad -d_{n-1}\,48(\Lambda-36n^2-54n-18)=0.
\end{aligned}
$$

2) $w=\sum_n a_n x^{2n+1}$, $v=\sum_n b_n x^{2n}$, $u=\sum_n c_n x^{2n+1}$, $t=\sum_n d_n x^{2n}, \pi=+.$

$$
\begin{aligned}
&a_{n+2}\,441(2n+4)(2n+5)+a_{n+1}(\Lambda 49-1908n^2-6678n-6606)\\
&\quad -a_n 4(\Lambda-36n^2-90n-54)-b_{n+2}\,45(2n+4)(18n+41)\\
&\quad -b_{n+1}\,45(\Lambda-36n^2-118n-110)+c_{n+2}\,819(2n+4)(2n+5)\\
&\quad +c_{n+1}7(\Lambda 13-936n^2-3456n-3402)\\
&\quad -c_n 7(\Lambda 13-468n^2-1350n-1062)+d_{n+2}63(2n+4)(26n+55)\\
&\quad +d_{n+1}7(\Lambda 13-936n^2-3096n-2682)\\
&\quad -d_n 7(\Lambda 13-468n^2-1170n-702)=0,
\end{aligned}
$$

$$
\begin{aligned}
&-a_{n+1}18(18n^2+49n+33)-a_n 9(\Lambda-36n^2-62n-40)+b_{n+2}18(2n+4)(2n+3)\\
&\quad +b_{n+1}2(\Lambda+90n^2+225n+107)+b_n 7(\Lambda-36n^2-54n-28)\\
&\quad -c_{n+1}\,42(2n+3)(3n+2)-c_n 7(\Lambda-72n^2-120n-46)\\
&\quad +c_{n-1}7(\Lambda-36n^2-42n-10)-d_{n+2}\,63(2n+4)(2n+3)\\
&\quad -d_{n+1}7(\Lambda-72n^2-216n-190)+d_n 7(\Lambda-36n^2-90n-82)=0,
\end{aligned}
$$

$$
\begin{aligned}
&a_{n+1}\,117(2n+2)(2n+3)+a_n(\Lambda 13-468n^2-990n-612)\\
&\quad -b_{n+1}\,15(2n+2)(6n+11)-b_n 5(\Lambda-36n^2-66n-28)\\
&\quad +c_{n+1}\,288(2n+2)(2n+3)+c_n 4(\Lambda 8-288n^2-720n-517)\\
&\quad +d_{n+1}\,24(2n+2)(24n+31)+d_n 4(\Lambda 8-288n^2-660n-397)=0,
\end{aligned}
$$

$$
\begin{aligned}
&a_{n+1}\,18(26n^2+75n+54)+a_n 13(\Lambda-36n^2-90n-54)\\
&\quad -b_{n+2}\,45(2n+3)(2n+4)-b_{n+1}\,5(\Lambda-36n^2-90n-82)\\
&\quad +c_{n+1}\,24(2n+3)(24n+29)+c_n 4(\Lambda 8-288n^2-780n-547)\\
&\quad +d_{n+2}\,720(2n+3)(2n+4)+d_{n+1}4(\Lambda 20-1152n^2-3600n-3493)\\
&\quad -d_n 48(\Lambda-36n^2-90n-54)=0.
\end{aligned}
$$

These linear equations, plus the relations $a_{n+1}(n)=a_n(n+1)$, allow us to solve for the coefficients.

2. COEFFICIENTS IN THE EXPANSION OF w, v, . . ., u, FOR STATES WITH $I \leqq 6, \lambda \leqq 9$.

I	λ	π_γ	a_0	a_1	b_0	b_1	c_0	d_0	$N_{I\lambda}$
0	0	+	1						4
0	6	+	−1	3					16/5
0	3	−	1						4/3
0	9	−	−3	5					16/7
2	1	−	1						4
2	5	−	1		−3				8
2	7	−	−1	5	−2				16/3
2	2	+			1				4
2	4	+	−3		1				8
2	8	+	−2		−1	5			16/3
3	3	−	1						8/3
3	9	−	−1	5					64/21
3	6	+	1						8/15
4	2	+	1						144
4	4	+	5				−9		9360
4	6	+	6		13		−3		12376/5
4	8	+	−5	85	60		−6		32640
4	3	−			1				88
4	5	−	11		6				2640
4	7	−	11		3		−15		4560
4	9	−	60		−7	95	−30		27968
5	4	+	1						8/3
5	8	+	1		−5				32/3
5	5	−			1				8/3
5	7	−	−5		1				32/3
6	3	−	1						2288/3
6	5	−	14				−11		418880/3
6	7	−	37		65		−13		553280/3
6	9	−	127	1615	1530		−135		797070976/21
6	9	−	16290	16184	41714		−10485	19279	780413920000/3
6	4	+			1				1040/3
6	6	+	13		9				208832/15
6	6	+	196		406			251	908017600/3
6	8	+	2002		1274		−1105	117	592067840/3

The normalization factor for the resultant wave functions is $\left[\frac{2I+1}{8\pi^2 N_{I\lambda}}\right]^{\frac{1}{2}}$.

References

1) A. Bohr, Mat. Fys. Medd. Dan. Vid. Selsk. **26** (1952) no. 14
2) A. Bohr and B. Mottelson, Mat. Fys. Medd. Dan. Vid. Selsk. **27** (1953) no. 16
3) A. Bohr and B. Mottelson, Beta and Gamma Ray Spectroscopy, edited by K. Siegbahn (Amsterdam, 1955) Ch. XVII
4) K. Alder, A. Bohr, T. Huus, B. Mottelson and A. Winther, Revs. Mod. Phys. **28** (1956) 432
5) L. Wilets and M. Jean, Phys. Rev. **102** (1956) 788
6) G. Rakavy, Nuclear Physics **4** (1957) 289
7) P. M. Morse and H. Feshbach, Methods of Theoretical Physics (McGraw-Hill, New York, 1953) Ch. 5

1.D.2:
2.C

Nuclear Physics **10** (1959) 386—394; © *North-Holland Publishing Co., Amsterdam*
Not to be reproduced by photoprint or microfilm without written permission from the publisher

RESONANT NEUTRON CAPTURE IN Er AND Hf

C. A. FENSTERMACHER †, J. E. DRAPER and C. K. BOCKELMAN
Yale University, New Haven, Connecticut ††

Received 12 January 1959

Abstract: The low energy portion of the gamma ray spectra has been studied following neutron capture in the 0.47, 0.58, 6.0 and 9.4 eV resonances in erbium and the 1.10 and 2.38 eV resonances in hafnium. Measurements of the absolute intensities of the 192, 285, 750 and 820 keV peaks in erbium give essentially the same results for the four resonances. The relative intensity of the 80 keV peak was measured for thermal capture. The 285, 192 and 80 keV peaks are associated with the 6^+, 4^+, 2^+ and 0^+ rotational levels of Er^{168} and all four resonances (previously unassigned) are assigned to the target isotope Er^{167}. There is evidence that the 192 keV peak is composite. In hafnium the 90,220 and 330 keV peaks are associated with the 0^+, 2^+, 4^+ and 6^+ rotational states of Hf^{178}. The relative intensities of the 220 and 330 keV peaks differ by the factor 2.7 for the 1.10 and 2.38 eV resonances producing Hf^{178}.

1. Introduction

Extensive and valuable information exists on the spectrum of gamma rays emitted after thermal neutron capture. The interpretation of such work is simplified in the few cases when it can be ascertained that the capture occurs by the excitation of an isolated level in the compound nucleus. This fact makes the study of resonance neutron capture gamma rays desirable. In addition, it is of interest to determine how the details of the gamma-ray cascades are related to other characteristics of the capture level. Resonant capture also has certain experimental davantages. The need for separated isotopes is removed. In addition, the time-of-flight techniques employed in the present work to select the resonant neutrons discriminate strongly against isomeric activity of half-lives longer than milliseconds, thereby removing a possible source of confusion in assignment of the gamma rays measured.

2. Experimental

The techniques used in the present work have been described in detail previously [2,3]). To summarize them briefly, the 6.5-MeV electron linear accelerator was used as a pulsed source (1 μsec) of neutrons, and the

† Present address: Los Alamos Scientific Laboratory, Los Alamos, New Mexico.

†† Supported by the U.S. Atomic Energy Commission. Preliminary accounts of this work have appeared [1]).

sample, placed at a distance of 3.3 m, was viewed by a 2.5-in. diam, 1.7-in. NaI(Tl) scintillator. The spectrum of the capture gamma rays was analysed only during an interval after the neutron burst which corresponds to the flight time interval of the neutron energy range of interest. The absolute intensities of the gamma rays were obtained by comparison with the 478-keV gamma ray from neutron capture by B^{10}. To supplement the data on resonance capture, thermal capture gamma rays were also examined by placing the sample beside the accelerator target and viewing it through a collimator with the NaI(Tl) scintillator at a sufficient distance to permit adequate shielding †.

3. Experimental Results

3.1. ERBIUM

The sample was in the form of Er_2O_3 powder in an Al container having 0.003″ walls. No measurable radiation has been observed from this type of sample container. The resonances at 0.47, 0.58, 6.0 and 9.4 eV have been investigated. Although the 0.47 and 0.58 eV resonances overlap [4]) they were partially isolated by gating one of the spectra over the interval 0.39 to 0.44 eV and the other over the interval 0.60 to 0.68 eV. The result of the former is given in fig. 1 which shows gamma rays at 190 ± 10, 285 ± 10, 750 ± 20 and 820 ± 20 keV. Additional runs at higher amplifier gain as well as the thermal capture spectrum of fig. 2 also show a gamma ray at 80 ± 6 keV. A more detailed investigation of the thermal capture spectrum further substantiated the two peaks at 750 and 820 keV and afforded a more precise determination of the energy of the 192 keV peak discussed below. Since the spectra for the other neutron resonances were of the same form, they are not shown.

The results of the intensity measurements are given in table 1. Sample absorption was taken into account, [3])and was 10—15 % for the 190 keV peak and less than 3 % for the higher energies. Since the 80 keV gamma ray is highly converted, as discussed later, and strongly absorbed in the sample, its intensity is listed only for thermal capture for which a 60 mg/cm² sample could be used. A 14 % correction for the absorption of the 80 keV gamma ray has been included in table 1. Similarly intensity limitations precluded an intensity assignment for the weak 285 keV gamma ray peak in the 9.4 eV resonance. Since the conversion coefficients for these transitions are not sufficiently well known, only the gamma ray intensity is listed in table 1. In order to detect changes in the spectra for various resonances the relative as well as the absolute intensities are listed since the former can be obtained with better precision.

† The results of an investigation by this means of thermal capture in many elements have been submitted for publication.

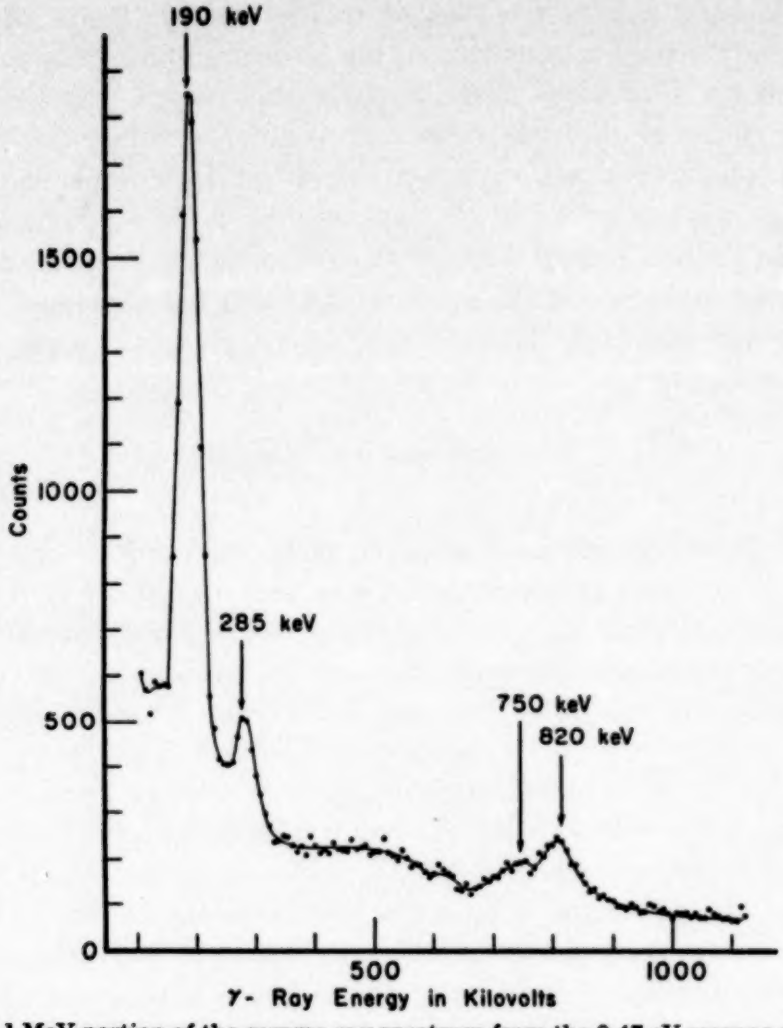

Fig. 1. 0.1 to 1 MeV portion of the gamma ray spectrum from the 0.47 eV resonance in erbium.

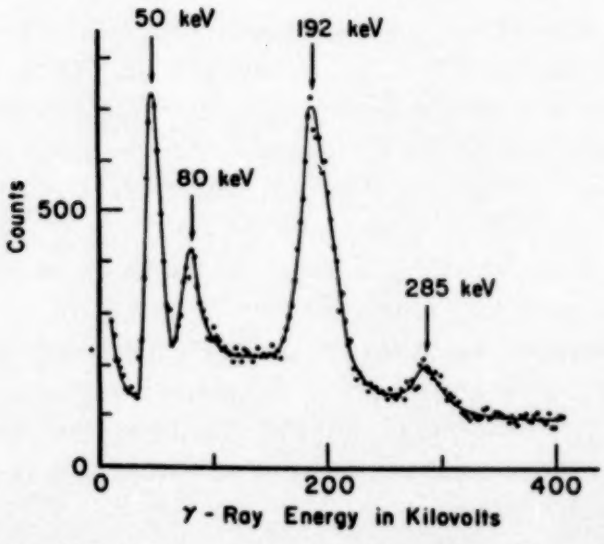

Fig. 2. 30 to 400 keV portion of the gamma ray spectrum from thermal neutron capture by erbium. The 50 keV peak is assigned as the X-ray.

TABLE 1

Intensity of neutron capture gamma rays

Product nucleus	E_n (eV)	E_γ (keV)	Relative gamma-ray intensity	Photons per 100 neutron captures
$_{68}Er^{168}$	0.47	185, 199	1	40±6
		285	0.15 ±0.04	...
		750	0.35 ±0.11	...
		820	0.70 ±0.18	...
	0.58	185, 199	1	33±4
		285	0.11 ±0.04	...
		750	0.32 ±0.10	...
		820	0.64 ±0.17	...
	6.0	185, 199	1	27±4
		285	0.076±0.025	...
		750	0.23 ±0.11	...
		820	0.72 ±0.17	...
	9.4	185, 199	1	25±5
		285	...	...
		750	0.16 ±0.11	...
		820	0.57 +0.24	...
	thermal	80	0.23 ±0.04 †	...
		185, 199	1	...
		285	0.13 ±0.02	...
		750	0.16 ±0.07	...
		820	0.70 ±0.13	...
$_{72}Hf^{178}$	1.10	90	0.21 ±0.03	...
		220	1	27±4
		330	0.096±0.043	...
		1150	...	14±8
	2.38	90	0.20 ±0.03	...
		220	1	42±8
		330	0.26 ±0.07	...
		1150	...	22±9
	thermal	90	0.30 ±0.04	...
		220	1	...
		330	0.28 ±0.04	...

† The relative rate of this transition is 1.95±0.35 using the conversion coefficient of ref. [8])

As discussed later, there was particular interest in the energy of the 192 keV peak shown in fig. 2. For this reason a 60 mg/cm^2 sample was used with thermal neutrons and a series of runs made which were alternated with various energy calibrations. Particular care was taken to avoid calibration shifts which could be caused by the accelerator flash. By comparisons with the 192 keV peak from In^{114} it was concluded that the peak indicated in fig. 2. does not differ in energy from that of the In^{114} peak by more than 4 keV. Further, the comparison shows that the Er peak is slightly wider than the In^{114} peak, indicating the presence of more than one gamma ray.

3.2. HAFNIUM

For most of the results the sample was a 2.5-in. square of 5-mil hafnium foil. The 1.10 and 2.38 eV resonances, both producing Hf^{178}, were examined and typical spectra are shown in fig. 3. Gamma rays of energies 90±5,

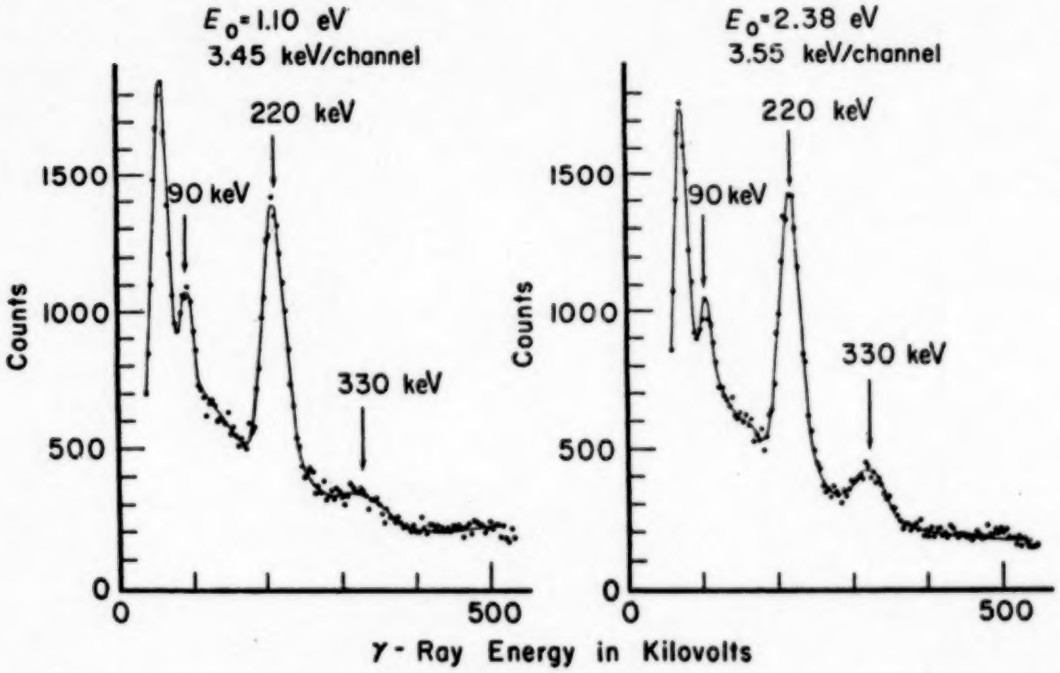

Fig. 3. Spectrum from neutron capture in the 1.10 and 2.38 eV resonances in hafnium. The 60 keV peak is assigned as the X-ray.

220±10 and 330±10 keV were found. The thermal capture spectrum also showed these and particularly clarified the 90 keV peak. The spectra from thermal neutron capture and from both resonances indicated several transitions having energies near 1150 keV. The intensities of these transitions are listed in table 1.

It is apparent in fig. 3 that the relative intensities of the 220 and 330 keV peaks are different for the two resonances. It is then important to known whether this reflects a real difference in the relative intensities of these two

transitions due solely to resonance neutron capture. One test of this was made by repeating the run with a thick B^{10} neutron absorber ($N\sigma = 1$ at 100 eV) inserted 20 in. upstream from the sample. The resulting spectrum showed a counting rate which was everywhere less than 20 % of the continuum under the peaks of fig. 3, and there was no evidence of structure in the vicinity of the 220 and 330 keV peaks. This B^{10} absorber left virtually unchanged the fast neutrons and the gamma rays in the beam caused by the accelerator flash and by neutron capture in the moderator. Thus the possibility of contributions from short-lived gamma-ray induced isomers or fast neutron induced isomers was eliminated.

The more conclusive test, however, was to use three pulse height analyses simultaneously; one with an 18-μsec gate centered on the 1.1 eV resonance, one with a 14-μsec gate centered on the 2.4 eV resonance, and one with a 14-μsec gate in the lowest part of the valley between resonances. Additional runs were made with the electronic systems interchanged. These runs would reveal any effects of slow neutron induced activities as well as any effects of activities produced by gamma rays or fast neutrons. Since the three spectra were obtained simultaneously, the possibility of confusion by a slow build-up of activity (e.g., the 5.5h Hf^{180m}) was avoided. The results of all these runs confirmed that the change in relative intensities of the 220 and 330 keV peaks in fig. 3 was due to the prompt (less than 10 μsec delay) gamma rays following neutron capture in the 1.1 and 2.4 eV resonances.

4. Discussion

The first conclusion to be drawn from the erbium data is that the 0.47, 0.58, 6.0 and 9.4 eV resonances and the majority of thermal capture are all due to the same isotope. The results obtained for many elements † show that the spectra of various nucleides bear little resemblance to each other. The spectra for these four resonances are closely similar in appearance, and this is indicated in table 1.

The second conclusion is that these four resonances and the majority of thermal capture all produce even-even compound nuclei since the gamma ray energy sequence 80, 185 and 285 keV matches well the rotational level sequence predicted by the collective model and based on the 2+ excited state in Er^{168} at 80 keV produced in Coulomb excitation [5]). If the 285, 185 and 80 keV gamma rays were respectively from the $6+ \rightarrow 4+$, $4+ \rightarrow 2+$ and $2+ \rightarrow 0+$ transitions there would be the further requirement that the above order be one of increasing intensity since cross-over transitions would be E4 and of negligible intensity. This requirement is satisfied as shown in table 1 when internal conversion is considered. An 80 keV E2 transition in Er^{166} has been found [6]) to have a total internal conversion coefficient of 7.6 ± 1.5.

† See footnote on p. 387.

From these considerations and the fact that the six natural isotopes of erbium include only one odd-neutron isotope, it was concluded in the preliminary account [1]) of this work that the majority of thermal capture and the resonances at 0.47, 0.58, 6.0 and 9.4 eV all produce Er^{168}. This conclusion is further substantiated by more recent results [7]) on Er^{168} in which 80, 185, 198, 448, 632, 742, 817 and 822 keV were the energies of the most intense gamma rays following K-capture in Tm^{168}. Six of these gamma rays can be identified with those reported here.

As noted earlier, the 192 keV peak of fig. 2 appears to be midway between the 185 and 198 keV gamma rays found by Michelich [7]) and is somewhat broader than a single peak. This result differs from that of Skliarevskii *et al.*[8]) who found the peak following thermal capture to be at 185 keV. In spite of the care with which the 192 keV calibration in fig. 2 was made, consideration of the small energy difference in question and the previously mentioned effect of the accelerator flash on the energy calibration of our scintillator system makes it difficult to evaluate precisely the energy and shape of this peak. However, the relative intensities of the two gamma rays can be made consistent with the requirements imposed by Michelich's level scheme [7]), wherein the 198 keV gamma ray feeds the 817 keV transition, while the 285 and 185 keV transitions are within the 6+, 4+, 2+, 0+ rotational sequence.

It is further concluded that the transitions listed in table 1 for erbium are of the same intensity, within the limits indicated, for all four resonances. A similar conclusion was made [2]) for three resonances producing Sm^{150}.

Comparison of figs. 2 and 3 and table 1 show that the three low energy gamma rays which are assigned to the $6+ \rightarrow 4+$, $4+ \rightarrow 2+$ and $2+ \rightarrow 0+$ rotational transitions are quite similar in pattern for both of the deformed even nuclei Er^{168} and Hf^{178}. A similar pattern is found † for Gd^{156} and Gd^{158} although the absolute intensity of each transition is somewhat lower for gadolinium. The evidence that these are rotational transitions in the neutron capture gamma ray spectrum at present consists in the energy relations and (less conclusively) the intensity relations of the gamma rays and the fact that when an E2 conversion correction is applied to the presumed $2+ \rightarrow 0+$ transition the resulting transition intensity is reasonable. The evidence that rotational levels play a prominent role in Hf^{178} is more extensive in radioactivity studies [9,10]). In those studies the entire $K = 0$ rotational cascade starting from the 8+ state has been observed. The transition intensities of all four of these were equal and the conversion coefficients confirmed the E2 assignment for each of the four. The gamma ray energies were 93.17, 213.7, 325.8 and 427.0 keV. The first three of these are in satisfactory

† To be published; see also ref. [8]).

agreement with those observed here following neutron capture in the first two resonances which are known[4]) to produce only Hf^{178}.

The peak at 1150 keV in Hf is presumed to be closely related to the intense band of at least five gamma rays observed[11]) with the Compton electron spectrometer following thermal neutron capture in elemental hafnium. Intensity and resolution limitations precluded an accurate assignment of the energies and intensities of the members of this band in the present experiment, but it was clear that the peak contained more than one gamma ray. The total intensity of this band reported in ref. [11]) is about twice that in table 1 if the band is assigned to transitions in Hf^{178}. However, we are reluctant to conclude that this intensity is different for thermal and resonant capture in view of the above limitations.

The final conclusion is that the relative intensities of the 220 and 330 keV gamma rays are different for the 1.10 and 2.38 eV resonances producing Hf^{178}. This is demonstrated in fig. 3. The experiments to verify this difference are described in the previous section. Similarly, a difference was found[3]) for three resonances producing In^{116}.

The ground state[12, 13]) of Hf^{177} is presumed to be $(\frac{7}{2}-)$. Consequently the compound state is (3−) or (4−), but the spins of these two resonances have not been measured. The radiation widths[14]) are 67 ± 2 meV for the 1.10 eV resonance and 60 ± 1 meV for the 2.39 eV resonance, and these are considered to be different. The neutron binding energy of Hf^{178} derived from mass values[15]) is 7.54 ± 0.06 MeV. Two measurements of the high energy gamma rays in thermal neutron capture appear to disagree. Campion and Bartholomew[16]) report gamma rays of 7.62 ± 0.02, 7.33 ± 0.03 and 6.77 ± 0.02 MeV. The highest energy gamma ray reported by Groshev *et al.*[11]) is 6.39 ± 0.04 MeV, although the data show that the energy region to at least 6.8 MeV was explored. The energy differences of the gamma rays of energy greater than 7 MeV do not correspond to differences between known energy levels, although the intensities are consistent with the single particle estimate for E1 radiation, modified by the ratio of level spacings at the initial and final state. Even though the position of these high energy radiations cannot be assigned uniquely in the level scheme it is clear that their intensities are far too low to influence appreciably the intensities of the low energy gamma rays observed in the present work. Hence, it appears that the change in intensity of the 330 keV transition is derived from cascaded transitions to the 633 keV level or from the onset of another transition of about 330 keV. The change may depend on the spin of the compound state, although this is not a requirement since energy levels are not completely characterized by total angular momentum and energy.

We are grateful to R. L. Hickok and T. S. Springer for their help with

some of the data and to P. S. Jewett for his maintenance of the accelerator. The work was initiated following preliminary experiments by A. E. Walters and R. G. Bennett. The erbium sample was kindly made available by Professor F. H. Spedding of Iowa State University. Thanks are due J. W. Michelich for several communications.

References

1) Fenstermacher, Draper and Bockelman, Bull. Am. Phys. Soc. **2** (1957) 41
2) Fenstermacher, Bennett, Walters, Bockelman and Schultz, Phys. Rev. **107** (1957) 1650
3) Draper, Fenstermacher and Schultz, Phys. Rev. **111** (1958) 906
4) D. J. Hughes and R. B. Schwartz, Neutron Cross Sections, Brookhaven National Laboratory Report BNL-325, second edition (Superintendent of Documents, U.S. Government Printing Office, Washington, D.C., 1958)
5) N. P. Heydenburg and G. M. Temmer, Phys. Rev. **100** (1955) 150
6) A. W. Sunyar, Phys. Rev. **93** (1954) 1345
7) J. W. Michelich and B. Harmatz, Phys. Rev. **106** (1957) 1232; and private communication
8) Skliarevskii, Stepanov and Obiniakov, Atomnaya Energiya **4** (1958) 22
9) Felber, Stephens and Asaro, University of California Radiation Laboratory Report UCRL-3882 (1957)
10) Bunker, Cochran, Mize and Starner, private communication
11) Groshev, Demidov, Lutsenko and Pelekhov, Atomnaya Energiya **4** (1958) 5
12) D. R. Speck and F. A. Jenkins, Phys. Rev. **101** (1956) 1831
13) B. R. Mottelson and S. G. Nilsson, Phys. Rev. **99** (1955) 1615
14) H. H. Landon, Phys. Rev. **100** (1955) 1414
15) W. H. Johnson, Jr. and V. B. Bhanot, Phys. Rev. **107** (1957) 1669
16) P. J. Campion and G. A. Bartholomew, Can. Journ. Phys. **35** (1957) 1361

4.E *Nuclear Physics* **10** (1959) 395—404; © *North-Holland Publishing Co., Amsterdam*
Not to be reproduced by photoprint or microfilm without written permission from the publisher

MEASUREMENT OF THE NEUTRON LIFE-TIME

A. N. SOSNOVSKY †, P. E. SPIVAK, Yu. A. PROKOFIEV, I. E. KUTIKOV
and Yu. P. DOBRININ †
Atomic Energy Institute, USSR Academy of Sciences, Moscow

Received 29 September 1958

Abstract: The half-life of the neutron has been measured and found to be 11.7 ± 0.3 min.

1. Introduction

The free neutron is the simplest of β-radioactive nuclei and the value of its half-life should yield useful information for elucidation of the mode of β-interaction. Interest in this problem has been revived recently and the demands on the accuracy of neutron half-life determinations have become more stringent. However, more accurate measurements of this important constant entail serious experimental difficulties and up to the present only an accuracy of 10—15 % has been attained. In the present work an attempt has been made to improve considerably the accuracy of the measurements.

Neutron half-life determinations have been made in the U.S.A. [1,2,3]) and U.S.S.R.[4]). In these investigations slow decay protons created in the intense neutron beams produced in nuclear reactors were accelerated to 10—15 kV and then recorded either directly [2,4]) or in coincidence with the decay electrons [1,3]). In all cases the accelerating electrodes were located near the beam and the decay protons were "pulled out" of the beam by the field. In order to find the half-life it was necessary to assess what fraction of the protons created in a certain part of the beam was recorded in the experiments. However, the results of the calculations depend not only on the experimental conditions but on the decay proton spectrum as well. Even at present this spectrum has not been sufficiently studied [4,5]) and its theoretical shape strongly depends on the choice of the β-interaction; at present the experimental basis of this choice cannot be considered to have been established to a satisfactory extent. Thus, in experiments performed with the accelerating electrode near the beam the half-life is measured with an error which is inherent in the very method employed and is due to deficient knowledge of the proton spectrum. As a result, the accuracy of the experiments is much impaired.

† The Editor regrets to state that he has been informed of the death of two of the authors, A. N. Sosnovsky and Yu. P. Dobrinin.

In early experiments of this type relatively rough values of the half-lives were obtained. Thus, Snell, Pleasonton and McCord [1]) cited a value lying between 10 and 30 min [1]), Robson [2]) indicated a value between 9 and 25 minutes and Spivak and Sosnovsky a half-life between 8 and 15 minutes [4]).

Later on Robson obtained a half-life value equal to 12.8 ± 2.5 min [3]) and Spivak and Sosnovsky one equal to 12.0 ± 1.5 min [4]). The latter value was obtained with an arrangement in which, though the beam passed through the proton accelerating field, the experimental conditions were such that the number of protons recorded by the counter exactly equalled the number of protons created in a definite part of the beam. In this experiment the half-life value did not depend on any uncertainty in the proton spectrum.

In the present investigation the life-time was also derived from directly measurable quantities and from geometrical factors which could be exactly determined. This was attained by first passing the decay protons through a system of diaphragms before permitting them to enter the accelerating field. Although the number of protons, N_p, selected in this way comprised a small fraction of the protons produced in the effective part of the beam, they nevertheless entered the accelerating field with a small angular spread and thus even at comparatively small voltages could be completely focussed on the window of the counter. Thus in the formula for the neutron half-life

$$T = K \frac{I}{N_p} \ln 2, \tag{1}$$

where I is the neutron density integral over the beam cross section, the coefficient K will depend only on the geometrical conditions of the experiment and on the distribution of the neutrons in the beam.

2. Description of the Experimental Arrangement

The measurements were performed with a neutron beam from the RFT reactor of the Atomic Energy Institute of the U.S.S.R. Academy of Sciences. A lengthwise section of the apparatus is shown diagramatically in fig. 1. A highly collimated neutron beam of 80 mm diameter passes through vacuum chamber 1 maintained at a pressure of $1-2 \times 10^{-6}$ mm. Hollow electrode 6 to which a positive voltage of 20 kV is applied is located in the chamber. Decay protons created in the beam opposite diaphragm 2 (diameter 78 mm) pass into the electrode (which is field-free inside) and reach grid 3 (diameter 100 mm). Diaphragm 2 and grid 3 are respectively 13.6 and 82.1 cm from the beam axis. After passing through grid 3 the decay protons enter a region in which an electric field between a grounded spherical grid (radius 3 cm) and high voltage electrode accelerates and focusses them on the window of counter 5. The accelerating field is nearly spherical and the proton motion in it can easily be calculated. According to the calculations all protons passing

through grid 3 should be focussed on the counter window at a voltage as low as 10 kV. A special study was made of the properties of this focussing system. Thus, the dependence of the proton counting rate on the voltage and on the position of counter 5 and dimensions of the entrance window 3 was investigated. These experiments confirmed the calculations and proved that with a voltage of 20 kV, which was employed to obtain a good ratio between the effect and background, all protons which entered the focussing field were certainly incident on the counter window.

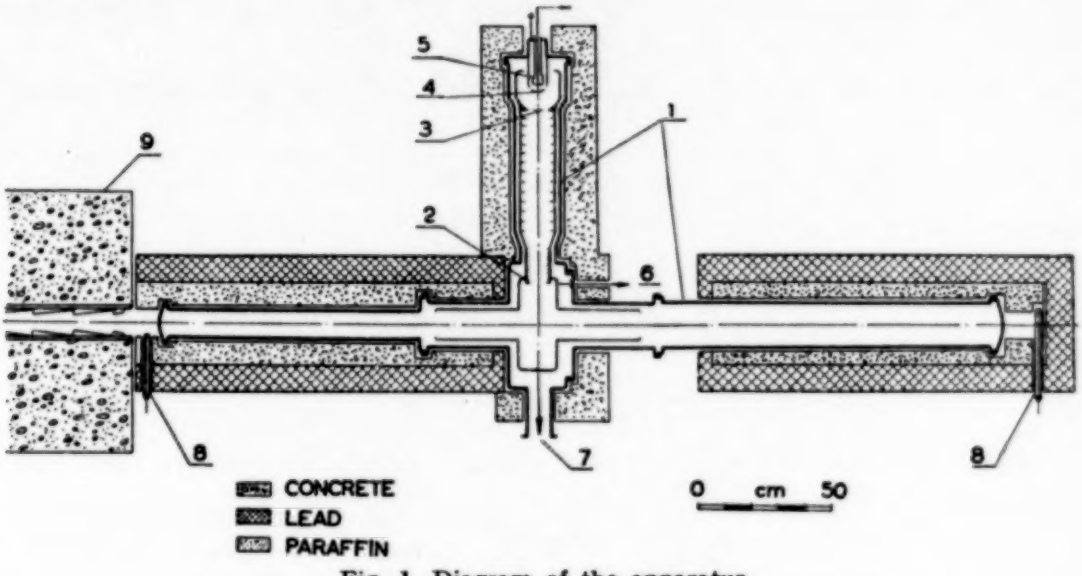

Fig. 1. Diagram of the apparatus

1. Body of apparatus;
2. Diaphragm;
3. Diaphragm with grid;
4. Spherical grid;
5. Proportional counter;
6. High voltage electrode;
7. Flange of diffusion pump;
8. Monitors;
9. Reactor shield.

For proton counting a ball proportional counter was employed. The design and properties of the counter have been described in detail [4]). The counter window (diameter 16 mm) was covered by a thin collodion film (0.07 micron thickness), which was supported from the vacuum side by a tungsten grid (wire $\varnothing 25\ \mu$, pitch 0.5 mm). A second grid ($\varnothing 20\ \mu$, pitch 0.9 mm) which screened the operating volume of the counter from charges accumulated on the film, was arranged on the other side of the film.

Four grids were interposed between the place of production of the decay protons and the working volume of the counter and hence some of the protons were absorbed and did not reach the counter. If the number of protons recorded by the counter is n_p, then

$$n_p = \alpha N_p,$$

where N_p is the number of protons reaching grid 3 and α is the resultant transmission of all the grids.

Grid 3, which covers the entrance window of the focussing system is made of 20 micron diameter wire, the cells being squares with 4 mm sides. The geometrical transparency of such a grid is close to 0.99. Actually it is even closer to unity due to the field being "suspended" in the cells. Absorption in this grid was therefore neglected; to account for this we somewhat increased the error in α. The geometrical transparency (for normal incidence) of spherical grid 4 was 0.913 and that of the grids in the counter window was 0.950 and 0.978. Thus, for normally incident protons the transparency of all the grids was 0.848. For the most obliquely incident protons the resultant transmission was somewhat smaller and equal to 0.838. Since the protons reach the grids at angles intermediate between those corresponding to these two extreme cases the value

$$\alpha = 0.843 \pm 0.006$$

was accepted.

3. Measurement of the Neutron Density

The neutron density was determined by activating a sodium target for which the cross section obeys the $(1/v)$-law [6]) and also by activating a gold target and introducing relevant corrections for the effect due to resonance neutrons.

In both methods absolute counting with a 4π-counter of β-electrons from Au^{198} was employed as the reference measurement. Neutron density measurements performed by activating gold was carried out with two targets. One of these was a thin gold film (0.06 mg/cm^2) evaporized in vacuum onto a metalized collodion film; the other was much thicker (40 mg/cm^2) and was made from a carefully weighed piece of gold foil.

After introduction of corrections to account for the effect from resonance neutrons the neutron density could be deduced from the absolute number of decays in the "thin" target as measured with a 4π-counter and from the relative activities of the two targets as determined by γ-ray measurements with a scintillation counter. The corrections were based on the measured values of the cadmium ratios for gold and the $(1/v)$-detector which equalled 2.84 and 23.4 respectively.

The neutron density determination based on activation of the sodium target was performed by measuring with a scintillation counter the intensity of the γ-rays emitted from the target. The proportionality coefficient between the unknown neutron density ρ and the measured γ-ray counting rate was found in a separate experiment. In this experiment the sodium target was placed in the path of a collimated neutron beam from a thermal column; the neutron density in the beam was determined from the absolute number of decays in the gold sample as described above. The ratio of the measured

neutron density to the γ-activity of the sodium target measured with the same scintillation counter yielded the value of the proportionality coefficient.

The correction for the interaction between the resonance neutrons and gold was insignificant in these experiments (0.7 %) as the cadmium ratios measured in the thermal column beam for Na and Au were respectively 4000 and 150. Thus one could be certain that the errors in the sodium activation measurements of the neutron density were determined only by the errors in the gold cross section value, $\sigma_c = (98 \pm 1.5) \times 10^{-24}$ cm^2 [7]) for $E = 0.025$ eV and by errors in the absolute measurements performed with the 4π-counter ($\pm$ 0.5 %) and errors in the relative measurements performed with the scintillation counter (± 0.5 %). The gold cross section error cited above includes 0.5×10^{-24} cm^2 to account for deviation from the $(1/v)$-law.

The results of the neutron density measurements performed by activation of gold and sodium in the centre of the beam (employed in the neutron life-time determinations) were found to be equal to within ± 0.5 %. These measurements yielded the value $\rho = 2.17 \times 10^3$ n/cm$^3 \pm 1.8$ %.

The neutron density integral I in formula (1) was determined by activation of a gold foil which completely intercepted the beam. The foil was then cut up into pieces and the activity of each of these was measured with the scintillation counter. The ratio of the total activity of the pieces to the specific activity of the central piece was then determined. The product of this ratio and the neutron density ρ in the centre of the beam yields the unknown value of the neutron density integral which turned out to be $I = (7.68 \pm 0.15) \times 10^4$ n/cm.

4. Measurement of Decay Protons

As was mentioned above the decay protons were recorded with a proportional counter, the window of which was covered by a thin film. The counter was filled with pure carbon tetrasfluoride (CF_4) at a pressure of 10 mm Hg. At this pressure the ranges of $\approx$ 20 keV protons were shorter than the counter dimensions.

The decay protons were recorded directly (not in coincidence with the electrons). Their number was determined as the difference of the counting rates measured with the accelerating voltage on and off. A point that required attention was that switching on of the accelerating voltage by itself led to a certain increase of the counting rate even in the absence of the neutron beam. An investigation of this effect showed [4]) that it was due to H_1^+ ions produced in the apparatus. By polishing and oxidizing the high voltage aluminium electrode and employing other measures inferred from earlier work, this effect could be made much smaller than the decay proton counting rate.

The H_1^+ ion counting rate slowly diminished as the apparatus was maintained at vacuum but it was always observed in a freshly evacuated system and this fact could be exploited in a number of control experiments. First of all it was shown that the magnitude of the effect did not depend on the degree of irradiation of the apparatus or on whether the neutron beam passed through the chamber or was intercepted. The effect from the H_1^+ ions could be determined by blocking the beam and measuring the difference of the counting rates in the presence and absence of the accelerating voltage.

Moreover, as long as the amount of H_1^+ ions was large the integral pulse height distribution could be measured for a selected multiplication value and a discrimination bias could be chosen so as to correspond to the "plateau" of this distribution (dotted curve, fig. 2). In the decay proton counting the

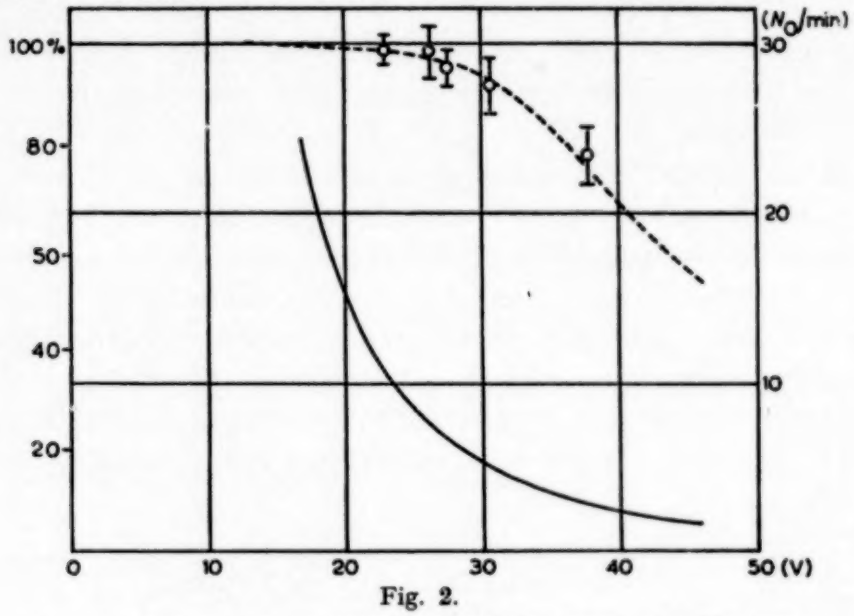

Fig. 2.

– – – – Integral pulse height distribution curve for H+ ions
——— Dependence of background on discriminator bias
Decay protons.

number of these particles and, to a greater extent, the number of H_1^+ ions was not large and the initial conditions (chosen in accord with the H_1^+ ions) were reproduced and periodically checked with the help of an α-particle source (Am^{241}) which could be moved within the vacuum chamber. Another reason why this was convenient is that if one suitably decreased the amplifier gain during the α-particle counting, the α-particle and H_1^+ ion integral pulse height distribution curves could be made almost identical with a good degree of accuracy.

The gas amplification of the counter was kept constant over a period of many hours of operation by employing a grid to screen the charges on the film, stabilizing the power supply, and suitably choosing the gas filling and using a large ballast volume connected to the counter.

Since the measurements were carried out over a relatively long period of time, possible variations in the beam intensity were monitored with two fission chambers, the stability of these in turn being checked by activation of the copper targets.

The decay proton counting procedure is illustrated in table 1 in which several measurement sets are presented, each of which consisted of four brief experiments.

TABLE 1

Neutron beam open			Neutron beam closed			
Accelerating voltage applied	Accelerating voltage removed	Decay protons and hydrogen ions	Accelerating voltage applied	Accelerating voltage removed	Hydrogen ions	Decay protons
(Number per 20 min)			(Number per 20 min)			(Number per min)
864	280	584	81	47	34	27.5
874	249	625	66	54	12	30.65
917	263	654	80	62	18	31.8
859	280	479	58	58	0	28.95
823	213	610	80	56	24	29.3

Twenty-five sets of measurements were carried out. From these the decay proton counting rate was found to equal 29.6 ± 0.4 min^{-1}. This quantity is reduced to the readings of the monitor chambers employed in the neutron density determinations. The deviation of the results of each set is in good agreement with the statistical error of the mean quantity.

The measurements were performed with a bias which was somewhat larger than which would permit all decay protons to be counted, but the effect-to-background ratio was much more favourable in this case than if smaller discriminator biases were used.

The result thus obtained is given in fig. 2 together with several control values measured at larger biases. It can be seen from the figure that extrapolation of the bias to zero could be performed with sufficient accuracy and the corresponding correction, (1.5 ± 0.5) %, was small. The extrapolated number of decay protons was $n_p = 30.0 \pm 0.4$ min^{-1} and with account of the grid transmission ($\alpha = 0.843$) it was $N_p = 35.6 \pm 0.54$ min^{-1}.

Regarding the errors inherent in the method the following should be noted. One difficulty was that for the slow decay protons to enter the accelerating field they had to travel over a comparatively large distance of about 80 cm. However, only a small part of low energy protons would be lost in scattering and charge exchange in collisions with the molecules of the residual gas at a pressure of $1-2 \times 10^{-6}$ cm Hg (measured directly in the chamber volume)

even if one accepts the most unfavourable cross sections of these processes and these proton losses could hardly exceed several tenths of a per cent.

In addition some of the protons scattered through small angles at the electrode walls could pass through the aperture in diaphragm 3 and thus somewhat increase the counting rate, providing that this effect was not compensated by charge exchange of the scattered protons.

The measurements described above were carried out with a large number of thin diaphragms in the electrode between diaphragms 2 and 3. The measurements were repeated with the same accuracy with the diaphragms removed; in this case the surface from which the protons could be scattered was a hundred times larger. The fact that the results were identical in both cases signified that the effect under consideration in reality did not occur.

5. Determination of Coefficient K

The magnitude of K in formula (1) is determined by the geometrical conditions of the experiments and by the neutron density distribution in a plane perpendicular to the beam axis.

In order to perform the calculations (which involved numerical integration) the operating volume of the beam was divided into 900 long parallelepipeds directed along the beam, each of which had a square cross section of 0.3×0.3 cm^2.

The number of decay protons striking the entrance window of the focussing system from the i^{th} parallelepiped is proportional to the product $P_i L_i$, where P_i is the neutron density in the i^{th} element and L_i is its geometrical "weight".

The total number of protons entering the counter from the whole volume of the beam is proportional to $\sum P_i L_i$. The ratio of this quantity to $\sum P_i$ yields

$$K = \frac{\sum P_i L_i}{\sum P_i}.$$

The "weights" L_i which depend only on geometrical conditions of the experiment were determined by an electronic computer.

The neutron density distribution was determined by activating a gold foil. For this purpose the foil was cut into 900 squares corresponding to the cross sections of the volume elements employed in the numerical integration and the specific activity of each of them (which is proportional to P_i) was determined. Fig. 3 illustrates the neutron density distribution in the beam.

Coefficient K was determined with the aid of a digital computer and found to equal $K = 7.87 \times 10^{-3}$ cm.

The magnitude of K weakly depends on the shape of the density distribution. Thus for a density distribution corresponding to a uniform beam with a

slightly smaller diameter ($\approx$ 70 mm) the value $K = 7.84 \times 10^{-3}$ cm was obtained. The error in the computation of K mainly depended on the accuracy with which the geometry of the apparatus was known and did not exceed several tenths of a per cent.

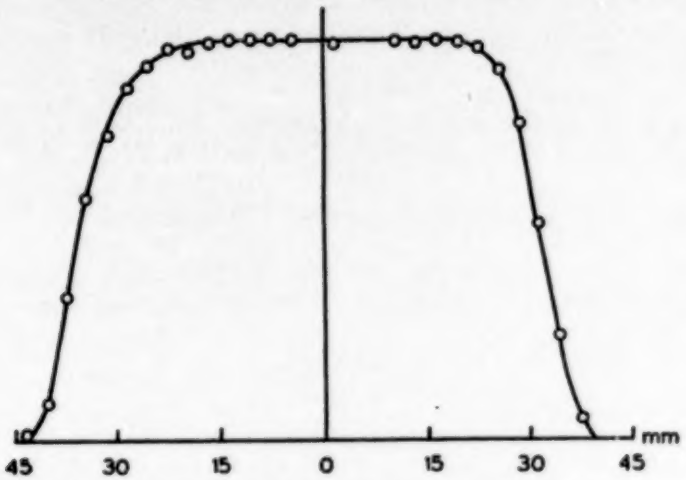

Fig. 3. Distribution of neutron density over beam cross section.

6. Results of the Measurements

By inserting the values of I, N_p and K in expression (1) the following value for the neutron half-period is obtained:

$$T = (11.7 \pm 0.3) \text{ min } \dagger.$$

Thus the reduced life-time of the neutron turns out to be $ft = 1180 \pm 40$ ††.

The value usually cited in the literature for tritium is $ft = 1060 \pm 40$ [9]. From a recent measurement of the mass difference between H^3 and He^3 the value $ft = 1132 \pm 40$ [10]) can be derived for tritium. Thus the ft-values for the neutron and tritium turn out to be almost equal. From the relation between ft and the ratio of the constants g_{GT} and g_F one can obtain, by comparing the ft-values for the neutron and O^{14} ($ft = 3103 \pm 62$ [11])), the value

$$\frac{g_{GT}^2}{g_F^2} = 1.42 \pm 0.08.$$

The authors are grateful to Academician I. V. Kurchatov for attention and continuous interest in this work. We are thankful to the members of the mathematical group, M. R. Shura-Bura, E. S. Kuznetsov and their colleagues, I. G. Krutikova, V. N. Toroptseva and O. B. Moskalev for performing the calculations on the computing machine. Thanks are also due to the operating crew of the RFT reactor.

† Here, as in all other cases, the mean square error is presented.

†† The value of f was computed on the basis of the tables of B. S. Dželepow and L. N. Zyrianova [8]).

References

1) A. H. Snell, F. Pleasonton and R. V. McCord, Phys. Rev. **78** (1950) 310
2) I. M. Robson, Phys. Rev. **78** (1950) 311
3) I. M. Robson, Phys. Rev. **83** (1951) 349
4) A. N. Sosnovsky and P. E. Spivak, Physical Investigations (Reports of Soviet Delegation at International Conference on the Peaceful Uses of Atomic Energy (Izd. Akad. Nauk SSSR. 1955) p. 235
5) I. M. Robson, Phys. Rev. **100** (1955) 933
6) S. P. Harris, C. O. Mülhause and G. E. Thomas, Phys. Rev. **79** (1950) 11
7) D. T. Hughes and J. A. Harvey, Neutron Cross Sections (McGraw-Hill Book Company, 1955)
8) B. S. Dželepow and L. N. Zyrianova, Effect of Atomic Electric Field on Beta Decay (Izd. Akad. Nauk SSSR)
9) O. Kofoed-Hansen and A. Winther, Mat. Fys. Medd. Dan. Vid. Selsk. **30** (1950) no. 20
10) M. Goldhaber, Report at the 1958 Annual International Conference on High Energy Physics at CERN
11) J. B. Gerhard, Phys. Rev. **109** (1958) 897

1.E.1: 3.A

Nuclear Physics **10** (1959) 405—411; © *North-Holland Publishing Co., Amsterdam*

Not to be reproduced by photoprint or microfilm without written permission from the publisher

Co^{57} DECAY SCHEME

J. M. FERGUSON †

Radioactivity Center, Department of Physics, Massachusetts Institute of Technology, Cambridge, Massachusetts ††

Received 3 December 1958

Abstract: The weak gamma radiations from Co^{57} were studied. In addition to the well known 14, 123, and 137 keV gamma rays, a 708 keV gamma ray was observed, having an intensity of 2×10^{-3} gamma rays per disintegration. No annihilation radiation was observed; an upper limit of 5×10^{-4} can be put on the number of positons per disintegration. There was no evidence for any other gamma rays. Although peaks appear in the pulse-height spectrum at 100 keV and 30 keV, they can be accounted for by scattering and X-ray escape effects in the scintillator.

1. Introduction

Although the important features of the Co^{57} decay scheme have been known for some time [1]), there are still conflicting results for the less intense

TABLE 1

		Crasemann and Manley [2])	Cork, Brice and Schmid [3])	This paper
β^+ relative intensity		none observed	very weak	$\leqq 5\times10^{-4}$
Gamma Rays (energies in keV)	1	14	14.6	14
	2	123	122.8	123
	3	137	137.5	137
	4	(no other γ's observed from 50 to 800 keV)	29	(neither 29 keV nor 100 keV gamma rays were observed)
	5		100	
	6		700	708

radiations emitted in the decay. Table 1 [1,2,3]) summarizes some of these results. It was decided to reinvestigate the gamma-ray spectrum with scintillation spectrometers.

† Now at U.S. Naval Radiological Defense Laboratory, San Francisco 24, California.

†† The work reported herein is supported in part by the U.S. Atomic Energy Commission, Division of Biology and Medicine, under Contract No. AT(30—1)—952.

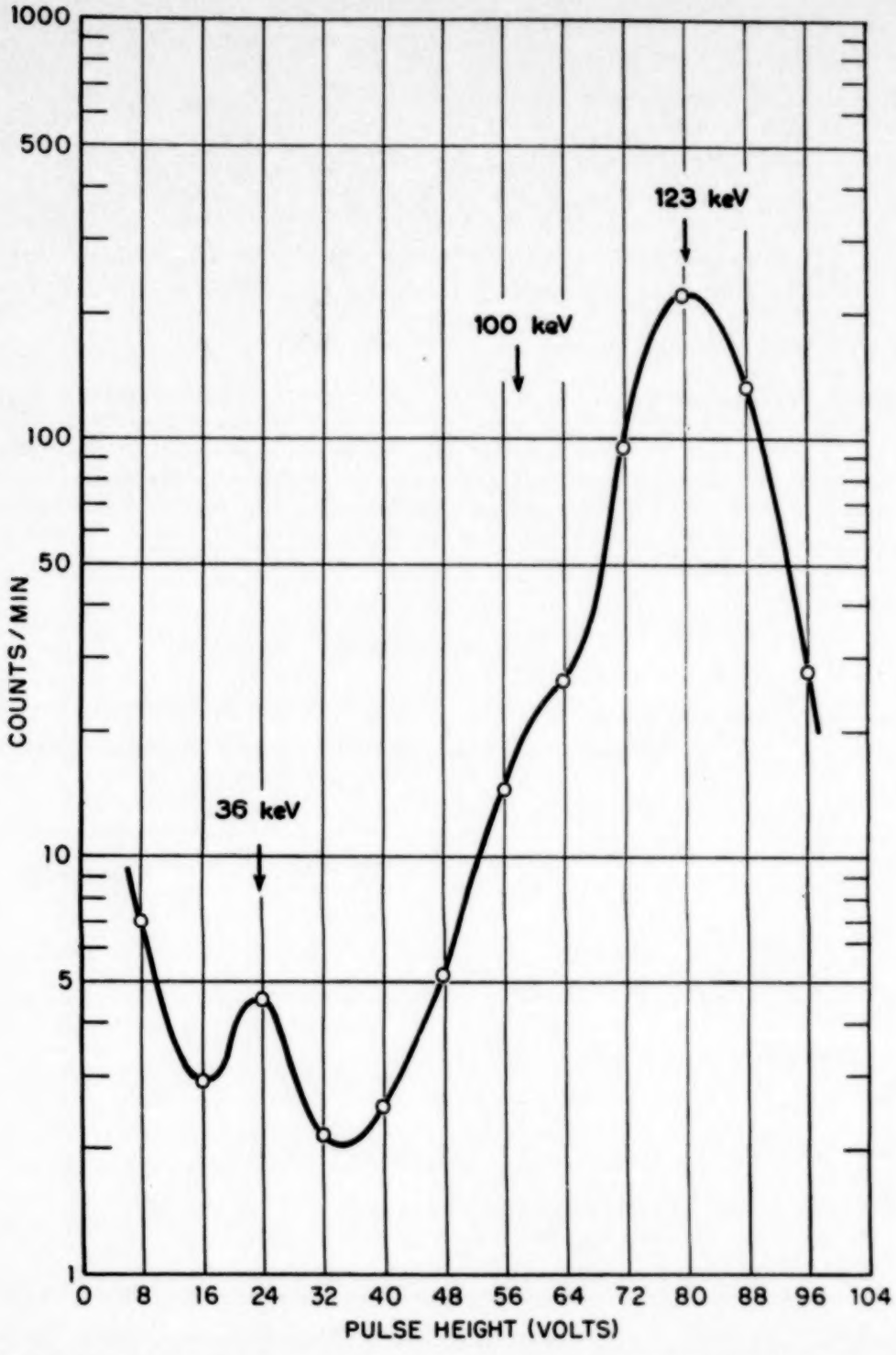

Fig. 1. Low energy gamma-ray pulse-height distribution taken with a $2 \times 2''$ NaI(Tl) crystal. The peaks are interpreted as follows: The 123 keV peak is a photopeak from the 123 keV gamma ray. The bulge at about 100 keV is due to the escape of an iodine K X-ray from the crystal after the photoelectric absorption of a 123 keV gamma ray. The peak at about 36 keV is due to Compton collisions of 123 keV gamma rays, with the subsequent escape of the scattered photon. In this particular distribution the 14 keV photopeak is not resolved. However, it can be resolved using this crystal with the proper gain setting and window setting.

2. Experimental Procedure and Results

The main part of this work was done at the MIT Radioactivity Center. The source used in that work was produced during α-bombardment of a nickel target. Fast neutrons from (α, n) reactions produce Ni^{57} from (n, 2n) reactions. Ni^{57} decays to Co^{57} with a 36 hour half period. The half period of Co^{57} is about 270 days. The advantage of this method of production is that virtually no Co^{56} is produced. After the bombardment in the cobalt was chemically separated from the nickel target. The source was used 9 months later, when the 71-day Co^{58} had decayed to a small value.

The gamma-ray spectrum of this source was investigated using a $2\times2''$ NaI(Tl) crystal and a CsI crystal with a thickness of about 50 mils.

The low energy pulse-height spectrum taken with the $2\times2''$ NaI(Tl) crystal is shown in fig. 1. Peaks appear at 36 and 123 keV. There is a bulge in the 100 keV region. The 14 keV peak is not resolved. The 100 keV bulge may be interpreted as due to the escape of the iodine K X-ray from the crystal after the 123 keV photon is absorbed. Since the entire 100 keV hump can be accounted for as an escape peak, there is no evidence for a 100 keV gamma ray. The peak at 36 keV may be accounted for as Compton absorption of the 123 keV gamma ray. The maximum energy left in the crystal in a single Compton collision is 40 keV, and the relative intensities of the 123 keV and 36 keV peaks have about the magnitudes expected for the Compton to total absorption ratio. The same spectrum was run with a series of absorbers between the source and the crystal. It was found that the intensity of the 36 keV peak stayed at a constant ratio to the 123 keV peak, even for the case where a 36 keV gamma ray should be attenuated by a factor of two relative to the 123 keV gamma ray.

The low energy gamma-ray activity from this source was also studied with an argon-methane proportional counter. The 14 keV photopeak was observed with a resolution of 20 percent. A search for a peak in the 30 keV region was made, but none was observed. From these data an upper limit of 0.01 30-keV gamma rays per disintegration was established.

Pulse-height spectra in the 400—1000 keV region are shown in fig. 2. These spectra were taken 150 days apart. The 800 and 500 keV peaks are due to Co^{58} activity, indicating that the 700 keV gamma ray is from a nucleide with a half period long compared to the 72 day Co^{58} half period. Since Co^{57} and Co^{60} are the only cobalt isotopes with half periods longer than 77 days, the 700 keV gamma ray must be attributed to Co^{57}. The relative intensity of this gamma ray is estimated to be 0.002 700-keV gamma rays per disintegration.

A run was made to establish whether or not the 700 keV gamma ray is in coincidence with any of the other gamma rays. One channel of the coinci-

dence unit was set to count all pulses in the 700 keV region in a 2×2″ NaI(Tl) crystal, and the other channel scanned the differential pulse-height spectrum from 10 to 200 keV in a thin CsI crystal. The counting rate over the entire region can be accounted for by chance coincidences. However, the expected ratio of true to chance coincidences is too low to positively establish a lack of true coincidences.

As a further check on the existence of the 700 keV gamma ray, another Co^{57} source has been investigated using a 4×4″ NaI(Tl) crystal and 100 channel pulse-height analyzer at the U.S. Naval Radiological Defense

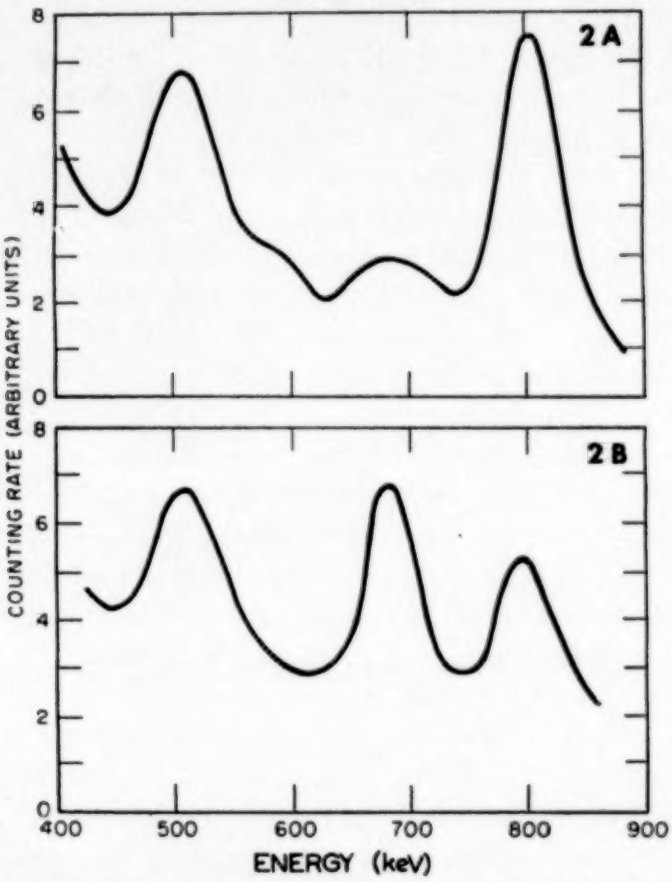

Fig. 2. Pulse-height distribution in the 400—1000 keV region, taken with a 2×2″ NaI(Tl) crystal. Both spectra were taken using the same source, but the spectrum in 2B was taken 5 months after the one in 2A. The two prominent peaks in 2A are from the 800 keV gamma rays with 411 keV annihilation radiation of Co^{58}. It is seen that a third peak at about 700 keV appears in the later run. This indicates that a longer-lived isotope with a 700 keV gamma ray is present in the source. The 511 keV peak appears to be relatively higher in 2B because it is sitting on the Compton edge of the 700 keV pulse-height distribution.

Laboratory. The source was very kindly loaned to the author by Dr. B. Crasemann of the University of Oregon. This source was produced by proton bombardment of nickel in 1954 [3]). Since the measurement was made in 1958, the small amounts of Co^{56} and Co^{58} originally present have decayed through about 15 half lives. The spectrum in the 700 keV region is shown in fig. 3.

It is seen that the 700-keV gamma ray is present in this source also. The measured relative intensity agrees with that quoted above within the limits of experimental error. The energy of the gamma ray, estimated from these data, is 708 ± 20 keV.

An upper limit on the number of positons per disintegration may be established from the lack of an annihilation radiation peak in the pulse-height spectrum of fig. 3. The upper limit is 5×10^{-4} positons per disintegration.

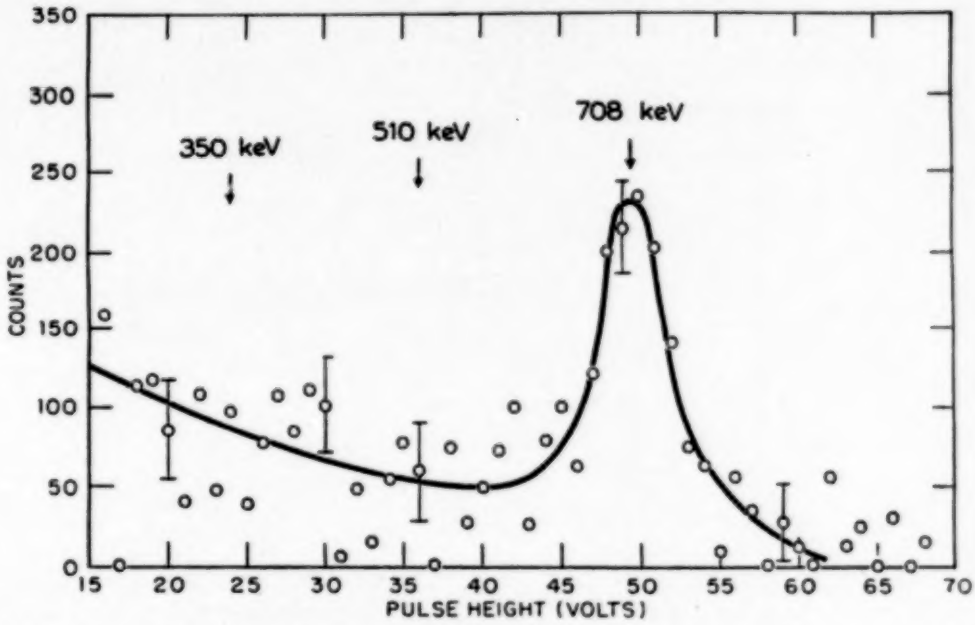

Fig. 3. The gamma-ray pulse-height distribution in the 200—900 keV region, taken with $4 \times 4''$ NaI(Tl) crystal and a 100 channel analyzer. This spectrum was taken with a different source from that used in fig. 2. No other cobalt isotopes are present in detectable amounts.

3. Discussion

The proposed decay scheme is shown in fig. 4. The lower energy radiations are of course well established. The only new feature is the 708 keV gamma ray. This gamma ray probably corresponds to the level in Fe^{57} at 705 ± 5 keV found by A. Sperduto using the (p, p') reaction [4]). Since our energy measurement has an assigned error of 20 keV, this gamma ray could be a transition either to the ground level or to the 14.4 keV level. Our energy value favors an assignment as a transition to the ground level. However, a gamma ray with an energy of 690 keV was observed in the decay of Mn^{57} by Cohen *et al.* [5]). This energy assignment favors a transition to the 14.4 keV level. Of course, the observed peak in the pulse-height spectrum may represent a mixture of gamma rays proceeding to both the 14.4 keV and ground levels.

Since there must be more than 700 keV available for the decay, it is

puzzling that a 350 keV gamma ray is not observed. G. F. Pieper and N. P. Heydenburg [6]) have observed a level in Fe^{57} at 365 keV by Coulomb excitation. This level decays principally to the 14 keV first excited level. The 365 keV level is assigned a character of $\frac{5}{2}^-$. Since the ground level of Co^{57} has a character of $\frac{7}{2}^-$ [1]), the transition to the 365 keV level should be

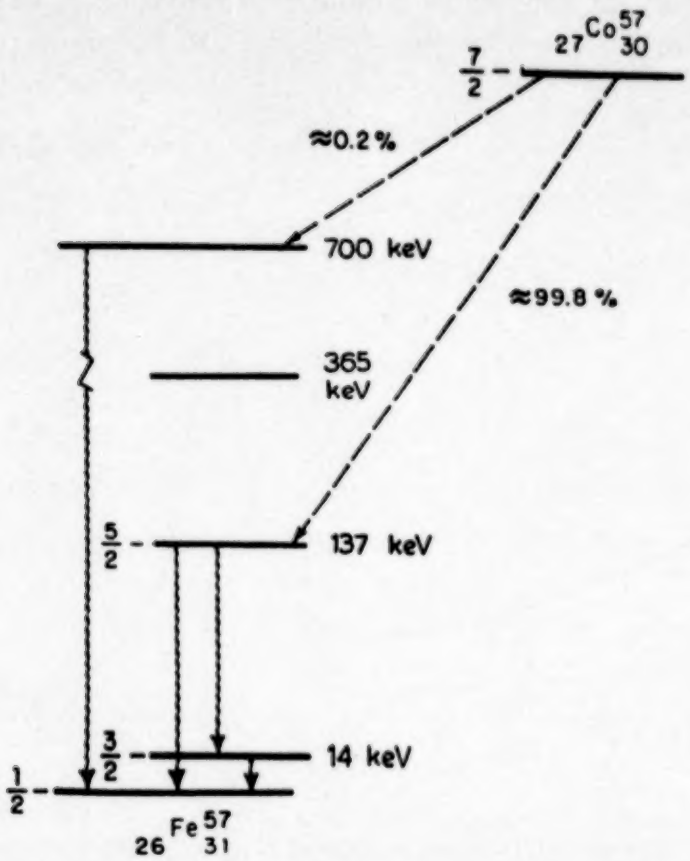

Fig. 4. Proposed Co^{57} decay scheme. The energies and angular momentum assignments for the ground levels of Co^{57} and Fe^{57} and the first two excited levels of Fe^{57} are taken from earlier work [1]). The 700 keV gamma ray is assigned as a direct transition to the ground level, although this has not been positively established. No gamma rays from a 365 keV level are observed. The upper limits on other radiations are as follows: positons, 5×10^{-4} per decay; 29 keV gamma rays, < 0.01 per decay; 100 keV gamma rays, < 0.03 per decay; 350 keV gamma rays, $< 3 \times 10^{-3}$ per decay.

allowed, and should be more intense than a transition to a level at 700 keV. The results presented here indicate that the character of the 365 keV level may be $\frac{3}{2}^-$ rather than $\frac{5}{2}^-$.

Thanks are due to the staff of the Radioactivity Center of the Massachusetts Institute of Technology, where most of this work was done, and also to the staff of the Nuclear Radiation Branch of the U.S. Naval Radiological Defense Laboratory, where the rest of the work was done. The author would particularly like to thank Professor Robley D. Evans of MIT and Dr. C. Sharp Cook of NRDL.

References

1) D. Strominger, Nuclear Level Schemes, TID-5300, June 1955;
J. M. Hollander and G. T. Seaborg, Revs. Mod. Phys. **30** (1958) 585
2) B. Crasemann and D. L. Manley, Phys. Rev. **98** (1955) 66
3) J. M. Cork, M. K. Brice and L. C. Schmid, Phys. Rev. **99** (1955) 703
4) A. Sperduto, MIT Lab. for Nuclear Science Progress Report (November 1957) p. 51
5) B. L. Cohen, R. A. Charpie, T. H. Handley and E. L. Olsen, Phys. Rev. **94** (1954) 953
6) C. F. Pieper and N. P. Heydenburg, Phys. Rev. **107** (1957) 1300

3.A *Nuclear Physics* **10** (1959) 412—417; © *North-Holland Publishing Co., Amsterdam*
Not to be reproduced by photoprint or microfilm without written permission from the publisher

GAMMA-GAMMA ANGULAR CORRELATIONS IN Tm^{169}

S. KOIČKI, J. SIMIĆ and A. KUKOČ
Institute of Nuclear Sciences "Boris Kidrič", Beograd, Yugoslavia

Received 29 December 1958

Abstract: The gamma-gamma angular correlations in Tm^{169} have been measured. It was found that both K-forbidden transitions of 177 and 198 keV are mixtures of M1 and E2 multipoles. The magnitudes and the interference signs of these mixtures have been determined.

1. Introduction

Fig. 1. presents the generally adopted part of the level diagram of Tm^{169}, including the $K = \frac{1}{2}$ rotational family and the first excited $\frac{7}{2}+$ ($K = \frac{7}{2}$) proton state [1-6]). The decay of this state occurs through three competing transitions, which are all strongly K-forbidden. The transition of 308 keV was definitely found to be of pure E2 type, but the existing multipolarity data about the 177 and 198 keV transitions are quite inconsistent [1-6]).

In this work we have measured the gamma-gamma angular correlations of the cascades lying below the metastable level at 316 keV, and from these measurements we have obtained informations about the M1—E2 mixing ratios of the 177 and 198 keV transitions.

For these measurements we used a conventional fast-slow coincidence system of two scintillation spectrometers, consisting of selected elements. Fig. 2 shows the spectra (below 200 keV), obtained in each of the detectors. In channel combinations a—e and c—d, the 198—110 and 177—131 keV cascades respectively were measured. The mutual purity of these cascades has been verified by measuring the coincidence counting rate in combination c—e, which was less than two percent of the rate in combination c—d (in d— there is the same counting rate as in e—).

The measurements were performed with a diluted solution of active $YbCl_3$ in HCl.

2. Results

2.1. 177—131 keV CASCADE

After correcting for finite angular resolution of the detectors, we obtained the following correlation:

$$W(\theta) = 1 + (0.269 \pm 0.003)\ P_2(\cos\theta) + (0.02 \pm 0.005)\ P_4(\cos\theta).$$

In fig. 3 the experimental coefficients are compared with the calculated values. Agreement exists when $\delta > 0$ and for $\delta = 0.255$ and $\delta = 0.66$. However, the value of A_4 clearly favours $\delta = 0.255$, which is also consistent with most of the conversion-electron data [2,3]).

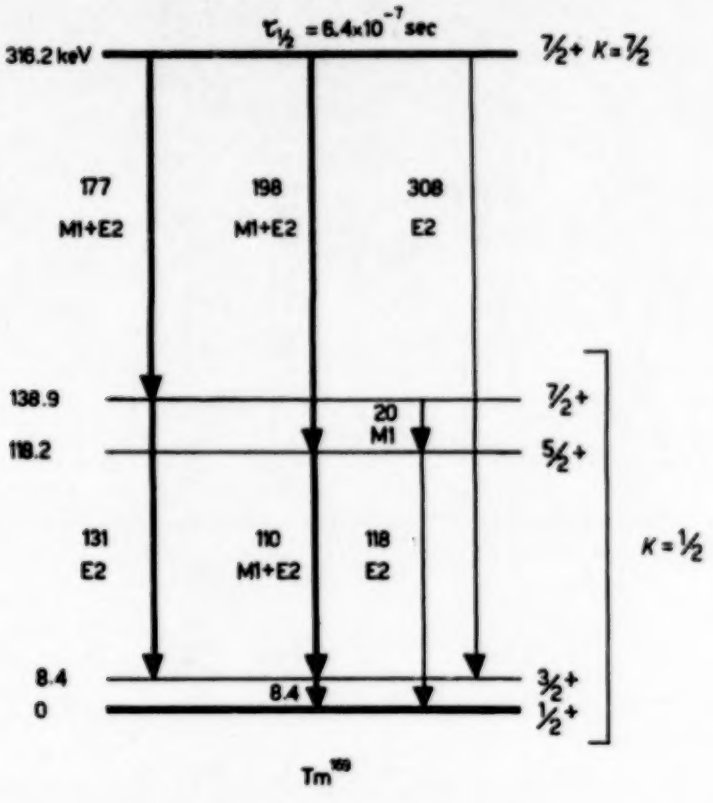

Fig. 1. Part of the level diagram of Tm^{169} (below the 0.64 μsec metastable state).

2.2. 198—110 keV CASCADE

After the correction for finite angular resolution was made, the following correlation was obtained:

$$W(\theta) = 1+(0.314\pm0.003)\ P_2(\cos\theta)-(0.003\pm0.005)\ P_4(\cos\theta).$$

From fig. 4 it can be seen that the agreement exists for $\delta_1 > 0$ and $\delta_2 \leqq 0$. The $\delta_1^2-\delta_2^2$ dependence, derived from the curves of fig. 4 and the measured value of A_2, is shown in fig. 5.

Both theoretical and experimental values of A_4 are very small and are therefore of little use in determination of the mixing ratio.

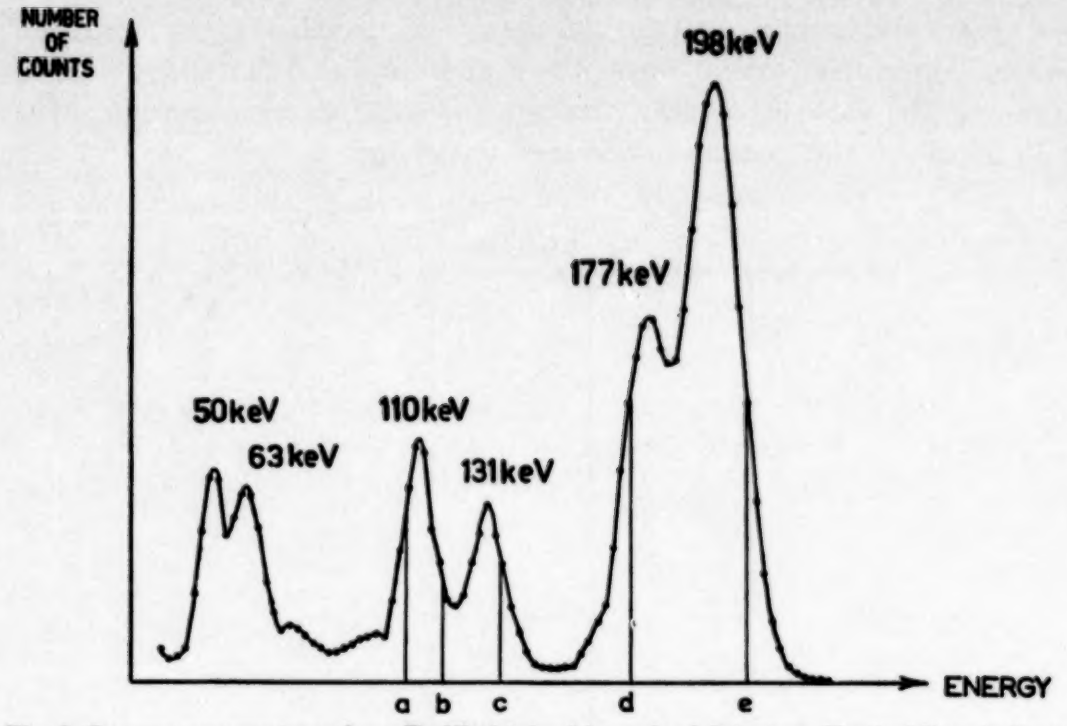

Fig. 2. Gamma-ray spectrum from Tm^{169} obtained in each of detectors. Vertical lines indicate the channel positions, but not their width.

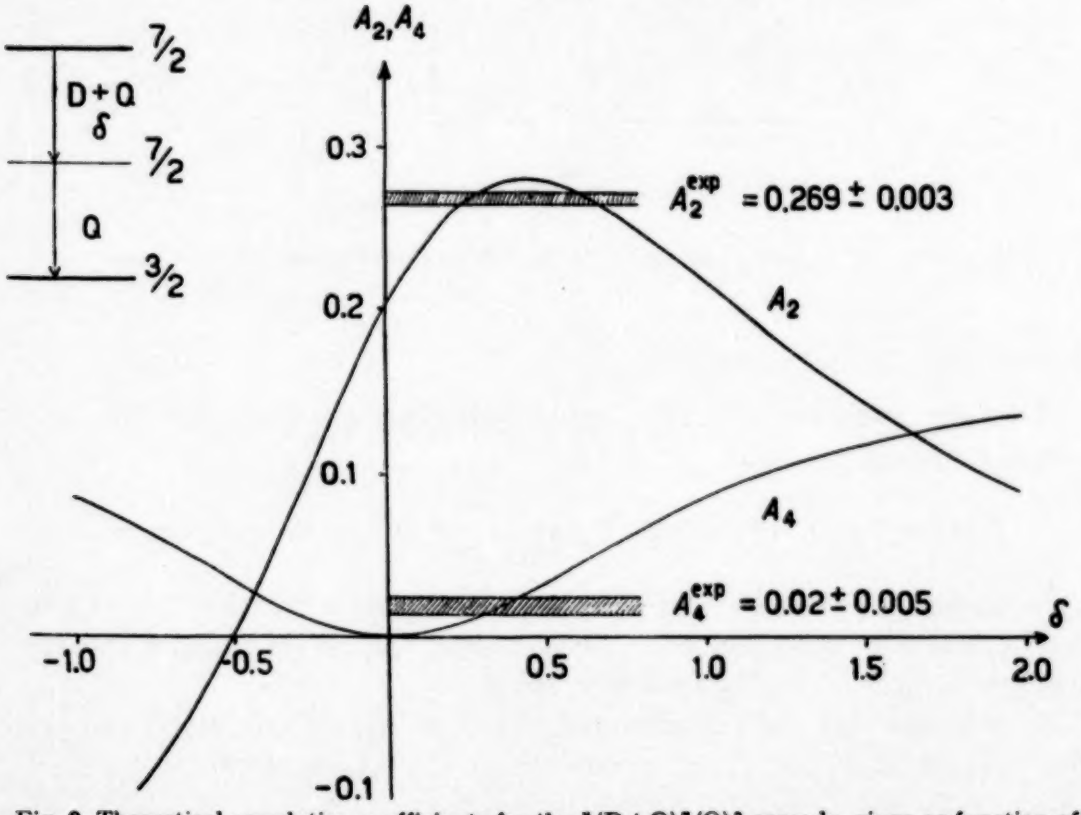

Fig. 3. Theoretical correlation coefficients for the $\frac{7}{2}(D+Q)\frac{7}{2}(Q)\frac{3}{2}$ cascade, given as function of δ. The shadowed area represents the measured values of A_2 and A_4 including errors of measurement.

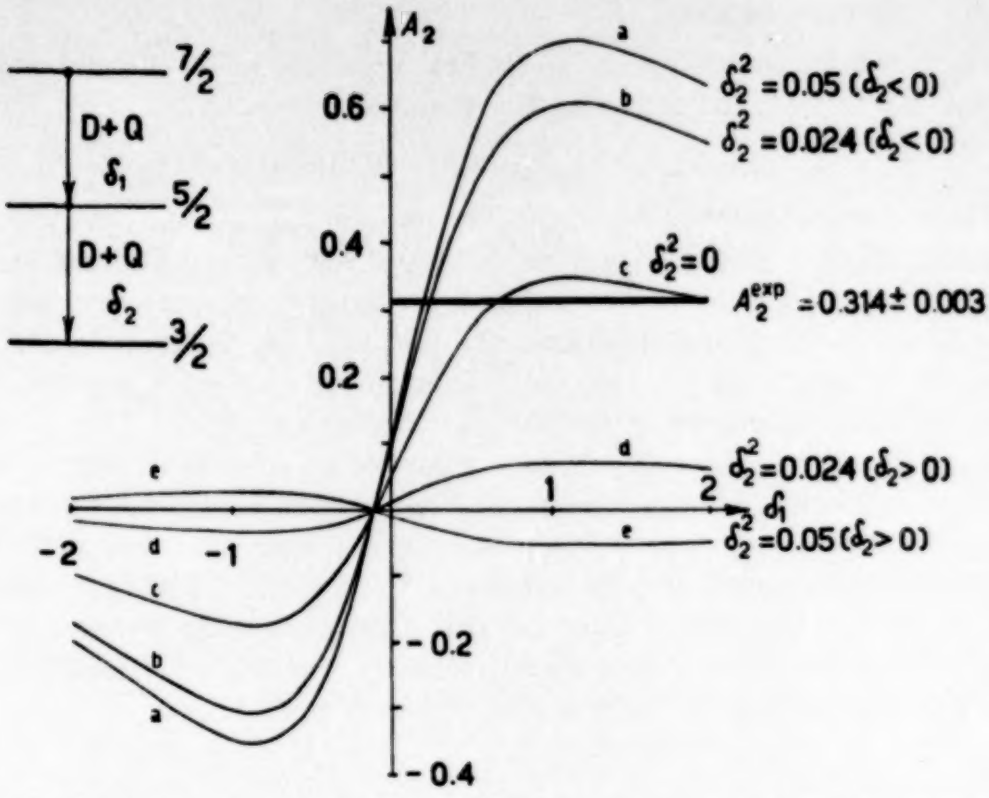

Fig. 4. Theoretical values of A_2 for the $\frac{7}{2}(D+Q)\frac{5}{2}(D+Q)\frac{3}{2}$ cascade, as function of δ_1 and δ_2^2. The full line represents the measured value of A_2, including errors of measurement.

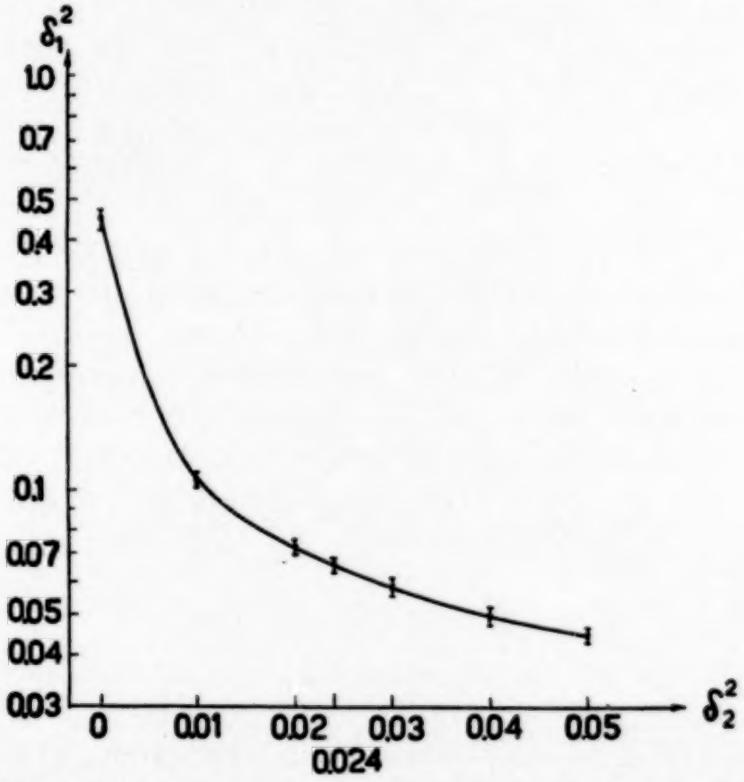

Fig. 5. The δ_1^2—δ_2^2 dependence for the 198—110 keV cascade, deduced from fig. 4.

2.3. 177—110 keV CASCADE

The first-third correlation, 177—110 keV, measured in the channel combination a—d, gives the following function:

$$W(\theta) = 1-(0.105\pm0.002)\ P_2(\cos\theta)-(0.016\pm0.004)\ P_4(\cos\theta).$$

The theoretical value of $A_2 = -0.356$ is obtained by use of $\delta_1 = 0.255$ for the first, $\delta_2 = 0$ for the second and $\delta_3 = -0.155$ for the third transition. Such a high value was not obtained from the experiment, but the deviation may be well understood if small amounts (only about 10 %) of adjacent lines in energy channels are present. These lines are very effective in producing large positive anisotropies.

Our correlation measurements give a particular value of mixing for the 177 keV transition, but only the $\delta_1^2-\delta_2^2$ dependence for the 198—110 keV cascade. However, a value of δ_2^2 may be calculated from rotational transition probabilities and gamma-ray intensity data [2]). As Mihelich *et al.* [3]) confirmed this value on the basis of their internal-conversion data, we have taken that $\delta_2^2 = 0.024$ is the correct mixing ratio for the 110 keV transition. In this case we obtained the mixtures as shown in table 1.

TABLE 1

E (keV)	δ	δ^2	Mixture
198	0.257 ± 0.006	0.066 ± 0.003	M1+(6.2±0.26) % E2
177	0.255 ± 0.025	0.065 ± 0.013	M1+(6.1±1.1) % E2
110	-0.155	0.024	M1+2.3 % E2

There is evidently great similarity between the transitions of 198 and 177 keV; the mixing ratios are, in the limit of experimental error, the same and the multipole interference signs are in both cases positive.

The metastable level $\frac{7}{2}+$ ($K = \frac{7}{2}$), at 316 keV, is depopulated by one M1 and one E2 family of radiations. The intensities of particular multipole components in both families tend to follow the simple energy dependence

$$I_{177}^{E2} : I_{198}^{E2} : I_{308}^{E2} = (177)^5 : 0.96 \cdot (198)^5 : 0.6 \cdot (308)^5$$

for E2 transitions and

$$I_{177}^{M1} : I_{198}^{M1} = (177)^3 : 1.18 \cdot (198)^3$$

for M1 transitions, where the coefficients indicate the departure from this dependence.

The E2 family of radiations is retarded to a lesser extent, which is consistent with the fact that their K-forbiddenness factor is one unit less than that

of M1 radiations. For both 177 and 198 keV transitions, the E2 components are less retarded by a factor of 3.5×10^2 than the corresponding M1 components.

A fuller account of this work will be published in the Bulletin of this Institute.

We are indebted to Prof. P. Savić for his interest in this work and to Mrs. A. Mijatović, Dr. G. Alaga and Dr. T. Novakov for valuable discussions.

References

1) J. M. Cork, M. K. Brice, D. V. Martin, L. C. Schmid and R. G. Helmer, Phys. Rev. **101** (1956) 1042
2) E. N. Hatch, F. Boehm, P. Marmier and J. W. M. DuMond, Phys. Rev. **104** (1956) 745
3) J. W. Mihelich, T. J. Ward and K. P. Jakob, Phys. Rev. **103** (1956) 1285
4) S. A. Baranov, R. M. Polevoj, Y. F. Rodionov and G. V. Shishkin, Atomnaya Energiya **9** (1957) 256
5) U. Cappeler and R. Klingelhofer, Z. für Physik **150** (1958) 375
6) K. Y. Gromov, B. S. Dželepow and B. K. Preobrazensky, Izv. Akad. Nauk URSS, Ser. Fiz. **22** (1958) 775

1.D.1:
2.A.1

Nuclear Physics **10** (1959) 418—422; © *North-Holland Publishing Co., Amsterdam*
Not to be reproduced by photoprint or microfilm without written permission from the publisher

(n, p) CROSS SECTIONS NEAR $Z = 50$

H. P. EUBANK, R. A. PECK, Jr. and M. R. ZATZICK

Brown University, Providence, R. I. †

Received 12 January 1959

Abstract: Forward differential (n, p) cross sections have been measured with a proportional counter-scintillation counter telescope for 14.1 MeV neutrons on the following nuclei: $_{45}Rh^{103}$, $_{47}Ag$ (natural), $_{48}Cd$ (natural), $_{49}In^{115}$, $_{50}Sn^{116}$, $_{50}Sn^{120}$, $_{51}Sb$ (natural) and $_{52}Te$ (natural). The measurements were made with an angular spread of about $\pm$ 15° and cover the proton energy range 4 MeV to 15 MeV. A decrease in differential cross section occurs with increasing Z reaching a minimum at $Z = 50$ of about 1 mb/s, thereafter rising abruptly at $Z = 51$ to 40 mb/s. At $Z = 52$, the cross section is again about 1 mb/s.

1. Introduction

Hughes and Sherman [1]) have noted a pronounced effect on neutron capture cross sections near $N = 50$, consequently, it was thought of interest to explore the effect of shell closure at $Z = 50$ upon (n, p) cross sections for 14.1 MeV neutrons to determine whether or not a similar behaviour exists.

2. Experimental

Neutrons of 14.1 MeV were produced by deuteron bombardment (175 keV) of tritiated zirconium films using a Cockcroft-Walton accelerator. Total neutron flux is measured with a BF_3 "long counter" arrangement which is compared with a standard polyethylene radiator employed with the counter telescope.

The proton detection system consists of two proportional counters and a 1 inch diameter by 1 mm thick cesium-iodide scintillator housed in a 4 inch diameter vacuum chamber. Argon + 5 % carbon dioxide at 1/10 atmosphere is employed as the counting gas. The cesium iodide crystal is bonded to a lucite cone with R313 Cement ††, the lucite forming the rear window to the counter chamber and coupling the scintillations to an RCA 6342, the output of which is fed, after suitable amplification and time delay, to a 20 channel analyzer. The front face of the crystal is covered with aluminized mylar or with magnesium oxide.

† Supported in part by the U.S. Atomic Energy Commission.
†† Carl H. Biggs Company, 2255 Barry Ave., Los Angeles 64, California.

The proportional counters serve to define the direction of the reaction protons and are employed in $\frac{1}{4}$ μ sec coincidence to generate a 2 μ sec gate for the pulse-height analyzer.

The geometry of the counting system is such that in relation to the neutron source there is an angular spread of about $\pm$ 15° at each angle of measurement. With a polyethylene radiator the energy resolution of the system is at best 12 %.

To detect protons at small angles with respect to the incident neutrons, it is necessary to use the counters in the primary flux without shielding. It is, therefore, not surprising that a severe background count is found, particularly at lower energies. The ratio of background to net count ranges from about 2 (as in the case of Sb) to values so large as to allow only the assignment of upper limits to cross sections (Sn^{116}, Sn^{122} and Te).

Above 5 MeV the purely accidental contribution to the background is negligible, the bulk arises apparently from the entrance window (0.0001 nickel foil), its support and the proportional counter cathodes. Both lead and graphite liners have been used for the wall of the vacuum container, the latter having such a large negative Q that protons are energetically impossible within the energy range of interest.

Targets of Rh, Ag, Cd, In and Sn were metallic foils 30 to 40 mg/cm², the two Sn samples were enriched to 98 %. Sb was evaporated onto lead backing to a thickness of 10 mg/cm² and Te powder was pressed into lead to about 40 mg/cm².

As a precaution against systematic uncertainties affecting absolute cross section the (n, p) reaction on $_{28}$Ni (natural) was examined for comparison with published results [2]): this reaction is also of significance in connection with the entrance window to the counter telescope. No analysis has been made of the Ni data beyond the desired comparison of cross section magnitude and energy variation, with which agreement is quite good.

3. Results

Figure 1 gives the proton yield as a function of energy for those cases in which the cross sections were sufficiently large to afford statistically significant results.

The 0° differential cross sections are tabulated in table 1. Only data on Rh is available for comparison, the comparable figures being 6 ± 1 mb/s for 9 MeV of excitation [3]), and 2.6 ± 0.6 mb/s for 7.5 MeV of excitation [2]), both consistent with the present observation.

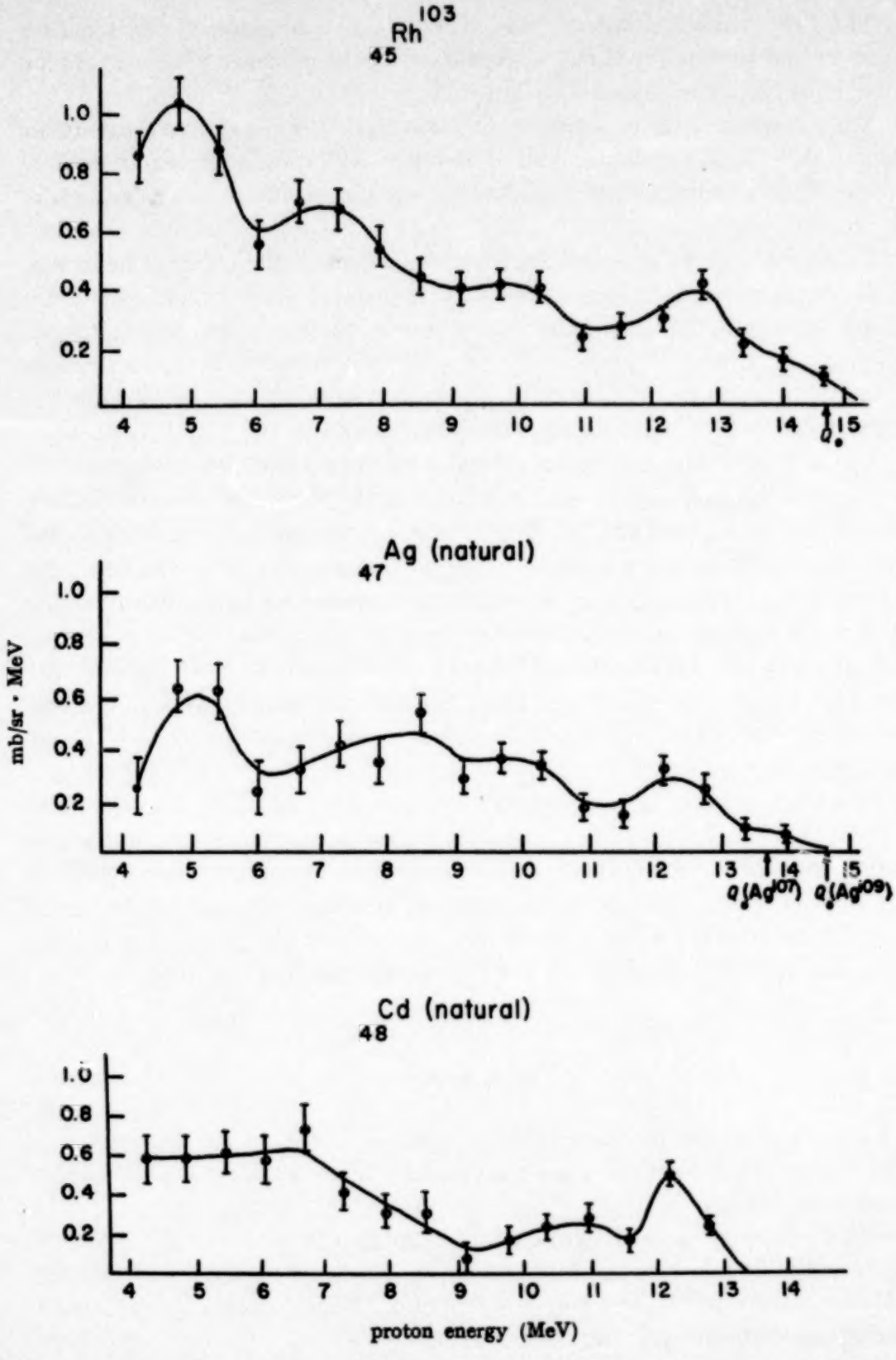

Fig. 1. Proton differential cross sections per MeV at 0°(±15° angular spread) as a function of excitation for those cases investigated in which the yield curve shape is statistically significant.

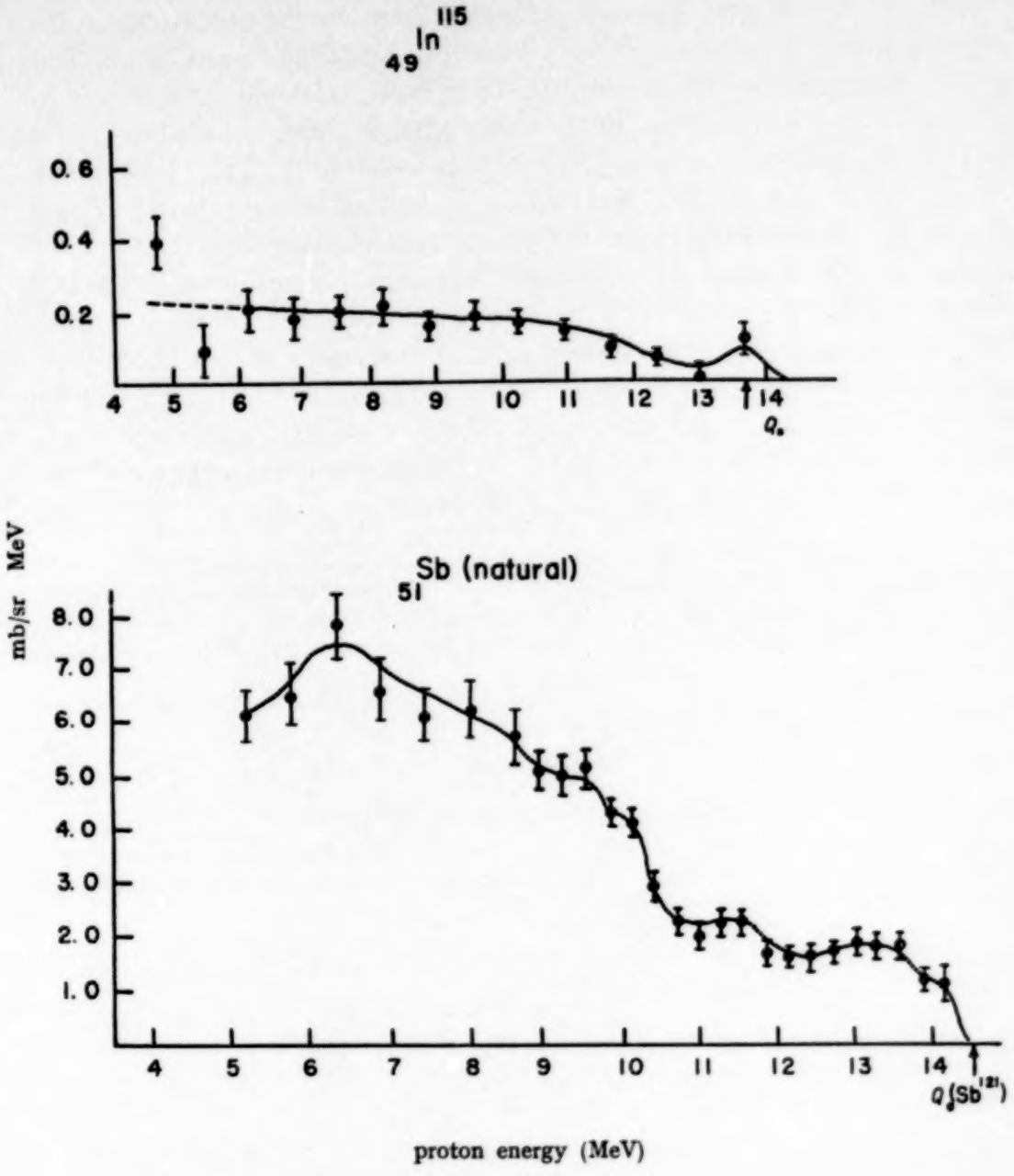

fig. 1 (continued)

TABLE 1

Proton differential cross sections at 0°(±15° angular spread)

Element	$_{45}$Rh	$_{47}$Ag	$_{48}$Cd	$_{49}$In	$_{50}$Sn^{116}	$_{50}$Sn^{120}	$_{51}$Sb	$_{52}$Te
σ(mb/steradian)	4.8±0.5	3.5±0.7	3.8±0.4	1.6±0.3	$<1^{+0}_{-1}$	$<1^{+0}_{-1}$	40±2	$<1^{+0}_{-1}$

Angular distributions have been obtained only in the case of Sb so far. These results will be presented at a later date with the results of emulsion studies of the angular distributions of Rh^{103}, In^{115}, Sn^{116} and Sn^{120}. It is quite clear that the yield, at least in the case of Sb, is strongly anisotropic, the yield at 60° is an order of magnitude less than that at 0°. From preliminary calculations it appears that the total cross section for Sb would be about 80 mb or a factor of 2 times the differential yield at 0° †.

The Sb cross section is a dramatic representation of the discontinuity expected with proton shell closure. The small value of cross section found for Te was surprising and suggests further measurements above $Z = 50$. Clearly, any attempt to account for these measurements must utilize level density formulae incorporating shell effects of which several are available [4, 5, 6]); the analysis of Rosenzweig seems most pertinent and predicts the large difference between Sb and Te as found.

† There is the chance of some significant deuteron contribution from Sb(n d)Sn since the Q values are only about −3.5 MeV and −4.7 MeV for Sb^{121} and Sb^{123}, respectively. However, upon lowering the voltage of the proportional counters to a value such that the counter unit is still deuteron sensitive but proton insensitive (4 MeV and greater) only about 10 % of the net count remains.

References

1) D. J. Hughes and D. Sherman, Phys. Rev. **78** (1950) 632 (L)
2) Verbinski, Hurlimann, Stephens and Winhold, Phys. Rev. **108** (1957) 799
3) Brown, Morrison, Muirhead and Morton, Phil. Mag. **2** (1957) 785 (see note included); L. Colli *et al.*, Nuovo Cimento **7** (1958) 400
4) Newton, Canad. J. Phys. **34** (1956) 804
5) C. Block, Phys. Rev. **93** (1954) 1094
6) Rosenzweig, Phys. Rev. **108** (1957) 817

2.1 *Nuclear Physics* **10** (1959) 423—428; © *North-Holland Publishing Co., Amsterdam*
Not to be reproduced by photoprint or microfilm without written permission from the publisher

PHOTONUCLEAR REACTIONS IN Pr^{141}

F. FERRERO, R. MALVANO and E. SILVA †
Istituto di Fisica dell'Università di Torino
Istituto Nazionale di Fisica Nucleare, Sez. di Torino,
J. GOLDEMBERG and G. MOSCATI
Universidade de S. Paulo

Received 16 January 1959

Abstract: The (γ, n) and $(\gamma, 2n)$ reactions in Pr^{141} have been studied up to 30 MeV by the method of residual activity. A comparison is made with the statistical theory of nuclear reactions finding a partial disagreement at high energies. The total photoabsorption cross section is evaluated and the integrated value is found to be greater than the theoretical predictions. The behaviour of the absorption cross section in the region above the giant resonance is discussed.

1. Introduction

Many experiments concerning $(\gamma, 2n)$ reactions have been carried out using the X-rays produced with electron accelerators, but only for F^{19} and Cu^{63} were the $(\gamma, 2n)$ excitation curves detected by means of the residual activity technique. The difficulty is to find elements that, irradiated with X-rays, present a residual activity of convenient half-life: actually this is the case of Pr^{141}. The Pr^{142} disturbing β^--activity (19.3 h half-life) that could be formed by neutron capture in Pr^{141}, is in our case avoided by counting the 0.51 MeV γ-rays from the β^+-annihilation: indeed, the $Pr^{141}(\gamma, n)Pr^{140}$ and $Pr^{141}(\gamma, 2n)Pr^{139}$ reactions give rise to β^+ residual activities of 3.4 min and 4.5 h respectively.

The evaluation of the $(\gamma, 2n)$ yield is usually made by subtracting the (γ, n) yield from the total neutron yield, measured by residual activity, and dividing the result by two. The difference between the two yields is in general very small in comparison with the total neutron yield: the $(\gamma, 2n)$ activation curve is therefore affected by much greater errors than the (γ, n) yield curve.

The $Pr^{141}(\gamma, 2n)Pr^{139}$ reaction is particularly interesting because Pr^{141} is magic in neutrons and in these cases it seems that an appreciable part of the absorption cross section is beyond the giant resonance. From this point of view one may clearly expect a rather strong $(\gamma, 2n)$ process. The independent

† Fellow of the National Council of Research of Brazil. On leave of absence from the University of S. Paolo, Brazil.

measurement of the two cross-sections, (γ, n) and (γ, 2n), allows us to build up the complete absorption cross section in the energy region beyond the giant resonance and to evaluate its integrated value.

2. Experimental Procedure

One gram powder samples of high purity (99.99 %) Pr_6O_{11} were irradiated by the X-ray beam of a 31 MeV Betatron. The distance of the sample from the internal target of the Betatron was as small as possible ($\approx$ 20 cm) in order to increase the incident dose.

The Pr_6O_{11} powder was enclosed in a small aluminium container which did not affect the measurements in view of the counting schedule. The activities were measured by detecting the 0.51 MeV annihilation radiation from the β^+-conversion in a convenient absorber placed around the samples. The NaI(Tl) well type (2″×2″) crystal was looked by a 6292 Dumont photomultiplier. A one channel pulse height analyser, set on the 0.51 MeV line, with a channel width of 10 %, allows only the annihilation radiation to be counted. The relative dose was measured by an aluminium ionization chamber and in the (γ, n) reaction measurement the electrometer was matched with a time constant equal to the mean life of Pr^{140}.

The two yield curves of the (γ, n) and (γ, 2n) processes were independently measured: the difference between the two half-lives is so great that one can obtain the best data for the short lived activity by irradiating the samples for a time comparable to the half-life with a consequent better evaluation of the effective dose. Although the samples contain oxygen, this does not appreciably affect the measurements because the oxygen activity will be a few per thousand of the total short lived praseodimium activity.

3. Results

In fig. 1 are plotted the yield curves for the two processes; the absolute value of the disintegrations/mole · 100r has been obtained by comparison with the (γ, n) activity in copper [1]); the ratio of the two activities, Pr^{140} and Pr^{139} was obtained in a single irradiation. The ratio $\beta^+/(\beta^+ + \text{E.C.})$ is 0.54 for Pr^{139} and 0.06 for Pr^{140} and has been taken into account [2,3]).

The $Pr^{141}(\gamma, 3n)Pr^{138}$ reaction (β^+, $T_{\frac{1}{2}} = 2$ h) has a threshold of approximately 24 MeV; this process, if important, could give an undesirable contribution very difficult to separate from the 4.5 h activity. In order to evaluate this contribution, we tried to separate it by analyzing the decay curves but we did not succeed to detect any appreciable distorsion of the 4.5 h half-life even at the maximum available energy. A trial to detect the 0.8 and 1.05 MeV γ-rays belonging to Pr^{138} [4]) also failed. These measurements prove that

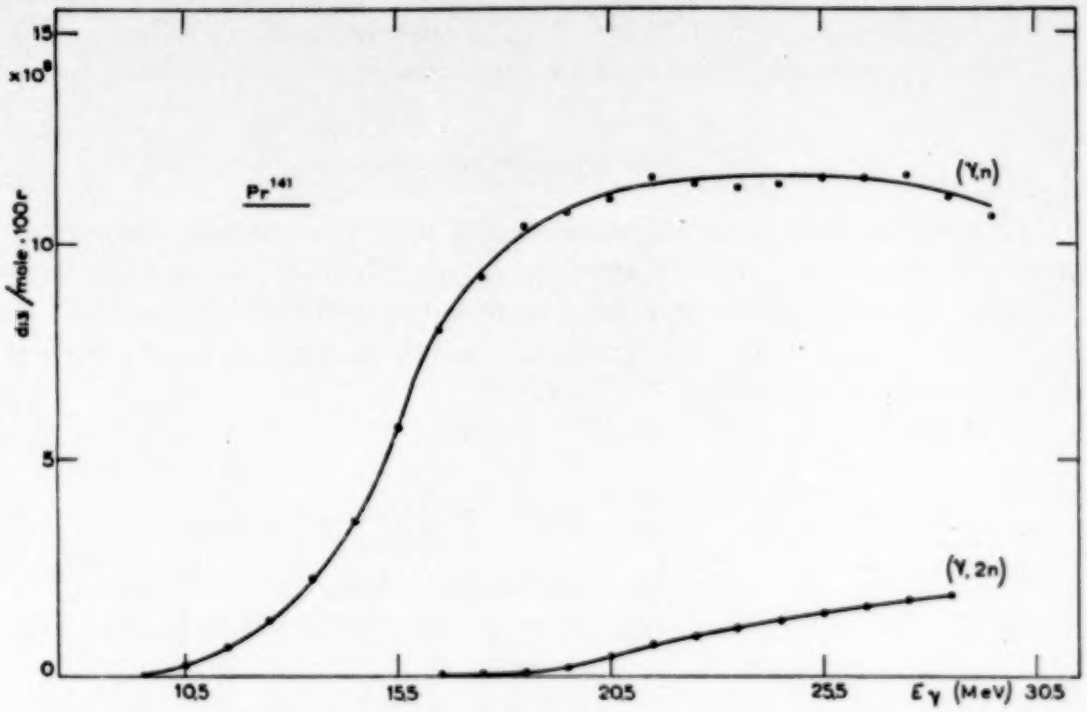

Fig. 1. Excitation functions for $Pr^{141}(\gamma, n)Pr^{140}$ and $Pr^{141}(\gamma, 2n)Pr^{139}$ reactions.

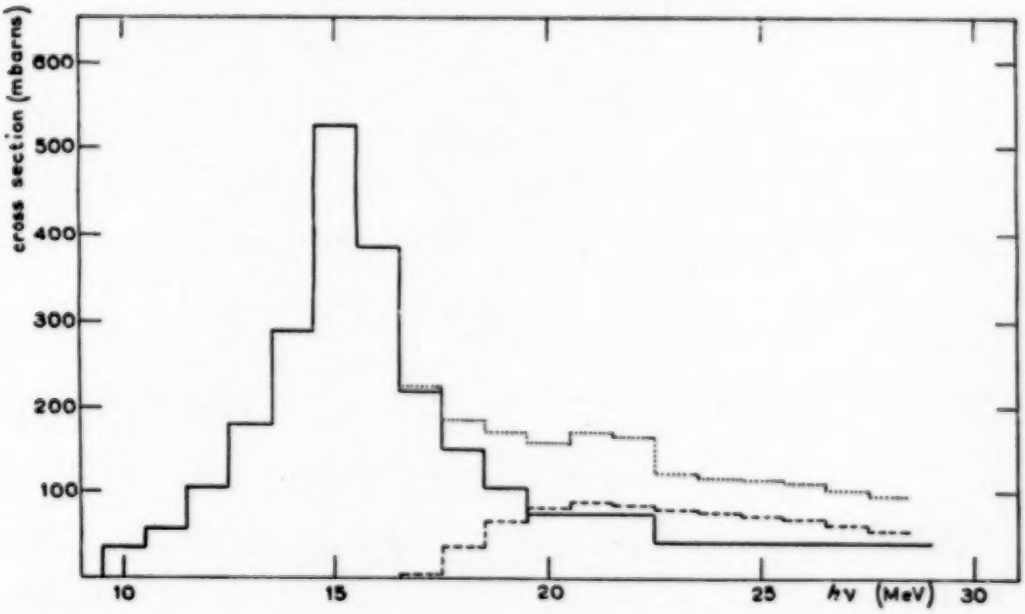

Fig. 2. Cross sections versus energy:
——— $Pr^{141}(\gamma, n)Pr^{140}$;
– – – – – – $Pr^{141}(\gamma, 2n)Pr^{140}$;
. . . . . sum of the two above processes.

the (γ, 3n) contribution, if it exists at these energies, is extremely small.

The Penfold-Leiss method [5]) was used to analyze the two yield curves of fig. 1 and the obtained cross sections are shown in fig. 2 †.

4. Discussion

The possibility to compare these results with the statistical model of nuclear reactions is quite good, since the (γ, n) and the (γ, 2n) reactions are probably the only important processes from 16 to 30 MeV, because of the high Coulomb barrier for proton emission and of the experimental evidence on the weakness of the (γ, 3n) reaction.

Following Blatt and Weisskopf [6]) we have

$$\frac{\sigma(\gamma, 2n)}{\sigma(\gamma, n)+\sigma(\gamma, 2n)} = 1-\left(1+\frac{\varepsilon_c}{\Theta}\right)\exp\left(-\frac{\varepsilon_c}{\Theta}\right)$$

where ε_c is the excess energy over the threshold of the (γ, 2n) reaction (16.5 MeV); $\Theta = (E'/a)^{\frac{1}{2}}$ is the temperature of the intermediate nucleus Pr^{140}; E' is the excess energy over the (γ, n) threshold (9.5 MeV) and a is a function of the mass number A (in our case $a = 9$). This ratio, together with that obtained experimentally, is plotted in fig. 3. A disagreement between the

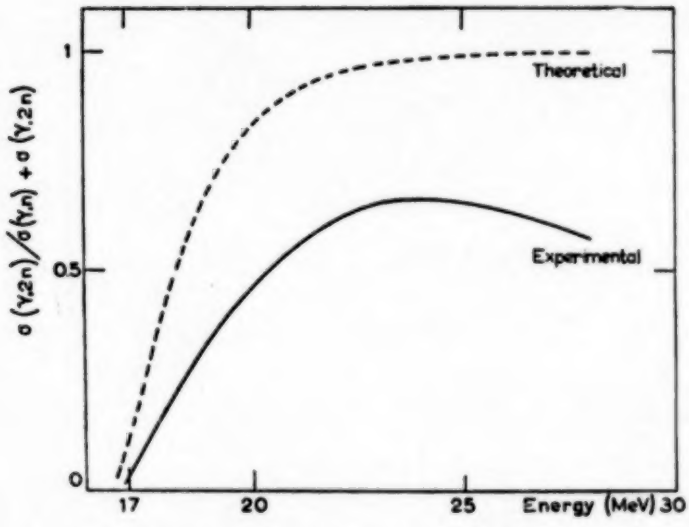

Fig. 3. Comparison between the statistical theory of nuclear reactions (theoretical) and the experimental ratio $\sigma(\gamma, n)/[\sigma(\gamma, n)+\sigma(\gamma, 2n)]$.

two curves is apparent and is supposed to be due to an appreciable direct photoneutron component that affects the (γ, n) process.

† O. Borello of the University of S. Paolo recently measured the total absorption coefficient of Pr^{141} using threshold detectors, and on subtracting the electronic absorption obtains results for the nuclear absorption which agree with the present work.

The integrated absorption cross section up to 30 MeV is evaluated as follows: the sum of the two measured processes (γ, n) and (γ, 2n) is 3.3 MeV · b; to this figure we must add at least 0.1 MeV · b for the (γ, p) process, because, taking into account the data for the (γ, p) reaction found in the literature, we see that a reasonable value of the integrated (γ, p) cross section is about 3 % of the correspondent (γ, n) integrated cross section. Neglecting the unknown contributions of the (γ, γ'), (γ, np), (γ, α) etc. processes, we obtain for the integrated cross section 3.4 MeV · b.

The Levinger and Bethe (L.B.) dipole sum rule †

$$\int \sigma \mathrm{d}E = 0.06 \frac{NZ}{A} (1+0.8x)$$

gives, for an exchange force fraction $x = 0.5$, a value of 2.88 MeV · b; we see, therefore, that the experimental result strongly exceeds the L.B. prediction †.

This experimental result is not, however, peculiar to Pr^{141}: in fact, in Ta^{181} Whalin and Hanson [9]), taking into account only the (γ, n) and (γ, 2n) processes, found a value of 3.6 MeV · b for the integrated cross section up to 22 MeV, and for the same element, Jones and Terwillinger [10]) found 5.1 MeV · b by integrating up to 80 MeV. The agreement with the L.B. prediction seems to be very difficult to obtain. For a detailed discussion on this point we refer to a paper by Levinger [11]).

Another expression for the integrated cross section, that is not confined to dipole transitions, is that of Gell-Mann *et al.* [12]):

$$\int_0^{\mu} \sigma(E)\mathrm{d}E = \frac{NZ}{A} \frac{e^2\hbar}{M} + \frac{1}{\pi} \int_{\mu}^{\infty} \mathrm{d}E(1-R(E))[Z\sigma_p(E)+N\sigma_N(E)].$$

Taking $R(\mu) = 0$; $\sigma_p/\sigma_N = 1.3$ and the experimental behaviour of σ_p versus energy, this relation becomes

$$\int_0^{\mu} \sigma(E)\mathrm{d}E = 0.06 \frac{NZ}{A} \left(1+0.1 \frac{A^2}{NZ}\right).$$

Now, the above expression, which takes into account higher order multipole transitions also, nevertheless gives nearly the same value as the L.B. formula with $x = 0.5$. This seems very peculiar and it lies outside the purpose of this paper to discuss the validity of the above expression. One thing, however, is certain: the experimental integrated cross section is greater than both the above theoretical predictions, even if one extends the integration only to 30 MeV and not up to the meson threshold.

† Even if, for the calibration, we had used the data on copper given in ref. [8]), which are much smaller than those usually employed, we would still get a value that exceeds the L. B. prediction by at least 0.3 MeV · b.

Danos and Steinwedel [13]) have pointed out that the hydrodynamical model of Jensen and Steinwedel [14]) would predict an absorption for quadrupole transition with a peak located at an energy 1.6 times the energy of the dipole one. The maxima for quadrupole and dipole absorption cross sections are correlated by the following relation

$$\frac{\sigma_{\text{res. qu.}}}{\sigma_{\text{res. d.}}} = 0.21 \left(\frac{E_d}{E_q}\right)^2 .$$

Taking into account the experimental data we get $E_q = 24$ MeV and therefore $\sigma_{\text{res. qu.}} = 43$ mb. Fitting a Lorentz line to the experimental values of the dipole resonance curve we get a contribution to the dipole tail of 20 mb. The difference from the experimental value is 100 mb and this last figure could be compared with the value of Danos and Steinwedel's calculation. Considering the uncertainty in the cross section values the results are not in contradiction with the quadrupole absorption mentioned above.

We thank Prof. M. Mandò, of the University of Florence, who kindly supplied pure praseodimium oxide, and Miss S. Menardi for computation work. One of us (E.S) wishes to express his gratitude to Prof. G. Wataghin, for the kind hospitality in the University of Turin.

References

1) L. Katz and A. G. W. Cameron, Can. J. of Phys. **29** (1951) 518
2) C. I. Browne, J. O. Rasmussen, J. P. Suris and D. F. Martin, Phys. Rev. **85** (1952) 146
3) B. J. Stover, Phys. Rev. **81** (1951) 8
4) T. H. Handley and E. L. Olson, Phys. Rev. **96** (1954) 1003
5) A. S. Penfold and J. E. Leiss, Analysis of photo-cross-sections (Phys. Res. Lab., University of Illinois, Champain, Ill., May 1958)
6) J. M. Blatt and V. F. Weisskopf, Theoretical Nuclear Physics, (John Wiley & Sons, New York, 1952) p. 379
7) J. S. Levinger and H. A. Bethe, Phys. Rev. **78** (1950) 115
8) A. I. Berman and K. L. Brown, Phys. Rev. **96** (1954) 83
9) E. A. Whalin and A. O. Hanson, Phys. Rev. **89** (1953) 324
10) L. W. Jones and K. M. Terwillinger, Phys. Rev. **91** (1953) 699
11) J. S. Levinger, Annual Rev. of Nuclear Science **4** (1954) 13
12) M. Gell-Mann, M. L. Goldberger and W. E. Thirring, Phys. Rev. **95** (1954) 1612
13) M. Danos and H. Steinwedel, Z. Naturforschg. **6a** (1951) 217
14) H. Steinwedel and J. H. D. Jensen, Z. Naturforschg. **5a** (1950) 413

2.B *Nuclear Physics* **10** (1959) 429—439; © *North-Holland Publishing Co., Amsterdam*
Not to be reproduced by photoprint or microfilm without written permission from the publisher

POLARIZATION OF NEUTRONS PRODUCED IN THE D—D REACTION

P. P. KANE †

Wesleyan University, Middletown, Conn., U.S.A.

Received 8 January 1959

Abstract: Polarization of neutrons from the d(d, n) He reaction was measured at an average deuteron energy of 93 keV and emission angles of 43° and 53° in the laboratory system. The values of P_n are found to be $-10.6\,\% \pm 2.3\,\%$ and $-9.5\,\% \pm 3.7\,\%$ respectively. These are in excellent agreement with previous results at higher energies. The results of all experiments suggest that the polarization is independent of deuteron bombarding energy between 93 keV and 700 keV.

1. Introduction

During the last few years, the production and use of medium energy polarized neutrons have resulted in a substantial contribution to our understanding of nuclear forces. Schwinger [1]) proposed the scattering of nucleons from helium as a mechanism for the production of polarization. This method of producing polarization, although successfully utilized at first by Heusinkveld and Frier [2]) and later by other workers for protons, is not particularly suitable for neutrons of a few MeV energy. The efficiencies of most detectors are only of the order of a few per cent and therefore it has not been possible so far to detect neutron polarization obtained in the above manner in the MeV region of kinetic energies. However, according to the original prediction of Wolfenstein [3]), the d(d, n)He^3 reaction has proved to be a convenient source of polarized neutrons in the energy range under consideration. The Li(p, n)Be^7 reaction [4–7]) has also been used extensively for obtaining polarized neutron beams. Our experiments are concerned exclusively with the d—d reaction.

The polarization of d—d neutrons has been studied by many workers [8–15]). Only the first of these experiments attempted to utilize deuteron bombarding energies less than 200 keV. At an energy of about 100 keV, Longley *et al.* [8]) obtained a value for $P_1(45°)$ of 40 ± 20 %. Here, $P_1(45°)$ is the polarization of neutrons at 45° in the centre of mass system. The experiments at higher deuteron energies give for the maximum neutron polarization a rather precise value in the neighbourhood of 10 %. Therefore, in order to understand

† Work supported in part by a grant from the Research Corporation.

better the dependence of the neutron polarization on the incident deuteron energy, it seemed necessary to us to increase the precision of the measurement of the neutron polarization at low incident deuteron energies. Our result for the neutron polarization at an average deuteron energy of 93 keV is in good agreement with the precise results obtained at the higher energies. The disagreement between our result and that of Longley *et al.* might be attributed to the large statistical error of the latter measurement or to the difference in technique. Following a suggestion of Schwinger [16]), Longley *et al.* employed the small angle scattering from a lead nucleus to detect the neutron polarization. This technique involves difficulties associated with very strong background and was therefore not used in the more recent experiments. Since the properties of carbon as an analyser had been studied in detail by Meier *et al.* [11]), we decided to employ carbon as an analyser. Among earlier workers, Pasma and Levintov *et al.* used scattering from helium for asymmetry measurements. The others used carbon scatterers. Previous work, particularly that of Levintov *et al.*, had shown that the results for neutron polarization obtained with thin deuterium targets were substantially the same as those obtained with thick targets. Therefore, no attempt was made to use thin targets.

The theoretical ideas underlying the experiment are well-known and are mentioned briefly in section 2. The experimental details are outlined in section 3. Results and conclusions are presented in the fourth section.

2. Theory

The notation is described in the caption to fig. 1. If $\mathbf{P}_n(\theta_1)$ is the polarization of the neutron beam incident on the carbon target, we have the relation

$$\mathbf{P}_n(\theta_1) = \mathbf{e}_1 P_n(\theta_1) \tag{1}$$

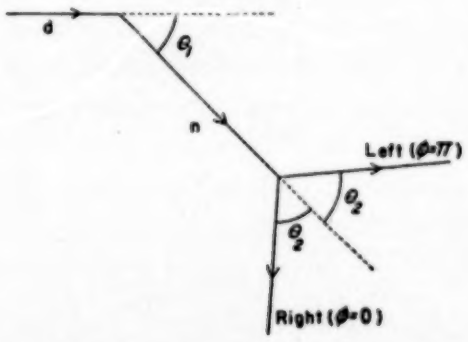

Fig. 1. Diagrammatic representation of the angles involved in the experiment. d and n represent the incident deuteron and the emitted neutron. θ_1 is the angle which the emitted neutron makes in the centre of mass system with the direction of incidence of the deuteron. θ_2 is the angle through which the neutron is scattered by the carbon nucleus in the centre of mass frame of the neutron and the nucleus. Directions, right and left, are defined in the diagram.

where

$$\mathbf{e}_1 = \mathbf{k}_d \times \mathbf{k}_n / |\mathbf{k}_d \times \mathbf{k}_n|. \tag{2}$$

Here $\mathbf{k}_d$ is the wave vector of the deuteron and $\mathbf{k}_n$ is the wave vector of the emitted neutron.

Let $\mathbf{P}_c(\theta_2)$ be the polarization of an initially unpolarized neutron beam after scattering from carbon through θ_2. Then we can write $\mathbf{P}_c(\theta_2)$ as

$$\mathbf{P}_c(\theta_2) = \mathbf{e}_2 P_c(\theta_2) \tag{3}$$

where

$$\mathbf{e}_2 = \mathbf{k}_n \times \mathbf{k}'_n / |\mathbf{k}_n \times \mathbf{k}'_n|. \tag{4}$$

In eq. (4), $\mathbf{k}_n$ and $\mathbf{k}'_n$ are the wave vectors of the incident and scattered neutrons respectively. The differential cross section for the scattering of a polarized neutron beam is given by the formula [17])

$$\sigma(\theta_2, \phi) = \sigma_u(\theta_2)\{1 + \mathbf{P}_n(\theta_1) \cdot \mathbf{P}_c(\theta_2)\} \tag{5}$$

where $\sigma_u(\theta_2)$ is the differential cross section for the scattering of an unpolarized neutron beam at θ_2 and ϕ is the azimuthal angle. In our experiment, scattering takes place in the plane defined by the direction of the deuteron beam and that of the emitted neutron. The asymmetry ε is given by the formula

$$\varepsilon(\theta_1, \theta_2) = \frac{\sigma(\theta_2, \phi = 0) - \sigma(\theta_2, \phi = \pi)}{\sigma(\theta_2, \phi = 0) + \sigma(\theta_2, \phi = \pi)}. \tag{6}$$

From the eqs. (1) to (6), we can derive the relation

$$\varepsilon(\theta_1, \theta_2) = P_n(\theta_1) P_c(\theta_2). \tag{7}$$

If $P_c(\theta_2)$ is known, experimental measurements of ε can be used to determine the required polarization $P_n(\theta_1)$. Along with McCormac *et al.*, we assume the validity of the phase shift analysis of Meier *et al.* for the scattering of neutrons from carbon between 2.4 and 3.6 MeV. On the basis of this assumption we get the relation

$$P_c(\theta_2) \approx -\sin(2\theta_2). \tag{8}$$

In deducing the polarization $P_n(\theta_1)$ from measurements of the asymmetry ε, we assumed complete equality between the two sides of (8).

3. Experimental Details

A beam of deuterons, accelerated through 120 kV, was allowed to impinge on an occluded deuterium target. The target was formed by adsorbing deuterium in an aluminium disc $\frac{1}{32}$ inch thick. After the target had been bombarded by a 100 μA deuteron beam for about 10 hours, it did not reveal any noticeable fluctuations in the deuterium content for at least two or three days. The experimental arrangement is shown in fig. 2. Europium

activated lithium iodide scintillator, available from Harshaw Chemical Company, was used for monitoring the neutron beam. The lithium iodide scintillator was a cylinder of diameter $1\frac{1}{2}$ inches and thickness $\frac{1}{2}$ inch. Pulses from the lithium iodide counter were amplified and then fed to a discriminator. The bias of the discriminator was set below the pulse height corresponding to the dissipation of the kinetic energies of the product triton and alpha-particle within the scintillator. Therefore, the lithium iodide monitor counts were rather insensitive to fluctuations in the gain of the electronics. This feature of the lithium iodide counter made it a satisfactory neutron monitor.

Neutrons, used for asymmetry measurements, were collimated as shown in fig. 2. The vertical height of the collimator was one inch all along its length. The maximum height of the neutron beam at the centre of the carbon target was somewhat less than $1\frac{1}{2}$ inches. An optical spectrometer was modified so

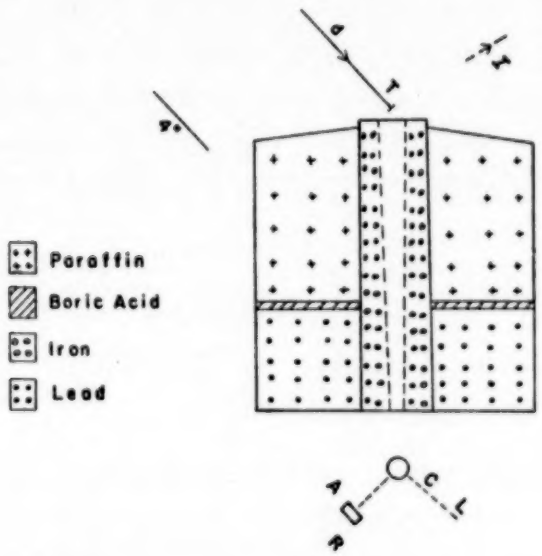

Fig. 2. Arrangement of shielding and counters. d represents the deuteron beam, T the deuterium target, C the carbon target and A the anthracene counter. The lithium iodide counter was placed at a distance of 58 inches from T in the direction of I.

as to support the carbon scatterer and the detector for scattered neutrons. The cylindrical carbon target was $1\frac{1}{2}$ inches in diameter. It had an average density of 1.76 g/cm^2. The spectrometer table had on it accurately marked circular grooves. So the target could be positioned quite accurately with reference to the centre of the spectrometer table. The scattered neutrons were detected with the help of an anthracene crystal, $1\frac{1}{2}$ inches in diameter and $\frac{3}{4}$ inch thick, mounted on a Dumont 6292 photo-multiplier. The anthracene counter was mounted in the movable arm of the spectrometer. The pulses from the anthracene counter were amplified and the amplified output was fed simultaneously to a single channel analyser and a discriminator. For given values of θ_1 and θ_2, counts were taken for an assigned number of

monitor counts on the right ($\phi = 0$) with and without the carbon target and on the left ($\phi = \pi$) again with and without the target. Such a set of four readings was repeated between ten to twenty times for each combination of θ_1 and θ_2 values. In order to cancel the effect of irregularities, the carbon target was rotated through approximately 180 degrees between successive sets of readings. From the above sets of observations, scattered neutron counts and asymmetries were determined in a straightforward manner. Only the single channel analyser counts were used in the measurement of the asymmetries. The counts obtained with the help of the discriminator were only used to study the effects of fluctuations in electronic gain. The values of asymmetries determined with the help of the discriminator for different bias settings were in agreement with the more reliable single channel values. The pulse height response of an anthracene counter to neutrons elastically scattered from carbon showed a rather flat distribution up to a certain critical value and then dropped off sharply. The window of the single channel analyser was set to accept only those pulses that had a height somewhat smaller than this critical value. This procedure helped considerably in reducing the number of unwanted background counts.

From previously published results on the scattering of 2.65 MeV neutrons [11]), it was expected that a systematic error of $\frac{1}{2}$ degree in the determination of zero degree scattering position would lead to asymmetries of about ± 0.01 at the values of θ_2 used in our measurements. Therefore, it was necessary to ensure accurate alignment of the scatterer and the detector with the beam axis. Accurate alignment of the centre of the spectrometer with the beam axis was achieved by means of an optical telescope. The correct zero degree position was determined by rotating the anthracene counter through small angles about the expected zero degree position and observing the approximate symmetry of the curve giving neutron count as a function of angle. The data are shown in fig. 3. The angles could be read to about one tenth of a degree on the spectrometer scale. The zero degree position, determined in this manner, was expected to be accurate to a quarter of a degree. A second check was provided by repeating the beam profile measurements with the carbon target in place. The zero degree position determined by the last procedure was found to be the same as that determined in the absence of the carbon target, thus revealing a proper alignment of the carbon target as well. The zero degree positions, determined before and after a series of asymmetry measurements, were found to be the same, indicating the absence of systematic drifts in the deuterium target or deuteron beam focus.

Two separate methods were used to detect instrumental asymmetries that might be present in spite of these careful alignment procedures. When θ_1 is zero, one would expect the polarization $\mathbf{P}_n$ of the emitted neutrons to vanish on the basis of eqs. (1) and (2). Therefore, asymmetry values for any

value of θ_2 should also vanish. The asymmetries, measured under these conditions, gave an average value of 0.004 ± 0.019. Further, eq. (8) suggests that $P_c(90°)$ should be zero and hence the asymmetry for a θ_2 value of 90° should also be zero. The experimental result is 0.007 ± 0.021. These measurements ensure the absence of appreciable instrumental asymmetries. An additional precaution was taken in the measurement of the non-vanishing asymmetries. From eqs. (1) to (6), we get the relation

$$\varepsilon(\theta_1, \theta_2) = +\varepsilon(-\theta_1, \theta_2). \tag{9}$$

In the case of the two values of θ_1 employed in our experiments, asymmetry measurements were made for the corresponding $-\theta_1$ values as well. The results satisfied eq. (9) within the experimental error. The values reported

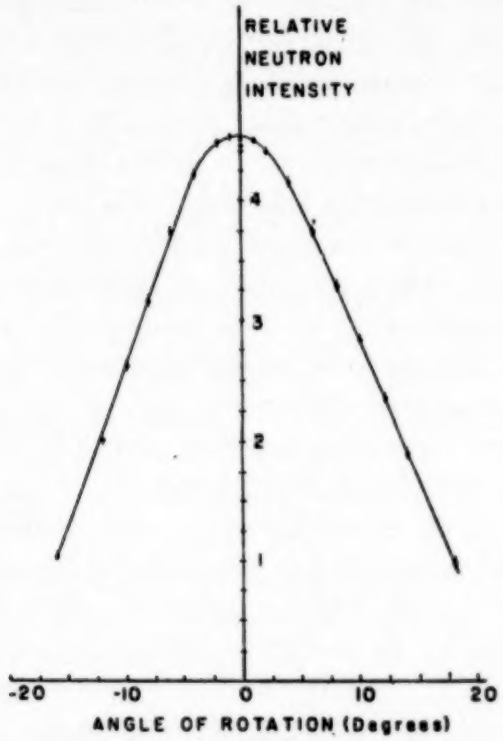

Fig. 3. Beam profile obtained with the help of the anthracene counter. The symmetry of the profile was used to determine the zero degree scattering position.

for the asymmetries in table 1 are the means of the two values of ε for θ_1 and $-\theta_1$.

The background was about 80 % of the counting rate in the presence of the carbon target. Under such conditions, the background may be substantially altered in an unpredictable manner by the use of the carbon target. For θ_2 larger than about 25 degrees, the background was almost independent of angle. This observation suggests that any asymmetries introduced by background differences were negligible.

The carbon target subtended an angle of ± 2 degrees at the centre of the deuterium target. The emission of neutrons from the d—d source is not isotropic. In a separate experiment, we have determined the angular distribution of neutrons emitted in the d—d reaction at an accelerating voltage of 120 kV. The anisotropy of the d—d source contributed an absolute asymmetry of about 0.003 in our experiment. In view of the fairly large statistical errors of the measurements, this correction has been considered to be negligible. However, it should be remarked here that the correction is of such a sign as to increase the observed asymmetries.

Appreciable multiple scattering of neutrons was present. However, an argument, that has been proposed before [12]), suggests that the measured asymmetries were probably not in error on this account.

Since a thick, adsorbed deuterium target was used in these experiments, it was desirable to know the average deuteron energy for neutron production. A knowledge of the dependence of the d(d, n)He^3 reaction cross section on deuteron energy was necessary in the calculation of the average energy of the deuterons. No previously published results were available at these energies †. So an auxiliary experiment was carried out to determine the energy dependence of the reaction cross section. For this purpose, the lithium iodide counter was placed at an angle of 90° in the laboratory system to the deuteron beam. A long boron tri-fluoride counter of the type suggested by Hanson and McKibben [18]) was also put at 90° to the deuteron beam on the other side. The insensitivity of such a long counter to neutron energy is well known. We also verified experimentally the absence of the dependence of the long counter sensitivity on neutron energy for a range of at least about 200 keV. If the energy of the deuterons is varied from 30 keV to 130 keV, the maximum variation in the energy of the neutrons emitted at 90° in the laboratory system is about 20 keV. The energy insensitivity of the long counter within such a narrow range could therefore be safely assumed. Lithium iodide and boron tri-fluoride counts were then taken for fixed intervals of time and for fixed values of deuteron current as the accelerating voltage was varied from 30 kV to 130 kV. The maximum variation in beam current was ± 1.5 % during these measurements. The mean value of the current was known probably to better than 1 %. Observations taken at a given voltage both before and after the complete set of readings revealed no significant fluctuations in the electronic gain. The data obtained with the long counter are presented in fig. 4. A moderately good fit to the data is obtained, if we take the d(d, n)He reaction cross section to be proportional to $E^{2.4}$, where E is the

† *Note added in proof:* The work of I. Bertholdson and G. Carlson [23]) has recently come to our attention. Although no attempt was made in that work to obtain an explicit functional relationship between the reaction cross section and deuteron energy, our results appear to be in agreement with those of above authors.

bombarding deuteron energy. The same energy dependence was shown within the experimental error by the lithium iodide counter, suggesting an absence of variation of the response of such a counter within a range of at least 20 keV in neutron energy. From the observed energy dependence of the reaction, we calculate the average deuteron energy to be 93 keV at an accelerating voltage of 120 kV. The error in the determination of the average deuteron energy is expected to be less than 7 keV. Among the earlier workers, Levintov *et al.* [14]) had assumed a linear dependence of the reaction

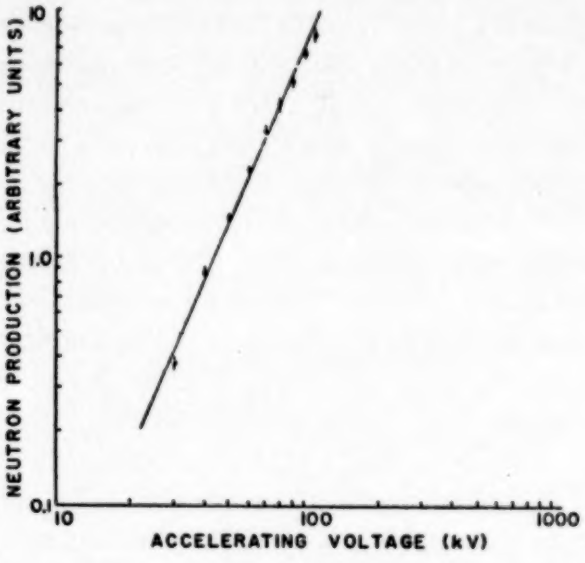

Fig. 4. Voltage dependence of the production of neutrons for a fixed beam current and a fixed interval of time. The straight line fit to the data suggests an $E^{2.4}$ dependence of the d—d reaction cross section at low deuteron energies E. This energy dependence has been used to compute the average energy of deuterons effective in producing neutrons.

cross section on voltage. But they used deuteron energies in the neighbourhood of 1 MeV. Further it should be pointed out that our determination of the energy dependence was achieved only with the help of a thick deuterium target.

4. Results and Discussion

The results are summarized in table 1. The observed polarization is in excellent agreement with other measurements both as regards magnitude and sign. Our value for the polarization is the same within the experimental error as that of Meier *et al.* [11]) around 600 keV, those of McCormac *et al.* [12]) between 500 and 700 keV, that of Levintov *et al.* [14]) at 400 keV and finally those of Pasma [15]) between 300 and 500 keV. An essential constancy of the polarization within the deuteron energy range 93 keV to 700 keV is suggested by all the experiments including the present one. Meier *et al.* analyse the

earlier results of Huber and Baumgartner [10]) by using the revised phase shift calculations and give a value of $-11\,\% \pm 5\,\%$ for the polarization at an energy of 600 keV and a laboratory emission angle of 45°. An earlier measurement of the polarization at 200 keV [15]) gives the somewhat lower value of

TABLE 1

Experimental results for the polarization of neutrons generated in a d—d reaction at an average deuteron energy of 93 keV in the laboratory system.

θ_{1L}	θ_1	θ_2	ε	$P_n(\theta_1)$	Mean $P_n(\theta_1)$
43.0°	45.7°	27.0°	0.082 ± 0.044	$-10.1\% \pm 5.4\%$	$-10.6\% \pm 2.3\%$
		32.4°	0.104 ± 0.032	$-11.5\% \pm 3.5\%$	
		43.0°	0.085 ± 0.031	$-\ 8.5\% \pm 3.1\%$	
		53.7°	0.116 ± 0.033	$-12.2\% \pm 3.5\%$	
53.0°	56.2°	32.4°	0.130 ± 0.054	$-14.4\% \pm 6.0\%$	$-\ 9.5\% \pm 3.7\%$
		48.4°	0.010 ± 0.050	$-\ 1.0\% \pm 5.0\%$	
		53.7°	0.124 ± 0.044	$-13.0\% \pm 4.6\%$	

θ_1 is the angle in the centre of mass frame that the neutron makes with the direction of the incident deuteron. θ_{1L} is the corresponding angle in the laboratory system. θ_2 is the angle through which the neutron is scattered by the carbon nucleus in the centre of mass frame of the neutron and the nucleus. ε is the observed asymmetry. The errors quoted are only statistical. ε is given by the relation

$$\varepsilon(\theta_1, \theta_2) = \frac{\sigma(\theta_2, \phi = 0) - \sigma(\theta_2, \phi = \pi)}{\sigma(\theta_2, \phi = 0) + \sigma(\theta_2, \phi = \pi)}.$$

The reported values for ε are the averages of the asymmetries for θ_1 and $-\theta_1$.

$-5.8\,\% \pm 2.5\,\%$ but the relative statistical error of the measurement is quite large. In view of the suggested independence of the polarization from energy, an average of all measurements mentioned in this paragraph was taken. This average value of the polarization at a laboratory emission angle between 43° to 50° turns out to be $-9.6\,\% \pm 0.7\,\%$. The suggested energy independence of the polarization could explain very well the fact that Levintov *et al.* noticed no significant changes in the polarization when thick deuterium targets were used instead of thin ones. The polarization of protons from the companion reaction d(d, p)H^3 has been measured previously [19–21]), although not with the same degree of precision. The proton polarization is of the same order of magnitude as the neutron polarization and is also found not to change rapidly with energy. This similarity is to be expected on the basis of charge independence of nuclear forces.

On the basis of the theory of the d—d reaction developed by Beiduk *et al.* [22]), Blin-Stoyle [23, 24]) deduced the following relation giving the neutron polarization as a function of energy E of the deuteron and centre of mass emission angle θ_1 of the neutron:

$$P_n(\theta_1) = B\frac{A(E)\sin 2\theta_1}{1+A(E)\cos^2\theta_1} \text{ for } E < 300\,\text{keV}. \quad (10)$$

In the above formula, the constant B depends upon a knowledge of the nuclear wave functions and so cannot be calculated at present. The coefficient $A(E)$ depends on the energy of the deuterons and is the same as the coefficient of $\cos^2(\theta_1)$ in the expression $1+A(E)\cos^2\theta_1$, which gives the angular distribution of the emitted neutrons. The suggested absence of the energy dependence of the polarization would imply in this theory a not too rapid variation of the coefficient $A(E)$ with energy. Since there was considerable disagreement between the measurements of the coefficient A in this energy region, it was determined by us in a separate experiment which will be reported shortly. Our value for A is in the neighbourhood of 0.9. It is higher than that reported earlier by some workers [25]). But it will extrapolate quite well to those of Preston *et al.* [26]) between 156 and 270 keV and those of Chagnon and Owen [27]) between 400 and 600 keV. Therefore, it appears that A varies between 0.9 and 1.8 as the deuteron energy is varied from 93 keV to about 400 keV. In that case, the form of eq. (10) certainly suggests a rather slow variation of the polarization with energy. The apparent lack of dependence of the experimentally observed polarization on energy is however not adequately explained at present. A further refinement of the theory is necessary before definite conclusions can be reached. We determined the polarization only for two values of θ_1 and therefore cannot make a significant comparison with the angular dependence exhibited in eq. (10).

It is a pleasure to thank Dr. F. I. Boley for making available the facilities of the electrostatic accelerator, Mr. B. D. Day, Mr. T. R. Fisher and Mr. J. A. Palsedge for assistance in taking data and Mr. D. B. Colby for some of the computations.

References

1) J. Schwinger, Phys. Rev. **69** (1946) 681
2) M. Heusinkveld and Frier, Phys. Rev. **85** (1952) 80
3) L. Wolfenstein, Phys. Rev. **75** (1949) 342
4) Willard, Bair and Kington, Phys. Rev. **95** (1954) 1359
5) Adair, Darden and Fields, Phys. Rev. **96** (1954) 503
6) A. Okazaki, Phys. Rev. **99** (1955) 55.
7) Striebel, Darden and Haeberli, Nuclear Physics **6** (1958) 188
8) Longley, Little and Slye, Phys. Rev. **86** (1952) 419
9) R. Ricamo, Nuovo Cimento **10** (1953) 1607
10) E. Baumgartner and P. Huber, Helv. Phys. Acta **26** (1953) 545
11) Meier, Scherrer and Trumpy, Helv. Phys. Acta **27** (1954) 577
12) McCormac *et al.*, Phys. Rev. **104** (1956) 718
13) Levintov *et al.*, Nuclear Physics **3** (1957) 221
14) Levintov *et al.*, Nuclear Physics **3** (1957) 237

15) P. J. Pasma, Nuclear Physics **6** (1958) 141
16) J. Schwinger, Phys. Rev. **73** (1948) 407
17) J. V. Lepore, Phys. Rev. **79** (1950) 137
18) A. O. Hanson and J. L. McKibben, Phys. Rev. **72** (1947) 673
19) Bishop *et al.*, Nature **170** (1952) 113
20) R. E. Segel and S. S. Hanna, Phys. Rev. **106** (1957) 536
21) B. Maglic and J. Vukovic, Nuclear Physics **6** (1958) 443
22) Beiduk *et al.*, Phys. Rev. **77** (1950) 622
23) R. J. Blin-Stoyle, Proc. Phys. Soc. A **64** (1951) 700
24) R. J. Blin-Stoyle, Proc. Phys. Soc. A **65** (1952) 949
25) Fuller, Dance and Ralph, Phys. Rev. **108** (1958) 91
26) Preston, Shaw and Young, Proc. Roy. Soc. **226** (1954) 212
27) P. R. Chagnon and G. E. Owen, Phys. Rev. **101** (1956) 1798
28) I. Bertholdson and G. Carlson, Arkiv f. Fysik **2** (1950) 289

1.E.1:
3.A:3.B

Nuclear Physics **10** (1959) 440—456; © *North-Holland Publishing Co., Amsterdam*
Not to be reproduced by photoprint or microfilm without written permission from the publisher

NUCLEAR SPECTROSCOPIC MEASUREMENTS ON MASS SEPARATED Pb^{198} SOURCES

BO JUNG

The Gustaf Werner Institute for Nuclear Chemistry, University of Uppsala

Received 29 December 1958

Abstract: The conversion electron spectrum of Pb^{198} was studied in a double focusing β-spectrometer and the γ-spectrum in a single channel scintillation spectrometer. For electrons, the energy range 15 keV—1500 keV was covered; and for gammas, the energy range 45 keV—2.3 MeV. Mass separated sources were used throughout. When measuring the γ-spectrum, disturbances from the daughter activity Tl^{198} were diminished by employing a continuous chemical separation method. A tentative level scheme involving 8 excited levels and 20 transitions has been constructed.

1. Introduction

The decay of Pb^{198} has been studied by Andersson *et al.* [1]). They found Pb^{198} to decay mainly by electron capture to Tl^{198} with a half-life of 2.4 hours (in contrast to an earlier reported value of 25 minutes [2])). From a β-spectroscopic investigation they assigned 21 conversion lines to the decay, and by electron-electron coincidence measurements they gathered some preliminary coincidence data. The transitions of the decay of 1.8 h Tl^{198m} [3]) were not found in the decay of Pb^{198}. Mass assignment of some conversion lines was made with electromagnetically mass separated sources but owing to low efficiency of the separator such sources were not used for energy or intensity measurements. As the Pb^{198} activity was produced by (p, xn) reactions with rather high proton energies, the chemically separated lead activity was a mixture of several isotopes which yielded a very complex electron spectrum. A more detailed study was therefore postponed until now. A reconstruction [4]) of the ion source has increased the efficiency of the mass separator considerably.

When the present study was started, it was intended to remeasure from mass separated sources only those conversion lines which in the earlier work [1]) had been affected by the presence of extraneous activities. As, however, the mass separated sources were found to be strong enough to permit the detection of new conversion lines, the scope was widened to cover the whole spectrum. With mass separated sources in combination with a continuous chemical separation method, it was also found possible to obtain the γ-spectrum of Pb^{198} without excessive interference from other activities.

2. Experimental Procedures

2.1. SOURCE PREPARATION

Pb^{198} was produced in the synchro-cyclotron of this Institute by bombardments of metallic Tl for 2-3 hours with protons of 100 MeV maximum energy. The targets were dissolved in hot nitric acid with 5 μg Pb^{2+} and 250 μg Fe^{3+} as carriers. All Tl was brought to the monovalent state by boiling with H_2O_2, and Pb and Fe were precipitated as hydroxides with NH_3. After being purified by reprecipitation and washing in water, the hydroxides were dissolved in 6 *N* HCl. The Fe-carrier was removed from the acid solution by extraction into ether and after addition of 5 mg stable $PbCl_2$, this was dried and the residue fed to the mass separator. (The role of the extra 5 mg $PbCl_2$ was to give stable running conditions in the ion source.) Similar chemical procedures have been used earlier [1,5]).

In the isotope separator the $A = 198$ ion current was collected behind a defining slit 1.5×15 mm, either on 2 mg/cm² Al-foil for e^--spectrometry or on Cu-foil for γ-measurements. (The use of this isotope separator for preparing radioactive samples has been discussed by Andersson [6]).) After the mass separations, which took about one hour, the Al-strips could be immediately transferred to the spectrometer, but the Cu-strips had to be treated chemically. The procedure employed was analogous to the treatment of the Tl targets after irradiation (cf. above) and the resulting active $PbCl_2$ solution was transferred to an ion-exchange column consisting of Dowex 2, 20—40 mesh, loaded with PO_4^{3-} ions. The Pb^{2+} ions were adsorbed on the column and the Tl, produced in the decay of Pb, could be washed away by a continuous flow of water through the resin. The efficiency of the separation was tested with tracer methods and no Tl was found to be adsorbed on the column. A similar method, used for rapid separation of Tl from lead, has been described by Andersson *et al.* [7]).

The efficiency of the mass separation stage was tested in a special run. In order to have a representative figure, this separation was made to simulate as closely as possible the normal ones, but in order to be able to use tracer methods, only Pb^{212} was incorporated in the charge. (The great variety of nucleides fed to the ion source in the normal separations prevented a similar study to be made with these.) An efficiency of about 7 % was found, and it should be remarked that this figure represents that which was actually utilized in the experiments, being the ratio of the activity collected as singly ionized Pb ions to the activity fed to the separator.

The isotopic purity of the mass separated samples was normally quite high, and any effects of impurities were completely neglected in the γ-spectroscopic work. In the conversion electron measurements some lines were found, however, which had to be identified as due to impurities. As can be seen from

table 4 the mass numbers of the contaminating activities were restricted to 197 and 199. The distortion of the spectrum caused by the presence of these impurities was rather limited, since at the start of the measurements the intensities of the strongest lines in the decays of Pb^{197} and Pb^{199} (207.1 and 281.5 keV respectively [1])) were normally less than 3 % of the intensity of the K-conversion line of the 290.3 keV transition in Tl^{198} (cf. table 1). In a special separation, when the ion currents of mass number 197, 198 and 199 were collected simultaneously on three 1.5×15 mm strips and all other experimental conditions were left unchanged, about 2 % of the total collected $A = 197$ and $A = 199$ activities was found on the $A = 198$ strip.

2.2. β-SPECTROMETER MEASUREMENTS

The conversion electron spectrum was measured in the double focusing spectrometer constructed by Arbman and Svartholm [8]). The momentum resolution was normally set at 0.35 % giving a transmission of about the same fraction of 4π. In some concluding measurements a resolution of 0.25 % was used in an attempt to resolve some lines which were thought to be composite. Two different windows for the Geiger-Müller counter were used, one made of 0.5 mg/cm² rubber hydrochloride film, the other of 0.25 mg/cm² film of VYNS [9]). The low energy part of the spectrum was measured with the thinner window.

The automatic registration facilities of the instrument were very convenient in a preliminary survey of the spectrum, but afterwards the whole energy region was covered by point-to-point measurements in order to increase the sensitivity and the energy and intensity accuracy. With the fresh samples the measurements were continued for about five hours. The decay periods of the lines were established by remeasuring them from the same source. The time limit was set by the short half-life of Pb^{198}, and several sources were needed before the whole energy region was covered.

The energy calibration of the spectrometer was made according to the procedure outlined by Arbman [10]). Used as reference lines were the 53.79 keV KL_IL_{II} Auger line [11]), and the K-conversion lines of the 411.77 and 675.75 keV transitions in the decay of Tl^{198}. The energy values of the last two lines have been obtained from measurements of the Au^{198} decay [12,13]), but corresponding lines have been measured, though with lower precision, in the decay of Tl^{198} [14]).

Relative intensities of the lines assigned to the Pb^{198} decay were calculated from the areas of the peaks, allowing for decay by a half-life of 2.4 hours and correcting for the absorption of the electrons in the detector window according to the diagram of Saxon [15]). The K-conversion line of the 290.3 keV transition (cf. table 1) was used as intensity standard and for this reason measured for every source. Because of the fluctuating yields in the cyclotron bombard-

ments, the sources were of rather different strengths. Every part of the energy region was, however, covered at least once with a rather strong source, and no lines of a relative intensity greater than 2 % of that of the standard line are thought to have escaped detection if not masked by near-lying, stronger lines. For the greater part of the spectrum the lower limit is less, as can be seen from tables 1 and 2 in section 3.1.

2.3. γ-SPECTROMETER MEASUREMENTS

The γ-rays were detected in a $1'' \times 1''$ NaI(Tl) crystal coupled directly to an EMI 6097B photomultiplier. After preamplification the pulses were fed to a single channel pulse height analyser constructed by Tove [16]). In this instrument the channel is fixed and the spectrum is scanned by varying the amplification in steps of 1.0133. The major advantage of such a scheme is that it provides a constant relative channel width.

The ion-exchange resin, which was loaded with the mass separated Pb^{198}, was contained in a glass tube $\varnothing\, 4 \times 20$ mm; and the wash-water was conveyed through a rubber tube to a lead shielded beaker. The distance between crystal and source was about 2 cm.

With the same source three spectra were recorded (cf. fig. 3). The first spectrum suffers from an overloaded amplifier, and intensity and energy calculations were made on the second one. Since the spectrum is rather complicated, only qualitative measurements were attempted, and so the efficiency curve of Lazar *et al.* [17]) was used for intensity calculations even though this curve had been constructed for a crystal of different size, $1.5'' \times 1''$.

3. Results

3.1. CONVERSION ELECTRON SPECTRUM

The mixture of Pb^{198} and Tl^{198} was found to have a complicated electron spectrum, and in some cases a resolution of 0.25 % was not sufficient to resolve conversion lines belonging to different transitions. The inevitable presence of Tl^{198} conversion lines in the spectrum was of some inconvenience, as they might have masked lines belonging to the decay of Pb^{198}, which were of the primary interest; on the other hand, some of them could conveniently be used as energy standards.

The assignment of the internal conversion lines to the decay of either Pb^{198} or Tl^{198} was based mainly on their measured half-lives, but when these could not be obtained with enough accuracy, energy and intensity relations were also used. Lines from impurities were identified from their energies and decay periods.

From the e^--spectroscopic measurements 14 transitions could be rather unambiguously assigned to the decay of Pb^{198} (cf. table 1). The multi-

TABLE 1

Gamma transitions in the decay of Pb^{198}
(Conversion ratios within parentheses from Rose [18]). Intensity scale: K 290.3 = 100)

Adopted transition energy (keV)	Calculated transition energy (keV)	Conv. shell (Tl)	Rel. line intensity	$T_{\frac{1}{2}}$ (h)	Remarks	Assignment of multipole order
30.8±0.1	30.79	L_I	60 ±20	2.3	Asym. shape, window corr.	M1
	30.77	L_{II}	6 ± 2	2.2	Asym. shape, window corr.	L_I/L_{II} = 10±2 (11)
	30.79	L_{III}	0.8 ± 0.5	<5	Poor statistics	L_I/L_{III} = 75 (82)
	30.83	M_I	15 ± 3	2.5	Asym. shape, window corr.	M_I/M = 0.9 (0.9)
	30.85	M_{II}	1.5 ± 0.5	≈3		M_{II}/M = 0.09 (0.09)
	30.84	M_{III}	0.5 ± 0.3		Poor statistics	M_{III}/M = 0.03 (0.009)
	30.79	M_V	0.4 ± 0.3		Poor statistics	M_{IV}/M < 0.01 (0.001)
	30.83	N_I	5 ± 1	2.2	$N_{II}-N_{VII}+0$ masked by K 116.9	M_V/M = 0.02 (0.01)
116.9±0.1	116.93	K	255 ±25	2.3		M1
	116.97	L_I	34 ± 4	2.3		
	116.96	L_{II}	2.1 ± 0.5		L_{III} < 0.4	K/L = 7.1±1.0 (6.3)
	117.02	M_I	9 ± 1	2.4		L_I/L_{II} = 16 ±2 (11)
	117.16	N_I	2.7 ± 0.4	2.4	High energy tail may be 0-line	L_I/L_{III} > 80
122.6±0.1	122.57	K	11 ± 2	2.3		M1
	122.67	L_I	2.3 ± 0.4	2.6	L_{II} < 0.3	K/L = 5±2 (6.3)
					L_{III} < 0.1	L_I/L_{II} > 7
	122.9	M_I	0.8 ± 0.3	4	Not resolved, N not resolved	L_I+L_{II}/L_{III} > 20
173.4±0.1	173.47	K	100 ±10	2.4		E2
	173.26	L_{II}	91 ± 9	2.5		K/L = 0.73±0.07 (0.7)
	173.41	L_{III}	48 ± 5	2.3		L_I+L_{II}/L_{III} = 1.9 ±0.2 (1.8)
	173.38	M_{II}	35 ± 4	2.4		
	173.35	N_I	8 ± 2	2.3	N_I not resolved from K 259.5	< 1 % M1
259.5±0.1	259.5	K	58 ± 5	2.4		M1 (+E2?)
	259.6	L_I	11 ± 1	2.7	L_{III} < 0.7	K/L = 5.3±0.7 (6.3 M1)
	259.5	M_I	3.4 ± 0.4		N not resolved from 259.3 line (cf. table 2)	L_I+L_{II}/L_{III} >14
290.3±0.1	290.3	K	100	2.4	Intensity standard	M1 (+E2?)

290.3±0.1	290.3 290.3 291.0 290.5	K L_I M_I N_I	100 19 ± 2 9 ± 1 1.3 ± 0.5	2.4 2.5 1.7	Intensity standard $L_{III} < 0.7$	M1 (+E2?) K/L = 5.3±0.5 (6.3 M1) $L_I+L_{II}/L_{III} > 24$
365.4±0.1	365.4 365.5 365.6 365.8	K L_I M_I N_I	88 ± 5 14 ± 1 3.5 ± 0.5 1.4 ± 0.5	2.4 2.4 2.8 3.3	 $L_{III} < 0.2$ Not resolved from L 382	M1 K/L = 6.0±0.6 (6.3) $L_I+L_{II}/L_{III} > 65$
382.0±0.1	382.0 382.0 382.2	K L_I M_I	12 ± 1 2.3 ± 0.2 0.5 ± 0.2	2.1 2.6 3	 $L_{III} < 0.1$ N not detected	M1 (+E2?) K/L = 5.1±0.8 (6.3 M1) $L_I+L_{II}/L_{III} > 20$
389.5±0.2	389.5 389.6 389.3	K L_I M_I	1.0 ± 0.2 0.5 ± 0.3 0.2 ± 0.1	3.5 4	Poor statistics Not resolved from 372.8 keV line (cf. table 3)	
397.7±0.1	397.7 397.6 397.8	K L_I M_I	7.0 ± 1.0 (3.4 ± 0.4) 0.6 ± 0.3	2.3 2.3 3	 Coincident with K 467.8 (cf. the text) $L_{III} < 0.07$	M1 $K/L_{III} > 80$
467.8±0.2	467.8 467.5	K L_I	(3.4 ± 0.4) 0.3 ± 0.1	2.3	Coincident with L 397.7 (cf. the text)	M1? Assignment from γ-spectrum
575.0±0.3	575.0 575.1 574.9	K L_I M_I	3.6 ± 0.4 0.6 ± 0.2 0.3 ± 0.1	2.5 3	 L_{III} coincident with K 649.0	M1? K/L = 6±2 (6.3) Assignment from γ-spectrum
649.0±0.4	649.0 649.1	K M_I	1.5 ± 0.3 0.1	2.5 5	L, M and N line excluded L coincident with 634 keV line (cf. table 3)	E2? Assignment from γ-spectrum
865.3±0.5	865.3 866.4 867.1	K L_I M_I	2.1 ± 0.2 0.4 ± 0.1 0.10± 0.05	2.4 4		M1? Assignment from γ-spectrum

polarity assignments are based mainly on comparisons between the experimental conversion ratios and corresponding ones interpolated from the theoretical internal conversion coefficients of Rose [18]). The theoretical K and L shell conversion coefficients include screening and finite nuclear size effects, but the M shell coefficients do not. It may be remarked, however, that according to Rose [18]) the effects of the finite nuclear size should not influence the M shell coefficients strongly, nor should the neglect of screening be harmful to the ratios between the M shell conversion coefficients. In table 1 the theoretical ratios are given within brackets after the experimental values. For the high energy transitions, information from the scintillation spectrum was used when multipolarity assignments were made.

The half-lives given in table 1 are in most cases rather crude since only the peak height intensities were used for their calculation; but to distinguish between Pb^{198} and Tl^{198}, the accuracy is sufficient.

The 173.4 keV transition has been found to be in delayed coincidence with the K X-ray by Johansson *et al.* [19]), who measured a half-life of 4.5 ± 1 ns, which is a value in accordance with the systematics [20]) of E2 transitions in this mass region. In fig. 1 the pertinent part of the conversion spectrum is given; and from the measured $L_I + L_{II}/L_{III}$ ratio, an upper limit of M1 admixture in this transition was calculated as 1 %.

The 259.5, 290.3, and 382.0 keV transitions have K/L ratios which are somewhat smaller than those predicted theoretically for pure M1 transitions and this may indicate an admixture of E2 into the M1 transitions, but the

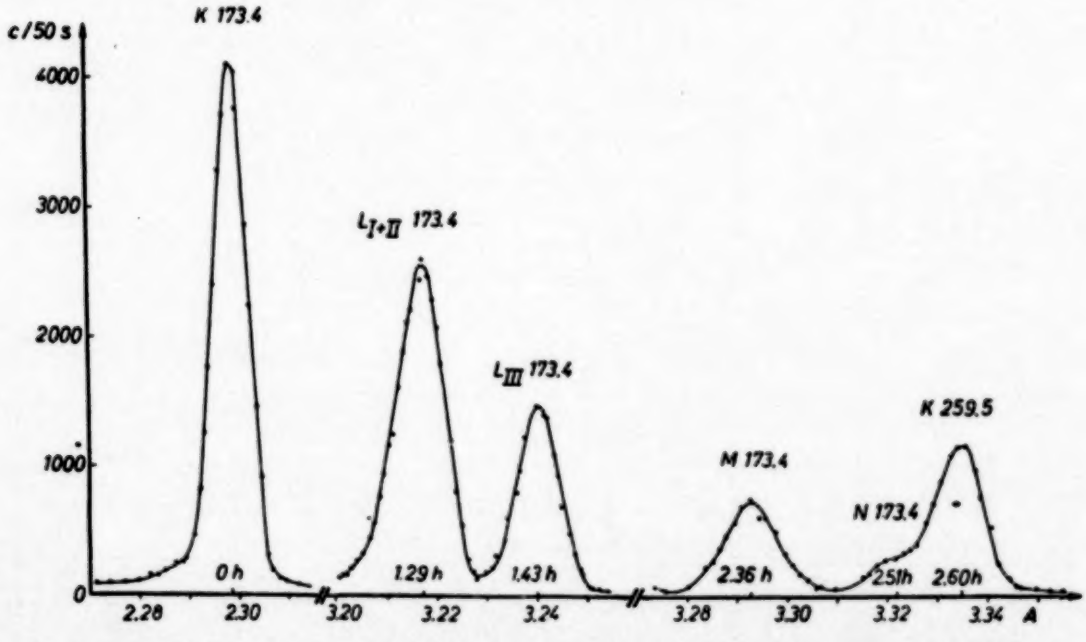

Fig. 1. Conversion spectrum of the 173.4 keV transition as measured with a momentum resolution of 0.35 %. Relative times of measurement are indicated on the abscissa. Counting time per point = 50 s.

possibility that the conversion lines are composite cannot be excluded.

The 389.5 keV transition is too weak to allow any multipolarity assignment; the L line, furthermore, has to be measured with high resolution in order to be separated from a neighbouring long-lived line (cf. table 3). The γ-spectrum gives no further information about the multipole order, because of its great complexity in this energy region.

The 397.7 keV transition needs a special discussion. As measured from the peak areas, the K/L conversion ratio was 2.0 which suggests an E2 or M4 character. The L_I+L_{II}/L_{III} ratio should then be 4.1 or 2.7, respectively, which is not in accordance with the measurements since these put a lower limit of 50 to the ratio. This suggests that the L line is composite which would also explain the unusually high L/M ratio of 5.7. The relevant part of the spectrum was measured with 0.25 % resolution, but as is shown in fig. 2,

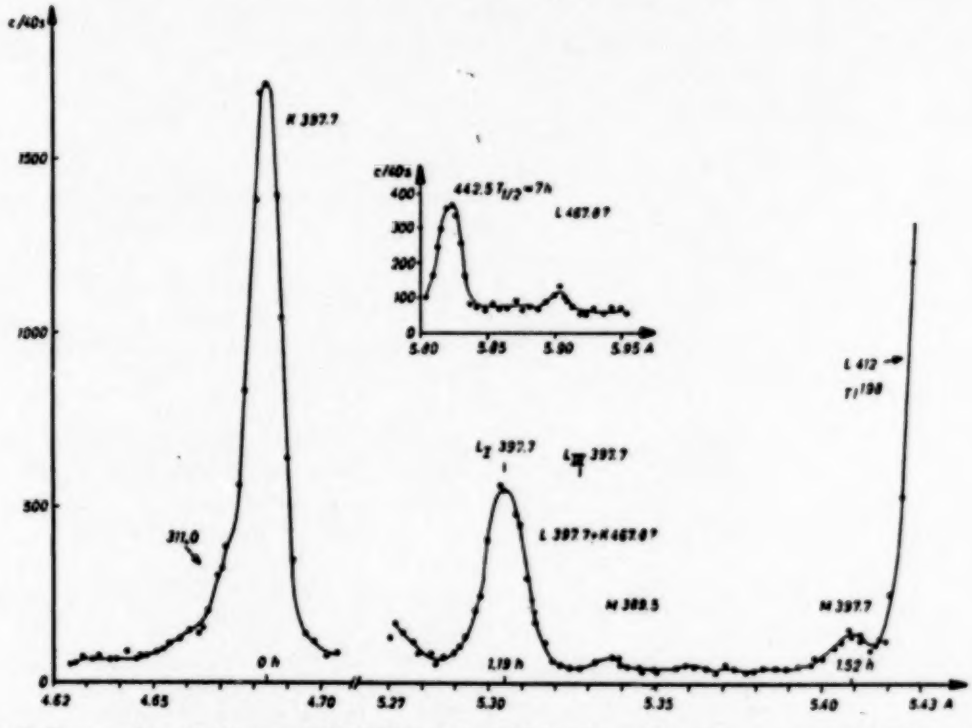

Fig. 2. Conversion spectrum of the 397.7 and 467.8 keV transitions as measured with a momentum resolution of 0.25 %. 311.0 is tentatively the K-conversion line of a 396.5 keV transition in Tl (cf. table 2). The inset shows the proposed L-conversion line of the 467.8 keV transition obtained from another source. Counting time per point = 40 s.

no composite character of the L line was revealed. A very weak line was found, however, in another measurement at the proper place for an L line converted in Tl with the corresponding K line composite with the L^- conversion line of the 397.7 keV transition. The γ-ray spectrum strengthens the assumption of a 468 keV transition by having a weak line at about this energy.

The half-life of Pb^{198} was checked by making accurate measurements on the intensities of the K 173.4, K 290.3 and K 365.4 keV lines at different times with the same source. As a mean value a half-life of 2.40 ± 0.10 hours was obtained.

Several of the electron lines attributed to the decay of Pb^{198} could not be assigned to a single conversion shell as firmly as those of table 1. These lines are collected in table 2. Some are rather weak which explains why no

TABLE 2

Electron lines in the decay of Pb^{198} not included in table 1
(Intensity scale: K 290.3 = 100)

Electron energy (keV)	Rel. line intensity	$T_{\frac{1}{2}}$ (h)	Possible conv. shell (Tl)	Proposed assignment	Remarks
21.8	1	<5	K, L, M	K 107.3 †	
36.7	1	<5	K, L, M		
37.4	0.2	<5	K, L, M		
52.8	10 ±2	<5	K, L	K 138.3 †	L 138.3 in 123.6 keV complex M 138.3 < 0.8
69.1	8	2.6	K	K 154.6	Too intense to be only $KL_{III}M$ Auger line
83.7	4	2.3	K	K 169.2	Too intense to be only KNN Auger line
103.7	0.7	<5	K, L		
119.8	0.6	<4	K, L		
123.6	8	2.8			Complicated mixture of several lines not resolved with 0.25 % resolution, not only L^- conversion lines
131.0	0.8	<3	K	K 216.5 †	
154.0	1			L 169.2	
181.2	2	2.5	K	K 266.7 †	L 266.7 in 251.3 keV line cf. table 3
189.8	4	2.5	K	K 275.4	L 275.4 in 259.3 keV line
200.9	2			L 216.5 †	Composite with Tl^{198} line?
259.3	1	<4			Broad line
300.4	0.4	<5	K	K 385.9	
311.0	0.8	<4	K	K 396.5 †	
342.8	1	<5	K	K 428.3	
520.4	1.8	2.6	K	K 605.9 †	
640	0.2	<5	K	K 726	
657	1.0	2.4	K	K 743	cf. the γ-spectrum
766	0.1	<5	K	K 852	

† Fit into the decay scheme (cf. fig. 4).

corresponding lines establishing the transition energy were found, others are too complex to allow any detailed interpretation. K/L ratios obtained from the calculations of Rose [18]) and the empirical rule $L/(M+N) \approx 3.2$ stated by Bäckström *et al.* [21]) were used for deriving the possible conversion shells. The others are excluded as corresponding lines should have been found. The tentatitive transitions stated in column 5 were derived mainly from the uniqueness of the conversion shell assignment, but in some cases the γ-

spectrum provides further confirmation. Some lines are rather loosely connected with transitions proposed by the decay scheme.

The conversion lines assigned to the decay of Tl^{198} are collected in table 3. No intensity relations are stated because of the complicated growth and decay features of a daughter activity; and, for the same reason, the half-lives given are very crude as no allowance was made for growth when they were calculated. Several of the lines can be recognized from earlier investigations of the decay of Tl^{198} [14, 22]), and, for the others, more detailed interpretations are deferred since the decay of Tl^{198} is the subject of a study in progress at this Institute.

Lines identified with contaminations are given in table 4. Many of the Tl^{199} lines were obtained from a source which was not equipped with a defining slit during the mass separation. The part of the spectrum which was measured with this source was, to a large extent, remeasured with other sources of higher purity.

The Auger region of the electron spectrum is very hard to interprete as Pb and Tl give Auger lines of nearly the same energies. The different Auger groups thus merge into each other. Intensity comparisons between corresponding Pb and Tl groups indicated, however, that some lines decaying with the shorter period were too strong to be only Auger lines. These lines are given in table 2.

3.2. γ-SPECTRUM

When measuring the γ-spectrum, the disturbances from the Tl^{198} decay were found to be rather limited since the whole spectrum decayed with a

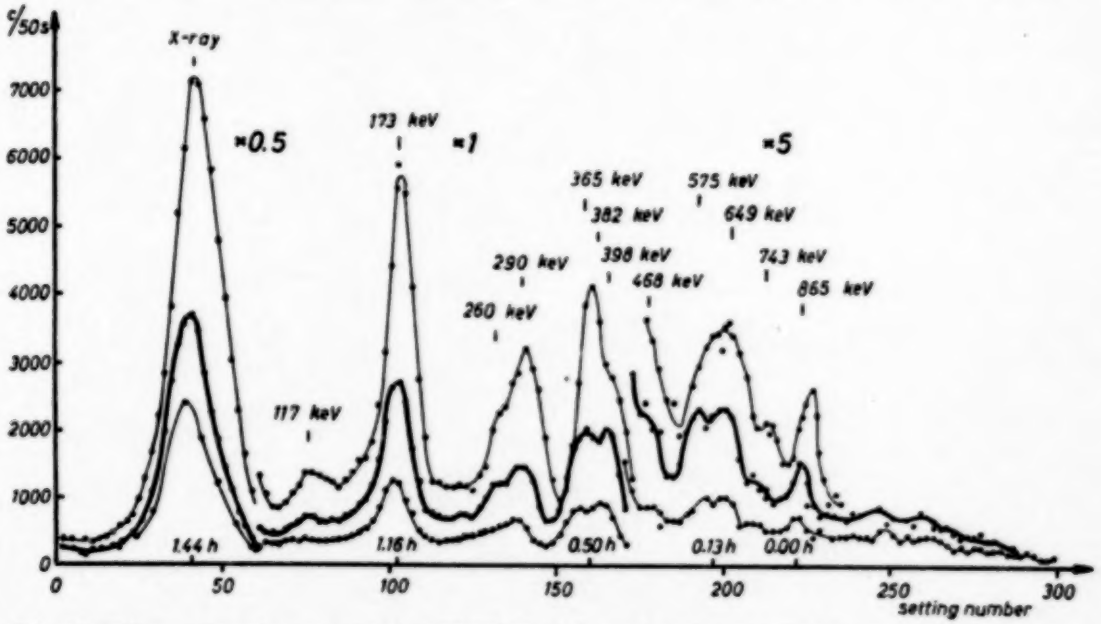

Fig. 3. Three successive γ-spectra of Pb^{198}. The time of measurement marked on the abscissa refer to the middle, bold-lined spectrum. Counting time per point = 50 s.

TABLE 3

Conversion electron lines assigned to the decay of Tl^{198}

Electron energy (keV)	$T_{\frac{1}{2}}$ (h)	Identified with	Reference
42.0	7		
46.3	5		
62.1	8		
121.4	6		
133.1	>10	Impurity?	
134.9	6		
137.3	4		
151.7	7		
155.3	5		
163.5	5		
199.3			
201.4	>10	K 284	[14]
219.9	7		
223.6	6		
224.9			
231.6	8		
242.2	6		
248.5	7		
293.5	7		
317.3	5	K 402	[14]
328.66		K 412 (standard)	[14]
344.0	7		
353.8	6		
372.8	11		
397.2	8	L 412	
408.3	8	M 412	
411.0	8	N 412	
442.5	7		
466.7	7		
503.4	7	K 586	[22]
514.9			
524.0	5		
554	14	K 635	[22]
581.7	13		
592.64	6	K 676 (standard)	[14]
603	11		
606	6		
622	10	L 635	
629	7		
634		M 635	
661	6	L 676	
674	10	M 676	
688	12		
705			
728			
757	5		

TABLE 3 (continued)

Electron energy (keV)	$T_{\frac{1}{2}}$ (h)	Identified with	Reference
834	>20		
840	7		
859	10		
907	5		
926	>5	924	[22])
963	7		
995	14		
1006	6	K 1088	[13])
1041			
1119	7	K 1198	[22])
1138	7		
1189	10		
1200	17		
1233	8		
1321	6		
1341	6		
1355	6		
1367	10		
1409	9		
1423	>5		
1435	>5		
1477	>5		
1515	>5		

TABLE 4

Internal conversion lines identified as due to impurities

Electron energy (keV)	$T_{\frac{1}{2}}$ (h)	Identified with	Reference
63.0	>20	L_I 77.6 Hg^{197}	[23])
63.6	>20	L_{II} 77.6 Hg^{197}	[23])
75.3	6	K 158 Tl^{199}	[14])
125.5	10	K 208 Tl^{199}	[14])
144.6	7	L_I+L_{II} 158 Tl^{199}	[14])
146.5	7	L_{III} 158 Tl^{199}	[14])
164.6	5	K 247 Tl^{199}	[14])
193.5	8	L_I+L_{II} 208 Tl^{199}	[14])
196.6	4	L_{III} 208 Tl^{199}?	[14])
207.5		L_{II} 222 Pb^{197m}	[1])
251.3	7	K 334 Tl^{199}	[14])
267.5	<3	K 352.8 Pb^{199}	[1])

half-life of about 3 hours and the prominent 412 keV transition in this decay did not appear as a peak, but was masked by the composite peak of 8 Pb^{198} transitions around 400 keV. The origin of the high-energy background is not completely understood; it may be due to Tl^{198} lines.

For the analysis of the spectrum, the transition energies found in the conversion electron measurements were used. The relative intensities of the γ-lines as calculated from the scintillation spectrum are given in table 5.

TABLE 5

Relative γ-intensities calculated from the γ- and the e^--spectrum. (The γ-intensities are normalized to the 173.4 keV γ-transition)

Transition energy (keV)	Relative intensity from γ-spectrum	Multipole assignment	Relative intensity from e^--spectrum
116.9	10	M1	13
173.4	100	E2	100
259.5	24	M1	27
290.3	50	M1	65
365.4		M1	
382.0	212	M1	130 [1]
389.5		M1	
397.7		M1	
467.8	9	M1	5
575.0		M1	
605.9	50	M1	55 [2]
649.0		E2	
743	8	M1	8
865.3	20	M1	25

[1]) The γ-spectrum might have been affected by the 412 keV transition in the Tl^{198} decay and by the three tentative transitions in this energy region given in table 2.

[2]) The E2 assignment for the 649.0 keV transition is based on the structure of the γ-peak. If M1 assignment the relative intensity from the electron spectrum is 30.

Because of the low resolution of the spectrometer, some lines were not resolved and had to be analysed as a group. Corresponding intensities were calculated from the intensities of the K-shell conversion electrons by using the theoretical internal conversion coefficients of Sliv and Band [24]). The intensity values were arbitrarily normalized to a γ-intensity of the 173.4 keV transition equal to 100. As can be seen from the table, the two intensity values are in good agreement except for the complex region around 400 keV. The reason for the discrepancy might be found in the 412 keV transition in the decay of Tl^{198} or in the three tentative transitions in this energy region which are proposed in table 2. As the γ-spectrum is rather complex and therefore hard to interprete, it is possible that the good agreement for some of the

other transitions might be fortuitous and the multipole assignments are thus less certain.

3.3. LEVEL SCHEME

The level scheme presented in fig. 4 is based mainly on energy relationships and must be regarded as tentative. For the sake of completeness the Tl branch of the decay of Tl^{198m} as given by Andersson and Bergström [25]) is included. All transitions given in table 1 are employed and some of the uncertain transitions of table 2, represented in the diagram by broken arrows, also fit nicely into the scheme.

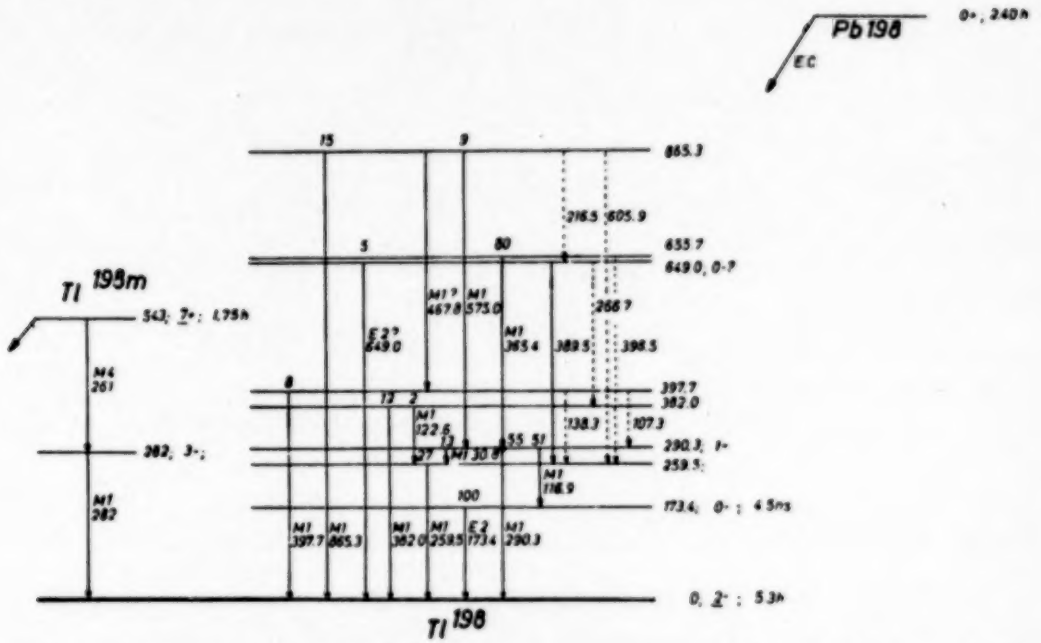

Fig. 4. Proposed level scheme for Pb^{198}. The energies are given in keV and the figures above the transition arrows refer to the total transition intensities, normalized to the 173.4 keV transition.

The coincidence measurements of Andersson *et al.* [1]) are in agreement with the scheme, except for the 397.7—290.3 keV pair, which according to the level scheme is not coincident as stated. This discrepancy called for a reinspection of the primary data from the coincidence measurements, and it was found that the coincidence effect for this pair was rather weak and thus may have been caused by impurities.

For the 290.3 and 365.4 keV pair the coincidence effect was strong, however, implying that these transitions are really in coincidence. The high intensity of the 365.4 keV transition makes it unlikely that there is an intermediate transition between this and the 290.3 keV transition and so they are placed in direct succession in the level scheme (cf. fig. 4).

The relative total transition intensities were calculated when possible by using the measured line intensities and the theoretical conversion coefficients

of Sliv and Band [24]). They are given as figures above the transition arrows in fig. 4. The total intensity of the 173.4 keV transition was arbitrarily equalled to 100.

The transitions suggested by the level scheme but which were not found are discussed in table 6.

TABLE 6

Transitions proposed by the level scheme for which corresponding conversion lines have not been found. (Energies in keV, intensity scale: K 290.3 = 100)

Transition between	Transition energy	Upper intensity limits or interfering electron lines
865.3 − 173.4	691.9	K masked by 606 keV line (cf. table 3)
− 382.0	483.3	K masked by 397 keV line (cf. table 3)
− 655.7	209.6	K in complex peak at 123.6 keV (cf. table 2)
655.7 − g.s.	655.7	K < 0.1
− 173.4	482.3	K masked by 397 keV line (cf. table 3)
− 382.0	273.7	K < 0.4
− 397.7	258.0	K coincides with N 173.4 (cf. table 1)
649.0 − 173.4	475.6	K < 0.2
− 290.3	358.7	K masked by L 290.3 (cf. table 1) L composite with K 428.3 (cf. table 2) and 344.0 keV line (cf. table 3)
− 397.7	251.3	K < 0.7
397.7 − 173.4	224.3	K < 0.4
382.0 − 173.4	208.6	K in complex peak at 123.6 keV (cf. table 2)
− 290.3	91.7	L masked by KMM Auger peak in Tl M coincident with K 173.4 (cf. table 1)
259.5 − 173.4	86.1	L masked by KLN Auger complex M < 0.8

From the existing information unambiguous spin and parity assignments cannot be given for most of the levels. The ground state spin has been measured by Lindgren *et al.* [26]) who found a spin of 2. For this state negative parity can be predicted by shell model considerations [25]).

The 173.4 keV transition between the first excited state and the ground state seems to be pure E2 and this may indicate a $\Delta I = 2$ transition. With a 2− ground state the 173.4 keV level should have spin and parity 0− or 4−, of which, however, the 4− assignment can be excluded since the level is not strongly fed in the decay of Tl^{198m}. The 290.3 keV level, decaying by M1 transitions both to the ground state and to the first excited state, should then have spin and parity 1−. The 649.0 keV level might be a 0− level as it seems to decay by an E2 transition to the ground state.

4. Discussion

The results on the decay of Pb^{198} obtained by Andersson *et al.* [1]) have been generally confirmed by the present work. All transitions which they assigned to the decay of Pb^{198} have been observed and the assigned multipole orders differ only for the 259.5 and 397.7 keV transitions where the earlier assignments were tentative. The transition energies are the same within the limits of error. The detection of a number of new transitions has made it possible to construct a tentative level scheme which needs checking with coincidence measurements before more definite conclusions can be drawn.

The similarity between the low lying levels in Tl^{200} and Tl^{198} may be worth mentioning. In Tl^{200} Åström *et al.* [27]) found the level sequence g.s. (2−), 148 keV (0−), 257 keV (1−), and 290 keV (?) while the corresponding levels in Tl^{198}, are, according to fig. 4, g.s. (2−), 173 keV (0−), 260 keV (?), and 290 keV (1−).

I wish to express my sincere thanks to Professor The Svedberg for his continuous interest in this work and to Professor Kai Siegbahn for stimulating contacts. To Dr. G. Andersson, Dr. E. Arbman and Dr. P. A. Tove, I am very much indebted for guidance and encouragement and for the opportunity of using their instruments. Thanks are due to Mr. Å. Svanheden and his cyclotron crew for the irradiations, to Miss I. B. Svensson for the chemical separations and to Mr. J. O. Burgman and Mr. R. Ringh for the mass separations.

The work has been financially supported by the Swedish Atomic Energy Commission.

References

1) G. Andersson, E. Arbman and B. Jung, Arkiv Fysik **11** (1957) 297
2) D. G. Karraker and D. H. Templeton, Phys. Rev. **81** (1951) 510
3) T. O. Passell, M. C. Michel and I. Bergström, Phys. Rev. **95** (1954) 999
4) J. O. Burgman and G. Andersson, Nuclear Instruments **3** (1958) 33
5) A. H. Wapstra, D. Maeder, G. J. Nijgh and L. Th. M. Ornstein, Physica **20** (1954) 169
6) G. Andersson, Arkiv Fysik **12** (1957) 331
7) G. Andersson, P. A. Tove, B. Jung and I. B. Svensson, Nuclear Physics **3** (1957) 493
8) E. Arbman and S. Svartholm, Arkiv Fysik **10** (1956) 1
9) B. D. Pate and L. Yaffe, Canadian Journal of Chemistry **33** (1955) 15
10) E. Arbman, Thesis (Uppsala, 1958)
11) I. Bergström and R. D. Hill, Arkiv Fysik **8** (1954) 21
12) D. E. Muller, H. C. Hoyt, D. J. Klein and J. W. M. DuMond, Phys. Rev. **88** (1952) 775
13) G. Bäckström and O. Bergman, Arkiv Fysik **13** (1958) 393
14) I. Bergström, R. D. Hill and G. de Pasquali, Phys. Rev. **92** (1953) 918
15) D. Saxon, Phys. Rev. **81** (1951) 639
16) P. A. Tove, Nuclear Instruments **2** (1958) 1
17) N. H. Lazar, R. C. Davis and P. R. Bell, Nucleonics **14** no. 11 (1956) 52

18) M. E. Rose, privately circulated tables (recently published in "Internal Conversion Tables" by M. E. Rose, North Holland Publishing Co., 1958)
19) B. Johansson, T. Alväger and W. Zuk, Arkiv Fysik **14** (1959) 439
20) I. Bergström and G. Andersson, Arkiv Fysik **12** (1957) 415
21) G. Bäckström, O. Bergman and J. Burde, Nuclear Physics **7** (1958) 263
22) J. D. Knight and E. W. Baker, Phys. Rev. **100** (1955) 1334
23) R. Joly, J. Brunner, J. Halter and O. Huber, Helv. Phys. Acta **28** (1955) 403
24) L. A. Sliv and I. M. Band, privately circulated tables
25) G. Andersson and I. Bergström, Nuclear Physics **3** (1957) 506
26) I. Lindgren, C. M. Johansson and S. Axensten, Phys. Rev. Letters **1** (1958) 473
27) B. Åström, B. Johansson and I. Bergström, Arkiv Fysik **12** (1957) 205

2.G *Nuclear Physics* **10** (1959) 457—467; © *North-Holland Publishing Co., Amsterdam*
Not to be reproduced by photoprint or microfilm without written permission from the publisher

THE INVESTIGATION OF THE MECHANISM OF THE Cr^{52} (d, p) Cr^{53} REACTION

IVO ŠLAUS

Institute "Rudjer Bošković", Zagreb, Yugoslavia

Received 2 January 1959

Abstract: The Cr^{52}(d, p)Cr^{53} reaction has been investigated at deuteron energies in the range 3.29 to 4.4 MeV. The measurements reveal the importance of the direct interaction process. The small angle part of the angular distribution could be fit with Butler's $L_a = 1$ curves. However, important deviations from the simple Butler theory have been found, which seem to be caused by the interference between stripping and compound nucleus formation. A pronounced secondary maximum evolved around 65°, and possible explanations of it are discussed.

1. Introduction

In the past few years a considerable effort has been made to understand the mechanism of (d, p) and (d, n) reactions. Though the simple Butler theory [1]) has been very sucessful in describing the main features of these reactions it has been realized that important modifications are required in order to interpret the existing data on angular distribution, angular correlations and polarization. Several measurements [2]) of the angular distributions performed at the energies below the Coulomb barrier have shown that, compared with the theory, the peaks are broader and somewhat shifted; the isotropic part is relatively much higher, the secondary maximum is almost as high as the main one and the absolute value of the cross section is appreciably reduced. A reasonably good fit to some of these measurements has been obtained [3]) by including in the theory Coulomb and nuclear interactions between the constituents of a reaction. Experiments on light nuclei have demonstrated the interference between direct interaction and compound nucleus formation [4]). Measurements of the excitation curves for Ca^{40}(d, p) Ca^{41} [5]) and Si^{28}(d, p) Si^{29} [6]) have indicated that the resonance structure persists even for heavier nuclei.

The purpose of the present experiment was to shed some light upon the mechanism of (d, p) reactions in the region of medium heavy nuclei. We chose Cr^{52} as a target nucleus. The Cr^{52}(d, p)Cr^{53} reaction has been previously investigated at a much higher energy [7]), and the spin and the parity of the ground state of Cr^{53} have been independently determined as $\frac{3}{2}-$ [8]). It seems that the ground state of Cr^{53} is, in agreement with the predictions of the

shell model, a $p_{\frac{3}{2}}$ level and that the stripping pattern is an $L_n = 1$ curve. The first excited state occurs at 0.54 MeV and is either [7]) $\frac{3}{2}-$ or $\frac{1}{2}-$. This level scheme is corroborated also by the measurement of the decay of V^{53}, [9]).

If the bombarding energy (3.2 MeV $\leqq E_d \leqq$ 4.4 MeV) is chosen to be considerably lower than the Coulomb barrier ($E_B \approx 7$ MeV), as it was done in this experiment, one expects to observe deviations from the Butler theory. Because the excitation energy in the compound nucleus Mn^{54} was about 18 MeV and our targets were usually about 130 keV thick one is inclined to interpret the results of the measurements as an average over the energy dependent features of the compound nucleus.

2. Experimental Arrangement

The deuteron beam was obtained from the University of Rochester 27" variable energy cyclotron [10]). The layout of the cyclotron and the associated equipment is shown in fig. 1. The beam was focussed by a quadrupole lens

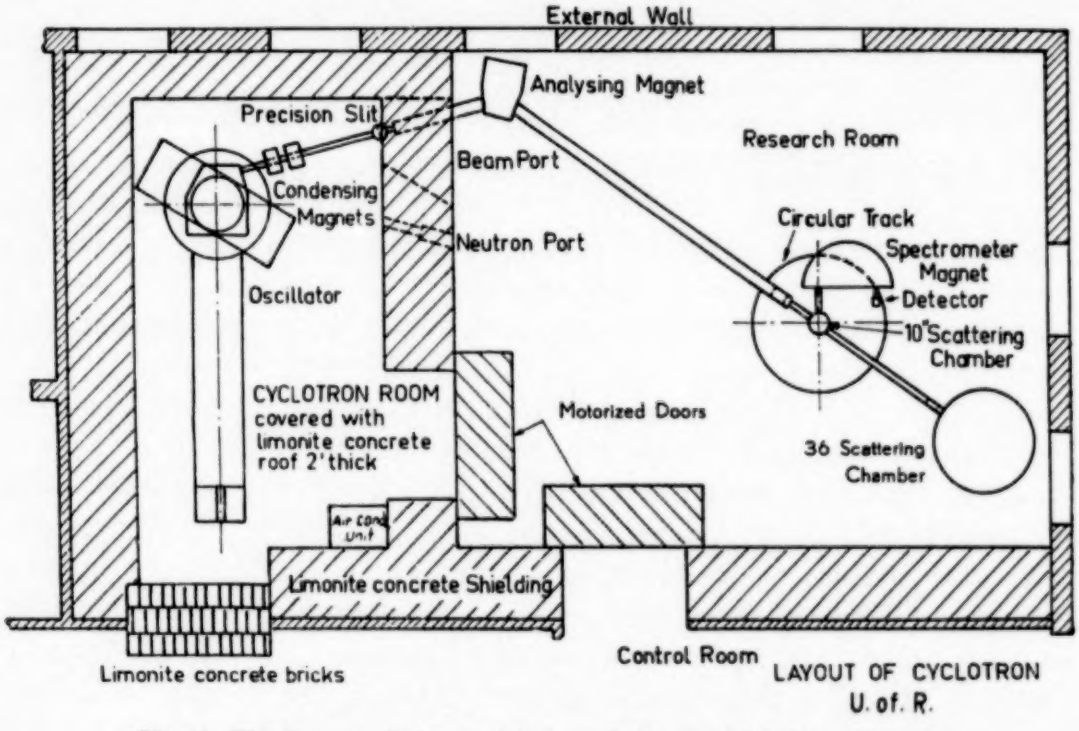

Fig. 1. The layout of the cyclotron and the associated equipment.

pair [11]) on a slit, which served as a source for a wedge analyzer magnet [11]). The energy resolution of this double focussing analyzer was 0.2 % and the energy calibration was accurate to 0.7 %. The analyzer magnet focussed part of the beam through the slit into two scattering chambers in tandem.

The experiment was performed in the 36" scattering chamber. An adjustable collimating system at the entrance to this chamber defined the

beam spot on the target. The beam was collected in a Faraday cup and the beam current was measured by an integrator.

A CsI(Tl) scintillation counter fixed at 45° relative to the beam direction monitored the elastically scattered deuterons from the target. The angular resolution of the monitor was 0.7°. Another CsI(Tl) scintillation counter, mounted on the rotating arm inside the scattering chamber, detected protons from the Cr^{52}(d, p)Cr^{53} reaction. A sandwich absorber made of aluminium and mylar was placed in front of the crystal. Its thickness was sufficient to stop protons of about 6 MeV. The counter could be set anywhere from 8° to 170° with an accuracy of 0.5°. The angular resolution was 0.9°. The zero of the angular scale was determined to $\pm 0.25°$ by measuring the Rutherford scattering from gold. Pulses from the detector, after passing through the preamplifier and the amplifier were analyzed by a 100 channel R.I.D.L. Model 3300 pulse height analyzer. The resolution of the detector was about 4 %.

The self supporting chromium targets were made by electroplating from a solution containing 250 g Cr_2O_3, 2.5 g H_2SO_4 and 1 litre of water. Thin copper foils were used as cathodes. After annealing by heating in a flame, the copper backing could be dissolved in a dilute nitric acid. Several targets from 0.1 to 2.5 mg · cm^{-2} in thickness were made by this method. The contamination due to light elements was determined to be less than a few per cents in all cases. The heavy element impurities were negligible. The isotopic composition of natural chromium is: Cr^{52} 83.8 %, Cr^{53} 9.5 %, Cr^{50} 4.3 % and Cr^{54} 2.4 %.

3. Measurements

Most of the measurements were performed using the 1.15 ± 0.15 mg · cm^{-2} thick chromium target set at an angle of $\pm 65°$ to the incident beam direction. Pulse height distributions obtained by the scintillation counter at incident energies of 3.29 MeV, 4.07 MeV and 4.27 MeV, at 60°, 150° and 65° respectively are shown in fig. 2. The proton group corresponding to the ground state and first excited state of Cr^{53} are labelled by "0" and "1". Although we used a natural chromium target, the Q-values of possible reactions are such that the proton groups "0" and "1" could interfere only with protons from Cr^{50}(d, p)Cr^{51} reaction and, if the target was contaminated with light elements, also with protons from C^{13}(d, p)C^{14} and O^{17}(d, p)O^{18} reactions. The contribution of these protons to the groups "0" and "1" is believed not to amount to more than 2 %. The few counts above the "0" group belong mostly to the Cr^{53}(d, p)Cr^{54} reaction.

The excitation curves for the ground state and first excited state groups were measured from 3.29 MeV to 4.4 MeV by the counter set at 20°. This

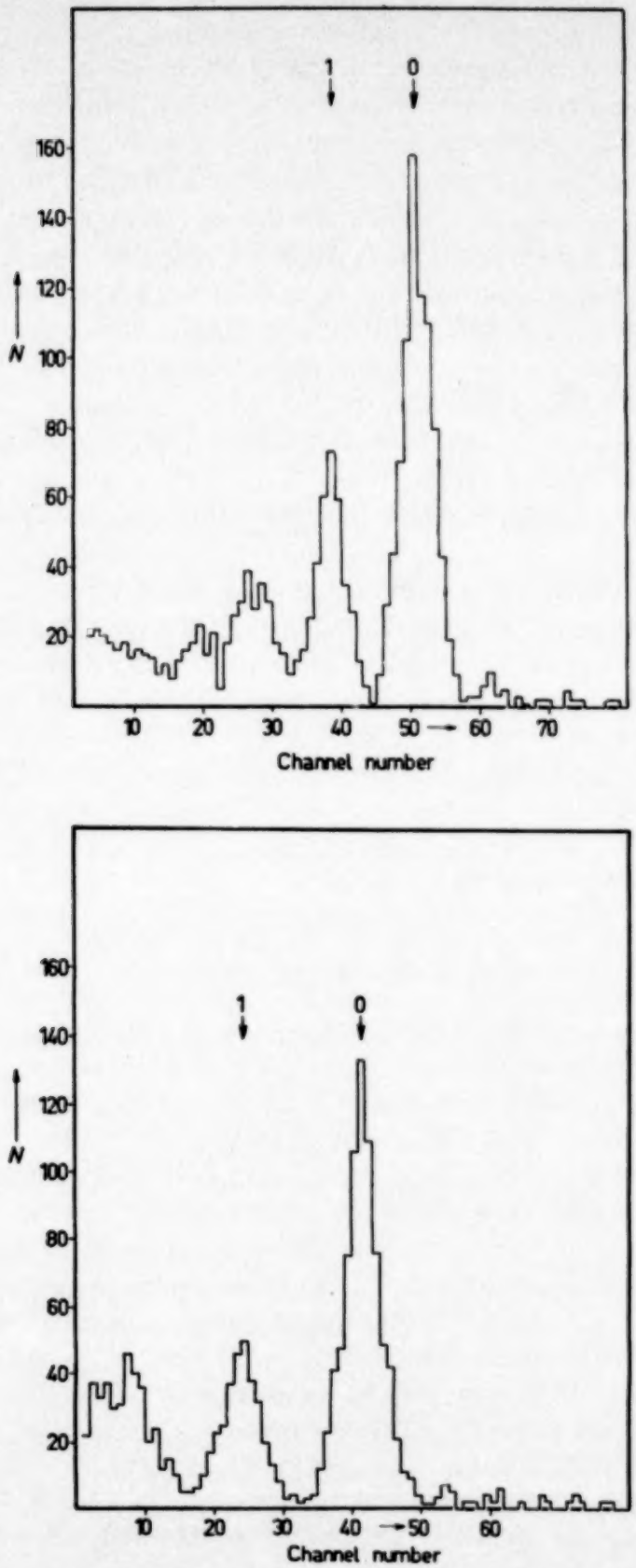

Fig. 2. Proton spectra from the Cr(d, p) reaction obtained at the incident energy of 3.29 MeV, 4.07 MeV and 4.27 MeV at 60°, 150° and 65° respectively. "0" and "1" indicate the proton groups corresponding to the formation of Cr^{53} in the ground state and in the first excited state.

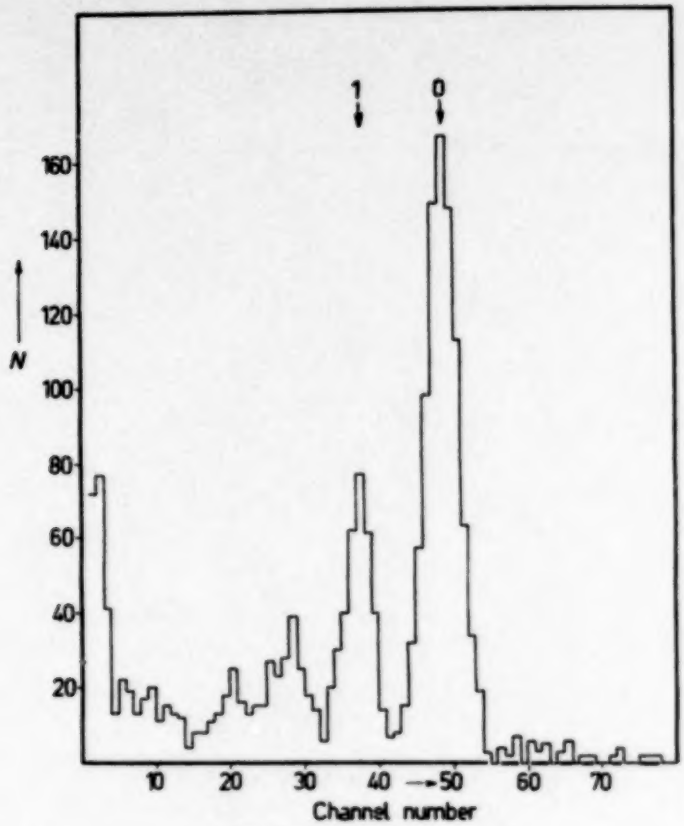

Fig. 2 (continued)

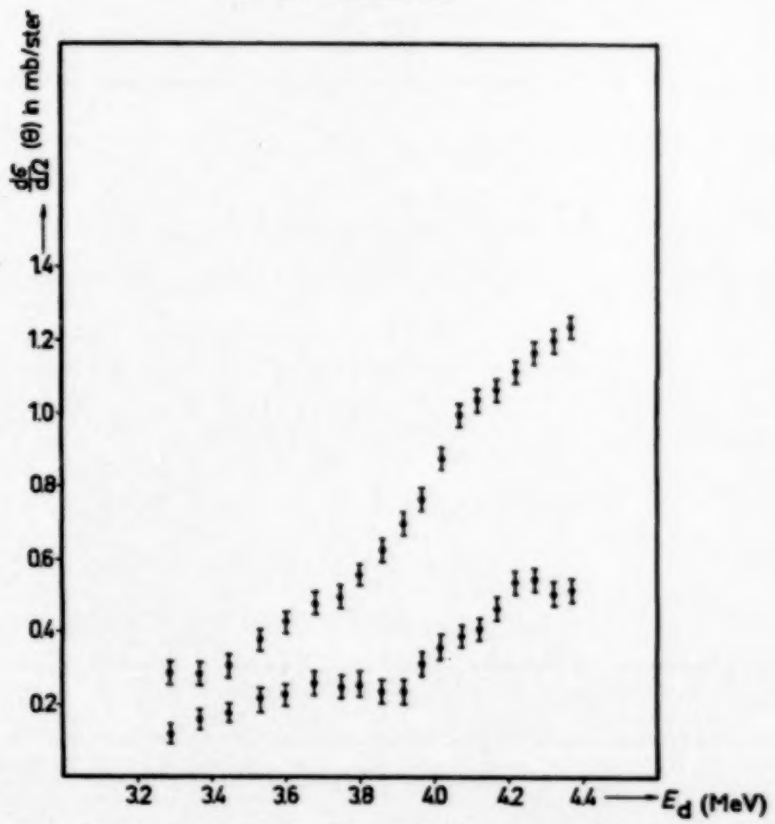

Fig. 3. The excitation curves for the Cr^{52}(d, p)Cr^{53} reaction. The cross section is measured with a counter set at 20°. The upper curve is for ground state protons and the lower for first excited state protons.

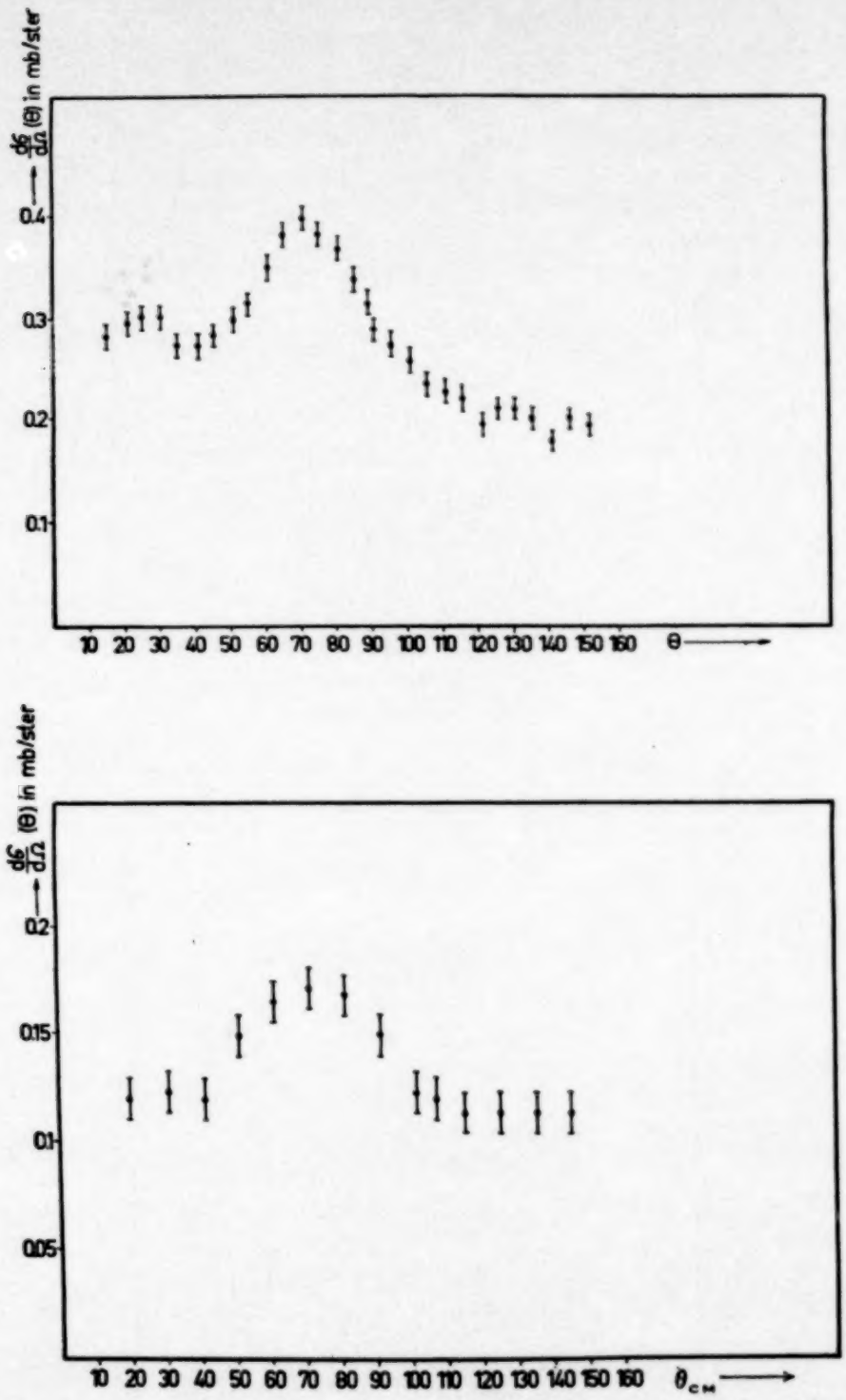

Fig. 4. The angular distributions of protons leaving Cr^{53} in the ground state and in the first excited state respectively. Incident energy: $E_d = 3.29$ MeV.

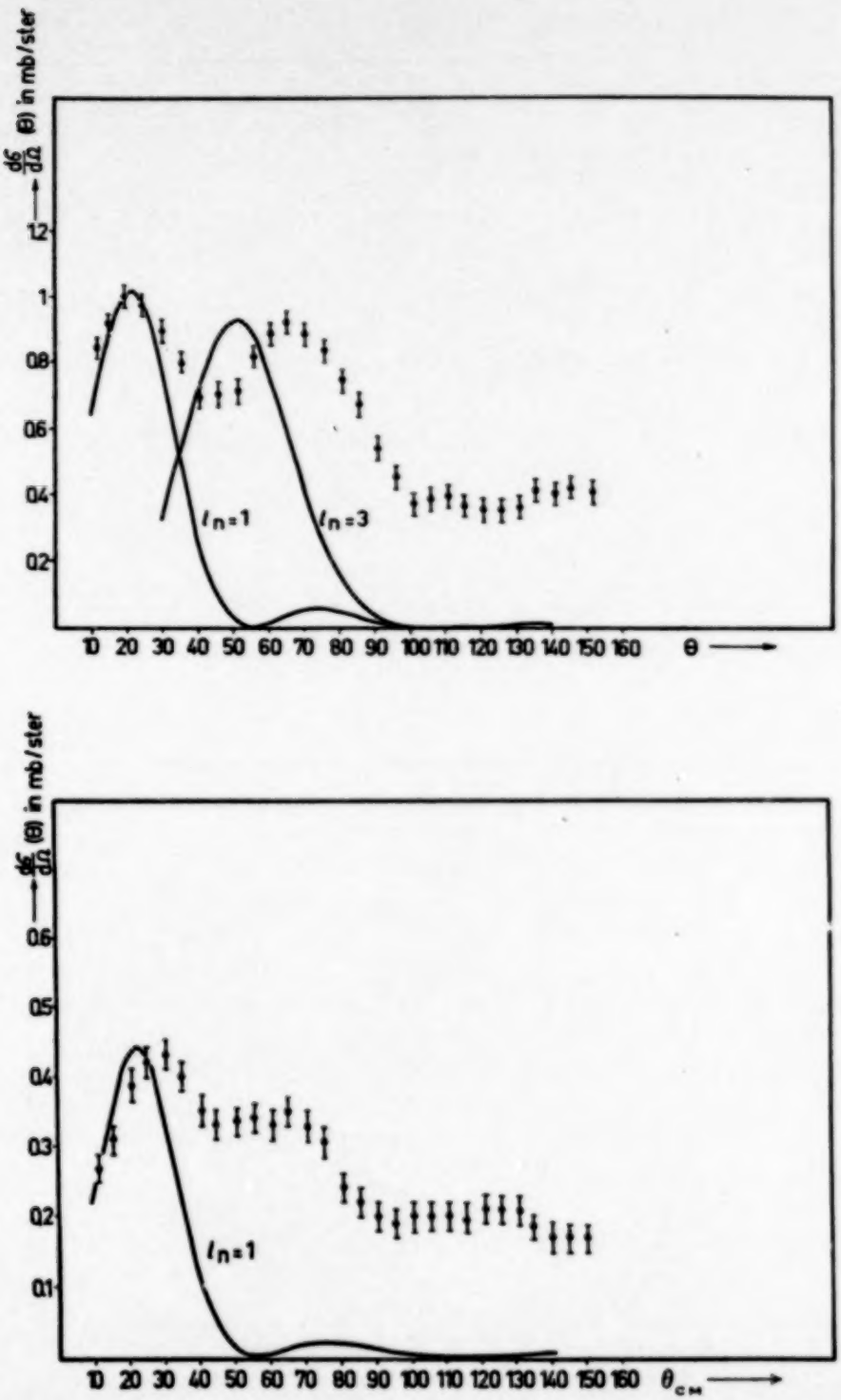

Fig. 5. The angular distributions of protons leaving Cr^{53} in the ground state and in the first excited state respectively. Incident energy $E_d = 4.07$ MeV. The solid curves are Butler's $L_n = 1$ and $L_n = 3$ curves calculated for $r_0 = 6.3 \times 10^{-13}$ cm.

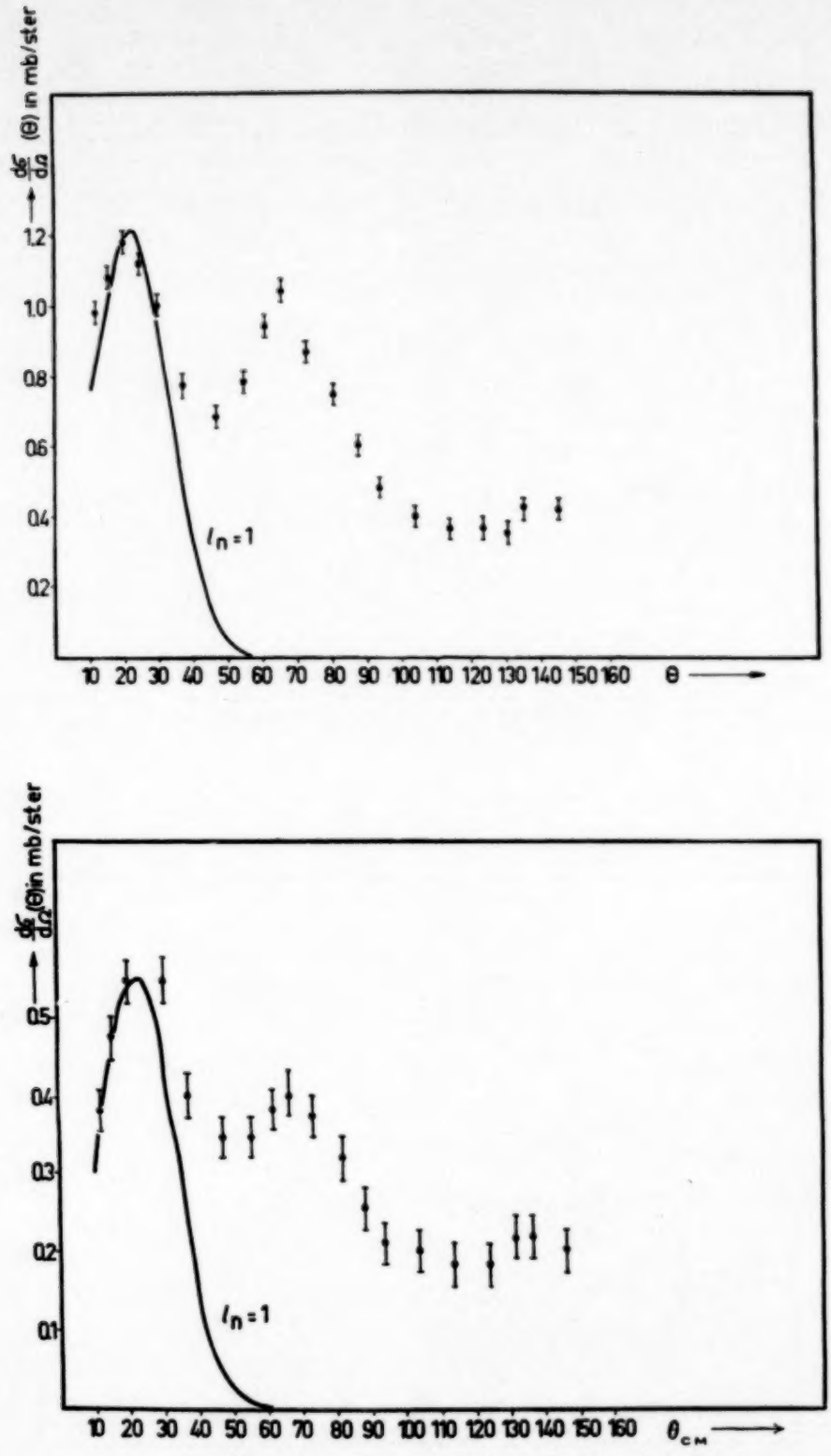

Fig. 6. The angular distributions of protons from the ground state and first excited state of Cr^{53}. Incident energy $E_d = 4.27$ MeV. The solid curves are Butler's $L_n = 1$ curves calculated for $r_0 = 6.3 \times 10^{-13}$ cm.

measurement was done on a (0.8 ± 0.1) mg · cm^{-2} thick target. The angular distributions were measured at the lowest energy we could reach: 3.29 MeV, and at two higher energies: 4.07 MeV and 4.27 MeV. The results are presented in figs. 3—6. The bars represent the statistical error.

Absolute differential cross sections were determined by comparing the proton yields with that of the elastically scattered deuterons using a monitor set at 45°. The elastic scattering of deuterons from chromium has been previously investigated [12]) and it has been shown that at 45° at low energies (up to about 4 MeV) there is no deviation from the Rutherford scattering. At higher energies the deviation increases steadily. The uncertainty in this fractional departure from the Rutherford scattering was estimated to be 3 %. The error introduced by counting protons from (d, p) reactions in the monitor was estimated to be less than 0.5 %. The angular position of the monitor was carefully determined with an uncertainty of 0.6°, which in turn causes at most a 6.5 % error in the absolute cross section. The error arising from variations in the beam intensity over the area of the beam spot on the target was estimated to be 3.5 %. An error of less than 1 % could be ascribed to the uncertainty of the deuteron energy. The overall accuracy of the absolute measurement is believed to be at least 10 %. The relative accuracy within an angular distribution is determined by the statistical errors.

4. Discussion

The prominent feature of this measurement is the pronounced forward peaking which indicates the importance of the direct interaction process even at energies only half as high as the Coulomb barrier. The forward-to-backward asymmetry increases as the incident energy increases and it is in general higher for the ground state group than for the first excited state group. The experimental data taken at 4.07 MeV and 4.27 MeV are compared with the Butler theory in figs. 5 and 6. The curves calculated for $L_n = 1$ and (following the suggestion of Holt and Marsham [13]))

$$r_0 = (1.22\, A^{\frac{1}{3}} + 1.7) \times 10^{-13}\ \text{cm} = 6.3 \times 10^{-13}\ \text{cm}$$

fit the first experimental maximum fairly well. The discrepancies between the theoretical curves and the experimental points at forward angles, namely, the broader maximum and the shift of the peak toward larger angles for the first excited state group can probably be explained in terms of Tobocman's refinements of the simple stripping theory. One can see that the shift is smaller as the incident energy increases.

The reduced width θ_0^2 for the ground state group, calculated at 4.07 MeV, is 0.08 %. Assuming that the spin of the first excited state of Cr^{53} is $\frac{3}{2}$, one obtains, at the same energy, $\theta_1^2 = 0.03$ %. The absolute value of the reduced widths is apparently too small due to the neglect of the Coulomb

and nuclear interactions. Correcting the cross section by a factor R_∞^2, as suggested by Butler [14]), one obtains for Θ_0^2 an unacceptably large value of about 160. However, by comparing the reduced widths for the two Cr^{53} levels one might conclude that the configuration of the first excited state is not so pure, in the sense of the single particle model, as that of the ground state.

The shape of the experimental angular distribution, with the exception of the small angle part just discussed, differs markedly from Butler's $L_n = 1$ curves. The first departure consists in a large isotropic part, the relative contribution of which increases as the incident energy decreases. It is difficult to estimate whether this isotropic background is entirely due to the reaction proceeding via compound nucleus formation, but it is probable that at least some part of it is. This can be coroborated by the excitation curve for the first excited state group, which shows some broad structure superimposed on a steep increase. The general trend of the excitation curves can be explained by barrier penetration.

The other important deviation is the marked maximum around 65°. Its shape and intensity are such that one is tempted to associate it with some other stripping curve, e.g. $L_n = 3$. Tests performed with other targets have demonstrated that this peak is not due to any possible contaminants. Also the level scheme of Cr^{53} is known well enough to rule out the possibility of two closely spaced levels, which could not be resolved in our measurement. It seems to us that the level spacings $1f_{\frac{5}{2}}-2p_{\frac{3}{2}}-1f_{\frac{7}{2}}$ [15]) and the character of Cr^{53} levels make the explanation of the shape of the angular distribution curves in terms of the spin-flip mechanism [16]) with a capture of a neutron in the 1f level improbable. It should be pointed out, moreover, that the $L_n = 3$ curve would have a maximum at 50° and the Coulomb interaction would have to be assumed in order to shift the maximum to 65° or 70°. Such a large shift seems inconsistent with almost no shift of the $L_n = 1$ curve. For that reason, one is inclined to conclude that the maximum around 65° is not an $L_n = 3$ stripping pattern. The regular variation of the angular distribution with energy suggests that it is not caused by any resonance effect.

The most probable explanation of this secondary maximum, which was also observed earlier for other target nuclei [2]), seems to be in terms of the nuclear interaction [3]) between the incident and outgoing particles with the initial and residual nuclei.

The author is indebted to Prof. W. P. Alford, Dr. Y. Hashimoto, Dr. K. Ilakovac and Dr. M. Cerineo for many stimulating discussions. He also wishes to express his gratitude to the University of Rochester, where this experiment was performed, for the hospitality, and to the Institute "R. Bošković" for a grant during his stay in U.S.A.

References

1) Butler, Proc. Roy. Soc. A **208** (1950) 559
2) Pratt, Phys. Rev. **97** (1955) 131;
Lee and Rall, Phys. Rev. **99** (1955) 1384;
Pratt, Phys. Rev. **95** (1954) 1517;
Teplov and Yuryev, J. Exptl. Theoret. Phys. USSR **33** (1957) 1313;
Teplov and Yuryev, J. Exptl. Theoret. Phys. USSR **34** (1958) 334
3) Tobocman, Phys. Rev. **94** (1954) 1655
Tobocman and Kalos, Phys. Rev. **97** (1955) 132;
Butler and Austern, Phys. Rev. **95** (1954) 605;
Horowitz and Messiah, J. Phys. Radium **14** (1953) 695
4) Baumgartner and Fulbright, Phys. Rev. **107** (1957) 219;
Stratton *et al.*, Phys. Rev. **98** (1955) 629;
McEllistrem *et al.*, Phys. Rev. **104** (1956) 1008;
Bonner *et al.*, Phys. Rev. **101** (1956) 209;
Marion and Weber, Phys. Rev., **103** (1956) 167;
Jurić, Phys. Rev. **98** (1955) 85
5) Lee and Schiffer, Phys. Rev. **107** (1957) 1340
6) Nemilov and Litvin, J. Exptl. Theoret. Phys. USSR **31** (1956) 719
7) Elwyn and Shull, Bull. Am. Phys. Soc. **1** (1956) 281
8) Halbach, Helv. Phys. Acta **27** (1954) 259;
Alder and Halban, Helv. Phys. Acta **26** (1953) 426;
Bowers, Proc. Phys. Soc. A **65** (1952) 860
9) Schardt and Dropesky, Bull. Am. Phys. Soc. **1** (1956) 162
10) Fulbright *et al.*, NYO report (1954) 6541
11) Bromley and Bruner, NYO report (1954) 3823
12) Slaus and Alford, to be published (NYO report 2137)
13) Holt, and Marsham, Proc. Phys. Soc. A **66** (1953) 1032
14) Butler, Nuclear Stripping Reactions (1957)
15) Nussbaum, Revs. Mod. Phys. **28** (1956) 423
16) Wilkinson, Phys. Rev. **105** (1957) 666;
A. P. French, Phys. Rev. **107** (1957) 1655;
Hensel and Parkinson, Phys. Rev. **110** (1958) 128
A. P. French and Evans, Phys. Rev. **109** (1958) 1272

8.B *Nuclear Physics* **10** (1959) 468—474; © *North-Holland Publishing Co., Amsterdam*
Not to be reproduced by photoprint or microfilm without written permission from the publisher

ON THE SECOND ORDER WAVE EQUATION OF FERMIONS II

G. MARX

Institute for Theoretical Physics, Roland Eötvös University
and
Central Research Institute for Physics, Budapest

Received 2 January 1959

Abstract: A new space reflection P′ and charge conjugation C′ can be readily introduced from the second order wave equation for fermion doublets. Strong as well as weak interactions are invariant with respect to P′ and C′ while electromagnetic interactions show only P′C′ invariance. The wave operator for the nucleon (and for other fermion doublets) is the irreducible representation of the Lorentz group extended by P′ and C′. Results obtained by this theory and by that of Gell-Mann disagree only as to decay of strange particles.

1. Introduction

The theory of universal Fermi interactions has increasing evidence in its favour. The basic idea is that vectors have to be constructed for various fermion pairs:

$$G_i(\mathrm{A},\mathrm{B}) = i\sqrt{f}\,(\bar{\psi}_\mathrm{A}\gamma_i\tfrac{1}{2}(1+\gamma_5)\psi_\mathrm{B}) \neq G_i^+(\mathrm{A},\mathrm{B}) \qquad (1)$$

($\sqrt{f}$ is real) and the universal Hamiltonian for weak interactions is given by the scalar product of such vectors:

$$H_\beta = G_i(\mathrm{A},\mathrm{B})G_i^+(\mathrm{C},\mathrm{D}) + G_i^+(\mathrm{A},\mathrm{B})G_i(\mathrm{C},\mathrm{D}). \qquad (2)$$

It is of interest to note, however, that such vectors cannot be built from any fermion pair and only certain pairings are allowed. Gell-Mann, for instance, proposes the following three classes [1]:

$$\begin{aligned}
&\text{I. Lepton pairs:} && (\mathrm{e},\nu),\ (\mu\nu).\\
&\text{II. Strangeness-conserving baryon pairs:} && (\mathrm{np}),\ (\Sigma^0\Sigma^+),\ (\Sigma^-\Sigma^0),\ (\Xi^-\Xi^0).\\
&\text{III. Strangeness-violating baryon pairs:} && (\Lambda\mathrm{p}),\ (\Sigma^0\mathrm{p}),\ (\Sigma^-\mathrm{n}),\ (\Xi^-\Lambda),\\
& && (\Xi^-\Sigma^0),\ (\Xi^0\Sigma^-).
\end{aligned} \qquad (3)$$

Class II is selected according to the unique rule that by the omission of the axial vector part in eq. (1) the current of the isobaric spin component $\mathcal{J}_-$ is obtained [2]. These pairs are products of π^+-dissociation. The only difference is that the latter selection principle would lead, in addition, to the $\Lambda^0\Sigma^+$ doublet. Products of K^+-meson dissociation are found in class III. Class I contains lepton pairs selected by the rule that in interaction processes an equal number of charged and neutral leptons should take part [3].

A closed theory of universal Fermi interaction would require that fermion pairs occurring in eq. (1) should be defined, instead of the specification given in the enumeration (3), by a rule "expressible in a single comprehensive sentence". In a previous paper [4]) we made the following attempt: it was assumed that the known fermions could be assigned to doublets according to a natural and unambiguous rule (e.g. (np), (eν)) and a fermion doublet could be described by a single field operator χ. This could be constructed in an unequivocal way from the Dirac wave operators of the doublet and would satisfy a four component second order wave equation of the Feynman type [5]).

2. The Theory of Ogievetsky and Chou

If we attempt to describe a fermion doublet, e.g. the proton and neutron, by a single multicomponent χ, it will not give an irreducible representation of the Lorentz group. The nucleon will be transformed irreducibly only in the combined Lorentz + isobaric group; a reference to the isobaric group is, however, not permitted for weak interaction since, contrary to strong interactions, they are not charge independent.

Recently Ogievetsky and Chou proposed [6]) to consider the nucleons, from the point of view of strong interactions, as the irreducible representation of the extended Lorentz group. Their hypothesis may be reformulated as follows: The usual operators for space reflection, (strong) time reflection and charge conjugation are given by

$$P\psi(\mathbf{r}, t)P^{-1} = \gamma_4\psi(-\mathbf{r}, t), \tag{4}$$

$$X\psi(\mathbf{r}, t)X^{-1} = i\gamma_5\gamma_4\psi(\mathbf{r}, -t), \tag{5}$$

$$C\psi(\mathbf{r}, t)C^{-1} = \gamma_c\bar{\psi}(\mathbf{r}, t) = \psi^c(\mathbf{r}, t), \tag{6}$$

respectively. (Symbols given in ref. [4]) are used.) Phase factors are chosen so that

$$P^2 = X^2 = C^2 = 1. \tag{7}$$

According to eqs. (4), (5), (6) the following relationships may be obtained:

$$PX = (-1)^N XP, \tag{8}$$

$$PC = (-1)^N CP, \tag{9}$$

$$XC = (-1)^N CX. \tag{10}$$

(N is the operator of the fermion number.) Geometrically the space reflection and the time reflection commute and therefore a new interpretation of time reflection is required so that the new time reflection operator Y should satisfy the following relations:

$$Y^2 = 1, \tag{11}$$

$$PY = YP, \tag{12}$$

while the validity of

$$YC = (-1)^N CY \tag{13}$$

remains unchanged.

It is easy to find such an operator Y; it has the concrete form

$$Y = XC\mathrm{e}^{-i\pi\mathscr{I}_2} = T\mathrm{e}^{-i\pi\mathscr{I}_2}, \tag{14}$$

where $T = XC$ is Wigner's weak time reflection, $\mathscr{I}_2$ is the 2nd component of the isobaric spin operator. Considering that [7])

$$[P, \mathscr{I}_2] = 0, \qquad [C, \mathscr{I}_2] = 0, \qquad \{X, \mathscr{I}_2\} = 0, \tag{15}$$

the validity of eqs. (11), (12) and (13) can be readily proved. Since the charge symmetry operator $\mathrm{e}^{-i\pi\mathscr{I}_2}$ leads to the interchange of p and n, we obtain by extending the group of proper Lorentz transformations L with P, Y, C an extended Lorentz group which can be irreducibly represented only by the eight component nucleon wave operator but not by the proton wave function in itself.

The electromagnetic interaction, on the other hand, is not invariant with respect to Y. Nor do weak interactions show isobaric invariance, but some invariance is found under charge symmetry transformation [8]). Now it seems very likely that a similar procedure may be used for the required interpretation of fermion doublets in weak interaction. Of course the Ogievetsky-Chou theory cannot be applied because of the important role played in it by P and C, for weak interactions are not invariant with respect to P and C.

3. P' and C' Operators

In this section our considerations will be restricted to the interactions of the nucleon doublet with γ and with $e\nu$: the study of strong interactions does not lead to new aspects, and the weak interactions of other elementary particles will be discussed in this respect in section 4.

The Dirac equation for free nucleons is written

$$(\gamma_i\partial_i + \kappa)\psi_\mathrm{p} = 0, \quad (\gamma_i\partial_i + \kappa)\psi_\mathrm{n} = 0. \tag{16}$$

The Hamiltonian for electromagnetic interaction is given by

$$H_\gamma = \tfrac{1}{2}iec\bar{\psi}_\mathrm{p}\gamma_i\psi_\mathrm{p}A_i + \text{charge conjugate}. \tag{17}$$

From eqs. (1) and (2) the Hamiltonian for β-interaction is obtained as

$$H_\beta = -f[(\bar{\psi}_\mathrm{n}\gamma_i\tfrac{1}{2}(1+\gamma_5)\psi_\mathrm{p})(\bar{\psi}_\nu\gamma_i\tfrac{1}{2}(1+\gamma_5)\psi_\mathrm{e}) + (\bar{\psi}_\mathrm{p}\gamma_i\tfrac{1}{2}(1+\gamma_5)\psi_\mathrm{n})(\bar{\psi}_\mathrm{e}\gamma_i\tfrac{1}{2}(1+\gamma_5)\psi_\nu)]. \tag{18}$$

It can be seen that all these equations are invariant under the proper Lorentz group L. (The transformation formulas for A_i are always the usual

expressions.) Formulae (16) and (17) are invariant with respect to the transformations P, C given in eqs. (4) and (5), the expression (18), however, shows only PC = K invariance. Usually, this phenomenon is interpreted as the reduced degree of symmetry of week interactions: they are not invariant under space reflection and charge conjugation. (There is no question of time reflection: the TCP theorem holds now, and from L and K invariance the T invariance follows throughout.)

Let us rewrite the above equations according to ref. [4]). By introducing the new operator

$$\chi = \tfrac{1}{2}(1+\gamma_5)\psi_p + \tfrac{1}{2}(1-\gamma_5)\psi_n^c, \tag{19}$$

one gets from eqs. (16), (17), (18) the following relations:

$$(\Box - \kappa^2)\chi = 0, \tag{20}$$

$$H_\gamma = iec\bar{\chi}\gamma_i \tfrac{1}{2}(1+\gamma_5)\chi + \text{charge conjugate}, \tag{21}$$

$$H_\beta = \tfrac{1}{4}f[\bar{\chi}^c\gamma_5\gamma_i\chi\ \bar{\eta}\gamma_5\gamma_i\eta^c + \bar{\chi}\gamma_5\gamma_i\chi^c\ \bar{\eta}^c\gamma_5\gamma_i\eta]; \tag{22}$$

η is the spinor constructed from ψ_ν and ψ_e similarly to eq. (19).

Equations (20), (21), (22) are completely equivalent to (16), (17) and (18) because ψ_p and ψ_n can be expressed from χ as

$$\begin{aligned} \psi_p &= [1+\kappa^{-1}\gamma_5\gamma_i\partial_i]\tfrac{1}{2}(1+\gamma_5)\chi = \tfrac{1}{2}(1+\gamma_5)\chi + \tfrac{1}{2}(1-\gamma_5)\xi^c, \\ \psi_n &= i[1+\kappa^{-1}\gamma_5\gamma_i\partial_i](\tfrac{1}{2}(1-\gamma_5)\chi)^c = \tfrac{1}{2}i(1+\gamma_5)\chi^c - \tfrac{1}{2}i(1-\gamma_5)\xi; \end{aligned} \tag{23}$$

ξ now denotes a subsidiary quantity constructed from the derivatives of χ:

$$\xi = -\kappa^{-1}\gamma_5\gamma_i\partial_i\chi^c. \tag{24}$$

Since the equations were simply rewritten, the formulae (20) and (21) continue to be invariant with respect to L, P, C and (22) is invariant with respect to L, K. The transformations P and C have, however, a very complex effect on the wave function χ:

$$P\chi(\mathbf{r}, t)P^{-1} = \gamma_4\xi^c(-\mathbf{r}, t) = [\kappa^{-1}\gamma_5\gamma_i\partial_i\gamma_4\chi]_{\mathbf{r}\to-\mathbf{r}}, \tag{25}$$

$$C\chi(\mathbf{r}, t)C^{-1} = \xi = -\kappa^{-1}\gamma_5\gamma_i\partial_i\chi^c(\mathbf{r}, t), \tag{26}$$

(there is no change in L). However, all transformations are such that through them the positive and the negative chirality part of χ each is transformed into itself, and therefore, as stated previously, the proton and neutron fields deduced from those according to (23) remain disconnected; χ is thus a reducible representation of group (E) = (L, P, T). With L, P we may write T instead of K according to the TCP theorem.

Now, let us forget for a moment the Dirac equation and consider eqs. (20), (21), (22) in themselves, expressed with χ. Obviously they are invariant with respect to L. Neglecting the electromagnetic interaction, the invariance of field equations, of weak (and strong) interaction Hamiltonians with

respect to space reflection becomes clearly apparent if the space reflection is interpreted in the most obvious way:

$$P'\chi(\mathbf{r},t)P'^{-1}=\gamma_4\chi(-\mathbf{r},t). \tag{27}$$

The same are also invariant with respect to charge conjugation according to the simple formulation

$$C'\chi(\mathbf{r},t)C'^{-1}=\gamma_c\bar{\tilde{\chi}}(\mathbf{r},t)\equiv\chi^c(\mathbf{r},t). \tag{28}$$

The electromagnetic interaction, however, shows only invariance with respect to P'C'. It is seen now that χ is an irreducible representation of the extended Lorentz group (E') = (L, P', T). A similar irreducible representation of (E') is given by the lepton wave function. Vector (1) is the only covariant quantity constructed from the irreducible χ field which

1) is not Hermitian,
2) does not contain derivatives,
3) does not violate the law of conservation of fermion number.

It can be seen that this treatment leads naturally to a set of fermion doublets and to the law of universal Fermi interaction (2). Of course, other bilinear vectors may also be constructed from χ, but these are Hermitian. Even scalars and tensors can be built without derivation in violating, however, the principle of fermion conservation, thus of baryon conservation, defined in equation (41) of ref. [4]).

If nucleons are separated into protons and neutrons according to their charges, we have to use spinors ψ_p and ψ_n instead of the comprehensive χ. Let us see what will be the effect of the new P', C' inversions on the usual Dirac wave operators. Departing from the inversion formula (23), we obtain

$$\begin{gathered}P'\begin{pmatrix}\psi_p\\ \psi_n\end{pmatrix}P'^{-1}=i\gamma_4\begin{pmatrix}\psi_n^c\\ \psi_p^c\end{pmatrix}_{-\mathbf{r}},\quad C'\begin{pmatrix}\psi_p\\ \psi_n\end{pmatrix}C'^{-1}=-i\begin{pmatrix}\psi_n\\ \psi_p\end{pmatrix},\\ P'C'\begin{pmatrix}\psi_p\\ \psi_n\end{pmatrix}C'^{-1}P'^{-1}=-\gamma_4\begin{pmatrix}\psi_p^c\\ \psi_n^c\end{pmatrix}_{-\mathbf{r}}.\end{gathered} \tag{30}$$

Now, we introduce the charge symmetry operator Z as reflection on the coordinate plane (1.3) of the isobaric space [7]):

$$Z=(-i)^N e^{-i\pi\mathcal{I}_2},\qquad Z\begin{pmatrix}\psi_p\\ \psi_n\end{pmatrix}Z^{-1}=-i\begin{pmatrix}\psi_n\\ \psi_p\end{pmatrix}, \tag{31}$$

which induces the interchange $p\rightleftarrows n$. Let us extend its interpretation to the leptons by the replacement of $p\to\nu$, $n\to e$. Then, the new inversion can be expressed with the usual operators P, C, Z in the form

$$P'=PCZ,\quad C'=Z,\quad P'C'=PC=K. \tag{32}$$

The weak interaction (18) is invariant, in the known way, with respect to K and with respect to the simultaneous interchange of $p\rightleftarrows n$, $\nu\rightleftarrows e$.

This explains the P′ and C′ invariance. The same is violated by (17).

From the above it can be stated that weak interactions show not fewer but other symmetry properties than electromagnetic interactions. Using electrical analysators, that is, if electromagnetic interactions come into prominence, it is suitable to use a description method based upon the Dirac equation; space reflection is best interpreted by P which does not mix the states with different charges. Dealing, however, with weak interactions the combined second order wave equation is more convenient because it leads readily to the space reflection operator P' which does not mix chirality states. The (ψ_n, ψ_p) doublet χ is an irreducible representation of the combined Lorentz group $(E, E') = (L, P, P', T)$ fitting to both cases.

4. Weak Interactions of Strange Particles

Some consideration is due to the weak interactions of strange particles. If we want to apply consistently the above considerations, it has to be assumed that all fermions appear in doublets and that, contrary to (3), a fermion is a member of only one doublet. How is this compatible with the singlet Λ and triplet Σ-hyperons? There are two possibilities:

(a) In weak interactions (as in the strongest π-interactions [9])) Λ and Σ are members of two doublets rather than of a singlet and of triplet.

(b) The only elementary baryon is the nucleon. The hyperons are bound states of N and $\overline{K}$ [10, 11]).

Case (b) may seem more natural. Group III, as written in (3), however, has to be left out in both cases; thus, the universal Fermi interaction is found to be useful only for the description of weak interactions occurring without change in strangeness. Consequently, the sum of vectors G_i is defined as the current of the $\mathcal{I}_-$ component of the isobaric spin — by generalizing its concept also for lepton doublets — with the modification that γ_i has to be replaced by $\frac{1}{2}\gamma_i(1+\gamma_5)$.

In order to represent weak interactions involving change in strangeness $\Delta S = \pm 1$, it is the most convenient to assume a direct weak interaction between charged K mesons and the vectors G_i:

$$H_\kappa = l \sum_{(AB)} (\partial_i \phi_K^+ G_i(A, B) + \partial_i \phi_K G_i^+(A, B)).$$

This represents, in first approximation, the transitions in question quite correctly [1]). To decide which one of the two possibilities is the correct one, would require some further calculations and measurements like, for instance, the comparison of the ft values in the β-decays of n and Λ. According to Gell-Mann's theory [1]) the renormalized coupling constant of the $(e\nu)$ interaction with the classes II and III of (3) may then be different, for group

III is no longer an isobaric spin component. Therefore, experimental tests become more difficult.

The role of the "strangest" particle, the muon, is still problematical. In the two-lepton doublets usually the same ν is taken to be involved and this is contradictory to our scheme. We suggest two possibilities:

(a) For some reason the electron in the doublet $(e\nu)$ may occur in two states: e^- and μ^-, and this phenomenon, violating the P′-invariance, does not occur for neutral components. Thus interaction $(e\nu)(\mu\nu)$ is one of the consequences of $(e\nu)(e\nu)$ interaction.

(b) We may assume [12]), besides the ν of -1 helicity, the existence of a particle η of $+1$ helicity, also of rest mass 0 and spin $\frac{1}{2}$, so that lepton doublets will be listed according to $(e^-\nu)$, $(\eta\mu^+)$. This means that instead of lepton conservation we may speak separately of the conservation of $e+\nu$ and the conservation of $\mu+\eta$. The theory leads, for all parity experiments and energy spectrum measurements, to the same results as those obtained by the two-component ν-theory.

Finally, we have to point out that the P′-invariance here introduced is spoiled by electromagnetic fields and electromagnetic mass splittings, whereas P is a constant of motion, the conservation of which is only violated by interactions which are weaker by several orders of magnitude. Therefore, the description of space reflection by P is from a practical point of view undoubtedly more important. In principle, however, it is of interest to attempt to find such symmetries of strong interactions which may be violated by electromagnetic interactions and hold for weaker interactions, because these symmetries may lead us to the recognition of the laws of weak interactions.

The author is indebted to Dr. Chou Kuang-Chao for valuable remarks.

References

1) M. Gell-Mann and A. Rosenfeld, Ann. Rev. Nucl. Sci. **7** (1957) 407
2) M. Gell-Mann, Phys. Rev. **111** (1958) 362
3) N. Menyhárd, Symposion on Elementary Particles, Balatonvilágos, Hungary (1958)
4) G. Marx, Nuclear Physics **9** (1958) 337
5) R. P. Feynman, M. Gell-Mann, Phys. Rev. **109** (1958) 193
6) V. J. Ogievetsky and Chou Kuang-Chao, JINR preprint (Dubna) (1958)
7) G. Marx and G. Györgyi, Nuovo Cimento Suppl. **5** (1957) 159
8) L. Michel, Progr. Cosmic Ray Phys. **1** (1952) 144
9) M. Gell-Mann, Rochester Conference (1957)
10) M. Goldhaber, Phys. Rev. **92** (1953) 1279
11) G. Györgyi, JETP **32** (1957) 152
12) J. Kawakami, Progr. Theor. Phys. **19** (1958) 459

1.E.1:
3.A

Nuclear Physics **10** (1959) 475—485: © *North-Holland Publishing Co., Amsterdam*
Not to be reproduced by photoprint or microfilm without written permission from the publisher

LEVELS IN Os^{190} POPULATED IN THE DECAY OF 11d Ir^{190}

O. B. NIELSEN, N. O. ROY POULSEN, R. K. SHELINE † and B. SKYTTE JENSEN ††
Institute for Theoretical Physics, University of Copenhagen

Received 13 January 1959

Abstract: 11d Ir^{190} was prepared in the $Re^{187}(\alpha, n)Ir^{190}$ reaction. The decay scheme was investigated in a six-gap β-ray spectrometer. Numerous e—γ coincidence experiments were performed with the spectrometer in connection with a γ-ray scintillation spectrometer and a 100 channel kicksorter.

Excited levels in Os^{190} at 186 (2^+), 548 (4^+), 557 (2^+), 754, 956, 1161, and 1683 keV were established. It is shown that Os^{190} possesses nuclear properties which characterize the elements in the region between the group of spherical nuclei around $A = 208$ and the strongly deformed nuclei in the rare-earth group.

1. Introduction

Ir^{190} has two long lived states [1, 2]) which decay by K-capture to Os^{190} with periods of 3 h and 11 d, respectively. A 10 min isomeric level in Os^{190} at 1700 keV is excited in the 3 h decay, and the 10 min activity can be studied separately after chemical separation of Os from Ir [3, 4]). The isomeric level probably has spin 10^-, since it decays by an M2 transition to the 8^+ member of the ground state rotational band. The three lower states in this band are revealed in the subsequent cascade of E2 transitions.

The decay scheme of the 11 d activity has not been studied in detail, but from the γ-ray spectrum [3]) it is evident that a number of levels not observed in the 10 min activity are excited. The case thus presents a possibility for the study of levels belonging to other low lying rotational bands in Os^{190}. The nucleus is one of a series exhibiting a gradual change in nuclear properties from the strongly deformed region with $152 < A < 190$ and the spherical group around the magic number 208. Certain excited states, which occur regularly in spherical even nuclei, are believed to be of collective origin and represent in the unified description modes of excitation having counterparts among the collective levels in the deformed nuclei [6, 7]). Experimental information on the occurrence of the states in question through the transition region evidently is an important contribution to the study of the relationship between the levels in the two types of nuclei.

† Permanent address: Department of Chemistry, Florida State University, Tallahassee, Florida.

†† Permanent address: Danish Atomic Energy Commission, Risø pr. Roskilde, Denmark.

2. Source Preparation

Ir^{190} was produced in the (α, n) reaction by bombarding natural rhenium with 20 MeV α-particles in the Copenhagen cyclotron. A target of satisfactory mechanical stability was obtained by pressing Re powder into a gold plate. The plate was soldered onto a water cooled target assembly in the cyclotron.

After the irradiation, the Re was scraped off and dissolved in a small amount of nitric acid. 5 μg iron carrier in solution as $FeSO_4$ was added and precipitated with concentrated ammonia as $Fe(OH)_3$ together with the iridium activity. The precipitate was dissolved again in nitric acid, reprecipitated and, after washing with water, taken up in 1 ml 0.5 *M* lactic acid. The activity was then electroplated onto a 250 $\mu g/cm^2$ nickel foil in a cell similar to that described by Joliot [8]). About 60 % adhered to the foil after plating with 100 mA/cm^2 for 1 hour. The deposition of the activity was followed continuously with a GM-operated count-rate meter, recording electrons passing a slit immediately behind the Ni-foil.

Apart from serving as a carrier, the iron was needed for securing adhering deposits of Ir which probably was adsorbed on the $Fe(OH)_3$ formed on the cathode. With no iron, the activity went back into solution immediately when the current was disrupted.

Unfortunately, the cross section for the $Re^{187}(\alpha, n)Ir^{190}$ reaction is extremely low at 20 MeV and, in spite of a bombardment of about 40 μA for 80 hours, only about 3 μC of the 11 d Ir^{190} were formed. The 3 h Ir^{190} and the 41 h Ir^{188} were also produced, but the source was sufficiently pure in the 11 d activity after about 10 d.

3. Experimental Methods

The conversion-line spectrum was measured in a recently constructed six gap β-ray spectrometer [9]). In e—γ coincidence measurements, the γ-ray spectra were recorded on a 100 channel kicksorter. The low source strength made it necessary to utilize the long half life for the coincidence measurements which went on continuously for about one month.

4. The Conversion-Line Spectrum

With a source area of about 5×10 mm^2, the resolution of the β-ray spectrometer was $1/R \approx 1.5$ % at higher energies, but, since the source was not ideally thin, the lines were broadened at lower energies corresponding to ≈ 3 % at 116 keV. The density of conversion lines is high (fig. 1), and some of the lines were not completely resolved, but, with the amount of activity available, the resolution could scarcely be much improved.

The experimental data on the conversion lines, which could be attributed to definite transition energies, are collected in table 1.

Obviously, the majority of the γ-rays indicated by the conversion lines cannot be resolved with the resolution obtainable in a scintillation spectro-

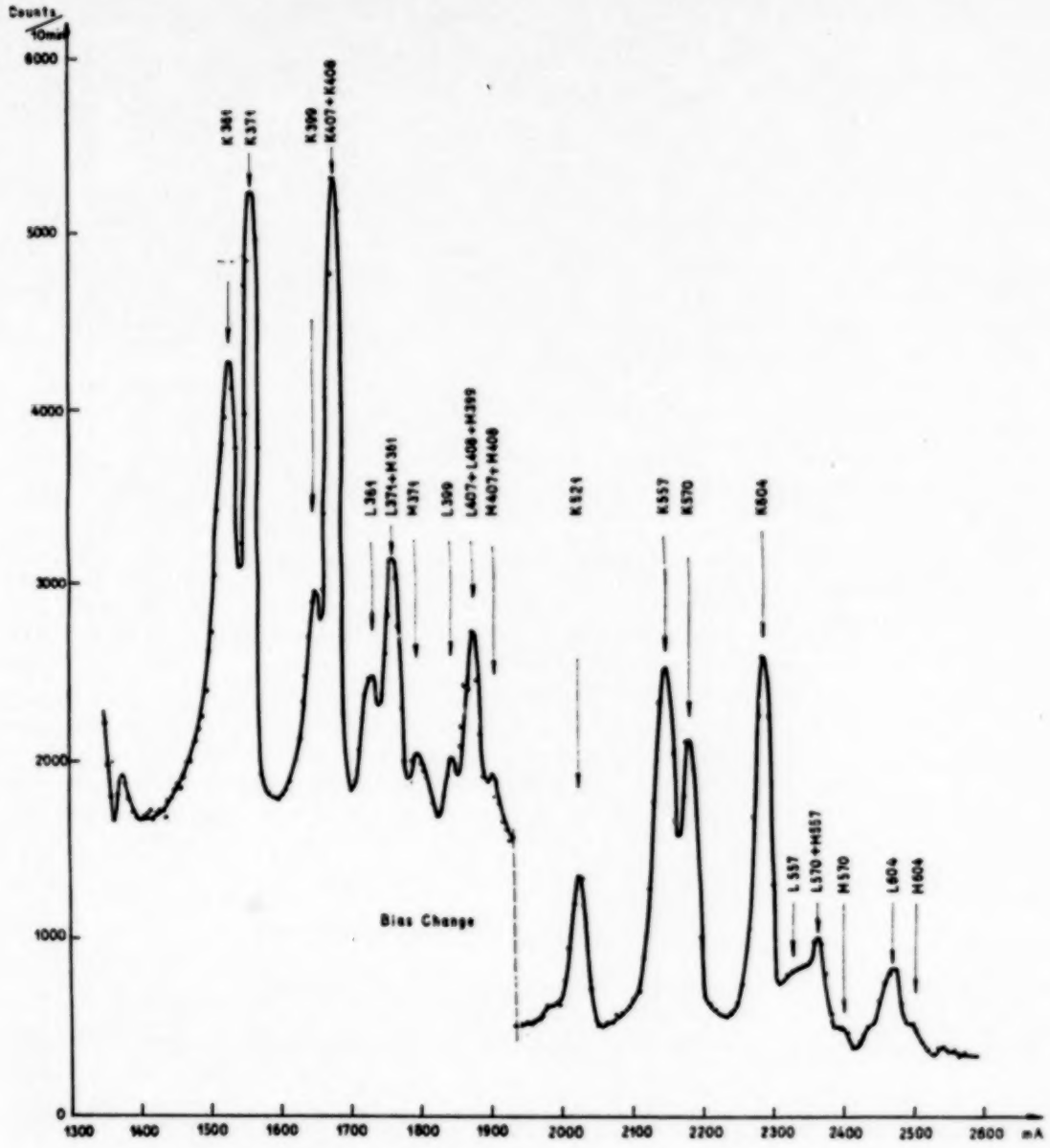

Fig. 1. Part of the conversion line spectrum.

meter. In the single γ-ray spectrum (fig. 2), only four peaks stand out, of which one is due to the X-rays and the second mainly to the strong 186 keV transition. The remaining two peaks represent unresolved groups of the γ-rays from 361 to 408 and 521 to 604 keV, respectively.

TABLE 1

Conversion line data

E_γ keV	Intensity of K Line %	K/L Ratios (exp.)	K/L Ratios (theoretical) E1	E2	M1	Assignment	α_K (theor.)	I_γ (calc.) %	I_γ (exp.) %	$I_{\text{Transition}}$ %
186	10.8	1.20	6.1	1.2	6.2	E2	0.21	51		75
196	2.4	†	6.1	1.3	6.3				$\lesssim 10$	$\lesssim 13$
205	0.34									
295	0.37									
361	0.42	2.9	6.5	2.9	6.3	E2	0.039	11		11
371	0.60	2.9	6.5	3.0	6.3	E2	0.037	16		17
399	0.21	3.1	6.5	3.1	6.3	E2	0.031	6.9		7
407+ 408	0.66	3.5	6.5	3.5	6.3	E2 E2	0.029	23		19 4.6
521	0.13	>4.5	6.6	4.0	6.4	E1	0.006	22	≈ 26	22
557	0.35	$\gtrsim 4.3$	6.7	4.3	6.4	E2	0.0145	24	≈ 24	25
570	0.28	$\gtrsim 3.4$	6.7	4.4	6.4	E2	0.0137	20	≈ 19	20
604	0.39	≈ 5	6.7	4.5	6.4	E2	0.0122	32	≈ 30	32

† K/M = 10.

The γ-ray intensities in column 9 are calculated from the K-conversion line intensities and the theoretical conversion coefficients. The experimental intensities in column 10 are obtained in e—γ coincidence experiments and form the basis for the multipole assignments in the cases these could not be inferred from the K/L ratios. Column 11 contains the total transition intensities with all conversion lines included.

5. e—γ Coincidence Measurements

The γ-ray spectra obtained in coincidence with the conversion lines not only establish the coincidence relations of the transitions, but from the known efficiency for γ-rays of different energies in the NaI-crystal the relative intensities of the transitions represented by the conversion line and the γ-ray can be estimated.

The results of the coincidence experiments are summarized in table 2. For each conversion line is given the energy of the coincident γ-rays and the percentage of the conversion electrons, which is accompanied by the γ-ray in question. The identification of the γ-rays is unambiguous, in spite of the low resolution in the γ-ray channel, since each transition was involved in the experiments both as conversion line and as γ-ray.

6. The Decay Scheme

In the decay of the 10 min isomer, levels with energies of 187, 547, 1047, 1663 and 1702 are excited (fig. 4). In addition to the 187 keV level, also a 2^+ level at about 560 keV has been Coulomb excited [10]).

The 186 keV transition is the most intense in the present decay and must represent the ground-state transitions from the first excited level. 361 keV is naturally identified as the transition from the 547 to the 186 keV level, and this interpretation is confirmed by the coincidence relations indicating strong coincidence only with the 186 keV γ-ray.

The γ-ray spectra coincident with the 371 and 557 keV conversion lines are quite similar in shape, except that 371 keV is totally coincident with

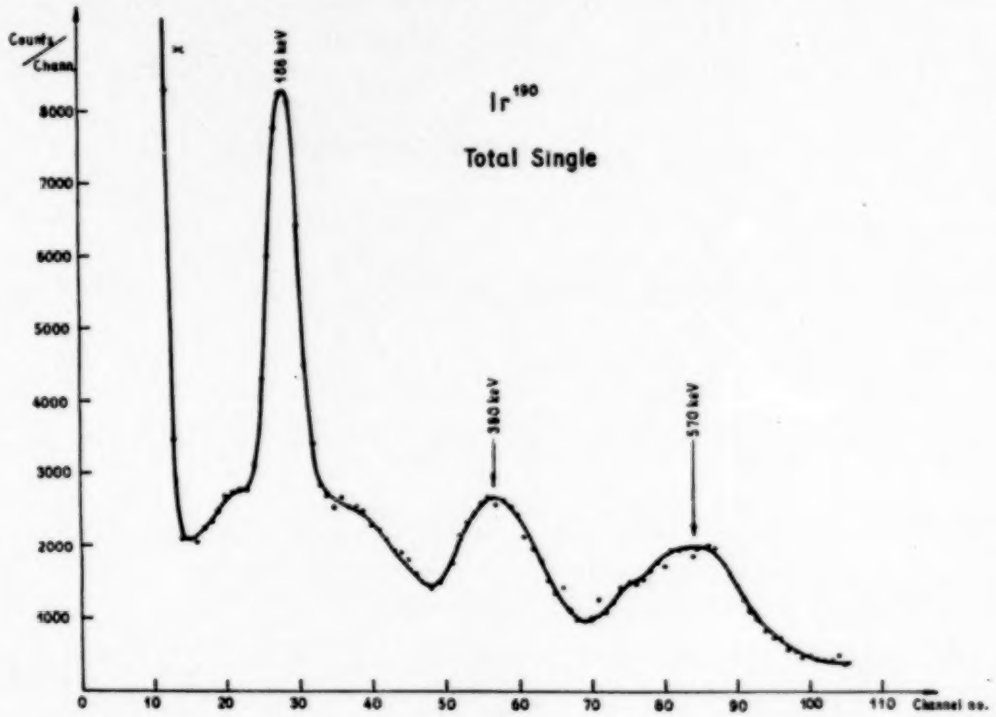

Fig. 2. The single γ-ray spectrum.

186 keV (fig. 3) and 557 keV not at all. As the 557 keV transition is of E2 nature (section 7), these two transitions represent de-excitations from a 557 keV 2^+ level, apparently the one known from Coulomb excitation.

The level at 1161 keV is established by the 604 keV transition in coincidence with 557 and 371 keV. The 521 keV γ-ray is also coincident with these as well as with 604 keV, but, since it appears weaker than 604 in the coincident spectra, it must be placed above, thus defining a level at 1683 keV.

The 407 and 570 keV lines are strongly coincident with each other as well as with the 186 keV transition, and to a smaller extent with 521 keV. These relations together with the energy fit places them as a cascade between

the 1161 and 186 keV levels. There is no experimental information on the order of the transitions, but the intermediate level is suggested at 754 keV, where it can be interpreted as the 3^+ member in the rotational band of the 557 keV 2^+ level.

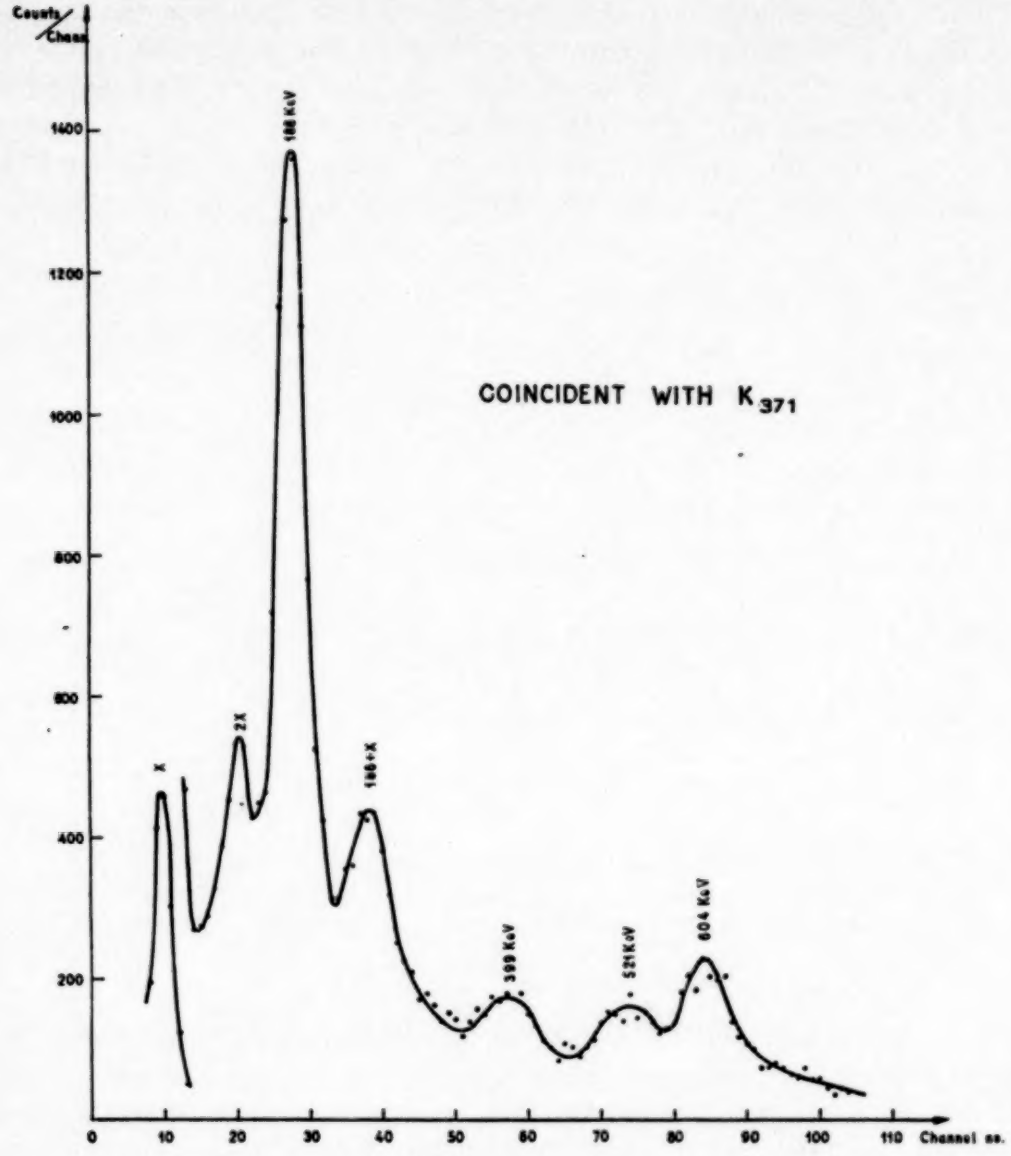

Fig. 3. The γ-ray spectrum coincident with the conversion line K_{371}.

In addition to the 407 keV transition in cascade with 570 keV, a weak ray $\approx$ 400 keV was observed in coincidence with 361 keV and another in coincidence with 371 and 557 keV. One of the conversion lines K_{399} or K_{407} is then probably double. The coincidence spectrum and intensity of the

399 keV transition suggest that it excites the 557 keV level from a level at 956 keV. A possible transition of 408 keV from this level to the 548 keV level almost coincides in energy with the strong 407 keV transition, and its existence was confirmed without much doubt, since also the spectrum coincident with the 407 keV K conversion line contains a weak γ-ray of about 360 keV.

The transitions of 196 and 205 keV could not be placed unambiguously into the decay scheme. 205 keV fits energetically between 548 and 754 keV, and also between 956 and 1161 keV. A coincidence experiment was not feasible, mainly because of interference from the tail of the line L_{186}. The relatively strong 196 keV transition fits between 754 and 557 keV, but this position was not consistent with the coincidence experiment. The coincident spectrum contained all the peaks of the single γ-ray spectrum, but the 371—408 keV peak was only half as intense as the suggested position would imply. Agreement with the experimental data would be obtained by assuming that the major part of the conversion lines was due to a transition exciting the 1161 keV level from a level at 1356, with a minor part representing a transition from 754 to 557 keV.

7. Multipole Orders and Intensities

The multipole assignments were made on the basis of the K/L ratios and of the γ-ray intensities found in the coincidence experiments (table 2). Although these intensities in the present experiments can only be considered

TABLE 2

γ-ray intensities measured in coincidence experiments

Conversion line	Coincident with
186	361—408 (87—74) 521—604 keV (80—67)
196	186 keV (55—?) 361—408 keV (70—?) 521—604 keV (105—?)
361	186 keV (85—100) 408 keV (37—41)
371	186 keV (100—100) 399 keV (26—18) 521 keV (31—40) 604 keV (64—78)
399	186 keV (50—40) 371 keV (31—40) 557 keV (74—60)
407+ 408	186 keV (90—100) 361 keV (22—19) 521+557 keV (110—121)
521	186 keV (74—63) 371+407 keV (75—63) 557+570+604 keV (110—138)
557	196? keV (16—?) 399 keV (30—18) 521 keV (37—40) 604 keV (73—78)
570	186 keV (110—100) 407 keV (80—90) 521 keV (40—50)
604	186 keV (40—40) 371 keV (44—40) 521+557+570 keV (110—110)

The figures after each γ-ray indicate the measured percentage and the percentage deduced from the decay scheme fig. 4, respectively. The values have been corrected for internal conversion (only important for the 186 keV γ-ray). The discrepancies are partly due to the fact that the 196 keV transition could not be placed in the decay scheme.

accurate to about 20 %, this is sufficient to distinguish between E1, E2, and M1 transitions, since the K conversion coefficients differ by at least a factor of 2, but considerable M1 admixtures in the E2 transitions are not excluded.

Table 1 contains the data pertinent to the multipole determinations. The experimental γ-ray intensities used for estimating the conversion coefficients are listed in column 10. These should be compared with the values in column 9 obtained by dividing the conversion line intensities with the theoretical conversion coefficients.

The K/L ratios for the 186, 361, 371 and 399 keV transitions indicate E2 nature. Also the ratio between the suggested (407+408) keV K and L lines point to this multipole order for at least the stronger 407 keV transition. The coincidence experiments in addition suggest that the conversion coefficients for the 407 and 408 keV transitions are similar. The intensity of the 408 keV γ-ray could thus be estimated to $\approx$ 4 % of all transitions or 0.18 times the compound (407+408) keV γ-ray from the coincidence spectrum of the 361 keV K conversion line, whereas the strength of the 361 keV γ-peak in coincidence with the (407+408) keV K line indicated that 0.22 of this line was due to K_{408}.

The 570 keV γ-ray must be about equal in intensity with the 407 keV ray, since these two transitions mutually are almost 100 % coincident.

The spectrum coincident with 604 keV reveals that the 557 keV γ-ray is about 1.5 times as intense as the 371 keV γ-ray. This is consistent only with an E2 assignment, which confirms the indentification of the 557 keV level as the level known from Coulomb excitation. Since the multipole order must be pure, the γ-ray intensity can be calculated safely from the conversion line and the theoretical E2 conversion coefficient.

The 604 keV transition is responsible for $\approx$ 70 % of the excitations of the 557 keV level (table 2), corresponding to about 30 % of all decays. Similarly, $\approx$ 50 % of the excitations of the 1161 keV level are due to the 521 keV γ-ray, and the intensity is consequently 0.5 $(I_{407}+I_{604}) \approx 26$ %. The corresponding conversion coefficient indicates E1 nature.

The line L_{196} was not resolved from the strong M_{186}, but the K/M ratio $\approx$ 10 for the 196 keV transition suggests a K/L ratio $\approx$ 3, which is higher than the E2 value of 1.3. The γ-ray intensity could not be inferred from any coincidence experiment, but from the spectrum coincident with the 186 and 557 keV conversion lines, an upper limit of about 10 % of all transitions could be set. The corresponding lower limit for $\alpha_K \approx 0.25$ is higher than α_K for E2 : 0.19. The conversion line thus probably represents one or more transitions which are at least partly of M1 nature.

Table 3 gives the intensities of the incoming and outgoing transitions for each level. K-capture transitions must be suggested to the levels for which the de-excitations significantly exceed the excitations by γ-transitions. The

ft-values in column 5 represent a rough estimate, assuming an energy difference between the ground states of Ir^{190} and Os^{190} ≈ 2.5 MeV, which is based on Levy's empirical atomic masses [12]).

TABLE 3

K-capture transitions

Level keV	Incoming γ-rays %	Outgoing γ-rays %	$I_{K\text{-capture}}$ %	Log *ft*
186	48	75	27	8.3
547	5	11	6	9.0
557	39	42	—	—
754	19	20	—	—
956	—	12	12	8.5
1161	26	51	25	8.0
1683	—	26	26	7.6

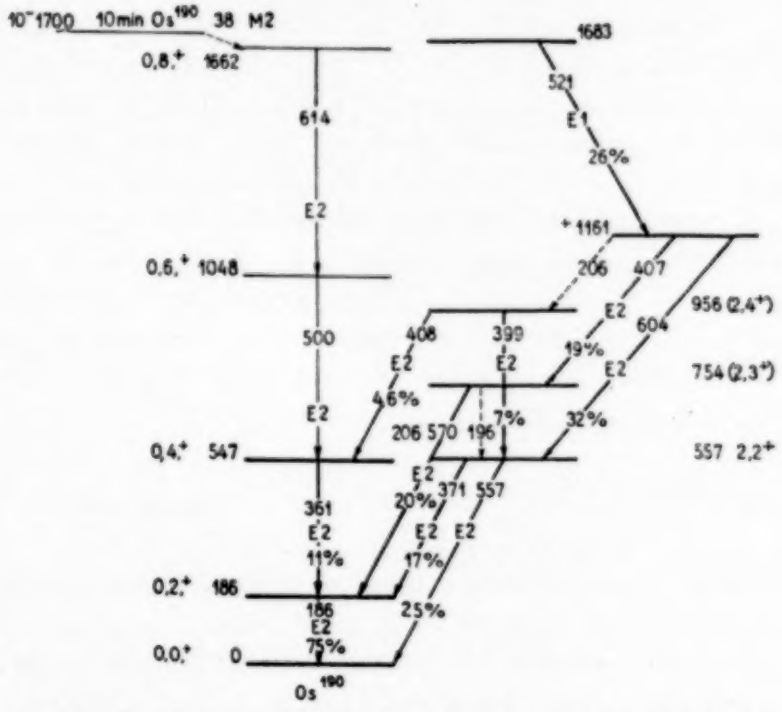

Fig. 4. The suggested level scheme of Os^{190}. Levels which are believed to belong to the same rotational family are placed above each other. The intensities are those based on the internal conversion lines.

8. Discussion

The level scheme of the neighbouring even isotope Pt^{192} is of the spherical type, but the relatively low energy of the first excited state in Os^{190} as well as the existence of a ground state rotational band are features which characterize the spheroidal group. Since it represents a limiting case, it is not surprising that it deviates even more than Os^{188} and Os^{186} from the spheroidal

nuclei of lower mass. The energy $E_1 = 186$ keV of the first excited level must be compared to $E_1 = 155$ keV in Os^{188}, 137 keV in Os^{186}, and ≈ 90 keV in the strongly deformed rare earth isotopes. The corresponding values for the second 2^+ level, probably representing a γ-vibration with $(K, I, \pi = 2, 2^+)$, are 557, 633, 764 and 800—1200 keV. The branching ratio, corrected for the energy dependence, of the γ-transitions from 557 keV to the ground state and to the 186 keV level is

$$\frac{I_{557}}{I_{371}} \left(\frac{671}{557}\right)^5 = 0.20,$$

compared to 0.3 and ≈ 0.3 for Os^{188} and Os^{186}, and between 0.4 and 0.6 for the more strongly deformed nuclei. The theoretical ratio for transitions from a (2, 2, +) level to levels (0, 0, +) and (0, 2, +) is 0.7 [11]), assuming no rotational-vibrational interaction.

In even spherical nuclei, the first excited level has spin 2^+ with only few exceptions. The next excited levels seem to be members of a triplet with spins 4^+, 2^+, and 0^+, at an energy between 2 and 2.5 times that of the first [6, 13, 14]). The levels of this triplet are believed to be analogous to the (0, 4, +) level of the ground state rotational band, the (2, 2, +) level of a γ-vibrational band, and the (0, 0, +) level of a β-vibrational band in deformed nuclei [6]). It is interesting to note that the levels in Os^{190} point to a smooth transition between the two types of level structures, since the (0, 4, +) state is only 10 keV below the (2, 2, +) state. It must be mentioned, however, that no information is available on low lying 0^+ levels in this region, and the nuclear level structures are probably more complicated than suggested by the simple picture outlined above.

The spins of the 754 and 965 keV levels are not unambiguously fixed experimentally, but the energies support an assignment as the 3^+ and 4^+ members of the γ-vibrational band. Since 11 d Ir^{190} decays with *ft*-values of the same order to levels with spin 2 and 4 (table 3), its spin is probably 3, and the spins of the 1161 and 1683 keV levels, which are also populated by K-capture, are then probably 2, 3 or 4. The absence of γ-transitions from these levels to the low-energy states demonstrates the effect of strong γ-selection rules. The result from the 557 keV level indicates that these neither can be described satisfactorily in terms of the K-selection rules for deformed nuclei [11]) nor the one-phonon selection rule for the vibrative nuclei [13]).

We wish to express our gratitude to Professor Niels Bohr for the excellent working possibilities in his Institute, and to Professor Aage Bohr and Dr. Ben R. Mottelson for continuous help and encouragement. One of us (B.S.J.) is grateful to the Danish Atomic Energy Commission, and especially to Dr. C. F. Jacobsen, for having given him the opportunity to participate in this work.

References

1) L. J. Goodman and M. L. Pool, Phys. Rev. **71** (1947) 288
2) T. C. Chu, Phys. Rev. **79** (1950) 582
3) A. H. W. Aten, G. D. de Feyfer, M. J. Sterk and A. H. Wapstra, Physica **21** (1955) 740, 990
4) G. Scharff-Goldhaber, D. E. Alburger, G. Harbottle and M. McKeown, Phys. Rev. **111** (1958) 913
5) R. M. Diamond and J. M. Hollander, Nuclear Physics **8** (1958) 143
6) A. Bohr, Physica **22** (1956) 959
7) R. K. Sheline, Proc. of the Univ. of Pittsburgh Conf. (June 6—8, 1957)
8) F. Joliot, J. Chim. Phys. **27** (1930) 119
9) O. B. Nielsen, to be published
10) R. Barloutaud, P. Lehmann and A. Levêque, C. R. **245** (1957) 523
11) G. Alaga, K. Alder, A. Bohr and B. R. Mottelson, Mat. Fys. Medd. Dan. Vid. Selsk. **29** (1955) no. 9
12) A. G. W. Cameron, Atomic Energy of Canada Limited, Report 433 (1957)
13) G. Scharff-Goldhaber and J. Weneser, Phys. Rev. **98** (1955) 212
14) K. Alder, A. Bohr, T. Huus, B. R. Mottelson and A. Winther, Revs. Mod. Phys. **28** (1956) 432

2.B:8.B *Nuclear Physics* **10** (1959) 486—491; © *North-Holland Publishing Co., Amsterdam*
Not to be reproduced by photoprint or microfilm without written permission from the publisher

RELATION BETWEEN INTRINSIC PARITIES AND POLARIZATIONS IN COLLISION AND DECAY PROCESSES

AAGE BOHR

Institute for Theoretical Physics, University of Copenhagen

Received 16 February 1959

Abstract: A simple rule is given which relates the polarizations of the particles involved in a collision process to the relative intrinsic parities in initial and final states. A similar rule applies to decay processes with conservation of parity. Some experiments are considered which could yield information on the intrinsic parities of hyperons and K-particles.

1. General Conservation Law

Considerable interest attaches at present to the experimental determination of the intrinsic parities of hyperons and heavy mesons, assuming parity to be conserved in the collision processes involving these particles. Various experiments have been suggested to this effect [1, 2, 3]).

The aim of the present note is to call attention to a simple rule relating the polarizations of the particles involved in a collision (or decay) process to their intrinsic parities, and to discuss some applications of this rule.

Consider a collision between two particles with relative momentum $\mathbf{p}_i$, leading to a final state of two particles emerging with relative momentum $\mathbf{p}_f$. For simplicity, let us first assume all the particles involved to have spin zero. Provided the interactions are parity conserving and the particles can be assigned intrinsic parities, the collision exhibits reflexion symmetry with respect to the *plane* containing $\mathbf{p}_i$ and $\mathbf{p}_f$. The initial and final states are thus eigenstates of the corresponding reflexion operator, which we denote by R, and the eigenvalues are the products $\mathscr{P}_i$ and $\mathscr{P}_f$ of the intrinsic parities in initial and final states. We now have the conservation law $\mathscr{P}_i = \mathscr{P}_f$, i.e., the process is forbidden if there is a change of intrinsic parity, as is also immediately evident from the fact that the relative orbital angular momentum l must be conserved.

If the particles possess spins, the eigenstates of R are those of spin quantization in the direction $\mathbf{n}$ perpendicular to the collision plane $(\mathbf{p}_i, \mathbf{p}_f)$. Since the reflexion R can be represented as a parity inversion followed by a rotation of 180° about $\mathbf{n}$, the eigenvalues of R are $\mathscr{P}e^{i\pi S_n}$, where S_n is the sum of the spin components along $\mathbf{n}$. We thus have the conservation law

$$\mathscr{P}_i e^{i\pi S_{in}} = \mathscr{P}_f e^{i\pi S_{fn}}$$

or

$$\Delta S_n = \begin{cases} \text{even} \\ \text{odd} \end{cases} \text{ according as } \mathscr{P}_f = \pm \mathscr{P}_i. \tag{1}$$

If the polarization of all the particles involved in the collision is measured, the relative intrinsic parity is thus obtained directly from (1).

For a photon, the eigenstates of R are those of linear polarization in the plane containing $\mathbf{n}$. Depending on whether the electric or the magnetic vector is parallel to $\mathbf{n}$, the photon contributes to R by a factor -1 or $+1$, respectively.

The relation (1) fully characterizes the direct implications of reflexion symmetry on the collision. It is thus seen to comprise the well-known theorem that, for unpolarized incident particles, the outgoing particles are polarized perpendicularly to the collision plane. In fact, the coherent polarization components for the outgoing particles then always differ by an even number of units. This theorem, however, in contrast to the relation (1), does not involve the intrinsic parities of the particles in the collision.

The extension of the relation (1) to collision processes with more than two particles in the final state and to decay processes will be briefly considered below.

The rule (1) contains, as a special case, a relation recently given by Bilenky [3]) for reactions of the type

$$\begin{aligned} \pi + \mathrm{p} &\to \Lambda(\Sigma) + \mathrm{K} \\ \overline{\mathrm{K}} + \mathrm{p} &\to \Lambda(\Sigma) + \pi \end{aligned} \tag{2}$$

assuming, as in the following discussion, the hyperons to have spin $\frac{1}{2}$ and the K-mesons spin zero. Denoting by $d\sigma$ and $d\sigma_0$ the cross sections for polarized and unpolarized targets, the relation referred to can be written

$$d\sigma = d\sigma_0(1 \pm \mathbf{P}_0 \cdot \mathbf{P}) \quad (\mathscr{P}_f = \pm \mathscr{P}_i), \tag{3}$$

where $\mathbf{P}_0$ is the polarization (2**s**) of the target and $\mathbf{P}$ that of the product for an unpolarized target. The relation (3) was obtained[3]) from an analysis of the general form of the collision matrix, but is also seen to follow directly from (1), if one writes the cross section in terms of the partial cross sections for targets polarized parallel and antiparallel to $\mathbf{n}$.

An intrinsic parity determination by means of the reactions (2) depends on the availability of polarized targets and thus presents difficult experimental problems. In the following, we restrict ourselves to a consideration of collisions with targets of spin zero, among which He^4-nuclei appear most promising in the present context. The projectiles are required to be either polarized or to have spin zero.

2. Projectiles of Spin Zero

Examples are provided by the processes

$$K^- + He^4 \rightarrow \begin{cases} \pi^- + {}_\Lambda He^4 \\ \pi^0 + {}_\Lambda H^4 \end{cases} \tag{4}$$

especially discussed by Dalitz [4]). Equivalent information can be obtained from the pion-induced reactions

$$\begin{aligned} \pi^+ + He^4 &\rightarrow K^+ + {}_\Lambda He^4 \\ \pi^- + He^4 &\rightarrow K^0 + {}_\Lambda H^4. \end{aligned} \tag{5}$$

The usefulness of these reactions for parity determination depends on the spins of the bound states of the hypernuclei [4]). If the doublet ${}_\Lambda H^4$, ${}_\Lambda He^4$ possesses only a single bound state of $s = 0$, the processes are forbidden for change of intrinsic parity. If there is a single bound state with $s = 1$, the hypernucleus is aligned ($s_{\mathbf{n}} = 0$ for $\mathscr{P}_f = \mathscr{P}_1$ and $s_{\mathbf{n}} = \pm 1$ for $\mathscr{P}_f = -\mathscr{P}_1$). Such an alignment could, e.g., be detected from an observation of the decay

$$\begin{aligned} {}_\Lambda H^4 &\rightarrow \pi^- + He^4 \\ {}_\Lambda He^4 &\rightarrow \pi^0 + He^4 \end{aligned} \tag{6}$$

whose angular distribution is

$$W(\theta, \varphi) = \begin{cases} \frac{3}{4\pi} \cos^2 \theta & (s_{\mathbf{n}} = 0) \\ \frac{3}{8\pi} \sin^2 \theta [1 + a \cos 2(\varphi - \varphi_0)] & (s_{\mathbf{n}} = \pm 1) \end{cases} \tag{7}$$

with θ and φ denoting the polar angles of the decay momentum with respect to the axis $\mathbf{n}$. In the case of $\mathscr{P}_f = -\mathscr{P}_1$, a coherent superposition of polarization states with $s_{\mathbf{n}} = +1$ and -1 is involved.

We are here assuming the processes (4) and (5) to be induced by particles in flight. If the capture takes place from an atomic orbit, the direction of incidence is affected by collisions with the electrons and by radiative atomic transitions. A corresponding averaging over directions $\mathbf{n}$ must then be performed. The angular distribution in the decay of ${}_\Lambda H^4$ produced by the capture of K^--mesons from atomic orbits has been discussed previously (cf., e.g., ref. [4])).

The analysis of the hypernuclear binding energies [4]) indicates, however, the possibility of two bound states ($s = 0$ and 1) with $s = 0$ for the ground state. An excited state with $s = 1$ is expected to decay to the ground state by M1 γ-radiation, and in this case a detection of an alignment of the hypernucleus in the processes (4) and (5) would require an observation of the angular distribution of the decay γ-ray.

In the unfavourable case of two bound states of the hypernucleus with

$s = 0$ as the ground state, a parity determination could in principle be obtained from an accurate determination of the Q-values in the reactions (4) or (5), which would reveal whether the ground state ($s = 0$) was formed directly in these reactions †.

An alternative process which may offer the possibility of determining the relative parities of K^- and Λ is

$$K^- + He^4 \rightarrow {}_\Lambda H^3 + n. \tag{8}$$

Provided the polarization of both products can be measured, the relative parity can be obtained from (1).

A detection of the neutron polarization, although difficult, would in principle be possible by a study of the azimuthal asymmetry in the scattering of the neutron on He^4 nuclei in a He bubble chamber.

The analysis of the ${}_\Lambda H^3$ binding indicates only a single bound state, and there is some preliminary evidence for $s = \frac{1}{2}$[4]). In this case, the decay

$${}_\Lambda H^3 \rightarrow He^3 + \pi^- \tag{9}$$

is expected to show an up-down asymmetry, which could be used to determine the polarization. If the spin of ${}_\Lambda H^3 = \frac{3}{2}$, the decay is expected to be predominantly by p-wave emission, in which case the decay (9) does not reveal the sign of s_n and so does not yield sufficient information for the parity determination. A polarization measurement of the He^3 daughter or of the products in the non-mesonic decay of H^3 would then be required.

As further examples of processes induced by K^--mesons, we may mention the reactions

$$K^- + He^4 \rightarrow \begin{cases} \Lambda^0 + H^3 \\ \Sigma^0 + H^3 \\ \Sigma^- + He^3. \end{cases} \tag{10}$$

While the hyperon polarization might be determined from decay asymmetries, the polarization of H^3 and He^3 would require the study of scatterings or perhaps other reactions of H^3 and He^3 with nuclei in the chamber.

The rule (1) may also be used to determine the parities of nuclear states. As an especially simple case, consider the inelastic scattering of α-particles (or π-mesons or other spin zero projectiles) from an even target nucleus. The state of polarization of the excited state will then be characterized by even or odd s_n, depending on whether its parity is even or odd. For instance, the observation of γ-rays associated with the decay to the ground state, and emitted in the direction of $\mathbf{n}$, implies $s_n = \pm 1$ and thus odd parity of the excited state.

† This was pointed out by E. M. Henley, who has also called attention to the possible interest of the reactions $K^- + C^{12} \rightarrow p + {}_\Lambda Be^{11}$ and $K^- + O^{16} \rightarrow p + {}_\Lambda C^{15}$, in case the Q-values can be measured sufficiently accurately to single out the ground state of these hypernuclei with expected spin of $\frac{1}{2}$.

3. Polarized Projectiles

If polarized nucleon beams are available, the reactions

$$\begin{aligned} p+He^4 &\rightarrow K^+ + {}_\Lambda He^5 \\ n+He^4 &\rightarrow K^0 + {}_\Lambda He^5 \end{aligned} \tag{11}$$

may be of interest. The hypernucleus is here expected to exist in only a single bound state with $s = \frac{1}{2}$, whose polarization can be determined from its decay asymmetry†.

With linearly polarized photons, one can study the reactions

$$\gamma+He^4 \rightarrow \begin{cases} K^+ + {}_\Lambda H^4 \\ K^0 + {}_\Lambda He^4 \end{cases} \tag{12}$$

which are similar to (4) or (5), except for the freedom in choice of polarization of the photon.

Incidentally, it may be noted that the process

$$\gamma+He^4 \rightarrow \pi^0+He^4 \tag{13}$$

may serve as an independent test of the π^0-parity. Thus, for a pseudoscalar π_0, the process requires incident γ-rays, polarized with the electric vector perpendicular to the collision plane.

4. Reactions with More than Two Products

If more than two particles emerge from the collision, the rule (1) still applies, provided all the momenta continue to lie in a plane.

As an example, consider the reaction

$$K^-+He^4 \rightarrow \overline{K}_0+\pi^-+He^4 \tag{14}$$

produced by K^--mesons in flight. If the two K-mesons have the same parity, the momenta of the outgoing particles cannot be co-planar with the direction of incidence (in view of the pseudoscalar character of the π^-). This would only be possible for opposite parities of the charged and neutral K-particles.

In the analysis of experiments one would not, of course, have to restrict oneself to the search for accurately co-planar events, since angular distributions only vary appreciably over angles of order of the reciprocal of the largest orbital angular momenta effectively involved. Thus, near threshold, where only relative s-states contribute, the reaction (14) becomes completely forbidden if the parities do not match.

Similarly, one might consider processes like

$$\Lambda^0+He^4 \rightarrow \begin{cases} \Sigma^+ + \pi^- + He^4 \\ \Sigma^0 + \pi^0 + He^4 \\ \Sigma^- + \pi^+ + He^4 \end{cases} \tag{15}$$

† *Note added in proof:* The possibility of an intrinsic parity determination by means of reaction (11) has been discussed recently [5]), together with an analysis of other reactions induced by polarized protons and antiprotons incident on a He^4 target.

if it becomes possible to study reactions initiated by polarized Λ^0-particles, and if the polarizations of the Σ's can be determined from their decay. While there are special advantages to using He^4 as a target, since it possesses only a single bound state, the absence of low-lying excited states in C^{12} and O^{16} might perhaps also be exploited.

5. Decay Processes

The relation (1) also applies to decay processes with conservation of parity. In a two-particle decay, there is a freedom in the choice of the reflexion plane, since this need only contain the single relative decay momentum. In a three-particle decay, the reflexion plane is defined by the two relative decay momenta.

Decay processes to which (1) applies include electromagnetic transitions, nuclear α-radioactivity, and the decay of virtual states formed in collisions.

Of special interest in the present context is the radiative decay process

$$\Sigma^0 \rightarrow \Lambda^0 + \gamma \qquad (16)$$

considered recently by Feldman and Fulton [2]), who pointed out that the relative $\Sigma^0 - \Lambda^0$ parity can be obtained from polarization measurements of the particles involved. This result also follows directly from (1) since, if we quantize the Σ^0 and Λ^0 polarizations along the direction of the electric polarization vector of the photon, the Σ^0 and Λ^0 spin components are seen to be equal or opposite, depending on whether the relative parity is odd or even. A polarization measurement of all three particles is thus required. While the Λ^0-polarization can be obtained from the asymmetry in the Λ^0-decay, the polarization of the Σ^0 along a given direction may be found from a measurement of the polarization of Λ^0-particles emitted in this direction. In fact, irrespective of the relative parities of Λ^0 and Σ^0, their spin components along the decay direction will necessarily be opposite as a consequence of conservation of angular momentum along this direction, since the photon has spin component ± 1.

The author is indebted to Drs. S. Barshay and E. Henley for valuable comments.

References

1) Proceedings of 1958 Annual International Conference on High Energy Physics, CERN Genève (also for references to previous literature);
A. Pais, Phys. Rev. **112** (1958) 624;
J. G. Taylor, Nuclear Physics **9** (1959) 357
2) G. Feldman and T. Fulton, Nuclear Physics **8** (1958) 106
3) S. M. Bilenky, Nuovo Cimento **10** (1958) 1049
4) Proceedings of the Sixth Annual Rochester Conference on High Energy Physics (Interscience Publishers, New York, 1956);
R. H. Dalitz and B. W. Downs, Phys. Rev. **111** (1958) 967
5) S. M. Bilenky and R. M. Ryndin, Nuovo Cimento

8.B *Nuclear Physics* **10** (1959) 492—507; © *North-Holland Publishing Co., Amsterdam*
Not to be reproduced by photoprint or microfilm without written permission from the publisher

ON PERIPHERAL INTERACTIONS OF ELEMENTARY PARTICLES

L. B. OKUN and I. Ya. POMERANCHUK
U.S.S.R. Academy of Sciences, Moscow

Received 20 September 1958

Abstract: The peripheral interaction of strongly interacting elementary particles is adequately described phenomenologically by modern meson theory. To separate the contribution of the peripheral interaction it is proposed to determine from the experimental data the amplitudes of processes corresponding to large orbital momenta, since large orbital momenta correspond to large impact parameters. A comparison of such experimentally determined amplitudes with theoretically computed values makes it possible to determine a number of important quantities characterizing the strong interactions of elementary particles, such as the renormalized interaction constants of π-mesons with nucleons and hyperons, the renormalized interaction constants of two π-mesons, of a π-meson and a K-meson, etc.

1. Introduction

An investigation of the existing meson theories has shown that the "naive" application of these theories to very small regions of space ($r \ll 10^{-13}$ cm) leads to serious contradictions [1]). It may be that a solution of these contradictions will necessitate a revision of the foundations of quantum mechanics and (or) relativity theory. Nevertheless, there is every ground for believing that the present theoretical concepts are quite adequate for describing the physical phenomena which occur at large distances ($r > 10^{-13}$ cm). The present paper deals with an analysis of strong interactions at such large distances.

When a collision occurs between two particles (say, two nucleons) a distance $r > 1/\mu$ apart, where μ is the mass of the π-meson, (we adopt the system of units in which $\hbar = c = 1$), their interaction is determined by the properties of the meson clouds surrounding them, and is practically independent of the properties of the regions inside these clouds. It is as if the peripheral regions of the nucleons touched. Many theoretical physicists (see, for example, [2])) realize that modern meson theory is capable of giving a phenomenological description of this peripheral interaction. In order to obtain such a description, however, one must be able to separate the contribution of the peripheral interaction. The experimental data on the interaction of elementary particles available to date depend but slightly on computable peripheral interactions. The phenomena investigated up to now are deter-

mined essentially by the character of the interaction at small distances, which cannot at present be computed.

A number of authors (Chew, Moravczik, Taylor, Uretsky, Tsifra *et al.* [3]) recently proposed a method of separating the contribution due to the exchange of one virtual meson †).

Chew's method consists essentially in extrapolating the function describing the angular distribution of the process under investigation into the non-physical region of values $|\cos\theta| > 1$. It can be shown (as will appear in the following) that for a certain value of $|\cos\theta| > 1$ the extrapolated angular distribution is determined by a one-meson amplitude proportional to g^2, where g is the renormalized π-meson-nucleon interaction constant. By comparing the values obtained from extrapolation of the experimental data on n—p scattering and the photoproduction of π-mesons with the corresponding theoretical values Chew *et al.* were able to determine the value of g.

In the following we propose another method of separating the contribution of the peripheral interaction by an analysis of the experimental data. This method is based on the well known fact that two particles with large relative orbital moment l interact effectively at a distance $\approx l\lambda\!\!\!^{-}$, where $\lambda\!\!\!^{-}$ is the wavelength of the particles, since penetration to smaller distances is prevented by the centrifugal barrier. Hence, it follows that in order to investigate the peripheral interaction one must separate from the experimental data relevant to a given process that part of the data which determines the amplitude of the process at sufficiently large values of l.

The possibility of separating and theoretically describing the peripheral interaction is based on the circumstance that two particles or systems of particles a sufficiently large distance apart effectively exchange the least possible number of mesons. Thus, the scattering of a π-meson by a nucleon at large distances is determined by the exchange of two π-mesons; the scattering of a nucleon by a nucleon is determined by the exchange of one π-meson, etc. In view of this, in considering, for example, the scattering of a nucleon by a nucleon one may describe the process at sufficiently large l within the limits of the one-meson approximation, neglecting the exchange of two, three and more π-mesons, as well as the contribution of other mesons and baryon pairs, these being taken into account in the renormalized interaction constant. We observe that in this case it is permissible to limit the calculations to the one-meson term, despite the circumstance that the interaction constant is much greater than unity ($g^2/4\pi \approx 15$). The expansion parameter, as will be seen below, is a quantity proportional to $(g^2/4\pi)\,e^{-\mu\lambda\!\!\!^{-}l}$, which at sufficiently large l is much less than unity. In a certain highly academic sense the one-meson approximation at large l is even more exact

† The authors are grateful to Prof. Chew for sending them the preprint of his paper.

than the one-photon approximation in electrodynamics, inasmuch as $e^2/4\pi = \text{const}$, whereas $(g^2/4\pi)e^{-\mu\lambda l} \to 0$ at $l \to \infty$.

The proposed method of analysis by orbital momenta, in addition to yielding the value of the constant g or similar constants, permits of establishing the relations between the various physical quantities (e.g., scattering phases) which characterize the given process.

In section 2 the method will be justified with the aid of a simple model. The following sections are devoted to a discussion of experiments by means of which the peripheral interaction of elementary particles could be studied. In section 3 we consider experiments involving nucleons and π-mesons; in section 4, experiments involving strange particles. Section 5 deals with the interaction of photons with strongly interacting particles. In section 6 we briefly discuss experiments involving leptons. Section 7 is devoted to a comparison of the data obtainable from the different experiments.

2. A Model of the Interaction

In order to explain the proposed method we consider the interaction of two similar scalar particles which exchange neutral scalar mesons. We shall not take into consideration the evident symmetry of the amplitude, due to the identity of the particles. Such a far-fetched example permits us to ignore details connected with the spin and isospin dependence of the amplitude.

Let us consider the behaviour at large l of the contribution of the one-meson approximation, as compared with the two-meson approximation. We shall also inquire as to how essential the dependence of the vertex part and Green's function of the virtual meson on q^2 is in the one-meson approximation.

The amplitude corresponding to the exchange of one virtual meson (diagram 1) equals

$$a^{(1)} = \mu f^{(1)}(k^2)\frac{d(q^2)\alpha^2(q^2)}{q^2-\mu^2}.$$

Here k is the momentum of one of the colliding particles in the centre-of-mass system; $q^2 = -|\mathbf{q}|^2 = -2k^2(1-\cos\theta)$; θ the scattering angle; μ the mass of the virtual meson. The dimensionless function $f^{(1)}$, which is proportional to the square of the renormalized interaction constant, depends on k^2 and is independent of q.

By limiting ourselves to the *exchange* of *one* virtual meson between the two particles we are taking into consideration *all* the virtual chains which contribute to the Green function of the virtual meson and to each of the vertex parts. This circumstance is reflected in the expression for $a^{(1)}$ in the factors $d(q^2)$ and $\alpha(q^2)$, respectively. We observe that $\alpha(\mu^2) = d(\mu^2) = 1$.

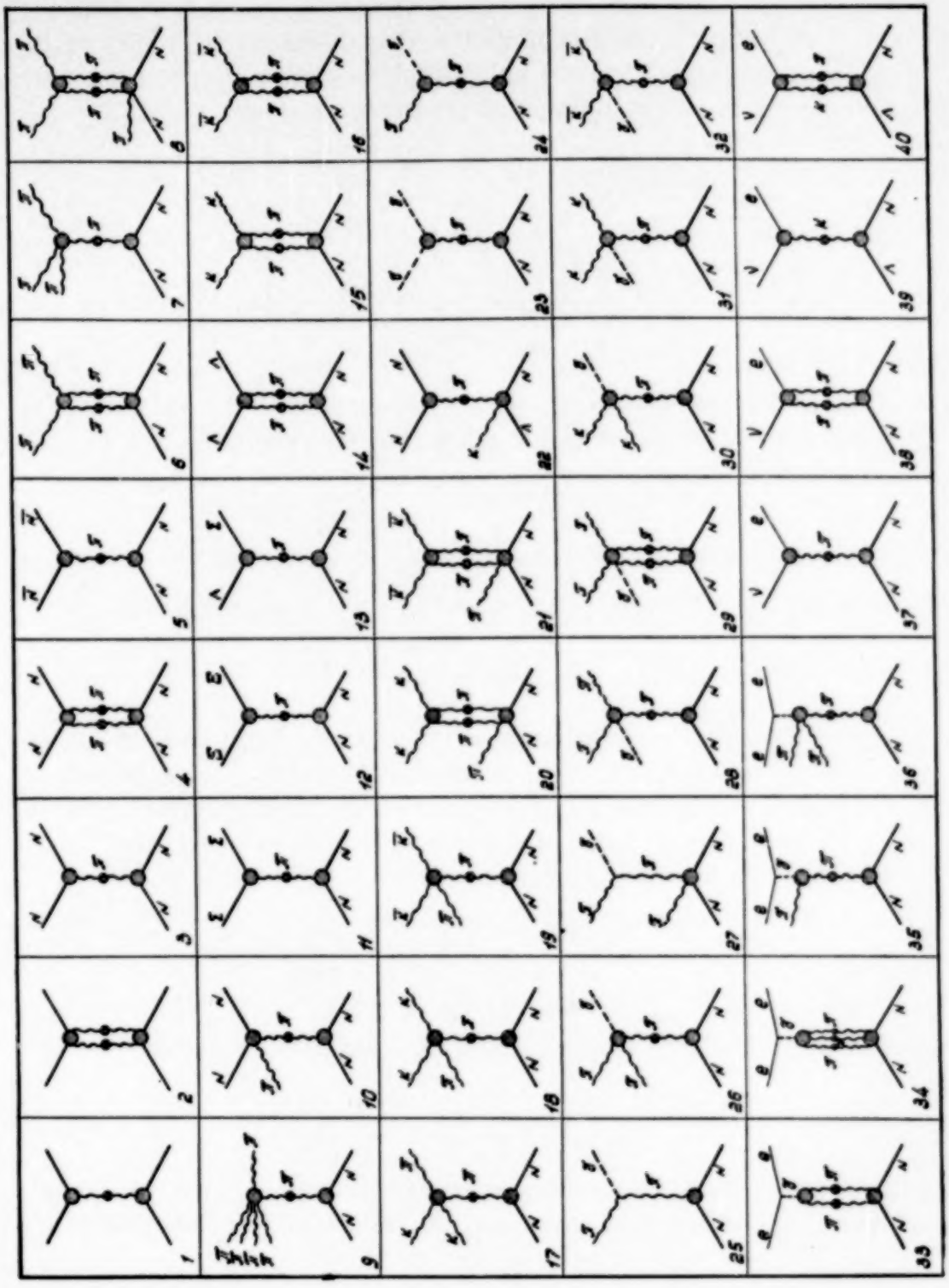

Fig. 1

In diagram 1 and the following diagrams the blocks containing all the possible virtual processes are marked by circles.

One easily obtains the contribution of the one-meson diagram 1 to the scattering amplitude in the state with orbital momentum l by resorting to the well known expansion in terms of Legendre polynomials:

$$a^{(1)} = \frac{1}{2ik}\sum_{l=0}(2l+1)\eta_l^{(1)}P_l(\cos\vartheta), \qquad \eta_l^{(1)} = e^{i2\delta_l^{(1)}}-1,$$

whence it follows that

$$\eta_l^{(1)} = \frac{i\mu f^{(1)}}{2k}\int_0^\pi \frac{P_l(\cos\vartheta)\mathrm{d}(\cos\vartheta)}{1+\frac{\mu^2}{2k^2}-\cos\vartheta} = \frac{i\mu f^{(1)}}{k}Q_l\left(1+\frac{\mu^2}{2k^2}\right),$$

where Q_l are the well known Legendre polynomials of the second kind. (For the analytical expression of Q_l see ref. [4]). For tables of Q_l see ref. [5]).) We observe that for $l \gg k/\mu \gg 1$,

$$Q_l\left(1+\frac{\mu^2}{2k^2}\right) \approx \sqrt{\frac{\pi k}{2\mu l}}\,e^{-\mu l/k}.$$

For $k/\mu \ll 1$ the exponential law is replaced by a power law:

$$Q_l\left(1+\frac{\mu^2}{2k^2}\right) \approx \frac{l!\,2^{l+1}}{(2l+1)!!}\left(\frac{k}{\mu}\right)^{2l+2}.$$

We now estimate the contribution at large l of the two-meson amplitude corresponding to diagram 2. Assuming that at large l the factors connected with the Green's functions of the mesons play the most important role, we neglect the dependence of the other terms on p and q and take these terms outside the integral. As a result we obtain

$$a^{(2)} = \frac{f^{(2)}(k^2)}{\mu}\int \frac{\mathrm{d}^4p}{[(p-\frac{1}{2}q)^2-\mu^2][(p+\frac{1}{2}q)^2-\mu^2]}$$

where $f^{(2)}$ is a dimensionless function of k^2. Combining the factors in the denominator and changing the variable of integration we obtain

$$a^{(2)} = \frac{f^{(2)}}{\mu}\int_0^1 \mathrm{d}x \int \frac{\mathrm{d}^4p}{[p^2+q^2(1-x)x-\mu^2]^2}.$$

In the integral over d^4p we now substitute integration over the real axis p^0 by integration over the imaginary axis (see ref. [6,7]). The denominator in this case becomes constant in sign, and we obtain

$$\eta_l^{(2)} = -\frac{f^{(2)}}{8\mu^2 k}\int_0^1 \frac{\mathrm{d}x}{(1-x)x}\int_0^\infty \frac{\partial}{\partial\mu}Q_l\left(1+\frac{\mu^2+t^2}{2k^2(1-x)x}\right)t^2\mathrm{d}t^2$$

where $t^2 = |p|^2+p_0^2$.

For $l \gg k/\mu \gg 1$ we use the asymptotic form of the function Q_l and, after integration, obtain

$$\eta_l^{(2)} = -\frac{\pi k f^{(2)}}{4\mu l^2} e^{-2\mu l/k}.$$

We thus see that for large l the two-meson amplitude is exponentially small compared to the one-meson amplitude. A more detailed analysis of the two-meson amplitude at large l will be given in another paper. Here we merely observe that in computing the contribution at large l the convergence of the integrals with respect to the momenta of the virtual particles is always guaranteed by the presence of $P_l(\cos\theta)$ in the integrand. Thus, in the integrals considered above, $t_{\text{eff}}^2 \approx \mu k/l$.

It is evident that the contribution of the three-meson amplitude at large $l (l \gg k/\mu \gg 1)$ should fall off as $l^{-(3\mu l/k)}$. In the case $k/\mu < 1$ this exponentially small term is replaced by a term of the type 2^{-2l-2} for the two-meson amplitude and 3^{-2l-2} for the three-meson amplitude.

Let us return to the one-meson amplitude. In deducing the formula for the one-meson amplitude we assumed $\alpha(q^2) = 1$ and $d(q) = 1$ on the ground that the essential values in the integral are $q^2 \approx \mu^2$. We shall now justify this approximation. Utilizing the spectral expansion of Green's function [8]) and the vertices [9]), we obtain

$$\frac{\alpha^2(q^2)d(q^2)}{q^2-\mu^2} = \frac{1}{q^2-\mu^2}(1+S_1(q^2))(1+S_2(q^2))^2$$

where

$$S_i = (q^2-\mu^2)\int_m \frac{\rho_i(\kappa^2)d\kappa^2}{q^2-\kappa^2}.$$

Limiting ourselves to linear terms in S_i, we obtain

$$\eta_l^{(1)} \approx \frac{i\mu f^{(1)}}{k}\left\{Q_l\left(1+\frac{\mu^2}{2k^2}\right) + \int_m^\infty Q_l\left(1+\frac{\kappa^2}{2k^2}\right)(\rho_1(\kappa^2)+2\rho_2(\kappa^2))\,d\kappa^2 + \ldots\right\}.$$

The quantity m is equal to the least sum of the masses of the particles into which a meson can be transformed. For a π-meson, for example, $m = 3m_\pi$, for a K-meson $m = 2m_\pi + m_k$. For a scalar meson we should have $m = 2\mu$. Hence, for $l \gg k/\mu \gg 1$ the correction terms, which are proportional to $e^{-(2\mu l/k)}$, are exponentially small compared to $Q_l(1+(\mu^2/2k^2) \approx e^{-\mu l/k})$. The contribution due to the factors $\alpha(q^2)$ and $d(q^2)$ is of the same order of magnitude as that due to the exchange of two and more mesons. In the case of virtual π-mesons this contribution is of the same order of magnitude as that due to the exchange of three π-mesons. It is easy to show that a consideration of the second- and third-order terms in S_i will not affect this conclusion.

A consideration of the isobaric and spin variables which are of importance in an analysis of concrete processes will slightly modify but not essentially affect the above results.

3. Interaction of π-Mesons and Nucleons

3.1. SCATTERING OF NUCLEONS BY NUCLEONS

A detailed analysis of this problem will be given elsewhere †. Hence, in the following we shall touch only the main questions.

The peripheral interaction of nucleons, as is evident from the preceding, is described by a one-meson amplitude

$$M = 4\pi g^2 \Big\{ (\bar{u}'_1 \gamma_5 \tau_\alpha u_1)(\bar{u}'_2 \gamma_5 \tau_\alpha u_2) \frac{\alpha^2(q^2) d(q^2)}{q^2 - \mu^2} - (\bar{u}'_2 \gamma_5 \tau_\alpha u_1)(\bar{u}'_1 \gamma_5 \tau_\alpha u_2) \frac{\alpha^2(p^2) d(p^2)}{p^2 - \mu^2}$$

corresponding to diagram 3.

Here g is the renormalized π-meson-nucleon interaction constant; $q = k - k'$, $p = k + k'$; k and k' are the 4-momenta of one of the particles before and after scattering, respectively. The factors α and d characterize the difference between the values of the vertex and the Green's function of the meson at $q^2 < 0$ and $p^2 < 0$ and their values at $q^2 = p^2 = \mu^2$.

The above expression for M allows us to compute the scattering amplitudes with a given value of the total angular moment, similar to the procedure for the scattering of scalar particles. Estimates carried out on various models show that for an energy of some tens of MeV the F-phase of nucleon-nucleon scattering should be closely described by the formula thus obtained.

As is well known [11]), in the non-relativistic approximation the nucleon-nucleon scattering amplitude may be represented in the form

$$\alpha + \beta(\boldsymbol{\sigma}_1 + \boldsymbol{\sigma}_2) \cdot \mathbf{n} + \gamma(\boldsymbol{\sigma}_1 \cdot \mathbf{n})(\boldsymbol{\sigma}_2 \cdot \mathbf{n}) + \delta(\boldsymbol{\sigma}_1 \cdot \mathbf{m})(\boldsymbol{\sigma}_2 \cdot \mathbf{m}) + \varepsilon(\boldsymbol{\sigma}_1 \cdot \mathbf{l})(\boldsymbol{\sigma}_2 \cdot \mathbf{l})$$

where $\alpha \ldots \varepsilon$ are scalar functions of the scattering angle, and $\mathbf{n}$, $\mathbf{l}$, $\mathbf{m}$ are unit vectors directed along $\mathbf{k} \times \mathbf{k}'$, $\mathbf{k} - \mathbf{k}'$, $\mathbf{k} + \mathbf{k}'$ respectively. The amplitude M contains all the terms of this expression, except the second: in the one-meson approximation $\beta = 0$. This means that the spin-orbital interaction is absent in the one-meson approximation, and in the effective potential [12]) of nucleon-nucleon interaction it should fall off with the distance at least as $e^{-2\mu r}$.

If we experimentally separate the term proportional to β and determine its contribution to the amplitudes at large l, we can find the magnitude of

† For the calculation of the nucleon-nucleon scattering phase-shifts in the one-meson approximation see also ref.[10]).

the two-meson diagram 4. We observe that in the one-meson approximation the dependence of the nucleon-nucleon scattering amplitude on the spin is more complex than the dependence on the spin of the antinucleon-nucleon or hyperon-nucleon scattering amplitude, since in the latter cases there are no exchange forces and, hence, no anti-symmetrization of the amplitude.

From nucleon-nucleon scattering one can establish the magnitude of g; simultaneously, since it is possible to compute the different phases and compare them with experiment, one can determine the trustworthiness of the results. Thus, the proposed method provides a criterion by which in each individual case one can estimate the accuracy of the results without having recourse to supplementary estimates.

3.2. SCATTERING OF ANTINUCLEONS BY NUCLEONS

Despite the difference in the magnitude of the cross sections and the character of nucleon-nucleon and nucleon-anti-nucleon interactions, the phases of antinucleon-nucleon scattering at large l should also be described by the one-meson diagram (diagram 5). The scattering phases for $\bar{p}+n \to \bar{p}+n$ and $\bar{n}+p \to \bar{n}+p$ should be equal to and opposite in sign to the scattering phases for $p+p \to p+p$ (or $n+n \to n+n$) in those states in which the latter processes may take place. The phases of $\bar{p}-p$ and $\bar{n}-n$ interaction should be equal to and opposite in sign to the phases of $p-n$ interaction, where one must once more take into consideration the additional symmetry of the two-nucleon system which is absent in the nucleon-anti-nucleon system. We observe that the one-meson scattering amplitude of the antinucleon has only one term of the type $\tau_1\tau_2(\sigma_1 \cdot \mathbf{l})(\sigma_2 \cdot \mathbf{l})$. It follows hence, in particular, that the amplitudes with $T = 0$ and $T = 1$ at large l should satisfy the relation

$$a_{T=0} = -3a_{T=1}.$$

Diffraction scattering due to inelastic processes in nucleon-antinucleon interaction may make it extremely difficult to separate out the contribution of the one-meson amplitude.

3.3. SCATTERING OF π-MESONS BY NUCLEONS

π-meson-nucleon scattering at large l is determined by the two-meson diagram 6, since the corresponding one-meson diagram is forbidden (due to pseudo-scalar nature of the π-meson the transition $\pi \to 2\pi$ is impossible).

As was shown by Lee and Yang [13]), the transformation of an even number of π-mesons into an odd number of π-mesons in vacuum is forbidden as a result of invariance of the Lagrangian of strong interactions under the combined transformation of rotation in isobaric spin space and charge

conjugation. Hence, only the diagrams describing the exchange of an even number of π-mesons can contribute to π-meson-nucleon scattering.

As appears from diagram 6, the phases of πN-scattering at large l are determined by the contributions of two blocks: π-meson-π-meson scattering and π-meson-nucleon scattering, which are connected by two virtual π-mesons.

3.4. PRODUCTION OF π-MESONS IN COLLISIONS OF π-MESONS AND NUCLEONS WITH NUCLEONS

In the production of mesons by mesons ($\pi+N \to N+2\pi$) the π-meson-π-meson scattering block mentioned above figures in the one-meson diagram 7. In this case an analysis based on angular momenta is more complicated, since there are three particles in the final state. To each given value of $\mathbf{j}_0$ of the colliding π-meson and nucleon there corresponds a collection of values of $\mathbf{j}_1$ and $\mathbf{j}_2$ which characterize the relative motion of the π-mesons and the motion of the nucleon, respectively. Diagram 7, as is easily seen, determines the amplitude of the transition corresponding to large values of the angular momentum $\mathbf{j}_2$. Hence, an experimental determination of these amplitudes would make it possible to find the value of the π-meson—π-meson scattering. By studying the dependence of the amplitude on $\mathbf{j}_1$–the relative angular momentum of the two π-mesons–one can determine in which orbital state the interaction of these π-mesons is strongest. Such a programme, however, demands for its fulfilment a great number of experimental points. The analysis based on angular moment $\mathbf{j}_2$ may possibly be simpler for cases when the two π-mesons are emitted with practically equal momenta. Depending on which value of $\mathbf{j}_1$ predominates, the emerging π-mesons will be in the isobaric state $T = 1$ (odd j_1) or $T = 0,2$ (even j_1). The two-meson diagram 8 is another diagram whose contribution at large l is small compared with that of diagram 7, but large compared with the other diagrams. For this diagram, as is easily seen, the large angular momentum on which the analysis should be based is that of one of the π-mesons (scattered) relative to the system nucleon + second π-meson (produced).

In similar manner one can analyze the production of a large number of π-mesons. Thus, for example, the process $\pi+N \to 4\pi+N$ (diagram 9) can yield information about the block containing six meson ends.

The amplitude of meson production upon the collision of nucleons $N+N \to N+N+\pi$ at large angular moments of the relative motion of the two nucleons in the final state is determined by the one-meson diagram 10, which contains, in addition to the vertex $NN\pi$, also the block of π-meson-nucleon scattering.

We observe that in investigating an inelastic process the analysis based on orbital momenta should be carried out sufficiently far from the threshold of

the process, since near the threshold the momentum transferred to the nucleon cannot be small.

4. Interaction of Strange Particles with π-Mesons and Nucleons

In turning to processes involving strange particles we must stress that the proposed method of analysis is greatly complicated in the case of processes for which the exchange of K-mesons is essential. This is due mainly to the circumstance that the mass of the K-meson is more than three times that of the π-meson. This makes it difficult to separate the contribution of the K-meson from the contribution of diagrams in which there may be one or two π-meson lines parallel to the virtual K-meson line. For this reason in the following we shall consider only such processes for which the amplitudes corresponding to large l are due to the exchange only of π-mesons.

4.1. SCATTERING OF HYPERONS BY NUCLEONS

Diagrams 11 and 12 correspond to scattering on nucleons at large momenta of Σ- and Ξ-hyperons, respectively. Diagram 13 corresponds to the process $\Sigma+N \to \Lambda+N$, and diagram 14 to the scattering of Λ-hyperons by nucleons. In the latter case the one-meson diagram is forbidden, since the vertex $\Lambda\Lambda\pi$ is isobarically non-invariant. For all these processes one can derive relations similar to those obtained for the scattering of nucleons and antinucleons. The amplitudes of antihyperon-nucleon scattering at large l bear a simple relation to the scattering amplitudes of hyperons. We observe that the form of the amplitude of the process $\Sigma+N \to \Lambda+N$ is determined by the relative parity of the Σ- and Λ-hyperons.

4.2. SCATTERING OF K-MESONS BY NUCLEONS

In the scattering of K-mesons, as in the case of the scattering of π-mesons, the one-meson diagram is forbidden due to the pseudo-scalar nature of the π-mesons, and at large angular momenta the two-meson diagram 15 predominates. This diagram is similar to diagram 6 and differs from the latter in that it contains the block of K-meson—π-meson scattering, instead of the $\pi-\pi$-scattering block. It is therefore of great interest to compare directly the phases of the processes $\pi+N \to \pi+N$ and $K+N \to K+N$ at large l. We observe that at large l the phase of K meson-nucleon scattering (diagram 16) is also determined by the block $\pi\pi KK$.

4.3. PRODUCTION OF K-MESONS AND PRODUCTION OF π-MESONS BY K-MESONS

The interaction block $\pi\pi KK$ in the diagram of K-meson-nucleon scattering also figures in a number of other diagrams. It is contained in particular, although for other values of the momenta of the particles, in diagram 17, which describes the process $\pi+N \to K+\overline{K}+N$. The analysis of this latter

process should be carried out similarly to the analysis of the reaction $\pi+N \to \pi+\pi+N$ by considering the relative motion of the K-mesons on the one hand, and the motion of their centre of mass with respect to the nucleon, on the other. The large angular momenta of the latter motion are due to diagram 17. The same block $\pi\pi KK$ figures in the one-meson diagrams 18 and 19, which describe the production of π-mesons by K- and $\overline{K}$-mesons: $K+N \to K+\pi+N$ and $\overline{K}+N \to \overline{K}+N+\pi$. The corresponding two-meson diagrams 20 and 21 are similar to diagram 5, differing from it in the upper block ($\pi\pi KK$ instead of $\pi\pi\pi\pi$). The production of K-mesons in the collision of nucleons $N+N \to N+\Lambda(\Sigma)+K$ is described for large l by diagram 22, which is similar to diagram 10 describing the production of π-mesons.

5. The Interaction of Photons with Mesons and Baryons

5.1. SCATTERING OF PHOTONS BY NUCLEONS

The phases of Compton scattering $\gamma+N \to \gamma+N$ at large l are determined by diagram 23. The existence of this diagram was indicated by Low [14]). The block $\pi\gamma\gamma$ figuring in it describes, as is easily seen, the decay of a π^0-meson to two γ-quanta. Thus, a measurement of the phases of Compton scattering of photons by nucleons at large l would be equivalent to a measurement of the life-time of the π^0-meson. We observe that the scattering phases determined by diagram 23 for the proton and neutron are equal in magnitude and opposite in sign.

5.2. PHOTOPRODUCTION OF π-MESONS

The peripheral production of charged π-mesons is described by diagram 24. In this case, in view of the generalized Ward theorem for the interaction of bosons and real photons [15]), diagram 24 is identically equal to diagram 25, in which the vertex $\gamma\pi\pi$ and the Green's function of the virtual meson are not renormalized. Thus, by measuring the amplitudes of the processes $\gamma+N \to \pi+N$ at large l one can find the pure block πNN.

We observe that the contribution of diagram 25 differs for the proton and the neutron only in sign. The reverse process to photoproduction — the emission of photons upon the capture of π-mesons by nucleons — is also described by diagram 25, if one considers it from right to left.

The photoproduction of a pair of π-mesons ($\gamma+N \to 2\pi+N$) at large angular moments of the pair relative to the nucleon is described by diagram 26, containing the block $\gamma\pi\pi\pi$. Diagram 27 is another one which will give a contribution at large angular moments of one of the mesons relative to the pair nucleon+second meson. The block $\gamma\pi\pi\pi$ in diagram 26 also figures in the one-meson diagram 28 which describes the emission of bremsstrahlung by the π-meson upon scattering by a nucleon. In the case of bremsstrahlung at large

impact parameters (large l) the main contribution comes from diagram 28, since due to the pseudo-scalar nature of the π-meson the usual "accompanying" bremsstrahlung is described by the two-meson diagram 29, the contribution of which at large l can be neglected. We observe that the bremsstrahlung may be accompanied by charge exchange of the π-mesons.

5.3. PHOTOPRODUCTION OF K-MESONS

Diagram 30 describing the photoproduction of the pair $K+\overline{K}$ contains the block $\gamma\pi KK$ which can be determined by studying the process $\gamma+N \to \overline{K}+K+N$. The same block figures in diagrams 31 and 32 describing the bremsstrahlung in the scattering of K- and $\overline{K}$-mesons by nucleons. We observe that bremsstrahlung may be accompanied by charge exchange of the K-mesons.

5.4. SCATTERING OF ELECTRONS BY NUCLEONS AND PRODUCTION OF π- AND K-MESONS BY ELECTRONS

At other values of the 4-momenta of the corresponding particles the blocks considered above figure in the diagrams which describe the interaction of electrons and nucleons. As is well known, the amplitude of electron-nucleon scattering contains two terms, one of which is proportional to τ_3, while the other is an isobaric scalar. As was shown by Goldberger and Bernstein [16]), the first of these terms corresponds to diagram 33, the second to diagram 34. The blocks $\gamma\pi\pi$ and $\gamma\pi\pi\pi$ contained in these diagrams and corresponding to virtual photons with $k^2 \neq 0$ also figure in the diagrams describing the processes of production of π-mesons by electrons:

$$e+N \to e+\pi+N \quad \text{and} \quad e+N \to e+2\pi+N$$

(diagrams 35 and 36).

The diagram of the process $e+N \to e+N+\overline{K}+\overline{K}$ is similar to diagram 36, differing from it in that the block $\gamma\pi\pi\pi$ has been replaced by the block $\gamma\pi KK$.

5.5. INTERACTION INVOLVING A NEUTRINO

The collision of electrons and protons may be accompanied by the process $e^-+p \to n+\nu$ due to the weak β-decay interaction. The peripheral part of this process corresponds to diagrams 37 and 38. These diagrams contain the blocks $\pi e\nu$ [17]) and $\pi\pi e\nu$ [18]), the first of which is due to axial vector interaction, and the second to vector interaction. Upon the collision of high-energy electrons with protons hyperons may also be produced, as, for example, $e+p \to \Lambda+\nu$. Diagrams 39 and 40 which describe this process contain the blocks $Ke\nu$ and $K\pi e\nu$. Both the blocks $\pi e\nu$ and $\pi\pi e\nu$, and the blocks $Ke\nu$ and $K\pi e\nu$ may be measured independently by measuring the decays: $\pi \to e+\nu$, $\pi \to \pi^0+e+\nu$,

$K \to e+\nu$, $K \to \pi+e+\nu$. Everything in this section holds also for the collisions of μ-mesons with nucleons, diagrams of the type 37 and 39 being in this case more important than in the case of electrons.

6. Comparison of the Different Processes

Table 1 lists the processes discussed above and the blocks of strong interactions which can be determined from an investigation of these processes. The figures 1, 2, 3 indicate the number of virtual mesons connecting these blocs in the corresponding diagrams. For example, in the line corresponding to the process $\pi+N \to 2\pi+N$, the figure 1 is situated at the intersections with the columns corresponding to the blocks $NN\pi$ and $\pi\pi\pi\pi$, and corresponds to diagram 7 in which these two blocks are connected by one virtual π-meson. For the same process the figure 2 corresponds to the diagram in which the blocks $\pi\pi\pi\pi$ and $\pi\pi\pi NN$ are connected by two mesons. On the example of one-meson diagrams we shall show how the blocks determined from the different processes can be compared.

The block $NN\pi$ (renormalized constant g) can be determined independently from the processes $N+N \to N+N$, $\overline{N}+N \to \overline{N}+N$, $\gamma+N \to \pi+N$, inasmuch as these processes do not contain any other unknown blocks. If the block $NN\pi$ is known, we can determine the following blocks:

$\pi\pi\pi\pi$	from the process	$\pi+N \to 2\pi+N$
$NN\pi\pi$	from the process	$N+N \to N+N+\pi$
$\Sigma\Sigma\pi$	from the process	$\Sigma+N \to \Sigma+N$
$\Sigma\Lambda\pi$	from the process	$\Sigma+N \to \Lambda+N$
$\Xi\Xi\pi$	from the process	$\Xi+N \to \Xi+N$
$\pi\pi KK$	independently from the three different processes	$\pi+N \to K+\overline{K}+N$ $K+N \to K+\pi+N$ $\overline{K}+N \to \overline{K}+\pi+N$
$\pi NK\Lambda$	from the process	$N+N \to N+\Lambda+K$
$\pi\gamma\gamma$	from the process	$\gamma+N \to \gamma+N$
$\gamma\pi\pi\pi$	from the processes	$\gamma+N \to 2\pi+N$ $\pi+N \to \pi+N+\gamma$
$\gamma\pi KK$	from the processes	$\gamma+N \to \overline{K}+K+N$ $K+N \to \gamma+K+N$ $\overline{K}+N \to \gamma+\overline{K}+N.$

As is easily seen, in determining a block from a one-meson diagram we obtain its value for the particular case when one of the ends of the block corresponds to a virtual π-meson.

In similar manner (see the table) from the two-meson diagrams we can determine the blocks containing two virtual π-meson ends. In a number of cases a particular block can be determined both from a one-meson diagram,

TABLE 1

Processes \ Blocks	
$\overline{N}+N \to \overline{N}+N$	1.1 2.2 3.3
$N+N \to N+N$	1.1 2.2 3.3
$\pi+N \to \pi+N$	2 2
$\pi+N \to 2\pi+N$	1 1.2 2
$N+N \to N+N+\pi$	1 1.2 2
$\Sigma+N \to \Sigma+N$	1 1 2 2
$\overline{\Xi}+N \to \overline{\Xi}+N$	1 1 2 2
$\Sigma+N \to \Lambda+N$	1 1
$\Lambda+N \to \Lambda+N$	2 2
$\overline{\Sigma}+N \to \overline{\Sigma}+N$	1 1 2 2
$\overline{\Sigma}+N \to \overline{\Lambda}+N$	1 1
$K+N \to K+N$	2 2
$\overline{K}+N \to \overline{K}+N$	2 2
$\pi+N \to K+K+N$	1 1
$K+N \to K+\pi+N$	1 1
$\overline{K}+N \to \overline{K}+\pi+N$	1 1
$N+N \to N+\Lambda+K$	1 1
$\gamma+N \to \gamma+N$	1 1
$\gamma+N \to \pi+N$	1 1
$\gamma+N \to 2\pi+N$	1 1 1 1
$\gamma+N \to K+\overline{K}+N$	1 1
$\pi+N \to \pi+\gamma+N$	1 1
$K+N \to K+\gamma+N$	1 1
$e+N \to e+N$	2 2 3 3
$e+N \to \nu+N$	1 1 2 2

and from a two-meson (or three-meson) diagram (for example, the block $\gamma\pi\pi\pi$). This allows of determining the magnitude of the block for such values of the momenta of the involved mesons, as correspond to a non-physical region. In this connection it is appropriate to stress once more that the same blocks determined from one-meson and from two-meson diagrams have different numerical values of the momenta of the particles involved.

In the preceding we considered the amplitudes of the different processes at orbital momenta $l \gg 1$. The experimental determination of amplitudes with very large l is, of course, practically impossible. It appears, however, that in the case of nucleon-nucleon scattering at low energies the experimental amplitude can be described by a peripheral one-meson interaction at $l = 3$. The character of the experimental angular distribution of nucleons in the process $\pi+N \to 2\pi+N$ indicates that the peripheral one-meson interaction can also be very large in this case and is a determining factor already at not very great l. Thus, an experimental investigation of the processes enumerated above, which will yield the data necessary for the proposed analysis, may fairly soon be possible in a number of cases.

We observe that relations similar to those existing between the different processes involving nucleons also exist for processes in which a neutron has been replaced by a deuteron or more complex nucleus. In particular, by comparing the scattering of nucleons and hyperons by nuclei, one can determine the ratio of the constants of interaction of π-mesons with nucleons and hyperons.

In conclusion it should be stressed that all the above conclusions relating to peripheral interaction are independent of the character of the interaction of strongly interacting particles at small distances. They are independent, in particular, of whether the π-meson is an elementary or a composite particle.

The authors are grateful to V. B. Berestetsky, N. N. Bogolubov, A. F. Grashin, B. L. Ioffe, L. D. Landau, A. P. Rudik, K. A. Ter-Martirosyan and I. I. Shmushkevich for discussions and valuable suggestions.

References

1) L. Landau and I. Pomeranchuk, Doklady AN SSSR **102** (1955) 489;
I. Pomeranchuk, Nuovo Cimento **3** (1956) 1186;
I. Pomeranchuk, V. V. Sudakov and K. A. Ter-Martirosyan, Phys. Rev. **10** (1956) 784;
E. C. Fradkin, JETP **28** (1955) 750;
G. Källen and W. Pauli, Mat. Fys. Medd. Dan. Vid. Selsk. **30** (1955) no. 7
2) Taketani *et al.*, Suppl. to Progr. Theor. Phys. **3** (1956);
G. Chew, Proc. of the Rochester Conf. (1957);
see also V. Khozyainov, JETP **27** (1954) 445
3) G. Chew, preprint;
G. Chew, Proceedings of the Geneva Conference on High energy Physics (1958)

4) M. M. Rizhik and I. S. Gradshtein, Tables of Integrals, Sums, Series and Products (GITTL, 1951)
5) Tables of Associated Legendre Functions (Columbia Univ. Press, 1945)
6) F. Dyson, Phys. Rev. **75** (1949) 1736
7) L. D. Landau, A. A. Abrikosov and I. M. Khalatnikov, Doklady AN SSSR **95** (1954) 497
8) H. Lehmann, Nuovo Cimento **11** (1954) 342
9) R. Karplus, C. Sommerfield and E. Wichmann, Phys. Rev. **111** (1958) 1187; further references in this paper
10) S. Otsuki, R. Tamagaki and W. Watari, Report at the Second Geneva Conference on Peaceful Application of Atomic Energy (1958)
11) R. Oheme, Phys. Rev. **98** (1955) 216;
L. Puzikov, F. Ryndin and Ya. Smorodinsky, JETP **32** (1957) 592
12) S. Okubo and R. Marshak, Ann. of Phys. **4** (1958) 166
13) T. D. Lee and C. N. Yang, Nuovo Cimento **3** (1956) 749
14) F. Low, Proceedings of the Geneva Conference on High energy Physics (1958), Chew's report
15) I. Pomeranchuk, Doklady AN SSSR **100** (1955) 41
16) J. Bernstein and M. Goldberger, Revs. Mod. Phys. **30** (1958) 465
17) M. Goldberger and S. Treiman, Phys. Rev. **110** (1958) 1178
18) R. Feynmann and M. Gell-Mann, Phys. Rev. **109** (1958) 193

10.D *Nuclear Physics* **10** (1959) 508; © *North-Holland Publishing Co., Amsterdam*

BOOK REVIEW

W. E. THIRRING, *Principles of quantum electrodynamics* (Academic Press, New York and London 1958, xv—234 p. 80s.)

Thirring's excellent treatise (which was, I think, the first book devoted to the new methods of quantum electrodynamics) is now translated, with some remodelling, into the common idiom of the physicists of the younger generation, which they innocently believe to be English. This treatment has fortunately not managed to destroy the eminent qualities which distinguish Prof. Thirring's style of exposition, in particular his endeavour to explain the structure of the mathematical formulae in terms of easily remembered semi-qualitative features of the formalism. This is of considerable didactic value, but when the author, in his preface, calls such formal features "the physical basis of the theory", I beg leave to dissent.

It makes good sense to say that the spatial part of the wave-function of a Dirac electron at rest (say) is spread (i.e. has significant values) over a domain of linear dimensions $\hbar/mc$; and to say that a transition matrix element occurring in a formula refers to a "virtual process" is a useful terminology inasmuch as it helps to visualize the structure of the formula. But it ought to be made clear to the beginner that such terminology belongs to the formalism itself, and by no means to its physical interpretation. A phrase like "the spreading of the charge due to virtual pairs" (p. 176) may be perfectly clear to the author and other initiates, but it is didactically preposterous in its deceptive suggestiveness of some vaguely imaginable physical process. This kind of loose talk constantly recurs throughout the book without the slightest warning of its danger in encouraging loose thinking. Indeed, the section on limitations of measurability, to which one would turn for a discussion of the basis for the actual physical interpretation of the mathematical symbols, is very weak in this respect; none of the crucial points is properly emphasized.

Another bone of contention is the use of the system of units based on $\hbar$, m and c, which the author tries to justify by specious arguments. The immediate result of wiping out $\hbar$ and c, however, is to deprive oneself of an easy means of recognizing at a glance whether a given phenomenon is classical or quantal, relativistic or unrelativistic. In fact, on p. 13 we find a telling footnote addressed to "the reader who gets confused with the dimensions": no such confusion could possibly arise if the formulae were written out without specialization of the units.

I hope the author will not mind my taking him as target for criticism which could just as well be aimed at others; but he has begged for it by his rashness in using the word "physics" in a rather uncongenial context. Anyhow, he will always find comfort in Dyson's review of the German edition.

L.R.

1.C *Nuclear Physics* **10** (1959) 509—526; © *North-Holland Publishing Co., Amsterdam*
Not to be reproduced by photoprint or microfilm without written permission from the publisher

UN DÉVELOPPEMENT DU POTENTIEL DE GIBBS D'UN SYSTÈME QUANTIQUE COMPOSÉ D'UN GRAND NOMBRE DE PARTICULES

III - LA CONTRIBUTION DES COLLISIONS BINAIRES

CLAUDE BLOCH et CYRANO DE DOMINICIS
Centre d'Études Nucléaires de Saclay, Gif-sur-Yvette (S & O)

Reçu le 8 décembre 1958

Abstract: Starting from an expansion derived in a previous work, we study the contribution to the Gibbs potential of the two-body dynamical correlations, taking into account the statistical correlations. Such a contribution is of interest for low density systems at low temperature. In the zero density limit, it reduces to the Beth-Uhlenbeck expression for the second virial coefficient. For a system of fermions in the zero temperature limit, it yields the contribution of the Brueckner reaction matrix to the ground state energy, plus, under certain conditions, additional terms of the form $\exp(\beta|\Delta|)$, where the Δ are the binding energies of "bound states" of the type first discussed by L. Cooper. Finally, we study the wave function of two particles immersed in a medium (defined by its temperature and chemical potential). It satisfies an equation generalizing the Bethe-Goldstone equation for an arbitrary temperature.

1. Introduction

L'étude des collisions binaires, qui ne fait intervenir que les corrélations dynamiques de deux particules, offre un intérêt lorsque la densité est assez basse pour que les effets des collisions multiples puissent être négligés.

Aux basses températures l'effet dû aux corrélations statistiques devient assez important pour nécessiter un développement du potentiel de Gibbs qui tienne compte de l'effet de ces corrélations [1]) (pour l'énergie, ce développement redonne à température nulle le développement de Goldstone et Hugenholtz [2])). Pour de faibles densités, considérer l'effet dû aux corrélations dynamiques de deux particules, revient alors à effectuer sur les diagrammes introduits dans [1]) une sommation partielle des diagrammes en échelle. Ceci est une généralisation à température non nulle de la sommation partielle considérée par Brueckner [3]) et une extension de celle considérée par Lee et Yang [4]) en tenant compte des corrélations statistiques.

Le cas d'interactions singulières (cœur dur répulsif par exemple) impose d'ailleurs une resommation préalable de diagrammes (en échelle), ce qui revient ici à introduire une interaction effective dépendant de la température β^{-1} et du potentiel chimique α.

April (2) 1959

La sommation partielle effectuée ici ne permet cependant pas, même à basse densité, une étude détaillée du voisinage de la surface de Fermi (au même titre d'ailleurs que la sommation partielle de Brueckner). Dans ce travail nous verrons les difficultés apparaître explicitement. Une telle étude nécessiterait un traitement plus symétrique des trous et des particules[5])

Dans les paragraphes 2 et 3 on met la contribution des collisions binaires sous une forme tenant compte des corrélations statistiques et qui s'exprime en fonction d'une matrice de réaction généralisée θ dépendant de α et β, ou en fonction de „déphasages propres" et „d'énergies de liaison" généralisés, relatifs au système de deux particules immergées dans le milieu.

A densité nulle, les corrélations statistiques devenant négligeables, cette forme donne comme cas particulier l'expression de Beth-Uhlenbeck[6]) pour le second coefficient du viriel (paragraphe 3).

La limite des températures nulles est examinée en détail au paragraphe 4 dans le cas d'un gaz de fermions et on montre qu'on obtient, outre la contribution à l'énergie donnée par la matrice t de Brueckner, un terme croissant exponentiellement lorsque $\beta \to \infty$, contribution d'états „liés" qui apparaissent de toute façon lorsque le potentiel est attractif au voisinage de la surface de Fermi.

Le paragraphe 5 est consacré à l'étude de quelques propriétés des solutions de l'équation régissant deux particules en interaction dans un milieu défini par α et β (équation qui à température nulle prend une forme équivalente à l'équation de Bethe et Goldstone[7]).

2. La Contribution des Collisions Binaires

Dans ce qui suit, nous utiliserons la notion de *„potentiel atténué"* introduite dans II (paragraphe 3,3). L'approximation des collisions binaires s'obtient alors en ne conservant dans le développement (II,38) que les diagrammes

a) sans interaction,

b) avec une interaction avec le champ self-consistant $\langle r|\mathscr{V}|m\rangle$,

c) avec une interaction entre deux particules $\langle rs|\mathscr{V}|mn\rangle$ itérée un nombre quelconque de fois (fig. 1).

En vertu des conditions de self-consistance la contribution des termes (b) est égale à moins deux fois la contribution des termes (c), exactement comme dans le calcul de l'état fondamental[2,3]). Nous aurons donc pour le potentiel de Gibbs, à l'approximation des collisions binaires,

$$A = A_0 + \frac{\Omega e^{2\alpha}}{\beta} b_2 + \ldots, \tag{1}$$

où b_2 est le coefficient habituellement introduit, qui est indépendant du volume, à la limite d'un volume Ω très grand. Il représente la contribution

des diagrammes de la fig. 1 et peut être écrit sous la forme

$$b_2 = \frac{1}{\Omega} \mathrm{Tr}\{e^{-\beta\mathscr{H}} - e^{-\beta H_0}\}_2, \tag{2}$$

où la trace est calculée seulement sur l'ensemble des fonctions d'onde à deux particules symétriques ou antisymétriques, suivant qu'on a affaire à des bosons ou à des fermions. Dans (1), A_0 est calculé pour le système de parti-

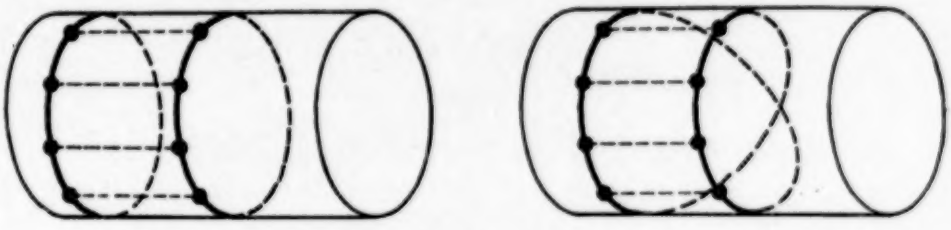

Fig. 1. Diagrammes pour le calcul de la contribution des collisions binaires.

cules indépendantes soumises au potentiel self-consistant $\langle r|\mathscr{V}|m\rangle$, et H_0 dans (2) est l'hamiltonien correspondant. Dans (2) $\mathscr{H}$ est l'hamiltonien de deux particules en interaction:

$$\mathscr{H} = H_0 + \mathscr{V} = H_0 + \tfrac{1}{4} \sum_{rsmn} \langle rs|\mathscr{V}|mn\rangle a_r^+ a_s^+ a_n a_m. \tag{3}$$

En mécanique statistique, on n'introduit généralement pas de potentiel self-consistant. Pour retrouver le résultat habituel, il faut développer $\mathscr{A}_0$ jusqu'au premier ordre en $\langle r|\mathscr{V}|s\rangle$. En exprimant ces éléments de matrice à l'aide des conditions de self-consistance, on retrouve l'expression habituelle

$$A = A_0 - \frac{\Omega e^{2\alpha}}{\beta} b_2 + \ldots, \tag{4}$$

où A_0 est maintenant calculé pour des particules libres dans le volume Ω, le facteur b_2 étant toujours donné par (2) et (3) (où H_0 est l'hamiltonien du système de particules libres).

Abordons maintenant le calcul proprement dit de b_2. En utilisant dans le plan complexe de la variable ε le contour C habituel composé d'une parallèle à l'axe réel en dessous de celui-ci parcourue dans le sens positif, et d'une parallèle au-dessus parcourue dans le sens négatif, nous pouvons écrire b_2 sous la forme

$$\begin{aligned} b_2 &= \frac{1}{2\pi i\Omega} \int_C d\varepsilon e^{-\beta\varepsilon} \mathrm{Tr} \left\{ \frac{1}{\varepsilon - \mathscr{H}} - \frac{1}{\varepsilon - H_0} \right\}_2 \\ &= \frac{1}{2\pi i\Omega} \int_C d\varepsilon e^{-\beta\varepsilon} \frac{d}{d\varepsilon} \mathrm{Tr\ Log} \left(1 - \frac{1}{\varepsilon - H_0} \mathscr{V} \right)_2. \end{aligned} \tag{5}$$

On vérifie, en effet, en dérivant le Log par rapport à ε que la seconde ligne est bien égale à la première. Cette expression peut également être établie à l'aide du développement (1.36). L'apparition du Log dans l'expression de b_2 s'explique alors immédiatement par la présence du facteur $1/p$ devant le terme d'ordre p en $\mathscr{V}$.

Les deux parallèles à l'axe réel constituant le contour C peuvent être prises infiniment proches de l'axe réel. Or on sait que si E est réel et ξ infiniment petit positif on a

$$\frac{1}{E\pm i\xi-H_0}=\frac{\mathscr{P}}{E-H_0}\mp i\pi\delta(E-H_0), \tag{6}$$

où $\mathscr{P}$ désigne la partie principale au sens de Cauchy. En posant

$$A=1-\frac{\mathscr{P}}{E-H_0}\mathscr{V}, \quad B=\pi\delta(E-H_0)\mathscr{V}, \tag{7}$$

on peut donc mettre b_2 sous la forme

$$b_2=-\frac{1}{2\pi i\Omega}\int_{-\infty}^{+\infty}\mathrm{d}E\mathrm{e}^{-\beta E}\frac{\mathrm{d}}{\mathrm{d}E}\mathrm{Tr}[\mathrm{Log}(A+iB)-\mathrm{Log}\,(A-iB)], \tag{8}$$

où l'intégrale est prise maintenant le long de l'axe réel. Or on a, même si les opérateurs A et B ne commutent pas l'un avec l'autre, la relation suivante †:

$$\mathrm{Tr}\,[\mathrm{Log}(A+iB)-\mathrm{Log}(A-iB)]=2i\,\mathrm{Tr}\,\mathrm{Arctg}(BA^{-1}). \tag{9}$$

Pour le voir, on peut, par exemple, remplacer dans cette relation B par λB et dériver par rapport à λ. La relation obtenue,

$$\mathrm{Tr}\,B[(A+i\lambda B)^{-1}+(A-i\lambda B)^{-1}]=2i\,\mathrm{Tr}\,BA^{-1}[1+(\lambda BA^{-1})^2]^{-1},$$

est facile à vérifier directement. Les déterminations des Log et de l'Arctg doivent naturellement être choisies de façon que la relation (9) soit exacte lorsqu'on fait tendre B vers zéro.

En introduisant la *matrice de réaction* θ définie par

$$\begin{aligned}\theta(E)&=\mathscr{V}\left(1-\frac{\mathscr{P}}{E-H_0}\mathscr{V}\right)^{-1}\\&=\mathscr{V}+\mathscr{V}\frac{\mathscr{P}}{E-H_0}\mathscr{V}+\mathscr{V}\frac{\mathscr{P}}{E-H_0}\mathscr{V}\frac{\mathscr{P}}{E-H_0}\mathscr{V}+\ldots,\end{aligned} \tag{10}$$

où tous les opérateurs sont des opérateurs à deux particules, nous pouvons mettre b_2 sous la forme

† La relation

$$\mathrm{Log}(A+iB)-\mathrm{Log}(A-iB)=2i\,\mathrm{Arctg}(BA^{-1}),$$

par contre, n'est exacte que si A et B commutent.

$$b_2 = -\frac{1}{\pi\Omega}\int_{-\infty}^{+\infty} \mathrm{d}E\mathrm{e}^{-\beta E}\frac{\mathrm{d}}{\mathrm{d}E}\,\mathrm{Tr}\,\mathrm{Arctg}[\pi\delta(E-H_0)\theta(E)]. \tag{11}$$

On notera que la matrice de réaction (10) dépend de β par l'intermédiaire des coefficients f^+ qui figurent dans $\mathscr{V}$.

3. Le Développement de Beth et Uhlenbeck

Le développement bien connu établi par Beth et Uhlenbeck [6]) pour le second coefficient du viriel peut être déduit comme un cas particulier de l'expression (11). Dans cette déduction la séparation du mouvement du centre de masse joue un rôle important, et il est indispensable de supposer que dans le mouvement de deux particules sans interactions décrit par H_0, le mouvement du centre de masse et le mouvement relatif sont dynamiquement indépendants. Dans la formulation générale qui précède, cette indépendance est détruite par le potentiel moyen $\langle r|\mathscr{V}|m\rangle$ figurant dans H_0 (sauf si on prend $\mathscr{V}$ de la forme $a+b\mathbf{p}^2$ qui conduit à la notion de masse effective). Nous allons donc, dans ce paragraphe, négliger le potentiel moyen dans H_0.

En désignant par $\mathbf{P}$ l'impulsion totale des deux particules et par $\mathbf{p}$ leur impulsion relative, on peut alors séparer le mouvement du centre de masse et écrire la matrice réaction sous la forme

$$\langle \mathbf{P}'|\theta(E)|\mathbf{P}''\rangle = \delta(\mathbf{P}'-\mathbf{P}'')\theta^{\mathrm{C.M.}}(\eta), \tag{12}$$

où $\theta^{\mathrm{C.M.}}(\eta)$ est la matrice de réaction dans le système du centre de masse exprimée en fonction de l'énergie relative:

$$\theta^{\mathrm{C.M.}}(\eta) = \mathscr{V}\left(1-\frac{\mathscr{P}}{\eta-H_0^{\mathrm{C.M.}}}\mathscr{V}\right)^{-1}, \tag{13}$$

où

$$E = \frac{\mathbf{P}^2}{4m}+\eta, \qquad H_0^{\mathrm{C.M.}} = \frac{\mathbf{p}^2}{m}. \tag{14}$$

Dans le cas d'un volume très grand, on peut, en reportant ces expressions dans (11) effectuer immédiatement la partie du calcul de la trace concernant les variables du centre de masse des deux particules. On obtient

$$b_2 = -\frac{4\pi}{h^3}\int_0^{+\infty} P^2\mathrm{d}P\mathrm{e}^{-\beta P^2/4m}\frac{1}{\pi}\int_{-\infty}^{+\infty}\mathrm{d}\eta\mathrm{e}^{-\beta\eta}\frac{\mathrm{d}}{\mathrm{d}\eta}\,\mathrm{Tr}\,\mathrm{Arctg}[\pi\delta(\eta-H_0^{\mathrm{C.M.}})\theta^{\mathrm{C.M.}}(\eta)], \tag{15}$$

où on a effectué l'intégration sur les directions du vecteur $\mathbf{P}$ en utilisant le fait que Tr Arctg [] ne dépend que de la grandeur de $\mathbf{P}$.

Considérons maintenant *l'équation d'onde du mouvement relatif de deux particules*:

$$(H_0^{\text{C.M.}}+\mathscr{V}-\eta)\Psi(\mathbf{r})=0. \tag{16}$$

Il convient de souligner que par suite de la présence des coefficients f^+ le potentiel atténué $\mathscr{V}$ qui figure dans cette équation *dépend de l'impulsion totale* **P**, et en particulier de l'angle des vecteurs **P** et **r**.

Si pour commencer nous négligeons la dépendance de l'équation (16) en **P**, nous retrouvons une équation à deux particules du type habituel. Cette équation pourra avoir des états liés $\eta_\nu < 0$. Les énergies positives correspondent aux phénomènes de diffusion, et à chaque $\eta > 0$ on peut associer les déphasages $\delta_\mu(\eta)$ des différentes ondes partielles. Naturellement, seuls les états liés et les ondes partielles ayant la symétrie correspondant aux particules étudiées (bosons ou fermions) doivent être pris en considération.

On sait que pour chaque état lié η_ν, l'élément diagonal de la matrice de réaction $\theta^{\text{C.M.}}(\eta)$ relatif à la fonction d'onde correspondante a un pôle simple et saute de $+\infty$ à $-\infty$ lorsque η traverse le pôle en augmentant. Il en résulte que

$$\text{Tr Arctg}[\pi\delta(\eta-H_0^{\text{C.M.}})\theta_0^{\text{C.M.}}(\eta)] \tag{17}$$

subit un saut de $-\pi$ à la traversée du pôle, et que chaque état lié donnera une contribution en $-\pi e^{-\beta\eta_\nu}$ dans l'expression (15).

On sait également [8]) (voir aussi l'appendice) que pour $\eta > 0$ les valeurs propres de $\theta^{\text{C.M.}}(\eta)$ sur la couche d'énergie sont égales à $-(1/\pi)\,\text{tg}\,\delta_\mu(\eta)$ où les $\delta_\mu(\eta)$ sont les différents déphasages à l'énergie η. Il en résulte que pour $\eta > 0$ l'expression (17) est égale à

$$-\sum_\mu \delta_\mu(\eta).$$

La généralisation de ces résultats au cas où on tient compte de la dépendance de l'équation (16) en **P** se fait sans difficulté et est indiquée en appendice. Les énergies des états liés dépendent alors de la grandeur P de l'impulsion totale. De plus, le potentiel $\mathscr{V}$ étant anisotrope, les ondes partielles habituelles sont couplées les unes aux autres, mais on peut définir des *dephasages propres* fonctions de P qui jouent le même rôle que les déphasages habituels. On obtient finalement pour b_2 l'expression

$$b_2=\frac{4\pi}{h^3}\int_0^\infty P^2\mathrm{d}P e^{-\beta P^2/4m}\left[\sum_\nu{}' e^{-\beta\eta_\nu(P)}+\frac{1}{\pi}\sum_\mu{}'\int_0^{+\infty}\mathrm{d}\eta e^{-\beta\eta}\frac{\partial\delta_\mu(\eta,P)}{\partial\eta}\right] \tag{18}$$

qui généralise le développement de Beth et Uhlenbeck, auquel elle se réduit exactement dans le cas limite où

$$f_r^+ \to (\text{quel que soit } r),$$

ce qui se produit en particulier aux basses densités où l'activité e^α tend vers zéro. Dans (18) les $\sum'$ sont, rappelons-le, les sommations étendues aux états

liés et aux déphasages propres ayant la symétrie correspondant au type de particules étudiées.

4. Le Cas Limite de la Température Nulle pour un Système de Fermions

Nous allons maintenant étudier le cas où les paramètres α et β tendent vers $+\infty$ de telle façon que leur rapport reste fini:

$$\frac{\alpha}{\beta} \to \varepsilon_\nu. \tag{19}$$

La quantité ε_ν qui a la dimension d'une énergie ne peut pas être assimilée sans précaution à l'énergie de Fermi. Cette grandeur est, en effet, toujours définie pour un système contenant un nombre déterminé de particules, alors que nous avons affaire ici à un ensemble grand canonique. Nous montrerons cependant, dans un travail ultérieur, que à la limite de la température nulle, les fluctuations du nombre de particules dans un ensemble grand canonique sont nulles, et que la définition (19) de l'énergie de Fermi coïncide avec la notion habituelle.

D'après (1) ou (4), la quantité dont il faut étudier la limite pour $\beta \to \infty$ n'est pas b_2 mais

$$e^{2\beta\varepsilon_\nu} b_2 = -\frac{1}{\pi\Omega}\int_{-\infty}^{+\infty} dE\, e^{\beta(2\varepsilon_\nu - E)} \frac{d}{dE} \operatorname{Tr} \operatorname{Arctg}[\pi\delta(E-H_0)\theta(E)], \tag{20}$$

où nous avons posé $\alpha = \beta\varepsilon_F$. Cette expression montre qu'à la limite, les contributions à l'intégrale ne viendront que des énergies

$$E \leqq 2\varepsilon_\nu. \tag{21}$$

Aux énergies plus élevées, en effet, l'exponentielle dans l'intégrale (20) tend vers zéro alors que le facteur en Arctg reste fini.

D'autre part, lorsque α et β tendent vers $+\infty$, on a

$$\begin{aligned} f_\nu^+ &\to 0, \quad \text{si} \quad \varepsilon_\nu < \varepsilon_\nu, \\ f_\nu^+ &\to 1, \quad \text{si} \quad \varepsilon_\nu > \varepsilon_\nu. \end{aligned} \tag{22}$$

Il en résulte que les éléments de matrice du potentiel atténué $\mathscr{V}$, pris entre des états dont l'un au moins a une énergie inférieure à ε_ν, tendent vers zéro. D'aprés (10), on voit que la matrice de réaction $\theta(E)$ possède la même propriété, tout au moins aux énergies telles que l'équation

$$\left(1 - \frac{\mathscr{P}}{E-H_0}\mathscr{V}\right)|> = 0 \tag{23}$$

n'ait aucune solution non identiquement nulle.

Commençons par examiner le cas simple où (23) n'a aucune solution non nulle pour toutes les énergies satisfaisant à (21), c'est-à-dire pour toutes les

énergies qui contribuent effectivement à (20) lorsque $\beta \to +\infty$. C'est ce qui se produit en particulier dans le cas des potentiels partout répulsifs. Tous les éléments de matrice de $\theta(E)$ figurant dans (20) tendent alors vers zéro, on peut développer l'Arctg en puissances de l'argument et ne garder que le premier terme. On obtient ainsi, après une intégration par parties,

$$\lim_{\beta \to +\infty} e^{2\beta\epsilon_\nu} b_2 = -\frac{\beta}{\Omega} \int_0^{2\epsilon_\nu} dE\, e^{\beta(2\epsilon_\nu - E)}\, \mathrm{Tr}[\delta(E-H_0)\theta(E)].$$

En explicitant le calcul de la trace, en effectuant l'intégration en E, qui est immédiate à cause de la présence de la fonction δ, cette expression devient

$$\lim_{\beta \to +\infty} e^{2\beta\epsilon_\nu} b_2 = -\frac{\beta}{\Omega} \sum_{m,n} e^{\beta(2\epsilon_\nu - \epsilon_m - \epsilon_n)} \langle mn|\theta(\varepsilon_m+\varepsilon_n)|mn\rangle$$

$$= -\frac{\beta}{\Omega} \sum_{m,n} f_m^- f_n^- \left[\langle mn|v|mn\rangle + \sum_{r,s} f_r^+ f_s^+ \frac{\langle mn|v|rs\rangle\langle rs|v|mn\rangle}{\varepsilon_m+\varepsilon_n-\varepsilon_r-\varepsilon_s} + \ldots \right].$$

Dans la seconde ligne, nous avons explicité le développement de θ, introduit l'expression (II,37) de $\mathscr{V}$ et tenu compte des relations

$$e^{\beta(\epsilon_\nu - \epsilon_m)} f_m^+ = f_m^-, \text{ etc.} \ldots .$$

Rappelons que pour les systèmes très grands que nous considérons ici, dans toutes les relations écrites, les sommations sur les états m, n, etc. . . . peuvent en réalité être remplacées par des intégrations que nous n'expliciterons pas, pour ne pas allonger l'écriture.

En faisant $\beta = +\infty$ dans les facteurs statistiques f^+ et f^-, nous obtenons enfin

$$\lim_{\beta \to +\infty} e^{2\beta\epsilon_\nu} b_2 = -\frac{\beta}{\Omega} \sum_{m,n} \langle mn|t|mn\rangle, \tag{24}$$

$$\text{avec } \varepsilon_m < \varepsilon_\nu \quad \text{et} \quad \varepsilon_n < \varepsilon_\nu,$$

où t est la *matrice de réaction de Brueckner* définie par †

$$\langle m'n'|t|mn\rangle = \langle m'n'|v|mn\rangle + \sum_{rs} \frac{\langle m'n'|v|rs\rangle\langle rs|v|mn\rangle}{\varepsilon_m+\varepsilon_n-\varepsilon_r-\varepsilon_s} + \ldots \tag{25}$$

$$\text{avec } \varepsilon_r > \varepsilon_\nu \quad \text{et} \quad \varepsilon_s > \varepsilon_\nu, \text{ etc.} \ldots .$$

Considérons maintenant le cas où l'équation (23) a des solutions non identiquement nulles pour certaines énergies du domaine qui nous intéresse. Pour simplifier, nous nous placerons dans un cas où le mouvement du centre de masse se sépare, et nous partirons, par conséquent, de l'expression (15) de b_2. Soit $\eta_\nu(P)$ une énergie telle que l'équation

† Dans l'approximation utilisée ici, on ne voit pas apparaître l'énergie d'excitation due au reste du diagramme à l'endroit où les échelles sont introduites.

$$\left(1-\frac{\mathscr{P}}{\eta_\nu-H_0^{\text{C.M.}}}\mathscr{V}\right)\Psi(\mathbf{r})=0 \tag{26}$$

relative à une quantité de mouvement totale P déterminée ait une solution non nulle. Si η_ν est négatif, nous retrouvons l'un des états liés apparaissant dans l'expression de Beth et Uhlenbeck (18). L'équation (26) aura également une solution non nulle (équation (A.21) de l'appendice) à chaque énergie positive telle que l'un des déphasages propres δ_μ soit égal à $\frac{1}{2}\pi$ (à π près). Ces énergies correspondent à des *niveaux virtuels*. Pour chacune de ces énergies, l'une des valeurs propres de la matrice $\theta^{\text{C.M.}}$ a un pôle. Il est alors facile de voir que pour β très grand, la matrice $\theta^{\text{C.M.}}(\eta)$ est très petite à toutes les énergies η telles que

$$\eta<\eta_{\max}=2\varepsilon_\nu-\frac{P^2}{4m},$$

sauf au voisinage des niveaux virtuels. Les déphasages sont alors infiniment voisins de $k\pi$ à toutes les énergies inférieures à $\eta_{\max}$, sauf au voisinage de chaque niveau virtuel, où l'un des déphasages varie brusquement de π. On peut montrer que dans le cas considéré ici, où les éléments de matrice de $\mathscr{V}$ sont très petits aux énergies inférieures à $\eta_{\max}$ les déphasages *augmentent* de π lorsqu'on traverse un niveau virtuel d'énergie inférieure à $\eta_{\max}$ dans le sens des énergies croissantes †. Ce sens de variation est d'ailleurs le même que pour un état lié véritable ayant une énergie négative.

Ces propriétés vont nous permettre d'étendre la relation (24) au cas où il existe des niveaux virtuels d'énergie inférieure à $\eta_{\max}$. En commençant par effectuer une intégration par parties dans l'expression (15), nous obtenons

$$\begin{aligned}e^{2\beta\varepsilon_\nu}b_2=\frac{4\pi\beta}{h^3}\int_0^{+\infty}P^2\mathrm{d}P e^{-\beta P^2/4m}\\ \cdot\frac{1}{\pi}\int_{-\infty}^{+\infty}\mathrm{d}\eta e^{\beta(2\varepsilon_\nu-\eta)}\mathrm{Tr}\,\mathrm{Arctg}[\pi\delta(\eta-H_0^{\text{C.M.}})\theta^{\text{C.M.}}(\eta)].\end{aligned} \tag{27}$$

Considérons maintenant l'un des déphasages $\delta_\mu(\eta)$, et supposons pour fixer les idées qu'il n'ait qu'un seul niveau virtuel η_ν d'énergie inférieure à $\eta_{\max}$. La contribution de ce déphasage à l'intégrale en η dans (27) est de la forme

$$\frac{1}{\pi}\int_{-\infty}^{+\infty}\mathrm{d}\eta e^{\beta(\eta_{\max}-\eta)}\mathrm{Arctg}[\mathrm{tg}\,\delta_\mu(\eta)] \tag{28}$$

où $\mathrm{tg}\,\delta_\mu(\eta)$ est une fonction très petite pour $\eta<\eta_{\max}$ sauf au voisinage de η_ν, où on a

† En général, à un niveau virtuel, les déphasages peuvent traverser la valeur $\frac{1}{2}\pi$ (à π près) dans le sens croissant ou le sens décroissant.

$$\operatorname{tg} \delta_\mu(\eta) \approx \frac{a}{\eta_\nu - \eta}, \quad \text{si} \quad \eta \approx \eta_\nu. \tag{29}$$

Pour calculer l'intégrale (28), nous isolerons alors un petit intervalle $\eta_\nu - \xi$, $\eta_\nu + \xi$ de sorte que

$$\begin{aligned} &\operatorname{Arctg}\,[\operatorname{tg} \delta_\mu(\eta)] \approx \operatorname{tg} \delta_\mu(\eta), \quad \text{si} \quad \eta < \eta_\nu - \xi, \\ &\operatorname{Arctg}\,[\operatorname{tg} \delta_\mu(\eta)] \approx \pi + \operatorname{tg} \delta_\mu(\eta), \quad \text{si} \quad \eta_\nu + \xi < \eta < \eta_{\max}. \end{aligned} \tag{30}$$

Pour évaluer la contribution à l'intégrale (28) de l'intervalle $\eta_\nu - \xi$, $\eta_\nu + \xi$, nous écrirons celle-ci sous la forme approchée

$$e^{\beta(\eta_{\max} - \eta_\nu)} \int_{\eta_\nu - \xi}^{\eta_\nu + \xi} d\eta \operatorname{Arctg}[\operatorname{tg} \delta_\mu(\eta)]. \tag{31}$$

D'après (29) on a pour $\eta \approx \eta_\nu$

$$\operatorname{Arctg}\,[\operatorname{tg} \delta_\mu] = \tfrac{1}{2}\pi + \text{fonction impaire de } \eta - \eta_\nu.$$

Il en résulte que (31) est approximativement égale à

$$e^{\beta(\eta_{\max} - \eta_\nu)} \tfrac{1}{2}\pi \cdot 2\xi \approx \int_{\eta_\nu}^{\eta_\nu + \xi} d\eta e^{\beta(\eta_{\max} - \eta)} \pi. \tag{32}$$

En rassemblant les contributions provenant de (30) et (32), nous voyons d'une part apparaître la *valeur principale* de l'intégrale de $\operatorname{tg} \delta_\mu(\eta)$, et d'autre part l'intégrale

$$\pi \int_{\eta_\nu}^{\eta_{\max}} d\eta e^{\beta(\eta_{\max} - \eta)} = \frac{\pi}{\beta} \left[e^{\beta(\eta_{\max} - \eta_\nu)} - 1 \right] \approx \frac{\pi}{\beta} e^{\beta(\eta_{\max} - \eta_\nu)}.$$

En revenant aux notations de la relation (24), nous pourrons finalement écrire †

$$\begin{aligned} \lim_{\beta \to +\infty} e^{2\beta\varepsilon_\nu} b_2 = &- \frac{\beta}{\Omega} \mathscr{P} \sum_{m,n} \langle mn|t|mn \rangle \\ &+ \frac{4\pi}{h^3} \sum_\nu \int_0^{+\infty} P^2 dP e^{\beta[2\varepsilon_\nu - \eta_\nu(P) - P^2/4m]}, \end{aligned} \tag{33}$$

où $\mathscr{P}$ indique qu'il faut, en chacun des pôles de la matrice t associés aux niveaux virtuels, prendre la valeur principale de l'intégrale. La contribution supplémentaire liée aux niveaux virtuels qui figurent dans (33) a exactement la même forme que la contribution des états liés dans le développement de Beth et Uhlenbeck (18). On remarquera d'ailleurs qu'il n'est pas impossible que le potentiel $\mathscr{V}$ donne lieu à un ou plusieurs états liés d'énergie η_ν négative,

† Pour ne pas allonger démesurément l'exposé, nous n'avons pas donné l'estimation des termes négligés dans les différentes approximations conduisant au résultat (33). On peut s'assurer qu'ils sont tous effectivement négligeables par rapport aux termes conservés à la limite $\beta \to +\infty$.

même à la limite de la température nulle, bien qu'en général cela ne se produise pas.

D'après la définition du potentiel de Gibbs, on doit s'attendre à ce que

$$\lim_{\beta \to +\infty} A(\beta\varepsilon_\nu, \beta) = E_0 - N\varepsilon_\nu, \tag{34}$$

où E_0 est l'énergie de l'état fondamental, et N le nombre de particules. La relation (24) montre qu'en l'absence de niveaux virtuels, le développement de A limité au terme b_2 redonne bien l'approximation de Brueckner pour E_0. Lorsqu'il y a des niveaux virtuels, l'expression de Brueckner contient une intégrale divergente. La relation (33) montre qu'il ne suffit pas alors de prendre la valeur principale de cette intégrale. Le pôle donne dans le potentiel de Gibbs une contribution supplémentaire qui *ne tend pas vers une limite* pour $\beta \to +\infty$, contrairement à ce qu'exige la relation (34). Dans ce cas, l'approximation des collisions binaires conduit donc à une inconsistance.

5. Remarques sur l'Équation d'Onde de deux Particules

Aux températures petites mais non nulles, les solutions de l'équation d'onde de deux particules dont l'interaction est donnée par le potentiel atténué $\mathscr{V}$ présentent le même comportement asymptotique que dans les problèmes de diffusion par des potentiels à courte portée (nous supposons naturellement que le potentiel véritable v est à courte portée). Pour toutes les énergies positives, les solutions sont à grande distance la somme d'une onde entrante et d'une onde sortante de la forme habituelle.

A température nulle, les propriétés asymptotiques deviennent différentes. L'équation d'onde devient alors très semblable à l'équation de Bethe et Goldstone [8]), puisque pour $\beta = +\infty$ les éléments de matrice du potentiel atténué $\langle rs|\mathscr{V}|mn\rangle$ sont égaux à ceux du potentiel véritable lorsque les énergies des états m, n, r, s sont toutes supérieures à l'énergie de Fermi, et nuls dans le cas contraire. La relation entre la fonction d'onde de Bethe et Goldstone $\Psi_{B.G}$ et la fonction d'onde que nous avons introduite ici Ψ est donnée par

$$\Psi_{B.G} \sim \lim_{\beta \to +\infty} [f^{(+)}(1) f^{(+)}(2)]^{\frac{1}{2}} \Psi$$

où le facteur de proportionnalité doit être choisi de façon que la limite soit finie.

Bethe et Goldstone [7]), puis Gomez, Walecka et Weisskopf [9]), ont montré que la solution a alors à grande distance la forme d'une onde libre. Mais ce résultat n'est pas valable pour une énergie correspondant à un niveau virtuel η_ν. Pour une telle énergie, Cooper [10]) a montré, en utilisant un potentiel particulier que la solution de l'équation d'onde a, à grande distance, une amplitude proportionnelle à $1/r^2$. Cette propriété résulte naturellement

immédiatement de (26), qui s'écrit à la température zéro, en passant à la représentation d'impulsion, sous la forme

$$\Psi(\mathbf{r}) = \frac{\mathscr{P}}{\eta_\nu - H_0^{\text{C.M.}}} \mathscr{V}\Psi(\mathbf{r}) = \int_{|\mathbf{k}|>k_{\max}} \mathrm{d}^3k e^{i\mathbf{k}\cdot\mathbf{r}} \frac{\Phi(\mathbf{k})}{k_\nu^2 - k^2}, \tag{35}$$

où $k_{\max}$ et k_ν sont définis par

$$\eta_{\max} = \frac{\hbar^2 k^2_{\max}}{m}, \qquad \eta_\nu = \frac{\hbar^2 k_\nu^2}{m}.$$

La forme exacte de $\Phi(\mathbf{k})$ importe peu (pourvu que sa décroissance pour les grandes valeurs de k soit assez rapide). La décroissance en $1/r^2$ de $\Psi(\mathbf{r})$ résulte en effet du fait que dans (35) le zéro du dénominateur est en dehors du domaine d'intégration puisque $k_\nu < k_{\max}$ (s'il était dans le domaine d'intégration, $\Psi(\mathbf{r})$ décroîtrait seulement en $1/r$).

Cette remarquable modification de la forme asymptotique à température nulle n'est possible que si dans ce cas limite le potentiel atténué $\mathscr{V}$ cesse d'être à courte portée, c'est-à-dire si les facteurs d'atténuation $(f^+)^{\frac{1}{2}}$ cessent d'être à courte portée lorsqu'on les exprime dans la représentation $\mathbf{r}$. C'est effectivement ce qui se produit, car on peut montrer que, en posant

$$\rho = |\mathbf{r} - \mathbf{r}''|, \quad \varepsilon_\nu = \frac{\hbar^2 k_\nu^2}{2m},$$

on a pour une *température finie*

$$\langle \mathbf{r}' | (f^+)^{\frac{1}{2}} | \mathbf{r}'' \rangle \sim \frac{k_\nu^{\frac{1}{2}}}{\hbar\beta^{\frac{1}{2}}(\pi\rho)^{\frac{3}{2}}} \sin(k_\nu\rho + \tfrac{1}{4}\pi) \exp\left(-\frac{\pi\rho}{\hbar^2\beta k_\nu}\right), \tag{36}$$

lorsque

$$\rho \gg \hbar^2\beta k_\nu;$$

alors qu'à la *température nulle* on a

$$\langle \mathbf{r}' | (f^+)^{\frac{1}{2}} | \mathbf{r}'' \rangle \approx \frac{k_\nu}{2\pi^2\rho^2} \cos k_\nu\rho, \tag{37}$$

lorsque

$$k_\nu\rho \gg 1.$$

La disparition du facteur exponentiel présent dans (36) lorsque la température devient nulle est caractéristique de la disparition de la propriété de courte portée.

6. Un Exemple Simple: Le Potentiel Séparable

La résolution d'une équation intégro-différentielle du type (16) est compliquée par la présence des facteurs statistiques. On peut, dans certains cas particulièrement simples, obtenir une solution explicite. A titre d'illus-

tration nous prendrons le cas d'une interaction séparable: $\langle \mathbf{r}|v|\mathbf{r}'\rangle = -v(\mathbf{r})v(\mathbf{r}')$. Soit

$$\langle \mathbf{p}+\tfrac{1}{2}\mathbf{P}, \mathbf{p}-\tfrac{1}{2}\mathbf{P}|\mathscr{V}|\mathbf{p}'+\tfrac{1}{2}\mathbf{P}, \mathbf{p}'-\tfrac{1}{2}\mathbf{P}'\rangle = -\frac{1}{h^3}\delta(\mathbf{P}-\mathbf{P}')\mathscr{V}(\mathbf{p},\mathbf{P})\mathscr{V}(\mathbf{p},\mathbf{P}), \quad (38)$$

où

$$\mathscr{V}(\mathbf{p},\mathbf{P}) = [1+\exp\{\alpha-\beta(\mathbf{p}+\tfrac{1}{2}\mathbf{P})^2/2m\}]^{-\frac{1}{2}}[1+\exp\{\alpha-\beta(\mathbf{p}-\tfrac{1}{2}\mathbf{P})^2/2m\}]^{-\frac{1}{2}}v(\mathbf{p}) \quad (39)$$

et

$$v(\mathbf{p}) = \int e^{i\mathbf{p}\cdot\mathbf{r}/\hbar}v(\mathbf{r})d^3r.$$

On peut alors immédiatement écrire les éléments de matrice de $\theta(E)$:

$$\langle \mathbf{p}+\tfrac{1}{2}\mathbf{P}, \mathbf{p}-\tfrac{1}{2}\mathbf{P}|\theta(E)|\mathbf{p}'+\tfrac{1}{2}\mathbf{P}', \mathbf{p}'-\tfrac{1}{2}\mathbf{P}'\rangle = -\frac{1}{h^3}\delta(\mathbf{P}-\mathbf{P}')\mathscr{V}(\mathbf{p},\mathbf{P})\mathscr{V}(\mathbf{p}',\mathbf{P})\left[1+\int\frac{d^3q}{h^3}\frac{\mathscr{V}^2(\mathbf{q},\mathbf{P})}{E-\left(\frac{q^2}{m}+\frac{P^2}{4m}\right)}\right]^{-1}. \quad (40)$$

En passant au système du centre de masse avec $E = \eta+(P^2/4m)$, et à des fonctions d'onde libres, du mouvement relatif, normalisées à l'unité d'intervalle d'énergie, on obtient, sur la couche d'énergie $\eta = p^2/m = p'^2/m$,

$$(\mathbf{p},\mathbf{P}|\theta^{\text{C.M.}}(\eta)|\mathbf{p}',\mathbf{P}) = -\frac{mp}{2h^3}\mathscr{V}(\mathbf{p},\mathbf{P})\mathscr{V}(\mathbf{p}',\mathbf{P})\left[1+\frac{m}{h^3}\int d^3q\,\frac{\mathscr{V}^2(\mathbf{q},\mathbf{P})}{p^2-q^2}\right]^{-1}. \quad (41)$$

La diagonalisation de $\theta^{\text{C.M.}}(\eta)$ conduit à résoudre l'équation séculaire

$$\int d\hat{p}'(\mathbf{p}',\mathbf{P}|\theta^{\text{C.M.}}(\eta)|\mathbf{p}',\mathbf{P})a^\mu(\hat{p}') = -\frac{1}{\pi}\operatorname{tg}\delta_\mu a^\mu(\hat{p}) \quad (42)$$

où $\hat{p} = \mathbf{p}/p$. La diagonalisation est immédiate et ne donne qu'une valeur propre non nulle:

$$\frac{1}{\pi}\operatorname{tg}\delta = \frac{mp}{2h^3}\int d\hat{p}\mathscr{V}^2(\mathbf{p},\mathbf{P})\left[1+\frac{m}{h^3}\int d^3q\,\frac{\mathscr{V}^2(\mathbf{q},\mathbf{P})}{p^2-q^2}\right]^{-1}, \quad (43)$$

d'où

$$b_2 = \frac{4\pi}{h^3}\int_0^\infty P^2 dP e^{-\beta P^2/4m}\left[e^{\beta|\eta_B(P,\beta)|}+\frac{1}{\pi}\int_0^\infty d\eta e^{-\beta\eta}\frac{\partial}{\partial\eta}\delta(\eta,P,\beta)\right]; \quad (44)$$

ici $|\eta_B|$ est défini par l'équation

$$1 = \int\frac{d^3q}{h^3}\frac{\mathscr{V}^2(\mathbf{q},\mathbf{P})}{|\eta_B|+q^2/m}. \quad (45)$$

Cette équation n'a d'ailleurs de solution que pour une interaction attractive assez forte.

On notera en outre que pour une interaction attractive même très faible, il existera toujours pour l'équation

$$1 = -\int \frac{d^3q}{h^3} \frac{\mathscr{V}^2(\mathbf{q}, \mathbf{P})}{\eta_0 - q^2/m} \tag{46}$$

une solution telle que $\eta_0 = 2\varepsilon_F - |\Delta(\beta, P)|$, pourvu que la température soit assez basse et le moment total P assez petit; pour une température ou un moment total croissants, la quantité $|\Delta(\beta, P)|$ décroit rapidement; (46) n'a plus de solution dès que $|\Delta|$ s'annule

Appendice

Nous allons ici établir élémentairement le développement (18) qui a été démontré aux paragraphes 2 et 3 par des transformations formelles d'opérateurs.

La relation (2) s'écrit dans la représentation $\mathbf{r}$ †

$$b_2 = \frac{1}{2\Omega} \int_\Omega d^3r_1 d^3r_2 \langle \mathbf{r}_1, \mathbf{r}_2 | e^{-\beta H_0} | \mathbf{r}_1, \mathbf{r}_2 \rangle, \tag{A.1}$$

où $|\mathbf{r}_1, \mathbf{r}_2\rangle$ est un ket normalisé, *symétrique ou antisymétrique* suivant qu'on s'occupe de bosons ou de fermions.

Nous supposerons, comme au paragraphe 3 qu'on n'a pas introduit de champ self-consistant; ce qui permet de séparer immédiatement le mouvement du centre de masse et d'écrire

$$b_2 = \tfrac{1}{2} \int \frac{d^3P}{h^3} e^{-\beta P^2/4m} \int d^3r \langle \mathbf{r} | e^{-\beta \mathscr{H}^{C.M.}} - e^{-\beta H_0^{C.M.}} | \mathbf{r} \rangle, \tag{A.2}$$

où

$$\mathbf{r} = \mathbf{r}_1 - \mathbf{r}_2, \qquad H_0^{C.M.} = \frac{\mathbf{p}^2}{m}, \quad \mathscr{H}^{C.M.} = \frac{\mathbf{p}^2}{m} + \mathscr{V}. \tag{A.3}$$

Le potentiel d'interaction des deux particules qui s'écrit

$$\mathscr{V}(1, 2) = [f^+(1) f^+(2)]^{\frac{1}{2}} v(1, 2)(1 + \varepsilon P_{12}) [f^+(1) f^+(2)]^{\frac{1}{2}} \tag{A.4}$$

dépend ici de la quantité de mouvement totale $\mathbf{P}$, car les facteurs statistiques f^+ qui figurent dans (A.4) sont donnés par

† Le facteur $\frac{1}{2}$ qui apparaît dans cette expression provient du fait que les intégrations sur $\mathbf{r}_1$ et $\mathbf{r}_2$ sont étendues à tout le volume Ω d'une manière indépendante. La trace devant être prise sur l'ensemble des fonctions d'onde symétriques ou antisymétriques doit être calculée en ne considérant pas comme distincts deux éléments d'intégration se déduisant l'un de l'autre par permutation de $\mathbf{r}_1$ et $\mathbf{r}_2$.

$$f^+(1) = \frac{1}{1-\varepsilon \exp\left[\alpha - \frac{\beta}{2m}(\tfrac{1}{2}\mathbf{P}+\mathbf{p})^2\right]},$$
$$f^+(2) = \frac{1}{1-\varepsilon \exp\left[\alpha - \frac{\beta}{2m}(\tfrac{1}{2}\mathbf{P}-\mathbf{p})^2\right]}. \tag{A.5}$$

On voit que $\mathscr{V}(1, 2)$ dépend non seulement de la grandeur de $\mathbf{P}$, mais aussi de l'orientation de $\mathbf{r} = \mathbf{r}_1 - \mathbf{r}_2$ par rapport à $\mathbf{P}$.

Considérons maintenant l'équation d'onde des deux particules dans le système du centre de masse:

$$(\mathscr{H}^{\text{C.M.}} - \eta)\Psi(\mathbf{r}) = 0. \tag{A.6}$$

La contribution à b_2 des états liés $\eta_\nu(P)$ de (A.6) se calcule facilement en écrivant

$$e^{-\beta \mathscr{H}^{\text{C.M.}}} = \sum_\nu |\nu\rangle e^{-\beta \eta_\nu(P)} \langle\nu| + \ldots,$$

où les termes non écrits se rapportent au spectre continu. Le ket $|\mathbf{r}\rangle$ figurant dans (A.2) est symétrique ou antisymétrique. On a donc, en désignant par $\psi_\nu(\mathbf{r})$ la fonction propre normalisée d'énergie

$$\langle\nu|\mathbf{r}\rangle = \frac{1+\varepsilon P_{12}}{\sqrt{2}}\psi_\nu(\mathbf{r}) = \frac{1}{\sqrt{2}}[\psi_\nu(\mathbf{r}) + \varepsilon\psi_\nu(-\mathbf{r})].$$

Les fonctions $\psi_\nu(\mathbf{r})$ sont soit symétriques, soit antisymétriques. Il en résulte que

$$\int d^3r \langle\mathbf{r}|e^{-\beta \mathscr{H}^{\text{C.M.}}}|\mathbf{r}\rangle = 2\sum_\nu{}' e^{-\beta \eta_\nu(P)} + \ldots,$$

où *la sommation* $\sum'$ *est étendue seulement aux valeurs propres correspondant aux fonctions d'onde ayant la symétrie appropriée aux particules considérées.*

En reportant cette expression dans (A.2) et en effectuant l'intégration sur les directions de $\mathbf{P}$, on obtient pour la contribution du spectre discret l'expression

$$\frac{4\pi}{h^3}\int_0^\infty P^2 dP e^{-\beta P^2/4m} \sum_\nu{}' e^{-\beta \eta_\nu(P)}, \tag{A.7}$$

compte tenu du fait que les $\eta_\nu(P)$ ne dépendent que de la grandeur du vecteur $\mathbf{P}$.

Les solutions de (A.6) dans le spectre continu décrivent la diffusion de deux particules sous l'action du potentiel $\mathscr{V}$. Celui-ci ne possédant pas la symétrie sphérique, les ondes de moment angulaire différent sont couplées entre elles. Le potentiel $\mathscr{V}$ tendant, par hypothèse, vers zéro rapidement lorsque la distance des particules augmente, la valeur asymptotique de la

solution la plus générale de (A.6) pour une énergie $\eta > 0$ et une température non nulle s'écrit

$$\Psi(\mathbf{r}) \to \sum_{l,m} Y_{lm}(\hat{r}) \frac{1}{r} [a_{lm} e^{-i(kr-\frac{1}{2}l\pi)} - b_{lm} e^{i(kr-\frac{1}{2}l\pi)}]. \tag{A.8}$$

On sait que les amplitudes b_{lm} des ondes sortantes s'expriment, pour tout problème de diffusion, en fonction des amplitudes a_{lm} des ondes entrantes à l'aide de la matrice S par la relation

$$b_{lm} = \sum_{l'm'} (lm|S|l'm') a_{l'm'}. \tag{A.9}$$

La matrice S étant unitaire, ses valeurs propres sont de la forme $e^{2i\delta_\mu}$. Nous désignerons par a^μ_{lm} les fonctions propres orthonormalisées correspondantes:

$$\sum_{l'm'} (lm|S|l'm') a^\mu_{l'm'} = e^{2i\delta_\mu} a^\mu_{lm}, \qquad \sum_{lm} a^{\mu *}_{lm} a^{\mu'}_{lm} = \delta_{\mu\mu'}. \tag{A.10}$$

L'invariance par renversement du sens du temps permet de choisir les phases des a^μ_{lm} de façon que

$$a^{\mu *}_{l,m} = (-)^m a^\mu_{l,-m}.$$

L'équation (A.6) a toujours une solution et une seule ayant à grande distance des amplitudes entrantes arbitrairement fixées. En particulier, il existe des solutions Ψ_μ dont la forme asymptotique est donnée par

$$\Psi_\mu \to \left(\frac{m}{\pi\hbar^2 k}\right)^{\frac{1}{2}} \sum_{lm} a^\mu_{lm} Y_{lm}(\hat{r}) \frac{\sin(kr + \delta_\mu - \frac{1}{2}l\pi)}{r}. \tag{A.11}$$

Les fonctions ainsi définies sont normalisées de façon que

$$\int d^3r \Psi_\mu^*(\mathbf{r}, \eta) \Psi_{\mu'}(\mathbf{r}, \eta') = \delta_{\mu\mu'} \delta(\eta - \eta'). \tag{A.12}$$

En l'absence d'interaction, les δ_μ sont nuls. Il existe alors des solutions de l'équation d'onde sans interaction dont la forme asymptotique soit donnée par

$$\Psi_\mu^0 \to \left(\frac{m}{\pi\hbar^2 k}\right)^{\frac{1}{2}} \sum_{lm} a^\mu_{lm} Y_{lm}(\hat{r}) \sin \frac{(kr - \frac{1}{2}l\pi)}{r}. \tag{A.13}$$

Retournant maintenant au calcul de b_2 nous pourrons écrire la contribution du spectre continu à l'intégrale

$$\int d^3r \langle \mathbf{r}| e^{-\beta \mathcal{H}^{\text{C.M.}}} - e^{-\beta H_0^{\text{C.M.}}} |\mathbf{r}\rangle \tag{A.14}$$

sous la forme

$$2 \int_0^\infty d\eta e^{-\beta\eta} \sum_\mu{}' \int d^3r (|\Psi_\mu|^2 - |\Psi_\mu^0|^2), \tag{A.15}$$

où, comme pour le spectre discret, *la sommation* $\sum'$ *est limitée aux ondes ayant la symétrie appropriée aux particules étudiées.*

En limitant d'abord l'intégration sur **r** à une sphère V de rayon R qu'on fera ensuite tendre vers l'infini, et en introduisant deux énergies voisines η et η', on peut écrire

$$\int_V d^3r|\Psi_\mu|^2 = \lim_{\eta' \to \eta} \int_V d^3r \Psi_\mu^* \Psi'_\mu$$

$$= \lim_{\eta' \to \eta} \frac{1}{\eta' - \eta} \int_V d^3r [\Psi_\mu^* (\mathcal{H}^{C.M.} \Psi'_\mu) - (\mathcal{H}^{C.M.} \Psi_\mu^*) \Psi'_\mu]$$

$$= \lim_{\eta' \to \eta} \frac{1}{\eta' - \eta} \frac{\hbar^2}{m} \int_S dS \left[\frac{1}{r} \frac{\partial}{\partial r} (r\Psi_\mu^*) \Psi'_\mu - \Psi_\mu^* \frac{1}{r} \frac{\partial}{\partial r} (r\Psi'_\mu) \right],$$

où Ψ_μ désigne la fonction d'onde pour l'énergie η', et où la dernière intégrale est étendue à la surface S de la sphère. La même transformation peut être faite sur l'intégrale de $|\Psi_\mu^0|^2$. La différence des deux intégrales de surface ainsi obtenues s'évalue immédiatement à l'aide des formes asymptotiques (A.11) et (A.13). On obtient, en faisant tendre η' vers η,

$$\int d^3r(|\Psi_\mu|^2 - |\Psi_\mu^0|^2) = \frac{1}{\pi} \frac{\partial \delta_\mu}{\partial \eta}. \tag{A.16}$$

En reportant cette expression dans (A.2) et en effectuant l'intégration sur les directions de **P** (qui est immédiate car les δ_μ ne dépendent que de la grandeur de **P**), on obtient finalement, compte tenu de (A.7), le développement (18).

Pour être complets, rappelons enfin comment on établit le lien entre la matrice $v^{C.M.}(\eta)$ et les déphasages δ_μ. Pour cela, remarquons que la fonction d'onde

$$\Phi_\mu = \Psi_\mu / \cos \delta_\mu,$$

dont la valeur asymptotique à grande distance est donnée par

$$\Phi_\mu \to \Psi_\mu^0 + \operatorname{tg} \delta_\mu \left(\frac{m}{\pi \hbar^2 k} \right)^{\frac{1}{2}} \sum_{lm} a_{lm} Y_{lm}(\hat{r}) \cos \left(\frac{kr - \frac{1}{2} l\pi}{r} \right) \tag{A.17}$$

satisfait à l'équation intégrale

$$\Phi_\mu = \Psi_\mu^0 + \frac{\mathscr{P}}{\eta - H_0^{C.M.}} \mathscr{V} \Phi_\mu, \tag{A.18}$$

dont la solution formelle s'écrit

$$\Phi_\mu = \left(1 - \frac{\mathscr{P}}{\eta - H_0^{C.M.}} \mathscr{V} \right)^{-1} \Psi_\mu^0.$$

D'autre part, compte tenu de (A.10), (A.13) et (A.17), on a

$$\int \Psi_\mu^{0*} \mathscr{V} \Phi_{\mu'} \mathrm{d}^3 r = \frac{\hbar^2}{m} \int_S [\Psi_\mu^{0*} \frac{1}{r} \frac{\partial}{\partial r} (r\Phi_{\mu'}) - \frac{1}{r} \frac{\partial}{\partial r} (r\Psi_\mu^{0*}) \Phi_{\mu'}] \mathrm{d}S$$

$$= -\frac{1}{\pi} \delta_{\mu\mu'} \operatorname{tg} \delta_\mu .$$

Cette relation, compte tenu de (A.19) et de la définition (13) de $\theta^{\text{C.M.}}(\eta)$, montre que

$$(\Psi_\mu^0 | \theta^{\text{C.M.}}(\eta) | \Psi_{\mu'}^0) = -\frac{1}{\pi} \delta_{\mu\mu'} \operatorname{tg} \delta_\mu . \tag{A.20}$$

Remarquons enfin que lorsque $\cos \delta_\mu = 0$, la fonction Ψ_μ est solution de l'équation

$$\Psi_\mu = \frac{\mathscr{P}}{\eta - H_0^{\text{C.M.}}} \mathscr{V} \Psi_\mu \tag{A.21}$$

à laquelle se réduit (A.18) dans ce cas.

Bibliographie

1) C. Bloch et C. De Dominicis, Nuclear Physics **7** (1958) 459; **10** (1959) 181; dénotés dans la suite par [I] et [II]
2) J. Goldstone, Proc. Roy. Soc. A **239** (1957) 267;
N. M. Hugenholtz, Physica **23** (1957) 481
3) K. A. Brueckner et C. Levinson, Phys. Rev. **97** (1955) 1344;
K. A. Brueckner, Phys. Rev. **100** (1955) 36
4) T. D. Lee et C. N. Yang, Phys. Rev. **105** (1957) 1119
5) N. N. Bogolubov, V. V. Tolmachev et D. V. Shirkov, A new method in the theory of super conductivity (Dubna, 1958);
L. P. Gorkov, JETP **34** (1958) 735;
P. C. Martin et J. Schwinger, B.A.P.S. **11** (1958) 202; et communication privée;
A. Migdal, communication à la conférence de Paris (1958);
J. G. Valatin, Nuovo Cimento **7** (1958) 843
6) E. Beth et G. E. Uhlenbeck, Physica **4** (1937) 915
7) H. A. Bethe et J. Goldstone, Proc. Roy. Soc. A **238** (1957) 551
8) B. A. Lippmann et J. Schwinger, Phys. Rev. **79** (1950) 469
9) L. C. Gomez, J. D. Walecka et V. F. Weisskopf, Ann. of Physics **3** (1958) 241
10) L. N. Cooper, Phys. Rev. **104** (1956) 1189

8.B *Nuclear Physics* **10** (1959) 527—540; © *North-Holland Publishing Co., Amsterdam*
Not to be reproduced by photoprint or microfilm without written permission from the publisher

ABSORPTION OF POLARIZED μ^--MESONS BY NUCLEI THE NEUTRON ANGULAR DISTRIBUTION

E. I. DOLINSKY and L. D. BLOKHINTSEV
Moscow State University

Received 5 September 1958

Abstract: The angular distribution of neutrons emitted in the absorption of polarized μ^--mesons by nuclei is calculated. Numerical computations are carried out for ${}_8O^{16}$ and ${}_{20}Ca^{40}$.

1. Introduction

Investigation of nuclear absorption of μ^--mesons may yield the form of non-electromagnetic interaction between μ-mesons and nucleons. Nuclear absorption of μ^--mesons occurs via an intermediate stage involving the formation of a mesic atom and can be described by the formula

$$\mu^- + \mathrm{P} \rightarrow \mathrm{N} + \nu + Q. \qquad (1)$$

According to this formula the proton absorbing the μ^--meson is transformed into a neutron (N) and neutrino (ν). A theoretical treatment of process (1) entails difficulties which are not only of a computational nature. The reason of this is that in μ^--meson capture a large amount of energy is released ($Q \approx 100$ MeV) and hence the neutrino and neutron ejected from the nucleus carry off sufficiently large angular momenta and the residual nucleus can acquire a large excitation energy. This leads to the necessity of taking into account transitions involving comparatively large changes of the angular momentum and to consider highly excited nuclear states. A complication which then arises is that at present no reliable information on the nuclear wave functions is available.

In most calculations pertaining to μ^--meson absorption by nuclei the latter are described by the nuclear shell model with j-j coupling. In this case the ratios of μ^--capture probabilities for various nuclei is found to depend on the type of μ-meson-nucleon coupling and this in turn permits one to differentiate between Fermi interaction (scalar, vector) and Gamow-Teller interaction (tensor, pseudovector) [1, 2, 3]).

The ratios of measured μ^--meson capture probabilities for six pairs of nuclei were compared in ref.[4]) with the calculations performed in ref. [3]). In the author's opinion [4]) the results indicate a possible predominance of

Gamow-Teller interaction. However, this conclusion does not appear to be sufficiently reliable as at best the calculations in ref. [3]) are of a semi-quantitative nature.

The discovery of parity non-conservation in weak interactions extends the number of phenomena which can be invoked to decide which type of μ-meson-nucleon interaction should be chosen. It has been suggested [5–9]) that for this purpose the asymmetry in the neutron angular distribution be analyzed for reaction (1) in which polarized μ^--mesons are absorbed. It has furthermore been shown [5, 9, 10]) that the nucleus formed after μ^--meson capture should be polarized and that the degree of polarization should depend on the type of μ-meson-nucleon interaction (the μ^--mesons can also be unpolarized). A study of circular polarization [8]) and angular distribution [8, 11]) of γ-quanta emitted in radiative capture (the μ^--mesons being assumed to be polarized in this second case) should also yield information on the type of interaction.

It should be emphasized that experiments on absorption of polarized μ^--mesons are not feasible in μ-mesic hydrogen because of the presence of a hyperfine structure in the mesic hydrogen atom and capture of the μ^--meson by one proton from another which leads to complete depolarization of the μ^--mesons [12]). Moreover, the probability of μ^--meson absorption of mesic hydrogen is very small. Thus of greatest interest should be a theoretical study of effects related to μ^--meson capture by complex nuclei. In the present paper the angular distribution of neutrons produced in reaction (1) as a result of absorption of polarized μ^--mesons by complex nuclei is considered. Some preliminary results have been reported earlier (ref.[13])).

2. Neutron Angular Distribution

μ^--mesons produced in the decay of π^--mesons are polarized along the direction of their motion. Depolarization of the μ^--mesons (which, however, may not be complete [14])) can occur when they are slowed down in matter and subsequently form a mesic atom. Part of the neutrons created in process (1) are ejected from the nucleus immediately after capture of the μ^--meson, that is, reaction (1) takes place as a direct process. Assuming that non-conservation of space parity holds in μ^--capture as in other weak interaction processes we find that the angular distribution should be of the form

$$1+P_\mu \alpha \cos\theta, \tag{2}$$

where P_μ is the degree of polarization of the μ^--mesons at the instant of capture, α is an asymmetry coefficient which depends on the type of μ-meson-nucleon four-fermion interaction and on the degree of parity non-

conservation; θ is the angle between the direction of μ^--meson polarization and direction of the emitted neutron.

It should be noted that an isotropic background of disintegration neutrons from the compound nucleus produced in reaction (1) is superimposed on the anisotropic angular distribution (2) of neutrons emitted from the nucleus as a result of the direct process. The spectrum of the isotropic background neutrons should have a peak at energies $E_N \approx 1$ to 1.5 MeV whereas the maximum of the probability for neutron emission in the direct process corresponds to $E_N \approx 5$ MeV (see section 3). Thus, by selecting neutrons with energies $E_N \gtrsim 3$ MeV the background can be appreciably lowered. It may be expected that for lighter nuclei neutrons from the direct process will comprise a significant fraction of the total number of neutrons.

If account is made for non-conservation of parity the μ-meson-nucleon four-fermion interaction Hamiltonian can be written in the form

$$H = \sum_k (\bar{\psi}_N O_k \psi_P)(\bar{\psi}_\nu [g_k - g'_k \gamma_5] O_k \psi_\mu) + \text{herm. conj.} \tag{3}$$

where $k = $ s, v, p, t, a denotes respectively scalar, vector, pseudoscalar, tensor and pseudovector coupling,

$$O_s = 1, \quad O_v^\alpha = \gamma_\alpha, \quad O_p = \gamma_5, \quad O_t^{\alpha\beta} = -\frac{i}{2\sqrt{2}}(\gamma_\alpha\gamma_\beta - \gamma_\beta\gamma_\alpha),$$
$$O_a^\alpha = -i\gamma_\alpha\gamma_5, \ (\alpha, \beta = 1, 2, 3, 4) \tag{4}$$

For $g'_k = -g_k$ we arrive at the longitudinal neutrino theory [15]) and as long as the Hamiltonian has the form as in (3) the neutrino produced in process (1) will be polarized in the direction of its motion. If, on the other hand, in absorption of the μ^--meson a neutrino is produced which is polarized opposite to its direction of motion the signs before the calculated values of asymmetry coefficient α should be changed.

Since in μ^--capture most of the released energy is carried off by the neutrino and only energy of the order of several MeV is left to the nucleons in the nucleus it should be permissible to use the non-relativistic approximation for nucleons in the case of s, v, t or a theory. For p-coupling (which vanishes in the non-relativistic approximation) the first approximation in v/c for nucleons has been employed, the small components of the wave functions (φ) being expressed in terms of the large ones (ψ) in accord with the well known formula $\varphi = [\boldsymbol{\sigma} \cdot \hat{\mathbf{p}}/2Mc]\psi$ where $\hat{\mathbf{p}} = -i\hbar\nabla$. Moreover, in p-theory terms of the order of λ_ν/a_μ can be neglected. ($\lambda_\nu \approx 2 \times 10^{-13}$ cm is the neutrino de Broglie wavelength, $a_\mu \approx 2 \times 10^{-11}/Z$ cm is the μ^--mesic K-orbit radius).

Since the binding energy of a μ^--meson on the K-orbit in a mesic atom is much smaller than its rest energy it should be sufficient to employ the non-relativistic approximation for the μ^--meson wave function. The nucleus will

be described by the shell model with j-j coupling and recoil energy will be neglected. The wave function of the emitted neutron will be that corresponding to a complex potential which takes into account the interaction between the neutron and residual nucleus. The shell model potential and neutron-nuclear interaction potential will be assumed to be spherically symmetrical.

Under the foregoing assumptions wave functions for the proton in the (n, j, l) shell, and for the neutron, μ^--meson and neutrino can be written in the form

$$\psi_P = R_{njl}(r)\Omega_{jlj_Z}(\mathbf{r}/r), \qquad \int_0^\infty R_{njl}^2(r)r^2\mathrm{d}r = 1, \tag{5}$$

$$\psi_N = \psi_N(\mathbf{r}) \cdot \chi_{s_N}, \qquad \psi_N(\mathbf{r}) = \sum_L i^L(2L+1)a_L(r)P_L(\mathbf{k}_N \cdot \mathbf{r}/k_N r) \tag{6}$$

$$\begin{gathered}\psi_N(\mathbf{r}) \approx (2\pi)^{-\frac{3}{2}}\left(e^{i\mathbf{k}_N\cdot\mathbf{r}} + \frac{f}{r}e^{-ik_N r}\right) \quad \text{if} \quad r \to \infty \ \dagger \\ \psi_\mu = (4\pi)^{-\frac{1}{2}}R_\mu(r)\chi_{s_\mu}, \quad \int_0^\infty R_\mu{}^2(r)r^2\mathrm{d}r = 1,\end{gathered} \tag{7}$$

$$\psi_\nu = (2\pi)^{-\frac{3}{2}}u_\nu e^{i\mathbf{k}_\nu\cdot\mathbf{r}}. \tag{8}$$

Here n, j, l are quantum numbers specifying the nuclear subshell in the j-j coupling model (n is the number of the energy shell, l is the orbital angular momentum, $j = l \pm \frac{1}{2}$ is the total angular momentum of the proton), χ are normalized spinors, u_ν is a normalized Dirac bispinor, Ω_{jlj_Z} is a spherical spinor [17]). If the finite size of the nucleus is neglected (which is permissible for $Z < 30$) one obtains

$$R_\mu(r) = 2a_\mu^{-\frac{3}{2}}\exp(-r/a_\mu) \quad \text{where} \quad a_\mu = \hbar^2/m_\mu e^2 Z.$$

The results of the calculations performed above are, strictly speaking, applicable to nuclei possessing completely filled proton subshells. In this case, with account of the Pauli principle, the state of protons in the nucleus can be described by a wave function which is of the form of a determinant constructed from the one-particle functions of the type (5). However, it is easy to show that if the calculations are carried out directly with wave function (5) for a single proton with subsequent summation over all projections of the total angular momentum j_Z and over all nuclear subshells (n, j, l) we arrive at the same result as in the calculations with the determinant. If, however, some subshell in the nucleus is not completely occupied one should, generally speaking, take into account the correlation between the angular momenta of separate protons in the subshell ††. It should also be

† This form of asymptotic expression takes into account neutron production [16]).

†† If the incomplete nuclear subshell (n, j, l) contains two protons with a total spin of zero, the formulas given below will remain valid providing that for this subshell in all the formulas in the appendix $(2j+1)$ is replaced by 2.

noted that if the nuclear spin is not zero and the protons contribute to the spin, then the hyperfine structure of the mesic atom should be taken into account in the calculations. Since the mesic atom hyperfine structure produces strong additional depolarization of the μ^--mesons, such cases will not be of special interest as far as the experiments discussed here are concerned and hence will not be considered by us.

From (3)–(8) we obtain by applying first order perturbation theory formulas the following expression for the probability of emission from the nucleus of a neutron possessing an energy between E_N and E_N+dE_N ($E_N = \hbar^2 k_N^2/2M$) and moving in the solid angle $d\Omega_N$ at an angle θ with respect to the direction of μ^--meson polarization †

$$\begin{aligned} dW(E_N,\theta) = \{&[(f_{ss}+2\,\mathrm{Re}\,f_{sv}+f_{vv})+3(f_{tt}+2\,\mathrm{Re}\,f_{ta}+f_{aa}))A_0(E_N) \\ &-2\,\mathrm{Re}(f_{pt}+f_{pa})A_1(E_N)+f_{pp}A_2(E_N)] \\ &+P_\mu[(-(h_{ss}+2\,\mathrm{Re}\,h_{sv}+h_{vv})+(h_{tt}+2\,\mathrm{Re}\,h_{ta}+h_{aa}))B_0(E_N) \\ &+2\,\mathrm{Re}(h_{pt}+h_{pa})B_1(E_N)-h_{pp}B_2(E_N) \\ &+2\,\mathrm{Im}(h_{st}+h_{sa}+h_{vt}+h_{va})G_0(E_N) \\ &+2\,\mathrm{Im}(h_{pt}+h_{pa})G_1(E_N)]\cos\theta\}\,dE_N\,d\Omega_N/4\pi, \end{aligned} \tag{9}$$

where $A_k(E_N)$, $B_k(E_N)$, $G_k(E_N)$ $(k = 0, 1, 2)$ are functions of the energy of the ejected neutron and depend on the properties of the nucleus under consideration ††.

Employing (9) we write the angular distribution of neutrons emitted from the nucleus in the following form:

$$q(E_N,\theta) = 1+P_\mu\alpha(E_N)\cos\theta, \tag{10}$$

where

$$\begin{aligned} \alpha(E_N) = \{&[(h_{ss}+2\,\mathrm{Re}\,h_{sv}+h_{vv})-(h_{tt}+2\,\mathrm{Re}\,h_{ta}+h_{aa})]\beta_0(E_N) \\ &-2\,\mathrm{Re}(h_{pt}+h_{pa})\beta_1(E_N)\gamma_1(E_N)+h_{pp}\beta_2(E_N)\gamma_2(E_N) \\ &+2\,\mathrm{Im}(h_{st}+h_{sa}+h_{vt}+h_{va})\delta_0(E_N) \\ &+2\,\mathrm{Im}(h_{pt}+h_{pa})\delta_1(E_N)\}\{(f_{ss}+2\,\mathrm{Re}\,f_{sv}+f_{vv}) \\ &+3(f_{tt}+2\,\mathrm{Re}\,f_{ta}+f_{aa})-2\,\mathrm{Re}\,(f_{pt}+f_{pa})\gamma_1(E_N)+f_{pp}\gamma_2(E_N)\}^{-1}. \end{aligned} \tag{11}$$

It may be recalled that if the hyperfine structure is neglected, for μ^--capture in mesic hydrogen [5]) one has †††

† The notations employed in formula (9) and in the following formulas in this section are defined in the appendix at the end of this paper.

†† In formulas (2) and (3) in ref. [13]) the terms describing interference between Fermi and Gamow-Teller interactions were not taken into account. The interference term which should be in (3) is given in formula (A12) in the appendix. Moreover, (2) and (3) should be multiplied by the function $\rho_{s/l}(E_N)$, the expression of which is also given in the appendix.

††† In ref. [5]) the tensor and pseudovector operators were defined correspondingly as $O_t^{\alpha\beta} = \frac{1}{2}(\gamma_\alpha\gamma_\beta-\gamma_\beta\gamma_\alpha)$ and $O_a^\alpha = \gamma_\alpha\gamma_5$. We employ here the usual definition (see eq. (4)).

$$\beta_k \equiv 1, \quad \delta_k \equiv 0, \quad \gamma_1 = 0.53\times 10^{-1}, \quad \gamma_2 = 0.28\times 10^{-2}. \tag{12}$$

The difference from mesic hydrogen is that now the quantities $\beta_k(E_N)$ and $\gamma_k(E_N)$ are functions of the neutron energy which depend on the particular properties of the nucleus; another difference is the appearance of additional terms containing $\delta_k(E_N)$. The order of magnitude of the functions $\gamma_k(E_N)$ for the nucleus is the same as that indicated in (12).

In the longitudinally polarized neutrino theory ($g'_k = -g_k$), formula (11) assumes the form

$$\begin{aligned}\alpha^{\text{long}}(E_N) = \{&(-|g_s+g_v|^2+|g_t+g_a|^2)\beta_0(E_N)\\ &+2\,\mathrm{Re}[g_p^*(g_t+g_a)]\beta_1(E_N)\gamma_1(E_N)-|g_p|^2\beta_2(E_N)\gamma_2(E_N)\\ &-2\,\mathrm{Im}[(g_s^*+g_v^*)(g_t+g_a)]\delta_0(E_N)-2\,\mathrm{Im}[g_p^*(g_t+g_a)]\delta_1(E_N)\}\\ &\times\{|g_s+g_v|^2+3|g_t+g_a|^2-2\,\mathrm{Re}[g_p^*(g_t+g_a)]\gamma_1(E_N)+|g_p|^2\gamma_2(E_N)\}^{-1}.\end{aligned} \tag{13}$$

In the absence of pseudoscalar interaction we obtain from (13)

$$\begin{aligned}\alpha^{\text{long}}_{\text{svta}}(E_N) = \{&(-|g_s+g_v|^2+|g_t+g_a|^2)\beta_0(E_N)\\ &-2\,\mathrm{Im}[(g_s^*+g_v^*)(g_t+g_a)]\delta_0(E_N)\}\times\{|g_s+g_v|^2+3|g_t+g_a|^2\}^{-1}.\end{aligned} \tag{13a}$$

For pure p-coupling

$$\alpha_p{}^{\text{long}}(E_N) = -\beta_2(E_N). \tag{13b}$$

If the integration is performed with respect to energy of the emitted neutron, E_N, we evidently obtain instead of (9), (10), (11), (13) and (13a, b) formulas of exactly the same form in which, however, the functions $A_k(E_N)$, $B_k(E_N)$, $G_k(E_N)$, $\beta_k(E_N)$, $\gamma_k(E_N)$, $\delta_k(E_N)$ are replaced respectively by the constants $\tilde{A}_k$, $\tilde{B}_k$, $\tilde{G}_k$, $\tilde{\beta}_k$, $\tilde{\gamma}_k$, $\tilde{\delta}_k$, which, of course, depend on the properties of the given nucleus.

In the particular case when the neutron and neutrino are emitted from the nucleus in opposite directions ($\mathbf{n}_N+\mathbf{n}_\nu = 0$) the angular distribution of the neutrons is the same as (10) in which the α is obtained from formulas (11), (13) for $\beta_k = 1$, $\delta_k = 0$ and the γ_k are very close to those given in (12).

Some remarks concerning the formulas obtained here should be made.

1. If the μ-meson-nucleon interaction be found to be consistent with the Gell-Mann-Feynman theory [18]) which assumes the existence of a and v coupling with a single common coupling constant then, as can be seen from (13), the asymmetry in the neutron angular distribution should vanish.

2. In all formulas the pseudoscalar coupling constant is larger by a factor of $\approx \frac{1}{20}$.

3. In the deduction of the foregoing formulas spin-orbit interaction between the emitted neutron and nucleus was not taken into account. If this interaction be taken into account the expression given in ref. [13]) should be obtained. Estimations performed for some special cases apparently indicate

that spin-orbit interaction should only slightly affect the neutron angular distribution. However, it may be important in calculations of the neutron polarization arising in process (1).

3. Numerical Calculations for $_8O^{16}$ and $_{20}Ca^{40}$

The quantities entering formulas (9) and (11) were evaluated for μ^--capture in $_8O^{16}$ and $_{20}Ca^{40}$ nuclei. The computations were carried out under the following assumptions.

(A) Wave functions in a rectangular potential well were employed for the radial wave functions of protons in the nucleus. The dependence of the well radius R on mass number A was assumed to have the form $R = r_0 A^{\frac{1}{3}}$. The dependence of the radial wave function on quantum number j was disregarded and hence the binding energy of the protons in the nucleus was completely specified by the values of quantum numbers n and l. Thus the order of filling up of the proton shells was assumed to be the following: $1s^2$, $1p^6$, $1d^{10}$, $2s^2$ etc. The potential well depth U_P was determined by well known formulas from the energy of separation of the proton from the nucleus, ε_P, for a prescribed well radius R. After this the binding energy of the other protons in the nucleus was determined. It should be mentioned that if the dependence on j of the radial wave function of a proton in the nucleus is neglected, one gets for nuclei with closed proton shells $G_k(E_N) \equiv 0$ which can easily be verified by direct summation over $j = l \pm \frac{1}{2}$ in formula (A4) in the appendix.

(B) The interaction between the neutron and nucleus, $V_N(r)$, was described by a complex rectangular well ($V_N(r) = -U_N(1+i\zeta)$ for $0 \leqq r \leqq R$ and $V_N(r) = 0$ for $r > R$), the radius R being the same on that for protons.

Use of a complex potential permits one to take into account definite probability of neutron absorption in the nucleus. In distinction to the scattering problem for which $\zeta > 0$, in our case the choice of the asymptotic neutron wave function in the same form as (6) implies that $\zeta < 0$.

(C) The coordinate dependence of the wave function of the μ^--meson in the K-orbit was neglected.

Parameters pertaining to the proton and neutron potentials and to the proton states in the nucleus are indicated in table 1. The values $r_0 = 1.45 \times 10^{-13}$ cm and $U_N = 42$ MeV were chosen in accord with ref. [19]).

The computations were performed on the "Strela" computer of Moscow University. In order to attain sufficient accuracy ($\approx 5\,\%$) it was necessary to take into account orbital angular momenta of emitted neutron L up to $L = 3$ inclusively for oxygen and $L = 4$ for calcium. It will be convenient for the following to replace the coupling constant g_k by a dimensionless coupling constant c_k:

TABLE 1

Nucleus	r_0 (10^{-13} cm)	U_N (MeV)	U_P (MeV)	Proton energy levels in nucleus (MeV)			
				1s	1p	1d	2s
$_8O^{16}$	1.45	42	32.3	22.1	12.1 [a])	—	—
$_{20}Ca^{40}$	1.45	42	31.7	25.6	19.3	11.6	8.35 [a])

[a]) Data on proton separation energy ε_P are taken from ref. [21]).

$$g_k = c_k \times (10^{-49}\ \text{erg} \cdot \text{cm}^3)$$

(and analogously for g'_k) and to measure the energy E_N in MeV. Then from (9) we obtain for the probability of neutron emission from the nucleus (as a result of the direct effect) in the energy interval between E_N and E_N+dE_N the following expression:

$$\begin{aligned} dW(E_N) = \{&[(\varphi_{ss}+2\,\mathrm{Re}\,\varphi_{sv}+\varphi_{vv})+3(\varphi_{tt}+2\,\mathrm{Re}\,\varphi_{ta}+\varphi_{aa})]W_0(E_N) \\ &-2\,\mathrm{Re}(\varphi_{pt}+\varphi_{pa})W_1(E_N)+\varphi_{pp}W_2(E_N)\}dE_N, \end{aligned} \tag{14}$$

where $\varphi_{ik} = c_i^* c_k + c_i'^* c'_k$ and the quantities $W_k(E_N)$ are related to the $A_k(E_N)$ in an evident manner. A completely similar formula for the total probability $\tilde{W} = \int dW(E_N)$ can be obtained by replacing $W_k(E_N)$ by $\tilde{W}_k = \int W_k(E_N)dE_N$.

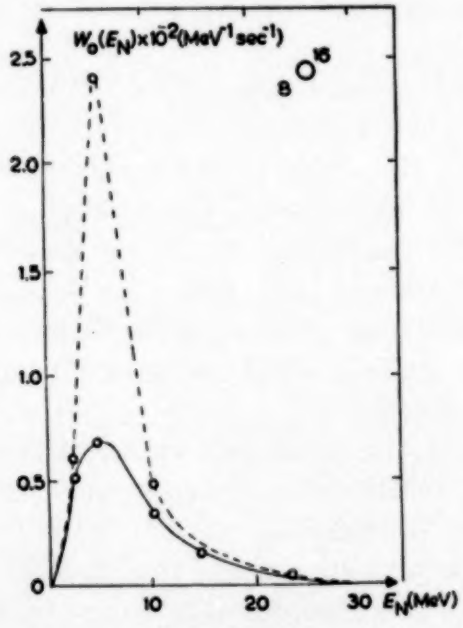

Fig. 1

The results of the calculations are presented in table 2 and in figs. 1—4. The dotted lines pertain to calculations without account of absorption of

TABLE 2

Nucleus	ζ	$\bar{W}_0$ (sec^{-1})	$\bar{W}_1$ (sec^{-1})	$\bar{W}_2$ (sec^{-1})	$\tilde{\beta}_0$	$\tilde{\beta}_1$	$\tilde{\beta}_2$	$\tilde{\gamma}_1$	$\tilde{\gamma}_2$	Ratio of μ^--capture probabilities in various shells [a]	Ratio of specific [a] (per proton) probabilities for μ^--capture in various shells
$_8O^{16}$	0	1.62×10^3	0.742×10^2	0.341×10^1	0.034	0.037	0.040	0.458×10^{-1}	0.210×10^{-2}	1 : 65 [b]	1 : 21.6 [b]
	−0.15	0.718×10^3	0.324×10^2	0.146×10^1	0.476	0.482	0.489	0.453×10^{-1}	0.203×10^{-2}	1 : 38 [b]	1 : 12.6 [b]
$_{20}Ca^{40}$	0	1.33×10^5	0.618×10^4	2.96×10^2	0.145	0.146	0.144	0.415×10^{-1}	0.222×10^{-2}	1 : 7.8 : 290 : 190 [c]	1 : 2.6 : 58 : 190 [c]
	−0.15	0.327×10^5	0.153×10^4	0.712×10^2	0.528	0.528	0.530	0.418×10^{-1}	0.218×10^{-2}	1 : 11.4 : 148 : 149 [c]	1 : 3.8 : 29.6 : 149 [c]

[a] Values referring to $(\bar{W}_{nl})_0$; the $(\bar{W}_{nl})_{1,2}$ yield similar results.
[b] 1s : 1p.
[c] 1s : 1p : 1d : 2s.

neutrons in the nucleus ($\zeta = 0$) and the full lines to calculations with account of absorption ($\zeta = -0.15$) †.

As can be seen from fig. 1 ($_8O^{16}$) and fig. 3 ($_{20}Ca^{40}$) the probability for

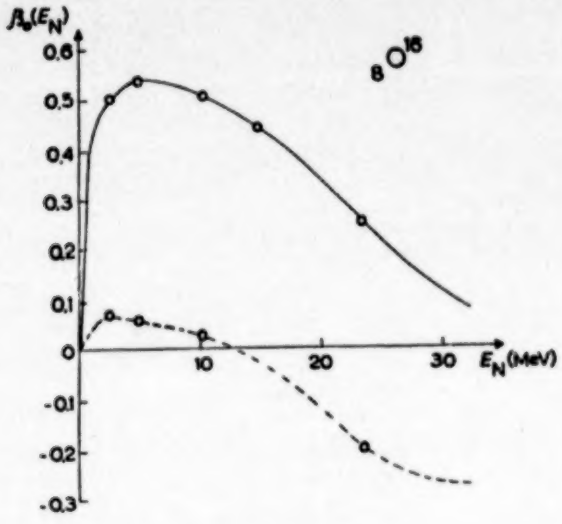

Fig. 2

neutron emission from the nucleus as a result of the direct effect possesses a pronounced peak for neutron energies $E_N \approx 5$ MeV. If absorption in the nucleus is taken into account the peak flattens out but its position does not

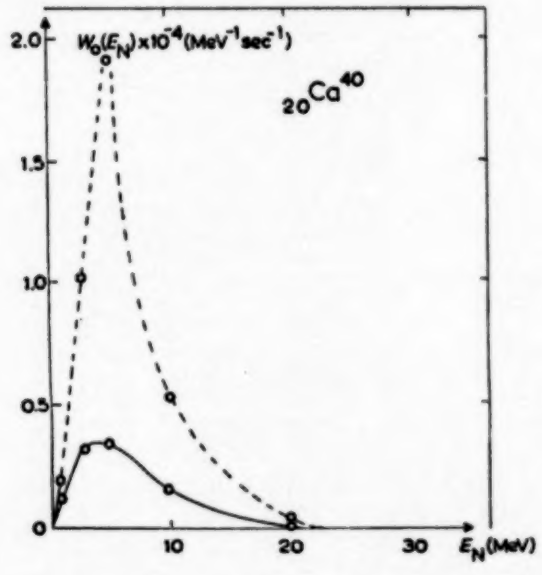

Fig. 3

change and the probability naturally becomes smaller. Values of $\bar{W}_0$, $\bar{W}_1$ and $\bar{W}_2$ obtained after integration over the neutron energy E_N are given in

† The energy dependence of $W_0(E_N)$ and $\beta_0(E_N)$ is shown in figs. 1–4. The shapes of the curves for $W_1(E_N)$ and $W_2(E_N)$ are practically the same as that of $W_0(E_N)$. The difference between $\beta_1(E_N)$ or $\beta_2(E_N)$ and $\beta_0(E_N)$ is not more than a few per cent.

columns 3, 4 and 5 in table 2. Ratios of the probabilities for μ^--capture in various shells integrated over E_N are given in columns 11 and 12 of table 2. The data show that at least for light nuclei μ^--meson capture is mainly due to protons belonging to the outer nuclear shells. Of the 8 protons in the ${}_8O^{16}$ nucleus only 6 protons from the outer 1p shell is efficient in respect to μ^--capture and of the 20 ${}_{20}Ca^{40}$ protons only 12 from the two outer shells (1d and 2s) are active. It is clear from column 12 that the assumption of approximately equal probability of μ^--meson absorption by nuclear protons (see e.g. ref.[20])) is not confirmed by the calculations.

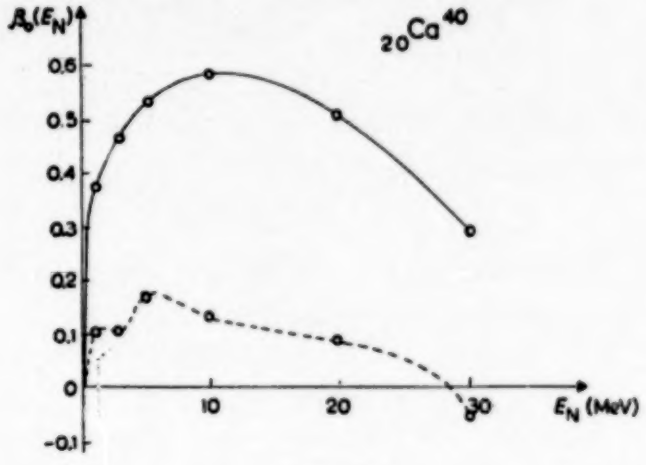

Fig. 4

The dependence of $\beta_0(E_N)$ on E_N is shown in fig. 2 (${}_8O^{16}$) and fig. 4 (${}_{20}Ca^{40}$). Account of neutron absorption in the nucleus is found to be very important as it appreciably increases $\beta_0(E_N)$ on the one hand and on the other yields a much smoother dependence on E_N †.

Values of $\tilde{\beta}_k$ and $\tilde{\gamma}_k$ are presented in columns 6—10 of table 2. Comparison of these data with (12) shows that in essence the difference from μ^--capture in mesic hydrogen is that the asymmetry coefficient α_H obtained for mesic hydrogen without account of the hyperfine structure, is multiplied by a positive factor smaller than 1. If absorption is taken into account for $\zeta = -0.15$ the decrease of α_H is approximately twofold. It can easily be demonstrated that for $E_N \to 0$, $\beta_k(E_N) \approx E_N^{\frac{1}{2}}$.

In order to ascertain how sensitive the results are to variation of the parameters some calculations were performed for ${}_8O^{16}$ with $r_0 = 1.3 \times 10^{-13}$ cm and $U_N = 52$ MeV (in accordance with ref. [19]) we assumed that $r_0 U_N^{\frac{1}{2}} = \text{const}$). Parameters referring to protons were as follows: $U_p = 36.6$ MeV, binding energy $\varepsilon_p^{1p} = 12.1$ MeV, $\varepsilon_p^{1s} = 24.3$ MeV. Within the accuracy of

† Calculations carried out by various authors on scattering of neutrons in nuclei indicate that the magnitude of absorption corresponding to $\zeta = -0.15$ is quite reasonable for the neutron well parameters chosen by us, and energies $E_N \approx 5$ to 15 MeV.

the calculations the results are identical with those for $r_0 = 1.45 \times 10^{-13}$ cm given above (e.g. for $\zeta = -0.15$; $\tilde{\beta}_0 = 0.491$ and the ratio of the capture probabilities in the 1s and 1p shells is 1 : 31, etc.).

4. Conclusion

Calculations on μ^--meson absorption in oxygen and calcium lead to the following results:

1. The energy spectrum of neutrons emitted from the nucleus immediately after μ^--capture possesses a pronounced peak at neutron energies $E_N \approx 5$ MeV.

2. Most of the μ^--mesons are absorbed by protons in the outer nuclear shells.

3. In a first approximation the angular distribution of neutrons $q(\theta)$ ejected as a result of absorption of polarized μ^--mesons by the nuclei can be represented in the form

$$q(\theta) = 1 + P_\mu \tilde{\beta} \alpha_H \cos\theta,$$

where α_H is the asymmetry coefficient for μ^--capture in mesic hydrogen (evaluated without consideration of the hyperfine structure of the latter). The factor $\tilde{\beta}(|\tilde{\beta}| \leqq 1)$ depends on the properties of the particular nucleus. For μ^--capture in ${}_8O^{16}$ and ${}_{20}Ca^{40}$, $\beta \approx +0.5$.

4. Since for μ^--mesons in the K-orbit of mesic atoms the degree of polarization is $P_\mu \approx 0.15-0.20$ [14,22]) and α_H varies between $-1 \leqq \alpha_H \leqq +\frac{1}{3}$ one should expect for $\tilde{\beta} \approx 0.5$ an asymmetry in the neutron angular distribution in the direct process of the order of 3—10 %.

A preliminary communication [23]) has recently appeared concerning measurements of the neutron angular distribution for μ^--capture in S, Zn and Pb. The results apparently indicate an isotropic distribution. However, it should be noted that the errors were comparatively large in these experiments (2 % for S, 3 % for Zn, 10 % for Pb). Since the expected asymmetry effect should be only several per cent, reliable conclusions can be drawn only if the measurements are carried out with an accuracy of several tenths of a per cent.

The authors express their deep appreciation to I. S. Shapiro for continuous interest in this work and discussion of the results. We consider it a pleasant duty to sincerely thank M. K. Akimova for performing the numerical calculations on the Moscow University "Strela" computor.

Appendix

The notations used in the paper are as follows:

$$f_{ab} = g_a^* g_b + g_a'^* g'_b, \quad h_{ab} = g_a^* g'_b + g_a'^* g_b, \quad (a, b = s, v, p, t, a) \quad (A1)$$

$$A_k(E_N) = C\sum_{njl}[(2j+1)/(2l+1)](E_\nu^{njl}/2Mc^2)^k A_{njl}(E_N)\rho_{njl}(E_N) \quad (A2)$$

$$B_k(E_N) = C\sum_{njl}[(2j+1)/(2l+1)](E_\nu^{njl}/2Mc^2)^k B_{njl}(E_N)\rho_{njl}(E_N) \quad (A3)$$

$$G_k(E_N) = C\sum_{njl}[(2j+1)/(2l+1)](E_\nu^{njl}/2Mc^2)^k G_{njl}(E_N)\rho_{njl}(E_N) \quad (A4)$$

$$\beta_k(E_N) = -B_k(E_N)/A_k(E_N),\quad \gamma_k(E_N) = A_k(E_N)/A_0(E_N),\quad \delta_k(E_N) = G_k(E_N)/A_0(E_N); \quad (A5)$$

$$\tilde{A}_k = \int A_k(E_N)dE_N,\quad \tilde{B}_k = \int B_k(E_N)dE_N,\quad \tilde{G}_k = \int G_k(E_N)dE_N; \quad (A6)$$

$$\tilde{\beta}_k = -\tilde{B}_k/\tilde{A}_k,\quad \tilde{\gamma}_k = \tilde{A}_k/\tilde{A}_0,\quad \tilde{\delta}_k = \tilde{G}_k/\tilde{A}_0,\quad (k=0,1,2); \quad (A7)$$

$$A_{njl}(E_N) = \sum_{L\Lambda}(2L+1)(2\Lambda+1)(C^{l0}_{L0\Lambda0})^2|b_{L\Lambda njl}(E_N)|^2; \quad (A8)$$

$$\begin{aligned}B_{njl}(E_N) = {}& \mathrm{Re}\sum_{L\Lambda}[(2L+1)(2L+2)(2L+3)(2\Lambda+1)(2\Lambda+2)(2\Lambda+3)]^{\frac{1}{2}}\\ &\times[C^{l0}_{L0\Lambda0}C^{l0}_{L+1\Lambda+10}W(L+1l\,1\Lambda;\Lambda+1L)b_{L\Lambda njl}(E_N)b^*_{L+1\Lambda+1njl}(E_N)\\ &+C^{l0}_{L+10\Lambda0}C^{l0}_{L0\Lambda+10}W(Ll\,1\Lambda;\Lambda+1L+1)b_{L+1\Lambda njl}(E_N)b^*_{L\Lambda+1njl}(E_N)]\end{aligned} \quad (A9)$$

$$\begin{aligned}G_{njl}(E_N) = {}& 6(2l+1)W(lj1\tfrac{1}{2};\tfrac{1}{2}l)\\ &\times\mathrm{Im}\sum_{L\Lambda}[(2L+1)(2L+2)(2L+3)(2\Lambda+1)(2\Lambda+2)(2\Lambda+3)]^{\frac{1}{2}}\\ &\times[C^{l0}_{L0\Lambda0}C^{l0}_{L+10\Lambda+10}X(L\Lambda l;L+1\Lambda+1l;111)b^*_{L\Lambda njl}(E_N)b_{L+1\Lambda+1njl}(E_N)\\ &+C^{l0}_{L0\Lambda+10}C^{l0}_{L+10\Lambda0}X(L\Lambda+1l;L+1\Lambda l;111)b^*_{L+1\Lambda njl}(E_N)b_{L\Lambda+1njl}(E_N)]\end{aligned} \quad (A10)$$

$$\begin{aligned}b_{L\Lambda njl}(E_N) &= \int_0^\infty R_\mu(r)a_L^*(r)j_\Lambda(k_\nu r)R_{njl}(r)r^2dr;\\ C &= (2M)^{\frac{1}{2}}\hbar^{-7}c^{-3};\qquad c = 3\times10^{10}\ \mathrm{cm/sec};\\ E_\nu^{njl} &= E_{N\,max}^{njl}-E_N;\qquad E_{N\,max}^{njl} = m_\mu c^2-\varepsilon_\mu-\varepsilon_p{}^{njl};\\ \rho_{njl}(E_N) &= E_N{}^{\frac{1}{2}}(E_{N\,max}^{njl}-E_N)^2;\end{aligned} \quad (A11)$$

$j_\Lambda(x) = (\pi/2x)^{\frac{1}{2}}J_{\Lambda+\frac{1}{2}}(x)$ is a spherical Bessel function,

$R_\mu(r)$ the normalized radial μ^--meson wave function for the ground state of the mesic atom,

W Racah coefficients [24]) (the definition of X is given in ref. [25])),

P_μ the degree of μ^--meson polarization at the instant of absorption,

ε_μ the binding energy of the mesic atom ground state,

m_μ the μ-meson mass,

$\varepsilon_p{}^{njl}$ the proton binding energy in the (n, j, l) subshell,

M the nucleon mass (the difference between the proton and the neutron masses is neglected).

If we disregard in formulas (A2), (A3) and (A4) the sum over (n, j, l) and insert the expressions thus obtained in (9) we obtain a formula for μ^--meson absorption in the given filled subshell (n, j, l).

It should be noted that for $l = 0$: $G_{nj0}(E_N) \equiv 0$.

$$
\begin{aligned}
&W^{svta}_{njl}(E_N, \theta) = (2j_0^1/3)(-)^{j-s}(2j+1) \\
&\times \sum_{IL\Lambda I'L'\Lambda' sfh} i^{L+\Lambda-L'-\Lambda'}(-)^{I+f+h}(2I+1)(2I'+1)(2L+1)(2L'+1) \\
&\times (2\Lambda+1)(2\Lambda'+1)(2g+1)(2f+1)(2h+1)C^{l0}_{L0\Lambda0}C^{l0}_{L'0\Lambda'0}C^{10}_{\Lambda0\Lambda'0}C^{11}_{L0\Lambda1} \qquad \text{(A12)} \\
&\times C^{11}_{L'0\Lambda1}W(I\tfrac{1}{2}\Lambda l;\ Lj)X(L'\Lambda' l;\ I'gj;\ \tfrac{1}{2}1\tfrac{1}{2})X(jI'g;\ If1;\ \Lambda1\Lambda') \\
&\times X(I1f;\ Lh1;\ \tfrac{1}{2}L'I')\ \mathrm{Re}\{[h_{st}+h_{sa}+h_{vt}+h_{va}] \\
&\times b^*_{IL\Lambda njl}(E_N)b_{I'L'\Lambda'njl}(E_N)\}\cos\theta.
\end{aligned}
$$

References

1) J. M. Kennedy, Phys. Rev. **87** (1952) 953
2) A. Rudik, Doklady AN SSSR **92** (1953) 739
3) H. A. Tolhoek and J. R. Luyten, Nuclear Physics **3** (1957) 679
4) J. C. Sens, R. A. Swanson, V. L. Telegdi and D. D. Yovanovitch, Phys. Rev. **107** (1957) 1464
5) I. S. Shapiro, E. I. Dolinsky and L. D. Blokhintsev, Doklady AN SSSR **116** (1957) 946; Nuclear Physics **4** (1957) 273
6) B. L. Ioffe, JETP **33** (1957) 308
7) H. Überall, Nuovo Cimento **6** (1957) 533
8) K. Huang, C. N. Yang and T. D. Lee, Phys. Rev. **108** (1957) 1340
9) L. Wolfenstein, Nuovo Cimento **7** (1958) 706
10) T. Fulton, Nuclear Physics **6** (1958) 319
11) Handelman, private communication
12) S. S. Gershtein, JETP **34** (1953) 463, 993;
A. E. Ignatenko, L. B. Yegorov, B. Khalupa and D. Chultham, JETP **35** (1958) 894
13) E. I. Dolinsky and L. D. Blokhintsev, JETP **34** (1958) 759
14) R. L. Garwin, L. M. Lederman and M. Weinrich, Phys. Rev. **105** (1957) 1415
15) L. D. Landau, JETP **32** (1957) 407;
T. D. Lee and C. N. Yang, Phys. Rev. **105** (1957) 1671;
A. Salam, Nuovo Cimento **5** (1957) 299
16) A. Sommerfeld, Structure of Atoms and Spectra (GITTL, Moscow, 1956) vol. 2
17) V. B. Berestetsky, A. Z. Dolginov and K. A. Ter-Martirosyan, JETP **20** (1950) 527
18) R. P. Feynman and M. Gell-Mann, Phys. Rev. **109** (1958) 193
19) H. Feshbach, C. E. Porter and V. F. Weisskopf, Phys. Rev. **96** (1954) 448
20) J. A. Wheeler, Revs. Mod. Phys. **21** (1949) 133
21) N. Feather, Advances in Physics **2** (1953) 141
22) L. B. Yegorov, A. E. Ignatenko, B. Khalupa and D. Chultham, Joint Institute of Nuclear Research, Materials of the IV Session of Scientific Council, Dubna (May 1958); JETP **35** (1958) 1131
23) C. T. Coffin, A. M. Sachs and D. H. Tycko, Bull. Amer. Phys. Soc. **3** (1958) 52
24) L. C. Biedenharn, J. M. Blatt and M. E. Rose, Revs. Mod. Phys. **24** (1952) 249
25) A. Simon and T. A. Welton, Phys. Rev. **90** (1953) 1042

8.A *Nuclear Physics* **10** (1959) 541—551; © *North-Holland Publishing Co., Amsterdam*
Not to be reproduced by photoprint or microfilm without written permission from the publisher

INTERACTION MODES IN BETA DECAY. DECAY OF Na^{24}

N. A. BURGOV and Yu. V. TEREKHOV
U.S.S.R. Academy of Sciences, Moscow

Received 22 September 1958

Abstract: Electron-neutrino correlation in the β-decay of Na^{24} has been investigated. The method of observation is based on the effect of nuclear resonance scattering of the γ-rays of Mg^{24} accompanying the β-decay of Na^{24}.

A gaseous source of Na^{24} was used.

The most probable value of the correlation constant which is in agreement with the measurements proved equal to

$$\lambda = -(0.22 \pm 0.12).$$

If one takes into consideration the isobaric spin and the experiments on the circular polarization of the γ-rays of Na^{24}, then it appears that the β-decay of Na^{24} is due only to interaction of the Gamow-Teller type.

It follows then from the results of the present paper that only the axial vector mode of interaction, corresponding to $\lambda = -\frac{1}{3}$, should be effective in the β-decay of Na^{24}.

1. Introduction

The determination of the modes of interaction in beta decay is an important problem in the theory of weak interactions. Since the discovery of parity non-conservation the number of experiments the data of which involve the interaction constants has greatly increased. However, the problem of determining the modes of interaction has not yet been solved.

Prior to the discovery of parity non-conservation it was generally believed that beta decay is due to tensor interaction and scalar interaction in the Hamiltonian. This view was based on measurements of electron-neutrino correlation in He^6 [1, 2]), in Ne^{19} [3, 4]) and also on the absence of the interference terms (Fierz term) in the experimental determinations of the beta spectrum.

However, as was shown by Lee and Yang [5]), the absence of the Fierz term does not denote that of all the interaction modes responsible for the Fermi transitions (scalar interaction S and vector interaction V) only one is realized. Neither does it justify the conclusion that of the axial vector and tensor modes of interaction leading to Gamow-Teller transitions, only one is realized.

The absence of the Fierz term merely denotes that the expression (notation as in ref. [5]))

$$\mathrm{Re}\,\{(C_V C_S^* + C'_V C_S^{*\prime})|M_F|^2 + (C_T C_A^* + C'_T C_A^{*\prime})|M_{GT}|^2\} \qquad (1)$$

is equal to zero; this occurs for

$$C_S = -C'_S, \quad C_V = C'_V; \quad C_T = -C'_T, \quad C_A = C'_A;$$

these relations follow from the data on beta electron polarization [6]).

Recently measurements have also been performed on angular electron-neutrino correlation for Ar^{35} [7]). There are grounds for believing that the β-decay of Ar^{35} is mainly due to Fermi-type interaction. As a result of the experiments the value $\lambda = 0.70 \pm 0.17$ was found for the correlation constant; this corresponds to a considerable contribution of the vector interaction. The results of the experiments on Ar^{35} can be satisfactorily explained by a combination of either vector and axial vector interactions or of vector and tensor interactions.

Hence, a contradiction with the previous conclusions arises. Further measurements of the interaction constants are necessary to determine which of them are responsible for beta decay.

2. Experimental Method

In all the above-mentioned papers [1, 2, 3, 4, 7]) on electron-neutrino correlation recoil nuclei were registered. One of us [8]) has suggested a different method of observing the correlation, based on observation of the nuclear resonance scattering of the gamma rays accompanying beta decay. The method is as follows.

Let the decay scheme of the nuclei be as shown in fig. 1, where beta decay is followed by two cascade gamma quanta with energies $E_{\gamma 1}$ and $E_{\gamma 2}$. In the apparatus shown in fig. 2, the gamma quanta $E_{\gamma 1}$ and $E_{\gamma 2}$ are counted

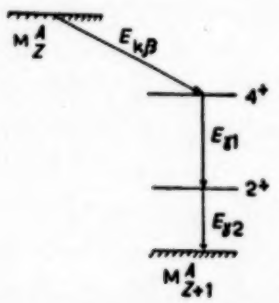

Fig. 1. Disintegration scheme.

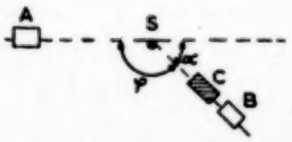

Fig. 2. Experimental set-up.

by detectors A and B, respectively. Between the source and B which registers the quanta corresponding to the ground state transitions, a target C is inserted, containing nuclei M^A_{Z+1}, the daughter nuclei of $M_Z{}^A$. The detectors A and B are connected in coincidence. The absorption of $E_{\gamma 2}$ gamma quanta in the target C is measured for various angles φ between the directions of the gamma quanta $E_{\gamma 1}$ and $E_{\gamma 2}$.

Apart from the usual absorption of gamma quanta due to the photoelectric effect, the Compton effect, and pair production an additional absorption arises in the target C owing to resonance scattering on the target nuclei. As is shown in ref.[8]), the average resonance scattering cross section depends not only on the level width Γ, but is also determined by the value of λ characterizing the interaction. This average cross section equals

$$\bar{\sigma} = \sigma_0 \frac{\pi}{4} \frac{\Gamma}{E_{\gamma 2}} \int_{\left|\frac{E_{\gamma 1}}{c}\cos\alpha - \frac{E_{\gamma 2}}{c}\right|}^{p_{\text{nuc max}}} \frac{m_1 c}{P_{\text{nuc}}} f(p_{\text{nuc}}) \mathrm{d}p_{\text{nuc}} \tag{2}$$

where

$$\sigma_0 = 2\pi\lambda^2 \frac{2j+1}{2i+1}; \tag{3}$$

λ is the wave length of the $E_{\gamma 2}$ gamma quantum; j the momentum of the excited level; i the momentum of the ground level; Γ the natural width of the excited level; m_1 the mass of the nucleus; $p_{\text{nuc max}}$ the maximum momentum received by the nucleus; $\alpha = \pi - \varphi$ (φ is the angle between the gamma quanta); $f(p_{\text{nuc}})$ is the distribution in momentum of the recoil nuclei. The function $f(p_{\text{nuc}})$ is normalized according to

$$\int_0^{p_{\text{nuc max}}} f(p_{\text{nuc}}) \mathrm{d}p_{\text{nuc}} = 1 \tag{4}$$

and depends on the correlation constant λ.

Formula (2) is derived on the assumption that the recoil nuclei are free, i.e., that their motion during the life-time of the excited levels is not disturbed by collisions with other nuclei. Another assumption is that there is no correlation between the directions of the beta particles and the gamma quanta.

Numerical calculations were made of the cross section for Na^{24}, whose decay scheme is similar to that presented in fig. 1. The following values were taken for the energies of the beta particles and gamma quanta:

$$E_{k\beta} = 1.4\ \text{MeV}, \qquad E_{\gamma 1} = 2.76\ \text{MeV}, \qquad E_{\gamma 2} = 1.38\ \text{MeV}.$$

The cross section has a maximum at

$$\cos\alpha = \frac{E_{\gamma 2}}{E_{\gamma 1}}, \tag{5}$$

i.e., at the angle $\alpha = 60°$. Fig. 3 shows the dependence of the calculated cross section on the angle α for three values of $\lambda = -1, 0, +1$. All the curves are normalized at $\sigma = \sigma_{\max}$. The diagram shows that the angular dependence of the cross section depends noticeably on the correlation constant λ.

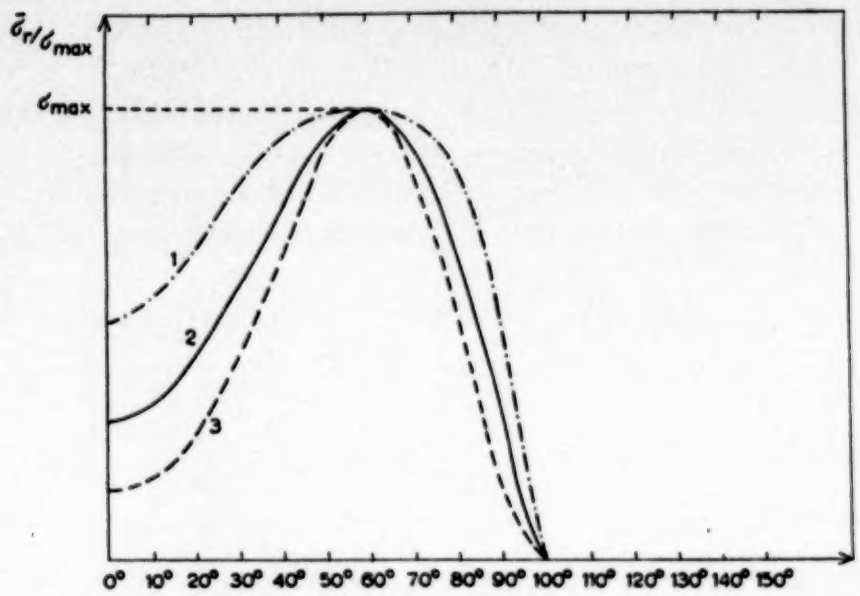

Fig. 3. Dependence of the cross section $\bar{\sigma}_r$ on the angle α. The solid curve corresponds to $\lambda = 0$, the dotted curve to $\lambda = -1$, the dot-dashed to $\lambda = +1$.

3. Apparatus and Experiments

In the present investigation experiments on electron-neutrino correlation were performed with a gaseous source of Na^{24}. The apparatus (see fig. 4) was in principle similar to that described in ref. [9]).

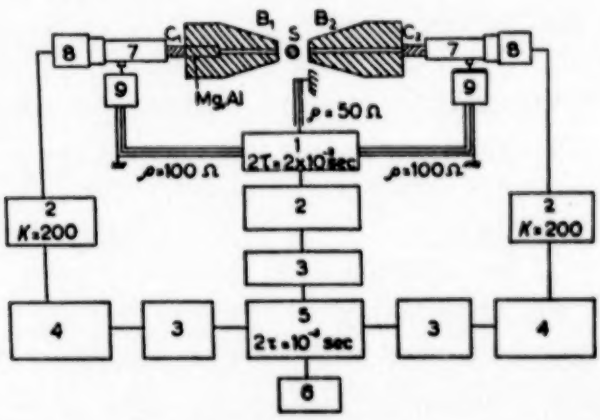

Fig. 4. Schematic diagram of the apparatus. S-source of gamma quanta; B_1 and B_2 — lead collimators, C_1 and C_2-tolane crystals.
1. Coincidence circuit; 2. Amplifiers; 3. Pulse shaping circuit; 4. Single-channel pulse-height analysers; 5. Triple coincidence circuit; 6. Counter; 7. FEU electron multiplier tubes; 8. Cathode followers; 9. Limiting amplifiers.

It is well known that the vapours of metallic sodium are monatomic. In order to achieve sufficient intensity, the source was kept at a temperature of about 900° C; this corresponds to a vapour pressure of metallic sodium in an air-tight stainless steel container of about 1 atm. At this pressure the time

interval between collisions exceeds 10^{-11} sec. From preliminary measurements performed in [9]) with a liquid sodium source we learnt that the life-time of the level with an energy $E_{\gamma 2} = 1.38$ MeV is less than 2×10^{-12} sec. Thus, one may consider the recoil nuclei in the gaseous source used to be free. As the source is warmed up, a part of the metallic sodium remains in the liquid phase; the lower part of the source container was therefore shielded by a lead screen, so that the number of gamma quanta from the liquid phase was about 1 per cent of the amount from the gaseous source.

The gamma quanta were registered by scintillation counters consisting of tolane crystals with FEU-33 electron multipliers. The angle $\alpha = \pi - \varphi$ could be varied by rotating one of the detectors about the axis of the source.

The pulse from each detector was fed to a fast coincidence circuit (resolving time $2\tau = 2 \times 10^{-9}$ sec) and simultaneously to a single-channel pulse-height analyser; this was adjusted to select pulses due only to gamma quanta of a certain energy.

From the analyser and the fast coincidence the pulses were fed to a slow coincidence circuit (resolving time 10^{-6} sec) and were then counted by a mechanical scaler.

A Mg target was placed before the counter registering the 1.38 MeV gamma quanta. An additional absorption of gamma quanta in the magnesium specimen was then observed for angles α from 0° to 100° due to resonance scattering. In a target containing Al nuclei there should be no resonance scattering.

The magnesium target was 80 mm long; the length of the aluminium target was chosen such that in the absence of resonance scattering, i.e., for angles $\alpha > 100°$, absorption should be the same in both targets.

4. Experimental Results

To exclude the ordinary absorption of gamma rays due to the photoelectric effect, the Compton effect, and pair production, the ratio of transparencies of the magnesium and aluminium targets

$$A_k = \frac{T_{Mg}}{T_{Al}} = \frac{N_{Mg}}{N} \Big/ \frac{N_{Al}}{N} = \frac{N_{Mg}}{N_{Al}} \quad . \tag{6}$$

was measured for different angles α. Here, N_{Mg} is the number of true coincidences of gamma quanta when a Mg target is used, N_{Al} is the number of true coincidences when an aluminium target is inserted; N is the number of true coincidences in the absence of a target; T_{Mg} and T_{Al} denote the transparencies of the magnesium and aluminium absorbers. Now,

$$T_{Mg} = T_{Mg,a} T_{Mg,r}; \qquad T_{Al} = T_{Al,a}, \tag{7}$$

where T_a is the transparency of the target due to the ordinary absorption and scattering of gamma quanta, T_r the transparency of the target due to the resonance scattering of gamma quanta. Hence

$$\frac{N_{Mg}}{N_{Al}}(\alpha) = \frac{T_{Mg,a}}{T_{Al,a}} T_{Mg,r}(\alpha). \tag{8}$$

The ratio $T_{Mg,a}/T_{Al,a}$ was determined experimentally without coincidence; it was found equal to 1.0006 ± 0.0002, i.e., practically equal to unity. Hence, we may take

$$T_{Mg,r}(\alpha) = \frac{N_{Mg}}{N_{Al}}(\alpha). \tag{9}$$

In table 1 the experimentally determined data on absorption due to the resonance scattering of gamma quanta are presented for different angles α.

TABLE 1

α	$1-T_{Mg,r}(\alpha)$
0°	0.011 ± 0.004
10°	0.016 ± 0.005
15°	0.017 ± 0.004
30°	0.032 ± 0.005
40°	0.036 ± 0.006
60°	0.052 ± 0.004
85°	0.025 ± 0.008
120°	0.001 ± 0.004

Since the experimentally determined transparencies differ but little from unity, we may write

$$1-T_{Mg,r}(\alpha) = n_{Mg} \bar{\sigma}_{Mg,r} d_{Mg}, \tag{10}$$

where $\sigma_{Mg,r}$ is the resonance scattering cross section determined according to formula (2); n_{Mg} denotes the number of nuclei of the Mg^{24} isotope per unit volume of the target; d_{Mg} the thickness of the target.

Using expression (10) one can compute the maximum resonance scattering cross section. It proves equal to

$$\sigma_{max} = (1.93 \pm 0.15) \times 10^{-25} \text{ cm}^2. \tag{11}$$

If we now denote the experimentally determined values by

$$D = \frac{1-T_{Mg,r}(\alpha)}{1-T_{Mg,r}(60°)} = \frac{\sigma_r(\alpha)}{\sigma_{max}} \tag{12}$$

and the theoretically computed values by D, we can obtain from the data of table 1 the ratio of the cross sections of resonance scattering at different angles to the maximum cross section; these results are represented in table 2 and in fig. 5.

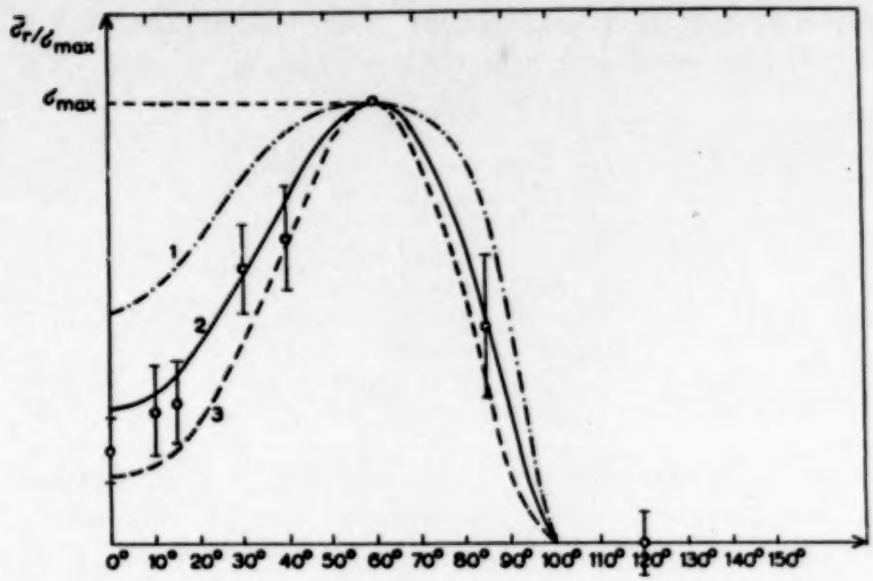

Fig. 5. Experimental results.
The solid curve corresponds to $\lambda = 0$, the dotted curve to $\lambda = -1$, the dot-dashed to $\lambda = +1$.

TABLE 2

α	$\bar{D}$
0°	0.21±0.07
10°	0.30±0.10
15°	0.32±0.09
30°	0.62±0.10
40°	0.69±0.12
60°	1.00
85°	0.49±0.16
120°	0.00±0.07

Table 2 and fig. 5 give the root mean square errors. For each point the errors $x = \bar{D} - D$ corresponding to values of λ from $+1$ to -1 will represent a continuous random variable characterized by a normal distribution law. Multiplying the probabilities of all the points, we find the most probable distribution of $x = \bar{D} - D$ in λ, which yields

$$\lambda = -0.26 \pm 0.15. \tag{13}$$

The experimental error is determined from the probability distribution for λ in the series of measurements performed. λ lies within the indicated limits with a probability of 67 %.

From (2) and (11) the width and life-time of the resonance level with energy $E_{\gamma 2}$ may be determined. For $\lambda = -0.26$ we obtain

$$\tau = (2.6 \pm 0.2) \times 10^{-13} \text{ sec.} \tag{14}$$

Measurements were performed with a solid source of Na^{24}. The method

was the same as with the gaseous source. The results obtained are presented in table 3. In this experiment, as in the investigation with a liquid source [9]),

TABLE 3

α	$1-T_{\mathrm{Mg},\,\mathrm{r}}(\alpha)$
100°	0.003±0.008
90°	0.000±0.008
65°	0.007±0.008
62°	0.010±0.008
60°	0.024±0.006

an additional resonance absorption was registered only in a rather narrow range about the angle $\alpha = 60°$. The interpretation of the results with the solid source is similar to that given in ref. [9]) for a liquid source. The presence of resonance scattering of gamma rays in the solid source denotes that the life-time of the 1.38 MeV excited level is comparable with the time of free flight of the recoil nucleus in the solid source (about 10^{-13} sec); this confirms the result obtained in ref. [13]).

In order to convince ourselves that the resonance scattering effects measured are not due to any instrumental asymmetry, we performed a control experiment with Co^{60} in place of Na^{24}; Co^{60} has a decay scheme similar to that of Na^{24}, but emits gamma quanta with energies $E_{\gamma 1} = 1.17$ MeV and $E_{\gamma 2} = 1.33$ MeV. The experimental results are given in table 4. It is evident

TABLE 4

α	$1-T_{\mathrm{Mg},\,\mathrm{r}}(\alpha)$
0°	0.001±0.004
40°	0.000±0.005
50°	0.003±0.005
60°	0.001±0.004
100°	0.001±0.004

that no angular dependence of the absorption arises. This points to the absence of asymmetry in the apparatus.

5. Discussion and Conclusions

The Na^{24} nucleus with momentum and parity 4^+ decays to the 4^+ level of the Mg^{24} nucleus. Thus, a $j-j$ transition takes place which is allowed both by the Fermi selection rules ($\Delta j = 0$, no) and by the Gamow-Teller selection rules ($\Delta j = 0, \pm 1$, no, $0 \to 0$ transition forbidden).

However, if the isobaric spin T and the results of the experiments on the

circular polarization of Na^{24} gamma rays are taken into consideration †, it follows that the matrix element for the transition obeying the Fermi selection rules should be much smaller than the matrix element for a transition obeying the Gamow-Teller selection rules.

In refs. [10]) and [11]) experiments on the circular polarization of gamma rays are described for different emitters including Na^{24}. The polarization coefficient α observed in these investigations is not large; from this we can conclude that the beta decay of Na^{24} is due either to Gamow-Teller or to Fermi interaction alone. If both interactions were present simultaneously, the interference term would increase considerably, and α would be large.

In view of the importance of the problem another experiment on the circular polarization of Na^{24} gamma rays was especially performed [12]). Whereas in refs. [10]) and [11]) the circular polarization was detected from the dependence of the number of scattered gamma quanta on the direction of the magnetic field, in ref. [12]) another method was applied; the gamma rays passed through a ferromagnetic alloy having a thickness several times the free path length of 2.76 MeV gamma quanta; thanks to this, the sensitivity of the method was increased several times as compared with the investigation reported in refs. [10]) and [11]).

The results of this investigation, within the limits of experimental error, also point to the absence of a noticeable interference term.

Let us take into consideration the isobaric spin T. For transitions of the Fermi type the selection rule ΔT holds, for Gamow-Teller transitions the selection rule $\Delta T = 0, \pm 1$ is valid.

The ground state of the Na^{24} nucleus has a projection of the isobaric spin $T_\xi = -1$. According to the rule that the ground state has the least possible isobaric spin, we can expect the isobaric spin of Na^{24} to be $T = 1$ and that of the Mg^{24} ground state $T = 0$.

It is well known that excited levels of the Mg^{24} nucleus with $T = 1$ appear only at excitation energies of about 10 MeV; all the lower levels have an isobaric spin $T = 0$.

It was shown in ref. [13]) that the β^+-transition of $Al^{24} \rightarrow Mg^{24}$ to the 9.35 MeV excitation level is superallowed ($\log ft = 3.35$) of the type $\Delta j = 0$, $\Delta T = 0$, $T = 1$, $A = 4n$; this is why for the 9.35 MeV level $T = 1$.

Wilkinson [14]) excluded the Coulomb term in the coupling energy of the Mg^{24} nucleus and thus calculated the first level with $T = 1$; he found it equal to 9.45 MeV, which is in close agreement with experiment. Hence, the 4.14 MeV level will have the isobaric spin $T = 0$.

If this is true, the Fermi type transition will appear only as a small

† We wish to thank A. I. Alikhanov, V. A. Liubimov and K. A. Ter-Martirosyan for drawing our attention to these possibilities.

admixture to the Gamow-Teller type transition due to the inaccuracy of the isobaric spin quantum number.

Thus, we may consider it established that the beta decay of Na^{24} is mainly due to Gamow-Teller interaction, i.e., that

$$|M_F|^2 \ll |M_{GT}|^2.$$

Hence, it follows from the data of the present investigation that in a β-transition with Gamow-Teller selection rules the axial vector mode of interaction corresponding to the correlation constant $\lambda = -0.33$ should be effective.

Bearing in mind that the errors of the present experiment are large, we may at any rate affirm that the tensor mode of interaction is not the only possible one as seemed to follow from the first experiments He^6 [2]).

The authors wish to thank A. I. Alikhanov, K. A. Ter-Martirosyan and V. A. Liubimov for many discussions and valuable suggestions.

The authors express their gratitude to their collaborators A. I. Zubkov, V. G. Alpatov and K. N. Rostovtsev for invaluable assistance in performing the experiment.

Note added in proof: Some time after the publication of ref. [8]), similar calculations were made by Curtis and Lewis [15]) and Morita and Morita [16]). They have shown that directional correlation between the recoil nucleus and ejected γ-quantum exists in the case of the Gamow-Teller interaction. The curves in fig. 3, therefore, hold true only for the Fermi interaction. The correlation between the recoil nucleus and the γ-quantum for the Gamow-Teller interaction does not essentially change the result obtained in the present paper. Treatment of the experimental data of table 1 by the least squares method, with due allowances for the above-stated correlation, leads to the value

$$\frac{1}{3}\,\frac{|C_T|^2-|C_A|^2}{|C_T|^2+|C_A|^2} = -(0.22\pm 0.12)$$

instead of the value $-(0.26\pm 0.15)$ given in the paper. The inference of the predominance of axial interaction will remain as it stood.

References

1) B. M. Rustad and S. L. Ruby, Phys. Rev. **89** (1953) 880
2) B. M. Rustad and S. L. Ruby, Phys. Rev. **97** (1955) 991
3) W. P. Alford and D. R. Hamilton, Phys. Rev. **95** (1954) 1351
4) D. R. Maxson, I. S. Allen and W. K. Jentschke, Phys. Rev. **97** (1955) 109
5) T. D. Lee and C. N. Yang, Phys. Rev. **104** (1956) 254
6) A. I. Alikhanov, V. A. Liubimov and G. P. Eliseyev, to be published

7) W. B. Hermannsfeldt, D. R. Mayson, P. Stühelin and I. S. Allen, Phys. Rev. **107** (1957) 641
8) N. A. Burgov, JETP **33** (1957) 655
9) N. A. Burgov and Yu. V. Terekhov, Atomnaya Energiya **2** (1957) 514
10) H. Shopper, Phil. Mag. **2** (1957) 710
11) F. Boehm and A. H. Wapstra, Phys. Rev. **109** (1958) 456
12) A. I. Alikhanov, V. A. Liubimov, M. Ya. Balatz, P. I. Lebedev and Yu. Obukhov (to be published)
13) M. Bolsterli and E. Feenberg, Phys. Rev. **97** (1955) 736
14) D. H. Wilkinson, Phil. Mag. **1** (1956) 1031
15) R. R. Lewis and R. B. Curtis, Phys. Rev. **110** (1958) 910
16) M. Morita and R. S. Morita, Phys. Rev. **111** (1958) 1130

7.A *Nuclear Physics* **10** (1959) 552—563; © *North-Holland Publishing Co., Amsterdam*
Not to be reproduced by photoprint or microfilm without written permission from the publisher

ON THE PROOF OF DISPERSION RELATIONS FOR INELASTIC SCATTERING

A. A. LOGUNOV and I. T. TODOROV

Laboratory of Theoretical Physics, Joint Institute of Nuclear Research, Dubna, U.S.S.R.

Received 28 August 1958

Abstract: A derivation of dispersion relations for the inelastic process ($p+\pi \to p'+\pi'+\pi''$) is presented based on a theorem of analytic continuation. The one-nucleon terms are correlated with the amplitudes of simpler processes.

1. Introduction

In refs. [1-3]) the dispersion relations for reactions of the type ($a+b \to a' + c+d$) have been obtained. For the processes ($N+b \to N'+\gamma+\gamma'$), in which under certain conditions there is no unobservable region, the proof of the dispersion relations has been given in ref. [4]).

In the paper by Kibble [1]) an attempt has been made to derive the dispersion relations in the general case based on a theorem of analytic continuation which is accepted without proof. However, in the derivation of the dispersion relations for an imaginary mass, the author makes an unjustified statement about the analyticity region of expression (6.2). As a result, the arguments about the analytic continuation of the dispersion relations (ref. [1]), section 7) lose their validity.

The present paper gives a consistent analysis of this problem. For definiteness we shall consider the process ($p+\pi \to p'+\pi'+\pi''$). The consideration of other processes of the type ($a+b \to a'+c+d$) is quite analogous. In the following we shall use the notations adopted in [2-4]).

2. Kinematics of the Fictitious Process

Let p and p' be the nucleon four-momenta in the initial and final states, and q, q', q'' the four-momenta of the incoming and outgoing mesons respectively. We adopt the Breit frame for the nucleons

$$\mathbf{p}+\mathbf{p}' = 0. \tag{2.1}$$

In this frame we put (cf. ref. [8]))

$$q'_0 = e^{\xi}\omega, \qquad q''_0 = e^{-\xi}\omega. \tag{2.2}$$

Introduce the vector

$$\Delta = \tfrac{1}{2}(e^{-\xi}q' - e^{\xi}q'') = (0, \boldsymbol{\Delta}), \tag{2.3}$$

$$-\Delta^2 = \boldsymbol{\Delta}^2 \equiv m_\Delta{}^2. \tag{2.4}$$

To study the analytic properties of the amplitude of the process $(p+\pi \to p'+\pi'+\pi'')$ we consider the kinematics of the fictitious process, with the 4-momenta particles defined by the following relations

$$q'^2 = q''^2 = \frac{\tau - m_\Delta{}^2}{\operatorname{ch}^2\xi}, \qquad q^2 = 4(\tau - M_\Delta{}^2), \qquad p^2 = p'^2 = M^2, \tag{2.5}$$

$$M_\Delta{}^2 \equiv \mu^2 \operatorname{ch}^2\xi + m_\Delta{}^2 - \tfrac{1}{4}\mu^2, \tag{2.6}$$

where τ is a certain parameter which will be determined later. For the real process of inelastic scattering $(p+\pi \to p'+\pi'+\pi'')$

$$\tau = \tau_0 \equiv \mu^2 \operatorname{ch}^2\xi + m_\Delta{}^2.$$

Introduce the vector Q in the following way:

$$Q = \tfrac{1}{2}[(1-\eta)e^{-\xi}q' + (1+\eta)e^{\xi}q''], \tag{2.7}$$

where

$$\eta \equiv \left(\frac{\tau}{m_\Delta{}^2} - 1\right) \operatorname{th}\xi. \tag{2.8}$$

It can easily be seen that

$$Q\Delta = -\mathbf{Q}\cdot\boldsymbol{\Delta} = 0, \tag{2.9}$$

$$Q^2 \operatorname{ch}^2\xi = \tau + \frac{\tau^2}{m_\Delta{}^2}\operatorname{sh}^2\xi. \tag{2.10}$$

In the following instead of the vectors q' and q'' we shall make use of the vectors Q and Δ:

$$q' = e^{\xi}[Q + (1+\eta)\Delta], \quad q'' = e^{-\xi}[Q - (1-\eta)\Delta]. \tag{2.11}$$

We assume that the vectors p, q, p', q', q'' are connected by the conservation law

$$p + q = p' + q' + q''. \tag{2.12}$$

From (2.12), after some elementary calculations, we find

$$\tfrac{1}{2}\mathbf{q} = \operatorname{ch}\xi\ \boldsymbol{\lambda}\mathbf{e} + t\boldsymbol{\Delta} - s\mathbf{r}, \qquad \mathbf{Q} = \boldsymbol{\lambda}\mathbf{e} - L\mathbf{r}, \tag{2.13}$$

where

$$m_\Delta{}^2 t = \tau \operatorname{sh}\xi - \tilde{p} m_\Delta \cos\alpha,$$

$$2\tilde{p}s \sin\alpha = M_\Delta{}^2 - \tilde{p}^2 \cos 2\alpha + 2\tilde{p}\frac{\tau}{m_\Delta}\operatorname{sh}\xi \cos\alpha,$$

$$2\tilde{p}L \operatorname{ch}\xi \sin\alpha = M_\Delta{}^2 - \tilde{p}^2 + 2\tilde{p}\frac{\tau}{m_\Delta}\operatorname{sh}\xi\cos\alpha, \tag{2.14}$$

$$\tilde{p} \equiv |\mathbf{p}|, \qquad \tilde{p} m_\Delta \cos\alpha = \mathbf{p}\cdot\boldsymbol{\Delta},$$

$$\lambda^2 = \omega^2 - Q^2 - L^2,$$

and $\mathbf{e}$, $\boldsymbol{\Delta}/m_\Delta$ and $\mathbf{r}$ are mutually orthogonal unit vectors.

For the following we must choose τ in such a way that the expression Q^2+L^2 is negative.

This condition may be written as follows:

$$\mathrm{sh}^2\xi\left(\frac{\tau}{m_\Delta}\right)^2+\left[\frac{M_\Delta{}^2-\tilde{p}^2}{\tilde{p}}\,\mathrm{sh}\xi\cos\alpha+m_\Delta\sin^2\alpha\right]\frac{\tau}{m_\Delta}+\frac{(M_\Delta{}^2-\tilde{p}^2)^2}{4\tilde{p}^2}<0. \quad (2.15)$$

For the existence of an interval of values of τ, for which the inequality (2.15) is fulfilled, it is necessary and sufficient that ($\tilde{p}<M_\Delta$)

$$\begin{aligned}(M_\Delta{}^2-\tilde{p}^2)\ \mathrm{sh}\xi &< 2m_\Delta\tilde{p}\cos^2\tfrac{1}{2}\alpha \quad \text{for} \quad \xi>0,\\ (M_\Delta{}^2-\tilde{p}^2)\ |\mathrm{sh}\xi| &< 2m_\Delta\tilde{p}\sin^2\tfrac{1}{2}\alpha \quad \text{for} \quad \xi<0.\end{aligned} \quad (2.16)$$

The condition (2.15) is fulfilled when τ lies between the zeros of the left-hand side of (2.15)

$$\tau_1<\tau<\tau_2. \quad (2.17)$$

In this case the root $\lambda=\sqrt{\omega^2-Q^2-L^2}$ will be real for any real values of ω.

3. Dispersion Relations for the Fictitious Process

The Fourier-transforms of the retarded and advanced matrix elements of the process ($\mathrm{p}+\pi\to\mathrm{p}'+\pi'+\pi''$) may be written in the form [1,2])

$$\begin{aligned}T^{\mathrm{ret}}(Q,\Delta)&=\iint_{\mathrm{G}}e^{i(Qx+\Delta y)}F^{\mathrm{ret}}(x,y)\mathrm{d}x\mathrm{d}y,\\ T^{\mathrm{adv}}(Q,\Delta)&=\iint_{\mathrm{G}'}e^{i(Qx+\Delta y)}F^{\mathrm{adv}}(x,y)\mathrm{d}x\mathrm{d}y,\end{aligned} \quad (3.1)$$

where the integration regions G and G′ are determined by the inequalities

$$\begin{aligned}\mathrm{G}&: x>0, \quad -(1-\eta)x<y<(1+\eta)x,\\ \mathrm{G}'&: x<0, \quad (1+\eta)x<y<-(1-\eta)x.\end{aligned} \quad (3.2)$$

For the fictitious process considered in the previous paragraph these amplitudes have the form

$$\begin{aligned}&T^{\mathrm{ret}}(\omega,\lambda\mathbf{e},\tau)\\ &=\iint_{\mathrm{G}}\exp\{i(\omega x_0-\sqrt{\omega^2-Q^2-L^2}\,\mathbf{e}\cdot\mathbf{x}-L\mathbf{r}\cdot\mathbf{x}-\boldsymbol{\Delta}\cdot\mathbf{y})\}F^{\mathrm{ret}}(x,y)\mathrm{d}x\mathrm{d}y,\\ &T^{\mathrm{adv}}(\omega,\lambda\mathbf{e},\tau)\\ &=\iint_{\mathrm{G}'}\exp\{i(\omega x_0-\sqrt{\omega^2-Q^2-L^2}\,\mathbf{e}\cdot\mathbf{x}-L\mathbf{r}\cdot\mathbf{x}-\boldsymbol{\Delta}\cdot\mathbf{y})\}F^{\mathrm{adv}}(x,y)\mathrm{d}x\mathrm{d}y.\end{aligned} \quad (3.3)$$

When τ changes in the interval (2.17) †

† In Kibble's paper [1]) it is asserted that expression (6.2) (analogous to expression (3.3) in the present paper) is an analytic function of ω and τ in the region where the inequality

$$\mathrm{Im}\,\omega>|\mathrm{Im}\,\sqrt{\omega^2-\tau}|$$

holds. This assertion is not evident and requires a special investigation since in the above-mentioned region the integral (6.2) may be meaningless. Actually the region of analyticity of expression (6.2) is determined by the inequality $\mathrm{Im}\,\omega>|\,\mathrm{Im}\,\lambda(\omega,\tau)|$.

$$\operatorname{Im}\omega > |\operatorname{Im}\sqrt{\omega^2-Q^2-L^2}| \tag{3.4}$$

and, therefore, the functions † $S_{\pm}T^{\mathrm{ret}}(\omega, \lambda\mathbf{e}, \tau)$ will be analytic in the upper half-plane of the complex variable ω, whereas $S_{\pm}T^{\mathrm{adv}}(\omega, \lambda\mathbf{e}, \tau)$ will be analytic in the lower half-plane.

We shall show that the functions $ST^{\mathrm{ret}}(\omega, \lambda\mathbf{e}, \tau)$ and $ST^{\mathrm{adv}}(\omega, \lambda\mathbf{e}, \tau)$ represent the same analytic function, i.e., that the function

$$ST(\omega, \tau) = \begin{cases} ST^{\mathrm{ret}}(\omega, \lambda\mathbf{e}, \tau), & \operatorname{Im}\omega > 0 \\ ST^{\mathrm{adv}}(\omega, \lambda\mathbf{e}, \tau), & \operatorname{Im}\omega < 0 \end{cases} \tag{3.5}$$

is an analytic function throughout the complex plane ω except for a finite number of points and cuts along the real ω-axis. For this purpose we consider the difference

$$ST^{\mathrm{ret}}(\omega, \lambda\mathbf{e}, \tau) - ST^{\mathrm{adv}}(\omega, \lambda\mathbf{e}, \tau) \equiv 2iSA(\omega, \tau) \tag{3.6}$$

for real values of ω.

Repeating the considerations of ref. [2]), it is easily shown that the poles of the δ-functions included in the expression for the absorptive part will be at the points $\pm\omega_l(n)$:

$$\begin{aligned}
\pm 2\operatorname{ch}\xi\sqrt{M^2+\tilde{p}^2}\,\omega_1(n) &= \mathrm{e}^{-\xi}\operatorname{ch}\xi(M_n^2-M^2)+(1-\operatorname{th}\xi)(m_\Delta^2-\tau) \\
&\quad +M_\Delta^2-\tilde{p}^2-2\mathrm{e}^{-\xi}m_\Delta\tilde{p}\cos\alpha, \\
\pm 2\operatorname{ch}\xi\sqrt{M^2+\tilde{p}^2}\,\omega_2(n) &= \mathrm{e}^{\xi}\operatorname{ch}\xi\,(M_n^2-M^2)+(1+\operatorname{th}\xi)(m_\Delta^2-\tau) \\
&\quad +M_\Delta^2-\tilde{p}^2+2\mathrm{e}^{\xi}m_\Delta\tilde{p}\cos\alpha, \\
\pm 2\operatorname{ch}\xi\sqrt{M^2+\tilde{p}^2}\,\omega_3(n) &= \tfrac{1}{2}(M_n^2-M^2)-2\tau+M_\Delta^2-\tilde{p}^2.
\end{aligned} \tag{3.7}$$

For $M_n = M$ we find six poles, $\pm\omega_1$, $\pm\omega_2$, $\pm\omega_3$, due to the one-nucleon states. The limits of the continuous spectra of the corresponding δ-functions are obtained from (3.7) for $M_n = M+\mu$.

It can be shown that for a certain region of values of ξ, α, $\tilde{p}$, m_Δ, the quantity $\omega_c \equiv \omega_{c_3}$ defined by

$$2\operatorname{ch}\xi\sqrt{M^2+\tilde{p}^2}\,\omega_c = M\mu+\tfrac{1}{2}\mu^2+M_\Delta^2-\tilde{p}^2-2\tau \tag{3.8}$$

is the lower limit of the continuous spectrum, while the poles of the one-nucleon states lie before the continuous spectrum

$$|\omega_l| < \omega_c, \qquad l = 1, 2, 3.$$

Separating the contribution of the one-nucleon states we may write the expression for the absorptive part of the amplitude (3.7) as follows:

† $S_{\pm}$ is the operation of symmetrization or antisymmetrization with respect to the vector $\mathbf{e}$.

$$SA(\omega,\tau)=\pi\sum_{l=1}^{3}\{g_l(\tau)\delta(\omega-\omega_l)-h_l(\tau)\delta(\omega+\omega_l)\}+\mathcal{F}(\omega,\tau), \tag{3.9}$$

where

$$\begin{aligned}
g_1(\tau)&=S\left|e^{-\xi}+\frac{\omega_1}{p_0}\right|V_{q'}(p'',p')D_{qq''}(p,p''),\\
g_2(\tau)&=S\left|e^{\xi}+\frac{\omega_2}{p_0}\right|V_{q''}(p'',p')D_{qq'}(p,p''),\\
g_3(\tau)&=S\left|\frac{1}{2\operatorname{ch}\xi}+\frac{\omega_3}{p_0}\right|D_{-q'q''}(p'',p')V_{q}(p,p''),\\
h_1(\tau)&=S\left|e^{-\xi}+\frac{\omega_1}{p_0}\right|D_{qq''}(p'',p')V_{q'}(p,p''),\\
h_2(\tau)&=S\left|e^{\xi}+\frac{\omega_2}{p_0}\right|D_{qq'}(p'',p')V_{q''}(p,p''),\\
h_3(\tau)&=S\left|\frac{1}{2\operatorname{ch}\xi}+\frac{\omega_3}{p_0}\right|V_{q}(p'',p')D_{-q'q''}(p,p'').
\end{aligned} \tag{3.10}$$

$$(p_0=\sqrt{M^2+\tilde{p}^2}).$$

(Operators V and D are considered in section 5.)

It is now clear that $ST^{\mathrm{ret}}(\omega,\lambda\mathbf{e},\tau)$ and $ST^{\mathrm{adv}}(\omega,\lambda\mathbf{e},\tau)$ actually represent a single analytic function $ST(\omega,\tau)$ (3.5), regular in the region $\operatorname{Im}\omega\neq 0$ with cuts along the real axis at $-\infty<\omega<-\omega_c$ and $\omega_c<\omega<\infty$ and with poles of the first order at the points $\pm\omega_l$.

It has been shown [5]) that functions of the type (3.3) increase at infinity ($|\omega|\to\infty$) no faster than a polynomial. Denote by n the degree of this polynomial. Then, applying the Cauchy theorem to the function

$$\frac{1}{(\omega-\omega_0)^{n+1}}ST(\omega,\tau),\qquad |\omega_0|<\omega_c,\quad \omega_0\neq\pm\omega_l,$$

we obtain

$$\begin{aligned}
&ST(\omega,\tau)\\
&=\frac{1}{\pi}(\omega-\omega_0)^{n+1}\int_{|\omega'|>\omega_c}^{\infty}\frac{\mathcal{F}(\omega'\tau)d\omega'}{(\omega'-\omega_0)^{n+1}(\omega'-\omega)}+\{\prod_l(\omega_l^2-\omega^2)\}^{-1}\mathcal{P}(\omega,\tau)
\end{aligned} \tag{3.11}$$

where $\mathcal{P}(\omega,\tau)$ is a polynomial of degree $n+6$ in ω:

$$\begin{aligned}
&\left\{\prod_{l=1}^{3}(\omega_l^2-\omega^2)\right\}^{-1}\mathcal{P}(\omega,\tau)\\
&=\sum_{l=1}^{3}\left\{\left(\frac{\omega_0-\omega}{\omega_0-\omega_l}\right)^{n+1}\frac{g_l(\tau)}{\omega_l-\omega}+\left(\frac{\omega_0-\omega}{\omega_0+\omega_l}\right)^{n+1}\frac{h_l(\tau)}{\omega_l+\omega}\right\}+\sum_{k=0}^{n}c_k(\omega_0,\tau)\omega^k.
\end{aligned} \tag{3.12}$$

4. Analytic Continuation of the Dispersion Relations

To perform the transition in (3.11) from the values of τ defined by (2.17) to the value $\tau = \tau_0 = \mu^2 \operatorname{ch}^2 \xi + m_\Delta^2$ (the real case), it is necessary to perform an analytic extension throughout a region of the τ-plane. For this purpose we make use of the following theorem †.

Theorem. For real ω, τ and $\lambda(\omega, \tau)$ (see (2.14)) the function $\mathscr{F}(\omega, \tau)$ (defined by expression (3.9)) may be presented in the form

$$\mathscr{F}(\omega, \tau) = \sum_{l=1}^{3} \{F_{l+}(\zeta_{l+}, \tau) + F_{l-}(\zeta_{l-}, \tau)\}, \tag{4.1}$$

where

$$\begin{gathered} \zeta_{l\pm} = \beta_l \tau \pm 2 p_0 \omega \operatorname{ch}\xi, \\ \beta_1 = 1 - \operatorname{th}\xi, \qquad \beta_2 = 1 + \operatorname{th}\xi, \qquad \beta_3 = 2. \end{gathered} \tag{4.2}$$

The functions $F_{l\pm}(\zeta, \tau)$ satisfy the following properties:

a) $F_{l\pm}(\zeta, \tau)$ are generalized integrable functions of the real variable ζ;

b) $F_{l\pm}(\zeta, \tau)$ are analytic functions of the complex variable τ, regular in the region

$$\mathscr{E}: \ \tau_1 < \operatorname{Re} \tau < \tau_0 + \rho\mu^2, \quad |\operatorname{Im} \tau| < \rho\mu^2; \tag{4.3}$$

c) $$F_{l\pm}(\zeta_l, \tau) = 0 \quad \text{if} \quad \zeta_l < \nu_l(2M\mu + \mu^2) + M_\Delta^2 - \tilde{p}^2 + \gamma_l, \tag{4.4}$$

where

$$\begin{gathered} \nu_1 = e^{-\xi} \operatorname{ch}\xi, \qquad \nu_2 = e^{\xi} \operatorname{ch}\xi, \qquad \nu_3 = \tfrac{1}{2}; \\ \gamma_1 = (1 - \operatorname{th}\xi) m_\Delta^2 - 2e^{-\xi} m_\Delta \tilde{p} \cos\alpha, \\ \gamma_2 = (1 + \operatorname{th}\xi) m_\Delta^2 + 2e^{\xi} m_\Delta \tilde{p} \cos\alpha, \qquad \gamma_3 = 0, \qquad \rho > 0. \end{gathered} \tag{4.5}$$

Using the above theorem and substituting (4.1) in (3.11) we obtain

$$\{ST(\omega, \tau) - \mathscr{N}(\omega, \tau)\} \prod_{l=1}^{3} (\omega_l^2 - \omega^2) = \mathscr{P}(\omega, \tau), \tag{4.6}$$

where

$$\begin{aligned} \pi\mathscr{N}(\omega, \tau) = (p_0 \operatorname{ch}\xi)^{n+1} (\omega - \omega_0)^{n+1} \sum_{l=1}^{3} \\ \cdot \left\{ \int_{-\infty}^{\infty} \frac{F_{l+}(\zeta, \tau) d\zeta}{(\zeta - \beta_l \tau + 2 p_0 \omega_0 \operatorname{ch}\xi)^{n+1} (\zeta - \beta_l \tau - 2 p_0 \omega \operatorname{ch}\xi)} \right. \\ \left. + \int_{-\infty}^{\infty} \frac{F_{l-}(\zeta, \tau) d\zeta}{(\zeta - \beta_l \tau + 2 p_0 \omega_0 \operatorname{ch}\xi)^{n+1} (\zeta - \beta_l \tau + 2 p_0 \omega \operatorname{ch}\xi)} \right\}. \end{aligned} \tag{4.7}$$

The function $\mathscr{N}(\omega, \tau)$ is an analytic function of ω and τ in the intersection of the regions $\mathscr{G} \cap \mathscr{E}$, where $\mathscr{E}$ is given by (4.3), and the region $\mathscr{G}$ is defined by the inequality

$$\mathscr{G}: |\operatorname{Im} \tau| < p_0 \operatorname{ch}\xi |\operatorname{Im} \omega|. \tag{4.8}$$

† An analogous theorem is advanced as a hypothesis by Kibble in his paper [1]).

On the other hand, as was shown previously, the function $ST(\omega, \tau)$ is regular in the region

$$\mathscr{D} : |\mathrm{Im}\ \omega| > |\mathrm{Im}\ \lambda(\omega, \tau)|. \tag{4.9}$$

Hence, the function

$$\{ST(\omega, \tau) - \mathscr{N}(\omega, \tau)\} \prod_{l=1}^{3} (\omega_l^2 - \omega^2)$$

is analytic in the intersection $\mathscr{E} \cap \mathscr{G} \cap \mathscr{D}$. But, by (4.6) it is a polynomial in ω for real values of τ limited by the inequality (2.17); hence, it is a polynomial in ω throughout the region of analyticity $\mathscr{E} \cap \mathscr{G} \cap \mathscr{D}$. In other words, the coefficients of the polynomial $\mathscr{P}(\omega, \tau)$ can be extended by analytic continuation throughout a certain region of the τ-plane. We shall show that this region includes the region $\mathscr{E}$.

Take any $\tau_\pm$ in the region $\mathscr{E}$, for which $\mathrm{Im}\ \tau \neq 0$:

$$\begin{gathered} \tau_\pm = \tau_r \pm i\delta, \\ 0 < \delta < \rho\mu^2, \qquad \tau_1 < \tau_r < \mu^2 \operatorname{ch}^2 \xi + m_\Delta^2 + \rho\mu^2. \end{gathered} \tag{4.10}$$

For a given $\tau_\pm$ choose $\omega_\pm$ as follows:

$$\omega_\pm = \omega_r \pm i \frac{b}{c} \omega_r \delta, \tag{4.11}$$

where

$$\begin{aligned} b\operatorname{ch}^2 \xi \sin^2 \alpha &\equiv \frac{\operatorname{sh}^2 \xi}{m_\Delta^2} \tau_r + \tfrac{1}{2} \sin^2 \alpha + \frac{M_\Delta^2 - \tilde{p}^2}{2\tilde{p} m_\Delta} \operatorname{sh}\xi \cos \alpha, \\ c\operatorname{ch}^2 \xi \sin^2 \alpha &\equiv \frac{\operatorname{sh}^2 \xi}{m_\Delta^2} (\tau_r^2 - \delta^2) \\ &\quad + \left(\sin^2 \alpha + \frac{M_\Delta^2 - \tilde{p}^2}{\tilde{p} m_\Delta} \operatorname{sh}\xi \cos \alpha \right) \tau_r + \frac{(M_\Delta^2 - \tilde{p}^2)^2}{4\tilde{p}^2}; \\ c &< \omega_r^2 < b^2 (M^2 + \tilde{p}^2) \operatorname{ch}^2 \xi \dagger. \end{aligned} \tag{4.12}$$

We shall show that upon such a choice of $\omega_\pm$ the points $(\omega_\pm, \tau_\pm)$ belong to the intersection $\mathscr{E} \cap \mathscr{G} \cap \mathscr{D}$. $\tau_\pm$ belong to the region $\mathscr{E}$ by construction. Let us check first that, for example, $(\omega_\pm, \tau_\pm)$ lies in the region $\mathscr{D}$. By (4.9) the region $\mathscr{D}$ is determined by the inequality

$$(\mathrm{Im}\ \omega)^2 > [\mathrm{Im}\ \lambda(\omega, \tau)]^2. \tag{4.13}$$

It is easy to show that the inequality (4.13) holds when and only when

$$\omega_r^2 > c \tag{4.14}$$

which coincides with the first inequality (4.12).

† It can be shown that there exists a certain region of values of the parameters $\xi, \alpha, \tilde{p}, m_\Delta$, in which

$$c < b^2 (M^2 + \tilde{p}^2) \operatorname{ch}^2 \xi,$$

and the one-nucleon poles $\pm\omega_l$ do not lie in the continuous spectrum. As is known, analogous restrictions occur in the proof of the dispersion relations for elastic scattering.

Thus, the point $(\omega_\pm, \tau_\pm)$ belongs to the region $\mathscr{D}$. It may be shown in a similar manner that $(\omega_-, \tau_-) \in \mathscr{D}$. We shall verify that $(\omega_\pm, \tau_\pm) \in \mathscr{G}$. In virtue of (4.8) this denotes that

$$c < p_0 \operatorname{ch}\xi \, b\omega_r. \tag{4.15}$$

Taking into account (4.14), the inequality (4.15) may be replaced by a stronger inequality

$$\omega_r < bp_0 \operatorname{ch}\xi$$

which is identical to the second inequality (4.12).

Thus, we have shown that the points $(\omega_\pm, \tau_\pm) \in \mathscr{E} \cap \mathscr{G} \cap \mathscr{D}$. It follows hence that the coefficients of the polynomial $\mathscr{P}(\omega, \tau)$ are analytic with respect to τ throughout the region $\mathscr{E}$ with a possible cut along the real axis τ. We shall show that such a cut does not in fact exist. Owing to (4.7)

$$\lim_{\delta \to 0} \mathscr{N}(\omega_\pm, \tau_\pm) = \lim_{\varepsilon \to 0} \mathscr{N}(\omega_r \pm i\varepsilon, \tau_r). \tag{4.16}$$

Using (4.7) and (4.16) we obtain

$$\lim_{\delta \to +0} [\mathscr{N}(\omega_+, \tau_+) - \mathscr{N}(\omega_-, \tau_-)] = 2i \sum_{l=1}^{3} \{F_{l+}(\beta_l \tau_r + 2p_0 \omega_r \operatorname{ch}\xi, \ \tau_r) + F_{l-}(\beta_l \tau_r - 2p_0 \omega_r \operatorname{ch}\xi, \ \tau_r)\} = 2i\mathscr{F}(\omega_r, \tau_r). \tag{4.17}$$

On the other hand since $(\omega_\pm, \tau_\pm) \in \mathscr{D}$, then on the basis of (3.3) we have

$$\lim_{\delta \to +0} [ST(\omega_+, \tau_+) - ST(\omega_-, \tau_-)] = ST^{\mathrm{ret}}(\omega_r, \tau_r) - ST^{\mathrm{adv}}(\omega_r, \tau_r) = 2i\mathscr{F}(\omega_r, \tau_r). \tag{4.18}$$

Combining (4.17) and (4.18) we obtain

$$\lim_{\delta \to +0} \{ST(\omega_+, \tau_+) - \mathscr{N}(\omega_+, \tau_+)\} = \lim_{\delta \to +0} \{ST(\omega_-, \tau_-) - \mathscr{N}(\omega_-, \tau_-)\}.$$

It follows hence that

$$\lim_{\delta \to +0} \mathscr{P}(\omega_r, \tau_+) = \lim_{\delta \to +0} \mathscr{P}(\omega_r, \tau_-), \tag{4.19}$$

i.e., there is no cut along the real axis τ and, therefore, $\mathscr{P}(\omega, \tau)$ is an analytic function of τ throughout the region $\mathscr{E}$.

It was established earlier that the function $\mathscr{N}(\omega, \tau)$ is analytic in the region $\mathscr{E} \cap \mathscr{G}$. We have now shown that the entire right-hand side of (3.11) is also an analytic function in this region. This means that we may extend the region of definition of the function $ST(\omega, \tau)$ so as to coincide with the right-hand side of (3.11) throughout the region $\mathscr{E} \cap \mathscr{G}$. This region also contains the value $\tau = \tau_0 (= \mu^2 \operatorname{ch}^2 \xi + m_\Delta^2)$ corresponding to the real process $(\mathrm{p} + \pi \to \mathrm{p}' + \pi' + \pi'')$ and, hence, the dispersion relations (3.11) are also valid at $\tau = \tau_0$. Defining (as usual) the Hermitian part of the amplitude by the equality

$$D(\omega) = \tfrac{1}{2}(T^{\mathrm{ret}}(\omega)+T^{\mathrm{adv}}(\omega)) \tag{4.20}$$

and taking into account that

$$\lim_{\varepsilon\to+0} ST(\omega\pm i\varepsilon, \tau) = \overset{\mathrm{ret}}{ST}{}^{\mathrm{adv}}(\omega, \tau) \tag{4.21}$$

we obtain the dispersion relations

$$SD(\omega) = \frac{(\omega-\omega_0)^{n+1}}{\pi}\mathrm{P}\int\frac{SA(\omega')\mathrm{d}\omega'}{(\omega'-\omega_0)^{n+1}(\omega'-\omega)} + \left\{\prod_{l=1}^{3}(\omega_l{}^2-\omega^2)\right\}^{-1}\mathscr{P}(\omega, \tau_0),$$
$$(\mathrm{Im}\,\omega = 0). \tag{4.22}$$

5. Analysis of the One-Nucleon Terms

In this section the coefficients $g_1(\tau_0)$, $g_2(\tau_0)$, $h_1(\tau_0)$, $h_2(\tau_0)$ of the expansion (3.9) will be related to the elastic scattering amplitudes. With this purpose we investigate the analytical properties of the vertex parts $V_{\varrho'}(p'', p')$, $V_{\varrho''}(p'', p')$, $V_{\varrho'}(p, p'')$, $V_{\varrho''}(p, p'')$ and the operators $D_{\varrho\varrho''}(p, p'')$, $D_{\varrho\varrho'}(p, p'')$ $D_{\varrho\varrho''}(p'', p')$, $D_{\varrho\varrho'}(p'', p')$.

Since the different vertex parts mentioned above are all investigated in similar manner, we restrict ourselves to only one of them, e.g.

$$V_{\varrho'}(p, p'') \equiv \langle p''|j_{\rho'}(0)|p\rangle. \tag{5.1}$$

According to (3.9) and (3.10)

$$p'' = p-q', \quad \omega = -\omega_1, \tag{5.2}$$

where

$$2\,p_0\omega_1\,\mathrm{ch}\xi = (1-\mathrm{th}\,\xi)(m_\Delta{}^2-\tau)+M_\Delta{}^2-\tilde{p}^2-2\mathrm{e}^{-\xi}m_\Delta\tilde{p}\cos\alpha. \tag{5.3}$$

Since at $\tau_1 < \tau < \tau_2$ the four-vector p'' is real, and $p''_0 > 0$, it can be considered as the four-momentum of a real nucleon, and therefore,

$$V_{\varrho'}(p, p'') = \frac{1}{(2\pi)^{\frac{3}{2}}}\bar{u}(p'')t^{\mathrm{ret}}(p''), \tag{5.4}$$

where

$$t^{\mathrm{ret}}(p'') = \int\left\langle 0\left|\frac{\delta j_{\rho'}(0)}{\delta\bar{\psi}(x)}\right|p\right\rangle \mathrm{e}^{ip''x}\mathrm{d}x. \tag{5.5}$$

In addition to the retarded amplitude (5.5) we shall need the advanced amplitude

$$t^{\mathrm{adv}}(p'') \equiv \int\left\langle 0\left|\frac{\delta\mathscr{J}(x)}{\delta\varphi_{\rho'}(0)}\right|p\right\rangle \mathrm{e}^{ip''x}\mathrm{d}x, \tag{5.6}$$

where $\mathscr{J}(x)$ is the fermion current:

$$\mathscr{J}(x) = i\frac{\delta S}{\delta\bar{\psi}(x)}\overset{+}{S}, \qquad \bar{\mathscr{J}}(x) = i\frac{\delta S}{\delta\psi(x)}\overset{+}{S} \tag{5.7}$$

(the variational derivative with respect to $\bar{\psi}(x)$ is taken on the left, and with respect to $\psi(x)$ on the right).

Using

$$\frac{\delta j_{\rho'}(0)}{\delta\bar{\psi}(x)} - \frac{\delta \mathcal{J}(x)}{\delta\psi_{\rho'}(0)} = i[j_{\rho'}(0), \mathcal{J}(x)],$$

it is easy to show that

$$t^{\mathrm{ret}}(p'') = t^{\mathrm{adv}}(p''), \tag{5.8}$$

if

$$\alpha_1 \equiv p_0 - 3\mu < p''_0 < M+\mu \equiv \alpha_2. \tag{5.9}$$

Further we shall make use of the following theorem of N. N. Bogolubov *et al.* [6,7]).

Let the generalized functions $\mathcal{F}^{\mathrm{ret}}(x)$ and $\mathcal{F}^{\mathrm{adv}}(x)$ possess the properties

$$\mathcal{F}^{\mathrm{ret}}(x) = 0 \quad \text{if} \quad x \lesseqgtr 0$$
$$\mathcal{F}^{\mathrm{adv}}(x) = 0 \quad \text{if} \quad x \gtreqless 0,$$

while their Fourier-transforms $\tilde{\mathcal{F}}^{\mathrm{ret}}(p)$ and $\tilde{\mathcal{F}}^{\mathrm{adv}}(p)$ coincide for real values of p, for which

$$\alpha_1 < p_0 < \alpha_2.$$

Then, there exists a function $\tilde{\Phi}(p)$ of the complex four-vector p, analytic in the region

$$|\mathrm{Im}\ \mathbf{p}| < |\mathrm{Im}\ \sqrt{(p_0-\alpha_1)(p_0-\alpha_2)}| \tag{5.10}$$

such that at real p, for which $\alpha_1 < p_0 < \alpha_2$,

$$\tilde{\Phi}(p) = \tilde{\mathcal{F}}^{\mathrm{ret}}(p) = \tilde{\mathcal{F}}^{\mathrm{adv}}(p).$$

Inequality (5.10), applied to the vector p'', may be written in the form

$$e^{\xi}|\mathrm{Im}\ \lambda(\omega,\tau)| < |\mathrm{Im}\sqrt{(p_0+e^{\xi}\omega_1-M-\mu)(e^{\xi}\omega_1+3\mu)}|.$$

At $\tau = \tau_0$ this inequality assumes the form

$$e^{2\xi}(Q^2+L^2) < 3\mu(M+\mu-p_0)+e^{\xi}(M-2\mu-p_0)\omega_1. \tag{5.11}$$

It is easy to verify that (5.11) actually holds under the corresponding restrictions on the parameters ξ, α, m_Δ and $\tilde{p}$ compatible with those imposed earlier (cf. footnote to formula (4.12)). Therefore, the function $t^{\mathrm{ret}}(p'')$ may be analytically extended with respect to τ up to $\tau = \tau_0$. Due to relativistic invariance the operator $V_{\sigma'}(p, p'')$ is of the form

$$V_{\sigma'}(p, p'') = \frac{1}{(2\pi)^{\frac{3}{2}}}\bar{u}(p'')\gamma_5\tau_{\rho'}g(q'^2)u(p), \qquad q'^2\mathrm{ch}^2\xi = \tau - m_\Delta^2. \tag{5.12}$$

Comparing (5.4) with (5.12), we find

$$t^{\mathrm{ret}}(p'') = \gamma_5\tau_{\rho'}g(q'^2)u(p). \tag{5.13}$$

Since we have shown that the left-hand side of (5.13) can be analytically extended to $\tau = \tau_0$, it follows hence that the function $g(q'^2)$ can also be analytically extended to $\tau = \tau_0$. In view of the hermiticity of the current $j_{\rho'}$, the function $g(q'^2)$ is real for $\tau_1 < \tau < \tau_2$; hence, it will also be real at $\tau = \tau_0$. The quantity $g(\mu^2)$ can be identified with the meson charge g (see Bogolubov *et al.* [6]).

Let us now investigate the analytical properties of the operators D. Consider, for example, the operator:

$$D_{\rho\rho''}(p'', p') = \int e^{\frac{1}{2}i(q+q'')x} \left\langle p' \left| \frac{\delta j_\rho(-\frac{1}{2}x)}{\delta\varphi_{\rho''}(\frac{1}{2}x)} + \frac{\delta j_{\rho''}(\frac{1}{2}x)}{\delta\varphi_\rho(-\frac{1}{2}x)} \right| p'' \right\rangle dx. \quad (5.14)$$

The momenta p', p'' are determined by the conservation law (2.12) and the relation (5.2).

Expression (5.14) is formally identical with the Hermitian part of the amplitude of the process ($p''+\pi \to p'+\pi''$). On considerations of relativistic invariance it can be written in the form

$$D_{\rho\rho''}(p'', p') = \sum_s \bar{u}(p') R_s u(p'') \operatorname{Re} \Omega^s(\nu, \nu_1), \quad (5.15)$$

where

$$\nu = \tfrac{1}{2}(p'+p'')q'', \qquad \nu_2 = -(\tfrac{1}{2}(q''-q))^2$$

In our case the momenta p'', p', q', q'' are connected not only by the conservation law

$$p''+q = q''+p'$$

but by relation (2.12) as well. Hence,

$$\begin{aligned} \nu &= -e^{\xi} p_0 \omega_1 - \frac{m_\Delta^2 + \tau \operatorname{ch} 2\xi}{2 \operatorname{ch}^2 \xi}, \\ 2\nu_1 \operatorname{ch}\xi &= \frac{m_\Delta^2 - \tau}{2 \operatorname{ch} \xi} + e^{\xi}(\operatorname{ch}^2 \xi - \tfrac{1}{4})\mu^2 + (e^{\frac{1}{2}\xi}\Delta - e^{-\frac{1}{2}\xi}\mathbf{p})^2. \end{aligned} \quad (5.16)$$

It is evident that $\nu_1(\tau) > \nu_1(\tau_0)$ where

$$2\nu_1(\tau_0) \operatorname{ch} \xi = \tfrac{1}{4}e^{3\xi}\mu^2 + (e^{\frac{1}{2}\xi}\Delta - e^{-\frac{1}{2}\xi}\mathbf{p})^2 > 0. \quad (5.17)$$

The dispersion relations for the elastic scattering process connect $\operatorname{Re} \Omega^s(\nu, \nu_1)$ with $\operatorname{Im} \Omega^s(\nu, \nu_1)$. Usually these dispersion relations are written in the frame in which

$$\mathbf{p}'_c + \mathbf{p}''_c = 0. \quad (5.18)$$

In this frame the invariants ν and ν_1 have the following significance:

$$\nu_1 = \mathbf{p}_c'^2, \qquad \nu = p'_{c0} E, \quad (5.19)$$

where $E = q_{c0} = q''_{c0}$ is the meson energy in the system (5.18).

It can be seen from formulas (5.16) and (5.19) that the quantity $\mathbf{p}_c'^2$

is positive for all $\tau \leqq \tau_0$. Hence, it can be concluded that D may be analytically extended up to $\tau = \tau_0$. But since at $\tau = \tau_0$ the quantity E lies below the threshold of the elastic process it should be calculated in terms of the dispersion integral.

In conclusion we wish to thank N. N. Bogolubov and V. S. Vladimirov for valuable discussions.

References

1) T. W. Kibble, Proc. Roy. Soc. **244** (1958) 355
2) A. A. Logunov and A. N. Tavkhelidze, Nuclear Physics **8** (1958) 374
3) A. A. Logunov and A. N. Tavkhelidze, Nuovo Cimento **10** (1958) 943
4) A. A. Logunov, S. M. Bilenky and A. N. Tavkhelidze, Nuovo Cimento **10** (1958) 953
5) N. N. Bogolubov and V. S. Vladimirov, Nauchniye Dokl. Vysshei Shkoly (in print)
6) N. N. Bogolubov, B. M. Medvedev and M. K. Polivanov, Problems related to the theory of dispersion relations (Moscow, 1958) pp. 106, 198
7) N. N. Bogolubov and V. S. Vladimirov, Izvestiya Akad. Nauk SSSR, ser. mat. **22** (1958) 15
8) J. C. Polkinghorne, Nuovo Cimento **4** (1956) 216

3.A *Nuclear Physics* **10** (1959) 564—570; © *North-Holland Publishing Co., Amsterdam*
Not to be reproduced by photoprint or microfilm without written permission from the publisher

INVESTIGATION OF THE 16.1 MeV EXCITATION LEVEL OF C^{12}

L. KESZTHELYI and I. FODOR
Central Research Institute for Physics, Budapest

Received 16 January 1959

Abstract: The radiation width for the transition to the ground state of the 16.1 MeV excitation level of C^{12} was determined by measuring the resonant absorption of γ-rays. The level width was found to be 7.5 ± 1.9 eV. The square of the matrix element for E2 transition, expressed in Weisskopf units, is 2.17 ± 0.55.

1. Introduction

It was shown recently by P. B. Schmidt and P. M. Endt that the cross section for resonance absorption of γ-quanta resulting from proton capture can be determined by absorption measurements of the γ-quanta as a function of the angle α at which the γ-rays are emitted with respect to the direction of motion of the bombarding protons [1, 2]). The compound nucleus proceeds in the direction of the bombarding protons, and owing to the Doppler effect the energy of the γ-radiation emitted in the reaction varies proportional to $\cos \alpha$. Thus, the difference between the energy E_γ of the γ-radiation and that of the excitation level, due to the recoil of the nuclei, can be compensated for. From absorption measurements one can determine by rather simple methods the ratio $\Gamma_{\gamma_0}/\Gamma_t$ of the width of the γ-transition level to the ground state to that of the total level for proton capture. By means of some additional data both Γ_{γ_0} and Γ_t can also be determined separately [1]).

In the present paper we attempt to show that the method described for the determination of Γ_{γ_0} may be simplified if Γ_t is known. This last quantity may be determined by measurements of the resonance parameters of (p, γ) reactions by means of an analysed proton beam. In our measurements the radiation width for the 16.1 MeV energy γ-radiation of the 16.1 MeV excitation level of C^{12} was determined.

Resonance of the nuclear reaction B^{11}(p, γ)C^{12} at 163 keV proton energy leads to the 16.1 MeV excitation level of C^{12} [3]). The total resonance width is $\Gamma_t = 5.3 \pm 1$ keV [4]). The excited state decays by emitting γ-quanta and α-particles. The γ-decay may be to the ground state by emission of 16.1 MeV energy γ-rays or by emission of 11.67 MeV and 4.43 MeV energy γ-quanta in cascade. Spin and parity assigned to the 16.1 MeV energy level are 2^+. Thus the 16.1 MeV γ-radiation is of E2 type. One obtains $\Gamma_{\gamma_0}/\Gamma_t \approx 10^{-3}$ from the relative cross sections for α-emission and γ-radiation [5]).

2. Measurements

The energy increment in 16.1 MeV energy γ-radiation due to the Doppler effect as a function of angle α is shown in fig. 1. The angle at which resonance occurs is calculated at 21° 30′. It can be seen from the figure that the 15°

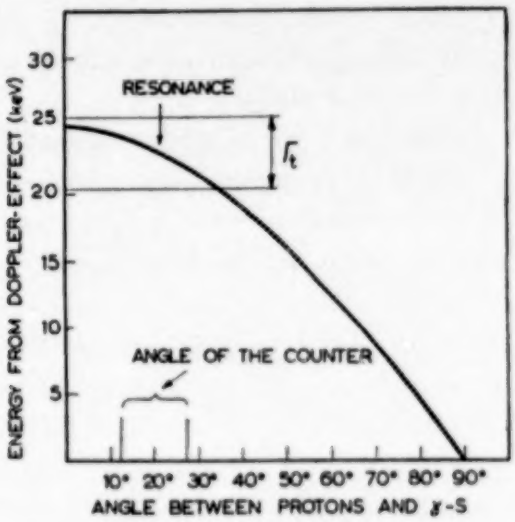

Fig. 1. The energy increment of γ-rays due to Doppler effect as a function of the angle between the direction of motion of the protons and that of the γ-rays. The half width of the resonance curve and the angular region measured by the measuring counter are shown in the figure.

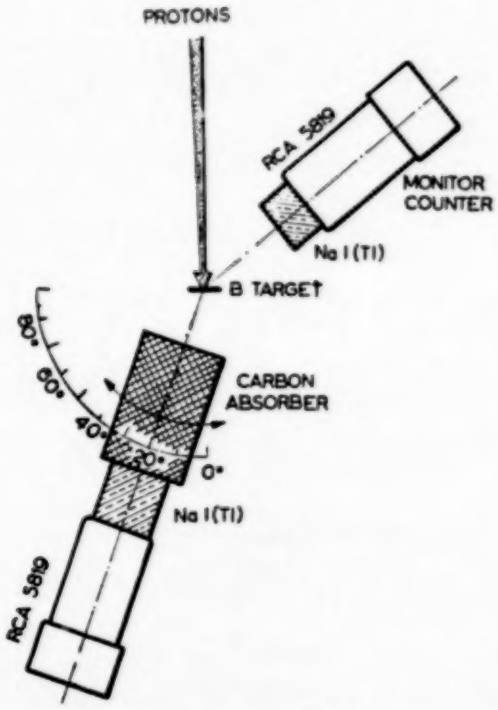

Fig. 2. Scheme of the measuring arrangement.

aperture angle of the detector used in our measurements is comparable to the half width of resonance. In the 0°—90° angular region only one half of the resonance absorption curve can be measured.

The measuring arrangement is shown schematically in fig. 2. A natural boron target was bombarded in a Cockcroft-Walton generator by means of a 300—400 μA unanalysed proton beam accelerated to 170 keV. At such low energy no other disturbing reactions occur.

An $1\frac{3}{4}$ in. $\times$ 2 in. NaI(Tl) crystal mounted on a RCA 5819 photomultiplier was used as a measuring counter while a $1\frac{1}{2}$ in. $\times$ 1 in. NaI(Tl) scintillation crystal mounted on a RCA 5819 photomultiplier served as a monitor counter. We applied a 10 cm long graphite cylinder as absorber and for comparison we used also an alternative absorber consisting of boron compressed in a thin-walled Al cylinder. In view of the large angular region — to avoid the error caused by the variations in the γ-intensity due to anisotropic angular distribution of the γ-radiation and to target absorption — relative measurements were carried out, i.e. the number of counts was recorded both for absorbers C and B and in a second run with absorber C and without absorber.

The integral pulse spectrum as measured by the measuring counter is plotted in fig. 3. At energies higher than 13.5 MeV, only pulses resulting from

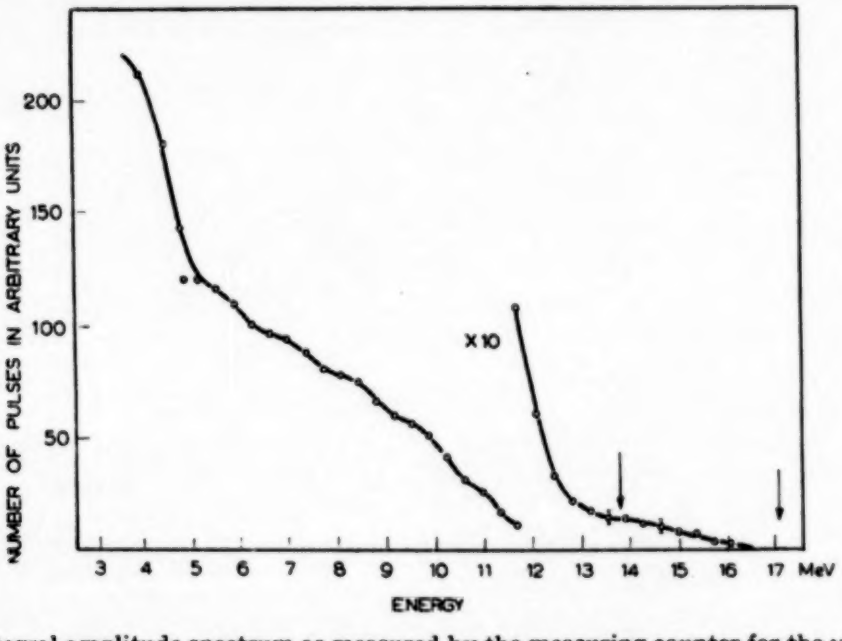

Fig. 3. Integral amplitude spectrum as measured by the measuring counter for the γ-radiation in the reaction $B^{11}(p, \gamma)\, C^{12}$.

16.1 MeV γ-radiation were accepted by the measuring counter. (In our arrangement the counts of pulses resulting from the simultaneous absorption of 11.67 and 4.43 MeV radiations amounted to less than 1.3 % of the

total number of counts in this region.) By the discriminator only pulses between 13.5 and 17 MeV (the region marked by arrows in fig. 3) were transmitted to the counter unit. Omitting pulses higher than 17 MeV, the background effect due to cosmic radiation was reduced by a factor of 3. On the average the counting rate for 16.1 MeV radiation was found to be about 1 count/s and that for background 0.082 ± 0.0013 count/s. The setting of the discriminator was checked approximately every hour during the measurement. The monitor counter monitored the 11.67 MeV γ-radiation. The number of pulses counted by the latter was higher by two orders of magnitude than that accepted by the measuring counter.

Results of the first set of measurements are shown in fig. 4. The ratio of

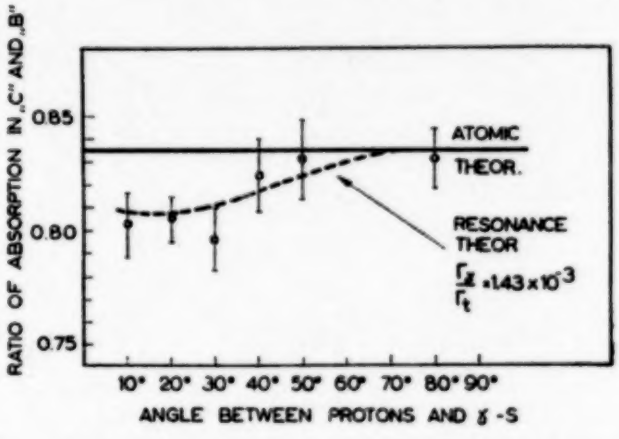

Fig. 4. The dependence of the ratio $R = \exp(-\mu_C x_C)/\exp(-\mu_{Ba} x_B)$ on the angle between the direction of motion of the protons and that of the γ-rays.

pulses counted with absorbers C and B, respectively, gives $R = \exp(-\mu_C x_C)/\exp(-\mu_{Ba} x_B)$, where x_C and x_B are absorber thicknesses of C and B, respectively. Absorption coefficient μ_C corresponding to C is composed of two parts: (1) atomic absorption coefficient μ_{Ca} which is independent of angle and (2) resonance absorption coefficient μ_{Cr} dependent on the angle of absorption. μ_{Ba} is the atomic absorption coefficient for boron. Upon extrapolating the values of μ_{Ca} and μ_{Ba} indicated in the table of ref. [6]) we obtain $R = 0.835$. The influence of the resonant absorption coefficient μ_{Cr} in the corresponding angular region is clearly shown by the result of our measurement (fig. 4).

In the second run pulses were counted with much higher accuracy at 20° and 80° without absorber as well as with absorber C. This measurement gives the value of the transmission $T = \exp(-\mu_C x_C)$; we found at 20° $T = 0.7435 \pm 0.00435$ and at 80° $T = 0.763 \pm 0.0044$. The value of μ_C was also computed and was found to be

$$\mu_C(20°) = 0.01807 \pm 0.00035 \text{ cm}^2/\text{g},$$
$$\mu_C(80°) = 0.0165 \pm 0.00035 \text{ cm}^2/\text{g}.$$

The value of $\mu_C(80°)$ is in agreement with the theoretical value of the atomic absorption coefficient 0.0165 cm²/g, i.e. the theoretical value is verified to an accuracy of 2 %. The absorption coefficient of unambiguously nuclear origin at 20° was evaluated as $\mu_{Cr}(20°) = 0.00157 \pm 0.00049$ cm²/g.

3. Discussion

In the present case the ratio $\Gamma_{\gamma_0}/\Gamma_t$ cannot be computed from the data of measurements on the basis of the absorption integral as indicated in ref. [1]). In our calculations the transmission resulting from the nuclear effect at energy $E' = E_\gamma + E_{Doppl}$ will be denoted by $T(E')$. It is obtained readily as

$$T(E') = \frac{2}{\pi\Gamma_t}\int_{-\infty}^{+\infty} \exp\left[-\sigma_0 N x \frac{1}{\left(\frac{E-E_0}{\frac{1}{2}\Gamma_t}\right)^2+1}\right] \cdot \frac{1}{\left(\frac{E-E'}{\frac{1}{2}\Gamma_t}\right)^2+1} \mathrm{d}E, \quad (1)$$

where N is the number of C atoms per gram, x the absorber thickness in g/cm²,

$$\sigma(E) = g\frac{\lambda^2}{2\pi}\frac{\Gamma_{\gamma_0}}{\Gamma_t}\frac{1}{\left(\frac{E-E_0}{\frac{1}{2}\Gamma_t}\right)^2+1} = \sigma_0 \frac{1}{\left(\frac{E-E_0}{\frac{1}{2}\Gamma_t}\right)^2+1}$$

is the cross section for resonance scattering, g the statistical factor, λ the wave-length of the γ-radiation and E_0 the resonance energy, while

$$f(E-E') = \frac{2}{\pi\Gamma_t}\frac{1}{\left(\frac{E-E'}{\frac{1}{2}\Gamma_t}\right)^2+1}$$

is the energy distribution of γ-rays at energy E' normalized to unity. The latter factor accounts for the fact that by proton capture at various points of resonance, γ-quanta with various energies are produced. The distribution is expressed by the Breit-Wigner formula for the variation in proton resonance cross section. The broadening of the resonance level due to thermal motion ($\approx$ 50 eV) may be neglected as compared to Γ_t.

Using the symbol

$$\sigma_0 N x = a$$

and substituting

$$\frac{E-E_0}{\frac{1}{2}\Gamma_t} = x, \quad \frac{E-E'}{\frac{1}{2}\Gamma_t} = x-s,$$

upon expanding the exponential factor, eq. (1) becomes

$$T(E')=\frac{1}{\pi}\int_{-\infty}^{+\infty}\left[\frac{1}{(x-s)^2+1}-a\frac{1}{(x^2+1)[(x-s)^2+1]}\right.$$
$$\left.+\frac{a^2}{2!}\frac{1}{(x^2+1)[(x-s)^2+1]}-\ldots\right]ds.$$

If we neglect in a all terms of higher than second order, the error will not exceed 1.5 % for $\Gamma_{\gamma^0}/\Gamma_t \approx 10^{-3}$. By integration we obtain

$$T(E') = 1-\frac{2a}{s^2+4}. \tag{2}$$

The measuring counter always responds to a given interval of energy E', i.e. to a corresponding angular region. The transmission to a given angular region α_1, α_2 is given by substituting the appropriate angle into eq. (2) and integrating, as follows:

$$T(\alpha_1,\alpha_2) = 1-\frac{ab\ \mathrm{arctg}\left\{\frac{(b^2+d^2+2d+1)\mathrm{tg}^2\frac{1}{2}\alpha+(b^2+d^2-1)}{2b}\right\}\Big|_{\alpha_1}^{\alpha_2}}{2(-\cos\alpha)} \tag{3}$$

where $b = \Gamma_t c/E_\gamma V$, $d = E_\gamma c/Mc^2V$. (M and V are the mass and velocity of the compound nucleus, respectively; c is the velocity of light.) By multiplying $T(\alpha_1, \alpha_2)$ with the transmission due to atomic absorption, it can be compared with experimental results. Making use of data obtained in both sets of measurements a was evaluated as 0.056 ± 0.014. From this $\Gamma_{\gamma^0}/\Gamma_t = (1.43\pm0.36)\times10^{-3}$ and the width of the level for 16.1 MeV energy γ-emission $\Gamma_{\gamma^0} = 7.6\pm1.9$ eV. The half life for the emission of γ-rays is obtained as $\tau = (8.8\pm2.2)\times10^{-17}$ sec. The error indicated here is of statistical origin with an additional uncertainty of 20 % in the value of Γ_t due to uncertainties in measurements of the energy of the bombarding protons and the thickness of the target.

The 16.1 MeV γ-radiation is an E2 radiation. From the measured value of Γ_{γ^0} the square of the transition matrix element is evaluated as $|M|^2 = 2.17\pm0.55$ in Weisskopf units. According to Wilkinson's estimations [7]) this value seems the most probable in E2 transitions occurring with light nuclei and it shows that even in the case of light nuclei considerable collective effects are involved in E2 transitions.

By means of the branching ratio of 16.1 MeV and 11.67 MeV energy radiations also Γ_γ(11.67 MeV) may be determined from Γ_{γ^0}, it is Γ_γ(11.67 MeV) $= 152\pm45$ eV.

The square of the matrix element of M1 transitions is obtained as $|M|^2 = 4.5\pm1.3$ in Weisskopf units.

In a comprehensive paper by Ajzenberg and Lauritsen [3]) the following values are given: $\Gamma_{\gamma^0} \leqq 3$ eV and Γ_γ(11.67 MeV) = 70 eV. They are based

on estimates of Beckmann *et al.* [5]). In their calculations the basis of estimation was the effective cross section for the nuclear reaction $B^{11}(p, \alpha)C^{12}$, the value of which was taken by the authors from measurements disagreeing in their results by a factor of 2 [8,9]). Besides, it is not quite apparent from these papers what proportion of the lower energy α-group is due to the very broad resonance level at 0.67 MeV. Consequently the discrepancy between our result of 7.6 eV and the 3 eV estimated by the above authors is probably to be attributed to the uncertainty in the value of the cross section for (p, α) reaction.

We have to thank our colleague Mr. Gy. Schmidt for his help in carrying out the measurements.

References

1) P. B. Schmidt and P. M. Endt, Phys. Rev. **110** (1958) 397
2) P. B. Schmidt and P. M. Endt, Phys. Rev. **110** (1958) 1442
3) F. Ajzenberg and T. Lauritsen, Revs. Mod. Phys. **27** (1955) 77
4) R. Tangen Kgl. Norske Videnskab. Selskabs Skrifter (1946)
5) O. Beckmann, T. Huus and C. Zupančić, Phys. Rev. **91** (1953) 606
6) C. M. Davisson, in Beta and gamma-ray spectroscopy, edited by K. Siegbahn (North-Holland Publishing Company, Amsterdam, 1955) p. 857
7) D. H. Wilkinson, in Proceedings of the Rehovoth Conference on nuclear structure, edited by H. J. Lipkin (North-Holland Publishing Company, Amsterdam 1958) p. 175
8) J. D. Cockcroft and W. B. Lewis, Proc. Roy. Soc. **154** (1936) 246
9) H. H. Williams, W. H. Wells, J. T. Tate and E. L. Hill, Phys. Rev. **51** (1937) 434

2.E *Nuclear Physics* **10** (1959) 571—582; © *North-Holland Publishing Co., Amsterdam*
Not to be reproduced by photoprint or microfilm without written permission from the publisher

CLASSICAL AND QUANTAL FLUX IN THE OPTICAL MODEL

R. M. EISBERG, I. E. McCARTHY and R. A. SPURRIER
School of Physics, University of Minnesota, Minneapolis, Minnesota

Received 8 December 1958

Abstract: In a semi-classical theory, direct interactions are described by two-body collisions at points in the nucleus. To describe the initial conditions for the collision we need to know the momentum of the incident particle, the probability of finding it at the collision point, and the probability of a collision occurring. These were calculated first by describing the particles by classical rays which can be refracted and absorbed by an optical potential. In the process of making these calculations it was found that the transmission coefficients for a particle following a given ray through the nucleus were not always in agreement with transmission coefficients calculated by quantum mechanics for the corresponding partial wave. To investigate this point the average flux and its divergence were calculated from the classical ray picture. The values of these quantities were found to be close to those of corresponding quantities calculated by quantum mechanics in the same potential where they are significantly large, but large differences were found where the flux and divergence are small. We conclude that the probability of a particle appearing at a point in the nucleus is, in general, not uniquely connected with the corresponding probability of finding it at a point outside, as is implied by a ray calculation. That is, the disturbance at any interior point is influenced by several partial waves. However, a classical flux calculation is sufficiently accurate to be useful in certain applications.

1. Introduction

In the theory of direct interactions there is a general feeling that it makes sense to speak of the momentum of particles which are localized to some extent in the nucleus. In the absence of an adequate many-body theory a semi-classical approach has often been used for such a description. In such an approach the reaction is described by a localized two-body collision, and it is necessary to know the following properties of the incident particle and the nucleus at the collision point:

(1) the momentum of the incident particle,
(2) the probability of the incident particle being located at the point,
(3) the probability of the collision occurring at the point.

The earlier calculations estimate the first two properties from the path of a classical ray in a square well potential. There is a question as to the region of the nucleus in which collisions which would lead to a direct interaction occur. Hayakawa, Kawai and Kikuchi [1]) assumed that collisions were distributed throughout the potential. Elton and Gomes [2]) showed that if a collision occurred inside the nuclear potential the reaction products were

almost certain to be totally internally reflected at the boundary. Their model of a collision in the classically forbidden region obtained quite good agreement with the inelastic (p, p′) scattering data [3]).

Recently Oda and Harada [4]) have obtained better results assuming a Thomas-Fermi gas model in a rounded well for the struck particles and using the same assumptions as Elton and Gomes for the incident particle.

The transition region for the optical potential is known to be large [5]), and therefore the inside and outside regions are not well defined. The first step in clarifying this point is to calculate the above three quantities in the optical model potnential. In the following sections we shall exhibit classical and quantal calculations of the three quantities in the optical model potential which will shed some light on the validity and meaning of the classical theory of the motion of particles in the nucleus.

2. Classical Ray Calculation

The obvious extension of the classical ray calculation in a square well is to calculate the trajectory of a particle in a real potential which gives the same trajectory as the complex optical potential. The ray is attenuated along its path and a calculation of this attenuation will enable us to find the probability of finding a particle at any point on the ray. Such a calculation has been concurrently suggested by Butler, Austern and Pearson [6]).

Consider a point in the complex optical model potential. We shall assume that the local wave number k and mean free path L are the same as those for a plane wave in an infinite uniform potential whose real and imaginary parts V_c and W_c are the same as the local values in the optical model. Trajectories are calculated by integrating (numerically) the classical equations of motion of particles moving through an equivalent real potential V' which is defined to be the one which would at each point give the same wave number k as would be evaluated for the complex potential:

$$\begin{aligned} V' &= -\tfrac{1}{2}\{[(E-V_c)^2+W_c^2]^{\frac{1}{2}}-E-V_c\}, \\ 1/L &= \frac{2}{\hbar}\{m(V_c-E+[(E-V_c)^2+W_c^2]^{\frac{1}{2}})\}^{\frac{1}{2}}, \end{aligned} \tag{1}$$

where E, m are the energy and mass of the incident particle respectively. The optical model potential is $(V+iW)f$ where

$$f = \{1+\exp[(r-R)/a]\}^{-1}. \tag{2}$$

Let the probability of finding a particle on a trajectory before entering the nucleus be unity. Then the probability of finding it at a point x, where x is the coordinate along the trajectory measured from some starting point outside the potential is evaluated by integrating the absorption of a particle

following the trajectory through the nucleus. This probability is

$$A(x) = \exp\left\{-\int_{-\infty}^{x} \mathrm{d}t/L(t)\right\}. \tag{3}$$

Let the ray be represented by a ray vector whose direction is that of the momentum of a particle and whose length is $A(x)$. The classical trajectories and ray vectors are represented in fig. 1 for 40 MeV protons in lead. The optical model parameters used are $V = -43$ MeV, $W = -20$ MeV, $R = 7.53\times10^{-13}$ cm, $a = 0.7\times10^{-13}$ cm. The same potential is used for all the calculations in this article.

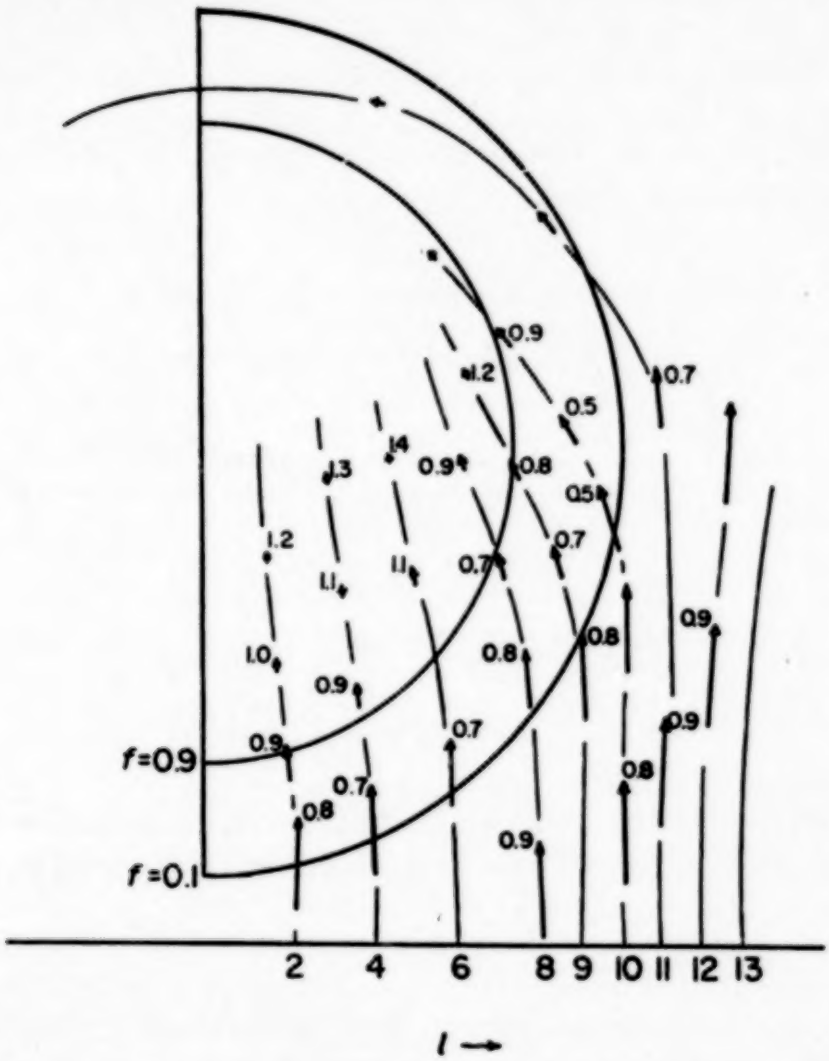

Fig. 1. Half classical trajectories of 40 MeV protons in lead. The remainder of the trajectory is symmetrical with the part illustrated about a line joining the end of the illustrated half to the centre of the nucleus. The arrows represent the classical ray vectors.

A useful check on the validity of this approximation is to calculate the transmission coefficient $A(\infty)$ and compare it with that for a partial wave

of the same angular momentum l in the quantal optical model where

$$l^2 = \frac{2mE}{\hbar^2} s^2, \tag{4}$$

s being the impact parameter of the classical trajectory. The quantal transmission coefficient is defined to be

$$1-(\sigma_R)_l/(2l+1)\pi\lambda^2 \tag{5}$$

where $(\sigma_R)_l$ is the partial reaction cross section for l calculated from the optical model (using the E.R.A. 1103 computer at the University of Minnesota), $(2l+1)\pi\lambda^2$ is the maximum possible partial reaction cross section, i.e. the cross section for an opaque nucleus.

The comparison is made in table 1 for the potential mentioned above and also for 160 MeV protons in lead using V = −15 MeV and the same values for the other parameters. The negative logarithms of $A(\infty)$ are compared to make the differences obvious.

TABLE 1

Negative logarithms of the transmission coefficient $A(\infty)$ compared with those of quantal transmission coefficients for 40 and 160 MeV protons in lead

40 MeV			160 MeV		
l	$-\ln A(\infty)$		l	$-\ln A(\infty)$	
	Classical	Quantal		Classical	Quantal
0	8.5	10.5	0	5.3	5.3
4	8.2	10.2	6	5.2	5.0
8	7.1	3.6	10	4.7	4.5
9	6.7	2.8	14	3.8	3.6
10	6.4	1.5	18	2.3	2.1
11	9.6	0.54	22	0.7	0.5
12	2.2	0.13	26	0.12	0.02

The classical and quantal calculations do not compare well when the rays depart appreciably from straight lines. In the 160 MeV case, the rays are almost straight everywhere and the comparison is good. For small values of l in the 40 MeV case, the rays are nearly straight. The quantal absorption is expected to be greater because of reflection in the potential gradient which is not included in the classical theory. When the rays bend appreciably their path length in the nucleus becomes very large. This is noticeable in the extreme case of $l = 11$. Evidently the quantal average behaviour of the particle does not follow the details of the path of the classical ray but seems to take a shorter course through the nucleus. We may express this in quantal language by saying that the disturbance at a point in the nucleus is not uniquely associated with the disturbance at a point outside.

In the next sections we explore this matter by calculating the average classical flux at a point in the potential and comparing it with a quantal calculation of the average flux.

3. Classical Flux Calculations

The three properties of the incident particle and the nucleus listed in section 1 can be derived from a knowledge of the classical flux. Assuming that the primary mechanism for nuclear reactions is an initial two-body collision [7]), the probability of a collision occurring at a point is proportional to the divergence of the flux at the point.

To calculate the absolute value of the classical flux $j(x)$, we must multiply the length of the ray vector $A(x)$ by a factor due to the focusing effect of the potential. We shall assume that the direction of the flux vector is the same as the direction of the ray vector, which is true if the flux is calculated by averaging the rays over a sufficiently small volume.

The focusing factor is determined by using two adjacent trajectories with impact parameters s and $s+\Delta s$. The flux is determined over an annular ring of inner and outer radii s and $s+\Delta s$ before entering the nucleus. When it reaches the point x, a distance R from the axis of the nucleus parallel to the incident direction, this flux will have been concentrated into an annular ring

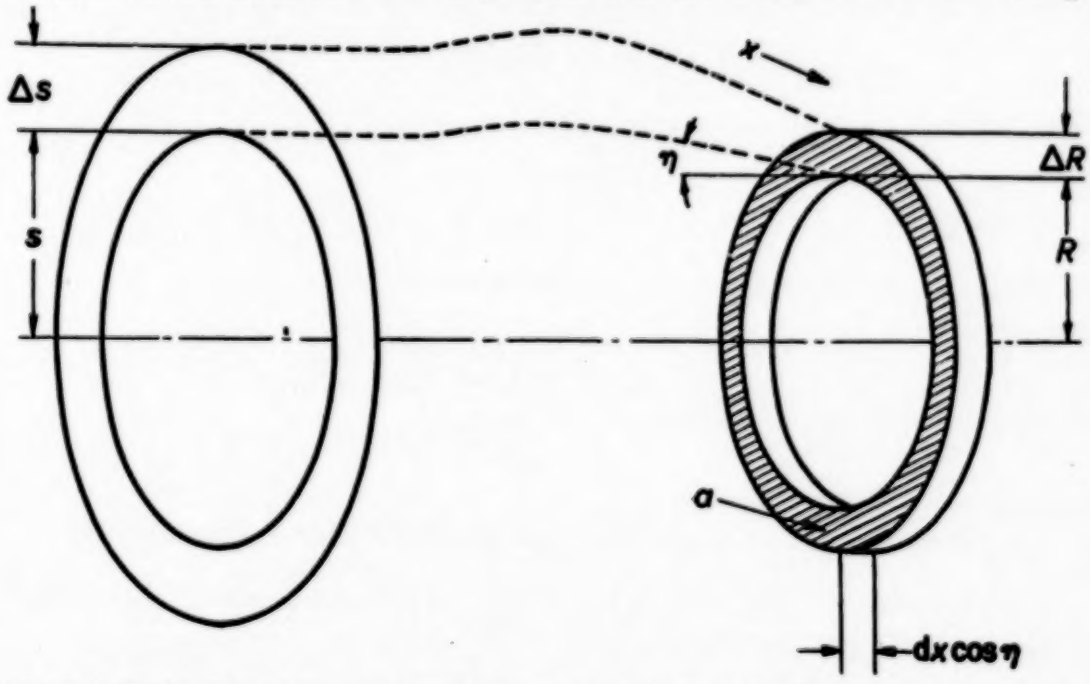

Fig. 2. Definition of the quantities referred to in the derivation of the classical flux and its divergence.

of inner and outer radii R and $R+\Delta R$. In the limit as $\Delta s \to 0$, the focusing factor $F(x)$ will be given by the ratio of the areas of the two annular rings

multiplied by the cosine of the angle η between the direction of the flux and the incident direction:

$$F(x) = \frac{s}{R}\frac{\Delta s}{\Delta R}\cos\eta. \tag{6}$$

This is illustrated in fig. 2. The magnitude of the flux is now given by

$$j(x) = F(x)\exp\left\{-\int_{-\infty}^{x} \mathrm{d}t/L(t)\right\}. \tag{7}$$

To calculate the divergence, consider a thin sheath of flux whose cross section is initially an annular ring, and which passes through the point x. Consider a short segment of length $\cos\eta\,\mathrm{d}x$ containing x. Let the area of the cross section of the segment be $a(x)$, where

$$a(x) = 2\pi R\Delta R. \tag{8}$$

Omitting explicit reference to the point x, the flux j is given by

$$j = n/(a\cos\eta), \tag{9}$$

where n is the number of particles crossing area a in unit time at an angle η to the normal. This is illustrated in fig. 2.

Differentiating (7) and using (6) we obtain

$$\mathrm{d}j = -j[\mathrm{d}x/L + \mathrm{d}(\Delta R)/\Delta R + \mathrm{d}R/R]. \tag{10}$$

The divergence of the flux is defined in the limit as $\mathrm{d}x \to 0$ by

$$\mathrm{d}n = \nabla\cdot\mathbf{j}\,\mathrm{dV} \tag{11}$$

where dV is the element of volume

$$\mathrm{dV} = a\,\mathrm{d}x\cos\eta. \tag{12}$$

Differentiating (9) we have

$$\mathrm{d}j = \mathrm{d}(n/a\cos\eta) = \mathrm{d}n/a\cos\eta - n\,\mathrm{d}a/a^2\cos\eta$$
$$= \nabla\cdot\mathbf{j}\,\mathrm{dV}/a\cos\eta - n\,\mathrm{d}a/a^2\cos\eta. \tag{13}$$

Substituting (10) in (13) and using (8) and (12) we have

$$\nabla\cdot\mathbf{j} = -j/L. \tag{14}$$

4. Comparison of Classical and Quantal Flux Calculations

The quantal flux calculation is the subject of a separate paper [8]) The flux is given by

$$\mathbf{j}(\mathbf{x}) = \frac{\hbar}{2im}[\bar{\psi}(\mathbf{x})\nabla\psi(\mathbf{x}) - \psi(\mathbf{x})\nabla\bar{\psi}(\mathbf{x})]. \tag{15}$$

In the potential (2), the divergence of the flux is

$$\nabla\cdot\mathbf{j}(\mathbf{x}) = (\hbar/m)Wf(\mathbf{x})\bar{\psi}(\mathbf{x})\psi(\mathbf{x}). \tag{16}$$

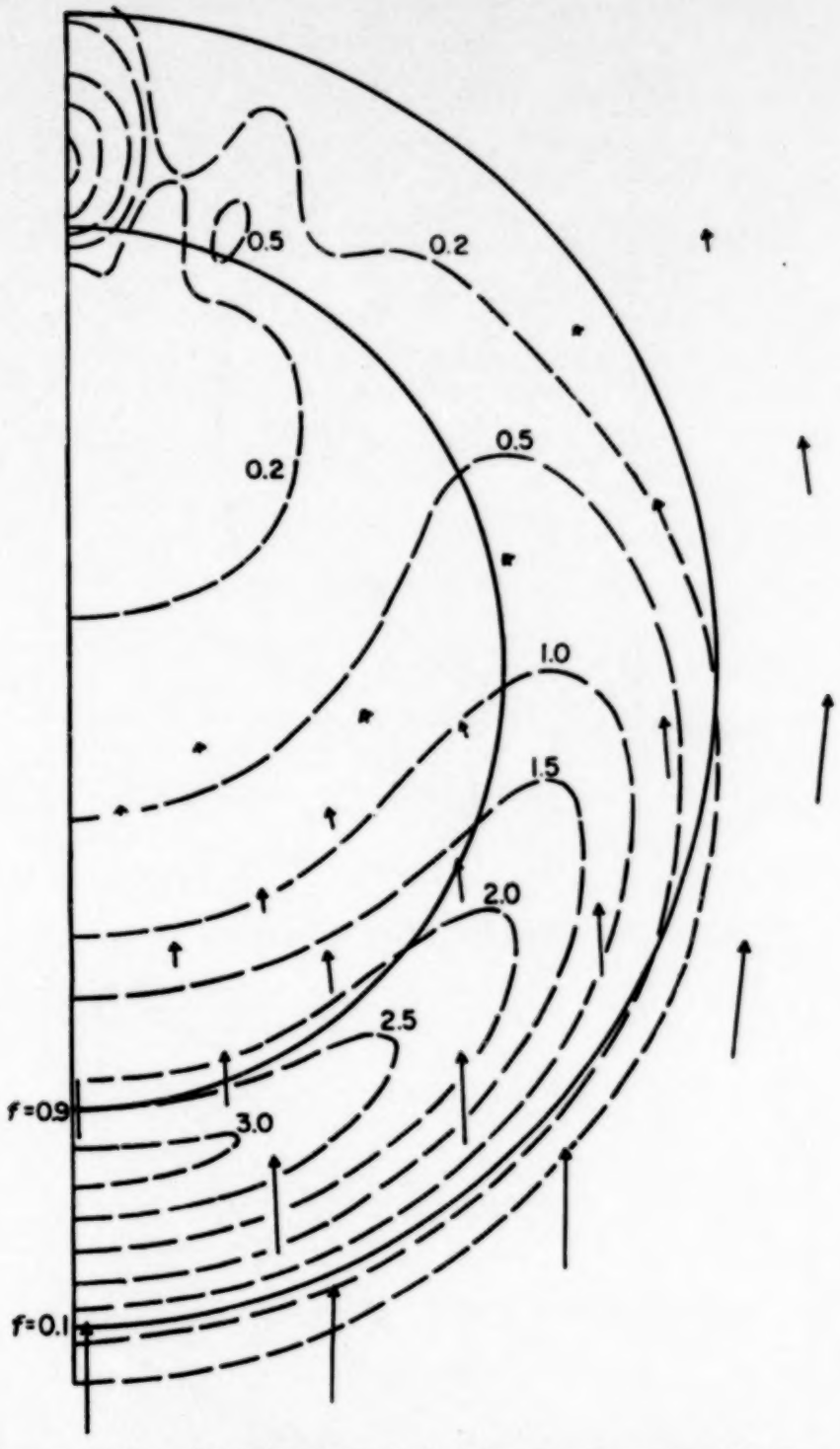

Fig. 3. The quantal flux of 40 MeV protons in lead. The arrows represent the flux vectors and the divergence is represented by contours in arbitrary units. The nuclear surface is illustrated by the circles for $f = 0.9$ and $f = 0.1$.

The flux and divergence were calculated by integrating the Schrödinger equation in the optical model potential using the E.R.A. 1103 computer of the University of Minnesota. The result in the case of 40 MeV protons in lead,

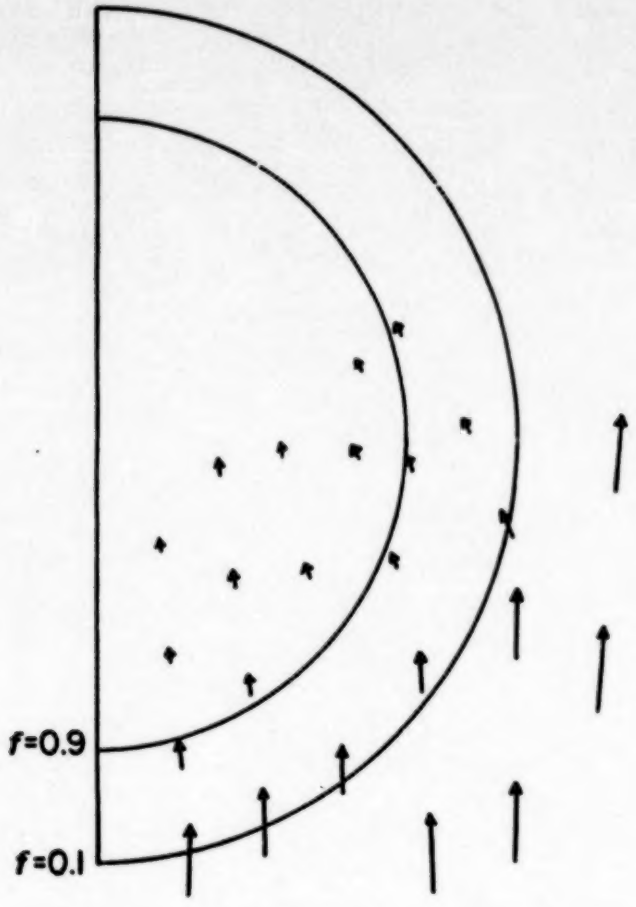

Fig. 4. The classical flux of 40 MeV protons in lead.

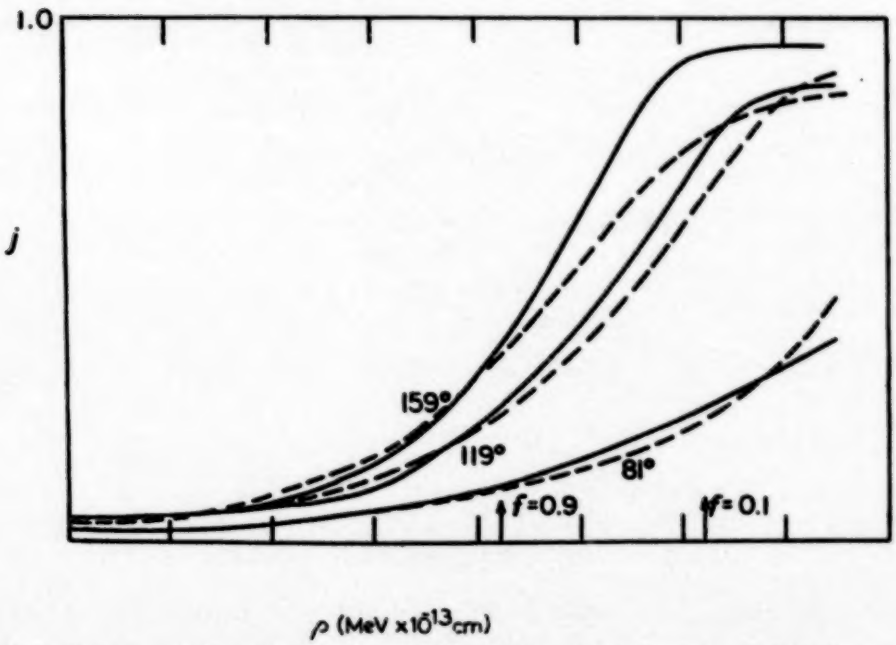

Fig. 5. Detailed comparison of the magnitudes of the classical and quantal fluxes at 159°, 119° and 81°.

is illustrated in fig. 3. The arrows represent the flux vector at the origin of the arrow. The divergence of the flux is represented by contour lines labelled in arbitrary units.

In the region where both fluxes are appreciable they are quite similar. There is a region with large flux and divergence in the far side of the nucleus in the quantal picture which is similar to the classical focus. This region will be examined in more detail in a future publication. Effects of reflection and dispersion, as well as those of focus, appear to be important. The classical flux was calculated graphically and is subject to error. In the case of the flux

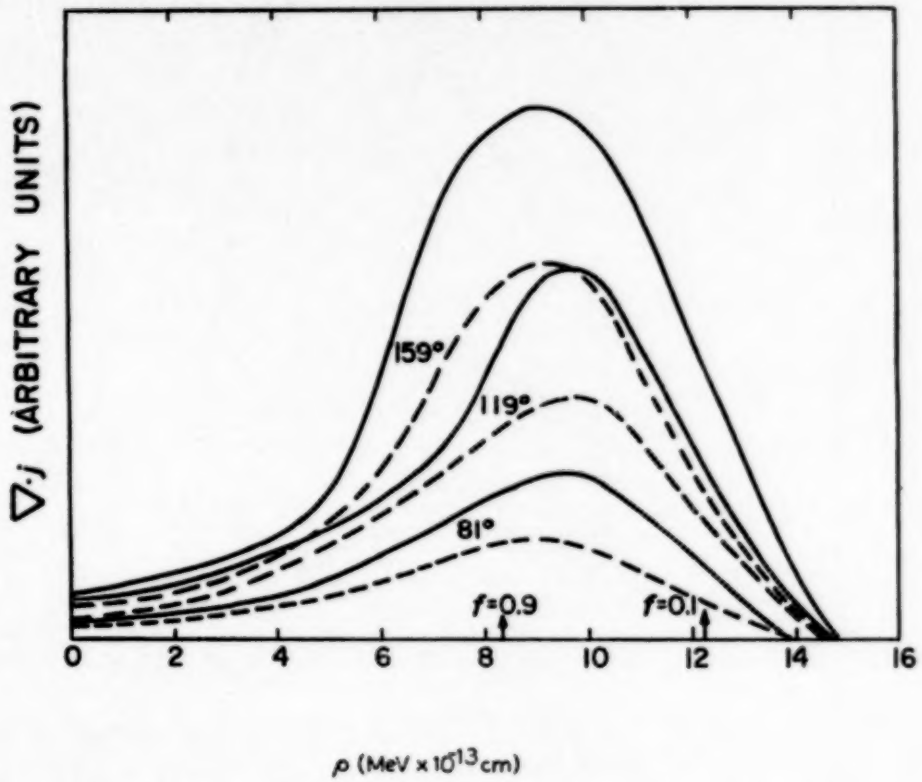

Fig. 6. Detailed comparison of the divergences of the classical and quantal fluxes at 159°, 119° and 81°.

and divergence the error is estimated to be about five percent and in the case of the angle η it is $\pm$ 2°. The classical flux is illustrated in fig. 4.

The two flux pictures can be compared in more detail by drawing the magnitude of the flux, the divergence of the flux, and the angle η as functions of r for different values of the polar angle θ measured from the incident direction. This comparison is made in figs. 5, 6 and 7 respectively for $\theta = 159°$, 119° and 81°. In general it confirms the conclusions drawn from table 1.

The classical flux is not calculated in the far side of the nucleus because of the difficulty of averaging over the tangled trajectories. The object of the classical calculation is to calculate the basic three quantities by a method

which has one great advantage over the quantal method. It does not require an electronic computer. Hence refinements which necessitate long computations are not justified. In both cases the magnitude of the flux in the far side of the nucleus is negligible except in the anomalous region near the axis, whose volume is relatively small. We can draw the qualitative conclusion that the classical approximation is bad in this region, which is the reason for the large differences in table 1.

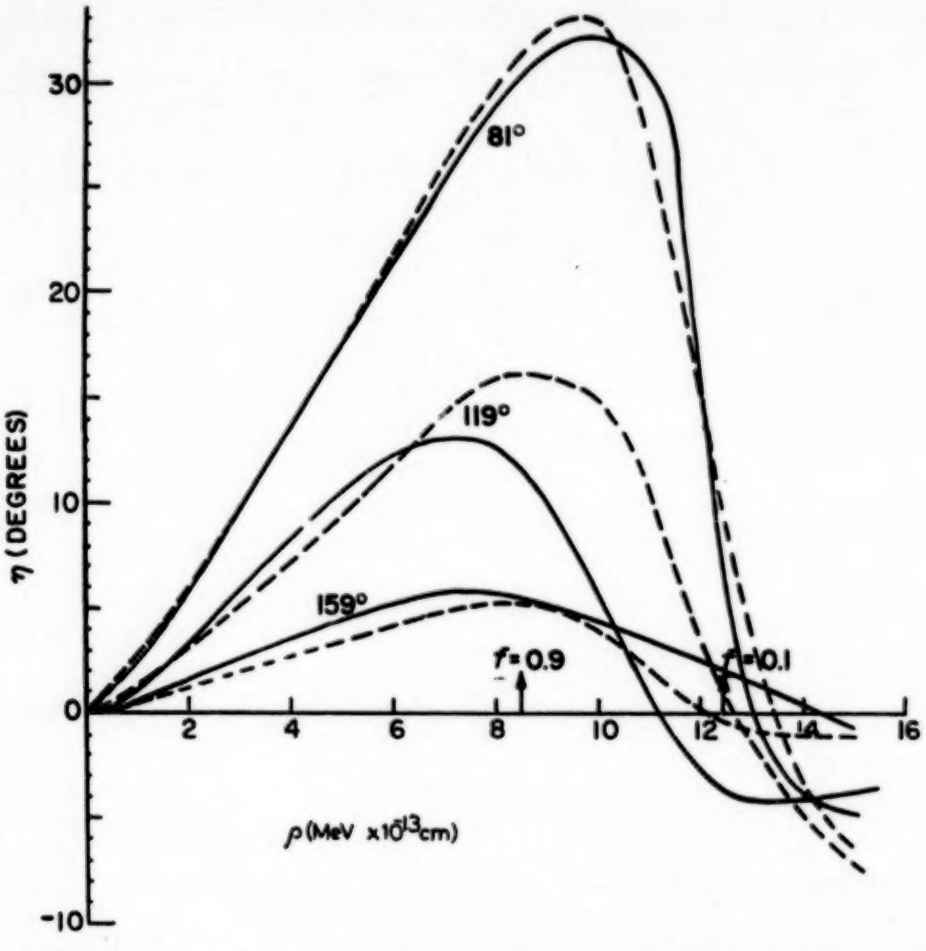

Fig. 7. Comparison of the angles η which the classical and quantal fluxes make with the incident direction at 159°, 119° and 81°. η is positive when the flux is bent towards the centre.

In the region where the flux is significant the differences may be accounted for by the fact that the classical theory does not describe the reflection of the beam in the potential gradient. The effect of a large potential gradient in the classical case is to bend the trajectories and hence increase the length over which the beam may be absorbed. In the quantal case it reflects the beam and in the part of the surface where the impact parameter is large, tends to hold it into the nucleus, thus increasing the flux at a point and bending it towards the centre.

This effect is seen in fig. 7 where the angle η is larger in the surface in the quantal case at 119°. At 159° the classical flux in the surface is considerably larger (fig. 5), but the classical divergence is also larger (fig. 6), so that at 119° and 81° the fluxes are comparable.

5. Conclusions

The calculations in this paper may be regarded in two ways, either as a check on the accuracy of the usual classical ray calculation, or as a method of gaining some idea of the validity of assigning properties to localized regions in the optical model.

It is clear that the classical ray approximation is bad. It neglects the effect of focusing of the beam in the potential. This effect is large in the surface where the rays are bent considerably. The surface is the interesting region from the direct interaction point of view. When the effect of focusing is taken into account as in the classical flux calculation, the classical theory does not differ greatly from the quantal one in the region where the flux is not very small, and when the advantage of simplicity of computation is considered, there is a good case for using it in direct interaction calculations where other assumptions, such as that of a static local potential, are crude.

Within the model, the results of the two calculations may be interpreted as follows. The properties of a small region in the potential are not uniquely determined by those of a similar region outside as they are assumed to be in the classical ray theory. In quantal language the disturbance at any interior point is influenced by several partial waves.

The differences between the two models in the region where the fluxes are appreciable seem capable of being accounted for by the fact that reflections in the potential gradient do not appear in the classical theory. However, the models are very different in the far side of the nucleus where the quantal quantities are determined by resonance and dispersion effects and bear no relation to the classical approximation. The region where the differences are qualitative has a small volume compared with that of the whole nucleus.

Calculations are at present being performed by the authors with the object of finding the total cross section for direct interactions by a method which is classical only in the sense that the collisions are localized. The initial conditions for the collision are described by the quantal flux and its divergence, and the probabilities for a product particle to escape from the potential are calculated in a quantal approximation. It is expected that this cross section will be very sensitive to the form factor of the imaginary potential inside the nucleus because this determines, for a given total reaction cross section, to what extent the divergence is concentrated near the surface where the product particles can escape without being totally internally reflected.

A comparison of the results of this calculation with the experimental cross section for direct interactions should provide a way of determining the form factor of the imaginary potential.

The authors would like to thank Drs. W. B. Cheston and D. R. Yennie for their interest and help.

References

1) S. Hayakawa, M. Kawai and K. Kikuchi, Prog. Theor. Phys. **13** (1955) 415
2) L. R. B. Elton and L. C. Gomes, Phys. Rev. **105** (1957) 1027
3) R. M. Eisberg and G. Igo, Phys. Rev. **93** (1954) 1039
4) N. Oda and K. Harada, Nuclear Physics **7** (1958) 251
5) Giassgold, Cheston, Stein, Schuldt and Erickson, Phys. Rev. **106** (1957) 1207
6) S. T. Butler, N. Austern and C. Pearson, Phys. Rev. (to be published)
7) E. V. Jezak, A. Kromminga and I. E. McCarthy, Nuclear Physics (to be published)
8) I. E. McCarthy, Nuclear Physics (to be published)

2.E *Nuclear Physics* **10** (1959) 583—589; © *North-Holland Publishing Co., Amsterdam*
Not to be reproduced by photoprint or microfilm without written permission from the publisher

FLUX OF PARTICLES IN THE OPTICAL MODEL

IAN E. McCARTHY
School of Physics, University of Minnesota,

Received 8 December 1958

Abstract: The flux of 18 MeV α-particles in argon is calculated with two optical model potentials which give similar elastic scattering and reaction cross sections. Although these potentials are similar in the nuclear surface, they give different fluxes inside the potential and in particular different values for the divergence of the flux which represents the probability of absorption of the beam at a point. The divergence for α-particles in both potentials is peaked more strongly at the surface than that for protons of the same momentum in a realistic potential, but it is not negligible in the centre. The divergence peaks are of different heights in the two potentials and hence may give different total cross sections for direct interactions.

1. Introduction

The elastic scattering of particles from nuclei can be well represented by scattering from a static optical model potential [1]) $(V+iW)f(r)$ where

$$f(r) = \{1+\exp[(r-R)/a]\}^{-1}. \qquad (1)$$

The potentials which fit a given angular distribution are not unique [2]). Igo has investigated sets of parameters which give similar angular distributions [3]) for the elastic scattering of 18 MeV α-particles from argon, 40 MeV α-particles from copper, and 48 MeV α-particles from lead. He found that the many potentials which fit a given set of data all give the same values for V and W in the nuclear surface (where the potential is $\gtrsim -10$ MeV). Some of these potentials also give total reaction cross sections which could not be experimentally distinguished.

Igo concluded that the nuclear surface in the optical model is well determined by entrance channel phenomena, but that they give no information about the centre of the potential. There has been a general feeling [13]) that this means that the potentials are such that the particle does not penetrate beyond the surface. To examine this point, and any questions that might depend on a knowledge of the potentials in the centre, it is useful to calculate the flux of particles in the potential, and the divergence of the flux which gives the probability of absorption of a particle at a point.

The flux and divergence for 18 MeV α-particles in argon has been calculated in each of Igos' two widely different potentials. In each, the flux in the centre is by no means negligible. It is less than that outside by a factor of

roughly 4 in the near side of the nucleus, i.e. the part first hit by the beam. There is a strong angular dependence of both the flux and divergence. Both are larger on the near side. The two potentials give similar fluxes and divergences on the near side in the region where the potentials are similar. On the far side the fluxes begin to differ because of resonances and dispersion effects which will be discussed in detail in a future publication. The divergence is peaked in the surface region.

The α-particle calculation was compared with one for protons of the same momentum (72 MeV) using potentials interpolated from existing data [2]). The flux does not fall off as quickly as in the α-particle cases, and the divergence is not peaked so strongly in the surface. It must be emphasized that in calculating the flux and its divergence in a given volume the volume element is proportional to $r^2 \sin \theta$, and therefore the centre of the potential is not nearly as important as the surface.

Several general questions about the interpretation of a flux calculation need to be discussed. Is it meaningful in the light of the uncertainty principle to talk about particles located at a point in the nucleus? This is discussed at length elsewhere [4]), but it is sufficient here to say that the flux calculated from a classical trajectory approximation is very similar to that calculated by quantum mechanics when 15 or more partial waves play a part in the calculation.

Is it meaningful to talk about an optical potential inside the nucleus? This question can be answered by finding experimental results that would depend on such a potential and comparing them with calculations based on that assumption. Thus it may be possible to define an optical potential in the nucleus. One such comparison has been suggested by the author and Dr. R. M. Eisberg [8]). If one assumes that the primary mechanism for nuclear reactions is an initial two-body collision † the divergence of the flux at a point represents the probability of a collision occurring at the point. If one of the collision products escapes from the nucleus without another collision, it would appear as a direct interaction particle. It is known [7]) that reflection effects make it difficult for a particle to escape from inside the potential, hence a potential that gives a large divergence in the surface should give a large total cross section for direct interactions.

In the two potentials studied for α-particles, the divergence peaks differ in height by about 15 %. The total reaction cross sections differ by only 3 %. Hence, on this argument, the direct interaction cross section may be much more sensitive to the value of V and W inside the nucleus than the total reaction cross section.

† Strong evidence for this in the case of proton-nucleus reactions has been given by recent experiments by Eisberg and Griffiths [5]). It will be discussed in another publication [6]).

2. Calculation of the Particle Flux and its Divergence

The flux of particles per unit time in a potential V_0 at the point $\mathbf{r}$ is [9])

$$\mathbf{S}(\mathbf{r}) = \frac{\hbar}{2im}[\bar{\psi}(\mathbf{r})\text{grad}\,\psi(\mathbf{r}) - \psi(\mathbf{r})\,\text{grad}\,\bar{\psi}(\mathbf{r})] \tag{2}$$

where $\psi(\mathbf{r})$ is the solution of the Schrödinger equation

$$\left(\frac{\hbar^2}{2m}\nabla^2 + E - V_0\right)\psi(\mathbf{r}) = 0; \tag{3}$$

E is the intitial energy of the beam of particles.

In the case when V_0 is the potential (1), the divergence of the flux is given by

$$\text{div}\,\mathbf{S}(\mathbf{r}) = (\hbar/m)Wf\bar{\psi}(\mathbf{r})\psi(\mathbf{r}). \tag{4}$$

If the Schrödinger equation (3) is separated in spherical coordinates the wave function may be expanded as follows:

$$\psi(\mathbf{r}) = \psi(\rho, \theta) = \frac{1}{k}\sum_L N_L \frac{u_L(\rho)}{\rho} P_L(\cos\theta) \tag{5}$$

where $u_L(\rho)$ is the solution of

$$\left[\frac{\mathrm{d}^2}{\mathrm{d}\rho^2} + 1 - \frac{L(L+1)}{\rho^2} - \frac{V_0}{E}\right]u_L(\rho) = 0, \tag{6}$$

with

$$\rho = kr, \qquad k = (2mE)^{\frac{1}{2}}/\hbar.$$

Owing to the axial symmetry of the problem, ϕ does not appear explicitly in the wave function.

N_L is a normalizing factor which is not important in the case of elastic scattering because only the logarithmic derivative u'_L/u_L enters the calculation. In our case we have a bilinear form with products of radial wave functions for different partial waves K and L, so we need to know N_L.

The solutions $u_L(\rho)$ for each L were normalized by matching them to the appropriate Coulomb functions at a point outside the nuclear potential.

The solution of the Schrödinger equation (3) in a Coulomb potential which is normalized to unit incident flux is

$$\psi_c(\rho, \theta) = \sum_L i^L(2L+1)\mathrm{e}^{i\sigma_L}[G_L(\rho) + iF_L(\rho)]P_L(\cos\theta), \tag{7}$$

$$\begin{aligned} F_L(\rho) &\approx \sin(\rho - \tfrac{1}{2}L\pi - \eta\ln 2\rho + \sigma_L), \\ G_L(\rho) &\approx \cos(\rho - \tfrac{1}{2}L\pi - \eta\ln 2\rho + \sigma_L), \end{aligned} \tag{8}$$

where $\eta = ZZ'e^2/\hbar v$, σ_L is the Coulomb phase shift. Hence,

$$N_L = i^L(2L+1)\mathrm{e}^{i\sigma_L}. \tag{9}$$

The calculation of $u_L(\rho)$, $G_L(\rho)$ and $F_L(\rho)$ has been programmed by Glassgold and Stein [10]) and this program was incorporated into the present one.

The components of **S** along and perpendicular to a given radius vector are respectively

$$S^\rho = \mathrm{Im} \sum_{KL} \bar{N}_K N_L \frac{1}{\rho^3} \bar{u}_K [\rho u'_L - u_L] P_K P_L,$$
$$S^\theta = \mathrm{Im} \sum_{KL} \bar{N}_K N_L \frac{1}{\rho^3} \bar{u}_K u_L P_K P'_L, \tag{10}$$

$$\mathrm{div}\, \mathbf{S} = Wf \sum_{KL} \bar{N}_K N_L \bar{n}_K u_L P_K P_L, \tag{11}$$

where the variables r and θ have not been written explicitly.

3. α-particle Flux

The two sets of optical parameters which Igo found to fit the elastic scattering of 18 MeV α-particles from argon are given in table 1.

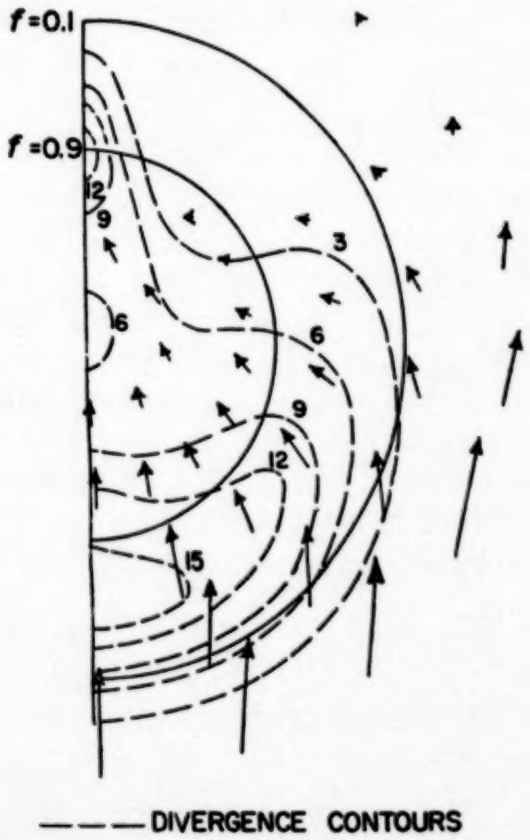

Fig. 1. α-particle flux in potential α_1.

TABLE 1

Two sets of optical parameters which fit the elastic scattering of 18 MeV α-particles from argon

	V(MeV)	W(MeV)	$R(10^{-13}$ cm)	$a(10^{-13}$ cm)
α_1	−87	−15	5.37	0.6
α_2	−40	− 8	6.05	0.5

Fig. 1 is a map of the particle flux in the potential α_1. An arrow represents the flux vector at the origin of the arrow. The divergence is represented by countour lines labelled in arbitrary units. The corresponding diagram for α_2 is similar, except that the flux is not bent towards the centre so sharply since the potentials are weaker. For detailed comparison of the pictures it is better to look at the absolute value of the flux and the divergence plotted against r for various values of θ.

In fig. 2, this is done for the absolute value of the flux at 179°, 139° and 81° for α_1 and α_2 and for 72 MeV protons using parameters $V = -30$ MeV, $W = -10$ MeV, $R = 4.5\times10^{-13}$ cm, $a = 0.8\times10^{-3}$ cm, denoted by p. This picture illustrates the fact that the flux is much larger on the near side

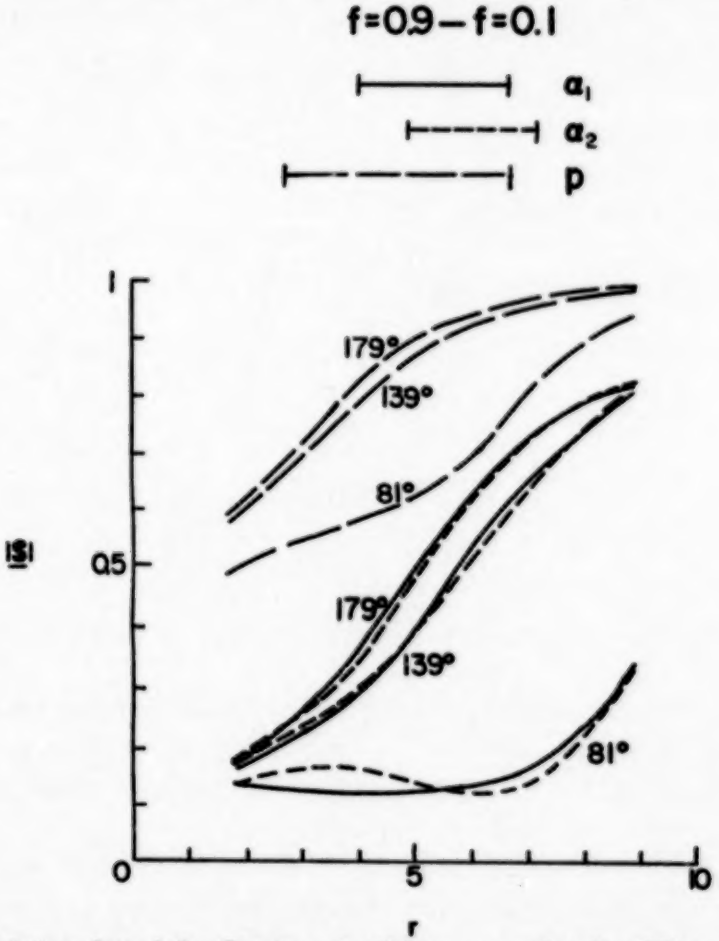

Fig. 2. Absolute value of the flux in potentials α_1, α_2 and p for different values of θ.

of the nucleus than the far side. Where it is large, its absolute values for the potentials α_1 and α_2 are almost indistinguishable. They fall off quite steeply towards the centre but are still 20 % of the outside value. For protons the fall-off is not as steep and the value in the centre is 50 % of the outside value. The size of the nuclear surface is illustrated by showing the distance between $f = 0.1$ and $f = 0.9$ for each potential.

Fig. 3 is a similar plot for the divergence. Here differences between α_1 and α_2 are more apparent. The divergence peaks for α_1 and α_2 are higher and

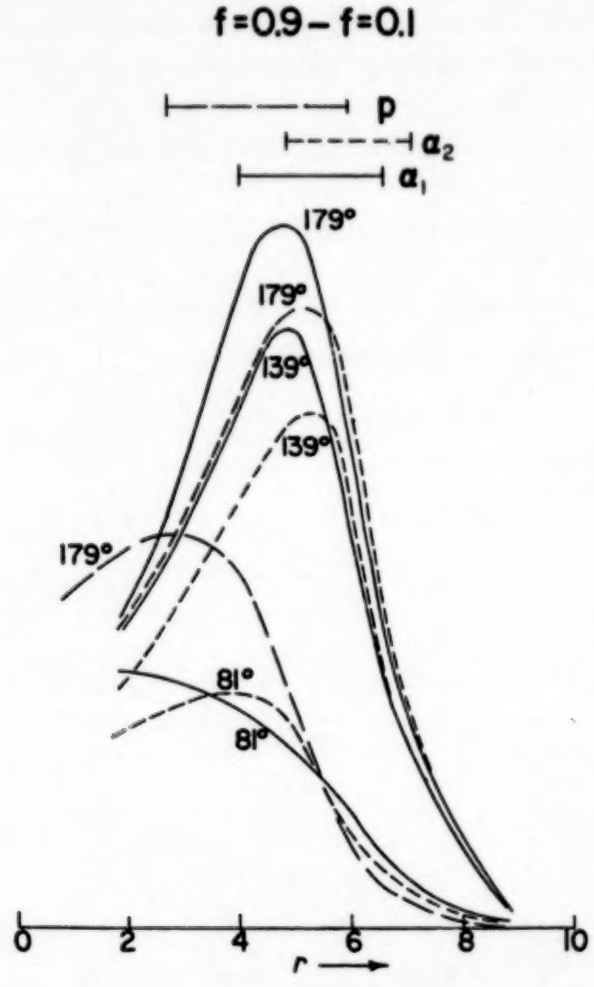

Fig. 3. Divergence of the flux in potentials α_1, α_2 and p for different values of θ.

wider and at a smaller value of r. The decreased volume in which the absorption occurs for α_1 makes up for the increased peaks. The total reaction cross sections for α_1 and α_2 are respectively 1313 mb and 1269 mb, a difference of 3.4 % which would be difficult to measure.

If we assume that an initial two body collision always occurs, we can divide the reaction cross section into the cross section for one particle escaping without a further collision and that for both particles being absorbed.

The probability of escape is very sensitive to the radial distance from the edge, since reflection in the potential is the chief mechanism for preventing escape. For α_1 the probability of a collision occurring near the edge is greater than for α_2, particularly in the far side of the nucleus (e.g. 81°) where the angle at which the reaction products strike the barrier is favorable for escape. The difference is about 15 %, but of course without knowledge of the transmission coefficient it is difficult to say whether this difference would show up in the direct interaction cross section. Work is being done to calculate the transmission coefficients and settle this point.

Such a calculation would probably have more meaning when applied to protons. However we do not have detailed comparisons of proton potentials such as those made by Igo for α-particles. There is reason to assume from the ambiguities found by Glassgold [2]) that a similar situation would apply. In the case of nucleons, Bjorklund and Fernbach [11]) have used an imaginary potential peaked in the surface. This potential arises from considerations of the exclusion principle [12]). It would give a much sharper divergence peak than the Saxon potential and should be easy to distinguish by this method.

I would like to thank Drs. W. B. Cheston, R. M. Eisberg, C. E. Porter, D. R. Yennie, and Messrs. A. J. Kromminga and D. H. Sowle for their continued interest and help with this work.

References

1) R. D. Woods and D. S. Saxon, Phys. Rev. **95** (1954) 1617
2) A. E. Glassgold and P. J. Kellogg, Phys. Rev. **107** (1957) 1372
3) G. Igo, Phys. Rev. Letters **2** (1958) 72
4) R. M. Eisberg, I. E. McCarthy and R. Spurrier, to be published
5) R. J. Griffiths and R. M. Eisberg, to be published
6) E. V. Jezak, A. J. Kromminga and I. E. McCarthy, to be published
7) L. R. B. Elton and L. C. Gomes, Phys. Rev. **105** (1957) 1027
8) R. M. Eisberg, Proceedings of the International Conference on Nuclear Physics, Paris, July 1958
9) L. I. Schiff, Quantum Mechanics (McGraw-Hill, 1955) 23
10) Glassgold, Cheston, Stein, Schuldt and Erickson, Phys. Rev. **106** (1957) 1207
11) F. Bjorklund and S. Fernbach, Phys. Rev. **109** (1958) 1295
12) S. Hayakawa, M. Kawai and K. Kikuchi, Prog. Theor. Phys. **13** (1955) 415
13) Proceedings of the Pittsburgh Conference on Nuclear Structure, pp. 214 and following

1.E.1: 3.A

Nuclear Physics **10** (1959) 590—605; © *North-Holland Publishing Co., Amsterdam*
Not to be reproduced by photoprint or microfilm without written permission from the publisher

THE Y^{89} (n, γ) Y^{90} REACTION

G. A. BARTHOLOMEW, P. J. CAMPION, J. W. KNOWLES and G. MANNING †

Chalk River Laboratory, Atomic Energy of Canada Limited, Chalk River, Ontario

Received 11 December 1958

Abstract: The thermal neutron capture gamma rays from the Y^{89}(n, γ)Y^{90} reaction were investigated in the energy region between 0.18 and 7.0 MeV with a pair spectrometer, a flat crystal spectrometer, and an angular correlation arrangement using two sodium iodide crystals. The prominent gamma rays in the spectrum, which is unusually simple for a nucleus of this mass number, can be fitted to a level diagram for Y^{90} with levels at 0.2024 $\pm$0.0003, 0.247$\pm$0.002, 0.7767$\pm$0.0002, 1.215$\pm$0.002 and 2.741$\pm$0.012 MeV. Angular correlation studies between cascading gamma rays, with certain assumptions based on the gamma ray intensities, lead to tentative assignments of 2+ and 3− for the levels at 0.7767 and 0.2024 MeV respectively. The neutron binding energy of Y^{90} is found to be 6.849$\pm$0.009 MeV. The observed level scheme is compared with shell model predictions.

1. Introduction

The neutron capture gamma ray spectra from odd Z and odd N product nuclei are usually very complex and the decay schemes more difficult to derive than those of neighbouring even Z product nuclei. An exception to this rule is found in the spectrum of Y^{90} which is very much simpler than the spectra of other odd nuclei of comparable mass, e.g., $Br^{80,82}$, As^{76}, or Nb^{94} [1,2]). As a result of this simplicity, an unambiguous decay scheme for the stronger radiations may be constructed and the energies and tentative spin assignments for some previously unobserved levels may be deduced.

Few reactions leading to energy levels of Y^{90} have been studied. The beta decay of Sr^{90} which proceeds only to the ground state of Y^{90}, has been examined by many workers [3]) and from these measurements the assignment 2− for the ground state of Y^{90} has been well established. Using the Y^{89}(d, p)Y^{90} reaction, Wall [4,5]) observed a (possibly complex) group corresponding to an excited state or states near 1.17$\pm$0.06 MeV. The stripping pattern for this group resembled that for an $l_n = 0$ distribution suggesting the presence of a level with a spin of 0 or 1 and negative parity. The neutron binding energy of Y^{90}, also obtained by Wall [4]), is 6.64$\pm$0.05 MeV. Since Y^{89} has a spin of $\frac{1}{2}$ and odd parity, the Y^{90} compound nucleus formed by thermal neutron capture is 0− or 1− or a mixture of these. No resonances have been reported [6]) in the neutron cross section curves for bombardment of Y^{89} with neutrons of energy

† Now at Norman Bridge Laboratory of Physics, California Institute of Technology, Pasadena, California.

up to 2 keV and the proportion in which the two possible spin states are formed at thermal energies is not known.

2. Experimental Method and Results

2.1. APPARATUS

The gamma rays from the $Y^{89}(n, \gamma)Y^{90}$ reaction were investigated using a target consisting of 400 g of yttrium oxide †, Y_2O_3, placed in an experimental hole of the Chalk River NRX reactor. Rare earth impurities in the target material were present in concentrations of less than a few parts per million. The gamma rays were detected with a pair spectrometer [7]) in the energy region above 3 MeV and with a flat crystal diffraction spectrometer [8]) in the region below that energy. The two instruments were arranged one behind the other so that the gamma ray beam from the target passed through the pair spectrometer to the flat crystal spectrometer. In a separate experiment, coincidences and angular correlations between cascade gamma rays were studied with the aid of two NaI(Tl) crystals 6" long by 4" diameter mounted on DuMont 6364 photomultipliers. In this arrangement [9]) a beam of thermal neutrons was used to bombard a target consisting of 16 g of Y_2O_3 in a Lucite capsule placed at the intersection of the axes of symmetry of the two NaI crystals. One crystal was mounted on a movable arm so that the angle between the two detectors could be varied between 90° and 220°.

2.2. ENERGY AND INTENSITY MEASUREMENTS

The spectra observed with both the flat crystal spectrometer and the pair spectrometer are presented together in fig. 1. In these curves the counting rate as a function of energy is shown without correction for variation of counting efficiency or for absorption of the gamma rays in the source or in various materials traversed by the gamma rays between the source and the spectrometers. For the low energy region between 180 and 300 keV the crystal diffraction spectrometer was operated as a single flat crystal instrument Laue diffracting from the (211) planes of calcite. With this arrangement (which provides a higher spectrometer efficiency to compensate for the high gamma ray absorption at these energies) the spectrometer resolution is about 2 percent at 200 keV. A germanium crystal, (440) planes, was employed in the single crystal arrangement to study a number of relatively weak lines in the higher energy region between 1 and 3 MeV. The resolution for these measurements was 4—8 percent. In the region between 0.4 and 1.5 MeV, double diffraction, using two calcite crystals, (211) planes, was used to give a nearly constant resolution of about 0.5 percent. With the pair spectrometer two arrangements of counter slits were employed to give

† We are very grateful to the U.S.A.E.C. for the loan of this material.

different combinations of counting rate and resolution as required at different parts of the spectrum. The highest resolution used was about 1 percent. The peak at 0.51094 MeV is produced by annihilation radiation and that at 4.17 MeV is probably background radiation from a bismuth

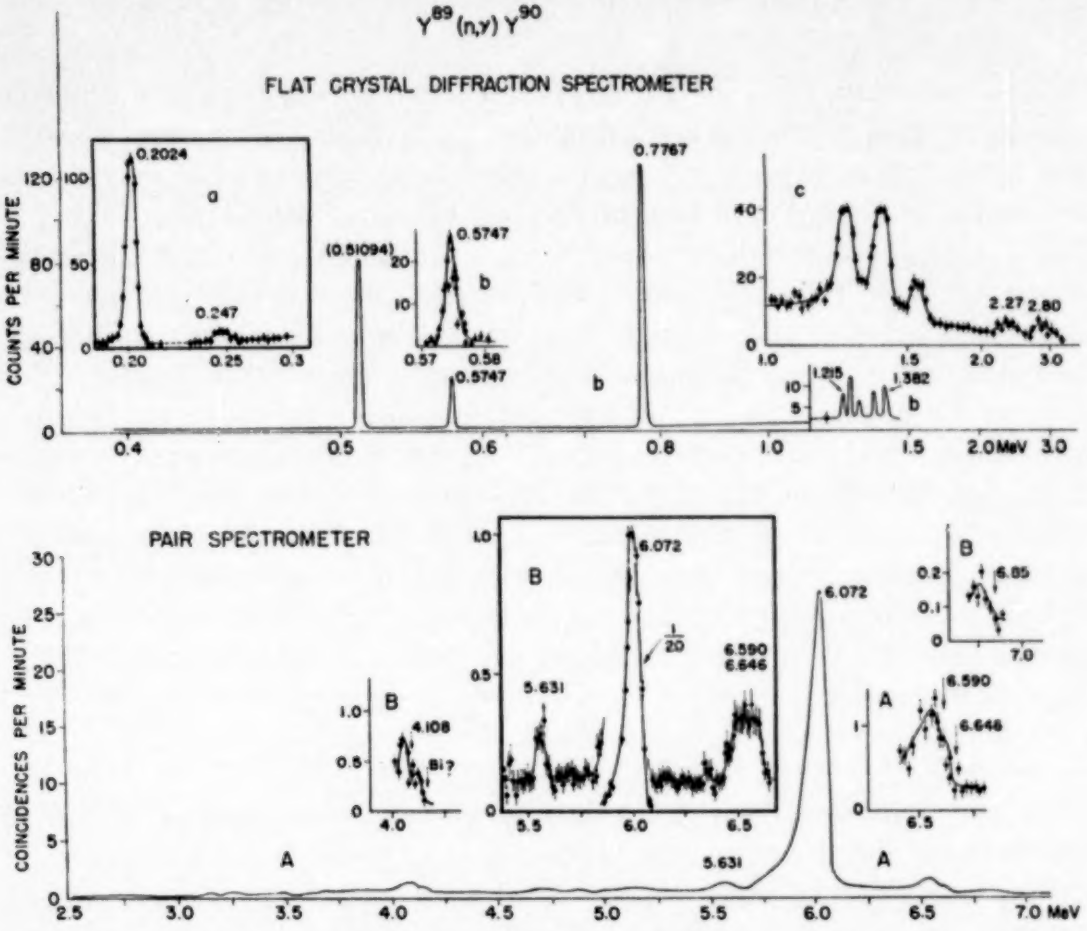

Fig. 1. Gamma-ray spectra from 0.18 to 7.0 MeV following thermal neutron capture in yttrium. The curves show the experimental data obtained with the flat crystal diffraction spectrometer below 3 MeV and with the pair spectrometer above 2.5 MeV. Corrections for spectrometer efficiency and absorption of the gamma rays have not been applied. Three arrangements of the flat crystal spectrometer were used: in region a, a system of Soller slits and diffraction from a single calcite crystal; in region b, double diffraction using two calcite crystals; in region c, Soller slits and a single crystal of germanium. Two arrangements of pair spectrometer slits giving different conditions of resolution and counting efficiency were used for regions A and B. The annihilation gamma ray at 0.51094 MeV was used as an energy calibration for the flat crystal spectrometer. The density and statistical accuracy of the experimental points shown in the insets is typical for the remainder of the observed spectrum.

plug placed between the target and the reactor core. The gamma ray at 6.85 MeV is extremely weak and there is a possibility that it is not produced by yttrium but by some impurity in the target or its container or by the reactor. Although the gamma ray doublet near 6.6 MeV is not well resolved, several examinations of this peak have shown that it has an abnormal width

and there can be little doubt that it is produced by two gamma rays of about equal intensity. The origin of the weak peak at 6.48 MeV is uncertain; it may be produced by a gamma ray from yttrium or from the background or it may be caused by a statistical fluctuation.

The energies and absolute intensities of the resolved gamma rays are given in table 1. The absolute intensities were determined with the aid of a target

TABLE 1

Energies and absolute intensities of resolved yttrium gamma rays

Energy (MeV)	Intensity (photons per 100 captures)
0.2024 ± 0.0003	9
0.247 ± 0.002	3
0.5747 ± 0.0003	10
0.7767 ± 0.0002	39
1.215 ± 0.002	1.5
1.240 ± 0.003	2.9
1.281 ± 0.005	1.6
1.335 ± 0.005	1.8
1.382 ± 0.003	3
1.55 ± 0.04	1
2.27 ± 0.07	1
2.80 ± 0.07	0.9
4.108 ± 0.010	9
5.631 ± 0.012	2
6.072 ± 0.009	45
6.590 ± 0.010	0.8
6.646 ± 0.009	0.8
6.85 ± 0.02	≦ 0.3

containing a mixture of weighed amounts of Y_2O_3 and V_2O_5. In this measurement the 6.868 MeV gamma ray following neutron capture in vanadium was used as the intensity standard for the gamma rays detected by the pair spectrometer. Its intensity was taken to be 0.08 ± 0.01 photons per capture [10]). The intensities of the low energy gamma rays detected with the flat crystal spectrometer were measured by comparing their counting rates with that of the 1.45 MeV gamma ray following beta decay of V^{52} †. Although the relative intensities of strong neighbouring gamma rays are known to a few percent, the accuracy of the absolute intensities given in table 1 is probably

† The product of the thermal neutron capture cross section of vanadium and the absolute intensity of the 1.45 MeV gamma ray in photons per neutron captured at equilibrium in natural vanadium enters into this evaluation. This quantity has been determined by direct comparison[11]) with the corresponding quantity for the 1.368 MeV radiation from sodium and found to be 4.73 ± 0.15 barn photon per capture. The cross sections of Y^{89} and Na^{23} were assumed to be 1.26 ± 0.08 b and 0.536 ± 0.010 b respectively [6]).

only ± 20 percent for strong well-resolved gamma rays and may be considerably worse for the weaker radiations. In fig. 2, the distribution of the unresolved continuum is shown as a graph of $\nu(E)$, the number of photons per capture per MeV, as a function of E. Since the counting rate between the

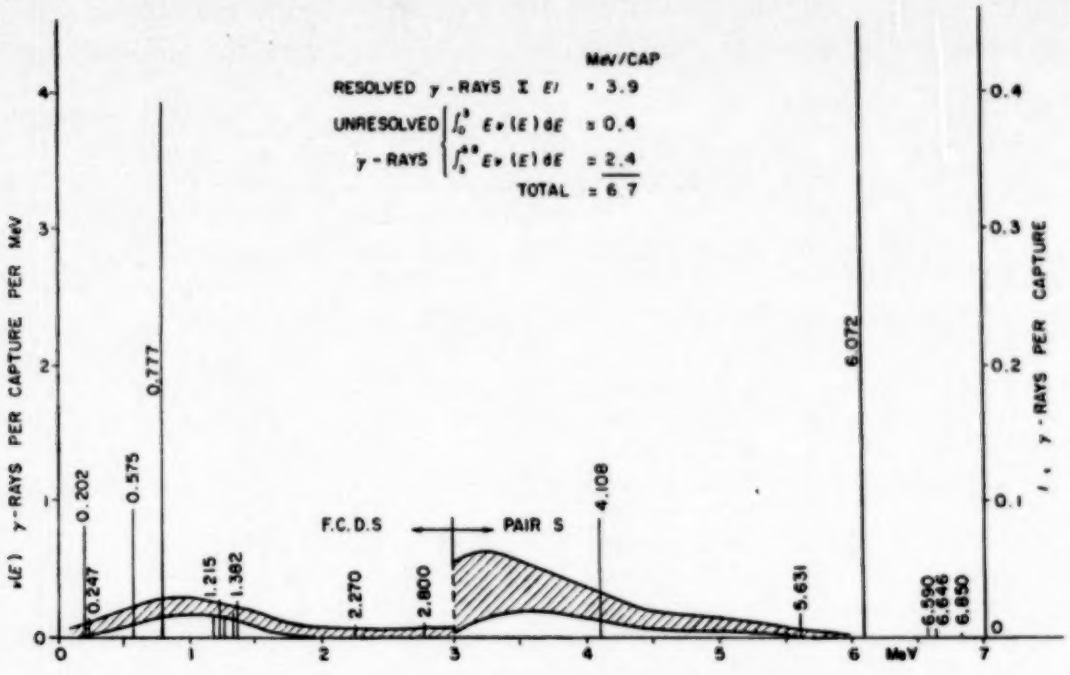

Fig. 2. Yttrium capture gamma ray spectrum corrected for spectrometer efficiency and absorption of the gamma rays. The resolved radiations are shown as vertical lines with heights representing the absolute intensities in gamma rays per capture (right hand scale). The intensity of radiation in the unresolved part of the spectrum, in gamma rays per capture per MeV is represented by the shaded band, (left hand scale). The width of the band is a measure of the uncertainty of the intensity determination for the unresolved radiation. The contributions of the resolved and unresolved parts of the spectrum to the total energy radiated per capture are listed.

peaks was very low and since the contribution from background radiation is not well known, rather wide limits of error are given for the continuum measurement. About 40 percent of the spectrum is apparently distributed among a large number of very weak transitions which were not resolved in the present experiment. The energy radiated per capture in both the resolved and unresolved parts of the spectrum is tabulated in fig. 2. In view of the probable errors involved in the intensity measurements the good agreement between the value obtained for the total energy radiated per capture, 6.7 MeV, and the binding energy, 6.849 MeV, (see below) is somewhat fortuitous but it provides a rough check of the consistency of the measurements.

2.3. COINCIDENCE AND CORRELATION MEASUREMENTS

The direct spectrum observed with one of the NaI scintillation spectrometers is shown in fig. 3. Gamma ray peaks at 6.7, 6.07, 4.11, 0.78, 0.55, and

0.20 MeV are clearly resolved. These peaks correspond to gamma rays or groups of gamma rays with energies (table 1) 6.85 plus 6.646 plus 6.590, 6.072, 4.108, 0.7767, 0.5747 plus 0.511, and 0.2024 MeV respectively. The region of the spectrum near 2.23 MeV is obscured by the gamma ray at this energy produced by neutron capture in the hydrogen in the Lucite sample container and is not shown in fig. 3.

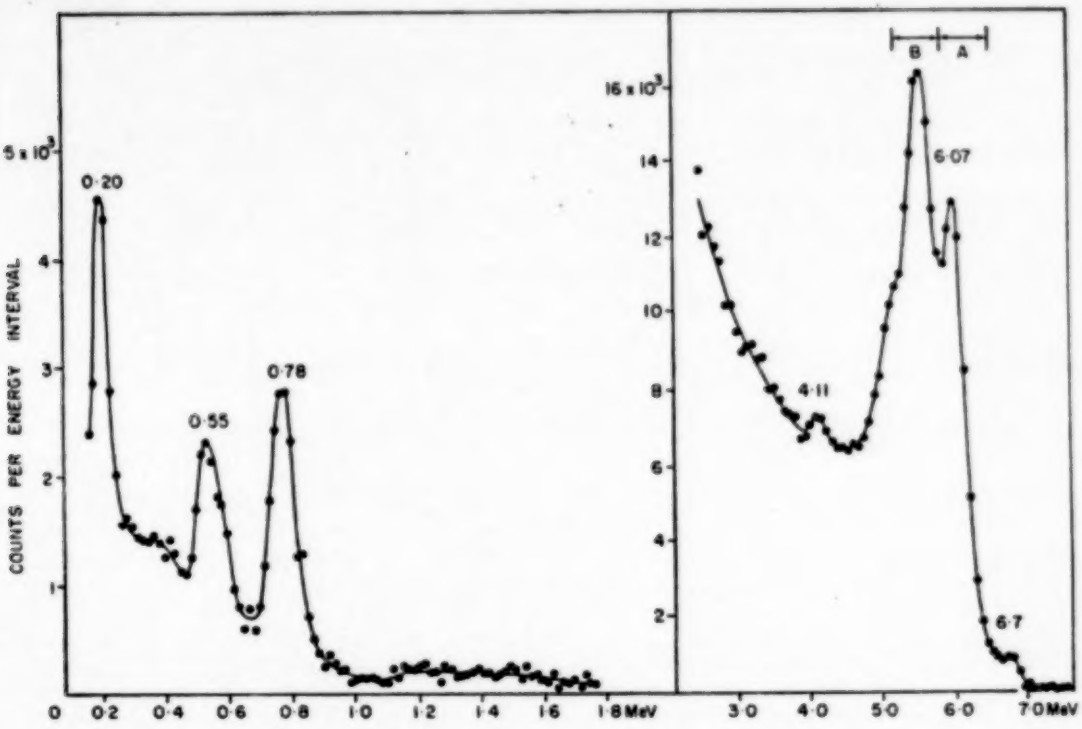

Fig. 3. Spectrum observed with one of the NaI scintillation spectrometers. The background spectrum (obtained with the yttrium target removed) has been subtracted. The energy intervals A and B correspond to the positions of the discriminator channels for the coincidence measurements shown in figs. 4 and 7 respectively.

The discriminators of a single channel pulse height analyser associated with the stationary crystal were adjusted so that the photopeak of the 6.072 MeV gamma ray was detected, as shown by the interval A, fig. 3. The spectrum from the moving crystal in coincidence with pulses in this interval was measured with the angle between the two crystals set alternatively at 90° and at 180°. The results are shown in fig. 4. In obtaining these particular curves the detector angle was alternately set at 90° and 180° some thirteen times and the alternate spectra added together channel by channel. Peaks corresponding to gamma rays at 0.78, 0.57 plus 0.51, and 0.20 MeV were observed. It was not possible to resolve the contributions from the 0.5747 MeV gamma ray and the 0.511 MeV annihilation gamma ray and therefore only a very approximate estimate can be made of the correlation of

the 0.5747 and 6.072 MeV gamma rays. However, the 0.7767 MeV gamma ray is well resolved and extensive measurements of the angular correlation between it and the 6.072 MeV gamma ray were made at six angles between 90° and 180° in equal intervals in $\cos^2\theta$ as shown in fig. 5.

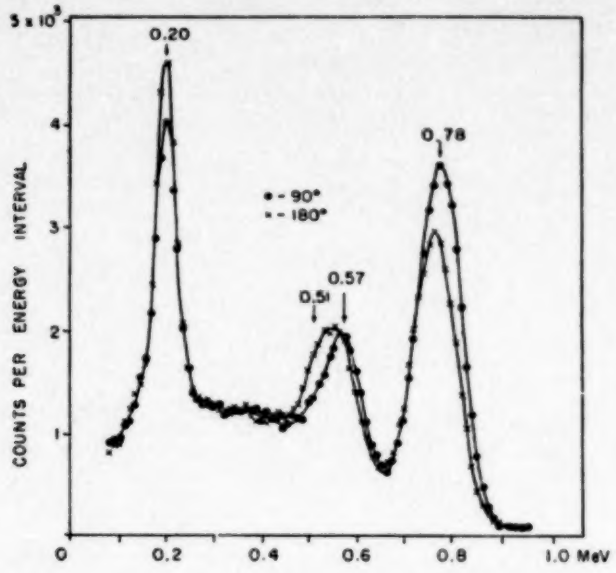

Fig. 4. Spectra in coincidence with pulses in the energy region A, fig. 3. Curves for counter angles of 90° and 180° are shown.

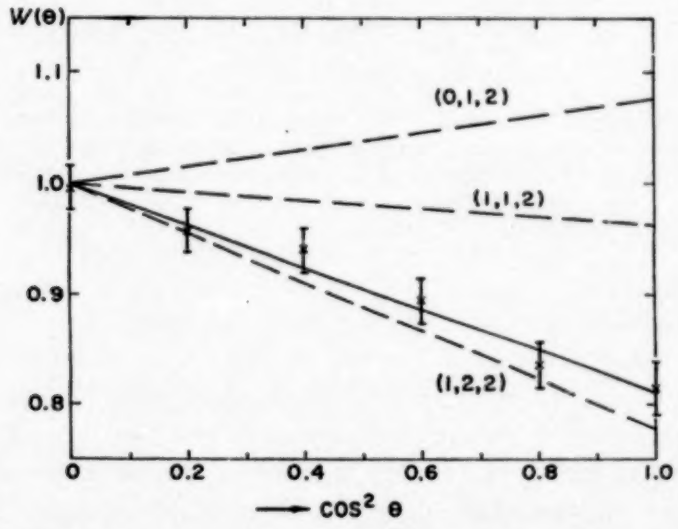

Fig. 5. Angular correlation of 6.072 and 0.7767 MeV gamma rays. The full line is a least squares fit of the experimental points to the expression $W(\theta) = 1+(a_2/a_0)P_2(\cos\theta)$. For comparison, the theoretical distributions (assuming dipole transitions only) suitably modified to allow for counter solid angle and finite source size, are shown as broken lines for three combinations of the spins (I_1, J, I_f) for the initial state, the intermediate state, and the final state. The least squares fitted function after geometry corrections is $W(\theta) = 1-(0.14\pm0.02)P_2(\cos\theta)$.

The positions of the discriminators of the single channel pulse height analyser used to observe coincidences between the 0.5747 and 0.2024 MeV gamma rays are shown in fig. 6a. The spectra in coincidence with pulses in this channel are shown in fig. 6b where again data obtained at counter angles of 90° and 180° are shown. The spectra were obtained by summing the

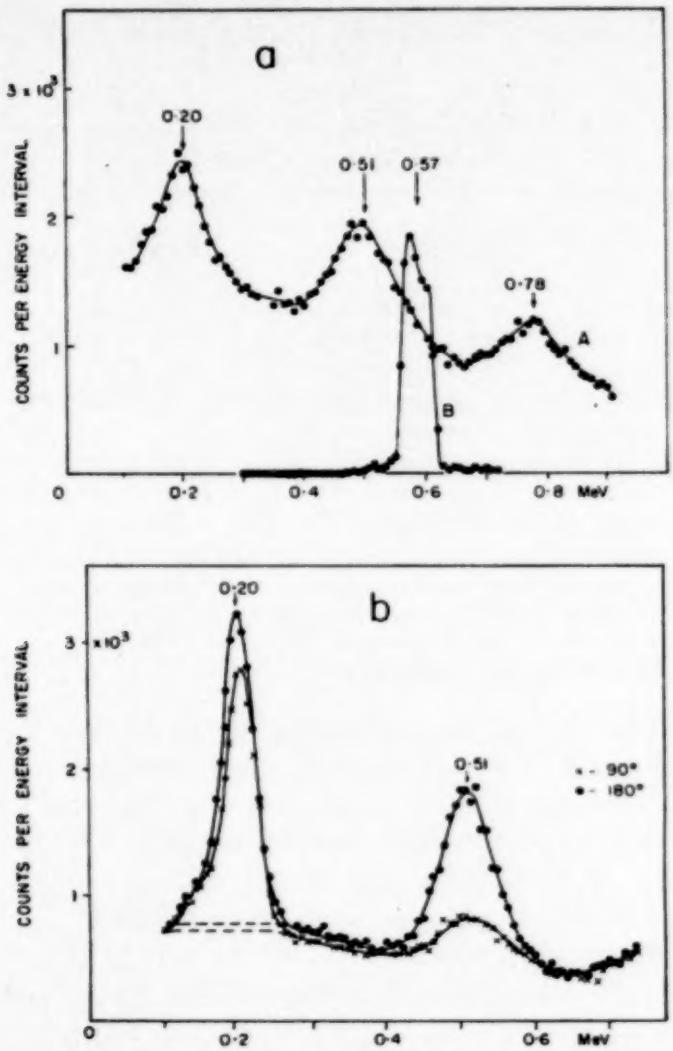

Fig. 6. The upper graph, a, shows the discriminator setting for the measurements of the 0.5747—0.2024 MeV correlation. Curve A is the spectrum from the stationary spectrometer. Curve B is a "self-gated" spectrum, from the same spectrometer, showing the part of curve A accepted by the discriminators during the correlation measurement. The lower graph, b, shows the spectrum from the moving spectrometer in coincidence with pulses in the discriminator channel. Curves for counter angles of 90° and 180° are shown. The 0.511 MeV gamma-ray peak is produced by annihilation radiation. Estimates of the background counting rates underlying the 0.20 MeV peaks were obtained from the shapes of the curves in the energy region immediately above the peaks and are shown as broken lines.

results of sixteen alternate measurements at each angle. The precision with which the 0.5747—0.2024 MeV correlation can be measured is limited by the detection of coincidences involving 0.511 MeV radiation produced by positrons annihilating in the target and surrounding materials. An additional uncertainty arises from the contribution to the 0.20 MeV peak from coincidences with gamma rays of energy greater than 0.5747 MeV for which pulses happen to fall in the channel shown in fig. 6a.

In the second column of table 2 are summarized the results of the measure-

TABLE 2

Experimental and theoretical coefficients a_2/a_0 for the angular correlation function $W(\theta) = 1 + (a_2/a_0) P_2(\cos\theta)$

Gamma-ray cascade energy in MeV	Observed a_2/a_0	Theoretical a_2/a_0						
		0, 1, 1, 2	0, 1, 2, 2	1, 1, 1, 2	1, 1, 2, 2	1, 2, 1, 2	1, 2, 2, 2	1, 2, 3, 2
6.072 —0.7767	-0.13 ± 0.02 †	+0.05	+0.05	−0.025	−0.025	−0.175	−0.175	−0.175
6.072 —0.5747	0.00 ± 0.08	−0.25	+0.05	+0.125	−0.025	+0.175	−0.175	+0.05
6.072 —0.2024	$+0.14 \pm 0.07$	−0.025	−0.175	+0.0125	+0.0875	+0.0175	−0.0875	+0.12
0.5747—0.2024	$+0.16 \pm 0.04$	−0.025	−0.175	−0.025	−0.175	+0.005	+0.175	+0.12

† Average of two separate determinations giving -0.12 ± 0.02 (fig. 4) and -0.14 ± 0.02 (fig. 5).
For the pairs of gamma rays listed in the first column, the observed coefficients are given in the second column and the theoretical coefficients, assuming dipole radiation only, for various combinations of the spins of the capturing state, the 0.7767 MeV level, the 0.2024 MeV level, and the ground state (in that order) are given in the last seven columns.

ments of the four correlations corrected for the finite geometry of the detectors and finite size of the target [9]). The correlations are expressed in terms of the coefficient a_2/a_0 in the Legendre polynomial expansion $W(\theta) = 1 + (a_2/a_0) P_2(\cos\theta)$. Rather liberal errors are quoted for these coefficients. These errors are based on the counting statistics and estimates of the underlying background and of possible systematic errors.

Attempts were made to observe the gamma rays in coincidence with the relatively weak, high energy radiations at 5.631 and 4.108 MeV (fig. 1). With the discriminators of the single channel pulse height analyser set to accept the photo-peak of the 5.631 MeV gamma ray as indicated by the setting B in fig. 3 †, a weak peak at 1.22 MeV was observed, fig. 7. A very complicated coincidence spectrum was observed with a gate set to include the 4.108 MeV radiation and, beyond the tentative statement that gamma rays near 2.7 and 1.38 MeV would appear to be in coincidence with that at 4.108 MeV, no conclusions can be drawn from this measurement.

† In this figure the 5.631 MeV photo-peak is obscured by the prominent escape peak from the 6.07 MeV gamma ray.

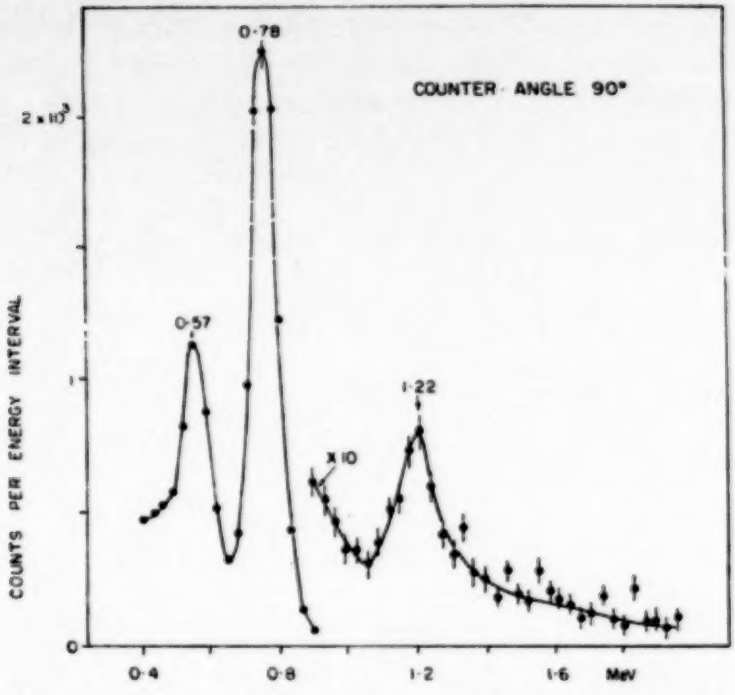

Fig. 7. Spectrum in coincidence with pulses in the differential discriminator setting B, fig. 3. The 1.22 MeV gamma ray is in coincidence with the 5.631 MeV gamma ray. The 0.57 and 0.78 MeV gamma ray peaks are produced by coincidences with pulses from the 6.072 MeV gamma ray which fall within the setting B.

3. Interpretation of Results

The decay scheme shown in fig. 8 was derived from the congruity of the summed energies of combinations of cascading gamma rays and the results of the coincidence experiments. Because of their high precision, the gamma ray energy measurements alone are almost sufficient to define a unique level pattern which includes most of the resolved radiation. However, the order of emission of cascading gamma rays is not determined in these experiments and the justification for drawing the decay scheme as shown with the highest energy gamma rays as primary transitions is based solely on the assumption that high energy gamma rays will be favoured in the decay of the initial state. This assumption is almost certainly correct for gamma rays above, say, 6 MeV but is much less certain in the case of the 4.108—2.80 MeV cascade. As mentioned above, the decay of the 2.741 MeV level appears to be very complicated. Only a fraction of the intensity of the 4.108 MeV gamma ray feeding this level is accounted for by the intensity of the 2.80 MeV gamma ray emitted in its decay. From energy considerations and from the spectrum in coincidence with the 4.108 MeV radiation, we surmise that the 2.741 MeV level may also decay by a cascade transition involving the 1.335 and 1.382 MeV gamma rays. Another possible cascade would involve the

1.240 and 1.55 MeV gamma rays. However, the order of the gamma rays in each of these cascades is not known and therefore these possible transitions are not included in fig. 8. The level energy, 1.17±0.06 MeV [4]), observed in the (d, p) reaction is in good agreement with the present determination of

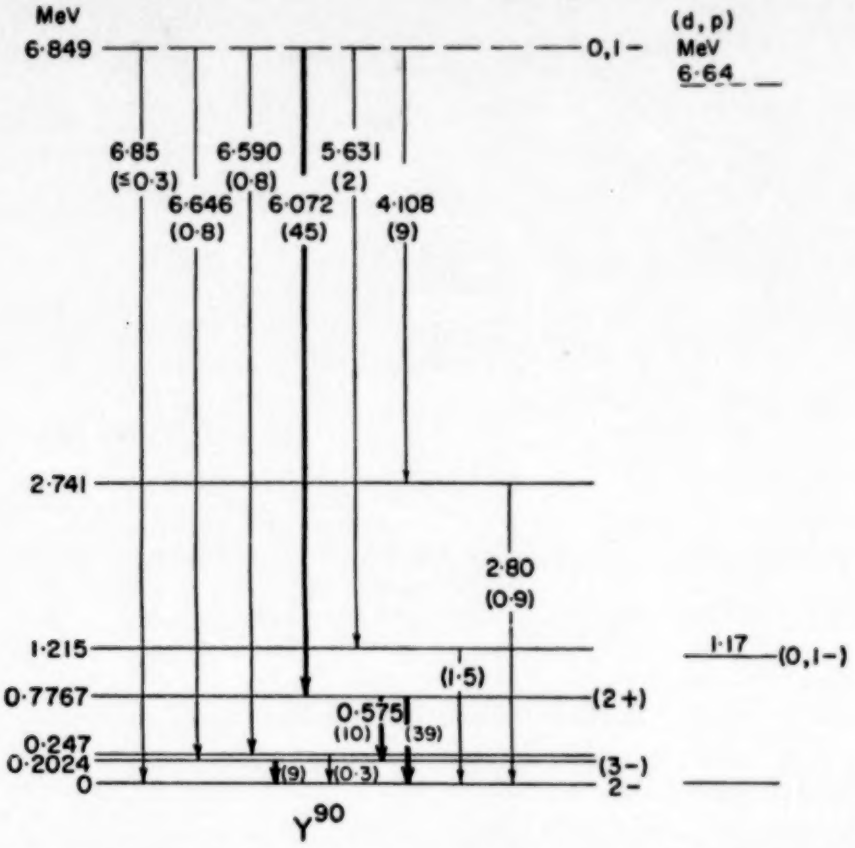

Fig. 8. Decay scheme for Y^{90}. The level energies on the left are obtained from the measured gamma ray energies with the assumption that the highest energy gamma rays in each cascade are emitted by the capturing state. The energies on the right are obtained from the (d, p) measurements of Wall [4]). Energies (in MeV) and absolute intensities in photons per 100 captures (in brackets) are given on the lines representing the transitions. The bracketed spin and parity assignments are tentative.

1.215±0.002 MeV and we shall assume that the same level is detected in both reactions. The neutron binding energy 6.64±0.05 MeV observed in the (d, p) reaction [4]) is somewhat lower than the value 6.849±0.009 MeV determined in the present measurements from the sum of the 6.072 and 0.7767 MeV gamma rays.

Since the parities of none of the excited states in fig. 8, except that at 1.215 MeV, have been measured it is not possible to derive unambiguous spin assignments from the present angular correlation measurements. In particular, if the parity of the level at 0.7767 MeV were odd, both the 6.072 and 0.7767 MeV transitions could contain mixtures of M1 and E2

radiation and several different spin values for the 0.7767 MeV level could be invoked, with suitable choices of the two multipole mixture parameters, to account for the observed correlation between these gamma rays. However, the 6.072 MeV gamma ray accounts for some 45 percent of all transitions from the capturing state in competition not only with the other strong gamma rays shown in fig. 8, but also, as mentioned above, with a number of other transitions each of which is too weak to be detected as a separate gamma ray. From the systematics of neutron capture gamma rays of different multipole types [12]) it would seem probable that the very prominent 6.072 MeV gamma ray and also that at 4.108 MeV, which has a comparable reduced matrix element, are of E1 type. In the following discussion, in the absence of more certain information, we shall therefore assume that the 6.072 MeV gamma ray is of E1 type. To be consistent with this assumption the 0.7767 MeV level then must have positive parity and the 0.7767 MeV gamma ray must be of E1 type. The possibility that the 0.7767 MeV level might be 0+ and the 0.7767 MeV gamma ray therefore of M2 type, is ruled out by the observation of anisotropy in the 6.072—0.7767 MeV correlation †. Since moreover, the reduced matrix elements of the 0.5747 and 0.7767 MeV gamma rays are comparable we infer that these two radiations probably have the same multipole order and that the parity of the 0.2024 MeV level is therefore probably negative. The fact that the ratio of reduced widths of the 6.646 and 6.072 MeV gamma rays is very nearly that expected from the single particle model if the 6.646 MeV gamma ray were M1 and the 6.072 MeV gamma ray E1, also tends to favour negative parity for the 0.2024 MeV level.

In table 2 the observed coefficients a_2/a_0 are compared with the theoretical values for various possible combinations of the spins of the four levels involved. The theoretical values are derived on the assumption that only dipole radiation is significant in each transition. Table 2 shows that, with this assumption, the only spin assignments for the capturing state, the 0.7767 and 0.2024 MeV states, and the ground state consistent with the observed correlations are 1, 2, 3, 2 respectively ††. On the basis of these arguments we tentatively assign spin and parities 2+ and 3— for the

† A spin of zero for the 0.2024 MeV level is also ruled out by the observation of anisotropy in the cascades involving this level as an intermediate state.

†† Assuming that the parities of the 0.7767 and 0.2024 MeV levels are even and odd respectively as argued above, all gamma rays in table 2 will be E1 except the 0.2024 MeV gamma ray which may be a mixture of M1 and E2 radiation. For only three of the seven spin combinations, viz., 1, 1, 2, 2; 1, 2, 2, 2; and 1, 2, 3, 2, is it possible to find values for the E2, M1 mixture which simultaneously satisfy the 6.072—0.2024 and 0.574—0.2024 MeV correlations within the quoted limits of error. While the 1, 1, 2, 2 case is quite effectively excluded by the 6.072—0.7767 MeV correlation, the rejection of the 1, 2, 2, 2 possibility depends on the 6.072—0.5747 MeV correlation. In spite of the low precision of this measurement it seems improbable that this correlation could have both the same strength and sign as the 6.072—0.7767 MeV correlation, as required by the 1, 2, 2, 2 case. For the favoured 1, 2, 3, 2 case the intensity of the E2 component in the 0.2024 MeV radiation is ≤ 0.01.

0.7767 and 0.2024 MeV levels respectively. Finally, it should be noted, that these measurements give no information concerning the relative proportions of spins 0 and 1 in the capturing state beyond implying that a large contribution from spin 1 is present.

4. Discussion

The applicability of the nuclear shell model [13]) to nuclei in the neighbourhood of $Z = 40$ and $N = 50$ is suggested by the level structure of Zr^{90} which exhibits typical "magic nucleus" properties [14]). This nucleus marks the filling of the $g_{\frac{9}{2}}$ neutron shell and the $p_{\frac{1}{2}}$ proton shell. The nucleus Y^{90} contains one proton hole in the $p_{\frac{1}{2}}$ shell and one $d_{\frac{5}{2}}$ neutron outside the $g_{\frac{9}{2}}$ shell and it seems reasonable to expect that it will also have a level structure which can be described, at least qualitatively, in terms of the shell model. A similar example occurs in Tl^{208} which contains one proton less and one neutron more than the doubly closed shell nucleus, Pb^{208}. Pryce [15]) has had considerable success in accounting for the low energy levels of Tl^{208} on a shell model basis.

In attempting to account qualitatively for the observed level scheme of Y^{90} we assume that the ground state will belong to the configuration in which the unpaired proton and unpaired neutron occupy the same orbits as in Y^{89} and Zr^{91} respectively and that the lowest excited states will belong either to the same configuration, or to configurations in which the proton only, or the neutron only, have been excited to higher orbits. It is assumed that configurations corresponding to the excitation of more than one nucleon, or to the excitation of the core †, do not give rise to exicted states near the ground state. From the known order of nuclear shells as given by Klinkenberg [17]) the proton orbit lying immediately above the $p_{\frac{1}{2}}$ is $g_{\frac{9}{2}}$. Above the $g_{\frac{9}{2}}$ orbit there is a considerable energy gap before the next orbit, $g_{\frac{7}{2}}$, is reached. The neutron orbit following the $d_{\frac{5}{2}}$ orbit is $g_{\frac{7}{2}}$ and this is followed closely in energy by $h_{\frac{11}{2}}$, $d_{\frac{3}{2}}$ and $s_{\frac{1}{2}}$. The number of excited states of Y^{90} arising from various combinations of these neutron and proton orbits is of course very large. However, we are immediately concerned only with those which will be excited by E1, M1, or E2 transitions from the capturing state since all of the levels shown in fig. 8 are formed by direct primary transitions ††. In table 3 the energies and the spin and parity assignments of the observed Y^{90} levels are given in the first and second columns. The various low energy configurations formed by excitation of one nucleon are given in the third column and all states which arise from these configurations and which combine with the capturing state with the emission of E1, M1, or E2 radiation

† There is evidence from the structure of Y^{89} [16]) that the energy required to remove a proton from the closed $p_{\frac{1}{2}}$ subshell may be 1.53 MeV.

†† It is assumed that M2 or higher multipoles have intensities too low to be detected.

are given in the fourth column. In the fifth column are given the zero order excitation energies for the excited configurations. These quantities are the energies of the levels which may be considered as the corresponding single particle excited states in neighbouring even-odd and odd-even nuclei. Thus the $g_{\frac{7}{2}}/d_{\frac{5}{2}}$ configuration, in the absence of perturbing forces between the particles, would be expected to lie at the same energy above the ground state of Y^{90} as the $g_{\frac{7}{2}}$ orbit lies above the ground state of Y^{89}, viz., 0.913 MeV. For a real nucleus, of course, the levels belonging to a given configuration are not degenerate and the displacement of a particular level from the nominal energy given in the fifth column of table 3 may be comparable to

TABLE 3

Energy levels of Y^{90}

Observed Levels		Possible Shell Model Levels		
Energy (MeV)	$J\pi$	Configuration	$J\pi$	Energy (MeV)
0	2−	$p_{\frac{1}{2}}d_{\frac{5}{2}}$	2−	0
0.2024	(3−)	$p_{\frac{1}{2}}d_{\frac{5}{2}}$	3−	
0.247		$p_{\frac{1}{2}}g_{\frac{7}{2}}$	3−	
—		$p_{\frac{1}{2}}d_{\frac{3}{2}}$	1− and 2−	
0.7767	(2+)	$g_{\frac{7}{2}}d_{\frac{5}{2}}$	2+	0.913[b]
1.215	(0− or 1−)[a]	$p_{\frac{1}{2}}s_{\frac{1}{2}}$	0− and 1−	(1.22)[c]

[a] See ref. [5]).

[b] Energy of $\frac{9}{2}+$ level in Y^{89} see ref. [18]).

[c] According to Bunker, Mize and Starner [19]), the beta decay of Y^{91} leading to the 1.22 MeV level of Zr^{91} has a log *ft* value of 8.80, indicating that this level is possibly $\frac{1}{2}-$. However, such a situation would be difficult to understand on the single particle model since the ground state of Zr^{91} is known to be $\frac{5}{2}+$. Way *et al.* [18]) favour $\frac{1}{2}-$ or $\frac{3}{2}+$ for the 1.22 MeV level.

The first column contains the energy and the second, the spin and parity assignments of the observed levels. The third column contains the low energy shell model configurations and the fourth column the spins of all states belonging to these configurations which might be expected to be excited appreciably in the Y^{89}(n, γ)Y^{90} reaction. The fifth column contains the zero-order estimate for the excitation energies of the configurations.

the excitation energy itself. It would appear from table 3 that the observed excited states, at least up to 1.215 MeV might be accounted for with some degree of plausibility in terms of these low energy configurations and although a comparison of this type may have little more than qualitative significance, a number of details call for some further discussion.

Firstly, the suggestion of 3— for the 0.247 MeV level is consistent with the observation that the 6.590 MeV primary transition from the capturing state has an intensity equal to that of the 6.646 MeV gamma ray feeding the first excited state which, as described above, is also probably 3—. Furthermore, the transition from the 0.7767 MeV level to the 0.247 MeV level is much weaker (at least by an order of magnitude) than the 0.575 MeV transition to

the 0.2024 MeV level as might be expected if the former transition involved a two particle jump, $g_{\frac{7}{2}}d_{\frac{5}{2}} \rightarrow p_{\frac{1}{2}}g_{\frac{7}{2}}$, while the latter involved a one particle jump †, $g_{\frac{7}{2}}d_{\frac{5}{2}} \rightarrow p_{\frac{1}{2}}d_{\frac{5}{2}}$. We also note, incidentally, that the assumption of 3— for the 0.2024 and 0.247 MeV levels is consistent with the fact that the beta decay of Sr^{90} (of total disintegration energy 0.535 MeV) has been observed to occur only to the ground state of Y^{90}, a state of affairs which would be difficult to understand if the spin and parity of the first or second excited state were $0\pm$, $1\pm$, or 2—.

Secondly, the $g_{\frac{7}{2}}d_{\frac{5}{2}}$ configuration is the only one among those expected to occur at low energies which can give rise to a spin and parity of 2+ for the 0.7767 MeV level. This, together with the agreement between the observed energy of this state and the $p_{\frac{1}{2}}$-$g_{\frac{7}{2}}$ splitting in Y^{89}, makes this configuration assignment seem plausible. It is also to be noted that the failure to observe a (d, p) stripping reaction leading to the 0.7767 MeV level is consistent with the requirement that, for the configuration assumed for this level in table 3, the proton orbit must change from $p_{\frac{1}{2}}$ to $g_{\frac{7}{2}}$, a process which must involve formation of an intermediate compound nucleus.

Thirdly, the observation [5]) of an $l_n = 0$ stripping pattern for the 1.17 MeV level is sufficient, on the single particle model, to specify its configuration uniquely as $p_{\frac{1}{2}}s_{\frac{1}{2}}$. The identification of this level as the 1.215 MeV level observed in the present experiment is consistent with the observation of the relatively weak 5.631 MeV gamma ray which would be of M1 type if the 1.215 MeV level were 0— or 1—.

Finally, it may appear at first sight somewhat strange that evidence was found for only one of the 0— or 1— levels of the $p_{\frac{1}{2}}s_{\frac{1}{2}}$ configuration and for neither the 1— nor the 2— level of the $p_{\frac{1}{2}}d_{\frac{5}{2}}$ configuration. If such levels are present in the energy range below 1.215 MeV we estimate that the primary transitions feeding them must have intensities less than 0.5 gamma rays per 100 captures ††. This limit is only four times less than the intensity of the 5.631 MeV gamma ray and therefore such levels are by no means ruled out by the present observations. Evidence for other levels, at least in the region below 2.741 MeV, is provided by the complex decay of the 2.741 MeV level and it would not be surprising if other levels of low spin were present below 1.215 MeV.

It is evident from these preliminary investigations of the properties of Y^{90} that further study of this nucleus using other reactions may lead to a better understanding of the shell model in this mass region.

† Both transitions in principle violate the orbital angular momentum selection rule. However, transitions corresponding to one particle jumps which violate the l-selection rule though somewhat weaker than normal, are observed. See, for example, refs. [20]).

†† See above discussion of the weak peak at 6.48 MeV.

References

1) P. J. Campion and G. A. Bartholomew, Can. J. Phys. **35** (1957) 1361
2) G. A. Bartholomew and B. B. Kinsey, Can. J. Phys. **31** (1953) 1025
3) D. Strominger, J. M. Hollander and G. T. Seaborg, Revs. Mod. Phys. **30** (1958) 585
4) N. S. Wall, Phys. Rev. **96** (1954) 664
5) N. S. Wall, Phys. Rev. **96** (1954) 670
6) D. J. Hughes and R. B. Schwartz, Neutron Cross Sections, Second Edition BNL325 (1958)
7) B. B. Kinsey and G. A. Bartholomew, Can. J. Phys. **31** (1953) 537
8) J. W. Knowles, Can. J. Phys. **37** (1959) 203
9) G. Manning and G. A. Bartholomew, to be published
10) See compilation by G. A. Bartholomew and L. A. Higgs, Atomic Energy of Canada Limited, Chalk River Report AECL 669 (1958)
11) Unpublished
12) B. B. Kinsey, Beta and Gamma Ray Spectroscopy, edited by K. Siegbahn (North-Holland Publishing Co., Amsterdam, 1955)
13) See J. P. Elliott and A. M. Lane, Handbuch der Physik (Springer-Verlag, Berlin) **39** (1957) 241
14) K. W. Ford, Phys. Rev. **98** (1955) 1516;
see also N. H. Lazar, G. D. O'Kelley, J. H. Hamilton, L. M. Langer and W. G. Smith, Phys. Rev. **110** (1958) 513;
and R. K. Sheline, Physica **23** (1957) 923
15) M. H. L. Pryce, Proc. Phys. Soc. A **65** (1952) 773
16) F. J. Shore, W. L. Bendel, H. N. Brown and R. A. Becker, Phys. Rev. **91** (1953) 1203
17) P. F. A. Klinkenberg, Revs. Mod. Phys. **24** (1952) 63
18) K. Way, R. W. King, C. L. McGinnis and R. van Lieshout, Nuclear Level Schemes, U.S.A.E.C. report TID-5300 (1955)
19) M. E. Bunker, J. P. Mize and J. W. Starner, Phys. Rev. **94** (1954) 1694
20) R. L. Graham and R. E. Bell, Can. J. Phys. **31** (1957) 377;
H. de Waard and T. R. Gerholm, Nuclear Physics **1** (1956) 281;
R. Lindqvist and I. Marklund, Nuclear Physics **3** (1957) 367

8.B *Nuclear Physics* **10** (1959) 606—619; © *North-Holland Publishing Co., Amsterdam*
Not to be reproduced by photoprint or microfilm without written permission from the publisher

THE CAPTURE OF MUONS BY COMPLEX NUCLEI

H. A. TOLHOEK †
Theoretical Study Division, CERN, *Geneva*

Received 29 December 1958

Abstract: A comparison is made of different theoretical approaches for calculating the total rates for capture of muons by complex nuclei. The merits of the closure approximation and shell model calculations are discussed. The application of the closure approximation to a statistical model of the nucleus is worked out in some detail. A tentative explanation of the experimental data in terms of a universal Fermi interaction is given.

1. Some General Features of Muon Capture Theory

Theoretical considerations on the capture of muons by complex nuclei have been published by Tiomno and Wheeler [1]), Kennedy [2]), Primakoff [3]) and Tolhoek and Luyten [4]). Recent experimental data were obtained by Sens, Swanson, Telegdi and Yovanovitch [5]) and by Asbury, Kemp, Lipman, Muirhead, Voss, Zangger and Kirk [6]). (Cf. ref. [4]) for references to older work.) The interpretation of the data has a special interest for the discussion of the Universal Fermi Interaction, in particular in the form proposed by Feynman and Gell-Mann [7]).

In this paper we want to compare certain features of the different theoretical approaches, which do not come out very clearly in the cited papers themselves. (Cf., e.g., the discussion in ref. [8])). In section 2 the use of the closure approximation for a statistical model of the nucleus is treated. In section 3 a discussion of the relative merits of the different approaches is given.

Muon capture differs from electron capture by one important feature, namely that the energy release (105 MeV) is considerably higher. This enables the final nucleus to reach many excited states. A 4-fermion interaction for muon capture may be written in the form

$$H_{\mu c} = g_{\mu c}(\psi_n^* \Gamma Q \psi_p)(\psi_\nu^* \Gamma \psi_\mu) \tag{1.1}$$

(Γ = Dirac matrix; Q = p → n transition operator). The total capture transition probability $\Lambda_{\mu c}$ is then calculated according to

$$\Lambda_{\mu c} = 1/\tau_{\mu c} = (2\pi/\hbar) g_{\mu c}^2 \sum_f |\langle f|M|i\rangle|^2 \rho(E), \tag{1.2}$$

† On leave of absence from the Physical Laboratory, University of Groningen.

where the transition matrix element can be written as

$$\langle \mathrm{f}|M|\mathrm{i}\rangle = \sum_{k=1}^{A} \int \mathrm{d}x [\Psi_\mathrm{f}^*(E_\mathrm{f}^{\mathrm{exc}}) \Gamma_k Q_k \Psi_\mathrm{i}][\psi_\nu^*(E_\nu) \Gamma \psi_\mu]_{\mathbf{r}=\mathbf{r}_k}; \qquad (1.3)$$

Ψ_i and Ψ_f are the wave functions of the initial and final nuclei (containing A nucleons); $\int \mathrm{d}x$ indicates the integration over space coordinates and summation over spin and isospin coordinates of the nucleons; Γ_k and Q_k are the operators for the k^{th}-nucleon; $\mathbf{r} = \mathbf{r}_k$ indicates that the lepton wave functions have to be taken at the place of the k^{th}-nucleon. The summation $\sum_\mathrm{f} = \sum_\mathrm{f}^{\mathrm{nucl}} \sum_\mathrm{f}^{\nu}$ indicates a summation over the different possible final states of the nucleus, as well as those of the neutrino. The energy of the neutrino E_ν is related to the excitation energy of the final nucleus by $E_\nu = m_\mu c^2 - E_\mathrm{f}^{\mathrm{exc}} \approx 105$ MeV $- E_\mathrm{f}^{\mathrm{exc}}$ (neglecting the energy difference of the ground states of initial and final nuclei). If one is interested in the total transition probability, making a summation over different nuclear excitations, the calculations may often be considerably simplified by introducing the following approximation: *the neutrino energy E_ν is put equal to an average value* $\bar{E}_\nu = 105$ MeV $- \langle E_\mathrm{f}^{\mathrm{exc}} \rangle_{\mathrm{av}}$. This approximation seems fairly good because the mean nuclear excitation is of the order of 15 MeV, which is relatively small in comparison with the total energy release of $m_\mu c^2 \approx 105$ MeV. In the cases of specific nuclear models, this approximation may then be used in the following way:

(a) *Group summation approximation.* In the case of shell model calculation for nuclei, which have a closed (sub)shell for either neutrons or protons (or both) the following holds †:

The total capture probability may be considered as the sum of the individual transition probabilities for transitions between definite initial proton and final neutron states. For each of these transitions an average is taken over all magnetic quantum numbers of the proton states and the neutron states.

This approximation was used by Tolhoek and Luyten [4]), mentioned concisely in ref. [8]) p. 683. One may make the refinement in the case of shell model calculations of taking a different neutrino energy for each of the various transition groups considered. In this way one should get a more accurate result than with the closure approximation, which uses one mean value of the neutrino energy.

(b) *Closure approximation.* When summing over a complete set of final states, one may use the property $\sum_\mathrm{f} |\mathrm{f}\rangle\langle\mathrm{f}| = 1$. This approximation may be applied to an "average nuclear model" as was first indicated by Primakoff [3]). This approach will be discussed in more detail in section 2. Burkhardt [11]) has applied the closure approximation to shell model calculations.

† A mimeographed note explaining this in more detail is available on request.

A further feature of muon-capture arises from the ratio of nuclear radii to the neutrino wave-length, $\lambda_\nu \approx 12.5\times 10^{-13}$ cm for $E_\nu = 100$ MeV. The fact that the neutrino wave-length is larger, but not much larger than the values of nuclear radii, has the following consequences:

(a) The different matrix elements which are designated as allowed, first forbidden, second forbidden etc. in the theory of β-radioactivity are not different in order of magnitude, but decrease only rather slowly in the case of muon-capture, so that matrix elements of more than one order must be calculated (or at least estimated).

(b) One should realize that of the two models proposed by Tiomno and Wheeler [1]: (I) "free particle model" ($R \gg \lambda\!\!\!^{-}_\nu$) and (II) "dipole transition model" ($\lambda\!\!\!^{-}_\nu \gg R$), the first model seems the less realistic one; furthermore the second one is rather easily improved (although this involves considerable work), by including higher order transition matrix elements.

Finally, one should bear in mind that the *Pauli principle* limits severely the possible individual nucleon transitions: the protons can only go to states which are not yet occupied by neutrons. If $N \geqq Z$, all neutron states corresponding to proton states will be occupied in an "average" nuclear model and *no "allowed" contributions to the capture rate will exist at all.* In view of this fact, Tiomno and Wheeler [1]) calculated in particular the first forbidden contribution in their "dipole transition model".

2. The Closure Approximation for an Average Model of the Nucleus

This approximation can be used for muon-capture calculations, as was first proposed by Primakoff [3]). As to the methods used, a similar application of the closure approximation by Gottfried [9]) and the introduction of (partial) density matrices for many-particle systems by Löwdin [10]) may be compared. Using the closure approximation for the final states of the nucleus, one obtains from (1.3)

$$\begin{aligned} M^2 &= \sum_{\mathrm{f}} |\langle \mathrm{f}|M|\mathrm{i}\rangle|^2 \\ &= \sum_{n=1}^{A}\sum_{n'=1}^{A}\int \mathrm{d}x \Psi_1^*(x)\Gamma_{n'}^{+} Q_{n'}^{+} Q_n \Gamma_n \Psi_1(x) F(\mathbf{r}_n, \mathbf{r}_{n'}) \end{aligned} \tag{2.1}$$

with

$$F(\mathbf{r}, \mathbf{r}') = \textstyle\sum_t^{\nu} [\psi_\nu^*(\mathbf{r}')\Gamma\psi_\mu(\mathbf{r}')]^*[\psi_\nu^*(\mathbf{r})\Gamma\psi_\mu(\mathbf{r})]; \tag{2.2}$$

x indicates the set of all space, spin and isospin coordinates of the A nucleons. The expression (2.1) has the form of an expectation value for the state Ψ_1. The expectation value of an operator Ω may be written with the aid of a density matrix ρ

$$\langle \Omega \rangle_{\mathrm{av}} = \langle \Psi|\Omega|\Psi\rangle = \mathrm{Tr}[\Omega\rho] \tag{2.3}$$

with

$$\rho = |\Psi\rangle\langle\Psi|, \tag{2.4}$$

using Dirac notation. In the case in which the operator Ω can be written in the form

$$\Omega = \Omega_0 + \sum_i \Omega_i + \sum_{ij}{}' \Omega_{ij}, \tag{2.5}$$

where $\sum'_{ij}$ means $\sum_{ij}$ with $i \neq j$, eq. (2.3) can be reduced to a form

$$\begin{aligned}\langle\Omega\rangle_{\mathrm{av}} = \Omega_0 &+ \int \mathrm{d}x_1 \int \mathrm{d}\bar{x}_1 \langle x_1|\Omega_1|\bar{x}_1\rangle\langle\bar{x}_1|\rho^{(1)}|x_1\rangle \\ &+ \int \mathrm{d}x_1 \int \mathrm{d}x_2 \int \mathrm{d}\bar{x}_1 \int \mathrm{d}\bar{x}_2 \langle x_1 x_2|\Omega_{12}|\bar{x}_1\bar{x}_2\rangle\langle\bar{x}_1\bar{x}_2|\rho^{(2)}|x_1 x_2\rangle,\end{aligned} \tag{2.6}$$

if the k-particle-density $\rho^{(k)}$ is introduced according to

$$\begin{aligned}&\langle x_1 \ldots x_k|\rho^{(k)}|x'_1 \ldots x'_k\rangle \\ &\quad = \frac{A!}{(A-k)!}\int \Psi(x_1 \ldots x_A)\Psi^*(x'_1 \ldots x'_k, x_{k+1} \ldots x_A)\mathrm{d}x'_{1\ldots k};\end{aligned} \tag{2.7}$$

$\int \mathrm{d}x'_{1\ldots k}$ indicates integration over all coordinates $x_{k+1}, \ldots, x_A$. Applying (2.6) to (2.1) we obtain

$$\begin{aligned}M^2 = &\sum_{\xi_1\eta_1\xi'_1\eta'_1} \int \mathrm{d}\mathbf{r}_1 \langle \mathbf{r}_1\xi_1\eta_1|D|\mathbf{r}_1\xi'_1\eta'_1\rangle\langle\mathbf{r}_1\xi'_1\eta'_1|\Omega_1|\mathbf{r}_1\xi_1\eta_1\rangle \\ &+ \sum_{\xi_1\eta_1\xi'_1\eta'_1}\sum_{\xi_2\eta_2\xi'_2\eta'_2} \int \mathrm{d}\mathbf{r}_1 \int \mathrm{d}\mathbf{r}_2 \langle \mathbf{r}_1\mathbf{r}_2\xi_1\eta_1\xi_2\eta_2|g|\mathbf{r}_1\mathbf{r}_2\xi'_1\eta'_1\xi'_2\eta'_2\rangle \\ &\qquad \cdot \langle \mathbf{r}_1\mathbf{r}_2\xi'_1\eta'_1\xi'_2\eta'_2|\Omega_{12}|\mathbf{r}_1\mathbf{r}_2\xi_1\eta_1\xi_2\eta_2\rangle\end{aligned} \tag{2.8}$$

with

$$\Omega_i = \Gamma_i^+ Q_i^+ Q_i \Gamma_i F(\mathbf{r}_i, \mathbf{r}_i), \tag{2.9}$$

$$\Omega_{ij} = \Gamma_i^+ Q_i^+ Q_j \Gamma_j F(\mathbf{r}_j, \mathbf{r}_i). \tag{2.10}$$

We have designated the one- and two-particle-densities $\rho^{(1)}$ and $\rho^{(2)}$ as D and g; because Ω_i and Ω_{ij} are diagonal in the space coordinates, we only need the diagonal matrix elements of D and g, with respect to the space coordinates; however, the non-diagonal elements with respect to spin and isospin are also needed. In the case of a system which can be specified by a Slater determinant (κ indicating the individual nucleon states ψ_κ)

$$\Psi(x_1 \ldots x_A) = (A!)^{-\frac{1}{2}} \sum_P \delta_P \prod_{\kappa=1}^{A} \psi_\kappa(x_{P\kappa}), \tag{2.11}$$

where $x_i = (\mathbf{r}_i, \xi_i, \eta_i)$ indicates the space coordinate $\mathbf{r}_i$, spin coordinate ξ_i, isospin coordinate η_i for the i^{th} particle, D and g are given by

$$\langle \mathbf{r}_1 \xi_1 \eta_1 | D | \mathbf{r}_1 \xi'_1 \eta'_1 \rangle = \sum_\kappa \psi_\kappa(\mathbf{r}_1 \xi_1 \eta_1) \psi_\kappa^*(\mathbf{r}_1 \xi'_1 \eta'_1), \tag{2.12}$$

$$\begin{aligned}\langle \mathbf{r}_1 \mathbf{r}_2 \xi_1 \eta_1 \xi_2 \eta_2 | g | \mathbf{r}_1 \mathbf{r}_2 \xi'_1 \eta'_1 \xi'_2 \eta'_2 \rangle \\ = \sum_{\kappa\lambda} [\psi_\kappa(\mathbf{r}_1 \xi_1 \eta_1) \psi_\lambda(\mathbf{r}_2 \xi_2 \eta_2) \psi_\kappa^*(\mathbf{r}_1 \xi'_1 \eta'_1) \psi_\lambda^*(\mathbf{r}_2 \xi'_2 \eta'_2) \\ - \psi_\kappa(\mathbf{r}_1 \xi_1 \eta_1) \psi_\lambda(\mathbf{r}_2 \xi_2 \eta_2) \psi_\lambda^*(\mathbf{r}_1 \xi'_1 \eta'_1) \psi_\kappa^*(\mathbf{r}_2 \xi'_2 \eta'_2)].\end{aligned} \tag{2.13}$$

In order to reduce the expressions for D and g further, one has to assume a specific nuclear model. For a simple first approach an "average" nuclear model will be introduced, using a Fermi gas, and having the following features:

(a) The pair correlation function is calculated as if the wave function were given by a Slater determinant for plane waves contained in a large cubic box (with periodic boundary conditions).

(b) However, the density distribution is assumed to be such that we have a spherical nucleus of radius $R = r_0 A^{\frac{1}{3}}$. (This density distribution also enters as a multiplicative factor in the pair correlation function.)

(c) Every space state, occupied by a nucleon with a certain spin, also contains a nucleon of the same type with the opposite spin.

(d) The calculation is also made for $N \neq Z$, as the dependence of the result on N/Z is a point of interest. Hence we have different Fermi limits for protons and neutrons

$$k_F^{(p)} = (3\pi^2)^{\frac{1}{3}} (Z/V)^{\frac{1}{3}}, \tag{2.14}$$

$$k_F^{(n)} = (3\pi^2)^{\frac{1}{3}} (N/V)^{\frac{1}{3}}, \tag{2.15}$$

where V is the nuclear volume

$$V = \tfrac{4}{3}\pi R^3 \quad (R = r_0 A^{\frac{1}{3}}). \tag{2.16}$$

It should be noted that assumptions (a) and (b) are only partially compatible, so that the result will hold only fairly well for "large" nuclei, i.e., for nuclei having $k_F R \gg 1$.

From the preceding starting points we then arrive at the following results for D and g for such nuclei:

$$\langle \mathbf{r}_1 \xi_1 \eta_1 | D | \mathbf{r}_1 \xi'_1 \eta'_1 \rangle = \tfrac{1}{2} \delta_{\xi_1 \xi'_1} V^{-1} C(r_1) [Z \Lambda_p^{(1)} + N \Lambda_n^{(1)}], \tag{2.17}$$

$$\begin{aligned}&\langle \mathbf{r}_1 \mathbf{r}_2 \xi_1 \eta_1 \xi_2 \eta_2 | g | \mathbf{r}_1 \mathbf{r}_2 \xi'_1 \eta'_1 \xi'_2 \eta'_2 \rangle \\ &= C(r_1) C(r_2) \{ \tfrac{1}{4} \delta_{\xi_1 \xi'_1} \delta_{\xi_2 \xi'_2} V^{-2} [Z \Lambda_p^{(1)} + N \Lambda_n^{(1)}][Z \Lambda_p^{(2)} + N \Lambda_n^{(2)}] \\ &- (6\pi^2)^{-2} \delta_{\xi_1 \xi'_2} \delta_{\xi_2 \xi'_1} [\nu_+(\eta_1) \nu_+(\eta'_2) k_F^{(p)3} S(k_F^{(p)} r) + \nu_-(\eta_1) \nu_-(\eta'_2) k_F^{(n)3} S(k_F^{(n)} r)] \\ &\times [\nu_+(\eta_2) \nu_+(\eta'_1) k_F^{(p)3} S(k_F^{(p)} r) + \nu_-(\eta_2) \nu_-(\eta'_1) k_F^{(n)3} S(k_F^{(n)} r)] \},\end{aligned} \tag{2.18}$$

where $r = |\mathbf{r}_1 - \mathbf{r}_2|$ is the distance between particles 1 and 2; $C(r)$ specifies the radial dependence of the density. In the simplest model one can take

$$C(r) = 1, \quad \text{if} \quad r \leqq R; \quad C(r) = 0, \quad \text{if} \quad r > R. \tag{2.19}$$

The operators Λ_p and Λ_n are the projection operators in isospin notation

$$\Lambda_p = \tfrac{1}{2}(1+\tau_3), \quad \Lambda_n = \tfrac{1}{2}(1-\tau_3). \tag{2.20}$$

The superscripts 1 and 2 of Λ_p and Λ_n indicate that one should take the matrix elements for the coordinates (η_1, η'_1) and (η_2, η'_2) respectively; ν_+ and ν_- are the isospin functions

$$\nu_+(\eta) = \begin{pmatrix}1\\0\end{pmatrix} \text{(proton)}; \quad \nu_-(\eta) = \begin{pmatrix}0\\1\end{pmatrix} \text{(neutron)}. \tag{2.21}$$

The function S is given by

$$S(x) = 3x^{-3}(\sin x - x\cos x) = 3(\tfrac{1}{2}\pi)^{\frac{1}{2}} x^{-\frac{3}{2}} J_{\frac{3}{2}}(x). \tag{2.22}$$

We shall now give the reduced expressions for Ω_i and Ω_{ij} according to (2.9) and (2.10), keeping only terms up to the order of the "first forbidden matrix elements". When using plane waves for the neutrino wave functions, normalized to one particle in a (large) normalization volume ω, one obtains, averaging over all directions:

Fermi interaction

$$\Omega_i = |\varphi_\mu(0)|^2(2\omega)^{-1}\tfrac{1}{2}(1+\tau_3^{(i)}), \tag{2.23}$$

$$\Omega_{ij} = |\varphi_\mu(0)|^2(2\omega)^{-1}Q_i^+ Q_j[1-\tfrac{1}{6}q^2|\mathbf{r}_i-\mathbf{r}_j|^2], \tag{2.24}$$

Gamow-Teller interaction

$$\Omega_i = 3|\varphi_\mu(0)|^2(2\omega)^{-1}\tfrac{1}{2}(1+\tau_3^{(i)}), \tag{2.25}$$

$$\Omega_{ij} = |\varphi_\mu(0)|^2(2\omega)^{-1}\boldsymbol{\sigma}^{(i)}\cdot\boldsymbol{\sigma}^{(j)}Q_i^+ Q_j[1-\tfrac{1}{6}q^2|\mathbf{r}_i-\mathbf{r}_j|^2]. \tag{2.26}$$

$|\varphi_\mu(0)|^2$ gives the square of the absolute value of the μ-meson wave function in its K-orbit at the place of the nucleus (averaged over the nuclear volume); $q = E_\nu/\hbar c$ is the average neutrino wave number.

The density of states per unit energy interval for the above-mentioned normalization of the neutrino wave functions is given by

$$\rho(E) = \omega q^2(2\pi^2\hbar c)^{-1}. \tag{2.27}$$

The result for M^2 can now be obtained from (2.8), (2.17), (2.18) and (2.23) ... (2.26). The results can be written as

Fermi interaction

$$M_F^2 = |\varphi_\mu(0)|^2(T_0+T_1)(2\omega)^{-1}, \tag{2.28}$$

Gamow-Teller interaction

$$M_{GT}^2 = 3|\varphi_\mu(0)|^2(T_0+T_1)(2\omega)^{-1}, \tag{2.29}$$

where T_0 and T_1 collect the terms of "allowed" and "first forbidden order" respectively. They are given by ($r = |\mathbf{r}_1-\mathbf{r}_2|$)

$$T_0 = Z - 2(6\pi^2)^{-2}\int d\mathbf{r}_1\int d\mathbf{r}_2 C(r_1)C(r_2)k_F^{(n)3}k_F^{(p)3}S(k_F^{(n)}r)S(k_F^{(p)}r), \tag{2.30}$$

$$T_1 = \tfrac{1}{3}q^2(6\pi^2)^{-2}\int d\mathbf{r}_1\int d\mathbf{r}_2 C(r_1)C(r_2)k_F^{(n)3}k_F^{(p)3}S(k_F^{(n)}r)S(k_F^{(p)}r)r^2. \tag{2.31}$$

One finally obtains the capture rate $\Lambda_{\mu c}$ from (1.2), (2.27), . . ., (2.31). If we suppose that we have a mixture of Fermi-interaction and Gamow-Teller interaction with coupling constants $g_{\mu c}^{F}$ and $g_{\mu c}^{GT}$, we can write the result as

$$\Lambda_{\mu c} = [(g_{\mu c}^{F})^2+3(g_{\mu c}^{GT})^2](2\pi c)^{-1}\hbar^{-2}q^2|\varphi_\mu(0)|^2(T_0+T_1). \tag{2.32}$$

For applications, one wants to have the final result, contained in (2.30), . . ., (2.32) in a more explicit form, for which the evaluation of the integrals is required.

The integral in (2.30) can be evaluated making use of the following result [12]) (putting $k_F^{(n)} = a$, $k_F^{(p)} = b$):

$$J_{a,b}^{(0)} = \int_0^\infty x^2 S(ax)S(bx)\mathrm{d}x = \begin{cases} \frac{3}{2}(\pi/a^3), & \text{if } a \geqq b, \\ \frac{3}{2}(\pi/b^3), & \text{if } b \geqq a. \end{cases} \tag{2.33}$$

In the case of fairly large nuclei ($k_F R \gg 1$), one can now write in first approximation, if $N \geqq Z$ (so that $a \geqq b$), making use of (2.14) and (2.33)

$$\begin{aligned} \int \mathrm{d}\mathbf{r}_1 \int \mathrm{d}\mathbf{r}_2 C(r_1)C(r_2)a^3b^3S(ar)S(br) &\approx Va^3b^3 4\pi \int_0^\infty r^2 S(ar)S(br)\mathrm{d}r \\ &= 6\pi^2 Vb^3 = \tfrac{1}{2}(6\pi^2)^2 Z. \end{aligned} \tag{2.34}$$

Hence one obtains from (2.30) and (2.34)

$$T_0 = Z-Z = 0. \tag{2.35}$$

If one would have nuclei with $Z > N$, one would find in the same way instead of (2.35): $T_0 = Z-N$.

We have arrived at the conclusion that $T_0 = 0$ for $N \geqq Z$ already in section 1: no allowed contributions should occur in this case, because of the Pauli principle (for an average nuclear model). However, it is seen that this conclusion should hold rigorously, while in (2.34) and (2.35) it is a result of an approximate calculation. This can be understood from the fact that the density and pair correlation functions represented by (2.17), (2.18) can only be approximate expressions, which can fulfil the preceding requirements (a) and (b) only if $k_F R \gg 1$. It is clear from the derivation of (2.35) that it just holds in the limit of large R.

For a more precise evaluation of (2.30) and (2.31), we can use the equation (for an arbitrary function $F(r)$, if $C(r)$ is given by (2.19); see appendix)

$$\int \mathrm{d}\mathbf{r}_1 \int \mathrm{d}\mathbf{r}_2 C(r_1)C(r_2)F(r) = \tfrac{1}{3}\pi^2 \int_0^{2R} F(r)[16R^3r-12R^2r^2+r^4]r\mathrm{d}r. \tag{2.36}$$

One may readily check with the aid of (2.36) that (2.35) is satisfied for the limit of large R, but that for actual nuclei this equation is not very well fulfilled. E.g. for ^{40}Ca the integral in (2.30) compensates only 65 % of the term Z. As we know, however, from the general argument of section 1 that (2.35) should hold strictly, for the correct D- and g-functions, we shall calculate $\Lambda_{\mu c}$ only with the term T_1 (dropping T_0). Using (2.36) (see appen-

dix), we obtain in this way from (2.32)

$$\Lambda_{\mu c} = \frac{[(g_{\mu c}^{F})^2+3(g_{\mu c}^{GT})^2]q^4 bR^3}{72\pi^3\hbar^2 c}|\varphi_\mu(0)|^2 J(\xi,\zeta), \tag{2.37}$$

where

$$J(\xi,\zeta) = \int_0^{2\xi} t^{-2}(\sin t - t\cos t)(\sin \zeta t - \zeta t\cos \zeta t)[16-12(t/\xi)+(t/\xi)^3]\mathrm{d}t, \tag{2.38}$$

$$\xi = bR, \tag{2.39}$$

$$\zeta = a/b = (N/Z)^{\frac{1}{3}}. \tag{2.40}$$

This gives the result in a form suitable for explicit calculation. Some numerical results are given in section 3. The application of the closure approximation to an average model of the nucleus was discussed in this section in some detail in order to show the approximations involved, in view of the comparison of the different methods in section 3. The method for the calculation was first indicated by Primakoff [3]). However, his final result does not vanish in the allowed order and seems to contain a major contribution from this order. But we have seen that the result should be zero in the allowed order and that non zero results can only be introduced by mathematical approximations.

3. Comparison of Different Methods

In this section we want to disscuss some relative merits of different theoretical approaches to the problem of muon-capture by complex nuclei:

A) use of the closure approximation for an "average" nucleus (Fermi-gas),

B) use of the closure approximation in connection with shell model wave functions,

C) use of the group summation approximation in connection with shell model wave functions.

The main aims of calculations of this kind are:

(1) to obtain the absolute value of the coupling constant, i.e. the value of the combination

$$g_{\mu c}^2 = (g_{\mu c}^{F})^2+3(g_{\mu c}^{GT})^2, \tag{3.1}$$

(2) to obtain information on the character of the interaction, i.e., on the mixing ratio of Gamow-Teller and Fermi interactions

$$X_{\mu c} = g_{\mu c}^{GT}/g_{\mu c}^{F}. \tag{3.2}$$

However, it may be that the muon-capture interaction is more complicated in nature and that even the absolute capture rates in complex nuclei cannot be adequately described in terms of the two constants $g_{\mu c}^{F}$ and $g_{\mu c}^{GT}$ only. In this paper we have confined ourselves to the consequences of Fermi interaction (S, V) and Gamow-Teller interaction (T, A) in the non-relativistic approximation for the nucleons. Those results provide probably the major

contribution, although detailed calculations on the effects of a large effective pseudoscalar coupling [13]) and the effect of Gell-Mann's "weak magnetism"[14]) are very much desirable.

If we now compare the different approaches the following points are to be noted:

(1) *The closure approximation for an "average nucleus"* has obviously the advantage of providing a result for any N and Z not requiring separate laborious calculations for every nucleus.

(2) The use of the *closure approximation* gives a substantial simplification by carrying out immediately the sum over the final states. However, the replacement of the neutrino energy E_ν by an average value $\bar{E}_\nu$ is an approximation which may introduce non-negligible errors: it is seen from (2.37) that the neutrino momentum q figures in the first forbidden contribution as q^4, so that the final result is quite sensitive to errors in q. This holds even more strongly for second forbidden contributions. Hence transitions to highly excited final states of the nucleus are strongly overestimated in this way. The absolute value of a result obtained with the closure approximation will therefore always have an appreciable uncertainty due to this cause.

(3) *The group summation approximation* can avoid this cause of error by taking separate energies for every "group" of levels of the final nucleus (cf. section 1). However, the simplification provided by this method is limited to nuclei with closed shells for either protons (and) or neutrons.

(4) In order to limit the amount of work, one is tempted to drop, e.g., the second forbidden contributions, when applying the *group summation approximation*. This may cause an underestimate of these contributions, in contrast with the overestimate in the closure approximation.

(5) A disadvantage of the use of an *"average" picture* of the nucleus, such as given in section 2, is that the allowed contributions are eliminated by the assumptions made. Hence one does not find in this way any influence of the character of the interaction on the total capture rates. On the other hand, in the case of the shell model [4]), it was calculated that the allowed contributions can be appreciable in the case of Gamow-Teller interaction. Thus the ratios of capture rates for different elements will be appreciably influenced by the character of the interaction (value of $X_{\mu c}$) according to the shell model picture, which must be considered as more realistic.

(6) It will be clear from the preceding point (5) and the considerations at the end of section 2 that the *closure approximation for an average nucleus* can only lead to *very rough results*. It is also difficult to diagnose what errors in the final result will be caused by the approximations made in the assumptions. Also it should be realized that for heavy nuclei account must be taken of the terms for contributions of second forbidden order, so that supplementary terms must be added to the expressions (2.23), . . ., (2.26).

(7) It is of interest to know to what extent the muon-capture rate is influenced by *dynamical correlations caused by the hard core of the nuclear potential.* An estimate of this effect could be obtained by means of the closure approximation for an average nucleus, when taking for example Jastrow wave functions [15]) for the description of the correlations (similar to the application of such wave functions by Gottfried [9]) on another problem).

The selection of the most suitable nuclei for the theoretical and experimental study of muon-capture is difficult because one would like to satisfy several conflicting requirements:

(a) The theoretical calculations give more reliable results for nuclei with well-known wave function: p and D are the best known, and nuclei in the neighbourhood of ^{16}O are better known than those near ^{40}Ca.

(b) Experiments become very difficult for low Z (say for $Z < 10$), because the free μ-decay rate is then greater than the μ-capture rate and in fact one often measures the sum of the two rates.

(c) Nuclei with doubly closed shells such as ^{16}O, ^{40}Ca seem very suitable for determining $(g^{\mathrm{F}}_{\mu c})^2+3(g^{\mathrm{GT}}_{\mu c})^2$, as they do not show any influence of the character of the interaction.

(d) In order to have a large dependence on the interaction type one should choose nuclei with large allowed contributions for the Gamow-Teller interaction (with a reasonably certain assignment of the configuration). The nuclei ^{51}V, ^{52}Cr, ^{54}Fe seem very suitable for this purpose. In order to have a large effect, one must not be very close to ^{16}O, ^{40}Ca, etc., because then only a few nucleons can provide an effect, while most partial transitions do not.

One should aim at a kind of "μ-mesic nuclear physics", in which theoretical predictions and experimental results can be compared for specific nuclei (separated isotopes) within errors of a few percent. Much work will be needed before this goal is attained.

For the purpose of comparison we give some numerical results obtained according to (A) (section 2 of this paper) and (C), the shell model calculations [2, 4]). We write the capture rate as

$$\Lambda_{\mu c} = K[(g^{\mathrm{F}}_{\mu c})^2+3(g^{\mathrm{GT}}_{\mu c})^2]. \tag{3.3}$$

The value for K (in c.g.s. units) according to (2.37) is calculated to be (in the numerical evaluation of (2.37) we have taken $\hat{E}_\nu = 90$ MeV and $r_0 = 1.1\times10^{-13}$ cm; $|\varphi_\mu(0)|^2$ was calculated making use of the results for Z_{eff} calculated by Sens [5]); see ref. [1]) for the definition):

$$\begin{aligned} K &= 2.48\times10^{101} \quad \text{for} \quad {}^{16}\mathrm{O}\ (N = Z = 8), \qquad \text{(a)} \\ K &= 80.2\ \times10^{101} \quad \text{for} \quad {}^{40}\mathrm{Ca}(N = Z = 20). \qquad \text{(b)} \end{aligned} \tag{3.4}$$

Comparable results, calculated on the basis of the shell model are

$$K = 135\times10^{101} \quad \text{for} \quad {}^{40}\text{Ca (Kennedy [2]) †)},$$
$$K = 146\times10^{101} \quad \text{for} \quad {}^{40}\text{Ca (Tolhoek and Luyten [4])}). \tag{3.5}$$

It is seen that an appreciable difference exists between the results for K calculated for ^{40}Ca on the basis of the closure approximation for an average model and on the basis of the shell model. We assume that the difference is due to the rough approximations made in the average model considered and that the shell model results are more reliable.

The value for the coupling constant obtained from the experimental data [5, 6]) for ^{40}Ca, using the shell model results (3.5), is

$$[(g_{\mu c}^{F})^2+3(g_{\mu c}^{GT})^2]^{\frac{1}{2}} = (4.3\pm0.4)\times10^{-49}\ \text{erg}\cdot\text{cm}^3. \tag{3.6}$$

The errors quoted in (3.6) and (3.8) are only related to *known* uncertainties in the experimental results and in the theoretical calculations. The value is appreciably larger than the comparable quantity for the β-interaction. It may be wondered whether this is in contradiction with the hypothesis of the V—A universal Fermi interaction. One should consider (3.4) as a rather preliminary result, as the absolute value of K may be strongly affected by the approximations made and the precise choice of the values of the parameters, and in particular by the neglect of the effects mentioned in refs.[13, 14]). Further the (less reliable) experimental result for ^{16}O seems to give a rather different value of the coupling constant (when comparing with the preliminary calculations of Burkhardt [11])). However, if the high value (3.4) for the coupling constant should persist after further consideration of these points (several calculations are at present in progress), the following hypothesis may be most attractive: a universal Fermi interaction of the type V—A exists for β-decay and μ-capture; the coupling constants for the Fermi parts of the interactions are equal (the value for g_β^{F} is taken from ref. [16])):

$$g_\beta^{F} = g_{\mu c}^{F} = (1.41\pm0.01)\times10^{-49}\ \text{erg}\cdot\text{cm}^3; \tag{3.7}$$

the ratios g^{GT}/g^{F} are different for μ-capture and β-decay. From (3.6) and (3.7) one would then obtain

$$|X_{\mu c}| = |g_{\mu c}^{GT}/g_{\mu c}^{F}| = 1.67\pm0.2, \tag{3.8}$$

which may be compared with a value of $|X_\beta| = 1.25\pm0.04$ for β-decay [16]). Such a high value for $X_{\mu c}$ would fit in very well with the interpretation of the experimental results [5, 6]) for the ratios of capture rates in different nuclei according to the shell model calculations [4]), as these results agree in fact with the pure Gamow-Teller predictions within the experimental and theoretical uncertainties. For the value (3.8) of $X_{\mu c}$ derived above, the Fermi and Gamow-Teller predictions of table 2 of ref. [4]) would be weighted

† The value quoted in ref. [2]) is divided by 2, because Kennedy apparently used a normalization of the neutrino wave function which is twice too large. This is equivalent to a definition of the coupling constant different from the usual definition given for β-decay.

in the ratio of $1 : 3X_{\mu c}^2 = 1 : 8.3$ giving predicted values practically the same as those for pure Gamow-Teller coupling within the present accuracy. It is of interest to note that a recent experimental result of Burgman, Fischer, Leontic, Lundby, Meunier, Stroot and Teja [17]) on μ-capture by carbon 12 ($\mu^- + {}^{12}\mathrm{C} \rightarrow {}^{12}\mathrm{B} \rightarrow {}^{12}\mathrm{C} + \beta^-$) may also be interpreted as $|g_{\mu c}^{\mathrm{GT}}/g_{\beta}^{\mathrm{GT}}| = 1.17 \pm 0.04$, to be compared with the value $|g_{\mu c}^{\mathrm{GT}}/g_{\beta}^{\mathrm{GT}}| = 1.34 \pm 0.2$, which is obtained from (3.8). However, it should be stressed that these interpretations are all very tentative.

It is seen that the N- and Z-dependence of (2.37) is not very simple and that formulae such as that of Primakoff (see eq. (1) of ref. [5])), should be considered essentially as interpolation formulae applying over a wide range of N and Z. Primakoff's formula can be written as

$$\Lambda_{\mu c} \propto |\varphi_{\mu}(0)|^2 Z[1-\alpha(N-Z)/A]. \tag{3.9}$$

It should be noted that one may try equally well to fit the data with formulae such as

$$\Lambda_{\mu c} \propto |\varphi_{\mu}(0)|^2 R^3[1-\beta(N-Z)/A] (R = r_0 A^{\frac{1}{3}}), \tag{3.10}$$

or

$$\Lambda_{\mu c} \propto |\varphi_{\mu}(0)|^2 R^4[1-\gamma(N-Z)/A], \tag{3.11}$$

where α, β and γ are parameters to be fitted. Such fits over a wide range appear to have only a limited value, and it seems more profitable to concentrate on the precise study of specific nuclei.

The author is indebted to Dr. N. H. Lipman, Dr. A. Lundby, Dr. J. C. Sens, Dr. J. D. Teja, Dr. Y. Yamaguchi, Dr. K. Wildermuth for valuable discussions, to Mr. W. Klein for calculating the numerical results (3.4) and to Dr. G. H. Burkhardt for sending his results before publication. The author thanks Professor C. J. Bakker and Professor B. Ferretti for the hospitality of CERN.

Appendix

REDUCTION OF THE INTEGRAL (2.36).

We want to reduce the left-hand side of (2.36) given by

$$J = \int \mathrm{d}\mathbf{r}_1 \int \mathrm{d}\mathbf{r}_2 C(r_1) C(r_2) F(r). \tag{A.1}$$

Introducing first r_1, r_2 and the angle ω between $\mathbf{r}_1$ and $\mathbf{r}_2$ as variables and by changing subsequently to the variables (r_1, r_2, r), r being related to ω according to

$$r^2 = r_1^2 + r_2^2 - 2r_1 r_2 \cos\omega, \tag{A.2}$$

one finds that the integral can be reduced to

$$J = 8\pi^2 \int \mathrm{d}r_1 \int \mathrm{d}r_2 \int \mathrm{d}r \quad r r_1 r_2 C(r_1) C(r_2) F(r). \tag{A.3}$$

When assuming for $C(r)$ the expression (2.19), this reduces to

$$J = 8\pi^2 \iiint_D \mathrm{d}r\mathrm{d}r_1\mathrm{d}r_2 F(r) r r_1 r_2, \tag{A.4}$$

where the domain D of integration is determined by the following inequalities:

$$\begin{aligned} &0 \leqq r_1 \leqq R, && \text{(a)} \\ &0 \leqq r_2 \leqq R, && \text{(b)} \\ &|r_1 - r_2| \leqq r \leqq r_1 + r_2. && \text{(c)} \end{aligned} \tag{A.5}$$

One may first carry out the integrations over r_1 and r_2; this provides

$$J = \tfrac{1}{3}\pi^2 \int_0^{2R} F(r)[16R^3 r - 12R^2 r^2 + r^4] r \mathrm{d}r. \tag{A.6}$$

This can be applied to the calculation of T_1 according to (2.31). By substituting

$$F(r) = a^3 b^3 S(ar) S(br) r^2 \tag{A.7}$$

in (A.6), the final result for T_1 is obtained:

$$T_1 = \tfrac{1}{9}\pi^2 q^2 (6\pi^2)^{-2} \int_0^{2R} r^3 a^3 b^3 S(ar) S(br)[16R^3 r - 12R^2 r^2 + r^4] \mathrm{d}r. \tag{A.8}$$

Notes added in proof:

(a) In a recent preprint, "Theory of muon capture", H. Primakoff gives the details of his work quoted in ref. [3]). The details of his calculations differ in several ways from our calculations in section 2. However, the conclusion of section 3 that the closure approximation for an average nucleus can only give a rough picture seems not to be changed. The fact that Primakoff uses a function $\sin qr/qr$, whereas we used only the first terms $1 - \frac{1}{6}q^2 r^2$ of the expansion of this function, makes only a rather small difference for medium-weight nuclei.

(b) A revised discussion of the experiment of Lundby *et al.* [17]) (private communication of Dr. Teja) has provided a lower value for their result: $g_{\mu c}^{GT}/g_{\beta}^{GT} = 1.08 \pm 0.05$. It is difficult to reconcile this value with our tentative proposal concerning the μ-capture interaction, formulated in section 3.

References

1) J. Tiomno and J. A. Wheeler, Revs. Mod. Phys. **21** (1949) 153
2) J. M. Kennedy, Phys. Rev. **87** (1952) 953
3) H. Primakoff, Proc. 5th Rochester Conf. (1955) 174; and private communication of Dr. Sens
4) H. A. Tolhoek and J. R. Luyten, Nuclear Physics **3** (1957) 679
5) J. C. Sens, R. A. Swanson, V. L. Telegdi and D. D. Yovanivitch, Phys. Rev. **107** (1957) 1464; J. C. Sens, Phys. Rev. to be published

6) A. Astbury, M. A. R. Kemp, N. H. Lipman, H. Muirhead, R. G. P. Voss, C. Zangger and A. Kirk, Capture rates for negative muons in various elements, to be published
7) R. P. Feynman and M. Gell-Mann, Phys. Rev. **109** (1958) 193
8) Proc. 1958 Ann. Int. Conf. High Energy Phys. (CERN) pp. 241—249
9) K. Gottfried, Nuclear Physics **5** (1958) 557
10) P. O. Löwdin, Phys. Rev. **97** (1955) 1474
11) G. H. Burkhardt and C. A. Caine, Nuclear shell effects in μ^--capture, private communication
12) W. Gröbner and N. Hofreiter, Integraltafel, II. Teil (Springer 1950) formula (551.5)
13) J. L. Lopes, Phys. Rev. **109** (1958) 509;
L. Wolfenstein, Nuovo Cimento **8** (1958) 882;
M. L. Goldberger and S. B. Treiman, Phys. Rev. **111** (1958) 354
14) M. Gell-Mann, Phys. Rev. **111** (1958) 362
15) R. Jastrow, Phys. Rev. **98** (1955) 1479;
F. Iwamoto and M. Yamada, Progr. Theor. Phys. **17** (1957) 543; **18** (1957) 345;
V. J. Emery, Nuclear Physics **6** (1958) 585;
J. Dabrowski, Proc. Phys. Soc. **71** (1958) 658; **72** (1958) 499;
C. D. Hartogh and H. A. Tolhoek, Physica **24** (1958) 721, 875, 896
16) Proc. 1958 Int. Conf. High Energy Phys. (CERN) pp. 238, 241
17) J. O. Burgman, J. Fischer, B. Leontic, A. Lundby, R. Meunier, J. P. Stroot and J. D. Teja, Phys. Rev. Letters **1** (1958) 469

2.B *Nuclear Physics* **10** (1959) 620—625; © *North-Holland Publishing Co., Amsterdam*
Not to be reproduced by photoprint or microfilm without written permission from the publisher

TIME-REVERSAL AND POLARIZED NUCLEAR REACTIONS

L. C. BIEDENHARN
Institute for theoretical Physics, University of Copenhagen †

Received 11 November 1958

Abstract: The generalized polarization-asymmetry theorem requires only reciprocity and not reversibility. The application of this result to complex potentials is discussed in detail.

1. Introduction

Satchler[1]) has recently published a paper, of the same title as above, in which he shows that the generalized polarization-asymmetry equality results only from the requirement of time reversibility on the interactions. It is the purpose of the present note to point out that this result actually holds for a rather more general situation and, in fact, requires only that the interaction obey *reciprocity* †† and not *time-reversibility*. These two terms are generally taken as equivalent [2]), and indeed time-reversibility implies reciprocity [3]), but the converse is not necessarily true. An important example in which the two terms must be distinguished is afforded by calculations involving complex potentials, and it was the examination of this case which prompted the present note. In the following section we show that the polarization asymmetry theorem requires only reciprocity — a result which is quite easily shown by direct construction. The next section is concerned with a general discussion of complex potentials, and a restriction based on reciprocity is postulated. Although not directly related to the problem at hand, this discussion of complex potentials allows a straightforward answer to the question of the proper final state to be utilized in distorted wave calculations with complex potentials. This is discussed briefly in the concluding section.

2. The Polarization-Asymmetry Theorem

The polarization-asymmetry theorem for the scattering of spin-$\frac{1}{2}$ particles was first proved by Blin-Stoyle; it asserts that the polarization $P(\vartheta)$ of particle c produced in the reaction a+b → c+d (with a, b unpolarized) is just the asymmetry $W(\vartheta)$ produced by the reaction c+d → a+b with

† Guggenheim Fellow 1958; permanent address: The Rice Institute, Houston, Texas.
†† The sense in which the term reciprocity is being used here is discussed in the following section.

c polarized, and the polarization of a, b unobserved [4]). This theorem was later shown to depend only on time-reversal symmetry, and not upon space-reversal symmetry for the interactions [5]) †. Satchler [1]) has shown that there exists a more general theorem which relates the general polarization (tensor parameters) of a particle produced in a given reaction to the asymmetry of the *inverse* reaction; his proof requires only time-reversal invariance, and employs the prescription of Coester [3]) that two reactions are to be defined as inverses if the two reactions are interchanges under time-reversal. Let us re-examine this theorem without introducing the requirement of time-reversibility; it is simplest to proceed by direct calculation.

Consider first the reaction $\alpha s \to j_1 j_2$, that is, the reaction produced by unpolarized alternatives α with channel spin s leading to the particles j_1 and j_2 (alternative β). We seek the polarization of j_1 with the polarization of j_2 unobserved. Using the results of ref. [6]), and, expressing the polarization of j_1 in terms of tensor parameters T_k^q — the expectation values of the multipole spin operators — one finds

$$T_k^q(\hat{\mathbf{k}}_\alpha, \hat{\mathbf{k}}_\beta)^* = \frac{\pi\lambda_\alpha^2}{2s+1} \sum_{\lambda L} Q_I(kL\lambda)\{(2\lambda+1)^{-\frac{1}{2}}(kLq\mu|\lambda, q+\mu) Y_{L\mu}(\hat{\mathbf{k}}_\beta) Y_{\lambda,\mu+q}(\hat{\mathbf{k}}_\alpha)^*\}, \tag{1a}$$

$$Q_I(kL\lambda) = \sum (1-S^{J_1\pi_1}_{\beta s_1 l'_1;\alpha s l_1})(1-S^{J_2\pi_2}_{\beta s_2 l'_2;\alpha s l_2})^* \times Z(l_1 J_1 l_2 J_2; s\lambda) W(j_1 k j_2 s_2; j_1 s_1)(l'_1 l'_2 00|L0)(-)^{s-J_1-l'_1} \tag{1b}$$

$$\times [(2j_1+1)(2s_1+1)(2s_2+1)(2l'_1+1)(2l'_2+1)(2J_1+1)(2J_2+1)]^{\frac{1}{2}} \begin{Bmatrix} l'_1 & l'_2 & L \\ s_1 & s_2 & k \\ J_1 & J_2 & \lambda \end{Bmatrix}.$$

The sum above is over $l_1 l_2 l'_1 l'_2 s_1 s_2 J_1 J_2 \pi_1 \pi_2$; the angular momentum functions appearing in this result have their standard meaning.

Consider next the reaction $j_1 j_2 \to \alpha s$ where j_1 is polarized (tensor parameters t_k^q) and j_2 is unpolarized. The angular distribution of alternatives αs (without polarization measurements) is given by

$$W(\hat{\mathbf{k}}_\alpha, \hat{\mathbf{k}}_\beta, \ldots) = \frac{\pi\lambda_\beta^2}{2j_2+1} \sum_{kq} t_k^q \sum_{\lambda L} Q_{II}(kL\lambda)(-)^{L+\lambda} \cdot \{(2\lambda+1)^{-\frac{1}{2}}(kLq\mu|\lambda, q+\mu) Y_{L\mu}(\hat{\mathbf{k}}_\beta) Y_{\lambda,\mu+q}(\hat{\mathbf{k}}_\alpha)^*\}, \tag{2a}$$

$$Q_{II}(kL\lambda) = \sum (1-S^{J_1\pi_1}_{\alpha s l_1;\beta s_1 l'_1})(1-S^{J_2\pi_2}_{\alpha s l_2;\beta s_2 l'_2})^* \times Z(l_1 J_1 l_2 J_2; s\lambda) W(j_1 k j_2 s_2; j_1 s_1)(l'_1 l'_2 00|L0)(-)^{s-J_1-l'_1} \tag{2b}$$

$$\times [(2j_1+1)(2s_1+1)(2s_2+1)(2l'_1+1)(2l'_2+1)(2J_1+1)(2J_2+1)]^{\frac{1}{2}} \begin{Bmatrix} l'_1 & l'_2 & L \\ s_1 & s_2 & k \\ J_1 & J_2 & \lambda \end{Bmatrix}.$$

† It should be noted that some of the remarks made in this note have already been made earlier in ref. [5]) for a more special situation. See also ref. [14]).

The sum in (2b) is over the same variables as in (1b). We have utilized the symmetry properties of the various angular momentum functions to put the result for (2b), as directly given by ref. [5]), in a similar form to (1b).

Comparing now eqs. (1) and (2), it is clear that if $S^{J\pi}$ is symmetric, then

$$(2j_1+1)\lambda_\alpha^2 W(\hat{\mathbf{k}}_\alpha, \hat{\mathbf{k}}_\beta, \ldots) = (2s+1)\lambda_\beta^2 \sum_{kq} t_k^q T_k^{q*}(-\hat{\mathbf{k}}_\alpha, -\hat{\mathbf{k}}_\beta). \qquad (3)$$

It follows that eq. (3), which is of the form of the generalized polarization-asymmetry theorem given by Satchler, requires only symmetry of the scattering matrix, a not unexpected result †.

The reactions $\alpha s \to j_1 j_2$, and $j_1 j_2 \to \alpha s$ (with reversed momenta according to eq. (3)) will be called *reciprocal*. The situation may then be expressed quite simply by saying that eq. (3) requires only *reciprocity*, and not reversibility. The distinction between these terms can be seen from the example of a scattering process involving both elastic and inelastic processes. The complex potential which describes this situation involves a loss of particles to the inelastic channels. Eq. (3) holds between the polarization of β produced by the reaction $\alpha \to \beta$ and the asymmetry produced in the reaction $\beta \to \alpha$ by polarized β, with either process being calculated from the complex potential. Since, however, both processes involve a *loss* of particles to the inelastic channels, the two processes are clearly not time inverses.

In the usual situation where time invariance holds, the symmetry of the scattering matrix is obtained as a consequence; reciprocity then relates inverse processes [3]). The general polarization-asymmetry theorem is itself only a special case of the results to be obtained from reciprocity. It is clear that reciprocity, as a weaker condition than reversibility, will suffice for these also.

3. Complex Potentials

Complex potentials have been introduced, originally by Bethe, as a schematic way to treat nuclear reactions, the complex part of the potential introducing absorption processes which are to represent in a direct way the overall loss of particles from the incident channels into the reaction channels. This is clearly a great oversimplification; more particularly, it is important to note that the introduction of true absorption has introduced an asymmetry in the direction of time, in schematically representing a problem which we will consider to have been originally time-reversible. We propose to examine in this section what are the consequences, if any, of this time asymmetry.

The essential content of Bethe's introduction of a complex potential can

† The use of a definite channel spin in eq. (3) is inessential, and occurs only as a convenience, Similarly the restriction to particle, as opposed to photon, channels is inessential.

be put in more general terms as the formal elimination of reaction channels by partitioning the scattering matrix. That is, one divides the channels into two classes: incident channels (i); and reaction channels (r) and considers only the sub-matrix S_{ii}, which we will call the reduced scattering matrix $\mathscr{S}$. Clearly this reduced scattering matrix is still symmetric; it is, however, no longer unitary.

An instructive, but fully equivalent, way to describe this has been given by Thomas [7]). Using the fact that the reaction channels contain outgoing waves, Thomas eliminated all explicit reference to these channels and obtained a reduced derivative matrix of the form

$$\mathscr{R} = R_{ii}+R_{ir}(L_r^{-1}-R_{rr})^{-1}R_{ri}. \tag{4}$$

(Here R refers to the original derivative matrix, and $L_r = S_r+iP_r$, where S_r and P_r are the shift and penetration factors respectively.) One may utilize this result for $\mathscr{R}$ to define, in a formal way, a complex 'equivalent potential'. Two general properties of such an equivalent potential can be obtained at once: (1) from the symmetry of the reduced scattering matrix it follows that $\mathscr{R}$ is symmetric, and hence the equivalent potential is reciprocal, and (2) although the equivalent potential is complex, the sign of the imaginary part of the diagonal terms is uniquely fixed to correspond to absorption.

In a sense these results are so immediate as to be almost trivial, particularly since we have dealt with a formal 'equivalent potential'. We postulate, however, that *for complex potentials that are to approximate the formal equivalent potentials both properties must still obtain.* This is a very natural requirement, and is equivalent to requiring that the time asymmetry of any admissible complex potential is to be a trivial asymmetry, and essentially of no consequence †.

The complex potential introduced by Feshbach, Porter and Weisskopf [8]), had one further, and novel, feature. This concerns the separation of a given channel into two parts, one part relating to processes through the compound nucleus, and the other part being the remainder. (FPW actually made this division only in the elastic channels, and spoke of compound-elastic and shape-elastic scattering, but this restriction is not essential — Coulomb excitation for example, is a type of shape inelastic scattering.) If the compound processes are considered to have a lifetime of Γ or longer, it is necessary to distinguish between the parts of a given channel by employing an energy average with a spread in energies of the order of $\hbar/\Gamma$.

For the purpose of the present work it is necessary only to note that the symmetry properties of the reduced S matrix are not affected by an averaging

† The second property is even more immediate physically, and it has been noticed many times that it implies that for a complex potential of the form $iV(r)\boldsymbol{\sigma}\cdot\mathbf{L}$ there must be a cut-off at high l. I am indebted to Dr. G. Igo for this remark.

over energy, and in consequence the reduced R matrix is also symmetric. (Since, however, the relation between R and S is not linear, the reduced R matrix even for purely elastic processes may now be complex.)

One further feature of the FPW complex potential should now be noted. This is the fact that the elastic processes described by their complex potential ("shape-elastic" scattering) cannot be physically distinguished from the "compound-elastic" processes (unless one utilizes time-of-flight experiments which are highly impractical as yet!). It is customary to separate off the latter processes by invoking statistical assumptions for the compound-elastic processes. Comparison between theory and experiment is thus more apt to be a test of these statistical assumptions, than of the complex potential †.

4. Distorted Wave Calculations

In calculation of direct nuclear reactions †† improvements in the accuracy of the results are often sought by using distorted waves for the incident and emergent nucleons; the distorted waves are considered as arising from the influence of a complex potential. In such calculations one is confronted with the evaluation of matrix elements of the form $\langle \mathrm{f}|V|\mathrm{i}\rangle$, where V is the direct interaction, and $|\mathrm{i}\rangle$ is the distorted incident wave in the complex potential, V_c, with an outgoing wave condition. The question then arises: what is the correct definition of $|\mathrm{f}\rangle$?

The usual discussions of this question [11]) are not immediately relevant, for time reversibility has been assumed. We can, however, extend these discussions to the present case in a simple physical way. For the actual distorted wave function (to which the complex potential wave function is but a schematization), the condition on ψ_f is that it contain *ingoing* scattered waves. Thus, in terms of Thomas' procedure to eliminate reaction channels, the appropriate complex potential has the opposite sign for i. Since we require reciprocal potentials it follows then that $\psi_f^{(-)}$ *is a distorted wave in the time-reversed complex potential with an ingoing wave condition.*

It should be noted that results equivalent to this are implicit already in the work of Hayakawa [12]), among others. Despite this, some results in the literature are ambiguous on this point, and a few are, in fact, incorrect.

Although it is perhaps not immediately obvious, the prescription given by Mott and Massey for real potentials is consistent with this result and therefore valid in general †††.

† A further discussion of this point is given in ref. [9]).

†† The literature is quite extensive and citations can be found in the forthcoming survey paper of N. Austern, Chap. V of ref. [10]).

††† This is the prescription used in ref. [13]). I am indebted to Dr. Levinson for a helpful correspondence on this matter.

5. Conclusions

The results contained in this note are simple and straightforward generalizations which are undoubtedly known already to a great many people. Nevertheless such questions are still of frequent occurrence, and a discussion, as above, is perhaps not superfluous.

The present note was initiated in discussions with Dr. A. M. Lane; the author would also like to thank Professor Leon Rosenfeld for his help and encouragement.

Note added in proof: Dr. G. R. Satchler has kindly brought to my attention the fact that time reversal, polarized particle reactions, and the polarization-asymmetry theorem have been discussed earlier by A. I. Baz', JETP **32** (1957) 628 (translation in Soviet Phys. JETP **5** (1958) 521) and by M. I. Shirokov, JETP **33** (1957) 975 (translation in Soviet Phys. JETP **6** (1958) 748). Results equivalent to those of ref. [1]) are obtained in these papers, but extension to the non-unitary case (complex potential) is not discussed.

References

1) G. R. Satchler, Nuclear Physics **8** (1958) 65
2) J. M. Blatt and V. F. Weisskopf, Theoretical Nuclear Physics (Wiley, New York, 1952) pp. 528–9
3) F. Coester, Phys. Rev. **84** (1951) 1259; Phys. Rev. **89** (1952) 619
4) R. J. Blin-Stoyle, Proc. Phys. Soc. A **65** (1951) 452;
L. Wolfenstein and J. Ashkin, Phys. Rev. **85** (1952) 947;
R. H. Dalitz, Proc. Phys. Soc. A **65** (1952) 175
5) J. S. Bell and F. Mandl, Proc. Phys. Soc. **71** (1958) 272, 867 (E)
6) A. Simon and T. A. Welton, Phys. Rev. **90** (1953) 1036; **93** (1954) 1435 (E)
7) R. G. Thomas, Phys. Rev. **97** (1955) 224;
see also A. M. Lane and R. G. Thomas, Revs. Mod. Phys. **30** (1958) 257
8) Feshbach, Porter and Weisskopf, Phys. Rev. **90** (1953) 166; **96** (1954) 448
9) Chase, Klahr and Temkin, WADC-58-79 (Feb. 1958) unpublished
10) Fast Neutron Physics, edited by J. L. Fowler and J. B. Marion (Interscience Publ., New York,)
11) K. M. Watson and K. A. Brueckner, AECU-2765 (1953);
M. Gell-Mann and M. L. Goldberger, Phys. Rev. **91** (1953) 398
12) S. Hayakawa, Trans. of Bose Res. Inst. (Calcutta) **20** (1955) 21
13) C. A. Levinson and M. K. Banerjee, Ann. Phys. **2** (1957) 471, 499
14) Chase, Wilets and Edmonds, Phys. Rev. **110** (1958) 1083

10.A

Nuclear Physics **10** (1959) 626; © *North-Holland Publishing Co., Amsterdam*

NEWS ITEM

NEW EDITOIAL STAFF FOR MATHEMATICAL TABLE AND OTHER AIDS TO COMPUTATION

The Division of Mathematics of the National Academy of Sciences, National Research Council, announces that Harry Polachek, Technical Director of the Applied Mathematics Laboratory of the David Taylor Model Basin, has been appointed Chairman of the Editorial Committee for the quarterly journal *Mathematical Tables and Other Aids to Computation* from January 1959. He succeeds C. B. Tompkins of the University of California at Los Angeles, who held the post since November 1954. The other members of the Editorial Committee are: C. C. Craig, A. Fletcher, E. Isaacson, D. Shanks, C. V. L. Smith, A. H. Taub, C. B. Tompkins and J. W. Wrench, Jr.

Mathematical Tables and Other Aids to Computation was founded in 1943 by R. C. Archibald with the aid of a grant from the Rockefeller Foundation and is published by the Division of Mathematics of the National Academy of Sciences, National Research Council. It publishes original papers in numerical analysis, high speed computer methods and other aids to computation as well as short articles reporting upon the latest developments in these fields. It serves as an information centre on tables and other aids to computation appearing in the current literature, not only in the fields of mathematics, physics, statistics, astronomy and navigation, but also in such areas as actuarial science, aeronautics, chemistry, engineering, geodesy, medicine and meteorology. A file of unpublished mathematical tables is maintained for use by subscribers.

Articles for publication in *Mathematical Tables and Other Aids to Computation* should be addressed to Harry Polachek, Editor, David Taylor Model Basin, Washington 7, D. C.

Information on subscriptions may be obtained from the National Academy of Sciences Printing and Publishing Office, 2101 Constitution Avenue, Washington 25, D. C.

10.D *Nuclear Physics* **10** (1959) 627; © *North-Holland Publishing Co., Amsterdam*

BOOK REVIEW

W. K. MANSFIELD, *Elementary Nuclear Physics* (Nuclear Engineering Monographs I) (Temple Press Ltd., London, 1958. viii—60 p., 10s 6d.)

J. J. SYRETT, *Nuclear Reactor Theory* (Nuclear Engineering Monographs II) (viii—80 p., 12s 6d.)

W. B. HALL, *Reactor Heat Transfer* (Nuclear Engineering Monographs III) (viii—68 p., 10s 6d.)

These three booklets are the first of a new series of monographs, which are intended to give an introductory treatment of nuclear engineering subjects for students, research assistants and others who might want it, but who have no time to derive full benefit from the more detailed special works available.

The first monograph is written to meet the need for a concise summary of the terminology and essential principles of nuclear physics. It has been prepared by the general editor of the series, W. K. Mansfield, of the Nuclear Engineering Laboratory, Queen Mary College, London. The book starts with a survey of the atomic theory of matter, giving a superficial explanation of the periodic system and the forces acting between atoms in molecules and solids. This is followed by an account of nuclear theory, touching on nuclear models, but with more attention to nuclear energetics and reactions. After a brief but instructive treatment of nuclear disintegrations, including radioactivity and fission, the author considers the interactions of neutrons and nuclear radiations with matter, emphasizing the concepts of cross-section and flux. The final chapter gives an appropriate description of methods and apparatus for detection and measurement of nuclear radiations.

In the second monograph J. J. Syrett, of the Reactor Division, A. E. R. E., Harwell, gives a survey of the physics of nuclear reactor design with particular emphasis on the heterogeneous natural uranium reactor with graphite moderator. The first chapters contain a qualitative explanation of the physical concepts of nuclear fission, chain reactions and neutron behaviour in reactors as well as their mathematical formulation in terms of elementary calculus, some special problems being deferred to two appendices. This provides the basis for a discussion of the calculations of critical size and lattice parameters. The variations of reactor properties due to temperature changes and neutron irradiation effects (fission product poisoning, fuel-burn-up and production of fissile material) are briefly discussed, and finally some of the possible reactor types and their fuel cycles are mentioned.

The third monograph (by W. B. Hall, Windscale Research and Development Laboratory) is devoted to the study of the heat transfer process in nuclear reactors. Since this problem bears directly upon the size and consequently the prize of a reactor, it demands much more consideration of reactor design than is required in many other industrial processes. The fundamental data of convective heat transfer are presented and discussed in the first part of the monograph, their application to reactor design and performance in the second part, while the last chapter is devoted to a discussion of some special aspects, such as the properties of liquid metal coolants and the efficiency of longitudinal and transverse fins on the surface of the fuel container.

In general the contents and the depth of treatment of these compact monographs appear to be adequate for their purpose. Particularly, it seems that the first of the series would serve as a very suitable introduction also for many readers who may be interested in the elementary principles of nuclear physics without being engaged in work in this field.

Svend Holm

10.E *Nuclear Physics* **10** (1959) 628: © *North-Holland Publishing Co., Amsterdam*

ERRATUM AND ADDENDUM

S. ONEDA, Strange Particle Decays and the Universal V—A Four-Fermion Interaction, (Nuclear Physics **9** (1958/59) 476).

The right hand side of eq. (41) should be multiplied by 4 and the right hand side of eq. (42) and (43) should be divided by 4. The value of R'' of (49) is not affected and is given by $R'' = \frac{1}{2}R'$ instead of $R'' = 2R'$. The following statement of p. 488, line 5 from top: "The case $\pi(1) = \pi^-$ and $\pi(2) = \pi^+$ could take place in higher order approximations or even in the lowest order if we allow the current $J_\alpha^{(1)}$ which satisfies $\Delta S/\Delta Q = -1$ from the outset", should be replaced by: "The case $\pi(1) = \pi^-$ and $\pi(2) = \pi^+$ must also be considered." The values of (59) and (62) should be read as

$$W(\Lambda^0 \to \mathrm{p}+\mathrm{e}^-+\bar{\nu})/W(\Lambda^0 \to \mathrm{p}+\pi^-) \approx 2.3\times 10^{-3} \tag{59}$$

and

$$W(\Lambda^0 \to \mathrm{p}+\mathrm{e}^-+\bar{\nu})/W(\Lambda^0 \to \mathrm{p}+\pi^-) \approx 8.4\times 10^{-4}. \tag{62}$$

The value of (62) is close to the presently available experimental ratio.

We did not discuss the contribution of fig. 6 in detail but inferred that it would not change drastically the conclusion drawn from the computation of the diagrams of the type of fig. 4. In fact the precise analysis has shown that no contributions would arise as long as we disregard the radiative corrections between the two black boxes of fig. 6. This follows from the charge conjugation invariance of the strong interactions and may be discussed in a forthcoming paper. Thus, to the approximation we adopted, the ratio $R' = W(\mathrm{K}_2^0 \to \pi^\pm+\mu^\mp+\tau)/W(\mathrm{K}_1^0 \to \pi^+ +\pi^-) \approx W(\mathrm{K}_2^0 \to \pi^\pm+\mathrm{e}^\mp+\nu)/W(\mathrm{K}_1^0 \to \pi^+ +\nu^-)$ would lie in the range $(3.0\times 10^{-3}-9.5\times 10^{-3})$ which seems to be significantly larger than the present experimental value $(3.1\times 10^{-4}-6.3\times 10^{-4})$. This may mean that either the coupling constant of the strangeness non-conserving baryon-lepton interaction is smaller than the usual Fermi coupling constant or the assumed form of the interaction (4) is not the correct one. Using a dispersion technique, Sakita obtained a similar conclusion from the analysis of the $\mathrm{K} \to \nu+\mu$ decay. (B. Sakita, Bull. Am. Phys. Soc. **4** (1959) 39).

7.B *Nuclear Physics* **10** (1959) 629—653; © *North-Holland Publishing Co., Amsterdam*
Not to be reproduced by photoprint or microfilm without written permission from the publisher

RADIATIVE CORRECTIONS TO BREMSSTRAHLUNG

A. N. MITRA
Department of Physics, Muslim University, Aligarh, U. P. India
and
P. NARAYANASWAMY and L. K. PANDE
Department of Physics, University of Delhi, Delhi-8, India

Received 2 January 1959

Abstract: The second order radiative corrections to bremsstrahlung have been evaluated by a straightforward application of Feynman-Dyson techniques, taking all the possible effects into account. The results are given in simplified forms for certain relativistic and extreme relativistic regions discussed in the text. The cross-section for double bremsstrahlung has also been evaluated in various limits, in order to cancel out the 'infra-red' terms appearing in the second order corrections. Our result for the extreme relativistic limit seems to disagree with one recently obtained by Fomin using 'mass operator' techniques.

1. Introduction

Quantum electrodynamics is perhaps the only branch of physics where the predictions of the theory have been borne out by observations to an accuracy which leaves almost nothing to be desired (viz. 10^{-9}). There hardly seems to be any conceivable process for which calculations of 'second order radiative corrections' (or even 4th order in many cases) have not been made and the results compared with experiment. The recent book by Jauch and Rohrlich [1]) is in fact the most concrete evidence in support of this statement. Perhaps the only notable exception is the calculation of radiative corrections to bremsstrahlung, and this had not been carried out so far presumably because of the extreme amount of calculational labour involved compared, e.g., with the corresponding calculation on Compton scattering [2]), and also because of the impossibility of a direct experimental check. Regarding this second point it was brought to the notice of one of us (ANM) about a year ago by Prof. Drell that large angle pair production by high energy γ-rays on protons represented fairly good conditions for providing still another test of quantum electrodynamics so far as finer effects like radiative corrections etc. were concerned.

Now, it is well known that bremsstrahlung and pair production are processes derivable from each other, simply by interchanging the role of the final negaton in the former with that of the final positon in the latter. Fur-

ther, one of us had in fact calculated the radiative corrections to bremsstrahlung in the non-relativistic limit [3]) a few years ago. For these reasons it was thought worthwhile to make a straightforward extension of the same process to the region of high energies, using Feynman's integration techniques, though it was quite apparent that the complexity involved was at least an order of magnitude higher than had been the case with Compton scattering [2]), for the simple reason that the 4-momentum transferred to the electromagnetic field of the nucleus was no longer a null vector †.

The calculations will be presented here for the bremsstrahlung process only, without any attempt being made to adapt them to the process of pair production, though the transition can in principle be made at any stage of the calculation. The next two sections are devoted to the main steps leading to the covariant matrix elements and cross sections for bremsstrahlung and its radiative corrections arising from various effects like vacuum polarization, self-energy, vertex and Compton parts. In sections 4 and 5 the cross sections for radiative corrections are derived in different relativistic regions. In section 6 we give the cross sections for double bremsstrahlung in the corresponding regions, with particular reference to the role of this process in eliminating the infra-red catastrophe. The evaluation of the various integrals appearing in the text and their tabulation are relegated to a series of appendices.

2. The Matrix Element and Cross Section for Bremsstrahlung

We shall use here the notational convention of Dyson [5]), viz. that the 4th component of a 4-vector is imaginary. p_λ, q_λ and k_λ represent respectively the 4-momenta of the initial and final electrons and the emitted quantum. The external field at x will be denoted by $A_\mu^{\,e}(x)$, with the index μ *reserved* for this purpose, so that eventually μ will take up only the value 4. The polarization of the emitted quantum will similarly have the index ν reserved for itself. Natural units, viz. $\hbar = c = m = 1$, will be used throughout.

From Feynman-Dyson techniques, the Hamiltonian density at x for bremsstrahlung is given by

$$H_0(x) = -e^2 \int \mathrm{d}^4x_1 A_\nu(k) A_\mu^{\,e}(x) \mathrm{e}^{-ikx_1} [\bar{\psi}(x)\gamma_\mu S_F(x_1-x)\gamma_\nu \psi(x_1) + \bar{\psi}(x_1)\gamma_\nu S_F(x-x_1)\gamma_\mu \psi(x)], \tag{1}$$

where

$$S_F(x) = (2\pi)^{-4} \int \mathrm{d}^4 s \, \mathrm{e}^{isx} (i\gamma s - m)/(s^2+m^2) \tag{2}$$

and

$$AB = \mathbf{A}\cdot\mathbf{B} + A_4 B_4 = \mathbf{A}\cdot\mathbf{B} - A_0 B_0.$$

† Very recently there came to the authors' notice a letter on the same subject by P. I. Fomin [4]), in which the author reported the results of similar calculations, using Schwinger's mass operator method which he claims to be considerably simpler than Feynman's method in this respect. Our results, however, seem to be somewhat different from his, in the extreme relativistic limit.

Taking

$$\psi(x) = u(p)e^{ipx}, \quad \bar{\psi}(x) = \bar{u}(q)e^{-iqx}$$

and

$$A_\nu(k) = (2k)^{-\frac{1}{2}} e_\nu, \tag{3}$$

where $\bar{u}(q) = u^*(q)\gamma_4$, the S-matrix element of (1) becomes

$$S^{(0)} = -e^2(2k)^{-\frac{1}{2}} A_\mu^{\,e}(Q)\bar{u}(q)B_{\mu\nu}e_\nu u(p), \tag{4}$$

where $Q_\lambda = p_\lambda - q_\lambda - k_\lambda$,

$$A_\mu^{\,e}(Q) = \int d^4x A_\mu^{\,e}(x)e^{iQx} = 2\pi i\delta(Q_0)V(Q), \tag{5}$$

$$V(Q) = 4\pi Ze/Q^2, \tag{6}$$

$$B_{\mu\nu} = \gamma_\mu S_F(p-k)\gamma_\nu + \gamma_\nu S_F(q+k)\gamma_\mu, \tag{7}$$

and

$$S_F(t) = (i\gamma t - 1)/(t^2+1). \tag{8}$$

The two terms of (7) correspond respectively to figs. 1(a) and 1(b).

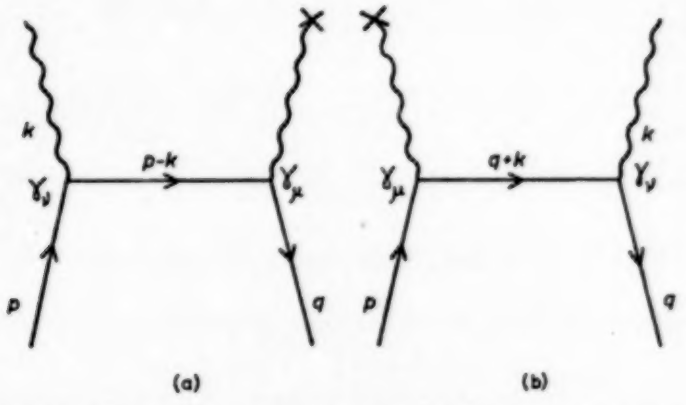

Fig. 1. Diagrams for the basic process. γ_μ and γ_ν indicate the respective vertices at which the external field and the photon field operate.

The Hermitian conjugate of (4) may be obtained most simply by working with adjoints [6]) which are so defined that adjoints of $u(p)$, i, A_λ and γ_σ are respectively $\bar{u}(p)$, $-i$, A_λ and $-\gamma_\sigma$, and the adjoint of a product of several operators is just the product of their adjoints in the reverse order. Thus we have from (4)

$$S^{(0)*} = -e^2(2k)^{-\frac{1}{2}} A_\mu^{\,e}(Q)\bar{u}(p)B_{\nu\mu}e_\nu u(q). \tag{9}$$

To obtain the unpolarized cross section it is convenient to sum over all the values of the index ν [7]) according to the relation

$$\sum_{\text{pol}} |e_\lambda c_\lambda|^2 = \sum_\nu c_\nu^* c_\nu, \tag{10}$$

where c_λ is any vector. (In our calculation $\bar{u}(q)B_{\mu\nu}u(p)$ plays the part of c_ν.) Finally the summation over the spins can be made by using the result

$$\langle u_\alpha(p)\bar{u}_\beta(p)\rangle_{\mathrm{AV}} = -(i\gamma p - 1)_{\alpha\beta}/4p_0. \tag{11}$$

Thus from (4), (5), (9—11), the unpolarized cross section for the electron to go into the solid angle $d\Omega$ is (after collecting all the factors)

$$\frac{d\sigma_0}{d\Omega} = -\tfrac{1}{4}\rho_t V^2(Q)\ \mathrm{Tr}\ [(i\gamma p - 1)B_{\nu\mu}(i\gamma q - 1)B_{\mu\nu}], \tag{12}$$

where

$$\rho_t = (q/p)\alpha_0^2(2\pi)^{-4}d^3k/k, \tag{13}$$

and

$$\alpha_0 = e^2/4\pi = 1/137. \tag{14}$$

The summation convention in (12) applies to ν, not to μ. The negative sign in front of (12) is compensated by another coming from the evaluation of the 'trace'.

Using the notation

$$\eta_1 = (-2pk), \quad \eta_2 = (2qk), \quad \eta_3 = (2pq), \tag{15}$$

and taking the case when η_3 dominates (in magnitude) over η_1 and η_2, (12) works out to be

$$d\sigma_0/d\Omega \approx \rho_t V^2(Q)[(q_\lambda/\eta_2) + (p_\lambda/\eta_1)]^2(2\eta_3 + 8p_0q_0). \tag{16}$$

Eq. (16) will be found to be useful for subsequent purposes.

3. Second Order Corrections

Fig. 2 gives all the processes leading to second order corrections to the S-matrix element. Figs. 2 (a), (b), (c), (d) represent the 'reducible processes' (in Dyson's sense) corresponding respectively to vacuum polarization, self-energy renormalization, self-energy part and vertex part. Fig. 2 (e) represents the so-called Compton part which is irreducible. These are briefly sketched as follows (as they are all well known).

3.1. VACUUM POLARIZATION

This modifies the external potential as [8])

$$A_\mu^{\,e}(Q) \to A_\mu^{\,e}(Q)\left[1 + \frac{\alpha_0}{2\pi}\int_0^1 dv\,\frac{2v^2(1-\frac{1}{3}v^2)Q^2}{4+Q^2(1-v^2)}\right], \tag{17}$$

where $Q_\lambda = p_\lambda - q_\lambda - k_\lambda$ is the 4-momentum transferred to the nucleus.

Setting $Q^2 = 4\sinh^2\beta$, the integral in (17) is easily evaluated to give the result

$$A_\mu^{\,e}(Q) \to A_\mu^{\,e}(Q)[1 + (\alpha_0/2\pi)W(\beta)], \tag{18}$$

where

$$W(\beta) = \tfrac{2}{9} + 2(1 - \tfrac{1}{3}\coth^2\beta)(\beta\coth\beta - 1). \tag{19}$$

In the extreme relativistic limit we have ($\beta \gg 1$)

$$W(\beta) \approx \tfrac{4}{3}\beta. \tag{19a}$$

The contribution to the S-matrix element is thus

$$S^{(p)} = (\alpha_0/2\pi)W(\beta)S^{(0)}. \tag{20}$$

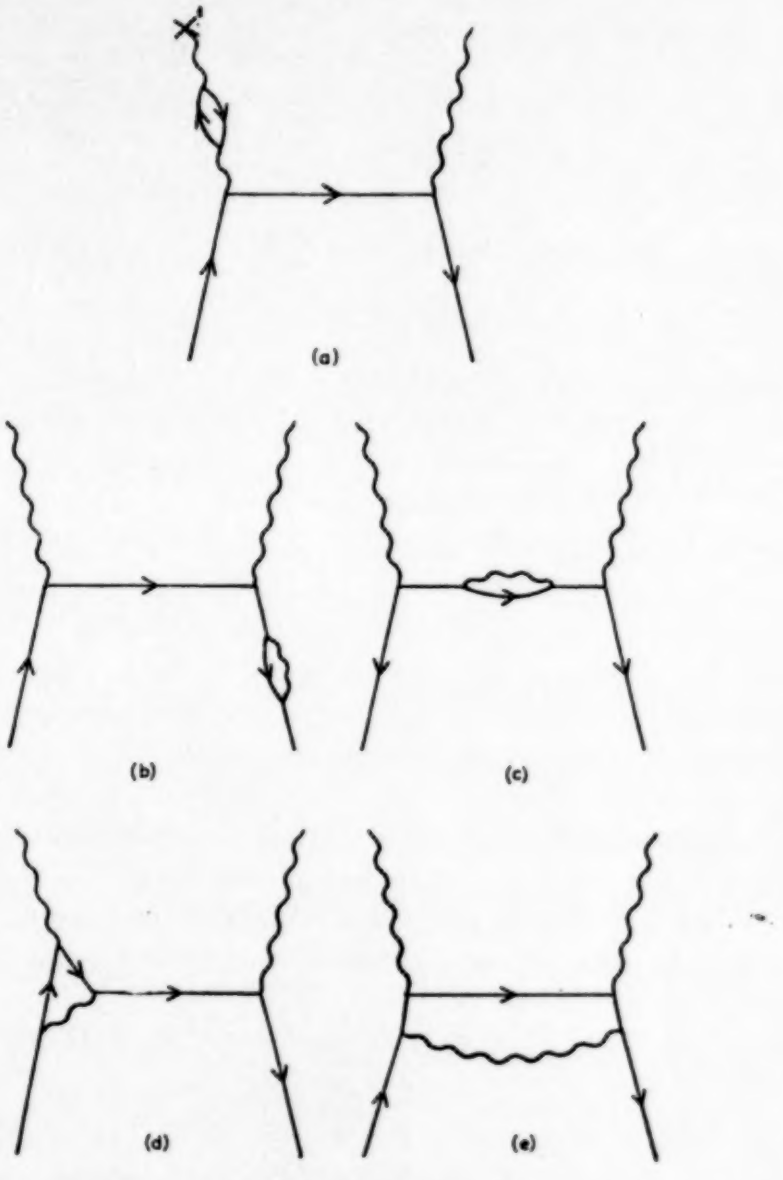

Fig. 2. Diagrams for the various second order corrections. The vacuum polarization correction applies only to the line marked X.

3.2. SELF-ENERGY RENORMALIZATION

This modification affects the spinors $u(p)$ and $u(q)$, which, it must be remembered, represent free electron lines, and as such give rise entirely to renormalization. The combined effect on $u(p)$ and $u(q)$ may be represented

by the modification of (4) by the overall factor (see BF for details)

$$Z_R = -(\alpha_0/4\pi)[\ln \Lambda^2 + 4 \ln \lambda + \tfrac{9}{2}], \tag{21}$$

where, in the notation of BF, Λ and λ represent the 'ultra-violet' and 'infrared' cut-off parameters respectively.

3.3. SELF ENERGY CORRECTION

This consists in the replacement

$$S_F(t) \to S_F(t) + S_F^{(2)}(t)$$

for an internal line with 4-momentum t_λ,
where

$$S_F^{(2)}(t) = (\alpha_0/4\pi) S_F(t)[\textstyle\sum(t) - \sum(t_0)] S_F(t), \tag{22}$$

$$\textstyle\sum(t) = (i/\pi^2) \int d^4 s \gamma_\lambda S_F(t-s) \gamma_\lambda / (s^2+\lambda^2), \tag{23}$$

and $\sum(t_0)$ is the free-particle part of $\sum(t)$ intended to cancel out the electron self-energy. Evaluation of (23) is straightforward as in BF, and one obtains

$$\begin{aligned} S_F^{(2)}(t) = \frac{\alpha_0}{4\pi} S_F(t) \Bigg[& -\ln \Lambda^2 - \tfrac{5}{2} + 2\eta \left(\frac{\eta-2}{2(\eta-1)^2} \ln \eta + \frac{1}{2(\eta-1)} \right) \\ & -2(i\gamma t - 1) \left(\frac{3\eta-2}{2(\eta-1)^2} \ln \eta - \frac{1}{2(\eta-1)} \right) \Bigg], \end{aligned} \tag{24}$$

where $\eta = t^2+1$. Thus in the notation of (15) η can represent either η_1 or η_2 according as the modification is made in the line with momentum $t_\lambda = p_\lambda - k_\lambda$ or $t_\lambda = q_\lambda + k_\lambda$ respectively. It may be noted that $\eta_1 > 0$ but $\eta_2 < 0$, so that $\ln \eta_2$ is complex. The imaginary part is relevant only in connection with the optical theorem which relates the total cross-section with the imaginary part of the forward scattering amplitude. However, since we are not interested in verifying this theorem here, we shall neglect the imaginary part in (24) and subsequent expressions, and this amounts to regarding $\ln \eta$ as $\ln|\eta|$ whenever η may be negative.

In the limits $|\eta| \ll |$ and $|\eta| \gg |$ respectively, eq. (24) reduces to

$$S_F^{(2)}(t) \approx (\alpha_0/4\pi) S_F(t)[-\ln \Lambda^2 - \tfrac{5}{2} + 4(\tfrac{1}{2} - \xi)], \tag{24a}$$

and

$$S_F^{(2)}(t) \approx (\alpha_0/4\pi) S_F(t)[-\ln \Lambda^2 + \xi - (3i\xi(\gamma t)/\eta)], \tag{24b}$$

where

$$\xi = \ln |\eta|. \tag{24c}$$

The contribution from the self-energy parts is thus

$$\begin{aligned} S^{(E)} &= -e^2 (2k)^{-\frac{1}{2}} (\alpha_0/4\pi) A_\mu^{\,e}(Q) \bar{u}(q) B_{\mu\nu}^{(E)} e_\nu u(p), \\ B_{\mu\nu}^{(E)}(\alpha_0/4\pi) &= \gamma_\mu S_F^{(2)}(p-k) \gamma_\nu + \gamma_\nu S_F^{(2)}(q+k) \gamma_\mu. \end{aligned} \tag{25}$$

3.4. VERTEX PARTS

The vertex correction is taken into account by the modification

$$\gamma_\lambda \to \gamma_\lambda + (\alpha_0/4\pi)\Lambda_\lambda(p', p''), \tag{26}$$

where

$$\Lambda_\lambda(p', p'') = (i/\pi^2)\int \mathrm{d}^4 s \gamma_\sigma S_F(p'-s)\gamma_\lambda S_F(p''-s)\gamma_\sigma D_F(s), \tag{27}$$

and

$$D_F(s) = 1/(s^2+\lambda^2), \quad (\lambda \to 0). \tag{27a}$$

Substitution of (26) in (4) gives the contribution from vertex parts as

$$S^{(V)} = -e^2(2k)^{-\frac{1}{2}}(\alpha_0/4\pi)A_\mu^{\ e}(Q)\bar{u}(q)B_{\mu\nu}^{(V)}e_\nu u(p), \tag{28}$$

where

$$\begin{aligned} B_{\mu\nu}^{(V)} = {} & \gamma_\mu S_F(p-k)\Lambda_\nu(p-k, p)+\Lambda_\nu(q, q+k)S_F(q+k)\gamma_\mu \\ & +\Lambda_\mu(q, p-k)S_F(p-k)\gamma_\nu+\gamma_\nu S_F(q+k)\Lambda_\mu(q+k, p). \end{aligned} \tag{29}$$

The general expressions Λ_ν, Λ_μ, unlike the general self-energy corrections (24) cannot unfortunately be given in a correspondingly simple form covering all the possible combinations occurring in (29), since the integrals involved here (particularly for the Λ_μ-terms) are quite complicated. Certain integrals of Λ_μ which were not encountered by BF are discussed in appendix A. These can be considerably simplified at appropriate limits like $|\eta| \ll 1$ or $|\eta| \gg 1$ etc., as listed in appendix B. The corresponding simplifications of (29) and their contributions to the cross-section are discussed in sections 4 and 5. It may be noted that the integrals in (29) contain some 'ultra-violet' divergences which must cancel out when the matrix elements for all the processes are added together. (29) does not contain any 'infrared' terms, however.

3.5. COMPTON PART

The matrix element for this part which corresponds to fig. 2 (e) is given by

$$S^{(C)} = -e^2(2k)^{-\frac{1}{2}}(\alpha_0/4\pi)A_\mu^{\ e}(Q)\bar{u}(q)B_{\mu\nu}^{(C)}e_\nu u(p), \tag{30}$$

where

$$\begin{aligned} B_{\mu\nu}^{(C)} = {} & (i/\pi^2)\int \mathrm{d}^4 s D_F(s)[\gamma_\lambda S_F(q-s)\gamma_\nu S_F(q+k-s)\gamma_\mu S_F(p-s)\gamma_\lambda \\ & +\gamma_\lambda S_F(q-s)\gamma_\mu S_F(p-k-s)\gamma_\nu S_F(p-s)\gamma_\lambda]. \end{aligned} \tag{31}$$

The expression (31) is even more complicated than (29) since the integrals involved here are the most difficult of all. Further, (31) contains certain 'infra-red' terms but no ultraviolet ones. The 'infra-red' terms are most easily picked out by noting that they will arise only from those terms of the numerator of (31) which are independent of s. Again, considerable simplifications are possible (as for the vertex terms) at appropriate limits as discussed below.

4. The Case of $|\eta_1|$ and $|\eta_2| \ll 1$

At this limit the lowest order matrix element (4) simplifies to

$$S^{(0)} \approx -e^2(2k)^{-\frac{1}{2}} A_\mu^{\,e}(P)\bar{u}(q)\left[\frac{2iq_\nu}{\eta_2}+\frac{2ip_\nu}{\eta_1}\right]\gamma_\mu u(p), \tag{32}$$

where $P_\lambda = p_\lambda - q_\lambda$.

As regards the various corrections, it will be enough to write only one type of terms, say the q-terms, since the other type can always be written down by the following transformations

$$q_\lambda \leftrightarrow p_\lambda, \quad \eta_2 \leftrightarrow \eta_1, \quad k_\lambda \leftrightarrow -k_\lambda. \tag{33}$$

Using (24a), the self-energy correction becomes

$$S^{(E)} \approx (\alpha_0/4\pi)[-\ln \Lambda^2 - \tfrac{5}{2} + 2(1-2\xi_2)]S^{(0)}, \tag{34}$$

where $S^{(0)}$ in (34) and in the subsequent expressions (37), (38) and (40) is supposed to stand only for the q-term of (32). The contributions from the vertex terms (2nd and 4th) of (29) reduce to the following:

$$\begin{aligned}&\bar{u}(q)\Lambda_\nu(q, q+k)S_F(q+k)\gamma_\mu u(p)\\ &\quad\approx (\eta_2)^{-1}\bar{u}(q)[4iq_\nu(-B_0^{(2)}+2C_0^{(3)}-2C_0^{(2)}+2G_0^{(2)})\\ &\quad +4iB_\nu^{(2)}-4iC_\nu^{(3)}]u(p),\end{aligned} \tag{35}$$

and

$$\begin{aligned}&\bar{u}(q)\gamma_\nu S_F(q+k)\Lambda_\mu(q+k, p)u(p)\\ &\quad\approx (2iq_\nu/\eta_2)\bar{u}(q)[-4(pq)\gamma_\mu G_0^{(1)}+2(\gamma_\mu\gamma_\lambda\gamma q+\gamma p\gamma_\lambda\gamma_\mu)G_\lambda^{(1)}\\ &\quad +2\gamma_\lambda\gamma_\mu\gamma_\sigma G_{\lambda\sigma}^{(1)}]u(p),\end{aligned} \tag{36}$$

in the notation of appendix A.

Substituting from the appendix B, for the various tensor integrals in (35) and (36) respectively, and simplifying, one obtains two different vertex part contributions as

$$S^{(V1)} \approx (\alpha_0/4\pi)[\ln \Lambda^2 + \tfrac{1}{2} + 4\xi_2] \tag{37}$$

and

$$\begin{aligned}S^{(V2)} \approx\ &(\alpha_0/4\pi)[-4c(2h(2\alpha)-h(\alpha)-\xi_2)+\ln \Lambda^2+\tfrac{1}{2}\\ &-2\alpha\coth\alpha+2b+4c]S^{(0)}\\ &-e^2(2k)^{-\frac{1}{2}}(\alpha_0/4\pi)b\bar{u}(q)(2iq_\nu/\eta_2)\sigma_{\mu\lambda}(p_\lambda-q_\lambda)u(p).\end{aligned} \tag{38}$$

Here

$$P^2 = (p-q)^2 = 4\sinh^2\alpha, \quad b = 2\alpha\,\mathrm{cosech}\,2\alpha, \quad c = 2\alpha\coth 2\alpha, \tag{38a}$$

and use has been made of the relation

$$\bar{u}(q)(ip_\mu+iq_\mu)u(p) = \bar{u}(q)[-2\gamma_\mu+\sigma_{\mu\lambda}(p_\lambda-q_\lambda)]u(p). \tag{39}$$

Finally, the contribution from the Compton part in the limit $|\eta| \ll 1$ is enormously simplified by noting, according to the results given in appendix B, that only the integral J_0 has a factor $(1/\eta_2)$ which alone makes a contribution comparable to (38). The higher tensor J-integrals do not have any such factor. Thus the Compton term gives simply

$$B_{\mu\nu}^{(C)} \approx 2iq_\nu(-4pq)\gamma_\mu J_0 + (1 \leftrightarrow 2).$$

Substituting for J_0 from appendix A one obtains

$$S^{(C)} \approx -8\alpha \coth 2\alpha(\xi_2 - \ln\lambda - h(2\alpha))S^{(0)}. \tag{40}$$

It is now an easy matter to collect all the contributions (34), (37), (38) and (40) in addition to the general expressions (20) and (21), and express the second order correction to the cross-section as a fraction † of the lowest order process, since most of the terms have already been expressed as multiples of $S^{(0)}$. The only exception is the second term of (38) for which the 'radiative' factor $((q_\nu/\eta_2)+(p_\nu/\eta_1))^2$ in the cross section remains unaltered, but the 'Rutherford factor' Tr $(i\gamma q-1)\gamma_\mu(i\gamma p-1)\gamma_\mu$ is replaced by

$$\text{Tr } (i\gamma q-1)\gamma_\mu(i\gamma p-1)\sigma_{\mu\lambda}(p_\lambda - q_\lambda).$$

The ratio of these two factors is simply

$$\rho = 2P^2/(4E^2 - P^2), \tag{41}$$

where $E(= p_0 \approx q_0)$ is the energy of the electron.

Collecting now all the terms together and simplifying, the second order radiative correction to the cross section may be expressed as

$$d\sigma_2 = d\sigma_0(\alpha_0/\pi)\delta_R, \tag{42}$$

where

$$\delta_R = W(\beta) + 2(c-1)(\ln\lambda + 1) - 2c(h(2\alpha) - h(\alpha)) - \alpha \tanh\alpha + \tfrac{1}{2}\rho b. \tag{43}$$

The case $|\eta| \gg 1$ also covers that of $p_0, q_0 \gg 1$ and $k_0 \ll p_0, q_0$ (though k need *not* necessarily be small by itself), provided the angles between the 3 vectors **p**, **q** and **k** are each small (viz. $\approx 1/p_0 \ll 1$). For, it is easily seen that under such conditions, $|\eta_2| = 2(kq_0 - kq\cos\theta_2) \approx (k/q_0)(1+\theta_2^2) \ll 1$, and the same holds for η_1. (In fact it is essentially from such small angles that the main contribution to the process comes about.) Further, $Q^2 = P^2 = (p-q)^2 \approx p_0 q_0 \theta^2 = O(1)$, so that the parameter ρ defined by (41) becomes

† It may be noted that the second order cross-section is not simply the lowest order cross-section times the sum of the various multiplying factors in (34), (38) etc. There is in addition a factor 2 which is seen to arise as follows. The cross section up to the second order is proportional to

$$(S^{(0)}+S^{(2)})^*(S^{(0)}+S^{(2)}) \approx S^{(0)*}S^{(0)} + 2\,\text{Re}\,S^{(0)*}S^{(2)},$$

where on the right hand side the factor 2 in the 2nd term is a consequence of the interference between $S^{(0)}$ and $S^{(2)}$.

vanishingly small. Using this result in (43) the expression for δ_R in this limit becomes

$$\delta_R = W(\beta)+2(c-1)(\ln\lambda+1)-2c(h(2\alpha)-h(\alpha))-\alpha\tanh\alpha. \qquad (44)$$

5. The Extreme Relativistic Limit

The general case of the E.R. limit when p_0, q_0, k_0 are all $\gg 1$ and the angles between any two of them may not be small, is characterized by the inequalities $\eta_1, |\eta_2|, |\eta_3| \gg 1$. The complete expression for the cross section in this case is extremely unwieldy and this is in fact borne out by the "size" of appendix C in which we have written down the contributions of the vertex and Compton parts to the second order cross section, expressed in terms of various tensor integrals, (which in turn, are listed in appendix B).

It was therefore decided to give the simplified form of the cross section only for one special case, viz. one in which the quantity $|\eta_3|$ dominates over η_1 or $|\eta_2|$, so that the following relations hold approximately:

$$Q^2 = P^2+\eta_1+\eta_2 \approx P^2 \approx -\eta_3. \qquad (45)$$

From (45) and (A7) it follows that

$$\alpha \approx \beta. \qquad (46)$$

It may be noted, however, that though it is not unreasonable to neglect η_1 and η_2 compared with η_3, it would *not* be a good approximation to do the same about their respective logarithms, since the latter are much more slowly varying quantities than the former. We shall, therefore (even in this approximation), retain $\ln\eta_1 = \xi_1$ and $\ln|\eta_2| = \xi_2$ as quantities of the *same* order of magnitude as α and large compared with unity. This seems to be a reasonable approximation from the numerical point of view.

In order to avoid working out the tensor integrals $J_{\lambda\sigma\nu}$ (which are extremely complicated) it was thought more practical to calculate the unpolarized cross sections averaged and summed over the initial and final spins respectively.

Thus the quantities to be evaluated, apart from statistical factors, are

$$\tfrac{1}{2}\sum_{\text{pol}} 2\,\text{Re}\,S^{(0)*}[S^{(E)}, S^{(V)}, S^{(C)}]. \qquad (47)$$

The corresponding factor from the lowest order process is

$$\tfrac{1}{2}\sum_{\text{pol}} S^{(0)*}S^{(0)},$$

which, from (12) and (16), reduces in this approximation to

$$(e^4/2k)[A_\mu{}^e(Q)]^2(2p_0q_0)^{-1}(-2\eta_3/\eta_1\eta_2)(\eta_3-4p_\mu{}^2). \qquad (48)$$

Here we have used the result

$$p_\mu \approx q_\mu = ip_0, \qquad (48a)$$

in the spirit of (45).

It is now most convenient, as in section 4, to write down the various contributions (47) as fractions of (48). Thus the fractional contribution from the self-energy part is simply given from (24a), (25) and (47) by

$$d\sigma_2^{(E)}/d\sigma_0 = (\alpha_0/2\pi)[-a+\tfrac{1}{2}(\xi_1+\xi_2)], \quad a = \ln \Lambda^2. \tag{49a}$$

The contribution from the vertex parts can be picked out fairly easily from the expressions (C1) and (C2), remembering that the $G^{(1)}$ and $G^{(2)}$ integrals go like $(1/\eta_3)$ and $(1/\eta_2)$ respectively, and that terms of $O(\eta_3, p_\mu^2)$ dominate over those of $O(\eta_1, \eta_2, k_\mu)$. Substitution for the various integrals from appendix B and subsequent simplification gives

$$\begin{aligned} d\sigma_2^{(V)}/d\sigma_0 = (\alpha_0/2\pi)[&2a+6\alpha-16\alpha^2+(6\alpha\xi_2-\tfrac{3}{2}\xi_2^2-\tfrac{3}{2}\xi_2) \\ &+(6\alpha\xi_1-\tfrac{3}{2}\xi_1^2-\tfrac{3}{2}\xi_1)], \end{aligned} \tag{49b}$$

where $\alpha \approx \beta$ has been used.

Finally the contribution from the Compton part in this approximation is obtained from (C3) and (C4) by noting that only the integrals J and $G^{(2)}$ contain a factor $(1/\eta_1)$ or $(1/\eta_2)$ and all others do not, so that only the terms involving these integrals need be considered at all. Here again we retain only the terms of order $(\eta_3^2/\eta_1\eta_2)$ or $(\eta_3 p_\mu^2/\eta_1\eta_2)$ etc., as the dominant terms compared with the rest. (There also happen to be terms of order (η_3^2/η_1^2), $(\eta_3 p_\mu^2\eta_2/\eta_1^3)$, etc. and these are also included.) After substituting for the integrals and simplifying we obtain

$$d\sigma_2^{(C)}/d\sigma_0 = (\alpha_0/2\pi)[8\alpha(\ln\lambda+\alpha)+(\eta_3-4p_\mu^2)^{-1}(\Omega_1+\Omega_2)], \tag{49c}$$

where

$$\begin{aligned} \Omega_2 &= (\xi_2+\tfrac{1}{2}\xi_2^2)(\eta_3-2p_\mu^2)-2p_\mu^2(\xi_2+\xi_2^2)+\chi_2 g(\eta_1, \eta_2, k_\mu), \\ g(\eta_1, \eta_2, k_\mu) &= \tfrac{1}{2}p_\mu^2(\eta_2/\eta_1)^2+\tfrac{3}{2}p_\mu^2(\eta_2/\eta_1)-p_\mu^2-\tfrac{1}{4}\eta_3(\eta_2/\eta_1) \\ &\quad +\tfrac{1}{2}\eta_3^2(k_\mu/\eta_1)^2-\tfrac{1}{2}p_\mu k_\mu(\eta_3/\eta_1)-p_\mu k_\mu(\eta_3\eta_2/\eta_1^2) \end{aligned} \tag{49d}$$

and

$$\chi_2 = 12\alpha^2-4\alpha\xi_2+\xi_2^2;$$

Ω_1 is obtained from Ω_2 by making the changes $k_\mu \to -k_\mu$, $\eta_1 \leftrightarrow \eta_2$ and $\xi_1 \to \xi_2$ in (49d).

Adding to (49a)—(49c) the contributions from vacuum polarization and self-energy renormalization from (20) and (21) the final result may be expressed in the form of (43) or (44) with

$$\begin{aligned} \delta_R = &\tfrac{13}{3}\alpha+2\ln\lambda\,(2\alpha-1)-4\alpha^2-\tfrac{1}{2}(\xi_1+\xi_2) \\ &-\tfrac{3}{4}(\xi_1^2+\xi_2^2)+3\alpha(\xi_1+\xi_2)+\tfrac{1}{2}(\eta_3-4p_\mu^2)^{-1}(\Omega_1+\Omega_2). \end{aligned} \tag{50}$$

It may be noted that (50) does not agree with (43) or (44) in the limit $\alpha \gg 1$. This apparent discrepancy may be traced to the fact that these expressions were derived under different approximations, viz $|\eta| \ll 1$ and $|\eta| \gg 1$ which are clearly incompatible with each other (see also discussion of the integral $G_0^{(1)}$ in appendix A).

6. Double Bremsstrahlung

As would be expected, 'infra-red divergences' appear in the expressions (43), (44) and (50) for the radiation corrections to bremsstrahlung. It is well known that these can be removed by simultaneously considering in addition the emission of a soft photon, which process is justified on the physical ground that it is impossible to detect a radiative process with strictly one photon emitted and that the best one can do is to have at least one soft photon accompanying it [2, 6]).

Proceeding as in BF (ref. [2]), sec. IV) it can be shown in a straightforward way that the cross section $d\sigma_D$ for double bremsstrahlung when the second quantum is a soft one, is approximately given by

$$d\sigma_D \approx \left(\frac{e^2}{4\pi}\right) d\sigma_0 \int_{k_{min}}^{k_{max}} \frac{d^3s}{4\pi^2} \left(\frac{q_\sigma}{qs} - \frac{p_\sigma}{ps}\right)^2, \tag{51}$$

where k_{max} and k_{min} are the maximum and minimum allowed magnitudes of the 'soft' quantum s as defined by Schwinger [9]) such that $k_{max} \ll m$ and k_{min} is related to the infra-red cut-off parameter λ by [10])

$$e\lambda = 2k_{min}. \tag{52}$$

Evaluation of (51) may be considerably facilitated by taking over a few steps from Schwinger's [9]) calculations, up to the stage where the equality of the magnitudes of p_λ and q_λ has not been assumed viz. from (2.80) to (2.88) of ref. [9]). Thus

$$\begin{aligned}\frac{d\sigma_D}{d\sigma_0} = &-\frac{\alpha_0}{\pi}\left[2\ln\frac{2k_{max}}{\lambda} - \frac{p_0}{2p}\ln\frac{p_0+p}{p_0-p} - \frac{q_0}{2q}\ln\frac{q_0+q}{q_0-q}\right] \\ &+ \frac{\alpha_0}{\pi}\int_{-1}^{+1} \frac{(1+\frac{1}{2}P^2)dv}{1+\frac{1}{4}(1-v^2)P^2}\left[\ln\frac{2k_{max}}{\lambda} - \frac{1}{2}\frac{p_{0v}}{|\mathbf{p}_v|}\ln\frac{p_{0v}+|\mathbf{p}_v|}{p_{0v}-|\mathbf{p}_v|}\right]\end{aligned} \tag{53}$$

where use has been made of (52) and $\mathbf{p}_v$, ip_{0v} are merely the four components of

$$p_{v\lambda} = \tfrac{1}{2}(p_\lambda+q_\lambda)+\tfrac{1}{2}v(p_\lambda-q_\lambda).$$

The evaluation of (53) is discussed in appendix D. Here we give only the results which are appropriate to the various limits already considered in sections 4 and 5 for the radiative corrections to the process. Thus, the expressions which may be added directly to (43), (44) and (50) are respectively given by

$$\delta_D(|\eta| \ll 1) = (2c-2)\ln\frac{2k_{max}}{\lambda} + \frac{p_0}{p}\ln\frac{p_0+p}{p_0-p} - \frac{p_0\cosh 2\alpha}{\sinh\alpha}\psi(\alpha), \tag{54a}$$

where $\psi(\alpha)$ is defined by (D9).

$$\delta_D(|\eta| \ll 1, \theta \ll 1) = (2c-2)\ln\frac{2k_{max}}{\lambda} + 2\ln(2p_0) - 2c\left[\ln\frac{p_0}{\sinh\alpha} + h(\alpha)\right] \quad (54b)$$

$$\delta_D(\alpha, \beta \gg 1) = (4\alpha-2)\ln\frac{2k_{max}}{\lambda} + \ln(4p_0q_0)(1-2\alpha) + 2\alpha^2. \quad (54c)$$

Here $c = 2\alpha\coth 2\alpha$. It may be noted that the expression (54c) is more general than (50) in so far as no assumption about the relative magnitudes of η_1, η_2, η_3 is involved in (54c).

The total correction to the cross section is obtained by adding (43), (44) and (50) to their respective counter parts in (54) and it is now seen that in each case the λ-terms cancel out, as expected. This completes our investigation. We note here that our result agrees with Fomin's [4]) for the first two cases but not for the third.

We now add a few final remarks. Eq. (50) of course is limited to a rather special case of the E.R. limit, but it is quite conceivable that it has a much wider range of validity (say covering the case for which all the η's may be comparable) except, perhaps with minor changes. It is the 'fractional' forms in which the various expressions have been obtained that lend credence to such a conjecture. In fact Fomin's result for the E.R. limit is already of this form though he does not seem to specify the relative magnitudes of the various η's. We are, however, unable to concede that our discrepancy with his result could be simply due to an error in our calculations. For, even allowing for the fact that the 'mass operator' method used by Fomin is superior from the calculational point of view, it is not clear why the results will not depend on the relative magnitudes of the various η's, particularly where integrals of the type $G_0^{(1)}$ are involved. (The integral $G_0^{(1)}$, e.g., depends, in a rather involved manner, on the parameters η_3 and η_2.) Thus, unless such 'controversial' integrals cancel out *algebraically* (and we are satisfied from our calculations that they do not), they would have a non-trivail effect on the nature of the final result.

Secondly, the results given here may be adapted to cover the case of pair production by high energy γ-rays by taking the final electron to be a negative energy one, in the E.R. limit. However, for this purpose, the results of sections 4 and 5 would not be valid, but that the more general expressions in appendix C would have to be used.

We are indebted to Professor R. C. Majumdar for his kind interest in the present investigation and for some helpful suggestions. We are also grateful to Professor S. D. Drell of Stanford University for having informed us about investigations on similar problems carried out at Stanford. Finally we record our deep appreciation of the help obtained from Mr. R. P. Saxena (Aligarh) in checking some of our algebraic calculations, particularly the vertex terms.

Appendix A

Most of the basic integrals appearing in this work are identical with those given in BF. However, the non-zero quantity Q^2 appearing in our work considerably complicates the derivation of at least some of them, compared with BF. We shall here discuss the derivation of only the more complicated ones which are not covered by BF's work. For this purpose we shall confine ourselves merely to the q-terms and use the following notation:

$$P_\lambda = p_\lambda - q_\lambda; \quad Q_\lambda = p_\lambda - q_\lambda - k_\lambda;$$
$$(0) = s^2+\lambda^2; \quad (1) = s^2-2ps; \quad (2) = s^2-2qs; \quad (3) = (s-q-k)^2+m^2.$$

The various scalar integrals are defined as

$$A_0 = (i/\pi^2)\int \mathrm{d}^4 s/(1)(2);$$
$$B_0^{(1)} = (i/\pi^2)\int \mathrm{d}^4 s/(1)(3); \quad B_0^{(2)} = (i/\pi^2)\int \mathrm{d}^4 s/(2)(3);$$
$$C_0^{(1)}, C_0^{(2)}, C_0^{(3)} = (i/\pi^2)\int \frac{\mathrm{d}^4 s}{(0)}\left\{\frac{1}{(1)}, \quad \frac{1}{(2)}, \quad \frac{1}{(3)}\right\},$$
$$G_0^{(1)}, G_0^{(2)} = (i/\pi^2)\int \frac{\mathrm{d}^4 s}{(0)(3)}\left\{\frac{1}{(1)}, \quad \frac{1}{(2)}\right\};$$
$$G_0^{(0)}, G_0^{(3)} = (i/\pi^2)\int \frac{\mathrm{d}^4 s}{(1)(2)}\left\{\frac{1}{(0)}, \quad \frac{1}{(3)}\right\};$$
$$J_0 = (i/\pi^2)\int \mathrm{d}^4 s/(0)(1)(2)(3).$$

Tensor integrals of corresponding types are defined analogously to BF, by replacing the subscript zero in the above expressions by the appropriate tensor indices.

It may be seen from the above list that only the quantities $G_0^{(1)}$, $G_0^{(3)}$ and J_0 are substantially more involved than in BF to warrant separate derivation. The higher tensors associated with them, present no additional difficulties if we follow BF's procedure of reduction to integrals involving smaller number of denominators (see appendix Y(e) of BF).

A.1. THE INTEGRAL J_0

Introducing auxiliary variables u, v, w, we may write

$$J_0 = (i/\pi^2)\int \mathrm{d}^4 s \int_0^1 \mathrm{d}v \int_0^1 2(1-u)\mathrm{d}u \int_0^1 3w^2 \mathrm{d}w/D,$$
$$D = [s^2+\eta_2 uw+\lambda^2(1-w)-2wsp_u]^4, \tag{A1}$$

where

$$p_{u\lambda} = p_{v\lambda}(1-u)+(q_\lambda+k_\lambda)u,$$
$$p_{v\lambda} = p_\lambda v+q_\lambda(1-v), \tag{A2}$$
$$\eta_2 = 2qk.$$

Using the result

$$\int d^4s/(s^2+A)^4 = i\pi^2/6A^2, \tag{A3}$$

we get from (A1)

$$J_0 = -\int_0^1 dv \int_0^1 (1-u)du \int_0^1 w^2 dw/[\eta_2 uw+\lambda^2(1-w)-w^2 p_u^2]^2. \tag{A4}$$

As in BF (appendix Y(d)) the integral (A4) can be split up into two parts J_I and J_{II} by introducing a small quantity ε (which is essentially linked with the infra-red cut-off parameter λ) such that for $u > \varepsilon$, $\lambda \to 0$ and for $u < \varepsilon$, $u^2 \ll u$. The derivation of J_{II} is identical with that of BF's (II) but J_I is now more involved. Thus

$$J_{II} = (1/2\eta_2) \int_0^1 dv p_v^{-2} \ln [\eta_2^2 \varepsilon^2/\lambda^2(-p_v^2)], \tag{A5}$$

and

$$J_I = -\int_0^1 dv \int_\varepsilon^1 du (1-u)/u\eta_2(u\eta_2 - p_u^2). \tag{A6}$$

To evaluate (A5) we note that

$$-p_v^2 = 1+v(1-v)P^2,$$

where we write

$$P^2 = 4\sinh^2\alpha, \quad Q^2 = 4\sinh^2\beta. \tag{A7}$$

The substitution $2v-1 = \tanh\theta/\tanh\alpha$ in (A5) brings the integral to the form

$$J_{II} = -\frac{1}{2\eta_2}\int_{-\alpha}^{\alpha} \frac{d\theta}{\sinh 2\alpha}\left[\ln\left(\frac{\eta_2^2\varepsilon^2}{\lambda^2\cosh^2\alpha}\right) + 2\ln\cosh\theta\right]. \tag{A8}$$

As regards J_I we have

$$u\eta_2 - p_u^2 = (1-u)^2 v(1-v)P^2 + 1 + uv(1-u)Q^2. \tag{A9}$$

It is the presence of the Q^2-term in (A9) that makes the *exact* evaluation of (A6) almost impossible. We shall therefore discuss its evaluation for the following special cases:

(1) $P^2 \gg 1$ and $Q^2 \gg 1$, which corresponds to the extreme relativistic limit;

(2) $P^2 \approx Q^2$ which corresponds to the case when the quantum emitted is soft compared with the electron energy. These cases will cover the requirements of the text.

Case 1: $P^2 \gg 1$, $Q^2 \gg 1$.

Carrying out the v-integration in a straightforward manner and simplifying we have

$$J_I \approx -\int_\varepsilon^1 \frac{du}{u\eta_2 e^\alpha}\frac{1}{x}\left[\ln\frac{(1-u)e^\alpha + (1/x)}{ue^{2\beta-\alpha}+(1/x)} + 2\ln x\right], \tag{A10}$$

where

$$x = (1-u)e^{\alpha}+ue^{2\beta-\alpha}, \tag{A11}$$

and free use has been made of $x \gg 1$ and

$$2\sinh\alpha \approx e^{\alpha}, \quad 2\sinh\beta \approx e^{\beta}.$$

It may be remarked that in (A10) though the terms $(1-u)e^{\alpha}$ and $ue^{2\beta-\alpha}$ are much larger than $(1/x)$ they are not so, near $u = 1$ and $u = 0$ respectively. To evaluate (A10) further we therefore break up the u-integration into 3 parts, viz.

$$\varepsilon \leqq u \leqq \varepsilon_1, \quad \varepsilon_1 \leqq u \leqq 1-\varepsilon_1 \quad \text{and} \quad 1-\varepsilon_1 \leqq u \leqq 1$$

such that for $u \leqq \varepsilon_1$, $(1-u)e^{\alpha} \gg (1/x) \gg ue^{2\beta-\alpha}$, and for $u \geqq 1-\varepsilon_1$, the opposite inequality holds. These conditions are easily seen to lead to

$$\varepsilon_1 \approx e^{-2\beta}. \tag{A11a}$$

Using the above inequalities we may now write (A10) approximately as (after carrying out some trivial integrations)

$$\begin{aligned} J_{\mathrm{I}} \approx{}& (-1/\eta_2 e^{2\alpha})[4\alpha \ln(\varepsilon_1/\varepsilon)+4\alpha^2-2\beta^2] \\ &+(-1/\eta_2 e^{2\alpha})\left[\int_{\varepsilon_1}^{1}\left(-\frac{dx}{x}\right)\ln\left(\frac{1-u}{u}\right)+\int_{\varepsilon_1}^{1}\frac{2\ln x}{u}du\right]. \end{aligned} \tag{A12}$$

In the second line the first integral remains finite at both limits (even when $\varepsilon_1 \to 0$). The second integral diverges only at the lower limit when $\varepsilon_1 \to 0$. If therefore, we neglect *finite* terms compared with $O(\alpha, \beta)$, we need consider only the contributions from those limits at which the integrals diverge when $\varepsilon_1 \to 0$. Thus we have finally

$$J_{\mathrm{I}} \approx (-1/\eta_2 e^{2\alpha})[-4\alpha \ln\varepsilon+4\alpha^2-4\alpha\beta-2\beta^2].$$

Adding the contribution from (A8) in the same approximation ($\alpha, \beta \gg 1$) which is

$$J_{\mathrm{II}} \approx (-1/\eta_2 e^{2\alpha})[4\alpha \ln(\varepsilon|\eta_2|/\lambda)-2\alpha^2],$$

we have finally:

$$J_0 = (-1/\eta_2 e^{2\alpha})[4\alpha\xi_2-4\alpha \ln\lambda+2\alpha^2-2\beta^2-4\alpha\beta]. \tag{A13}$$

Case 2: $P^2 \approx Q^2$

In this case (A9) becomes simply

$$u\eta_2-p_u^2 = 1+4\sinh^2\alpha y(1-y), \tag{A14}$$

where $y = v(1-u)$. Changing the integration variable from v to y and then setting

$$2y-1 = \tanh\theta/\tanh\alpha, \tag{A15}$$

the y-integration is carried out trivially, giving

$$J_1 = -\frac{1}{\eta_2 \sinh 2\alpha}\left[-2\alpha \ln \varepsilon + 2 \tanh \alpha \int_0^1 \frac{du \ln u}{1-(1-2u)^2 \tanh^2 \alpha}\right],$$

where a partial integration with respect to u has been used and ε has been set equal to zero in the 2nd integral. Then the substitution $(1-2u) \tanh \alpha = \tanh \phi$ gives

$$J_1 = \left(-\frac{1}{\eta_2 \sinh 2\alpha}\right)\left[-2\alpha \ln \varepsilon + \int_{-\alpha}^{\alpha} d\phi \ln \frac{\sinh(\alpha-\phi)}{2 \sinh \alpha \cosh \phi}\right].$$

The term involving $\sinh(\alpha-\phi)$ may be simplified by the transformation $\alpha-\phi = \phi'$. Next (A8) may be added to the last expression, yielding

$$\eta_2 J_0 = -2\alpha \operatorname{cosech} 2\alpha[\xi_2 - \ln \lambda - \ln \sinh 2\alpha + (2\alpha)^{-1} \int_0^{2\alpha} \ln \sinh \phi \, d\phi].$$

Finally an integration by parts leads to the expression

$$\eta_2 J_0 = -2\alpha \operatorname{cosech} 2\alpha[\xi_2 - \ln \lambda - h(2\alpha)], \tag{A16}$$

where $h(\alpha)$ is defined after BF as

$$h(\alpha) = \alpha^{-1} \int_0^{\alpha} \theta \coth \theta \, d\theta. \tag{A17}$$

As a check it is easily seen that in the limit $\alpha \gg 1$ (A16) leads to (A13) for $\alpha \approx \beta$.

We have deliberately discussed the J_0-integral in some detail for both the cases, in order to bring out clearly the nature of the approximations considered, thus setting a pattern for the calculations. The remaining integrals may therefore be sketched only briefly.

A.2. THE INTEGRAL $G_0^{(1)}$

By straightforward calculation this integral may be brought to the form

$$G_0^{(1)} = -\int_0^1 dv(1+v(1-v)Q^2 - v\eta_2)^{-1} \ln [(1+v(1-v)Q_2)/v\eta_2]. \tag{A18}$$

This is exact so far.

For $|\eta_2| \ll 1$ (A18) can be evaluated very simply by neglecting the term $v\eta_2$ in the denominator, and setting

$$2v-1 = \tanh \theta / \tanh \beta. \tag{A19}$$

Thus

$$G_0^{(1)} = -\int_{-\beta}^{\beta} \operatorname{cosech} 2\beta \, d\theta [\ln \sinh 2\beta - \xi_2 - \ln \cosh \theta + \ln \cosh \beta - \ln \sinh(\theta+\beta)].$$

Manipulation as in (A15)—(A17) leads finally to

$$G_0^{(1)} = -2\beta \operatorname{cosech} 2\beta[-\xi_2 + 2h(2\beta) - h(\beta)]. \tag{A20}$$

In the extreme relativistic case when *both* Q^2 and $|\eta_2|$ are $\gg 1$ and comparable to each other the term unity in the denominator may be neglected provided the lower limit of v-integration is modified to

$$\varepsilon_2 = (Q^2-\eta_2)^{-1}. \tag{A21}$$

(A18) may be written as

$$G_0^{(1)} \approx -\int_{\epsilon_2}^1 \frac{dv}{Q^2-\eta_2}\left[\frac{1}{v}+\frac{Q^2}{(1-v)Q^2-\eta_2}\right]\left(\ln\frac{Q^2}{\eta_2}+\ln(1-v)\right). \tag{A22}$$

Here again we use the same approximation as employed for the evaluation of (A12), viz. only those terms which are of $O(\beta, \xi_2)$ etc. may be retained and those of $O(1)$ neglected. Thus the terms involving $\ln(1-v)$ in (A22) make no contribution at all, and we have

$$G_0^{(1)} \approx -(Q^2-\eta_2)^{-1}[\ln(Q^2/\eta_2)][-\ln\eta_2+2\ln(Q^2-\eta_2)]. \tag{A23}$$

Further simplification of (A23) will depend on the relative magnitudes of Q^2 and η_2. For the case considered in the text (sec. 5), we have taken $Q^2 \gg \eta_2$ though $\ln\eta_2$ has not been neglected compared with $\ln Q^2$. (This is quite reasonable since $\ln x$ varies much more slowly than x itself.) For this case (A23) gives

$$G_0^{(1)} \approx -e^{-2\beta}(2\beta-\xi_2)(4\beta-\xi_2). \tag{A24}$$

It may be noted that unlike the case of J_0(A24) does not reduce to (A20) in the limit $\beta \gg 1$. This is simply because η_2 did not appear explicitly in the evaluation of the J_0 integral (except as an overall multiplicative factor) whereas for $G_0^{(1)}$ the magnitude $|\eta_2|$ played a more vital role and it would therefore be unreasonable to expect the results based on $|\eta_2| \ll 1$ and $|\eta_2| \gg 1$ to agree.

A.3. THE INTEGRAL $G_0^{(3)}$

This integral, after integration over the virtual momentum s_λ, may be written as

$$G_0^{(3)} = -\int_0^1 dv \int_0^1 (1-u)du/(u\eta_2-p_u^2), \tag{A25}$$

where $p_{u\lambda}$ is defined as in (A2) so that (A9) holds for this case as well.

Case 1: $p^2 \gg 1$, $Q^2 \gg 1$

Proceeding as for the evaluation of J_1 we get, analogously to (A10) and in the same notation,

$$G_0^{(3)} \approx -e^{-\alpha}\int_0^1 (du/x)[\ln(1-u)-\ln u+2\ln x+2\alpha-2\beta], \tag{A26}$$

since the absence of the factor $1/u$ in (A26) unlike in (A10), enables us to neglect $1/x$ compared with $(1-u)e^\alpha$ and $ue^{2\beta-\alpha}$, throughout the entire range of u-integration. The rest of the integration in (A26) can now be performed

exactly by changing to the variable x from u, leading in a straightforward manner to

$$G_0^{(3)} = -2(\alpha^2-\beta^2)/(e^{2\alpha}-e^{2\beta}). \tag{A27}$$

Case 2: $P^2 \approx Q^2$

For this case, we may use (A14) and (A15) and obtain after integration over θ,

$$G_0^{(3)} = -\int_0^1 du \operatorname{cosech} 2\alpha[\alpha+\tanh^{-1}((1-2u)\tanh\alpha)].$$

The further substitution

$$(1-2u)\tanh\alpha = \tanh\phi$$

leads in a simple way to the final result

$$G_0^{(3)} = -\alpha \operatorname{cosech} 2\alpha. \tag{A28}$$

It may be noted that (A27) and (A28) agree in the simultaneous limits $\alpha \gg 1$ and $\alpha \approx \beta$, as one would expect, since the magnitude of η_2 does not play any role in (A27) or (A28).

Appendix B

The various tensor integrals encountered in the text are listed here as follows (in the notation of appendix A):

$$a = \ln \Lambda^2, \quad P^2 = (p-q)^2 = 4\sinh^2\alpha;$$
$$\xi_2 = \ln|\eta_2|, \quad Q^2 = (p-q-k)^2 = 4\sinh^2\beta.$$

TWO-DENOMINATOR INTEGRALS

$$A_0 = -a+2\alpha\coth\alpha-1;$$
$$A_\lambda = \tfrac{1}{2}(p_\lambda+q_\lambda)(-a+2\alpha\coth\alpha-\tfrac{1}{2});$$
$$B_\lambda^{(1)} = \tfrac{1}{2}(p_\lambda+q_\lambda+k_\lambda)(-a+2\beta\coth\beta-\tfrac{1}{2});$$
$$B_0^{(2)} = 1-a;$$
$$B_\lambda^{(2)} = \tfrac{1}{2}(2q_\lambda+k_\lambda)(-a+\tfrac{3}{2});$$
$$C_0^{(1)} = C_0^{(2)} = -(a+1);$$
$$C_\lambda^{(1)} : p_\lambda = C_\lambda^{(2)} : q_\lambda = \tfrac{1}{2}(-a+\tfrac{1}{2});$$
$$B_0^{(1)} = -a+2\beta\coth\beta-1;$$
$$C_0^{(3)} = -(a+1)+[\xi_2\eta_2/(\eta_2-1)];$$
$$C_\lambda^{(3)} = (q_\lambda+k_\lambda)[-\tfrac{1}{2}a+\tfrac{1}{4}-\tfrac{1}{2}(\eta_2/\eta_2-1)+\tfrac{1}{2}\xi_2\eta_2^2(\eta_2-1)^{-2}].$$

These formulae are exact.

THREE-DENOMINATOR INTEGRALS

These quantities will be given only for the limits

a) $\eta_1, |\eta_2| \ll 1$ and b) $\eta_1, |\eta_2|, |\eta_3| \gg 1$ with $|\eta_3| \gg \eta_1, |\eta_2|$.

We use the notation: $b = 2\alpha \operatorname{cosech} 2\alpha$; $c = 2\alpha \coth 2\alpha$.

a) $\eta_1, |\eta_2| \ll 1$: In this case, $\beta \approx \alpha$.

$$
\begin{aligned}
G_0^{(0)} &= -b(-\ln\lambda + h(\alpha) - h(2\alpha)); \quad \text{(exact)} \\
G_0^{(1)} &= -b(-\xi_2 + 2h(2\alpha) - h(\alpha)); \\
G_0^{(2)} &= \xi_2 - 1 + \tfrac{1}{2}\eta_2(\xi_2 - \tfrac{1}{2}) + O(\eta_2^2); \\
G_0^{(3)} &= -\tfrac{1}{2}b; \\
G_\lambda^{(1)} &\approx G_\lambda^{(0)} = -\tfrac{1}{2}b(p_\lambda + q_\lambda); \\
G_{\lambda\sigma}^{(1)} &\approx G_{\lambda\sigma}^{(0)} = (p_\lambda p_\sigma + q_\lambda q_\sigma)\theta_1(\alpha) + \delta_{\lambda\sigma}\theta_3(\alpha) + (p_\lambda q_\sigma + p_\sigma q_\lambda)\theta_2(\alpha); \\
\theta_1(\alpha) &= \tfrac{1}{2}(1-c)\operatorname{cosech}^2\alpha, \quad \theta_2(\alpha) = \tfrac{1}{2}(b-1)\operatorname{cosech}^2\alpha, \\
\theta_3(\alpha) &= -\tfrac{1}{4}a - \tfrac{3}{8} + \tfrac{1}{2}\alpha \coth\alpha.
\end{aligned}
$$

b) $|\eta_3| \gg \eta_1, |\eta_2| \gg 1$:

In this case, $\eta_3 = -2\cosh 2\alpha \approx -e^{2\alpha}$; $\beta \approx \alpha$.

$$
\begin{aligned}
G_0^{(0)} &= 4\alpha(-\ln\lambda - \tfrac{1}{2}\alpha)/\eta_3; \\
G_0^{(1)} &= (2\beta - \xi_2)(4\beta - \xi_2)/\eta_3; \\
G_0^{(2)} &= -\tfrac{1}{2}\xi_2^2/\eta_2; \\
G_0^{(3)} &= -2\alpha/\eta_3; \\
G_\lambda^{(0)} &= (2\alpha/\eta_3)(p_\lambda + q_\lambda); \\
G_\lambda^{(1)} &= (1/\eta_3)[(2\beta - \xi_2)(q_\lambda + k_\lambda) + 2\beta p_\lambda]; \\
G_\lambda^{(2)} &= (1/\eta_2)[-\xi_2 k_\lambda + (\xi_2 - \tfrac{1}{2}\xi_2^2)q_\lambda]; \\
G_\lambda^{(3)} &= (\alpha/\eta_3)[2q_\lambda + k_\lambda]; \\
G_{\lambda\sigma}^{(1)} &= (1/\eta_3)[\beta p_\lambda p_\sigma + (\beta - \tfrac{1}{2}\xi_2)(q_\lambda + k_\lambda)(q_\sigma + k_\sigma)] + \tfrac{1}{4}\delta_{\lambda\sigma}(2\beta - a); \\
G_{\lambda\sigma}^{(2)} &= (1/\eta_2)[(\tfrac{3}{2}\xi_2 - \tfrac{1}{2}\xi_2^2)q_\lambda q_\sigma - \tfrac{1}{2}\xi_2 k_\lambda k_\sigma - \xi_2(q_\sigma k_\lambda + q_\lambda k_\sigma)] \\
&\quad + \tfrac{1}{4}\delta_{\lambda\sigma}(\xi_2 - a).
\end{aligned}
$$

THE J-INTEGRALS

a) $\eta_1, |\eta_2| \ll 1$

$$
\begin{aligned}
J_0 &= -(b/\eta_2)(\xi_2 - \ln\lambda - h(2\alpha)); \\
J_\lambda &= \tfrac{1}{2}\operatorname{cosech}^2 2\alpha[\alpha \tanh\alpha(p_\lambda + q_\lambda) + (\xi_2 - 1)(q_\lambda \cosh 2\alpha - p_\lambda) \\
&\quad + (2h(2\alpha) - h(\alpha) - \xi_2)(bq_\lambda - cp_\lambda)]; \\
J_{\lambda\sigma} &= \tfrac{1}{4}\operatorname{cosech}^2 2\alpha(1-c)(p_\lambda p_\sigma - q_\lambda q_\sigma + p_\lambda q_\sigma + p_\sigma q_\lambda) \\
&\quad + \tfrac{1}{2}\operatorname{cosech}^2 2\alpha(b - \cosh 2\alpha)q_\lambda q_\sigma - \tfrac{1}{4}b\delta_{\lambda\sigma}.
\end{aligned}
$$

b) $|\eta_3| \gg \eta_1$, $|\eta_2| \gg 1$

We set $\chi_2 = 12\alpha^2 - 4\alpha\xi_2 + \xi_2^2$.

$$
\begin{aligned}
J_0 &= (1/\eta_2\eta_3)[4\alpha\xi_2 - 4\alpha \ln \lambda - 4\alpha^2];\\
J_\lambda &= -\tfrac{1}{4}\chi_2(\eta_1\eta_3)^{-1}p_\lambda + \tfrac{1}{4}(\chi_2 + 2\xi_2^2)(\eta_2\eta_3)^{-1}q_\lambda + \tfrac{1}{4}\chi_2(\eta_1\eta_2)^{-1}k_\lambda;\\
J_{\lambda\sigma} &= \alpha_\lambda p_\sigma + \beta_\lambda q_\sigma + \gamma_\lambda k_\sigma - \tfrac{1}{8}\delta_{\lambda\sigma}(\chi_2/\eta_1),\\
\alpha_\lambda &= (\chi_2\eta_2/4\eta_1^2)[(p_\lambda/\eta_3) - (k_\lambda/\eta_2)];\\
\beta_\lambda &= \tfrac{1}{4}(\eta_2\eta_3)^{-1}[\chi_2 + 2\xi_2^2 - 4\xi_2]q_\lambda + \tfrac{1}{4}(\eta_1\eta_2)^{-1}\chi_2 k_\lambda;\\
\gamma_\lambda &= -\tfrac{1}{4}(\chi_2/\eta_1^2)p_\lambda + \tfrac{1}{4}(\chi_2/\eta_1\eta_2)q_\lambda + \tfrac{1}{4}(\chi_2\eta_3/\eta_1^2\eta_2)k_\lambda.
\end{aligned}
$$

Appendix C

We give here the general extreme relativistic limits for the various contributions to the second order cross-section $d\sigma_2$ arising from the 'vertex' and 'Compton' parts. The common multiplicative factor for all the following expressions is $-\rho_f(\alpha_0/2\pi)V^2(Q)$, where $V^2(Q)$ and ρ_f are given by (6) and (13) of the text respectively.

(C1) the Λ_μ-vertex terms (multiplied by $(-1/\eta_1\eta_2)$)

$$
\begin{aligned}
&B_0^{(1)}[2\eta_1^2 + 2\eta_3^2 - 2\eta_1\eta_3 - 2\eta_2\eta_3 + 4\eta_2 p_\mu(p_\mu + q_\mu) - 4\eta_3(p_\mu^2 + q_\mu^2)\\
&\quad + 4\eta_1(2p_\mu^2 + q_\mu^2 - p_\mu q_\mu)]\\
&+G_0^{(1)}[4\eta_1^2\eta_3 - 2\eta_1^3 - 4\eta_1\eta_3^2 - 2\eta_2\eta_3^2 + 2\eta_3^3 + 2\eta_1\eta_2\eta_3 - 8\eta_1^2 p_\mu^2 - 4p_\mu^2\eta_2^2\\
&\quad - 4q_\mu^2(\eta_1^2) + 4\eta_3^2(-q_\mu^2 - p_\mu^2) + 8\eta_1\eta_3(p_\mu^2 + q_\mu^2)\\
&\quad - 8\eta_1\eta_2 8p_\mu(p_\mu + q_\mu)]\\
&+G_\lambda^{(1)}[p_\lambda(4\eta_1\eta_3 - 4\eta_3^2 + 8\eta_2\eta_3 - 2\eta_2^2 - 4\eta_1^2 - 2\eta_1\eta_2 + 8\eta_3 k_\mu^2 - 8\eta_2 q_\mu^2\\
&\quad + 8\eta_2 p_\mu k_\mu - 8\eta_1 q_\mu^2 - 8\eta_1 p_\mu q_\mu)\\
&\quad + q_\lambda(16\eta_1 p_\mu^2 - 8\eta_1 k_\mu^2 - 2\eta_1^2 + 8\eta_2 p_\mu^2 - 8\eta_3 k_\mu^2 - 16\eta_3 q_\mu k_\mu\\
&\quad - 2\eta_1\eta_2 + 4\eta_2\eta_3 + 4\eta_1\eta_3 - 4\eta_3^2)\\
&\quad + k_\lambda(2\eta_1\eta_3 - 4\eta_1^2 - 8\eta_1 q_\mu^2 - 8\eta_2 p_\mu^2 - 8\eta_2 p_\mu q_\mu + 8\eta_3(p_\mu + q_\mu)^2\\
&\quad - 4\eta_3^2 - 4\eta_1\eta_3 + 2\eta_2\eta_3)]\\
&+G_\mu^{(1)}[8\eta_3^2 p_\mu - 8\eta_1\eta_3 p_\mu - 8\eta_2\eta_3 p_\mu + 4\eta_1\eta_2 q_\mu + 4\eta_2^2 p_\mu + 4\eta_1\eta_2 p_\mu + 8\eta_1^2 p_\mu]\\
&+G_{\mu\mu}^{(1)}[-4\eta_1^2 - 4\eta_3^2 + 4\eta_1\eta_3 + 4\eta_2\eta_3]\\
&+G_{\lambda\mu}^{(1)}[p_\lambda(8\eta_3 p_\mu - 8\eta_2 p_\mu - 8\eta_1 k_\mu) - 8k_\lambda(\eta_1 p_\mu + \eta_3 q_\mu)\\
&\quad + 8q_\lambda(-\eta_1 p_\mu + \eta_3 q_\mu - \eta_2 p_\mu - \eta_1 q_\mu)].
\end{aligned}
$$

(C2) the Λ_ν vertex terms (multiplied by (-1))

$$
\begin{aligned}
&B_0^{(2)}(\eta_1\eta_2)^{-1}[-4\eta_1^2-16p_\mu k_\mu\eta_1+8p_\mu q_\mu\eta_3-2\eta_3^2+4k_\mu^2\eta_3+2\eta_1\eta_3-4p_\mu^2\eta_2\\
&\quad+2\eta_2\eta_3-4p_\mu q_\mu\eta_2-4p_\mu q_\mu\eta_1-4q_\mu^2\eta_1]\\
&+C_0^{(2)}(\eta_1\eta_2)^{-1}[2\eta_1^2+8\eta_1p_\mu k_\mu+2\eta_3^2-4\eta_3(p_\mu^2+q_\mu^2)+4p_\mu q_\mu(\eta_1+\eta_2)\\
&\quad-2\eta_1\eta_3+4p_\mu^2\eta_2+4q_\mu^2\eta_1-2\eta_2\eta_3]\\
&+C_0^{(3)}(\eta_1\eta_2)^{-1}[2\eta_1^2+4\eta_1(p_\mu^2+p_\mu k_\mu)+4\eta_1q_\mu^2-4\eta_3(p_\mu^2+q_\mu^2)+2\eta_3^2-2\eta_1\eta_3\\
&\quad-2\eta_2\eta_3+4p_\mu^2\eta_2+4p_\mu q_\mu\eta_2]\\
&+G_0^{(2)}(\eta_1)^{-1}[8p_\mu q_\mu\eta_3-4q_\mu k_\mu\eta_3-2\eta_3^2+2\eta_3\eta_2-4q_\mu^2\eta_1-4p_\mu q_\mu\eta_2]\\
&+G_\mu^{(2)}(\eta_1)^{-1}[4k_\mu\eta_1+4p_\mu(\eta_3-\eta_2)]+4G_{\mu\mu}^{(2)}\\
&+G_{\lambda\mu}^{(2)}(\eta_1\eta_2)^{-1}[-24\eta_1p_\mu q_\lambda-8\eta_3k_\mu k_\lambda+8\eta_2p_\mu k_\lambda-8\eta_1q_\mu k_\lambda-8\eta_2q_\mu p_\lambda]\\
&+G_\lambda^{(2)}[(p_\lambda/\eta_1)(-2\eta_1+2\eta_2-8p_\mu q_\mu-8q_\mu k_\mu)\\
&\quad+(q_\lambda/\eta_2)(8p_\mu k_\mu-32p_\mu q_\mu+2\eta_2-4\eta_3+16q_\mu^2)\\
&\quad+(8q_\lambda/\eta_1\eta_2)(\eta_2p_\mu q_\mu+\eta_3^2-2\eta_3p_\mu^2-2\eta_3q_\mu^2+2p_\mu^2\eta_2-\eta_2\eta_3)\\
&\quad+(2k_\lambda/\eta_1\eta_2)(\eta_1\eta_3-3\eta_2\eta_3+2\eta_3^2-8\eta_3q_\mu^2-4p_\mu q_\mu\eta_1+8q_\mu^2\eta_1+8p_\mu q_\mu\eta_2)]\\
&+G_{\lambda\nu}^{(2)}\left[\frac{4p_\nu p_\lambda}{\eta_1}+(p_\nu q_\lambda)\left(\frac{12}{\eta_2}-\frac{8\eta_3}{\eta_1\eta_2}+\frac{4}{\eta_1}+\frac{32p_\mu q_\mu}{\eta_1\eta_2}\right)+\frac{4p_\nu k_\lambda}{\eta_1\eta_2}(-\eta_2-\eta_3+4p_\mu q_\mu)\right.\\
&\quad+\frac{4q_\nu q_\lambda}{\eta_2^2}(\eta_2+2\eta_1-2\eta_3+8p_\mu k_\mu+4p_\mu q_\mu)\\
&\quad+(q_\nu k_\lambda)\left(-\frac{8\eta_3}{\eta_2^2}+\frac{8\eta_1}{\eta_2^2}+\frac{4\eta_3}{\eta_1\eta_2}+\frac{4}{\eta_2}+\frac{32p_\mu^2}{\eta_2^2}-\frac{16p_\mu q_\mu}{\eta_1\eta_2}\right)\\
&\quad\left.+(4k_\nu k_\lambda/\eta_1\eta_2)(\eta_3-4p_\mu q_\mu)\right].
\end{aligned}
$$

(C3) *the Compton I terms* (multiplied by $(1/\eta_1)$)

$$
\begin{aligned}
&\eta_3J_0[4\eta_3(p_\mu^2+q_\mu^2)-4\eta_2p_\mu(p_\mu+q_\mu)-4\eta_1q_\mu(p_\mu+q_\mu)-2\eta_3^2+2\eta_3(\eta_1+\eta_2)]\\
&\quad+(J_\lambda k_\lambda)(-8\eta_3k_\mu q_\mu)+(k_\lambda J_{\lambda\mu})(8\eta_3q_\mu)\\
&\quad+\eta_3J_\mu[4\eta_1(q_\mu+2p_\mu)-4\eta_3(q_\mu+2p_\mu)]+4\eta_3J_{\mu\mu}(\eta_3-\eta_2).\\
&\quad+G_0^{(3)}\eta_3(8q_\mu^2-2\eta_3+2\eta_2)\\
&\quad+G_\lambda^{(3)}p_\lambda(-16q_\mu^2+4\eta_3-4\eta_2)\\
&\quad+(G_0^{(3)}-G_0^{(1)})\eta_3(2\eta_3+4k_\mu q_\mu)\\
&\quad+p_\lambda(G_\lambda^{(3)}-G_\lambda^{(1)})(-4\eta_3+4\eta_2+4\eta_1-8k_\mu q_\mu)\\
&\quad+4\eta_3q_\mu(G_\mu^{(1)}-G_\mu^{(3)})+8p_\lambda q_\mu(G_{\lambda\mu}^{(3)}-G_{\lambda\mu}^{(1)})\\
&\quad+(G_0^{(3)}-G_0^{(2)})[4\eta_3^2-4\eta_2\eta_3-2\eta_1\eta_3-4\eta_3(p_\mu^2+q_\mu^2-q_\mu k_\mu)\\
&\qquad+4(p_\mu+q_\mu)(\eta_1q_\mu+\eta_2p_\mu)]\\
&\quad+(G_\lambda^{(3)}-G_\lambda^{(2)})[4p_\lambda(\eta_2-\eta_3-2k_\mu q_\mu)+8k_\lambda q_\mu(p_\mu+q_\mu)]\\
&\quad+(G_\mu^{(3)}-G_\mu^{(2)})[8p_\mu(\eta_3-\eta_2)-4q_\mu(\eta_1+\eta_2+\eta_3)]\\
&\quad+8q_\mu(G_{\lambda\mu}^{(3)}-G_{\lambda\mu}^{(2)})(p_\lambda-k_\lambda)\\
&\quad+G_{\mu\mu}^{(3)}-(G_{\mu\mu}^{(2)})(4\eta_2-4\eta_3).
\end{aligned}
$$

(C4) *the Compton II terms* (multiplied by $(1/\eta_2)$)

$$
\begin{aligned}
&-2\eta_2\eta_3 J_0(\eta_1+4p_\mu k_\mu)+4\eta_2\eta_3(J_\mu k_\mu+J_{\mu\mu})\\
&+2\eta_3(J_\lambda k_\lambda)(\eta_1-\eta_2+4p_\mu k_\mu)+4\eta_3(J_{\lambda\nu}k_\lambda k_\nu)\\
&+2\eta_3 G_0^{(1)}(\eta_3-\eta_1-4p_\mu{}^2)+4\eta_3 G_\mu^{(1)}p_\mu-4G_\mu^{(3)}(k_\mu\eta_3+q_\mu\eta_1)\\
&+G_\lambda^{(1)}[2q_\lambda(\eta_1-2\eta_3+4p_\mu{}^2)+2p_\lambda(\eta_2-4p_\mu q_\mu)-2k_\lambda\eta_3]\\
&+G_0^{(3)}[-2\eta_2(\eta_1+\eta_3)+(\eta_1 q_\mu+\eta_2 p_\mu)(4p_\mu+8q_\mu)+4k_\mu{}^2(\eta_3-\eta_2)\\
&\quad+8\eta_3 q_\mu k_\mu+4\eta_3 p_\mu k_\mu]\\
&+G_\lambda^{(3)}[k_\lambda(2\eta_3-8p_\mu q_\mu)-2p_\lambda\eta_2+q_\lambda(4\eta_3-2\eta_1-8p_\mu{}^2-8p_\mu q_\mu)]\\
&+(G_0^{(3)}-G_0^{(1)})(\eta_1{}^2+\eta_1\eta_2-2\eta_1\eta_3+2\eta_3{}^2-4\eta_3 p_\mu q_\mu-4\eta_3 p_\mu{}^2\\
&\quad+4\eta_1 p_\mu{}^2+4\eta_2 p_\mu q_\mu)\\
&+(G_\lambda^{(3)}-G_\lambda^{(1)})[4q_\lambda(\eta_1-\eta_3)+2k_\lambda(\eta_1-4p_\mu{}^2)]\\
&+4(G_{\mu\mu}^{(3)}-G_{\mu\mu}^{(1)})(\eta_1-\eta_3)+8p_\lambda p_\mu(G_{\lambda\mu}^{(3)}-G_{\lambda\mu}^{(1)})\\
&+(G_\mu^{(3)}-G_\mu^{(1)})[8p_\mu(\eta_3-2\eta_2-2\eta_1)+8q_\mu(\eta_3-\eta_1)]\\
&+(G_0^{(3)}-G_0^{(2)})(\eta_1\eta_2+\eta_2{}^2+4\eta_2 k_\mu{}^2)\\
&+(G_\lambda^{(3)}-G_\lambda^{(2)})[2p_\lambda\eta_2+2q_\lambda(\eta_1+2\eta_2-2\eta_3)+2k_\lambda(4p_\mu q_\mu-\eta_2-\eta_3)]\\
&+(G_\mu^{(2)}-G_\mu^{(3)})4\eta_2(p_\mu+q_\mu)\\
&+8(p_\mu q_\lambda)(G_{\mu\lambda}^{(3)}-G_{\mu\lambda}^{(2)}).
\end{aligned}
$$

Appendix D

We give here a short derivation of (54) from (53). Clearly,

$$1+\tfrac{1}{2}P^2=\cosh 2\alpha. \tag{D1}$$

The infra-red terms in (53) may be evaluated by the substitution $v\tanh\alpha=\tanh\phi$ and their contribution to δ_D is found to be

$$\delta_D(\lambda)=(4\alpha\coth 2\alpha-2)\ln(2k_{\max}/\lambda). \tag{D2}$$

Eq. (D2) covers all the 3 cases to be considered. The evaluation of the other integral, however, depends on the nature of the approximation, appropriate to each particular case. We set

$$I=\int_0^1\frac{dv}{1+\frac{1}{4}(1-v^2)P^2}\left(\frac{p_{0v}}{|\mathbf{p}_v|}\right)\ln\frac{p_{0v}+|\mathbf{p}_v|}{p_{0v}-|\mathbf{p}_v|}. \tag{D3}$$

Case 1:

$$p_0,\ q_0\gg k,\ \text{so that}\ p_0\approx q_0. \tag{D4}$$

In this case, $p_{0v}\approx p_0$ and

$$|\mathbf{p}_v|^2=p^2-(1-v^2)\sinh^2\alpha=J^2,\ \text{say}. \tag{D5}$$

Also

$$1+\tfrac{1}{4}(1-v^2)P^2=(p_0{}^2-J^2). \tag{D6}$$

We now change the integration variable from v to J according to (D5) so that

$$J\mathrm{d}J = v\mathrm{d}v \sinh^2\alpha. \tag{D7}$$

Using the results in (D3), we have

$$I = \int_{(p^2-\sinh^2\alpha)^{\frac{1}{2}}}^{p} \frac{p_0 \mathrm{d}J \operatorname{cosech}^2\alpha}{v(p_0^2-J^2)} \ln\left(\frac{p_0+J}{p_0-J}\right) = p_0 \operatorname{cosech}\alpha\, \psi(\alpha), \tag{D8}$$

where

$$\psi(\alpha) = \int_{(p^2-\sinh^2\alpha)^{\frac{1}{2}}}^{p} \mathrm{d}J (J^2+\sinh^2\alpha-p^2)^{-\frac{1}{2}}(p_0^2-J^2)^{-1} \ln\left(\frac{p_0+J}{p_0-J}\right). \tag{D9}$$

Case 2:

$$p_0, q_0 \gg 1; \quad k \ll p_0, q_0; \quad \theta_1, \theta_2, \theta = \mathrm{O}(1/p_0) \ll 1.$$

In this case it is easily seen that

$$P^2 \approx p_0^2\theta^2 = \mathrm{O}(1),$$

and

$$|\mathbf{p}_v|^2 = p^2-\tfrac{1}{4}(1-v^2)P^2 \approx p^2. \tag{D10}$$

Further,

$$p_{0v}+|\mathbf{p}_v| \approx 2p_0 \approx 2p, \tag{D11}$$

and,

$$p_{0v}-|\mathbf{p}_v| \approx (P^2/8p_0)(1-v^2) = (\sinh^2\alpha/2p_0)(1-v^2). \tag{D12}$$

Using (D10)—(D12) in (D3) we have

$$I \approx \int_0^1 \mathrm{d}v(1+\sinh^2\alpha(1-v^2))^{-1}[2\ln(2p_0/\sinh\alpha)-\ln(1-v^2)]. \tag{D13}$$

This integral may now be evaluated without any further difficulty by the substitution

$$v = \tanh\phi/\tanh\alpha, \tag{D14}$$

following the methods of appendix A. The final result is

$$I = 4\alpha \operatorname{cosech} 2\alpha[\ln(p_0 \operatorname{cosech}\alpha)+h(\alpha)]. \tag{D15}$$

Case 3:

$$p_0, q_0 \gg 1 \quad \text{and} \quad P^2 \gg 1.$$

The transformation (D14) brings I to the form

$$I = \operatorname{cosech} 2\alpha \int_{-\alpha}^{\alpha} \mathrm{d}\phi \frac{p_{0v}}{|\mathbf{p}_v|} \ln\frac{p_{0v}+|\mathbf{p}_v|}{p_{0v}-|\mathbf{p}_v|}. \tag{D16}$$

By algebraic manipulation it is easy to show that

$$p_{0v} \approx \frac{p_0 e^{\phi}+q_0 e^{-\phi}}{2\cosh\phi}, \quad |\mathbf{p}_v| \approx p_{0v}-\tfrac{1}{8}p_{0v}^{-1}e^{2\alpha}\operatorname{sech}^2\phi, \tag{D17}$$

where $\alpha \gg 1$ has been made use of. Substituting in (D16) from (D17) we obtain

$$I \approx 2e^{-2\alpha}\int_{-\alpha}^{\alpha} 2d\phi \ln[2e^{-\alpha}(p_0e^{\phi}+q_0e^{-\phi})]. \tag{D18}$$

Using the fact that the two terms p_0e^{ϕ}, $q_0e^{-\phi}$ in (D18) contribute respectively in the regions $0 \leqq \phi \leqq \alpha$ and $-\alpha \leqq \phi \leqq 0$, (D18) can be immediately evaluated to give

$$I \approx 4e^{-2\alpha}[\alpha \ln (4p_0q_0)-\alpha^2]. \tag{D19}$$

References

1) Jauch and Rohrlich, The theory of photons and electrons (Addison Wesley and Co., Cambridge, U.S.A. 1955)
2) L. M. Brown and R. P. Feynman, Phys. Rev. **85** (1952) 231; referred to as BF
3) A. N. Mitra, Nature **169** (1952) 1009
4) P. I. Fomin, JETP **34** (1958) 227
5) F. J. Dyson, Phys. Rev. **75** (1949) 486, 1736
6) A. N. Mitra, Ph. D. thesis, Delhi University (1952) unpublished
7) R. P. Feynman, Phys. Rev. **76** (1949) 749
8) R. Karplus and N. M. Kroll, Phys. Rev. **77** (1950) 536
9) J. Schwinger, Phys. Rev. **76** (1949) 790
10) R. P. Feynman, Phys. Rev. **74** (1948) 1430

1.D.2 *Nuclear Physics* **10** (1959) 654—662; © *North-Holland Publishing Co., Amsterdam*
Not to be reproduced by photoprint or microfilm without written permission from the publisher

ON THE SHAPE OF EVEN ATOMIC NUCLEI

A. DAVYDOV and G. FILIPPOV
Moscow State University, Moscow

Received 18 October 1958

Abstract: A nuclear model which consists of a core and of two nucleons in a shell of angular momentum j is considered. The energy as a function of parameters β and γ is found for various values of the total angular momentum of the nucleons. It is shown that if $j > \frac{1}{2}$ the shape for minimum energy of the nucleus in the ground state is not axially symmetric. In the limit of very strong coupling of the nucleons to deformations of the nuclear surface, the equilibrium shape of the nucleus approaches one possessing axial symmetry.

1. Introduction

It was long believed by physicists that atomic nuclei are spherical formations. This belief was supported by the success of the liquid drop model of the nucleus. However, extensive studies of ground and excited nuclear states indicated that the shape of many nuclei was not spherical. This was found to be especially true for nuclei with mass numbers in the regions

$$A > 225, \qquad 155 < A < 185 \quad \text{and} \quad A \approx 24.$$

Deviation of the shape of the nucleus from spherical symmetry could also be inferred from the existence of a rotational spectrum of the excited states and from the large quadrupole electric moments of the stationary nuclear states, which could be studied in greater detail as a result of application of the method of Coulomb excitation of nuclei and investigation of transitions in nuclei. During a large period of time no explanation of the equilibrium shape of the nucleus from spherical symmetry was offered. The first explanation of this type was suggested by J. Rainwater [1]) on basis of an investigation of the interaction between the nuclear surface and external nucleons, i.e., nucleons located in incompletely filled shells. However, in this work as well as in other successive investigations [2–5]) it was assumed that the nucleus possessed axial symmetry. Formally this reduced to neglection of those terms in the Hamiltonian which were not diagonal in the quantum numbers of the angular momentum projections on one of the nuclear axes. Thus in essence the interaction energy between the outer nucleons and nuclear surface was averaged only over the states of nucleons possessing definite values of the angular momentum projections on this axis.

It has recently been shown [6]) that many properties of the first excited states of even atomic nuclei, such as the spin sequence of the excited states, the energy of these states and the probabilities of electromagnetic transitions between them, can be satisfactorily explained if one assumes that in a first approximation the equilibrium shape of the nucleus can be represented by a triaxial ellipsoid. In Bohr's work the ellipsoidal shape of the nucleus was specified by two parameters, β and γ, related by the equations

$$a_0 = \beta \cos\gamma, \qquad a_1 = a_1 = 0, \qquad a_2 = a_{-2} = \frac{\beta \sin\gamma}{\sqrt{2}}$$

with the parameters a_μ which determine the shape of the nucleus

$$R(\vartheta\varphi) = R_0 + R_0 \sum_{\mu=-2}^{2} a_\mu Y_{2\mu}(\vartheta\varphi)$$

in a coordinate system fixed to the nucleus. For a given value of β variation of the "non-axiality" parameter γ between 0 and $\frac{1}{3}\pi$ signified a change of the nucleus from a prolate to oblate ellipsoid of revolution. The value $\gamma = 30°$ corresponds to a shape intermediate between those of an oblate and prolate ellipsoid of revolution. In order to explain the experimental facts it was assumed in ref. [6]) that in some nuclei the equilibrium value of γ may be close to 30°. This appreciable deviation from axial symmetry requires a theoretical explanation.

The possibility of violation of axial symmetry of the equilibrium shape of nuclei was first demonstrated by Gursky [7]); the results of the calculations of this author are presented in a paper by Wilets and Jean [8]). According to these calculations the minimum energy of a system of nucleons consisting of 55 protons and 91 neutrons moving in the field of a triaxial ellipsoid corresponds to $\beta = 0.04$ and $\gamma = 7.5$. Similar calculations in the same approximation were performed by Geilikman [9]) for a three dimensional oscillator potential and by Zaikin [10]) for a rectangular potential. It was also shown in these papers that in a number of cases minimum of energy of a system of nucleons corresponds to a non-axial shape of the nucleus. Unfortunately, neglection of the spin-orbit interaction and the specific choice of the potential somewhat invalidate the numerical estimations.

In the present paper a new method, based on an extension of Bohr's method to non-axial nuclei, is proposed which should permit one to investigate the possibility of deviation of the equilibrium shape of the nucleus from axial symmetry.

2. Statement of the Problem

Consider a system consisting of a certain number of nucleons forming the core of a nucleus and of two equivalent external nucleons in a shell with a

definite value of the angular momentum j. In accord with the Pauli principle the total angular momentum of two nucleons can assume only even values

$$J = 0,\ 2, \ldots 2j-1. \tag{2.1}$$

In the zero approximation, when coupling with deformations of the nuclear surface is ignored (the nucleons move in the field of the nuclear core), the total angular momentum of the nucleons J and its projection M on the axis ζ in the coordinate system $\xi\eta\zeta$ fixed to the nucleus, are integrals of motion, the energy being specified by the operator H_{p}. States ψ_{JM} differing by their values of J and M have the same energy, that is,

$$(H_{\mathrm{p}}-E_{\mathrm{p}})\psi_{JM} = 0. \tag{2.2}$$

Suppose, furthermore, in accord with the unified nuclear model of Bohr and Mottelson, that the properties of the nuclear core can be specified by the collective motion operators

$$H_{\mathrm{r}} = \tfrac{1}{2}\{a(\hat{I}_\xi-\hat{J}_\xi)^2+b(\hat{I}_\eta-\hat{J}_\eta)^2+c(\hat{I}_\zeta-\hat{J}_\zeta)^2\}, \tag{2.3}$$

$$H_{\mathrm{vib}} = -\frac{\hbar^2}{2B}\left\{\frac{1}{\beta^4}\frac{\partial}{\partial\beta}\left(\beta^4\frac{\partial}{\partial\beta}\right)+\frac{1}{\beta^2\sin 3\gamma}\frac{\partial}{\partial\gamma}\left(\sin 3\gamma\frac{\partial}{\partial\gamma}\right)+\tfrac{1}{2}C\beta^2\right\}, \tag{2.4}$$

where

$$a = \hbar^2[4B\beta^2\sin^2(\gamma-\tfrac{2}{3}\pi)]^{-1}, \qquad b = \hbar^2[4B\beta^2\sin^2(\gamma+\tfrac{2}{3}\pi)]^{-1}, \qquad c = \hbar^2[4B\beta^2\sin^2\gamma]^{-1}; \tag{2.5}$$

C is an elasticity parameter of the nuclear surface, B is a mass parameter; $\hat{I}_\xi, \hat{I}_\eta, \hat{I}_\zeta$ are projections of the operator of total angular momentum of the nucleus; $\hat{J}_\xi, \hat{J}_\eta, \hat{J}_\zeta$ are projections of the operator of total angular momentum of the outer nucleons.

Suppose that the pair of external nucleons interact with the core as a whole. The interaction operator in this case can be written as

$$H_{\mathrm{int}} = \beta T[\cos\gamma(3\hat{J}_\zeta^2-\hat{J}^2)+\sqrt{3}\sin\gamma(J_\xi^2-J_\eta^2)], \tag{2.6}$$

where T is a parameter which defines the magnitude of the coupling between the pair of nucleons in shell j and the nuclear surface.

The assumption underlying expression (2.6) of course requires an overall analysis. It is a limiting case opposite to the assumption made in Ford's paper [5]) regarding the independent interaction of the external nucleons with the surface. The H_{int} introduced by Ford completely ignores the interaction between the external nucleons. Thus Ford's Hamiltonian cannot be employed to investigate problems related to pairing of the nucleons. Interaction (2.6) will be postulated in the present paper. Moreover, those terms in the total Hamiltonian which lead to non-diagonal matrix elements in the magnetic quantum numbers will not be neglected (in contrast to ref. [2-5])): in other words we shall not assume that $j_3 = \Omega$ is a good quantum number and hence we shall not restrict the class of permissible nucleon states to

those states for which $\sum_i \Omega_i = 0$. (2.7) It is quite natural that in the investigations in which only the states satisfying auxiliary condition (2.7) are investigated, the equilibrium shape of nucleus is always axially symmetric.

If the motions connected with changes in β and γ are slow compared with the motion of the external nucleons, one may apply the adiabatic approximation employed in ref. [2-5]). Computing thereafter the energy of the complete system for fixed but arbitrary values of β and γ, one can find those values β_0 and γ_0 which correspond to a minimum of the energy. It is just these values which determine the equilibrium shape of the nucleus.

In the adiabatic approximation the operators corresponding to kinetic energy can be neglected in (2.4) and the surface vibration operator will then assume the form

$$H^{\mathrm{a}}_{\mathrm{vib}} = \tfrac{1}{2} C\beta^2. \tag{2.4a}$$

In the ground state of an even nucleus the total angular momentum of the nucleus is zero and hence the rotational energy operator (2.3) for the ground state can be written in the form

$$H_{\mathrm{r}}^{0} = \tfrac{1}{2}\{aJ_\xi^2 + bJ_\eta^2 + cJ_\zeta^2\}. \tag{2.3a}$$

Thus, the total Hamiltonian for a nucleus in the ground state has the following form in the adiabatic approximation:

$$H = H_{\mathrm{p}} + H_{\mathrm{r}}^{0} + H^{\mathrm{a}}_{\mathrm{vib}} + H_{\mathrm{int}}. \tag{2.8}$$

The solution of the equation

$$[H - E(\beta\gamma)]\psi = 0, \tag{2.9}$$

which defines the energy of the system as a function of β and γ, will be presented in the following section.

3. Calculation of the Nuclear Energy as a Function of β and γ

For the calculation of the energy $E(\beta\gamma)$ in equation (2.9) we shall write the wave function ψ in the form

$$\psi = \sum_{JM} a_{JM} |JM\rangle, \qquad |JM\rangle = [2(1+\delta_{M0})]^{-\frac{1}{2}}[\psi_{JM} + \psi_{J-M}], \tag{3.1}$$

where J assumes the values in (2.1) and $M = 0, 2, 4, \ldots J$. Inserting (3.1) in (2.9) we find a set of equations for coefficients a_{JM}. From the condition of solubility of this set of equations we obtain an equation for $E(\beta, \gamma)$.

Taking into consideration that the non-vanishing matrix elements of operators (2.3a) and (2.6) are

$$\begin{aligned}
&\langle JM|H_r^0|JM\rangle = \tfrac{1}{4}(a+b)\{J(J+1)-M^2\}+\tfrac{1}{2}cM^2,\\
&\langle JM|H_r^0|JM+2\rangle = \tfrac{1}{8}(a-b)F(JM),\\
&\langle JM|H_{\text{int}}|JM\rangle = T\beta\cos\gamma[3M^2-J(J+1)],\\
&\langle JM|H_{\text{int}}|JM+2\rangle = \tfrac{1}{2}\sqrt{3}\beta T\sin\gamma\cdot F(JM),
\end{aligned} \tag{3.2}$$

where

$$F(JM) = \sqrt{(1+\delta_{M0})(J-M)(J-M-1)(J+M+1)(J+M+2)},$$

we easily see that J is an integral of motion. Thus the equation for $E(\beta, \gamma)$ breaks up into several simpler equations for each value of J.

For $J = 0$ (pairing of nucleons with opposite angular momenta) the interaction between the deformation of the nuclear surface and the nucleon pair vanishes in our approximation. In this case the nuclear energy will depend on β and γ only through the dependence of E_p and the deformation potential energy $\frac{1}{2}C\beta^2$. Since $\frac{1}{2}C\beta^2$ is independent of γ and E_p is apparently a slowly varying function of γ in our investigation of the dependence of the nuclear energy on γ we neglect, for the sake of simplicity, the dependence of E_p on γ. Introducing

$$\varepsilon = E(J)-E(0),$$

where $E(0)$ is the nuclear energy for $J = 0$, we arrive at an equation for the energy ε when $J = 2$

$$\begin{vmatrix} \frac{3}{2}(a+b)-6\beta T\cos\gamma-\varepsilon, & 6\beta T\sin\gamma+(a-b)\frac{1}{2}\sqrt{3} \\ 6\beta T\sin\gamma+(a-b)\frac{1}{2}\sqrt{3}, & \frac{1}{2}(a+b)+6\beta T\cos\gamma+2c-\varepsilon \end{vmatrix} = 0.$$

Inserting (2.5) and expanding the determinant we obtain a quadratic equation

$$x^2-\frac{9x}{2\sin^2(3\gamma)}+\frac{9}{2\sin^2(3\gamma)}-\frac{27\cos(3\gamma)}{4\sin^2(3\gamma)}l-\tfrac{9}{4}l^2 = 0, \tag{3.3}$$

where

$$x = \varepsilon\left(\frac{\hbar^2}{B\beta^2}\right)^{-1}, \qquad l = 4\beta T\left(\frac{\hbar^2}{B\beta^2}\right)^{-1}, \tag{3.4}$$

$\hbar^2/B\beta^2$ being the energy of the first excited nuclear level.

To obtain a rough estimate of l we put $T \approx 40$ MeV, $\hbar^2/B\beta^2 \approx 400$ keV, $\beta = 0.2$. Then (3.4) yields $l \approx 80$. With increase of the deformation the parameter l increases $\propto \beta^3$.

Solutions of equation (3.4) as functions of γ for $l = 10$, 15 and 150 are represented in fig. 1.

If the pair of external nucleons exists in a state with $J = 4$, the equation defining the total nuclear energy is

$$x^3-\frac{45x^2}{2\sin^2(3\gamma)}-\left[39l^2+117l\,\frac{\cos(3\gamma)}{\sin^2(3\gamma)}-\frac{81}{\sin^4(3\gamma)}-\frac{78}{\sin^2(3\gamma)}\right]x$$
$$-70l^3\cos(3\gamma)+5\left[42-\frac{9}{\sin^2(3\gamma)}\right]l^2 \qquad (3.5)$$
$$+5\left(\frac{81\cos 3\gamma}{\sin^4(3\gamma)}+42\right)l-\frac{270}{\sin^4(3\gamma)}-\frac{70}{\sin^2(3\gamma)}=0,$$

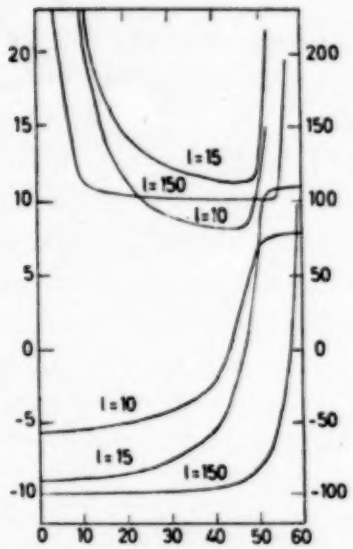

Fig. 1. Energy of nucleus as a function of γ and of the quantity l which specifies the coupling between a pair of outer nucleons and deformations of the nuclear surface. For $l = 10$ and 15 the energy is read off the left hand scale and for $l = 150$ off the right hand scale.

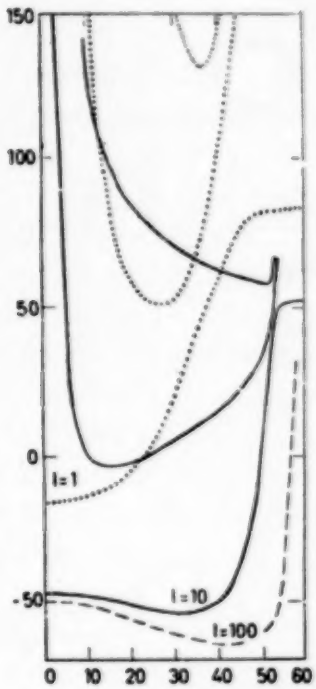

Fig. 2. Energy as a function of γ and l. For $l = 1$ the energy should be decreased 10 times and for $l = 100$, increased 10 times.

where x and l are defined in (3.4). The dependence of the three roots of eq. (3.5) on γ for $l = 10$ (full curve) is depicted in fig. 2. The dependences of the smallest roots of equation (3.5) on γ for $l = 1$ (dotted curve) and $l = 100$ (broken curve) are represented in the same figure.

4. Shape of the Nucleus as a Function of the Coupling Energy Between the Particles and Nuclear Surface

We now apply the results of the preceding section to find the equilibrium shape of the nucleus.

If each of the external electrons is in a state $j = \frac{1}{2}$, pairing will be possible only for the value $J = 0$. Such a pair of nucleons will not affect the shape of the nucleus.

If the nucleons are in a state with $j = \frac{3}{2}$, pairing can occur at $J = 0$ and 2. According to fig. 1, the state with $J = 2$ corresponds to the smaller energy. In this case an axial shape of the nucleus ($\gamma_0 = 0$) corresponds to the minimum energy. Thus the pair of outer nucleons in states with $j = \frac{3}{2}$ does not violate axial symmetry of the nucleus.

If the nucleons are in states with $j = \frac{5}{2}$, pairing can occur for $J = 0, 2, 4$. A comparison of fig. 1 and 2 shows that for a given value of l the minimum energy corresponds to the largest possible angular momentum ($J = 4$). In this case, for $l = 1$ the equilibrium shape of the nucleus is also an ellipsoid of revolution ($\gamma_0 = 0$). However, with increase of l the nuclear shape corresponds to $\gamma_0 \neq 0$. When l reaches the value 10, the equilibrium shape corresponds to $\gamma_0 \approx 30°$. Non-axiality of the nucleus is maximum in this case and the nuclear shape is intermediate between that of an oblate and prolate ellipsoid of revolution. For $l = 100$, $\gamma_0 \approx 42°$; for $l \to \infty$, $\gamma_0 \to 60°$, i.e., the nucleus is again axially symmetric. Thus in the limiting case of very strong coupling between the nucleons and the surface (large values of l) the result is the same as that obtained by Bohr and Ford.

If the nucleons are in any of the states with $j \geqq \frac{7}{2}$, the qualitative regularities established for $j = \frac{5}{2}$ still remain. The minimum energy corresponds to the highest possible value of J. With the growth of l the equilibrium value of γ changes between 0 and 60°. For large values of J deviation from axial symmetry sets in at correspondingly smaller values of l.

Thus, the interaction of a pair of nucleons with the nuclear surface favours pairing of nucleons possessing the highest possible values of J. This effect thus acts in a direction opposite to that due to the attractive interaction of fermions on the Fermi surface (in momentum space); in some cases (superconductivity of metals) this interaction leads to a bound state of fermions whose spins and momenta are in opposite directions. For sufficiently small values of l states with $J = 0$ will be favoured, whereas for large values of l the energetically favourable states are those with the highest possible values of J. Due to Coulomb repulsion between protons this will apparently occur in the case of protons at smaller values of l than in the case of neutrons.

If the number of nucleons in a shell of angular momentum j is that

required to fill the shell, only a single total angular momentum $J = 0$ will correspond to this state. If two nucleons are required to fill the shell, it is usually said that there are two holes in the shell. We may hope that the interaction of these two holes with the deformations of the nuclear surface will differ from the interaction between two nucleons only by the sign of parameter T in (2.6). Taking this assumption into consideration, one can easily apply the preceding results to describe the effect of two holes on the nuclear shape. The substitution $T \to -T$ corresponds to the transformation $l \to -l$ in equations (3.3), (3.4) and (3.5). Thus the values γ_h corresponding to the equilibrium shape of the nucleus, when two holes are present in a shell of angular momentum j, can be deduced from the corresponding equilibrium values of γ_0 defining the shape of the nucleus, when only two nucleons are present in the same shell, by means of the simple transformation

$$\gamma_h \approx 60^\circ - \gamma_0.$$

Employing the formulas in ref. [6]), one can determine, with a latitude corresponding to the transformation $\gamma' \rightleftarrows 60^\circ - \gamma_0$, the equilibrium value γ_0 from the experimental ratios of the energy of the second excited state of spin 2 to the energy of the first level. The uncertainty is due to the fact that the level spacing and transition probabilities do not depend on the sign of the quadrupole moment. It can be demonstrated by such calculations that the greatest non-axiality ($30^\circ > \gamma_0 > 27^\circ$) is observed in

$$_{46}Pd^{108},\ _{46}Pd^{106},\ _{48}Cd^{114},\ _{52}Te^{122},\ _{52}Te^{126},\ _{78}Pt^{192},\ _{78}Pt^{196}$$

and several other nuclei in which the number of protons differ from the magic numbers 50 and 82 by 2 or 4 units. For $T = 40$ MeV and values of β computed from Coulomb excitation data, the parameter l which determines the energy dependence of the ground state of the nucleus on γ lies between 20 and 80.

For nuclei with a ratio $E(2')/E(2)$ lying between 20 and 2.9 which corresponds to γ in the region $10^\circ < \gamma_0 < 20^\circ$, or $50^0 > \gamma_0 > 40^\circ$, the parameter l will equal 300—600. Finally, for nuclei which are almost axially symmetrical and for which $E(2')/E(2) > 23$ ($\gamma_0 < 10$ or $\gamma_0 > 50^\circ$) the parameter $l \approx 1000$. These experimental data qualitatively agree with the theoretical results.

References

1) J. Rainwater, Phys. Rev. **79** (1950) 432
2) A. Bohr, Mat. Fys. Medd. Dan. Vid. Selsk. **26** (1953) 14
3) A. Bohr and B. Mottelson, Mat. Fys. Medd. Dan. Vid. Selsk. **27** (1953) 16
4) J. Davidson and E. Feenberg, Phys. Rev. **89** (1953) 856
5) K. Ford, Phys. Rev. **90** (1953) 29
6) A. S. Davydov and G. F. Filippov, JETP **35** (1958) 440; **35** (1958) 703; Nuclear Physics **8** (1958) 237
7) M. Gursky, Phys. Rev. **98** (1955) 1205
8) L. Wilets and M. Jean, Phys. Rev. **102** (1956) 788
9) B. T. Geilikman, JETP **35** (1958) 989
10) D. A. Zaikin, JETP **35** (1958) 529

7.C *Nuclear Physics* **10** (1959) 663—687; © *North-Holland Publishing Co., Amsterdam*
Not to be reproduced by photoprint or microfilm without written permission from the publisher

A THEORETICAL APPROACH TO LOW ENERGY PION PHYSICS

B. BOSCO †, S. FUBINI †† and A. STANGHELLINI †††
CERN, *Geneva*

Received 28 November 1958

Abstract: We wish to propose a new approach for the study of problems involving low energy pions.

The method starts from a determination of the pion-nucleon scattering state vector in terms of the physical nucleon state vector and of the renormalized coupling constant.

Such a determination can be performed in the one-meson approximation and leads in a simple and natural way to the same results as the Chew and Low approach to scattering and photoproduction.

The method is then applied to the problem of radiative pion-nucleon scattering where we obtain an expression for the T matrix in a closed form which has the same degree of validity as the result for photoproduction.

Although the method has its natural field of application in the framework of the static model, it can be applied to obtain the recoil effects due to the motion of the physical nucleon. In the case of pion-nucleon scattering we obtain results closely analogous to those obtained in the framework of relativistic dispersion theory.

1. Introduction

During the last few years our theoretical understanding of the phenomena involving pions and nucleons has greatly improved. General relations involving the renormalized coupling constant and the scattering amplitudes, the so-called "dispersion relations", have been recently derived in the framework of quantum field theory. One has then tried to "solve" these relations, i.e. one has looked for an explicit form of the scattering matrix satisfying these dispersion relations and other physical requirements like unitarity and a reasonable high energy behaviour.

The method of dispersion relations has been first applied to the so-called "static p-wave theory", a simplified version of the general theory, in which a fixed extended nucleon source can only emit and absorb p-wave mesons. One has thus obtained expressions for the pion-nucleon scattering amplitudes which are in good agreement with experiment. Those expressions involve the renormalized coupling constant and the cut-off. The latter determines essentially only the position of the resonance and therefore it is possible to

† Present adress: Istituto di Fisica dell'Università, Torino.
†† On leave of absence from Istituto di Fisica dell'Università, Torino.
††† On leave of absence from Istituto di Fisica dell'Università, Bologna.

obtain an accurate cut-off independent determination of the coupling constant.

In the case of the photoproduction of mesons the success of the method is even more striking: all experimental photo-production can be explained simply from the knowledge of the scattering phase-shifts and of the magnetic moments of the nucleons.

The dispersion method has subsequently been applied to the full relativistic theory. The result of this more general, but also much more complicated, investigation fully confirms the simpler static calculations. Apart from some small corrections, one arrives at essentially the same results as those of the static model. An excellent account of this approach can be found in the review articles by Wick [1]) and Chew [2]), and in the original papers [3, 4]).

In this paper we want to discuss an alternate approach to pion problems which leads to final results closely analogous to those obtained by means of dispersion relations. The method we use is an "old-fashioned" one in the sense that its central problem is the determination of the pion-nucleon scattering state vector and, more specifically, of its component in the state formed by one physical nucleon plus one free pion.

We shall first obtain a rigorous integral equation for this "wave function". The kernel is very analogous to the right-hand side of the Low equation. The solution of such an integral equation can be obtained if one evaluates the kernel using the "one-meson approximation", which consists of neglecting the cross-sections for inelastic processes.

Our method is the generalization of a simple approach introduced by Friedman, Lee and Christian [5]), in which the scattering state vector has been approximated by a superposition of states with one physical nucleon and one physical nucleon plus one pion. Those authors then use the Tomonaga approximation for the physical nucleon state vector. It has been subsequently pointed out by Stroffolini [6]) that, as in the dispersion approach, the scattering phase-shifts can be reasonably computed in terms of the renormalized coupling constant independently of any detailed assumption on the physical nucleon. Our treatment fully confirms such a result.

We shall first discuss (section 2) the general problem of the determination of the scattering state vector and of the pion-nucleon scattering phase-shifts. This determination can be performed consistently in the "one-meson approximation" leading to results analogous to the ones obtained by Chew and Low [3]). Such a discussion is also useful for a better understanding of the still open problem of the uniqueness of the solution of the Low equation.

Once a form for the scattering state vector has been obtained, this can be applied to the computation of the matrix elements for pion photoproduction and for radiative pion-nucleon scattering. The solution of such problems

(section 3) does not involve any integral equation but only some integrations involving the scattering "wave function".

Our results for photoproduction coincide with those of Chew and Low [3]). In the case of radiative pion-nucleon scattering we obtain, in the same approximation of photoproduction, a compact expression which involves only the nucleon magnetic moments, the scattering phase-shifts, and which is independent of the cut-off. In a subsequent work such expressions will be numerically evaluated and compared with the results of other calculations [7]) based on the Chew-Low method.

The present approach is essentially a non-relativistic one. Pair effects are neglected and therefore the physical pion (in contrast with the physical nucleon) will be identified with a bare one. However, we shall be able (section 4) to account, in a simple and natural manner, for the recoil effects due to the motion of the physical nucleon. Comparison with the analogous results obtained by Chew *et al.* [4]) in the framework of the relativistic dispersion theory may be useful to clarify which corrections to the static model are simply due to the use of the correct kinematics, and which terms come from an essential improvement in the treatment of the dynamical problem.

The method is, of course, less general than the relativistic dispersion one. It has, however, some advantages: it is simple and it leads to explicit solutions in the shortest possible way; it finally allows the use of the correct kinematics. Such advantages are particularly evident in the case of radiative pion-nucleon scattering and also in the case of the reactions

$$\pi+\mathrm{N} \to \pi+\pi+\mathrm{N}$$
$$\gamma+\mathrm{N} \to \pi+\pi+\mathrm{N}$$

which will be treated in a subsequent paper.

2. Pion-Nucleon Scattering

2.1. THE GENERAL PROBLEM

In all our treatment, the usual static interaction Hamiltonian

$$H' = \sum_q (a_q V_q + a_q^+ V_q^+), \tag{2.1}$$

$$V_q = if_0 \sqrt{\frac{2\pi}{\omega_q}}\, u(q^2)\tau_q \boldsymbol{\sigma}\cdot\mathbf{q} \tag{2.1'}$$

will be used †. However, in the derivation it will become apparent that all the results obtained are valid for a much wider class of Hamiltonians.

The eigenstates of the total Hamiltonian will be denoted by ψ_n, where n indicates the number of incoming pions; so ψ_0 will denote one of the four

† The index q denotes both the momentum $\mathbf{q}$ and the isospin of the pion.

physical nucleon states †, $\psi_1(q)$ the scattering state produced by an incoming meson q on a nucleon r, and so on ††. Let us define

$$\phi(q) = a_q^+\psi_0 - \sum_{\alpha=0,2,3\ldots} \psi_\alpha \langle \psi_\alpha a_q^+ \psi_0 \rangle \tag{2.2}$$

where the Greek index α denotes all eigenstates of H, but the pion-nucleon scattering states ψ_1. It is easy to verify that

$$\langle \phi(q), \psi_\alpha \rangle = 0 \qquad (\alpha = 0, 2, 3 \ldots). \tag{2.3}$$

This shows that the $\phi(q)$ all lie in the sub-space of the ψ_1. On the other hand, the fact that the $a_q^+\psi_0$ represent the incoming part of the $\psi_1(q)$ shows that there is a one-to-one correspondence between the $\psi_1(q)$ and the $\phi(q)$. We are therefore authorized to expand the $\psi_1(q)$ in terms of the $\phi(q)$:

$$\psi_1(q) = \sum_{q'} \phi(q')\chi(q', q). \tag{2.4}$$

The determination of the function χ will be the problem of this section.

From the asymptotic form of χ one obtains the pion-nucleon scattering phase-shifts. On the other hand, the knowledge of χ will enable us to compute matrix elements involving the scattering states: this will lead us to the simple derivation of closed expressions for photoproduction of pions and radiative pion-nucleon scattering.

The function χ will be determined by requiring that

$$\langle \phi(q')(H-\omega)\psi_1(q) \rangle = \sum_{q'} \langle \phi(q')(H-\omega)\phi(q'') \rangle \chi(q'', q) = 0. \tag{2.5}$$

Using eqs. (2.2) and (2.3) one gets

$$\langle \phi(q')(H-\omega)\phi(q'') \rangle = \langle \psi_0 a_{q'}(H-\omega)a_{q''}^+\psi_0 \rangle - \sum_{\alpha=0,2,3\ldots} \langle \psi_0 a_{q'}\psi_\alpha \rangle \langle \psi_\alpha a_{q''}^+ \psi_0 \rangle (E_\alpha - \omega). \tag{2.6}$$

The first term in the right-hand side of eq. (2.6) can be put in a more convenient form using the identity

$$[a_{q'}, [H, a_{q''}^+]] = \omega_{q'}\delta_{q'q''}$$

which leads to

$$\langle \psi_0, a_{q'}(H-\omega)a_{q''}^+\psi_0 \rangle = \delta_{q'q''}(\omega'-\omega) - \langle \psi_0 a_{q''}^+(H+\omega)a_{q'}\psi_0 \rangle. \tag{2.7}$$

The simple transformation (2.7) is the essential point in our whole derivation. The matrix element on the right-hand side of eq. (2.7) has the advantage of having the meson field operators "well ordered" in such a way that only destruction operators operate on the physical nucleon. In this way, if we insert between a_q^+ and a_q the complete set of eigenstates of H, the role of

† Our total Hamiltonian is normalized in such a way that $H\psi_0 = 0$.

†† The nucleon indexes are suppressed; all our matrix elements have to be understood as operators in the spin and isospin spaces of the nucleon.

the states other than those of the physical nucleon is comparatively unimportant, because a_q on the physical nucleon cannot excite states which have mesons at large distance from the nucleon. The same would not be true if we inserted directly the complete set of states in the left-hand side of (2.7).

The integral equation for χ can be written as

$$(\omega-\omega')\chi(q', q) = -\sum_{q''} K(q', q'')\chi(q'', q) \tag{2.8}$$

where

$$\begin{aligned} K(q', q'') &= \sum_{n=0,1,2\ldots} \langle\psi_0 a^+_{q''}\psi_n\rangle\langle\psi_n a_{q'}\psi_0\rangle(E_n+\omega) \\ &\quad + \sum_{\alpha=0,2,3\ldots} \langle\psi_0 a_{q'}\psi_\alpha\rangle\langle\psi_\alpha a^+_{q''}\psi_0\rangle(E_\alpha-\omega) \\ &= \sum_{n=0,1,2\ldots} \langle\psi_0 V_{q''}\psi_n\rangle\langle\psi_n V^+_{q'}\psi_0\rangle \frac{(E_n+\omega)}{(E_n+\omega')(E_n+\omega'')} \\ &\quad + \sum_{\alpha=0,2,3\ldots} \langle\psi_0 V^+_{q'}\psi_\alpha\rangle\langle\psi_\alpha V_{q''}\psi_0\rangle \frac{(E_\alpha-\omega)}{(E_\alpha-\omega')(E_\alpha-\omega'')}. \end{aligned} \tag{2.9}$$

It is convenient to rewrite our kernel in an angular momentum representation:

$$K(q', q'') = \sum_{l,m} \langle q'|l, m\rangle K^l_{mm'}(\omega', \omega'')\langle l, m'|q''\rangle \tag{2.10}$$

where

$$\langle l, m|\mathbf{q}\rangle = \sqrt{\frac{8\pi^2}{q\omega_q}}\, Y_m{}^l(\mathbf{q}); \qquad \text{for}^\dagger\ l = 1, \langle m|\mathbf{q}\rangle = \sqrt{\frac{6\pi^2}{q^3\omega}}\, q_m; \tag{2.11a}$$

$$\sum_{\mathbf{q}} \langle lm|\mathbf{q}\rangle\langle\mathbf{q}|l'm'\rangle\delta(\omega-\omega') = \delta_{ll'}, \delta_{mm'}; \tag{2.11b}$$

$$\delta(\omega-\omega')\sum_{lm} \langle\mathbf{q}|lm\rangle\langle lm|\mathbf{q}'\rangle = \delta_{\mathbf{q},\mathbf{q}'}. \tag{2.11c}$$

Only the p-wave part of K will be different from zero and will be given by

$$\begin{aligned} K_{mm'}(\omega', \omega'') &= C(q')C(q'')\{\sum_{n=0,1,2\ldots} \langle\psi_0 V_{m'}\psi_n\rangle\langle\psi_n V_m\psi_0\rangle \\ &\quad \times \frac{E_n+\omega}{(E_n+\omega')(E_n+\omega'')} \\ &\quad + \sum_{\alpha=0,2,3\ldots} \langle\psi_0 V_m\psi_\alpha\rangle\langle\psi_\alpha V_{m'}\psi_0\rangle \frac{E_\alpha-\omega}{(E_\alpha-\omega'-i\varepsilon)(E_\alpha-\omega''-i\varepsilon)}, \end{aligned} \tag{2.12}$$

$$C(q) = \sqrt{q^3}u(q^2). \qquad V_m = \frac{f_0}{\sqrt{3}\pi}(\sigma\tau)_m. \tag{2.13}$$

Until now our derivation has been rigorous. The contributions to the kernel (2.12) can be divided into three groups:

† The index $l = 1$ is usually suppressed.

a) the contributions coming from the physical nucleon state can be simply evaluated in terms of the renormalized coupling constant f;

b) the contributions coming from the pion-nucleon scattering states, using the well-known results of Low and Wick, can be related to the pion-nucleon scattering amplitudes;

c) the contribution coming from higher states can be related to the matrix elements for inelastic pion-nucleon collisions.

We shall introduce the "one-meson approximation" which consists of neglecting the contribution c). Those terms are indeed of the same order of magnitude as the terms neglected in the one-meson approximation to the Low equation [8]).

In the one-meson approximation the kernel is given by

$$K_{mm'} = \frac{C(q)C(q')}{\omega}\left\{\frac{\omega f^2}{3\omega'\omega''}[(\sigma\tau)_m(\sigma\tau)_{m'} - (\sigma\tau)_{m'}(\sigma\tau)_m] + \sum_i \int d\bar{\omega}\, \frac{\omega+\bar{\omega}}{(\omega'+\bar{\omega})(\omega''+\bar{\omega})}\, \frac{\sin^2\delta_i(\bar{\omega})}{C^2(\bar{\omega})} \langle m'|P_i|m\rangle\right. \tag{2.14}$$

where P_i are the well-known projection operators on the different J and T states.

The kernel (2.14) can be written as

$$K_{mm'} = \sum_i K_i(\omega'\omega'')\langle m|P_i|m'\rangle \tag{2.15}$$

where

$$K_i(\omega'\omega'') = \frac{C(q')C(q'')}{\pi}\left\{\frac{\lambda_i\omega}{\omega'\omega''} + \sum_j A_{ij}\int \frac{(\omega+\bar{\omega})}{(\omega'+\bar{\omega})(\omega''+\bar{\omega})}\, \frac{\sin^2\delta_j(\bar{\omega})}{\bar{q}^3 u^2(\bar{q})}\, d\bar{\omega}\right\}, \tag{2.15'}$$

$$\lambda_i = \tfrac{2}{3}f^2 \begin{pmatrix} -4 \\ -1 \\ 2 \end{pmatrix} \begin{matrix} (1) \\ (2) \\ (3) \end{matrix}$$

and A_{ij} is the crossing matrix defined by †

$$\langle m'|P_i|m\rangle = \sum_j A_{ij}\langle m|P_j|m'\rangle, \tag{2.16}$$

$$A_{ij} = \tfrac{1}{9}\begin{pmatrix} 1 & -4 & 16 \\ -2 & -1 & 4 \\ 4 & 2 & 1 \end{pmatrix}. \tag{2.17}$$

Eq. (2.15) clearly shows the nature of our problem. In order to obtain the "wave function" χ and therefore the scattering matrix, we have to compute the kernel (2.15) which is a function of the scattering phase-shifts.

† The notation $1 = 11$, $2 = 13 = 31$, $3 = 33$ for the phase-shifts is used.

Therefore, we have first to make a guess about the form of the scattering phase-shifts, then solve the integral equation (2.8) and finally verify that the scattering matrix thus obtained coincides with our initial guess.

In order to do this we shall first discuss the simple solution, already found by Stroffolini, which is obtained by completely neglecting the term containing the scattering phase-shifts in the kernel (2.15). Such a solution will coincide with the solution of the Low equation in the one-meson approximation and neglecting the cross-term. This is not surprising since the second term on the right-hand side of (2.15) is closely analogous to the cross-term in the Low equation. We shall refer to this as the "no-crossing approximation".

We shall then take the no-crossing approximation as a guidance in order to postulate a form for the scattering phase-shifts. In this way we shall be able to find a solution to our self-consistent problem. Such a solution will have many of the features of the no-crossing approximation from which it will differ only slightly for the dominant (33) phase-shift. The problem of the uniqueness of such a solution will finally be discussed.

2.2. THE NO-CROSSING APPROXIMATION

The solution of eq. (2.8) in the no-crossing approximation is indeed a trivial problem. We first divide eq. (2.8) by $(\omega-\omega')$ by imposing the outgoing boundary condition on χ

$$\chi(q'q) = \delta_{qq'} - \frac{1}{\omega-\omega'-i\varepsilon}\sum_{q''} K(q', q'')\chi(q'', q). \tag{2.18}$$

Let us transform χ in the angular momentum representation:

$$\chi(q', q) = \sum_{m, m', i} \langle q'|m'\rangle\langle m'|P_i|m\rangle\langle m|q\rangle\chi_i(\omega', \omega) \tag{2.19}$$
$$+ \text{ s-waves} + \text{d-waves} + \ldots .$$

Of course, only the p-wave part of χ is affected by the potential K. The integral equation for χ_i becomes

$$\chi_i(\omega, \omega') = \delta(\omega-\omega') - \frac{C(q')}{\omega'}\,\frac{\omega}{C(q)}\,\frac{h_i(\omega)}{\pi(\omega-\omega'-i\varepsilon)}, \tag{2.20}$$

$$h_i(\omega) = C(\omega)\lambda_i \int \frac{C(\omega'')}{\omega''}\chi_i(\omega'')\mathrm{d}\omega''. \tag{2.21}$$

From the asymptotic form of eq. (2.20) one immediately recognizes that

$$h_i(\omega) = \mathrm{e}^{i\delta_i}\sin\delta_i$$

where δ_i is the scattering phase-shift corresponding to the energy ω.

Let us now substitute eq. (2.20) in (2.21). We get for $h_i(\omega)$

$$h_i(\omega) = \frac{\lambda_i \dfrac{q^3}{\omega} u^2(q)}{1+\lambda_i \dfrac{\omega}{\pi}\displaystyle\int_\mu^\infty \frac{u(q')q'^3 \mathrm{d}\omega'}{(\omega-\omega'-i\varepsilon)\omega'^2}}, \tag{2.22}$$

$$\operatorname{tg}\delta_i(\omega) = \frac{\lambda_i \dfrac{q^3}{\omega} u^2(q)}{1-\dfrac{\lambda_i \omega}{\pi}\,\mathrm{P}\displaystyle\int_\mu^\infty \frac{q'^3 u^2(q')\mathrm{d}\omega'}{\omega'^2(\omega'-\omega)}}. \tag{2.22'}$$

Eq. (2.22') can be put in a very convenient form by considering that the integral in the denominator is dominated by the high values of q and therefore is a slowly varying function of ω (effective range approximation). So we simply have

$$\operatorname{tg}\delta_i(\omega) = \frac{C^2(q)}{\omega}\frac{\lambda_i}{1-\lambda_i I\omega} \tag{2.23}$$

where

$$I \approx \frac{1}{\pi}\int_\mu^\infty \frac{q'^3}{\omega'^2} u^2(q')\mathrm{d}\omega', \tag{2.24}$$

which shows clearly that only the (3.3) phase-shift is passing through a resonance, while the other phase-shifts are small and negative.

It is interesting to remark that not only the scattering amplitude given in (2.22), but also the "wave function" χ(2.20), are closely related to dispersion theory. In appendix 1 it will be shown that χ satisfies a dispersion relation similar to the one appearing in the theory of photoproduction.

For the sake of future reference, we give a compact form for χ. Using eqs. (2.18), (2.19) and (2.20) we have

$$\chi(q', q) = \delta_{qq'} - \frac{1}{\pi(\omega-\omega'-i\varepsilon)}\frac{C(\omega')}{\omega'}\frac{\omega}{C(\omega)}\sum_{i,m}\langle q'|m\rangle\langle m|P_i h_i(\omega)|q\rangle. \tag{2.25}$$

Finally, from eq. (2.21) one gets

$$\sum_{q'}\langle m|q'\rangle\frac{C(q')}{\omega'}\chi(q', q) = \sum_i \frac{h_i(\omega)}{\lambda_i C(\omega)}\langle m|P_i|q\rangle, \tag{2.25'}$$

$$\begin{aligned}
\langle m|P_{11}|q\rangle &= \tfrac{1}{9}\sqrt{\frac{6\pi^2}{q^3\omega}}\,\sigma_m(\boldsymbol{\sigma}\cdot\mathbf{q})\tau_m\tau_q \\
\langle m|P_{31}|q\rangle &= \tfrac{1}{9}\sqrt{\frac{6\pi^2}{q^3\omega}}\,(3\delta_{mq}-\tau_m\tau_q)\sigma_m(\boldsymbol{\sigma}\cdot\mathbf{q}) \\
\langle m|P_{13}|q\rangle &= \tfrac{1}{9}\sqrt{\frac{6\pi^2}{q^3\omega}}\,(3\delta_{mq}-\sigma_m(\boldsymbol{\sigma}\cdot\mathbf{q}))\tau_m\tau_q \\
\langle m|P_{33}|q\rangle &= \tfrac{1}{9}\sqrt{\frac{6\pi^2}{q^3\omega}}\,(3\delta_{mq}-\sigma_m(\boldsymbol{\sigma}\cdot\mathbf{q}))(3\delta_{mq}-\tau_m\tau_q).
\end{aligned} \tag{2.25''}$$

2.3. THE CROSSING CORRECTIONS

Let us go back to our original kernel (2.15). In order to give an estimate to the term depending on $\sin^2 \delta_i$ we shall take as a guidance the solution of the last section. We shall assume that

a) only $\sin^2 \delta_3$ is appreciable;

b) $\sin^2 \delta_3$ is appreciable only in a small energy range around the resonance energy ω_r.

Around resonance $\operatorname{tg} \delta_3$ can be approximated by

$$\operatorname{tg} \delta_3 = C^2(k) \frac{\gamma}{\omega - \omega_r}. \tag{2.26}$$

For sufficiently small γ we have

$$\frac{1}{\pi} \int \frac{\sin^2 \delta_3}{C^2(\bar{q})} \frac{(\omega+\bar{\omega})\mathrm{d}\bar{\omega}}{(\omega'+\bar{\omega})(\omega''+\bar{\omega})} = |\gamma| \frac{\omega+\omega_r}{(\omega'+\omega_r)(\omega''+\omega_r)}. \tag{2.27}$$

For the moment, ω_r and γ are two unknown parameters subject to the limitation that ω_r is sufficiently below the cut-off and that the resonance is sufficiently narrow that eq. (2.27) is approximatively valid. We now insert eq. (2.27) in (2.15) in order to solve the resulting integral equation and get an expression for the scattering phase-shifts in terms of ω_r and γ.

The identification of such an expression with eq. (2.26) will enable us to obtain an unambiguous determination of γ and ω_r.

The kernel K can be written as

$$K_i = \frac{C(q')C(q'')}{\pi} \left[\frac{\lambda_i}{\omega'\omega''} + \frac{\mu_i(\omega+\omega_r)}{(\omega'+\omega_r)(\omega''+\omega_r)} \right] \tag{2.28}$$

where

$$\mu_i = \tfrac{1}{9} |\gamma| \begin{pmatrix} 16 \\ 4 \\ 1 \end{pmatrix}. \tag{2.28'}$$

The integral equations for the χ_i are

$$(\omega-\omega')\chi_i(\omega', \omega) = -\frac{C(\omega')}{\pi} \left[\frac{F_i(\omega)}{\omega'} + \frac{G_i(\omega)}{\omega'+\omega_r} \right] \tag{2.29}$$

where

$$\begin{aligned} F_i(\omega) &= \lambda_i \omega \int \frac{C(\omega'')}{\omega''} \chi_i(\omega, \omega'')\mathrm{d}\omega'' \\ G_i(\omega) &= \mu_i(\omega+\omega_r) \int \frac{C(\omega'')}{\omega''+\omega_r} \chi_i(\omega, \omega'')\mathrm{d}\omega''. \end{aligned} \tag{2.30}$$

It is convenient to obtain directly an expression for $\operatorname{tg} \delta_i$. Therefore we shall impose on χ stationary boundary conditions

$$\chi_i(\omega') = \delta(\omega-\omega') - \frac{C(\omega')}{\omega-\omega'} \frac{\mathrm{P}}{\pi} \int \left[\frac{F_i(\omega')}{\omega'} + \frac{G_i(\omega')}{\omega'+\omega_\tau} \right] \mathrm{d}\omega'. \tag{2.31}$$

From the asymptotic form of eq. (2.9) one immediately sees that

$$\mathrm{tg}\, \delta_i(\omega) = \frac{C(\omega)}{\omega} F_i(\omega) + \frac{C(\omega)}{\omega+\omega_\tau} G_i(\omega). \tag{2.32}$$

Let us determine F and G by substituting (2.31) into (2.30):

$$\begin{aligned} F_i(\omega) &= \lambda_i C(\omega) - \lambda_i \omega [I_{FF} F_i(\omega) + I_{FG} G_i(\omega)] \\ G_i(\omega) &= \mu_i C(\omega) - \mu_i (\omega+\omega_\tau) [I_{GF} F_i(\omega) + I_{GG} G_i(\omega)], \end{aligned} \tag{2.33}$$

$$\begin{aligned} I_{FF} &= \frac{\mathrm{P}}{\pi} \int \frac{C^2(q')}{\omega'^2(\omega'-\omega)} \mathrm{d}\omega' \\ I_{FG} = I_{GF} &= \frac{\mathrm{P}}{\pi} \int \frac{C^2(q')}{\omega'(\omega'+\omega_\tau)(\omega'-\omega)} \mathrm{d}\omega' \\ I_{GG} &= \frac{\mathrm{P}}{\pi} \int \frac{C^2(q')}{(\omega'+\omega_\tau)^2(\omega'-\omega)} \mathrm{d}\omega'. \end{aligned} \tag{2.33'}$$

The main contribution to the integrals (2.33') comes from values of K near the cut-off. So we shall neglect ω and ω_τ as compared to ω' (effective range approximation):

$$I_{FF} = I_{GF} = I_{FG} = I_{GG} = I = \frac{1}{\pi} \int \frac{C^2(q')}{\omega'^3} \mathrm{d}\omega',$$

$$F_i(\omega) = \lambda_i C(\omega) \left[1 - \frac{\omega(\lambda_i+\mu_i) I}{1-[\lambda_i \omega + \mu_i(\omega+\omega_\tau)]} \right]$$

$$G_i(\omega) = \mu_i C(\omega) \left[1 - \frac{(\omega+\omega_\tau)(\mu_i+\lambda_i) I}{1-[\lambda_i \omega + \mu_i(\omega+\omega_\tau)]} \right]$$

and finally

$$\mathrm{tg}\, \delta_i = C^2(\omega) \left\{ \frac{\lambda_i}{\omega} + \frac{\mu_i}{\omega+\omega_\tau} + \frac{(\lambda_i+\mu_i)}{\omega - \dfrac{1-I\omega_\tau\mu_i}{I(\lambda_i+\mu_i)}} \right\}. \tag{2.34}$$

Eq. (2.34) gives the scattering phase-shifts in terms of the two parameters I and ω_τ. We have now to verify that our result reproduces our starting assumptions.

Let us first consider the (3.3) phase-shift. Eq. (2.34) shows that there can indeed be a resonance for

$$\omega_\tau = \frac{1-I\mu_3\omega_\tau}{I(\lambda_3+\mu_3)}.$$

Around such resonance the last term in the bracket gives the most important contribution. Comparing such a term with eq. (2.26) and using the definitions

(2.16) and (2.28') of λ_i and μ_i we obtain

$$\begin{aligned} &\tfrac{4}{3}f^2+\tfrac{1}{9}|\gamma| = \gamma, \\ &\frac{1-\tfrac{1}{9}|\gamma|\omega_r I}{I(\tfrac{4}{3}f^2+\tfrac{1}{9}|\gamma|)} = \omega_r. \end{aligned} \tag{2.35}$$

The two parameters γ and ω_r are therefore

$$\gamma = \tfrac{3}{2}f^2, \qquad \omega_r = \tfrac{3}{5}\frac{1}{f^2 I}. \tag{2.36}$$

Let us now consider the other phase-shifts. One has

$$\lambda_1+\mu_1 = 4(\lambda_2+\mu_2) = -\tfrac{8}{3}f^2+\tfrac{16}{9}|\gamma| = 0. \tag{2.37}$$

This means (see eq. (2.34)) that those phase-shifts do not pass through any resonance and are always small.

The solution (2.34) (with the values of γ and ω_r given by (2.36)) does, indeed, reproduce the starting assumptions a) and b) and therefore is a solution of our self-consistent problem.

It is interesting to compare our result with the one obtained by Chew and Low in the framework of the effective range approximation.

Let us define

$$\operatorname{Re} g_a = \frac{\lambda_a}{\omega} q^3 u^2(q) \operatorname{cotg} \delta_a. \tag{2.38}$$

TABLE 1

	Improved solution	No-crossing approximation	CL
$\frac{1}{\operatorname{Re} g_1}$	$\frac{1}{1+\frac{\omega}{\omega_r}}$	$\frac{1}{1+\frac{2\omega}{\omega_r}}$	$\frac{1}{1+\frac{\omega}{\omega_r}}$
$\frac{1}{\operatorname{Re} g_2}$	$\frac{1}{1+\frac{\omega}{\omega_r}}$	$\frac{1}{1+\frac{\omega}{2\omega_r}}$	1
$\frac{1}{\operatorname{Re} g_3}$	$\frac{-\frac{1}{8}}{1+\frac{\omega}{\omega_r}}+\frac{\frac{9}{8}}{1-\frac{\omega}{\omega_r}}$	$\frac{1}{1-\frac{\omega}{\omega_r}}$	$\frac{1}{1-\frac{\omega}{\omega_r}}$
	$\omega_r = \frac{3}{5f^2 I}$	$\omega_r = \frac{3}{4f^2 I}$	$\omega_r = \frac{1}{4f^2 I}$

From table 1 one can see that our result is formally very similar to the CL one, but differs strongly from it in the determination of the resonance energy as a function of the cut-off. This discrepancy is not a serious one since

the position of the (33)-resonance is very dependent on details of the theory, such as the small-size phase-shifts †.

In all our treatment, the cut-off enters only through the integral I which can be empirically fitted to the experimental value of the (33)-resonance energy.

The quoted CL result for g_2, which is the most different from ours, is also the less justified in the framework of the CL theory.

In CL it is shown that the exact g_α have to satisfy to the following crossing relation:

$$\frac{1}{g_\alpha(\omega)} = \sum_\beta B_{\alpha\beta} \frac{1}{g_\beta(-\omega)} \tag{2.39}$$

where

$$B_{\alpha\beta} = -\frac{1}{\lambda_\alpha} A_{\alpha\beta}\lambda_\beta .$$

The effective range approximation consists essentially in neglecting $\operatorname{Im} g_\alpha = -\lambda\alpha q^3/\omega$ compared to $\operatorname{Re} g_\alpha$ (for small $q/q_{\max}$). Therefore, in this approximation the crossing relation (2.39) can be written as

$$\frac{1}{\operatorname{Re} g_\alpha(\omega)} = \sum_\beta B_{\alpha\beta} \frac{1}{\operatorname{Re} g_\beta(-\omega)} . \tag{2.40}$$

It is interesting to verify that our solution satisfies exactly eq. (2.40).

The scattering phase-shifts obtained above are a solution of our self-consistent problem. However, we have not excluded the possibility that other solutions exist. In appendix 2 it will be shown that this is indeed the case.

The multiplicity of the solutions of our scattering problem is due to the fact that no assumptions have been made on the physical nucleon and that our results are valid for many kinds of static Hamiltonian. A way of removing such an ambiguity is to try to calculate the physical nucleon state using a well-defined Hamiltonian. This has been done (with the static Hamiltonian (1)) by Friedman, Lee and Christian using the intermediate coupling approximation: the resulting scattering phase-shifts have only one (3)-resonance and therefore are in favour of the solution discussed in section 2.3.

3. Electromagnetic Phenomena

3.1. INTRODUCTION

In this section we shall study the phenomena of pion photoproduction and of radiative pion-nucleon scattering. The matrix elements for such processes are

$$H_k(q) = \langle \psi_0, j(\mathbf{k})\psi_1^{\text{out}}(\mathbf{q})\rangle, \tag{3.1}$$

† In ref. [4]) it is shown that the dispersion relations for pion-nucleon scattering can be approximately satisfied for any position of the (33)-resonance.

$$H_k(q, p) = \langle \psi_1^{\text{in}}(\mathbf{q}), \quad j(-\mathbf{k})\psi_1^{\text{out}}(\mathbf{p})\rangle, \tag{3.2}$$

where

$$j(\mathbf{k}) = -\int \mathbf{j}(x)\cdot\mathbf{A}(x)\mathrm{d}v = -\frac{1}{(2k)^{\frac{1}{2}}}\int \mathbf{j}(x)\cdot\boldsymbol{\varepsilon}\mathrm{e}^{-i\mathbf{k}\cdot\mathbf{r}}\mathrm{d}v; \tag{3.3}$$

$\mathbf{j}(x)$ is the total current of the system composed of the nucleon plus the meson field.

The matrix elements (3.1) and (3.2) will be computed by using the scattering state vector $\psi_1(q)$ discussed in the last section.

Before entering into such a detailed calculation, we want to list some well-known properties of the operator $j(\mathbf{k})$ which will be needed in the further developments. Let us first consider the expectation value in the physical nucleon state. Using invariance under rotations, space and time inversion, and charge conservation we can write

$$\langle \psi_0, j(\mathbf{k})\psi_0\rangle = -\frac{i}{\sqrt{2k}}G(k^2)\boldsymbol{\sigma}\cdot\mathbf{t}, \qquad \mathbf{t} = \mathbf{k}\times\boldsymbol{\varepsilon}. \tag{3.4}$$

The left-hand side of eq. (3.4) represents the interaction of a physical nucleon with a magnetic field of frequency k. So for small k^2 we have

$$G(k^2) = \tfrac{1}{2}(\mu_{\mathrm{P}}+\mu_{\mathrm{N}})+\tfrac{1}{2}(\mu_{\mathrm{P}}-\mu_{\mathrm{N}})\tau_3$$

where μ_{P} and μ_{N} are the static magnetic moments of the nucleons.

Let us now consider the commutator between $j(\mathbf{k})$ and a_q^+. The contributions to this commutator come from two sources: a) the meson current

$$-ie(\varphi_1\nabla\varphi_2-\varphi_2\nabla\varphi_1);$$

b) the interaction current due to the variation in time of the charge of the nucleon when mesons are emitted and absorbed. Such a term can be formally obtained by making the usual substitution $\nabla \to \nabla - ie\mathbf{A}$ in the static interaction Hamiltonian:

$$-\sqrt{4\pi}ef_0\boldsymbol{\sigma}\cdot\boldsymbol{\varepsilon}(\tau_1\varphi_2-\tau_2\varphi_1).$$

We therefore have†

$$[a_q, j(k)] = \tfrac{1}{2}ief_0\left(\frac{\pi}{k\omega}\right)^{\frac{1}{2}}[\tau_q, \tau_3]\boldsymbol{\sigma}\cdot\boldsymbol{\varepsilon} - ie\frac{\mathbf{q}\cdot\boldsymbol{\varepsilon}}{(k\omega)^{\frac{1}{2}}}\int \mathrm{e}^{-i(\mathbf{k}-\mathbf{q})\cdot\mathbf{r}}(\delta_{q1}\varphi_2-\delta_{q2}\varphi_1)\mathrm{d}v. \tag{3.5}$$

The expectation value of (3.5) in the physical nucleon state is simply obtained in terms of the renormalized coupling constant f:

$$\begin{aligned} H_k^0(q) &= \langle \psi_0, [j(k), a_q^+]\psi_0\rangle \\ &= \tfrac{1}{2}ief\left(\frac{4\pi}{k\omega}\right)^{\frac{1}{2}}[\tau_q, \tau_3]\left\{\boldsymbol{\sigma}\cdot\boldsymbol{\varepsilon} - \frac{2\boldsymbol{\sigma}\cdot(\mathbf{q}-\mathbf{k})\mathbf{q}\cdot\boldsymbol{\varepsilon}}{(\mathbf{q}-\mathbf{k})^2+1}\right\}. \end{aligned} \tag{3.6a}$$

The p-wave part of the commutator (3.6a) is

† We denote by e the rationalized charge ($e^2/4\pi = 1/137$).

$$H_k^0(q) = \tfrac{1}{2}ief\sqrt{\frac{q^3}{6\pi k}}\,[\tau_q, \tau_3]\{F_M(k,q)(\boldsymbol{\sigma}\times\mathbf{t})_m + F_Q(k,q)[(\boldsymbol{\sigma}\cdot\mathbf{k})\varepsilon_m + (\boldsymbol{\sigma}\cdot\boldsymbol{\varepsilon})k_m]\}\langle m|q\rangle, \tag{3.6b}$$

with

$$F_M(k,q) = \frac{3}{8qk}\left[\frac{2}{u} - \frac{1-u^2}{u^2}\log\left(\frac{1+u}{1-u}\right)\right], \qquad u = \frac{2kq}{\omega_q^2+k^2},$$
$$F_Q(k,q) = \frac{1}{k^2} - \frac{\omega_q^2}{k^2}F_M(k,q). \tag{3.6c}$$

Finally, using eq. (3.5) we get

$$\langle\psi_0[[a_q, j(k)], a_p^+]\psi_0\rangle = ie\,\frac{\mathbf{q}\cdot\boldsymbol{\varepsilon}}{(2k\omega_q\omega_p)^{\frac{1}{2}}}\,\delta_{\mathbf{p},\mathbf{q}-\mathbf{k}}(\delta_{q1}\delta_{p2} - \delta_{q2}\delta_{p1}). \tag{3.7}$$

From the development of the next sections we shall see that the expectation values (3.4), (3.6) and (3.7) are the only information needed about the current in order to give a complete evaluation of photoproduction and radiative scattering.

3.2. PHOTOPRODUCTION

Let us introduce in eq. (3.1) the form (2.4) for the scattering state vector:

$$H_k(q) = \sum_{q'}\langle\psi_0 j(k)\phi(q')\rangle\chi(q', q). \tag{3.8}$$

Since χ is well known, our problem is to evaluate the matrix element $\langle\psi_0, j(k)\phi(q')\rangle$.

By introducing eq. (2.2) one has

$$\langle\psi_0 j(k)\phi(q')\rangle = \langle\psi_0 j(k)a_{q'}^+\psi_0\rangle - \sum_{\alpha=0,2,3\ldots}\langle\psi_0 j(k)\psi_\alpha\rangle\langle\psi_\alpha a_{q'}^+\psi_0\rangle. \tag{3.9}$$

In complete analogy to, and with the same philosophy as in the evaluation of the kernel of the scattering equation, we shift the operator a_q^+ onto the left of the current, and then we introduce between them the complete set of states ψ_n

$$\langle\psi_0 j(k)\phi(q')\rangle = \langle\psi_0, [j(k), a_{q'}^+]\psi_0\rangle + \sum_{n=0,1,2\ldots}\langle\psi_0 a_{q'}^+\psi_n\rangle\langle\psi_n j(k)\psi_0\rangle - \sum_{\alpha=0,2,3\ldots}\langle\psi_0 j(k)\psi_\alpha\rangle\langle\psi_\alpha a_{q'}^+\psi_0\rangle. \tag{3.10}$$

The expression (3.10) is rigorous. In order to obtain a simple evaluation we apply the one-meson no-crossing approximation which consists in keeping only the contribution coming from the physical nucleon state.

The corrections due to the one-meson states are given as a product of a photoproduction and a scattering matrix element, and could be computed by reinserting the no-crossing approximation in those terms. Since those terms have only $\omega+\omega'$ denominators and involve the crossing matrix, such correction, as in scattering, would turn out to be quite small.

We thus obtain

$$\langle\psi_0 j(k)\phi(q')\rangle = \langle\psi_0[j(k), a^+_{q'}]\psi_0\rangle + \langle\psi_0 a^+_{q'}\psi_0\rangle\langle\psi_0 j(k)\psi_0\rangle - \langle\psi_0 j(k)\psi_0\rangle\langle\psi_0 a^+_{q'}\psi_0\rangle. \quad (3.11)$$

The matrix element (3.11) is therefore reduced to the well-known results of eqs. (3.4) and (3.6) and to

$$\langle\psi_0 a^+_{q'}\psi_0\rangle = \frac{if}{\sqrt{3\pi}}\frac{C(q')}{\omega'}(\sigma\tau)_m\langle m|q'\rangle.$$

We now insert in eq. (3.8) the form of χ obtained with the no-crossing approximation in section 2.2. The results of the summations on q' can be classified by using a convenient notation introduced by Chew and Low. We call H^π the contribution coming from the commutator, and H^N the remaining part.

$$H_k(q) = H_k{}^\pi(q) + H_k{}^N(q), \quad (3.12)$$

$$H_k{}^N(q) = \frac{f}{\sqrt{6\pi k}}\sum_{q',m}\frac{C(q')}{\omega'}[(\sigma\tau)_m G(k^2)\boldsymbol{\sigma}\cdot\mathbf{t} - G(k^2)\boldsymbol{\sigma}\cdot\mathbf{t}(\sigma\tau)_m]\langle m|q'\rangle\chi(q', q), \quad (3.13)$$

and using eq. (2.25′),

$$H_k{}^N(q) = \frac{f}{C(q)\sqrt{6\pi k}}\sum_{i,m}[(\sigma\tau)_m G(k^2)\boldsymbol{\sigma}\cdot\mathbf{t} - G(k^2)\boldsymbol{\sigma}\cdot\mathbf{t}(\sigma\tau)_m]\langle m|\frac{P_i h_i(\omega)}{\lambda_i}|q\rangle; \quad (3.14)$$

$$H_k{}^\pi(q) = \sum_{q'} H_k{}^0(q')\chi(q', q), \quad (3.15)$$

or using (2.25)

$$H_k{}^\pi(q) = H_k{}^0(q) - \sum_{q',i}\frac{C(\omega')\omega}{\omega' C(\omega)}\frac{H_k{}^0(q')}{\pi(\omega-\omega'-i\varepsilon)}\langle q'|m\rangle\langle m|P_i h_i(\omega)|q\rangle. \quad (3.16)$$

In the second term in the right-hand side of eq. (3.16) the summation on q' selects only the p-wave part of $H^0(k, q)$ given in eq. (3.6c) The result is

$$H_k{}^\pi(q) = H_k{}^0(q) + \sum_i h_i(\omega)U_m(k, q)\langle m|P_i|q\rangle \quad (3.17)$$

where

$$U_m(k, q) = -\frac{ief}{\sqrt{6\pi k}}\frac{\omega}{C(\omega)}[\tau_m, \tau_3] \cdot \tfrac{1}{2}\{I_M(k, q)(\boldsymbol{\sigma}\times\mathbf{t})_m + I_Q(k, q)[(\boldsymbol{\sigma}\cdot\mathbf{k})\varepsilon_m + (\boldsymbol{\sigma}\cdot\boldsymbol{\varepsilon})k_m]\}, \quad (3.18)$$

$$I_{M,Q}(k, q) = \frac{1}{\pi}\int\frac{q'^3 u^2(q')}{\omega'(\omega-\omega'-i\varepsilon)}F_{M,Q}(k, q')\mathrm{d}q'.$$

Our result for photoproduction expressed in eqs. (3.12), (3.17) and (3.18) coincides completely with the result obtained by Chew and Low, neglecting the cross terms in their integral equations.

It is interesting to compare the two ways in which the same result has been obtained. In the CL approach, different dispersion relations have to be solved for different processes. In the present method we are confronted with the solution of an integral equation only in the scattering problem; in the case of photoproduction we had just to evaluate some matrix elements.

3.3. RADIATIVE SCATTERING

We introduce eq. (2.4) in eq. (3.2):

$$H_k(q, p) = \sum_{q' p'} \chi^{+\mathrm{in}}(q, q') B_k(q', p') \chi^{\mathrm{out}}(p', p). \tag{3.19}$$

As in the case of photoproduction, we are reduced to the calculation of the matrix element

$$\begin{aligned} B_k(q', p') &= \langle \phi(q'), j(k) \phi(p') \rangle = \langle \psi_0 a_{q'} j(k) a_{p'}^+ \psi_0 \rangle \\ &- \sum_{\alpha=0,2,3\ldots} \langle \psi_0 a_{q'} j(k) \psi_\alpha \rangle \langle \psi_\alpha a_{p'}^+ \psi_0 \rangle \\ &- \sum_{\alpha=0,2,3\ldots} \langle \psi_0 a_{q'} \psi_\alpha \rangle \langle \psi_\alpha j(k) a_{p'}^+ \psi_0 \rangle + \sum_{\alpha,\beta=0,2,3\ldots} \langle \psi_0 a_{q'} \psi_\alpha \rangle \langle \psi_\alpha j(k) \psi_\beta \rangle \langle \psi_\beta a_{p'}^+ \psi_0 \rangle. \end{aligned} \tag{3.20}$$

We neglect the effect of states with more than one meson.

As usual, we have to order our operators in such a way that a_q acts directly on the left of ψ_0 and a_q^+ on the right, and then use the complete set ψ_n.

For the second and third term of eq. (3.20) we are in the same situation of photoproduction. For the first term we use the identity

$$a_{q'} j(k) a_{p'}^+ = [[a_{q'}, j(k)], a_{p'}^+] + j(k)\delta_{q'p'} + [j(k), a_{p'}^+] a_{q'} - a_{p'}^+ [j(k), a_{q'}] + a_{p'}^+ j(k) a_{q'}$$

where the simple and double commutators are given in eqs. (3.5) and (3.7).

We introduce between all operators the complete set ψ_n and, in the spirit of the no-crossing approximation (which has been very successful in scattering and photoproduction) we keep only the nucleon contribution.

The neglected terms coming from one-meson states could be computed in terms of scattering, photoproduction and radiative scattering. Here also, because of our "good ordering", all those terms involve only $\omega+\omega'$ denominators, so we can expect those corrections to be small.

The final result is

$$B_k(q', p') = B_k^{\pi}(q', p') + B_k^{\mathrm{N}}(q', p'), \tag{3.21}$$

$$\begin{aligned} B_k^{\pi}(q', p') &= \langle \psi_0 [[a_{q'}, j(k)], a_{p'}^+] \psi_0 \rangle \\ &- \langle \psi_0 a_{q'} \psi_0 \rangle \langle \psi_0 [j(k), a_{p'}^+] \psi_0 \rangle + \langle \psi_0 [j(k), a_{p'}^+] \psi_0 \rangle \langle \psi_0 a_{q'} \psi_0 \rangle \\ &- \langle \psi_0 [a_{q'}, j(k)] \psi_0 \rangle \langle \psi_0 a_{p'}^+ \psi_0 \rangle + \langle \psi_0 a_{p'}^+ \psi_0 \rangle \langle \psi_0 [a_{q'} j(k)] \psi_0, \end{aligned} \tag{3.22}$$

$$\begin{aligned} B_k^{\mathrm{N}}(q', p') &= \langle \psi_0 j(k) \psi_0 \rangle \delta_{q'p'} \\ &+ \langle \psi_0 a_{q'} \psi_0 \rangle \langle \psi_0 j(k) \psi_0 \rangle \langle \psi_0 a_{p'}^+ \psi_0 \rangle - \langle \psi_0 a_{q'} \psi_0 \rangle \langle \psi_0 a_{p'}^+ \psi_0 \rangle \langle \psi_0 j(k) \psi_0 \rangle \\ &+ \langle \psi_0 a_{p'}^+ \psi_0 \rangle \langle \psi_0 j(k) \psi_0 \rangle \langle \psi_0 a_{q'} \psi_0 \rangle - \langle \psi_0 j(k) \psi_0 \rangle \langle \psi_0 a_{q'} \psi_0 \rangle \langle \psi_0 a_{p'}^+ \psi_0 \rangle. \end{aligned} \tag{3.23}$$

Eqs. (3.21), (3.22) and (3.23), together with (3.19), show that the problem of radiative pion-nucleon scattering is reduced to the computation of some integrals. Indeed, all the matrix elements appearing in those equations are known (see eqs. (3.4), (3.6), (3.7)) and the function χ has been given in section 2.2.

Our solution of radiative scattering has exactly the same degree of reliability as the solution of photoproduction which (see CL) has given an excellent fit of existing experiments.

Before going into the details of the explicit calculation of $H_k(q, p)$, we want to discuss the physical meaning of our terms.

The matrix element B has been separated in a "nucleon part" B^N which is proportional to the static magnetic moments of the nucleons, and a meson part B^π which contains the direct interaction of the photon with pion field and the effects of the interaction current.

The first term of $B^{N,\pi}$ corresponds to a "disconnected graph" in which the photon interact with the nucleon (pion) while the other particle travels freely. The contributions to real processes coming from the disconnected terms are due only to rescattering effects represented by the outgoing part of χ.

We shall therefore separate both H^N and H^π into a connected part $H_c^{N,\pi}$ and a disconnected part $H_d^{N,\pi}$.

$$H = H_c^N + H_d^N + H_c^\pi + H_d^\pi. \tag{3.24}$$

Let us first consider the nucleon part

$$\begin{aligned} H_c^N = &-\frac{if^2}{3\pi}\frac{1}{C(q)C(p)\sqrt{2k}}\sum_{ij}\frac{h^i(q)}{\lambda_i}\frac{h^j(p)}{\lambda_j} \\ &\cdot\sum_{mm'}\langle q|P_i|m\rangle\{(\tau\sigma)_{m'}G(k^2)\boldsymbol{\sigma}\cdot\mathbf{t}(\tau\sigma)_m \\ &+(\tau\sigma)_m G(k^2)\boldsymbol{\sigma}\cdot\mathbf{t}(\tau\sigma)_{m'} - G(k^2)\boldsymbol{\sigma}\cdot\mathbf{t}(\tau\sigma)_m(\tau\sigma)_{m'} \\ &-(\tau\sigma)_m(\tau\sigma)_{m'}G(k^2)\boldsymbol{\sigma}\cdot\mathbf{t}\}\langle m'|P_j|p\rangle, \end{aligned} \tag{3.25}$$

$$\begin{aligned} H_d^N = &-\frac{i}{\pi}\frac{1}{\sqrt{2k}}\Bigg\{\Bigg[\sum_{\substack{ij\\m}}\langle q|P_i g_i(q)|m\rangle \\ &\cdot G(k^2)\boldsymbol{\sigma}\cdot\mathbf{t}\langle m|P_j h_j(p)|p\rangle\frac{\omega_p C(q)}{\omega_q C(p)}\frac{1}{\omega_p-\omega_q} \\ &+\sum_{\substack{ij\\m}}\langle q|P_i h_i(q)|m\rangle G(k^2)\boldsymbol{\sigma}\cdot\mathbf{t}\langle m|P_j g_j(p)|p\rangle\frac{\omega_q C(p)}{\omega_p C(q)}\frac{1}{\omega_q-\omega_p}\Bigg] \\ &+\frac{\omega_q\omega_p}{C(p)C(q)}\frac{I(p)-I(q)}{\omega_q-\omega_p}\sum_{\substack{ij\\m}}\langle q|P_i h_i(q)|m\rangle G(k^2)\boldsymbol{\sigma}\cdot\mathbf{t}\langle m|P_j h_j|p\rangle\Bigg\} \end{aligned} \tag{3.26}$$

where we have defined $g_i(p) = \cos\delta_i e^{i\delta_i}$ and

$$I(p) = \frac{1}{\pi}\int \frac{q^3 u^2(q)\,d\omega}{(\omega_p - \omega)\omega^2}. \tag{3.27}$$

Recalling eq. (2.22') we have

$$I(p) = \frac{\frac{4}{3}f^2\frac{p^3}{\omega}\operatorname{cotg}\delta_3 - 1}{\frac{4}{3}f^2\omega}. \tag{3.28}$$

Eqs. (3.25), (3.26) and (3.28) show that the nucleon contribution can be computed in terms of the magnetic moment of the nucleon and of the scattering phase-shifts only.

As in the case of photoproduction, a reasonable approximation for H^N should be to keep only the vector part of $G(k^2)$ and to neglect the small scattering phase-shifts.

Let us now turn our attention to the meson contribution H^π. The connected part is given by

$$\begin{aligned} H_c^\pi = &-\frac{if}{\sqrt{3\pi}}\Big\{\sum_{i,m}\langle q|P_i|m\rangle\frac{h_i(q)}{\lambda_i C(q)}[(\sigma\tau)_m,\ H_k^0(p)] \\ &-\sum_{i,m}[H^0_{-k}(q),\ (\sigma\tau)_m]\frac{h_i(p)}{\lambda_i C(q)}\langle m|P_i|p\rangle\Big\} \\ &+\frac{if}{\sqrt{3\pi}}\sum_{\substack{ij\\m,m'}}h_i(q)h_j(p)\langle q|P_i|m\rangle\Big\{\frac{[(\sigma\tau)_m, U_{m'}(kp)]}{\lambda_i C(q)} \\ &+\frac{[U_m(k,q),\ (\sigma\tau)_{m'}]}{\lambda_j C(p)}\Big\}\langle m'|P_j|p\rangle. \end{aligned} \tag{3.29}$$

The rescattering corrections appearing in the second term of eq. (3.29) are given in terms of the operator U_m which has been defined in eq. (3.17) in connection with the rescattering corrections to photoproduction. Finally, the disconnected contribution is

$$\begin{aligned} H_d^\pi = &-ie\frac{\mathbf{q}\cdot\boldsymbol{\varepsilon}}{\sqrt{2k\omega_q\omega_{q-k}}}\frac{1}{\pi(\omega_p-\omega_{q-k})}\frac{C(q-k)}{\omega_{q-k}}\frac{\omega_p}{C(p)} \\ &\cdot\sum_i\langle q-k,\alpha|P_i h_i(p)|p\rangle\varepsilon_{q\alpha 3} \\ &+ie\frac{(\mathbf{p}+\mathbf{k})\cdot\boldsymbol{\varepsilon}}{\sqrt{2k\omega_p\omega_{p+k}}}\frac{1}{\pi(\omega_q-\omega_{k+p})}\frac{C(p+k)}{\omega_{p+k}}\frac{\omega_q}{C(q)} \\ &\cdot\sum_i\langle q|P_i h_i(q)|k+p,\alpha\rangle\varepsilon_{p\alpha 3} \\ &+\frac{ie}{\pi\sqrt{2k}}\frac{\omega_p\omega_q}{C(p)C(q)}\sum_{\substack{mn\\ij}}\langle q|P_i h_i(q)m\rangle\{R_M(q,p)(\varepsilon_n K_m-\varepsilon_m K_n) \\ &+R_Q(q,p)(\varepsilon_n K_m+\varepsilon_m K_n)\}\varepsilon_{mn3}\langle n|P_j h_j(p)|p\rangle \end{aligned} \tag{3.30}$$

where

$$R_{\mathrm{M}}(q,p)=-\frac{3}{16\pi^2}\int\left(q'^2-\frac{(\mathbf{q}',\mathbf{k})^2}{k^2}\right)\frac{1}{\omega_{q'}^2(\omega_q-\omega_{q'}-i\varepsilon)}\,\frac{\mathrm{d}^3q'}{\omega_{q'-k}^2(\omega_p-\omega_{q'-k}-i\varepsilon)}, \tag{3.31}$$

$$R_{\mathrm{Q}}(q,p)=\frac{3}{16\pi^2}\int\left(\frac{2\mathbf{q}'\cdot\mathbf{k}}{k^2}-1\right)\left(q'^2-\frac{(q'k)^2}{k^2}\right)\frac{\mathrm{d}^3q'}{\omega_{q'}^2(\omega_q-\omega_{q'}-i\varepsilon)}\,\frac{1}{\omega_{q'-k}^2(\omega_p-\omega_{q'-k}-i\varepsilon)}.$$

The two integrals R_{M} and R_{Q} are convergent without cut-off. The terms containing R_{M} and R_{Q} are important when $\omega_p\approx\omega_q$ on the resonance. In this situation one has

$$R_{\mathrm{Q}}\approx 0, \qquad R_{\mathrm{M}}\approx -\frac{3}{2\pi}\int_{\mu}^{\infty}\frac{q^3}{\omega^3}\,\frac{\mathrm{d}\omega}{(\omega_p-\omega-i\varepsilon)^2}. \tag{3.32}$$

The terms coming from the meson current are therefore known in terms of quantities already computed for photoproduction and of the convergent integrals R_{Q} and R_{M} given in eqs. (3.31) and (3.32).

A general discussion of the results together with an explicit evaluation of the cross-sections for radiative scattering will be made elsewhere. An interesting feature of the solution is that the matrix element

$$\langle\psi_\alpha{}^{\mathrm{in}}|j(k)|\psi_\beta{}^{\mathrm{out}}\rangle$$

has the phase $\delta_\alpha+\delta_\beta$, if ψ_α and ψ_β are eigenstates of J, T and of the total energy. Such property is quite general and can be proved using invariance under time reversal and unitarity of the S-matrix [9]).

4. Recoil Effects

Until now all our development has followed a strict static approximation where all recoil effects have been consistently neglected.

It is clear that our approach is essentially non-relativistic since we are unable to deal with pair effects. However, we want to show that it is possible to include in a simple way the recoil effects due to the use of the correct relativistic kinematics. We shall here discuss pion-nucleon scattering: photoproduction and radiative scattering do not offer any new essential difficulty.

The states will be labelled using the notation $\psi_n(W_n, \mathbf{p}, \alpha)$, where W denotes the mass of the state (i.e. the total energy in the CM system), $\mathbf{p}$ is the total momentum and α are all other variables identifying the state. We have †

$$H\psi_n(W_n,\mathbf{p},\alpha)=\sqrt{W_n{}^2+p^2}\;\psi_n. \tag{4.1}$$

We follow the same procedure as in section 2. The only difference is that now

† Of course, in this section we use the convention that the rest energy of the nucleon is M and not zero.

we take into account momentum conservation and eq. (4.1) will enable us to account for recoil effects.

We develop the scattering state vector $\psi_1(W, 0, q)$ $(W = E_q+\omega_q)$ as in eq. (2.4). In the one-meson approximation the integral equation for χ is

$$\sum_{q'} \{\langle\psi_0(-q')a'_{q'}(H-W)a^+_{q''}\psi_0(q'')\rangle + (W-M)\langle\psi_0(-q')a_{q'}\psi_0(0)\rangle\langle\psi_0(0)a^+_{q''}\psi_0(-q'')\rangle\}\chi(q'', q) = 0. \quad (4.2)$$

Using eq. (4.1) and following, step by step, the calculation between eqs. (2.6) and (2.9) we get

$$(W-W')\chi(q', q) = -\sum_{q''} K(q', q'')\chi(q'', q) \quad (4.3)$$

where

$$K(q', q'') = \sum_{n=0,1} \frac{\sqrt{W_n^2+(q'+q'')^2}+W-E'-E''}{(\omega''-E'+\sqrt{W_n^2+(q'+q'')^2})(\omega'-E''+\sqrt{W_n^2+(q'+q'')^2})} \cdot \langle\psi_0(-q')V_{q''}\psi_n(W_n, -q'-q'')\times\psi_n(W_{n'}-q'-q'')V^+_{q'}\psi_0(-q'')\rangle - \frac{W-M}{(W'-M)(W''-M)}\langle\psi_0(-q')V^+_{q'}\psi_0(0)\rangle\langle\psi_0(0)V_{q''}\psi_0(-q'')\rangle.$$

We have arrived at eq. (4.3) only by using the correct kinematical properties of the physical states.

Our problem is reduced to the evaluation of matrix elements of the type $\langle\psi_0 V_q\psi_n\rangle$ where the operators V_q contain only nucleon variables.

Such matrix elements depend on the detailed form of the pion-nucleon interaction. Since here we are interested only in kinematic corrections to the static model we shall evaluate such terms using the static Hamiltonian (2.1). Taking the non-relativistic form for the kinetic energies of the nucleons we have

$$K(q', q'') = \frac{f^2}{3\pi} C(q')C(q'')\langle q'|n\rangle \left\{ \frac{\bar\omega+\dfrac{\mathbf{q}'\cdot\mathbf{q}''}{M}}{\left(\bar\omega'+\dfrac{\mathbf{q}'\cdot\mathbf{q}''}{M}\right)\left(\bar\omega''+\dfrac{\mathbf{q}'\cdot\mathbf{q}''}{M}\right)}(\sigma\tau)_m(\sigma\tau)_n - \frac{\bar\omega}{\bar\omega'\bar\omega''}(\sigma\tau)_n(\sigma\tau)_m + \frac{3\gamma}{\pi}\frac{\bar\omega+\omega_\tau+\dfrac{(\mathbf{q}'\cdot\mathbf{q}'')}{M}}{\left(\bar\omega'+\omega_\tau+\dfrac{(\mathbf{q}'\cdot\mathbf{q}'')}{M}\right)\left(\bar\omega''+\omega_\tau+\dfrac{(\mathbf{q}'\cdot\mathbf{q}'')}{M}\right)}\langle m|P_3|n\rangle \right\} \langle m|q''\rangle \quad (4.4)$$

where here and in the following $\bar\omega = \sqrt{q^2+1}+q^2/2M$

and

$$\gamma = \frac{1}{\pi}\int \frac{\sin^2\delta_3}{p^3 u^2(p)}\,\mathrm{d}p \simeq \tfrac{3}{2}f^2.$$

Taking only the $1/M$ corrections we have

$$K = K^{\mathrm{p}} + K' \tag{4.5}$$

$$K^{\mathrm{p}}(q'q'') = \frac{f^2}{3\pi} C(q')C(q'')\langle q'|n\rangle \left\{ \frac{\bar{\omega}}{\bar{\omega}'\bar{\omega}''}\left[(\sigma\tau)_m(\sigma\tau_n) - (\sigma\tau)_n(\sigma\tau)_m\right] + \frac{3\gamma}{\pi}\,\frac{\bar{\omega}+\omega_{\mathrm{r}}}{(\bar{\omega}'+\omega_{\mathrm{r}})(\bar{\omega}''+\omega_{\mathrm{r}})}\langle m|P_3|n\rangle \right\} \langle m|q''\rangle, \tag{4.5'}$$

$$K'(q', q'') = f^2 \frac{2\pi}{\sqrt{\omega'\omega''}} \left\{ \frac{1}{\bar{\omega}'\bar{\omega}''}\left(1 - \frac{\bar{\omega}}{\bar{\omega}'} - \frac{\bar{\omega}}{\bar{\omega}''}\right)\frac{(\mathbf{q}'\cdot\mathbf{q}'')}{M}(\boldsymbol{\sigma}\cdot\mathbf{q}'')(\boldsymbol{\sigma}\cdot\mathbf{q}')\tau_{q''}\tau_{q'} + \frac{3\gamma}{(\bar{\omega}'+\omega_{\mathrm{r}})(\bar{\omega}''+\omega_{\mathrm{r}})}\left(1 - \frac{\bar{\omega}+\omega_{\mathrm{r}}}{\bar{\omega}'+\omega_{\mathrm{r}}} - \frac{\bar{\omega}+\omega_{\mathrm{r}}}{\bar{\omega}''+\omega_{\mathrm{r}}}\right)\frac{\mathbf{q}'\cdot\mathbf{q}''}{M} \times \left(\tfrac{1}{3}\delta_{q'q''} - (\boldsymbol{\sigma}\cdot\mathbf{q}'')(\boldsymbol{\sigma}\cdot\mathbf{q}')\right)\left(\tfrac{1}{3}\delta_{q'q''} - \tau_{q''}\tau_{q'}\right) \right\}; \tag{4.5''}$$

K^{p} contains only p-waves and becomes identical to the static approximation if one replaces ω by $\bar{\omega}$.

One immediately obtains a form for the scattering matrix by introducing such a kernel in eq. (4.3). Apart from a small shift in the resonance energy (which, of course, can be adjusted by a corresponding change in the cut-off) the result is

$$\mathrm{tg}\,\delta_i = \mathrm{tg}\,\delta_i^{\mathrm{s}}(\bar{\omega})\,\frac{\mathrm{d}\omega}{\mathrm{d}\bar{\omega}} = \mathrm{tg}\,\delta_i^{\mathrm{s}}(\bar{\omega})\,\frac{1}{1+\omega/M} \tag{4.6}$$

where $\mathrm{tg}\,\delta_i^{\mathrm{s}}(\bar{\omega})$ are the phase-shifts obtained in the static approximation in section 2.

The extra coefficient $\mathrm{d}\omega/\mathrm{d}\bar{\omega}$ is the proper recoil correction to the statistical factor and comes in the transformation of the sum on q'' into an integral on $\bar{\omega}$. In CLGN, such a factor does not appear explicitly because it is almost cancelled by some other terms which appear in their relativistic treatment and which are usually associated to pair effects †.

The term K' gives rise only to s- and d-waves. Since such effects are small, we can solve the corresponding equation in the Born approximation. We obtain

† Such a compensation can be seen very clearly in the Born approximation (see ref. [10]).

$$T(q', q'') = -2\pi^2 \frac{\mathbf{q}' \cdot \mathbf{q}''}{\omega M} f^2 \frac{\boldsymbol{\sigma} \cdot \mathbf{q}''(\boldsymbol{\sigma} \cdot \mathbf{q}')\tau_{q''}\tau_{q'}}{\omega^2} + 3\gamma \frac{[(\mathbf{q}' \cdot \mathbf{q}'') - \frac{1}{3}(\boldsymbol{\sigma} \cdot \mathbf{q}'')(\boldsymbol{\sigma} \cdot \mathbf{q}')](\delta_{q'q''} - \frac{1}{3}\tau_{q''}\tau_{q'})}{(\omega+\omega_r)^2}, \tag{4.7}$$

$$\delta_s^{\frac{1}{2}} = \lambda_s \left(\frac{1}{\omega^2} - \frac{4}{(\omega+\omega_r)^2}\right), \quad \delta_s^{\frac{3}{2}} = \lambda_s \left(\frac{-2}{\omega^2} - \frac{1}{(\omega+\omega_r)^2}\right), \quad \lambda_s = \tfrac{1}{3}\frac{f^2 q^5}{M}; \tag{4.8}$$

$$\delta_{D\frac{3}{2}}^{\frac{1}{2}} = \lambda_D \left(\frac{-1}{\omega^2} - \frac{14}{(\omega+\omega_r)^2}\right), \quad \delta_{D\frac{3}{2}}^{\frac{3}{2}} = \lambda_D \left(\frac{2}{\omega^2} - \tfrac{7}{2}\frac{1}{(\omega+\omega_r)^2}\right), \tag{4.9}$$

$$\delta_{D\frac{5}{2}}^{\frac{1}{2}} = \lambda_D \left(\frac{4}{\omega^2} - \frac{4}{(\omega+\omega_r)^2}\right), \quad \delta_{D\frac{5}{2}}^{\frac{3}{2}} = \lambda_D \left(\frac{-8}{\omega^2} - \frac{1}{(\omega+\omega_r)^2}\right),$$

$$\lambda_D = \tfrac{1}{15}\frac{f^2 q^5}{M}.$$

The d-waves given by eq. (4.9) coincide with the ones obtained by CLGN [4]).

We are very grateful to Prof. V. F. Weisskopf for the kind interest he has shown in this investigation; without his advice and encouragement this work would never have been done. We also would like to thank Prof. B. Ferretti for several illuminating discussions and for his criticism.

Appendix 1

A DISPERSION RELATION FOR THE FUNCTION χ

We discuss here some interesting properties of our "wave function" χ which are useful in order to clarify the relation between the dispersion method and our method.

We start from the orthogonality relation between two scattering state vectors corresponding to different energies ω_p and ω_q:

$$\langle \psi_1(p),\ \psi_1(q) \rangle = \delta_{pq}. \tag{A.1.1}$$

We insert for $\psi_1(q)$ the expression (2.4):

$$\sum_{p'} \langle \psi_1(p) a_{p'}^+ \psi_0 \rangle \chi(p', q) = \delta_{pq}. \tag{A.1.2}$$

We recall from Wick's paper [1]) that

$$\langle \psi_1(p) a_{p'}^+ \psi_0 \rangle = \delta_{p'p} - \frac{1}{\omega_{p'} - \omega_p - i\varepsilon} \langle \psi_1(p) V_{p'} \psi_0 \rangle \tag{A.1.3}$$

where the matrix element $\langle \psi_1(p) V'_q \psi_0 \rangle$ can be simply expressed in terms of the scattering phase-shifts.

The "wave function" χ in the angular momentum representation does satisfy the following integral equation:

$$\chi_i(p, q) = \delta(\omega_q - \omega_p) - \frac{1}{\pi} \frac{h_i(p)}{C(p)} \int \frac{\chi_i(p', q) C(q')}{\omega_{p'} - \omega_p - i\varepsilon} \mathrm{d}\omega_{p'}. \qquad \text{(A.1.4)}$$

Eq. (A.1.4) is a rigorous relation between the wave function χ and the scattering amplitudes h_i.

One can put eq. (A.1.4) in a well-known form by defining

$$\frac{h_i(q)}{C(q)} \chi_i(p, q) \frac{C(p)}{h_i(p)} = \xi_i(p, q), \qquad \text{(A.1.5)}$$

$$\xi_i(p, q) = \delta(\omega_q - \omega_p) - \frac{1}{\pi} \int_\mu^\infty \frac{h_i(p') \xi_i(p', p)}{\omega_{p'} - \omega_p - i\varepsilon} \mathrm{d}\omega_{p'}. \qquad \text{(A.1.6)}$$

Eq. (A.1.6) appears in all dispersion treatments of meson photoproduction and similar processes. Its explicit solution has been given by Omnès [11]).

We have to prove that our solution for scattering is consistent with eq. (A.1.4). Indeed, it is easy to verify that if h_i is given by

$$h_i(q) = \frac{\lambda_i \dfrac{q^2}{\omega} u^2(q)}{1 + \lambda_i \dfrac{\omega}{\pi} \displaystyle\int_\mu^\infty \frac{q'^3 u^2(q')}{\omega'^2(\omega - \omega' - i\varepsilon)} \mathrm{d}\omega'}$$

the corresponding "wave function"

$$\chi(p, q) = \delta(\omega_p - \omega_q) - \frac{C(p)}{\omega_p} \frac{\omega_q}{C(q)} \frac{h_i(q)}{\pi(\omega_q - \omega_p - i\varepsilon)}$$

satisfies eq. (A.1.4).

Appendix 2

THE MULTIPLICITY OF THE SOLUTIONS

We would like to discuss the self-consistency problem considered in section 2.3. starting from a less restrictive hypothesis on the scattering phase-shifts.

We assume that $\operatorname{tg} \delta_i$ can be written in the form

$$\operatorname{tg} \delta_i = C^2(q) \sum_n \frac{g_i^{(n)}}{\omega - \omega_i^{(n)}} \qquad \text{(A.2.1)}$$

where $\omega_i^{(n)}$ are the positions of different resonances in the channel (i) sufficiently narrow and well spaced.

As in section 2.3 we have

$$\frac{1}{\pi} \int_{\text{around } \omega_i^{(n)}} \frac{\sin^2 \delta_i}{C^2(\bar{q})} \frac{(\bar{\omega} + \omega) \mathrm{d}\bar{\omega}'}{(\omega' + \bar{\omega})(\bar{\omega} + \omega'')} \approx \frac{\gamma_i^{(n)} (\omega + \omega_i^{(n)})}{(\omega' + \omega_i^{(n)})(\omega'' + \omega_i^{(n)})}. \qquad \text{(A.2.2)}$$

where

$$\gamma_i^{(n)} = |g_i^{(n)}| f(\omega_i^{(n)}), \qquad f(x) = \begin{cases} 1 & \text{for } 1 < x < \omega_{\max} \\ 0 & \text{for } x < 1,\ x > \omega_{\max}. \end{cases} \tag{A.2.3}$$

Eq. (A.2.3) shows that only when the resonances take place in the physical interval $(1-\omega_{\max})$ they can give an appreciable contribution to eq. (A.1.3).

The resulting integral equation for χ can be solved in effective range approximation using the same procedure as in section 2.3. The solution is

$$\operatorname{tg} \delta_i = C^2(q) \left\{ \frac{\lambda_i}{\omega} + \sum_{j,n} \frac{A_{ij}\gamma_j^{(n)}}{\omega+\omega_j^{(n)}} + \frac{I(\lambda_i + \sum_{jn} A_{ij}\gamma_j^{(n)})^2}{1 - I[\sum_{jn} A_{ij}\gamma_j^{(n)}(\omega+\omega_j^{(n)})]} \right.$$

Eq. (A.2.4) shows a very peculiar feature: in the effective range approximation each phase-shift can only pass through one single resonance. Thus the index n can be dropped. The identification of eqs. (A.2.4) and (A.2.1) gives

$$\begin{aligned} &\text{(a)} \quad (g_1+\tfrac{1}{9}\gamma_1) = \tfrac{8}{3}f^2+\tfrac{8}{9}\gamma_2-\tfrac{16}{9}\gamma_3, \\ &\text{(b)} \quad (g_2+\tfrac{7}{9}\gamma_2) = \tfrac{2}{3}f^2+\tfrac{2}{9}\gamma_1-\tfrac{4}{9}\gamma_3, \\ &\text{(c)} \quad (g_3+\tfrac{7}{9}\gamma_3) = -\tfrac{4}{3}f^2-\tfrac{4}{9}\gamma_1-\tfrac{4}{9}\gamma_2; \end{aligned} \tag{A.2.5}$$

$$\begin{aligned} &\text{(a)} \quad -(g_1-\tfrac{1}{9}\gamma_1)\omega_1 = \frac{1}{I}+\tfrac{8}{9}\gamma_2\omega_2-\tfrac{16}{9}\gamma_3\omega_3, \\ &\text{(b)} \quad -(g_2-\tfrac{7}{9}\gamma_2)\omega_2 = \frac{1}{I}+\tfrac{2}{9}\gamma_1\omega_1-\tfrac{4}{9}\gamma_3\omega_3, \\ &\text{(c)} \quad -(g_3-\tfrac{1}{9}\gamma_3)\omega_3 = \frac{1}{I}-\tfrac{4}{9}\gamma_1\omega_1-\tfrac{4}{9}\gamma_2\omega_2. \end{aligned} \tag{A.2.6}$$

Eqs. (A.2.3), (A.2.5) and (A.2.6) are the conditions for the determination of g_i, γ_i, ω_i. Since eq. (A.2.3) is a non-linear relation between the g_i and the γ_i we have to expect a multiplicity of solutions. We have, indeed, to consider separately the different possible values of $f(\omega_i)$.

We first show that if ω_3 is outside the interval $(1-\omega_{\max})$ (and therefore $\gamma_3 = 0$), ω_2 and ω_3 become negative. In such a case, from eq. (A.2.5) one has $g_1 > 0$; $g_2 > 0$; $g_3 < 0$. Inserting in eq. (A.2.1), one finally has $\omega_1 < 0$, $\omega_2 < 0$.

The (33)-state has a privileged situation: if there is only one single resonance this must necessarily be in the state (33).

We now want to show that our system does not exclude the possibility of the existence (in addition to the (3.3)) of a (1) and (2) resonance.

This can be understood by transforming (A.2.5) into

$$\begin{aligned} &(g_1+\gamma_1)+4(g_2+\gamma_2)+4(g_3+\gamma_3) = 0, \\ &(g_1+\gamma_1)-2(g_2+\gamma_2)+(g_3+\gamma_3) = 0, \\ &(g_1-\gamma_1)+(g_2-\gamma_2)-2(g_3-\gamma_3) = 0. \end{aligned} \tag{A.2.7}$$

Because of eq. (A.2.5c) $g_3 < 0$, and using eq. (A.2.3),

$$g_3+\gamma_3 = 0. \tag{A.2.8}$$

This means that the only two solutions of (A.2.7) are $g_1+\gamma_1 = 0$ and $g_2+\gamma_2 = 0$, which give

$$g_1 = -\gamma_1 < 0, \qquad g_2 = -\gamma_2 < 0. \tag{A.2.9}$$

Since C_1, C_2, C_3 are different from zero all equations in (A.2.6) will be meaningful. We shall use the following combinations of (A.2.6):

$$\begin{aligned} &\text{(a)} \quad (\gamma_1-g_1)\omega_1+4(\gamma_2-g_2)\omega_2+4(\gamma_3-g_3)\omega_3 = 9/I, \\ &\text{(b)} \quad (\gamma_1+g_1)\omega_1+ (\gamma_2+g_2)\omega_2-2(\gamma_3+g_3)\omega_3 = 0, \\ &\text{(c)} \quad (\gamma_1-g_1)\omega_1-2(\gamma_2-g_2)\omega_2+ (\gamma_3-g_3)\omega_3 = 0. \end{aligned} \tag{A.2.10}$$

Eqs. (A.2.8) and (A.2.9) show that eq. (A.2.10b) is always identically satisfied.

Therefore the only conditions we can impose on our resonances are

$$\begin{aligned} &2\gamma_3-\gamma_1-\gamma_2 = 9/f^2, \\ &\omega_1\gamma_1+4\omega_2\gamma_2+4\omega_3\gamma_3 = \tfrac{9}{2}/I, \\ &\omega_1\gamma_1-2\omega_2\gamma_2+\omega_3\gamma_3 = 0. \end{aligned} \tag{A.2.11}$$

Eq. (2.7) does, indeed, admit an infinity of γ_i and ω_i in the interval $(1-\omega_{\max})$, each corresponding to tg δ_i acceptable from our point of view.

References

1) G. C. Wick, Revs. Mod. Phys. **27** (1955) 339
2) G. F. Chew, Encyclopedia of Physics
3) G. F. Chew and F. E. Low, Phys. Rev. **101** (1956) 1570, 1579
4) G. F. Chew, M. L. Goldberger, F. E. Low and Y. Nambu, Phys. Rev. **106** (1957) 1337, 1345
5) M. H. Friedman, T. D. Lee and R. Christian, Phys. Rev. **100** (1955) 1496
6) R. Stroffolini, Phys. Rev. **104** (1956) 1146
7) R. E. Cutkosky, Phys. Rev. **109** (1958) 209;
   B. Bosco and R. Stroffolini, Nuovo Cimento **10** (1958) 688
8) F. E. Low, Phys. Rev. **97** (1955) 1392
9) S. Fubini, Y. Nambu and V. Wataghin, Phys. Rev. **111** (1958) 329
10) H. W. Wyld Jr., Phys. Rev. **96** (1954) 1661
11) R. Omnès, Nuovo Cimento **8** (1958) 316

1.C *Nuclear Physics* **10** (1959) 688—697; © *North-Holland Publishing Co., Amsterdam*
Not to be reproduced by photoprint or microfilm without written permission from the publisher

THE SOLUTION OF THE BETHE-GOLDSTONE EQUATION FOR NON-ZERO CENTRE-OF-MASS MOMENTUM

E. WERNER

Institut für theoretische Physik der Universität des Saarlandes, Saarbrücken

Received 2 January 1959

Abstract: The problem of the motion of two particles with non-zero centre-of-mass momentum is discussed for nuclear matter. In a mathematically rigorous treatment the equation of motion is reduced to a set of integro-differential equations that couple together the contributions of the various angular momentum substates present in the total wave-function.

1. Introduction

The Schrödinger equation for the motion of a pair of particles in nuclear matter has been derived by various authors [1, 3, 4]) under the assumption of the validity of the independent-pair model [3, 4]). A discussion of the solution of this equation has been given by Bethe and Goldstone [1]), Brueckner and Gammel [2]), and Gomes, Walecka and Weisskopf [3]) for the special case that the centre-of-mass of the two interacting nucleons is at rest. An approximate solution of the general problem was given by Brueckner and Gammel [2]) who used the angular average of the projection operator on the outside of the Fermi-sphere, thus restoring the spherical symmetry.

In this paper we give a rigorous treatment of the full problem. In section 2 we state the problem and derive the general formalism; in section 3 we evaluate explicitly the projection operator on the outside of the Fermi-sphere. In section 4 we are dealing with the derivation of the integro-differential equations describing the formal solution of the problem. Finally in section 5 we give a comparison with earlier work and a discussion of the results.

2. General Formalism

We consider the motion of two nucleons in nuclear matter (Fermi momentum k_F). We assume for simplicity that the interaction between the nucleons can be described by a local, spherically symmetric two-body potential $v(|\mathbf{r}_i - \mathbf{r}_j|)$.

In the effective-mass approximation the reaction matrix G satisfies the following integral equation [1]):

$$(\mathbf{k}|\tilde{G}|\mathbf{k}_0, \mathbf{P}) = (\mathbf{k}|\tilde{v}|\mathbf{k}_0) - \frac{1}{(2\pi)^3}\int \frac{\theta_{\text{out}}^{(k')}(\mathbf{k}|\tilde{v}|\mathbf{k}')(\mathbf{k}'|\tilde{G}|\mathbf{k}_0, \mathbf{P})}{\frac{1}{m^*}(k'^2 - k_0^2)}\,\mathrm{d}\tau_{k'} \qquad (1)$$

Here $\mathbf{k}$ is the relative momentum of two nucleons, $2\mathbf{P}$ is their centre-of-mass momentum, and m^* is the effective mass. $\theta_{\text{out}}^{(k')}$ is a projection operator on the outside of the Fermi-sphere, acting in k'-space.

The volume over which the k'-integration in the second term of the right side of eq. (1) has to be carried out depends on the total momentum $2\mathbf{P}$. In section 3 we shall have to discuss this dependence on $2\mathbf{P}$ in detail; here we have only to remark that the excluded volume has rotational symmetry around the direction of $2\mathbf{P}$.

This rotational symmetry suggests not to use the usual plane wave states as a basic set of zero-order wave-functions, but instead to employ linear combinations of plane wave states whose absolute values are rotationally symmetric around the direction of total momentum.

We now choose the direction of $\mathbf{P}$ as the z-axis of a polar coordinate system in k-space. A plane wave-state of relative motion can then be characterized by the coordinates $k, \vartheta_k, \varphi_k : |\mathbf{k}\rangle = |k, \vartheta_k, \varphi_k\rangle$. The above mentioned linear combinations can be written

$$|k, \vartheta_k, \mu\rangle = \frac{1}{\sqrt{2\pi}}\int_0^{2\pi} |k, \vartheta_k, \varphi_k\rangle \mathrm{e}^{i\mu\varphi_k}\,\mathrm{d}\varphi_k, \qquad (2)$$

μ integer.

In configuration space $|k, \vartheta_k, \mu\rangle$ is of the form

$$\begin{aligned}
&\varphi_{k,\vartheta_k}^{\mu}(r, \vartheta, \varphi) = \varphi_{k,\vartheta_k}^{\mu}(\mathbf{r}) \\
&= \frac{1}{\sqrt{2\pi}}\int_0^{2\pi} \mathrm{e}^{i\mu\varphi_k}\Big[\sum_{l=0}^{\infty}(2l+1)i^l j_l(kr)\sum_{m=l}^{+l}\alpha_l{}^m P_l{}^m(\cos\vartheta)P_l{}^m(\cos\vartheta_k)\mathrm{e}^{im(\varphi-\varphi_k)}\Big]\mathrm{d}\varphi_k \\
&= \sqrt{2\pi}\sum_{l=0}^{\infty}(2l+1)i^l j_l(kr)\alpha_l{}^{\mu} P_l{}^{\mu}(\cos\vartheta)P_l{}^{\mu}(\cos\vartheta_k)\mathrm{e}^{i\mu\varphi}; \qquad (3)
\end{aligned}$$

$$\alpha_l{}^{\mu} = \frac{(l-\mu)!}{(l+\mu)!} \quad \text{if} \quad |\mu| \leqq l; \quad \alpha_l{}^{\mu} = 0 \quad \text{if} \quad |\mu| > l.$$

The functions $\varphi_{k,\vartheta_k}^{\mu}(\mathbf{r})$ satisfy the orthogonality relation

$$\int \varphi_{k',\vartheta_{k'}}^{\mu'*}(\mathbf{r})\varphi_{k,\vartheta_k}^{\mu}(\mathbf{r})\mathrm{d}\tau_r = \delta(k-k')\delta(\vartheta_k - \vartheta_{k'})\delta_{\mu\mu'}, \qquad (4)$$

and the completeness relation

$$\int \varphi^{\mu^*}_{k,\vartheta_k}(\mathbf{r}')\varphi^{\mu}_{k,\vartheta_k}(\mathbf{r})\mathrm{d}\tau_k = \delta(r-r')\delta(\vartheta-\vartheta')\delta(\varphi-\varphi'), \tag{5}$$

where

$$\int \mathrm{d}\tau_k = \sum_{\mu}\int\int k^2\mathrm{d}k \sin\vartheta_k \mathrm{d}\vartheta_k.$$

The reaction matrix satisfies in the new representation $|k, \vartheta_k, \mu\rangle$ formally the same integral equation as in the $|k, \vartheta_k, \varphi_k\rangle$-representation:

$$\langle k, \vartheta_k, \mu|\tilde{G}|k_0, \vartheta_{k_0}, \mu_0\rangle$$
$$= \langle k, \vartheta_k, \mu|\tilde{v}|k_0, \vartheta_{k_0}, \mu_0\rangle - \frac{1}{(2\pi)^3}\int \frac{\langle k, \vartheta_k, \mu|\tilde{v}|k', \vartheta_{k'}, \mu'\rangle\langle k', \vartheta_{k'}, \mu'|\tilde{G}|k_0, \vartheta_{k_0}, \mu_0\rangle\theta^{(k')}_{\mathrm{out}}}{\frac{1}{m^*}(k'^2-k_0^2)}\,\mathrm{d}\tau_{k'}. \tag{6}$$

From (6) we now derive an integro-differential equation for the wave-function $\psi^{\mu_0}_{k_0,\vartheta_{k_0}}(\mathbf{r})$ in configuration space and an explicit expression for the reaction matrix-elements, which give the potential energy.

We define a wave-function

$$\tilde{\psi}^{\mu_0}_{k_0,\vartheta_{k_0}}(k', \vartheta_{k'}, \mu')$$
$$= (2\pi)^3\delta[(k', \vartheta_{k'}, \mu')-(k_0, \vartheta_{k_0}, \mu_0)] - \frac{\langle k', \vartheta_{k'}, \mu'|\tilde{G}|k_0, \vartheta_{k_0}, \mu_0\rangle\theta^{(k')}_{\mathrm{out}}}{\frac{1}{m^*}(k'^2-k_0^2)}. \tag{7}$$

Here the subscripts $k_0, \vartheta_{k_0}, \mu_0$ indicate that we are dealing with the wave-function which developed from $|k_0, \vartheta_{k_0}, \mu_0\rangle$ under the influence of the perturbation.

From (7) we obtain the wave-function in configuration-space

$$\psi^{\mu_0}_{k_0,\vartheta_{k_0}}(\mathbf{r}) = \frac{1}{(2\pi)^3}\int \tilde{\psi}^{\mu_0}_{k_0,\vartheta_{k_0}}(k, \vartheta_k, \mu)\varphi^{\mu}_{k,\vartheta_k}(\mathbf{r})\mathrm{d}\tau_k$$
$$= \varphi^{\mu_0}_{k_0,\vartheta_{k_0}}(\mathbf{r}) - \frac{1}{(2\pi)^3}\int \varphi^{\mu}_{k,\vartheta_k}(\mathbf{r})\,\frac{\langle k, \vartheta_k, \mu|\tilde{G}|k_0, \vartheta_{k_0}, \mu_0\rangle\theta^{(k')}_{\mathrm{out}}}{\frac{1}{m^*}(k^2-k_0^2)}\,\mathrm{d}\tau_k. \tag{8}$$

Comparison of (6) and (7) gives

$$\langle k, \vartheta_k, \mu|\tilde{G}|k_0, \vartheta_{k_0}, \mu_0\rangle = \frac{1}{(2\pi)^3}\int \langle k, \vartheta_k, \mu|\tilde{v}|k', \vartheta_{k'}, \mu'\rangle\tilde{\psi}^{\mu_0}_{k_0,\vartheta_{k_0}}(k', \vartheta_{k'}, \mu')\mathrm{d}\tau_{k'}. \tag{9}$$

Substituting (9) into (8) and making use of

$$\langle k, \vartheta_k, \mu|\tilde{v}|k', \vartheta_{k'}, \mu'\rangle = \int \varphi^{\mu^*}_{k,\vartheta_k}(\mathbf{r}'')v(r'')\varphi^{\mu'}_{k',\vartheta_{k'}}(\mathbf{r}'')\mathrm{d}\tau_{r''}$$

and of

$$\tilde{\psi}^{\mu_0}_{k_0,\vartheta_{k_0}}(k',\vartheta_{k'},\mu') = (2\pi)^3\int\varphi^{\mu^*}_{k,\vartheta_k}(\mathbf{r}')\psi^{\mu_0}_{k_0,\vartheta_{k_0}}(\mathbf{r}')\mathrm{d}\tau_{r'} \tag{8a}$$

we obtain an integral equation for $\psi^{\mu_0}_{k_0,\vartheta_{k_0}}(\mathbf{r})$:

$$\psi^{\mu_0}_{k_0,\vartheta_{k_0}}(\mathbf{r})-\varphi^{\mu_0}_{k_0,\vartheta_{k_0}}(\mathbf{r})$$
$$=-\frac{1}{(2\pi)^3}\int\int\int\int\frac{\theta^{(k)}_{\text{out}}\varphi^{\mu'^*}_{k',\vartheta_{k'}}(\mathbf{r}')\varphi^{\mu^*}_{k,\vartheta_k}(\mathbf{r}'')\varphi^{\mu}_{k,\vartheta_k}(\mathbf{r})\varphi^{\mu'}_{k',\vartheta_{k'}}(\mathbf{r}'')v(r'')\psi^{\mu_0}_{k_0,\vartheta_{k_0}}(\mathbf{r}')}{\frac{1}{m^*}(k^2-k_0^2)}\mathrm{d}\tau_k\mathrm{d}\tau_{k'}\mathrm{d}\tau_{r'}\mathrm{d}\tau_{r''}. \tag{10}$$

If we use (4) and (5) the k'-integration and the r''-integration drops out and we get

$$\psi^{\mu_0}_{k_0,\vartheta_{k_0}}(\mathbf{r})-\varphi^{\mu_0}_{k_0,\vartheta_{k_0}}(\mathbf{r})$$
$$=-\frac{1}{(2\pi)^3}\int\frac{\theta^{(k)}_{\text{out}}\varphi^{\mu^*}_{k,\vartheta_k}(\mathbf{r}')\varphi^{\mu}_{k,\vartheta_k}(\mathbf{r})v(r')\psi^{\mu_0}_{k_0,\vartheta_{k_0}}(\mathbf{r}')}{\frac{1}{m^*}(k^2-k_0^2)}\mathrm{d}\tau_k\mathrm{d}\tau_{r'}. \tag{11}$$

We can transform this integral equation into an integro-differential equation if we multiply both sides by $(1/m^*)(\nabla^2+k_0^2)$; then we have

$$\frac{1}{m^*}(\nabla^2+k_0^2)\psi^{\mu_0}_{k_0,\vartheta_{k_0}}(\mathbf{r}) = v(r)\,\psi^{\mu_0}_{k_0,\vartheta_{k_0}}(\mathbf{r})-\int g(\mathbf{r}',\mathbf{r})v(r')\psi^{\mu_0}_{k_0,\vartheta_{k_0}}(\mathbf{r}')\mathrm{d}\tau_{r'} \tag{12}$$

where $g(\mathbf{r}',\mathbf{r})$ is defined as

$$g(\mathbf{r}',\mathbf{r}) = \frac{1}{(2\pi)^3}\int\theta^{(k)}_{\text{in}}\varphi^{\mu^*}_{k,\vartheta_k}(\mathbf{r}')\varphi^{\mu}_{k,\vartheta_k}(\mathbf{r})\mathrm{d}\tau_k. \tag{13}$$

Here we have performed the integration over the outside of the Fermi-sphere by first integrating over all k-space and then subtracting the contribution from the inside of the Fermi-sphere. Therefore $\theta^{(k)}_{\text{in}}$ in eq. (13) is a projection operator on the inside of the Fermi-sphere.

The interpretation of eq. (12) is analogous to the interpretation of the corresponding equation if plane-wave states are used (see for example ref. [1]) and [3]): the perturbation of the wave-function through the action of the two-body potential $v(r)$ can contain only states permissible by the Pauli-principle.

The energy of relative motion of the state $\psi^{\mu_0}_{k_0,\vartheta_{k_0}}(\mathbf{r})$ is given by

$$E^{\mu_0}_{k_0,\vartheta_{k_0}} = \frac{k_0^2}{m^*}+\langle k_0,\vartheta_{k_0},\mu_0|\tilde{G}|k_0,\vartheta_{k_0},\mu_0\rangle.$$

With the help of eqs. (9) and (9a) we obtain

$$E^{\mu_0}_{k_0,\vartheta_{k_0}} = \frac{k_0^2}{m^*}+\int\varphi^{\mu_0^*}_{k_0,\vartheta_{k_0}}(\mathbf{r})v(r)\psi^{\mu_0}_{k_0,\vartheta_{k_0}}(\mathbf{r})\mathrm{d}\tau_r. \tag{14}$$

3. Evaluation of the Projection Operator

We now calculate the projection operator

$$g(\mathbf{r}',\mathbf{r}) = \frac{1}{(2\pi)^3}\int \theta_{\text{in}}^{(k)}\varphi_{k,\vartheta_k}^{\mu *}(\mathbf{r}')\varphi_{k,\vartheta_k}^{\mu}(\mathbf{r})\mathrm{d}\tau_k .$$

First we have to make clear the geometry of the problem (see fig. 1). The integral in (13) must be taken over all states for which either the momentum-vector of one nucleon or the momentumvectors of both nucleons lie inside the Fermi-sphere. In fig. 1 we have drawn a cross-section through the

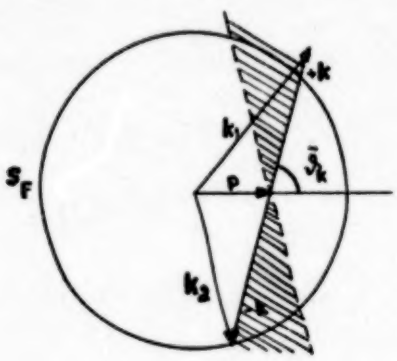

Fig. 1

Fermi-sphere S_F along the direction of $\mathbf{P}$. If $k^2+P^2 < k_F^2$ at least one of the two vectors $\mathbf{k}+\mathbf{P}$ and $\mathbf{P}-\mathbf{k}$ lies inside the Fermi-sphere. Therefore for these states no restriction as to the angular integration exists. If $k_F+P > k > \sqrt{k_F^2-P^2}$ the shaded area between $\bar{\vartheta}_k$ and $\pi-\bar{\vartheta}_k$ must be excluded from the range of integration. Obviously, $\bar{\vartheta}_k$ is given by the relation

$$\cos\bar{\vartheta}_k = \left|\frac{k_F^2-P^2-k^2}{2Pk}\right| . \tag{15}$$

As we have already mentioned in section 2 the problem is rotationally symmetric around the direction of $\mathbf{P}$.

Making use of eq. (3) we obtain for $g(\mathbf{r}',\mathbf{r})$

$$\begin{aligned} g(\mathbf{r}',\mathbf{r}) = \frac{1}{(2\pi)^2}\sum_{\mu,l',l''}(2l''+1)(2l'+1)(-i)^{l''}i^{l'}\alpha_{l''}^{\mu}\alpha_{l'}^{\mu}P_{l''}^{\mu}(\cos\vartheta')P_{l'}^{\mu}(\cos\vartheta)\mathrm{e}^{i\mu(\varphi-\varphi')} \\ \times\Big\{\int_{k=0}^{\sqrt{k_F^2-P^2}}k^2\mathrm{d}k\int_{\vartheta_k=0}^{\pi}\sin\vartheta_k\mathrm{d}\vartheta_k j_{l''}(kr')j'_{l'}(kr)P_{l''}^{\mu}(\cos\vartheta_k)P_{l'}^{\mu}(\cos\vartheta_k) \\ +\int_{k=\sqrt{k_F^2-P^2}}^{k_F+P}k^2\mathrm{d}k\Big[\int_{\vartheta_k=0}^{\bar{\vartheta}_k}\sin\vartheta_k\mathrm{d}\vartheta_k j_{l''}(kr')j_{l'}(kr)P_{l''}^{\mu}(\cos\vartheta_k)P_{l'}^{\mu}(\cos\vartheta_k) \\ +\int_{\vartheta_k=\pi-\bar{\vartheta}_k}^{\pi}\sin\vartheta_k\mathrm{d}\vartheta_k j_{l''}(kr')j_{l'}(kr)P_{l''}^{\mu}(\cos\vartheta_k)P_{l'}^{\mu}(\cos\vartheta_k)\Big]\Big\} \end{aligned} \tag{16}$$

Because of the symmetry properties of $P_l^{\mu}(\cos\vartheta)$ the sum of the two integrals in the square bracket is different from zero only if l' and l'' are either

both even or both odd. We want to indicate this by a prime at the summation sign for the double sum. Then we can write for (16)

$$g(\mathbf{r}', \mathbf{r}) = \frac{1}{2\pi^2} \sum_{\mu, l'} (2l'+1)\alpha_{l'}^{\mu} P_{l'}^{\mu}(\cos\vartheta') P_{l'}^{\mu}(\cos\vartheta) e^{i\mu(\varphi-\varphi')} h_{l'}(r', r)$$
$$+ \frac{1}{2\pi^2} \sum_{\mu, l', l''}' (2l''+1)(2l'+1)(-i)^{l''} i^{l'} \alpha_{l''}^{\mu} \alpha_{l'}^{\mu} P_{l''}^{\mu}(\cos\vartheta') P_{l'}^{\mu}(\cos\vartheta) e^{i\mu(\varphi-\varphi')} h_{l''l'}^{\mu}(r', r) \tag{17}$$

where we have used the following abbreviations:

$$h_l(r', r) = \int_{k=0}^{\sqrt{k_F^2 - P^2}} j_l(kr') j_l(kr) k^2 \, dk \tag{17a}$$

$$h_{l''l'}^{\mu}(r', r)$$
$$= \int_{k=\sqrt{k_F^2 - P^2}}^{k_F+P} k^2 dk \int_{\vartheta=0}^{\bar{\vartheta}_k} \sin\vartheta_k d\vartheta_k j_{l''}(kr') j_{l'}(kr) P_{l''}^{\mu}(\cos\vartheta_k) P_{l'}^{\mu}(\cos\vartheta_k). \tag{17b}$$

The integrals in (17a) and (17b) must be computed numerically.

4. Derivation of the Schrödinger Equation for Partial Waves

We are now in the position to derive the Schrödinger-equation for the radial wave functions in the partial wave expansion of $\psi_{k_0, \vartheta_{k_0}}^{\mu_0}(\mathbf{r})$. Without loss of generality we can make the following ansatz for $\psi_{k_0, \vartheta_{k_0}}^{\mu_0}(\mathbf{r}')$:

$$\psi_{k_0, \vartheta_{k_0}}^{\mu_0}(\mathbf{r}') = \sqrt{2\pi} \sum_l (2l+1) i^l \chi_{k_0, \vartheta_{k_0}, l}^{\mu_0}(r') \alpha_l^{\mu_0} P_l^{\mu_0}(\cos\vartheta') P_l^{\mu_0}(\cos\vartheta_{k_0}) e^{i\mu_0\varphi'}. \tag{18}$$

If we substitute this expression together with the expression for $g(\mathbf{r}', \mathbf{r})$ from eq. (17) into the Schrödinger equation (12) we obtain

$$\sum_l (2l+1) i^l \left\{ \frac{1}{m^*} \left[+ \frac{1}{r^2} \frac{d}{dr} \left(r^2 \frac{d}{dr} \right) + l(l+1) + k_0^2 \right] - v(r) \right\} \chi_{k_0, \vartheta_{k_0}, l}^{\mu_0}(r) \alpha_l^{\mu_0} P_l^{\mu_0}(\cos\vartheta) P_l^{\mu_0}(\cos\vartheta_{k_0}) e^{i\mu_0\varphi}$$
$$= -\frac{1}{2\pi^2} \sum_{\mu, l, l'} \int (2l+1) i^l (2l'+1) \alpha_{l'}^{\mu} \alpha_l^{\mu_0} P_{l'}^{\mu}(\cos\vartheta') P_{l'}^{\mu_0}(\cos\vartheta) P_l^{\mu_0}(\cos\vartheta_{k_0}) P_l^{\mu_0}(\cos\vartheta')$$
$$\times \chi_{k_0, \vartheta_{k_0}, l}^{\mu_0}(r') h_{l'}(r', r) e^{i\mu\varphi} e^{i(\mu_0-\mu)\varphi'} d\tau_{r'}$$
$$- \frac{1}{2\pi^2} \sum_{\mu, l, l', l''} \int (2l+1)(2l'+1)(2l''+1) i^l i^{l'} (-i)^{l''} \alpha_l^{\mu_0} \alpha_{l'}^{\mu} \alpha_{l''}^{\mu} P_{l'}^{\mu}(\cos\vartheta) \tag{19}$$
$$\cdot P_{l''}^{\mu}(\cos\vartheta') P_l^{\mu_0}(\cos\vartheta') P_l^{\mu_0}(\cos\vartheta_{k_0}) \times \chi_{k_0, \vartheta_{k_0}, l}^{\mu_0}(r') h_{l'l''}^{\mu_0}(r', r) e^{i\mu\varphi} e^{i(\mu_0-\mu)\varphi'} d\tau_{r'}$$
$$= -\frac{2}{\pi} \sum_l (2l+1) i^l \alpha_l^{\mu_0} P_l^{\mu_0}(\cos\vartheta) P_l^{\mu_0}(\cos\vartheta_{k_0}) e^{i\mu_0\varphi} \int \chi_{k_0, \vartheta_{k_0}, l}^{\mu_0}(r') v(r') h_l(r', r) r'^2 dr'$$
$$- \frac{2}{\pi} \sum_{l, l'}' (2l+1)(2l'+1) i^{l'} \alpha_l^{\mu_0} \alpha_{l'}^{\mu_0} P_l^{\mu_0}(\cos\vartheta_{k_0}) P_{l'}^{\mu_0}(\cos\vartheta) e^{i\mu_0\varphi} \int \chi_{k_0, \vartheta_{k_0}, l}^{\mu_0}(r') v(r') h_{ll'}^{\mu_0}(r', r) r'^2 dr'.$$

Because of the orthogonality of the spherical harmonics this separates in the following way:

$$\frac{1}{m^*}\left[+\frac{1}{r^2}\frac{\mathrm{d}}{\mathrm{d}r}\left(r^2\frac{\mathrm{d}}{\mathrm{d}r}\right)+l(l+1)+k_0^2\right]\chi^{\mu_0}_{k_0,\vartheta_{k_0},l}(r)P_l^{\mu_0}(\cos\vartheta_{k_0})$$
$$=v(r)\chi^{\mu_0}_{k_0,\vartheta_{k_0},l}(r)P_l^{\mu_0}(\cos\vartheta_{k_0})-\frac{2}{\pi}P_l^{\mu_0}(\cos\vartheta_{k_0})\int\chi^{\mu_0}_{k_0,\vartheta_{k_0},l}(r')v(r')h_l(r',r)r'^2\mathrm{d}r' \quad (20)$$
$$-\frac{2}{\pi}\sum_{l'}{}'(2l'+1)\alpha_{l'}^{\mu_0}P_{l'}^{\mu_0}(\cos\vartheta_{k_0})\int\chi^{\mu_0}_{k_0,\vartheta_{k_0},l'}(r')v(r')h^{\mu_0}_{l,l'}(r',r)r'^2\mathrm{d}r'.$$

In the last line in (20) the prime at the summation sign has the following meaning: If l is even the l'-sum goes only over even values, if l is odd the l'-sum goes over odd values only. Because of the parity conservation in scattering to intermediate states this result was to be expected. The coupling of wave-functions of different angular momentum arises since the projection operator $g(\mathbf{r}', \mathbf{r})$ is not spherically symmetric.

Whereas eq. (20) is exact we can derive a much simpler approximate equation if we assume that the dependence of the wave-function $\chi^{\mu_0}_{k_0,\vartheta_{k_0},l}(r)$ on the parameter ϑ_{k_0} is weak compared to the ϑ_{k_0}-dependence of $[P_l^{\mu_0}(\cos\vartheta_{k_0})]^2$. If we make this assumption and multiply (20) by $P_l^{\mu_0}(\cos\vartheta_{k_0})$ and integrate we obtain

$$\frac{1}{m^*}(D_{r,l}+k_0^2)\chi^{\mu_0}_{k_0,l}(r)=v(r)\chi^{\mu_0}_{k_0,l}(r)$$
$$-\frac{2}{\pi}\int\chi^{\mu_0}_{k_0,l}(r')v(r')h_l(r',r)r'^2\mathrm{d}r'-\frac{2}{\pi}\alpha_l^{\mu_0}(2l+1)\int\chi^{\mu_0}_{k_0,l}(r')v(r')h^{\mu_0}_{ll}(r',r)r'^2\mathrm{d}r'. \quad (21)$$

Eq. (21) can be interpreted as the Schrödinger equation for a radial wave-function which has been averaged over the direction of the incident particle. In this equation the coupling between states of different angular momentum is removed. Physically this is plausible since the averaging over the directions of the incident particles restores the spherical symmetry of the projection operator $g(\mathbf{r}', \mathbf{r})$.

If we know the solutions of the integro-differential equations (20) we can evaluate the energy of relative motion of the state $\psi^{\mu_0}_{k_0,\vartheta_{k_0}}(\mathbf{r})$ according to eq. (14).

If we want to compute single particle energies we have to express the matrix elements $\langle k, \vartheta_k, \varphi_k|\bar{G}|k, \vartheta_k, \varphi_k\rangle$ in the plane wave representation $|k, \vartheta_k, \varphi_k\rangle$ by the matrix elements of $\bar{G}$ in the $|k, \vartheta_k, \mu\rangle$ representation.

To this end we first expand

$$\mathrm{e}^{\mathrm{i}\mathbf{k}\cdot\mathbf{r}}=\sum_{\mu}\beta_\mu\psi^{\mu}_{k,\vartheta_k}(\mathbf{r})$$

or

$$\sum_{m,l}(2l+1)i^l j_l(kr)\alpha_l^m P_l^m(\cos\vartheta)P_l^m(\cos\vartheta_k)\mathrm{e}^{\mathrm{i}m(\varphi-\varphi_k)}$$
$$=\sqrt{2\pi}\sum_{\mu,l}\beta_\mu(2l+1)i^l j_l(kr)\alpha_l^\mu P_l^\mu(\cos\vartheta)P_l^\mu(\cos\vartheta_k)\mathrm{e}^{\mathrm{i}\mu\varphi}. \quad (22)$$

Term-by-term comparison of both sides of eq. (22) gives $\beta_\mu = (2\pi)^{-\frac{1}{2}} e^{-i\mu\varphi_k}$ and therefore

$$e^{i\mathbf{k}\cdot\mathbf{r}} = \frac{1}{\sqrt{2\pi}} \sum_{\mu=-\infty}^{+\infty} e^{-i\mu\varphi_k} \varphi^{\mu}_{k,\vartheta_k}(\mathbf{r}); \quad \mathbf{k} = (k, \vartheta_k, \varphi_k). \tag{23}$$

Now we can evaluate the matrix elements

$$\langle \mathbf{k}|\bar{G}|\mathbf{k}\rangle = \frac{1}{2\pi} \sum_{\mu\mu'} e^{i(\mu-\mu')\varphi_k} \langle k, \vartheta_k, \mu|\bar{G}|k, \vartheta_k, \mu'\rangle. \tag{24}$$

For the matrix elements on the right side of eq. (24) we can write according to eq. (9)

$$\langle k, \vartheta_k, \mu|\bar{G}|k, \vartheta_k, \mu'\rangle = \frac{1}{(2\pi)^3} \int \varphi^{\mu^*}_{k,\vartheta_k}(\mathbf{r}) v(r) \varphi^{\mu'}_{k,\vartheta_k}(r) \mathrm{d}\tau_r. \tag{25}$$

Substituting (3) and (18) we obtain

$$\begin{aligned}
&\langle k, \vartheta_k, \mu|\bar{G}|k, \vartheta_k, \mu'\rangle \\
&\quad = \frac{1}{(2\pi)^2} \sum_{l,l'} (2l+1)(2l'+1)(-i)^l i^{l'} \alpha_l{}^{\mu} \alpha^{\mu'}_{l'} P_l{}^{\mu}(\cos\vartheta_k) P^{\mu'}_{l'}(\cos\vartheta_k) \\
&\quad\quad \cdot \int v(r) j_l(kr) \chi^{\mu}_{k,\vartheta_k,l'}(r) P_l{}^{\mu}(\cos\vartheta) P^{\mu'}_{l'}(\cos\vartheta) e^{i(\mu'-\mu)\varphi} \mathrm{d}\tau_r \\
&\quad = \frac{1}{\pi} \delta_{\mu\mu'} \sum_{l} (2l+1) \alpha_l{}^{\mu} [P_l{}^{\mu}(\cos\vartheta_k)]^2 \int v(r) j_l(kr) \chi^{\mu}_{k,\vartheta_k,l}(r) r^2 \mathrm{d}r \\
&\quad = \delta_{\mu\mu'} \langle k, \vartheta_k, \mu|\bar{G}|k, \vartheta_k, \mu'\rangle.
\end{aligned} \tag{26}$$

Finally we have

$$\langle k, \vartheta_k, \varphi_k|\bar{G}|k, \vartheta_k, \varphi_k\rangle = \frac{1}{2\pi} \sum_{\mu} \langle k, \vartheta_k, \mu|\bar{G}|k, \vartheta_k, \mu\rangle. \tag{27}$$

Relation (27) gives the diagonal elements of the reaction matrix in the plane wave representation expressed by matrix elements of the reaction matrix in the $|k, \vartheta_k, \mu\rangle$-representation. The evaluation of the single-particle energies from the known matrix elements (27) was already discussed by Brueckner and Gammel [2]) and will not be repeated here.

5. Comparison with Earlier Work and Discussion of Results

We want to compare our results with earlier work, especially with the papers of Bethe and Goldstone [1]) and Brueckner and Gammel [2]).

To this end we first treat the special case $P = 0$. From (17), (17a) and (17b) we now obtain

$$\begin{aligned}
g(\mathbf{r}', \mathbf{r}) = \frac{1}{2\pi^2} \int_{k=0}^{k_F} &\sum_{\mu,l} (2l+1) \alpha_l{}^{\mu} P_l{}^{\mu}(\cos\vartheta') \\
&\cdot P_l{}^{\mu}(\cos\vartheta) e^{i\mu(\varphi-\varphi')} j_l(kr) j_l(kr') k^2 \mathrm{d}k.
\end{aligned} \tag{28}$$

The sum under the integral in (28) can be evaluated † and gives $j_0(kr_0)$; $r_0 = |\mathbf{r}'-\mathbf{r}|$. Therefore we have

$$g(\mathbf{r}', \mathbf{r}) = \frac{1}{2\pi^2}\int_{k=0}^{k_F} k^2 j_0(kr_0)\,\mathrm{d}k = \frac{\sin k_F r_0 - k_F r_0 \cos k_F r_0}{2\pi^2 r_0^3}.$$

This is identical with the result of Bethe and Goldstone ††.

No direct comparison with the results of Brueckner and Gammel can be given since these authors work with the integral equation for the wave-function. Nevertheless we can compare their treatment of the exclusion principle in the evaluation of the Green's function with our procedure †††.

We want to show now which approximations in the treatment of the exclusion principle lead to equation (34) of ref. [2]).

We start with the expression for $g(\mathbf{r}', \mathbf{r})$ as given by equations (17), (17a) and (17b). As a first approximation we neglect the coupling between angular momentum states of different l. Then we have

$$h^{\mu}_{l'l''} = \delta_{l'l''}\int_{k=\sqrt{k_F^2-P^2}}^{k_F+P} k^2 f_l{}^{\mu}(k, P) j_l(kr) j_l(kr')\,\mathrm{d}k$$

where

$$f_l{}^{\mu}(k, P) = \int_{\vartheta=0}^{\bar{\vartheta}_k} [P_l{}^{\mu}(\cos\vartheta_l)]^2 \sin\vartheta_k \mathrm{d}\vartheta_k$$

is a weighting function which varies from 1 to 0 when k goes from $\sqrt{(k_F{}^2-P^2)}$ to k_F+P. Now we make a further approximation by dropping the l- and μ-dependence of the weighting factor; then we simply use

$$f(k, P) = f_0{}^0(k, P) = \int_{\vartheta=0}^{\bar{\vartheta}_k} \sin\vartheta_k \mathrm{d}\vartheta_k \qquad (29)$$

as a weighting factor for all angular momentum states. The function $f(k, P)$ given by eq. (29) is the angular average of a function which is zero for states forbidden by the Pauli-principle and unity for permissible states (see fig. 1 and eq. (15)). This coincides with the definition of $f(P, k')$ in ref. [2]), eq. (34).

The error introduced by the replacement of $f_l{}^{\mu}(k, P)$ by $f(k, P)$ is probably small, since this replacement only changes the details of the behaviour of $f_l{}^{\mu}(k, P)$ when it drops from 1 to 0 while k varies from $\sqrt{(k_F{}^2-P^2)}$ to k_F+P.

On the other hand it is not clear what the effect of the neglect of the non-diagonal terms $h^{\mu}_{l'l''}(r', r)$ will be. As we have seen above (see eq. (21)) this neglect can only be justified if the dependence of the radial wave-function $\chi^{\mu}_{k,\vartheta_k,l}(r)$ on the parameter ϑ_k is weak. At least for large values of P this seems doubtful.

† See for example, Morse and Feshbach, Methods of Theoretical Physics, Vol. 2, p. 1574.
†† See ref. [1]), p. 555, eq. (2.26).
††† See ref. [2]), p. 1026, eq. (34).

In order to check this question one should start with the solutions of the simplified equations (21) and use them as test-functions in the integrals on the right side of eq. (20). Then one has to solve an inhomogeneous differential equation; if it turns out that the effect of the admixtures of angular momentum states with $l' \neq l$ is small, the decoupled equations (21) will be a good approximation.

The work of Brueckner and Gammel has shown that only S-, P-, and D-states have to be included for the computation of properties of nuclear matter. Since this feature has its origin in the short range of nuclear forces and the rather low density of nuclear matter, it is surely also true for our treatment. This means that for a fixed value of μ the system (20) reduces to a set of three integro-differential equations; because of parity conservation only the equations for $\chi_{k,\vartheta_k,0}(r)$ and $\chi^0_{k,\vartheta_k,2}(r)$ are coupled together, whereas the equation for $\chi^\mu_{k,\vartheta_k,1}(r)$ is uncoupled, provided we do not want to include states with $l = 3$. The fact that the equation for $\chi^\mu_{k,\vartheta_k,1}(r)$ is uncoupled means that $\chi^\mu_{k,\vartheta_k,1}(r)$ is independent of the parameter ϑ_k; therefore apart from the function h^μ_{11} the equation for the radial function of a P-state is identical with the equation that would be obtained with the Brueckner-Gammel treatment of the exclusion principle.

On the other hand it seems unplausible that the coupling between $\chi_{k,\vartheta_k,0}$ and $\chi^0_{k,\vartheta_k,2}$ can be neglected, particularly since the numerical value of the binding energy of nuclear matter depends sensitively on the behaviour of the wave-function within the potential range. But definite conclusions on this point can be drawn only after numerical solutions of eqs. (20) have been obtained.

A paper on numerical results is in preparation.

References

1) H. A. Bethe and J. Goldstone, Proc. Roy. Soc. A **238** (1957) 551
2) K. A. Brueckner and J. Gammel, Phys. Rev. **109** (1958) 1023
3) L. C. Gomes, J. D. Walecka and V. F. Weisskopf, Ann. of Phys. **3** (1958) 241
4) W. Brenig, Nuclear Physics **4** (1957) 363

AUTHOR INDEX

ABRAHAM, G., *see* WARKE
ALIKHANIAN, A. I. and F. R. ARUTYUNIAN, Scattering of μ-mesons in lead 244
ALLAN, D. L., The energy and angular distribution of protons from 14 MeV neutron reactions with Fe^{54} 348
ALMEIDA, I. G., *see* MARQUEZ
ARUTYUNIAN, F. R., *see* ALIKHANIAN
BARTHOLOMEW, G. A., P. J. CAMPION, J. W. KNOWLES and G. MANNING, The $Y^{89}(n, \gamma)Y^{90}$ reaction 590
BÈS, DANIEL R., The γ-dependent part of the wave functions representing γ-unstable surface vibrations 373
BIEDENHARN, L. C., Time-reversal and polarized nuclear reactions . 620
BISI, A. and L. ZAPPA, Relation between circular polarization and energy for external bremsstrahlung from beta-rays 331
BLOCH, CLAUDE et CYRANO DE DOMINICIS, Un développement du potentiel de Gibbs d'un système composé d'un grand nombre de particules (II) 181
BLOCH, CLAUDE et CYRANO DE DOMINICIS, Un développement du potentiel de Gibbs d'un système quantique composé d'un grand nombre de particules (III) — La contribution des collisions binaires 509
BLOKHINTSEV, L. D., *see* DOLINSKY
BOCKELMAN, C. K., *see* FENSTERMACHER
BOHR, AAGE, Relation between intrinsic parities and polarizations in collision and decay processes 486
BO JUNG, Nuclear spectroscopic measurements on mass separated Pb^{198} sources 440
BOSCO, B., S. FUBINI and A. STANGHELLINI, A theoretical approach to low energy pion physics 663
BURGOV, N. A. and Yu. V. TEREKHOV, Interaction modes in beta decay. Decay of Na^{24} 541
CAMPION, P. J., *see* BARTHOLOMEW
CHOU KUANG-CHAO, *see* OGIEVETSKY
COSTA, N. L., *see* MARQUEZ
CYBULSKA, E. W., *see* MARQUEZ
DAVYDOV, A. and G. FILIPPOV, On the shape of even atomic nuclei 654
DE DOMINICIS, CYRANO, *see* BLOCH

DOBRININ, Yu. P., *see* SOSNOVSKY
DOLINSKY, E. I. and L. D. BLOKHINTSEV, Absorption of polarized μ^--mesons by nuclei. The neutron angular distribution 527
DRAPER, J. E., *see* FENSTERMACHER
EISBERG, R. M., I. E. MCCARTHY and R. A. SPURRIER, Classical and quantal flux in the optical model 571
ELBEK, B., M. C. OLESEN and O. SKILBREID, Inelastic scattering from separated lutecium isotopes 294
EUBANK, H. P., R. A. PECK, Jr. and M. R. ZATZICK, (n, p) cross sections near $Z = 50$ 418
FENSTERMACHER, C. A., J. E. DRAPER and C. K. BOCKELMAN, Resonant neutron capture in Er and Hf 386
FERGUSON, J. M., Co^{57} decay scheme 405
FERGUSON, J. M., *see* KERN
FERRERO, F., R. MALVANO, E. SILVA, J. GOLDEMBERG and G. MOSCATI, Photonuclear reactions in Pr^{141} 423
FIERZ, M., Wolfgang Pauli (1900—1958) 1
FILIPPOV, G., *see* DAVYDOV
FINK, RICHARD W. and BEROL L. ROBINSON, On the half-life of Tl^{204} 82
FODOR, I., *see* KESZTHELYI
FUBINI, S., *see* BOSCO
GEMMELL, D. S., A. H. MORTON and E. W. TITTERTON, A study of the giant resonance regions of Be^8 and C^{12} through the inverse reactions $Li^7(p, \gamma)Be^8$ and $B^{11}(p, \gamma)C^{12}$ 33
GEMMELL, D. S., A. H. MORTON and W. I. B. SMITH, Gamma radiation from the capture of 5 to 7.7 MeV protons in F^{19}, Na^{23}, Al^{27} and P^{31} 45
GLASHOW, SHELDON, L., The renormalizability of vector meson interactions 107
GOLDEMBERG, J., *see* MARQUEZ
GOLDEMBERG, J., *see* FERRERO
GRASHIN, A. F., *see* LOMANOV
GYÖRGYI, G., Bound states in meson pair theory (a possible physical model of hyperons) 197
HULTBERG, SÖLVE, *see* NATHAN
KANE, P. P., Polarization of neutrons produced in the D—D reaction 429
KERN, B. D., W. E. THOMPSON and J. M. FERGUSON, Cross sections for some (n, p) and (n, α) reactions 226
KESZTHELYI, L. and I. FODOR, Investigation of the 16.1 MeV excitation level of C^{12} 564
KNOWLES, J. W., *see* BARTHOLOMEW
KOIČKI, S., J. SIMIĆ and A. KUKOČ, Gamma-gamma angular correlations in Tm^{169} 412

KRÓLIKOWSKI, W., On the second neutral pion 213
KUKOČ, A., *see* KOIČKI
KURATH, D. and L. PIČMAN, Simplified intermediate-coupling procedure in the 1p-shell 313
KUTIKOV, I. E., *see* SOSNOVSKY
LOGUNOV, A. A. and L. D. SOLOVYOV, Dispersion relations for virtual photoproduction 60
LOGUNOV, A. A., On the theory of dispersion relations for virtual processes 71
LOGUNOV, A. A. and I. T. TODOROV, On the proof of dispersion relations for inelastic scattering 552
LOMANOV, M. F., A. G. MESHKOVSKY, YA. YA. SHALAMOV, V. A. SHEBANOV and A. F. GRASHIN, Observation of the bremsstrahlung of π-mesons interacting with nuclei 283
MALVANO, R., *see* FERRERO
MANNING, G., *see* BARTHOLOMEW
MARIĆ, Z. and P. MÖBIUS, Nuclear Raman effect 135
MARKOV, M., An example of a field theory with indefinite metric in Hilbert space (I) 140
MARQUEZ, L., E. W. CYBULSKA, N. L. COSTA, I. G. ALMEIDA and J. GOLDEMBERG, The disintegration of Ga^{73} 28
MARX, G., On the second order wave equation of fermions II 468
MCCARTHY, I. E., Flux of particles in the optical model 583
MCCARTHY, I. E., *see* EISBERG
MESHKOVSKY, A. G., *see* LOMANOV
METZGER, F. R. and W. B. TODD, Internal conversion of gamma-ray transitions in As^{75} 220
MITRA, A. N., P. NARAYANASWAMY and L. K. PANDE, Radiative corrections to bremsstrahlung 629
MÖBIUS, P., *see* MARIĆ
MORTON, A. H., *see* GEMMELL
MOSCATI, G., *see* FERRERO
NAKAGAWA, KIMIKO, The isobaric selection rule for hyperons and K-mesons 20
NAQVI, M. A., Surface corrections to the Fermi-Thomas statistical theory 256
NARAYANASWAMY, P., *see* MITRA
NATHAN, OVE and SÖLVE HULTBERG, Measurements of the γ-radiations from Eu^{152} by the method of external conversion 118
NIELSEN, O. B., N. O. ROY POULSEN, R. K. SHELINE and B. SKYTTE JENSEN, Levels in Os^{190} populated in the decay of 11d Ir^{190} 475
OGIEVETSKY, V. I. and CHOU KUANG-CHAO, Charge symmetry proper-

ties and representations of the extended Lorentz group in the theory of elementary particles 235
OKUN, L. B. and I. Ya. POMERANCHUK, On peripheral interactions of elementary particles. 492
OLESEN, M. C., *see* ELBEK
PANDE, L. K., *see* MITRA
PECK, Jr., R. A., *see* EUBANK
PIČMAN, L., *see* KURATH
POMERANCHUK, I. Ya. *see* OKUN
PROKOFIEV, Yu., A., *see* SOSNOVSKY
RAMAKRISHNAN, ALLADI, N. R. RANGANATHAN and S. K. SRINIVASAN, Meson production in nucleon-nucleon collisions 160
RAMASWAMY, M. K., K-capture to positon branching ratios in the decay of Ga^{68} 205
RANGANATHAN, N. R., *see* RAMAKRISHNAN
RICCI, R. A. and R. VAN LIESHOUT, On the decay of ^{67}Ge 360
ROBINSON, BEROL L., *see* FINK
ROY POULSEN, N. O., *see* NIELSEN
SAAVEDRA, I., Symmetries of leptonic interactions 6
SAWICKI, JERZY and SHIGUEO WATANABE, High energy nucleon-deuteron elastic scattering and the nucleon-nucleon forces 151
SHALAMOV, Ya. Ya., *see* LOMANOV
SHEBANOV, V. A., *see* LOMANOV
SHELINE, R. K., *see* NIELSEN
SILVA, E., *see* FERRERO
SIMIĆ, J., *see* KOIČKI
SIMONS, LENNART, Spin and parity of the 760 keV resonance level in the reaction $Si^{30}(p,\gamma)P^{31}$ and of the intermediate levels in P^{31} . . . 215
SKILBREID, O., *see* ELBEK
SKYTTE JENSEN, B., *see* NIELSEN
ŠLAUS, IVO, The investigation of the mechanism of the $Cr^{52}(d, p)Cr^{53}$ reaction 457
SMITH, W. I. B., *see* GEMMELL
SOLOVYOV, L. D., *see* LOGUNOV
SOSNOVSKY, A. N., P. E. SPIVAK, Yu. A. PROKOFIEV, I. E. KUTIKOV and Yu. P. DOBRININ, Measurement of the neutron life-time 395
SPIVAK, P. E., *see* SOSNOVSKY
SPURRIER, R. A., *see* EISBERG
SRINIVASAN, S. K., *see* RAMAKRISHNAN
STANGHELLINI, A., *see* BOSCO
TEREKHOV, Yu. V., *see* BURGOV
THIRRING, W., On the number of fundamental fields 97

THOMPSON, W. E., *see* KERN
TITTERTON, E. W., *see* GEMMELL
TODD, W. B., *see* METZGER
TODOROV, I. T., *see* LOGUNOV
TOLHOEK, H. A., The capture of muons by complex nuclei 606
VAN DER SPUY, E., The effective atomic field for electron scattering . 53
VAN LIESHOUT, R., *see* RICCI
VILLI, C., A remark on the interpretation of the electron-nucleus scattering experiments 166
WARKE, C. S. and G. ABRAHAM, Holes in the 1p shell in the unified model 306
WATANABE, SHIGUEO, *see* SAWICKI
WERNER, E., The solution of the Bethe-Goldstone equation for non-zero centre-of-mass momentum 688
ZAPPA, L., *see* BISI
ZATZICK, M. R., *see* EUBANK
ZIMÁNYI, J., Circular polarization of gamma rays following the emission of polarized heavy particles 88

SUBJECT INDEX

1. Nuclear Structure

1.B *Two- and three-body problems*

High energy nucleon-deuteron elastic scattering and the nucleon-nucleon forces, Jerzy Sawicki and Shigueo Watanabe 151

1.C *Many-particle systems*

Un développement du potentiel de Gibbs d'un système composé d'un grand nombre de particules (II), Claude Bloch et Cyrano de Dominicis . . . 181
Surface corrections to the Fermi-Thomas statistical theory, M. A. Naqvi . 256
Un développement du potentiel de Gibbs d'un système quantique composé d'un grand nombre de particules (III) - La contribution des collisions binaires, Claude Bloch et Cyrano de Dominicis 509
The solution of the Bethe-Goldstone equation for non-zero centre-of-mass momentum, E. Werner 688

1.D *Nuclear models*

1.D.1 *Shell model*

(n, p) cross sections near $Z = 50$, H. P. Eubank, R. A. Peck, Jr. and M. R. Zatzick. 418

1.D.2 *Collective model*

Measurements of the γ-radiations from Eu^{152} by the method of external conversion, Ove Nathan and Sölve Hultberg. 118
Inelastic scattering from separated lutecium isotopes, B. Elbek, M. C. Olesen and O. Skilbreid 294
Holes in the 1p shell in the unified model, C. S. Warke and G. Abraham 306
The γ-dependent part of the wave functions representing γ-unstable surface vibrations, Daniel R. Bès 373
Resonant neutron capture in Er and Hf, C. A. Fenstermacher, J. E. Draper and C. K. Bockelman. 386
On the shape of even atomic nuclei, A. Davydov and G. Filippov . . 654

1.D.4 *Relationship between different models*

Simplified intermediate-coupling procedure in the 1p-shell, D. Kurath and L. Pičman 313

1.E *Properties of nuclei*

1.E.1 *Energy levels*

Measurements of the γ-radiations from Eu^{152} by the method of external conversion, Ove Nathan and Sölve Hultberg 118
Spin and parity of the 760 keV resonance level in the reaction $Si^{30}(p, \gamma)P^{31}$ and of the intermediate levels in P^{31}, Lennart Simons 215
Co^{57} decay scheme, J. M. Ferguson 405
Nuclear spectroscopic measurements on mass separated Pb^{198} sources, Bo Jung 440

Levels in Os^{190} populated in the decay of 11d Ir^{190}, O. B. Nielsen, N. O. Roy Poulsen, R. K. Sheline and B. Skytte Jensen . . 475
The $Y^{89}(n, \gamma)Y^{90}$ reaction, G. A. Bartholomew, P. J. Campion, J. W. Knowles and G. Manning 590

1.E.5 *Nuclear radii; matter distributions*

A remark on the interpretation of the electron-nucleus scattering experiments, C. Villi 166

2. Nuclear Reactions

2.A *General properties*

2.A.1 *Cross-sections, energy relations*

A study of the giant resonance regions of Be^8 and C^{12} through the inverse reactions $Li^7(p, \gamma)Be^8$ and $B^{11}(p, \gamma)C^{12}$, D. S. Gemmell, A. H. Morton and E. W. Titterton 33
Gamma radiation from the capture of 5 to 7.7 MeV protons in F^{19}, Na^{23}, Al^{27} and P^{31}, D. S. Gemmell, A. H. Morton and W. I. B. Smith 45
Cross sections for some (n, p) and (n, α) reactions, B. D. Kern, W. E. Thompson and J. M. Ferguson. 226
(n, p) cross sections near $Z = 50$, H. P. Eubank, R. A. Peck, Jr. and M. R. Zatzick. 418

2.B *Angular distributions; correlations; polarization*

Circular polarization of gamma rays following the emission of polarized heavy particles, J. Zimányi 88
Spin and parity of the 760 keV resonance level in the reaction $Si^{30}(p, \gamma)P^{31}$ and of the intermediate levels in P^{31}, Lennart Simons 215
The energy and angular distribution of protons from 14 MeV neutron reactions with Fe^{54}, D. L. Allan 348
Polarization of neutrons produced in the D—D reaction, P. P. Kane . . . 429
Relation between intrinsic parities and polarizations in collision and decay processes, Aage Bohr 486
Time-reversal and polarized nuclear reactions, L. C. Biedenharn 620

2.C *Resonance reactions; R-matrix theory*

Gamma radiation from the capture of 5 to 7.7 MeV protons in F^{19}, Na^{23}, Al^{27} and P^{31}, D. S. Gemmell, A. H. Morton and W. I. B. Smith . . 45
Resonant neutron capture in Er and Hf, C. A. Fenstermacher, J. E. Draper and C. K. Bockelman 386

2.D *Statistical model*

The energy and angular distribution of protons from 14 MeV neutron reactions with Fe^{54}, D. L. Allan 348

2.E *Optical model*

Classical and quantal flux in the optical model, R. M. Eisberg, I. E. McCarthy and R. A. Spurrier. 571
Flux of particles in the optical model, Ian E. McCarthy 583

2.F *Direct interaction (other than stripping)*

The energy and angular distribution of protons from 14 MeV neutron reactions with Fe^{54}, D. L. Allan 348

2.G *Stripping and pick-up*

The investigation of the mechanism of the $Cr^{53}(d, p)Cr^{55}$ reaction, Ivo Šlaus 457

2.H *Coulomb excitation*

Inelastic scattering from separated lutecium isotopes, B. Elbek, M. C. Olesen and O. Skilbreid 294

2.I *Photonuclear processes*

A study of the giant resonance regions of Be^{9} and C^{13} through the inverse reactions $Li^{7}(p, \gamma)Be^{8}$ and $B^{11}(p, \gamma)C^{12}$, D. S. Gemmell, A. H. Morton and E. W. Titterton. 33
Nuclear Raman effect, Z. Marić and P. Möbius 135
Photonuclear reactions in Pr^{141}, F. Ferrero, R. Malvano, E. Silva, J. Goldemberg and G. Moscati 423

2.L *Scattering processes (except two-nucleon system and meson scattering)*

The effective atomic field for electron scattering, E. van der Spuy 53
High energy nucleon-deuteron elastic scattering and the nucleon-nucleon forces, Jerzy Sawicki and Shigueo Watanabe 151
Inelastic scattering from separated lutecium isotopes, B. Elbek, M. C. Olesen and O. Skilbreid 294

3. Electromagnetic Radiation

3.A *Gamma radiation*

Co^{57} decay scheme, J. M. Ferguson 405
Gamma-gamma angular correlations in Tm^{169}, S. Koički, J. Simič and A. Kukoč 412
Nuclear spectroscopic measurements on mass separated Pb^{198} sources, Bo Jung 440
Levels in Os^{190} populated in the decay of 11d Ir^{190}, O. B. Nielsen, N. O. Roy Poulsen, R. K. Sheline and B. Skytte Jensen 475
Investigation of the 16.1 MeV excitation level of C^{13}, L. Keszthelyi and I. Fodor 564
The $Y^{89}(n, \gamma)Y^{90}$ reaction, G. A. Bartholomew, P. J. Campion, J. W. Knowles and G. Manning 590

3.B *Internal conversion*

Internal conversion of gamma-ray transitions in As^{75}, F. R. Metzger and W. B. Todd 220
Nuclear spectroscopic measurements on mass separated Pb^{198} sources, Bo Jung 440

3.C *Extranuclear effects*

Measurements of the γ-radiations from Eu^{152} by the method of external conversion, Ove Nathan and Sölve Hultberg 118

4. Beta Decay; Parity

4.D *K-capture*

K-capture to positon branching ratios in the decay of Ga^{68}, M. K. Ramaswamy 205

4.E *Analysis of data*

The disintegration of Ga^{73}, L. Marquez, E. W. Cybulska, N. L. Costa, I. G. Almeida and J. Goldemberg 28
On the half-life of Tl^{204}, Richard W. Fink and Berol L. Robinson 82
On the decay of ^{67}Ge, R. A. Ricci and R. van Lieshout 360
Measurement of the neutron life-time, A. N. Sosnovsky, P. E. Spivak, Yu. A. Prokofiev, I. E. Kutikov and Yu. P. Dobrinin 395

6. Methods and Instruments

6.D *Tables and Computational aids*

The γ-dependent part of the wave functions representing γ-unstable surface vibrations, Daniel R. Bès 373

7. Quantum field theory

7.A *General*

Dispersion relations for virtual photoproduction, A. A. Logunov and L. D. Solovyov 60
On the theory of dispersion relations for virtual processes, A. A. Logunov 71
The renormalizability of vector meson interactions, Sheldon L. Glashow . 107
On the proof of dispersion relations for inelastic scattering, A. A. Logunov and I. T. Todorov 552

7.B *Quantum electrodynamics*

Radiative corrections to bremsstrahlung, A. N. Mitra, P. Narayanaswamy and L. K. Pande 629

7.C *π-meson field (scattering and nuclear forces)*

Meson production in nucleon-nucleon collisions, Alladi Ramakrishnan, N. R. Ranganathan and S. K. Srinivasan 160
Observation of the bremsstrahlung of π-mesons interacting with nuclei, M. F. Lomanov, A. A. Meshkovsky, Ya. Ya. Shalamov, V. A. Shebanov and A. F. Grashin 283
A theoretical approach to low energy pion physics, B. Bosco, S. Fubini and A. Stanghellini 663

8. Elementary particles

8.A *Experimental*

The effective atomic field for electron scattering, E. van der Spuy 53
Relation between circular polarization and energy for external bremsstrahlung from beta-rays, A. Bisi and L. Zappa 331

Interaction modes in beta decay. Decay of Na^{24}, N. A. Burgov and Yu. V. Terekhov 541

8.B *Theory: interactions, transformation properties*

Symmetries of leptonic interactions, I. Saavedra 6
The isobaric selection rule for hyperons and K-mesons, Kimiko Nakagawa 20
On the number of fundamental fields, W. Thirring. 97
On the second neutral pion, W. Królikowski 213
Charge symmetry properties and representations of the extended Lorentz group in the theory of elementary particles, V. I. Ogievetsky and Chou Kuang-Chao 235
On the second order wave equation of fermions II, G. Marx 468
Relation between intrinsic parities and polarizations in collision and decay processes, Aage Bohr 486
On peripheral interactions of elementary particles, L. B. Okun and I. Ya. Pomeranchuk 492
Absorption of polarized μ^--mesons by nuclei. The neutron angular distribution, E. I. Dolinsky and L. D. Blokhintsev 527
The capture of muons by complex nuclei, H. A. Tolhoek. 606

8.C *Fundamental theory of matter*

An example of a field theory with indefinite metric in Hilbert space (I), M. Markov 140
A remark on the interpretation of the electron-nucleus scattering experiments, C. Villi 166
Bound states in meson pair theory (a possible physical model of hyperons), G. Györgyi 197

9. Cosmic Radiation

9.B *Passage of particles through matter*

Scattering of μ-mesons in lead, A. I. Alikhanian and F. R. Arutyunian . . 244

10. News Items

10.A *News items*

1958 Nobel Prize for Physics 93
International conference on high energy accelerators and their instrumentation (CERN, Geneva, 1959) 95
Conference on Nuclear Physics at Oxford (8—10 April 1959) 203
Conference on nuclear forces and the few-nucleon problem at University College, London (8—11 July 1959) 204
New editorial staff for mathematical tables and other aids to computation 626

10.C *Obituaries*

Wolfgang Pauli (1900—1958), M. Fierz 1

10.D *Book reviews*

Akhiezer, A. I. and V. B. Berestetsky, Quantum Electrodynamics (addition) 92
Beck, H. R. *et al.*, Leitfaden des Strahlenschutzes für Naturwissenschafter,

Techniker und Mediziner (J. A. Cohen) 312
FERRETTI, B., editor, 1958 Annual international conference on high energy physics at CERN (L. R.) 311
FLÜGGE, S. V., editor, Encyclopedia of physics, vol. 38, part 1: External properties of atomic nuclei (L. R.) 311
HALL, W. B., Reactor heat transfer (Nuclear engineering monographs III) (Svend Holm) 627
MANSFIELD, W. K., Elementary nuclear physics (Nuclear Engineering monographs I) (Svend Holm) 627
MATHER, K. B. and P. SWAN, Nuclear scattering (L. R.). 92
Sonderausschuss Radioaktivität, Erster Bericht (L. R.) 92
SYRETT, J. J., Nuclear reactor theory (Nuclear engineering monographs II) (Svend Holm) 627
THIRRING, W. E., Principles of quantum electrodynamics (L. R.) 508
WAPSTRA, A. H., G. J. NIJGH, and R. VAN LIESHOUT, Nuclear spectroscopy tables (L. R.) 311

10.E *Errata*

A. Z. DOLGINOV and N. P. POPOV, Nuclear Physics **7** (1958) 591—598 . . 96
B. S. DŽELEPOW and N. N. ZHUKOVSKY, Nuclear Physics **6** (1958) 655—668 96
K. V. LAURIKAINEN, Nuclear Physics **8** (1958) 210 96
RIAZUDDIN, Nuclear Physics **7** (1958) 217. 96
RIAZUDDIN, Nuclear Physics **7** (1958) 223. 96
S. ONEDA, Nuclear Physics **9** (1958/59) 476 628